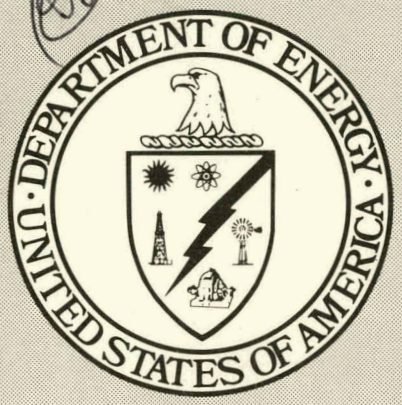
410
7-30-81

(2)

Rec.-410
Bins-171
Special-164
NTIS-75



MASTER

CONF-800433

NUCLEAR METHODS IN ENVIRONMENTAL AND ENERGY RESEARCH

Fourth International Conference Held at
Columbia, Missouri, April 14–17, 1980

Work Performed Under Contract No. AC02-80EV10318

University of Missouri
Columbia, Missouri

TECHNICAL INFORMATION CENTER
UNITED STATES DEPARTMENT OF ENERGY

DISCLAIMER

This report was prepared as an account of work sponsored by an agency of the United States Government. Neither the United States Government nor any agency Thereof, nor any of their employees, makes any warranty, express or implied, or assumes any legal liability or responsibility for the accuracy, completeness, or usefulness of any information, apparatus, product, or process disclosed, or represents that its use would not infringe privately owned rights. Reference herein to any specific commercial product, process, or service by trade name, trademark, manufacturer, or otherwise does not necessarily constitute or imply its endorsement, recommendation, or favoring by the United States Government or any agency thereof. The views and opinions of authors expressed herein do not necessarily state or reflect those of the United States Government or any agency thereof.

DISCLAIMER

Portions of this document may be illegible in electronic image products. Images are produced from the best available original document.

DISCLAIMER

"This book was prepared as an account of work sponsored by an agency of the United States Government. Neither the United States Government nor any agency thereof, nor any of their employees, makes any warranty, express or implied, or assumes any legal liability or responsibility for the accuracy, completeness, or usefulness of any information, apparatus, product, or process disclosed, or represents that its use would not infringe privately owned rights. Reference herein to any specific commercial product, process, or service by trade name, trademark, manufacturer, or otherwise, does not necessarily constitute or imply its endorsement, recommendation, or favoring by the United States Government or any agency thereof. The views and opinions of authors expressed herein do not necessarily state or reflect those of the United States Government or any agency thereof."

This report has been reproduced directly from the best available copy.

Available from the National Technical Information Service, U. S. Department of Commerce, Springfield, Virginia 22161.

Price: Printed Copy A99
Microfiche A01

CONF-800433
Distribution Category UC-11

PROCEEDINGS

OF THE

FOURTH INTERNATIONAL CONFERENCE ON

NUCLEAR METHODS

IN

ENVIRONMENTAL AND ENERGY RESEARCH

Edited by

JAMES R. VOGT

Held at

Columbia, Missouri

April 14-17, 1980

SPONSORED BY

AMERICAN NUCLEAR SOCIETY
Division of Isotopes and Radiation

U.S. DEPARTMENT OF ENERGY
Office of Health and Environmental Research

RESEARCH REACTOR FACILITY
University of Missouri

COLLEGE OF ENGINEERING
ENGINEERING EXTENSION
NUCLEAR ENGINEERING PROGRAM
University of Missouri-Columbia

MEETING CHAIRMEN

General Chairman:	James R. Vogt, Program Director, Research Reactor Facility and Professor of Nuclear Engineering
Vice Chairman:	Walter Meyer, Professor and Chairman, Nuclear Engineering Program
Coordinator:	Frank Seibert, Program Supervisor, Engineering Extension

Work Performed Under Contract No. DE-AC02-80EV10318

CONTENTS

Hevesy Award Presentation and Response viii

SOFTWARE AND MATHEMATICAL METHODS 1

The INAA Advance Prediction Computer Program--Its Uses In Environmental and Energy Research 2
Vincent P. Guinn (Plenary Lecture)

Comparisons of Peak-Search and Photopeak-Integration Methods in the Computer Analysis of Gamma-Ray Spectra 15
Philip A. Baedecker (Plenary Lecture)

Accuracy in Activation Analysis: Count Rate Effects 25
Richard M. Lindstrom and Ronald F. Fleming (Plenary Lecture)

The Random Search Algorithm For Spectrum Analysis 36
Yasushi Takeda

Environmental Radionuclide Concentrations: Statistical Model to Determine Uniformity of Distribution 45
Ervin J. Fenyves, D. Blair Spitzberg, John Wiorkowski and M. Taghi Chehroudi

Direct Image Reconstruction with Limited Angle Projection Data for Computerized Tomography 54
T. Inouye

NUCLEAR METHODS IN ATMOSPHERIC AND WATER RESEARCH 60

Resolving the Sources of Airborne Particles for the Regional Air Pollution Study 61
Daniel J. Alpert and Philip K. Hopke

Identifying Locations of Dominant Point Sources of Elements in Urban Atmospheres from Large, Multielement Data Sets 82
Scott W. Pheingrover and Glen E. Gordon

Nuclear Activation Analysis Methods and the Evaluation of Volcanic Deposits and Emissions 96
W.H. Zoller, D.L. Anderson, M.P. Failey and M.S. Germani

Neutron Activation Analysis in the Survey of River Water Quality and Trace Element Distribution 106
M.T. Ganzerli Valentini, N. Genova, L. Maggi, S. Meloni, R. Stella, A. Albini and F. Salghetti

Non-Destructive Multi-Element Photon Activation Analysis of River Sediments 119
Ch. Berthelot, G. Carraro and V. Verdingh

CONTENTS

Neutron Activation for the Determination of Total Halogenated Organics 127
C.D. Reach, Jr., P.F. Meiburger, and J.T. O'Connor

A Model for Pb-210 in Sediments Influenced by Mixing and Compaction 135
Erik R. Christensen and Nan-Kwang Chien

Elemental Analysis by PIXE of Environmental Samples of the Brazilian Cerrado 147
A.S. Paschoa, G.B. Baptista, E.C. Montenegro, C.V. Barros Leite and T.L. Cullen

Multielement Analysis of Soil of a Sewage-Farm by Photon and Neutron Activation Analysis Using Waste Incineration Ash as Reference Material 159
B.F. Schmitt, and C. Segebade

Study of Heavy Elements (Cd, Hg and Se) in the Aquatic Environment Around Bombay by Radiochemical Neutron Activation Analysis 169
R. Ganesan, P.K. Shah, A.R. Turel and B.C. Haldar

Atmospheric Deposition of Heavy Metals Studied by Analysis of Moss Samples Using Neutron Activation Analysis and Atomic Absorption Spectrometry 175
J.P. Rambaek and E. Steinnes

NUCLEAR AND ATOMIC METHODOLOGY 180

The Use of Neutron-Capture Prompt Gamma-Ray Activation Analysis in Environmental and Energy Research 181
Glen E. Gordon (Plenary Lecture)

Activation-Analysis Prospects by Using a Concentric $5 \cdot 10^{12}$ N/S Sealed Neutron Tube Combined with a Fast Rabbit System 195
H.U. Fanger, R. Pepelnik and W. Michaelis

Neutron Activation Without Multi-Element Standards 205
A. Ahmad, T.D. Mac Mahon, M. Macwani, M.J. Minski, J.G. Williams

The Feasibility of Trace Multielement Analysis by 14-MeV Neutron Activation 216
Robert E. Williams and Philip K. Hopke and Richard Meyer

Environmental Trace Element Analysis Using Short-Lived Nuclides 231
A. Chatt and K.N. DeSilva

CONTENTS

Prompt Neutron Capture Gamma Ray Analysis of Nuclear Fuel Materials with a Pair Spectrometer 247
B.R.S. Pecequilo, G.C. Vandenput, C.R.S. Stopa and A.A. Suarez

Measurement of Moisture Depth Distribution in Composite Materials Using Positron Lifetime Technique 258
Jag J. Singh, W.H. Holt, W. Mock, Jr. and Gerald Mall

The Use of a Synchrotron Radiation X-Ray Microprobe for Elemental Analysis at the National Synchrotron Light Source . . 268
B.M. Gordon

Laser Isotope Dating: A New Technique of Radioisotope Dating Using Lasers 275
R.H. McFarland, Javed Husain and L.D. Schearer

The Feasibility of Using a Novel Pulsed Neutron Source for In Vivo Prompt Gamma Analysis 286
H.C. Biggin and W.D. Morgan

NAA as Viewed from the Perspective of International Atomic Energy Agency Intercomparison Tests 296
Rajmund Dybczynski

PIXE Analysis of Biological and Environmental Samples Using a Proton Microprobe 306
H.R. Wilde, W. Bischof, B. Raith and B. Gonsior

Ultra-Sensitive Trace Element Analysis of Environmental Samples Using Advanced TRXRF Techniques 313
H. Schwenke, J. Knoth and W. Michaelis

Microautoradiography: A Useful Technique for Investigating Radionuclide Transport in Geologic Media 321
J.L. Thompson, W.R. Daniels, S. Maestas, E.N. Vine and K. Wolfsberg

Instrumental Photon Activation Analysis of Cd and Pb in Zinc Ores, with a Rotating Device for Intermittent Irradiations . . 326
Ch. Berthelot and G. Carraro

Error-Free Binary Dilution Method for the Preparation of ppb-Level Liquid Standards 332
Miguel Wiernik

Activation Analysis with Short Lived Nuclides in Environmental Research 337
F. Grass

CONTENTS

NUCLEAR METHODS IN BIOLOGY AND MEDICINE 353

The Chemist in the Clinic 354
J.M.A. Lenihan (Plenary Lecture)

Neutron Activation Analysis of Hair from Breast Cancer Patients 360
Ibrahim Othman and Nicholas M. Spyrou

Toxicokinetic Studies Possible After Acute Inhalation Administration of Compounds Labeled with Short-Lived Isotopes 369
Ray S. Kutzman, Geerd-J. Meyer and Alfred P. Wolf

Application of PIXE and INAA to Biological Materials: Analysis of Serum and Serum Albumin 378
W. Maenhaut, L. De Reu, U. Tomza and J. De Roose

In Vivo Measurement of Cadmium in an Occupationally-Exposed Population 388
K.J. Ellis, W.D. Morgan, S. Yasumura, D. Vartsky, I. Zanzi and S.H. Cohn

A Feasibility Study for the In Vivo Measurement of Silicon and Beryllium by Nuclear Technique 398
K.V. Ettinger, W.D. Morgan, U. Miola, D. Vartsky, K.L. Ellis, L. Wielopolski, S.H. Cohn

Evaluation of the Diagnostic Sensitivity of Scattering Measurements of Bone Density 409
J.G. Roberts, E. DiTomasso and C.E. Webber

Nuclear Magnetic Resonance Method for Observation of Ferromagnetic Pulmonary Contaminants 415
K.V. Ettinger, D. Vartsky, A. Kronenberg and S.H. Cohn

Application of Neutron Activation Analysis in a Regulatory Agency 424
William B. Stroube, Jr. and James T. Tanner

Distribution Pattern of Small and Trace Elements in Human Cancerous Tissues and Normal Human Tissues 427
M. Terai, M. Yasuda, A. Akabane, M. Matsumoto and K. Hashimoto

Neutron Activation Analysis of Copper and Silver in Environmental Samples 437
Parag K. Shah and B.C. Haldar

Trace Element Analysis of Human Hair by Proton Induced X-ray Excitation PIXE 442
A. Aframian, H. Shakiba and A. Housseiney

CONTENTS

In Vivo Neutron Activation Analysis in a Study of Cadmium and Hypertension in South Wales 449
W.D. Morgan, P.E. Cummins, P.C. Elwood, C.J. Evans, J. Dutton and A. Sivyer

INAA Studies of Normal and Diseased Human Brain 459
W.D. Ehmann, W.R. Markesbery, M. Alauddin, D.T. Goodin and T.I.M. Hossian

Biogeochemical Prospecting for Gold by Neutron Activation Analysis 470
I.M. Valente, M.J. Minski and P.J. Peterson

Retention of Metabolized Trace Elements in Rat Tissues: Silver, Cerium, Caesium, Manganese, Scandium and Tin 480
G.V. Iyengar, K. Kasperek and L.E. Feinendegen

Influence of Post Mortem Changes on the Elemental Composition of Rat Liver Studied by Atomic Absorption Spectrometry and Neutron Activation Analysis 491
G.V. Iyengar, K. Kasperek and L.E. Feinendegen

NUCLEAR METHODS IN ENVIRONMENTAL MONITORING 500

A New Technique of Radiation Dosimetry Based on Lyoluminescence 501
K.V. Ettinger, J.R. Mallard and D. Vartsky

Analysis of Fluroine Contamination from Industrial Sources . . 512
John M. Skelly, A. Keith Furr, H. Gene Knight and T.F. Parkinson

In Situ Determination of Transuranic and Fission Product Radionuclides 524
Michael A. Kay

Evaluation of Airborne Radioactive Iodine and Noble Gas Environmental Monitors Using Short-Lived Research Reactor-Produced Radionuclides 534
W.A. Jester and J.H. Wallace

Autoradiographic Studies of Actinide Sorption in Groundwater Systems 540
G.D. O'Kelley, G.W. Beall and B. Allard

Trace Element Analysis of Wild Rodent Tissues Using the PIXE Method 549
Max W. Hill, Nolan F. Mangelson, John F. Ryder, N. Duane Atwood and Benjamin W. Wood

Determination of ^{210}Pb and ^{210}Po in the Environment 560
W.L. Raines, J.W. Dillard, L.G. Kanipe and B.B. Hobbs

CONTENTS

NUCLEAR METHODS IN ENERGY RESEARCH 570

Development of Novel Radiochromatographic Techniques for Investigation of Trace Element Behavior in Coal Liquefaction . . 571
R.H. Filby, A.K. Das Gupta and D.D. Barbee
(Plenary Lecture)

Nuclear Methods in Coal Research 587
W.S. Lyon (Plenary Lecture)

Instrumental Prompt Gamma Activation Analysis of Energy-Related Samples and Standards 597
D.L. Anderson, M.P. Failey, G.E. Gordon and W.H. Zoller

Assessments of Accuracy and Precision of Multi-Element Determinations in Whole Coal by Non-destructive Neutron Activation Analysis 604
George E. Miller, Don R. Burtner and Paul A. Jerabek

Study of Coal Oxidation by Charged Particle Activation Analysis 612
David J. Schlyer and Alfred P. Wolf

Classification of Coal by Trace Analysis Using INAA-Clusteranalysis and Leaching of Precipitator Ash 621
H.A. van der Sloot

Studies of Oxygen and Nitrogen in Coal Conversion Liquids by 14 MeV INAA 636
Samir R. Khalil, David W. Koppenaal and William D. Ehmann

Nuclear Techniques for the On-Line Bulk Analysis of Coal 645
B.D. Sowerby and J.S. Watt

Radiochemical-NAA Studies of Biological Samples in Connection with Marine Production of Petroleum 662
Keith de Lancey and Vincent P. Guinn

Substoichiometric Isotope Dilution Analysis of Tin in Coal Fly Ash 671
Nobuo Suzuki and Hisanori Imura

Variation of Minor and Trace Elements in Coals From Known Geologic Settings 685
A. Bailey and J. Jones

Determination of Mineral Matter in Coal by Target Transformation Factor Analysis 692
Bradley A. Roscoe and Philip K. Hopke

CONTENTS

On-Line Monitoring of Plutonium in Mixed Uranium-Plutonium Solutions 705
K.J. Hofstetter, T.V. Rebagay and G.A. Huff

NUCLEAR METHODS IN TRACER STUDIES 718

Plutonium as a Tracer for Studies of Settling Processes in a Slow Body of Running Water 719

Approach to Cadmium Speciation in Natural Waters Using ^{109}Cd as Radiotracer 729
L. Maggi, V. Caramella-Crespi, N. Genova and S. Meloni

Soil Homogeneity Evaluation by Radionuclide Tracer Breakthrough Curve Interpretation 742
J.S. Brenizer, Jr., A.R. Jarret and W.A. Jester

New Developments in the Use of Stable Activable Tracers in Environmental Science 753
W. Loveland, K. Keasler, L. Ghannam and A. Borovik

LIST OF PARTICIPANTS 763



Professor Vincent P. Guinn Being Presented With The Hevesy Award Certificate and Medal for 1979 By W.S. Lyon Representing the Editorial Board of the Journal of Radioanalytical Chemistry

PROFESSOR VINCENT P. GUINN

PRESENTED WITH THE HEVESY MEDAL FOR 1979

Professor Vincent P. Guinn of the University of California at Irvine is the 1979 receipient of the George Hevesy Medal. Dr. Guinn was cited for his pioneering work in radiochemistry, neutron activation analysis, and his leadership in educating the public, other professions, and students in these applied nuclear techniques.

Dr. Guinn received his Ph. D. degree from Harvard University in 1949 and returned to the Emeryville Research Center, Shell Development Company, Emeryville, California where he had previously been employed as a chemist. From 1949 to 1961 he worked as a radiochemist and advanced to Head of the Radiochemistry Group. His first papers were concerned with the use of radioactive tracers in refinery processes and problems, and counting techniques. In 1961 Dr. Guinn moved to the General Atomic Division, General Dynamics Corporation, San Diego, California where he became Technical Director of the Activation Analysis Program. Thus began his fruitful and innovating career in NAA.

Dr. Guinn early recognized the potential of NAA for forensic applications and his papers and talks strongly influenced developments in this field. In addition to formal scientific presentations, he produced for the AEC a 40-minute film "Neutron Activation Analysis" (1964) and a 28-minute film "Activation Analysis in Crime Investigation" (1966). In 1964 he was co-receipient of the American Nuclear Society's Special Award for Novel Applications of Nuclear Energy, being specifically cited for the forensic activation analysis work. His interest in this application has continued and he often appears as an expert witness or as a consultant in court trials.

Dr. Guinn was also one of the first to recognize the problem of mercury pollution and was chairman of the IAEA Expert Meeting on Mercury Contamination in the Biosphere in Amsterdam in 1967. This activity logically grew from his forensic activities, and during the 1960's and 1970's he helped organize and was several times chairman or honorary president, of, many international conferences. He has been intimately associated with the Modern Trends in Activation Analysis Conferences, and no one who was present at l'Hotel d'Ville in 1972 will ever forget his gracious response to the welcome given the conference delegates by the representative of the City of Paris. Dr. Guinn's diplomatic and delightful manner of handling meetings and interactions between scientists from many nations has put him in wide demand as a meeting organizer and lecturer. His list of consultanties, invited lectureships, and meeting participations is too lengthy for inclusion here. His name is almost synonymous with activation analysis.

During his years at General Atomic Dr. Guinn provided training for a number of scientists both in the USA and from abroad. He also lectured at many universities and institutions throughout the world. With this background and interest in education his move to the University of California at Irvine as Professor of Radiochemistry in 1970 was quite natural. He has remained there since, helping educate another generation of students in the mysteries of nuclear and radio-chemistry. A number of these people have already established positions of leadership in science.

Professor Guinn's contributions continue to be significant. He was among

the first to use computers in predicting and implementing NAA sensitivity. Instrumental NAA is another of his interests, and he and his collaborators have used the technique for many environmental and archeological applications.

Professor Guinn has been active in scientific organizations both in the USA and abroad. He has held many offices, and is a Fellow of the American Nuclear Society, the American Association for the Advancement of Science, and the American Academy of Forensic Sciences. His publication list has passed 200. But Professor Guinn is not the austere white-coated laboratory recluse so often depicted in motion pictures; rather he is an outgoing social person who enjoys meeting with and entertaining his colleagues. Many delightful evenings have been spent by visiting scientists at the Guinn's pleasant La Jolla home with its spectacular view. Often he has hosted informal social hours at his hotel in other cities. Whether in the laboratory, the classroom, the courtroom, or a drawing room, Vincent P. Guinn, this year's Hevesy Medal winner is always at home, always interesting to be with, and always a gentleman.

W.S. Lyon

Nuclear Activation Analysis 45 Years after George Hevesy's Discovery

(Response upon Receipt of the George Hevesy Medal for 1979)

by
Vincent P. Guinn
Department of Chemistry
University of California
Irvine, California 92717

First, may I say how deeply honored and pleased I feel to be selected to receive the George Hevesy Medal for 1979. I am most grateful for the kind and effective efforts of those esteemed peers who nominated me for the award. Their efforts are indeed heart-warming. Also, of course, I am indebted to the Editors of the Journal of Radioanalytical Chemistry, who created this award, in 1968, and to Max Peisach's selection committee.

One of the nicest aspects of receiving this award has been my receipt of congratulatory letters and telephone calls from so many good friends in the field of nuclear activation analysis, from many parts of the world--not only friends whom I see often, but also some friends whom I have not seen in years. One of the most interesting letters was one from Professor Gustaf Arrhenius, of the Scripps Institution of Oceanography, who mentioned that he was closely acquainted with George Hevesy, when both were at the University of Stockholm. Professor Arrhenius is not only an eminent

scientist, but he comes from a well known eminent family of chemists, and his wife is the daughter of George Hevesy.

Another aspect of my receipt of this award that has proved most interesting is that it spurred me to look into the many accomplishments of George Hevesy. He was fantastically creative and productive. Most of us, I am sure, think of George Hevesy primarily for his origination, in 1935 (published in 1936) of a method close to our collective hearts--neutron activation analysis. Yet only 2 of his 397 scientific publications dealt with NAA. Perhaps it will be a surprise to many, as it was to me, to learn that George Hevesy also

(1) performed the first radiotracer study (with RaD, in 1913),
(2) was the first to measure self-diffusion (jointly with G. Gróh),
(3) discovered the element hafnium (in 1923, jointly with D. Coster),
(4) was the first to use radiotracers in biology (in 1923),
(5) was the first to use radiotracers in medical research (in 1923),
(6) invented the method of X-ray fluorescence (in 1931, jointly with E. Alexander),
(7) invented the method of isotope dilution analysis (in 1932, jointly with R. Hobbie), and
(8) was the first to use an artificially-produced radiotracer (P-32, in 1935).

In 1943, he received the Nobel Prize for these many pioneering discoveries in the field of radiochemistry.

George Hevesy, more correctly known as György von Hevesy, or George de Hevesy, was Hungarian--born in Budapest in 1885. He was educated in Budapest, Berlin, and Freiburg, receiving his Ph.D. in 1908. After his Ph.D., his research was conducted in Zurich, in Karlsruhe (with Fritz Haber), in Cambridge (with Ernest Rutherford), in Vienna (with H. Paneth), in England (with H.G. Mosely), and in Copenhagen (with Niels Bohr). When the Nazis came to power in the 1930's, he left Germany to return to Copenhagen, where he and Hilde Levi originated the method of NAA in 1935. When the Nazis invaded Denmark, he fled to Sweden, to the University of Stockholm. George Hevesy died in Freiburg in 1966, almost at his

81st year. For those interested in more complete accounts of the career of this great man, four good sources are listed as references.[1-4]

Initially, the development and application of the method of nuclear activation analysis grew slowly, since in the 1930's work was hampered by the limitations of low-flux isotopic neutron sources, early cyclotrons of limited performance, lack of detectors efficient for gamma-ray detection, and no methods for gamma-ray spectrometry measurements. Around 1945, however, the method experienced a much more rapid growth rate, brought about by the availability of the very first nuclear reactors, with their vastly higher fluxes of thermal neutrons. The Oak Ridge National Laboratory, with the world's first regularly operating reactor (the X-10 graphite-moderated, air-cooled, natural-uranium, 10^{12}-flux reactor) became the fountainhead of the now accelerating growth rate of the methodology and applications of the neutron activation analysis (NAA) method. For a number of these early years, the Oak Ridge NAA group was headed by the late George W. Leddicotte, a good friend of mine for many years. Since the time that Leddicotte left Oak Ridge, the NAA group there has been under the capable direction of William S. Lyon, also a good friend of mine of long standing. Today, some 35 years after it first began NAA work, the Oak Ridge group continues to contribute significantly to progress in the field of NAA.

During the second half of the decade of the 1940's, the method, although now having access to high fluxes of thermal neutrons in a few nuclear reactors, was still hampered by the necessity of employing radiochemical separations, with carriers, since induced activities still had to be beta-counted separately, usually with an end-window Geiger-Müller or gas-proportional counter.

With the advent of the first high-efficiency, energy-proportional detector for gamma radiation--the thallium-activated sodium iodide (NaI(Tl)) scintillation detector, development of the instrumental, nondestructive form of the NAA method experienced a rapid growth rate during the 1950's. Single-channel and very soon multichannel pulse-height analyzers rapidly also became commercially available, as well as progressively larger canned single-crystal NaI(Tl) detectors, coupled to improved photomultiplier tubes. By the second half of the decade of the 1950's, the first international conferences devoted solely or significantly to NAA

studies were already being held. During the 1950's, many additional research-type nuclear reactors were put into operation in many other countries, besides additional ones in the United States. During this period, the NAA group at Harwell, in England, under the direction of Albert A. Smales, soon joined the Oak Ridge group as a leader in this field. The group at the University of Michigan, in the U.S., headed by W. Wayne Meinke, also became an early major contributor to progress in the field during the 1950's. In recognition, particularly, of their early pioneering work, it was most appropriate that Wayne Meinke was selected as the first recipient, and Albert Smales as the second recipient, of the George Hevesy Medal.

Just as the NaI(Tl) scintillation detector initiated, in about 1950, the rapid expansion of the NAA method, particularly in its purely instrumental form, and held the center of the stage during roughly the 15-year period of 1950-1965, so the lithium-drifted germanium (Ge(Li)) semiconductor detector initiated a new era of rapid growth of the instrumental NAA (INAA) method in the early 1960's. Ge(Li) gamma-ray spectrometry (nowadays also including the use of intrinsic germanium detectors) has dominated the field of INAA for the 15-year period from about 1965 to the present.

The development of the INAA method, first with the scintillation detector and then with the semiconductor detector, also involved several necessary concurrent developments. Rapidly, commercially available pulse-height analyzers advanced from single-channel units, to scanning single-channel units, to multichannel units of a moderate number of analysis and storage channels (suitable for NaI(Tl) spectra), to improved transistorized multichannel analyzers (replacing the older vacuum-tube circuitry), to all solid-state analyzers with many thousands of channels--needed to capitalize on the 20-30 fold better energy resolution of the germanium detector, compared with the NaI(Tl) scintillation detector. With the wealth of digital data available in even a single germanium pulse-height spectrum, the development of suitable computer programs for the optimum and rapid processing of such data also advanced rapidly beyond the extensive programs already developed for NaI(Tl) spectra. Another development during this period was a coupling of the older individual-element radiochemical separation form of the NAA method with the newer instrumental

form, namely, the use of group radiochemical separations, followed by gamma-ray spectrometry measurements.

During the 1960's and 1970's, in particular, the early pioneering NAA studies of Meinke and Smales were greatly extended by other recipients of the George Hevesy Medal--particularly by Julian Hoste in Belgium, Philippe Albert in France (charged-particle activation analysis), Francesco Girardi in Italy, the late and greatly missed Saadia Amiel in Israel, and Robert E. Jervis in Canada. I consider it a real privilege to have had all of these eminent scientists as close friends of mine for many years.

As for my own work in the field of NAA, I will make only a few remarks. My first work in the field of radiochemistry occurred in 1951, while I was with the Shell Development Company, and this has been my major field of research ever since. In 1957, with the availability in my laboratory of a 10^8 thermal-neutron flux (using a 3 MeV electron Van de Graaff), my studies in the field of NAA commenced. Shortly, my facilities at Shell were augmented by a 14 MeV neutron generator. These studies produced such developments as the first multi-element INAA system,[5] the first routine (40 hours per week) use of INAA, the first INAA determinations of pesticide residues,[6] and some of the first sensitive oxygen determinations.

Late in 1961, I joined General Atomic, as Technical Director of the Activation Analysis Program. There, for the first time, I had a nuclear reactor at my disposal. My 8 years at General Atomic were busy ones, with quite a few new developments. Those that at least I consider to be the more significant ones were the development of (1) a comprehensive Activation Analysis Service, (2) the first NAA method for the detection of gunshot residues,[7] (3) INAA methods involving second and sub-second induced activities,[8] (4) a method of improving the detection sensitivities for such elements by means of 1000 MW reactor pulses,[9] (5) a statistical method of establishing INAA upper limits for undetected elements, (6) comprehensive studies of potential applications of NAA in scientific crime investigation,[10] (7) a routine, computerized multi-element INAA scanning procedure, and (8) various advanced computer programs for the processing of INAA data (largely developed by H.P. Yule). Other interesting projects at General Atomic were the production of two films for the AEC: a 40-minute film on "Neutron Activation Analysis" and a 28-minute film enti-

tled "The Nuclear Witness--Activation Analysis in Crime Investigation"; and organization and hosting at GA of an Advanced Seminar on Activation Analysis, in 1965, and the First International Conference on Forensic Activation Analysis, in 1966.

Being a frustrated teacher, I at long last decided to join the ranks of academia, joining the faculty of the Department of Chemistry at the University of California at Irvine as professor of radiochemistry in 1970--again, with a TRIGA reactor to work with. At U.C. Irvine, with my various graduate students and postdoctoral fellows, I have been able to continue and extend many of my earlier NAA interests, such as pulsing and non-pulsing studies with very short-lived activities,[11] various forensic studies such as the INAA comparison of bullet-lead specimens,[12] studies of early and current levels of mercury in seafoods involving museum specimens of tuna,[13] and studies of marine pollution.[14] Undoubtedly the most important new development in my research at U.C. Irvine, in my opinion, is the development of an INAA Advance Prediction Computer Program,[15,16] the most recent aspects of which are the subject of my Plenary Lecture at this conference. Other interesting studies at U.C. Irvine have included my recent analyses of the bullet-lead evidence specimens involved in the President Kennedy assassination,[17] and studies related to the SLA Shootout, the Michigan Coed murders, the Oscar Bonavena murder, and many other fascinating cases.

To conclude, let me say that I have been remarkably fortunate throughout my scientific life--fortunate first of all to obtain my doctorate at Harvard University under the great G.B. Kistiakowsky, and then to be initiated to the field of radiochemistry early in 1952 by an outstanding teacher, R.T. Overman. Both at Shell and at General Atomic, my closest colleague was the outstanding radiochemist, H.R. Lukens, with whom I have some 26 joint publications. Fortunate, also, to be urged to join the U.C. Irvine faculty by the eminent hot-atom chemist, F.S. Rowland, and to be able to collaborate at Irvine closely with radiochemist/Reactor Supervisor, G.E. Miller. I thoroughly enjoyed my years at Shell Development, enjoyed my years at General Atomic even more, and my enjoyment of the mix of teaching and research at U.C. Irvine is even greater still. Both at Shell Development and General Atomic I had the good fortune to work with excellent colleagues. At Irvine, I have been most fortunate in having many outstanding radiochemists in my

research group: many postdoctoral fellows, graduate students, IAEA trainees, and undergraduate research students. Four of my present graduate students and two of my current postdoctoral fellows are attending this Conference.

Nuclear activation analysis is a fascinating field, with outstanding experts in it all over the world--most of whom I see often or periodically, and am happy to know as good friends. George Hevesy, we thank you!

References

1. G. Hevesy, Adventures in Radioisotope Research (2 volumes), (Oxford University Press, 1962).

2. H. Levi etal, "George de Hevesy", Intl. J. Appl. Rad. & Isotopes, 16 (1965) 505.

3. H. Levi, "George de Hevesy", Nucl. Physics, 98 (1967) 1.

4. F. Szabadváry, "George Hevesy", Journal of Radioanalytical Chemistry, 1 (1968) 97. See also: Dictionary of Scientific Biography, VI, ed. by C.C. Gillispie (Charles Scribner's Sons, N.Y., 1972) 365.

5. V.P. Guinn and C.D. Wagner, Analytical Chemistry, 32 (1960) 317.

6. V.P. Guinn and J.C. Potter, J. Agricultural and Food Chemistry, 10 (1962) 232.

7. R.R. Ruch, V.P. Guinn, and R.H. Pinker, Nuclear Science and Engineering, 20 (1964) 381.

8. V.P. Guinn, in Production and Use of Short-Lived Radioisotopes from Reactors (International Atomic Energy Agency, Vienna, 1963), p. 3.

9. H.P. Yule and V.P. Guinn, in Radiochemical Methods of Analysis (International Atomic Energy Agency, Vienna, 1965), p. 111.

10. V.P. Guinn, H.R. Lukens, and H.L. Schlesinger, U.S. AEC Report GA-9807 (1970), 263 pages.

11. D.A. Miller and V.P. Guinn, Journal of Radioanalytical Chemistry, 32 (1976) 179.

12. V.P. Guinn and M.A. Purcell, Journal of Radioanalytical Chemistry, 39 (1977) 85.

13. G.E. Miller, P.M. Grant, R. Kishore, F.J. Steinkruger, F.S. Rowland, and V.P. Guinn, Science, 175 (1972) 1121.

14. J.J.M. de Goeij, V.P. Guinn, D.R. Young, and A.J. Mearns, in Comparative Studies of Food and Environmental Contamination, IAEA-SM-175/15 (Intl. Atomic Energy Agency, Vienna, 1974), p. 189.

15. V.P. Guinn, Journal of Radioanalytical Chemistry, 15 (1973) 473.

16. V.P. Guinn, E. Garzanov, and E. Cortes T., Journal of Radioanalytical Chemistry, 43 (1978) 599.

17. V.P. Guinn, Analytical Chemistry, 51 (1979) 484A.

SOFTWARE AND MATHEMATICAL METHODS

Session Chairman

R.H. Filby

THE INAA ADVANCE PREDICTION COMPUTER PROGRAM-- ITS USES IN ENVIRONMENTAL AND ENERGY RESEARCH

by

Vincent P. Guinn
Department of Chemistry
University of California
Irvine, California 92717

Abstract

The instrumental neutron activation analysis (INAA) Advance Prediction Computer Program (APCP) is described, and some of its advantages and uses are presented. For any given sample matrix type (e.g., seawater, blood, coal, igneous rock, etc.) of only approximately known typical or average elemental composition, the APCP rapidly computes the principal details of its Ge(Li) pulse-height spectrum; the energy and net photopeak area (and its standard deviation) of each statistically-significant peak; and all Compton levels and Compton edges produced by the various input elements--for any thermal-neutron flux, irradiation period, decay time, counting time, detector, and counting geometry specified. The APCP routinely makes such calculations for 12 stepped sets of irradiation, decay, and counting periods. For each set of conditions, the maximum allowable sample size is calculated, with subsequent calculations based on that size. INAA lower limits of detection are also readily calculated for additional elements of interest not known to be present. The program output readily shows the optimum conditions for the measurement of any element of interest in such a matrix. Experimental tests on various materials have shown that the APCP is remarkably effective. Current improvements and extensions are described, as well as a number of illustrative applications.

Introduction

Over the years, many compilations of interference-free limits of detection (LOD) have been published, for various specified conditions of thermal-neutron flux (ϕ_{th}), maximum irradiation period (t_i), decay time (t_d), counting period (t_c), type and size of detector, counting geometry, and criterion for minimum detectability. For example, two such compilations have been published by the author--one for a standard NaI(Tl) detector,[1] and one for a medium-sized Ge(Li) detector.[2] Such compilations are very useful, but they only indicate the smallest amount of an element detectable, under the stated conditions, in the absence of any other significant activity. If the half life of a species is long enough, such limits of detection can be reached, in practice, if a good high-yield radiochemical separation of the element of interest is carried out prior to counting.

Especially with the advent of sizable high-resolution Ge(Li) and intrinsic Ge detectors, and of suitable computer programs for data reduction, interest in the use of the nondestructive, purely instrumental form of the NAA method (INAA) has rapidly increased in recent years. This is a powerful multi-element method, enabling one, in some cases, to detect and measure induced activities from as many as 25-30 elements in a single pulse-height spectrum. However, under given conditions, the INAA LOD for an element is usually quite a bit larger than its interference-free LOD, since each photopeak must be measured on top of the cumulative Compton level produced by higher-energy γ-rays from other induced activities, rather than on top of a zero baseline. How much larger the INAA LOD for an element will be, via a particular γ-ray of one of its (n,γ) products, depends upon the overall elemental composition of the sample matrix and the particular t_i, t_d, and t_c conditions. Depending upon these various factors, the INAA LOD for a given element may be as much as 10 to 50 times larger than its interference-free LOD under otherwise the same conditions.

About 9 years ago, the author decided that it would be quite valuable to have a method of predicting INAA limits of detection, for various kinds of sample-matrix types for which at least approximate typical or average compositions were known for the major and minor elements of the matrix. It was soon established that such a method was feasible, using a simplified model of γ-ray pulse-height spectra. The author presented a paper on this subject, for NaI(Ti) pulse-height spectra, utilizing this model, at the 1972 Modern Trends conference at Saclay, published the following year in the Journal of Radioanalytical Chemistry.[3] Since that time, in our laboratory the method has been greatly extended, refined, computerized, and tested experimentally for INAA with Ge(Li) detectors, and several papers have been published describing various aspects of these developments.[2,4-7]

Present Nature of the INAA Advance Prediction Computer Program

The APCP is not a method of processing actual INAA data. Rather, it is a method to guide the analyst to optimum INAA procedures and to provide him in advance with reasonably good predictions of attainable precisions and detectabilities for any sample matrix type for which approximate average or typical major/minor elemental composition data are available. Various aspects of the APCP, in its present form, are summarized below.

Useful APCP Output Information. The APCP output provides ad-

vance information of considerable usefulness. For each of 12 stepped sets of t_i, t_d, t_c conditions, increasing from $t_i = t_d = t_c = 0.1$ minute each (Set I) in steps of 3 up to $t_i = t_d = t_c = 100$ minutes each (Set VII), then to $t_i = t_d = 300$ minute each, but with t_c remaining at 100 minutes (Step VIII), and thereafter t_i remaining at 300 minutes and t_c remaining at 100 minutes, but t_d increasing to 1000, then 3000, then 10,000, and finally 30,000 minutes (Sets IX, X, XI, XII), the output gives the following information (for a given flux, detector, counting geometry, and maximum allowable sample size):

a. The maximum sample weight that will not result in appreciable spectrum distortion by pulse pileup.
b. A list of all (n,γ) products that are deleted from further consideration (for that Set) because the total γ-ray counting rate (in cps) at start of count (SOC) of each is less than 0.01% of the total sample counting rate.
c. For all remaining (n,γ) products, a listing of the cumulative sample Compton level (in counts per keV) between each of the Compton edges produced by each γ-ray energy of all the products, arranged in descending energy.
d. A listing of each photopeak that should be measurable to a relative standard deviation (% σ_{rel}) of less than ±100%, arranged in descending energy. Each such peak is identified as to radionuclide, energy in keV, integrated number of net photopeak counts (NPPC) obtained during the counting period t_c, the standard deviation of the NPPC (σ_{NPPC}), and the percent relative standard deviation of the NPPC (% σ_{rel}).
e. Wherever a photopeak will partially overlap with a Compton edge, attention is drawn to it by an asterisk in the output. Wherever a photopeak will partially overlap with another photopeak, two asterisks are shown. If both situations occur, three asterisks are shown.
f. For high-energy γ-rays, the magnitudes and standard deviations of the first and second escape peaks are also printed out (identified the same way as for the primary peaks).
g. For high-energy γ-rays, the contribution of each to the 511 keV photopeak (via pair-production interaction in the shield) is also printed out.
h. If lower limits of detection for elements not included in the known approximate input composition (or included in the input but not appearing in the output) are desired, these can be calculated and printed out for each such specified element of interest.
i. If desired, any or all of the predicted pulse-height spectra can be computer plotted, as log (counts per keV) versus keV. Each plot shows each cumulative Compton level, each Compton edge, and each statistically-significant peak (the latter shown as a vertical line of height proportional to the peak area, superimposed on top of the underlying Compton level at that energy).

Additional Information. By manual inspection of the outputs for all 12 sets of conditions, the following additional valuable information can be readily obtained:

a. For each set of conditions, the total number of input elements detectable, under such conditions.
b. For each input element that exhibits only one detectable activity, the particular set of conditions that provides the most precise measurement of it.
c. For each input element that exhibits two or more detectable

activities, the radionuclide product that provides the most precise measurement of that element (and the best set of conditions for its measurement).

d. For each detectable activity that generates more than one photopeak, the energy of the peak that provides the most precise measurement of that radionuclide (and the best set of conditions for its measurement).

e. Similarly, the optimum conditions for the detection of each non-input or non-detected input element of interest (i.e., giving the lowest INAA LOD for that element in that matrix), via the best γ-ray of its best (n,γ) product, are rapidly seen from the printouts.

Later, these various additional pieces of useful information may also be computerized, replacing the present manual scanning procedures.

Other Uses of the APCP. The APCP is also very useful for rapidly determining the weight of an element to be used as a standard, for any or all of the 12 sets of t_i and t_d conditions. For each such calculation, the input composition is simply the pure element, and the sample weight limit is usually set as that which gives a total counting rate, at SOC, of 1000 cps. The APCP can also be used for NAA with either pre- or post-irradiation chemical separations of interfering elements (e.g., Na), or of groups of elements, by simply deleting the removed elements from the input elemental composition. In cases for which insufficient even approximate elemental composition information is available for some kind of matrix, just a small amount of exploratory experimental INAA work--involving just two irradiation periods and a few decay periods--will provide suitable approximate input composition data for use in the APCP. If the activity limitation at SOC, for a given neutron flux, irradiation time, and decay time, results in limitation to a sample size that is too small to be representative and/or too small to be weighed and handled conveniently, a larger sample at a correspondingly lower flux can be employed. For example, if a 10^{13} flux for 100 minutes, followed by a decay period of 100 minutes, would result in a sample size of only one milligram (giving a total count rate of 5000 cps at SOC), one could instead use the same irradiation and decay times, but use a 100 mg sample and a 10^{11} flux. Other sets of conditions, besides the 12 standard sets, can readily be input, or various of the standard sets can be deleted, as desired.

Principal Assumptions of the APCP. The original objective, which is still the main objective, was to make use of a simple model of γ-ray pulse-height spectra that would be sufficiently accurate for the intended purposes, yet compatible with even a rather small computer. The model introduced for this purpose, in 1972, was that of a flat, horizontal Compton region, ending abruptly at the Compton edge, for each γ-ray. For statistical calculations, the effective base width of each photopeak is taken as 3 times its FWHM. This very simple model has proved to be surprisingly accurate and effective.

Permanent Input Data. The APCP permanently-stored data include "best" values for all relevant nuclear data for all stable nuclides and their γ-emitting (n,γ) radionuclide products (atomic weights, isotopic abundances, thermal-neutron (n,γ) cross sections, half lives, γ energies and yields). Also permanently stored are equations for the response curves of two of our Ge(Li) detectors, a "5%" and a "15%" detector, each for a given counting geometry. These equations are fittings to experimentally-determined parameters, versus γ-ray energy, of detection efficiency, photofraction, and resolution--and for high-energy γ-rays, the relative sizes of the

first and second escape peaks, and the contribution to the 511 keV peak via pair-production interaction in the detector shield. Also stored is the calculated saturation total cps per gram of element of each (n,γ) product, for a 10^{13} flux and zero decay time, for the standard counting geometry, for each detector. Also stored is the experimentally-determined equation for the relationship between sample-to-detector distance and counting geometry.

Variable Input Data. For each matrix to be considered, the variable input data include the known approximate elemental composition (in weight fraction of each element), the desired flux, the maximum allowable total counting rate at SOC (usually set at 5000 cps), the maximum sample size (in grams), the detector to be used, and the counting distance to be used.

Experimental Tests of the APCP. To date, the APCP has been used to predict the pulse-height spectra from each of the 12 stepped sets of conditions for a number of widely used reference materials and Standard Reference Materials (e.g., Bowen's Kale, Orchard Leaves, Bovine Liver, IAEA Animal Muscle, NBS Coal, etc.), followed by experimental measurements to ascertain how closely the APCP predicts the actual experimental results for such materials, for which extensive and accurate (as opposed to only approximate) elemental-composition data are available. A number of these comparisons are in progress or are planned for the near future, but those carried out to date indicate that the computer model is quite effective. For example, the results published[6] for one set of conditions for IAEA Animal Muscle H-4 showed that all predicted photopeaks were observed experimentally (and none that were not predicted to be significant), that the mean ratio of measured to predicted NPPC was 1.06 ± 0.36, for the 15 peaks, and that the mean ratio of the 9 major Compton levels (measured vs. predicted) was 0.93 ± 0.23.

An Example--NMS Standard Coal (SRM 1632)

It is instructive to examine an illustrative case of the application of the APCP to a material for which extensive accurate elemental-composition data are available--to show the kinds of useful output information that result. The example chosen here is that of NBS Standard Coal, SRM 1632. In an excellent and extensive four-laboatory INAA study of this NBS Coal, Ondov et al[8] report values for 37 elements, covering a wide range of radionuclide half lives. Their mean values for these 37 elements were used as input to our APCP program for a 10^{13} thermal-neutron flux, a 5% Ge(Li) detector at a 2 cm distance, and a maximum sample size of 5 grams or 5000 total cps at SOC (whichever was smaller). All 12 standard sets of t_i, t_d, t_c conditions (I-XII) were calculated.

The APCP output provided a wealth of information, summarized in Tables I and II. Table I shows, for each of the 12 sets of conditions: the maximum allowable sample weight, the number of elements detectable, the number of radionuclides detectable, and the number of significant photopeaks. It is seen that the maximum sample weight ranges from around one milligram, for the shorter t_i/t_d conditions, up to over two grams, for Set XII (long t_i, long t_d). Also, it is seen that the number of elements detectable in a single spectrum increases from only 4 (Set I) up to 21 elements (Set VI), decreases to 19 elements (Sets VII-IX), then increases up to 28 elements (Set XI), and then down to 24 elements (Set XII). This sort of bimodal frequency distribution is observed for many complex matrices, of a wide variety of types. The average number of (n,γ) products detectable, per element detected, only ranges from 1.00 up to 1.24. The average number of photopeaks observed, per (n,γ) pro-

duct detected, however, increases from 1.67 on up to 5.30. It is thus obvious (as we of course know from general experience) that the pulse-height spectra generally become increasingly complex, for such materials, with increasing t_i, t_d, and t_c: more elements become detectable, more radionuclides, and many more peaks. For condition Set XI, NBS Coal should produce 175 statistically-significant photopeaks that are at least 1 keV apart, from 33 radionuclides of 28 elements. As discussed later, this increased number of peaks of course results in an increased number of overlapping peaks, especially at the lower energies.

In Table II, the detectabilities of the 37 NBS Coal input elements are presented for each of the 12 sets of conditions. They are coded as follows: 3 = precisely detectable, to ±0-4% σ_{rel}; 2 = detectable to σ_{rel} of ±4-20%; 1 = detectable to σ_{rel} of ±20-40%; 0 = borderline detectability, i.e., to σ_{rel} of ±40-100%; and -- = not detectable, i.e., σ_{rel} > 100% of the value. A study of Table II reveals many things, such as the condition set (or sets) that provides the most precise INAA measurement of any element of interest, in the NBS Coal matrix; which elements are not detectable in this matrix (Ni and Ag), etc. It is seen that, for example, Se is measurable, but only to a borderline precision, under Sets I and II (via its 17.5 s Se-77m product), then not at all (Sets III-IX), and finally to a good precision, under Set XII (via its 120 d Se-75 product). Similar two-radionuclide examples may be seen for Ca, Sc, Co, Sr, Cs, Ba, Hf, Th, and U. The measurement precisions for elements that form only one gamma-emitting (n,γ) product (e.g., Na, Mg, Al, etc.), or essentially only one, instead merely improve and then decline in just one series of condition sets--usually being best (lowest % σ_{rel}) in a condition set that is somewhere near the radionuclide half life.

Table III merely provides a view of a small portion of the Compton level printout for a 0.72 g sample of NBS Coal under condition Set XI (t_i = 5 hrs, t_d ~ 1 week, t_c = 100 min). It shows just 10 consecutive Compton levels (counts/keV) in the range of Compton edges between 904 and 801 keV--out of a total printout of 155 Compton edges at energies > 50 keV.

Similarly, Table IV merely provides a view of a small portion of the printout of significant (% σ_{rel} < 100%) photopeaks for NBS Coal, again for condition Set XI. It shows just 10 consecutive photopeaks, in the energy range from 920 keV to 752 keV. The total printout for this condition set includes 175 significant photopeaks.

Table V presents a simple example of how the APCP predicts, again for NBS Coal, which (n,γ) product would give the better measurement precision for cobalt--10.5 m Co-60m or 5.27 y Co-60. It is seen that both products can give good precisions, but that condition Set XII, using the 1173 keV peak of Co-60, results in a better relative precision (ca 0.5%) than does the 58 keV peak of Co-60m in Set V (ca 4%). Table V also shows, in a very simple example, how the APCP indicates which of the two γ-rays of Co-60 would produce better measurement precision for cobalt in this matrix. It is seen that the 1173 keV is slightly the better of the two.

Another valuable piece of resulting information, not shown in the Tables, pertains to the frequency of occurrence of overlapping peaks, mentioned earlier. For NBS Coal, it turns out that there is considerable crowding together of peaks in the low-energy region, as would be expected. However, the printouts provide much more semi-quantitative detail than would otherwise be available in any reasonable period of time. For example, under condition Set XI, of the 175 statistically-significant photopeaks, only 55 of these do not overlap with one or more peaks, for a Ge(Li) detector of typical

energy resolution. Even in the high-energy region (>1000 keV), there are six doublets, one triplet, and one quadruplet. In the intermediate-energy region (500-1000 keV), the extent of overlapping is more severe, with even one region (552-564 keV) of 7 overlapping peaks. In the low-energy region (50-500keV), large numbers of peaks overlap, especially below 152 keV. There are 36 overlapping peaks in the 87-152 keV region, forming a long part of the spectrum in which no single peak is entirely resolved. The same situation occurs in the 52-72 keV region, with 21 overlapping peaks. The very low-energy region is thus of limited usefulness. Even if a detector of better resolution, such as a low-energy photon detector (LEPD), were used, many overlapping peaks would still be encountered in this region. The very low-energy region (< 115 keV) might be significantly worse yet if K X-rays, resulting from EC decays and internal conversion, were also included in the treatment.

The NBS Coal example described was presented just to show the kind of useful detail that is rapidly produced with the APCP, in this case, however, from a very accurate and comprehensive input elemental composition. In real use, of course, the value of the APCP is in predicting such parameters with reasonable accuracy for samples of a matrix for which only typical or average elemental composition data are available. In this connection, it is interesting to note that very similar results were also obtained when average composition data from a large suite of Illinois Basin coals[9] were used as input, instead of data for NBS Coal. Even though the ratios of the concentration in NBS Coal to the correspondingg average concentration in Illinois coal ranged from as low as 0.12 (for Zn) to as high as 4.6 (for Sr), the mean ratio was only 1.46, for the 37 elements for which data were available for both. Of these 37 elements, 25 have higher concentrations in the NBS Coal and 12 are higher in the Illinois coal. Thus the variations in composition from one coal to another considerably offset one another, so far as the cumulative Compton levels are concerned, with a similar partial offsetting of short-lived activities vs. long-lived activities. The lower limit of detection of an element is a function of the square root of the Compton counts in the region where its best peak should occur, rather than being a function of the Compton level itself, thus making such LOD's less sensitive to moderate variations in Compton levels, and hence compositions, than would otherwise be the case.

Conclusions

The APCP continues to be improved and further tested. In the U.C. Irvine laboratory, it is used routinely, and is proving to be remarkably effective and useful. In a matter of minutes, it provides a detailed output that would require months of steady hand calculation to duplicate. In this laboratory, it has now been applied to a host of different kinds of matrices, many of which are of practical interest in environmental and energy research--reference materials, Standard Reference Materials, and materials for which only average composition data are available. After making frequent changes/improvements in the APCP during the last year and a half, it should soon be possible to fill the many requests that have been received for copies of the basic program, written in BASIC-PLUS and used at U.C. Irvine with a PDP-11/45 computer. From time to time, auxiliary programs, adding to the basic program, will also become finalized and available for distribution, as will the main program written in FORTRAN-IV.

Progress on the development of the APCP during the period of

1972 to mid 1979 was slow, due to lack of funding. Since then, with the availability of NSF funding, its development is proceeding much faster. Two graduate students, Miss Jeanne Leslie and Miss Leiko Nakazawa, with the author, have now almost completed several important additions to the basic program, such as inclusion of all (n,n'), (n,p), (n,α), and (n,2n) fast-neutron products. Visiting professor Dr. Roger Naeumann, from Norway, has also made good progress on incorporating fission products into the APCP, for matrices containing appreciable concentrations of natural uranium. Radioactive daughters, only a few of which are currently included in the program (e.g., Pa-233 and Np-239) and these only approximately, will soon be included.

Acknowledgements

The author is deeply appreciative of the financial support provided by the National Science Foundation (Grant No. CHE 79-11877), and to the scientific contributions to this work of Jeanne Leslie, Leiko Nakazawa, and Dr. Roger Naeumann.

References

1. V.P. Guinn, Chapter in Volume 1, Part III D of Physical Methods of Chemistry, edited by A. Weissberger and B.W. Rossiter (John Wiley and Sons, N.Y., 1972), p. 447.

2. V.P. Guinn and J. Hoste, chapter 7 in IAEA Technical Report No. 197 on Elemental Analysis of Biological Materials, ed. by R.M. Parr (IAEA, Vienna,1980), p. 105.

3. V.P. Guinn, Journal of Radioanalytical Chemistry, 15 (1973), 473.

4. V.P. Guinn, D. Chambless, E. Cortes T., K. de Lancey, E. Garzanov, D.A. Miller, G.E. Miller, and M.A. Purcell, Proceedings of the Fourth European Conference of TRIGA Users (Vienna, Sept. 28-30, 1976). General Atomic Company, San Diego, California, 1976, p. 4-11.

5. V.P. Guinn, Jeanne C. Leslie, and L.E. Murray, Trans. Amer. Nucl. Soc., 27 (1977) 218.

6. V.P. Guinn, E. Garzanov, and E. Cortes T., Journal of Radioanalytical Chemistry, 43 (1978) 599.

7. V.P. Guinn, O.I. Asubiojo, J.C. Leslie, and C.C. Perkins, Trans. Amer. Nucl. Soc., 32 (1979) 191.

8. J.M. Ondov, W.H. Zoller, I. Olmez, N.K. Aras, G.E. Gordon, L.A. Rancitelli, K.H. Abel, R.H. Filby, K.R. Shah, and R.C. Ragaini, Anal. Chem., 47 (1975) 1102.

9. H.J. Gluskoter, R.R. Ruch, W.G. Miller, R.A. Cahill, G.B. Dreher, and J.K. Kuhn, Trace Elements in Coal: Occurrence and Distribution, (Illinois State Geological Survey Circular 499, Urbana, Ill., 1977), 153 pages.

TABLE I

Main Features of Predicted INAA Pulse-Height Spectra of NBS Coal

Condition Set No.	Maximum Sample Wt. (mg)	Number of Elements Detectable	Number of Radionuclides Detectable	Number of Significant Photopeaks > 50 keV
I	4.2	4	4	8
II	1.6	6	6	10
III	0.67	8	8	15
IV	0.54	9	9	19
V	2.4	17	19	47
VI	6.6	21	26	73
VII	3.5	19	21	76
VIII	2.9	19	19	79
IX	8.6	19	20	83
X	38	25	30	109
XI	720	28	33	175
XII	2300	24	29	145

TABLE II

Predicted INAA Precision Profiles for 37 Elements in NBS Coal

Element	Coded Measurement Precision for Condition Set No.											
	I	II	III	IV	V	VI	VII	VIII	IX	X	XI	XII
Na	–	–	0	1	3	3	3	3	3	3	3	–
Mg	–	–	–	0	2	2	–	–	–	–	–	–
Al	3	3	3	3	3	0	–	–	–	–	–	–
Cl	–	0	0	2	3	3	3	0	–	–	–	–
K	–	–	–	–	0	2	3	3	3	3	2	–
Ca	–	–	0	1	2	2	–	–	–	–	1	2
Sc	2	2	2	–	–	–	0	1	2	3	3	3
Ti	–	–	0	2	3	2	–	–	–	–	–	–
V	–	0	2	2	3	0	–	–	–	–	–	–
Cr	–	–	–	–	–	–	–	–	–	2	3	3
Mn	–	–	0	2	3	3	3	3	3	–	–	–
Fe	–	–	–	–	–	–	–	–	0	2	3	3
Co	–	–	–	0	3	2	–	–	–	1	3	3
Ni	–	–	–	–	–	–	–	–	–	–	–	–
Zn	–	–	–	–	–	–	0	1	1	1	2	3
As	–	–	–	–	–	2	2	3	3	3	3	–
Se	0	0	–	–	–	–	–	–	–	0	2	3
Br	–	–	–	–	2	2	2	3	3	3	3	0
Rb	–	–	–	–	–	–	–	–	–	–	2	2
Sr	–	–	–	–	2	3	3	3	2	–	1	2
Ag	–	–	–	–	–	–	–	–	–	–	–	–
In	–	–	–	–	1	2	2	0	–	–	–	–
Sb	–	–	–	–	–	–	1	2	2	3	3	3
Cs	–	–	–	–	–	1	2	1	–	0	2	3
Ba	–	–	–	–	2	3	3	–	0	2	3	3
La	–	–	–	–	–	2	2	3	3	3	3	3
Ce	–	–	–	–	–	–	0	0	2	2	3	3
Sm	–	–	–	–	1	2	3	3	3	3	3	3
Eu	–	–	–	–	2	3	3	3	3	3	3	3
Tb	–	–	–	–	–	–	–	–	–	0	2	3
Yb	–	–	–	–	–	–	–	–	–	1	3	3
Lu	–	–	–	–	–	–	0	0	0	2	3	3
Hf	0	0	–	–	–	–	–	–	–	1	3	3
Ta	–	–	–	–	–	–	–	–	–	0	2	3
W	–	–	–	–	–	–	1	2	2	2	2	–
Th	–	–	–	–	–	0	–	–	0	2	3	3
U	–	–	–	–	2	2	–	0	1	2	3	0

TABLE III

Illustrative Portion of Compton Level Printout
(NBS Coal, Condition Set XI)

(Total of 155 Compton edges > 50 keV and levels)

Compton Edge (keV)	Compton Counts/keV
904	8036
892	9037
879	9061
872	9108
843	9112
840	9115
839	9519
834	9520
804	9545
801	9550

TABLE IV

Illustrative Portion of Photopeak Printout
(NBS Coal, condition Set XI)

(Total of 175 photopeaks > 50 keV)

Radionuclide	E_γ (keV)	NPPC	$\pm \sigma_{NPPC}$	$\pm \%\sigma_{rel,NPPC}$
La-140	920	3141	460	14.64
Sc-46	889	13356	472	3.53*
La-140	868	7968	464	5.83
Na-24	858	7561	463	6.12
Eu-152m	842	20015	475	2.37*
Br-82	828	17205	474	2.75
La-140	816	38095	495	1.30
Br-82	777	67015	520	0.78**
W-187	773	493	452	91.67**
La-140	752	8491	462	5.44

TABLE V

Example (Cobalt) of Best Radionuclide and Best Gamma Ray (NBS Coal)

Condition Set	Radionuclide and γ-Ray Energy (with ± % σ_{rel})		
	Co-60m, 58 keV	Co-60, 1173 keV	Co-60, 1332 keV
IV	±43%	---	---
V	4.0	---	---
VI	4.6	---	---
X	---	±36%	±45%
XI	---	1.7	2.1
XII	---	0.49	0.55

Comparisons of Peak-Search and Photopeak-Integration Methods in the Computer Analysis of Gamma-Ray Spectra

Philip A. Baedecker
U.S. Geological Survey
Reston, Virginia 22092

Introduction

Myriad methods have been devised for extracting quantitative information from gamma-ray spectra by means of a computer, and a critical evaluation of the relative merits of the various programs that have been written would represent a Herculean, if not an impossible, task. The results from the International Atomic Energy Agency (IAEA) intercomparison, which may represent the most straightforward approach to making such an evaluation, showed a wide range in the quality of the results - even among laboratories where similar methods (or the same program!) were used (1). The most clear-cut way of differentiating between programs is by the method used to evaluate peak areas: by the iterative fitting of the spectral features to an often complex model, or by a simple summation procedure. Previous comparisons (2, 3) have shown that relatively simple algorithms can compete favorably with fitting procedures, although fitting holds the greatest promise for the detection and measurement of complex peaks. However, fitting algorithms, which are generally complex and time consuming, are often ruled out by practical limitations based on the type of computing equipment available, cost limitations, the number of spectra to be processed in a given time period, and the ultimate goal of the analysis. Comparisons of methods can be useful, however, in helping to illustrate the limitations of the various algorithms that have been devised. This paper presents a limited review of some of the more common peak-search and peak-integration methods, along with some empirical evaluations of their effectiveness.

Peak-search procedures

Most peak-search procedures, although differing in approach, are similar in practice and involve the convolution of the spectral data into a new spectrum, which facilitates the location of peaks, by using a transform function that has zero area in the absence of a peak. One class of procedures is that which computes derivative spectra (4, 5), generally by least squares fitting using the now classical procedures of Savitzky and Golay (6). Various cross correlation procedures have been proposed that generally use a square wave or rectangular wave correlator (7, 8) or a normal distribution (9). The application of five different convolutes to a weak gamma-ray line is illustrated in Fig. 1. The signal is computed as:

$$S_j = \sum_{i=-m}^{i=n} c_i d_{j+i} \qquad (1)$$

where j is the channel number, c_i is the coefficient and d_j is the number of counts in channel j, and i is the ith channel relative to channel j within the convolute. The convolution procedure involves moving an m+n+1 channel "window" across the spectrum or region of interest. j is the centermost channel in the window, and for a convolute having an odd number of channels, n=m, whereas for an even number of channels, n=m-1. When derivative spectra are computed, the channels within the "window" are fit to a polynomial by least squares (c_i being the least squares coefficient for data point i), and the derivative at i=0 is computed as the derivative of the spectrum at channel j. In the correlation procedure, c_i is a coefficient that gives the correlator function the approximate shape of the signal sought. The standard deviation of the signal, based on

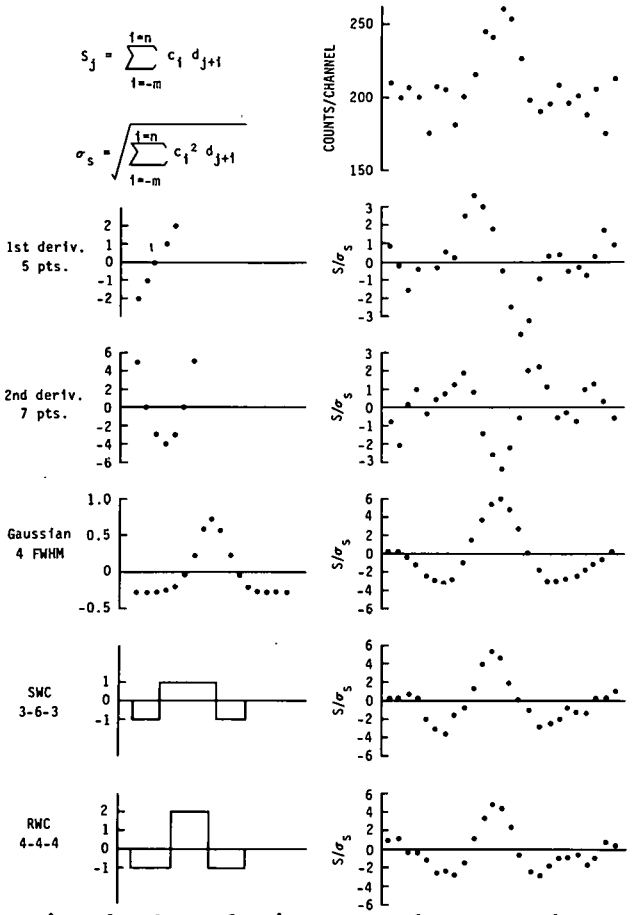


Fig. 1. Convolution procedures used for the location of photopeaks in gamma-ray spectra.

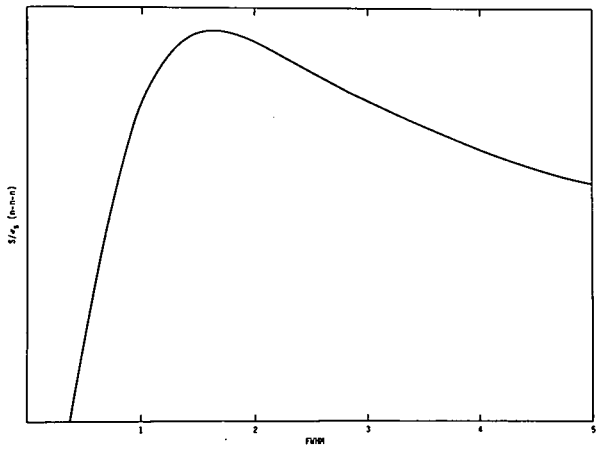


Fig. 2. Signal to noise ratio for a rectangular wave correlator as a function of the ratio of correlator width to peak width.

the Poisson counting error, is:

$$\sigma_s = \sqrt{\sum_{i=-m}^{i=n} c_i^2 \, d_{j+1}} \qquad (2)$$

Plotted on the left-hand side of Fig. 1 are the coefficients used, and on the right is the ratio of the signal to its standard deviation. The first two examples are first and second derivative spectra using the Savitzky-Golay coefficients for fitting 5 and 7 channels, respectively, to a quadratic, and determining the derivative of the centermost channel. The last three examples represent cross correlation procedures. One would expect, a priori, that the best correlator would be a signal that is virtually identical with the signal sought (10): a symmetrical normal distribution, normalized to zero area within the width of the convolute, with a full width at half maximum (FWHM) which is the same as the gamma-ray line sought. The last two examples represent the simplest type of cross correlation function in which the coefficients have values of -1, 1 or 2, and therefore are the easiest to program with a computer. The fifth method, the rectangular wave (or "n-n-n") convolute (RWC), has some advantages over the fourth, square wave (or "n-2n-n") convolute (SWC), in that the central positive component can be any integer number of channels, and, for a given width of the central component, produces a stronger signal to noise ratio. The cross-correlation procedures can be seen to produce a signal which is an inverted second derivative spectrum. The signal to noise ratio produced by a correlator of fixed width is dependent on the width of the photopeak sought. This is shown in Fig. 2 which is a plot of signal-to-noise ratio as a function of the ratio of correlator width to peak width for an RWC correlator applied to a normal distribution on a linear baseline. The RWC signal is a maximum when n is approximately 1.5 FWHM. The signal falls off slowly above 2 FWHM, and sharply below 1 FWHM, this illustrates that the optimum results for a peak-search procedure using the RWC signal would utilize relatively broad convolutes.

The Savitzky-Golay, SWC, and RWC convolutes were tested using the IAEA intercomparison spectrum 200, which is a 2048 channel spectrum containing 22 peaks of varying intensity, that are near the limit of detection. The spectrum was synthesized from a Ge(Li) detector spectrum, and a computer was used to multiply the channel contents by a constant factor, shift the photopeak locations, and

superimpose the photopeaks on a synthetic compton continuum. The continuum was constructed in the form of a step function providing about 10^4 counts/channel in the lower half of the spectrum, and about 200 counts in the upper half. The resulting spectrum was then subjected to a random-number generation process to simulate the effect of counting statistics (i.e. the channel contents all conform to Poisson statistics) (1). The resolution (FWHM) of the peaks in the spectrum ranged from 2.7 to 5.0 channels, which is comparable with the range in values found in a typical 4096 channel Ge(Li) spectrum, where a detector was used that had a FWHM of 2.0 keV for the 1332 keV photopeak of Co(60), calibrated at 0.5 keV/channel. The response of each convolute was tested against the response from the normal distribution convolute (NDC), where the coefficients were recomputed at each channel based on a FWHM vs. channel-number correlation obtained from the IAEA reference spectrum number 100. This latter approach represents an overly cumbersome approach to peak location, but is an interesting basis for comparison with the other simpler convolutes. The result of this comparison showed that the RWC correlator had a sensitivity comparable with the NDC correlator (that has a width of 4 FWHM) when the width of the positive central component had an integer value closest to 1.5 FWHM, based on the FWHM calibration. The relative signal strengths of the two approaches for the 22 peaks in the IAEA intercomparison spectrum are shown in Fig. 3. Most peak-search procedures test the strength of the signal at each channel location against its associated standard deviation to accept or reject a provisional photopeak. As suggested by the work of Hnatowicz (11), a 3σ cutoff was found to be the most effective limit for all the procedures tested. Where this limit was used the RWC and NDC procedures reported no spurious peaks, except near the compton edge (which can be rejected using other criteria). Fig. 3 shows that the RWC had 18 peaks above the 3σ cutoff, whereas the NDC procedure had 17. If a limit lower than 3σ was used in order to include the difficult peaks at channels 119, 353, 870, and 1517, then spurious peaks were introduced. The Savitzky-Golay procedures were found to be less sensitive, because fewer channels were used for the convolute, and those convolutes having a larger number of channels involve large values for the coefficients.

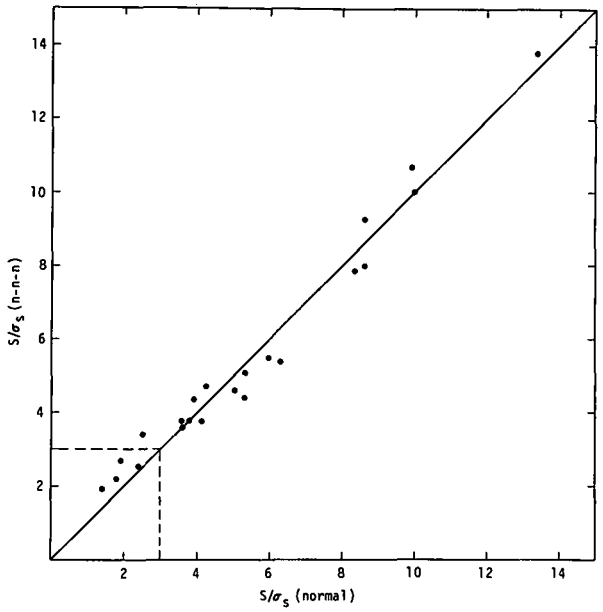


Fig. 3. Response of a variable width rectangular wave correlator relative to a variable width normal distribution correlator applied to the IAEA test spectrum 200.

The RWC filter used to determine the relative signal strengths shown in Fig. 3 had a total width of all three loops ranging from 12 to 21 channels. Although the use of relatively broad convolutes enhances the sensitivity for the detection of well-resolved photopeaks, they can be less successful for the detection of weak components near strong spectral lines. This is demonstrated in Fig. 4 which shows a weak 1115 keV Zn(65) line next to a strong 1120 keV peak of Sc(46) in a spectrum from an irradiated chondritic meteorite. Also shown is the RWC signal for three different widths of the central loop. The Zn(65) photopeak would be detected only by the 3-3-3 channel convolute, as broader convolutes all provide signals below the 3σ limit. The signals from the broader convolutes are all lowered because of the strong negative component in the inverted second erivative signal from the 1120 keV peak.

In the program "SPECTRA" used in the instrumental neutron activation analysis (INAA) program (12) of the U.S. Geological Survey, provisional photopeaks are

located by an examination of the first derivative spectrum using a 5-point Savitzky-Golay convolute. When the first derivative is observed to change sign once from negative to positive within a three channel region, both the narrow 3-3-3 and the broader 5-5-5 RWC signals are examined in a region from -2 to +2 channels. Where either RWC signal is above the 3σ limit, the peak is accepted.

The detection of poorly resolved components should be treated as a separate problem, because relatively narrow convolutes, and weak statistical criteria for acceptance or rejection are required. The detection of overlapping peaks can, therefore, best be effected by a dual pass procedure. In the "SPECTRA" program, the initial pass is halted when the separation between two neighboring peaks is greater than 5 FWHM. After a peak, or a group of partially resolved peaks, has been identified, minima on each side of the region of interest are defined by an examination of the first derivative to establish a linear baseline. A second pass of the region of interest can then be made to identify additional components by looking for minima in the second derivative spectrum. Alternatively, the third derivative spectrum can be examined for changes in sign from negative to positive values as shown in Fig. 5.

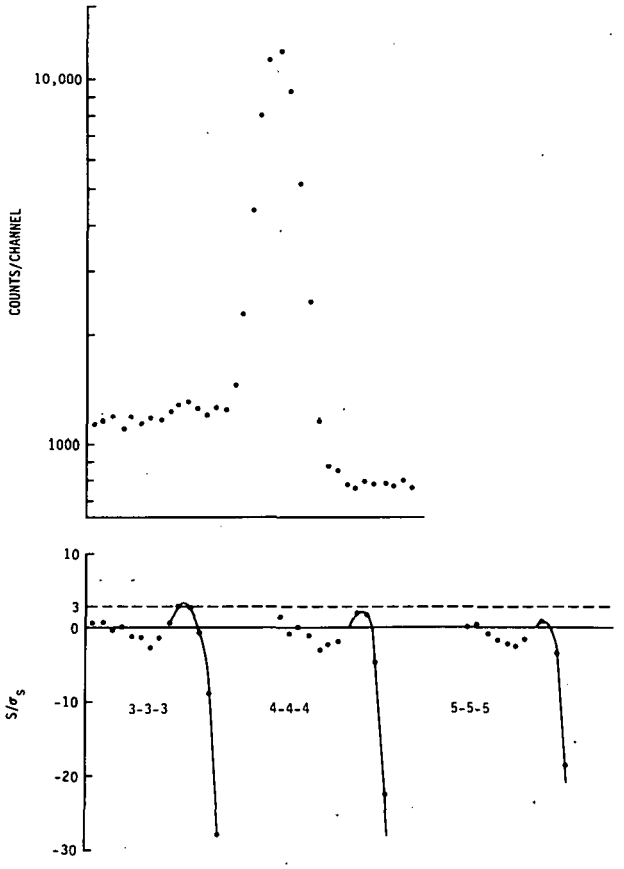


Fig. 4. Response of rectangular wave correlators of different widths to a peak near the limit of detection next to a prominent gamma-ray line.

Photopeak integration procedures

Procedures for peak-area estimation can generally be divided into two categories: non-iterative (or digital) methods of summing the channels within peak boundary limits, and iterative least squares fitting techniques. A third approach to processing gamma-ray spectra (not treated in this paper) does not involve the integration of gamma-ray photopeaks directly but rather uses the strength of the signal from the convolution procedure as a measure of peak intensity (8). In previous studies (2, 3), the relative precision attainable by several digital methods of photopeak integration was evaluated empirically, including the "total peak area" (TPA) method, and methods proposed by Covell (14), Sterlinsky (15, 16), Quitner (17) and Wasson

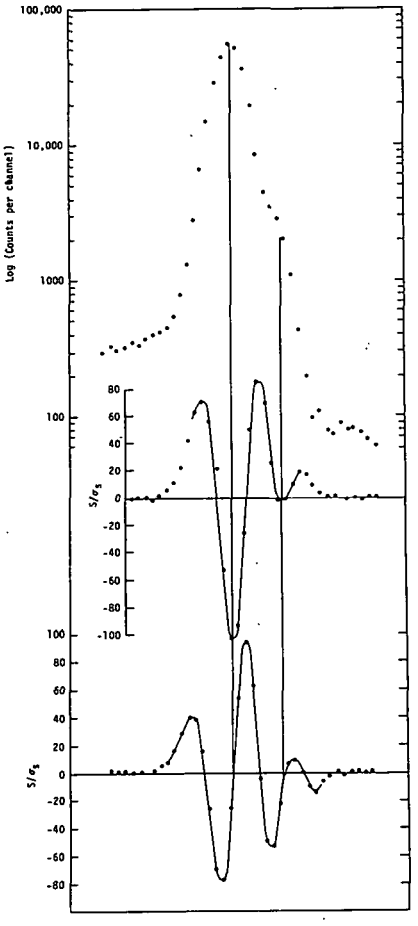


Fig. 5. The location of an unresolved peak using second (middle) or third derivative (bottom) spectra.

(personal communication in (2)) (as well as some modifications of those methods). The last four methods involve fixed limits of integration and different procedures for baseline determination and for weighting the data during the summation process. The Wasson method yielded a precision comparable with or better than that of the other methods tested, but where comparable precision was obtained, the Wasson method was favored because of its relative simplicity. All digital methods that involve fixed limits of integration are susceptible to errors due to peak broadening at higher counting rates. The TPA method is less sensitive to this effect, whereas those suggested by Covell and Sterlinsky show the greatest variation. For experiments that require the comparison of peak areas between spectra obtained with substantial differences in counting rate, the TPA method may be used to advantage, or where fixed integration methods are prefered, a correction factor can be computed from the relative widths of strong, well resolved lines (18).

Most of the digital methods can be carried out by means at a computer or small calculator. In addition to these methods, many procedures have been devised for the computer analysis of photopeaks by non-linear least-squares fitting of the spectral features to a variety of functional forms. Because of their complexity and the fact that chi-squared must be minimized by a time-comsuming iterative procedure, the fitting techniques require a much greater investment in computer time than the simple digital techniques. Iterative fitting methods have been reviewed by Campbell and co-workers (19-21) who compared reduced chi-squared values obtained with various analytical forms for Si(Li) and Ge(Li) photopeaks. Yule (22) and Baedecker (3) have made earlier empirical evaluations of the relative precision attainable using digital and iterative fitting techniques. Both authors observed that for weak lines, the digital and iterative procedures yield comparable results. Yule and Baedecker, in their experiments used the analytical expressions for peak shape suggested by Routti and Prussin (23) in their program "SAMPO", which was identified by the IAEA intercomparison as outperforming three other programs of the four most commonly used. (1).

Campbell and Jorch (21) found that the optimum fits were obtained with four additive components: 1) a symmetrical normal distribution, 2) a linear or quadratic baseline, 3) a tailing term which consisted of an exponential tail on the left and a normal term on the right, and 4) a step function. In SAMPO, the analytical forms use a simpler expression to fit the low energy tail, and a quadratic to define the baseline. Although McNelles and Campbell (19) reported less satisfactory fits using the SAMPO tailing equation, it has the advantage that both the equation and its first derivative are continuous with the normal distribution used to fit the upper and right hand side of the photopeak, and it introduces only one additional adjustable parameter in the fitting process. The tailing term of Campbell and Jorch is additive and introduces four additional terms. In the experiments carried out for this report, we have continued to use the SAMPO analytical form to account for low energy tailing but have introduced a step function to describe the baseline. Thus the data were fitted to the sum of two functions, one representing the peak and the second representing the base area:

$$Y(x) = F(x) + B(x) \qquad (3)$$

The peak is defined by a normal distribution:

$$F(x) = \sum_{i=1}^{N} H_i \exp\left[-(x_i - C_i)^2/2\sigma^2\right] \qquad (4)$$

which is joined to an exponential tail on the low energy side:

$$F(x) = \sum_{i=1}^{N} H_i \exp\{t\,[t+2(x-C_i)]\,/2\sigma^2\} \text{ for } x<(C_i-t) \qquad (5)$$

where N is the number of peaks in the fitting region, H_i is the height and C_i is the centroid of the ith component. σ is the standard deviation of the normal distribution and t is the junction (distance from the centroid) where the normal distribution changes to an exponential tail. The baseline is defined by the height of the background at the right-hand side of the fitting interval, plus a

step function for each component:

$$B(x) = B + \sum_{i=1}^{N} \frac{(B_l - B_r)\, H_i}{\sum_{j=1}^{N} H_j} \{\mathrm{erfc}\,[(x-C_i)/\sigma 2]\} \qquad (6)$$

where B_r and B_l are the baseline values defined for the right-and left-hand sides of the fitting interval respectively. H_i, C_i, B_l, and B_r are adjustable parameters in the fitting process. The parameters σ and t are the same for all components in the fitting region. Initial estimates of σ and t are obtained from gamma-ray calibration spectra and could be held fixed or allowed to vary in the fitting process. Chi squared is minimized by the Gauss-Seidal procedure (24) modified as suggested by Hartley (25) to minimize the possibility of convergence to local minima in the parameter hypersurface. The quantity χ^2 is defined as follows:

$$\chi^2 = \sum_{i}^{N} w_i\, [y_i - Y(x_i)]^2 \qquad (7)$$

where x_i is the channel number and y_i is the measured number of counts in channel x_i, with n channels in the fitting interval. w_i is the weight for datum y_i and is generally taken as $1/\sigma_i^2$ where σi is the standard deviation. In counting experiments w_i is therefore usually replaced by $1/y_i$ based on the Poisson counting error. As recently discussed by Phillips (26), this may lead to biased results when fitting peaks with very low statistics, because those channels that have the fewest counts are given the greatest weight in the fitting process. Phillips has observed that the problem can be alleviated by using a three-point average or a five-point smoothing of the data to calculate the weights. Awaya (27) has recently addressed the same problem and suggested an alternative fitting procedure from χ^2 minimization. Kohman (28) has shown that the use of the geometric mean of the input and calculated value as the weight has the advantage that both high and low data with the same error factors each make the same contribution to the sum of the squares. In this work, we have followed Kohman's suggestion and set $W_i = 1/\sqrt{Y(x_i)\,y_i}$ (8)

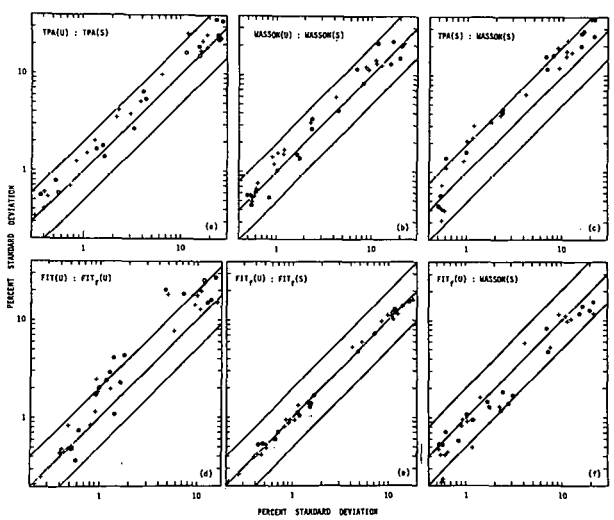


Fig. 6. Log-log plots of the percent standard deviation observed for one method of spectral analysis plotted against that of a second (captioned as y:x) for 21 photopeaks in 12 replicate spectra (+) and the same spectra with varying contributions of Co(60) (o). (U:unsmoothed; S: smoothed; f:peak shape parameters fixed on values derived from calibration spectra).

Precision

Test spectra to evaluate the precision of the various integration procedures considered were produced by using a neutron irradiated chondritic meteorite sample. Two weeks after irradiation the sample was counted 12 times in succession using a Ge(Li) detector with a resolution of 2.1 keV for the 1333 keV photopeak of Co(60) and a peak to Compton ratio of 33:1. The resulting spectra were recorded on magnetic tape along with reference spectra of gamma-ray standards. The principal activities in the sample were Sc(46), Cr(51), Fe(59), Co(58), Co(60), Zn(65) and Ir(192). The peaks used and their relative intensities are listed in Table 1. In order to check for systematic variations in measured peak area with decreasing peak to background ratio, spectra of Co(60) were accumulated for increasing lengths of time and added to 11 of the 12 chondrite spectra. The net Co counts varied by one order of magnitude between the first and last spectrum in the set of spectra.

The results of the experiment are presented in Fig. 6. Shown are log-log plots of the percent standard deviation for one procedure against that of a

second. Figures 6(a), and 6(b) show the effect of smoothing on the TPA and Wasson methods respectively, for which a five-point Savitzky-Golay convolute was used. Lines drawn at 45° represent ratios of 2,1 and 0.5. Nearly all the data points lie between the upper two lines, and smoothing tended to improve the precision of the digital methods tested by as much as a factor of 2. Mean values for the ratio of unsmoothed to smoothed precision values were 1.25±.11 and 1.14±.09 for the TPA and Wasson methods respectively, where the error values are 95% confidence limits on the mean. Figure 6(e) shows that for the iterative fitting techniques (designated FIT), smoothing of the data had little effect on the precision obtained. The relative performance of the Wasson and TPA procedures is indicated in Fig. 6(c). Except for the most intense peaks, the Wasson method yielded improved precision over the TPA method with an average precision ratio of 1.49±.17. In figure 6(d) the relative precision obtained where the peak shape parameters were variable in the fitting process is compared to that obtained where the shape parameters were fixed to the values derived from the calibration spectra. The data show considerable scatter but, in general, fixing the peak-shape parameters tended to improve precision, particularly for the peaks of moderate to low intensity.

Table 1

Photopeaks used in evaluating the relative precision at integration methods

Peak	142	192	205	296	308	316*	320*
Area+	11428	28037	1939	12914	12525	34792	229873
σ(%)	1.3	.96	9.7	.96	.91	.83	.44
Peak	335	468	484	588	604	612	810
Area+	1442	13020	822	971	1802	1031	2120
σ(%)	10.2	.94	11.8	11.3	5.1	11.0	5.9
Peak	889	1099	1115*	1121*	1173	1291	1332
Area+	59759	100952	798	48111	158697	66208	141519
σ(%)	.42	.42	16.	.49	.22	.49	.26

* doublets + as determined by least squares fitting

A comparison of the precision attainable by means of the fitting algorithm to that obtained by means of the Wasson method is shown in Fig. 6f. In general, the fitting algorithm showed improved precision, although the Wasson procedure gave comparable or higher precision in 1/5 of the test cases for peaks having a wide range in intensity. The mean precision ratio for the FIT to Wasson plot was 0.81±.07.

Doublet Analysis

In order to test the accuracy of procedures for doublet resolution, 11 spectra with synthetic open doublets (doublets with a discernable valley between the peaks) were produced by counting a Co(60) source for a preset time and changing the zero offset of the ADC by five to eight channels and continuing to count for an additional period of time. The ratio of the intensities of the left peak to the right peak in the doublets varied from .0101 to 99.0. The Ge(Li) detector used in this experiment had a resolution of 2.2 keV and a peak to Compton ratio of 40:1. In the same experiment, 10 spectra with closed doublets were produced that had the same range in peak ratios. The degree of separation varied from five to seven channels, so that the two peaks were detectable using a second or third derivative convolute.

The test spectra were subjected to both iterative and non-iterative fitting procedures. The non-iterative procedure used the same equations to represent the doublets as the iterative fitting procedure. The peak shape parameters (σ and t) were derived from iterative fits of the calibration spectra, and it was assumed that the centroids were well determined from the second derivative spectra during the peak search procedure. B_l and B_r in equation 4 were determined by averaging five channels on each side of the doublet, the peak limits

having been determined by a first derivative search for minima. The solution then reduces to solving N equations in N unknowns for a multiplet of N components, in order to determine the relative heights of each component.

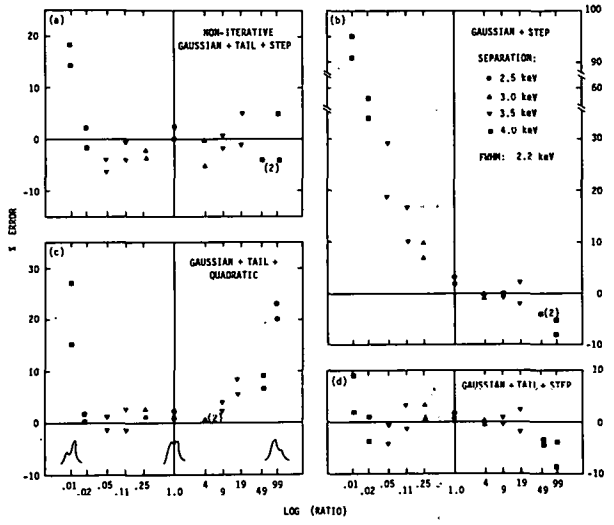


Fig. 7. The percent error in the determination of the relative intensities of the components in synthesized open doublets plotted against the log of the true ratio of the intensities of the lower energy to the higher energy peak. The symbols designate the degree of separation of the two peaks, as indicated. The two data points at each ratio represent the results from the 1173 keV and 1333 keV lines of the spectrum. A "(2)" represents overlapping data points.

In the SPECTRA program, the tailing parameter is not used in the analysis, because the iterative fitting algorithm is not included in the program. The area of a multiplet is summed, as in the TPA method, and the reported area of each component is the fraction of the total area that is determined from the peak heights, which are measured by the non-iterative fit (3).

The percent errors in the analysis of the synthesized open doublets with variations in the ratio of the lower to higher energy peaks are presented in Fig. 7. Fig. 7a presents the data for the non-iterative method. In general, the results are quite good, and all are less than or equal to 5 percent except for the errors of 14 and 19% for the peak area ratio of .0101. The iterative fit was more successful as demonstrated in Fig. 7d. The principal source of error in the non-iterative procedure is in the centroid determination. The error in the separation of approximately +1 channel for the 0.0101 multiplet should result in a negative error of nearly 20% (3). Apparently the correction for tailing was too small, and the resulting positive error more than compensated for the error due to the centroid determination.

The effects on the iterative fitting process of deleting either the step function (replaced by a quadratic baseline) or the tailing correction are shown in Fig. 7(b) and 7(c). Failure to correct for tailing results in large positive errors for a small component on the low energy side of a photopeak. Fig. 7(c) shows that the use of quadratic (or linear) baseline results in positive errors for a small component on either the high or low energy side of the peak; this indicates that the step function is a better representation for the baseline under a photopeak. The small negative errors for the ratios of 49 and 99 in figures 7(b) and 7(d) indicate that the complimentary error function has under estimated the baseline at a separation of 4 keV.

The results for the analysis of closed doublets are shown in Fig. 8. The data show many of the same features as shown in Fig. 7. The non-iterative fit was less successful owing to positive errors of up to one channel in the observed separation. This is the source of the positive error for ratios > 1. and negative errors for ratios < 1. For roughly half of the doublets, the errors were < 10%. The iterative fitting procedure was successful in treating closed doublets with an error of less than about 6% in nearly all cases, when the peak shape parameters were held fixed in the fitting process (Fig. 8(d)). Allowing the peak-shape parameters to vary (Fig. (8c)) resulted in large negative errors in the peak-area ratio for ratios less than 0.25 in spite of the fact that lower chi-squared values were obtained. This demonstrated one of the pitfalls of treating a complex situation with functional forms having several unconstrained adjustable parameters. Figures 8(b) and 8(c) show the same features as their counterparts in Fig. 7. The positive errors for ratios greater than 1 indicate that the use of a quadratic baseline has overestimated the baseline on the high

energy side of the major component in the doublets tested.

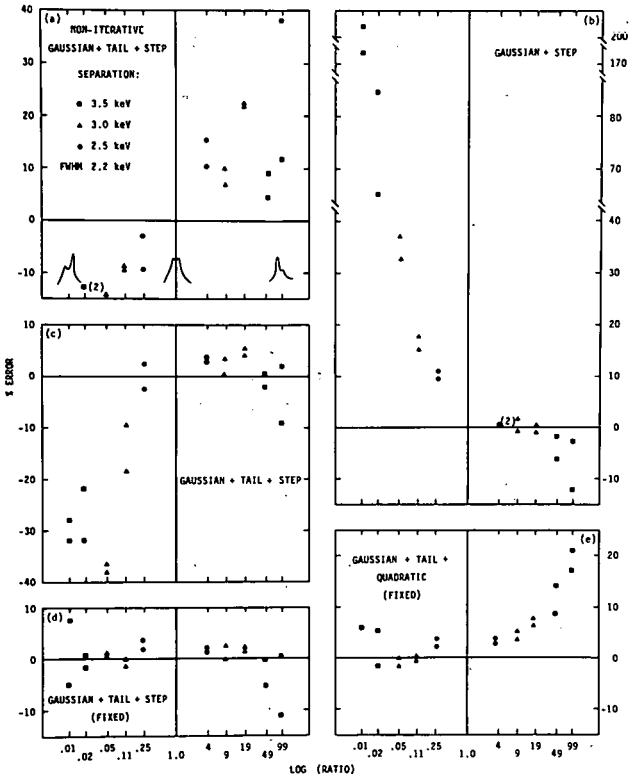


Fig. 8. The percent error in the determination of the relative intensities of the components in synthesized closed doublets. The abscissa is the same as that in Fig. 7.

Conclusions

Peak-search algorithms which use either derivative spectra or correlation techniques have been examined. A rectangular-wave convolution has been shown to give sensitivity comparable with a variable width correlator based on a normal distribution when applied to the IAEA test spectrum 200. Optimum sensitivity of the RWC convolute is achieved when the central loop of the convolute has a width of approximately 1.5 FWHM. However, narrower convolutes may be required for the detection of small peaks within 3 to 4 FWHM of a larger peak. When peaks and peak boundaries have been established for well to moderately resolved photopeaks, a second pass with a narrow convolute to evaluate the second or third derivative can help to define poorly resolved peaks.

In a test to evaluate the relative precision of both digital and iterative least squares fitting procedures, a preliminary smoothing of the data was found to increase the precision of the digital methods but had no effect on the precision of the fitting procedure. For the most part, the fitting algorithm gave improved precision over the Wasson method over a wide range in intensity. Iterative least squares fitting is useful for the analysis of closed multiplets providing that the models used for the fit can properly account for low-energy tailing and the shape of the baseline. Fits of the data with simpler models may generate larger errors than a simple non-iterative treatment. A non-iterative approach appears to be adequate for the treatment of open doublets.

The iterative least squares fitting of gamma-ray spectra has its greatest application in nuclear spectroscopy, where it has the advantage of greater accuracy for fitting complex peaks and where the residuals from the fitting process can be searched for components that are undetected in the peak search process. It has the disadvantage of increasing computer time by at least an order of magnitude over simple digital methods of analysis, and in general requires greater supervision by the user to see that the fits to the data are proper. Although fitting algorithms are useful for nuclear physics applications, they are less appropriate for activation analysis programs that involve the processing of a large number of spectra.

References

1. R.M. Parr, H. Houtermans, and K. Schaert, The IAEA Intercomparison of Methods for Processing Ge(Li) Gamma-Ray Spectra: A Preliminary Report in Computers in Activation Analysis and Gamma-Ray Spectroscopy, B.S. Carpenter, M.D. Agostino, H.P. Yule (Eds.), DOE Symposium Series: 49, pp. 544-562 (1979).
2. P.A. Baedecker, Digital Methods of Photopeak Integration in Activation Analysis, Anal. Chem., 43: 405-410 (1971).
3. P.A. Baedecker, the Precision and Accuracy of Iterative and Non-Iterative Methods of Photopeak Integration in Activiation Analysis with Particular Reference to the Analysis of Multiplets, J. Radioanal. Chem., 39:239-254 (1977).

4. M.A. Mariscotti, A Method for Automatic Identification of Peaks in the Presence of Background and its Application to Spectrum Analysis, Nucl. Instr. and Meth., 50: 309-320 (1967).
5. H.P. Yule, Computation of Lithium-Drifted Germanium Detector Peak Areas for Activation Analysis and Gamma-Ray Spectrometry,Anal.Chem.,54:1480-1486 (1968).
6. A. Savitzky and M.J.E. Golay, Smoothing and Differentiation of Data by Simplified Least Squares Procedures, Anal. Chem., 36: 1627-1639 (1964).
7. A. Robertson, W.V. Prestwich, and T.J. Kennett, An Automatic Peak Extraction Technique, Nucl. Instru. and Meth., 100: 317-324 (1972).
8. J. Op de Beeck, Gamma-Ray Spectrometry Data Collection and Reduction by Simple Computing Systems, Atomic Energy Rev., 13: 743-805 (1975).
9. W.W. Black, Application of Correlation Techniques to isolate Structure in Experimental Data, Nucl. Instr. and Meth., 71: 317-327 (1969).
10. N.A. Anstey, Correlation Techniques - A Review, Geophys.Prospecting, 12: 355-382 (1964).
11. V. Hwatowicz, Identification of Weak Lines in Gamma-Ray Spectra Nucl. Instr. and Meth., 133: 137-141 (1976).
12. P.A. Baedecker, the INAA Program of the U.S. Geological Survey, in Computer in Activation Analysis and Gamma-Ray Spectroscopy, B.S. Carpenter, M.D. Agostino, H.P. Yule (Eds.), DOE Symposium Series: 49, pp. 554-562 (1979).
13. J. Hertogen, J. De Donder, and R. Gijbels, Experimental Data on Photopeak Integration Methods in Activation Analysis, Nucl. Instr. and Meth., 115: 197-212 (1974).
14. D.F. Covell, Determination of Gamma-Ray Abundance Directly from the Total Absorption Peak, Anal. Chem., 31: 1785-1790 (1959).
15. S. Sterlinski, Analysis of Digital Data from a Multichannel Pulse Height Analyzer on Gamma-Ray Total Absorption Peaks in Activation Analysis, Anal. Chem., 40: 1995-1998 (1968).
16. S. Sterlinski, Features of the Modified Covell Method for Computation of Total Absorption Peak Areas in Complex Gamma-Ray Spectra, Anal. Chem., 42: 151-155 (1970).
17. P. Quitner, Precise Peak Area Determination for Ge(Li) Detectors, Anal. Chem., 41: 1504-1506 (1969).
18. J. Yellen, A Systematic Error from Count Rates in Neutron Activation Analysis of Archaelogical Materials, Anal. Chim. Acta, 113: 159-164 (1980).
19. L.A. McNelles and J.L. Campbell, Analytic Approximations to Peak Shapes Produced by Ge(Li) and Si(Li) Spectrometers, Nucl. Instr. and Meth., 127: 73-81 (1975).
20. H.H. Jorch and J. L. Campbell, On the Analytic Fitting of Full Energy Peaks from Ge(Li) and Si(Li) Detectors, Nucl. Instr. and Meth.,143:551-559 (1977).
21. J.L. Campbell and H.H. Jorch, On the Analytic Fitting of Full Energy Peaks from Ge(Li) and Si(Li) Photon Detectors, II, Nucl. Instr. and Meth., 159: 163-170 (1979).
22. H.P. Yule, Computer Analysis of Weak Spectral Components in Gamma-Ray Spectra, J. Radioanal. Chem., 15: 695-705 (1973).
23. J.T. Routti and S.G. Prussin, Photopeak Method for the Computer Analysis of Gamma-Ray Spectra from Semiconducter Detectors, Nucl. Instr. and Meth., 72: 124-142 (1969).
24. R.H. Moore and R.K. Zeigler, The Solution of the General Least Squares Problem with Special Reference to High Speed Computers, Los Alamos Scientific Laboratory Report LA-2367 (1960).
25. H.O. Hartley, The Modified Gauss-Newton Method for the Fitting of Non-Linear Regression Functions by Least Squares, Technometrics, 3: 269-280 (1961).
26. G.W. Phillips, Fitting Peaks with Very Low Statistics, Nucl. Instr. and Meth., 153: 449-455 (1978).
27. T. Awaya, A New Method for Curve Fitting to the Data with Low Statistics Not Using the Method, Nucl. Instr. and Meth., 165: 317-323 (1979).
28. T.P. Kohman, Least Squares Fitting of Data with Large Errors, J. Chem. Ed., 47: 657-658 (1970).

Accuracy in Activation Analysis: Count Rate Effects

Richard M. Lindstrom and Ronald F. Fleming
Center for Analytical Chemistry
National Bureau of Standards
Washington, D.C. 20234

Abstract

The accuracy inherent in activation analysis is ultimately limited by the uncertainty of counting statistics. When careful attention is paid to detail, several workers have shown that all systematic errors can be reduced to an insignificant fraction of the total uncertainty, even when the statistical limit is well below one percent.

A matter of particular importance is the reduction of errors due to high counting rate. The loss of counts due to random coincidence (pulse pileup) in the amplifier and to digitization time in the ADC may be treated as a series combination of extending and non-extending dead times, respectively. The two effects are experimentally distinct. Live timer circuits in commercial multichannel analyzers compensate properly for ADC dead time for long-lived sources, but not for pileup. Several satisfactory solutions are available, including pileup rejection and dead time correction circuits, loss-free ADCs, and computed corrections in a calibrated system. These methods are sufficiently reliable and well understood that a decaying source can be measured routinely with acceptably small errors at a dead time as high as 20 percent.

Introduction

We define accuracy in measurement to be the absence of systematic error. An accurate measurement in activation analysis, then, is one whose result is indistinguishable from the truth within the bounds of precision set by the statistics of counting (1).

There are very many sources of inaccuracy in activation analysis (2,3). Some limitations are set by the analytical sample itself, such as sampling inhomogeneity (4) or contamination before irradiation. Error may be incurred during irradiation because of variations of the neutron spectrum shape or intensity with respect to space or time. Analyte may be lost from the sample due to hot-atom effects during irradiation or because of incomplete chemical separations. Errors in counting may result from variations in counting geometry, absorption, or effects dependent on counting rate. Finally, systematic error may be incurred in the data reduction process because of bias in peak area determinations or by using inaccurate values of nuclear constants.

Despite all these opportunities for error, activation analysis can in practice often be performed in such a manner as to make all these errors smaller than counting statistics, even when that limit is well below one percent (5). Since "knowledge increases ... not by the direct perception of truth but by a relentless bias toward the perception of error (6)", a desirable approach toward attaining accuracy is to search for inaccuracy, devise correction procedures, and test the adequacy of these procedures under conditions more stringent than those encountered in routine practice.

An essential consideration in the search for high accuracy in radioactivity measurements is that the distorting effects due to high count rates be kept small. Consider, as an example, the measurement of Au-198 with a large Ge detector. If we aim at a relative accuracy of 0.1 percent, then Poisson statistics require that at least 10^6 net counts be accumulated. If the counting time is to be kept reasonably short, say an hour, then (since 20 percent of the counts accumulated fall in the full-energy peak) the count rate to be dealt with is 1500 per second. At this rate, errors of several percent may be incurred under certain experimental conditions. In many measurements, particularly when the source decays rapidly, rates of tens of thousands per second must be dealt with.

Mechanisms and Magnitude of Rate-related Losses

Rate-related loss of counts is due to the finite resolving time of the electronic system composed of the detector, amplifier, and analog-to-digital converter (ADC). In the following discussion we model the losses as the result of two dead times in series. The longer dead time is due to the ADC; for an event of energy corresponding to channel 4096, an ADC with an oscillator frequency of 100 MHz requires 41 μs, plus about 5 μs for logic, to determine the channel address and to add one count to that channel. During this time the ADC is unable to accept another pulse for analysis, but the arrival of another pulse does not extend the insensitive interval further. This is the classical case of non-extending dead time (7). All modern multichannel analyzers compensate for this loss of sensitive time by using the ADC busy interval to gate the live-time clock; compensation can be essentially perfect.

A second effect, pulse pileup, is usually not compensated by the ADC. Whenever two gamma rays arrive at the detector within a time short compared to the shaping time of the amplifier (a few μs), the output pulse height of the amplifier reflects the sum of the two events. The result of this random coincidence is that counts are lost from the low energy portion of the spectrum and reappear as higher-energy sum events. Rejection of piled-up events after their detection by a fast discriminator will remove the false high-energy events but will not compensate for their loss from the low-energy portion of the spectrum. Unlike the ADC, the amplifier is always sensitive to an input and succeeding events add to their predecessors, so that the busy time during which an amplifier signal exceeds a discriminator level is approximated by the classical extending dead time formulation (7). Even though the amplifier resolving time is an order of magnitude shorter than the ADC dead time, the effect of pileup on measured counting rates can be substantial, as may be seen in Figure 1. The losses can be substantial even when the counting rate is moderate: 2-4 percent at an integral input rate of 4000 s^{-1}, which corresponds to only 10 percent ADC dead time.

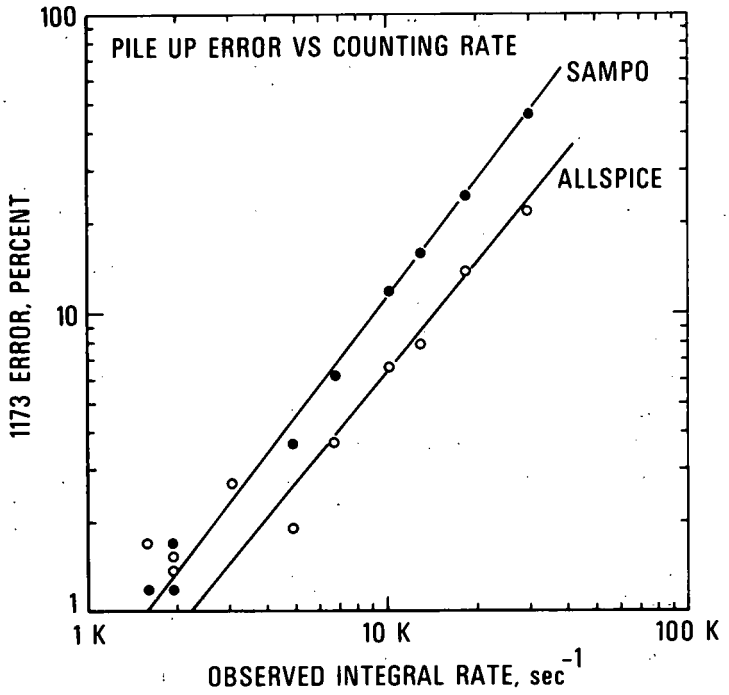
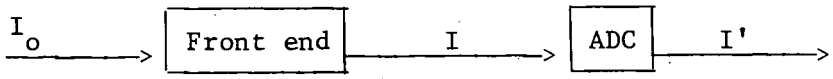


Figure 1. Loss of counts due to pulse pileup in counting a Co-60 source with a dead-time compensated ADC. The difference between the two curves reflects peak broadening: a peak integration procedure (SAMPO) which does not allow for the fact that peaks observed at high rate are wider than the calibration spectrum is more seriously in error than is one (ALLSPICE) which determines the peak boundaries from the observed spectrum.

Theory of Count of Rate Losses

We will treat in some detail the simplest case of a single decaying source, using as a model for the counting system a detector and amplifier combination with extending deadtime followed by an ADC with non-extending deadtime. The model is schematically:



Here I_o, I, and I' are the event rates into the detector, into the ADC, and out of the ADC respectively. The relations among these rates are

$$I'(t) = \frac{I(t)}{1+\theta I(t)} \quad \text{[Non-extending]} \tag{1a}$$

$$I(t) = I_o(t)e^{-\alpha I_o(t)} \quad \text{[Extending]} \tag{1b}$$

$$I_o(t) = I_o(o)e^{-\lambda t} \quad \text{[Decay]} \tag{1c}$$

We have expressed the system in terms of three constants: the decay constant λ, the pulse pileup factor α, and the mean ADC deadtime per event θ. The number of counts recorded in clock time CT is

$$C = \int_{t_1}^{t_1+CT} I'(t)dt$$

$$= \int_{t_1}^{t_1+CT} \frac{I_o(o)e^{-\lambda t}\, e^{-\alpha I_o(o)e^{-\lambda t}}\, dt}{1+\theta I_o(o)e^{-\lambda t}\, e^{-\alpha I_o(o)e^{-\lambda t}}} \qquad (2)$$

In order to avoid numerical integration, we now make the assumption that the pulse pileup and the ADC deadtime effects are approximately separable. This is valid for some α if the source decay is moderate during the counting interval CT; that is, if the effect of pileup on dead time is small. This assumption gives

$$C \approx e^{-\alpha I_o(o)e^{-\lambda t_1}} \int_{t_1}^{t_1+CT} \frac{I_o(o)e^{-\lambda t}dt}{1+\theta I_o(o)e^{-\lambda t}} \qquad (3)$$

The integral can now be carried out to give

$$C = I_o(o)e^{-\lambda t_1}\, e^{-\alpha I_o(o)e^{-\lambda t_1}}\, \frac{(1-e^{-\lambda \cdot LT})}{\lambda} \left[\frac{\lambda \cdot DT}{e^{\lambda \cdot DT}-1}\right] \qquad (4)$$

where the dead time DT = CT - LT. Grouping the experimental quantities together we obtain

$$A(t_1) \equiv \frac{\lambda C\, e^{\lambda t_1}}{1-e^{-\lambda \cdot LT}} \left[\frac{e^{\lambda \cdot DT}-1}{\lambda \cdot DT}\right] = I_o(o)e^{-\alpha I_o(o)e^{-\lambda t_1}} \qquad (5)$$

If we take the logarithm of both sides we obtain

$$\ln[A(t_1)] = \ln[I_o(o)] - \alpha I_o(o)e^{-\lambda t_1}, \qquad (6)$$

and we see that the slope of a plot of $\ln[A(t_1)]$ vs. $e^{-\lambda t_1}$ will yield the pulse pileup parameter α. A plot representing a six-halflife decay for a Cu-64 source (Figure 2) demonstrates that this simple model is valid within the uncertainty of the data points, the standard deviation of which ranges from 0.06 percent to 0.25 percent (8).

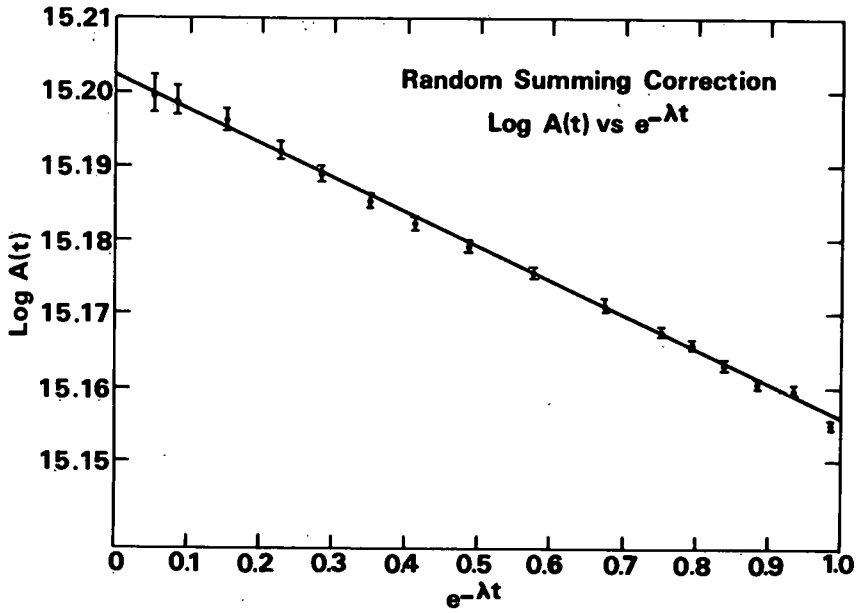


Figure 2. Experimental test of equation 6. The fact that the points are fitted by a straight line shows that the model is adequate.

Once the value of α has been determined for a particular nuclide and counting system, the pileup correction factor (F_P) with which to correct the observed A_o may be determined. That is:

$$A_o(\text{true}) = F_P \cdot A_o(\text{obs})$$

We recognize that for the general case, for which $I_o(o)$ is not known, the factor is given by

$$F_P = e^{\alpha I_o(o) e^{-\lambda t_1}} \qquad (8)$$

Therefore we rewrite equation (5) as

$$Y = Xe^{\alpha Y}$$

where $Y = I_o(o)e^{-\lambda t_1}$ and $X = A(t_1)e^{-\lambda t_1}$. The solution of this equation is, by iteration,

$$Y = X\exp(\alpha X\exp(\alpha X\exp(\ldots))))$$

and therefore

$$F_P = \exp(X\exp(X\exp(...))), \quad (9)$$

which may be solved numerically and quickly converges.

A slightly different formulation has been given by Wyttenbach (9). Treating pileup as represented by an extending dead time gives the pileup correction factor, the ratio of observed to true count rate in the peak of interest,

$$F_P = A(true)/A(obs) = \exp(2I_o t) \quad (10)$$

where I_o is, as before, the integral count rate into the amplifier and t a time which is approximately the interval during which the amplitude of an average pulse exceeds the ADC's input discriminator. Wyttenbach pointed out that for a given spectral shape (a given t) and a multichannel analyzer in the live time mode, the dead time

$$DT \equiv CT - LT = KI_o \quad (11)$$

where K is a constant. Combining equations 10 and 11 we obtain

$$F_P = A(true)/A(obs) = \exp(P \cdot DT/LT) \quad (12)$$

where $P = 2t/K$ is a constant to be measured (10). Wyttenbach showed experimentally that when spectra of similar shapes are compared the correction is excellent. Verheijke's modification of the method (11) allows for varying spectrum shape through calculation of the weighted mean channel number.

The pileup parameter P is conveniently measured by an extension of the classical two-source method of determining detector dead times (12,13). A source, conveniently Co-60 or Y-88, of moderate activity is counted several times in the presence of large and varying amounts of another source which does not contain this nuclide. The strong source may be a Cs-137 or, better, an irradiated sample of the matrix to be analyzed. Both live and clock times are measured. For this calibration the range of dead times should bracket that expected for samples.

Taking logarithms of both sides of equation 12 and rearranging, we have

$$\ln A(obs,i) = \ln A(true) + P[DT(i) / LT(i)] \quad (13)$$

which is a linear equation in the two unknowns A(true) (the peak count rate of the calibration nuclide at zero dead time) and the parameter P. The subscript i indicates an individual measurement of the peak count rate and live and dead times. For three or more observations, equation 13 may be solved by weighted least squares (14) to determine A(true) and P and their uncertainties.

Since pileup is a measure of the amplifier resolving time, the pileup correction should become less important as the shaping time constant τ of the amplifier is reduced. As can be seen in Figure 3, this is observed experimentally. For each value of τ the dependence of F_P upon dead time is approximately exponential (strictly, an exponential in DT/LT, while the usual definition of fractional dead time is DT/CT). From Wyttenbach's derivation we see that the pileup parameter P is proportional to τ, as is shown in Figure 4 which is derived from the same data set as is the preceding figure. Clearly the smaller the value

of τ, the smaller the pileup correction and its uncertainty. There is a limit, set by the charge collection time in the detector, to how small τ can be without serious loss in energy resolution. On the same axis on Figure 4 we show the dependence of resolution on τ for the counting system used in these experiments. The optimum performance for this counting system is achieved when τ is set at one or two microseconds.

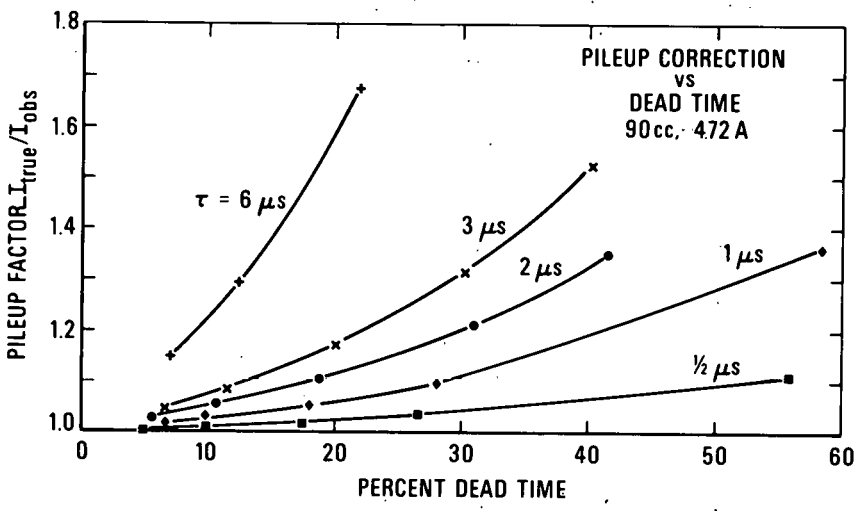


Figure 3. Dependence of pileup correction factor on dead time. The reference source is Co-60, with varying amounts of Cs-137 to change the counting rate.

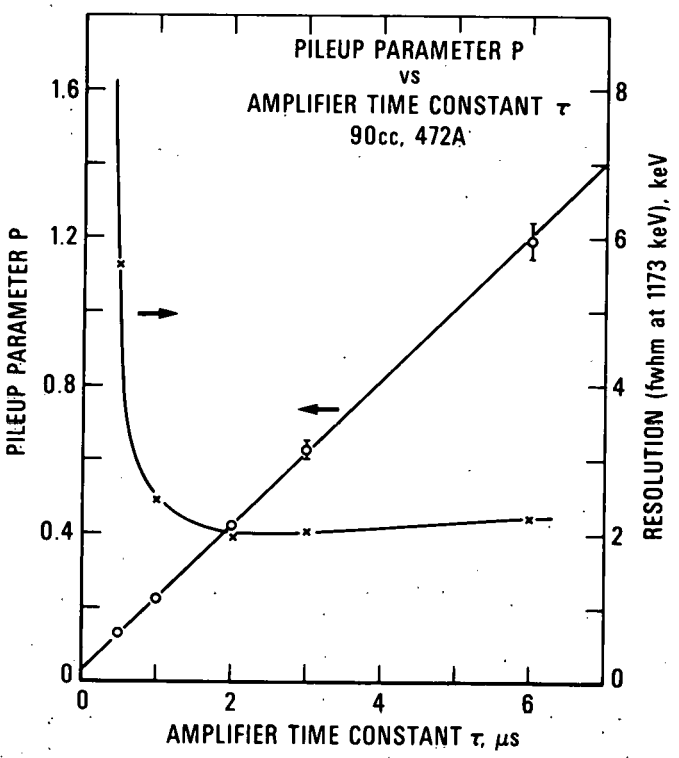


Figure 4. Pileup parameter P derived from the data set of Figure 3. The optimum balance between small pileup correction and good resolution is reached for a time constant of 1-2 μs.

An estimate of the uncertainty of the computed pileup correction factor F_P can be derived by conventional propagation of errors (15). The uncertainty σ_P in the pileup parameter P is obtained as part of the calibration process just described. Most multichannel analyzers count elapsed live and clock time (LT and CT) only to the nearest second, and thus at least one of these times and their difference DT has an uncertainty σ_{DT}. This quantity is not strictly a standard deviation since it has finite bounds, for instance +1 to -0 sec, which must be determined for any given system. Treating σ_{DT} as a formal standard deviation and assuming that the elapsed live time is known exactly (as is true to 10 msec for some commercial instruments), we find the relative uncertainty in the pileup correction

$$\left[\frac{\sigma_{F_P}}{F_P} = \left(\frac{DT}{LT}\ \sigma_P\right)^2 + \left(\frac{P}{LT}\ \sigma_{DT}\right)^2\right]^{1/2} \qquad (14)$$

This modified Wyttenbach model of the pileup correction may be tested with the data of Figure 2. A chi-squared test shows that the exponential model of equation 14 represents the data well within their 0.3 percent counting statistics.

Hardware Methods

A number of approaches are available to correct for rate-related counting losses with hardware. A pulser may be used (16,17,18) to correct the observed rates for both pileup and deadtime. A small additional correction is necessary in the most accurate work to allow for the fact that a periodic pulser cannot be coincident with itself (19,20). Another approach is to detect nearly-coincident events in the detector with a fast discriminator, reject these events from the spectrum, and extend the ADC dead time by a compensating amount. These circuits are available commercially and, as will be shown, correct very well for random coincidence with reasonably long-lived radioactive samples.

A disadvantage of most hardware methods is that the correction of the observed average count rate for decay during its counting interval cannot be performed exactly unless the dead time as a function of time is known (21, 22) or the pulser rate is made proportional to the dead time (18,23,24). In practice, often one of the two limiting cases is nearly correct: either the dead time is constant or it decays exponentially with a single half-life (22,25).

An elegant hardware solution to the general case of multiple decay constants has been devised by Harms (26) and further developed by Westphal (27) and by Byrd and Goosey (28). By the addition of circuits to detect and count the arrival of n events at the ADC and the amplifier during busy intervals, and then adding 1 + n instead of 1 to the memory cell addressed, full compensation for both ADC and amplifier dead time is achieved. Moreover, since compensation is performed on an event-by-event basis the spectral shape is undistorted for all half-lives much longer than the interval between pulses (29) and, since the live time and clock time are equal, the decay equations are easier to solve. Such "loss-free" ADC's are not at present commercially available.

Experimental Tests

An intercomparison which was designed to test the adequacy of dead time and pileup corrections was recently conducted by the International Atomic Energy Agency (IAEA) (30). The IAEA distributed a set of five sources, each containing four radionuclides with a total activity of 100 to 1600 kBq (1 Bq = 1 disintegration/sec). Participants were requested to arrange the counting efficiency such that the lowest activity source produced an integral countin rate of 1000 sec^{-1}, and

then to determine the activities of all nuclides in the other samples relative to the first source using whatever procedures they deemed appropriate. After the results were reported the participants were informed of the correct ratios. Our laboratory chose to perform the measurements in two ways. The first set of measurements used a 90-cm^3 Ge(Li) detector, a Nuclear Data 6600 computer-based analyzer with its internal live time clock and the modified Wyttenbach pileup correction (Eq. 12) with a fixed-boundary peak integration procedure (31). The second set used a 63-cm^3 Ge(Li) detector coupled through a Canberra model 1468 pileup rejector/livetime corrector to a Nuclear Data ND100 4096-channel analyzer, using the ALLSPICE program (32) for peak boundary determination and total-peak-area integration.

The results are displayed in Figure 5, where the ratio of the relative activity found to that provided by IAEA is plotted against source strength. The error bars represent one standard deviation based upon propagated counting statistics and, for the first method, the additional uncertainty due to the pileup correction. (For the latter it was found that the uncertainty in P was dominant at high counting rates and the uncertainty in DT more important at low rates). Inspection of the figure shows that the two approaches used were substantially equivalent and, since no significant slope is present in the lines, both give correct values for the relative activities. It may then be satisfyingly concluded that there is more than one acceptable method for removing the distortion of count-rate related errors in relative radionuclide assay, and that this important source of error in high-accuracy activation analysis is under control (33).

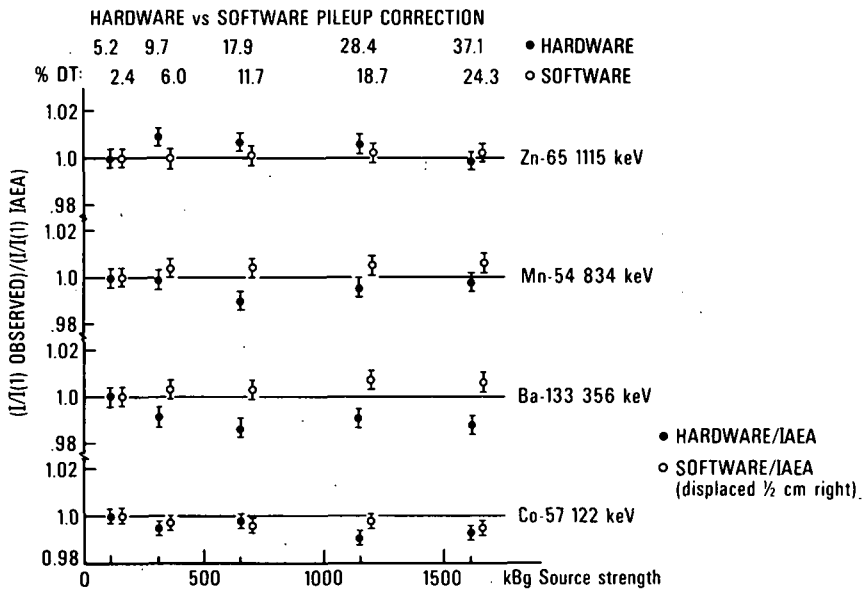


Figure 5. Performance of hardware and software (equation 12) methods of pileup correction for the IAEA G2 source set. Both are satisfactory.

References and Notes

(1) L. A. Currie, The Limit of Precision in Nuclear and Analytical Chemistry, Nucl. Inst. Methods, 100, 387-395 (1972).

(2) D. Gibbons, Errors in Activation Analysis, in J. M. A. Lenihan and S. J. Thomson, eds., "Activation Analysis Principles and Applications", Academic Press, London (1965).

(3) J. P. Cali, J. R. Weiner, and G. G. Rocco, The Accuracy of Radioactivation Analysis, Proc. 1965 Int. Conf. Modern Trends in Act. Anal., College Station, Texas, pp. 253-258.

(4) C. O. Ingamells and P. Switzer, A Proposed Sampling Constant for Use in Geochemical Analysis, Talanta, 20, 547-568 (1973).

(5) R. M. Lindstrom, S. H. Harrison, and J. M. Harris, Accurate Calibration of Gold Film Standards by Neutron Activation and Gravimetry, J. Appl. Phys., 49, 5903-5908 (1978).

(6) K. E. Boulding, Science: Our Common Heritage, Science, 207, 831-836 (1980).

(7) L. J. Rainwater and C. S. Wu, Applications of Probability Theory to Nuclear Particle Detection, Nucleonics, 1, (2), 60-69 (Oct. 1947).

(8) R. F. Fleming, A Direct Measurement of Random Summing Losses in Gamma Counting, Trans. Am. Nucl. Soc., 33, 234 (1979).

(9) A. Wyttenbach, Coincidence Losses in Activation Analysis, J. Radioanal. Chem., 8, 335-343 (1971).

(10) Our equation 12 differs from Wyttenbach's equation 10 in that we use the exponential rather than approximating it by the first few terms of a series expansion.

(11) M. L. Verheijke, Some Practical Procedures in Computerized Thermal Neutron Activation Analysis with Ge(Li) Gamma-ray Spectrometry, J. Radioanal. Chem., 35, 79-93 (1977).

(12) R. D. Evans, "The Atomic Nucleus", McGraw-Hill, New York (1955).

(13) G. F. Knoll, "Radiation Detection and Measurement", Wiley, New York (1979).

(14) P. R. Bevington, "Data Reduction and Error Analysis for the Physical Sciences", McGraw-Hill, New York (1969). A Fortran program for determination of the pileup parameter is available on request from the present authors.

(15) H. H. Ku, Notes on the Use of Propagation of Error Formulas, J. Res. NBS (US) 70C, 263-273 (1966). Reprinted in H. H. Ku, ed., "Precision Measurement and Calibration", NBS Spec. Pub. 300 (Vol. 1) 1969.

(16) M. A. Strauss, L. L. Sifter, F. R. Lankszus, and R. Brenner, Ultra Stable Reference Pulser for High Resolution Spectrometers, IEEE Trans. Nucl. Sci., NS-15, (3), 518-530 (1968).

(17) O. U. Anders, Experiences with the Ge(Li) Detector for High Resolution Gamma-ray Spectrometry and a Practical Approach to the Pulse Pileup Problem, Nucl. Inst. Methods, 68, 205-208 (1969).

(18) H. H. Bolotin, M. G. Strauss, and D. A. McClure, Simple Technique for Precise Determinations of Counting Losses in Nuclear Pulse Processing Systems, Nucl. Inst. Methods, 83, 1-12 (1970).

(19) K. Debertin, Relative Aktivitätsbestimmungen mit Ge(Li)-Detektoren, Atomkernenergie, 17, 97-102 (1971).

(20) E. J. Cohen, Live time and Pileup Correction for Multichannel Analyzer Spectra, Nucl. Inst. Methods, 121, 25-32 (1974).

(21) E. Schonfeld, ALPHA — A Computer Program for the Determination of Radioisotopes by Least Squares Resolution of the Gamma-ray Spectra, Nucl. Inst. Methods, 42, 213-218 (1966).

(22) E. Junod, Corrections of Counting Losses in Gamma-Spectrometry of Short-Lived Radionuclides, J. Radioanal. Chem., 20, 113-134 (1974).

(23) W. Görner and G. Höhnel, An Automatic Life Time Correction in Multichannel Counting of Short-lived Nuclides, Nucl. Inst. Methods, 88, 193-196 (1970).

(24) B. A. Roscoe and A. K. Furr, Time Dependent Deadtime and Pileup Corrections for Gamma Ray Spectroscopy, Nucl. Inst. Methods, 140, 401-404 (1977).

(25) D. DeSoete, R. Gijbels, and J. Hoste, "Neutron Activation Analysis", Wiley-Interscience, London (1972).

(26) J. Harms, Automatic Dead-Time Correction for Multichannel Pulse-Height Analyzers at Variable Counting Rates, Nucl. Inst. Methods, 53, 192-196 (1967).

(27) G. P. Westphal, On the Performance of Loss-free Counting — a Method for Real-Time Compensation of Dead-Time and Pileup Losses in Nuclear Pulse Spectroscopy, Nucl. Inst. Methods, 163, 189-196 (1979); and references therein to earlier work.

(28) J. S. Byrd and M. H. Goosey, A Pulse Height Analyzer with Automatic Differential Deadtime Correction, Nucl. Inst. Methods, 158, 565-569 (1979).

(29) C. F. Masters and L. V. East, An Investigation into the Harms Dead Time Correction Procedure for Pulse Height Analyzers Using Monte Carlo Modeling Techniques, IEEE Trans. Nucl. Sci., NS-17, 383-389 (1970).

(30) IAEA: Intercomparison of High Precision Gamma-ray Spectrometry Results G-2, organized by G. B. Cook, H. Schaerf, and H. Houtermans (1979).

(31) R. M. Lindstrom, and R. F. Fleming, Program SUM. A description and listing are available on request.

(32) H. P. Yule, ALSPIS — Activation Analysis Peak Area Program, in NBS Tech. Note 548 (1970) pp. 128-135. See also H. P. Yule, Computer Data Reduction in Activation Analysis, in Proc. NATO Advanced Study Inst: Act. Anal. in Geochem. and Cosmochem. (Kjeller, Norway, 1971).

(33) In this work it has been necessary to identify suppliers of commercial equipment in order adequately to describe the procedures. In no case should this identification be construed as endorsement by the National Bureau of Standards, or indeed by the authors.

THE RANDOM SEARCH ALGORITHM FOR SPECTRUM ANALYSIS

Yasushi Takeda

Department of Nuclear Engineering, Faculty of Engineering
Tohoku University
Aramaki-aza-Aoba, Sendai, Japan

ABSTRACT

The random search algorithm was applied to various spectrum analyses and related curve fitting problems. This algorithm has several advantages over other conventional methods. Especially its robust and easily applicable properties are outstanding. These characteristics of this algorithm are shown through analyzing various kinds of spectra. The possibility to reduce the total computing time is also discussed.

1 Introduction

Not only in the spectrum analyses but also in most of the experimental data processing procedures, it is very common to perform fitting of experimental data to some functions. These procedures of data analysis are carried out to guarantee a consistency in obtained results among experimental runs as well as automations of data processing. The required physical quantities are derived directly from the fitted adjustable parameters. Consequently, fitting functions are desired to reflect the physical aspects as precisely as possible. For example, explicit functions predicted theoretically seem best. In the fitting procedure, the least squares method is usually used. For those complicated nonlinear fitting functions, however, the least squares (normal) equations are also nonlinear and solutions cannot be obtained in a straightforward manner. To solve such nonlinear least squares equations, many sophisticated methods have been developed and adopted to many computer codes. These sophisticated algorithms can give their successful results for some specific problems. However on the other hand, they are practically very weak against such conditions as large statistical fluctuations of experimental data, poor degree of initial estimates and changes of fitting functions. These conditions are realized very often. In these cases, there occur oscillations and/or divergences of solutions and, for the most cases, one has to use some other fitting algorithm so that it causes losing consistency and giving rise to random errors in the course of data analysis procedures. Considering these present situations of data processing, the use of the algorithm is expected which is robust for the actual data analysis and easily applicable in changes of fitting functions, even if it is not so refined.

I have applied a random search algorithm to a wide variety of spectrum analyses. The advantages of this algorithm over other sophisticated methods are:

1) algorithmic logic is very simple,
2) successful convergence to a true optimum is guaranteed,
3) only rough initial estimates are required,
4) very little increase of computer storage occurs with increasing the number of adjustable parameters,
5) applications to a variety of fitting problems are very easy,
6) program is easily prepared.

The only disadvantage of this method is to require a comparatively large computing time. However this point has been overcome by the development of high speed computing machines. Moreover, those advantages can completely compensate this point. Especially, this seems to cause no problem in the environmental research field where the sufficient computing time is given.

This paper describes its robustness, effectiveness and good applicability to spectrum analyses by showing several examples of applications. The possibility to reduce the total computing time is also discussed.

2 Principle and Method

The principle of the random search algorithm is very simple. Sophistications of the algorithm is to involve information which appears on the spectrum into algorithm so as to obtain solutions faster and more precisely. On the contrary it also means growth of a danger that spurious information will

lead the solution to spurious optimum. In the sense, it can be said that the simplicity of the present algorithm guarantees its robustness and giving a true optimum. Although this algorithm can also be naturally refined in the frame of the principle, the simplest algorithm was used in this work in order not to lose its robustness at all. As the details of this algorithm are described elsewhere (Ref. 1), I will give it here very briefly.

(a) In an n-dimensional parameter space, set the limited region (LR) and search region (SR) in the LR. The LR should be as large as the true optimum point P* exists 100% inside. The volume of SR is quite arbitrary. The central point P0 of this SR with lengths of their sides represents the position of SR. (b) Generate trial point P1 randomly in SR and compare the variance (sum of squared residuals) S1 at P1 with S0 at P0. (c) If S1 is smaller than S0, move search region to P1. When S1 is larger than S0, try the opposite point P1'. (d) Iterate these moves until locating SR over P*. (e) When fault trials are repeated for some preset number of times successively and move is no longer performed, narrow the SR by multiplying a factor less than 1 and repeat the same procedures as above. (f) Repeat these procedures of moving and narrowing until the very small SR could at least cover the true optimum points so that the representative point of SR can be approximated as a most probable point.

Iteration is interrupted by several convergence criteria. Most generally, it is limited by two criteria. One of them is the number of successive fault trials and/or of total fault trials. This is mainly used to interrupt iterations for a fixed SR. Another is a smallness of search region or the number of narrowing times. Other than these, it can be naturally performed by some restrictions from a physical consideration of the problem. In this work, another criterion is discussed later.

Most of the computations were performed on the ACOS77/700 and 900 computer of Tohoku University Computer Center. The required memory storages depended on the problems. However it did not exceed 15kw at the largest including a comparatively large area for data storage. It is expected that refinement of programming can make it smaller than 10kW. Procedures applying to many examples were very easy because the main program is common to every problem and just exchanging subroutines of fitting function was needed.

3 Applications

(a) Gamma-ray Spectrum (Ref. 1 and 2)

In analyzing gamma ray spectrum, positions and areas of peaks are ususally computed from fitted values of parameters in a fitting function. Single Gaussian or Gaussian plus exponential function is commonly used for peak and some other various functions for background. A fitting function for a single component has 6-15 adjustable parameters including background function, and thus, for multiple peak it becomes over 12-30 including background function. More than 100 peaks with various shapes were analyzed and every computation could give reasonable results. For comparison, all the data were also analyzed by the variable metric method (Davidon method) with the same fitting function. Very good agreements were obtained between results by two algorithm. However for some examples, variable metric method could not give solutions showing oscillations or divergences, while the present method could give good fitting results. This fact made it evident that this algorithm is very robust against a diversity of experimental data and that convergences do not depend on the initial estimates.

(b) TOF-neutron Spectrum (Ref. 3)

Typical properties of this kind of spectra are poor counting statistics, asymmetrical peak shape against a time channel and that continuous components are as important as peak components. These characteristics require to analyze whole spectrum simultaneously and it causes the increasing number of adjustable parameters. The example spectrum used here was of secondary neutrons from an inelastic neutron scattering. The spectrum was composed of 3 peaks and 1 continuous component. Fitting function was made by a combination of Gaussian and exponential functions. The number of parameters was 13. Although this spectrum was tried to resolve each components by using the variable metric method at first, it showed a violent oscillation of solution. The present method could give a good fitting result. The spectrum was well reproduced, and physical quantities evaluated from fitted parameters showed good agreement with the previously known values.

(c) Two-dimensional Data (Ref. 4)

In recent years, multidimensional measurement has become very common. It seems very difficult to analyze such types of experimental data by hand so that it requires a computer fitting. However up to date, very little computer code has been developed (Ref. 5). The present method is easily applicable to this kind of problem also. The example here is a spectrum for mass identification of recoiling heavy ions. The number of data point in the fitting area was 300-500. Analyses were performed by using two kinds of fitting functions. They include 9 and 15 adjustable parameters. The result showed very robust properties and easy applicability of the present method. It was also suggested to design fitting functions which reflect all characteristic patterns appearing in the spectrum as precisely as possible.

(d) Ion Beam Scattering Spectrum (Ref. 6)

Back scattering of ion beam is now widely used in research of surface properties of metals, amorphouses and other materials. The spectrum is continuous and its structure largely depends on materials and specimens. However its original shape showing some structure for a single component can be derived theoretically by assuming some surface conditions. In this example it was assumed that a specimen is composed of 3 components and 1 layer. The original spectrum is expressed as:

$$F(x) = H - ax \quad ; \ x \leq t_1$$

$$= G \quad ; \ t_1 < x < t_2$$

Adjustable parameters are t_1, t_2, H, G, and a. The difference, $t_2 - t_1$, corresponds to thickness of the layer and H,G,a represent its fraction for this component. A fitting function was determined by a convolution of this spectrum with a resolution function R.

$$S(x) = \int_{+\infty}^{+\infty} F(t)R(x-t)dt, \quad R(y) = \frac{1}{\sqrt{2\pi}\sigma} \exp\left(\frac{-y^2}{2\sigma^2}\right)$$

It gives a function of linear combination of error functions.

$$S(x) = \frac{G-ax}{2}\left[\mathrm{erf}\left(\frac{x-t_1}{\sqrt{2}\sigma}\right)+0.5\right] + \frac{a\sigma}{\sqrt{2\pi}}\exp\left[-\frac{(x-t_1)^2}{2\sigma^2}\right] \quad ; x<t_{1}$$

$$= \frac{H}{2}\left[\mathrm{erf}\left(\frac{x-t_1}{\sqrt{2}\sigma}\right) - \mathrm{erf}\left(\frac{x-t_2}{\sqrt{2}\sigma}\right)\right] \quad ; x>t_1$$

The number of parameters is 8 for a single component. Since an experimental spectrum looks non-structural as a result of sum of several components, there seemed too much freedom to separate them. And so, some physical relationships between parameters and between components were utilized in setting search region and in generating random trial points. Analyses were performed for data with 200 points and with 3 components which required 25 parameters. One of the results is shown in Fig. 1. Resolution among 3 components looks very reasonable and in fact, physical quantities such as peak position were in a very good agreement with that obtained by other methods used previously. This is the first time that the physical quantities were obtained for all the components and between components since all components were completely separated.

(e) Infection of Tuberculosis (Ref. 7)

The present algorithm is quite useful not only for spectrum analysis but also for most fitting problems. As an example, fitting of the experimental curve for infection of tuberculosis was performed. Generally, fitting problems in a field of public health have the characteristics of small number of data points and nonlinear fitting function determined empirically. The problem treated here was essentially a fitting of 2-dimensional data with a function having 3 adjustable parameters. Since the data points were very scarce it was treated as a one-dimensional problem. Analysis was very successful (Fig. 2) and it could give good agreement with previsously predicted values.

4 Convergence Criteria

As mentioned in the introduction, the only disadvantage of this method is to require a comparatively large computing time. In order to make it shorter without losing any advantage of the algorithm, it seems best to interrupt the iteration at much less iterations. The principle of the least squares method is to minimize a variance (sum of squared residuals; S) and usually one obtains solutions from equating all partial derivatives of S along parameter axes to be zero:

$$\left|\frac{\partial S}{\partial a_i}\right|_j = \left|\left[S_j(..a_i+\delta a_i,..) - S_j(..a_i,..)\right]\right|/\delta a_i$$

However, direct utilization of these derivative values leads to a loss of robustness and compactness of the algorithm, especially in cases with larger number of parameters. And thus, I have tried to use the behavior of improvement rate in variance as a function of successful iterations instead

of monitoring the derivatives. The improvement rate was defined as:

$$\Delta_j = \frac{|S_j - S_{j-1}|}{S_{initial}}$$

By using gamma ray spectra as examples, variation of the improvement rate was compared with that of derivatives. (Fig. 3). A very similar behavior of variation could be observed between them. Both of improvement rate and derivatives reach saturations at iteration less than total iteration times at which the present criteria terminated the iteration. It is very important that the saturation point of improvement rate is beyond that of derivatives. This behavior could be observed for all the examples analyzed and the iteration number of this saturation point corresponds to less than 1/5 of the total iterations. Consequently it can be expected to utilize this behavior as a measure of convergence. By using this, the total computing time can be largely reduced compared with the one now performed in those applications.

5 Conclusion

Applications of the random search algorithm to several kinds of spectrum analyses and fitting problems were described. The excellent property of robustness and the wide applicability of this algorithm were shown. It has also been shown that present method can completely compensate the difficulties in conventional sophisticated algorithms. The advantage of the method can sufficiently overcome the disadvantage of large computing time. Moreover, it was recognized that computing time can be reduced by using more appropriate convergence criteria.

This method can be a powerful tool in a field where a small computer is used such as in environmental research. In using this method, the users have only to design fitting functions which are physically and/or theoretically reasonable, and in which each adjustable parameter corresponds to each physical quantity. Other problems can be overcome by the use of this robust algorithm.

ACKNOWLEDGMENT

The author expresses his gratitude to Dr. M. Kitamura with his helpful discussions and suggestions and his continuing encouragements throughout this work. He is also thankful to Prof. K. Sugiyama and Assoc. Prof. S. Toda for their understanding and helpful supports.

REFERENCES

1. M. Kitamura et al., Nucl. Instru. Meth., 136 (1976) 363
2. Y. Takeda et al., ibid, 136 (1976) 369
3. M. Bada, private communication
4. Y. Takeda et al., Nucl. Instru. Meth., 166 (1979) 561
5. V. B. Zlokazov, Comp. Phys. Comm., 18 (1979) 281
6. S. Yamaguchi et al., to be published
7. A. Kochi, private communication

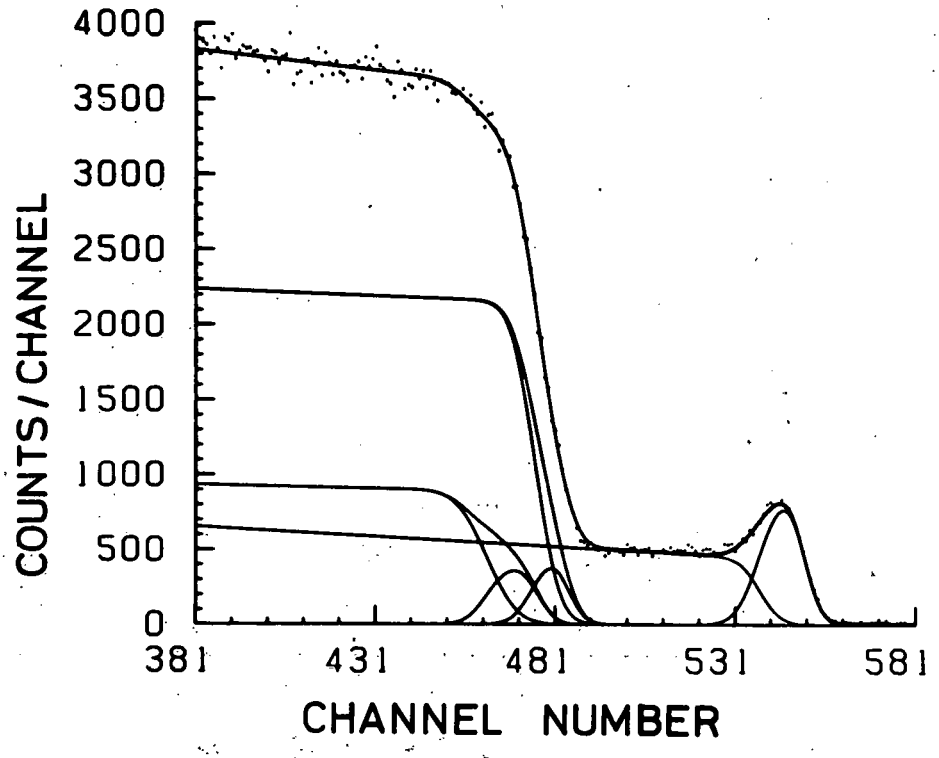


Fig. 1: Result in ion beam back scattering spectrum (Application d)

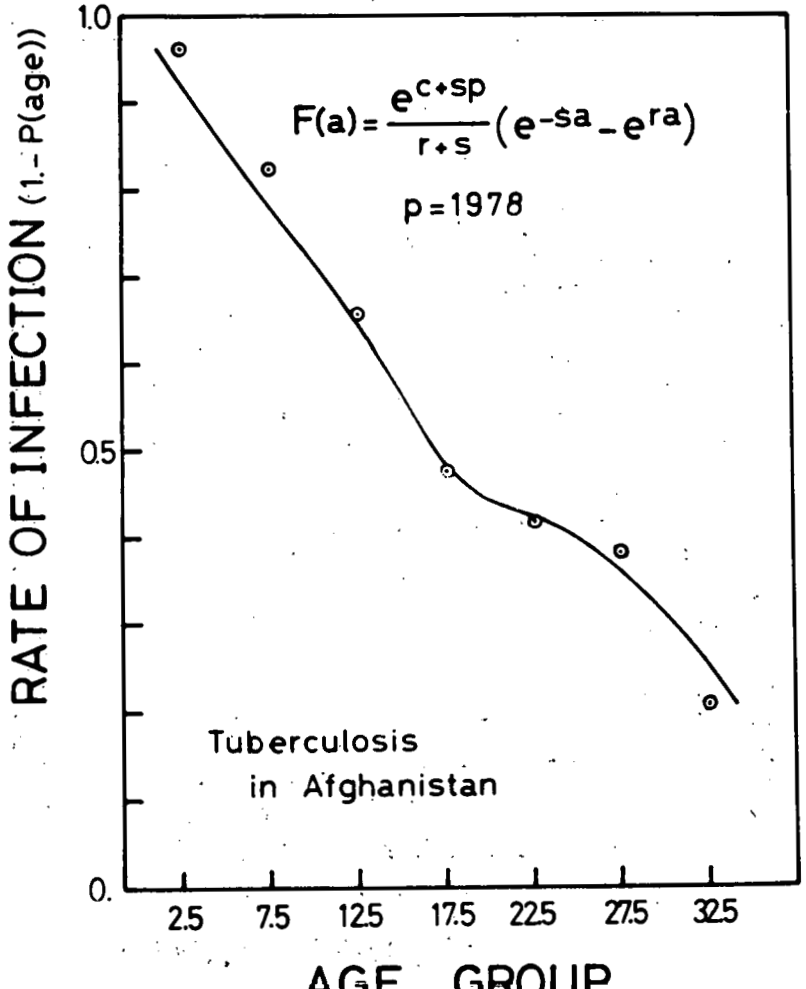


Fig. 2: Result in fitting problem in infection of tuberculosis (Application e).

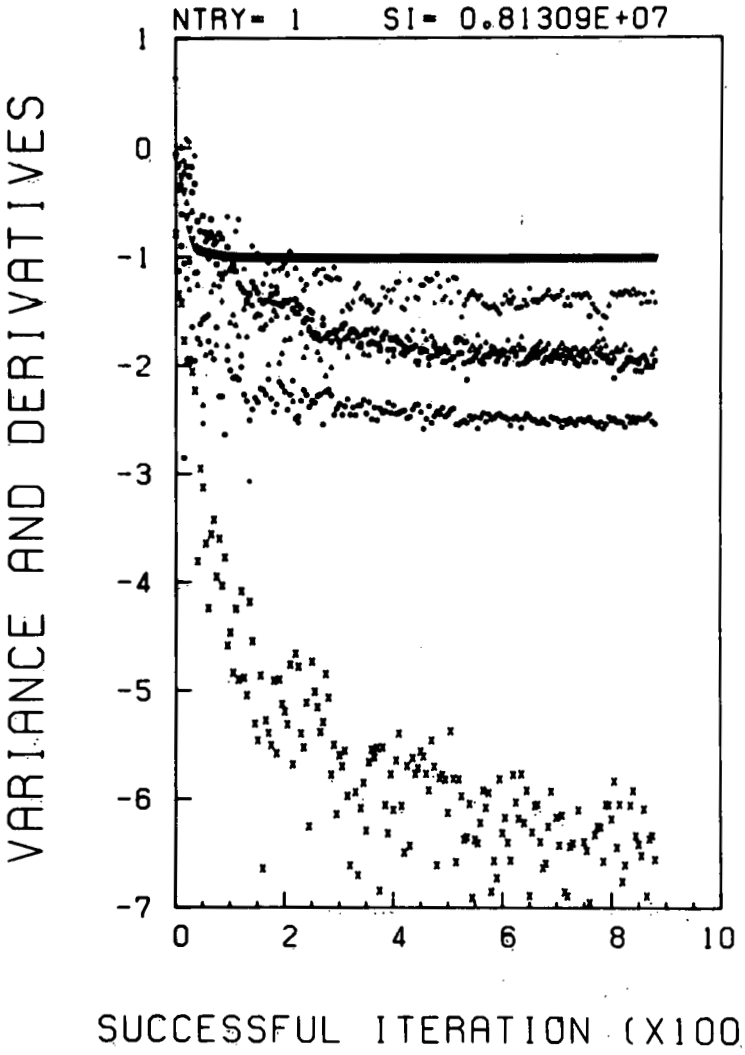


Fig. 3: Variations of improvement rate and partical derivative values against successful iterations. The ordinate is logarithmic values. Mark V represents variances, X improvement rate and others partial derivatives.

Environmental Radionuclide Concentrations: Statistical Model to Determine Uniformity of Distribution

Charles N. Cawley
Cornell University

Ervin J. Fenyves, D. Blair Spitzberg,
John Wiorkowski
The University of Texas at Dallas

M. Taghi Chehroudi
Teheran University

ABSTRACT: In the evaluation of data from environmental sampling and measurement, a basic question is whether the radionuclide (or pollutant) is distributed uniformly. Since physical measurements have associated errors, it is inappropriate to consider the measurements alone in this determination. Hence, a statistical model has been developed. It consists of a weighted analysis of variance with subsequent t-tests between weighted and independent means. A computer program to perform the calculations is included.

INTRODUCTION: To determine whether or not a radionuclide (or pollutant) is distributed uniformly in a system is a basic question in the evaluation of data from environmental sampling and measurement. Because physical measurements have associated errors, it is inappropriate to consider the measurements alone in this determination (1-4). The size of the errors among the measurements may differ substantially. Hence, a statistical model which evaluates the error contribution of each measurement has been developed.

MODEL DESCRIPTION: A weighted analysis of variance has been performed in order to determine whether or not there is a significant difference in concentration

at any location(s):

$$F_{calc} = \frac{\dfrac{\sum_i \sum_j w_{ij}(X_{ij} - \bar{X})^2 - \sum_i \sum_j w_{ij}(X_{ij} - \bar{X}_i)^2}{K - 1}}{\dfrac{\sum_i \sum_j w_{ij}(X_{ij} - \bar{X}_i)^2}{N-K}} \quad (1)$$

in which X_{ij} = Measurement

$\bar{X}_i$ = Group mean

$\bar{X}$ = Grand mean

N = Number of measurements

K = Number of sites

w_{ij} = Inverse of the square of the error of the measurement

The group mean and variance for each site can be calculated from:

$$\bar{X}_i = \frac{\sum_i w_{ij} X_{ij}}{\sum w_{ij}} \quad (2)$$

$$S_i^2 = \frac{\sum_j w_{ij} (X_{ij} - \bar{X}_i)^2}{N_i - 1} \quad (3)$$

in which N_i= number of observations at one site. The formulas for the grand mean and total variance are:

$$\bar{X} = \frac{\sum_i \sum_j w_{ij} X_{ij}}{\sum_i \sum_j w_{ij}} \quad (4)$$

$$S^2 = \frac{\sum_i \sum_j (X_{ij} - \bar{X}_i)^2}{N - K} \quad (5)$$

The number of degrees of freedom for the calculated F-value is (K - 1, N - K).

If $F_{calculate}$ is greater than $F_{critical}$, then it is appropriate to perform t-tests of weighted and independent means in order to determine at which sites the deviations are significant using the following formula:

$$t = \sqrt{\frac{\bar{X}_i - \bar{X}_k}{\frac{s_i^2}{\sum_j w_{ij}} + \frac{s_k^2}{\sum_j w_{kj}}}} \qquad (6)$$

in which X_i and X_k are the weighted average, and S_i and S_k are their respective variances.

APPLICATION: The model has been used to analyze data on environmental trituum concentrations in selected reservoirs in North Central Texas. In Table I, there are measurements and associated errors for the reservoirs. The purpose of the survey is to establish the baseline concentrations for various radionuclides before the nuclear power plant at Commanche Peak near Glen Rose, Texas, goes online in 1981.

Table I: Tritium Concentration in Reservoirs in North Central Texas (April 17-19, 1978)

Reservoir	Concentration (pCi/l)
Possum Kingdom	104 ± 30
Lake Granbury	190 ± 40
Commanche Peak	117 ± 25
Lake Whitney	205 ± 42
Garza Little Elm	52 ± 37
Lake Waxahatchie	167 ± 33
Lake Waco	166 ± 45
Lake Belton	30 ± 24

The variation in tritium concentrations can be explained by interaction of micrometerological events, hydrologic differences, and unique site geochemistry related to soil type and particulate suspension in the reservoir. To determine whether or not tritium is uniformly distributed in the reservoirs, the model

has been used. For a .05 level of significance and (7,112) degrees of freedom, $F_{critical}$ is 2.09. Since $F_{calculate}$ is 45.55, we reject the null hypothesis and accept the alternate hypothesis: There is a non-uniform concentration of tritium in the reservoirs.

Subsequent to the weighted analysis of variance, t-tests of the weighted and independent means have been made. At the .05 level of significance and for 28 degrees of freedom, the critical value is 2.048. The calculated t-values are in Table II and it is apparent that tritium concentrations in:

1. Garza Little Elm differ significantly from those of Lake Granbury and Lake Whitney,
2. Lake Waxahatchie differs significantly from Lake Granbury, Commanche Peak, Lake Whitney, and Lake Waco, and
3. Lake Belton differs significantly from Lake Granbury, Commanche Peak Reservoir, Lake Whitney, and Lake Waco.

Table II: t-Tests of Weighted and Independent Means of Selected Reservoirs in North Central Texas

Reservoir	Lake Granbury	Commanche Peak	Lake Whitney	Garza Little Elm	Lake Waxahatchie	Lake Waco	Lake Belton
Possum Kingdom	-1.43	-0.26	-1.61	0.86	1.38	-0.90	1.17
Lake Granbury		2.01	-0.28	2.74	3.22	0.39	3.01
Commanche Peak			-2.14	1.76	2.42	-0.99	2.13
Lake Whitney				2.84	3.30	-0.61	3.10
Garza Little Elm					0.64	-1.88	0.40
Lake Waxahatchie						-2.34	-0.24
Lake Waco							2.15

1. W.G. Cochran, (1954). Biometrica 10, 101.

2. W.G. Cochran and S.P. Carroll, (1953). Biometrica 9, 447.

3. D.V. Hinkley, (1979). Scandinavian Journal of Statistics 6, 37.

4. G.S. James, (1956). Biometrica 43, 301.

```
MESSY: PROC OPTIONS(MAIN);
   GET LIST (N,M);  L = N*M;

ONE: BEGIN;
DCL MEEN FLOAT INIT (0);                    /*  MEAN  */
DCL (NOM, DNOM) FLOAT INIT(0);
DCL (TSUM, SWERR, S1, S2, SUMW ) INIT (0);
DCL ( X (N,M),XBAR(N), WERR(N,M), S (N,M), SSQ(N), VAR(N),
      SW2(N), T(L), WT_ERR(N));
DCL HEADER CHAR(80) VAR INIT(' ');
DCL WIJ(N);   WIJ = 0;

   II = M;  K = 1;
                  /* + + + + + + + + + + */
GET LIST(NN);
                  /* WHERE NN EQUALS    */
                  /* # MEASUREMENTS     */


X=0;
XBAR = 0;
WERR = 0;
S = 0;
SSQ = 0;
VAR = 0;
SW2 =0;
T = 0;
WT_ERR = 0;

ON ENDFILE (SYSIN) STOP;


   IN: DO I = 1 TO N;
   GET SKIP EDIT(HEADER)(A(80));
   PUT SKIP (3) EDIT (HEADER)(A(80));
   PUT SKIP LIST('MEASUREMENT AND ERROR');
      IN2: DO J = 1 TO M;
           GET LIST (X(I,J), S(I,J) );
           PUT SKIP DATA (X(I,J), S(I,J));
      END IN2;
   END IN;

CALC1: DO I = 1 TO N; DO J = 1 TO M;
       IF S(I,J) = 0 THEN WERR(I,J) = 0;
                     ELSE WERR (I,J) = 1. / S(I,J) ** 2;
```

```
      END CALC1;
E_ONE: DO I = 1 TO N;
       WT_ERR(I) = 1 / (SUM (WERR(I, *)) ** .5);
       END E_ONE;

TWO: DO I = 1 TO N;
     WIJ(I) = 1 / SUM(WERR(I, *));
     END TWO;
CALC2: DO I = 1 TO N; DO J = 1 TO M;
       TSUM = TSUM + WERR(I,J) * X(I,J);
       SWERR = SWERR + WERR (I,J);
         END;
       XBAR(I) = TSUM / SWERR; TSUM, SWERR = 0;
     END CALC2;
   PUT SKIP(2);
   OUT: DO I = 1 TO N;
        PUT SKIP DATA (XBAR(I), WT_ERR(I),WIJ(I) );
        END OUT;
        PUT SKIP(2);
CALC3: DO I = 1 TO N; DO J = 1 TO M;
       SSQ(I) = SSQ(I) + WERR(I,J) * ((X(I,J) - XBAR(I)) ** 2) /
              (II - K);
        END CALC3;
CALC4: DO I = 1 TO N; DO J = 1 TO M;
       NOM = NOM + WERR(I,J) * X (I,J);
       DNOM = DNOM + WERR(I,J);
       END CALC4;
   MEEN = NOM / DNOM;          /*  GRAND MEAN  */
   PUT SKIP(3) LIST ('+++++++GRAND MEAN  =', MEEN);
 KK = N;                       /* # OF SITES  */
CALC5: DO I = 1 TO N; DO J = 1 TO M;
       S1 = S1 + WERR(I,J) * (X(I,J) - MEEN) ** 2;
       S2 = S2 + WERR(I,J) *(X(I,J) - XBAR(I) ) ** 2;
       END CALC5;
FCALC = ((S1 - S2) /(KK - 1)) / (( DNOM * S2) / (NN - KK));
PUT SKIP(2) DATA (FCALC);

CALC6:  DO I = 1 TO N; DO J = 1 TO M;
        SUMW = SUMW + WERR(I,J);
         END;
       VAR(I) = SSQ(I) / SUMW;
       SUMW = 0; PUT SKIP;
        END CALC6;
CALC7:  DO I = 1 TO N; DO J = 1 TO M;
        SW2(I) = SW2(I) + WERR(I,J);
        SW2(I) = 1 / SW2(I);
        END CALC7;

   PUT SKIP (2);
ALLOUT: DO I = 1 TO N;
        PUT SKIP DATA (VAR(I), SSQ(I), SW2(I));
        END ALLOUT;
PUT SKIP (2);
K = 0;
CALC8:DO I = 1 TO N - 1; DO J = I + 1 TO N;
```

```
        K = K +1;
        T1 = SSG(I) / SW2(I);
        T2 = SSQ(J) / SW2 (J);
        T3 = T1 + T2;
        T(K) = (XBAR(I) - XBAR(J) ) / SQRT(T3);
        PUT SKIP(2) DATA(I, J); PUT DATA (T(K));
        PUT DATA (T1, T2);
        END CALC8;
END MESSY;
```

Direct Image Reconstruction with Limited Angle Projection Data for Computerized Tomography

T. Inouye

Toshiba Research and Development Center
Kawasaki 210, Japan

Abstract

Discussions are made on the minimum angle range for projection data necessary to reconstruct the complete CT image. As is easily shown from the image reconstruction theorem, the lack of projection angle provides no data for the Fourier transformed function of the object on the corresponding angular directions, where the projections are missing. In a normal situation, the Fourier transformed function of an object image holds an analytic characteristic with respect to two-dimensional orthogonal parameters. This characteristic enables uniquely prolonging the function outside the obtained region employing a sort of analytic continuation with respect to both parameters. In the method reported here, an object pattern, which is confined within a finite range, is shifted to a specified region to have complete orthogonal function expansions without changing the projection angle directions. These orthogonal functions are analytically extended to the missing projection angle range and the whole function is determined. This method does not include any estimation process, whose effectiveness is often seriously jeopardized by the presence of a slight fluctuation component. Computer simulations were carried out to demonstrate the effectiveness of the method.

1. Introduction

Gamma-ray emission from injected radio-isotopes in the human body or x-ray transmission through the body provides useful information for medical diagnosis. This diagnostic information is actually obtained by using emission or transmission type computerized tomography (CT) scanners. In a CT scanner, projection data through the object concerning gamma-ray emission or x-ray transmission are supplied to solve integral equations and the original source intensity distribution is calculated using a computer. Many sophisticated computer algorithms have been proposed for this purpose. However, in the commercially available CT scanners, only analytical reconstruction algorithms based on two-dimensional Fourier transform method are used. These analytical algorithms are mathematically equivalent and can provide high resolution images in relatively short processing time. This mathematical principle for image reconstruction is described as follows:

A component of two-dimensional Fourier transform of object pattern on an oblique line is obtained by one-dimensional Fourier transform of projection on the oblique line in the same direction.

In the conventional method using this mathematics, the whole two-dimensional Fourier transform function of the object pattern is obtained by taking the whole angle projection data around the object. For this reason, in any kind of CT scanner, projection data have to be collected for angles between 0 and 180 degrees around the object. However, the Fourier transformed function of an object holds an analytic characteristic, so the function can be uniquely prolonged from the partial data employing a sort of analytic continuation. By applying this principle, it seems to be possible to reconstruct an image from projections for smaller angle range less than 180 degrees around the object.

The author previously reported a method for image reconstruction from partial projection angle data[1)], which obtains angular parameters for analytic continuation by estimation. This estimating process is often seriously affected by the presence of a slight fluctuation component in the real data.

This paper proposes a new image reconstruction algorithm using smaller angle range projections less than 180 degrees, which does not include any estimation process. This deterministic image reconstruction method from partial projection angle data can be applied to any reconstruction problem, provided the object pattern is confined within a finite range area.

2. Mathematical Theory

The object pattern distribution is expressed in polar coordinates as $f(r,\theta)$. As indicated in Fig. 1, projection $g(p,\phi)$ for this function is obtained by integrating $f(r,\theta)$ along a line $\ell(p,\phi)$, where p and ϕ are the length and direction of normal line to ℓ from the origin:

$$g(p,\phi) = \int_{\ell(p,\phi)} f(r,\theta)\,ds \quad . \tag{1}$$

Since $f(r,\theta)$ and $g(p,\phi)$ are periodic functions with respect to angle θ and ϕ with a period of 2π, both functions are able to be expanded into a Fourier series as follows:

$$f(r,\theta) = \sum_{n=-\infty}^{\infty} f_n(r)\exp(in\theta) \quad , \tag{2-a}$$

$$g(p,\phi) = \sum_{n=-\infty}^{\infty} g_n(p)\exp(in\psi) \quad . \tag{2 b}$$

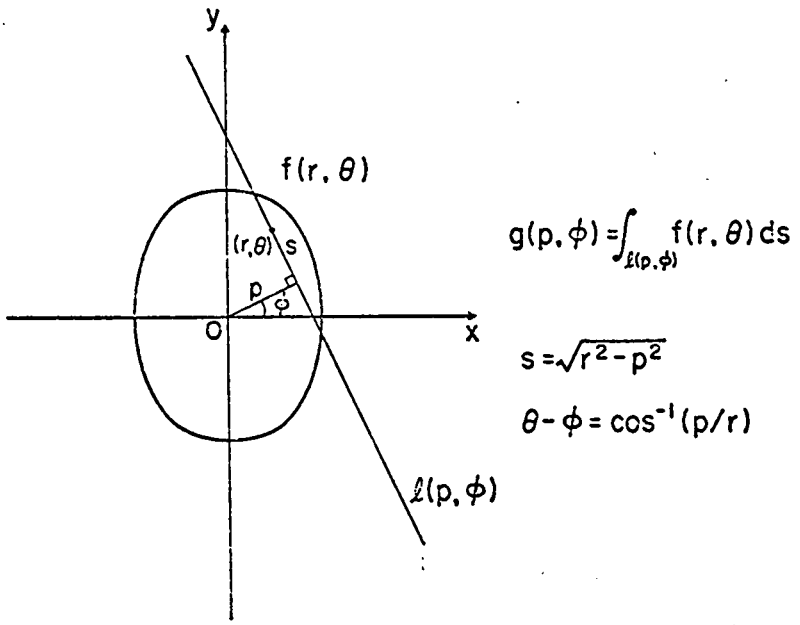


Fig. 1 Relationship between object and its projection.

By substituting these expressions into Eq. (1), the following relationship holds:

$$g_n(p) = 2\int_p^\infty \frac{f_n(r)T_n(p/r)}{\sqrt{1-(p/r)^2}}\,dr \tag{3}$$

where $T_n(\cdot)$ is a Tschebyscheff polynomial of n-th order. A solution for this integral equation with respect to $f_n(r)$ was presented by Cormack[2] as follows:

$$f_n(r) = -\frac{1}{\pi}\frac{d}{dr}\int_r^\infty \frac{g_n(p)T_n(p/r)}{\sqrt{(p/r)^2-1}\cdot p}\,dp \tag{4}$$

By substituting these equations into Eq. (2-a), the original image distribution $f(r,\theta)$ is obtained.

It should be noted that the reconstructed image $f(r,\theta)$ at radius r is uniquely determined using projections $g(p,\phi)$ at higher radial length p than r only. For this reason, if the object pattern is located within the innermost tangential lines of projection missing angles, the projection data outside of the limited angular range are not taken into the calculation.

Presuming that the projection data are missing at indicated angular range in Fig. 2, the object pattern within the hatched area is uniquely determined by applying Eq. (4). This process to allocate the object is always possible, if the original object distribution is confined within a finite range area. In Fig. 2, the center circle can be so chosen to contain the object distribution area, and the projection data at allowed angular region $g_0(X,\phi)$ is able to be shifted without changing the projection angle ϕ. This modification of projection data is attained by parallelwise shifting $g_0(X,\phi)$ to $g(p,\phi)$ according to the relationship

$$g(p,\phi) = g_0(p - s\cos\phi, \phi) \tag{5}$$

as shown in Fig. 3, where s is shifted pattern center in the allowed area.

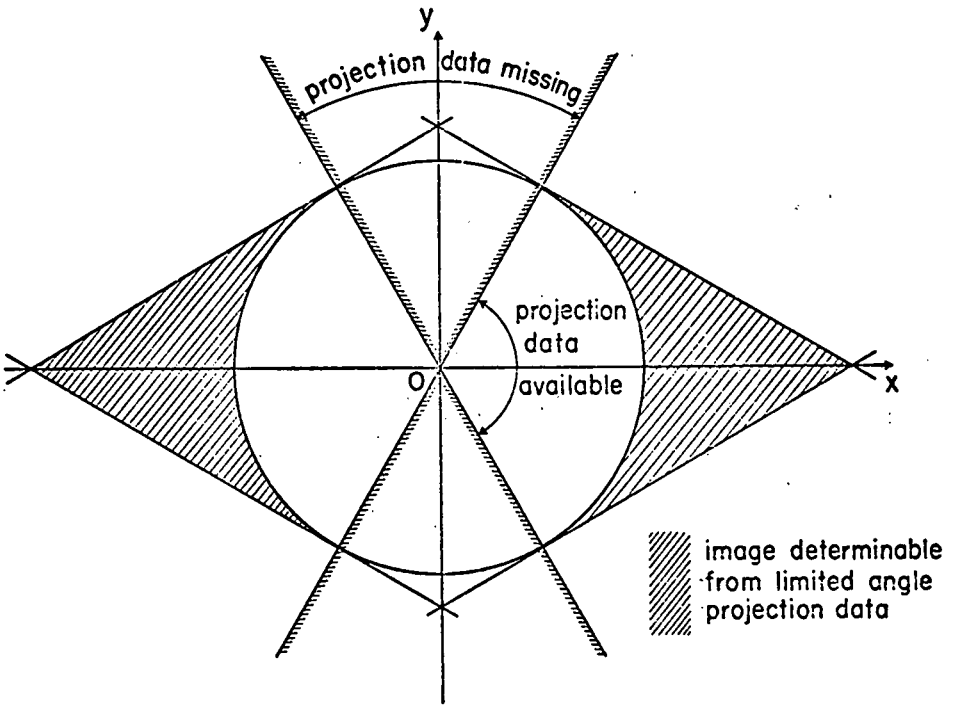
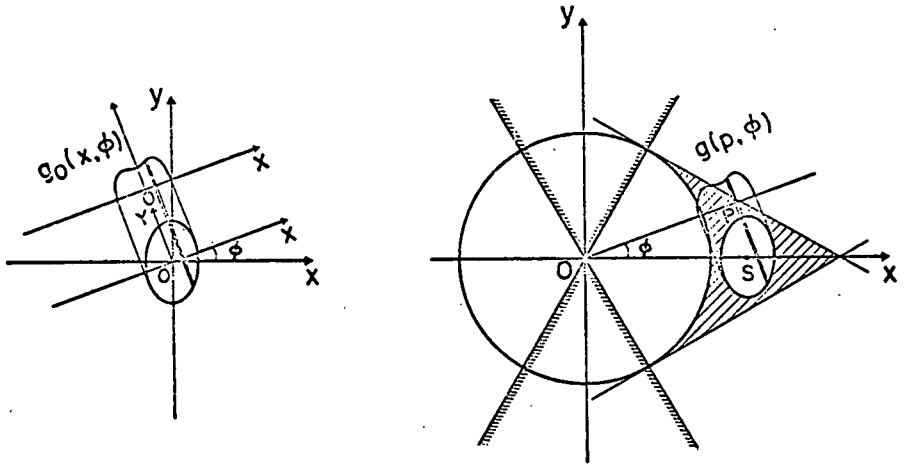


Fig. 2 Object area where image is reconstructed from limited angle projection data.



$$g(p,\phi) = g_0(p - s\cos\phi, \phi)$$

Fig. 3 Shift of projection for object confinement within area where image is reconstructed from limited angle projection data.

After obtaining these modified projection data, Eq. (4) is applied to calculate the Fourier series coefficient of the object distribution. Mathematically speaking, this process expressed by Eq. (4) is a sort of analytic continuation in the radial direction using Tschebyscheff polynomials.

Another image reconstruction based on this method is also attained by calculating projections for missing angular range. If Fourier series component of the object pattern $f_n(r)$ is substituted into Eq. (3), projections are calculated by a simple integration operation for angular regions, where original projections are missing. Since the position of object is limited within the designat-

ed outside area of a circle with radius p_0 in this instance, the integration in Eq. (3) is actually performed on a definite range as follows:

$$g_n(p) = 2\int_{p_0}^{p_{max}} \frac{f_n(r)\cdot T_n(p/r)}{\sqrt{1-(p/r)^2}}\, dr \qquad (6)$$

where p_{max} is the maximum value for p of the object pattern.

The projection data for missing angular range are obtained by calculating $g(p,\phi)$ using Eq. (2-b). The thus obtained projections all around the object can provide necessary data for a conventional image reconstruction method, such as the filtered-back projection algorithm. This combined method for image reconstruction is practically effective, because projection data at allowed projection angles are directly taken into calculation.

3. Numerical Calculations

Some typical calculation examples are shown in Figs. 4 and 5. In the case shown in Fig. 4, a cylinder is put on the indicated area, where 67 % projection angle range between -60° and +60° is sufficient to reconstruct an image. In an actual calculation, the maximum expansion order has to be limited. In the case shown in Fig. 4, Fourier series and Tschebyscheff coefficients up to the 16-th order are taken into calculation. Using Eqs. (4) and (2-a), a cross-section of reconstructed image is obtained and plotted. The result at $\theta = 0°$ is shown in comparison with the exact value. A similar comparison is made for the calculated projection data at $\phi = 90°$ for the same cylinder in Fig. 4. For the same object pattern, the result of reconstructed image with higher order Fourier series and Tschebyscheff coefficients up to the 24-th order is shown in Fig. 5.

In both examples, due to the limited number of expansion terms for Tschebyscheff polynomials as well as for Fourier series, the resolution of reconstructed image is rather deteriorated. However, this problem is easily overcome by increasing the maximum order of expansion.

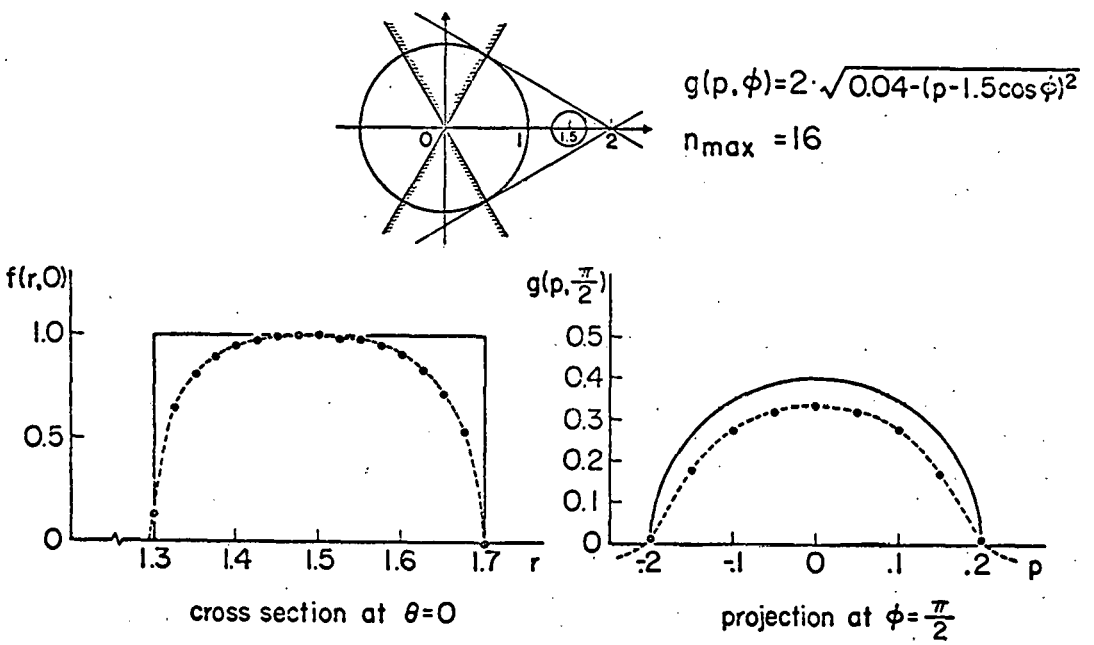


Fig. 4 Example of limited view angle reconstruction calculation. Projection data available between $-\pi/3 < \varphi < \pi/3$ around horizontal line.

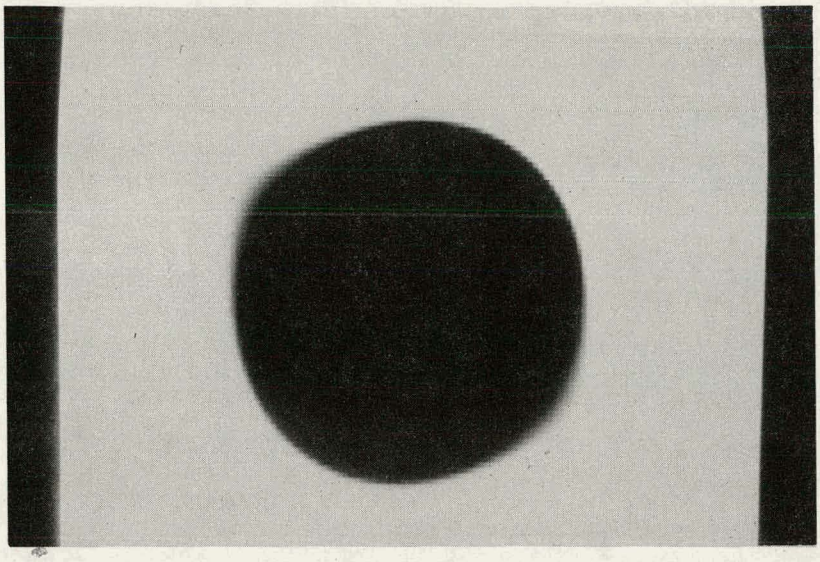


Fig. 5 Example of image reconstruction of cylinder. Maximun expansion order of Fourier series and Tschebyscheff polynomial: 24. Projection data available for 67% angle range between $0 < \varphi < 2\pi/3$.

In the actual calculation of Eq. (4), the analytically extended Tschebyscheff polynomial is a rapidly increasing function of p/r. In a normal numerical integration method, this integral has to be carried out with a large number of intervals. This restriction determines the maximum order of Fourier series and Tschebyscheff polynomial expansion terms.

4. Discussion

This image reconstruction technique with limited angle projection data provides a direct method to restore the original object pattern. It does not include any kind of estimating process, which is the case in other proposed methods.

Higher resolution is attained by increasing the number of expansion terms, whose process might take a longer computation time. The case shown in Fig. 5, a processing took about 4 minutes using a Cyber 176 computer. This drawback for practical applications would be solved by improvements in computer technology and this method for limited view angle reconstruction would be soon applied to practical cases.

Using this technique, a quite different type of CT scanner is feasible. For instance, a fan-beam scanning with a linear motion of x-ray source provides sufficient data for this method. Therefore, using this image reconstruction technique, a linear scan CT is attained. As for normal CT scanners, this technique provides a data collection method with smaller radiation dose, because the scanning range can be reduced to a smaller angle rotation.

References

1) T. Inouye, IEEE Trans. Nucl. Sci. NS-26, No.2, 2666 (1979).
2) A. M. Cormack, J. Appl. Phys. 34, 2722 (1963), and J. Appl. Phys. 35, 2908 (1964).

NUCLEAR METHODS

IN

ATMOSPHERIC AND WATER RESEARCH

Session Chairman

G.E. Gordon

RESOLVING THE SOURCES OF AIRBORNE PARTICLES FOR THE REGIONAL AIR POLLUTION STUDY

Daniel J. Alpert and Philip K. Hopke
Institute for Environmental Studies
and
Nuclear Engineering Program
University of Illinois
Urbana, Illinois

Abstract

Target transformation factor analysis (TTFA) has been applied to an analysis of a subset of the aerosol-composition data acquired during the Regional Air Pollution Study (RAPS) for St. Louis, MO. The RAPS program collected a large number of samples with ten, continuously operated, dichotomous samplers from March 1975 to March 1977. The purpose of the present study was to evaluate the capability of TTFA to resolve sources of airborne particulate matter in a set of ambient-aerosol samples. Only the samples from one sampling station, for July and August 1976, both fine and coarse fractions, were examined in this study. Because of the large number of missing values and values below the detection limits, it was necessary to exclude a sizable fraction of the data from the analyses. Separate analyses were performed on the samples from the fine and coarse fractions. In the fine-fraction data, secondary sulfate aerosol particles accounted for 64% of the mass of the average sample. Motor vehicle emissions accounted for another 15%. In the coarse fraction, soil and limestone particles accounted for 80% of the average sample mass.

Introduction

There is growing concern over possible deleterious effects associated with exposure to anthropogenic airborne particulate matter. Moreover, studies have isolated potentially mutagenic compounds in the carbonaceous particles that arise from the combustion of fossil fuels. Large scale efforts are now being made to reduce the potential hazard to public health and welfare by identifying the sources of airborne particulate matter and, where possible, applying appropriate control technologies. Because of the complexities of urban ecosystems, quantitatively apportioning the aerosol particles between the various sources is a very difficult problem. Modern receptor methodologies for determining the contribution of the various sources to the total level of

suspended particulate matter (TSP) require the collection and elemental analysis of large sets of ambient aerosol samples. It is then necessary to examine the voluminous amounts of data in order to provide recommendations that can be used by local officials to mandate the necessary controls. The volume of data necessitates the use of statistical analysis techniques to resolve the contributions of the various sources. The majority of recent source-resolution work has used the chemical element balance method (CEB) developed by Miller, Friedlander, and Hidy (1). In this method, it is assumed that the number and composition of the sources are known. The observed elemental concentrations in a set of ambient aerosol samples are fit by means of a multiple regression analysis. CEB has produced very good fits to the data in recent studies of Washington, D.C. (2), St. Louis, MO (3), and Portland, OR (4). Chemical element balance methods, however, have a major drawback in that they require an a priori knowledge of both the number and composition of the suspected source emissions. The only quantities calculated are the contributions of each of the presumed sources to each of the measured samples. Another form of statistical analysis, factor analysis, has also been used to identify sources of airborne particulate matter. A major advantage of this method is that it requires no prior assumptions about the nature of the system under study. Factor analysis has been used to identify sources of airborne particulate matter in Boston, MA, (5), Tuscon, AZ (6), and St. Louis, MO (7). In these applications of factor analysis, the actual mass contribution of each of the identified sources to each sample could not be determined. Several recent studies (8,9) have employed a new form of factor analysis called target transformation factor analysis (TTFA). Originally developed by Malinowski and co-workers (10), TTFA permits an analysis, similar in nature to the chemical element balance method, but without the presumptions as to the number or nature of the sources in the system. Unlike the earlier applications of factor analysis, TTFA allows the direct calculation of the contribution of each source to each sample. This paper presents an analysis of particulate samples collected as part of the Regional Air Pollution Study (RAPS) of St. Louis, MO using target transformation factor analysis. By providing reliable quantitative source resolutions, TTFA could be an important tool in the development of cost-effective strategies for the control of airborne particulate matter.

Target Transformation Factor Analysis

The fundamental assumption of factor analysis is that the amount of each element in each aerosol sample can be represented by a sum of the contributions from each of the sources that comprise the system. This model is of the form

$$x_{ij} = \sum_{k=1}^{p} a_{ik} f_{kj}$$

where x_{ij} is the amount of element i in sample j and p is the number of independent sources. The contribution from each source is represented as a product of two cofactors, a_{ik} and f_{kj}. The former represents the concentration of the ith element in the particles emitted by the kth source and the latter is the amount of particulate matter per unit volume contributed by source k to sample j. The entire set of aerosol samples can be resolved into source contributions given by the matrix equation

$$X = AF$$

The objectives of a factor analysis are 1) To determine p, the number of independent sources that contribute to the system, 2) To identify the components of matrix A, the elemental-source profiles, and 3) To calculate F, the contribution of each source to each sample.

The number of sources is determined by performing an eigenvalue analysis on the matrix of correlations between the samples. A target transformation analysis (10) is used to identify the nature of the sources. Target transformation determines the degree of overlap between an input source profile and one of the calculated factor axes. The input source profiles, called test vectors, are developed from existing knowledge of the emission profiles of various sources. Uniqueness test vectors, having values of all but one element equal to zero are also analyzed. The uniqueness test can resolve sources that are identified primarily with only one element. To give each element an equal weight in the target transformation, a weighting scheme has been added to the analysis. Weighting factors for each element are the calculated variance of the element weighted with the experimental error for each datum point. The weighted rotation has greatly enhanced the ability of the target transformation to resolve sources with similar concentration profiles. When a complete set of plausible sources has been isolated, they are scaled to reflect the actual concentration of each element in the source material. Correct scaling factors for all source profiles are determined from the calculated source contributions and the total measured sample weights by means of a multiple regression analysis (8). The scaled test vectors are then used to calculate contribution of each source to each sample. A more detailed description of factor analysis may be found in Alpert and Hopke (9).

Description of Data

The data used in this study were produced as part of the Regional Air Pollution Study (RAPS) for St. Louis, MO. In the RAPS program, automated dichotomous samplers were operated over a two year period at ten sites in the St. Louis metropolitan area. Over 30,000 samples were collected. Ambient aerosol samples were collected in fine, <2.4 μm, and coarse, 2.4 to 20 μm,

fractions (11). The samples were analyzed for total mass by beta-gauge measurements and for twenty-seven elements by x-ray fluorescence (12). For the present study, the data for the months of July and August 1976 were analyzed. This paper will present the results of a factor analysis of the fine and the coarse-fraction samples collected during these two months at one station. The selected station, RAPS station 112, was located near Washington University, west of downtown St. Louis. During the sixty-two days of July and August, filters were changed at twelve hour intervals producing a total of 124 samples in each the fine and coarse fractions. Data were missing for forty-eight of the samples leaving a total of 200; 99 in the fine fraction and 101 in the coarse fraction. Of the twenty-seven elements determined for each sample, a majority of the determinations of ten elements were either missing or had values below detection limits. Since a complete and accurate data set is required to perform a factor analysis, these ten elements were eliminated from the analysis. Unfortunately, arsenic was among the excluded elements. Arsenic data may be important to the differentiation of coal flyash and crustal material; two materials with very similar source profiles.

Results and Discussion

The first step in the analysis was to determine the minimum number of factors needed to represent the two data sets. The results of the tests that aid this determination are given in Table 1. For each number of retained factors, the chi-square value, exner (13), and average percent error give an indication of the point-by-point error between the original data and the data reproduced with that number of factors. In the fine-fraction data, the large change in the magnitude of the eigenvalues indicated that four factors should be retained. The test results for the coarse fraction are not conclusive, indicating either four or five factors. The nature of the sources in each fraction was determined with a target transformation analysis. In addition to uniqueness vectors, seventeen different source profiles were tested to determine the degree of overlap with any of the calculated factor axes. The seventeen test vectors included nine different crustal factors, two determinations of coal flyash, three motor vehicle factors, and three industrial type sources. In the fine-fraction data, potassium was found to be unique but related to the concentration of Al, Cl, Zn, Sr, and Ba. This factor is attributed to the presence of fireworks particles resulting from the July 4th Bicentennial display near station 112. The resolution of a fireworks factor, though present in only four of the ninety-nine samples, illustrates the source resolution power of this method. To examine the effects caused by the presence of the fireworks factor, the fine-fraction data were analyzed both with and without the samples from July 4th and 5th. One sample from July 4th was excluded from the coarse

fraction. Table 2 compares the average concentration of the elements in the fine fraction both with and without the July 4th samples. Removal of only four of the ninety-nine samples resulted in significant changes in the average concentrations of four elements: Al, K, Sr, and Ba. These elements are the primary constituents of the fireworks particles. The results of the dimensionality tests for the fine-fraction data without July 4th and 5th are given in Table 3. There are large changes in the magnitude of the eigenvalues and chi-square test with both three and five retained factors. Since the tests indicated only four factors when the July 4th samples are included, it appears that in addition to the fireworks factor, there are three major and two minor factors in the fine-fraction data. The two weaker factors were not resolved when the samples from July 4th were included.

The target transformation analysis for the fine fraction without July 4th and 5th indicated the presence of a motor vehicle source, a sulfur source, a soil or flyash source, a titanium source, and a zinc source. The presence of the sulfur, titanium, and zinc factors was determined by the uniqueness test for those elements. The concentration of sulfur was not related to any other elements and probably represents a secondary sulfate aerosol resulting from primary emissions of sulfur oxide. Titanium was found to be associated with the elements sulfur, calcium, iron, and barium. Rheingrover (14) identified the source of titanium as a paint-pigment factory located to the south of station 112. The zinc factor, associated with the elements chlorine, potassium, iron, and lead, is attributed to refuse-incinerator emissions. This factor may also represent particles from zinc and/or lead smelters, though a high chlorine concentration is usually associated with particles from refuse incinerators (15). With July 4th and 5th included, the results indicated, in addition to the fireworks source, only the presence of motor vehicle, sulfate, and soil or flyash sources. Thus, we conclude that the presence of the fireworks factor inhibits the resolution of the weaker paint-pigment and refuse factors. Based on the degree of alignment with the data, a motor vehicle, paint-pigment, and crustal source were selected from the set of input source profiles. Since the fireworks and sulfate factors had no prior source determinations, and the refuse factor differed from that measured by Greenberg (15) in the relative concentration of chlorine, source vectors predicted by the uniqueness test were used for these source profiles. Each of the profiles were refined by replacing the original values for each element with the values predicted by the target transformation.

The absolute concentrations of the source profiles predicted by the target transformation may not correspond exactly to those found in the St. Louis area. The predicted source profiles were scaled to absolute concentrations by means

of a multiple regression analysis. The scaled source profiles that best reproduced the fine data are listed in Table 4. The sulfur concentration in the refined sulfate factor is consistent with that of ammonium sulfate. The calculated lead concentration in the motor vehicle factor of ten percent and a lead to bromine ratio of about 0.28 are typical of values reported in the literature (16). The concentration of lead in motor vehicle exhaust will vary from city to city and is dependent on the ratio of leaded gasoline to unleaded and diesel powered vehicles. Except for the chlorine concentration, the calculated source profile for the refuse factor, with high concentrations of zinc and lead, is similar to that measured by Greenberg, et al (15) for the Nicosia Municipal Incinerator near Chicago. In the paint-pigment component, the titanium and iron concentrations are similar to those calculated by Dzubay (3). There are no previous determinations of a fireworks component but the main ingredients of gunpowder are carbon, sulfur, and saltpeter (KNO_3) so a calculated potassium concentration of 58% seems reasonable. The nature of the calculated soil/flyash factor is more like that of coal flyash than soil, though the calculated sulfur concentration is higher than would be expected in flyash. Differentiating soil and coal flyash, because of the similarity of their elemental profiles, is a problem often encountered in aerosol source resolution work. Coal flyash emissions are expected to be found primarily in the fine fraction while crustal material should be found in the coarse fraction. Thus, we conclude, that this factor is primarily the result of coal-burning power plant emissions. Reliable data for elements, such as arsenic, would be needed to clearly differentiate the contributions of soil and coal flyash.

For the coarse fraction, the target transformation indicated the presence of a sulfate factor, a paint-pigment factor, and two crustal factors, one an alumino-silicate type and the other of limestone or cement origin. In an earlier factor analytical study of aerosol sources in the St. Louis area, Gatz (7) found the element calcium to be associated with other than crustal sources. The high calcium loading at one site was attributed to cement plants in the sampling area. Kowalczyk (2) reports finding potassium to calcium ratios of 0.8 in plume aerosols collected over a cement plant near Washington, D.C. The uniqueness test for calcium shows no strong correlation between calcium and potassium, indicating the origins of the sources are probably crustal. The refined source profiles that best reproduced the coarse fraction are listed in Table 5. The calculated profiles of the two crustal components follow those of Miller (1) and Mason (17). The paint-pigment profile strongly resembles that calculated for the fine-fraction data. The only major difference is in the concentration of barium; unlike the fine fraction, the coarse fraction

profile does not associate barium with the paint-pigment factor. The calculated sulfur concentration in the coarse-fraction sulfate factor is much less than that in the fine-fraction and there are sizable concentrations of other elements such as aluminum, iron, and lead. This factor could result from a small part of the sulfate particles in the fine fraction ending up in the coarse samples, though a correction for this possibility was made by Goulding, et al (12) in the original analyses of the samples. Another possible explanation of the origin of this source is the transformation of gaseous sulfur dioxide into sulfates on the surfaces of the coarse particles. Carbon soot and iron- or manganese-containing particles can catalyze the conversion of SO_2 to sulfates that would adhere to the particles in the coarse fraction.

Tables 6 and 7 summarize the average elemental concentrations along with the average observed concentrations for the fine fraction. The major elements, Al, Si, S, K, Ca, Fe, and Pb, are fit very closely. The overall fit for the remaining elements is also fairly good. However, the average point-by-point errors in the reproduced data range up to a value of 350% for barium in the data without July 4th and 5th. Note, that despite the large point-by-point error, the average predicted and observed concentrations are very close, 16 and 15 ng/m^3, respectively. The disparity is in part due to the tendency of the target transformation rotation to produce profiles that represent the average composition of each source. Thus, even though the average fit for barium is very good, the point-by-point error indicates that this element has not been well reproduced. The problem is compounded by the large number of missing values and values below the detection limits for many of the less abundant elements. The presence of source components that are not resolved can lead to the underprediction of elements. For example, a paint-pigment factor was resolved in the data without July 4th and 5th but is concealed when the data for those two days are included. The unresolved paint-pigment factor in the data with July 4th and 5th would account for the underprediction of titanium in the data that included the two days. With the addition of the two extra factors to the data without July 4th and 5th, a much better fit for the concentrations of zinc and titanium was obtained. Table 8 summarizes the mass contributions for the coarse fraction. Here, all the elements are fit well.

A comparison of the predicted and measured masses for each sample is another indicator of the quality of fit produced by the target transformation. The average deviations in the mass predictions were 16% for the fine data and 12% for the coarse. Figure 1 summarizes the average mass contribution for each source to the total measured sample mass. The low percentage of unaccounted sample mass is expected in this type of analysis since the regression fit

calculates scaling factors so as to minimize the overall difference between the measured and predicted sample mass. Secondary sulfate aerosol particles account for 64% of the mass of the fine-fraction data, an average concentration of nearly 19 $\mu g/m^3$. Motor vehicle emissions account for another 15%. The measured lead concentration is divided among the refuse and motor vehicle factors. Here the lead contribution is 70% from motor vehicle emissions and 10% from refuse incinerators. In the coarse fraction, the two crustal components account for 80% of the total mass.

Conclusions

Target transformation factor analysis has been used to resolve sources of airborne particulate matter in samples collected as part of the RAPS study of St. Louis, MO. A source profile for fireworks was resolved in the fine-fraction data even though this factor was present in only four of the one hundred samples. The presence of the fireworks factor, however, was found to conceal the presence of other, weaker, sources. Additional factors were resolved when the samples from July 4th and 5th were excluded. Five factors were needed to represent the fine-fraction data without the samples from July 4th and 5th: sulfate, motor vehicles, flyash/soil, paint-pigment, and refuse incinerators. A source profile for coal-burning power plant emissions was tentatively identified, though distinguishing crustal material from coal flyash would be more certain if data for additional elements were available. Four factors were needed to represent the coarse-fraction data: soil, limestone, sulfate, and paint-pigment.

Acknowledgement

This work was supported in part by the Environmental Protection Agency (USEPA PO D6004NAEX). One of us (D.J.A.) wishes to express his appreciation to the Public Health Service, Department of Health, Education, and Welfare, National Research Award Number 5 T32 ES07001-04, for their support.

References

1. Miller, M.S., S.K. Friedlander, and G.M. Hid . A Chemical Element Balance for the Pasadena Aerosol. J. Colloid Interface Sci., 39:165-176, 1972.

2. Kowalczyk, G.S. Concentration and Sources of Elements on Washington, D.C. Area Atmospheric Particles. PhD Thesis, University of Maryland, College Park, Maryland, 1979.

3. Dzubay, T.G. Chemical Element Balance Method Applied to Dichotomous Sampler Data. Annals of the New York Academy of Sciences, 338:(in press).

4. Watson, J.G., Jr. Chemical Element Balance Receptor Methodology For the Sources of Fine and Total Suspended Particulate Matter in Portland, Oregon. PhD Thesis, Oregon Graduate Center, Beaverton, OR, 1979.

5. Hopke, P.K., E.S. Gladney, G.E. Gordon, W.H. Zoller, and A.G. Jo The Use of Multivariate Analysis to Identify Sources of Selected Elements in the Boston Urban Aerosol. Atmos. Environ., 10:1015-1025, 1976.

6. Gaarenstroom, P.D., S.P. Perone, and J.L. Moyers. Application of Pattern Recognition and Factor Analysis for Characterization of Atmospheric Particulate Composition in Southwest Desert Atmosphere. Environ. Sci. & Tech., 11:795-800, 1977.

7. Gatz, D.F. Identification of Aerosol Sources in the St. Louis Area Using Factor Analysis. J. Appl. Met., 17:600-608, 1978.

8. Hopke, P.K., R.E. Lamb, and D.F.S. Natusch. Multielemental Characterization of Urban Roadway Dust. Environ. Sci. & Tech., 14:164-172, 1980.

9. Alpert, D.J. and P.K. Hopke. A Quantitative Determination of Sources in the Boston Urban Aerosol. Atmos. Environ., (in press).

10. Weiner, P.H., E.R. Malinowski, and E.R. Levinston. Factor Analysis of Solvent Shifts in Proton Magnetic Resonance. J. Phys. Chem., 74:4537-4542, 1970.

11. Nelson, E. Regional Air Pollution Study: Dichotomous Aerosol Sampling System. EPA-297 310, U.S. Environmental Protection Agency, Research Triangle Park, NC, 1979.

12. Goulding, F.S., J.M. Jaklevic, and B.W. Loo. Aerosol Analysis for the Regional Air Pollution Study -- Interim Report. EPA-600/4-78-034, U.S. Environmental Protection Agency, Research Triangle Park, NC, 1978.

13. Exner, O. Additive Physical Properties. Collection of Czech. Chem. Commun., 31:3222-3253, 1966.

14. Rheingrover, S.W. A Statistical Model for Titanium Pollution Transport and Dispersion in the Atmosphere of St. Louis. M.S. Thesis, Florida State University, Tallahassee, Florida, 1977.

15. Greenberg, R.R., G.E. Gordon, and W.H. Zoller. Composition of Particles from the Nicosia Municipal Incinerator. Environ. Sci. & Tech., 12:1329-1332, 1978.

16. Dzubay, T.G., R.K. Stevens, and L.W. Richards. Composition of Aerosols Over Los Angeles Freeways. Atmos. Environ., 13:653-659, 1979.

17. Mason, B. Principals of Geochemistry, 3rd Ed. John Wiley & Sons, Inc., New York, NY, 1966.

Table 1. Results of Dimensionality Tests

RAPS Station 112, July and August 1976

Fine Fraction

Factor	Eigenvalue	Chi Square	Exner	Average % Error
1	98.	8.9	.324	204
2	5.0	3.9	.214	164
3	1.7	1.7	.141	129
4	1.3	0.3	.064	93
5	0.16	0.2	.047	72
6	0.09	0.1	.034	68
7	0.03	0.06	.027	67
8	0.02	0.04	.021	58
9	0.02	0.02	.016	49

Coarse Fraction

Factor	Eigenvalue	Chi Square	Exner	Average % Error
1	96.	3.6	.216	73
2	2.4	1.2	.125	50
3	0.6	0.6	.089	45
4	0.29	0.3	.064	41
5	0.19	0.1	.040	35
6	0.07	0.06	.028	33
7	0.03	0.03	.019	28
8	0.02	0.01	.013	23
9	0.01	0.01	.009	22

Table 2. Comparison of Data With and Without Samples From July 4th and 5th. (ng/m^3)

RAPS Station 112, July and August 1976

Fine Fraction

Element	With July 4th & 5th Mean	Without July 4th & 5th Mean[a]
Al	220 ± 30	200 ± 30
Si	440 ± 60	450 ± 60
S	4370 ± 310	4400 ± 320
Cl	90 ± 10	80 ± 9
K	320 ± 130	150 ± 9
Ca	110 ± 10	110 ± 10
Ti	63 ± 13	64 ± 13
Mn	17 ± 3	17 ± 3
Fe	220 ± 20	220 ± 20
Ni	2.3 ± 0.2	2.3 ± 0.2
Cu	16 ± 3	15 ± 3
Zn	78 ± 8	75 ± 8
Se	2.7 ± 0.2	2.7 ± 0.2
Br	140 ± 9	130 ± 8
Sr	5 ± 4	1.1 ± 0.1
Ba	19 ± 5	15 ± 4
Pb	730 ± 50	720 ± 50

[a]Mean value and standard deviation of the mean.

Table 3. Results of Dimensionality Tests

RAPS Station 112, July and August 1976

Fine Fraction July 4th and 5th Excluded

Factor	Eigenvalue	Chi Square	Exner	Average % Error
1	87.	7.5	.304	197
2	4.9	2.6	.304	197
3	2.8	0.4	.070	123
4	0.2	0.2	.050	98
5	0.1	0.1	.037	73
6	0.04	0.07	.029	69
7	0.02	0.05	.023	69
8	0.02	0.03	.019	67
9	0.01	0.02	.015	53

Table 4. Refined Source Profiles. (mg/g)

RAPS Station 112, July and August 1976

Fine Fraction Without July 4th and 5th

Element	Motor Vehicle	Sulfate	Flyash/ Soil	Paint	Refuse
Al	5.	1.1	53.	0.7	0.0
Si	0.0	2.2	130.	0.0	7.
S	0.0	240.	20.	78.	0.0
Cl	2.4	1.1	0.0	4.6	22.
K	1.3	1.6	15.	5.7	48.
Ca	10.	0.0	16.	34.	1.2
Ti	0.0	0.7	2.5	110.	0.0
Mn	0.0	0.0	0.7	4.8	8.6
Fe	0.0	1.1	36.	90.	36.
Ni	0.08	0.04	0.042	0.011	0.7
Cu	0.6	0.01	0.0	0.0	8.7
Zn	0.8	0.0	0.0	0.5	65.
Se	0.1	0.1	0.001	0.2	0.2
Br	30.	0.2	2.5	0.0	0.0
Sr	0.09	0.01	0.15	0.1	0.0
Ba	0.7	0.03	0.08	26.	0.5
Pb	107.	6.5	5.	0.0	46.

Table 5. Refined Source Profiles. (mg/g)

RAPS Station 112, July and August 1976

Coarse Fraction

Element	Soil	Limestone	Sulfate	Paint
Al	71.	30.	28.	5.
Si	274.	150.	0.0	0.0
S	4.9	0.0	90.	37.
Cl	1.4	16.	3.6	6.9
K	19.	15.	9.3	0.0
Ca	40.	188.	0.08	25.
Ti	0.0	1.5	0.0	128.
Mn	0.8	1.6	1.	1.2
Fe	40.	34.	43.	65.
Ni	0.01	0.2	0.2	0.06
Cu	0.0	0.6	0.9	0.0
Zn	0.0	4.2	4.3	0.3
Se	0.01	0.02	0.13	0.001
Br	0.5	3.1	3.8	1.3
Sr	0.2	0.3	0.2	0.1
Ba	0.6	0.7	0.4	3.2
Pb	1.5	11.	13.	6.7

Fine Fraction, Including July 4th and 5th

Element	Vehicle	Sulfate	Flyash/ Soil	Fireworks
Al	3.	0.9	62.	60.
Si	0.0	2.8	140.	0.0
S	0.0	232.	14.	26.
Cl	5.2	1.6	0.31	19.
K	0.0	0.06	43.	580.
Ca	12.	0.006	17.	0.27
Ti	2.8	1.8	2.3	0.0
Mn	1.5	0.1	0.8	3.6
Fe	5.8	3.8	38.	9.
Ni	0.2	0.06	0.05	0.3
Cu	1.9	0.2	0.03	4.6
Zn	9.8	1.4	0.0	24.
Se	0.1	0.1	0.0	0.01
Br	26.	0.0	2.7	2.
Sr	0.0	0.0	0.9	12.
Ba	1.45	0.3	0.8	15.
Pb	105.	8.	3.8	0.0

Table 6. Summary of Mass Contributions. (ng/m^3)

RAPS Station 112, July and August 1976

Samples From July 4th and 5th Excluded

Fine Fraction

Element	Motor Vehicle	Sulfate	Flyash/ Soil	Paint	Refuse	Total Predicted	Total[a] Observed	Average[b] % Error
Al	22.	21.	170.	0.3	0.0	220	200 ± 24	29
Si	0.0	42.	430.	0.0	9.	480	450 ± 59	17
S	0.0	4530.	66.	34.	0.0	4630	4360 ± 320	7
Cl	11.	21.	0.0	2.0	28.	61	80 ± 9	163
K	6.	30.	49.	2.5	60.	150	150 ± 9	28
Ca	45.	0.0	53.	15.	1.5	110	110 ± 10	52
Ti	0.0	12.	8.	49.	0.0	68	64 ± 13	250
Mn	0.0	0.0	2.3	2.1	11.	15	17 ± 3	122
Fe	0.0	21.	120.	39.	45.	220	220 ± 19	15
Ni	0.4	0.8	0.1	0.0	0.9	2.1	2.2 ± 0.2	106
Cu	2.6	0.2	0.0	0.0	11.	14	15 ± 2	210
Zn	3.6	0.0	0.0	0.2	82.	86	75 ± 8	78
Se	0.4	2.1	0.0	0.1	0.2	2.8	2.7 ± 0.2	89
Br	130.	4.2	8.2	0.0	0.0	146	132 ± 8	26
Sr	0.4	0.2	0.5	0.0	0.0	1.2	1.1 ± 0.1	88
Ba	3.1	0.6	0.3	11.	0.6	16	15 ± 4	353
Pb	480.	120.	16.	0.0	58.	670	720 ± 53	7

[a]Uncertainty is the standard deviation of the mean value.

[b]Average point-by-point error in predicted and measured data.

Table 7. Summary of Mass Contributions. (ng/m^3)

RAPS Station 112, July and August 1976

Including Samples From July 4th and 5th

Fine Fraction

Element	Motor Vehicle	Sulfate	Flyash/ Soil	Fireworks	Total Predicted	Total[a] Observed	Average[b] % Error
Al	16.	17.	176.	20.	230	220 ± 31	29
Si	0.0	54.	398.	0.0	450	440 ± 57	12
S	0.0	4495.	40.	8.5	4540	4370 ± 310	5
Cl	28.	31.	0.9	6.2	66	85 ± 9.	194
K	0.0	1.2	122.	190.	310	320 ± 130	11
Ca	64.	0.1	48.	0.1	112	112 ± 10	72
Ti	15.	35.	6.5	0.0	56	63 ± 13	655
Mn	8.0	2.7	2.2	1.2	14	17 ± 3	175
Fe	31.	74.	108.	3.0	215	217 ± 19	49
Ni	1.0	1.1	0.1	0.1	2.3	2.3 ± 0.2	128
Cu	10.	3.5	0.1	1.5	15	16 ± 2	261
Zn	52.	27.	0.0	7.9	87	78 ± 8	131
Se	0.6	2.1	0.0	0.0	2.8	2.7 ± 0.2	89
Br	138.	0.0	7.7	0.7	146	137 ± 9	31
Sr	0.0	0.0	2.5	3.8	6.3	5.3 ± 4.0	294
Ba	7.7	5.8	2.3	4.9	21	19 ± 5	303
Pb	557.	155.	11.	0.0	723	725 ± 51	2

[a]Uncertainty is the standard deviation of the mean value.

[b]Average point-by-point error in predicted and measured data.

Table 8. Summary of Mass Contributions. (ng/m^3)

RAPS Station 112, July and August 1976

Coarse Fraction

Element	Soil	Limestone	Sulfate	Paint	Total Predicted	Total[a] Observed	Average[b] % Error
Al	1365.	272.	111.	125.	1760	1840 ± 180	12
Si	5266.	1359.	0.0	0.0	6630	6400 ± 580	4
S	94.	0.0	356.	92.	543	490 ± 32	35
Cl	27.	145.	14.	17.	208	210 ± 213	72
K	365.	136.	37.	0.0	540	540 ± 50	9
Ca	769.	1703.	0.3	62.	2540	2380 ± 141	8
Ti	0.0	14.	0.0	320.	330	300 ± 43	107
Mn	15.	15.	4.0	3.0	37	39 ± 4	37
Fe	769.	308.	168.	162.	1410	1470 ± 158	11
Ni	0.2	2.0	0.8	0.1	3.2	3.6 ± 0.4	155
Cu	0.0	5.8	3.6	0.0	9.4	8.9 ± 0.8	149
zn	0.0	38.	17.	0.7	56	56 ± 6	126
Se	0.2	0.2	0.5	0.0	0.9	0.7 ± 0.04	154
Br	8.8	28.	15.	3.2	55	51 ± 3	51
Sr	3.8	2.4	0.7	0.3	7.2	7.9 ± 0.8	21
Ba	11.	6.3	1.4	8.0	27	27 ± 3	53
Pb	29.	100.	52.	17.	197	193 ± 11	47

[a]Uncertainty is the standard deviation of the mean value.

[b]Average point-by-point error in predicted and measured data.

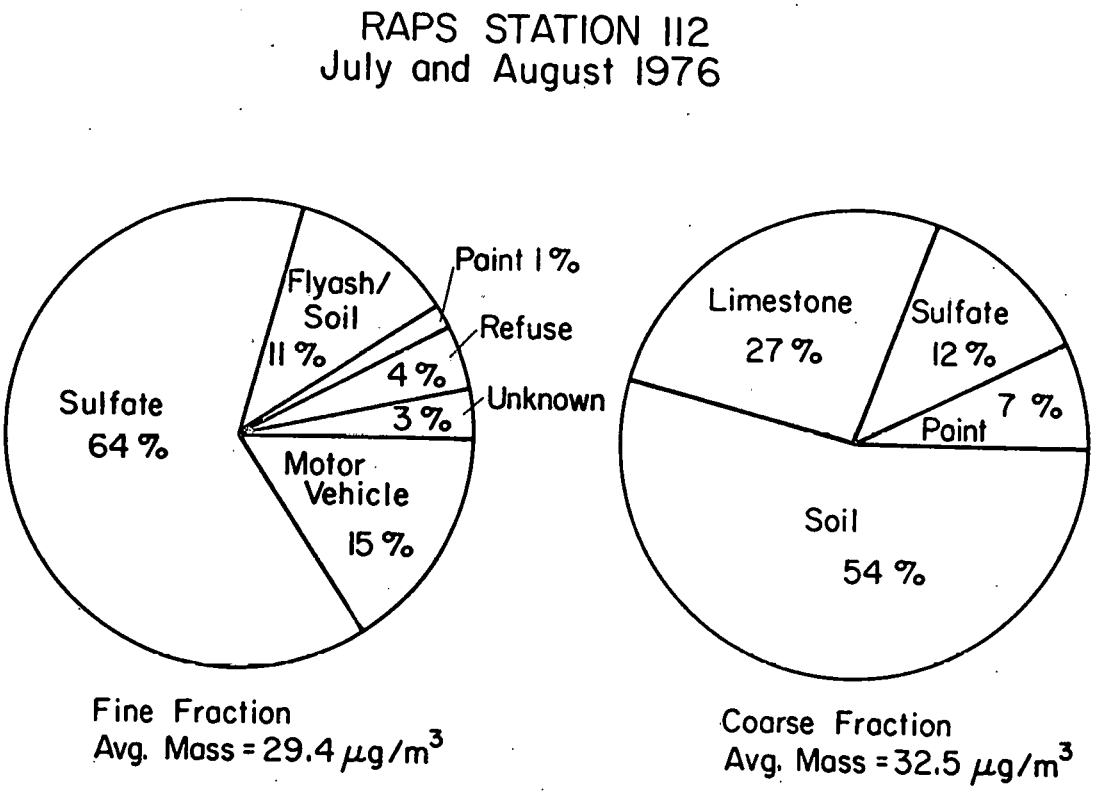


Figure 1. Average percent contribution of each source to the total average mass. The data are the fine- and coarse-fraction samples from RAPS station 112 for the months of July and August 1976.

Table 1. Results of Dimensionality Tests

RAPS Station 112, July and August 1976

Fine Fraction

Factor	Eigenvalue	Chi Square	Exner	Average % Error
1	90.	8.9	.324	204
2	5.0	3.9	.214	164
3	1.7	1.7	.141	129
4	1.3	0.3	.064	93
5	0.16	0.2	.047	72
6	0.09	0.1	.034	68
7	0.03	0.06	.027	67
8	0.02	0.04	.021	58
9	0.02	0.02	.016	49

Coarse Fraction

Factor	Eigenvalue	Chi Square	Exner	Average % Error
1	96.	3.6	.216	73
2	2.4	1.2	.125	50
3	0.6	0.6	.089	45
4	0.29	0.3	.064	41
5	0.19	0.1	.040	35
6	0.07	0.06	.028	33
7	0.03	0.03	.019	28
8	0.02	0.01	.013	23
9	0.01	0.01	.009	22

Table 2. Comparison of Data With and Without Samples From July 4th and 5th. (ng/m^3)

RAPS Station 112, July and August 1976

Fine Fraction

Element	With July 4th & 5th Mean	Without July 4th & 5th Mean[a]
Al	220 ± 30	200 ± 30
Si	440 ± 60	450 ± 60
S	4370 ± 310	4400 ± 320
Cl	90 ± 10	80 ± 9
K	320 ± 130	150 ± 9
Ca	110 ± 10	110 ± 10
Ti	63 ± 13	64 ± 13
Mn	17 ± 3	17 ± 3
Fe	220 ± 20	220 ± 20
Ni	2.3 ± 0.2	2.3 ± 0.2
Cu	16 ± 3	15 ± 3
Zn	78 ± 8	75 ± 8
Se	2.7 ± 0.2	2.7 ± 0.2
Br	140 ± 9	130 ± 8
Sr	5 ± 4	1.1 ± 0.1
Ba	19 ± 5	15 ± 4
Pb	730 ± 50	720 ± 50

[a]Mean value and standard deviation of the mean.

Table 3. Results of Dimensionality Tests

RAPS Station 112, July and August 1976

Fine Fraction July 4th and 5th Excluded

Factor	Eigenvalue	Chi Square	Exner	Average % Error
1	87.	7.5	.304	197
2	4.9	2.6	.304	197
3	2.0	0.4	.070	123
4	0.2	0.2	.050	98
5	0.1	0.1	.037	73
6	0.04	0.07	.029	69
7	0.02	0.05	.023	69
8	0.02	0.03	.019	67
9	0.01	0.02	.015	53

Table 4. Refined Source Profiles. (mg/g)

RAPS Station 112, July and August 1976

Fine Fraction Without July 4th and 5th

Element	Motor Vehicle	Sulfate	Flyash/ Soil	Paint	Refuse
Al	5.	1.1	53.	0.7	0.0
Si	0.0	2.2	130.	0.0	7.
S	0.0	240.	20.	78.	0.0
Cl	2.4	1.1	0.0	4.6	22.
K	1.3	1.6	15.	5.7	48.
Ca	10.	0.0	16.	34.	1.2
Ti	0.0	0.7	2.5	110.	0.0
Mn	0.0	0.0	0.7	4.8	8.6
Fe	0.0	1.1	36.	90.	36.
Ni	0.08	0.04	0.042	0.011	0.7
Cu	0.6	0.01	0.0	0.0	8.7
Zn	0.8	0.0	0.0	0.5	65.
Se	0.1	0.1	0.001	0.2	0.2
Br	30.	0.2	2.5	0.0	0.0
Sr	0.09	0.01	0.15	0.1	0.0
Ba	0.7	0.03	0.08	26.	0.5
Pb	107.	6.5	5.	0.0	46.

Fine Fraction, Including July 4th and 5th

Element	Vehicle	Sulfate	Flyash/ Soil	Fireworks
Al	3.	0.9	62.	60.
Si	0.0	2.8	140.	0.0
S	0.0	232.	14.	26.
Cl	5.2	1.6	0.31	19.
K	0.0	0.06	43.	580.
Ca	12.	0.006	17.	0.27
Ti	2.8	1.8	2.3	0.0
Mn	1.5	0.1	0.8	3.6
Fe	5.8	3.8	38.	9.
Ni	0.2	0.06	0.05	0.3
Cu	1.9	0.2	0.03	4.6
Zn	9.8	1.4	0.0	24.
Se	0.1	0.1	0.0	0.01
Br	26.	0.0	2.7	2.
Sr	0.0	0.0	0.9	12.
Ba	1.45	0.3	0.8	15.
Pb	105.	8.	3.8	0.0

Table 5. Refined Source Profiles. (mg/g)

RAPS Station 112, July and August 1976

Coarse Fraction

Element	Soil	Limestone	Sulfate	Paint
Al	71.	30.	28.	5.
Si	274.	150.	0.0	0.0
S	4.9	0.0	90.	37.
Cl	1.4	16.	3.6	6.9
K	19.	15.	9.3	0.0
Ca	40.	188.	0.08	25.
Ti	0.0	1.5	0.0	128.
Mn	0.8	1.6	1.	1.2
Fe	40.	34.	43.	65.
Ni	0.01	0.2	0.2	0.06
Cu	0.0	0.6	0.9	0.0
Zn	0.0	4.2	4.3	0.3
Se	0.01	0.02	0.13	0.001
Br	0.5	3.1	3.8	1.3
Sr	0.2	0.3	0.2	0.1
Ba	0.6	0.7	0.4	3.2
Pb	1.5	11.	13.	6.7

Table 6. Summary of Mass Contributions. (ng/m^3)

RAPS Station 112, July and August 1976

Samples From July 4th and 5th Excluded

Fine Fraction

Element	Motor Vehicle	Sulfate	Flyash/ Soil	Paint	Refuse	Total Predicted	Total[a] Observed	Average[b] % Error
Al	22.	21.	170.	0.3	0.0	220	200 ± 24	29
Si	0.0	42.	430.	0.0	9.	480	450 ± 59	17
S	0.0	4530.	66.	34.	0.0	4630	4360 ± 320	7
Cl	11.	21.	0.0	2.0	28.	61	80 ± 9	163
K	6.	30.	49.	2.5	60.	150	150 ± 9	28
Ca	45.	0.0	53.	15.	1.5	110	110 ± 10	52
Ti	0.0	12.	8.	49.	0.0	68	64 ± 13	250
Mn	0.0	0.0	2.3	2.1	11.	15	17 ± 3	122
Fe	0.0	21.	120.	39.	45.	220	220 ± 19	15
Ni	0.4	0.8	0.1	0.0	0.9	2.1	2.2 ± 0.2	106
Cu	2.6	0.2	0.0	0.0	11.	14	15 ± 2	210
Zn	3.6	0.0	0.0	0.2	82.	86	75 ± 8	78
Se	0.4	2.1	0.0	0.1	0.2	2.8	2.7 ± 0.2	89
Br	130.	4.2	8.2	0.0	0.0	146	132 ± 8	26
Sr	0.4	0.2	0.5	0.0	0.0	1.2	1.1 ± 0.1	88
Ba	3.1	0.6	0.3	11.	0.6	16	15 ± 4	353
Pb	480.	120.	16.	0.0	58.	670	720 ± 53	7

[a]Uncertainty is the standard deviation of the mean value.

[b]Average point-by-point error in predicted and measured data.

Table 7. Summary of Mass Contributions. (ng/m^3)

RAPS Station 112, July and August 1976

Including Samples From July 4th and 5th

Fine Fraction

Element	Motor Vehicle	Sulfate	Flyash/ Soil	Fireworks	Total Predicted	Total[a] Observed	Average[b] % Error
Al	16.	17.	176.	20.	230	220 ± 31	29
Si	0.0	54.	398.	0.0	450	440 ± 57	12
S	0.0	4495.	40.	8.5	4540	4370 ± 310	5
Cl	28.	31.	0.9	6.2	66	85 ± 9	194
K	0.0	1.2	122.	190.	310	320 ± 130	11
Ca	64.	0.1	48.	0.1	112	112 ± 10	72
Ti	15.	35.	6.5	0.0	56	63 ± 13	655
Mn	8.0	2.7	2.2	1.2	14	17 ± 3	175
Fe	31.	74.	108.	3.0	215	217 ± 19	49
Ni	1.0	1.1	0.1	0.1	2.3	2.3 ± 0.2	128
Cu	10.	3.5	0.1	1.5	15	16 ± 2	261
Zn	52.	27.	0.0	7.9	87	78 ± 8	131
Se	0.6	2.1	0.0	0.0	2.8	2.7 ± 0.2	89
Br	138.	0.0	7.7	0.7	146	137 ± 9	31
Sr	0.0	0.0	2.5	3.8	6.3	5.3 ± 4.0	294
Ba	7.7	5.8	2.3	4.9	21	19 ± 5	303
Pb	557.	155.	11.	0.0	723	725 ± 51	2

[a]Uncertainty is the standard deviation of the mean value.

[b]Average point-by-point error in predicted and measured data.

Table 8. Summary of Mass Contributions. (ng/m^3)

RAPS Station 112, July and August 1976

Coarse Fraction

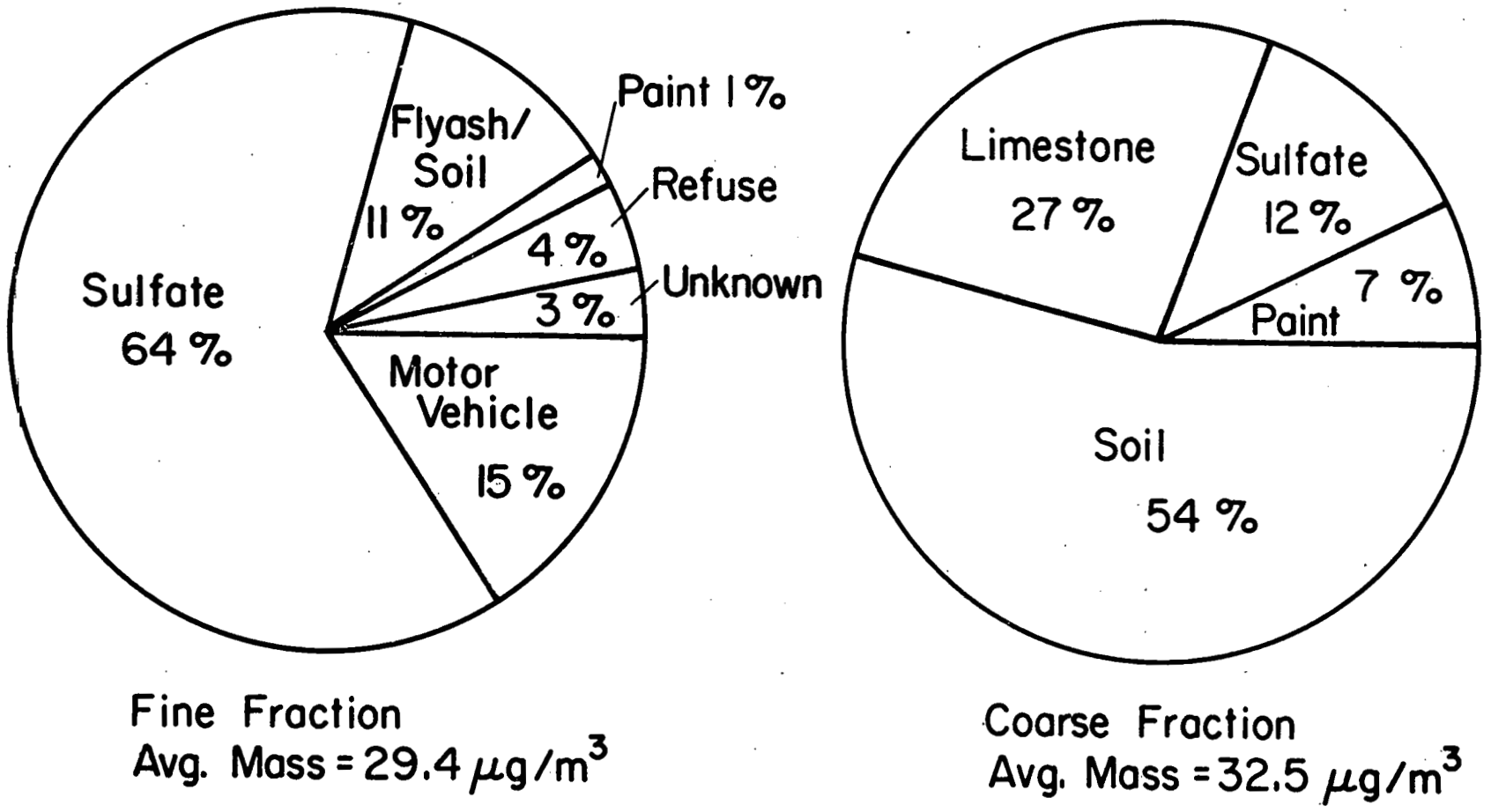
Element	Soil	Limestone	Sulfate	Paint	Total Predicted	Total[a] Observed	Average[b] % Error
Al	1365.	272.	111.	125.	1760	1840 ± 180	12
Si	5266.	1359.	0.0	0.0	6630	6400 ± 580	4
S	94.	0.0	356.	92.	543	490 ± 32	35
Cl	27.	145.	14.	17.	200	210 ± 213	72
K	365.	136.	37.	0.0	540	540 ± 50	9
Ca	769.	1703.	0.3	62.	2540	2380 ± 141	8
Ti	0.0	14.	0.0	320.	330	300 ± 43	107
Mn	15.	15.	4.0	3.0	37	39 ± 4	37
Fe	769.	308.	168.	162.	1410	1470 ± 158	11
Ni	0.2	2.0	0.8	0.1	3.2	3.6 ± 0.4	155
Cu	0.0	5.8	3.6	0.0	9.4	8.9 ± 0.8	149
zn	0.0	38.	17.	0.7	56	56 ± 6	126
Se	0.2	0.2	0.5	0.0	0.9	0.7 ± 0.04	154
Br	8.8	28.	15.	3.2	55	51 ± 3	51
Sr	3.8	2.4	0.7	0.3	7.2	7.9 ± 0.8	21
Ba	11.	6.3	1.4	8.0	27	27 ± 3	53
Pb	29.	100.	52.	17.	197	193 ± 11	47

[a]Uncertainty is the standard deviation of the mean value.

[b]Average point-by-point error in predicted and measured data.

RAPS STATION 112
July and August 1976

Figure 1



Average percent contribution of each source to the total average mass. The data are the fine - and coarse - fraction samples from RAPS station 112 for the months of July and August 1976.

IDENTIFYING LOCATIONS OF DOMINANT POINT SOURCES OF ELEMENTS IN URBAN ATMOSPHERES FROM LARGE, MULTIELEMENT DATA SETS*

Scott W. Rheingrover and Glen E. Gordon
Department of Chemistry
University of Maryland
College Park, Maryland 20742

ABSTRACT

Because of the inaccuracies of source-emissions inventories and dispersion models, air pollution control authorities are beginning to use receptor models (e.g., chemical element balances and factor analysis) to determine contributions of various sources to total suspended particulate matter in urban areas. A major limitation of receptor models is the poor quality of existing data on compositions and size distributions of particles from the important types of sources in some urban areas. A new method for determining compositions for particles from sources is proposed. Samples heavily impacted by certain sources are identified by searching large data sets for samples with unusually high concentrations of certain elements that were obtained during periods of small wind fluctuation. The mean wind directions for these groups of samples often form clusters about angles pointing to major sources of the elements. By triangulation of wind trajectories from several sampling stations, one can pinpoint the source of the element to within a 1.5- x 1.5-km area in favorable cases. Samples heavily influenced by a source can be analyzed in detail to obtain the composition of particles from the source in question.

*Work supported in part by the U. S. Environmental Protection Agency under Cooperative Agreement No. CR 806263-02-0.

INTRODUCTION

There is increasing interest among air pollution authorities in the use of receptor models to determine contributions of various types of sources to total suspended particulate matter (TSP) in urban areas (1). The traditional methods have serious deficiencies caused by inaccuracies in the source-emissions inventories and the associated dispersion models as well as the fact that many non-ducted, fugitive emissions are not included in the treatment.

According to the receptor approach, one determines concentrations of a large number of chemical elements or species at many times and places in an urban area and then uses various statistical methods to resolve the observed concentration patterns into components originating from various sources. Two

major interpretive methods have been used: chemical element balances (2-6) and a variety of methods under the general category of "pattern recognition", e.g., multivariate or factor analysis (7,8). Recently, Alpert and Hopke have developed a hybrid approach which they call, "target transformation factor analysis" (9).

In order to perform chemical element balances (CEBs), one must know the concentration patterns of particles from the important types of sources present in the region under study. The concentration pattern of each urban particulate sample is assumed to be a linear combination of the patterns of the components, with coefficients (source strengths) determined by a least-squares fit to the observed concentrations of a subset of the measured elements called the "marker elements" (chosen to be strong indicators of particles from the various sources). The quality of the fit may be tested by comparing predicted and observed concentrations of the remaining "floating" elements not used in the least-squares fit.

In pure factor analysis, no assumptions are made about the number or compositions of components: all individual concentrations in samples are normalized with respect to the mean and standard deviation for the element and a search is made for the minimum number of factors that will explain most of the variations of the elements about their mean values. Because of the normalizations, one cannot obtain the composition patterns of the components -only the portion of the variance about the mean that is accounted for by each factor. In the target-transformation factor analysis of Alpert and Hopke, there is no normalization to the mean, so it provides concentrations of elements for each factor, while retaining most other advantages of factor analysis. The factors obtained as solutions may be thought of as vectors in elemental concentration space. They will not necessarily line up with vectors representing the compositions of known source particles in the area; however, the vector solutions obtained can be "rotated" so that certain of them do line up with vectors of known sources as is done by Alpert and Hopke (9).

Tests of receptor models as applied to Boston (7,9) and Washington (4,5), which have few industrial sources, have been reasonably successful. For example, Kowalczyk (5) used concentrations of nine marker elements (Na, Al, Ca, V, Mn, Fe, Zn, As and Pb) to determine strengths of seven sources (coal, oil and refuse combustion, soil, limestone, motor vehicle emissions and marine aerosols) via CEBs on compositions of aerosols from the Washington, D.C. area. On the average, concentrations of the 28 non-volatile floating elements were predicted to within a factor of two.

The success of receptor models, especially CEB and target-transformation methods, depends on the availability of reliable concentration patterns of particles from major sources in an area. Components are needed as input to the former and at least some of the components are needed in the latter for rotation of the vector solutions. Components are not used directly in factor analysis, but some knowledge of them is needed for association of the resulting factors with sources in the area.

Our present knowledge of concentration patterns of components is barely adequate for use in cities with rather simple atmospheric mixtures, but totally inadequate for industrialized cities such as Chicago, St. Louis or Pittsburgh. We are attempting to perform CEBs on the huge data set obtained by Loo et al. (10) from a network of dichotomous samplers operated in and near St. Louis in connection with the Regional Air Pollution Study (RAPS). The components available for our study are quite inadequate, first because the St. Louis area has several types of sources for which there are little or no data (10-12): a pigment plant, zinc and lead smelters, a steel mill, etc. Second,

even if there were detailed analyses available on particles collected from the stacks of these and other sources, they would not necessarily represent the composition pattern of the particles observed at the receptor sites some distance away. If the stack gases are hot, some volatile species may be present in the vapor phase, but later condense upon cooling after release to the atmosphere, the so-called "condensibles" (1). Very large particles in the stack may settle out before reaching the sampling stations (although this may not be a problem if compositions of particles of various size ranges in the stack are known). Finally, not all emissions from a complex source come from the stack. The fugitive process emissions and dust raised by handling of materials, transportation, construction, etc. are handled poorly, if at all, by source-emissions inventories.

Below we present a method whereby it may be possible to determine compositions of particles from various sources by proper selection and treatment of data from ambient sampling networks.

WIND TRAJECTORY ANALYSIS

The St. Louis data set was obtained by collection of samples with ten dichotomous samplers operated between mid-1975 and early-1977 (10,11,13). Consecutive 12-hr samples were taken at most sites, 6-hr samples at two sites and, for a 5-week intensive sampling period, 2-hr samples were taken at three sites. Fine and coarse fractions were analyzed for about twenty elements by x-ray fluorescence (XRF) and for total mass by β-particle attenuation. Other groups in the RAPS project collected data on wind speed and direction, temperature, dew point, light scattering, pollutant gas concentrations, etc.

To develop components for sources unique to St. Louis, we identified samples from the network that were heavily impacted by material from specific sources by searching the data set for samples having unusually large concentrations of elements whose ambient levels are dominated by emissions from one or a few large sources. We first determined average concentrations and standard deviations ($\bar{x}\pm\sigma$) for the 1976 data set, which covered a full year at most stations. Then, samples at each station were searched for those having unusually high concentrations ($x>\bar{x}+z\sigma$; where z is a parameter typically set at about 3) of each element in the two size fractions. The average wind direction for the collection of samples obtained for some of the elements appeared to point in the direction of probable sources of the elements. We thought this might be a way of identifying dominant sources of the elements. However, we found that this procedure did not yield definitive results for a number of elements, mainly for two reasons: first, the wind directions may be highly variable during a sampling period. Although the wind may bring a high concentration of particles from a particular source to the sampler during a portion of the sampling period, a wind shift may produce a mean wind direction for the period that is far away from the trajectory toward the source. Second, for some elements there may be two or more sources in the area that cause unusually high concentrations at the sampler. In that case, the mean wind direction of the high concentration sampling periods will be a weighted average of the trajectories towards the several dominant sources of the element, but will not usually point to a particular source.

A better way in which to locate sources of certain elements is that of searching the data set for sampling periods that meet two criteria: (1) concentration of the element $x>\bar{x}+z\sigma$ and (2) the standard deviation of hourly wind directions, $\sigma(\theta)\leq 20$ deg. Furthermore, instead of simply determining the overall mean wind direction from all of the sampling periods meeting these criteria, we make a histogram of the mean wind directions from each sampling period.

Examples of histograms of wind directions obtained from all 6-hr samples meeting both criteria at Station 103 are shown in Fig. 1. The events obtained for Ti in both fine and coarse fractions cluster around angles of about 211 deg. The trajectories indicated for Ti point to the well known major Ti source in St. Louis (14), a paint pigment plant to the southwest of Station 103.

Some elements show clusters around more than one angle, and the fine and coarse fractions often yield different results. For example, the coarse-particle Zn distribution in Fig. 1 has only one cluster, at 188 deg, associated with a primary Zn smelter slightly west of south of the station. By contrast, the fine-particle Zn distribution has one cluster at 10 deg and another at 194 deg. The former is associated with iron and steel production NNE of the station and the latter, with the primary Zn smelter (perhaps with some influence by a primary Pb smelter located at an angle more west of south).

For some elements, there are no narrow clusters, e.g., coarse Si and Ca in Fig. 1. These elements are mostly lithophile ("crustal") elements which have so many sources, such as fugitive dust associated with traffic, that there are no dominant point sources at specific angles. One must use caution in interpreting cases for which the events are broadly distributed in angle. For a few elements there are very broad distributions centered between 150 and 210 deg. However, before attempting to associate these distributions with particular sources, one must examine the populations of wind directions from which these samples were selected.

In Fig. 2 are histograms of mean wind directions for all sampling periods and for those sampling periods for which $\sigma(\theta) \leq 20$ deg (shaded portions) for the 6-hr samples at Station 103 (lower) and 12-hr samples at Station 115 (upper). The Station 103 histogram has two maxima centered at $\bar{\theta}$ = 181 and 321 deg with $\sigma(\bar{\theta})$ values of 11 and 22 deg, respectively. Because of these distributions, some elements may display broad maxima at these angles whether or not there are point sources located along those trajectories. The best confirmation of the presence of a dominant source of an element is the observation of maxima at different angles at other stations of the network. Note that there are very few sampling periods with $\sigma(\theta) \leq 20$ deg for wind directions around 60-105 and 185-260 deg at Station 115. Thus, if no trajectories for elements are found at those directions, it does not necessarily mean that there are no point sources at those angles: even if they are present, we could not observe them with this condition on fluctuations of the wind direction. The percentage of sampling periods with $\sigma(\theta) \leq 20$ deg ranged from about 75% for the 6-hr samples taken at Stations 103 and 105 to about 50% for the 12-hr samples taken at the eight remaining stations. Station 115 is located to the NE of St. Louis (Fig. 3) and the dearth of samples with $\sigma(\theta) \leq 20$ from directions 185-260 (Fig. 2) severely limited the possibility of finding trajectories for many elements.

A summary of the wind-direction histograms for the various elements at Station 103 is given in Table I. For each element that displayed clusters, we assigned events to each cluster and used the mean wind values of the cluster to calculate an overall average $\bar{\theta}$ and standard deviation of the mean value, $\bar{\sigma}(\theta)$, as in Table I. The z value used as the criterion for high concentrations was usually set at about 2.75, but was varied somewhat from one element to another to obtain a reasonable number of events for each element. Note that we have selected a very unusual set of samples. At Station 103, for example, we have selected about 10-30 sampling periods for each element out of the total of 1938 6-hr samples taken at Station 103. The ratios of

concentrations of elements in the selected samples to the station average for the element, $\bar{x}$, usually ranged from about 5 to 15.

This procedure was performed on data from each station to determine the values of $\bar{\theta}$ and $\bar{\sigma}(\theta)$, for each cluster for elements that yielded clusters. Then maps were made for each element showing the wind trajectories from each of the stations. For example, trajectories for fine-particle Mn (solid arrows) pointing to an iron works located near Station 106 are shown in Fig. 3. Typical $\bar{\sigma}(\theta)$ values about the mean trajectory are shown by the dashed lines for Station 118. With $\bar{\sigma}(\theta)$ values of 3 deg and trajectories of 15 km from receptor to source the arc length at the source is about 1.5 km. Thus, we were able to locate the source of the high concentrations of fine-particle Mn in Fig. 3 within a 1.5- x1.5-km area. Additional trajectories for fine-particle Mn point to an iron and steel plant located between Stations 103 and 108.

As shown in Table I, several elemental trajectories for several groups of elements agree in angle to within their respective $\bar{\sigma}(\theta)$ values. In Table II is a summary of various groups of elements at Station 103 with similar trajectories that are associated with dominant sources identified by our procedure. As noted above, the trajectory for fine-particle Zn at 194 deg is likely to be a combination from the Zn and Pb smelters. The copper products plant and the primary Zn smelter are located within 2 km of one another and thus the designations for Ni and Sn are not known with certainty. Although the data shown are all of Station 103 these elemental groupings and associations have been confirmed by their appearance at appropriate angles in data from other stations. There is possibly one addition element group in Table I: coarse-particle K, S and P at about 60 deg, which is probably associated with a fertilizer plant, but this has not be confirmed.

At this time we do not have trajectories to sources such as soil, motor vehicles, or power plants. The soil and motor-vehicle sources may be too widespread for distinct clusters of associated elements and tall stacks probably cause the lack of trajectories to power plants. Arsenic has been the best indicator from CEBs for coal-fired power plants (4,5) but the As K x-ray has strong interference of Pb L x-rays, so the As values are probably not very reliable (13).

DISCUSSION

The wind trajectory method as applied to concentration data for many elements on ambient samples from a network is promising as a method of determining identities of point sources that are dominant sources of specific elements. From the data presented above it appears that locations of such sources can be determined to within areas as small as 1.5 x 1.5 km. In so doing, we identify samples that are strongly impacted by emissions from these sources. This process can perhaps be improved. Note, for example, that we have not used observed concentrations to hlep determine locations of sources. In the case of ground-level sources, the highest concentrations would be observed at stations closest to the source. But for sources with tall stacks, there is not a simple relationship between distance and ground-level concentration.

Once the samples containing large contributions from the various sources are identified, we will obtain the samples from the archives to perform additional analysis by instrumental neutron activation analysis (INAA). This will provide data on several elements that are very useful for characterizing sources, but which cannot be observed accurately, if at all, by XRF, e.g., As, Se, Sb. The question will then arise, how can we use the analyses of these

samples to determine compositions of particles from the sources? One cannot simply subtract the average concentrations at the station and attribute the residuals to the source. In some cases one may be able to subtract a background based on samples taken at a station upwind of the source. However, there is such a concentration of sources of various types in the St. Louis area that there may well be other sources between the upwind and downwind stations.

Another approach may be that of determining linear regressions of the concentrations of various elements with that of the element used as a marker for the source. For example, scatter plots of the concentrations of fine-particle Fe and Ti vs. fine-particle Mn, along with their regression lines, are shown in Fig. 4. The samples used in these regressions are the 27 fine-particle Mn-criteria samples which made up the four station trajectories shown in Fig. 3. The relationship between Fe and Mn is quite strong with a probability of no correlation $P<0.001$, whereas Ti vs. Mn has $P>0.5$. Results of linear regressions of several elements with fine-particle Mn are listed in Table III. Many elements appear to be associated with the Mn concentrations from the iron works: surely, the elements down through Sn in Table III. However, one must use caution in interpreting the correlation coefficients: the trajectories from some stations towards the source of Mn may also have other sources along the same line, causing some correlation.

As a first approximation for elements that are strongly correlated, the slopes of the regression lines (Col. 4 of Table III) could be taken as the concentrations of elements relative to Mn on particles from the source in question. That is, for the iron works, the relative concentrations could be taken as Si/Fe/K/Cr/Cu/Sn/Mn = 2.58/1.11/0.309/0.017/0.039/0.014/1.00. Perhaps the best approach will be that of applying the target-transformation method of Alpert and Hopke (9) to the collection of samples impacted by the source in order to extract the source of interest from the other sources contributing to the samples.

If compositions of particles from the sources can be obtained in this way from network samples, this approach will have many advantages over the traditional methods:

(1) Most condensibles will have condensed before reaching the sampling site and very large particles will have fallen out. (One can perhaps check composition vs. distance by analysis of samples from stations at different distances from the source.)

(2) The component received at the sampling stations should include fugitive particles of size small enough to remain airborne for a significant time.

(3) The source components are determined at the same time as the ambient samples are taken -which is often not the case.

(4) This method identifies the impact of specific point sources, not just the class of source. Thus, it may be possible to distinguish emissions of three or so major sources within a class.

(5) Since we are selecting samples containing very high concentrations of elements, the method may be effective for elements whose concentrations are below detection limits for a majority of the sampling periods.

Thus, the wind trajectory method may provide components that are appropriate for use in receptor models. However, if successful, it will simply complement other methods and not completely supplant them. At this time, it is not clear, for example, that it will be able to handle components from sources with very tall stacks. It may also not be useful for sources that are widely distributed, e.g., motor vehicles, home heating, gravel quarries. Thus, it will probably still be necessary to make collections from sources followed by detailed analyses of the composition of particles and vapors collected.

The success of the wind-trajectory method as we have applied it depends on the analysis of a very large number of samples taken simultaneously with accurate wind-direction data. The RAPS network was very expensive to operate, so it would be beyond the means of most localities to collect similar data sets. Thus, one of our tasks will be that of determining the minimum and optimum set of data required to obtain the information, i.e. how many sampling sites are needed, what is the minimum number of samples that must be collected and what should be the collection time for each sample? Regarding the latter, it is clear that 24-hr sampling times are too long because of large wind fluctuations. Six-hour samples are better than 12-hr, but with shorter periods, the amount of material collected may be too small for good analyses.

REFERENCES

1. National Research Council. Controlling Airborne Particles. National Academy of Sciences, Washington, D.C., 1979.

2. S. K. Friedlander, Chemical element balances and identification of air pollution sources, Environ. Sci. Technol. 7, 235-240 (1973).

3. D. F. Gatz, Relative contributions of different sources of urban aerosols: application of a new estimation method to multiple sites in Chicago, Atmos. Environ. 9, 1-18 (1975).

4. G. S. Kowalczyk, C. E. Choquette and G. E. Gordon, Chemical element balances and identification of air pollution sources in Washington, D.C, Atmos. Environ. 12, 1143-1153 (1978).

5. G. S. Kowalczyk, Concentrations and sources of trace elements on Washington, D.C. area atmospheric particles. Ph.D. thesis, Univ. of Maryland, 1979.

6. J. G. Watson, Jr., Chemical element balance receptor methodology for assessing the sources of fine and total suspended particulate matter in Portland, Oregon. Ph.D. Thesis, Oregon Graduate Center, Beaverton, OR, 1979.

7. P. K. Hopke, E. S. Gladney, G. E. Gordon, W. H. Zoller and A. G. Jones, The use of multivariate analysis to identify sources of selected elements in the Boston urban aerosol, Atmos. Environ. 10, 1015-1025 (1976).

8. P. D. Gaarenstroom, S. P. Perone and J. L. Moyers, Application of pattern recognition and factor analysis for characterization of atmospheric particulate composition in the Southwest Desert atmosphere, Environ. Sci. Technol. 11, 795-800 (1977).

9. D. J. Alpert and P. K. Hopke, A quantitative determination of the sources in the Boston urban aerosol, Atmos. Environ. (in press, 1980).

10. B. W. Loo, W. R. French, R. C. Gatti, F. S. Goulding, J. M. Jaklevic, J. Llacer and A. C. Thompson, Large-scale measurement of airborne particulate sulfur, Atmos. Environ. 12, 759-771 (1978).

11. R. K. Stevens, T. G. Dzubay, G. Russwurm, and D. Rickle, Sampling and analysis of atmospheric sulfates and related species, Atmos. Environ. 12, 55-68 (1978).

12. D. F. Gatz, "Identification of aerosol sources in the St. Louis area using factor analysis", in Proc. of the 4th Joint Conf. on Sensing of Environmental Pollutants, New Orleans, Nov. 1977 (Amer. Chem. Soc., Washington, D.C., 1978) pp. 443-445.

13. T. G. Dzubay and R. K. Stevens, Ambient air analysis with dichotomous sampler and x-ray fluorescence spectrometer, Environ. Sci. Technol. 9, 663-668 (1975).

14. S. W. Rheingrover, "A statistical model for titanium pollution transport and dispersion in the atmosphere of St. Louis", J. Appl. Meteor. (submitted, 1980).

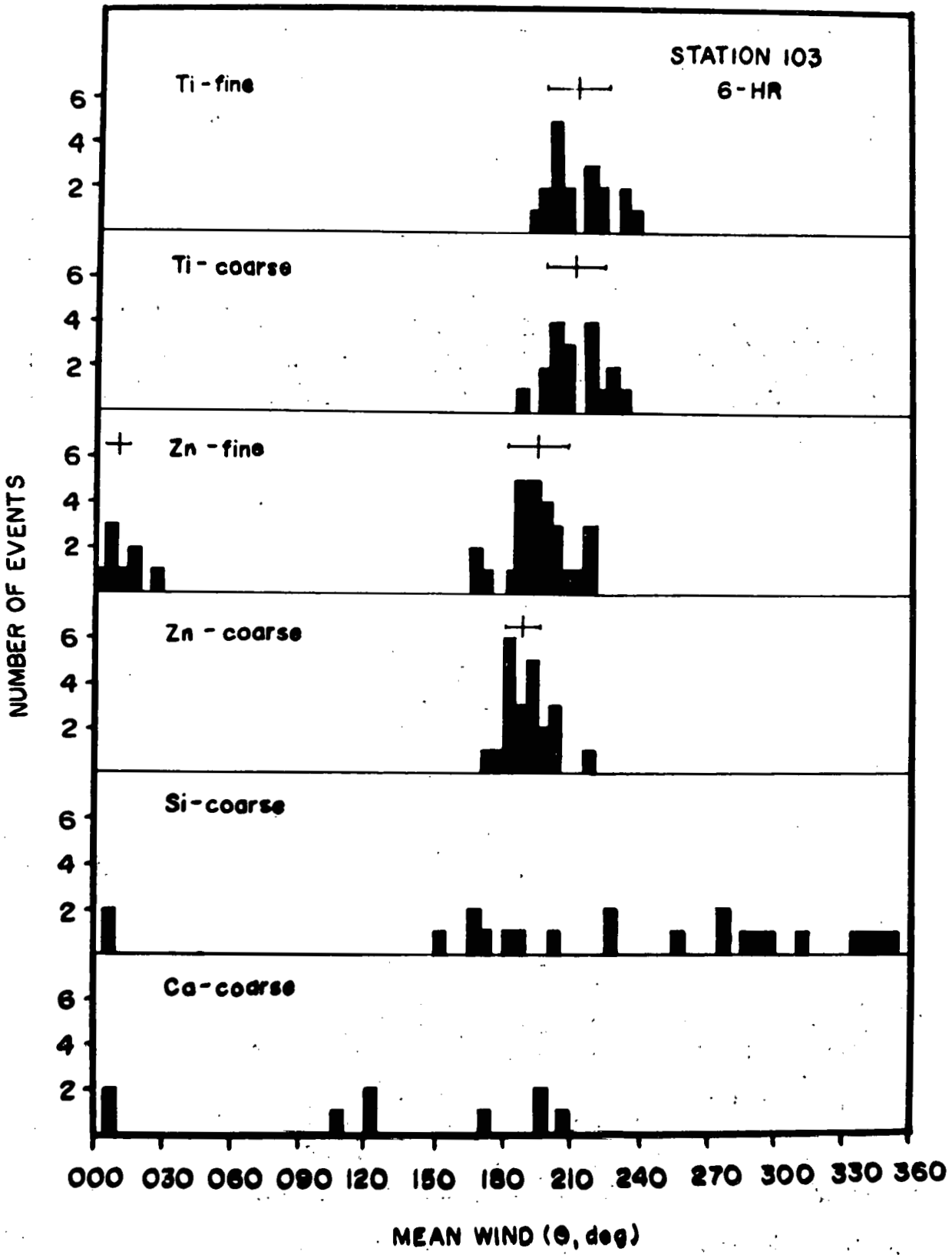


Fig. 1. Histograms of mean wind direction (Θ) for samples meeting two criteria of indicated elemental concentration $x > \bar{x} + z\sigma$ and $\sigma(\Theta) < 20$ deg. Mean wind direction (vertical bar) and standard deviation of a single observation (horizontal bar) are shown above the clusters.

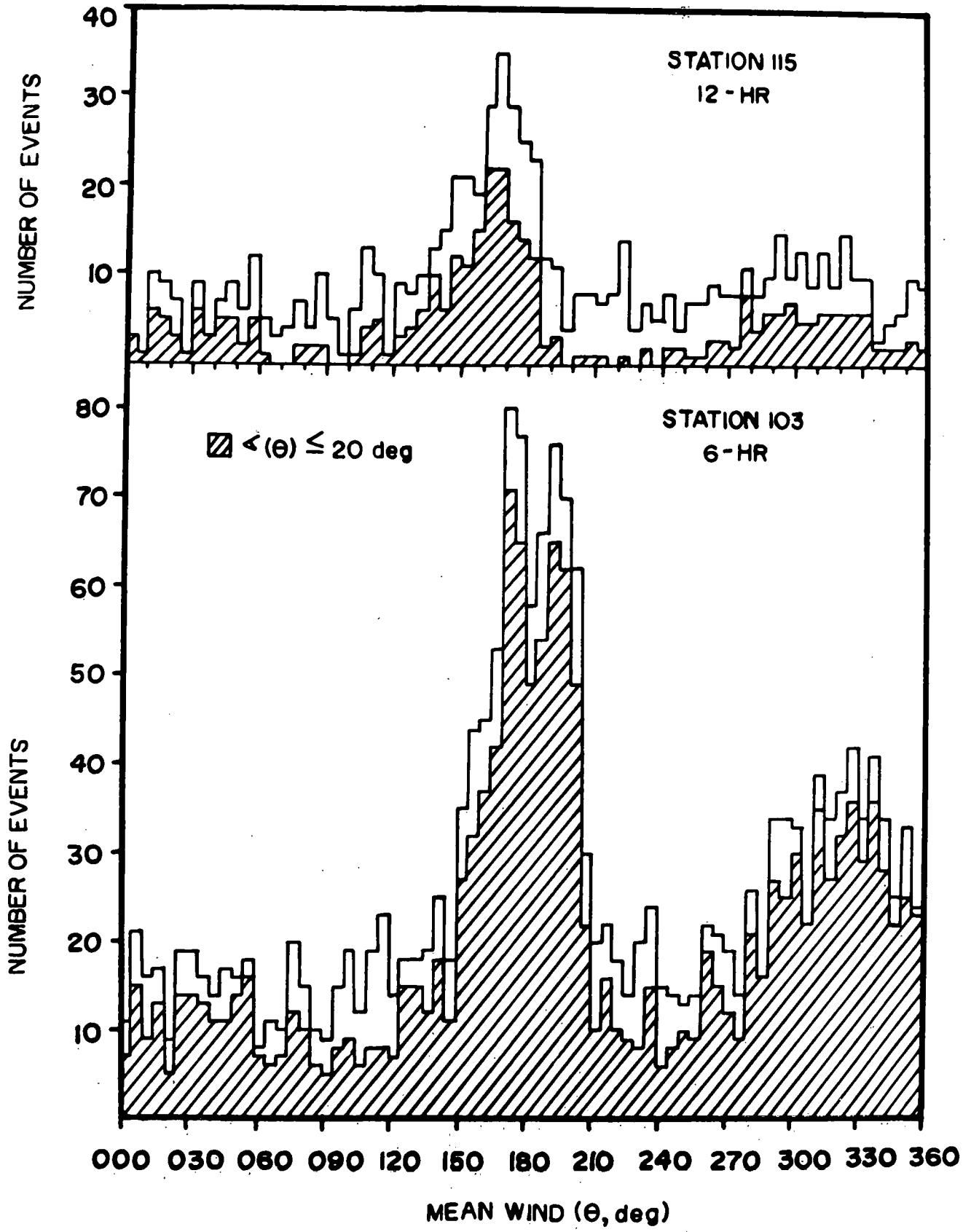


Fig. 2. Histograms of mean wind direction (θ) for all sampling periods and for those sampling periods for which $\sigma(\theta)<20$ deg. (shaded) at Stations 103 and 115.

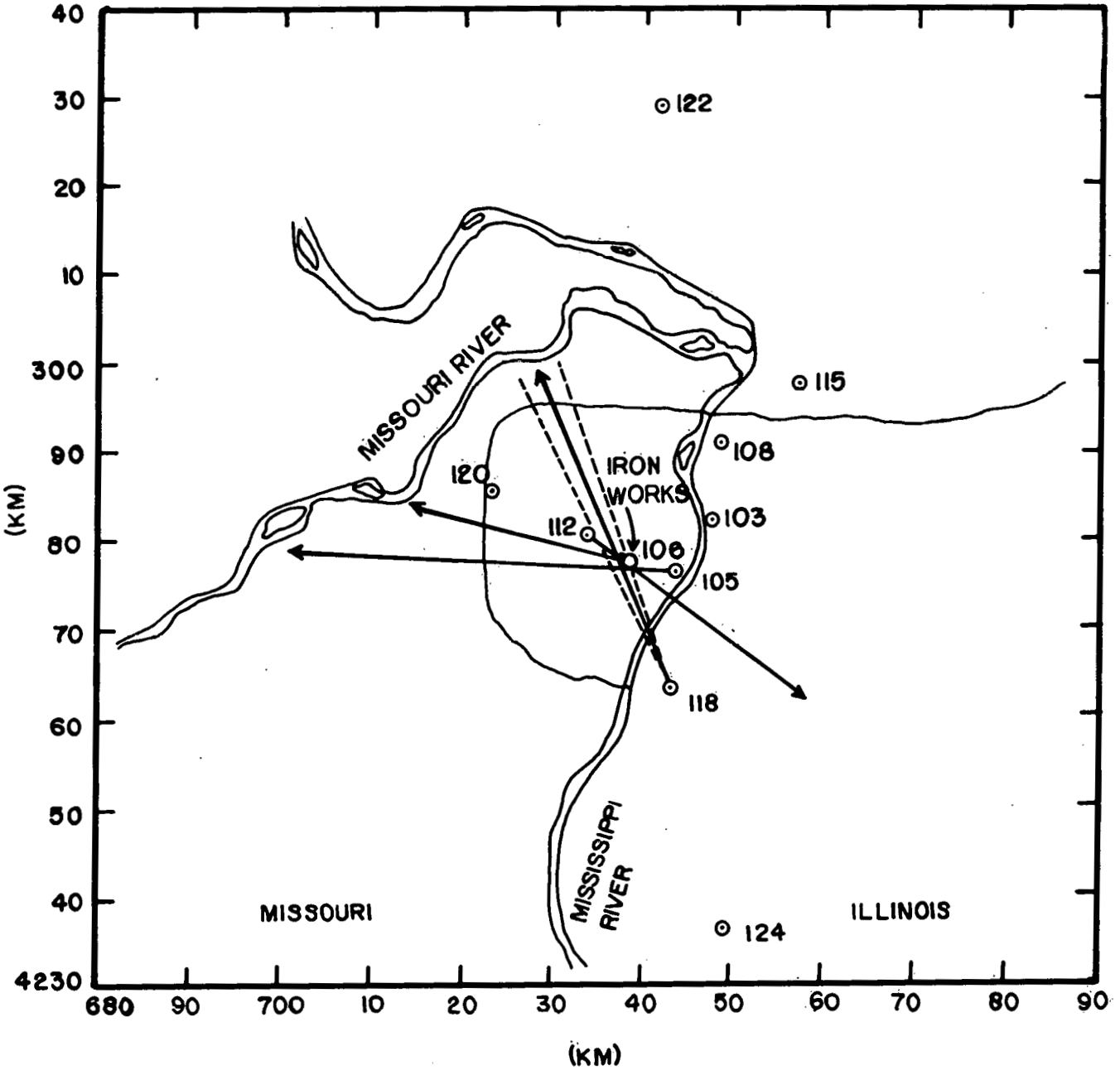


Fig. 3. A map showing fine-particle Mn trajectories (solid arrows) from Stations 105, 106, 122 and 118 locating an iron works. Dashed lines represent $\bar{\sigma}(\Theta)$ for the Station 118 clusters.

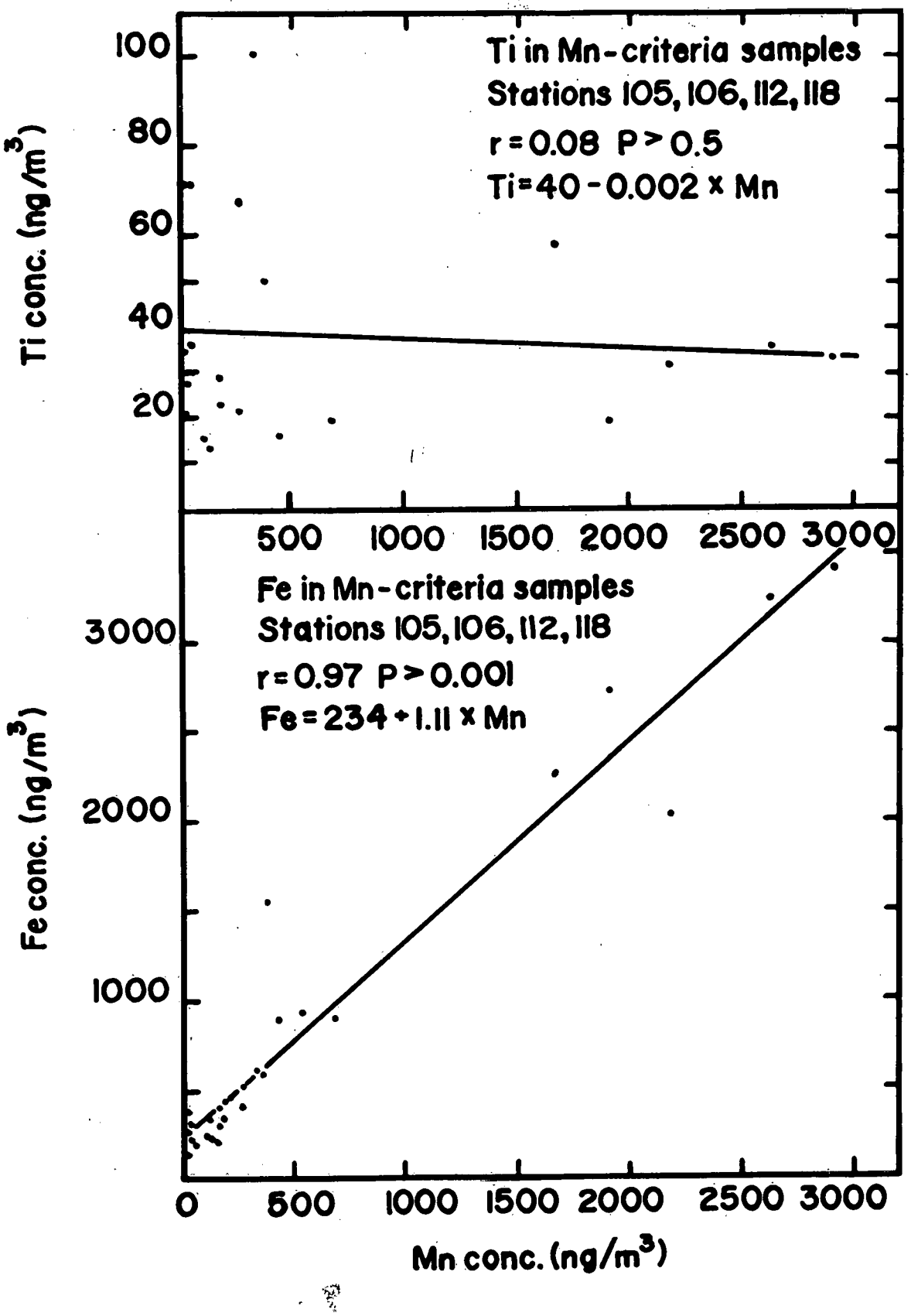


Fig. 4. Scatter plots of fine-particle Fe and Ti concentrations vs. fine-particle Mn concentration from the Mn-criteria samples at Stations 105, 106, 112 and 118. Regression lines are shown with indicated correlation coefficient (r) and probability of no correlation (P).

Table I. Wind-Direction Clusters Observed at Station 103 (Six-hr samples)

Species	Fine Fraction				Coarse Fraction			
	Z	Cases	Mean Wind ($\bar{\theta}$) (deg)	$\sigma(\bar{\theta})$	Z	Cases	Mean Wind ($\bar{\theta}$) (deg)	$\sigma(\bar{\theta})$
Al	No clusters				3.0	13	292.4	2.7
Si	No clusters				No clusters			
P	6.0	19	183.3	2.0	2.75	4	62.2	3.9
						6	109.2	3.6
S	No clusters				2.0	5	59.8	3.1
Cl	2.5	15	194.3	3.3	No clusters			
K	2.5	8	324.8	2.8	2.0	4	62.2	3.9
		4	21.8	3.5		7	110.6	4.2
Ca	3.0	4	5.8	2.1	No clusters			
Ti	2.5	18	211.4	3.3	2.0	18	210.4	3.0
V	3.0	11	16.9	2.6	No clusters			
Cr	2.25	10	356.2	4.3	2.25	11	352.9	2.8
Mn	3.0	4	9.2	1.7	3.0	4	5.8	2.1
Fe	2.75	11	8.4	1.5	2.5	4	5.8	2.1
Ni	3.5	23	187.8	2.1	3.0	10	187.7	3.3
		4	9.2	2.8				
Cu	2.75	27	188.8	1.6	2.5	25	184.4	1.9
Zn	2.75	7	10.3	2.1	2.0	21	188.4	1.8
		26	194.1	2.7				
Se	3.25	29	197.3	0.9	No clusters			
Br	2.75	15	177.8	2.1	No clusters			
Sr	No clusters				2.5	21	291.3	2.3
Cd	2.75	13	198.8	2.8	2.75	15	188.5	2.0
Sn	2.75	13	189.7	4.2	2.75	8	353.2	4.3
Ba	No clusters				2.5	4	287.0	3.8
Pb	2.5	23	186.9	2.6	2.75	13	196.9	1.6

Table II. Groups of Elements Associated with Particles from Specific Sources in the St. Louis Area

Source	Element	Fine ($\bar{\theta}$)	Coarse ($\bar{\theta}$)	Source	Element	Fine ($\bar{\theta}$)	Coarse ($\bar{\theta}$)
Copper	Cu	188.8	184.4	Steel	Cr	356.2	352.9
Products	Sn	189.7		Foundry	Sn		353.2
Plant	Ni	187.8	187.7				
				Iron	Ni	9.2	
Primary	Pb	186.9		and	Fe	8.4	5.8
Zn	Cd		188.5	Steel	Mn	9.2	5.8
Smelter	Zn		188.4	Plant	Ca	5.8	
					Zn	10.3	
	Zn	194.1					
				Paint	Ti	211.4	210.4
Primary	Pb		196.9	Pigment			
Pb	Se	197.3		Plant			
Smelter	Cd	198.8					

Table III. Correlations of Concentrations of Various Elements with Manganese on the Fine-Particle Fraction of Samples Strongly Impacted by Emissions from a Iron Works near Station 106

Element	No. Cases	Regression Line		Correlation coefficient	Probability of no correlation
		Intercept (ng/m^3)	Slope		P
Si	26	179	2.58	0.98	<0.001
Fe	27	234	1.11	0.97	<0.001
K	27	200	0.309	0.93	<0.001
Cr	22	14	0.017	0.81	<0.001
Cu	27	24	0.039	0.75	<0.001
Sn	21	16	0.014	0.70	<0.001
Zn	27	117	0.089	0.56	~0.0025
Ni	24	6.2	0.0032	0.55	~0.005
Pb	27	746	0.290	0.53	~0.005
Cl	26	150	0.052	0.43	~0.025
Ca	27	84	0.023	0.32	~0.1
Br	27	193	0.033	0.23	~0.25
Ti	21	40	-0.002	-0.08	>0.5
Al	25	168	0.0007	0.005	>0.5

NUCLEAR ACTIVATION ANALYSIS METHODS AND THE EVALUATION OF VOLCANIC DEPOSITS AND EMISSIONS*

W. H. Zoller, D. L. Anderson, M.P. Failey and M.S. Germani
Department of Chemistry
University of Maryland
College Park, Maryland 20742

J. L. Moyers
Department of Chemistry
University of Arizona
Tucson, Arizona 85721

B. W. Mosher
Graduate School of Oceanography
University of Rhode Island
Kingston, Rhode Island 02881

ABSTRACT

Samples of volcanic deposits from the top of Mt. Erebus, an active volcano on the coast of Antarctica, were collected for chemical analysis. Filters were used to collect particles in the plume of the volcano for comparison with the deposits. Vapor-phase forms of the halogens and arsenic were collected using charcoal traps and treated filters. Analyses were performed using prompt γ-ray activation analysis (PGAA) and instrumental neutron activation analysis (INAA) for approximately 40 elements.

Non-destructive nuclear analytical techniques make it possible to determine chemical compositions of valuable samples without modification. Analyses of the plume samples showed that large fractions of the halogens were in the gas phase and rather large quantities of Cl and As are being emitted by the volcano. The deposits found in the vicinity of the plume on the summit of the volcano were variable, but were, in general, water soluble and contained large abundances of F and Cl, as well as Na, Al, Si and Fe. Using x-ray diffraction, we identified several previously unknown minerals all of which are relatively water soluble and unique to volcanoes. Most of the volatile trace metals, such as Sb, Cd, Zn and In, are highly enriched in the plume and in deposits relative to their abundances in the magma. Since this volcano has a permanent lava lake, it is postulated that the volatile elements leave the magma in a molecular form (e.g., SiF_4, AlF_3, etc.) which has a high vapor pressure at the temperatures of the melt.

*Work supported in part by the National Science Foundation under Contract DPP-762342301 and the U. S. Department of Energy under Contract DE-AS05-76ER0-5173-M003.

INTRODUCTION

Recently there has been an enhanced interest in the chemistry of volcanic emissions and deposits. The literature has been filled with discussions of the importance of volcanic emissions and their relation to climate. One of the fundamental questions is that of the composition and quantity of the ash and gaseous emissions. The mechanism for the formation of the deposits as well as the fractionation of magma require detailed chemical analyses as well as mineralogical studies in order to help resolve the current uncertainties in the processes involved.

Most of the data available on volcanic emissions have been obtained from studies of ash that has fallen near the volcano and of fumarolic deposits in the vicinity of active vents. Fallen ash usually has a composition similar to that of the erupted magma or previously ejected lava (1-3). Much of the ash deposited near a volcano consists of large particles which had very short atmospheric residence times, which are of little importance in the atmosphere. Particles suspended in volcanic plumes have been collected by Cadle et al. (4) at Kilauea Volcano, Hawaii; Mroz and Zoller (5) at Heimaey, Iceland; Lepel et al. (6) at Mt. Augustine, Alaska; Buat-Menard and Arnold (7) at Mt. Etna, Sicily and Lazrus et al. (8) at Central American volcanoes. Most of these studies were carried out on the ground near hot vents or areas where hot volcanic gases were being emitted. These studies have all indicated that varying quantities of volatile elements are released by volcanic activity. In some cases, the plumes contain large quantities of ash as well as the volatile elements, so that a comparison of the data is difficult. The elements that have been routinely observed in these volcanic plumes include the chalcophilic elements and the halogens. In some cases, these elements are enriched relative to the lava or ash by factors of up to tens of thousands.

The chemistry of the sublimates or fumarolic deposits found near active vents has been extensively investigated by White and Waring (9) in Alaskan volcanoes, by Naughton (10) at Kilauea volcano, and by Stoiber and Rose (11) in the Central American volcanoes. Most of these studies have involved chemical analyses only for the major elements present or the identification of mineral species. Few studies have attempted to analyze the salts or sublimates for trace elements that may have been present. A study by Lepel (12) showed that up to 40 major and trace elements could be measured by neutron activation analysis. The results demonstrated that some of the trace elements, especially the chalcophilic elements, are enriched in selected deposits. Because of the complex nature of volcanic phenomena, it has been difficult to correlate the chemistry of deposits with atmospheric emissions as well as the mechanism of their formation. Much work still needs to be completed before we will have even an rudimentary idea of the chemistry of volcanic emissions.

SAMPLE COLLECTION AND ANALYSIS

Mt. Erebus is a large stratovolcano on Ross Island near the coast of the Antarctic continent. The summit crater is at an altitude of 3970 m and has a diameter of nearly 600 m (see Kyle et al. 13). The nearly flat main crater floor is ~160 m below the summit and ~100 m below the lowest part of the main run. A circular pit, ~250 m in diameter and 100 m deep, called the inner crater, is situated at the north end of the main crater. A molten northoclase phenolite lava lake fills most of the inner crater. A noisy, high pressure vent is situated near the edge of the lava lake, which occasionally has explosive events which eject lava bombs up to several hundred meters. The lake has been present for at least the past six years and appears

to be increasing in size while the explosive events have decreased during the last few years (13).

We collected plume samples during Jan. 1979 on the rim, where one can stand in a sulfur-rich plume as it leaves the main crater. These samples were collected on 47-mm Nuclepore filters which were followed by a charcoal sampling train to collect vapor-phase species. A small, battery-powered vacuum pump was used to pull the air through the sampling system at a flow rate of 10 ℓ/min. Additional plume samples were collected using a sampling system aboard an LC-130 Hercules aircraft operated by the U. S. Navy for the National Science Foundation during Dec. 1977 and 1978. The aircraft samples were not as useful as those collected on the rim, as they did not properly represent plume material, but contained contributions from other sources, and only brief samples could be collected due to the high speed of the aircraft (300 kts).

The entire rim of the volcanic crater is covered with yellowish-white deposits that have been called "sulfur" by volcanologists. We collected several samples from the rim area as well as from the slope of the volcano for comparison. The deposits ranged in color from brillant yellow and yellow-white to white and even a blend of brownish-white. After the samples were returned to the United States, they were prepared for analysis by a combination of analytical techniques, to obtain as much information as possible. Since only a few samples were obtained, the analyses needed to be done non-destructively if possible. We, therefore, analyzed them by prompt gamma-ray activation analysis (PGAA) followed by conventional instrumental neutron activation analysis (INAA). Additional elements such as Pb, Li, Ni, which could not be measured by INAA or PGAA, as well other elements for comparison, were determined by atomic absorption. Duplicates of the salt samples were run by each of the techniques and compared for as many elements as possible. For the plume samples and salt deposits, 25 and 47 elements, respectively, were determined.

RESULTS AND DISCUSSION

Plume Chemistry

The plume samples yielded results which were similar to those observed at other volcanoes by our group and others. We define the crustal enrichment factor EF_{crust} by the equation:

$$EF_{crust} = \frac{(X/Al)_{sample}}{(X/Al)_{crust}} ,$$

where X is the concentration of the element of interest whose concentration is normalized to that of Al. The crustal values are those of Taylor (14). The chalcophilic elements and the halogens were all highly enriched, as they usually are in volcanic plumes from magmatic eruptions. The surprising results were for the alkali metals and rare earth elements, which were also highly enriched as shown in Table I.

This is the first time that the rare earth elements (REE) have been observed at concentrations strongly in excess of predictions based on other crustal elements. This result suggests that a chemical fractionation must be occurring in the lava lake, with perhaps gaseous emissions of a volatile form of the rare earths, especially Ce being released. Since the boiling points of the REE themselves are very high (Table I), a more volatile chemical form must have been formed. The alkali metal enrichments are unusual, but possible when one considers the very high temperatures that are involved in a volcanic

eruption. In this case, one has a constant source of hot (>800°C) lava from which the alkali metals can be emitted. The boiling points of the alkali metals (Table I) are indeed low enough so that, if the free metals could be formed, they would be volatile. It is interesting to note that the elements with the highest enrichments also have the lowest boiling points. When these and other volatile species are emitted, they are probably in the vapor state. But by the time they reach the rim, the gases have cooled and condensed onto the surfaces of particles or hydrometers present in the plume.

Table II gives the results for the charcoal samples. Only three elements could be measured above the blanks (F, Cl and As) and these showed significant percentages in the gas phase. The halogens had particularly high concentrations in the plume samples, e.g., up to 2 mg/m^3 of gaseous Cl (probably HCl), most of which is in the vapor phase. The ratio of F/Cl in this volcano is higher than usually observed at other volcanoes (8), which may indicate why the salt compositions are so unique (see below). When one compares the enrichment factors observed in this study with those of others, a pattern begins to emerge, as shown in Fig. 1. There are three areas of the periodic table in which elements are enriched in certain volcanic systems, but not in others: the alkali metals, some transition metals, and the heavy elements. In another area encompassing the chalcophilic elements and halogens, the elements are almost always highly enriched. Therefore, one should focus attention on the elements whose enrichments vary from one volcano to another so that we can begin to identify the mechanisms involved in the enrichments process. Nuclear analytical methods are the best for these elements and, thus the most useful in this area of research.

Deposits

Most of the deposits analyzed exhibited similar compositions and properties. For most samples between 45 and 50 elements were determined and, as with the plume samples, the highest enrichments were found for chalcophilic elements and the halogens. Most other elements were not enriched with respect to their normal crustal abundances, or were even depleted relative to Al. Concentrations for some elements measured in four samples covering the range in coloration and type are given in Table III. All of the samples are high in Al and Na and remarkably low in Si and S. The brown samples have higher Si concentrations than the others, but concentrations of most other elements shown are comparable. This sample, as well as the yellow sample, are believed to have been formed by the reaction of gas-phase HCl and HF with volcanic lava away from the rim area. The yellow (rim) samples were collected on the summit of the volcano on the crater rim. The last sample, which showed no coloration, was believed to have been formed by gas alterations of lava, as it was found several km from the rim. The question is, how does this salt relate to the others? Bulk characterization shows that the white salt has some properties which are similar to those of the rim salts and some to those of others. Calcium is found at concentrations 10 times higher in the first two samples than in the yellow rim and white sample. The rim sample is much higher in Pb and As, but lower in sulfur and sulfate. It should be noted that all four salts are mostly water soluble. The white salt contains a rather large percentage of sulfate and low concentrations of Cl and Na, probably indicating a certain degree of weathering.

Since the plume data indicated that the rare earth elements were enriched, the concentrations of these elements may give a clue to the mechanism of formation if the distribution patterns are different for these elements. In Fig. 2, the rare earth distribution patterns normalized to the chondritic meteorite distribution are shown. Patterns of the REEs in the brown and yellow salts are similar to that of lava, and those of the rim and white salts are similar to each other, but different from the others in that

they have more heavy REEs. From this evidence it would appear that the white salt was formed by deposition on an older rim during earlier phases of the volcano's growth, and that alteration by leaching, etc., has removed some of the minerals and volatile compounds. Since this salt is so soluble it may be the residue of salts formed on an older active area of the volcano, moved to other areas by run-off, and deposited by evaporation.

Since this material was so complex, we decided to have a mineralogist examine some samples using x-ray diffraction (15). This examination has indicated that at least two, and probably more, new minerals are present. So far, three distinct phases have been found. These minerals, as yet unnamed, have the formulas indicated in Table IV. It is obvious from these studies that the chemistry of the salts is quite complex and much further work still must be done. At volcanoes in most other locations, the water-soluble minerals would have been destroyed, but in the cold, dry environment of the summit area, they are preserved.

The complex chemistry of the salt formation is not at present understood. Measurements of some of the trace elements will probably be necessary to obtain a better understanding of the chemical processes that are responsible for the formation of the salts and their relation to the volcano's emissions.

From our studies on volcanic samples, we believe that it is essential to have information on as many elements as possible. It is obvious that the nuclear analytical techniques offer the best chance to obtain the needed information from these samples.

REFERENCES

1. R. E. Stoiber and W. I. Rose, Jr., Bulletin Volcanologique 33-2, 475 (1969).

2. W. I. Rose, Jr., S. Bonis, R. E. Stoiber, M. Keller and T. Bickford, Bulletin Volcanologique 37-3, 338 (1973).

3. S. Thorarinsson and G. Sigvaldason, Bulletin Volcanologique 36, 269 (1972).

4. R. D. Cadle, A. F. Wartburg and F. E. Grahek, Geochim. Cosmochim. Acta 35, 503 (1971).

5. E. J. Mroz and W. H. Zoller, Science 190, 461 (1975).

6. E. A. Lepel, K. M. Stefansson and W. H. Zoller, J. Geophys. Res. 83, 6213 (1978).

7. P. Buat-Menard and M. Arnold, Geophys. Res. Lett. 5, 245 (1978).

8. A. L. Lazrus, R. D. Cadle, B. W. Gandrud, J. P. Greenberg, B. J. Huebert and W. I. Rose, Jr., J. Geophys. Research 84, 7869 (1979).

9. D. E. White and G. A. Waring, U. S. Geol. Surv. Prof. Paper 440-K, 1 (1963).

10. J. J. Naughton, V. A. Greenberg and R. Goguel, J. Volcanology and Geothermal Res. 1, 149 (1976).

11. R. E. Stoiber and W. I. Rose, Geochim. Cosmochim. Acta 38, 495 (1974).

12. E. A. Lepel, M.S. Thesis, Department of Chemistry, University of Maryland, 1978.

13. R. R. Kyle, R. R. Dibble, W. F. Giggenbach and J. Keys, Symp. Antarctic Geology and Geophys., Madison, WI, Aug., 1977.

14. P. S. Taylor and R. E. Stoiber, Geol. Soc. Amer. Bull. 84, 1031 (1973).

15. W. I. Rose, private communication (1979).

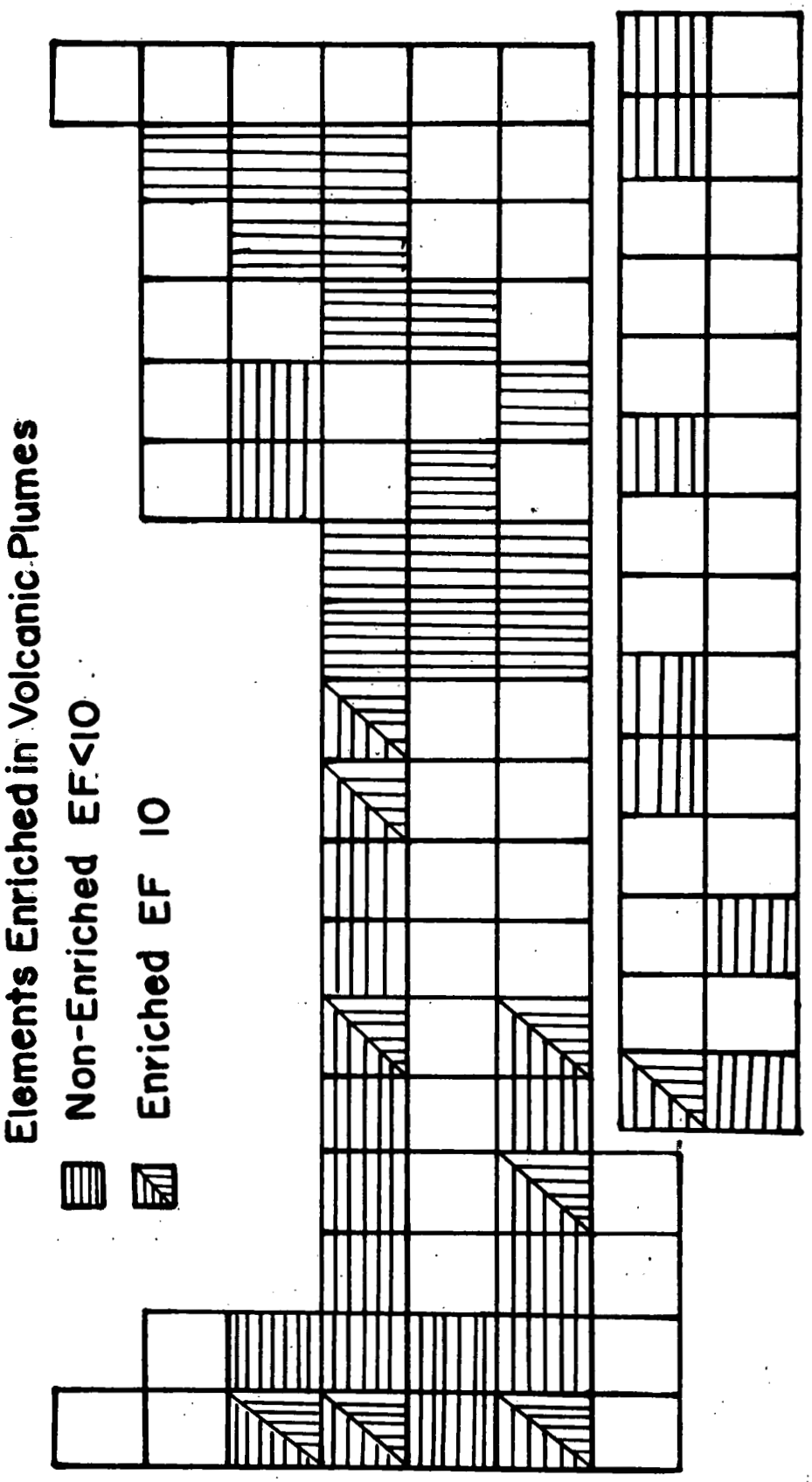


Fig. 1. Elements which have been observed in volcanic plumes as reported in the literature and this report.

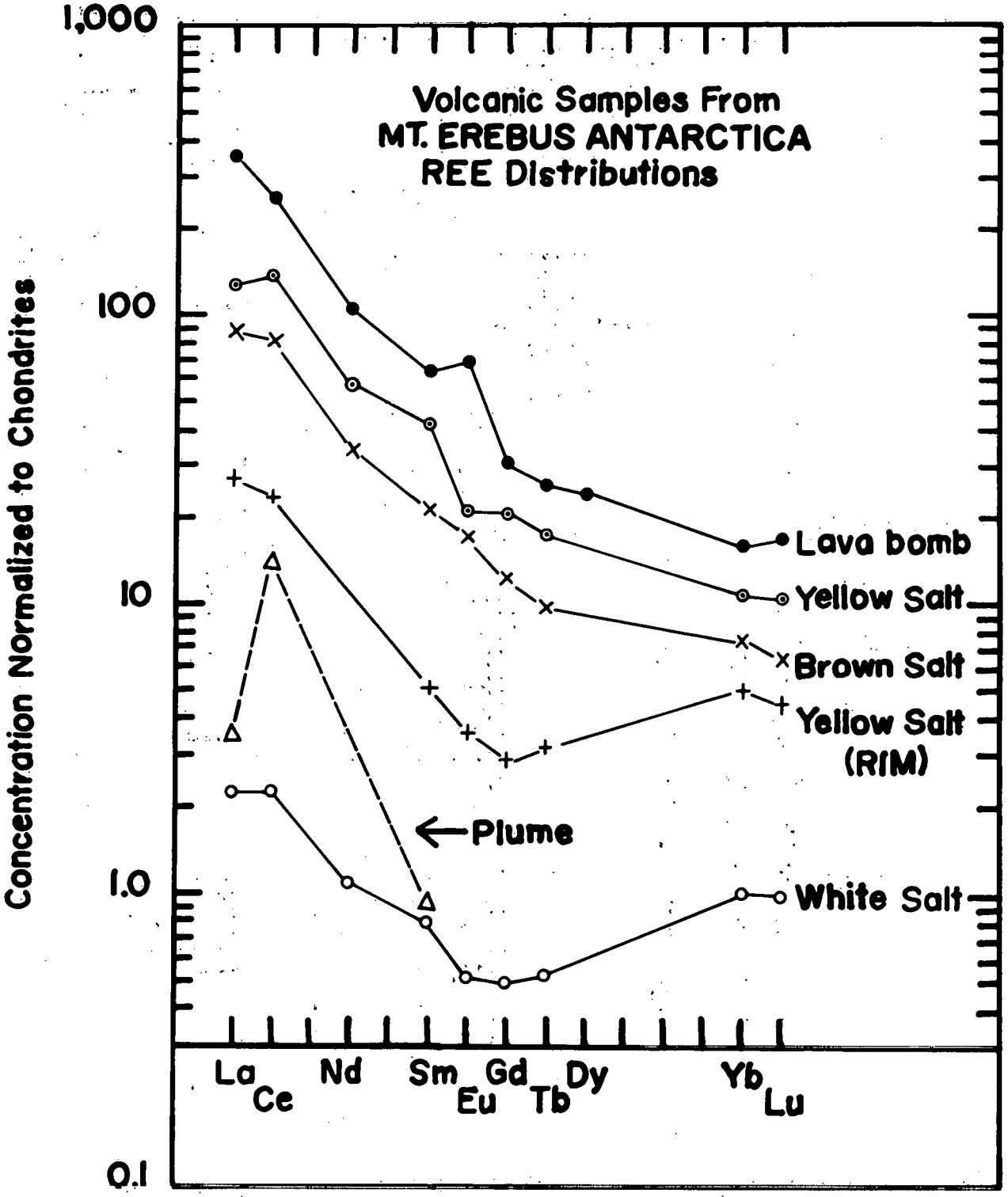


Fig. 2. Rare earth element distribution for volcanic salts from Mt. Erebus normalized to chondrites.

Table I. Crustal Enrichments of Elements in Volcanic Plumes

	EF_{crust}		
Element	Mt. Erebus	Augustine	Elemental Boiling Point (°C)
Na	15-80	1.0-2.0	882
K	32-61	1.2-2.5	774
Cs	80-120	1.2-2.8	678
La	17	1.5-2.2	3454
Ce	81	1.7-3.0	3257
Sm	12	1.2-1.7	1778

Table II. Vapor-Phase Species in Mt. Erebus Plume Samples

Element	Concentration ($\mu g/m^3$)	% Vapor Phase
F	200-500	>90%
Cl	500-2200	94-96%
As	0.6-2.1	25%

Table III. Compositions of Mt. Erebus Salts

Element	Brown	Yellow	Yellow (Rim)	White
Al (%)	12.4	12.0	11.5	11.7
Si (%)	3.9	0.55	0.72	0.23
Fe (%)	1.23	0.64	2.32	0.30
Na (%)	9.1	8.8	10.1	2.1
Ca (%)	0.55	0.52	0.060	0.055
Zn (ppm)	71	320	150	294
As (ppm)	60	39	167	13.2
Cd (ppm)	9.6	24	20.2	39.6
Pb (ppm)	30	58	205	16.8
U (ppm)	2.1	5.7	3.4	7.8
S (%)	3.4	1.51	0.68	10.9
SO_4 (%)	9.3	4.1	2.0	32.4
Cl (%)	13.0	19.4	20.7	4.9
Solubility (%)	76	84	81	96

Table IV. Mt. Erebus Minerals

$FeCl_3 \cdot 6H_2O$	Hydromolysite
AlF_3	?
$NaAl_4O_4Cl_5$	?
or	
$NaAl_4O_4(Cl,F)_5$	

NEUTRON ACTIVATION ANALYSIS IN THE SURVEY OF RIVER WATER QUALITY AND TRACE ELEMENT DISTRIBUTION.

M.T. Ganzerli Valentini, N. Genova, L. Maggi, S. Meloni, R. Stella

(Laboratorio di Radiochimica e Centro di Radiochimica e Analisi per Attivazione del CNR - Viale Taramelli 12 - 27100 Pavia (Italy)).

A. Albini, F. Salghetti

(C.I.S.E. - C.P. 3986 - 20100 Milano (Italy)).

SUMMARY

Neutron Activation Analysis has been employed to characterize river water samples, either with instrumental analysis (INAA) or after simple radiochemical separations (for Hg, Cd and Cu), within a study on the dispersion of inorganic pollutants in water systems. In particular, five grain-size fractions of suspended particulate matter have been analyzed by this tecnique while Atomic Absorption has been used for the aqueous phase (filtered through 0.45 μm) in equilibrium.

The results are presented, as obtained with two different samples of river water.

INTRODUCTION

In recent years public concern with the quality of water in rivers, streams and lakes has stimulated renewed scientific interest in the aquatic environment. Italian National Research Council (CNR) is promoting and supporting many interdisciplinary research programmes on this subject: the present work is part of one of such programmes, and is concerned with the study of the most important interactions and distribution of some pollutants in the Po river (Northern Italy).

In order to have a general picture of the system under investigation the complete analysis of all parameters affecting water quality and the trace element distribution among the aquatic components were carried out.

Neutron Activation Analysis (NAA) was adopted as the most useful multielemental analytical technique when applied to complex matrices of both inorganic and organic origin, such as suspended particulate previously divided in five granulometric fractions (1,2). Atomic absorption, that also is widely adopted for environmental analysis (3,4), in this work was coupled and sometimes preferred to the NAA, as in the case of water samples.

EXPERIMENTAL

a) sampling

Large samples of 1200 liters of river water were necessary to perform all the required experiments: two samples were collected in two different periods of the year from a boat suitably equipped also for preliminary analyses.

A 200 liters aliquot sample was divided in smaller subsamples which in part were immediately filtered through a 0.45 μm pore size membrane filter and then added with the proper reagent for the following determinations:

1) Alkalinity
2) Anionic detergents
3) Soluble sulphides
4) Nitrogen (total,organic,ammonia)
5) Trace Elements (by Atomic Absorption)

One sample of the entire water, stored at 4 °C, was processed within 24 hours after collection for the following determinations;

1) Nitric and nitrous nitrogen
2) Chlorides, sulphates, phosphates
3) TOC (Total Organic Carbon)
4) TIC (Total Inorganic Carbon)
5) BOD
6) COD
7) Colloidal silica
8) Hardness

b) treatments of sample

Within 24 hours from collection a large sample (1000 liters) was submitted to a multistep wet filtration in order to obtain five fractions of the suspended matter, corresponding to the following diameter ranges: > 250 μm, 250-125 μm, 125-63 μm, 63-22 μm, and 22-0.45 μm.

The employed equipment consisted in four ASTM sieves of the appropriate retention capacity mounted on vibrating plates in serial sequence:

the finest fraction was obtained after filtration through Millipore membranes of decreasing porosity. The whole equipment is drawn in Fig. 1.
All fractions obtained were centrifuged for 30 min at 2000 rpm and finally

dried at 110 °C for 24 hours:

samples of about 150 mg were submitted to nuclear activation analysis.

c) INAA of suspended matter

In order to improve the sensitivity and selectivity of the neutron activation method, the nuclear characteristics of the elements were exploited by submitting the samples to four diverse types of irradiations differing in time and flux exposure. The samples were irradiated in the TRIGA Mark II Reactor of the University of Pavia : Irradiation positions and related fluxes, times and determined elements are listed in Table I.

All samples were irradiated in polyethylene vials, with exception of samples irradiated in Central Thimble position, that were sealed in quartz vials. After suitable cooling time, ranging from 5 minutes for samples irradiated in the Thermal Column to two days for samples irradiated in the Lazy Susan position, gamma countings were performed with a Ge-Li detector linked to a multichannel computer assisted analyzer (LABEN).

In Instrumental Neutron Activation Analysis (INAA) with multielement standards the complexity of the resulting gamma-ray spectra may lead to erroneous results when the composition of the standard samples is strongly different from the unknowns ones. This was checked by simoultaneously irradiating several different NBS standards (sediments, coal, fly ash, rocks such as GSN, W1, BCR) and also pure salts solution aliquots (for Hg, Cd, Cu).

Results showed that the differences in the specific activities of different standards for most of the elements were small compared to statistical error. The nuclear data for the determined elements are listed in Table II.

Most of the nuclear and spectrometric interferences were avoided by performing irradiations in selected flux conditions: the contribute of reactions such as $^{27}Al(n,p)\ ^{27}Mg$ and $^{56}Fe(n,p)\ ^{56}Mn$, which are known to interfere with the determinations of magnesium and manganese respectively, was reduced to a negligible extent by irradiating in a highly thermalized neutron flux, which is available in the Thermal Column.

d) Radiochemical separation

The instrumental measurement of ^{64}Cu (511 Kev peak) is obviously subject to interferences from pair-production by high energy gamma radiation, especially from ^{24}Na. In the case of mercury the count rate of the isotope ^{203}Hg (279.2 Kev peak) is affected by the 279.6 Kev photopeak of ^{75}Se, the latter having also half-life longer (120 d) than ^{203}Hg (47 d).

An highly selective radiochemical separation was thus devised, that in addition to copper and mercury could also insure cadmium activity isolation. The latter element is in fact often present in amounts that are too near the detection limit for instrumental neutron activation analysis to obtain reliable results.

The procedure for the radiochemical separation of copper, cadmium, and mercury from neutron irradiated suspended matter samples was the following

1) Samples were dissolved at 160 °C in teflon lined stainless steel autoclave with 12 cm^3 of HCl, HNO_3, and HF mixture in the 1:3:3 volume ratio. Cadmium and copper carriers were previously added.

2) The resulting solution was diluted to triple volume with distilled water and Hg carrier was added.

3) The solution was passed through a column (0.4 cm I.D., 5 cm length) filled with granular copper metal freshly precipitated with metallic zinc from

copper sulfate solution. Metallic copper holding ^{197}Hg and ^{203}Hg radioisotopes was dissolved with 3M HNO_3.

4) The solution eluted through the copper column was concentrated almost to dryness. The residue was recovered with 15 cm^3 of 0.5M HNO_3 - 0.1M HBr solution.

5) The resulting solution was passed through a Dowex 1x8 (100-200 U.S.mesh) column (0.8 cm I.D., 12 cm length)pretreated with 0.5M HNO_3 - 0.1M HBr solution. After washing with 30 cm^3 of the same solution, ^{115}Cd was eluted with 40 cm^3 3M HNO_3.

6) To the washing solution a few metallic cadmium grains were added and then packed in a column (0.4 cm I.D., 5 cm length), and the solution was passed through it. Cadmium grains, holding ^{64}Cu, were dismantled from the column and gamma counted.
Atomic Absorption Spectrometry was also employed as an intercomparison technique for these analyses and results were generally found in good agreement.

e) Elements determination in water

Trace elements in natural waters, filtered through 0.45 μm pore size membrane filters, may be present in a variety of inorganic and organic dissolved species and colloidal forms (5): their total concentrations are near or below the ppb level, and this level is on the borderline of the detection sensitivities of many of the popular techniques presently in use. Neutron Activation Analysis is one of those capable of determining the greatest number of elements with high sensitivities, but its application to water samples is limited by the fact that during long irradiations as the ones required to meet the necessary sensitivity, the production of radiolysis gas would damage the containers. The determination of elements requiring long irradiations is thus impossible by INAA, unless the evaporation of the matrix or other preconcentration steps are carried out.
All these treatments present the risks of losses and contaminations. For this reason Atomic Absorption Spectrometry (AAS) was preferred to INAA.
The relative merits of this technique are increased by non-flame devices, and the following equipments were employed:
PYE UNICAM SP1900, VARIAN AA5, HITACHI 170-70.

RESULTS AND DISCUSSION - The analytical results obtained are presented in table III and IV and in figures. In particular the results reported in figures 2 and 3 illustrate the peculiar distributions of many elements within the different fractions of suspended particulate matter.
Fig. 4 and 5 show the percentage amounts of the different elements in the total suspended matter: here again a great variety in behaviours is apparent, plotted against the element atomic numbers.
A detailed discussion of such results, and their correlation to the chemical, biological and mineralogical characteristics of the analysed samples is beyond the scope of this paper.
What is important to point out here is that such peculiar behaviours demand for a large number of data, to take into account the many parameters involved as it often occurs in environmental studies. In such a framework, the multielemental character, the sensitivity and the relative simplicity and speed of neutron activation analysis - coupled to a careful choise of irradiation conditions and to simple radiochemical separations for peculiar elements - represents a powerful analytical tool, scarcely equalled by other techniques.

ACKNOWLEDGEMENTS

The helpful co-operation of L. Beccalli, E. Croce, F. Pioltini and F. Calvenzi is gratefully acknowledged.

This work was sponsored by CNR (the Italian Council for Research) in the framework of the Project "Promozione della Qualità dell'Ambiente".

REFERENCES

1) E.A. Uken, P. Hahn-Weinheimer, H. Stark, Procedings of the "1976 International Conference on Modern Trends in Activation Analysis", 13-17 September 1976, Munchen, FRG, p 474

2) L. Kosta, J. Radioanal. Chem., 44, 317 (1978)

3) R. Wagemann, NBS Spec. Publ. 422, Proceedings of the "7th IMR Symposium, 7-10 October 1974, Gaithersburg (USA), p 247

4) A. Rattonetti, Ibid., p 633

5) D.E. Robertson, Ibid., p 805

TABLE I - Irradiation positions and related characteristics in the TRIGA Mark II Reactor of the University of Pavia.

Position	Flux: n cm^{-2} sec^{-1}	Irradiation time	Determined elements
Thermal column	7.7×10^{9}	20 min	Na, Mg, Al, K, Ca, Mn, Ti,
Rabbit (pneumatic system)	2.5×10^{12}	0.1 - 1 min	Na, K, Ca, Al, Mn, V, Ti,
Central Thimble	9.0×10^{12}	12 hours	Cu, Cd, Hg,
Lazy Susan (rotatory specimen rack)	1.2×10^{12}	32 hours	Sc, Cr, Fe, Co, Ni, Zn, Rb, Cs, Ba, La, Ta, Th,

TABLE II - Nuclear characteristics of investigated elements

Element	Produced Isotope	Gamma energy (KeV)	Half-life $t_{\frac{1}{2}}$	Interferences
Na	^{24}Na	1369 - 1733	15.0 h	$^{24}Mg(n,p)^{24}Na$, $^{27}Al(n,\alpha)^{24}Na$
Mg	^{27}Mg	1014	9.56 m	^{27}Al (n,p) ^{27}Mg
Al	^{28}Al	1779	2.32 m	^{28}Si (n,p) ^{28}Al
K	^{42}K	1525	12.4 h	
Ca	^{49}Ca	3084	8.80 m	
Sc	^{46}Sc	889	84 d	
Ti	^{51}Ti	320	5.79 m	
V	^{52}V	1434	3.75 m	
Cr	^{51}Cr	320	27.8 d	
Mn	^{56}Mn	847	2.58 h	^{56}Fe (n,p) ^{56}Mn
Fe	^{59}Fe	1099 - 1292	45 d	
Co	^{60}Co	1173 - 1332	5.26 y	
Ni	^{58}Co	811	71.3 d	^{52}Eu (811)
Cu	^{64}Cu	511	12.8 h	high energy gamma rays
Zn	^{65}Zn	1116	243 d	
Rb	^{86}Rb	1077	18.7 d	
Cd	^{115}Cd	336 - 528	2.25 d	
Cs	^{134}Cs	796	2.05 y	
Ba	^{131}Ba	496	12.1 d	
La	^{140}La	816 - 1597	40.2 h	
Ta	^{182}Ta	1222	115 d	
Hg	^{197}Hg	78	2.71 d	
	^{203}Hg	279	47 d	
Th	^{233}Pa	312	27.4 d	

TABLE III- Overall Analytical Data of first sample. Element concentrations in water (ppb) and in suspended matter (ppm) by NAA or AAS (*).

Element	Water (<0.45 µm)	Suspended matter					Per cent element in suspended matter
		FRACTION 1 (0.45 ÷ 22 µm)	FRACTION 2 (22 ÷ 63 µm)	FRACTION 3 (63 ÷ 125 µm)	FRACTION 4 (125 ÷ 250 µm)	FRACTION 5 (> 250 µm)	
Li	2 *	37.6*	33.0*	26.4 *	23.4 *	20.0 *	40.09
Na	23000 *	6300	7760	4370	3650	2300	1.06
Mg	12000 *	22)00	15400	21280	14400	8790	5.89
Al	25 *	72860	68700	52280	40520	27750	99.05
Si	4720 *	243)00 *	270000 *	210200 *	208300 *	186800 *	67.16
K	3100 *	13)87	12805	10860	8267	6892	13.80
Ca	58000 *	52)00	52540	37660	34990	29140	3.25
Sc	n.d.	9.99	8.57	6.22	5.48	4.45	-
Ti	< 100 *	5)20	4550	4710	4190	3300	-
V	< 25 *	64.05	60.07	57.91	47.28	33.70	-
Cr	< 10 *	524.5	502.1	576.2	467.8	436.7	-
Mn	25 *	1)78.3	802.2	660.0	623.4	504.6	61.80
Fe	36 *	45)18	36915	28362	24393	21409	97.75
Co	< 10 *	19.31	16.13	14.46	11.76	10.22	-
Ni	25 *	178 *	156 *	164*	134 *	127*	20.80
Cu	13 *	764.6	912.3	1087.6	875.2	658.7	71.67
Zn	95 *	1)90	1519	1767	1500	1490	40.36
As	< 10 *	2.28*	1.50*	3.06 *	2.92 *	4.0*	-
Se	280 *	29.6 *	35.0 *	18.1 *	17.5 *	13.4*	0.41
Rb	3 *	103.2	86.4	65.1	52.9	44.4	54.27
Sr	42 *	285 *	250 *	208*	204*	167 *	19.61
Cd	2 *	27.4	20.2	39.6*	24.4*	20.9*	
Cs	< 5 *	3.12	2.50	2.03	1.63	1.49	-
Ba	100 *	705.2	613.6	608.1	492.3	426.5	20.37
Ta	n.d.	1.59	1.46	1.29	0.98	0.84	-
Hg	< 20 *	1.93	4.57	4.85	12.28	13.91	-
Pb	50 *	745 *	628*	814 *	622 *	559 *	35.60
Th	n.d.	7.33	6.48	4.30	4.37	3.45	-
TOC	3600	80)00	73700	209800	200000	297000	-
Weight of fraction in g (relative to 1000 liters)		21.17	11.50	2.90	2.10	1.66	-

n.d. = not determined

TABLE IV - Overall Analytical Data of second sample. Element concentrations in water (ppb) and in suspended matter (ppm) by NAA or AAS (*).

Element	Water (<0.45 µm)	Suspended matter					Per cent element in suspended matter
		FRACTION 1 (0.45 ÷ 22 µm)	FRACTION 2 (22 ÷ 63µm)	FRACTION 3 (63 ÷ 125µm)	FRACTION 4 (125 ÷ 250 µm)	FRACTION 5 (>250 µm)	
Na	13230 *	6535	9099	14243	13933	14962	10.97
Mg	10000 *	22247	18639	15638	18126	26033	21.48
Al	15 *	58392	58415	55150	53775	52708	99.79
Si	3600 *	n.d.	n.d.	n.d.	n.d.	n.d.	-
K	9090 *	12935	13144	11566	0497	13605	14.73
Ca	50000 *	51469	32750	67410	27705	23135	8.13
Sc	n.d.	0.35	0.09	0.10	0.46	0.19	-
Ti	< 100 *	3852	3760	4342	2910	<1000	-
Cr	< 10 *	203.5	186.8	174.9	93.9	63	-
Mn	4 *	1855	1473	1031	631	419	96.67
Fe	60 *	47900	20240	13480	28160	19500	98.41
Co	< 10 *	24.2	20.24	13.48	11.22	10.82	-
Ni	< 5 *	197 *	420 *	n.d.	n.d.	n.d.	
Cu	4 *	158.6	148.5	13.5	13.0	9.9	61.48
Zn	120 *	1127 *	475 *	n.d.	n.d.	n.d.	-
Se	n.d.	6.95	6.04	9.46	6.86	2.05	-
Rb	< 10 *	109.2	167.6	< 50	83.4	113.9	-
Sr	410 *	414.3	468	561.4	< 200	< 200	-
Cd	1 *	18.3	10.7	1.82	< 1	< 1	-
Cs	0.015*⊙	3.5	3.2	1.6	1.2	1.4	94.15
Ba	950 *	2244	2341	2410	1815	1218	19.85
Ta	n.d.	0.83	0.10	0.92	0.53	0.45	-
Hg	< 10 *	0.57	2.32	0.24	0.15	< 0.10	-
Pb	< 2 *	139 *	143 *	n.d.	n.d.	n.d.	-
Th	n.d.	9.65	9.1	1.9	8.0	6.0	-
TOC	3600	24900	22900	8700	1700	2250	-
Weight of fraction in g (relative to 1000 liters)	-	26.04	7.40	8.02	53.42	35.52	-

n.d. = not determined ⊙ = previous preconcentration on NCFC column

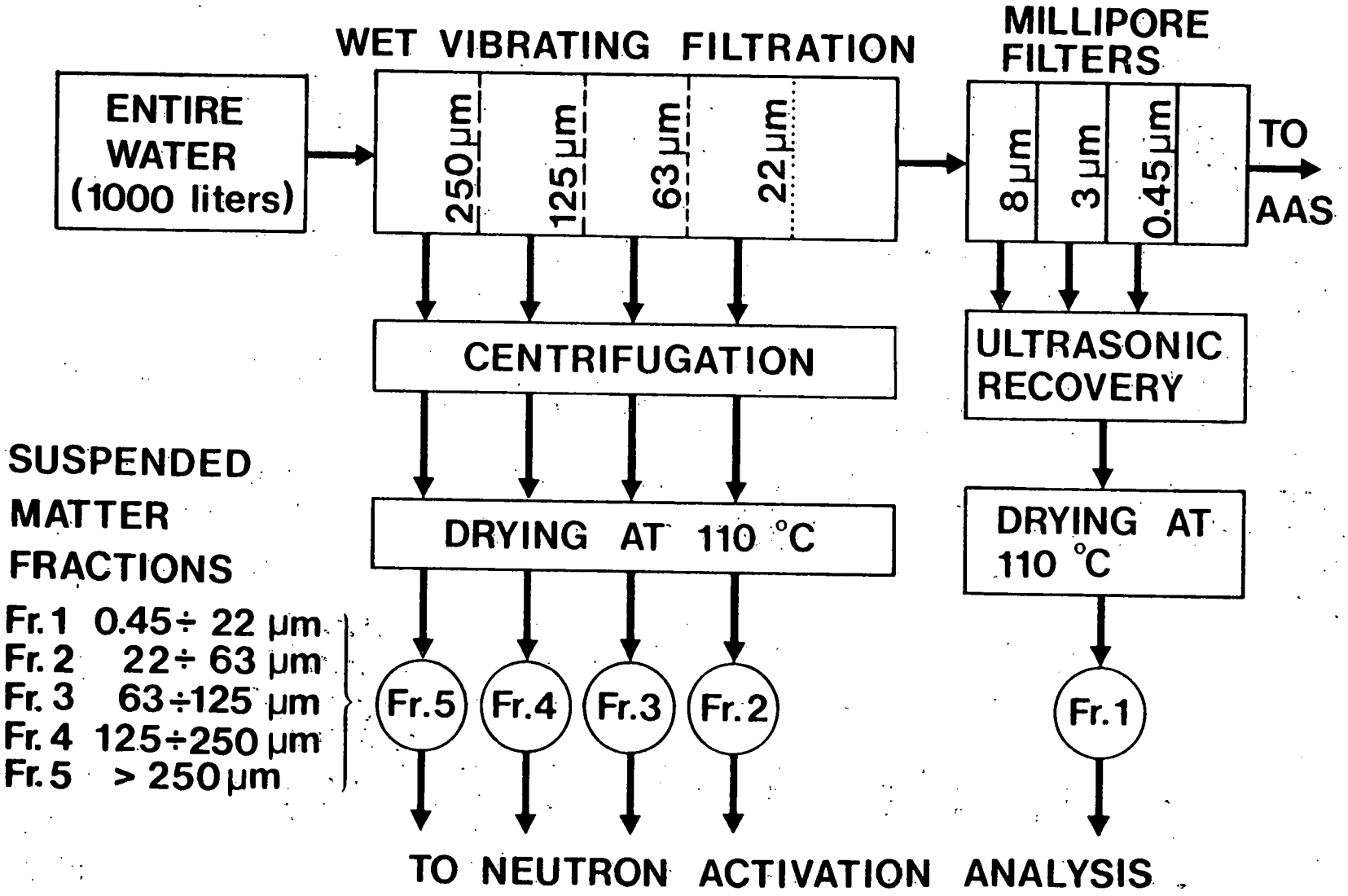


FIGURE 1 - Suspended matter filtration procedure.

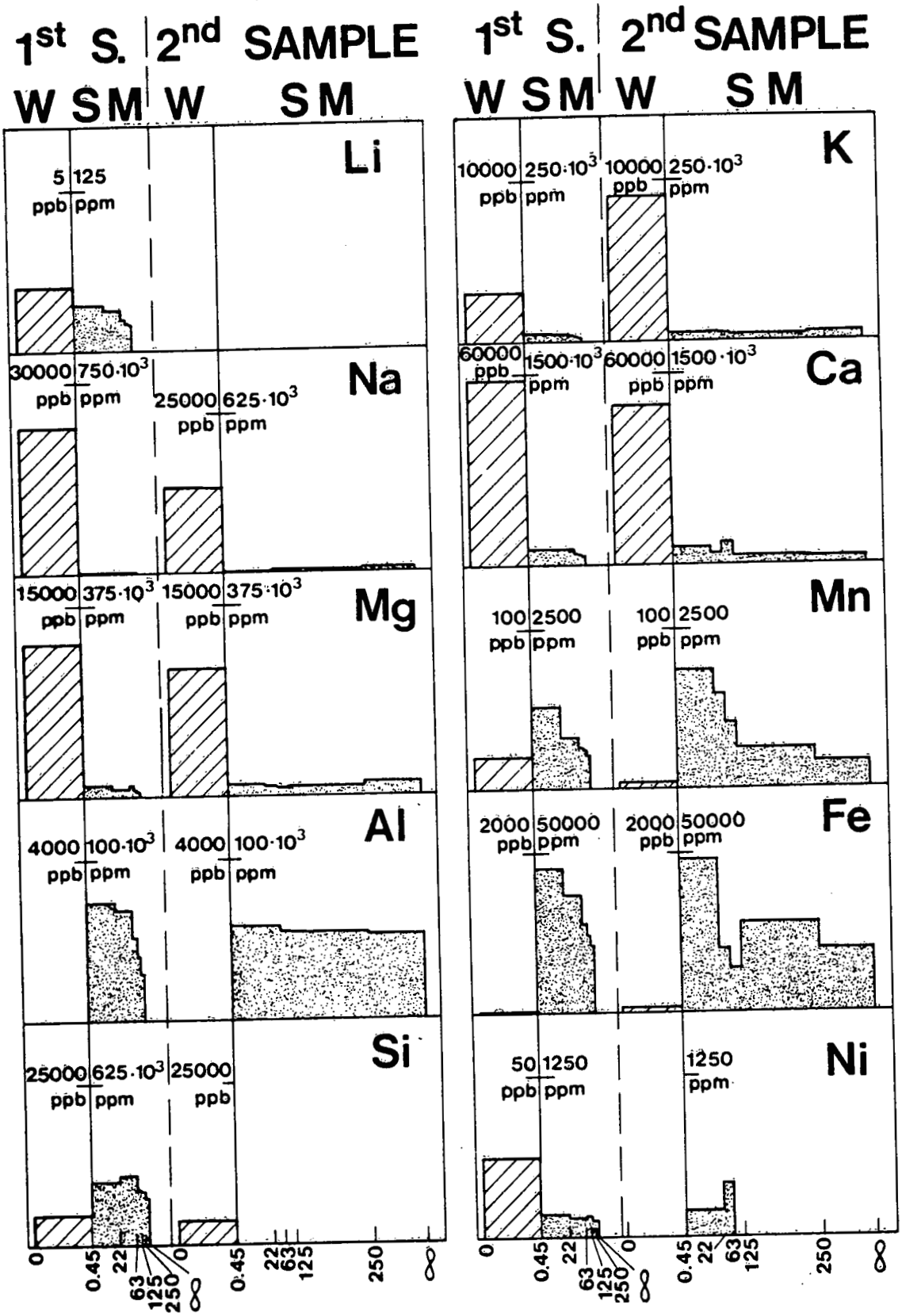


FIGURE 2 - Element distribution between water (W) and 5 grain-size fractions of suspended matter (SM).

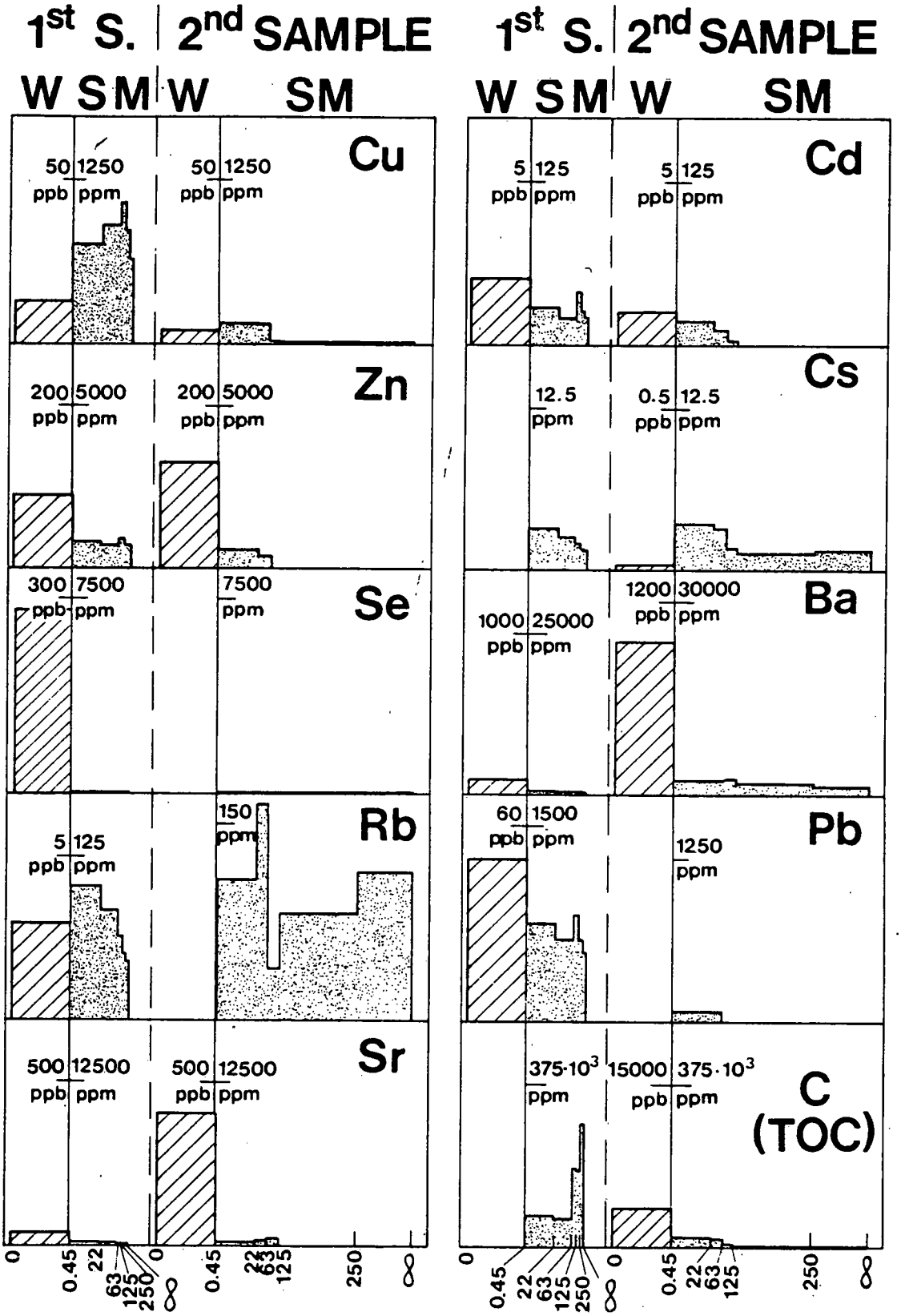


FIGURE 3 - Element distributions between water (W) and 5 grain-size fractions of suspended matter (SM).

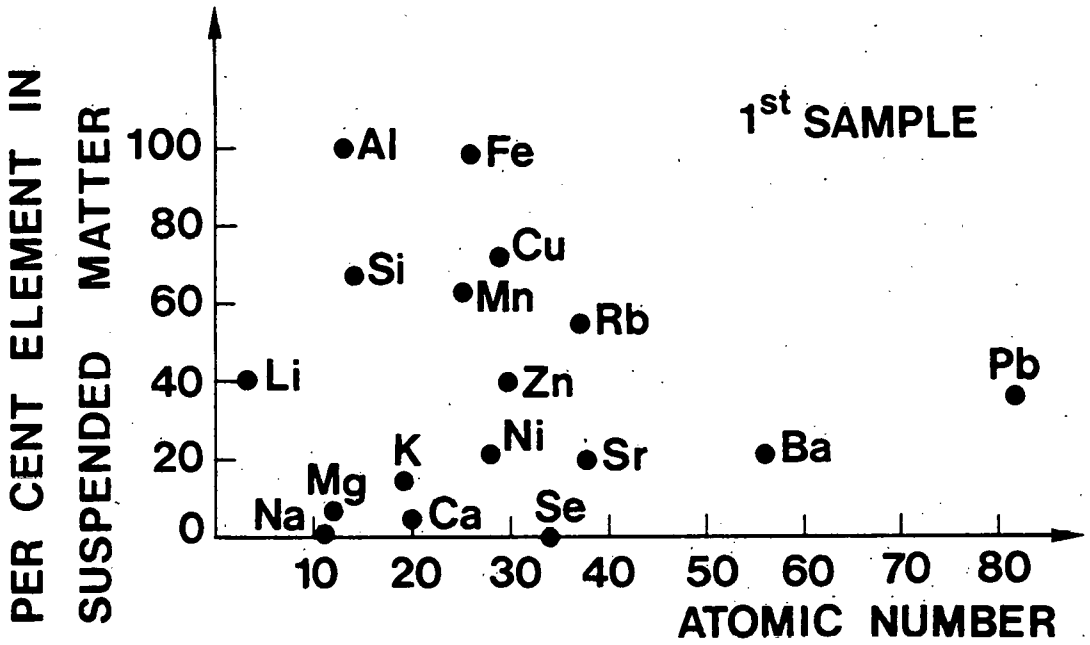


FIGURE 4 - Per cent partition of elements between water and suspended matter.

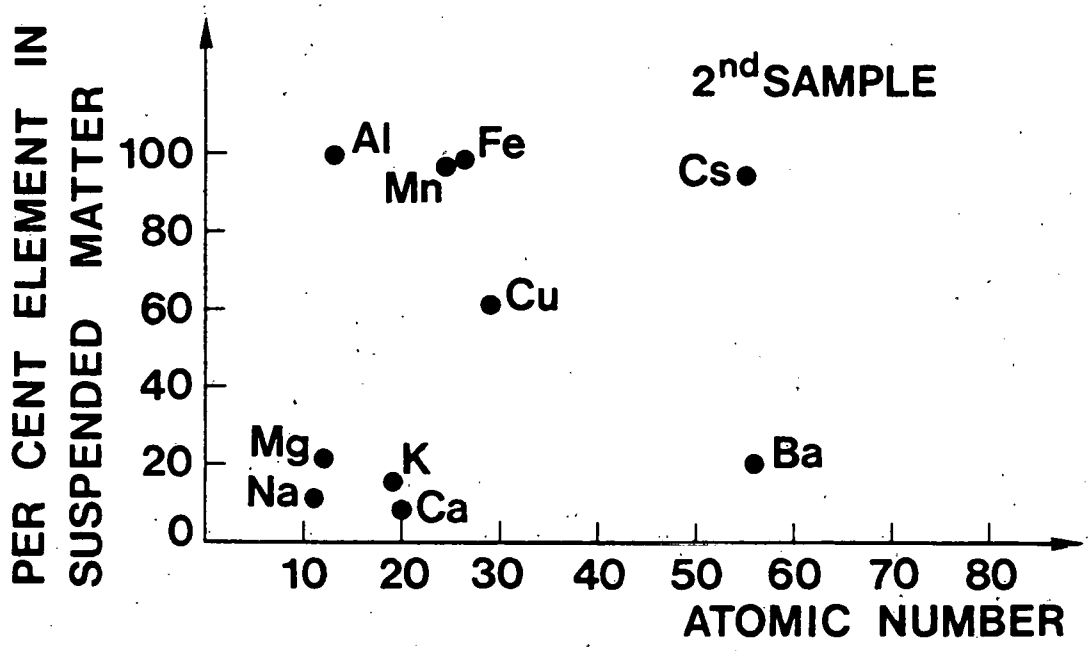


FIGURE 5 - Per cent partition of elements between water and suspended matter.

NON-DESTRUCTIVE MULTI-ELEMENT PHOTON ACTIVATION ANALYSIS OF RIVER SEDIMENTS

by Ch. Berthelot, G. Carraro and V. Verdingh

Central Bureau for Nuclear Measurements

B-2440 GEEL, BELGIUM

INTRODUCTION

An instrumental photon activation analysis method has been developed for the determination of multi-element concentrations in Scheldt and National Bureau of Standards (NBS) river sediments. The intact analysis of a complex matrix, such as the sediment, is attractive as difficulties and errors associated with sample dissolution, are eliminated. The absorption of high energy photons by the sediments, composed mainly of low-Z elements, is small and the bulk sample can be activated homogeneously. A large number of toxic elements, including the actinides Th and U at low levels, have been determined non-destructively by photon activation.

EXPERIMENTAL

The analyses are performed at the Geel linear accelerator using the bremsstrahlung produced by the impact of an electron beam (44 - 45 MeV) on a water-cooled platinum target.

Irradiation arrangement

The standards are placed at the front and back of the sample (sandwich arrangement) and the whole assembly is contained in the central part of an Al block. The sample holder itself is locked in the head of a cylindrical rabbit (Ø 52 mm) which can be rotated (12 rpm) during the continuous γ-irradiation in front of the conversion target and at a distance of about 10 mm [1]. The axis of the rabbit lies along the electron beam. The length of irradiation varies between 1 1/2 hours with an electron beam of 65 μA for short-lived nuclides and 7-18 hours with an electron beam of 35-58 μA for long-lived nuclides.

Sampling and counting system

The sediment samples (300 mg) are directly encapsulated in very pure Al cans ($\emptyset_i$ 10 mm). Synthetic standards containing the elements to be analysed are also encapsulated in Al cans. The activities of the samples and the standards, after irradiation, are measured directly with the activated Al cans (Fig. 1). To minimize the interfering reactions induced by neutrons, the sediment powder is also mixed with 50 w.% of very pure lithium sulphate, pressed into pellets (400 mg) and then wrapped in Al foils. After irradiation, the pellets are extracted from the Al foils and transferred to inactive Al cans for γ-counting using a Philips single open-ended coaxial Ge(Li) detector (54.6 cm^3) in conjunction with a Canberra 8180 multichannel analyser. The counting without the activated Al can gives a lower background of the spectrum and allows the determination of magnesium by the reaction $^{25}Mg(\gamma,p)^{24}Na$, free of the reaction $^{27}Al(n,\alpha)^{24}Na$ from aluminium, (Fig. 2).

Photopeak integrations are calculated using the total peak area method [2] and the Cutipie program [3] adapted to the IBM 370 computer, after substraction of the intrinsic background of the Ge(Li) detector from each spectrum.

RESULTS AND DISCUSSION

Depending on the half-life of the radionuclide, the decay time before the counting can vary from 1 hour to 6 weeks. The concentration of an element is determined according to the specific activity of the sample in comparison to

the mean specific activity of the two standards. The following elements have been determined:

TABLE 1

Element concentrations in river sediments

Element (μg/g)	Scheldt 5/6	Scheldt 17/18	NBS 1645	NBS 1645 certified values
Th	22	21	1.8	1.62
U	4.5	4.1	1.4	1.11
Ag	22	21		
As	101	85	87	
Ba	190	150		
Bi	12	9.5		
Ca	4.12 w.%	4.04 w.%		
Cd	11	13	11	10.2
Ce	86	83	28	
Co	18	19	24	
Cr	420	357	2.98 w.%	2.96 w.%
Cs	30	24		
Cu	170	150	106	109
Ga	18	22		
Ge	⩽ 2	2.4		
Hg	0.36	0.78	1.3	1.1
I	168	165		
In	1.1	1.2		
Mg	0.502 w.%	0.485 w.%		
Mo	11	9	25	
Na	0.873 w.%	0.931 w.%		
Nb	17	18		
Ni	37	38	48	45.8
Pb	238	231	724	714
Rb	73	72		
Sb	5.2	5.1	52	
Se	9.1	9.3		
Sn	13	12.5		
Sr	245	364	862	
Ta	1.5	1.9		
Te	7.1	5.7		
Tl	2.3	2.2	1.9	1.44
Ti	0.439 w.%	0.396 w.%	825	
W	⩽ 0.60	0.92		
Zn	753	663	1730	1720
Zr	747	386	71	

The two Scheldt sediment samples are taken in different locations and it shows large variation of concentration for Zr, and to a smaller extent for some elements, like Sr. Depending on the concentration, the specific activity and the half-life of the radionuclide, the accuracy is of the order of 2% to 30%.

The best limits of detection of all elements analysed by photon activation are given in the following table:

TABLE 2

Nuclear Reactions and Detection Limits (3x background standard deviation of the blank sample spectra at appropriate energy)

Element	Nuclear Reaction	$T_{1/2}$ [4]	γ-ray [5] (keV)	Detection Limit (μg)
Th	$^{232}Th(\gamma,n)^{231}Th$	25.52 h	25.64 84.21	0.14
U	$^{238}U(\gamma,n)^{237}U$	6.75 d	59.54 99.43(Np Kα) 208.01	0.028
Ag	$^{107}Ag(\gamma,n)^{106m}Ag$	8.5 d	450.95	
	$^{107}Ag(\gamma,2n)^{105}Ag$	41.3 d	344.52	0.35
As	$^{75}As(\gamma,n)^{74}As$	17.8 d	595.89 634.76	0.037
Ba	$^{134}Ba(\gamma,n)^{133m}Ba$	38.9 h	275.63	
	$^{136}Ba(\gamma,n)^{135m}Ba$	28.7 h	268.24	0.53
Bi	$^{209}Bi(\gamma,3n)^{206}Bi$	6.24 d	803.10 880.91	0.39
Ca	$^{44}Ca(\gamma,p)^{43}K$	22.2 h	372.84 617.66	1.5
Cd	$^{111}Cd(\gamma,\gamma')^{111m}Cd$ $^{112}Cd(\gamma,n)$	48.6 m	245.8	
	$^{116}Cd(\gamma,n)^{115}Cd \xrightarrow{\beta^-} {}^{115m}In$	53.4 h 4.5 h	527.76 336.24	0.13
Ce	$^{140}Ce(\gamma,n)^{139}Ce$	137.6 d	165.85	0.027
	$^{142}Ce(\gamma,n)^{141}Ce$	32.55 d	145.44	
Co	$^{59}Co(\gamma,n)^{58}Co$	70.78 d	810.76	0.033
Cr	$^{52}Cr(\gamma,n)^{51}Cr$	27.7 d	320.07	0.28
Cs	$^{133}Cs(\gamma,n)^{132}Cs$	6.474 d	667.6	0.016
Cu	$^{63}Cu(\gamma,2n)^{61}Cu$	3.41 h	283.35 656.02	5.6
Ga	$^{69}Ga(\gamma,n)^{68}Ga$	68.4 m	1077.4	
	$^{69}Ga(\gamma,2n)^{67}Ga$	78.3 h	300.21	0.90
Ge	$^{70}Ge(\gamma,n)^{69}Ge$	39.1 h	871.93 1106.65	0.40
	$^{74}Ge(\gamma,p)^{73}Ga$	4.86 h	297.36	
Hg	$^{198}Hg(\gamma,n)^{197m}Hg$	23.8 h	133.96	
	$^{198}Hg(\gamma,n)^{197}Hg$	64.1 h	68.18(Au Kα) 77.35+77.84(Au Kβ)	0.084
I	$^{127}I(\gamma,n)^{126}I$	13.0 d	388.67 666.34	0.13

Element	Nuclear Reaction	$T_{1/2}$ [4]	γ-ray [5] (keV)	Detection Limit (μg)
In	$^{113}In(\gamma,\gamma')^{113m}In$	99.5 m	392.20	
	$^{115}In(\gamma,n)^{114m}In$	49.51 d	190.26	0.090
			558.24	
Mg	$^{25}Mg(\gamma,p)^{24}Na$	15.0 h	1368.56	0.10
			1732.17 DE	
Mo	$^{97}Mo(\gamma,p)^{96}Nb$	23.35 h	778.22	
	$^{100}Mo(\gamma,n)^{99}Mo \downarrow \beta^- {}^{99m}Tc$	66.0 h	739.47	
		6.01 h	140.51	0.069
Na	$^{23}Na(\gamma,n)^{22}Na$	2.602 y	1274.53	0.36
Nb	$^{93}Nb(\gamma,n)^{92m}Nb$	10.14 d	934.51	0.053
	$^{93}Nb(\gamma,3n)^{90}Nb$	14.6 h	1129.20	
Ni	$^{58}Ni(\gamma,n)^{57}Ni$	36.0 h	127.19	
			1377.59	0.051
			1919.43	
Pb	$^{204}Pb(\gamma,\gamma')$, $^{206}Pb(\gamma,2n)$ ^{204m}Pb	66.9 m	899.2	
			911.8	
	$^{204}Pb(\gamma,n)$, $^{206}Pb(\gamma,3n)$ ^{203}Pb	52.0 h	72.17 (Tl Kα)	
			279.19	0.15
Rb	$^{85}Rb(\gamma,n)^{84}Rb$	32.77 d	881.60	0.025
Sb	$^{121}Sb(\gamma,n)^{120}Sb$	5.76 d	197.31	
			1023.18	
	$^{123}Sb(\gamma,n)^{122}Sb$	2.68 d	564.01	0.032
Se	$^{76}Se(\gamma,n)^{75}Se$	118.5 d	264.65	0.80
	$^{82}Se(\gamma,n)^{81m}Se$	57.3 m	103.04	
Sn	$^{112}Sn(\gamma,p)^{111}In$	2.83 d	171.29	0.54
	$^{117}Sn(\gamma,\gamma')^{117m}Sn$, $^{118}Sn(\gamma,n)$	14.0 d	245.35	0.54
			158.58	
Sr	$^{86}Sr(\gamma,n)^{85m}Sr$	68.0 m	231.68	
	$^{86}Sr(\gamma,n)^{85}Sr$	64.7 d	513.99	
	$^{87}Sr(\gamma,\gamma')$, $^{88}Sr(\gamma,n)$ ^{87m}Sr	2.805 h	388.46	0.050
Ta	$^{180}Ta(\gamma,\gamma')$, $^{181}Ta(\gamma,n)$ ^{180m}Ta	8.01 h	55.38 (Hf Kα)	0.094
			63.18 (Hf Kβ)	
			93.4	
Te	$^{122}Te(\gamma,n)^{121}Te$	16.8 d	573.02	0.70
	$^{130}Te(\gamma,n)^{129}Te$	69.5 m	459.54	
Tl	$^{203}Tl(\gamma,n)^{202}Tl$	12.23 d	70.15 (Hg Kα)	
			439.56	0.031

Element	Nuclear Reaction	$T_{1/2}$ [4]	γ-ray [5] (keV)	Detection Limit (μg)
Ti	$^{48}Ti(\gamma,p)^{47}Sc$	3.42 d	159.39	0.062
	$^{49}Ti(\gamma,p)^{48}Sc$	43.7 h	1037.48	
W	$^{182}W(\gamma,n)^{181}W$	121 d	57.10 (Ta Kα) 65.12 (Ta Kβ)	0.12
Zn	$^{66}Zn(\gamma,n)^{65}Zn$	244 d	1115.52	0.48
Zr	$^{90}Zr(\gamma,n)^{89}Zr$	78.4 h	909.15	0.023
	$^{96}Zr(\gamma,n)^{95}Zr$	64.0 d	756.72	

$$X\ K\alpha = X\ K\alpha_{1,2}\ ,\quad X\ K\beta = X\ K\beta_{1,3}$$

CONCLUSION

The instrumental photon activation analysis method is very useful for multi-element determinations in river sediments, from percent levels to sub-ppm levels, such as As, Cd, Ce, Co, Cs, Hg, I, In, Mg, Mo, Nb, Ni, Pb, Rb, Sb, Sr, Ta, Th, Ti, Tl, U, W and Zr.

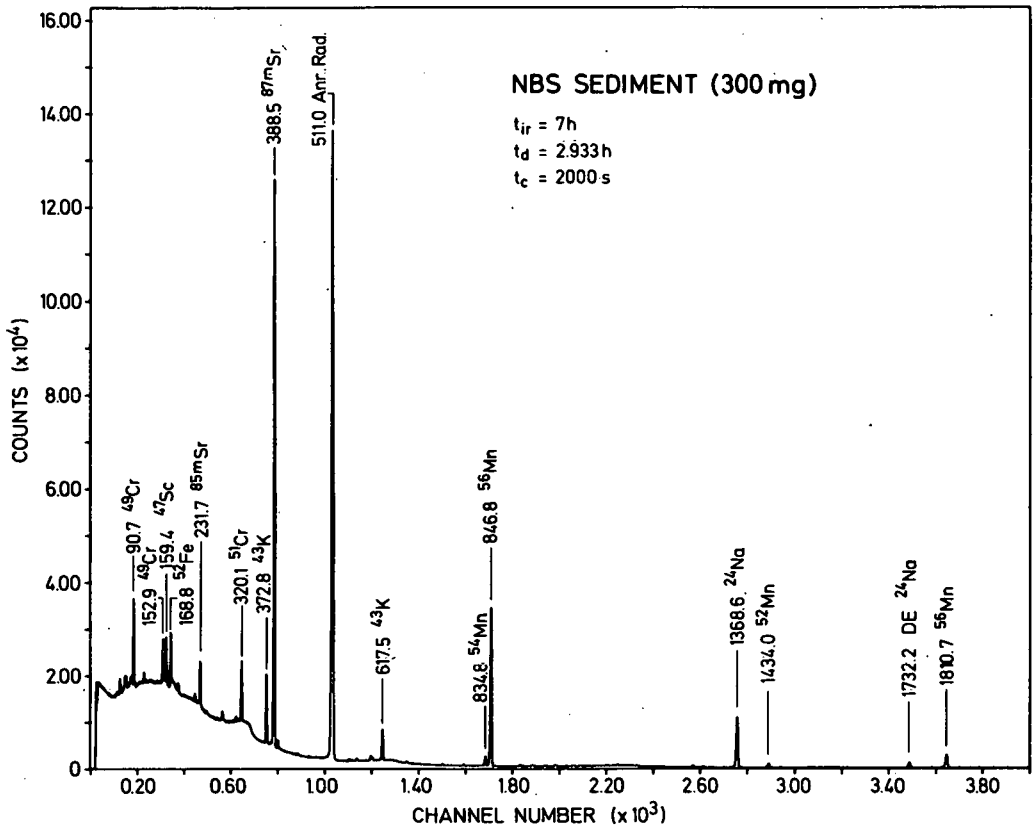
ACKNOWLEDGEMENT

The authors express their gratitude to Dr. R. Batchelor and Dr.B.Rose for their advice and support to this project, and to Dr. H.L. Eschbach for helpful discussions. The samples were prepared by T. Mencarelli and H. Ruts. The authors also wish to thank Dr. C. Bastian for the Angela program (substraction of the background or blank sample spectrum from the activated sample spectrum) and D. Reher for the adaptation of the Cutipie program to the IBM 370 computer. The assistance of the Linac machine group is greatly appreciated.

REFERENCES

1. Ch. Berthelot, G. Carraro, V. Verdingh - J. Radioanal. Chem. 50 (1979) 185.
2. P.A. Baedecker - Anal. Chem. 43 (1971) 405.
3. W. Teoh - Nucl. Instr. and Meth. 109 (1973) 509.
4. C.M. Lederer, V.S. Shirley, eds. - Table of Isotopes, Wiley-Interscience Publ. (1978)
5. a. E.W. White, G.G. Johnson, Jr. - X-Ray Emission and Absorption Wavelengths and Two-Theta Tables - ASTM Data Series DS 37A, 2nd ed., Philadelphia (1970)
   b. P. Anderson, J.S. Hislop, D.R. Williams - High resolution γ spectra of 40-44 MeV γ photon activation products: Pt. 1 - The elements Sodium to Molybdenum - Harwell AERE-R 7823 (1974)
   c. D.R. Williams - Ibid, Pt. 2 - The elements Ruthenium to Uranium - AERE-R 9021 (1978)
   d. R.L. Heath - Gamma-Ray Spectrum Catalogue, Ge(Li) and Si(Li) Spectrometry, vol. 2, 3rd ed., USAEC ANCR-1000-2 (1975)
   e. J.J. Legrand et al. - Table de Radionucléides - CEA, BNM, Lab. de Métrologie des Rayonnements Ionisants (1977)

5.f.G. Erdtmann, W. Soyka - The Gamma Rays of the Radionuclides, Tables for Applied Gamma Ray Spectrometry, vol. 7 Verlag Chemie (1979)



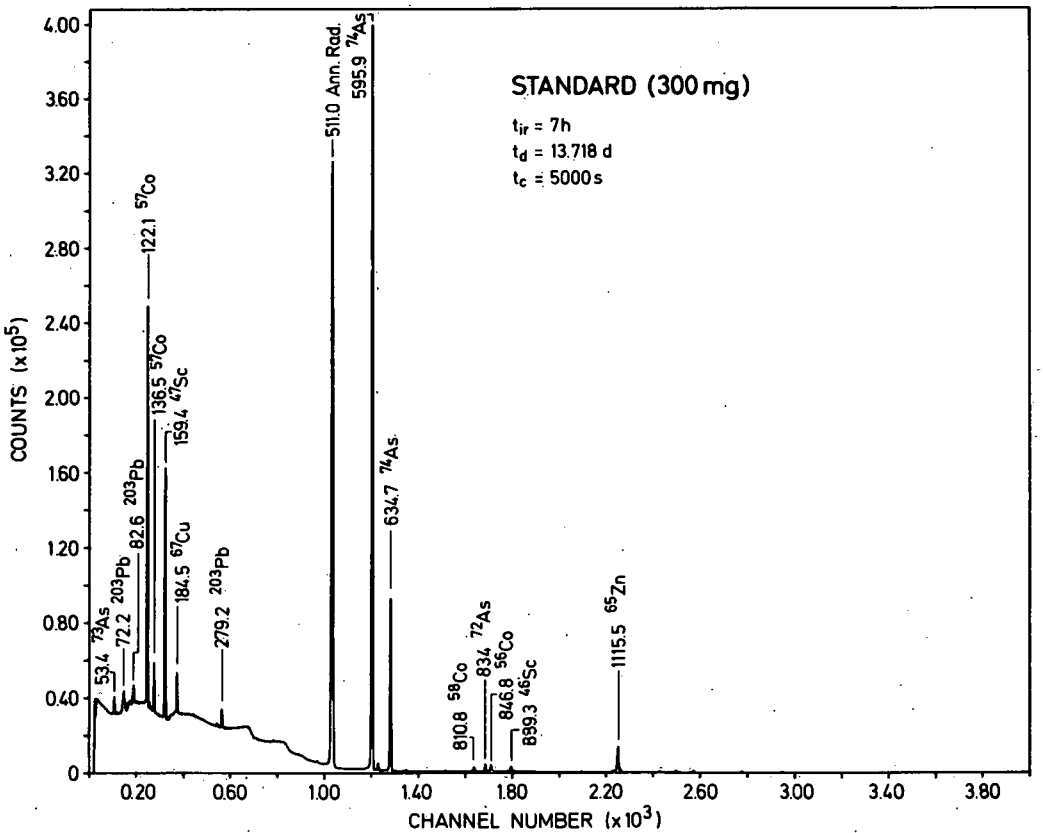
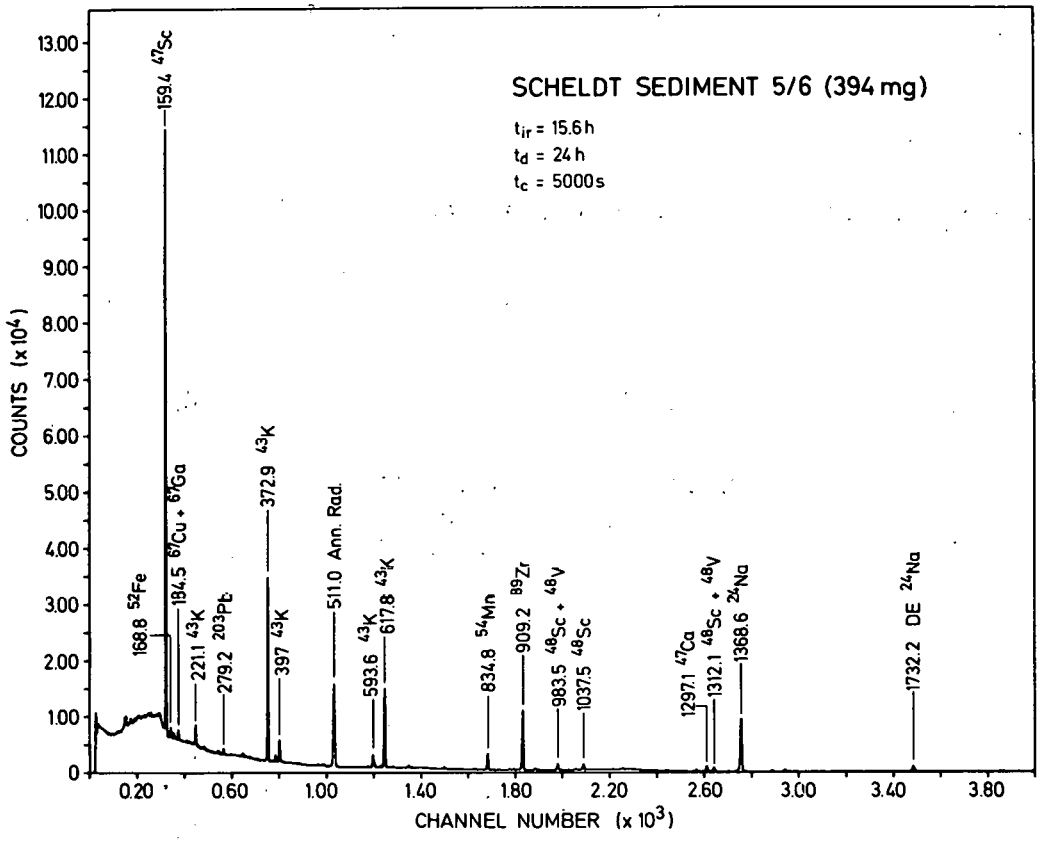


Figure 1 Gamma-ray spectra of NBS river sediment sample and standard. t_{ir} = irradiation time, t_d + time from end of irradiation, t_c = counting time



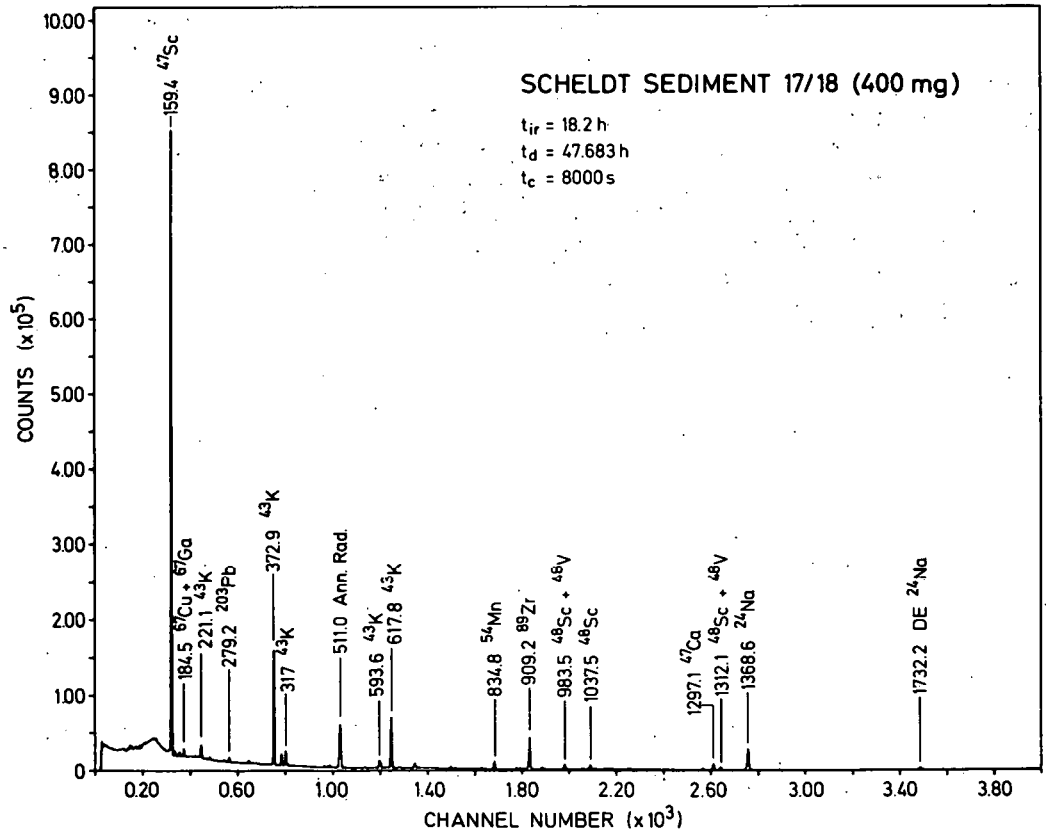


Figure 2 Gamma-ray spectra of Scheldt river sediment 5/6 and 17/18 samples.

Neutron Activation for the Determination of Total Halogenated Organics

by

C.D. Reach, Jr., P.F. Meiburger, and J.T. O'Connor

Department of Civil Engineering
University of Missouri-Columbia
Columbia, MO 65211

ABSTRACT

The disposal of hazardous chemical wastes is one of the most critical and far-reaching problems facing the industrialized world. Enforcement of new federal and state regulations will require the development of a cost effective analytical procedure which is sensitive to many toxic waste substances. The application of neutron activation analysis for organohalide detection is presented as a predisposing and complementary method to gas and liquid chromatography procedures for priority pollutant analyses. The concept is introduced that NAA offers an unprecedented broad-spectrum monitoring technique in the ability to determine a toxic substance parameter known as the "organohalides".

Introduction

Approximately 35 million tonnes of hazardous chemical wastes are produced annually in the United States. In November, 1978, the U.S. Environmental Protection Agency (EPA) released a report estimating that some 32,000 waste chemical dumps exist throughout the country. A more recent (February 1980) report to Congress has indicated that while significant reductions in air and surface water pollution have been achieved, land and ground water contamination by synthetic organic chemicals (SOCs) has increased to a critical level in many areas.

Reports of chemical contamination due to spills, negligent usage, and improper waste disposal (past and present) are received almost daily by State and Federal agencies. Nation-wide damages to personal and public properties have totaled into the upper hundreds of millions of dollars. Costs to correct environmental contamination have been estimated to exceed several hundred billion dollars. Most disturbing, however, are the unknown and possibly long term adverse health effects related to SOC contamination. Laboratory results have shown that many synthetic organic waste components produce carcinogenic, mutagenic and/or teratogenic effects in one or more test organisms.

Analytical Needs

Because of the scope of the SOC problem, new and stringent hazardous waste disposal regulations are being promulgated by the EPA as amendments to the 1976 Resource Conservation and Recovery Act. Many states have recently passed legislation supporting the new federal laws and have begun to outline programs to control the transportation/disposal of hazardous chemical agents.

The "cradle-to-grave" hazardous waste regulations, issued by the U.S. Environmental Protection Agency face several major legal, technical and financial obstacles. Unfortunately, the bottom line to these regulations, ultimate waste disposal, must contend with all three obstacles at once. This compound problem is to a significant degree associated with the need to establish an environmental monitoring system for waste containment sites. Current technology provides no readily available, cost effective method for broad-spectrum monitoring to observe the intrusion or migration of toxic chemical contaminates.

The most widely used analytical techniques of Atomic Absorption (AA), Total Organic Carbon (TOC), Gas Chromatography (GC), High-Performance Liquid Chromatography (HPLC), and Gas Chromatography-Mass Spectrometry (GC-MS) are not individually adequate as general environmental monitoring methods. Although GC-MS and HPLC are unmatched in their quantification and identification of specific organic compounds,these methods are exceedingly time consuming and expensive. Conversely, TOC analysis provides a cost effective determination for the total organic material present, but yields no information as to the nature of the compounds or their structure. Atomic absorption, while both selective and inexpensive, is only applicable to elemental metal analysis.

The nature of the major analytical techniques indicates that each is either too costly, too general or too limited to be utilized as an operational, environmental monitoring parameter. A parallel combination of AA, TOC, and GC-MS analyses is necessary to provide a comprehensive data base for determining the presence or threat of SOC contamination. The total cost per sample, however, makes the implementation of a multi-analysis scheme economically infeasible. An obvious need exists for the application and/or development of a single analytical technique which is sensitive to a wide range of elements and compounds, yet economical to utilize on a per sample basis.

Nuclear analysis techniques, particularly neutron activation, may have significant potential as a broad-spectrum hazardous waste pollution indicator. Neutron activation analysis (NAA) is extremely sensitive for most "toxic" metals with the exception of lead. Moreover, utilization of an activated carbon sorption matrix in conjunction with NAA allows the determination of a group parameter designated as the "organohalides" (OX or OHa; organic compounds containing Cl^-, Br^-, or I^-). The ramifications of the ability to quantatively determine the organohalide parameter can be readily seen in Table 1 which shows that halogenated organic compounds comprise 48 of the 93 substances listed by the U.S. EPA as priority pollutants. Approximately half of the 500,000 tonnes of pesticides used in the farming industry each year belong to the chlorinated hydrocarbon group. Additionally, several of the most toxic substances known (e.g., dioxins) are halogenated by-products resulting from the manufacture of pesticides, industrial/household solvents and polymeric materials.

Origin of Organic Halide Analysis

Interest in the OX parameter was first generated by Rook (1) during an investigation to observe the reaction between chlorine and naturally-occurring fulvic and humic acids. Although Rook's data showed a pronounced formation of chlorine-substituted methane groups, it was questioned whether significant amounts of larger molecular weight chlorinated organic substances were also produced. Such larger molecular weight organohalides, if produced, were considered important because of their possible resemblance to pesticides and industrial chemical by-products known to be toxic.

As the interest in measuring OX became more wide-spread, Wegmen and Greve(2) studied a technique in which ether extracts from river water samples were burned in an oxygen-rich atmosphere. Furnace out-gases were titrated with silver ions(3) to determine the mass of halogen liberated from the extracted organic molecules. This determination of ether-extracted organic-bound halides became known as EOX and was shown to concentrate specific organic substances by a factor of 1000. The EOX analysis was later modified by Glaze, et.al.(4) with the utilization of a macroreticular resin to absorb the halogenated organics from aqueous samples. Sorbed organics were eluted from the resin matrix with a small volume of ether and pyrolized for halogen content. Concurrent with the work of Wegmen and Greve, other researchers including Thurman(5), Suffet(6) investigated additional concentrating matrix materials and various sorption procedures for determining organically bound halides.

OX Analysis by NAA

In the current state-of-the-art, the OX analysis procedure, as accepted by the U.S. EPA, utilizes an activated carbon microcolumn system to sorb organohalides from solution. Once sufficient OX has been accumulated the carbon is rinsed with 5,000 ppm nitric acid solution to remove inorganic chloride ion interference. Rinsed carbon undergoes oxidative pyrolysis followed by microcoulometric titration as silver chloride. Schematic diagrams of the complete microcoulometric titration system (MCTS) are presented in Figures 1 and 2.

The MCTS system has several inherent limitations. The system requires the use of activated carbon as the sample concentrating matrix. Activated carbon is not as effective for the sorption of neutral and polar organic compounds as it is for non-polar organics. The MCTS system, therefore, measures only the "carbon adsorbable" fraction (CAOX) of the "total organic halide" (TOX) concentration present. Although study results indicate that activated carbon will concentrate 90% to 95% of the organohalides present in drinking water, the efficiency for recovery of OX compounds from complex chemical wastes is unknown.

The microcoulometric system for OX determination is additionally limited to the analysis of aqueous samples containing low levels of suspended solids.

While the technique is theoretically capable of handling semi-liquid (i.e., sludges) and solid samples, pyrolysis of complex organic materials such as polymers, soil and vegetation readily contaminates the titration cell.

Neutron activation analysis for the determination of organohalides may provide several major advantages over the MCTS method. The principal advantage of NAA is the ability to analyze many various solid samples. This aspect of NAA is particularly important for liquid samples in that carbonaceous resins can be utilized as sample concentrating matrixes in addition to activated carbon. Resin matrixes increase the classes (i.e., neutral and polar) of organic substances which can be extracted from aqueous samples. Subsequently, neutron activation analysis yields OX values much closer to the actual amount of total organic halide present than would a comparative analysis using the MCTS system.

In addition to a more comprehensive analysis, carbonaceous resins used in conjunction with NAA could provide a certain degree of compound selectivity. Utilization of various resins in a series concentration procedure could result in an effective molecular sieve similar to gas chromatography. Such a resin separation technique would be functional over a broad molecular size range of trace organic compounds. Broad spectrum molecular sieving would promote the usefulness of the OX/NAA method for toxic chemical monitoring.

One of the most important aspects of OX analysis by neutron activation is the ability to distinguish between the total brominated (TOBr) and the total chlorinated (TOCl) organohalide species. This differentiation is particularly significant in light of the indications that brominated organic substances are many times more mutagenic than their chlorinated homologues. Chlorinated SOCs can undergo substitution reactions in an environment where bromide ions are present and become increasingly more toxic to plant and animal life.

Preliminary Investigation of OX by NAA

The primary application for organohalide analysis via neutron activation is in the determination of bulk halogenated organic compounds from hazardous waste disposal site leachates and monitoring wells. The ability to detect bulk OX is largely dependent on the utilization of interference-free sorption matrixes. Table 2 presents a preliminary investigation of several different adsorbent materials commonly used to remove organic compounds from aqueous solution. Results show the detectable elements for potential matrix materials in the raw state and following treatment with 1+1 HNO_3, CH_3OH and/or 1+1 NH_4OH.

The "XE" series carbonaceous resin exhibited the broadest trace element content for all 'short-shot' raw matrix materials. Conversely, the polystyrene based XAD resins showed only two elements to be detectable. As expected, the lignite coal activated carbon contained the overall greatest quantity of interference elements, particularly with respect to manganese.

Initially, the element of most concern is chloride since the background will establish the sensitivity limit for OX analysis. With the exception of XE-340, raw matrix materials exhibit large amounts of intrinsic chloride contamination. The application of various chemicals for ion exchange or extraction can reduce chloride levels by 85% to 99%. For optimum determination of OX compounds, background matrix chloride levels should be reduced to less than one microgram per gram following short irradiation.

The second largest concern resulting from the Table 1 data is the appreciable concentration of elements with broad cross-sections and half-lives equal to or greater than chlorine. The sodium and manganese levels observed in the preliminary investigation are examples of primary interference elements. Fortunately, data results indicate that Na and Mn can be removed from the matrix materials with chemical pretreatment.

Future research efforts will be directed in three main areas. First, matrix materials will be treated with various chemicals to determine lowest background interference levels which can be reasonably achieved. Second, single and multi organohalide solute systems will be investigated to establish the recovery efficiency for OX compounds. Third and most important, various irradiation/decay periods will be investigated to determine the optimum sensitivity for both chlorinated and brominated organic substances.

Summary

A large potential exists for the application of OX determination by NAA as a predisposing, complementary method to GC-MS and HPLC analyses for evaluating synthetic organic chemical contamination. Organic halide analysis by neutron activation would provide a sensitive, broad-spectrum scanning method for monitoring hazardous waste disposal facility leachates and ground water wells. The NAA method would have several major advantages over the current oxidative pyrolysis-microcoulometric titration technique. Most importantly, OX/NAA determinations would be easily obtainable and cost effective.

Greater than thirty facilities operating nation-wide contain the ability to determine toxic metals and organohalides at the one microgram level. With sufficient development of the OX/NAA method, it may be possible to determine levels of organic chloride, organic bromide plus several toxic metals for under $200 per sample. On a cost basis OX/NAA analysis could provide an overall superior monitoring tool for determining the presence of hazardous chemical contaminates than would an analysis for priority pollutants costing $800 to $1000 per sample.

REFERENCES

1. Rook, J.J., Jour. of Amer. Water Works Assoc., 68:168 (1976).
2. Wegman, R.C. and P.A. Greve, Sci. of the Total Environ., 7:235(1977).
3. Kuhn, W. and H. Sontheimer, Vom Wasser, 41:65 (1973).
4. Glaze, W.H., et al., Environ. Sci. and Tech., 11:685 (1977).
5. Thurman, E.M., et al., Anal. Chem., 50:775 (1979).
6. Suffet, I.H., et al., Environ. Sci. and Tech., 12:1315 (1978).
7. Takahashi, Y., and R.T. Moore, "Measurement of Total Organic Halides (TOX) in Water by Carbon Adsorption/Microcoulometric Determination", presented before the Division of Environmental Chemistry, Amer.Chem.Soc., Honolulu, Hawaii, April 1979.

BIBLIOGRAPHY

Disposal of Hazardous Wastes-Report to Congress, U.S. Environmental Protection Agency, Office of Solid Waste Management Programs, SW-115 (1974).

Industrial Waste Management: Seven Conference Papers, U.S. EPA, OSW, SW-156 (1975).

Hazardous Waste Management Facilities in the United States-1977, U.S. EPA, OSW SW-146.3 (1977).

Hazards of Difficult to Handle Waste Survey Report, North Carolina Dept. of Human Resources, U.S. EPA, PB-292-968 (1978).

Public Hearing of Proposed Hazardous Waste Regulations, U.S. EPA, OSW, SW-51p, (1979).

"Chemical Waste Disposal: A Costly Problem", Chemical and Engineering News, Vol. 57, No. 11, March 12, 1979.

TABLE 1

Master List of Individual Organic Chemicals Considered as Hazardous Wastes by the U.S. Environmental Protection Agency

Acenaphthene
Acrolein
Acrylonitrile
Benzene
Benzidine
Chlorobenzene
1,2,4-Trichlorobenzene
Hexachlorobenzene
1,2-Dichloroethane
1,1,1-Trichloroethane
1,1-Dichloroethane
1,1,2-Trichioroethane
Chloroethane
Bis(chloromethyl) ether
Bis(2-chloroethyl) ether
2-Chloroethyl vinyl ether (mixed)
2-Chloronaphthalene
2,4,6-Trichlorophenol
p-Chloro-*m*-cresol
2-Chlorophenol
1,3-Dichlorobenzene
3,3-Dichlorobenzidine
1,1-Dichloroethylene
1,2-*trans*-Dichloroethylene
2,4-Dichlorophenol
1,2-Dichloropropane
1,2-Dichloropropylene (1,3-dichloropropene)
2,4-Dimethylphenol
2,4-Dinitrotoluene
2,6-Dinitrotoluene
1,2-Diphenylhydrazine
Ethylbenzene
Fluoranthene
4-Chlorophenyl phenyl ether
4-Bromophenyl phenyl ether
Bis(2-chloroisopropyl) ether
Bis(2-chloroethoxy) methane
Methyl chloride (chloromethane)
Bromoform (tribromomethane)
Dichlorobromomethane
Trichlorofluoromethane
Dichlorodifluoromethane
Chlorodibromomethane
Hexachlorobutadiene
Hexachlorocyclopentadiene
Isophorone
2-Nitrophenol
4-Nitrophenol
4,6-Dinitro-*o*-cresol
N-Nitrosodimethylamine
N-Nitrosodiphenylamine
N-Nitrosodi-*n*-propylamine
Pentachlorophenol
Bis(2-ethylhexyl)phthalate
Butyl benzyl phthalate
Di-*n*-butyl phthalate
Di-*n*-octyl phthalate
Diethyl phthalate
Dimethyl phthalate
Benzo(a)anthracene (1,2-benzanthracene)
Benzo(a)pyrene (3,4-benzopyrene)
3,4-Benzofluoranthene
Benzo(k)fluoranthane (11,12-benzofluoranthene)
Chrysene
Acenaphthylene
Anthracene
Benzo(g,h,i)perylene (1,12-benzoperylene)
Fluorene
Phenanthrene
Dibenzo(a,h)anthracene-(1,2,5,6-dibenzanthracene)
Indeno(1,2,3-c,d) pyrene (2,3-*o*-phenylenepyrene)
Pyrene
Toluene
Vinyl chloride (chloroethylene)
Aldrin
Chlordane (technical mixture & metabolites)
a-Endosulfan-alpha
b-Endosulfan sulfate
Endosulfan sulfate
Endrin aldehyde
Heptachlor
Heptachlor epoxide
BHC-alpha (1,2,3,4,5,6-hexachlorocyclohexane)
BHC-beta
BHC-delta
PCB-1242
PCB-1254
PCB-1221
PCB-1232
PCB-1248
PCB-1260
PCB-1016
2,3,7,8-Tetrachlorodibenzo-*p*-dioxin(TCDD)

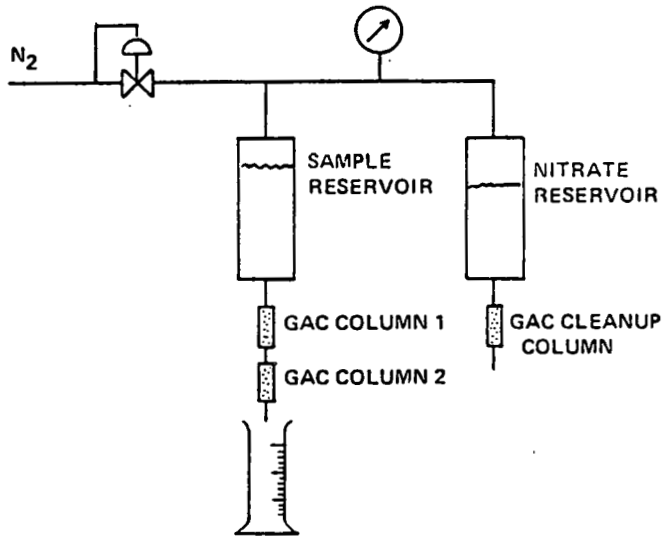


Figure 1. Microcolumn Activated Carbon Concentration of Aqueous Organohalides(7).

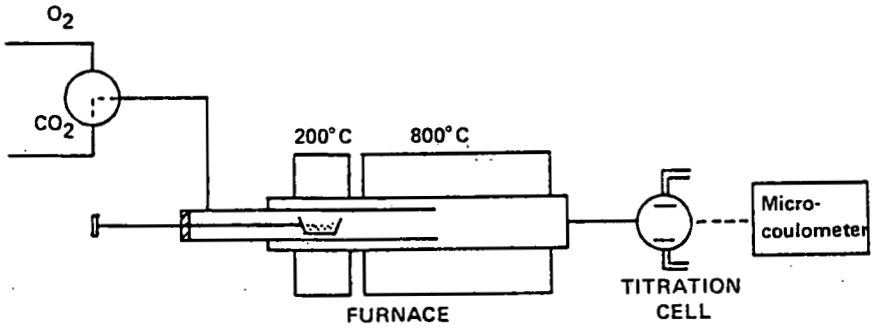


Figure 2. Pyrolysis and Microcoulometric Titration of Carbon Adsorbed Organohalides(7).

TABLE 2

Neutron Activation Analysis of Raw and Treated Sorption Matrixes: Elements Detected with Less than 20% Error After a Ten-Second Irradiation at 1×10^{14} Neutrons/Square Centimeter/Second

ELEMENT (ug/g) \ MATRIX	ICI-4000 (raw)	ICI-4000 (HNO_3;CH_3OH)	XAD-2 (raw)	XAD-2 (NH_4OH)	XAD-4 (raw)	XAD-4 (NH_4OH)	XE-340 (raw)
Na	---	---	3040	435	6180	322	690
Al	---	---	---	---	---	---	4
Cl	1985	284	4170	87	8930	41	35
Ca	2030	---	---	---	---	---	1749
V	90	---	---	---	---	---	>0.1
Mn	1094	13	---	---	---	---	2

A Model for Pb-210 in Sediments Influenced by Mixing and Compaction

Erik R. Christensen and Nan-Kwang Chien

Department of Civil Engineering
University of Wisconsin-Milwaukee
Milwaukee, Wisconsin 53201

Abstract

A unified model for the activity of radionuclides in sediments has been set up based on the one-dimensional advection-diffusion equation. The model considers sedimentation, mixing and compaction. Observed distributions of deposit-feeding organisms, and the nature of physical disturbances, indicate that a gaussian diffusion coefficient may be appropriate. Two-layer models with constant and gaussian mixing, respectively, in the upper layer are compared with measured Pb-210 profiles for two cores from Green Bay, Lake Michigan, and it is found that the maximal diffusion coefficient D_o=4 cm^2/yr for the gaussian model is considerably greater than the constant D value of 0.2 cm^2/yr, if compaction effects are neglected. The solution for the gaussian model is based on an approximate power series method. Compaction can be taken into account using an exponential sedimentation rate or sediment density. By comparing with measured data for a Lake Ontario core it is seen that compaction alone can give an appreciable flattening of the activity curves near the top layers. An exponential sedimentation rate tends to overestimate this flattening, while it is slightly underestimated using an exponential sediment density.

1. Introduction

Dating of lake and nearshore ocean sediments by the Pb-210 method has received considerable attention since its first successful demonstration in the early 1970's [1,2]. Mixing in the upper sediment layers induced by biological activity or physical stirring by bottom currents can have a significant impact on the measured Pb-210 profiles [3,4]. Evidence for mixing of abyssal sediments has also been given through the dispersal of microtektite layers [5,6].

Information on the magnitude and vertical extent of mixing is important, not only for the proper interpretation of historical records of substances introduced to the sediments, but also for an evaluation of the possible role of the sediments as a source of these substances to the water column. While compaction of sediments usually is of minor importance it may also have an impact on the activity profiles. Both mixing and compaction have the effect of flattening the activity profile near the water-sediment interface.

Several models that include mixing have been described. Berger and Heath [7] considered a homogeneous mixing layer above undisturbed historical layers. Models based on the advection-diffusion equation were set up by Goldberg and

Koide [8], Guinasso and Schink [9], and Nozaki [10]. Nozaki's model is the only one that allows for a continuously decreasing diffusion coefficient vs. depth. The need for this had been pointed out previously [9,4] and is also suggested by other data, for example those of Nozaki et al. [11] who studied the C-14 age of abyssal sediments. However, Nozaki's model [10] includes zero sedimentation rate, and an apparently unrealistic exponentially decreasing diffusion coefficient vs. depth. Based on the observations of Robbins et al. [4] on the density of biological species vs. depth it appears that an exponential decrease would fail to give the experimentally found well-defined mixing zone.

Both mixing and compaction were taken into account by Robbins and Edgington [3] and Robbins et al. [4]. They considered an upper homogeneous layer with rapid mixing, and undisturbed layers below. Robbins et al. [12] found that compaction alone could explain several Pb-210 profiles from the Great Lakes. In no case was the compaction model based on the advection-diffusion equation.

A signal theory approach has also been proposed [9,13].

The purpose of the present work is to present a unified model for radionuclides in sediments influenced by mixing and compaction. The model is based on the advection-diffusion equation with a gaussian diffusion coefficient and an exponential sedimentation rate or sediment density.

2. The general advection-diffusion equation

The activity of Pb-210 in sediments is dependent upon sedimentation, mixing, and radioactive decay as expressed by the one-dimensional advection-diffusion equation:

$$-\frac{\partial}{\partial z}(vc) + \frac{\partial}{\partial z}\left(D\frac{\partial c}{\partial z}\right) - \lambda c = \frac{\partial c}{\partial t} \quad , \tag{1}$$

where $c(dpm/cm^3)$ is the Pb-210 activity, $z(cm)$ is the depth below the water-sediment interface, $t(yr)$ is the time, $v(cm/yr)$ is the sedimentation rate, $D(cm^2/yr)$ is the mixing coefficient, i.e., the eddy diffusion coefficient, and $\lambda(yr^{-1})$ is the radioactive decay constant for Pb-210. Under the assumption of steady-state conditions we obtain the following equation:

$$-\frac{d}{dz}(vc) + \frac{d}{dz}\left(D\frac{dc}{dz}\right) - \lambda c = 0 \ . \tag{2}$$

This equation forms the basis for the present model. The diffusion coefficient D and the sedimentation rate v are generally dependent on the depth z, reflecting maximal mixing and minimal compaction, respectively, at the top sediment layers.

In the simple case of undisturbed sedimentation we have no mixing or compaction so that D=0 and v is a constant. The sediment density $\rho(g/cm^3)$ will then also be constant vs. depth under the usually reasonable assumption of constant sedimentation rate. Thus, the activity per weight unit s (dpm/g) is proportional to the activity per volume unit, $s=c/\rho$, independently of depth, and equation (2) reduces to

$$-v\frac{ds}{dz} - \lambda s = 0 \ , \tag{3}$$

with the solution

$$s = s_0 e^{-\frac{\lambda}{v}z} \tag{4}$$

where s_0 is the activity at the water-sediment interface. This is the usual exponential expression for the activity vs. depth in non-compacting sediments.

3. Two-layer model with constant mixing in the upper layer

Since benthic mixing normally is confined to the uppermost sediment layers, we will consider, as a first step, a two-layer model with D equal to a constant in the upper layer and zero below. If compaction effects are neglected we obtain from equation (2):

$$\left.\begin{aligned} D\frac{d^2s}{dz^2} - v\frac{ds}{dz} - \lambda s = 0 \qquad & z \leq z_o \\ - v\frac{ds}{dz} - \lambda s = 0 \qquad & z > z_o \end{aligned}\right\} \tag{5}$$

This set of equations with proper boundary conditions were solved by Goldberg and Koide [7]. The solution may be written as:

$$\left.\begin{aligned} s &= s_2[Ke^{\alpha_1 z} + e^{\alpha_2 z}] \qquad z \leq z_o \\ s &= s_3\, e^{-\frac{\lambda}{v} z} \qquad z > z_o \end{aligned}\right\} \tag{6}$$

with

$$K = -\frac{\alpha_2}{\alpha_1} e^{\frac{v}{D}\sqrt{1 + \frac{4\lambda D}{v^2}}\, z_o}$$

$$\alpha_1 = \frac{v}{2D}\left(1 - \sqrt{1 + \frac{4\lambda D}{v^2}}\right)$$

$$\alpha_2 = \frac{v}{2D}\left(1 + \sqrt{1 + \frac{4\lambda D}{v^2}}\right)$$

The solution is compared to measured Pb-210 activities in two cores from Green Bay, Lake Michigan [14] (Table 1). The activities are plotted in Fig. 1. Although the boundary z_o between the two layers can only be ascertained as being between 3 and 4 cm we have chosen z_o=4cm for the sake of comparison with the gaussian model. The listed diffusion coefficients D=0.2 and 1.0 cm^2/yr can therefore be considered to be lower limits.

Table 1

Mixing and sedimentation parameters for Green Bay Cores*

Parameter	Station No 1	Station No 7
Latitude (N)	45°59'00"	44°56'30"
Longitude (W)	87°29'00"	87°37'30"
Water depth (m)	26	15
Two-layer boundary, z_o (cm)	4	4
Sedimentation rate, v (cm/yr)	0.11	0.52
Diffusion coefficient, D (cm^2/yr)	0.2	1.0
s_2 (dpm/g)	0.437	0.243
s_3 (dpm/g)	42	28
K	171.89	130.97

* Based on two-layer model with constant D in the upper layer.

The two-layer model with constant mixing in the upper layer is clearly inadequate at the boundary z_0. While the continuity of the flux of activity requires the slope to be horizontal at the boundary in the mixed zone, the resulting breakpoint is an artifact not found in actual distributions. The model may provide a reasonable first approximation, but there is obviously a need for a model with a continuously decreasing diffusion coefficient.

4. Two-layer model with gaussian mixing in the upper layer

There are strong arguments for choosing a gaussian diffusion coefficient. Deposit-feeding animals such as oligochaete worms, responsible for benthic reworking, are mainly found in the top layers in the area of their food source and would only by chance move to deeper layers. The distributions of Pontoporeia affinis and tubificid oligochaetes found by Robbins et al. [4] are indeed close to being gaussian. Furthermore, if physical disturbances induced by bottom currents play a role in the mixing process, this activity would be confined to the upper layers and decrease rapidly with depth. We will therefore assume that the diffusion coefficient has the following form:

$$D = D_0 \, e^{-\frac{z^2}{2\sigma^2}} \tag{7}$$

where D_0 (cm^2/yr) is the diffusion coefficient at the water-sediment interface, z (cm) is the depth, and σ (cm) is an effective mixing depth below which mixing becomes less important.

If compaction effects are neglected, equation (2) reduces to:

$$D_0 \frac{d^2s}{dz^2} - \left(v \, e^{\frac{z^2}{2\sigma^2}} + \frac{z}{\sigma^2} D_0\right) \frac{ds}{dz} - \lambda s \, e^{\frac{z^2}{2\sigma^2}} = 0 \tag{8}$$

An approximate solution to this equation is obtained by introducing a boundary z_0 above which s obeys equation (8) and below which there is no mixing, that is, s can be found from equation (4). We further require the activity s and its first derivative to be continuous at z_0. The solution for $0<z\leq z_0$ is obtained as a power series:

$$s = \sum_{n=0}^{N} a_n \, y^n$$

where $y = z - z_0$. Details of the mathematical treatment will be published elsewhere.

The results of the calculations are compared to the measured activities for the two Green Bay cores in Fig. 2. In this figure, z_0 = 4 cm, σ = 2.5 cm, and N = 80. Note that if $D_0 \to 0$ we expect the solution for $0<z\leq z_0$ to be a linear extrapolation of the activity curve for $z>z_0$ in the semi-logarithmic plot. Although the D_0=0.5 cm^2/yr curve for Station 1 is not convergent for N = 80, this curve is approaching the linear extrapolation of the curve beyond z_0. For large values of D_0 the activity plot should have a horizontal tangent at the the sediment-water interface. As can be seen from Fig. 2, this condition is approximately fulfilled.

By comparing the gaussian with the constant-D model (Figs. 1,2) it is clear that the maximal diffusion coefficient D_0 is considerably greater than D as would be expected, and further, that the breakpoint at $z=z_0$ has disappeared in the gaussian model.

5. Compaction

Particulates settle loosely on the lake or sea bottom and may be subjected to significant compaction under the weight of additional settled material. As

in the case of mixing, the result is a flattening of the Pb-210 activity profiles near the sediment-water interface. While existing compaction models [3,4] do not rely on the advection-diffusion equation, we shall develop such models based on this equation.

Using the cumulative weight data for core KB from Lake Ontario [4], the sediment density for this core has been calculated as a function of depth and plotted in Fig. 3. This distribution is given by the curve labeled best ρ -fit, and is approximately represented by the exponential distribution:

$$\rho = \rho_0 - \rho_1 e^{-az} , \tag{10}$$

where $\rho_0 = 0.38$ g/cm^3, $\rho_1 = 0.28$ g/cm^3, and $a = 0.12$ cm^{-1}.

To arrive at the sedimentation rate in the absence of mixing, consider equation (2) for the sediment particulates with $c=\rho$, $D=0$, and $\lambda=0$:

$$\frac{d}{dz}(v\rho) = 0 , \tag{11}$$

reflecting the fact that the mass sedimentation rate $r = v\rho$ is constant under steady-state conditions. Since $r = 0.057$ g/cm^2/yr [4], we have $v = 0.057/\rho$ which is shown in Fig. 3 together with the following approximate representation:

$$v = v_0 + v_1 e^{-bz} \tag{12}$$

where $v_0 = 0.15$ cm/yr, $v_1 = 0.32$ cm/yr, and $b = 0.20$ cm^{-1}.

The Pb-210 activity in the absence of mixing can now be obtained from equation (2) with $D=0$, v from equation (12) or $v = r/\rho$ with ρ given by equation (10).

5.1 Exponential sedimentation rate

Using the exponential expression, equation (12), for v we obtain from equation (2):

$$-(v_0 + v_1 e^{-bz})\frac{dc}{dz} + cv_1 e^{-bz} - \lambda c = 0 . \tag{13}$$

With the substitution

$$c = f(z)\, e^{-\frac{\lambda}{v_0} z} , \tag{14}$$

equation (13) can be written

$$\frac{df(z)}{dz} = \frac{v_1(b + \frac{\lambda}{v_0})e^{-bz}}{v_0 + v_1 e^{-bz}}$$

with the solution

$$f(z) = f(o)\, e^{I(z)} , \tag{15}$$

where I(z) is the integral

$$I(z) = \int_o^z \frac{v_1 (b+\frac{\lambda}{v_0})e^{-b\eta}}{v_0 + v_1 e^{-b\eta}}\, d\eta \tag{16}$$

By substitution of equation (15) into equation (14) we obtain the activity distribution:

$$c = f(o)\, e^{I(z) - \frac{\lambda}{v_0} z} \tag{17}$$

The integral in equation (16) is evaluated by Simpson integration [15] and the resulting activities are converted to a weight basis by the equation $s = c/\rho$ using the best ρ-fit indicated in Fig. 3. The activity distribution derived in this manner provides a reasonably good fit to the measured activities (Fig. 4). Note that the curve is exponential for large z-values and significantly flattened in the upper layers for z less than about 8 cm.

5.2 Exponential sediment density

Introducing $c = \rho s$ we obtain from equation (2):

$$\frac{d}{dz}(v\rho s) + \lambda s\rho = 0 \ . \tag{18}$$

But since $r = v\rho$ is constant we have:

$$\frac{ds}{dz} = -\frac{\lambda}{r}\rho s$$

with the solution

$$s = s_o \, e^{-\frac{\lambda}{r}m} \ , \tag{19}$$

where m is the cumulative weight

$$m = \int_o^z \rho dn \tag{20}$$

Using the exponential expression, equation (10), for ρ we obtain

$$s = s_o \, e^{-\frac{\lambda}{r}\left[\rho_o z - \frac{\rho_1}{a}(1 - e^{-az})\right]} \tag{21}$$

The results for core KB are plotted in Fig. 4. The curve fits the measured activities well. The calculated distribution is exponential for large z-values, and is gradually flattened in the upper layers.

6. Discussion

An important advantage of the present approach is that the treatment of both mixing and compaction is based on the advection-diffusion equation. This gives added insight in the physical mechanisms responsible for the actual Pb-210 profiles, and more flexibility in the modeling.

The gaussian diffusion coefficient introduced here appear to give a fairly well defined mixing layer but at the same time a smooth transition to the deeper historical layers. It is suggested that this form of the diffusion coefficient can explain the gradual fall-offs in the Cs-137 activities found by Robbins et al. [4], and also the gradual increase vs. depth of the C-14 age found in abyssal sediments by Nozaki et al. [11].

While compaction can have a significant impact on the activity curves, there is some indication that nearshore cores are more affected than offshore cores, especially in the upper 10 to 20 cm [3]. This is supported by data for three cores from central Lake Michigan [14]. For these cores having a sedimentation rate of between 0 and 0.05 cm/yr, there was no measurable deviation of the activity profile from the exponential form. Other data for cores from Lake Erie and Ontario are less conclusive but show similar trends [12].

It should be noted that the degree of compaction observed is strongly dependent on the depth over which it is measured. Thus, one reason why compaction does often not show in activity profiles in cores from locations of great water depth, is that the sedimentation rate is so low that measurable excess Pb-210 activities are confined to the upper 3-4 cm over which depth the compaction usually is small.

Both mixing and compaction give rise to flattening of the otherwise exponential activity curve in the upper layers. Thus, a given activity profile may falsely be interpreted as being influenced by mixing when the flattening actually is caused by compaction, and vice versa. This means in particular that estimated diffusion coefficients may be too large if compaction effects are neglected.

Note that it can not be ascertained whether the deviations from the exponential forms of the activity curves for the two Green Bay cores are caused by mixing, compaction or both of these processes, without access to sediment density data. We have assumed here, however, that the deviations are caused by mixing for the sake of comparison between the two-layer models with constant and gaussian mixing, respectively.

To resolve the general problem of determining activity profiles in the presence of both mixing and compaction, it is suggested to measure the sediment density distribution, insert this, using equation (10) and (11), or (12), into equation (2), and solve this equation with D_0 and σ as parameters.

Mixing is measured most accurately with radionuclides for which $\lambda D_0 >> v^2$ while maintaining measurable activities over the depths of interest. Thus, in addition to Pb-210 with a half-life of 22.26 years, other radionuclides such as the cosmic-ray produced Be-7 with the considerably shorter 53-day half-life [16] may provide valuable information on the diffusion coefficient.

Once the mixing and compaction parameters have been derived, equation (1) can be used in connection with proper input functions, reflecting the time-dependent flux to the sediments of various radioactive or non-radioactive (λ=0) substances, to predict their profiles in the sediments as a function of time. Such predictions are of particular value in the interpretation of historical records of pollutants found in sediments.

7. Conclusions

A unified model for the activity of radionuclides in sediments has been set up based on the one-dimensional advection-diffusion equation. The model considers sedimentation, mixing and compaction.

It is shown that a gaussian diffusion coefficient holds considerable promise to describe the mixing in the relatively well-defined mixing zone near the sediment-water interface. By comparing two-layer models with constant and gaussian mixing, respectivley, in the upper layer, it is concluded that the maximal diffusion coefficient D_0 is considerably greater than the constant D for a given core. This is illustrated by the data for a Green Bay core where D_0=4 cm^2/yr and D=0.2 cm^2/yr under the assumption of negligible compaction.

The treatment of compaction is based on an exponential form of the sedimentation rate or the sediment density. Good agreement with Pb-210 activities measured in a Lake Ontario core [12] is obtained using both of these distributions. It is seen that compaction alone gives a significant flattening of the activity curve in the top layers. While this flattening is overestimated using the exponential sedimentation rate, it is slightly underestimated on the basis of an exponential sediment density.

Although the model is based on steady-state mixing and sedimentation parameters, it would be fully capable of accepting a time-dependent input in the form of fluxes of radioactive or non-radioactive substances reaching the

sediments, and make predictions for the resulting distributions in the sediments of these substances as a function of time.

References

1 S. Krishnaswami, D. Lal, J.M. Martin and M. Meybeck, Geochronology of lake sediments, Earth Planet. Sci. Lett. 11 (1971) 417-414.

2 M. Koide, A. Soutar and E.D. Goldberg, Marine geochronology with ^{210}Pb, Earth Planet. Sci. Lett. 14 (1972) 442-446.

3 J.A. Robbins and D.N. Edgington, Determination of recent sedimentation rates in Lake Michigan using Pb-210 and Cs-137, Geochim. Cosmochim. Acta 39 (1975) 285-304.

4 J.A. Robbins, J.R. Krezoski and S.C. Mozley, Radioactivity in the sediments of the Great Lakes: post-depositional redistribution by deposit-feeding organisms, Earth Planet. Sci. Lett. 36 (1977) 325-333.

5 B.P. Glass, Reworking of deep-sea sediments as indicated by the vertical dispersion of the Australasian and Ivory Coast microtektite horizons, Earth Planet. Sci. Lett. 6 (1969) 409-415.

6 B.P. Glass, R.N. Baker, D. Storzer and G.A. Wagner, North American microtektites from the Caribbean Sea and their fission track age, Earth Planet. Sci. Lett. 19 (1973) 184-192.

7 W.H. Berger and G.R. Heath, Vertical mixing in pelagic sediments, J. Mar. Res. 26 (1968) 134-143.

8 E.D. Goldberg and M. Koide, Geochronological studies of deep-sea sediments by the ionium/thorium method, Geochim. Cosmochim. Acta 26 (1962) 417-450.

9 N.L. Guinasso, Jr. and D.R. Schink, Quantitative estimates of biological mixing rates in abyssal sediments, J. Geophys. Res. 80 (1975) 3032-3043.

10 Y. Nozaki, Distributions of natural radionuclides in sediments influenced by bioturbation, J. Geol. Soc. Japan 8 (1977) 699-706.

11 Y. Nozaki, J.K. Cochran, K.K. Turekian and G. Keller, Radiocarbon and ^{210}Pb Distribution in submersible-taken deep-sea cores from project FAMOUS, Earth Planet. Sci. Lett. 34 (1977) 167-173.

12 J.A. Robbins, D.N. Edgington and A.L.W. Kemp, Comparative ^{210}Pb, ^{137}Cs, and pollen geochronologies of sediments from Lakes Ontario and Erie, Quat. Res. 10 (1978) 256-278.

13 T.J. Goreau, Quantitative effects of sediment mixing on stratigraphy and biogeochemistry: a signal theory approach, Nature 265 (1977) 525-526.

14 E.R. Christensen and N.K. Chien, Arsenic, mercury and other elements in dated Green Bay sediments, Internat. Conf. on the Management and Control of Heavy Metals in the Environment, London, England, Conf. Proc. CEP Consultants, Edinburgh, UK (1979) 373-376.

15 M.C. Potter, Mathematical Methods in the Physical Sciences (Prentice-Hall, Englewood Cliffs, N.J., 1978).

16 S. Krishnaswami and D. Lal, Radionuclide limnochronology, in: Lakes: Chemistry, Geology, Physics (Springer, New York, 1978).

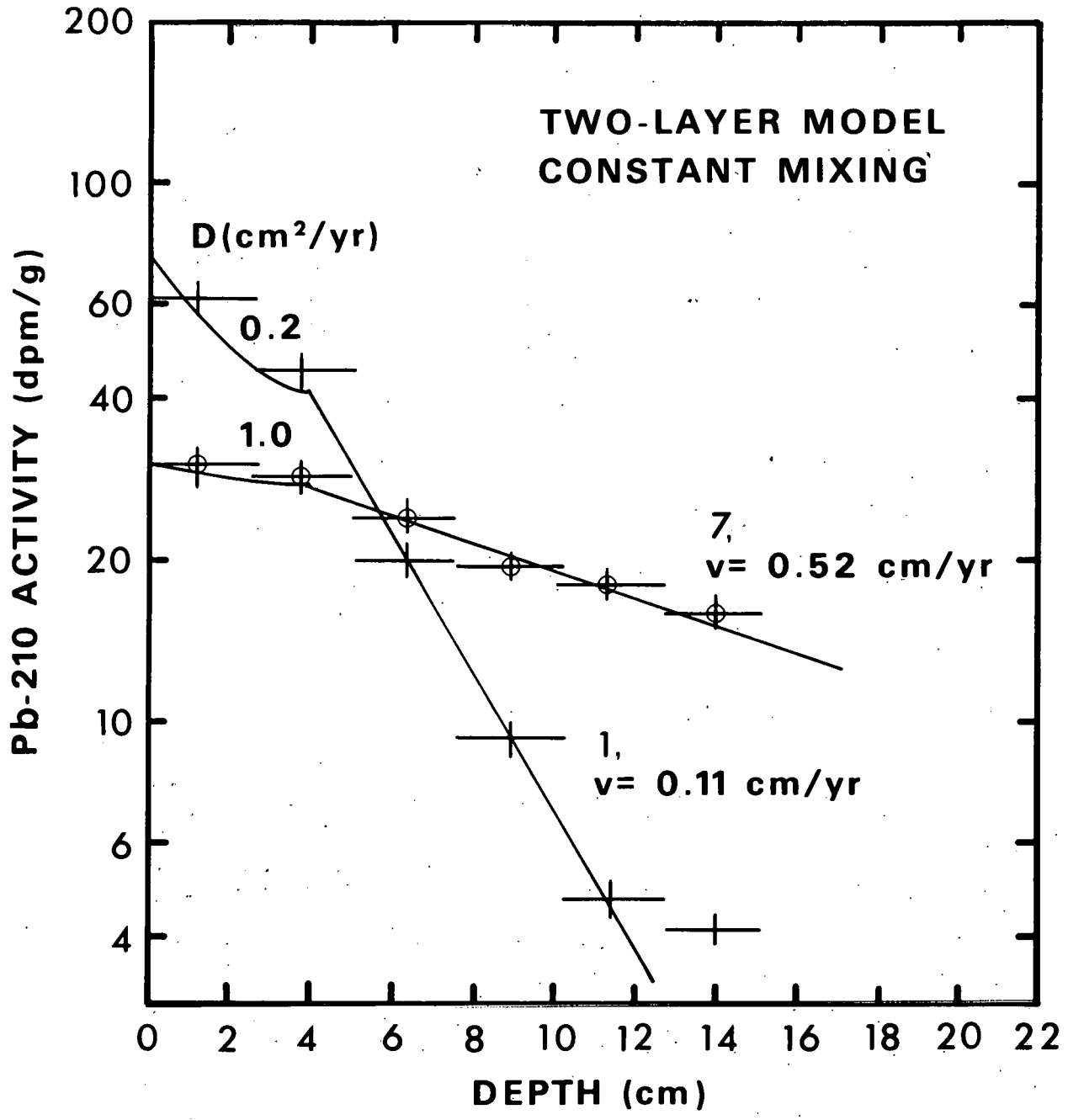


Fig. 1. Pb-210 activity vs. depth in Green Bay cores 1 and 7. Measured activities are compared to a two-layer model with constant mixing in the upper layer of thickness 4 cm.

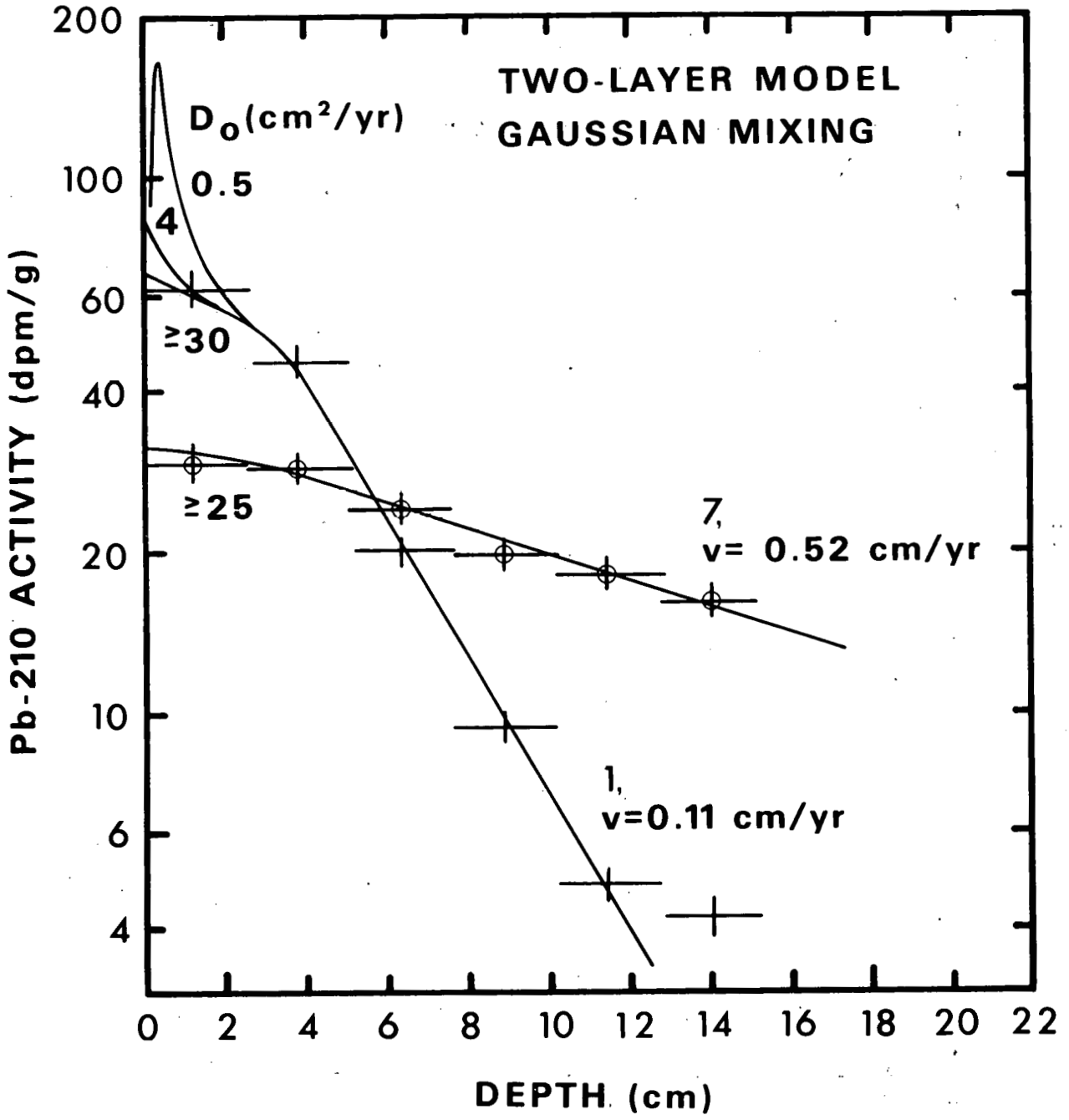


Fig. 2. Pb-210 activity vs. depth in Green Bay cores 1 and 7. Measured activities are compared to a two-layer model with gaussian mixing in the upper layer of thickness 4 cm.

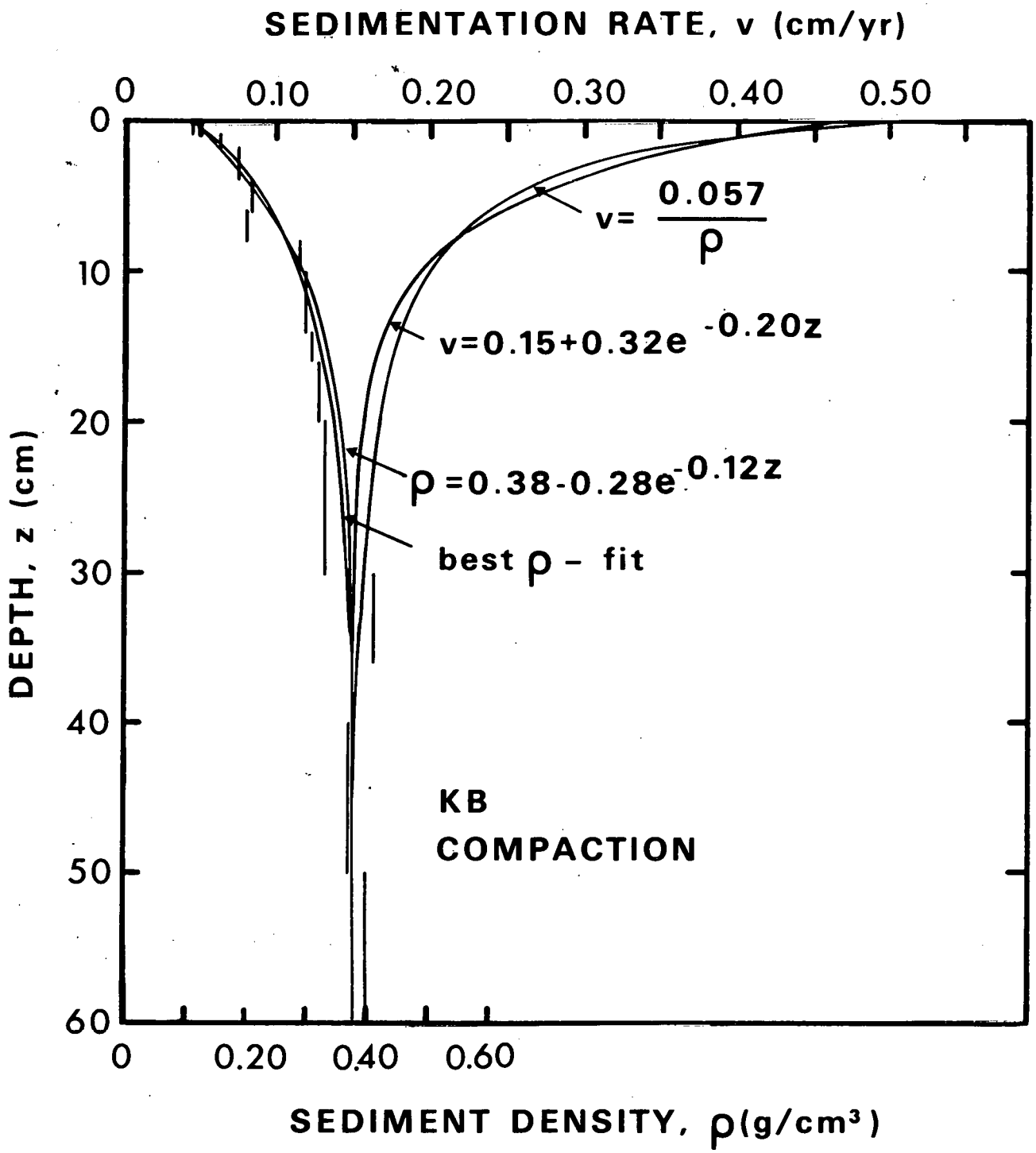


Fig. 3. Sedimentation rate and sediment density vs. depth based on cumulative weight data for core KB from Lake Ontario [12].

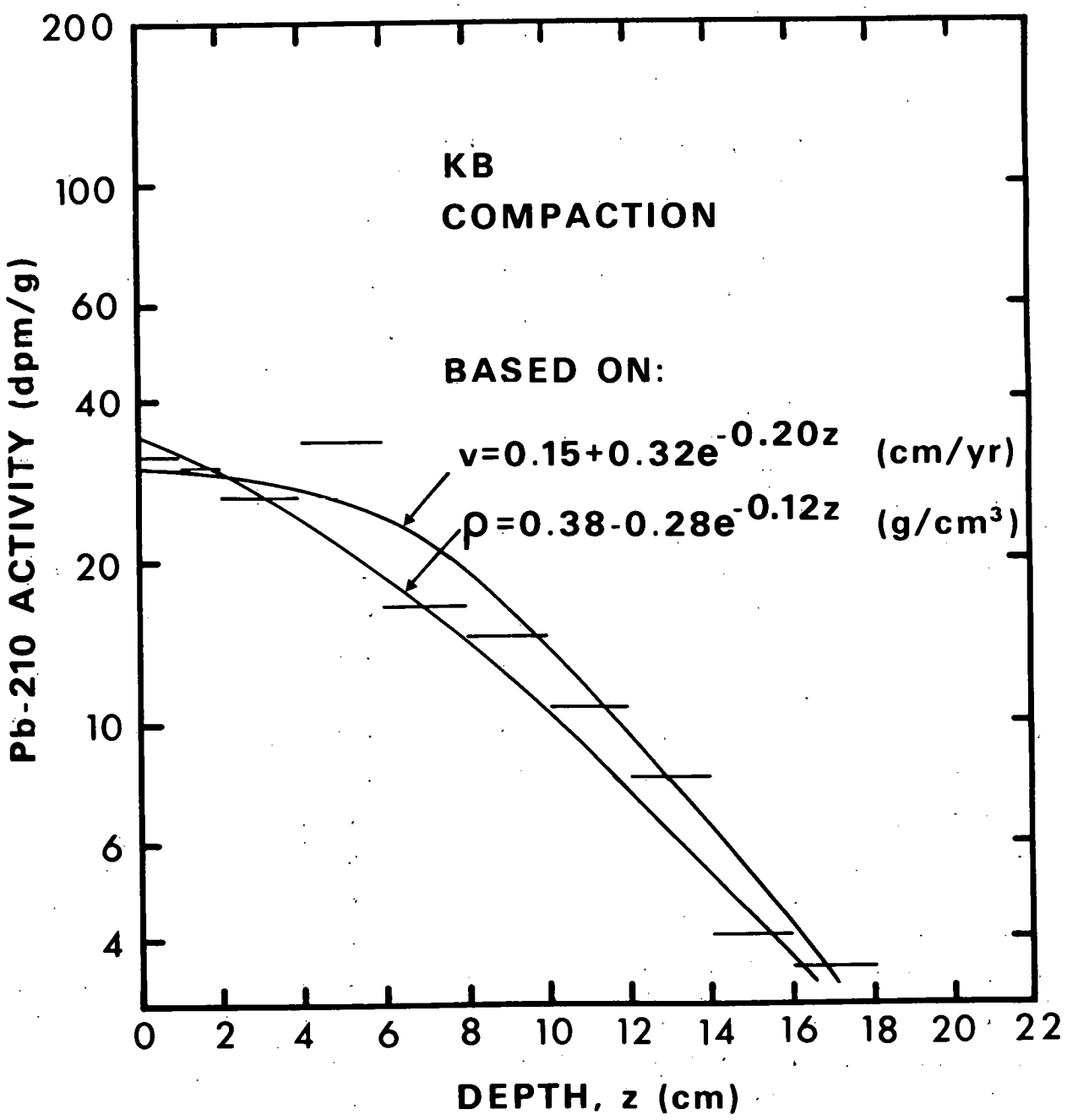


Fig. 4. Excess Pb-210 activity vs. depth in Lake Ontario core KB. Measured activities [12] are compared to a compaction model based on exponential sedimentation rate and sediment density, respectivley .

ELEMENTAL ANALYSIS BY PIXE OF ENVIRONMENTAL SAMPLES OF THE BRAZILIAN CERRADO*

A.S. Paschoa, G.B. Baptista, E.C. Montenegro, C.V. Barros Leite and T.L. Cullen

Pontifícia Universidade Católica do Rio de Janeiro, Depto. de Física, C.P. 38071, Rio de Janeiro, RJ 22453, Brasil

ABSTRACT. A vast region in the brazilian central plateau is characterized by a flora denominated Cerrado and a somewhat peculiar fauna. An area of about 13 km^2 in this region is maintained as an ecological reserve. A number of scientists, including biologists, chemists, geologists, botanists and physicists are involved in several research projects in this ecological reserve. The present paper deals only with the contribution to the study of soil and particulate matter suspended in natural springs and rainwater of the area, by using the PIXE technique as an analytical tool to determine the metal concentrations in these materials. The concentrations of titanium, zinc, chromium, copper and calcium in relation to iron have been determined in samples of soil and suspended materials in springwater to serve as a basis for future comparisons with similar samples from several origins. Variations in the concentrations of potassium, calcium, titanium, chromium, nickel, copper and zinc in relation to iron have been monitored in the suspended matter found in rainwater collected within the area.

* Work supported by Fundação Instituto Brasileiro de Geografia e Estatística (IBGE), International Atomic Energy Agency (IAEA), Conselho Nacional de Desenvolvimento Científico e Tecnológico (CNPq) and Financiadora de Estudos e Projetos (FINEP).

I. INTRODUCTION

A vast region in the brazilian central plateau is characterized by a flora denominated Cerrado and a somewhat peculiar fauna. An area of about 13 km^2 in this region, the Roncador Ecological Reserve (RER), is maintained by the Fundação Instituto Brasileiro de Geografia e Estatística (IBGE). The geographical position of RER in relation to the brazilian territory is indicated in the map presented in the upper part of Figure 1. The RER is located at about 50 km south of Brasília, the political capital of Brazil. The RER is removed from any industrial areas and human conglomerates, and is regarded as a non-developed area which has not been used thus far for grazing and agricultural purposes. Besides that, the RER can be viewed as a relatively non-polluted area, at least as far as local environmental pollutants are concerned. Accordingly, the RER seems to have the potential to be used as a convenient baseline for comparative studies on air and water pollution and environmental contamination. A number of investigational groups, including biologists, botanists, chemists, geologists and physicists are involved in several research projects related to the RER area. Classification of vegetal and animal species of the Cerrado has been undertaken by some of these investigational groups.

The present paper deals only with the contribution to the study of soil and particulate matter suspended in natural springs and rainwater of RER. The PIXE (Particle Induced X-Ray Emission) technique was used as a tool to investigate the metal concentrations in samples of soils and particulate matter suspended in water collected in the RER area. The concentrations of titanium, zinc, chromium, copper and calcium in relation to iron have been determined in samples of soil and suspended materials in springwater to serve as a baseline for future comparisons with similar samples from several origins. Variations in the concentrations of potassium, calcium, titanium, chromium, nickel, copper and zinc in relation to iron have been monitored in the suspended matter found in rainwater collected within the RER area.

The use of the PIXE technique for the analysis of environmental samples of the brazilian Cerrado is interesting in that there is the possibility to determine simultaneously the concentrations of heavy metals and the calcium content of soils.

II. SAMPLE COLLECTION AND ANALYSIS

Soil samples and one species of orchard leaves were collected from the sites indicated by numbers from 1 to 7 in Figure 1. The description of the sampling sites appears in Table I. Samples of water from natural springs were also collected whenever available near the soil collection sites. Soil and springwater samples are identified by S and SW in Tables I and II respectively. Samples of rainwater were collected using a plastic funnel, 50 cm diameter in the larger openning of the hollow cone, placed at 7 meters high in the site indicated as "tower" in Figure 1. Each rainwater sample corresponds to one month accumulation period starting in August 1978.

The soil samples were prepared by simply dissolving small amounts of soil in bi-distilled water and then dripping on a Nuclepore filter. The samples of suspended matter in water were prepared by filtering 100 ml of water through a Nuclepore filter, 0.4μm pore size, to collect the material in suspension. All samples were framed in aluminium rings 1.2 cm diameter to become suitable to be irradiated in a scattering chamber described elsewhere[1].

The target samples were irradiated with a 2.0 MeV proton beam produced in a 4 MV Van de Graaff accelerator. The overall experimental arrangement was already described in an earlier paper[1]. The X-rays emitted by the target-sample upon proton bombardment reach a Si(Li) detector after crossing a mylar window 4 mm diameter. The detector is placed at a 90^{o} angle with respect to the proton beam. The characteristics of the proton beam and its diffusing system is described in detail in another paper[2].

The uncertainties involving the elemental quantitative analysis by PIXE have been discussed elsewhere[3], mainly as far as the non-uniformity of the particle beam and the target sample thickness are concerned. Although the system is calibrated for quantitative analysis[1], in this paper only the relative concentrations in relation to iron rather than the absolute elemental mass concentrations are reported. The iron contents of the samples analysed are in the order of percent and can be easily determined through more conventional methods.

The mass, M_i, of an element i present in a sample can be evaluated through PIXE analysis by using the following expression[1]:

$$M_i = K \frac{A_i \; S \; N_{xi}}{\frac{\Omega}{4\pi} \varepsilon_i \; \sigma_{xi}(E) Q} \qquad (1)$$

where K is a factor related to the units used; A_i is the atomic mass of an element i; S is the beam area, defined by the collimator; N_{xi} is the number of observed characteristic X-rays of an element i; Ω is the solid angle defined by the detector; ε_i is the detection efficiency of the system for characteristic X-rays of an element i; $\sigma_{xi}(E)$ is the cross section, for an element, for X-ray production by protons with energy E; and Q is the integrated beam current.

Thus, the concentration C(i/Fe) for an element relative to that of iron in a target sample can be readily determined by the expression

$$C(i/Fe) = \frac{(A_i/A_{Fe})(N_{xi}/N_{xFe})}{(\varepsilon_i/\varepsilon_{Fe})(\sigma_{xi}/\sigma_{Fe})} \qquad (2)$$

III. RESULTS AND DISCUSSION

The results obtained for the concentrations relative to iron of the elements detected in all samples analysed are shown in Tables II, III and IV. Table II shows, on the one hand, that the soils from RER seem to be low in calcium, which was detected in only one sample with 5.5% relative concentration to iron while on the other hand, the concentrations of titanium relative to iron in the same soils range from 7.5 to 22%. This indicate a high concentration of titanium in soils of RER, particularly near the Monjol riverhead where there is also the highest zinc concentration in relation to iron.

Figure 3 shows as an illustration, a X-ray spectrum of a soil sample from RER. Table III allows one to observe that the relative concentration of titanium to iron in the suspended matter in waters of the Monjol's riverhead is 18% which, as expected, is nearly the same relative concentration found in the soil sample from the same area. Accordingly, the X-ray spectrum of suspended matter in the springwater sample from the Monjol riverhead, with conspicuous K_α and K_β titanium peaks, is shown in Figure 4. Curious, and thus far unexplained satisfactorily, is the fact that in the samples of suspended matter in waters from the riverheads of the Taquara and Roncador brooks the titanium is absent, while the relative concentra-

tions of titanium to iron in the soils collected near these sites are, respectively, 16 and 20%.

The concentrations of chromium relative to iron in the analysed soil samples varies from 0.28 to 0.55%, however, this element is not present in the samples of suspended matter in waters from the riverheads of the brooks Taquara, Monjol and Roncador.

The concentrations of copper relative to iron in the analysed soil samples are encountered in a narrow range varying from 0.20 to 0.55%, while the relative concentrations of the same element reaches 25 and 27% in the samples of suspended matter in waters from the riverheads of the Taquara and Roncador, respectively. Here it is interesting to observe from Table III that nickel and copper are high in the samples where titanium is not present, while titanium is high in the sample without nickel and low copper. Further studies are necessary to explain these observed differences.

Table II also shows that the concentrations of zinc relative to iron in the soil samples present a wide range from 0.32 to 27%. The highest concentration occurs in the soil sample collected near the Monjol riverhead while no zinc was detected in the samples of suspended matter in water collected in this site.

Table IV and Figure 2 show the relative elemental concentration in suspended matter in rainwater. The relative concentrations of zinc to iron in samples of suspended matter in rainwater present a significant variation for the period of sampling. The highest concentration appears in the sample corresponding to the period from October 17 to November 17, 1978. One may expect that the zinc found in the suspended matter in rainwater comes from the soil dust of the region suspended in the air and carried by the rain fall. The variation of the relative concentration of copper to iron in the suspended matter in rainwater follows a pattern similar to that of zinc, as can be seen in Figure 2. The variety of elements detected in suspended matter in rainwater is illustrated by Figure 5.

Another interesting aspect to be further investigate is the apparent constant relative concentration of titanium to iron in the suspended matter in rainwater that can be observed in Figure 2.

IV. CONCLUDING REMARKS

The limited data presented here constitutes an illustration on how the PIXE technique can be applied as a helpful investigatio

nal tool to examine peculiar aspects of local soils. The confirmation in Table II of the property that low calcium soils tend to have relatively high concentrations of heavy metals[4] serves to exemplify the applicability of PIXE in the study of soils. The PIXE technique offers an important contribution in the understanding of the ecological aspects of plant nutrition. Of course, there is still a long way to go in the study of floras which are characteristic of soils containing high concentrations of heavy metals. However, the high amount of titanium present in the soil samples from RER makes that area of the brazilian Cerrado a potential candidate to host a unique flora occurring naturally, as a result of the characteristics of the local soil and weathering.

A successful study in the RER area will have to be supplemented with a variety of additional data, as for example: local pluviometric precipitation; variations in riverflow; local micrometeorological studies including short and long term variations of vertical mixing and wind direction, geological formation, determination of pH and its variation with soil composition, etc.

REFERENCES

1. Paschoa A.S., E.C. Montenegro, W. Margulis, A.G. de Pinho, C.V. Barros Leite, and G.B. Baptista (1977). In Proceedings of the Third International Conference on Nuclear Methods in Environmental and Energy Research. (James R. Vogt, editor), CONF. 771072, 21-48.

2. Montenegro E.C., G.B. Baptista, C.V. Barros Leite, A.G. de Pinho and A.S. Paschoa (1979) Nuclear Instruments and Methods, 164, 231-234.

3. Montenegro E.C., G.B. Baptista, A.S. Paschoa and C.V. Barros Leite (1979) Nuclear Instruments and Methods, 159, 153-156.

4. Epstein E. (1971) Mineral Nutrition of Plants: Priciples and Perspectives. John Wiley & Sons, Inc. 358.

Table I. Description of the sampling sites.

1 - Taquara riverhead.
2 - Thick Cerrado - Experimental site of the reserve.
3 - Thin Cerrado.
4 - Prairie.
5 - Sciatic forest - Near the Roncador river.
6 - Monjol riverhead.
7 - Roncador riverhead.

Table II. Relative elemental concentration in soil (element/iron).

Sample	Concentration	Ca $\times 10^{-2}$	Ti $\times 10^{-1}$	Cr $\times 10^{-3}$	Cu $\times 10^{-3}$	Zn $\times 10^{-2}$
S-1		-	1.6	5.0	-	-
S-2		-	0.75	-	5.5	1.1
S-3		-	0.76	4.3	5.1	0.33
S-4		-	1.2	2.8	2.1	-
S-5		-	1.3	4.4	2.5	-
S-6		-	2.2	0.53	-	27
S-7		5.5	2.0	3.8	3.1	0.32

Table III. Relative elemental concentration in suspended matter in springwater (element/iron).

Sample	Concentration	Ti $\times 10^{-1}$	Ni $\times 10^{-1}$	Cu $\times 10^{-1}$
SW-1		-	4.3	2.5
SW-6		1.8	-	0.06
SW-7		-	1.3	2.7

Table IV. Relative elemental concentration in suspended matter in rainwater: (element/iron).

Sampling period	Concentration	K $\times 10^{-2}$	Ca $\times 10^{-2}$	Ti $\times 10^{-3}$	Cr $\times 10^{-3}$	Cu $\times 10^{-3}$	Zn $\times 10^{-3}$
08/03-09/06		5.6	1.8	12	3.1	3.9	4.4
09/06-10/17		-	14	8.1	4.7	6.9	27
10/17-11/17		-	-	-	-	66	69
11/17-12/17		-	-	16	8.4	8.2	29
12/18-01/17		-	-	7.3	12	18	38
01/18-02/20		-	-	11	-	3.0	10

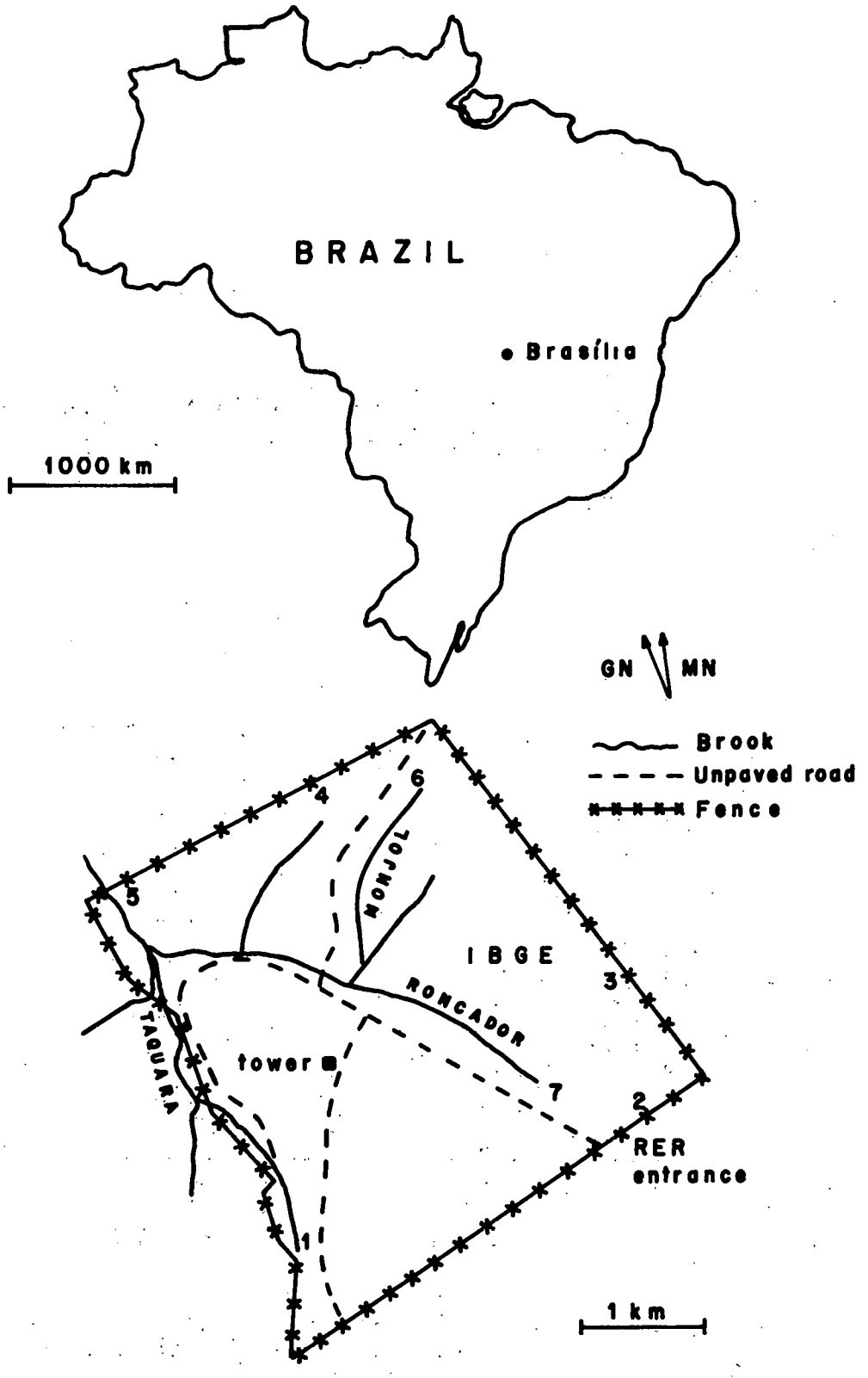


Figure 1 Upper-part - Contour map of Brazil, indicating the political capital, Brasilia; lower-part - sampling sites in the RER.

---- M^{Ti}/M^{Fe}; —— M^{Zn}/M^{Fe}; **** M^{Cr}/M^{Fe};
×××× M^{Cu}/M^{Fe}; '''' M^{Ca}/M^{Fe}; oooo M^{K}/M^{Fe}.

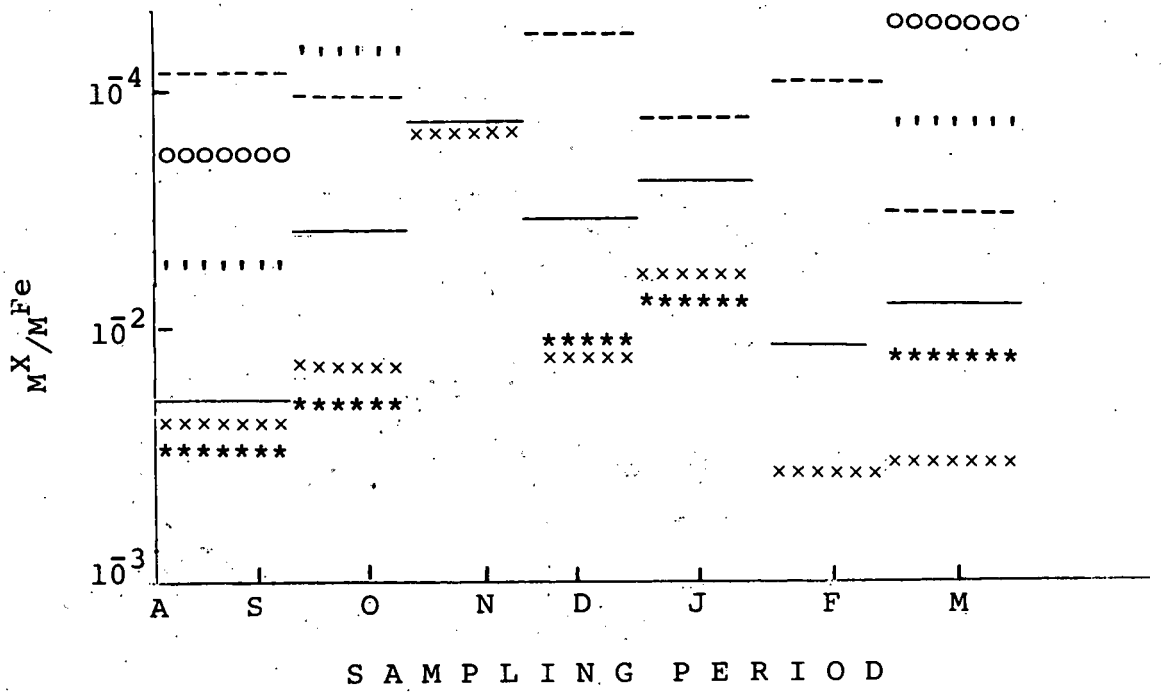


Figure 2 Relative elemental concentration in suspended matter in rainwater (element/iron)

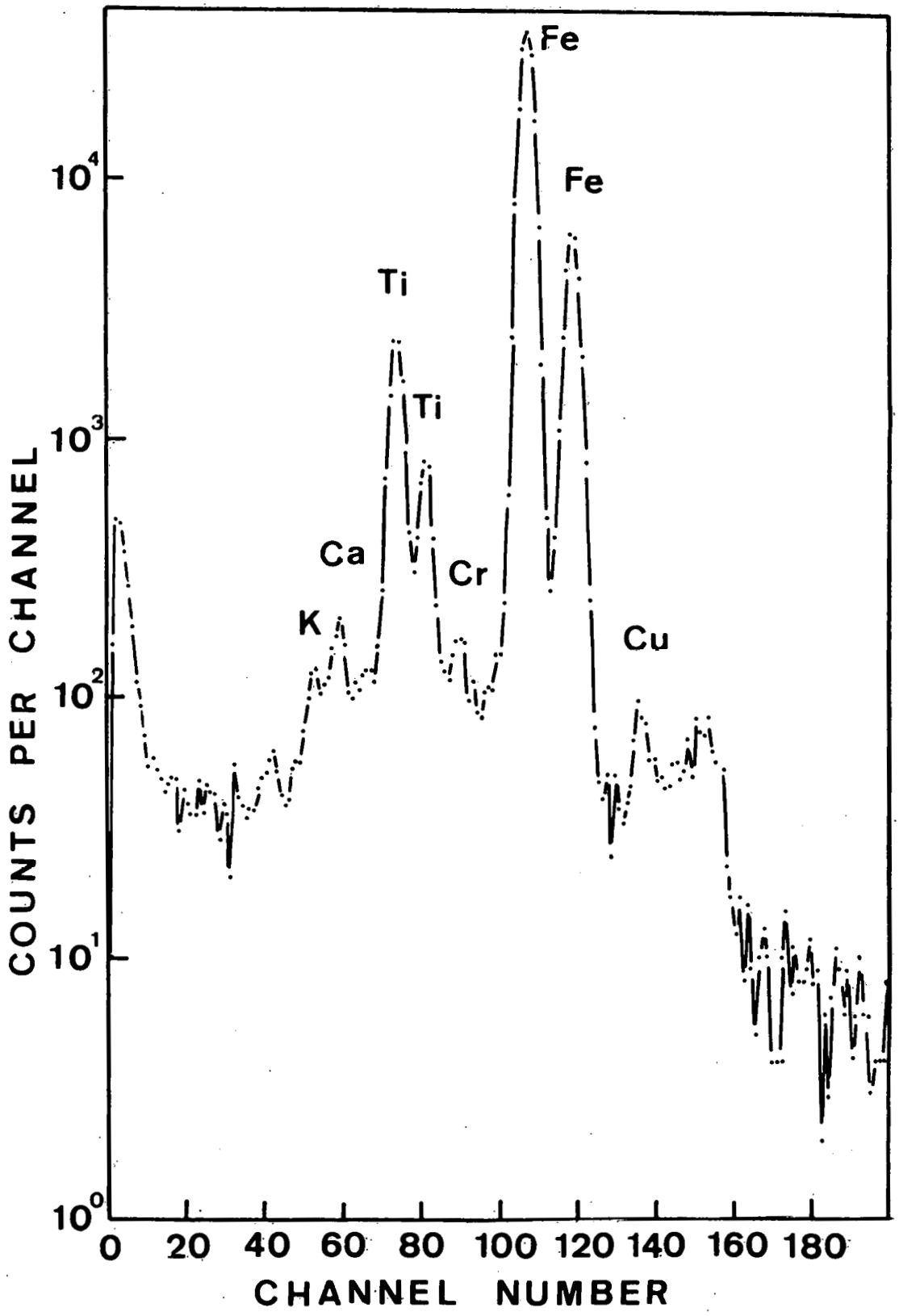


Figure 3 X-ray spectrum of soil sample from RER.

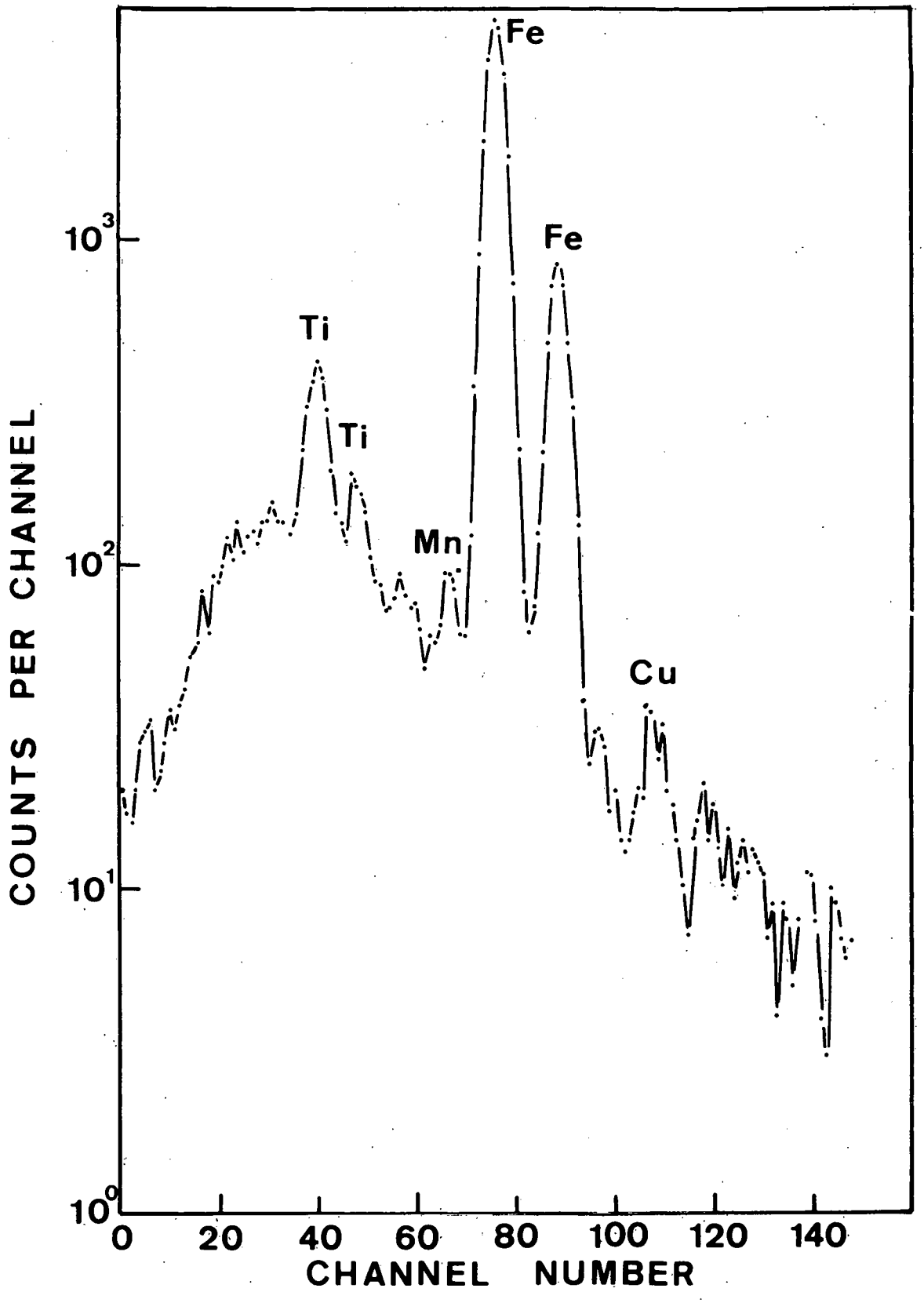


Figure 4 X-ray spectrum of suspended matter in the springwater sample from the Monjol riverhead.

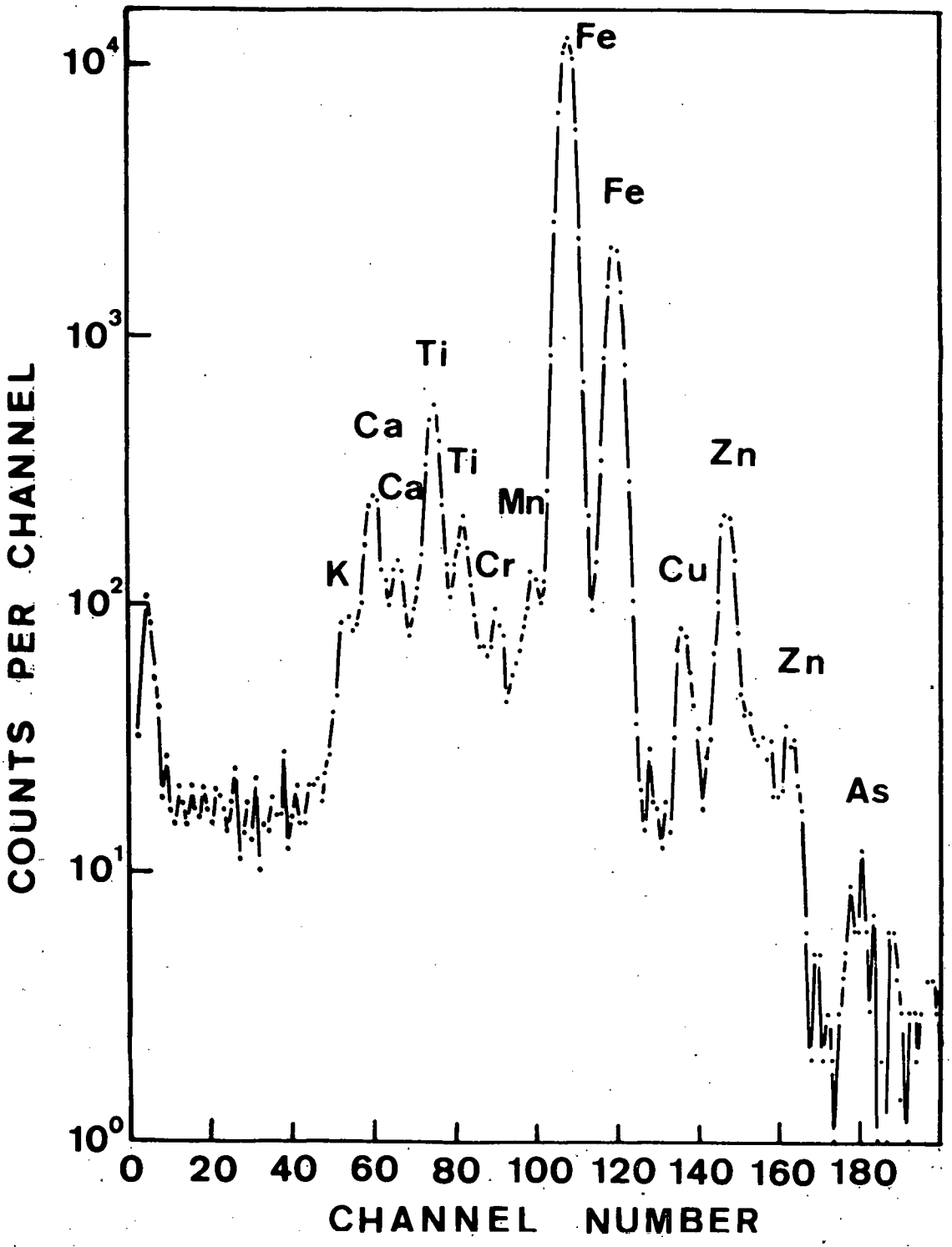


Figure 5 X-ray spectrum of suspended matter in rainwater sample from RER.

Multielement Analysis of Soil of a Sewage-Farm by Photon and Neutron Activation Analysis Using Waste Incineration Ash as Reference Material

B.F. Schmitt, C. Segebade, H.-U. Fusban
Bundesanstalt für Materialprüfung (BAM)
Unter den Eichen 87, D-1000 Berlin 45
F.R. Germany

Summary

Soil samples from a waste water cleaning facility in Berlin have been analyzed using several activation analysis methods. 43 elements have been determined by instrumental high energy photon activation analysis, instrumental thermal neutron activation analysis and 14 MeV-neutron activation analysis. Conventional gamma ray spectroscopy and low energy photon spectroscopy have been applied for product activity measurement. It has turned out that these methods in combination offer a large spectrum of analytical information. Fly ash of a waste incineration facility in Berlin has been used as a reference material. This ash has been found to be suitable particularly for environmental analyses, since toxic elements are present in comparably high concentration levels. Both the preparation of this multielement reference material and its application for the soil analysis are discussed.

1. Introduction

At many places of the world, especially in regions with high density of population and high level of industrialisation, the ground water level drops by the consumption of household and for industrial purpose such as cooling or cleaning. Seasons with low precipitation intensify this phenomenon. One consequence of this development is the shortage of drinking water. Therefore one tries to elevate the ground water level by an enrichment using surface water of rivers or lakes. This procedure is surely the cheapest way to convert more or less polluted surface water into drinking water by the cleaning effect of soil by filtering, precipitation, adsorption or ion exchange.

The aim of the investigations presented in this paper is threefold: Firstly, analyses were performed in order to collect detailed information about the elemental composition and especially the minor and trace element patterns of the soils under investigation with respect to many parameters. Secondly, it was intended to test the applicability of two of the methods used to environmental analyses in general (fNAA and PAA). Thirdly, the applicability of waste incineration ash as a multielement reference material was investigated. This work was performed within a large-scale research project about the chemical exchange capacity of soils charged by highly polluted urban and industrial waste wa-

ters [1]. The behaviour of components which are injurious to health were emphasized, and hence analysis methods had to be applied, which are suitable for fast, accurate and precise determinations of these elements.

2. The origin of the soil samples

The North German Low Plain is one part of a region of glacial end moraines which ranges from Russia through Poland to the North Sea. The soil of this region is characterized by a high content of sand with occasional islands of loess or loam. To determine the retaining quality of a soil sewage-farms are the most suitable objects. Therefore, the sewage-farm Berlin-Karolinenhöhe was selected for detailed investigation.

Between 1874 and 1909 the city of Berlin laid out 8,500 hektars for sewage-farms for daily 400,000 m^3 of waste water. The sewage-farm Karolinenhöhe is running since 1900. The charge before World War II was about 7 m^3/m^2 per year and after the war the charge rate dropped to 2 $m^3/(m^2 \cdot a)$. Since 1967 only one section has been operating.

In cooperation with the Federal Health Institute (BGA) and the Geochemical Institute of the Free University of Berlin four groups of sewage-farm soil samples, taken from different locations and depths, were analyzed. Samples were dried at 105 °C for 24 h and then ground with a ball mill to a particle size of $\leq$ 100 µm.

3. Analysis methods

Analyses were performed using instrumental methods exclusively. Since large amounts of sample material were available (> 50 g), major and some of the minor constituents could be analyzed by 14 MeV-neutron activation analysis (NAA) and high energy bremsstrahlung photon activation analysis (PAA). Using these methods it was possible to analyze following elements: Na, Mg, Al, Si, Cl, K, Ca, Sc, Ti, Cr, Mn, Fe, Co, Ni, Cu, Zn, Ga, As, Se, Br, Rb, Sr, Y, Zr, Nb, Mo, Ag, Cd, Sn, Sb, I, Cs, Ba, La, Ce, Nd, Sm, Eu, Yb, Hf, Ta, W, Pt, Au, Hg, Tl, Pb, Th, U.

4. Activation procedures

Activation with fast neutrons

30 g of sample material were filled into a polyethylene vial. A copper disc with 5 cm diameter and 0.5 mm thickness served as a flux monitor which was fixed to the irradiation vessel. Irradiations were carried out with a SAMES d,T neutron generator [2]. Irradiation time was 400 s, the measured flux density was $5 \cdot 10^8$ cm^{-2} s^{-1}. After irradiation the flux monitor was removed and the sample was measured with a coaxial Ge(Li) high resolution gamma detector. The properties of the spectrometer used will be described below. The very short-lived product nuclides ($T < 2$ m) were allowed to decay within a cooling period of 5 m. The nuclear reactions used for analysis are presented in table 1. Samples are measured twice; activities with half-lives of < 10 m were counted during the first measuring period of 5 m. Product nuclides with half-lives $\geq$ 10 m were measured then during a counting time of 50 m. The spectra were stored on a magnetic disc and processed as described below. The ^{62}Cu activity of the flux monitor was allow-

ed to decay to zero. The ^{64}Cu activity induced by the reaction ^{65}Cu (γ,n) ^{64}Cu was then counted with a NaJ(Tl) crystal detector connected with a single channel analyzer plus scaler measuring the 511 keV annihilation radiation of the isotope.

Photon activation analysis

The photonuclear reactions used for analysis are given in ref. [3]. 100 - 200 mg of sample material were wrapped into an aluminium foil sheet, transferred into an aluminium irradiation rabbit and then irradiated with 30 MeV-bremsstrahlung of the electron linear accelerator of the Bundesanstalt für Materialprüfung in Berlin. The mean electron beam current was set to 150 µA. The properties and physical parameters of the linac are described in detail in ref. [4]. After 2 hours bremsstrahlung exposure the sample was unwrapped, mixed with 300 mg Cellulose powder and pressed into a pellet with 20 mm diameter and 1 mm thickness. After a cooling period of 2 hours the product activities with half-lives of 0.5 to 25 hours were measured for 30 m. After a total decay period of 1 day the gamma spectrum of the long-lived product nuclides was collected within a counting time of 20 h. Thereafter, the low energy photon spectrum was taken with the planar intrinsic Ge-diode spectrometer described below. The particular advantages of low energy photon spectroscopy (LEPS) after photon activation was reported in detail in ref. [5,6]. The short-lived ($T < 30$ m) activation products were analyzed in a few cases only. A separate short-time irradiation ($t = 5$ m) was performed. The samples were then uncapsuled and transferred into small polyethylene vials. After a total cooling period of 5 - 10 m the sample was measured for 5 m using coaxial Ge(Li)-spectrometry.

Neutron activation analysis

100 mg of the sample material were prepared as done in the PAA procedure and irradiated with thermal neutrons of the research reactor BER II of the Hahn-Meitner-Institute for Nuclear Research in Berlin. The flux density was $7 \cdot 10^{12}$ cm^{-2} s^{-1}. After an irradiation period of 2 h and a decay time of 1 day samples were transferred into small polyethylene vials and measured with the coaxial gamma spectrometer described below. The reactions used for analysis are compiled in ref. [3].

5. Gamma- and LEP-spectrometry

High resolution semiconductor spectrometry exclusively was used for product activity measurements. The physical parameters of the detectors were as follows:

coaxial detector (ORTEC):

active volume:	50 cm^3
efficiency:	20 % of a 3" x 3" NaJ(Tl) crystal at 662 keV
resolution:	2.1 keV FWHM at 1333 keV

planar detector (intrinsic germanium, ORTEC):

active area:	500 mm^2
active thickness:	10 mm
resolution:	350 eV FWHM at 6 keV 600 eV FWHM at 122 keV

Gamma spectra were stored in 2048 channels of a 4096 channel pulse height analyzer (CANBERRA Ser. 80); 1024 channels were used for LEP-spectra storage. The counting geometry for both spectroscopy methods was as presented in fig. 1.

6. Data processing

Spectra were stored in a magnetic disc data storage unit. Peak integration, net peak area calculation, energy calibration and storage of energies and peak areas in special data files were performed with a semiautomatic interactive program using a Hewlett-Packard 64 K-computer (HP 21 MX) [7]. Peak assignment and concentration calculation were then performed using a separate program [8] printing out a complete results list.

7. Interferences

Caused by the large number of different nuclear reaction types various kinds of interference have to be considered, if activation is performed with high energy particles. These interferences have to be accounted for when using fNAA and especially in PAA [9,10, 11]. Interference calculation in soil analysis is described in detail in ref. [3].

8. Waste incineration ash as a reference material

Several years ago we searched for materials with which we would be able to check the analytical capacity of our electron linear accelerator. Fly ash of the combined urban and industrial waste incineration facility in Berlin-Ruhleben seemed to be suitable for analysis purpose. We analysed the fly ash for toxic elements and detected more than 50 elements. A batch of 10 kg was sieved, ground, sieved again and homogeneized. Within two years we analysed this material using different activation methods. We used the purest available elements or oxides with a stoichiometric composition as primary standards. For Cl, Br and I analysing we used NaCl, $NaBrO_3$ and $NaIO_3$ [12].

The waste incineration ash is an alumino-silicate with high contents of calcium and iron. The complete concentration list of all components detected is presented in table 3. We have used this ash as our internal reference material. It is suitable particularly for the analysis of silicate materials as ashes and soils, but also for dust analysis. Also other laboratories are interested in this reference material. So we have prepared a new batch of 100 kg in cooperation with BCR, Brussels. This batch will have another composition since the waste slightly changes its composition daily, but first analyses indicated that the content of toxic materials is as high as or higher than in our first batch. We hope that this material will be available in one or two years as a good RM for environmental analyses.

9. Sensitivity, accuracy and precision

The sensitivity of the presented analysis methods strongly depend on the nuclear parameters of the target nuclide, the nuclear reaction and the product nuclides under consideration. In the case of fNAA they generally are found in the milligram region [13]. In NAA and PAA sensitivity of micrograms to nanograms are achievable [6]. In ref. [6] a comparison of sensitivities of conventional

gamma spectroscopy and LEPS applied to PAA is presented.

Accuracy of the obtained values was determined by parallel analysis of different certified RMs (NBS-SRM 1571, NBS-SRM 1632, NBS-SRM 1633). The results generally were in satisfactory agreement with the certified or recommended values of the RMs. The precision data are presented in ref. [3]; 1 σ standard deviations generally ly between 4 and 12; they are calculated taking into account following influence factors:

1. the 1 σ standard deviation of the values based on the counting statistics;
2. a quasi-assumed deviation of a singly determined value caused by apparative parameters and systematically occuring errors.

The latter source of error was determined by multiple analysis of a self-prepared standard soil; this procedure was selected since each soil sample was analysed only once. It turned out that the precision data of the methods used generally did not differ significantly.

10. Results and discussion

Complete analysis data are given in ref. [3]. The first investigation was the analysis of bore-cores with a length of 14 m. In fig. 2 the relative concentration profile is shown for the elements silicon, chromium, iron, zinc and lead. The maximum value is set to a hundred percent. One can see the influence of the ground water level at about 10 m depth, where the concentrations of heavy metals decrease to low values. We did not find significant differences between soil of a forest area in the neighbourhood and the soil of the sewage-farm. In a second run we analysed samples of two digs of only 2 m depth with smaller distances from sample to sample. We analysed five samples of soil of the forest area and four samples of the sewage-farm. As shown in table 2 significant differences can be detected in the first 20 cm from the surface only. Significant enrichment can be stated for nickel, zinc, barium and lead. The values of arsenic show no differences between the charged and the virgin soil. The reason may be that we have low content of As in the waste water. Unfortunately there are no concentration data of toxic elements in the waste water available yet.

11. Cited literature

[1] Report on the research project 02WA 744 of the Institut für Wasser-, Boden- und Lufthygiene; activities until December 31, 1978

[2] R. Neider, P. Reimers, E. Santner, B.F. Schmitt, Atomwirtschaft 15 (1970), 382

[3] H.-U. Fusban, Ch. Segebade, B.F. Schmitt, Instrumental Multielement Activation Analysis of Soil Samples, in print

[4] P. Jost, P. Reimers, H.-P. Weise, BAM-BER 026 (1974)

[5] H.-P. Weise, Chr. Segebade, Journ. Radioanal. Chem. 37 (1977), 195

[6] Chr. Segebade, H.-P. Weise, ibidem 45 (1978), 209

[7] P. Reimers, H.-U. Fusban, "Fast Subroutines for Interactive Computer Programs in Activation Analysis" presented on the 5th Symposium on the Recent Developments in Activation Analysis, July 17 - 21, 1978, St. Catherine's College, Oxford, U.K.

[8] H.-U. Fusban, Chr. Appel, unpublished data

[9] Chr. Segebade, G.J. Lutz, H.-P. Weise, Journ. Radioanal. Chem. 39 (1977), 179
[10] A. Chattopadhyay, R.E. Jervis, Anal. Chem. 46 (1974), 1630
[11] Chr. Segebade, Journ. Radioanal. Chem. 43 (1978), 243
[12] H.-U. Fusban, Chr. Segebade, B.F. Schmitt, "Multielement Analysis of Waste Incineration Ash as a First Step to an Environmental Reference Material", Proceedings of the International Symposium on the Production and Use of Reference Materials, November 13 - 16, 1979, Bundesanstalt für Materialprüfung (BAM), D-1000 Berlin (in print)
[13] G. Erdtmann, Neutron Activation Tables, Verlag Chemie Weinheim, New York, 1976
[14] J.S. Hislop, "Photon Activation Analysis of Biological and Environmental Samples: A Review", Proceedings of the International Conference on Photonuclear Reactions and Applications, March 26 - 30, 1973, Asilomar Conference Grounds, Pacific Grove/California, U.S.A.

Table 1: Reactions used for 14 MeV-neutron activation analysis of soil samples

Element	Reaction	Half-life	E_γ [keV]	Interference*
Mg	^{24}Mg (n,p) ^{24}Na	15 h	1369, 2754	^{27}Al (n,α) ^{24}Na
Al	^{27}Al (n,p) ^{27}Mg	9.46 m	844, 1014	^{56}Mn (847)
Si	^{28}Si (n,p) ^{28}Al	2.246 m	1779	^{31}P (n,α) ^{28}Al
	^{29}Si (n,p) ^{29}Al	6.6 m	1273	
Ca	^{44}Ca (n,p) ^{44}K	22.2 m	1157	
Fe	^{56}Fe (n,p) ^{56}Mn	2.58 h	846, 1811	
Ba	$^{138}Ba(n,2n)^{137m}Ba$	2.55 m	662	

see ref. [11]

Element		0 – 5 cm	5 – 20 cm	20 – 50 cm	50 – 100 cm	100 – 200 cm
Ni	A	4	3	3	4	2
	B	27		0,8	4	5
Zn	A	40	119	190	27	6
	B	220		15	44	30
As	A	18	13	6	2	7
	B	11		2	2	2
Ba	A	350	370	320	460	310
	B	1200		170	240	150
Pb	A	23	15	27	12	29
	B	237		8	24	6

A: Soil of forest
B: Soil of sewage-field, irrigated 1900 – 1967
Distance A – B about 100 m

Table 2: Comparison of analysis results of sewage-farm and virgin soil

Table 3: Element concentrations in waste incineration fly ash; batch URM 1, given in µg/g or as indicated

Element	Concentration	S.D.	Element	Concentration	S.D.
C %	2.5	0.1	Rb	139	3
F %	0.15	0.03	Sr	778	38
Na %	1.65	0.04	Y	34	1
Mg %	1.80	0.07	Zr	152	10
Al %	8.28	0.07	Nb	15.9	0.7
Si %	14.00	0.07	Mo	24	2
P %	0.3	0.1	Ag	42	2
Cl %	1.28	0.02	Cd	250	30
K %	2.3	0.15	Sn %	0.324	0.015
Ca %	10.16	0.18	Sb	220	12
Sc	20	2	I	24	1
Ti %	0.710	0.001	Cs	16	1
Cr	379	13	Ba %	0.441	0.008
Mn %	0.102	0.007	Ca	34	1
Fe %	7.89	0.16	Ce	56	3
Co	38	1	Nd	44	5
Ni	126	4	Sm	6	1
Cu	769	70	Eu	0.23	0.03
Zn %	1.24	0.05 %	Tb	0.59	0.04
Ga	261	28	Yb	1.6	0.2
Ge	16.4	0.4	Lu	0.6	0.2
As	93	3	Hf	3.6	0.1
Se	22	3	Ta	1.85	0.14
Br	136	13	W	36	2
			Au	0.60	0.06
			Hg	0.27	0.01
			Tl	82	3
			Pb %	0.635	0.018
			Th	11.3	0.3
			U	4.2	0.2

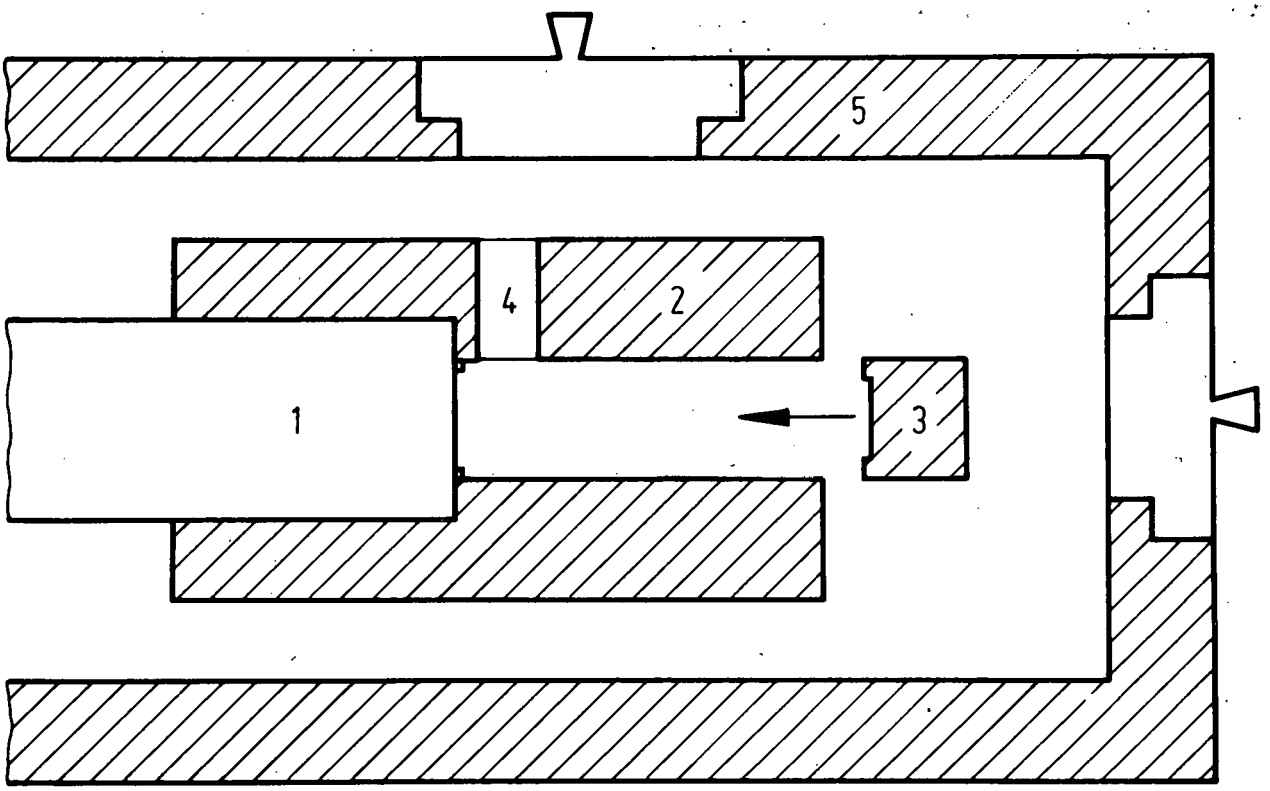


Fig. 1: Counting geometry for gamma (LEP)-spectroscopy

1: Detector housing
2: Fe-(Al-) collimator
3: Movable sample holder
4: Opening for test tube sample container
5: Pb-(Fe-) shielding

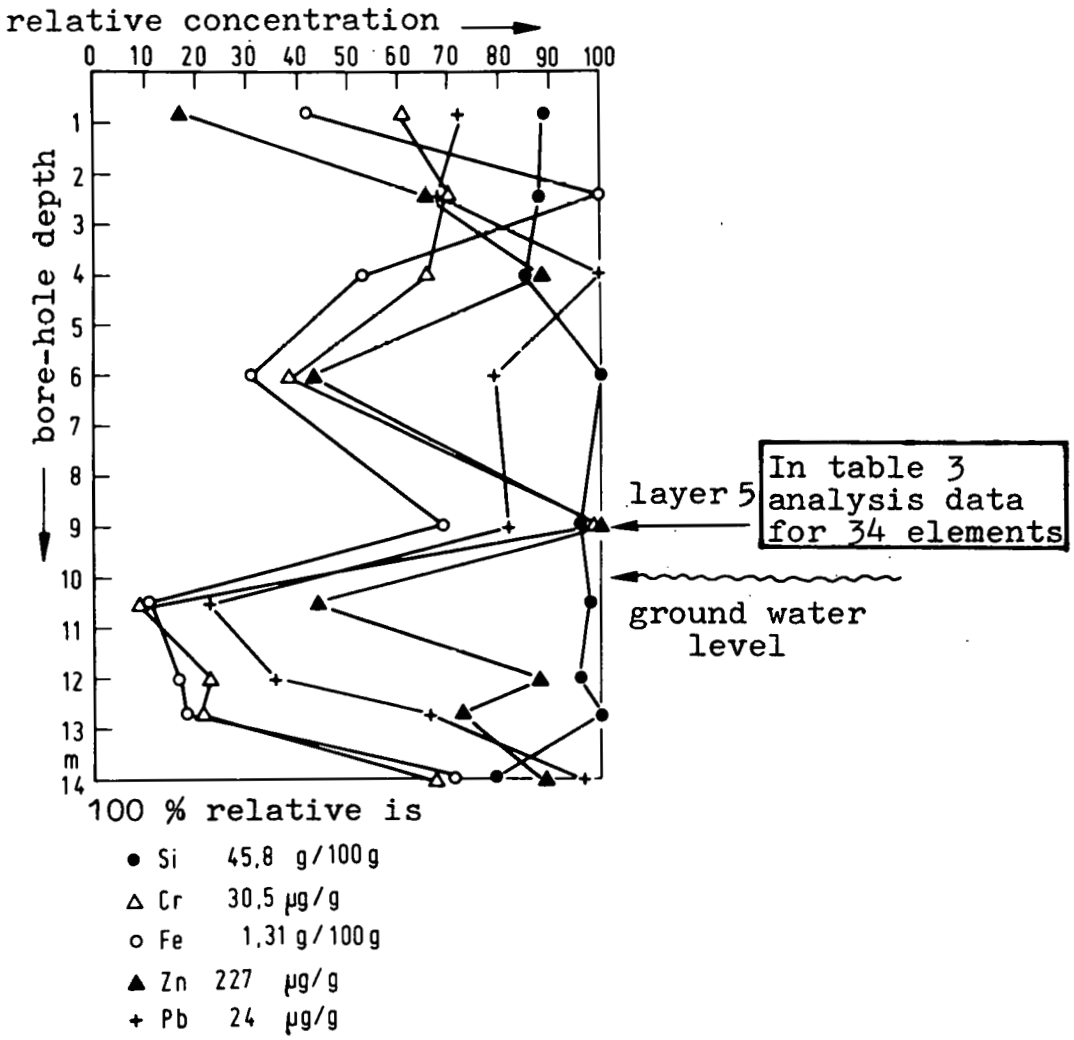


Fig. 2: Concentration profile of a 14 m bore-core

Study Of Heavy Elements (Cd, Hg and Se) In The Aquatic Environment Around Bombay By Radiochemical Neutron Activation Analysis.

R. Ganesan, P.K. Shah and Z.R. Turel,
Department of Nuclear Chemistry
and
B.C. Haldar
Environmental Chemistry Laboratory,
The Institute of Science,
Bombay-400032, INDIA.

ABSTRACT

Hg, Cd and Se in water, sediment and tissues of crabs collected from five locations around Bombay have been measured by radiochemical neutron activation analysis. The results are discussed to throw light on the heavy metal contamination of the aquatic environment.

INTRODUCTION

Some of the coastal areas of Bombay are receiving idustrial wastes rich in toxic heavy metal pollutants, which may lead to depletion of marine resource and pose a health hazard problem. It is, therefore considered worthwhile to employ radiochemical neutron activation analysis to measure the concentrations of Hg, Cd and Se in water, sediments and crustaceans from locations such as Nariman Point (NP), Worli (W), Mahim Creek (MC), Versova (V) and Thana Creek (TC) around Bombay.

EXPERIMENTAL

Sampling: All collections were made from a distance of 1-3 km. from the shoreline under the condition of low tide. Samples of water were collected in polyethylene bottles cleaned by treating with a dilute solution of nitric acid and then with 0.05M $K_2Cr_2O_7$ solution and washing with deionized water. Conc. HNO_3 was added to lower the pH of the water to 4. Water samples when received at the laboratory, were filtered through Whatman 41 filter paper and stored at 4^oC. It was tested to find out whether any of the three elements being analyzed were released from the filter paper. None of these elements were detected in the blank run. Analysis of water samples was completed within 72 hours of their collection.

The crustaceans were dissected after bringing each collection to the laboratory and each of the tissues (muscle, hepatopancreas and gills) of the same species was kept in pretreated polythene bags and preserved in a refrigerator. The samples were lyophilized, ground to a fine powder and used for analysis. Some of the animals were separated according to their size and sex prior to dissection. A 1-g. sample was used to determine the loss on weight at 110^oC.

Sediments were air dried at room temperature (26 ± 2^oC) before analysis. A 1-g. portion of the sediment from each location was dried at 110^oC in an air oven to find out its dry weight.

All analytical data were normalized to the oven-dry (110^oC) weight of the sample.

Chemicals and Reagents: Chemicals, solvents and reagents used were of A.R. grade. 1-amidino 2-thiourea (ATU) was prepared by the method given by Kurzer.[1] Carrier solutions of Cd, Se and Hg were prepared by diluting an appropriate aliquot of the stock solution with double distilled water. The strength of each stock solution was determined by the procedure given in Scott.[2]

Counting of Samples: Samples were counted on a Gamma-ray spectrometer in conjunction with a single-channel pulse-height analyzer and a 3.5 cm x 3.5 cm NaI(Tl) well-type detector.

Procedure for the Estimation of Se, Cd and Hg:

Irradiation: 2 quartz ampoules each containing 100 mg of tissue or sediment or 2 gm of water (evaporated to dryness by gentle heating) and an ampoule containing 20 µg of Cd, 10 µg of Se and 10 µg Hg standards were sealed at liquid nitrogen temperature. They were taken in an aluminium can and irradiated in

the CIRUS reactor of Bhabha Atomic Research Centre, Trombay at a thermal neutron flux of $5x10^{12}$-10^{13} n/cm^2/sec., for a duration of 4-8 days.

The irradiated sample was dissolved in 10 ml of aqua-regia in the presence of 4-20 miligram carriers of Se, Cd and Hg. The nitrous fumes were expelled by heating with 5 ml of concentrated HCl. 5 ml of conc. HCl and 5 ml of 2% ATU were added. The solution was stirred vigorously and chilled for 10 minutes. The precipitate of Se was centrifuged. It was washed with 10 ml of hot water, dissolved in 3 ml of aqua-regia in the presence of 1 mg of each of Cu, As, Cd, Hg hold-back carriers and the solution was evaporated to dryness after adding 5 ml of conc. HCl. The residue was treated with 5 ml of conc. HCl. 5 ml of 2% ATU was added and Se was precipitated. The precipitate was centrifuged, washed twice with (10 + 10 ml) hot water and then with 10 ml of alcohol, transferred to a weighed counting tube, dried at 110^{0}C, weighed and counted.

To the supernatant was added 5 ml of 2% ATU and the pH of the solution was made 7.5 with NH_3. The solution was boiled for two minutes and centrifuged. The precipitate was washed with 10 ml of hot water and treated with 10 ml of 1N HCl. The precipitate of HgS was separated. The supernatant containing Cd was concentrated to 1 ml and then diluted to 10 ml with water. The solution was transferred to a 150-ml separating funnel and Cd was extracted substoichiometrically with 10 ml of 0.012% solution of isonitrosoacetophenone in chloroform[3] after adjusting the pH of the aqueous phase to 7.2. The organic phase was centrifuged and a 4-ml aliquot was taken for counting.

HgS was washed with 10 ml of hot water. It was dissolved in aqua-regia and the nitrous fumes were removed by heating with 5 ml of conc. HCl. The solution was scavenged with Se and Au metal and Hg was finally precipitated as HgS with 5 ml of 2% ATU after raising the pH of the solution to 7.5 with NH_3. The precipitate was centrifuged, washed twice with 10 + 10 ml of hot water and 10 ml of alcohol, transferred to a weighed counting tube, dried at 110^{0}C to a constant weight, weighed and counted.

The standards were treated identically. The amount of the element present in the sample was calculated in the usual way.

RESULTS AND DISCUSSION

The measured values of the γ - energies, β - energies and half-lives of the separated isotopes are in agreement with those reported in the literature. The precision and accuracy of the method for Se, Cd and Hg are 4.9% and 6.4%, 6.4% and 7.8% and 5.3% and 6.1% respectively. 2 samples and a standard can be processed and counted within 3 hours. The sensitivities are 10 ppb for Se, 2 ppb for Cd and 3 ppb for Hg, which are obtained by irradiating samples at a thermal neutron flux of $1x10^{13}$ n/cm^2/sec. for one week and counting the sample after 32 hours from the end of the irradiation. The activity counted is found to be double the background. A chemical recovery of 55-70% was obtained for Hg and Se.

The results of the analysis are given in Table I. The average values for Cd in water give the following order:

$V < W < MC < NP < TC$,

while those of Hg and Se follow the series,

$V \simeq W < MC \simeq NP < TC$ and $V < W \simeq MC < NP < TC$

respectively. Water from a relatively non-industrial area like V contains

less Cd, Hg and Se compared to that from other areas. The highest concentrations of Se (76 µg/l) and Hg (72 µg/l) are found in water from TC, whereas the concentration of Cd is maximum (80 µg/l) in water from NP. Cd in coastal water around Bombay is much more than that[4] in shoreline water from most industralized area of the Eastern Irish sea.

TABLE - I.
Se, Cd and Hg in Water Collected From Five Sites Around Bombay.

Locations	µg/l					
	Se		Cd		Hg	
	Range	Average	Range	Average	Range	Average
NP	11-68	44 (4)	17-80	41 (4)	13-30	23 (4)
V	4-10	7.0(3)	1-5.8	2.9(3)	14-18	16 (3)
MC	4-25	14 (6)	5-57	34 (6)	10-35	22 (6)
W	4-29	13 (6)	16-31	22 (5)	10-31	16 (4)
TC	16-76	51 (6)	34-69	51 (5)	16-72	42 (5)
Shore line water[4] (Eastern Irish sea most industralized).	-		0.41		-	
Least industralized.	0.05		0.46		0.18	

NP = Nariman Point, MC = Mahim Creek, TC = Thana Creek, V = Versova, W = Worli. The figures in parenthesis indicate the number of samples analyzed.

The values for Se, Cd and Hg in Sediments (Table II) are in the ranges 0.05-0.65 µg/g, 0.5-3.5 µg/g and 0.1-9.7 µg/g respectively. Sediments from Versova contains at least seven

TABLE - II.
Se, Cd and Hg in Sediments.

Location	µg/g-dry weight		
	Se	Cd	Hg
MC	0.58-0.65	0.50-0.60	1.1-1.7
NP	0.19	0.60	9.7
V	0.05	3.5	0.10

times more Cd than those from Nariman Point and Mahim Creek. Hg concentration in sediments from Nariman Point (9.7 µg/g-dry weight) exceeds that in sediments from Versova and Mahim Creek by factors of 97 and 5.7 respectively. The high value for Hg in sediments from Nariman Point area is surprising because

it is considered to be a clean zone of the aquatic environment around Bombay.

TABLE - III.
Se, Cd and Hg In Tissues Of Crabs.

Location	Sample	µg/g-dry weight		
		Se	Cd	Hg
V	M-S	2.7-3.3	0.85-7.2	1.22-5.5
	G-S	0.25-20	5.6-17	0.84-0.86
	H-S	3.2-6.7	0.68-9.9	3.6-4.5
MC	M-S	2.0-6.6	0.80-13	1.6-23
	G-S	1.1-36	2.0-21	2.4-37
	H-S	1.5-34	2.2-11	1.3-5.6
NP	M-S	1.1-4.7	0.37-1.9	1.7-15
	G-S	1.5-14	0.65-14	3.8-15
	H-S	0.51-4.8	1.1-13	9.0-11
TC	M-S	2.3-21	1.9-7.7	1.6-44
	G-S	2.8-38	1.5-9.6	0.31-41
	H-S	4.4-20	2.3-5.8	7.8-66
W	M-O	2.0-8.9	1.1-3.4	16.7-25
	G-O	7.3-21	4.2-13	6.9-44
	H-O	2.4-15	3.4-12	1.2-14

M = Muscle, G = Gills, H = Hepatopancreas, S = Scylla serrata and O = Ozius reguloris.

Scylla serrata and Ozius reguloris show higher concentrations of Se and Cd in gills than in hepatopancreas and muscles (Table III). However, no systematic trend could be discerned for Hg. The maximum value (66 µg/g) for Hg is found in hepatopancreas of Scylla serrata collected from Thana Creek. Its muscle and gills show Hg concentrations of 44 µg/g and 41 µg/g respectively. These values are certainly abnormally high compared to the value of less than 0.025 µg/g found in tissues of Scylla serrata from the coastal area near Ratnagiri, which is least industralized and is free from environmental pollution.

Levels of Cd, Hg and Se in tissues do not seem to depend significantly on the size and sex of the crabs examined.

****

This work was supported by a grant from the Department of Science and Technology, Government of India.

REFERENCES

1. F. Kurzer, J. Chem. Soc., 1 (1955).

2. W.W. Scott, "Standard Methods of Chemical Analysis". (D. Van Nostrand and Co., New York), (1939).

3. Z.R. Turel and B.C. Haldar, Radiochem. Radioanal. Letters, 39,201 (1979).

4. A. Preston, D.F. Jeffries, J.W.R. Dutton, B.R. Harvey and A.K. Stee, Envir. Pollut. 3,39 (1972).

ATMOSPHERIC DEPOSITION OF HEAVY METALS STUDIED BY ANALYSIS OF MOSS SAMPLES USING NEUTRON ACTIVATION ANALYSIS AND ATOMIC ABSORPTION SPECTROMETRY

J.P. Rambæk[1] and E. Steinnes[2]

1. Institute for Energy Technology, 2007 Kjeller, Norway
2. Department of Chemistry, University of Trondheim - NLHT, 7055 Dragvoll, Norway

ABSTRACT

In a study of the atmospheric deposition of trace elements in different parts of Norway samples of the moss Hylocomium splendens were analyzed with respect to 26 elements. The determination of Cu, Zn, Pb, Cd and Ni was carried out by flame atomic absorption spectrometry, while an additional 21 elements were determined by instrumental neutron activation analysis. Several elements showed a substantially higher deposition in the southernmost parts of Norway than in places located further north. As regards Pb, As and Sb, the difference amounted to a factor of ten or more. A similar but less pronounced trend was evident for elements such as V, Zn, Cd, Se and Ag. In some cases local pollution sources or marine aerosols had a significant effect on the results. For several heavy metals however long-distance transport from areas to the south and the south-west of Norway was responsible for a major part of the air pollution.

INTRODUCTION

Mosses are useful indicators of atmospheric pollution because they absorb nutrients from the air and have a high capacity to retain many ions. The use of moss samples in deposition studies is advantageous because samples can be obtained simultaneously from a great number of places without the need of specific sampling equipment. A number of reports on moss surveys based on atomic absorption spectrometry (AAS) have appeared in the literature recently. It is shown here that the information obtained in this kind of pollution study can be considerably extended by the use of instrumental neutron activation analysis (INAA) in combination with AAS.

The feasibility of mosses as indicators of trace element deposition was first demonstrated by Rühling and Tyler (1) who were able to show that the atmospheric fall-out of certain heavy metals is distinctly larger in the southern and southwestern parts of the Scandinavian peninsula than in the northernmost part of the area. An initial moss survey in Norway (2), involving samples from 40 different sites, clearly indicated the great promise of INAA in this kind of study. The present paper presents some results from a more extensive survey of trace element deposition in Norway based on moss analysis.

EXPERIMENTAL

Samples of the forest moss Hylocomium splendens were collected during the summer of 1977 at about 500 sites regularly distributed all over the country. Each sample typically consisted of five sub-samples taken within an area of 10^4 m^2 or less. Since the aim of this investigation was to study regional trends, sampling sites in the close proximity of industrial plants or larger population centra were avoided. The sampling always took place at a distance of at least 300 m from roads or agricultural fields. The material was collected in polyethylene bags, and disposable polyethylene gloves were used during the sampling as well as the subsequent handling of the material.

In the laboratory the samples were dried to constant weight at room temperature. After removal of foreign matter, sub-samples were taken for trace element determination by INAA and by AAS.

For the INAA aliquots of about 0.3 g were weighed into either polyethylene or quartz containers and irradiated in the JEEP-II reactor (Kjeller, Norway) at a thermal neutron flux of about 1.5×10^{13} n $cm^{-2}s^{-1}$. After appropriate decay intervals the samples were assayed by γ-spectrometry using coaxial Ge(Li) detectors with associated electronics interfaced to a small digital computer. Standards for each element to be determined were irradiated simultaneously, and the quantitative analyses were based on peak areas calculated according to standard methods. Two different procedures were employed:

A. Determination via short-lived nuclides according to the following sequence: 30 sec. irradiation - 12 min. decay - 5 min. counting. The samples and standards were irradiated two at a time in sealed polyethylene tubes, assuming no appreciable temporal variation in the neutron flux. The elements determined in this way were Na, Al, Cl, V, Mn and I.

B. Determination via more long-lived nuclides ($t_{\frac{1}{2}}$ > 1d). In this case 20 hours' irradiation in sealed quartz tubes was used. The samples were removed from the quartz ampoules and counted after five days (As, Br, Mo, Sb, La, Sm) and three weeks (Sc, Cr, Fe, Co, Se, Rb, Ag, Cs, Th).

For the AAS-analyses 2-gram portions were digested with 10 ml of concentrated HNO_3 for 20 hours. After removal of undissolved organic matter by filtration and dilution to 25 ml with water, the resulting solutions were analyzed with

respect to Pb, Zn, Cd, Cu and Ni by flame atomic absorption spectrometry using an air/acetylene flame. A blank was run along with every 25 samples. The method of standard additions was used on a number of samples to check that remaining traces of undissolved organic material did not interfere significantly with the determinations.

RESULTS AND DISCUSSION

As indicated in Table I, 22 elements were determined in the moss samples by INAA. For most of the elements the concentrations observed were above the detection limit in all, or nearly all, samples investigated. Not all of these elements are of primary interest in air pollution studies, but many of them are, and the introduction of INAA clearly extends the scope of moss surveys. The use of flame AAS normally allows the determination of pollutants such as Cr, Co, Ni, Cu, Zn, Cd and Pb, while the determination of V requires a graphite furnace. By means of INAA additional elements such as As, Se, Br, Mo, Ag and Sb can be readily determined in most samples, and improved data may be obtained for V, Cr and Co. On the other hand, INAA alone is not adequate, since the determination of the important elements Ni, Cd and Pb is not possible by this technique. Thus a combination of INAA and AAS appears to be advantageous for moss surveys and similar air-pollution related studies.

Some typical results from the regional study of trace element deposition in Norway are shown in Figs. 1-8. The deposition of many trace elements is distinctly higher in the southernmost parts of Norway than in areas further north. For Pb, As and Sb the difference appears to be as much as a factor of ten. Also for Se, V, Cd and Ag substantial differences are evident. The largest differences are observed for relatively volatile elements, known to be preferentially concentrated on the small-size fraction of air particulates. The deposition patterns indicate that a major fraction of the fall-out of these elements in Norway is associated with long-range atmospheric transport from sources in the densely populated and heavily industrialized parts of Europe.

Effects from local point-sources, however, are also evident for some elements. The iso-concentration maps for V and Cr show clear contributions from ferro-alloy industrial plants in Western Norway. In the case of Cu, Ni and As a large smelter in the Soviet Union is the source of the abnormal deposition patterns observed in the far north-east of Norway.

The results for Br and I indicate that the contents of these elements in the moss are mainly derived from marine aerosols. Se appears to have a somewhat similar distribution pattern, showing high concentrations on the coast relative to corresponding areas inland at all latitudes. This pattern is similar to that previously observed for selenium in Norwegian surface soils (3,4) and may be explained by assuming two components in the atmospheric supply of Se: The one component originating from pollution - showing a distribution similar to that of Pb, As and Sb - and the other originating from natural processes, possibly associated with the marine environment.

REFERENCES

1. Å. Rühling and G. Tyler, Water, Air, Soil Poll. 2 (1973) 445.
2. E. Steinnes, Report KR-154. Institutt for atomenergi, Kjeller, Norway (1977).
3. J. Låg and E. Steinnes, Ambio 3 (1974) 237.
4. J. Låg and E. Steinnes, Geoderma 20 (1978) 3.

Element	Radionuclide used	Concentration observed (ppm)	Approximate detection limit (ppm)
Na	^{24}Na	70 - 1700	10
Rb	^{86}Rb	1.2 - 40	0.5
Cs	^{134}Cs	<0.01 - 2.0	0.01
Sc	^{46}Sc	0.03 - 1	0.01
La	^{140}La	0.1 - 10	0.02
Sm	^{153}Sm	0.01 - 1	0.01
Th	^{233}Pa	0.02 - 2	0.02
V	^{52}V	<0.5 - 60	0.5
Cr	^{51}Cr	0.3 - 120	0.2
Mo	^{99m}Tc	<0.2 - 1.6	0.2
U	^{239}Np	<0.03 - 0.2	0.03
Mn	^{56}Mn	30 - 1000	1
Fe	^{59}Fe	110 - 4300	20
Co	^{60}Co	0.05 - 4	0.01
Ag	^{110m}Ag	0.05 - 0.7	0.05
Hg	^{197}Hg	0.05 - 0.20	0.05
Al	^{28}Al	170 - 4700	20
As	^{76}As	0.05 - 3.5	0.05
Sb	^{122}Sb	0.03 - 2.0	0.03
Se	^{75}Se	<0.1 - 2.8	0.1
Cl	^{38}Cl	30 - 800	10
Br	^{82}Br	1.3 - 34	0.1
I	^{128}I	<1 - 20	1

Table I. Some typical results obtained by analysis of moss samples using INAA.

Figs. 1-4. Regional distribution of trace elements in moss (ppm).

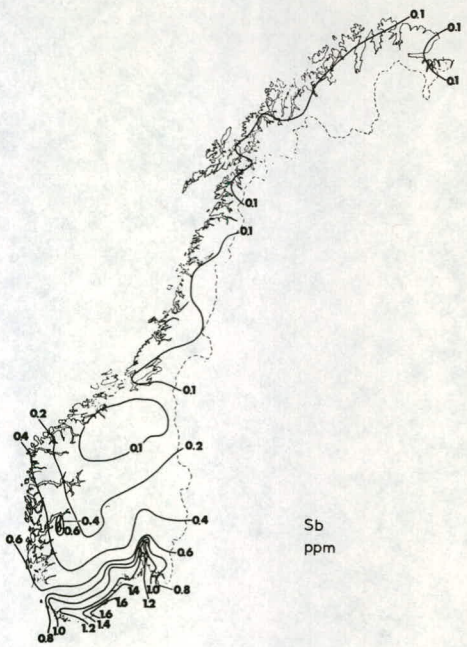


Fig. 1. Antimony.

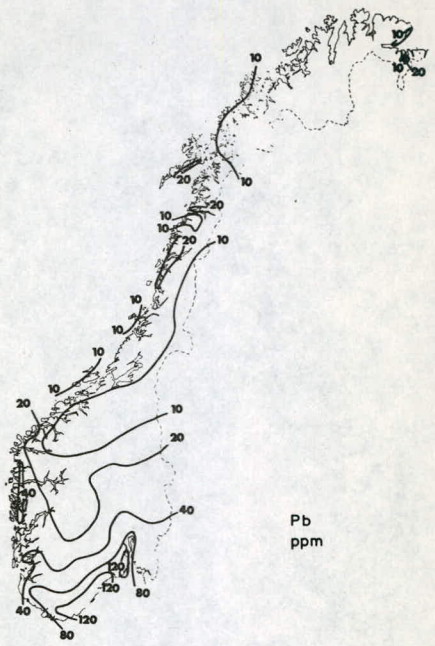


Fig. 2. Lead.

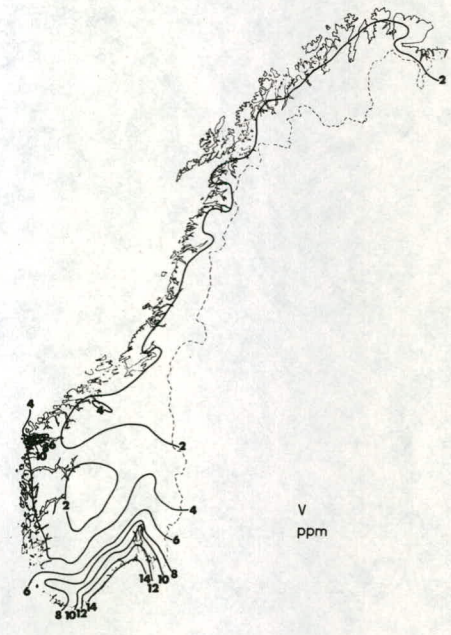


Fig. 3. Vanadium.

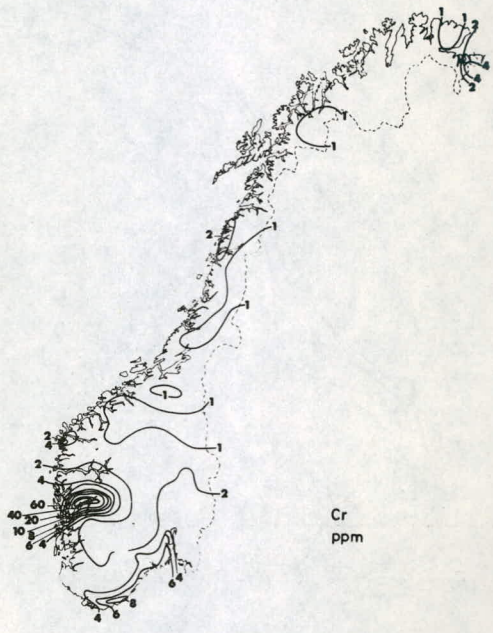


Fig. 4. Chromium.

Figs. 5-8. Regional distribution of trace elements in moss (ppm).

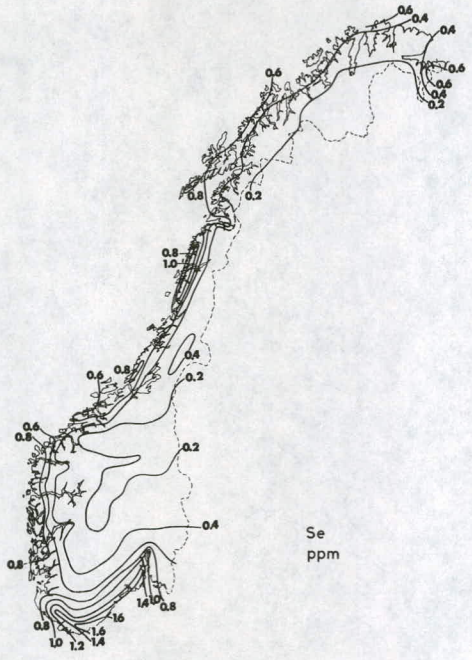


Fig. 5. Selenium.

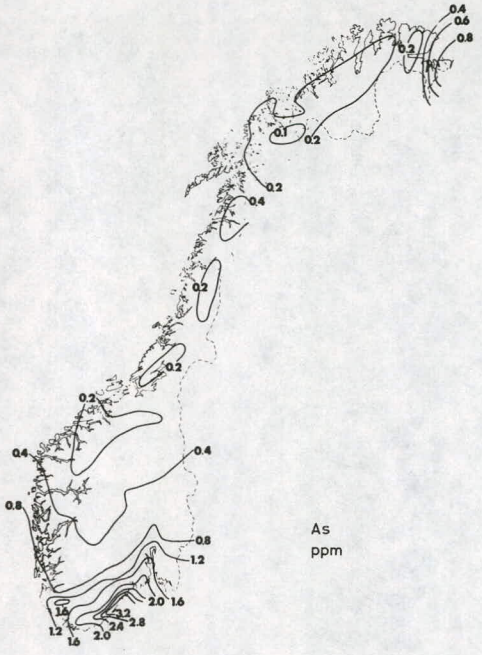


Fig. 6. Arsenic.

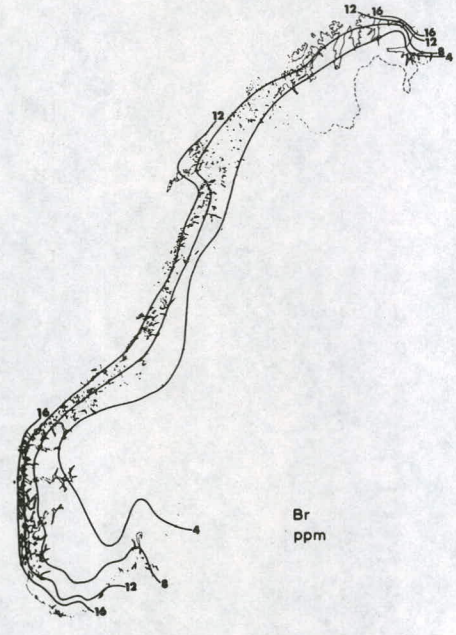


Fig. 7. Bromine.

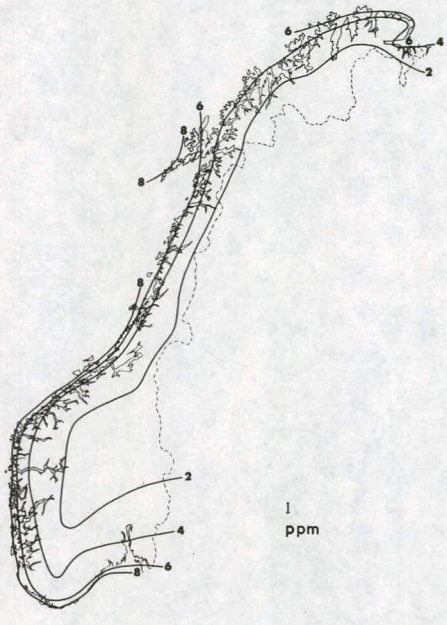


Fig. 8. Iodine.

NUCLEAR AND ATOMIC METHODOLOGY

Session Chairmen

V.P. Guinn

P.A. Baedecker

THE USE OF NEUTRON-CAPTURE PROMPT GAMMA-RAY ACTIVATION ANALYSIS IN ENVIRONMENTAL AND ENERGY RESEARCH*

Glen E. Gordon
Department of Chemistry
University of Maryland
College Park, Maryland 20742

ABSTRACT

Reactor-based neutron-capture prompt γ-ray activation analysis (PGAA) can be used for several trace elements (e.g., B, Cd, Sm, Gd), but it is mainly a major and minor element method. Among the 15 to 20 elements that can be determined in a particular type of sample, the major elements C, H, N and S can usually be measured in coals and biological samples and the elements of geochemical interest, Na, Al, Si, K, Ca, Ti, Fe and others in rocks, coal and other crustal samples. When used along with instrumental neutron activation analysis (INAA), the combined techniques can be used to analyze for 40 to 50 elements in crustal samples. Suggestions for further development of reactor-based PGAA include: the need to reduce low-energy γ-ray backgrounds for observations of species having intense lines only at low energy, more development of biological and special materials applications, the use of beam choppers to look for very short-lived species, and demonstrations of analyses of samples too large, precious or hazardous to be irradiated inside reactors. The greatest potential for applications of PGAA may be in the use of systems detached from reactors, i.e. those using ^{252}Cf or other isotopic neutron sources. This may be the only method for elemental analyses of large, inhomogeneous process streams in various industries, power plants, etc. Fluxes comparable to those of external beams from reactors are feasible with the use of mg quantities of ^{252}Cf. Practical systems for use on coal have been developed. Many other applications would be possible: field prospecting for valuable ore deposits, studies of nutrients in soil and plants, *in situ* measurements in remote locations such as planetary surfaces, mines, bore holes, etc.

*Work in part supported by the U. S. Department of Energy under Contract No. DE-AS05-76ER05173.

INTRODUCTION

At the time of the Third Conference, several groups had demonstrated the use of neutron-capture prompt γ-ray activation analysis (PGAA) to determine concentrations of a few elements in a limited number of samples (1). Morrison and coworkers had performed calculations on sensitivities of various elements by PGAA and demonstrated the method by analyzing mixtures of B and Gd oxides (2-5). Comar *et al.* used a curved neutron guide to remove fast neutrons and γ rays from a thermal neutron beam from the Saclay reactor to measure B, N, Na, P, Cl and Ca in biological samples (6). Henkelmann and Born (7) used a cold source and a curved neutron guide at the high flux Grenoble reactor to analyze rocks for rare earths, Th, Al and several other elements. Heurtebise and

coworkers applied PGAA to the analysis of petroleum hydrodesulfurization catalysts for water (via H), Co, Mo and Ni (8-10). Gladney et al. at Los Alamos had analyzed various samples for B, Cd and S outside of the reactor (11, 12). Our group, in cooperation with the National Bureau of Standards (NBS) had installed a system for PGAA studies at the NBS reactor and were just beginning to use it (1).

Despite this variety of activities (including work with isotopic sources noted below), the full capabilities of PGAA had not been explored nor, with rare exceptions, had the method been applied to practical or scientific problems other than the development of the method itself. Since the Third Conference there has been a great deal of development and exploitation of the PGAA method. Although many fundamental developments remain to be done, it is already clear that the method has great potential for use in scientific and practical applications. Many of the latter require the use of neutron sources other than reactors and considerable progress is being made in that area.

Below, I have summarized the present status of this field and offered some suggestions of new directions that should be pursued. I have not attempted a comprehensive review of every use of PGAA: despite the relative youth of the field there is already substantial literature. Gladney recently prepared a detailed literature survey of PGAA that includes 190 references, of which probably 100 are on PGAA itself (13).

REACTOR-BASED PGAA STUDIES

The basic idea of PGAA is that of bombarding samples with neutrons and observing the prompt γ rays emitted within a fraction of a second after neutrons are captured by stable nuclides in the sample. This method has the advantage relative to off-line methods that it does not depend on formation of a radioactive product. Regardless of the stability of the ground state of the product, with rare exceptions, one or more prompt γ rays are emitted in the de-excitation of the highly excited states formed by neutron capture.

Various arrangements of irradiation, shielding and detector facilities are used. Most groups bring a neutron beam out of the reactor, the major exception being the LASL group, which irradiates samples in a thermal column (11, 12). The flux on the sample is much greater inside, but this is approximately balanced by the much greater sample-to-detector distance required when the sample is internal. Otherwise, there are many advantages of external beams: samples are subjected to much lower fluxes and no heating, so the method is almost totally non-destructive; large or hazardous samples can be irradiated externally; one has better control over fast neutrons and γ-ray backgrounds; absorbers can be placed in the beam to remove neutrons of certain energy ranges; and more sophisticated detector arrangements can be used (e.g., coincidence counting).

The detection system, at least for research purposes, must have very good resolution, as there is a high density of lines, especially below 2 MeV (14, 15). Thus, Ge(Li) or intrinsic Ge detectors must be used for research purposes. The system must handle γ rays with energies from about 100 keV to 11 MeV. Calculations based on capture cross sections, prompt γ-ray intensities and detection efficiencies invariably predict that the highest sensitivities for analyses for most elements are those based on γ rays of <2 MeV, mainly because of the strong fall-off of the detector efficiency curve at higher energies. However, in practice, it is usually desirable to base analyses on much higher energy γ rays despite their much lower counting rates, as there is much less overlap of peaks at high energy and the general spectrum background is lower. Unfortunately, in some nuclides, the decay of the

excited state may proceed by a cascade of low-energy γ rays, with few γ rays of several MeV. Thus, whereas elements such as N, Fe, Si can be observed by high energy γ rays, several elements such as Cd and B can be observed only via γ rays of below 1 MeV, so the system must be effective from 0.1 to 11 MeV to observe all possible elements. Note, however, that there may be some practical applications in which it is necessary to measure only a few dominant lines, e.g., of H or Fe. In those cases, it may be better to sacrifice resolution for an enormous gain in counting efficiency by using NaI or $Bi_4Ge_3O_{12}$ (16) scintillation crystals.

For research on PGAA, some groups (including our own) have large NaI detectors surrounding the Ge(Li) crystal for operation in Compton-suppression or pair spectrometer modes (15). This is useful in fundamental studies in making unambiguous identifications of full energy and single- and double-escape peaks. We have discovered some peaks, previously thought to be free of interference, had other peaks of these types under them. Also, the Compton-suppression mode reduces general spectrum background by factors of three to five between 1 and 10 MeV, reducing limits of detectability and statistical uncertainties in determinations of species with lines close to background levels. However, it does not make a dramatic difference in the spectra, e.g., it does not reveal lines of elements that were not previously observable. To surround the Ge detector with a NaI crystal, one must move the Ge detector farther from the sample. For most applications, it is probably preferable not to use a shield detector so the Ge detector can be moved closer to the sample to enhance sensitivity.

A major problem of PGAA is that of backgrounds. Accompanying the thermal neutrons, which are usually the desirable species, are fluxes of γ rays and fast neutrons that must be prevented from reaching the detection system. Our approach to these problems has been rather "brute force", but effective. First, we made the external beam tube large (about 14 cm I.D.) so that little of the fluxes would strike the wall. Second, we used three concentric Plexiglas tubes around the beam and filled the spaces between them with Li_2CO_3, boron carbide (B_4C), and paraffin to thermalize and absorb scattered neutrons. Third, the NaI detector was surrounded with 10 cm of Pb and, outside of that, B_4C in polystyrene. Since neutron capture in boron yields a 477-keV γ ray, there must be γ-ray absorber between boron and the detection system. Finally, there is a Pb collimator containing a small $^6Li_2CO_3$ plug in front of the detector. Since ^6Li yields no capture γ rays, it is an excellent neutron absorber, but very expensive. With these measures, the neutron background was reduced to negligible levels and the boron background line was of low enough intensity that we can measure boron at very low levels in samples.

The low energy γ-ray background poses a serious problem. As shown in Fig. 1, the general background below 300 keV is so high that only very intense γ rays can be observed. For the most part, this background is not caused by Compton or other partial energy events in the detector, as it is not strongly reduced by Compton suppression. Instead it appears to result from scattering of γ radiation in the beam by the sample.

It is important to reduce the low-energy γ-ray background: as Henkelmann and Born (7) have shown, detection limits are quite low for many elements via γ rays below 300 keV. They removed both the fast neutron and γ-ray backgrounds very elegantly with a curved neutron wave guide. Thermal neutrons follow the curve, but fast neutrons and γ rays do not, so the beam from the wave guide is almost purely thermal neutrons. As shown in Fig. 1, the low-energy background with their system is quite low. A simpler method of removing much of the γ-ray and fast neutron background is that of placing a

single crystal of a heavy element such as Bi in the beam (17). If the crystal axis is aligned parallel to the neutron beam and cooled to liquid nitrogen temperature, thermal neutrons undergo "channeling" in the crystal and are transmitted with small attenuation. But γ rays are strongly absorbed and fast neutrons scattered out of the beam upon passage through the crystal.

ELEMENTS OBSERVABLE WITH PGAA

Extensive studies of application of PGAA to several types of samples have been performed by the LASL group and our group. Because of the complex spectra, it is difficult to identify spectral features to use for determinations of the various elements. After lines associated with capture in an element are identified, one must obtain the element's complete spectrum in order to determine its possible interferences under peaks of other elements. Compilations of spectra of elements are not completely reliable, as the elemental standards used often contain impurities of elements with large capture cross sections. In one compilation (18), for example, a γ ray of about 558 keV is reported for 38 elements, many of which are due to Cd impurities in the standards. We have investigated elemental spectra carefully and identified interferences with lines used for analysis (14, 15).

In Table I, I have compiled the elements observable in several types of materials by PGAA. A total of 32 elements have been observed in one kind of sample or another, but usually only twenty or fewer are observed in a specific class of substances. (Some additional elements are observable in very unusual types of samples that have compositions quite different from those of crustal or biological materials.) Although PGAA is quite sensitive for several trace elements (mainly B, Cd and some rare earths), it is much more applicable to major and minor elements than instrumental neutron activation analysis (INAA). Elements such as H, C, N and S can be measured in coal and biological samples with PGAA. Most elements traditionally measured by geochemists in rocks and minerals (Na, Mg, Al, Si, P, K, Ca, Ti and Fe) can be measured in rocks. When one uses the geochemical method of expressing concentrations as common oxides of the elements (e.g., Al_2O_3, K_2O, CaO, etc.), the sum of these oxide concentrations (plus C, H, N and S for coal) is usually between 90 and 100%.

The PGAA method has not been as successful for biological samples. In part, this results from lower concentrations of many "crustal" elements in biological material and in part, from interferences, especially by Cl lines. The classic problem of INAA of marine samples is that of the huge activities of Na or K and Cl that make it almost impossible to observe other products of half lives less than a few days. In PGAA, Na and K do not cause much interference, but Cl has many strong lines throughout the spectra. Little work has been done on PGAA of biological materials, so considerable improvements may be possible. However, in order greatly to extend the method for these samples, some pre-irradiation chemistry may be needed (e.g., removal of Cl).

Any laboratory equipped for reactor-based PGAA is also equipped to do INAA. Thus, the former should be considered as a complement to the latter, not a replacement. The two methods combined can be used to measure a very large number of elements in many types of samples. Mainly with the use of PGAA and INAA, our group measured concentrations of 51 elements in the NBS bituminous coal standard (SRM 1632a) and 43 elements in the subbituminous (SRM 1635) (21).

ADVANTAGES OF REACTOR-BASED PGAA

The PGAA method shares many advantages with other instrumental nuclear methods (INAA plus activation with photons or 14-MeV neutrons) relative to other methods for multi-element measurements on complex samples: many elements can be observed in an individual sample; the sample doesn't have to be dissolved (saving labor and avoiding contamination or losses of material); although inter-element interferences occur, they can be observed and usually corrected; and self-absorption effects are usually negligible. The latter is a particularly important advantage relative to the main competing instrumental, multi-element method, x-ray fluorescence, XRF. X-rays of most elements are so strongly absorbed in material that samples must be very thin and homogeneous for XRF analysis. However, even with such ideal samples as thin deposits of atmospheric particles on air filters, elements below Ca can be measured only with great care (22).

In comparison with INAA and other off-line nuclear methods, PGAA has several advantages, especially with the use of an external beam:

1. Rapid turn-around time: Data are ready for final interpretation at the end of the irradiation with PGAA, whereas at least two weeks are needed to observe long-lived species in off-line applications.

2. Greater accuracy for some elements: Especially in the case of species determined off-line by short-lived activities (Al, V, Ti, Ca, S, Mg), one avoids errors due to timing and change of dead-time fraction.

3. Less destruction: There is little heating, radiation damage or residual activity caused by small fluxes of external beams.

4. More flexible sample requirements: Samples that are too large, hazardous or precious to be placed in a reactor can be irradiated externally. Samples could be placed in an inert gas, be frozen or be subjected to other conditions during external irradiations.

5. Easier control of neutron flux: The energy spectrum of neutrons in the external beam can be modified by absorbers, or one could install a "chopper" to produce short beam bursts for observation of species with half lives of seconds or less.

6. No losses of recoils: In INAA, Szilard-Chalmers reactions release the reaction products from their chemical bonding and volatile elements, especially Hg and Br, may be lost from the sample (23). In PGAA, prompt γ rays are emitted before the residual nucleus can move away.

The PGAA method has some disadvantages relative to INAA (aside from the differences in the elements that can be observed):

1. Longer irradiations and larger samples needed: In general, to achieve the same accuracy, for many elements, longer irradiation times and larger samples are needed for PGAA.

2. Single-sample irradiations: Unlike common INAA practice, most systems for PGAA have provision for irradiating only one sample at a time. With more experience in handling external neutron beams, we may be able to place several target/counting stations on neutron beams without interference between experiments.

3. No time separation: Almost no time separation of events involving different elements is obtained via PGAA. Thus, we cannot check for interferences or identify unknown peaks, as in off-line methods, by observation of decay.

4. Post-irradiation chemistry not possible: When chemical separations are required for off-line methods, they are performed after irradiation, if possible, as there is no danger of contamination by reagents, containers, etc. after irradiation. However, there is no "post-irradiation" of PGAA - any separations must be done prior to irradiation, with the attendant possibilities for error.

FURTHER DEVELOPMENTS - REACTOR-BASED PGAA

Exploratory studies of PGAA have been so promising that groups at several research reactors are setting up PGAA facilities. The method is well enough understood that our group is using it for analyses of atmospheric and volcanic samples (see W. H. Zoller *et al.*, This Conference). The LASL group has used their facility for studies of boron in meteorites (23). The technique is sufficiently reliabile for many of elements that the activation analysis group at NBS is beginning to use it for analyses leading to certification of standards.

Despite these advances, much remains to be done to fully exploit PGAA:

1. Backgrounds need to be reduced in order that more species can be observed. The low-energy γ-ray background should be reduced as Henkelmann and Born (7) have done with a curved neutron guide or as with a single crystal Bi absorber (17, 25).

2. More study of applications to biological samples, including the use of chemical separations, is needed.

3. The application of PGAA in many additional fields is needed, e.g., high-purity materials for solar batteries, semiconductors and light pipes, and other materials in which small concentrations of certain elements may degrade its performance.

4. Demonstrations are needed of the application of PGAA to hazardous or irreplacable samples, e.g., forensic samples, art objects, forgeries, explosives, gasoline.

5. Beam choppers should be installed to allows searches for elements observable via very short-lived activities between beam bursts, e.g., 19-sec ^{46m}Sc, 17-sec ^{77m}Se, 1.3-min ^{165m}Dy and 19-sec ^{179m}Hf. This technique would be a variation of the cyclic irradiation method of Spyrou and Kerr (26). To obtain reasonable sensitivity, the detector should be moved close to the target.

6. The enhancement of sensitivity of determinations of some elements via epithermal neutrons should be investigated by the use of absorbers in the neutron beam.

7. Since lines from several isotopes of some elements are observed, PGAA could be used to detect variations of isotopic abundances.

8. The uses of PGAA as applied to nuclear fuel materials should be investigated (see B. R. S. Pecequilo *et al.*, This Conference).

PGAA WITH ISOTOPIC NEUTRON SOURCES

Reactor-based PGAA systems with external beams provide optimum conditions for fundamental development of the method and routine analyses of samples that can be brought to reactors. However, the most important applications of PGAA will probably be those involving the use of field units containing isotopic neutron sources. Many kinds of analytical problems could be solved by on-the-spot, real-time analyses of samples so inhomogenous that one must average over considerable volumes of samples. Possible applications include in situ analysis of process streams in various industries such as steel mills, non-ferrous smelters, coal-fired power plants or coal-conversion plants; monitoring compositions of construction materials on site; field prospecting for minerals; testing soils; measurement of nutrients in grains; analyses in remote locations such as surfaces of planets, the ocean floor or in mines and oil wells.

Few techniques have even the potential to handle these very difficult analytical problems. Few methods have inherent depth ranges great enough to integrate over considerable bulk of sample. Methods based on microwave attenuation and change of electrical capacitance could be used to measure the moisture content of bulk coal in real time (27). But the only method that appears to have a chance of measuring elemental concentrations of bulk samples in real time is PGAA.

Many studies of PGAA with isotopic neutron sources have been made. For example, Duffey and coworkers investigated the use of ^{252}Cf sources in analyses of coal (28), copper-smelting process streams (29), concrete (30), the sea floor and manganese nodules (31). Gladney lists references to many other works involving the use of isotopic sources (13).

Several isotopic sources are available, e.g., ^{241}Am-Be, ^{239}Pu-Be and ^{252}Cf (32). For most purposes, ^{252}Cf sources are probably the most convenient, as the neutron fluxes obtainable can be comparable to those of external beams from reactors. Sources up to a few mg of ^{252}Cf can be obtained and safely handled with shields of about 1 m^3 volume. To achieve the same neutron flux as a ^{252}Cf source, a typical (α,n) source would need about a thousand-fold greater α activity, causing problems of heating and ^4He gas build-up in very intense sources. Some (α,n) sources would be totally impractical at 10^{10} n/sec levels, e.g., the amount of ^{226}Ra needed would exceed supplies and that of ^{239}Pu would be a critical mass. A 1-mg source of ^{252}Cf costs about $10,000 and releases about 2.5×10^9 n/sec. Each fission is accompanied by several γ rays - some from the continuum of prompt fission γ rays (up to about 10 MeV), others following β^- decay of fission products (up to about 4 MeV), and low energy γ rays associated with α decay of ^{252}Cf. Thus, γ rays from the source must be shielded from the detector. Most (α,n) sources emit considerable γ radiation, but of generally much lower energy than that from ^{252}Cf, making them easier to shield. Obviously, (γ,n) sources containing ^{124}Sb and Be have very intense γ radiation of rather high energy, making them difficult to shield.

Neutrons from most isotopic sources have energies up to several MeV. For ^{252}Cf, the neutron energy spectrum is typical of the fission process, with a most-probable energy of about 1 MeV, tailing off to a ten-fold reduction in intensity at 6 MeV. Most of the neutrons initially have energies too high to be captured strongly. In hydrogenous material, neutrons must travel about 5 cm before becoming reasonably thermalized. Thus, the maximum thermal neutron flux is down about two orders of magnitude from the neutron emission rate, so a 1-mg ^{252}Cf source produces a maximum thermal flux of about 10^7 n/cm^2-sec.

Although the fluxes are low, in most applications this is balanced by irradiation of large volumes of material, e.g., the order of 1 kg of coal at an average flux of 5 x 10^5 n/cm^2-sec. With use of a large-volume Ge(Li) detector at about 30 cm from the center of the coal sample, the counting rate would be about 400 c/sec for the H capture line. Unfortunately, it is not possible to make a simple calculation of the expected intensities of capture γ rays from all elements, as the neutrons are not well enough thermalized to allow use of thermal-neutron capture cross-sections. The capture spectra obtained by Gozani et al. (27) with ^{252}Cf neutrons bombarding coal are quite different from those obtained for fly ash by our group using a well-thermalized beam: very strong lines from trace elements with enormous thermal-neutron cross sections (e.g., Sm, Gd) in our spectra are absent from theirs. This change causes lines from some major elements (e.g., the 841-keV line of S) to stand out more clearly from interferences with ^{252}Cf than with a well-thermalized neutron beam. It is difficult to calculate the energy spectrum of neutrons vs. distance in a complex matrix such as coal, but it appears that major portions of the neutrons are captured before they become truly thermal.

As far as I have been able to determine, little work has been done in which the neutrons were strongly thermalized without capture before allowing them to enter the sample, e.g., by placing moderators of low mass number and cross section (such as Be and D) around the ^{252}Cf source. Of course, if this is done, the flux will be decreased approximately as $1/R^2$ and the zone of neutron captures in the sample will be greatly expanded, thus reducing the geometry for γ-ray spectrometry. Despite the disadvantage, such an approach should be investigated. The minimum radius for such a moderator would be about 12 cm, so the thermal-neutron flux at the surface around a 1-mg ^{252}Cf source would be about 10^6 n/cm^2-sec or less. However, if one is wishes to measure trace elements with very high cross sections at thermal energies, this approach will be needed. The system should be flexible enough that one can remove the moderator, if desirable, to irradiate the sample directly if the major interest is in using the highest possible flux to determine major element concentrations.

APPLICATIONS OF PGAA WITH ISOTOPIC SOURCES

Many applications of PGAA with isotopic sources have been demonstrated (see Ref. 13). The most thoroughly investigated application is that of on-line analyses of coal (27, 28, 33). Herzenberg et al. (28) demonstrated analyses for H, Fe, Si, S, Cl, Ca and Ti in coal with ^{252}Cf sources surrounding a pipe containing coal. By irradiating a bin of coal with neutrons from ^{252}Cf, Gozani et al. (27) analyzed for the same elements plus C, N, Na, Al and K. These systems are ready to be put into use in coal-fired plants for real-time measurements of the concentrations of total sulfur, nitrogen, ash and other species noted above. If it would be useful to the plant operators to have information of this type over averaging times down to about 5 min, it could be done with ^{252}Cf sources of practical sizes.

Although the greatest attention has been given to the analysis of coal streams, PGAA might be useful for many other process streams, e.g., limestone, cement, ferrous and non-ferrous ores and their product streams. As noted above, there are many potentially important field applications of PGAA, if a transportable system of high efficiency and ruggedness can be developed. It is unlikely that a "back-pack" device can be made because of the necessary biological shielding, but devices that can be carried in a van or small truck are certainly feasible. Perhaps the most spectacular application of PGAA with an isotopic source was the work at the Third Conference by Vartsky et al. (34), who used an 85-Ci ^{238}Pu-Be source for irradiation of the kidneys and

liver of persons suspected of overexposure to Cd. Over a 30-min irradiation period, with a local radiation dose to the patient of about 670 mrem, they can measure Cd at normal levels and above to an accuracy of about ±15%.

In summary, the potential for applications of PGAA is enormous, limited mainly by our imaginations and abilities to obtain developmental support.

REFERENCES

1. G. E. Gordon, D. L. Anderson, M. P. Failey, W. H. Zoller, W. B. Walters and R. M. Lindstrom, "Prompt Gamma-Ray Neutron Activation Analysis". In Proc. of the Third Int. Conf. on Nuclear Methods in Environmental and Energy Research, J. R. Vogt, ed. (University of Missouri, Columbia, MO, 1978), TID Document CONF 771071, pp. 83-89.

2. T. L. Isenhour and G. H. Morrison, "Modulation Technique for Neutron Capture Gamma Ray Measurements in Activation Analysis", Anal. Chem. 38, 162 (1966).

3. T. L. Isenhour and G. H. Morrison, "Determination of Boron by Thermal Neutron Activation Analysis Using a Modulation Technique", Anal. Chem. 38, 167 (1966).

4. S. M. Lombard, T. L. Isenhour, P. H. Heintz, G. L. Woodruff and W. E. Wilson, "Neutron-Capture Gamma-Ray Activation Analysis, Design of Apparatus for Trace Analysis", J. Appl. Rad. Isotopes 19, 15 (1968).

5. S. M. Lombard and T. L. Isenhour, "Neutron-Capture Gamma-Ray Activation Analysis Using Lithium-Drifted Germanium Semiconductor Detectors", Anal. Chem. 40, 1990 (1968).

6. D. Comar, C. Crouzel, M. Chasteland, R. Riviere and C. Kellershohn, "The Use of Neutron Capture Gamma Radiations for the Analysis of Biological Samples". In Modern Trends in Activation Analysis, J. R. DeVoe, ed., Nat'l. Bureau of Stds. Special Publication No. 312, 1969, pp. 114-117, Vol. 1.

7. R. Henkelmann and H.-J. Born, "Analytical Use of Neutron-Capture Gamma-Rays", J. Radioanal. Chem. 16, 473 (1973).

8. M. Heurtebise and J. A. Lubkrowitz, "Determination of Metals in Alloys by Neutron Capture Gamma-Ray Spectrometery", J. Radioanal. Chem. 31, 503 (1976).

9. M. Heurtebise, H. Buenafama and J. A. Lubkrowitz, "Determination of Cobalt, Molybdenum, and Nickel in Hydrodesulfurization Catalysts by Neutron Capture γ-Ray Spectrometry and Neutron Activation Analysis", Anal. Chem. 48, 1969 (1976).

10. M. Heurtebise and J. A. Lubkrowitz, "Determination of Water in Hydrodesulfurization Catalysts by Neutron Capture γ-ray Spectrometry", Anal. Chem. 48, 2143 (1976).

11. E. S. Gladney, E. T. Jurney and D. B. Curtis, "Nondestructive Determination of Boron and Cadmium in Environmental Materials by Thermal Neutron-Prompt γ-ray Spectrometry", Anal. Chem. 48, 2139 (1976).

12. E. T. Jurney, D. B. Curtis and E. S. Gladney, "Determination of Sulfur in Environmental Materials by Thermal Neutron Capture Prompt Gamma-Ray Spectrometry", Anal. Chem. 49, 1741 (1977).

13. E. S. Gladney, "A Literature Survey of Chemical Analysis by Thermal Neutron Induced Capture Gamma Ray Spectrometry", Los Alamos Scientific Laboratory Report LA-8028-MS, Sept. 1979.

14. M. P. Failey, D. L. Anderson, W. H. Zoller, G. E. Gordon and R. M. Lindstrom, "Neutron Capture Prompt γ-Ray Activation Analysis for Multi-Element Determination in Complex Samples", Anal. Chem. 51, 2209 (1979).

15. M. P. Failey, "Neutron-Capture Prompt Gamma-Ray Activation Analysis: A Versatile Nondestructive Technique for Multi-Element Analysis of Complex Matrices", Ph.D. Thesis, Univ. of Maryland, 1979.

16. O. H. Nestor and C. Y. Huang, "Bismuth Germanate: A High-Z Gamma-Ray and Charged Particle Detector", Technical Paper, Harshaw Chemical Co., 1978.

17. H. Zwittlinger, "Neutron Capture Gamma-Ray Activation Analysis of Refined Steel", J. Radiochem. Anal. 14, 147 (1973).

18. N. C. Rasmussen, Y. Hukai, T. Inoue and V. Orphan, "Thermal Neutron Capture Gamma-Ray Spectra of the Elements", Report AFCRL-69-0871, U. S. Air Force Cambridge Research Lab., Bedford, MA, Jan. 1969.

19. E. S. Gladney, D. B. Curtis and E. T. Jurney, "Simultaneous Determination of Nitrogen, Carbon, and Hydrogen Using Thermal Neutron Prompt Gamma-Ray Spectrometry", Anal. Chim. Acta 110, 339 (1979).

20. E. S. Gladney, D. B. Curtis and E. T. Jurney, "Multielement Analysis of Major and Minor Elements by Thermal Neutron Induced Capture Gamma-Ray Spectrometry", J. Radioanal. Chem. 46, 399 (1978).

21. M. S. Germani, I. Gokmen, A. C. Sigleo, G. S. Kowalczyk, I. Olmez, A. Small, D. L. Anderson, M. P. Failey, M. C. Gulovali, C. E. Choquette, E. A. Lepel, G. E. Gordon and W. H. Zoller, Concentrations of Elements in the National Bureau of Standards Bituminous and Subbituminous Coal Standard Reference Materials, Anal. Chem. 52 , 240 (1980).

22. T. G. Dzubay, ed., X-Ray Fluorescence Analysis of Environmental Samples (Ann Arbor Science, Ann Arbor, MI, 1977).

23. L. C. Bate, "Loss of Mercury from Containers in Neutron Activation", Radiochem. Radioanal. Lett. 6, 139 (1971).

24. D. B. Curtis, E. S. Gladney and E. T. Jurney, "The Cosmochemistry of Boron", Geochim. Cosmochim. Acta, in press.

25. M. R. Najam, M. Anwar-Ul-Islan, A. F. M. Ishaq, J. A. Mirza, A. M. Khan and I. H. Qureshi, "In-Beam Neutron Activation Analysis of Stainless Steel and Iron Ore", J. Radioanal. Chem. 27, 115 (1975).

26. N. M. Spyrou and S. A. Kerr, "Multielement Trace Analysis Using Cyclic Activation and a Low Energy Photon Detector", in Proc. 3rd. Int. Conf. on Nuclear Methods in Environmental and Energy Research, Columbia, MO, 1977, J. R. Vogt, ed., CONF-771072, pp. 108-125.

27. T. Gozani, E. Elias and H. Bozorgmanesh, "Nuclear Assay of Coal: Determination of Total Hydrogen Content of Coal by Nuclear Techniques", Electric Power Research Institute Report FP-989, Vol. 3, Jan. 1979; G. Reynolds, H. Bozorgmanesh, E. Elias, T. Gozani, T. Maung and V. Orphan, ibid., Vol. 1, "Coal Composition by Prompt Neutron Activation Analysis - Basic Experiments", Jan. 1979.

28. C. L. Herzenberg, N. M. O'Fallon, B. S. Yarlagadda, R. W. Doering, C. E. Cohn, K. G. Porges and D. Duffey, "Neutron-Induced Gamma Spectrometry for On-Line Compositional Analysis in Coal Conversion and Fluidized-Bed Conbustion Plants", in Proc. of 3rd Int. Conf. on Nuclear Methods in Environmental and Energy Research, Columbia, MO, 1977, J. R. Vogt, ed., CONF-771072, 1977, pp. 412-424.

29. D. Duffey, J. P. Balagna, P. F. Wiggins and A. A. El-Kady, "Copper Mining and Mill Analyses by Gamma-Rays from Capture of ^{252}Cf Neutrons", Anal. Chim. Acta 79, 149 (1975).

30. D. Duffey, P. F. Wiggins, F. E. Senftle and A. A. El-Kady, "Concrete Analysis by Neutron Capture Gamma Rays Using ^{252}Cf", Highw. Res. Rec. 412, 13 (1972).

31. P. F. Wiggins, D. Duffey and A. A. El-Kady, "Neutron Capture Gamma-Ray Studies of Marine Manganese Nodules Using a Nuclear Reactor and a ^{252}Cf Source", Anal. Chim. Acta 61, 421 (1972).

32. W. C. Reinig and A. G. Evans, "Californium-252: A New Neutron Source for Activation Analysis". In Modern Trends in Activation Analysis, J. R. DeVoe, ed., Nat'l. Bureau of Stds. Special Publication No. 312, 1969, pp. 953-957, Vol. 2.

33. M R. Ghavi and C. O. Cogburn, "Coal Analysis by Cf-252 Induced Capture-Gamma Spectroscopy", in Proc. of 3rd Int. Conf. on Nuclear Methods in Environmental and Energy Research, Columbia, MO, 1977, J. R. Vogt, ed., CONF-771072, 1977, pp. 404-411.

34. D. Vartsky, K. J. Ellis, N. S. Chen and S. H. Cohn, "In-Vivo Measurement of Kidney and Liver Cadmium by Neutron Capture Prompt Gamma-Ray Analysis", ibid., pp. 639-648.

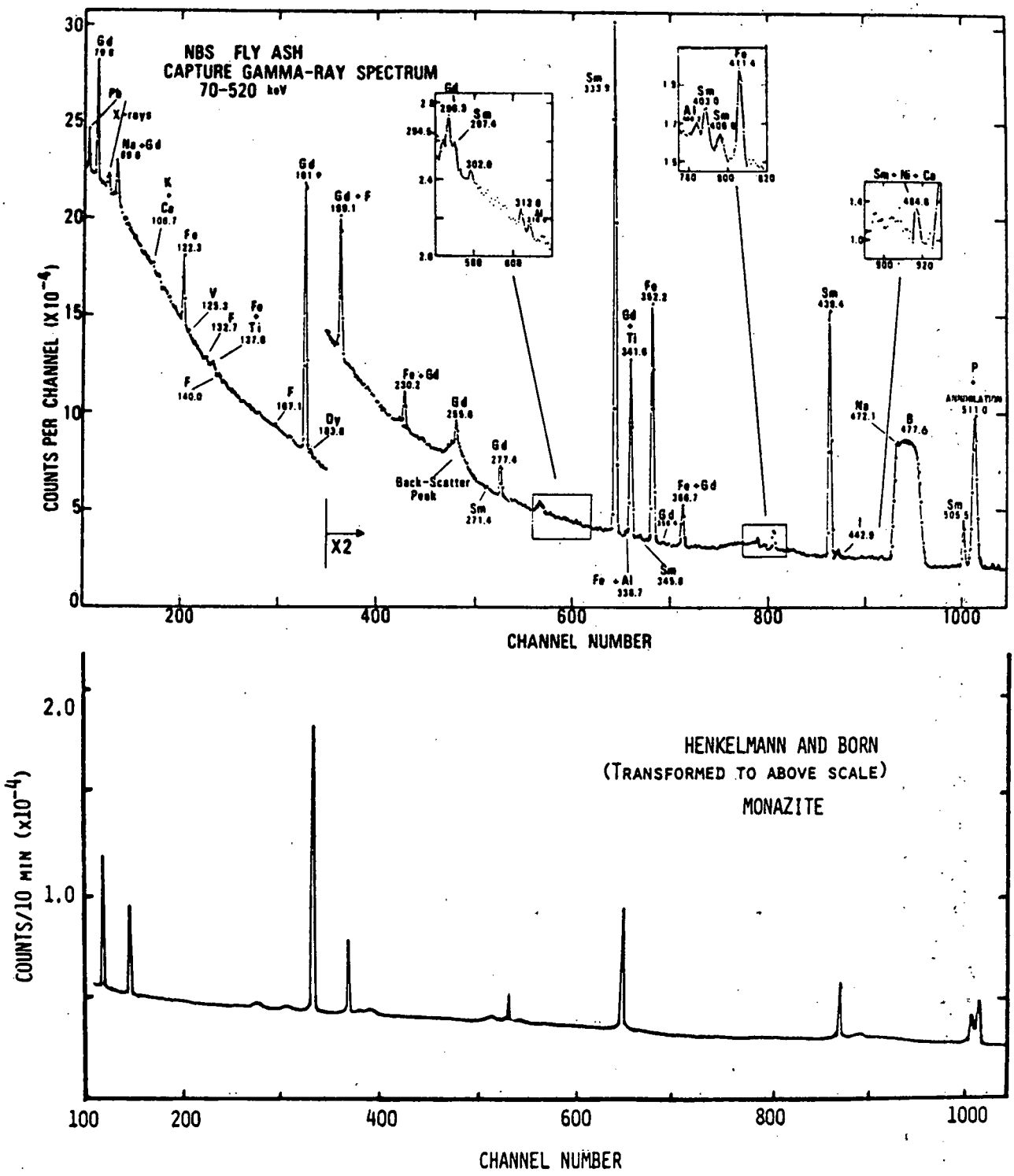


Fig. 1. Upper portion: Prompt γ-ray spectrum of fly ash from Failey et al. (14).
Lower portion: Prompt γ-ray spectrum of a monazite sample from Liberia taken by Henkelmann and Born (7) and transformed approximately to the same energy scale as the fly ash spectrum above.

Table I. Elements Observed in Various Types of Samples by PGAA

Element	Coal[a,b,c]	Fly Ash[a,b]	Granite[d,e]	Peridotite[d,e]	Manganese Nodule[e]	Monazite[f]	Catalyst[g]	Bovine Liver[a,b,c]	Orchard Leaves[a,b,c]
H	S		S	S	S		S	S	S
B	S	S	S	S	S			W	S
C	W							S	S
N	S							S	S
Na (D)	M	W	S	M	M			W	
Mg		M	W	S					W
Al (D)	S	S	S	S	S				
Si	S	S	S	S					
P		M	M	M					
S	S	W						S	S
Cl	S		W	W	S			S	S
K	S	S	S		W			S	S
Ca	S	S	S	W					S
Ti	S	S	S	W					
V (D)		W	W	W	W				
Cr				S					
Mn (D)	W	W	W	S	S			M	W
Fe	S	S	S	S	S				
Co				W	W		S		
Ni				W	W		S		
Cu					W				
Sr			W						
Mo	W						S		
Cd		W	M		S			W	
Ba			W						

Table I. Elements Observed in Various Types of Samples by PGAA

Element	Coal[a,b,c]	Fly Ash[a,b]	Granite[d,e]	Peridotite[d,e]	Manganese Nodule[e]	Monazite[f]	Catalyst[g]	Bovine Liver[a,b,c]	Orchard Leaves[a,b,c]
La	M					S			
Nd	S	W	W		W	S			
Sm		S	S	M	S	S			W
Eu	S					S			
Gd		S	S		S	S			
Dy						S			
Th						S			

[a]Ref. (14).
[b]Refs. (11, 12).
[c]Ref. (19).
[d]Ref. (15).
[e]Ref. (20).
[f]Ref. (7).
[g]Refs. (8, 9).

S = sensitive; can be determined in most samples of type indicated
W = weak; can usually be determined by with large error or long counting time
M = marginal; can be determined in some samples, but not all
D = unusually measured (at least in part) by radioactive decay

ACTIVATION-ANALYSIS PROSPECTS BY USING A CONCENTRIC $5 \cdot 10^{12}$ N/S SEALED NEUTRON TUBE COMBINED WITH A FAST RABBIT SYSTEM

H.U. Fanger, R. Pepelnik and W. Michaelis
Institut für Physik
GKSS - Forschungszentrum, D-2054 Geesthacht, Germany

ABSTRACT

A new type of intense 14 MeV neutron generator with cylindrical acceleration structure is being installed at the GKSS Research Center Geesthacht. The system represents a modification of a sealed neutron tube originally designed for medical therapy. In combination with a fast pneumatic rabbit system which transports samples within 140 ms to a remote detector station at 16 m distance, the facility has particular capabilities for neutron activation analysis and cross section studies involving short-lived reaction products. The averaged neutron flux available for activation is $5.5 \cdot 10^{10}$ n/cm^2 s with inhomogeneities of less than 7 % within sample volumes of about 3 cm^3. Detailed calculations reveal that half the ensemble of 78 elements can be detected below a 1 µg level. Thus, the new facility might also provide favourable conditions for applications in environmental studies like surveillance of air pollution or water quality.

I. INTRODUCTION

14 MeV NAA is generally accepted as being a well established technique for the fast determination of elements like oxygen, silicon, fluorine, nitrogen (for protein), phosphorus and others unsuited for analysis by means of reactor neutrons. With the advent of neutron generators with yields of $5 \cdot 10^{12}$ n/s which originally had been developed for medical purposes the analytical capabilities both with respect to sensitivity and selectivity have been extended considerably, as will be discussed in this paper. Since the source of 14 MeV neutrons - a D-T reaction target - is depleted within hours for open generators through some hundreds of hours for sealed neutron tubes, short-lived reaction products with half-lives centered in the region of minutes have always been preferred in fast NAA. In order to take full advantage of the analytical potential, however, extension of the half-life range down to 1/10 of a second, at least, seems to be promising. Statistical considerations suggest that up to 80 radionuclides in the half-life range between 10 ms and 10 s might be useful for 14 MeV NAA [1]; but many of the cross sections relevant to these reactions have not been measured up to now.

The combination of an intense sealed neutron tube and a fast rabbit system is just being realized at the GKSS Research Center Geesthacht. In the following section, technical specifications and characteristic features of the facility will be revealed. Thereupon, the procedure for predicting the analytical prospects will be discussed and the results of sensitivity calculations for the new facility considering 78 elements will be presented and, finally, be confronted with some typical trace element concentrations in environmental samples.

II. NEUTRON GENERATOR AND RABBIT SYSTEM

One of the most intense 14 MeV neutron generators hitherto available is a sealed neutron tube with a cylindrical acceleration structure developed by Schmidt [2]. It is manufactured under licence by Emile Haefely & Co. Ltd., Basel (Switzerland). The guaranteed neutron source strength of the cylindrical target is $5 \cdot 10^{12}$ n/s.

The neutron tube with its annular ion source, acceleration electrode and inner ScTD target is presented in fig. 1. The ion beam current, about one third of the total current, is 150 mA at an acceleration voltage of 200 kV. The neutron flux at the axis within the target is about $5 \cdot 10^{10}$ n/cm^2 s, whereas the neutron flux at the lower end outside the tube has the rather conventional value of 10^9 n/cm^2 s. The guaranteed lifetime of the neutron tube is 300 h.

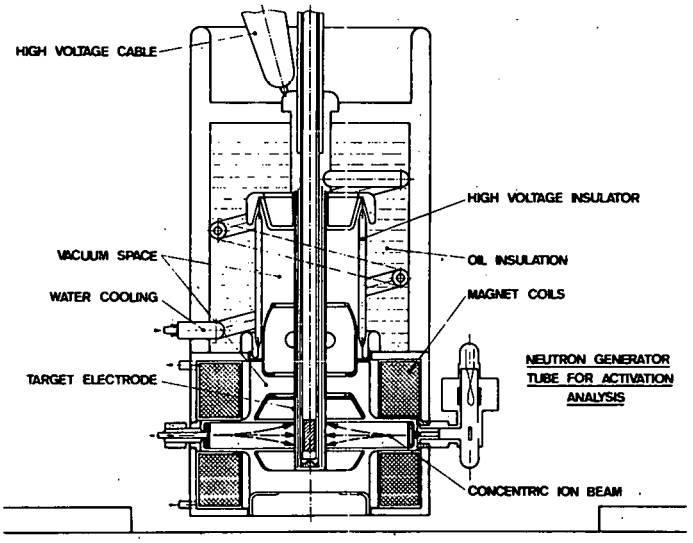


Fig. 1 Schematic view of a sealed neutron tube with cylindrical acceleration structure for activation analysis (by courtesy of Haefely & Co. Ltd., Basel).

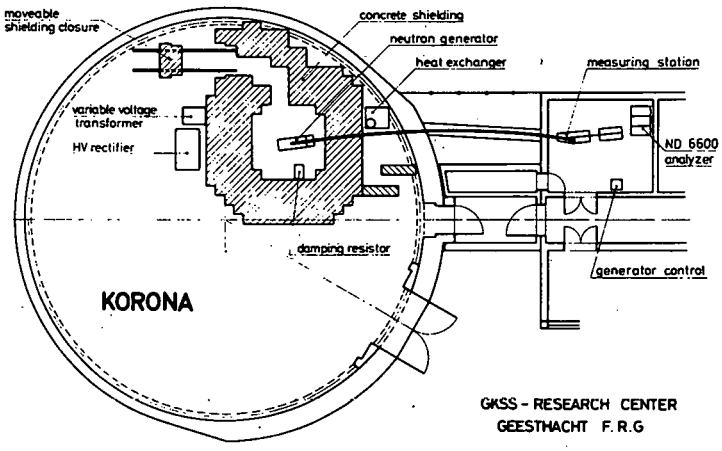


Fig. 2 Set-up of the facility KORONA with rabbit system and heavy-concrete shielding.

In order to meet the requirements for 14 MeV neutron activation analysis of short-lived nuclides, the interior space of the earlier closed-end neutron tube had to be made accessible for a fast sample transfer system. Therefore, based on suggestions and specifications made by the authors, modifications had to be performed both on the medical version of the neutron tube and the existing rabbit transfer device. The resulting facility, called KORONA, is now being installed at the GKSS Research Center. The set-up of KORONA is shown in fig. 2. The neutron generator is shielded with heavy concrete of 2.5 m wall thickness. Samples activated in the interior of the neutron tube are pneumatically transferred within less than 140 ms to a 16 m distant detector station with a computerized multi-channel analyzer in a separate building. A special feature of the transport system developed by Kreiner [3] is the separation of carrier rabbit and sample capsule by means of centrifugal force in a curved branch of the pneumatic tube near the detector.

With the geometrical conditions of the neutron tube (with inner hole diameter of 29 mm), this principle, however, confines the sample volume to 0.55 cm^3. Sacrificing the advantage of sample separation from the rabbit for the sake of larger amounts of material allows a sample volume of 2.8 cm^3. Finally, substitution of the fast rabbit system by a conventional one would raise the maximum value to 25 cm^3.

It is a special feature of the cylindrical neutron tube structure that the neutron flux within the interior is rather homogenous. Both geometric flux distributions and mean flux values for different sample sizes and ion beam distributions have been calculated in detail [4]. As an example, fig. 3 displays the local neutron flux distribution within the cylindrical target of KORONA. The maximum relative deviation from the mean flux value is ± 2 % or ± 6.5 % for the capsule with 0.55 cm^3 or 2.8 cm^3 sample volume, respectively. This homogeneity of the neutron flux clearly demonstrates the superiority of irradiation in cylindrical target geometry compared with minimum-distance activation in plane target geometry which is known to be a severe source of systematic error.

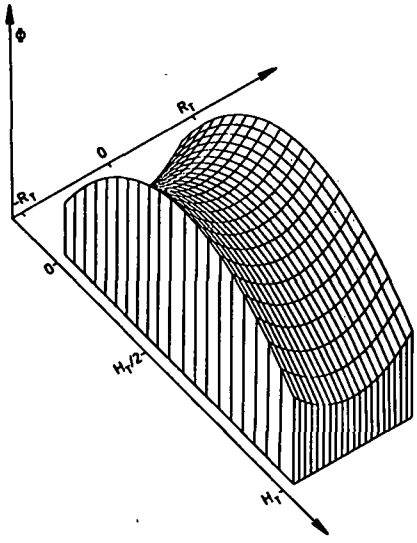


Fig. 3 Local neutron flux distribution within the cylindrical neutron source (42 mm diam. x 60 mm) of KORONA.

III. TIME FUNCTIONS IN ACTIVATION ANALYSIS

In order to make a reasonable estimate of the lower limits of detection for all elements that can be both activated by 14 MeV neutrons and identified by γ radiation, a procedure has to be found with respect to the time functions involved. Obviously, the saturation assumption which is often met for simplicity in compilations of similar kind, suffers from the fact that short-lived reactions products with half-life $\tau = \lambda^{-1} \cdot \ell n2$ are handicapped due to the τ dependence of the counting response. On the other hand, this disadvantage can partly be overcome by repetitive measurements in the so-called 'cyclic activation' technique [5], as will be discussed more quantitatively in the following.

The period p (i.e. one activation cycle) is defined by the sum of irradiation time t_i, waiting time t_w, measuring time t_m, and sample return time t_r

$$p = t_i + t_w + t_m + t_r, \tag{1}$$

and the saturation γ activity be noted by A.

Then, the cumulative total number $\Gamma_{4\pi}$ of γ quanta emitted within all measuring intervals t_m of N activation cycles is

$$\Gamma_{4\pi} = A \cdot f(t_i, t_w, t_m) \cdot g(N, p, \tau) = A \cdot F \tag{2}$$

with

$$f = (1 - e^{-\lambda t_i})\, e^{-\lambda t_w} (1 - e^{-\lambda t_m})\, \lambda^{-1} \tag{3}$$

and

$$g = \frac{N}{1 - e^{-\lambda p}} - \frac{e^{-\lambda p}\ (1 - e^{-N\lambda p})}{(1 - e^{-\lambda p})^2} . \qquad (4)$$

Thus, the intensity P of a peak at energy E in a γ spectrum recorded by a detector with absolute efficiency $\varepsilon(E)$ is

$$P = \varepsilon(E)\ \Gamma_{4\pi} . \qquad (5)$$

The time behaviour of conventional one-cycle activation analysis is determined by the function f. Optimum conditions are obtained with $t_i = t_m \equiv t$, and the detection response as a function of τ is highest for $\tau = 0.552\ t$ (neglecting t_w). For short-lived nuclides ($t >> \tau$) the response f is proportional to τ, and, viceversa, for long-lived isotopes ($t << \tau$) the function f decreases with $1/\tau$.

With cyclic activation, there appears an additional function in eq. (2), the gain factor g. This factor is strongly dependent on the number N of cycles, but it exceeds N because of remainder activities of the preceding irradiations.

Suppose, there is a fixed total time T of activation analysis available and the task given to determine, under optimum conditions, some element by a reaction product with half-life τ (neglecting matrix effects). This means optimizing the function $F = f \cdot g$ by variation of the number N of cycles which controls the period time p and activation (or measuring) time t according to

$$p = T/N \qquad (6)$$

and

$$t = t_s = t_m = \frac{T/N - t_w - t_r}{2} . \qquad (7)$$

This is the procedure applied for the diagram in fig. 4 and for the compilation of elemental sensitivities in tab. I.

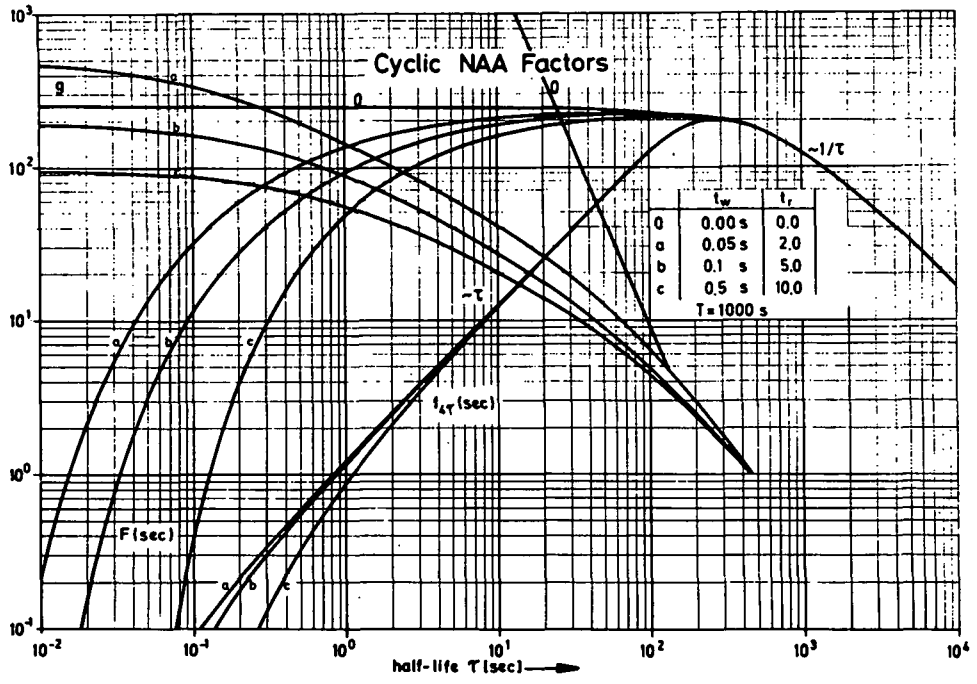


Fig. 4 Time functions f and F for conventional and cyclic activation analysis, respectively, as well as repetition gain factor g. For details see text.

The curves in the diagram reveal the time behaviour for a fixed total time of T = 1000 s and four assumed combinations of t_w and t_r. In one-cycle activation, for favourable conditions of f the time $t = t_i = t_m$ may be chosen, e.g., equal to 4τ or 500 s - t_w - t_r whichever is less. This has been done for f indexed by 4τ in fig. 4. On the other hand, for optimizing $F = f \cdot g$ for cyclic activation the factor f has not necessarily to be optimum; it might be better to shorten the period time p, i.e. to loose somewhat in f, but to obtain greater gain g by increasing the number N of cycles.

It is interesting to note that with cyclic activation analysis the loss of response to short-lived radionuclides is well compensated if $t_w = t_r = 0$. In all other cases, due to finite t_w and t_r values, the compensation deteriorates with shortening half-life. The case b with $t_w = 0.15$ and $t_r = 5.0$ s represents roughly the conditions for KORONA. A short-lived nuclide with τ = 100 ms, e.g., has to compensate by a factor of 20 in more favourable nuclear data for having equal chances to be detected compared to radionuclides with half-lives between 10 s and 400 s.

IV. ELEMENTAL SENSITIVITIES

Although in practice all experimental conditions have to be adjusted to the particular analytical problem, the procedure utilized in the foregoing discussion of the cyclic NAA time functions seems to be quite adequate for comparative sensitivity considerations. Calculations of this kind, neglecting matrix effects, have been performed using T = 2000 s corresponding to about 15 min maximum duty time of neutron activation, $t_w = 0.14$ s, $t_r = 5$ s and $\phi = 5 \cdot 10^{10}$ n/cm^2 · s.

The results are presented in tab. I. A total of 78 elements has been compiled this way by selecting that reaction for each of them which is most prominent with respect to detection response. For fluorine and chlorine also the second strongest reactions have been included because, on cross section arguments, these reactions are usually expected to be the superior ones. The most recent nuclear data compilations available were used [6, 7, 8] supplemented by literature on single measurements as quoted in tab. I. For the indication of the minimum mass detectable (m_{min}), the efficiencies of a 15 % Ge(Li) diode and a 7.5 cm diam. x 7.5 cm NaI(Tl) crystal (values in brackets) were taken as a basis.

A statistical evaluation of the calculated sensitivity data in terms of m_{min} is given in fig. 5. The histograms reveal the number of elements plotted versus their lower limits of detection. All 78 elements of the compilation for 14 MeV NAA with KORONA have been used in the upper part of this figure, whereas in the lower part a similar representation of reactor neutron activation sensitivities [9] is given including 60 elements. For either histogram Ge(Li) detector efficiencies were utilized. In all cases except for nitrogen, reactions leading to strong annihilation quanta radiation have been neglected in the statistics as being unspecific.

When comparing both histograms, one has to keep in mind that (i) the reactor neutron flux is still 1000 times higher than that of KORONA, (ii) the total time of reactor activation analysis assumed in the calculations is 170 times longer than for KORONA, and (iii) the cross sections for thermal neutron reactions tend to higher values. Thus, it is rather astonishing that there is no greater difference in the averaged sensitivities of these methods.

To be able to judge the analytical potential of KORONA for practical work in environmental studies and surveillance routine, it is useful to compare the elemental sensitivity data of tab. I with typical heavy metal concentrations in natural samples. For this purpose, results of measurements of air-dust filter samples performed at the authors' institute [11], of air-dust 'fall-down' samples

Table I

Calculated lower limits of detection for elements activated by 14 MeV neutrons

Reaction	Ab.[a] [%]	$\sigma_{14.7}$[b] [mb]	τ[a] [sec]	E_γ[a,c] [keV]	I[a,c] [%]	N[d]	$\Gamma_{4\pi}$[e] [ng^{-1}]	m_{min}[f] [ng]	
$^{11}B(n,p)^{11}Be$	80.2	25	13.8	2125	33	41	7.2	2340	(460)
$^{12}C(n,p)^{12}B$	98.89	1.9	0.02	4439	1.3	367	$5.0\cdot10^{-6}$	-	
$^{14}N(n,2n)^{13}N$	99.63	7.5	598	511	199.6	1	13.0	294	(57)
$^{16}O(n,p)^{16}N$	99.76	37	7.13	6129	69	62	16.9	2370	(490)
$^{19}F(n,p)^{19}O$	100	18	26.9	197	91	26	11.0	130	(34)
[$^{19}F(n,\alpha)^{16}N$	100	23	7.13	6129	69	62	8.9	4500	(940)]
$^{23}Na(n,\alpha)^{20}F$	100	150	11.0	1633	100	47	75	172	(34)
$^{26}Mg(n,\alpha)^{23}Ne$	11.01	75	37.6	440	33	21	1.46	2280	(460)
$^{27}Al(n,p)^{27}Mg$	100	75	568	844	73	1	25.0	258	(50)
$^{28}Si(n,p)^{28}Al$	92.23	220	134.4	1779	100	7	97	145	(29)
$^{31}P(n,\alpha)^{28}Al$	100	117	134.4	1779	100	7	51	277	(55)
$^{34}S(n,p)^{34}P$	4.21	75	12.4	2127	15	44	0.17	100 000	(19600)
$^{37}Cl(n,p)^{37}S$	24.23	37	300	3103	94	3	3.1	8100	(1580)
[$^{37}Cl(n,\alpha)^{34}P$	24.23	101	12.4	2127	15	44	1.21	14 000	(2750)]
$^{40}Ar(n,p)^{40}Cl$	99.60	18	81	1461	77	12	4.6	2440	(480)
$^{39}K(n,2n)^{38}K$	93.26	4.3	457	2167	100	2	1.3	13 300	(2630)
$^{44}Ca(n,p)^{44}K$	2.09	35	1326	1157	58	1	0.10	91 000	(17000)
$^{45}Sc(n,2n)^{44}Sc$	100	190	14148	1157	100	1	5.9	1530	(295)
$^{46}Ti(n,p)^{46m}Sc$	8.2	66[g]	18.7	143	62	34	0.86	1190	(380)
$^{51}V(n,p)^{51}Ti$	99.75	35	348	320	94	2	8.1	290	(64)
$^{52}Cr(n,p)^{52}V$	83.79	95	226	1434	100	4	20.2	550	(108)
$^{55}Mn(n,\alpha)^{52}V$	100	32	226	1434	100	4	7.7	1450	(283)
$^{56}Fe(n,p)^{56}Mn$	91,8	103	9284	847	99	1	3.5	1870	(360)
$^{59}Co(n,\alpha)^{56}Mn$	100	30	9284	847	99	1	1.0	6540	(1250)
$^{61}Ni(n,p)^{61}Co$	1.13	100	5940	67	86	1	0.05	13 300	(5600)
$^{63}Cu(n,2n)^{62}Cu$	69.2	550	584	511	196	1	140.0	27	(5)
$^{65}Cu(n,\alpha)^{62}Co$	30.8	7	834	1173	83	1	0.3	27 000	(5200)
$^{64}Zn(n,2n)^{63}Zn$	48.6	180	2286	511	186	1	17.0	226	(44)
				670	8.4	1	0.8	6700	(1280)
$^{69}Ga(n,2n)^{68}Ga$	60.1	1010	4086	511	180	1	67.0	57	(11)
				1077	3.0	1	1.1	7600	(1480)
$^{76}Ge(n,2n)^{75m}Ge$	7.8	1000	48	140	39	18	5.5	181	(58)
$^{75}As(n,p)^{75m}Ge$	100	15	48	140	39	18	1.03	970	(310)
$^{78}Se(n,2n)^{77m}Se$	23.5	840[+]	17.4	162	52.5	35	16.0	73	(21)
$^{79}Br(n,2n)^{78}Br$	50.69	970	388	511	184	2	140.0	27	(5)
$(n,n')^{79m}Br$	50.69	653[h]	4.9	207	76	77	31	48	(13)
$^{84}Kr(n,p)^{84}Br$	57.0	8.5	1908	882	42	1	0.2	35 600	(6800)
$^{87}Rb(n,2n)^{86m}Rb$	27.83	750	61.2	556	98	15	32	130	(26)
$^{88}Sr(n,2n)^{87m}Sr$	82.6	290[+]	10080	388	82	1	4.3	675	(138)
$^{89}Y(n,n')^{89m}Y$	100	350[i]	16.1	909	99	37	47	149	(29)
$^{90}Zr(n,2n)^{89m}Zr$	51.5	150[k]	251	588	89.5	4	9.9	450	(88)
$^{93}Nb(n,2n)^{92m}Nb$	100	465	876 960	934	99	1	0.1	59 500	(11100)
$^{92}Mo(n,2n)^{91}Mo$	14.8	177	929	511	188	1	5.7	675	(130)
^{91m}Mo		15	65	653	48	14	0.15	33 000	(6300)
$^{99}Tc(n,\alpha)^{96}Nb$	100 *	2.0	84 240	778	97	1	$5.0\cdot10^{-3}$	10^6	$(2\cdot10^5)$

Table I (continued)

Reaction	Ab. [a)] [%]	$\sigma_{14.7}$ [b)] [mb]	τ [a)] [sec]	E_γ [a,c)] [keV]	I [a,c)] [%]	N [d)]	$\Gamma_{4\pi}$ [e)] [ng^{-1}]	m_{min} [f)] [ng]
$^{104}Ru(n,2n)^{103}Ru$	18.7	1440	3404160	497	86	1	0.01	$3\cdot10^5$ (50000)
$^{103}Rh(n,\alpha)^{100}Tc$	100	11	15.8	540	7.0	37	0.09	45 000 (8900)
$^{108}Pd(n,2n)^{107m}Pd$	26.7	517	21.3	215	68	31	11.0	142 (36)
$^{107}Ag(n,2n)^{106}Ag$	51.83	800	1440	511 + 512	144	1	49.9	76 (15)
$^{109}Ag(n,2n)^{108}Ag$	48.17	740	144	633	1.75	7	0.78	6100 (1200)
$^{112}Cd(n,2n)^{111m}Cd$	24.1	600	2916	245	94	1	6.8	263 (64)
$^{113}In(n,2n)^{112m}In$	4.3	1380	1254	155	13	1	0.6	1850 (510)
$^{124}Sn(n,2n)^{123m}Sn$	5.64	547	2406	160	85.5	1	1.4	820 (240)
$^{121}Sb(n,2n)^{120}Sb$	57.3	1090	948	511	88	1	50.0	76 (15)
$^{123}Sb(n,2n)^{122m}Sb$	42.7	710	252	76	18.4	4	6.0	119 (46)
$^{130}Te(n,2n)^{129}Te$	34.5	660 [l)]	4140	460	7.1	1	0.5	6400 (1280)
$^{127}J(n,2n)^{126}J$	100	1650	1123200	389	35	1	0.08	35 000 (7140)
$^{136}Xe(n,2n)^{135m}Xe$	8.9	750	936	527	81	1	4.5	880 (170)
$^{133}Cs(n,2n)^{132}Cs$	100	1550	559008	668	97.5	1	0.4	12 000 (2300)
$^{138}Ba(n,2n)^{137m}Ba$	71.7	1150 [+)]	153	662	90	6	72	69 (13)
$^{139}La(n,p)^{139}Ba$	99.91	4.9	4974	166	22	1	0.03	42 000 (12300)
$^{140}Ce(n,2n)^{139m}Ce$	88.5	1180	56	754	92.5	16	92	62 (12)
$^{141}Pr(n,2n)^{140}Pr$	100	1850	203	511	97	5	169	23 (4)
				1596	0.47	5	0.82	15 200 (2970)
$^{142}Nd(n,2n)^{141m}Nd$	27.2	640	61	756	91	15	14.7	390 (76)
$^{144}Sm(n,2n)^{143m}Sm$	3.1	540	66	754	90	14	1.34	4300 (830)
$^{151}Eu(n,2n)^{150m}Eu$	47.9	540	45 360	334	3.9	1	0.03	83 000 (16700)
$^{160}Gd(n,2n)^{159}Gd$	21.8	1660	66 960	363	10	1	0.07	40 300 (7700)
$^{159}Tb(n,2n)^{158m}Tb$	100	451 [m)]	10.5	110	0.9	49	0.29	2690 (1010)
$^{164}Dy(n,\alpha)^{161}Gd$	28.1	6	222	361	61	4	0.08	32 000 (6700)
$^{165}Ho(n,2n)^{164m}Ho$	100	1750	2220	57	6.7	1	4.9	140 (57)
$^{168}Er(n,2n)^{167m}Er$	27.1	700 [+)]	2.28	208	42	118	3.7	400 (105)
$^{169}Tm(n,2n)^{168}Tm$	100	2000	8043840	198	50	1	0.01	95 000 (25000)
$^{168}Yb(n,2n)^{167}Yb$	0.14	1850 [l)]	1050	113	56	1	0.1	8850 (3300)
$^{175}Lu(n,2n)^{174m}Lu$	97.39	650	12268800	67	7.4	1	$5\cdot10^{-4}$	10^6 ($5\cdot10^5$)
$^{180}Hf(n,2n)^{179m}Hf$	35.2	600 [+)]	18.7	214	95	34	13.8	113 (29)
$^{181}Ta(n,2n)^{180m}Ta$	99.99	1810	29160	93	5	1	0.35	1900 (800)
$^{186}W(n,2n)^{185m}W$	28.6	540	100	132	4.3	10	0.49	1910 (600)
$^{187}Re(n,2n)^{186}Re$	62.6	1500	326160	137	9.3	1	0.03	32 000 (10500)
$^{190}Os(n,n')^{190m}Os$	26.4	15 [n)]	594	616	99	1	0.25	18 800 (3600)
$^{191}Ir(n,2n)^{190m_2}Ir$	37.3	190	11520	616	94	1	0.6	7960 (1540)
$^{198}Pt(n,2n)^{197m}Pt$	7.2	1030	5640	346	11	1	0.1	18 300 (3800)
$^{197}Au(n,n')^{197m}Au$	100	291 [g)]	7.7	278	73	59	11.6	175 (40)
$^{200}Hg(n,2n)^{199m}Hg$	23.1	780 [+)]	2556	158	52	1	2.9	390 (115)
$^{203}Tl(n,2n)^{202}Tl$	29.5	1900	1054080	440	91	1	0.05	66 000 (13500)
$^{208}Pb(n,2n)^{207m}Pb$	52.3	1650 [+)]	0.81	570	98	190	19.6	220 (43)
$^{226}Ra(n,2n)^{225}Ra$	100 *	1600	1278720	41	33	1	0.04	17 000 (7000)
$^{232}Th(n,2n)^{231}Th$	100	1260	91872	84	6.5	1	0.08	8500 (3500)
$^{238}U(n,2n)^{237}U$	99.28	660	583200	208	23	1	0.02	76 000 (18000)

Table I (continued)

a) Isotopic abundance of the target nuclide Ab, half-live τ, γ-ray energy E_γ and intensity I of the product nuclide. Values preferably taken from:
C.M. Lederer and V.S. Shirley: Table of Isotopes, 7th ed (1978), John Wiley & Sons, N.Y.

b) Cross sections for 14.7 MeV neutrons; values interpolated - if not indicated otherwise - from:
M. Bormann, H. Neuert, W. Scobel: Handbook on Nuclear Activation Cross-Sections, Technical Reports Ser. No. 156 (1974), IAEA Vienna.

c) γ-ray energy E_γ and intensity I;
G. Erdtmann, W. Soyka: The Gamma Rays of the Radionuclides, Top. Present. in Nucl. Chemistry 7 (1979), Verlag Chemie, Weinheim/New York.

d) Optimum number N of activation cycles p within total time Np = 2000 s; delay times due to sample transfer and sample return are t_w = 0.14 s and t_r = 5 s, respectively.

e) Total number of gamma quanta emitted per ng of sample within the sum of all measuring intervals in total time Np = 2000 s for neutron flux $\Phi = 5 \cdot 10^{10}$ n/cm^2 · s.
Formula used:

$$\Gamma = \frac{a \cdot m \cdot L}{A} \Phi \sigma I \left(1 - e^{-\lambda t_s}\right) e^{-\lambda t_w} \left(1 - e^{-\lambda t_m}\right) \lambda^{-1} \left\{\frac{N}{1 - e^{-\lambda p}} - \frac{e^{-\lambda p}\left(1 - e^{-N\lambda p}\right)}{\left(1 - e^{-\lambda p}\right)^2}\right\}$$

with $t_s = t_m$.

f) Minimum mass (ng) of element that can be determined by means of a 15 % Ge(Li)diode (7.62 cm x 7.62 cm diam NaI(Tl)detector, respectively) with 100 counts-per-peak assumption.

g) F. Özek, H. Özyol, A. Z. Ortaovali: Radiochem. Radioanal. Letters 41 (1) (1979) 87 - 94

h) S.L. Sothras, G.N. Salaita: Proc. of Int. Conf. on the Interactions of Neutrons with Nuclei, Vol. II, p. 1391, Jul. 6 - 9, 1976, Lowell, Mass. USA.

i) A. Abboud, P. Decowski, W. Grochulski, A. Marcinkowski, K. Siwek, I. Turkiewicz, Z. Wilhelmi: Acta Phys. Polonica B2 (1971) 527

k) Y. Kanda: Nucl. Physics A 185 (1972) 177

l) G. Erdtmann: Neutron Activation Tables (1976), Verlag Chemie, Weinheim/New York

m) V. Krivan, K. Krivan: J. of Radioanal. Chemistry, Vol. 29 (1976) 145

n) E. Rurarz, J. Chwaszczewska, Z. Haratym, M. Pietrzykowski, A. Sulik: Acta Phys. Polonica B2 (1971) 553

*) Instable element; 100 % - abundance assumption made for calculation.

+) Including the (n,n')reaction leading to the same metastable state.

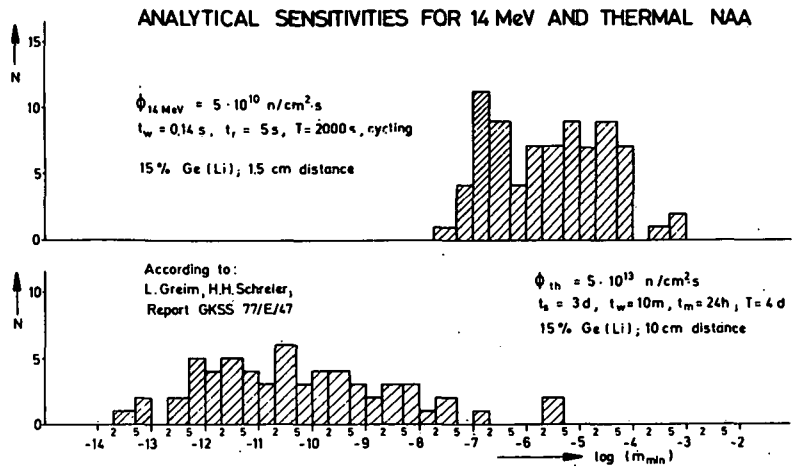


Fig. 5 Histograms of calculated elemental sensitivities for NAA with 14 MeV neutrons at KORONA (upper part) and with reactor neutrons (lower part)

collected in the city of Munich [12], and selected data of heavy metal ranges in waters [13, 14] are presented in tab. II. One may expect that more than 50 % of the elements quoted, namely V, Cr, Mn, Fe, Zn, Br, Sb, and Pb can be analyzed by 14 MeV NAA with excellent sensitivity, As, Se, Cd, and, perhaps, Hg with probably sufficient sensitivity, and Co, Ni, Cu with rather poor sensitivity.

Table II

KORONA sensitivities related to trace element concentrations in waters and air

Element	Nat. waters[a] [µg/ℓ]	Air dust[b] [µg/0.1 g]	Air dust[c] [µg/0.1 g]	KORONA sensitivity [µg]
V			51	0.3
Cr	0.6 - 130	0.6 - 50	23	0.55
Mn	10 - 580		80	1.5
Fe	90 - 3400		1380	1.9
Co	0.3 - 3	0.2 - 19	-	6.5
Ni	1.0 - 44		25	13
Cu	1.8 - 128	4 - 3400	20	27
Zn	20 - 520	42 - 4500	400	6.7
As		0.1 - 30	23	1.0
Se		0.03 - 2	4	0.07
Br		13 - 675	35	0.05
Cd	0.05 - 26 [d]	0.05 - 200	?	0.3
Sb		0.34 - 6.4	-	0.1
Hg	0.01 - 6.5 [d]	0.002 - 1.6	-	0.4
Pb	0.5 - 49		290	0.2

a) Ref. 13

b) Samples obtained by the Bergerhoff method from different stations in the city of Munich; dust level 0.3 mg/m^3; ref. 12

c) Filter-collected samples from Schauinsland (Black Forest, Germany); dust level 0.1 mg/m^3; ref. 11

d) Ref. 14

V. CONCLUSIONS

There is no doubt that the theoretical estimates given in the preceding section need experimental confirmation which will require some effort during the first years of operation. With the theoretical data verified, the new facility is expected to be an interesting tool for many practical applications as has been shown for the example of environmental samples. On the other hand, during the study of literature (s. also ref. 10), great lack of relevant nuclear data concerning cross sections, half-lives and decay schemes has become evident. For systematic investigations of this kind, KORONA will be a helpful instrument, too.

ACKNOWLEDGEMENT

The authors are obliged to Dr. B. Anders, University of Hamburg, Bundesrepublik Deutschland, for his cooperation in the search for cross section and other nuclear data.

REFERENCES

[1] H.U. Fanger, R. Pepelnik, W. Michaelis: J. of Radioanal. Chemistry (in press)

[2] K.A. Schmidt, H. Dohrmann: Atomkernenergie (ATKE) 27 (1976) 159

[3] H.J. Kreiner: Atomkernenergie (ATKE) 25 (1975) 227

[4] P. Rybaczok, H.-U. Fanger: GKSS 80/E/2

[5] W.W. Givens, W.R. Mills and R.L. Caldwell: Nucl. Instr. and Meth. 80 (1970) 95

[6] M. Bohrmann, H. Neuert, W. Scobel: Handbook on Nuclear Activation Cross Sections, Techn. Reports Ser. No. 156 (1974), IAEA Vienna

[7] G. Erdtmann, W. Soyka: The Gamma Rays of the Radionuclides, Top. Present. in Nucl. Chemistry 7 (1979), Verlag Chemie, Weinheim/New York

[8] C.M. Lederer and V.S. Shirley: Table of Isotopes, 7th ed. (1978), John Wiley & Sons, New York

[9] L. Greim. H.H. Schreier: GKSS 77/E/47

[10] W. Michaelis: Nuclear Techniques in Marine Metal Exploration, Proc. Int. Conf. on Nuclear Cross Sections for Technology, Oct. 22 - 26, 1979, Knoxville, Tennessee

[11] K. Freitag, J. Knoth, H. Schwenke: GKSS 79/E/9

[12] P. Schramel, K. Samsahl, J. Parlu: J. of Radioanal. Chem. 19 (1974) 329

[13] U. Förstner, G. Müller: Schwermetalle in Flüssen und Seen; Springer Verlag, Berlin - Heidelberg - New York 1974

[14] Deutsche Kommission zur Reinhaltung des Rheins, Zahlentafeln 1978, Sept. 1979

Neutron Activation Analysis without Multi-element Standards

A. Ahmad, T.D. Mac Mahon, M. Macwani, M.J. Minski, J.G. Williams

University of London Reactor Centre, Silwood Park, Ascot, Berkshire SL5 7PY England.

T. Bereznai*

Max-Planck Institut für Metallforschung, Stuttgart, F.R. Germany.

*Present address: Institut für Radiochemie der Technischen Universität München, Garching, F.R. Germany.

ABSTRACT

The extra information which is required to carry out neutron activation analysis without the use of multi-element standards is discussed. Particular emphasis is placed on the characterization of the neutron flux in the irradiation, and a rationalized self-consistent flux convention is described in some detail.

1. INTRODUCTION

Reactor neutron activation analysis combined with high resolution Ge(Li) gamma ray spectrometry has proved to be a powerful instrumental multi-element analytical technique for sub-ppm concentrations. The features of the relative, comparator, and absolute versions of the technique have recently been reviewed by Bereznai(1). It has been pointed out that the preparation of multi-element standards to be irradiated under the same conditions as the unknown sample is time-consuming, and is a possible source of inaccuracies. The relative technique also has the drawback of requiring prior knowledge of the elements in the unknown matrix. These factors provide the incentives for the development of methods not requiring multi-element standards.

The calculation of element masses from a neutron activation analysis experiment without standards is carried out using equation 1:

$$m = \frac{N\,M}{N_{Av}\,\theta\,P_\gamma\left[\sigma_{th}\,\Phi_{th} + I_o(\alpha)\,\phi_e\right]\varepsilon_\gamma\,S\,D\,C\,t_m} \qquad \ldots 1$$

where N is the net peak area of the photopeak, corrected for dead-time and pulse pile-up losses,
M is the atomic mass,
N_{Av} is Avogadro's number,
θ is the natural isotopic abundance,
P_γ is the gamma ray emission probability,
$\left[\sigma_{th}\,\Phi_{th} + I_o(\alpha)\,\phi_e\right]$ is the reaction rate, or saturated activity, per target atom in an irradiation site where the conventional thermal flux is Φ_{th} and the epithermal neutron flux is described by the parameters ϕ_e and α which are defined in section 4 below together with σ_{th} and $I_o(\alpha)$.
ε_γ is the gamma ray photopeak detection efficiency,

$S = 1-\exp(-\lambda t_i)$; $D = \exp(-\lambda t_d)$; and $C = \left[1-\exp(-\lambda t_m)\right](\lambda t_m)^{-1}$

are, respectively, the factors taking into account saturation during irradiation, decay between irradiation and gamma counting, and decay during counting.

In equation 1, and all further equations in this paper, the effects of self-shielding in the sample have been ignored. The equations can only, therefore, be applied to materials which are sufficiently dilute, or to cases where the necessary self-shielding corrections have been applied.

The use of equation 1 requires information not required when standards of each element are irradiated. The additional information is in three categories:

(i) the counting efficiency of the gamma ray detector measured under conditions identical to those used in counting the unknown samples;
(ii) nuclear data for each reaction used, encompassing thermal neutron activation cross-sections, resonance integrals and effective resonance energies, gamma ray emission probabilities and half-lives;
(iii) neutron flux parameters for the irradiation position, representing both the thermal and epithermal neutron flux density spectrum on an absolute scale.

These items are covered in turn in the sections below.

In constructing equation 1 it was found necessary to review the various neutron flux conventions and to arrive at a self-consistent, rationalized convention suitable for application in NAA. This is described in detail in section 4.

2. GAMMA DETECTOR EFFICIENCY

Techniques for the efficiency calibration of Ge(Li) detectors have become well established in recent years. Gehrke et al (2) have provided a comprehensive list of precise relative gamma ray intensities, while Schotzig et al. (3) and Debertin et al (4,5,6) have discussed in detail the problems of absolute efficiency calibration, including the treatment of pulse pile-up and coincidence summing effects. Using ^{152}Eu (7) and other calibration nuclides, efficiency calibration uncertainties of about 1% in the energy range 300-2000 keV can be obtained. Below 300 keV attainable uncertainties are a factor of two higher (3).

The more general problems encountered in the treatment and analysis of gamma ray spectra are dealt with by several authors in the proceedings of the 1978 Topical Conference on Computers in Activation Analysis and Gamma Ray Spectroscopy (8). In particular, Cline (9) describes a technique for the calculation of detector efficiencies for extended sources, which are commonly encountered in NAA.

3. STATUS OF NUCLEAR DATA

For many years uncertainties in nuclear data were the major source of systematic errors in attempts to carry out neutron activation analysis in an absolute manner. However, recent compilations, such as the seventh edition of "Table of Isotopes" (10), show a steady convergence in nuclear data for most isotopes of importance in NAA.

Half life data for most radionuclides of interest are now known with an uncertainty of 1% or less, though it has been pointed out (1) that the analysis is not sensitive to errors in half-life data unless the cooling time between irradiation and gamma counting is significant compared to the half-life. The situation regarding gamma-ray emission probabilities has also been improving with uncertainties reduced to 1 or 2% in most important cases. In general, errors in decay scheme data (half-lives and gamma ray emission probabilities) are not the factors which limit the accuracy of absolute NAA.

Thermal neutron cross-sections, which basically determine the reaction rate in mainly thermal neutron spectra have uncertainties of, typically, 5 to 10%. In general, the values given in "Table of Isotopes" (10) are in good agreement with those in the earlier compilation, BNL-325 (11). As far as resonance integrals are concerned, the uncertainties may be as much as a factor of 10 greater than for thermal neutron cross-sections. The scatter in resonance integrals is well illustrated in the compilations of Gryntakis and Kim (12,13) where no attempt was made to evaluate the data. It is now believed that the scatter in the data is due, to a certain extent, to a failure of the measurers to determine the shape of the epithermal neutron spectrum in which the resonance integrals were measured. It has been pointed out (14,15) that deviations from the commonly assumed 1/E shaped epithermal spectrum frequently occur in nuclear reactors and that these deviations can lead to severe changes in the apparent resonance integral. Without knowledge of the relevant epithermal shape parameter it is not possible to evaluate the data listed in references 12 and 13. Until the situation improves, the resonance integrals given in BNL-325 (11) and in the Chart of the Nuclides (16) are judged (1) to be the most reliable.

Simonits et al (17) have introduced a compound nuclear constant, $k_{o,Au}$, for use in NAA:

$$k_{o,Au} = \frac{\theta\, P_\gamma\, g\, \sigma_o\, M^{-1}}{(\theta\, P_\gamma\, g\, \sigma_o\, M^{-1})_{Au}} \qquad \ldots 2$$

where M, θ and P are as defined in section 1 above,
σ_o is the 2200 m s^{-1} cross-section,
and g^o is the Westcott factor accounting for the deviation of the cross-section from the 1/v law in the thermal region, omitted in ref. 17.
The advantages of the $k_{o,Au}$ constants are that, although the individual component nuclear data may not be known precisely, the $k_{o,Au}$ constants themselves can be measured with an accuracy of about 1% (18). Measured $k_{o,Au}$ constants have been tabulated by Simonits et al (19).

4. NEUTRON FLUX CONVENTION

The purpose of a neutron flux convention is to simplify the calculation of reaction rates in typical reactor spectra in which both thermal and epithermal neutron contributions are significant. The well known conventions of Westcott (20,21), Stoughton and Halperin (22) and Høgdahl (23) make use of the assumption that the flux density can be represented as the sum of a Maxwellian thermal component and an epithermal slowing down component proportional to 1/E. In their simplest form these conventions assume that the epithermal component has a low energy cut-off at energy μkT, where T is the characteristic temperature of the Maxwellian component, k is Boltsmann's constant and μ is a number usually taken as 5 in H_2O or D_2O moderated systems.

The assumption of a 1/E slowing down spectrum is often not adequate in practical irradiation facilities. A better approximation (24,25,26,27) is to assume that the epithermal flux density is proportional to $1/E^{1+\alpha}$, where α is a parameter which has to be determined experimentally for each irradiation position.

The convention adopted here is similar to that used by Bereznai and Mac Mahon (14) and also has features in common with that of De Corte et al (18, 15). The effects of departures from the 1/v law in activation cross-sections at low energies are also included in the present formalism.

Following the Stoughton and Halperin (22) convention, but taking into account the departure from the 1/E spectrum shape, the reaction rate, or saturated activity, per target atom for an (n,γ) type nuclear reaction in a thermal reactor is given by

$$A = \Phi_{th}\, \sigma_{th} + \phi_e\, I_o(\alpha) \qquad \ldots 3$$

where Φ_{th} is the conventional Maxwellian thermal flux equal to $n_{th}\, v_o$ the product of the thermal neutron density and the reference speed of 2200m.s^{-1},
ϕ_e is the epithermal flux per unit lnE at energy E_1, which is an arbitrary energy chosen for convenience to be 1 eV.

i.e. $$\phi_e = E_1^{-\alpha}\, E^{1+\alpha}\, f_e(E), \quad (E \geqslant \mu kT) \qquad \ldots 4$$

where $f_e(E)$ is the epithermal neutron flux density per unit energy, assumed proportional to $1/E^{1+\alpha}$,

σ_{th} is the effective activation cross-section for cadmium absorbable neutrons,

$$\text{i.e.} \quad \sigma_{th} = g\sigma_o + \frac{\phi_e}{\phi_{th}} \int_{\mu kT}^{E_{Cd}} \sigma(E) \frac{E_1^\alpha}{E^{1+\alpha}} \, dE \qquad \ldots 5$$

$I_o(\alpha)$ is the effective resonance integral, which depends on the value of α:

$$I_o(\alpha) = \int_{E_{Cd}}^{\infty} \sigma(E) \frac{E_1^\alpha}{E^{1+\alpha}} \, dE \qquad \ldots 6$$

In order to deal with the integral from μkT to E_{Cd} which appears in equation 5 we introduce the dimensionless quantity $W'(\alpha)$:

$$W'(\alpha) = \frac{1}{\sigma_o} \int_{\mu kT}^{E_{Cd}} \left(\sigma(E) - \frac{g\sigma_o v_o}{v}\right) \frac{E_1^\alpha}{E^{1+\alpha}} \, dE \qquad \ldots 7$$

In the case where $\alpha=0$, W' is the quantity tabulated by Ryves and Zieba (28), which accounts for deviation of the cross-section from the 1/v law in the energy range μkT to E_{Cd}. Because the correction is usually small we are nearly always justified in replacing $W'(\alpha)$ with W'. We then obtain:

$$A = \Phi_{th}\, g\sigma_o + \phi_e \left[\sigma_o W' + g\sigma_o f_1(\alpha) + I_o(\alpha)\right] \qquad \ldots 8$$

$$\text{where} \quad f_1(\alpha) = \int_{\mu kT}^{E_{Cd}} \frac{v_o}{v} \frac{E_1^\alpha}{E^{1+\alpha}} \, dE \qquad \ldots 9$$

which can be easily evaluated for any value of α.

Finally we need a means of evaluating $I_o(\alpha)$ from available nuclear data. It may be easily shown that:

$$I_o(\alpha) = g\sigma_o \left[\left(\frac{E_1}{\bar{E}_r}\right)^{\alpha} \left(\frac{I_o}{g\sigma_o} - f_2(o)\right) + f_2(\alpha)\right] \qquad \ldots 10$$

where I_o is the resonance integral for $\alpha=o$

$$f_2(\alpha) = \int_{E_{Cd}}^{\infty} \frac{v_o}{v} \frac{E_1^\alpha}{E^{1+\alpha}} \, dE \qquad \ldots 11$$

$\bar{E}_r$ is the effective resonance energy as defined by Moens et al in reference 29, which also contains tabulated values.

Combining equations 8 and 10 we obtain

$$A = \Phi_{th} g\sigma_o + \phi_e g\sigma_o \left[\frac{W'}{g} + f_1(\alpha) + \left(\frac{E_1}{\bar{E}_r} \right)^{\alpha} \left(\frac{I_o}{g\sigma_o} - f_2(o) \right) + f_2(\alpha) \right] \quad \ldots 12$$

A simplification to equation 12 which has been adopted by Moens et al (30) arises if we ignore deviations from the 1/v law in the activation cross-section below E_{Cd}, and from 1/E in the epithermal flux density below E_{Cd}. In that case g=1, $W' \equiv o$ and $\Phi_{th} + \phi_e f_1(o) = \Phi_s$, the conventional sub-cadmium flux as used in the Høgdahl convention (23). In our opinion it is unwise to ignore the g factor because of its slight departure from unity in the very important case of ^{197}Au(g ≃ 1.01). We then obtain:

$$A = \Phi_s g\sigma_o + \phi_e g\sigma_o \left[\left(\frac{E_1}{\bar{E}_r} \right)^{\alpha} \left(\frac{I_o}{g\sigma_o} - f_2(o) \right) + f_2(\alpha) \right] \quad \ldots 13$$

This equation is equivalent, except for the inclusion here of the g factor, to that used by the workers at INW, Gent and KFKI, Budapest (15,17,18,19,29,30).

5. DETERMINATION OF FLUX PARAMETERS

In order to apply equation 1 we need to be able to estimate the three flux parameters Φ_{th}, ϕ_e and α. Methods of finding the parameters fall into three categories involving measurement of (a) cadmium ratios of two or more isotopes to estimate Φ_{th}/ϕ_e and α, (b) cadmium covered absolute activities of at least two isotopes to estimate ϕ_e and α, and (c) absolute activities without cadmium cover of at least three isotopes to obtain all three parameters, or of a single isotope to obtain only Φ_{th} if the other parameters are already known. Examples of the use of these methods may be found in references 14, 15 and 18 , where the choice of suitable materials is also discussed.

The basis of all of the methods involves finding values of the parameters which satisfy equation 12 or the equivalent one for a cadmium covered irradiation:

$$A_{Cd} = \phi_e g\sigma_o \left[\left(\frac{E_1}{\bar{E}_r} \right)^{\alpha} \left(\frac{I_o}{g\sigma_o} - f_2(o) \right) + f_2(\alpha) \right] \quad \ldots 14$$

In the case of cadmium ratio measurements we do not know A or A_{Cd} separately, but only $R_{Cd} = A/A_{Cd}$ for each isotope. The relevant equation is easily derived from 12 and 14:

$$R_{Cd}-1 = \frac{\Phi_{th}/\phi_e + W'/g + f_1(\alpha)}{(E_1/\bar{E}_r)^{\alpha}(I_o/g\sigma_o - f_2(o)) + f_2(\alpha)} \quad \ldots 15$$

The best method of estimating flux parameters using equations 12, 14 or 15 is the generalised least squares method (31) which requires more measured quantities than the minimum numbers referred to above in order to produce an over-determined set of simultaneous equations. The technique, which has not been applied to this problem in any previously published work, will be described here with reference to cadmium ratio measurements and equation 15, but the principles are the same for the other two methods also. Cadmium ratio measurements should provide the best determination of the epithermal flux parameters provided the effects of shadowing and reactor flux perturbations are properly treated (32).

When more than two cadmium ratios are measured no single pair of values of Φ_{th}/ϕ_e and α can be found in general which exactly reproduce the measured values when applied in equation 15. This is because of the presence of errors in all measured quantities which must be taken into account by seeking the values of Φ_{th}/ϕ_e and α which minimise the appropriately weighted squared deviations between measured and calculated values. Since the nuclear data are also based on measurements with uncertainties, the best values of these must not be assumed equal to the values taken from the literature. Instead we seek new values for the nuclear data which best satisfy equation 15, in the least squares sense, by including the appropriately weighted squared deviations between the literature values and the new values in the minimization procedure.

The function to be minimised to find the least squares estimates of the flux parameters and nuclear data is:

$$\chi^2 = [E-C]^T[V_e]^{-1}[E-C] + [P_o-P_1]^T[V_p]^{-1}[P_o-P_1] \qquad \ldots 16$$

where the quantities in square brackets are matrices, T indicates the transpose of a matrix and -1 the inverse.

E	is the vector of experimental $(R_{Cd}-1)$ values,
C	is the vector of calculated $(R_{Cd}-1)$ values,
V_e	is the covariance matrix of experimental cadmium ratios,
P_1	is the vector of input parameters (flux parameters and nuclear data) containing the prior information,
P_o	is the vector of current estimated parameters from which C is calculated, and for which the best estimate is sought,
V_p	is the covariance matrix of input parameters

The covariance matrices V_e and V_p must be obtained by considering the experimental information to which they relate. In many cases we can assume that the experimental data are uncorrelated, in which case V_e and V_p are diagonal matrices containing only the variances, which are equal to the square of the standard deviations usually specified as the 'errors' of the experiments. In this case equation 16 reduces to a simple sum of squares.

The CERN library code MINUIT (33) has been used to perform the minimization on the University of London CDC 7600. The code provides the best estimates of the parameters P_o, which include Φ_{th}/ϕ_e, α, $I_o/g\sigma_o$ and $\bar{E}_r$ and their associated uncertainties in the form of standard deviations and correlation coefficients. Any attempt to calculate error propagation without taking into account these correlation terms can be very misleading.

Table 1 shows illustrative results obtained using this technique with experimental data for the ULRC ICIS irradiation position taken from ref. (14) and nuclear data from refs. (11) and (29). Not shown in the table are the correlation coefficients. For α and Φ_{th}/ϕ_e this coefficient is equal to -.91 which means that the parameter values are nearly completely negatively correlated.

6. NUCLEAR DATA ADJUSTMENTS

The generalised least-squares method as outlined in the previous section provides, each time it is applied, a new and improved estimate of the nuclear data included in the model. The output values given in Table 1 should not be taken too seriously as improved estimates of the fundamental constants $(I_o/g\sigma_o)$ because such a claim should only be made after including a number of careful measurements in different irradiation facilities, preferably from many labora-

TABLE I

Parameter	Input Values	Output Values
α	0.002 ± .4*	-0.025 ± .016
$\frac{\Phi_{th}}{\phi_e}$	25.0 ± 10.0*	17.6 ± .9
$(\frac{I_o}{g\sigma_o})_{Au}$	15.79 ± .41	15.81 ± .41
$(\frac{I_o}{g\sigma_o})_{Co}$	2.03 ± .04	2.01 ± .04
$(\frac{I_o}{g\sigma_o})_{Mn}$	1.053 ± .035	1.082 ± .032
$(\frac{I_o}{g\sigma_o})_{Cu}$	1.090 ± .092	1.023 ± .066
$\bar{E}_{r\ Au}$ (eV)	5.47 ± .56	5.47 ± .55
$\bar{E}_{r\ Co}$ (eV)	133 ± 13	132 ± 12
$\bar{E}_{r\ Mn}$ (eV)	412 ± 41	414 ± 41
$\bar{E}_{r\ Cu}$ (eV)	742 ± 74	741 ± 73
$\chi^2_4 = 4.94$		

*These values are merely starting guesses with large enough uncertainties that the output values are not influenced by them.

tories. Such a procedure can be carried out cumulatively using at each stage the relevant output parameters, with their covariance matrices from the previous step as input parameters in equation 16.

In Table 1 the reductions in the uncertainties for the nuclear data for these isotopes are quite small, mainly because the data for these isotopes are all among the best available. If isotopes with poorly known data were included with these better known ones then the improvement would be dramatic, even in only one step.

The method can be applied not only to cadmium ratio measurements, but also to absolute activities of bare or cadmium covered samples. In this case I_o and $g\sigma_o$ appear as separate quantities and not only as ratios. In addition the set of parameters found in the k_o factor and ε_γ must be included in the vectors P_o and P_1 and improved knowledge of these would be obtained in a similar way.

International collaborative efforts to improve the data for I_o, $g\sigma_o$ and k_o are clearly very desirable. The method proposed here is the only systematic and unequivocal approach to this task which is available.

7. ILLUSTRATIVE NAA RESULTS

The ideas discussed above are now being applied to practical NAA problems at U.L.R.C. Results obtained using multi-element standards are being compared to those using the 'absolute' technique. Initially irradiations are being carried out in a position of the CONSORT II reactor (34) where the epithermal shape parameter, α, is known (14) to be close to zero.

The value of Φ_{th}/ϕ_e has been determined both from cadmium ratio measurements and from the Zr double isotope technique to be 17.8 ± 1.0. Variations of this ratio with moderator temperature and control rod positions have not been detectable within the quoted error.

Rainwater samples have been analysed using both the relative technique with multi-element standards, and a single comparator technique with a dilute gold foil. In the latter technique the mass of an element x in the sample being studied is calculated by means of equation 17 below, which is derived from equations 1, 2 and 8.

$$m_x = \frac{m_{Au}}{k_{o,Au,x}} \cdot \frac{N_x}{N_{Au}} \cdot \frac{\left[\Phi_{th}/\phi_e + f_1(\alpha) + \left\{\frac{W'}{g} + \frac{I_o(\alpha)}{g\sigma_o}\right\}_{Au}\right]}{\left[\Phi_{th}/\phi_e + f_1(\alpha) + \left\{\frac{W'}{g} + \frac{I_o(\alpha)}{g\sigma_o}\right\}_{x}\right]} \cdot \frac{\varepsilon_{Au}}{\varepsilon_x} \cdot \frac{(S\ D\ C\ t_m)_{Au}}{(S\ D\ C\ t_m)_x} \qquad \ldots 17$$

where the parameters are as defined earlier in the paper and the subscripts x and Au refer to element x in the sample and to the gold foil respectively. $k_{o,Au,x}$ is the k_o factor for element x relative to gold, as defined in eq. 2.

Table 2 lists concentrations of elements in the rainwater samples determined by the two techniques:

TABLE 2

Element	Elemental Concentrations in μg/100 ml.	
	Relative Technique	Single Comparator Technique
Manganese	4.73 ± 0.25	5.32 ± 0.3
Sodium	433 ± 8	458 ± 44
Vanadium	0.84 ± 0.06	0.94 ± 0.07
Aluminium	4.73 ± 0.69	5.33 ± 0.57
Chlorine	964 ± 14	993 ± 83

Future comparisons of the two techniques will be made using irradiation positions with significant deviations from the 1/E shape in the epithermal region.

REFERENCES

1. T. Bereznai, Z. Anal. Chem. (in press).

2. R.J. Gehrke, R.G. Helmer, R.C. Greenwood, Nucl. Instr. & Meth. 147 (1977) 405-423.

3. U. Schötzig, K. Debertin, K.F. Walz, Nucl. Instr. & Meth. 169 (1980) 43-51.

4. K. Debertin, U. Schotzig, K.F. Walz, H-M. Weiss, Proc. E.R.D.A. Symp. on X- and gamma-ray sources and applications, N.T.I.S. (1976) 59.

5. K. Debertin, U. Schötzig, Nucl. Instr. & Meth., 140 (1977) 337.

6. K. Debertin, U. Schötzig, Nucl. Instr. & Meth., 158 (1979) 471-477.

7. K. Debertin, Nucl. Instr. & Meth., 158 (1979) 479-486.

8. B.S. Carpenter, M.D. D'Agostino, H.P. Yule (Editors), Proc. A.N.S. Topical Conf. on Computers in Activation Analysis and Gamma-Ray Spectroscopy, Mayaguez, Puerto Rico, 1978, CONF-780421, Department of Energy Symposium Series 49, (1979).

9. J.E. Cline, ibid, pp 185-196.

10. C.M. Lederer, V.S. Shirley (Editors) "Table of Isotopes" 7th edition (1978) J. Wiley & Sons, Inc., New York.

11. S.F. Mughabghab, D.I. Garber, "Neutron Cross-Sections" BNL-325 3rd edition, vol. 1. (1973), Brookhaven National Laboratory, New York.

12. E.M. Gryntakis, J.I. Kim, J. Radioanal. Chem. 29 (1976), 175-224.

13. E.M. Gryntakis, J.I. Kim, J. Radioanal. Chem. 42 (1978) 181-278.

14. T. Bereznai, T.D. Mac Mahon, J. Radioanal. Chem. 45 (1978) 423-434.

15. F. De Corte, L. Moens, K. Sordo-El Hammami, A. Simonits, J. Hoste, J. Radioanal. Chem. 52 (1979) 305-316.

16. F.W. Walker, G.J. Kirouac, F.M. Rourke, Chart of the Nuclides, 12th edition, (1977), Knolls Atomic Power Lab., Schenectady, New York.

17. A. Simonits, F. De Corte, J. Hoste, J. Radioanal. Chem. 24 (1975) 31-46.

18. F. De Corte, L. Moens, A. Simonits, A. de Wispelaere, J. Hoste, J. Radioanal. Chem. 52 (1979) 295-304.

19. A. Simonits, L. Moens, F. De Corte, J. Hoste, A. de Wispelaere, A. Elek, paper presented to 5th Symp. on Recent Developments in Activation Analysis". July 1978, Oxford.

20. C.H. Westcott, J. Nucl. Energy, 2 (1955) 59-76.

21. C.H. Westcott, W.H. Walker and T.K. Alexander, Proc. 2nd Int. Conf. Peaceful Uses of Atomic Energy, Geneva, A/ConF./15/P/202, U.N., New York (1958).

22. R.W. Stoughton and J. Halperin, Nucl. Sci. & Engng., 6 (1959) 100-118.

23. O.T. Høgdahl, MMPP-226-1 (1962).

24. L.C. Schmid, J.H. Lauby, W.P. Stinson and V.O. Uotinen, Phys. Res. Quart. Rept., HW-84608 (1965).

25. P. Schumann and D. Albert, Kernenergie, 8, (1965) 88.

26. K.W. Geiger and L. Van der Zwan, Metrologia, 2 (1966) 1.

27. T.B. Ryves and E.B. Paul, J. Nucl. Energy, 22 (1968) 759.

28. T.B. Ryves and K.J. Zieba, J. Phys. A: Math., Vol. 7 No. 18 (1974) 2318.

29. L. Moens, F. De Corte, A. Simonits, A. De Wispelaere, J. Hoste, J. Radioanal. Chem. 52 (1979) 379-387.

30. L. Moens, A. Simonits, F. De Corte, J. Hoste, J. Radioanal. Chem. 54 (1979) 377-390.

31. B.R. Martin, Statistics for Physicists, Academic Press, London (1971).

32. A. Ahmad and J.G. Williams, ULRC/RES/27, University of London Reactor Centre (1979).

33. F. James and M. Roos, Computer Physics Communications 10 (1975) 343.

34. G.D. Burholt, T.D. Mac Mahon, J. Radioanal. Chem. 53 (1979) 365-372.

THE FEASIBILITY OF TRACE MULTIELEMENT ANALYSIS BY 14-MeV NEUTRON ACTIVATION

Robert E. Williams and Philip K. Hopke
Institute for Environmental Studies
University of Illinois, Urbana

and

Richard A. Meyer
Lawrence Livermore Laboratory

Abstract

Instrumental Fast Neutron Activation Analysis of NBS Fly Ash, Orchard Leaves, and Bovine Liver was performed using the ICT (Insulated Core Transformer) intense neutron source at LLL. The high 14-MeV neutron flux allowed concentration determinations of up to 20 elements from the set of Na, Mg, Al, Si, P, K, Sc, Ti, Fe, Co, Ni, Zn, As, Se, Rb, Sr, Y, Zr, Mo, Sb, Ba, Ce, Tl, and Pb. Problems with interferences and steep flux gradients are discussed. The elemental profile obtained is the most complete analysis to date using FNAA.

In the last twenty years, there has been extensive use of 14-MeV neutron activation analysis utilizing small neutron generators. The vast majority of this work has been single element determinations of O and Si. An excellent review of Fast Neutron Activation Analysis (FNAA) is presented by Nargolwalla and Przybylowicz (1). Determinations of trace elements have been difficult because of flux limitations on neutron generators. Typically, the fast neutron flux is $10^9 n/cm^2$-sec with maximum fluxes of $10^{10} n/cm^2$-sec. Compounding this problem, fast-neutron cross sections are generally lower than thermal neutron absorption cross sections.

High intensity fast neutron sources are being developed, however, with the growing need to study neutron radiation damage to fusion reactor materials. The Lawrence Livermore Laboratory has two such sources, RTNS-I, henceforth referred to as the ICT (Insulated Core Transformer), and RTNS-II (Rotating Target Neutron Source) that can provide the high neutron flux required for trace element determinations. The maximum flux of the ICT source is $2\times10^{12} n/cm^2$-sec, and when RTNS-II reaches its optimum operating conditions, a flux of $4\times10^{13} n/cm^2$-sec is expected.

With access to the ICT, we have begun to develop procedures for trace multielemental analysis by 14-MeV neutron activation. There are several reasons why FNAA will be a very useful analytical tool. A number of elements difficult or impossible to determine by thermal activation (such as Si, P, Tl, and Pb) may be determined by FNAA. Secondly, biological samples with large amounts of Na and Cl, often requiring chemical separations because of intense ^{24}Na and ^{38}Cl activities, may be analyzed without separations by FNAA. Finally, a higher fraction of the total sample mass may be analyzed because of the ability to determine the abundant, low-Z elements like Si. Thus, the goal of this initial effort is to explore the potential of this new technique for trace multielemental analysis and to determine if FNAA can be developed to parallel thermal

neutron activation.

In the experiments reported here, NBS Fly Ash, Bovine Liver, and Orchard Leaves have been analyzed for 24 elements. Fast-neutron reaction products with half lives ranging from 11 seconds to 11 years were observed in the four irradiations per sample. The irradiation-counting protocol used in this analysis is similar to procedures for thermal activation. A pneumatic transfer system was used to transport samples from the ICT target room to the counting facilities in 3 to 5 seconds to count short lived activities.

METHOD

FNAA differs from thermal neutron activation in two major respects: source geometry and induced reactions. The fast neutron source is the area of deuteron beam on the tritium target, almost a point source less than 1 cm in diameter. Thus, the flux has pronounced spatial variations over a few centimeters (2), and is also influenced by beam and target conditions. Severe flux gradients are rarely the case for thermal neutrons.

Fast neutron reactions are totally different from radiative capture of thermal neutrons. Three major reaction paths are available for fast neutron interactions with a target nucleus: (n,p), (n,α), and (n,2n). In addition, there are many exotic but much less probable reactions such as (n,d), (n,t), (n,^{3}He), (n,γ), and others. Although some of the reaction products are stable nuclei, the possibility of creating three radioisotopes allows more flexibility for activation analysis than thermal neutron absorption. At the same time, however, these multiple reactions may lead to many interferences. Primary interferences occur when a particular radionuclide used for an elemental determination is produced from a second target element via another reaction path. Secondary interference occurs when two different radioisotopes emit identical energy gamma rays. Corrections for interferences require the concentration of the interfering element, which must be determined independently using another reaction product. Primary interferences are not often a problem in thermal activation analysis.

Previous experiments using the ICT were performed to ascertain how these differences between fast and thermal neutrons manifest themselves in FNAA. Following several irradiations of flyash, over 50 radioisotopes were identified and the experiments gave some acceptable quantitative analysis (3). Problems were encountered with several interferences and by the use of liquid standards. Effects of interferences can be reduced by carefully mixing standards containing combinations of elements that do not interfere with each other. Water present in the liquid standards attenuated the fast neutron flux. Because fast neutron reaction cross sections decrease rapidly with decreasing neutron energy, all reactions, including elastic and inelastic scattering, remove neutrons from the energy range needed for reactions of interest. In particular, a neutron can lose all of its energy in a single elastic collision with hydrogen, not only attenuating the fast flux but enhancing the thermal flux. This problem has been greatly reduced by the use of dry standards.

EXPERIMENT

Unlike the earlier experiments, this work provides a test of FNAA to determine a comprehensive elemental profile of three standard reference materials. Forty elements were included among the standards to maximize the number of elements in the analysis. The experiment was conducted in two parts; the first part, three irradiations per sample, was performed without the use of the fast transfer system. Later, short irradiations were repeated and radionuclides with half lives as small as 11 seconds were observed by employing the transfer system.

Samples Three NBS Standard Reference Materials, representing a variety of sample matrices, were chosen for analysis: Flyash (SRM 1633), Bovine Liver (SRM 1577), and Orchard Leaves (SRM 1571). Samples containing approximately

500 mg of material were used for each irradiation to ensure both sample homogeneity and adequate induced radioactivity. The samples, packaged in square polyethylene bags, were rather large, about 2×2 cm and up to 0.5 cm thick. Much smaller samples, 0.6 cm squares and 0.2 cm thick, were prepared for use in the rabbit system. Space limitations inside the rabbits dictated samples of 30-70 mg. The biological samples were dried at 85°C overnight before packaging.

Standards For the first part of the experiment nine standards were necessary because a sample-standard pair was used for each run. These standards were also packaged in 2-cm square bags to allow intimate contact with the samples during irradiation, lessening the effects of neutron flux gradients. Each standard contained nearly the same amount of every element of interest as the sample with which it was irradiated. Most elements, in the form of liquid standards, were measured into the bags and allowed to dry in air on a clean bench for two weeks, evaporating the solute and leaving only the elements of interest. Major constiuents, as either metal powders or other solid powders, were then added to complete the standard. (For example, the standard for the short irradiation of Bovine Liver included dried liquid standards of V, Cr, Mn, Fe, Cu, Zn, Br, Rb, Zr, and Sb along with 23 mg of Al_2O_3, 21 mg SiO_2, 11 mg KCl, and 28 mg $CaCo_3$.) Finally, six additional standards containing Cd, Pt, Tl, and Pb were prepared for these specific elemental determinations.

Only two standards were needed for the rabbit irradiations, one with matrix elements similar to fly ash and one similar to the biological materials. These standards were irradiated separately as sample-standard pairs would not fit into rabbits allowing both to receive sufficient neutron flux.

Irradiations The irradiations were performed at LLL on the ICT neutron source capable of producing 5×10^{12}n/sec. The source strength varied over the irradiation period from 1.4 to 2.9×10^{12}n/sec creating a flux of 0.6 to 1.1×10^{12}n/cm^2-sec at the optimum beam spot. This intense source is achieved by accelerating a 20 mA beam of deuterons through a 400 kV potential incident upon a rotating, tritiated target. The beam spot on the target was 0.6 cm in diameter. This unique facility is described in detail by Booth et al (4).

Sample-standard pairs were rolled into cylinders (2 cm long and 1 cm diameter) and placed in a sample holder attached to the face of the target assembly in the primary beam spot. The target assembly moves enabling beam to strike an unused band of the target. Since the sample holder was fixed to the face of the assembly, it could not be moved without positioning the sample holder away from the beam spot. Thus, in the course of a four hour irradiation, the source strength fell by a factor of two as tritium was depleted. The irradiation end of the rabbit system is not attached to the ICT, eliminating this constraint.

Table I lists all the irradiations and the counting schedule for each sample.

Counting The samples were counted repeatedly on one of four Ge(Li) detectors and the spectra collected on 4096 channel multichannel analyzers. The counts, also listed on Table I, ranged in length from 30 seconds for the first counts after the short runs to 20,000 seconds for the long counts. All of the spectra taken at the irradiation facility were stored on a disk using a Nuclear Data 6620 and brought to the University of Illinois for analysis by standard peak comparison methods on the ND6620. Spectra from rabbit runs were recorded on tape with an ND 6603 and analyzed on an ND 6620 at LLL. The remaining spectra were taken on a calibrated Ge(Li) detector system in the LLL Nuclear Chemistry Division and the peak energies and intensities were determined using the LLL GAMANA code (5).

RESULTS AND DISCUSSION

The analysis of the three samples yielded the concentrations of 24 elements. The reactions and radioisotopes used are listed in Table II, along with cross sections (6), gamma-ray energies, and elemental abundances of the target nuclei. In general, the cross sections for (n,p) reactions are larger than (n,2n) for

low-Z nuclei. This trend is gradually reversed so that (n,2n) reactions dominate in heavy nuclei. An asterisk by a nuclide in Table II indicates that this nuclide is formed through more than one reaction. A list of these primary interference reactions is given in Table III, along with the only troublesome secondary interference, ^{203}Hg. While several of these reactions produced negligible activity, others required corrections to elemental concentrations. Two were very severe: the ^{24}Na activity from Al was larger than from Mg in flyash and the ^{51}Cr activity from Cr was totally obscurred by the ^{54}Fe interference. Correction of the remaining interferences was eased because care was taken to avoid mixing interfering elements in the standards (7).

Since many (n,p) and (n,α) reaction products are also produced by thermal neutron absorption of lower-Z elements, a large thermal flux in the target room would have presented a major source of interference. To determine the thermal and fast neutron fluxes, a sample of Co powder was irradiated at the optimum beam spot for 45 minutes. The thermal neutron flux was determined from the measured activity of ^{60}Co. It was assumed that the thermal flux was nearly constant in the vicinity of the target because scattering from the walls and a large,water-filled shield provided the source of thermal neutrons. The flux was measured to be 1.1×10^{7}n/cm^2-sec, a factor of 10^4 less than the 14-MeV neutron flux and, therefore, a negligible source of interference.

A larger, but still negligible interference for a few elements may be caused by radiative capture (n,γ) of fast neutrons. More ^{24}Na, ^{27}Mg, ^{28}Al, and ^{54} Mn was produced this way than produced by thermal neutron capture, even though the cross sections are less than a millibarn (1). Radiative capture of fast neutrons can be an important interference under special circumstances. Single element irradiations are needed to quantitate the magnitude of this interference because of variations in thermal-, epithermal-, and fast-neutron cross sections and the relative neutron fluxes.

Results of the analysis are given in Tables IV and V along with literature values for comparison. Detection limits were reported when there was no gamma-ray peak in the sample at the same energy of an identifiable peak in the standard. The unobservable activity is assumed to be less than twice the background standard deviation over that portion of the sample spectrum containing the peak in the standard spectrum.

The concentrations for NBS Fly Ash are compared to a compilation by Ondov et al (8). Concentrations are determined for 20 elements and detection limits are given for 6 more elements. Several determinations differed from accepted values by more than 20%; concentrations of Sc, Se, Y, Zr, and Tl were too large while Sr and Ba concentrations were too small. The remaining determinations are within the range of typical results by neutron activation. It is unfortunate Ca, Cr, Zn, and Pb determinations were not possible. A Tl determination was made although the concentration was found to be much greater than that reported by Chattopadhyay and Jervis (9) using Instrumental Photon Activation Analysis. Tl and Pb are important environmental toxins which cannot be determined by thermal neutron activation.

The irradiations of biological samples yielded very low activity and several more elements are below detection limits. Of the 27 elements listed in Table V, there are only 12 determinations for Orchard Leaves and 10 for Bovine Liver. Detection limits are listed as a measure of the sensitivities of FNAA for this experiment. The analysis of Orchard Leaves is in good agreement with NBS certified values as only Ni and Sb concentrations differ by more than 20%. It is significant that a Pb determination was possible. In the case of Bovine Liver, however, the concentrations of several elements (Na, Mg, P, K, Fe, and Zn) were too low.

In general, several determinations varying widely from certified values are major constituents (Na, Mg, K, Fe, and Ba) included in the standards as powdered solids. It is clear this method of packaging standards was a factor. This

fact is underscored by the steep flux gradients in the vicinity of the optimum flux position. It was difficult to insure the elements added as solids were as well mixed as they are in the samples. In addition, the dimensions of the sample-standard pairs were larger than the primary beam spot. Thus, if a majority of an element was pushed into a corner of the standard package, it would have received less flux than if it were well mixed throughout the standard and the measured concentration of that element would be too large. Likewise, an element located chiefly in the center of the standard would result in too much activity from that element. Since each element is spread evenly across the flux gradients through the sample, this case would cause the determination to be too small. Thus, the major source of error in this experiment is the combined effect of inhomogeneous standards and geometric factors resulting in flux gradients across the sample-standard pairs. Standards used in the rabbit runs were well mixed, eliminating the problem.

Most of the remaining determinations differing from accepted concentrations were found to be too large. Inhomogeneous mixing is less likely (but not impossible) for those elements added as liquids to the standards. Certain elements may have been depleted by forming volatile compounds in the liquid mixture which evaporated with the solute during drying, accounting for a few determinations being too large while several are close to accepted values. Tl and Pb were placed in standards separate from those imitating the sample matrices which contributed to discrepancies and large detection limits.

Of the 40 elements included in the standards, results have been tabulated for 31. Five elements (V, Br, Cu, Ga, and I) were not detected in the standard spectra and four others (B, Mn, Cd, and Pt) with gamma-ray peaks in the standards resulted in detection limits too large to be of any value.

CONCLUSIONS

Several facts emerge from this work demonstrating the feasibility of trace multielemental FNAA. Neither thermal neutron absorption nor interfering fast neutron reactions seriously impair quantitative analysis by 14-MeV neutron activation. Concentrations of 20-30 elements can be accurately determined in three or four irradiations using multielemental standards. At least five elements, Si, P, Mo, Tl, and Pb, difficult or impossible to observe by thermal neutron activation, have been determined by FNAA.

This analysis provides the most complete elemental profiles of standard reference materials yet determined by 14-MeV neutron activation. Improvements in the rabbit system and methods of preparing and packaging samples and standards, already underway, will increase accuracy, sensitivity, and the number of elements that can be analyzed.

Acknowledgement

We wish to thank the Nuclear Chemistry Division of Lawrence Livermore Laboratory for their encouragement and support of this work. One of us (R.E.W.) would like to thank the Nuclear Engineering Program of the University of Illinois for their partial support of his trip to LLL to conduct these experiments, and the Associated Western Universities, Inc. for granting a fellowship to complete this work at LLL.

REFERENCES

1. Nargolwalla, S.S.; Przybylowicz, E.P., "Activation Analysis with Neutron Generators", John Wiley & Sons: New York, 1973.

2. Van Grieken, R.; Speeche, A.; Hoste, J., J. Radioanal. Chem., 10, 95 (1970).

3. Hopke, P.K.; Williams, R.E.; Meyer, R.A., The Feasibility of Trace Multielemental Analysis by High Flux 14-MeV Neutron Activation, presented to the 173rd Meeting of the American Chemical Society, March 1977.

4. Booth, R. et al, Nucl. Instr. and Meth., 145, 25 (1977).

5. Gunnink, R.; Niday, J.B., Lawrence Livermore Report No. UCRL-51051 (unpublished), 1972, Vol. I-IV.

6. "Handbook on Nuclear Activation Cross-Sections", Technical Reports Series No. 156, IAEA: Vienna, 1974.

7. Krivan, V.; Krivan, K., J. Radioanal. Chem., 26, 145 (1976).

8. Ondov, J.M. et al, Anal. Chem., 47, 1102 (1975).

9. Chattopadhyay, A.; Jervis, R.E., Anal. Chem., 46, 1630 (1974).

TABLE 1: Irradiations† and Counting Times

	Flyash	Bovine Liver	Orchard Leaves
Rabbit Runs	30 second irrad.	1 minute irrad.	1 minute irrad.
decay times to counts	30 seconds 1 minute 3 minutes 9½ minutes	30 seconds 1 minute 3 minutes 9½ minutes	30 seconds 1 minute 3 minutes 9½ minutes
Short Runs	10 second irrad.	1 minute irrad.	1 minute irrad.
decay times to counts	4 minutes 27 minutes	4 minutes 27 minutes	4 minutes 36 minutes
Intermediate Runs	25 minute irrad.	1 hour irrad.	1 hour irrad.
decay times to counts	70 minutes 5½ hours 20 hours 2 days 3 days	34 minutes 6 hours 25 hours 1½ days 2½ days	34 minutes 4½ hours 22 hours 2 days
Long Runs	4 hour irrad.	5 hour irrad.	11 hour irrad.*
decay times to counts	4 days 5 days 15 days	3 days 13 days	3 days 12 days

† maximum flux was 1×10^{12} neutrons/sec-cm^2

* not in primary flux position

TABLE II: Radioisotopes Used in Elemental Determinations

Element Sought	Reaction and product	Target abundance %	14.9-MeV cross section[a] (mb)	Product[b] Half life	Gamma-ray Energy (keV)
SHORT RUNS					
B	$^{11}B(n,p)^{11}Be$	80.	25 ± 4	13.8 S	2125
F	$^{19}F(n,p)^{19}O$	100.	18 ± 5	26.9 S	197,1357
Na	$^{23}Na(n,p)^{23}Ne^{*}$	100.	43 ± 5	37.6 S	440
	$^{23}Na(n,\alpha)^{20}F$	100.	150 ± 20	11.0 S	1634
Mg	$^{25}Mg(n,p)^{25}Na$	10.0	40 ± 4	60. S	975,390,585
Al	$^{27}Al(n,p)^{27}Mg^{*}$	100.	75 ± 7	9.45 M	844,1014
Si	$^{28}Si(n,p)^{28}Al^{*}$	92.23	210 ± 20	2.24 M	1779
	$^{29}Si(n,p)^{29}Al$	4.67	147 ± 18	6.50 M	1273
P	$^{31}P(n,\alpha)^{28}Al$	100.0	115 ± 12		
Cl	$^{35}Cl(n,2n)^{34m}Cl$	75.77	12	32.0 M	146(IT)2128,1176
	$^{37}Cl(n,p)^{37}S$	24.23	41 ± 4	5.0 M	3103
K	$^{39}K(n,2n)^{38}K$	93.26	5.1 ± 0.5	7.61 M	2168
Ca	$^{44}Ca(n,p)^{44}K^{*}$	2.09	36 ± 7	22.1 M	1157
Fe	$^{56}Fe(n,p)^{56}Mn^{*}$	91.8	103 ± 6	2.58 H	847,1811
Rb	$^{85}Rb(n,2n)^{84m}Rb$	72.17	650	20.4 M	248,464
Zr	$^{90}Zr(n,2n)^{89m}Zr$	51.5	130	4.10 M	588(IT)
INTERMEDIATE RUNS					
Mg	$^{26}Mg(n,p)^{26}Na^{*}$	79.0	180 ± 18	15.02 H	1369,1732
K	$^{41}K(n,p)^{41}Ar^{*}$	6.73	48 ± 10	1.83 H	1293
Sc	$^{45}Sc(n,2n)^{44m}Sc$	100.	155 ± 15	58.6 H	271(IT)
Ti	$^{48}Ti(n,p)^{48}Sc^{*}$	73.7	61 ± 6	43.7 H	1312,983,1037
	$^{47}Ti(n,p)^{47}Sc$	7.45	120 ± 20	3.41 D	159
Fe	$^{54}Fe(n,p)^{54}Mn$	5.8	315 ± 25	312 D	835
Ni	$^{58}Ni(n,2n)^{57}Ni$	68.3	35 ± 3	36.1 H	1378
Zn	$^{67}Zn(n,p)^{67}Cu$	4.1	40	61.7 H	185
	$^{70}Zn(n,2n)^{69m}Zn$	0.62	744 ± 100	13.8 H	439(IT)
Sr	$^{86}Sr(n,2n)^{85m}Sr$	9.84	276 ± 30	67.7 M	232,151
	$^{88}Sr(n,2n)^{87m}Sr$	82.6	354 ± 30	2.81 H	388(IT)
Zr	$^{90}Zr(n,2n)^{89}Zr$	51.5	790 ± 50	78.5 H	909
Sb	$^{121}Sb(n,2n)^{120m}Sb$	57.3	600	5.76 D	197,89
	$^{123}Sb(n,2n)^{122}Sb$	42.7	1300	2.72 D	564
Pb	$^{204}Pb(n,2n)^{203}Pb^{*}$	1.42	1840 ± 130	52.1 H	279
LONG RUNS					
Na	$^{23}Na(n,2n)^{22}Na$	100.	54 ± 5	2.60 Y	1274
Ti	$^{46}Ti(n,p)^{46}Sc$	8.25	270 ± 25	83.8 D	889,1120
Cr	$^{52}Cr(n,2n)^{51}Cr^{*}$	83.8	358 ± 25	27.7 D	320
Co	$^{59}Co(n,p)^{59}Fe^{*}$	100.	82 ± 8	44.6 D	1099,1292
	$^{59}Co(n,2n)^{58}Co^{*}$	100.	735 ± 55	70.8 D	811
Ni	$^{58}Ni(n,d)^{57}Co$	68.3	520 ± 50 (1)	271 D	122,136
	$^{60}Ni(n,p)^{60}Co$	26.1	109 ± 8	5.27 Y	1173,1332
As	$^{75}As(n,2n)^{74}As$	100	1085 ± 75	17.8 D	596,635
Se	$^{77}Se(n,p)^{77}As$	7.6	36 ± 10	38.8 H	239
	$^{76}Se(n,2n)^{75}Se$	9.0	944 ± 65	120 D	265
Rb	$^{85}Rb(n,2n)^{84}Rb$	72.2	1430	33 D	881
Y	$^{89}Y(n,2n)^{88}Y$	100.	1015 ± 70	107 D	898,1836
Mo	$^{100}Mo(n,2n)^{99}Mo$	9.6	1390 ± 60	66 H	140
Ba	$^{132}Ba(n,2n)^{131}Ba$	0.10	1600	11.7 D	496,124,216
	$^{136}Ba(n,2n)^{135m}Ba$	7.9	700	28.7 H	268(IT)
	$^{134}Ba(n,2n)^{133}Ba$	2.4	940 ± 80	10.7 Y	356
Ce	$^{140}Ce(n,2n)^{139}Ce$	88.5	1760 ± 110	138 D	166
Hf	$^{176}Hf(n,2n)^{175}Hf$	5.2	2200 ± 115	70 D	343
Au	$^{197}Au(n,2n)^{196}Au$	100.	2250 ± 120	6.17 D	333
Hg	$^{198}Hg(n,p)^{198}Au$	10.0	4	2.7 D	412
Tl	$^{203}Tl(n,2n)^{202}Tl$	29.5	1850 ± 180	12.2 D	439

* Have interfering reactions

a) Bormann, et al, Handbook on Nuclear Activation Cross Sections, Technical Reports Series No. 156, IAEA, 1974

b) Table of Isotopes, Seventh Edition, Lederer and Shirley, John Wiley & Sons, New York, 1978

TABLE III: Summary of Interferences Encountered

Element	Interfering Reaction	Target Abundance (%)	14.9 MeV* Cross Section (mb)	Comments
Na	$^{26}Mg(n,\alpha)^{23}Ne$	10.0	72 ± 10	
Mg	$^{27}Al(n,\alpha)^{24}Na$	100.	111 ± 4	Severe in flyash
K	$^{44}Ca(n,\alpha)^{41}Ar$	2.09	35 ± 8	Ca was not determined; NBS value used
Ti	$^{51}V(n,\alpha)^{48}Sc$	99.8	19 ± 4	Negligible correction
Cr	$^{54}Fe(n,\alpha)^{51}Cr$	5.8	96 ± 10	Totally obscured Cr
Fe	$^{59}Co(n,\alpha)^{56}Mn$	100.	29 ± 3	Negligible
Fe	$^{55}Mn(n,2n)^{54}Mn$	100.	850 ± 60	Negligible
Co	$^{58}Ni(n,p)^{58}Co$	68.3	330 ± 30	Use ^{59}Fe if possible
Pb	$^{204}Hg(n,2n)^{203}Hg$	6.9	2190 ± 150	Same gamma-ray energy

* Handbook on Nuclear Activation Cross-Sections, Technical Report Series No. 156, IAEA, Vienna, 1974.

TABLE IV: Elemental Concentrations in NBS Fly Ash (SRM 1633) Determined by FNAA (μg/g unless % indicated)

element	this work	others [a]
Na	3150 ± 110	3200 ± 400
Mg (%)	1.5 ± 1.3	1.8 ± 0.4
Al (%)	13.6 ± 0.5	12.7 ± 0.5
Si (%)	22.8 ± 0.8	21 ± 2
K (%)	1.9 ± 0.5	1.61 ± 0.15
Sc	41 ± 5	27 ± 1
Ti	7300 ± 150	7400 ± 300
Cr	< 150	125 ± 6
Fe (%)	6.95 ± 0.15	6.20 ± 0.30
Co	45 ± 16	41.5 ± 1.2
Ni	105 ± 3	98 ± 9
Zn	< 420	210 ± 2
As	68 ± 12	61 ± 3
Se	35 ± 13	10.2 ± 1.4
Rb	137 ± 4	125 ± 10
Sr	1310 ± 50	1700 ± 300
Y	150 ± 7	62 ± 10
Zr	410 ± 20	301 ± 20
Mo	28.0 ± 1.3	--
Sb	<15	6.9 ± 0.6
Ba	2100 ± 100	2700 ± 200
Ce	136 ± 5	146 ± 15
Hf	<17	7.9 ± 4
Au	<8	--
Hg	<8	0.15 ± 0.01
Tl	18 ± 6	4 [b]

a) Ondov et al, Anal. Chem., 47, 1102 (1975).

b) Chattopadhyay and Jervis, Anal. Chem., 46, 1630 (1974).

TABLE V: Elemental Concentrations in NBS Orchard Leaves (SRM 1571) and Bovine Liver (SRM 1577) Determined by FNAA (μg/g unless % indicated)

element	Orchard Leaves		Bovine Liver	
	this work	other values[a]	this work	other values[a]
F	<240	(4)	<350	--
Na	< 360	82 ± 6	1600 ± 100	2430 ± 130
Mg	7030 ± 170	6200 ± 200	290 ± 40	(605)
Al	322 ± 22	409[b]	<80	(46)
P (%)	0.20 ± 0.01	0.21 ± 0.01	0.64 ± 0.06	(1.1)
Cl	<1400	(690)	<5400	2750[b]
K (%)	1.57 ± 0.25	1.47 ± 0.03	0.63 ± 0.11	0.97 ± 0.06
Ca (%)	<3	2.09 ± 0.33	<0.5	(120 ppm)
Sc	<2	0.2[b]		
Ti	26 ± 3	--	3.2 ± 1.0	--
Cr	<2	2.6 ± 0.3	<0.3	0.5 - 3.5[b]
Fe	348 ± 10	300 ± 20	137 ± 5	270 ± 20
Co	<8	(0.2)	0.31 ± 0.12	(0.18)
Ni	2.2 ± 0.7	1.3 ± 0.2	<9	0.21[b]
Zn	<110	25 ± 3	78 ± 25	130 ± 10
As	10.6 ± 0.3	10 ± 2	<1.3	(0.055)
Se	--	0.08 ± 0.01	< 2	1.1 ± 0.1
Rb	12.8 ± 0.6	12 ± 1	18.1 ± 0.6	18.3 ± 1.0
Sr	53 ± 4	(37)		
Y	<1.1	--	<14	--
Zr	<5	--	<3	--
Mo	<1.4	0.3 ± 0.1	2.6 ± 0.4	(3.2)
Sb	5.1 ± 1.1	2.9 ± 0.3	--	0.034[b]
Ba	<240	(44)	--	2.92[b]
Ce	<2	1.0[b]	<3	--
Hg	<5	0.155 ± 0.015	--	0.016 ± 0.002
Pb	57 ± 12	45 ± 3	5	0.34 ± 0.08

a) NBS certified and uncertified () values.

b) Nadkarni and Morrison, Anal. Chem., 45, 1957 (1973).

TABLE 1: Irradiations† and Counting Times

	Flyash	Bovine Liver	Orchard Leaves
Rabbit Runs	30 second irrad.	1 minute irrad.	1 minute irrad.
decay times to counts	30 seconds 1 minute 3 minutes 9½ minutes	30 seconds 1 minute 3 minutes 9½ minutes	30 seconds 1 minute 3 minutes 9½ minutes
Short Runs	10 second irrad.	1 minute irrad.	1 minute irrad.
decay times to counts	4 minutes 27 minutes	4 minutes 27 minutes	4 minutes 36 minutes
Intermediate Runs	25 minute irrad.	1 hour irrad.	1 hour irrad.
decay times to counts	70 minutes 5½ hours 20 hours 2 days 3 days	34 minutes 6 hours 25 hours 1½ days 2½ days	34 minutes 4½ hours 22 hours 2 days
Long Runs	4 hour irrad.	5 hour irrad.	11 hour irrad.*
decay times to counts	4 days 5 days 15 days	3 days 13 days	3 days 12 days

† maximum flux was 1×10^{12} neutrons/sec-cm^2

* not in primary flux position

TABLE II: Radioisotopes Used in Elemental Determinations

Element Sought	Reaction and product	Target abundance %	14.9-MeV cross section[a] (mb)	Product[b] Half life		Gamma-ray Energy (keV)
SHORT RUNS						
B	$^{11}B(n,p)^{11}Be$	80.	25 ± 4	13.8	S	2125
F	$^{19}F(n,p)^{19}O$	100.	18 ± 5	26.9	S	197,1357
Na	$^{23}Na(n,p)^{23}Ne^{*}$	100.	43 ± 5	37.6	S	440
	$^{23}Na(n,\alpha)^{20}F$	100.	150 ± 20	11.0	S	1634
Mg	$^{25}Mg(n,p)^{25}Na$	10.0	40 ± 4	60.	S	975,390,585
Al	$^{27}Al(n,p)^{27}Mg^{*}$	100.	75 ± 7	9.45	M	844,1014
Si	$^{28}Si(n,p)^{28}Al^{*}$	92.23	210 ± 20	2.24	M	1779
	$^{29}Si(n,p)^{29}Al$	4.67	147 ± 18	6.50	M	1273
P	$^{31}P(n,\alpha)^{28}Al$	100.0	115 ± 12			
Cl	$^{35}Cl(n,2n)^{34m}Cl$	75.77	12	32.0	M	146(IT)2128,1176
	$^{37}Cl(n,p)^{37}S$	24.23	41 ± 4	5.0	M	3103
K	$^{39}K(n,2n)^{38}K$	93.26	5.1 ± 0.5	7.61	M	2168
Ca	$^{44}Ca(n,p)^{44}K^{*}$	2.09	36 ± 7	22.1	M	1157
Fe	$^{56}Fe(n,p)^{56}Mn^{*}$	91.8	103 ± 6	2.58	H	847,1811
Rb	$^{85}Rb(n,2n)^{84m}Rb$	72.17	650	20.4	M	248,464
Zr	$^{90}Zr(n,2n)^{89m}Zr$	51.5	130	4.10	M	588(IT)
INTERMEDIATE RUNS						
Mg	$^{24}Mg(n,p)^{24}Na^{*}$	79.0	180 ± 18	15.02	H	1369,1732
K	$^{41}K(n,p)^{41}Ar^{*}$	6.73	48 ± 10	1.83	H	1293
Sc	$^{45}Sc(n,2n)^{44m}Sc$	100.	155 ± 15	58.6	H	271(IT)
Ti	$^{48}Ti(n,p)^{48}Sc^{*}$	73.7	61 ± 6	43.7	H	1312,983,1037
	$^{47}Ti(n,p)^{47}Sc$	7.45	120 ± 20	3.41	D	159
Fe	$^{54}Fe(n,p)^{54}Mn$	5.8	315 ± 25	312	D	835
Ni	$^{58}Ni(n,2n)^{57}Ni$	68.3	35 ± 3	36.1	H	1378
Zn	$^{67}Zn(n,p)^{67}Cu$	4.1	40	61.7	H	185
	$^{70}Zn(n,2n)^{69m}Zn$	0.62	744 ± 100	13.8	H	439(IT)
Sr	$^{86}Sr(n,2n)^{85m}Sr$	9.84	276 ± 30	67.7	M	232,151
	$^{88}Sr(n,2n)^{87m}Sr$	82.6	354 ± 30	2.81	H	388(IT)
Zr	$^{90}Zr(n,2n)^{89}Zr$	51.5	790 ± 50	78.5	H	909
Sb	$^{121}Sb(n,2n)^{120m}Sb$	57.3	600	5.76	D	197,89
	$^{123}Sb(n,2n)^{122}Sb$	42.7	1300	2.72	D	564

Pb	$^{204}Pb(n,2n)^{203}Pb^{*}$	1.42	1840 ± 130	52.1	H	279

LONG RUNS

Na	$^{23}Na(n,2n)^{22}Na$	100.	54 ± 5	2.60	Y	1274
Ti	$^{46}Ti(n,p)^{46}Sc$	8.25	270 ± 25	83.8	D	889,1120
Cr	$^{52}Cr(n,2n)^{51}Cr^{*}$	83.8	358 ± 25	27.7	D	320
Co	$^{59}Co(n,p)^{59}Fe^{*}$	100.	82 ± 8	44.6	D	1099,1292
	$^{59}Co(n,2n)^{58}Co^{*}$	100.	735 ± 55	70.8	D	811
Ni	$^{58}Ni(n,d)^{57}Co$	68.3	520 ± 50 (1)	271	D	122,136
	$^{60}Ni(n,p)^{60}Co$	26.1	109 ± 8	5.27	Y	1173,1332
As	$^{75}As(n,2n)^{74}As$	100	1085 ± 75	17.8	D	596,635
Se	$^{77}Se(n,p)^{77}As$	7.6	36 ± 10	38.8	H	239
	$^{76}Se(n,2n)^{75}Se$	9.0	944 ± 65	120	D	265
Rb	$^{85}Rb(n,2n)^{84}Rb$	72.2	1430	33	D	881
Y	$^{89}Y(n,2n)^{88}Y$	100.	1015 ± 70	107	D	898,1836
Mo	$^{100}Mo(n,2n)^{99}Mo$	9.6	1390 ± 60	66	H	140
Ba	$^{132}Ba(n,2n)^{131}Ba$	0.10	1600	11.7	D	496,124,216
	$^{136}Ba(n,2n)^{135m}Ba$	7.9	700	28.7	H	268(IT)
	$^{134}Ba(n,2n)^{133}Ba$	2.4	940 ± 80	10.7	Y	356
Ce	$^{140}Ce(n,2n)^{139}Ce$	88.5	1760 ± 110	138	D	166
Hf	$^{176}Hf(n,2n)^{175}Hf$	5.2	2200 ± 115	70	D	343
Au	$^{197}Au(n,2n)^{196}Au$	100.	2250 ± 120	6.17	D	333
Hg	$^{198}Hg(n,p)^{198}Au$	10.0	4	2.7	D	412
Tl	$^{203}Tl(n,2n)^{202}Tl$	29.5	1850 ± 180	12.2	D	439

* Have interfering reactions

a) Bormann, et al, Handbook on Nuclear Activation Cross Sections, Technical Reports Series No. 156, IAEA, 1974

b) Table of Isotopes, Seventh Edition, Lederer and Shirley, John Wiley & Sons, New York, 1978

TABLE III: Summary of Interferences Encountered

Element	Interfering Reaction	Target Abundance (%)	14.9 MeV* Cross Section (mb)	Comments
Na	$^{26}Mg(n,\alpha)^{23}Ne$	10.0	72 ± 10	
Mg	$^{27}Al(n,\alpha)^{24}Na$	100.	111 ± 4	Severe in flyash
K	$^{44}Ca(n,\alpha)^{41}Ar$	2.09	35 ± 8	Ca was not determined; NBS value used
Ti	$^{51}V(n,\alpha)^{48}Sc$	99.8	19 ± 4	Negligible correction
Cr	$^{54}Fe(n,\alpha)^{51}Cr$	5.8	96 ± 10	Totally obscured Cr
Fe	$^{59}Co(n,\alpha)^{56}Mn$	100.	29 ± 3	Negligible
Fe	$^{55}Mn(n,2n)^{54}Mn$	100.	850 ± 60	Negligible
Co	$^{58}Ni(n,p)^{58}Co$	68.3	330 ± 30	Use ^{59}Fe if possible
Pb	$^{204}Hg(n,2n)^{203}Hg$	6.9	2190 ± 150	Same gamma-ray energy

* Handbook on Nuclear Activation Cross-Sections, Technical Report Series No. 156, IAEA, Vienna, 1974.

TABLE IV: Elemental Concentrations in NBS Fly Ash (SRM 1633) Determined by FNAA (μg/g unless % indicated)

element	this work	others [a]
Na	3150 ± 110	3200 ± 400
Mg (%)	1.5 ± 1.3	1.8 ± 0.4
Al (%)	13.6 ± 0.5	12.7 ± 0.5
Si (%)	22.8 ± 0.8	21 ± 2
K (%)	1.9 ± 0.5	1.61 ± 0.15
Sc	41 ± 5	27 ± 1
Ti	7300 ± 150	7400 ± 300
Cr	< 150	125 ± 6
Fe (%)	6.95 ± 0.15	6.20 ± 0.30
Co	45 ± 16	41.5 ± 1.2
Ni	105 ± 3	98 ± 9
Zn	< 420	210 ± 2
As	68 ± 12	61 ± 3
Se	35 ± 13	10.2 ± 1.4
Rb	137 ± 4	125 ± 10
Sr	1310 ± 50	1700 ± 300
Y	150 ± 7	62 ± 10
Zr	410 ± 20	301 ± 20
Mo	28.0 ± 1.3	--
Sb	<15	6.9 ± 0.6
Ba	2100 ± 100	2700 ± 200
Ce	136 ± 5	146 ± 15
Hf	<17	7.9 ± 4
Au	<8	--
Hg	<8	0.15 ± 0.01
Tl	18 ± 6	4 [b]

a) Ondov et al, Anal. Chem., 47, 1102 (1975).

b) Chattopadhyay and Jervis, Anal. Chem., 46, 1630 (1974).

TABLE V: Elemental Concentrations in NBS Orchard Leaves (SRM 1571) and Bovine Liver (SRM 1577) Determined by FNAA (μg/g unless % indicated)

	Orchard Leaves		Bovine Liver	
element	this work	other values[a]	this work	other values[a]
F	<240	(4)	<350	--
Na	< 360	82 ± 6	1600 ± 100	2430 ± 130
Mg	7030 ± 170	6200 ± 200	290 ± 40	(605)
Al	322 ± 22	409[b]	<80	(46)
P (%)	0.20 ± 0.01	0.21 ± 0.01	0.64 ± 0.06	(1.1)
Cl	<1400	(690)	<5400	2750[b]
K (%)	1.57 ± 0.25	1.47 ± 0.03	0.63 ± 0.11	0.97 ± 0.06
Ca (%)	<3	2.09 ± 0.33	<0.5	(120 ppm)
Sc	<2	0.2[b]		
Ti	26 ± 3	--	3.2 ± 1.0	--
Cr	<2	2.6 ± 0.3	<0.3	0.5 - 3.5[b]
Fe	348 ± 10	300 ± 20	137 ± 5	270 ± 20
Co	<8	(0.2)	0.31 ± 0.12	(0.18)
Ni	2.2 ± 0.7	1.3 ± 0.2	<9	0.21[b]
Zn	<110	25 ± 3	78 ± 25	130 ± 10
As	10.6 ± 0.3	10 ± 2	<1.3	(0.055)
Se	--	0.08 ± 0.01	< 2	1.1 ± 0.1
Rb	12.8 ± 0.6	12 ± 1	18.1 ± 0.6	18.3 ± 1.0
Sr	53 ± 4	(37)		
Y	<1.1	--	<14	--
Zr	<5	--	<3	--
Mo	<1.4	0.3 ± 0.1	2.6 ± 0.4	(3.2)
Sb	5.1 ± 1.1	2.9 ± 0.3	--	0.034[b]
Ba	<240	(44)	--	2.92[b]
Ce	<2	1.0[b]	<3	--
Hg	<5	0.155 ± 0.015	--	0.016 ± 0.002
Pb	57 ± 12	45 ± 3	5	0.34 ± 0.08

a) NBS certified and uncertified () values.

b) Nadkarni and Morrison, Anal. Chem., 45, 1957 (1973).

ENVIRONMENTAL TRACE ELEMENT ANALYSIS

USING SHORT-LIVED NUCLIDES

A. Chatt* and K.N. DeSilva

Trace Analysis Research Centre
Department of Chemistry
Dalhousie University
Halifax, N.S., B3H 4J1
Canada

ABSTRACT

Pseudo-cyclic, cyclic thermal, and cyclic epithermal instrumental neutron activation analysis methods have been developed for the simultaneous determination of multielement concentrations through short- and medium-lived nuclides. The methods have been successfully applied to a number of environmental and biological sample matrices. Precision, accuracy, and limits of detection of these methods have been observed to be superior to conventional INAA methods. Various aspects of the methods are described here.

INTRODUCTION

A number of elements produce short-lived (half-life <65s) nuclides on thermal and resonance neutron activation. These nuclides cannot easily be detected by conventional irradiation, decay and counting procedures which require several minutes of experimental time. Methods based on the principles of cyclic activation are being developed in this and other laboratories for the simultaneous detection of a number of short-lived nuclides.

There are several elements which give long-lived (half-life >65d) neutron activation products whose detections normally require lengthy irradiation, decay, and counting periods. Some of these elements can also be determined through short-lived isomers of the long-lived nuclides. The application of short-lived nuclides in routine measurements can reduce total analysis time and provide superior detection limits in many cases. The objective of this study is to develop instrumental neutron activation analysis (INAA) methods for the simultaneous determinations of multielement concentration in biological and environmental materials using short-lived nuclides.

The cyclic activation technique is based on the principles of irradiating a sample for a short time, transferring it quickly to a detector, counting the induced activities, and repeating the process several times. Cyclic INAA (CINAA) was first used by Anders in 1960 (1) for the determination of F, and later by Anders (2) and Givens *et al.* (3) for measuring a few selected elements. The theory of CINAA has been well described by Givens *et al.* (3,4)

and by Spyrou and Kerr (5). Recently, Spyrou and coworkers (6-12), and Grass and coworkers (13-16) have used reactors as neutron sources for CINAA of trace elements.

Two INAA methods, a pseudo-cyclic and a cyclic, have been developed in this work for the simultaneous determination of trace elements in biological and environmental materials. Both reactor flux (mainly thermal) and epi-boron neutrons have been utilized in developing PCINAA and CINAA methods. A rapid automated transfer cyclic system has been designed for studying very short-lived nuclides. Precision and accuracy of measurements have been evaluated. Limits of detection for a few elements have been calculated and reported here. Several boron compounds have been analyzed for contaminants in order to evaluate their suitability in CINAA. Advantage factors relative to V, Al, and Na have been measured for a few selected nuclides. Applications of both PCINAA and CINAA methods are reported here.

EXPERIMENTAL

Multielement comparator standards were prepared by spotting Nuclepore polycarbonate membrane filters with microlitre portions (containing microgram amounts) of atomic absorption standard solutions, and evaporating them to dryness at low heat under an infrared lamp. The filters were placed in precleaned polyethylene envelopes which were then heat-sealed.

Standard reference materials (SRM) were obtained from the U.S. National Bureau of Standards (NBS) and the International Atomic Energy Agency (IAEA). The SRM were dried according to the procedures prescribed by the respective suppliers. The SRM were weighed into precleaned 1.5-mL polyethylene vials which were then closed by sealing with heat.

Elemental boron and boron compounds were obtained from several commercial suppliers. Samples of atmospheric particulate matter were collected from the Halifax area using an Anderson 5-stage sampler. The Fish Flour sample was obtained from the International Council for the Exploration of the Seas(ICES, 1975). A sample of hair was collected from a resident of the San Francisco Bay area.

Samples and standards were irradiated in the Dalhousie University SLOWPOKE-2 Reactor (DUSR) at a thermal flux of 5×10^{11} n cm^{-2} s^{-1} (40). Gamma-ray spectra of irradiated materials were recorded using two different spectrometry systems. One system consisted of a 60-cm^3 Canberra Ge(Li) detector (full width at half-maximum, FWHM, of 1.9 keV at the 1332.4 keV gamma-ray of ^{60}Co, peak-to-Compton ratio of 35:1, and an efficiency of 9.5%) coupled to a Tracor Northern TN-11 model 4096-channel pulse height analyzer. The other system consisted of a 35-cm^3 PGT Ge(Li) detector (FWHM of 2.4 keV, peak-to-Compton ratio of 30:1, and an efficiency of 7.1%) in conjunction with a TN-1700 model 4096-channel pulse height analyzer.

A sample recycling system was designed in collaboration with the Atomic Energy of Canada Limited, Commercial Products, and was installed at the DUSR facility. This system has been described by Chatt *et.al.* (17). The transit time of an irradiation capsule from reactor core to counting position was approximately 600 ms at best. Due to complexeity of diverters used in this recycling system, the capsule transit time occasionally reached values greater than 1s. In rare cases, capsules got stuck in the system. Moreover, the heat-sealed caps of the capsules sometimes came off after striking the diverters. Consequently, the recycling system was modified. A schematic diagram of the considerably improved recycling system is shown in Fig. 1. This system

has two counting positions. The transit time of a sample from reactor core to the horizontal (Pin) counting position is always less than 400 ms, and that to the vertical counting position is about 550 ms. A detailed description of the modified recycling system is given elsewhere (18). The CINAA methods reported here have been developed using this modified system.

Several factors could influence the transit time of an irradiation capsule. The factors studied included air pressure in the pneumatic tube, shape of the top and bottom portions of a capsule, weight of a capsule, and capsule sealing technique (19). It was observed that a properly sealed capsule weighing between 4 and 6 g could be easily transferred to the pin counting position within 400 ms at an air pressure of about 40 p.s.i., and could be used for more than 100 cycles.

RESULTS AND DISCUSSION

More than 38 elements are known to produce both short- and long-lived nuclides on thermal neutron activation (20). Nuclear data of some of these elements, which are of particular interest in this study, are shown in Table I. Except F, the other seven elements give both short- (half-life <5.1 min) and long-lived (half-life >12.8h) products which emit gamma-rays during their decay. The isotopic abundances and cross-sections generally favor the production of short-lived nuclides. These observations have been used in developing PCINAA and CINAA methods for simultaneous multielement determinations.

The nuclides detected in several biological and environmental materials by PCINAA and CINAA methods are given in Table II. Gamma-rays used are generally free from interference under the experimental conditions used here. Several interfering nuclear reactions have been studied in detail. Possible interferences from epithermal and fast neutron reactions, viz. (n,p.), (n,α) and (n,2n), of the neighboring isotopes to the thermal neutron activation products of interest have been studied. The $^{19}F(n,\gamma)^{20}F$ reaction has been observed to be seriously interfered with by the $^{23}Na(n,\alpha)^{20}F$; consequently, appropriate correction factors have been applied for calculating F levels. The other interfering reaction, $^{20}Ne(n,p)^{20}F$, has been found to contribute very little to observed F concentrations. Levels of Mg and Al have been corrected for interferences from $^{27}Al(n,p)^{27}Mg$ and $^{28}Si(n,p)^{28}Al$ reactions, respectively.

During the early stages of our investigation on short-lived nuclides, a pseudo-cyclic INAA (PCINAA) method has been developed (21). The method involves irradiation of a sample for either 10 or 30 s, manual transfer of the sample from a lead receiver to a Ge(Li) detector within 10 s from the end of irradiation, and counting for 30 s. The sample is allowed to decay for 3 min prior to next irradiation. The irradiation-transfer-counting cycle is repeated four times and the cumulative gamma-ray spectrum is recorded at the end of each cycle.

Concentrations of Ag, Rb, Sc and Se in 3 biological SRM have been determined using the PCINAA method; the results are given in Table III. Precision, expressed in terms of relative standard deviation, has improved from first through fourth cycle, in some cases by as much as seven times. Both qualitative detection limits, L_D, and quantitative determination limits, L_Q, as defined by Currie (22), have decreased with increasing number of cycles. Accuracy of measurement has also improved in a similar fashion. The agreement between our values and those reported in literature (23-25) is generally good.

The length of irradiation, t_i, in PCINAA depends very much on the concentrations of major elements present in samples being analyzed. A t_i of 10 s has been observed to be superior to that of 30 s for samples containing large amounts of Al and Mn (e.g., botanical SRM such as Orchard Leaves, Pine Needles, Pepperbush, etc.) whereas the opposite condition (i.e., t_i of 30 s) is suitable for samples with low activity (e.g., Zoological SRM such as Bovine Liver, Oyster Tissue, Animal Muscle, etc.). The criteria developed for selecting appropriate t_i for multielement determination by PCINAA in a variety of sample matrices are reported elsewhere (26).

The PCINAA method offers several advantages: (i) short experimental time; (ii) simultaneous measurement of short- and medium-lived nuclides; (iii) significant improvement of precision, accuracy, and detection limits; (iv) no need for expensive instrumentation and extensive dead time correction; (v) no interference from ^{24m}Na and ^{38m}Cl; and (vi) capability of determining degree of homogeneity of a sample by analyzing several portions of it. The PCINAA method has two main disadvantages. Firstly, it is not suitable for detecting nuclides with half-lives less than 10 s. Secondly, errors in timing may occur during manual transfer of a sample and triggering of a detector system within a short interval. Although such errors are generally rare, they may be encountered.

An automated rapid transfer cyclic system was subsequently designed and installed. This system can be used for detecting nuclides with half-lives as short as 400 ms (27). The application of very short-lived (half-life <1s) nuclides in routine elemental determinations is presently being studied. In the meantime, CINAA methods have been developed for simultaneous multielement determinations in various sample matrices using nuclides with half-lives greater than 5 s. A computer program, based on the cyclic activation equation, has been developed to theoretically determine the optimum timing parameters for detecting a number of short-lived nuclides in biological and environmental materials (28, 29).

The CINAA method reported here involves the following timing parameters: irradiation time (t_i) = 10 s, decay time (t_d) = 2 s, counting time (t_c) = 10 s, and number of cycles (n) = 12. Gamma-ray spectra of a sample of Orchard Leaves (one of the difficult matrices because of high ^{28}Al activity) obtained using these timing parameters and recorded after 1st., 6th., and 12th. cycle are shown in Fig. 2. Number of counts under the photopeaks of interest has increased significantly from 1st. to 12th. cycle leading to reliable determinations of several elements. Improvement in precision of measurement with increasing number of cycles can be better understood by examining Fig. 3 which shows the determination of Sc in Orchard Leaves cycle by cycle. The overall improvement in precision is almost four-fold. It can be seen that the relative standard deviation has decreased from 34% at n=1 to 10% at n=8. A further increase of 4 cycles has resulted in only 1% reduction. Accuracy of measurement by the CINAA method has been evaluated by analyzing several SRM, and has been observed to be very good. The agreement between values obtained by PCINAA and CINAA methods is generally good. The Sc content of Orchard Leaves determined by PCINAA (0.052 ± 0.002 ppm, Table III, n=4) differs slightly from that obtained by CINAA (0.043 ± 0.004 ppm, Fig. 3, n=12). This small difference can perhaps be explained in terms of comparatively high dead time (mostly due to build-up of ^{28}Al) in CINAA. Samples are allowed to decay for 3 min between two successive irradiations in PCINAA compared to 12 s in CINAA; contribution from ^{28}Al towards dead time is far less in PCINAA than in CINAA (dead time corrections have been made in CINAA). The relative standard deviation of Sc measurements is also better in PCINAA.

In an effort to reduce swamping activities of several thermal neutron activation products, such as ^{24}Na, ^{28}Al, ^{38}Cl, ^{52}V, ^{56}Mn, etc., as well as to detect short-lived nuclides in biological and environmental materials, a cyclic epithermal neutron activation analysis (CENAA) method is being developed. In the past, Cd has been widely used as a thermal neutron shield for conventional ENAA of various matrices (30-33). Rossitto *et al.* (34) have described the possibility of utilizing B shields. A few scientists have used B shields for determining selected elements (35-38).

Boron shields are superior to Cd shields for CENAA of short-lived nuclides because of several reasons. Firstly, B can be used to absorb a larger fraction of the low-energy neutrons than Cd; B can easily absorb neutrons of up to 300 eV whereas the energy cut-off for Cd is only 0.4 eV. Secondly, since the effective neutron cut-off energy of B can be changed by varying its thickness as a shield, it can be used for selective enhancement of activities of certain nuclides. The most important advantage of using B in CENAA lies in the observation that B forms only one nuclide (^{12}B with a half-life of 20 ms and decays by emitting hard β-rays) on thermal neutron absorption while Cd forms several nuclides of which ^{111m}Cd (half-life of 49 min, 150- and 246-keV gamma-rays) is very intense and interfering. Consequently, the use of B shields reduces radiation hazard to experimenter and eliminates interference from gamma-rays of the shield.

In order to detect short-lived nuclides by CENAA, the sample needs to be counted along with its shield. It is, therefore, necessary to have as pure a boron shield as possible. Several boron compounds have been obtained from commercial suppliers and analyzed for contaminants. Concentrations of a few of the elements detected in a selected number of boron compounds are given in Table IV. Some of these compounds have been specially prepared and purified. Finally, the boron nitride #6 has been chosen for CENAA reported here.

Most boron compounds are generally obtained in powder form; it is difficult to fabricate rigid and reproducible shields with these compounds. Different techniques have been used initially to fabricate shields. One such design consisted of pouring a mixture of boron compounds and melted paraffin wax in an irradiation vial, solidifying the mixture, and making a hole in the center for sample. This design was later discarded due to problems of irreproducible shields, partial melting of shields on lengthy irradiations, breaking of shields, and contamination. Finally, the design of a novel shield of boron has been accomplished for use in pseudo-cyclic, cyclic, and conventional activation analysis (39). This shield is solid, stable, re-usable, and reproducible. It can be fabricated in any normal chemical laboratory to desired thickness, and it can withstand a temperature of at least 150°C without compromising its integrity. It can be made to fit any shape and size of irradiation capsule; thus it should be universally applicable. This shield has been used here for CENAA of biological and environmental materials.

In ENAA, the term "advantage factor" is often used. We have developed an advantage factor which describes the extent of reduction of interference due to ^{24}Na, ^{28}Al, ^{38}Cl, ^{52}V and ^{56}Mn on several nuclides of interest. Advantage factors of a few selected nuclides are given in Table V. It is obvious that several elements can be better determined by epi-boron neutrons in presence of large interfering activities rather than by thermal neutrons.

Several types of sample material have been analyzed for multielement content using a combination of CINAA and CENAA. Concentrations of several elements in a few selected matrices are shown in Table VI. Detailed descriptions of the significance of these data are beyond the scope of this paper.

CONCLUSION

Multielement concentrations of biological and environmental materials have been determined using short- and medium-lived nuclides. Pseudo-cyclic and automated cyclic methods have been found to be very useful in improving precision, accuracy, and detection limits. The cyclic system needs to be further modified for detecting nuclides with half-lives less than 200 ms. An in-depth study on the short-lived nuclides produced on epi-boron neutron activation is presently being carried out.

ACKNOWLEDGEMENT

The authors thankfully acknowledge the cooperation of the SLOWPOKE-2 Operations Group, Dalhousie University SLOWPOKE-2 Reactor, for their assistance in irradiations. This research was supported by a research operating grant (#A-9977) from the Natural Sciences and Engineering Research Council Canada. The award of a Killam Postgraduate Fellowship to one of the authors (K.N. DeSilva) is gratefully acknowledged.

REFERENCES

1. O.U. Anders, Anal. Chem., 32 (1960) 1368.

2. O.U. Anders, Anal. Chem., 33 (1961) 1706.

3. W.W. Givens, W.R. Mills, R.L. Caldwell, Nucl. Instr. and Meth., 80 (1970) 95.

4. W.W. Givens, W.R. Mills, R.L. Caldwell, Proc. 1968 Intern. Conf. on Modern Trends in Activation Analysis, J.R. DeVoe, Ed., NBS Spec. Publ. 312, II (1969) 929.

5. N.M. Spyrou, S.A. Kerr, J. Radioanal. Chem., 48 (1979) 169.

6. N.M. Spyrou, K. Ingle, F. Ozek, Proc. 2nd. Intern. Conf. on Nuclear Methods in Environmental Research, J.R. Vogt and W Meyer, Eds., Univ. of Missouri-Columbia, MO, (1974) 106.

7. N.M. Spyrou, P. Maheswaran, K. Nagy, F. Ozek, Proc. Intern. Symp. on Measurement, Detection and Control of Environmental Pollutants, International Atomic Energy Agency, Vienna, (1976) 151.

8. A. Egan, N.M. Spyrou, Anal. Chem., 48 (1976) 1959.

9. A. Egan, N.M. Spyrou, J. Radioanal. Chem., 37 (1977) 775.

10. A. Egan, S.A. Kerr, M.J. Minski, Radiochem. Radioanal. Letters, 28 (1977) 369.

11. N.M. Spyrou, S.A. Kerr, Proc. 3rd. Intern. Conf. on Nuclear Methods in Environmental and Energy Research, J.R. Vogt, Ed., Univ. of Missouri-Columbia, MO, (1977) 108.

12. S.A. Kerr, N.M. Spyrou, J. Radioanal. Chem., 44 (1978) 159.

13. F. Grass, Atomkernenergie, 19 (1972) 117.

14. F. Grass, Atomkernenergie, 25 (1975) 243.

15. F. Grass, G.P. Westphal, Nucl. Instr. and Meth., 140 (1977) 97.

16. F. Grass, R. Niesner, Nucl. Instr. and Meth., 151 (1978) 589.

17. A. Chatt, K.N. DeSilva, J. Holzbecher, D.C. Stuart, R.E. Tout, D.E. Ryan, Can. J. Chem., submitted (1980).

18. A. Chatt, K.N. DeSilva, R.E. Tout, J. Radioanal. Chem., accepted (1980).

19. A. Chatt, K.N. DeSilva, R.E. Tout, Proc. 1st. Ann. Conf. Can. Nucl. Soc., accepted (1980).

20. R.E. Tout, A. Chatt, Anal. Chim. Acta, accepted (1980).

21. A. Chattopadhyay, K.N. DeSilva, Trans. Am. Nucl. Soc., 32 (1979) 185.

22. L.A. Currie, Anal. Chem., 40 (1968) 586.

23. National Bureau of Standards, Certificate of Analysis, Standard Reference Material 1577, Bovine Liver, Washington, D.C., (1977).

24. H.A. van der Sloot, G.D. Walls, C.A. Weers, H.A. Das, Anal. Chem., 52 (1980) 112.

25. International Atomic Energy Agency, Intercomparison H-4 Animal Muscle, Preliminary Report, Vienna, (1979).

26. K.N. DeSilva, A. Chatt, Anal. Chim. Acta, submitted (1980).

27. A. Chatt, K.N. DeSilva, R.E. Tout, Trans. Can. Nucl. Soc., 1 (1980) 80.

28. R.E. Tout, A. Chatt, Trans. Am. Nucl. Soc., 33 (1979) 233.

29. R.E. Tout, A. Chatt, Anal. Chim. Acta, accepted (1980).

30. N.V. Bagdavadze, L.M. Mosulishvili, J. Radioanal. Chem., 24 (1975) 65.

31. E. Steinnes, J.J. Rowe, Anal. Chim. Acta, 87 (1976) 451.

32. M. Janssens, B. Desmet, R. Dams, J. Hoste, J. Radioanal. Chem., 26 (1975) 305.

33. P.A. Baedecker, J.J. Rowe, E. Steinnes, J. Radioanal. Chem., 40 (1977) 115.

34. F. Rossitto, M. Terrani, S. Terrani, Nucl. Instr. and Meth., 103 (1972) 77.

35. J.D. Jones, P.B. Kaufman, W.L. Rigot, J. Radioanal. Chem., 50 (1979) 261.

36. E.S. Gladney, D.R. Perrin, Anal. Chem., 51 (1979) 2015.

37. A. G. Hanna, H. Al-Shahristani, J. Radioanal. Chem., 37 (1977) 581.

38. L.E. Wangen, E.S. Gladney, Anal. Chim. Acta, 96 (1978) 271.

39. K.N. DeSilva, A. Chatt, to be published.

40. D.E. Ryan, D.C. Stuart, A. Chattopdahyay, Anal. Chim. Acta, 100 (1978) 87.

TABLE I. Comparison of Nuclear Data of Short- and Long-Lived Neutron Activation Products

Element	Short-lived nuclide				Long-lived nuclide			
	Target isotope	Cross section, b	Nuclide	Half-life	Target isotope	Cross section, b	Nuclide	Half-life
Ag	^{109}Ag	89	^{110}Ag	24.0 s	^{109}Ag	3.2	^{110m}Ag	253d
Cu	^{65}Cu	2.3	^{66}Cu	5.1 min	^{63}Cu	4.5	^{64}Cu	12.8h
F	^{19}F	0.0098	^{20}F	11.2 s	-	-	-	-
Hf	^{178}Hf	52	^{179m}Hf	18.6 s	^{180}Hf	12.6	^{181}Hf	42.5d
Rb	^{85}Rb	0.10	^{86m}Rb	1.04 min	^{85}Rb	0.91	^{86}Rb	18.7d
Sc	^{45}Sc	11	^{46m}Sc	20.0 s	^{45}Sc	23	^{46}Sc	84d
Se	^{76}Se	21	^{77m}Se	17.5 s	^{74}Se	30	^{75}Se	120d

TABLE II. Nuclides Detected in Biological and Environmental Materials

Element	Nuclide	Half-life	Gamma-ray used, keV
Ag	^{110}Ag	24.0 s	658
Al	^{28}Al	2.3 min	1779
Br	^{80}Br	17.6 min	617
Ca	^{49}Ca	8.5 min	3083
Cl	^{38}Cl	37.3 min	1642
Cu	^{66}Cu	5.1 min	1039
F	^{20}F	11.2 s	1633
Hf	^{179m}Hf	18.6 s	214
I	^{128}I	25 min	443
K	^{42}K	12.5 h	1525
Mg	^{27}Mg	9.5 min	1014
Mn	^{56}Mn	2.58 h	1811
Na	^{24}Na	15 h	1369
Rb	^{86m}Rb	1.04 min	556
Sc	^{46m}Sc	20.0 s	142
Se	^{77m}Se	17.5 s	162
Ti	^{51}Ti	5.8 min	320
V	^{52}V	3.8 min	1434

TABLE III. Elemental Concentrations of Biological Materials Determined by PCINAA

Element	Material	Reported value[a]	No. of cycles	This work[a,b]	Rel. std. dev., %	Limits[a] L_D	Limits[a] L_Q
Ag	Bovine Liver (NBS SRM-1577)	(0.06)[c]	1	0.085 ± 0.072	85	0.089	0.48
			2	0.060 ± 0.028	47	0.063	0.28
			3	0.055 ± 0.032	58	0.060	0.22
			4	0.066 ± 0.021	32	0.052	0.19
Rb	Bovine Liver (NBS SRM-1577)	18.3 ± 1.0[c]	1	18.6 ± 3.2	17	6.0	29.2
			2	19.4 ± 1.6	8	3.6	16.2
			3	17.6 ± 0.9	5	2.9	12.0
			4	17.6 ± 0.9	5	2.4	9.2
Sc	Orchard Leaves (NBS SRM-1571)	0.054 ± 0.004[d]	1	0.096 ± 0.018	19	0.028	0.113
			2	0.061 ± 0.005	8	0.017	0.073
			3	0.052 ± 0.002	4	0.013	0.047
			4	0.052 ± 0.002	4	0.011	0.031
Se	Animal Muscle (IAEA H-4)	(0.275)[e]	1	0.307 ± 0.065	21	0.087	0.382
			2	0.289 ± 0.028	10	0.061	0.240
			3	0.277 ± 0.009	3	0.053	0.184
			4	0.277 ± 0.009	3	0.041	0.162

[a]all values are in ppm, dry-weight basis. [b]average of 4 determinations. [c]Ref. 23. [d]Ref. 24. [e]Ref. 25. The values in parentheses are either for information only or provisional listing.

TABLE IV. Comparison of Trace Element Content of Boron Compounds

Compound	Content, in arbitrary units						
	Br	Co	Mn	Ta	Ti	V	W
Boron Carbide	N.D.	20	2.8	N.D.	1.2	130	3.9
Boron Nitride #1	N.D.	175	3.8	N.D.	1.5	6.5	4.6
Boron Nitride #2	1	250	1.7	N.D.	3.5	35	55
Boron Nitride #3	N.D.	1	N.D.	N.D.	2.6	16	1
Boron Nitride #4	N.D.	15	13	1.5	1	1	1
Boron Nitride #5	1.1	5	1	N.D.	N.D.	1.9	N.D.
Boron Nitride #6	N.D.	1.5	N.D.	1	N.D.	3.5	N.D.
Enriched Boron	1.7	3060	22	1790	160	6.7	205

TABLE V. Advantage Factors for Nuclides under a Boron Shield

Nuclide	γ-ray, keV	Advantage factors relative to		
		^{52}V	^{28}Al	^{24}Na
^{110}Ag	658	9.6	7.5	4.5
^{76}As	559	17	14	8.2
^{20}F	1633	7.2	5.7	3.4
^{116m}In	417	8.6	6.9	4.1
^{86m}Rb	556	10	8.1	4.8
^{239}U	74	1.9	16	9.2

TABLE VI. Elemental Content of Biological and Environmental Materials Determined by CNAA and CENAA

Element	Hair (ppm)	Fish Flour (ppm)	Air particulate (ng/m^3)
Ag	1.2	0.055	0.4
Al	32	53.9	2100
Br	17.5	43.6	94
Ca	190	16700	2300
Cl	10900	7330	970
Cu	167	4.84	220
F	-	55	-
Hf	-	-	0.012
I	0.26	3.05	2.2
K	3500	16300	1020
Mg	52	1087	960
Mn	2.9	15.0	65
Na	3000	5800	520
Rb	3.3	3.72	1.8
Sc	0.023	-	0.085
Se	0.15	1.35	1.2
Ti	1.9	-	26
V	0.08	0.22	6.4

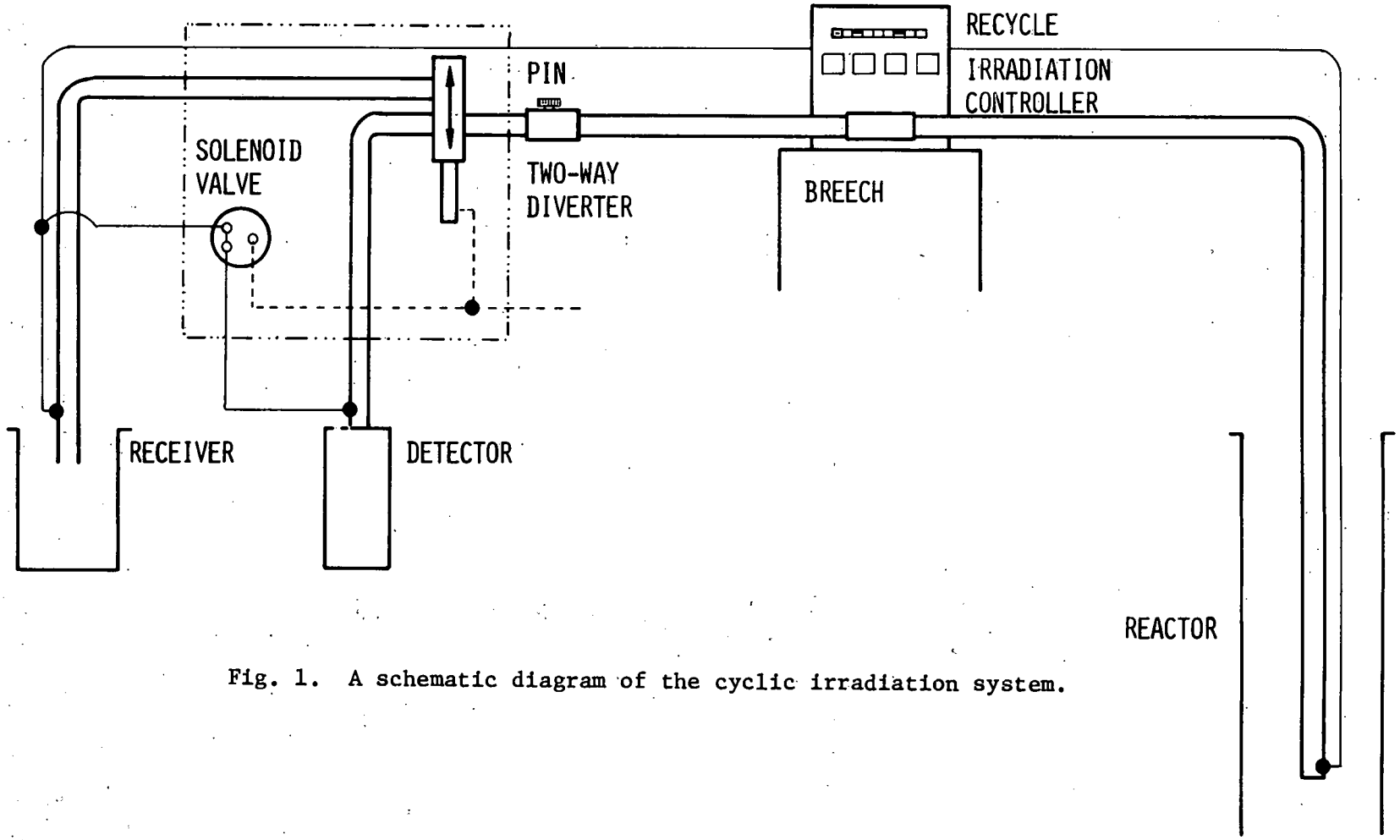


Fig. 1. A schematic diagram of the cyclic irradiation system.

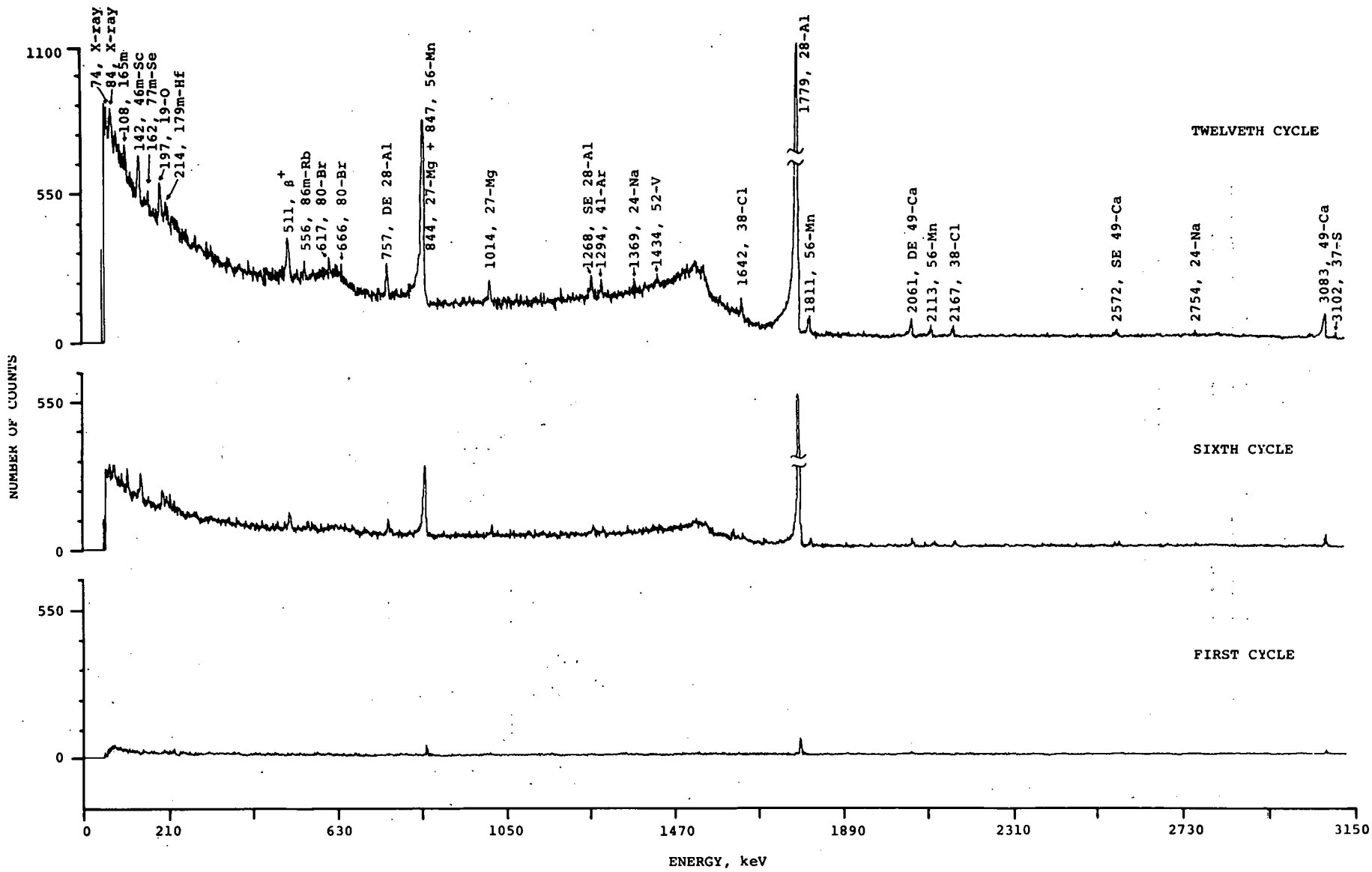


Fig. 2. Gamma-ray spectra of a sample of Orchard Leaves by CINAA.

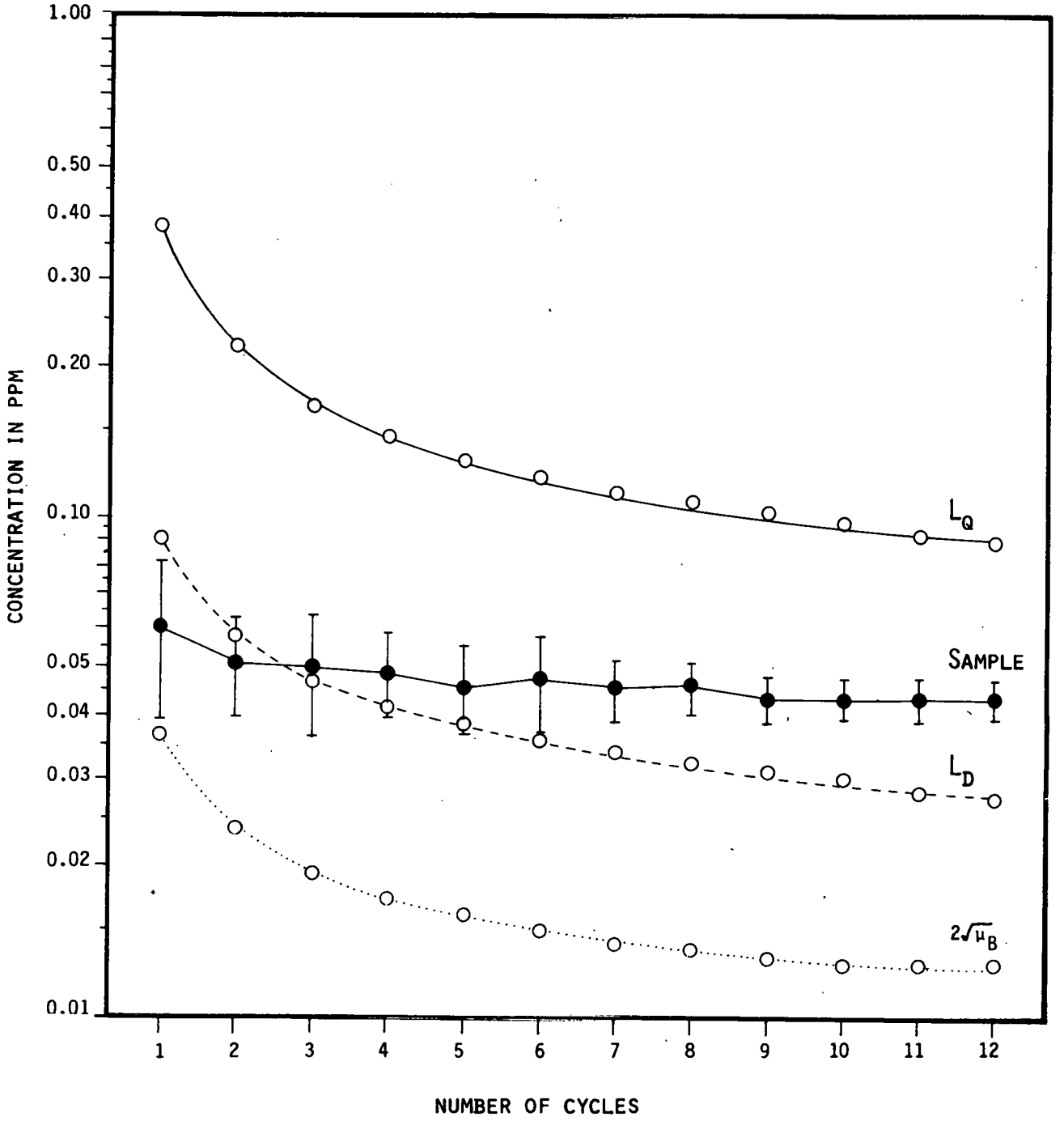


Fig. 3. Determination of Sc content of Orchard Leaves by CINAA.

PROMPT NEUTRON CAPTURE GAMMA RAY ANALYSIS OF NUCLEAR FUEL MATERIALS WITH A PAIR SPECTROMETER*

B.R.S. Pecequilo, G.C. Vandenput**, C.R.S. Stopa*** and A.A. Suarez
Instituto de Pesquisas Energéticas e Nucleares
C.P. 11049 - Pinheiros, 01000 São Paulo, S.P. - Brasil

ABSTRACT

Prompt gamma rays following thermal neutron capture are used to determine fuel material impurities in a reactor internal geometry. In order to increase the detection sensitivity for weak lines and simplify the analysis of the spectra, a 3-crystal coincidence spectrometer was mounted and the gain in peak-to-background ratio calculated for several spectra was about a factor of 6. The calibration of the experimental arrangement was performed with UO_2 targets contamined by controlled amounts of Gd and Sm.

* Work partially sponsored by the International Atomic Energy Agency(IAEA) and Comissão Nacional de Energia Nuclear(CNEN-Brazil).

** Now at SCK/CEN B-2400 MOL, Belgium.

*** Now at CTA, São José dos Campos, Brazil.

INTRODUCTION

Man's interest in atomic power has increased with the world power crisis.Thus, special care has been devoted to the improvement of techniques of purification and analysis of the nuclear fuel materials. Some typical contaminants of those materials are Al, B, Be, Cd, Ni, W, V and rare earths like Gd, Sm, Dy and Eu[1].

There exist already several techniques which are quite sensitive for the determination of trace impurities present in nuclear materials, however some of them loose precision when measuring quantities greater than 30 ppm. Spectrographic analysis have high sensitivity only for trace element analysis and needs a previous chemical separation. Neutron activation analysis relies on the properties of the product nucleus and in numerous cases the product nucleus may have a short half-life, a long half-life or a stable composition or it may not be a gamma emitter at all. In the specific case of nuclear materials (like uranium, for example) the neutron activation analysis of the contaminants is difficulted by the production of fission fragments in the matrix.

In view of the increasing interest and necessities of new techniques for determinations of impurities in nuclear fuel materials, like uranium compounds, we developed and presented in previous papers[2,3] an alternative method of analysis of fuel material impurities using prompt gamma rays following thermal neutron capture.

Prompt gamma-ray spectrometry offers advantages over many of other techniques in that it provides a relatively rapid and nondestructive trace and major multielement analysis requiring a minimum of physical preparation and no chemical processing.

Prompt gamma-rays are typical of each isotope. Thus, the analysis of gamma-ray spectra obtained for a certain sample permits the identification of the contaminants of the sample.

The main advantage of this technique proceeds from the relatively low neutron binding energy(~ 4.8 MeV) of nuclear fuel materials which allows all high energy capture gamma-rays belonging to the impurities to be detected in relatively low background conditions.

We showed the viability of this method by measuring with a single coaxial Ge(Li) detector samples of uranium oxide(UO_2) with controlled amounts of rare-earth impurities and the prompt high energy gamma rays of these elements were easily seen since above 4.8 MeV there are no more prompt gamma rays emitted by the uranium matrix[2,3].

However, neutron capture γ-ray spectra of isotopes in the medium and heavy mass region, obtained with Ge(Li) detectors, tend to become very complex due to characteristically high level densities of the product nuclei. They are further complicated by the presence of single and double escape peaks, apart from the one corresponding to full energy absorption, for every gamma ray detected with energy E_γ>1022 keV and unresolved multiplets are therefore a common feature.

Moreover, Compton scattering and subsequent escape of scattered gamma-rays from the detector are the source of an important continuous background distribution on which lower energy peaks are superposed.

This complicates the analysis of the spectra, limits the detection sensitivity for weak lines and reduce the precision of peak area estimates.

Nevertheless, greatly simplified and significantly "cleaner" spectra can be obtained by a slight sofistication of the detection system, namely by introducing a three-crystal coincidence technique. The double escape peaks result from the (e^+-e^-) pair production in the detector followed by positron annihilation and the subsequent escape from detection of both 511 keV γ-rays produced in the process. If this annihilation radiation is allowed to strike two additional detectors surrounding the central Ge(Li) crystal, then single escape and full energy peaks can be eliminated by imposing triple time coincidence. The only peaks retained in the spectra result from double escape and, it should be emphasized, are free of Compton distributions.

The pair spectrometer used in our measurements consists of a Ge(Li) detector and two optically separated NaI(Tl) crystals. With this system we measured several UO_2 samples with controlled samarium (Sm_2O_3) and gadolinium (Gd_2O_3) impurities and we observed that although the coincidence requirement drastically reduces the detection efficiency, a very substancial gain in peak-to-background ratio is obtained, so we could detect lower intensity peaks than in the single mode and the peak area estimates also became more accurate.

EXPERIMENTAL FACILITIES AND TARGETS

The experimental set up for this experiment is installed at the tangential tube of the IEA-R1 reactor of São Paulo and the basic features of our internal target facility are illustrated in fig. 1.

The internal target geometry is definitely superior to the external one in sensibility (higher signal-to-background ratio). In the external target geometry there are two solid angles: one for the neutrons at the target and other for the gamma rays at the detector, whereas in the internal geometry there is only one solid angle from the target to the detector. So, despite the difficulty in handling the samples we choose the internal target geometry.

The samples to be analysed are positioned close to the reactor core and the neutron flux is typically about $5 \times 10^{11} cm^{-2}.s^{-1}$ at the target position.

The γ-beam is collimated by a set of internal graded lead collimators and a 4mm diameter final collimator focusing on the compensated annular area of a Ge(Li) crystal situated outside of the reactor biological shield at a distance of 654cm from the target. In this conditions, the solid angle seen by the Ge(Li) detector is 1.03×10^{-7}sr.

A $^6Li_2CO_3$ thermal neutron absorber is installed in front of the Ge(Li) detector to protect it against probable thermal neutron existing in the γ-beam.

There are also some other aspects observed in order to reduce the background:

a - The lead collimators inside the aluminium tangential tube of the reactor are conical behind the target in order to prevent that no radiation from the beam tube wall close the core reach the detector directly.

b - The reactor beam tube was covered with a nuclear pure graphite tube of 37/8" internal diameter on the whole inner surface where there are no collimators. Since gamma rays from the aluminium tube can be scattered at the target, we covered the wall with graphite which it is a material emitting very few thermal neutron capture gamma rays.

c - The reactor beam tube was evacuated by a rotary pump to less than 10^{-3}torr in order to decrease the scattered neutron to the Ge(Li) spectrometer as well the capture gamma rays from the nitrogen in the air.

d - The target holder was of nuclear pure graphite due to its low capture cross section and rather simple gamma spectrum.

The calibration of the experimental arrangement was performed with UO_2 targets contamined by controlled amounts of Gd and Sm. The total weight of the samples utilized was around 5 grams.

THE PAIR SPECTROMETER

The pair spectrometer developed for our measurements consists of a 42.5cc true coaxial Ge(Li) detector which fits into a cylindrical opening in the common housing of two optically separated 6" x 6" NaI(Tl) crystals facing the central Ge-crystal from opposite sides (Fig. 2). The electronics also showed in fig.2 comprise standard coincidence hardware. The fast output signals from three linear amplifiers trigger 3 timing single channel analyzers and are subsequently fed into a fast coincidence module operating with a time resolution $2\tau \sim 100$ns.

The coincident events generate a gate pulse for a gated biased amplifier (for choosing high energy ranges) allowing the linear signal from the unipolar output of the Ge(Li) amplifier to be processed. The selection of 511 keV annihilation radiation in the scintillators is accomplished by a proper adjustment of the discriminator levels at the single channel analyzer. By using analog stabilization the variation of photomultiplier and amplifier gain are offset. The energy signal from the Ge(Li) detector is digitally stabilized at the ADC level and this is essential for maintaining energy resolutions of ~7.0 keV at 4.1 MeV during long measuring periods.

RESULTS AND DISCUSSION

The data analysis of the γ-ray spectra was done by using the GAUSS V program[4] in operation in our computer center. In the program, the peak is represented by a Gaussian function and the underlying spectral background by a linear function. The basic mathematical operation is the nonlinear least-squares fit by which the parameters of the Gaussian (height, width and position) are determined. For the energy calibration we used the quite well known capture gamma rays of nitrogen[5] (for more details, see reference[6]).

Some of the UO_2 targets with rare earth impurities was measured even in the single and in the coincidence mode and the direct and pair spectra obtained are showed in figs. 3 and 4.

We observed that although the coincidence requirement reduces the detection efficiency by a factor of about 4.5 in comparison with the single mode, the gain in peak-to-background ratio calculated for several spectra is about a factor of 6. So, we obtained a very substantial decrease in the background and we could detect lower intensity peaks.

For example in fig. 3 some peaks of lower intensity like the double escape of the 6670 keV(I_γ = 0.08%) and 6913.4 keV(I_γ = 0.07%) γ -transition of ^{158}Gd are more proeminent in the pair spectrum. Also, the 6913 DE peak is no more overlapped by the 5902.9 keV γ transition, visible only in the direct spectrum.

Moreover, in fig. 4 the single escape of the 6750 keV γ transition of ^{158}Gd in the direct spectrum difficults the double escape peak of the 7283 keV γ transition of the ^{156}Gd. However, in the pair spectrum the 7283 keV DE peak is quite "clear", and the spectral background is also lower. It's interesting to point that the detection probability of the more intense γ-transition of the

^{156}Gd(7283 keV) is lower by a factor of 14 comparing with that one of the more intense γ-transition of the ^{158}Gd(6750 keV), i.e, σ = 61000 barns for ^{155}Gd and I_γ = 0.4% for ^{156}Gd and σ = 250000 barns for ^{157}Gd and I_γ = 1.32% for ^{158}Gd.

The peak-to-background ratio gain calculated for several spectra was about a factor of 6, but in the lower energy region this gain is more significant. In those regions, the background radiation is increased by Compton effect in higher energies and the peak-to-background ratio in the direct spectrum is lower than 1. As an example, for the double escape peak of the 4060 keV γ-transition of the ^{239}U we have a 0.58 ratio in the direct spectrum and a 9.19 ratio in the pair one. So, in the lower energy region the gain in identifying weak transitions is about a factor of 15.

With the UO_2 targets with controlled rare earth impurities of Sm and Gd we also have determined calibration curves of the experimental system. The impurity content is proportional to the peak area and is expressed in ppm(ratio of micrograms of impurity to grams of uranium oxide).

The calibration curves are presented at fig. 5. The impurity content in the uranium oxide expressed in ppm plotted against the peak area ratio of impurity to uranium (strongest transitions) results in a straight line which has a slope proportional to the sensibility of the arrangement to that particular impurity.

The reproducibility of this method of analysis using prompt neutron capture gamma-rays was checked previously and the results are presented in previous papers[2,3]. The observed deviation was less than 2%.

The multielement capability of analysis, the rather convenient sensibility for impurities contents greather than 20 ppm and the gain obtained in peak-to-background ratio by using a three-crystal pair spectrometer permits to say that this method of analysis acts as a complementary method to the existing techniques.

Also, we would like to point out that the analysis of impurities using radioactive thermal neutron capture could be used not only for the nuclear fuel materials, but also for biological and geological applications.

ACKNOWLEDGEMENT

We thank the International Atomic Energy Agency (IAEA) and the Comissão Nacional de Energia Nuclear(CNEN-Brazil) for the financial support of this work.

REFERENCES

1 - "Analytical Methods in the Nuclear Fuel Cycle" - Proc. Symposium Vienna, 1971 - IAEA, Vienna, 1972 p. 137.

2 - B.R.S. Pecequilo - Ph.D. thesis, IEA-D5-078(1978).

3 - "Fuel material analysis using radioactive thermal neutron capture", B.R.S. Pecequilo and A.A. Suarez in "Neutron Capture Gamma-Ray Spectroscopy" ed. by R.E.Chrien and W.R.Kane, Plenum Press, 1979 p. 710-13.

4 - Helmer, R.G. & Putnam, M.H. - Gauss V, a computer program for the analysis of gamma-ray spectra from Ge(Li) spectrometers. Idaho-Falls, Aerojet Nuclear Company, Jan. 1972(ANCR-1043).

5 - Ajzenberg-Selove, F. Energy levels of light nuclei A=13-15 Nucl. Phys. A268 p.138, 1976.

6 - Stopa, C.R.S. & Pecequilo, B.R.S. - Energy and Relative Efficiency calibration of a Ge(Li) gamma-ray spectrometer, to be published.

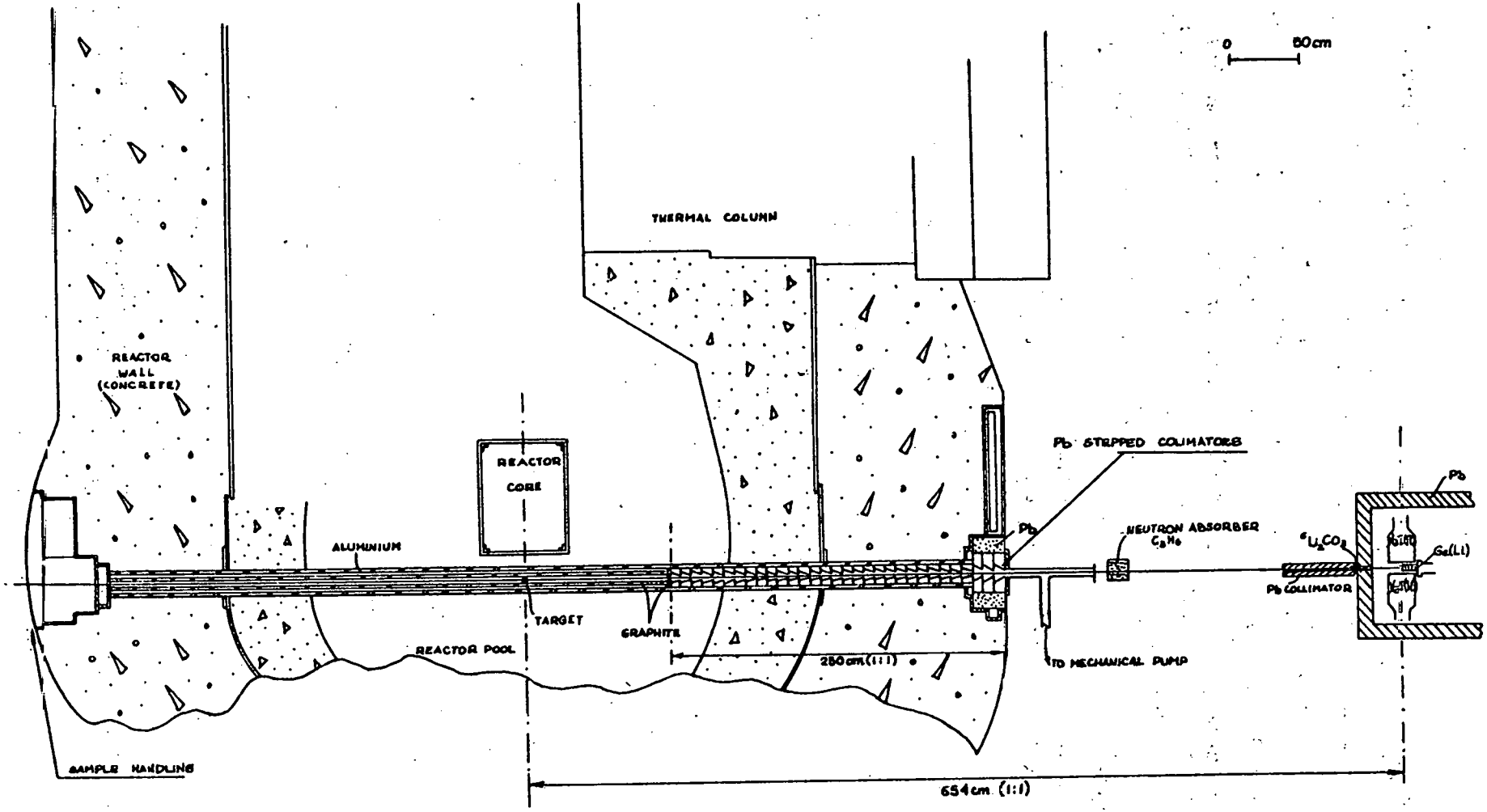
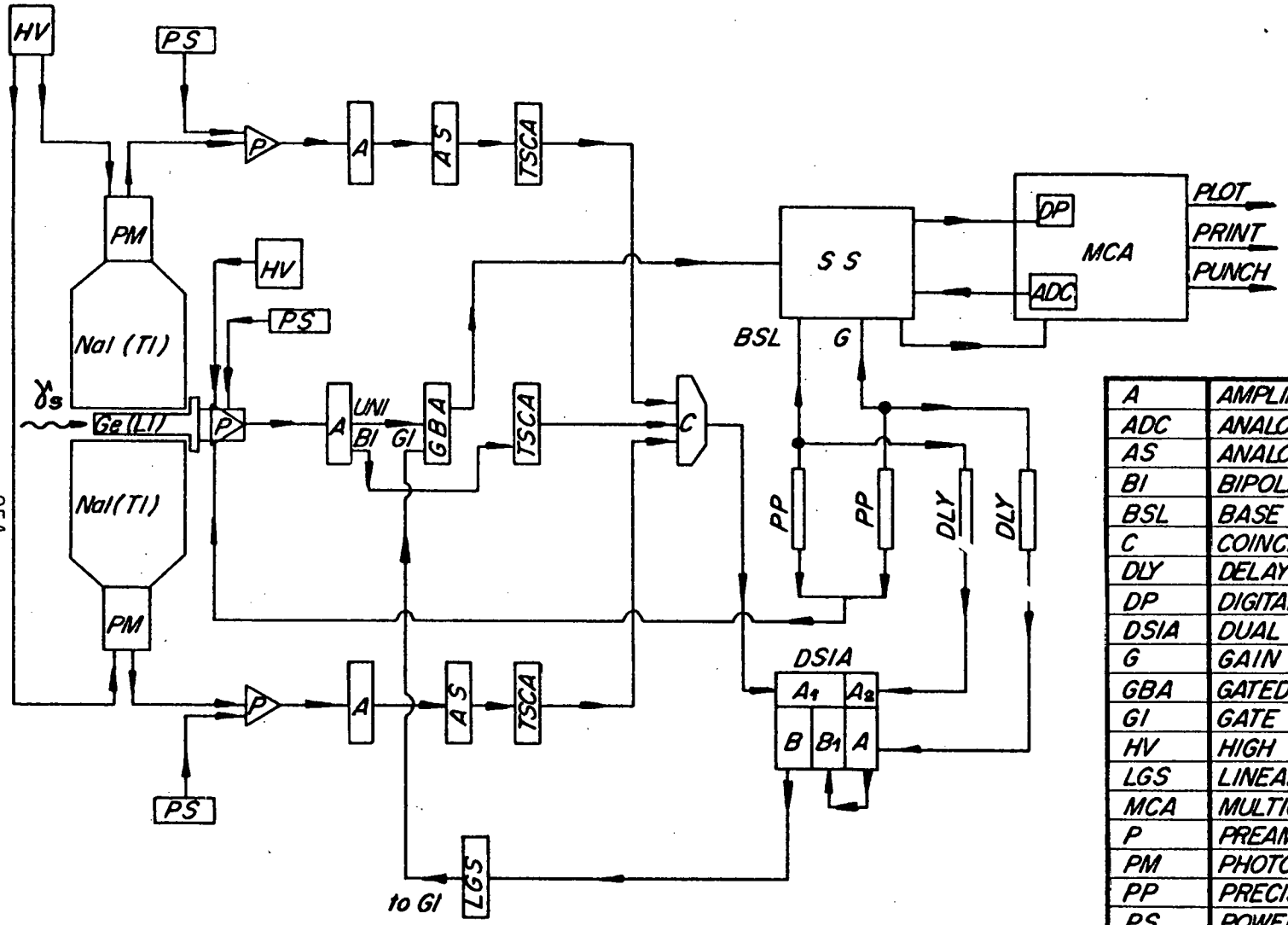


FIG. 1 - Experimental arrangement installed at the tangencial beam tube of the IEA-R1 reactor



A	AMPLIFIER
ADC	ANALOG-TO-DIGITAL CONVERTER
AS	ANALOG STABILIZER
BI	BIPOLAR
BSL	BASE LINE
C	COINCIDENCE
DLY	DELAY
DP	DIGITAL PROCESSOR
DSIA	DUAL SUM INVERT AMPLIFIER
G	GAIN
GBA	GATED BIASED AMPLIFIER
GI	GATE IN
HV	HIGH VOLTAGE
LGS	LINEAR GATE STRETCHER
MCA	MULTICHANNEL ANALYZER
P	PREAMPLIFIER
PM	PHOTOMULTIPLIER
PP	PRECISION PULSER
PS	POWER SUPPLY
SS	SPECTRUM STABILIZER (DIGITAL)
TSCA	TIMING SINGLE CHANNEL ANALYZER
UNI	UNIPOLAR

FIG.2 - Electronics of the 3-crystal pair spectrometer

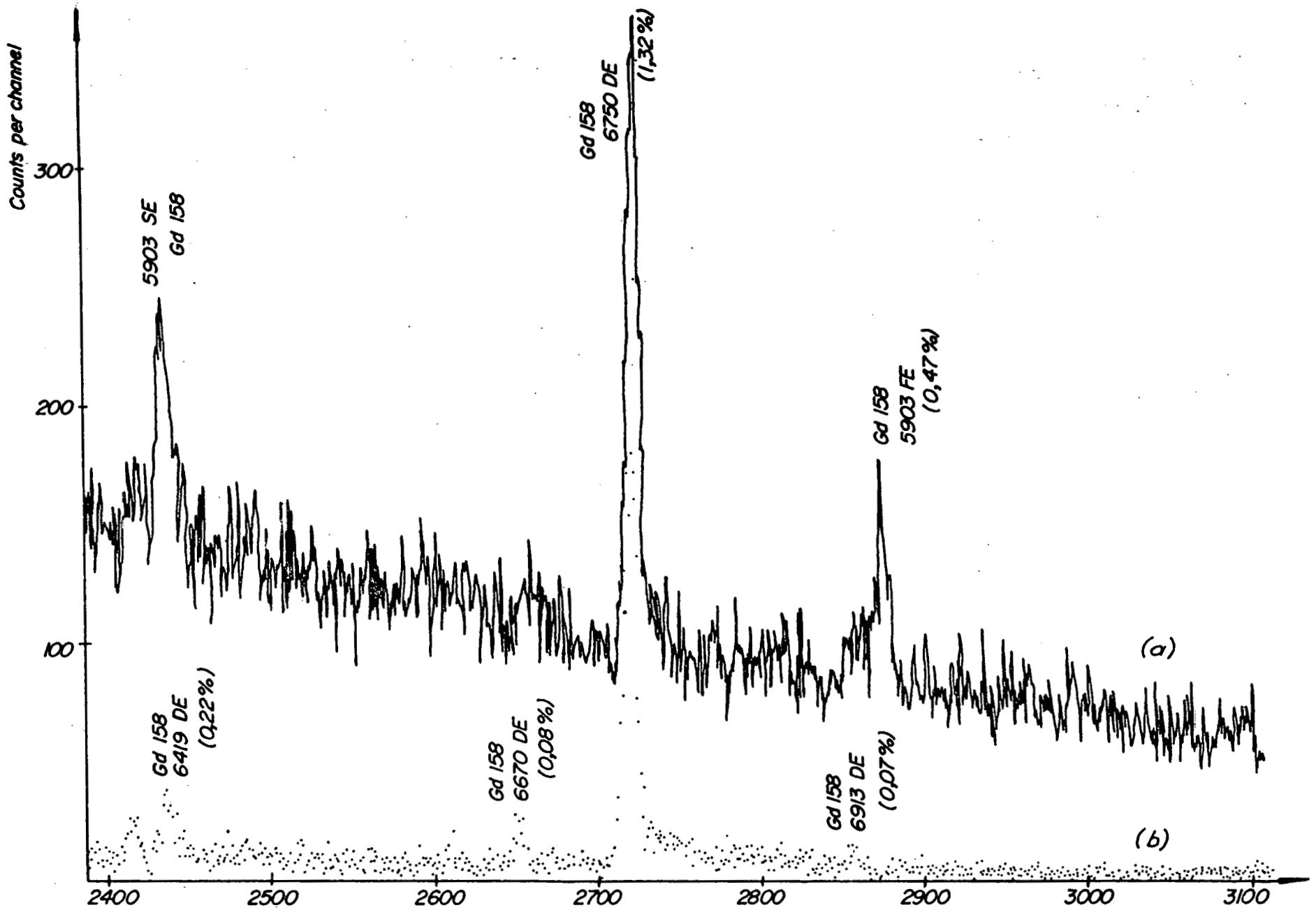


FIG. 3 - Prompt γ-ray spectrum of the UO_2 + 48ppm Gd sample in the region of 5300 to 6200 kev. FE, SE and DE are full, single and double-escape peaks. a) direct spectrum, run of 13 hs. b) pair spectrum, run of 34 hs.

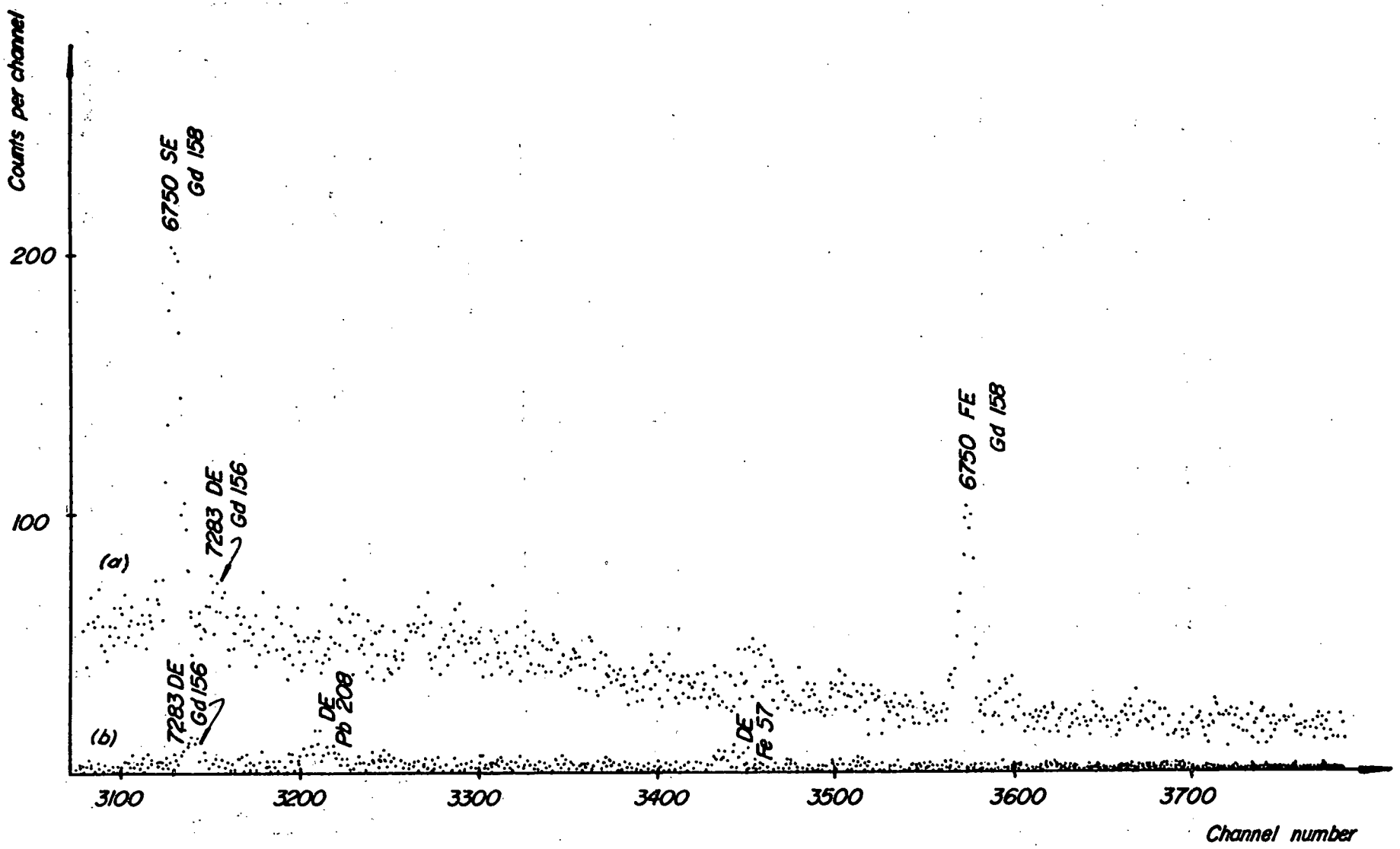


FIG 4 - Prompt γ-ray spectrum of the UO_2 + 48ppm Gd sample in the region of 6200 to 7000 kev. The iron and lead impurities are from the target holder.

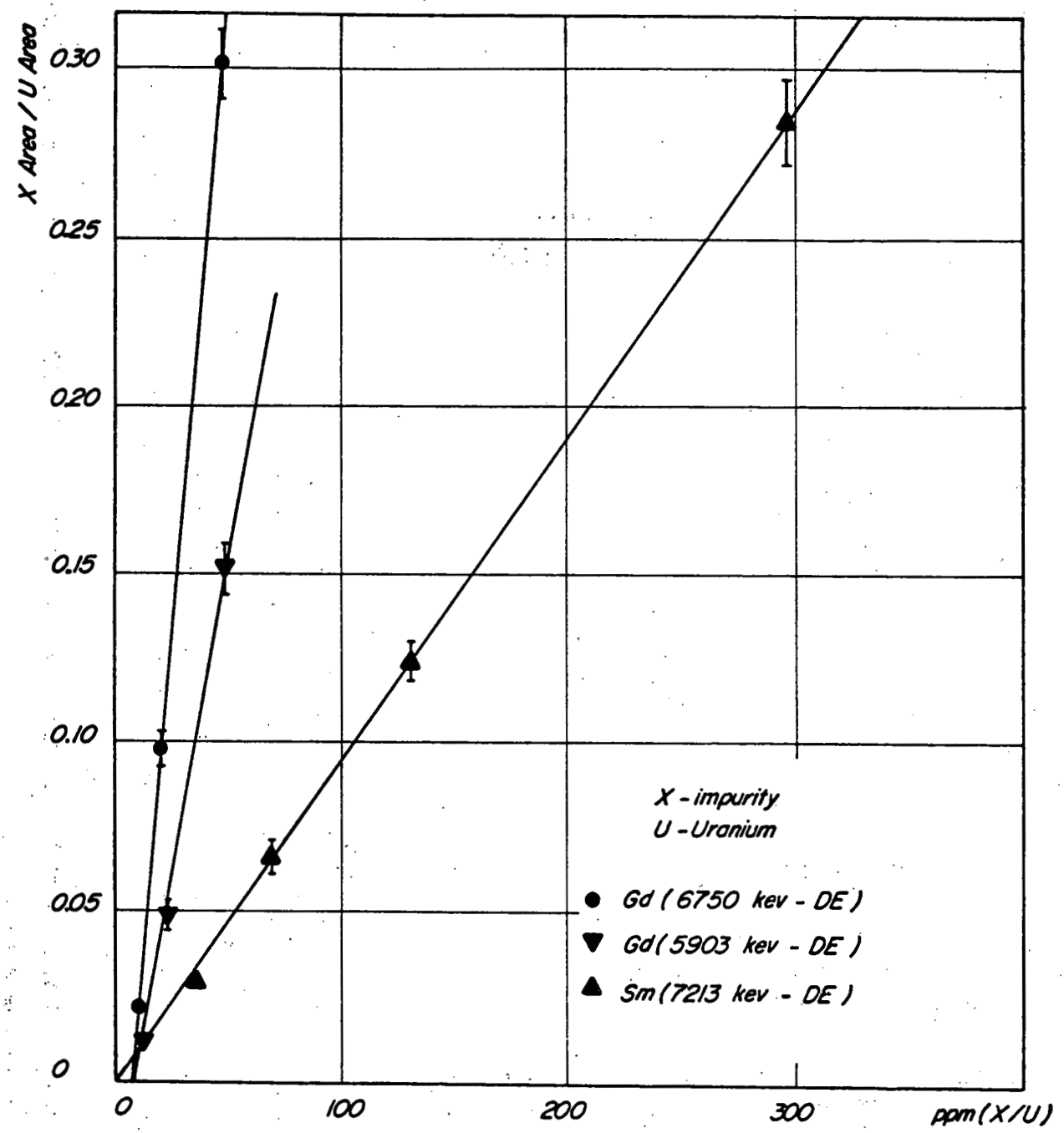


FIG. 5 - Calibration curves of the experimental arrangement with the pair spectrometer

DE = double - escape peak

MEASUREMENT OF MOISTURE DEPTH DISTRIBUTION IN COMPOSITE MATERIALS USING POSITRON LIFETIME TECHNIQUE

Jag J. Singh
NASA Langley Research Center
Hampton, VA 23665

W. H. Holt and W. Mock, Jr.
Naval Surface Weapons Center
Dahlgren, VA 22448

Gerald H. Mall
Computer Sciences Corporation
Hampton, VA 23665

ABSTRACT

Fiber-reinforced resin matrix composites reportedly suffer significant degradation in their mechanical properties when exposed to hot, moist, environments for extended periods. Moisture weakens the fiber matrix bond as well as the matrix shear strength. An important factor in determining the extent of degradation is the depth distribution of moisture in the resin matrix. Despite the importance of measuring moisture distribution and its effects on composite material properties, not enough data are available on suitable nondestructive techniques for detecting and measuring moisture diffusion in organic composite materials. This paper addresses itself to the problem of measuring the moisture content of such materials, with special emphasis on its depth distribution, using positron lifetime technique.

INTRODUCTION

Fiber-reinforced polymeric composites are attractive candidates for lightweight structures in aerospace applications, because of their low density and high strength. However, several recent studies[1-5] have shown that these materials pick up moisture when exposed to hot, moist, environment for an extended period. The equilibrium moisture pickup is a strong function of the temperature and relative humidity of the ambient air at the material surface--being maximum at noontime and minimum at night.[6-8] The presence of moisture in these materials degrades their mechanical properties. Water vapors migrate along the fiber-matrix interface thereby weakening the fiber-matrix bond. Water also diffuses through the polymeric matrix itself and degrades the matrix dominated properties of the composite materials. Furthermore, the daily absorption-desorption cycles experienced by the polymeric composites in service cause cyclic stress conditions in the outer layers of these materials and produce fatigue damage in their mechanical properties. A proper understanding of the factors affecting the moisture absorption is necessary before any effective steps can be taken to minimize the degrading effects of environmental moisture on the plastic composites. An equally important requirement is the data on moisture depth distribution for properly analyzing the cyclic stresses accompanying the absorption-desorption cycles in the test samples. These data require the development of sensitive nondestructive techniques for measuring the moisture

PAGES 259 to 274

WERE INTENTIONALLY

LEFT BLANK

LASER ISOTOPE DATING: A NEW TECHNIQUE OF RADIOISOTOPE DATING USING LASERS*

R. H. McFarland, Javed Husain, and L. D. Schearer

Department of Physics, UMR, Rolla, MO 65401

*Supported by the Office of Naval Research.

ABSTRACT

The selective detection of radioisotopes has important applications in many areas of science and technology including environmental and energy problems. At present the most sensitive technique of selective isotope detection is the one that is based on MeV range accelerators. In this paper we discuss some of the aspects of a recently introduced technique of selective isotope detection. We call it Laser Isotope Detection (L.I.D.) and show that L.I.D. sensitivities could be one or two orders of magnitude better than accelerator detection. We also present some ideas that may be useful for the enhancement of L.I.D. sensitivity.

INTRODUCTION

Radioisotopes have a vast number of applications these days [1 to 9]. The selective detection of low concentrations of radioisotopes is of importance for many areas of science and technology including environmental and energy problems.

At present, the most sensitive technique for the selective detection of isotopes is based on accelerator detection [10]. In this technique the sample, prior to detection, is accelerated in an accelerator to energies of the order of several MeV's. The sensitivity of this technique is several orders of magnitude better than conventional dating. However, this method suffers because of the rather poor efficiency of production of the utilized ions in the accelerator. Typically efficiencies only of the order of 10^{-4} are achieved. The accelerator technique is the state-of-the-art in present day work on dating. The smallest ratio reported for accelerator work for any isotope has been for ^{36}Cl [11]. This ratio was 2×10^{-16} in 20 minutes which implies 2.4×10^{-13} per second. The conversion efficiency of the the utilized ions, η_c, was 7×10^{-3} [12]. This then yields for the sensitivity a value of 3.4×10^{-11}. Although these accelerator developments are now only about three years old their importance has already been realized by the U. S. National Science Foundation, which has funded a $1.24 million accelerator dating facility for the University of Arizona [13].

Recently [14] we proposed the use of laser techniques for radioisotope dating and detection and pointed out that the use of lasers could cut down the price of a dating set-up by at least a factor of ten. We shall refer to the use of lasers for radioisotope dating as Laser Isotope Dating (L.I.D.). In a more general sense we shall also mean Laser Isotope Detection.

In this paper we present detailed calculations of L.I.D. sensitivity and also present some novel ideas that may turn out to be useful for L.I.D. and therefore need further exploration.

It is important to point out that only due to the recent developments in lasers and related techniques [15 to 19] is it possible to achieve the high sensitivities mentioned in this paper. Specially important for L.I.D. is the recent research attempting to extend the CW region of lasers into the UV [20 to 25]. At present the tuning range of stabilized CW dye lasers is limited to 3620 Å to 7800 Å. However, it can be safely expected that this range would vastly increase in the matter of a few years. In this regard ring CW dye lasers are very promising [20, 21, 24]. Another idea is the use of intra-cavity harmonic generation. This has already yielded [20] a reasonable 10 mW CW with a limited tuning range around 3000 Å. It can therefore be expected that the present 4000 Å limit can be extended to 2500 Å and modest powers can be obtained.

CALCULATIONS

Let us consider a fluorescence approach for L.I.D. Other approaches are also possible and will be discussed later. We consider a crossed beam resonant absorption and fluorescence situation in which a laser beam crosses at right angles an atomic beam having A atoms sec^{-1} cm^{-2} in it with $\bar{v}$ the average velocity of the atoms. One may work with a non-90° angle also. For a 90° angle for a two-level system the number of photons scattered by each atom is $\frac{n_e}{n_o}\frac{d}{\bar{v}\tau}$ where d is the diameter of the laser beam and τ is the lifetime of the excited state. n_o and n_e are the populations of the ground and excited states. Thus at saturation ($I_s = \frac{\hbar w}{2\sigma\tau}$) we can scatter $d/\bar{v}\tau$ photons/atom. The induced emission, of course, does not come into the picture because it all takes place in the forward direction. Since the active volume is very small, radiation trapping also does not cause any problem. We have already ignored small corrections to volume shape.

If η_d represents the efficiency of the photon detection processes and Ω the fraction of the solid angle in which the emission is collected, then the number of photons that can be detected per atom is $\Omega\eta_d d/\bar{v}\tau$. Thus if n_{min} is the minimum number of detected atoms, then we have

$$n_{min} = \frac{\bar{v}\tau}{\Omega\eta_d d} B \frac{S}{N}$$

where B is the background rate and S/N is the lowest signal-to-noise level of the detector. The sensitivity achieved in time t is then

$$s = \frac{\bar{v}\tau}{\Omega\eta_d\eta_c dAt} B \frac{S}{N} \qquad (1)$$

where η_c is the efficiency of conversion of the sample to the utilized beam.

The Rayleigh scattering background is given, in usual notation, by

$$I_{scatt} = \frac{4\bar{\Lambda}}{3}\left(\frac{2\bar{\Lambda}}{\lambda}\right)^4 N \alpha^2 I_{inc.}$$

Here N is the number of scatterers and α is the polarizability. For typical values of λ = 5000 Å, $N = 10^8$ atoms and $\alpha = 10^{-24}$ cm^2 this yields

$$I_{scatt} = 10^{-20} I_{inc.}$$

Since the resonant scattering for the isotope of interest can be saturated with a laser power of less than 10^{16} photons/sec the Rayleigh scattering does not present any problem. We can also ignore power, collision and Doppler broadenings. For the simple scheme described above the largest contribution to the background in Equation (1) comes from the natural broadening. Notice that both the signal and the background depend in the same way on A, Ω and η_d. Also, n_{min} can be of the order of unity and the amount of time taken to detect a single atom cannot be larger than $d/\bar{v}$.

Taking the conservative estimate for the detection time discussed above and using the Lorentzian function for natural broadening and a Gaussian laser beam we obtain for the sensitivity

$$S = \left[\frac{\int_0^{\infty} \frac{\exp\{-16\pi^2 (\ell n 2)(\nu-\nu_2)^2/\Gamma^2\}\, d\nu}{(\nu-\nu_1)^2 + (\frac{1}{4\pi\tau})^2}}{\int_0^{\infty} \frac{\exp\{-16\pi^2 (\ell n 2)(\nu-\nu_2)^2/\Gamma^2\}\, d\nu}{(\nu-\nu_2)^2 + (\frac{1}{4\pi\tau})^2}} \right] \frac{S}{N} \frac{d}{\bar{\nu}\eta_c \tau} \qquad (2)$$

where $(\nu_1 - \nu_2)$ is the isotope shift and Γ the laser bandwidth.

Notice here that a simple observation of the signal would not suffice since in this case the signal would be overwhelmed by the noise. Therefore multi-channel analysis of the signal must be performed.

It should be noted here that the amount of time taken to detect fluorescence from an atom or molecule could be made of the order of τ without much difficulty.

In order to evaluate the integrals in (2) we first observe that for practical cases of interest the limits of integration can be changed to $-\infty$ to $+\infty$ without affecting the results. The error made should be easily possible to calculate and should be negligible. With this change the integrals become the Voigt integrals whose properties have been most recently reviewed by Armstrong and Nicholls [26]. Introducing

$$x = 4\pi\ (\ell n\ 2)^{1/2}\ (\Delta\nu)/\Gamma$$

and

$$y = (\ell n\ 2)^{1/2}/(\Gamma\tau)$$

we obtain for the ratio, R, of the integrals in Eq. (2) the value

$$R = K(0,y)/K(x,y)$$

where

$$K(x,y) = \frac{y}{\pi} \int_{-\infty}^{\infty} \frac{e^{-u^2}}{(x-u)^2 + y^2}\, du$$

K(0,y) is related to the complementary error function erfc (y) [27] through the relation

$$K(0,y) = e^{y^2}\ \mathrm{erfc}(y)$$

Tables of K(x,y) for limited ranges are available in a few places, all referenced in [26]. However, since in this paper we would need to explore a large range of values of the parameter x (corresponding to a large range of values of the laser band-width) we would, besides the use of the tabulated values, also make use of truncated series expansions for K(x,y) and erfc(y). At this point we notice that for the typical values $\tau = 10^{-8}$ sec and $\Delta\nu = 10^9$ Hz., a typical value of the parameter $a = 1/(4\pi\tau(\Delta\nu))$ is $a = 8 \times 10^{-3}$. Hence for $x<1$, $y=ax<<1$. Using the Maclaurin expansion (3.7.25) of reference [26] and the expansion (7.1.5) of [27] and truncating the two after the second terms we obtain

$$R = \frac{\sqrt{\pi}\ -2y\ -\ \sqrt{\pi}\ (x^2-y^2)}{2\ e^{y^2}\ (1-y^2)}$$

For $x \gtrsim 1$ we have used tabulated values of K(0,y) and K(x,y). For x>>1 and y>1 we have used the asymptotic expansions (3.7.26) of [26] and (7.1.23) of [27] and upon similar truncation obtain

$$R = \frac{y^4[2(x^2+y^2) + (3x^2-y^2)]}{(2y^2-1)\ (x^2+y^2)^3}$$

Finally connecting all the different regions we show the results in Fig. 1 for some values of a. From it we notice that for $x=10^2$ a value of 10^{-6} results for R. The value of $x=10^2$ corresponds to a laser band-width of about 10^8 Hz. Considering the fact that these days lasers have been developed with remarkable frequency stability [15] (close to a few Hz.), the operation of a laser with a bandwidth of 10^8 Hz does not pose any serious problems. Assuming a value of η_c=10% and with typical values for the other quantities in Eq. (1) we obtain a value of the order of 10^{-11} per sec. for the sensitivity of L.I.D. The above being a very conservative estimate, sensitivities better than this by one or two orders of magnitude should not be difficult to achieve, and the subject certainly needs further theoretical and experimental development.

Notice that the graph of R vs. x presented by us is quite general and would also be good for other L.I.D. techniques not based on the fluorescence method discussed above.

From Fig. 1 we note that the value of R and hence of the sensitivity can be easily improved by about an order of magnitude simply by increasing $\Delta\nu$ or by decreasing Γ by about a factor of two.

POTENTIALLY USEFUL IDEAS FOR L.I.D.

We list here some ideas that may or may not turn out to be useful for L.I.D. However, it does seem that they are worth exploring.

The use of intracavity absorption techniques [28 to 30] could be useful in enhancing absorption and therefore in increasing the sensitivity.

In some cases the difference in the nuclear spin of two isotopes and the resulting difference in the hyperfine structure [31] may be utilizable. This idea has already been explored for Laser Isotope Separation. The hyperfine effect is larger for heavier atoms than for lighter atoms.

Correlations between the signal photons can be utilized for discriminating against the scattered light [32]. The correlations amongst the photons generated by the fluorescence of the background isotope may be different compared to the correlations amongst the photons coming from the signal isotope. Differentiation between these correlations could improve the sensitivity.

The use of multiphoton techniques [33] could be promising for two reasons. One, they could be useful where single-photon absorption is not possible due to the lack of the availability of a laser. Secondly, the use of more than one photon also increases the isotopic selectivity very dramatically [34] in those cases in which the transition takes place through a real state. The subject of multiphoton line-shapes is not yet fully developed. One question that is not fully understood is the line-shape of a state which cannot be reached by single-photon absorption from the ground state but can fluoresce to a state (which is not the ground state). The development of double-wavelength lasers [35] is specially promising for multiphoton work.

Another idea that may be of some help could be to utilize the change in polarization of the fluorescence when one scans through different hyperfine levels with a narrow bandwidth laser [36]. Such effects being different for different isotopes, it may be possible to increase the sensitivity by a small factor if the experiment is done with polarized light.

In some cases electric and magnetic fields could be of help in increasing the isotope shift. This idea would be specially useful if one isotope has a hyperfine structure whereas the other one does not. Further, one may also combine the excitation of magnetic sub-levels (after having split them in a field) and utilize the resultant difference in the polarization of the fluorescence from different isotopes.

There are also ways of "beating" the natural broadening [37 to 39]. By observing the fluorescence from only the long-lived atoms one can narrow down the natural broadening to levels below those required by the uncertainty principle. Of course, this requires that only a subset of the sample (the long-lived atoms) be detected at any given time. This requirement would have an adverse effect on the sensitivity because it would tend to increase the time required for dating. But on the other hand it is possible that this advantage may become offset by the narrower bandwidths that would become available. These narrower bandwidths could help in cutting down the sample size. Resolution better than the natural line-width can also be obtained by using optical Ramsey fringes [40].

The use of derivative spectroscopy [41] may be useful in some cases in untangling complicated spectra.

Heterodyne detection techniques may also play a role for L.I.D.

It has been observed recently [32] that the detection of several scattered photons from an atom leads to much narrower line-widths than under normal circumstances. This could be useful for L.I.D.

Differences in the angular distribution of the two isotopes may be exploited for L.I.D. These differences will probably be even more pronounced for multiphoton processes than for single photon processes.

Another technique that may be useful for L.I.D. could be the use of nozzle beams [42,43].

REFERENCES

1. See the other articles in these Proceedings.

2. G. Faure, Principles of Isotope Geology, (John Wiley and Sons, New York, 1977).

3. R.E.M. Hedges, "Radioisotope clocks in archaeology", Nature 281, 19 (1979).

4. R. Gannon, "How Old Is It? - The Elegant Science of Dating Ancient Objects", Popular Science, Nov. 1979, p. 76.

5. R.E.M. Hedges, "Physics in Archaeology", Nature 278, 691 (1979).

6. R. D. Reeves and R. R. Brooks, Trace Element Analysis of Geological Materials, John Wiley, New York (1978).

7. M. E. Bickford and W. R. Vanschmus, "Geochronology and Radiogenic Isotope Research", Rev. of Geophysics & Space Physics 17, 824 (1979).

8. E. Jaeger, Lectures in Isotope Geology, Springer-Verlag, New York (1979).

9. S. Jefferson, Radioisotopes: A New Tool for Industry, Philos. Lib. (1958).

10. H. E. Gove, D. Elmore, R. Ferraro, R. P. Beukens, K. H. Chang, L. R. Kilius, H. W. Lee, A. E. Litherland, and K. H. Purser, "Radioisotope Detection with Tandem Electrostatic Accelerators", Nuclear Instrum. Meth. 168, 425 (1980), and the references therein.

11. K. Nishiizumi, J. R. Arnold, D. Elmore, R. D. Ferraro, H. E. Gove, R. C. Finkel, R. P. Beukens, K. H. Chang, and L. R. Kilius, "Measurements of ^{36}Cl in Antarctic Meteorites and Antarctic Ice Using a Van de Graaf Accelerator", Earth and Planet, Sci. Lett. 45, 285 (1979).

12. K. H. Purser, A. E. Litherland, and H. E. Gove, "Ultra-sensitive particle identification systems based upon electrostatic accelerators", Nucl. Instr. Meth. 162, 637 (1979).

13. Physics Today 32, no. 2, p. 20 (1979).

14. J. Husain, "New Sensitive Approaches to Radioisotope Dating", Opt. Commun. 29, 197 (1979).

15. J. L. Hall, "Stabilized Lasers and Precision Measurements", Science 202, 147 (1978).

16. C. R. Pidgeon and M. J. Colles, "Recent developments in tunable lasers for spectroscopy", Nature 279, 377 (1979).

17. H. Walther and K. W. Rothe, ed., Laser Spectroscopy IV, Springer-Verlag, New York (1979).

18. T. F. George, "Overview of Laser Applications to Chemistry", Opt. Eng. 18, 167 (1979).

19. C. L. Tang, ed., Quantum Electronics, parts A and B, Acad. Press, New York (1979).

20. C. E. Wagstaff and M. H. Dunn, "2nd-harmonic ring dye laser for the generation of continuous-wave, single-frequency uv-radiation", J. Phys. D 12, 355 (1979).

21. S. M. Jarrett and J. F. Young, "High-efficiency single-frequency cw ring dye laser", Opt. Lett. 4, 176 (1979).

22. B. Burghardt, W. Jitschin and G. Meisel, "Precise rf Tuning for cw Dye Lasers", App. Phys. 20, 141 (1979).

23. K. Jain, "A milliwatt-level cw laser source at 224 nm", Appl. Phys. Lett. 36, 10 (1980).

24. C. M. Marshall, R. E. Stickel, F. B. Dunning and F. K. Tittel, "Computer Controlled Intracavity Second Harmonic Generation in a CW Ring Dye Laser", Appl. Opt. (in press, 1980).

25. W. Huffer, R. Schieder, H. Telle, and R. Rave, "New Efficient Laser Dye for Pulsed and cw Operation in the Ultraviolet", Advance Program, Conf. on Laser & Electro-Optical Systems, San Diego, Feb. 1980, p. 41.

26. B. H. Armstrong and R. W. Nicholls, Emission, Absorption and Transfer of Radiation in Heated Atmospheres (Pergamon Press, Oxford, 1972).

27. W. Gautschi, in Handbook of Mathematical Functions, ed. by M. Abramowitz and I. Stegun (National Bureau of Standards, Applied Math. Series No. 55, Washington, D.C., 1964).

28. For a review see R. A. Keller and J. C. Travis, in N. Omenetto, ed., Analytical Laser Spectroscopy, John Wiley, New York (1979), p. 49.

29. W. T. Hill, III, R. A. Abreau, T. W. Hansch, and A. L. Schawlow, "Sensitive Intracavity Absorption at Reduced Pressures", Opt. Communic. 32, 96 (1980).

30. P. Kumar, G. O. Brink, S. Spence and H. S. Lakkaraju, "Line Shape Studies in cw Dye Laser Intracavity Absorption", Opt. Communic. 32, 129 (1980).

31. P. Jacquinot and R. Klapisch, "Hyperfine spectroscopy of radioactive atoms", Rep. Prog. Phys. 42, 773 (1979).

32. D. A. Lewis, J. F. Tonn, S. L. Kaufman, and G. W. Greenless, "Photon-Burst Method in High-Resolution Spectroscopy", Phys. Rev. A 19, 1580 (1979).

33. S. Stenholm, "Laser-induced Multiphoton Transitions", Contemp. Phys. 20, 37 (1979).

34. V. S. Letokhov and V. I. Mishin, "Highly Selective Multistep Ionization of Atoms by Laser Radiation", Opt. Communic. 29, 168 (1979).

35. S. Blit, A. Olsson, and C. L. Tang, "Double-wavelength electro-optically tuned synchronously pumped cw laser", Opt. Lett. 4, 245 (1979).

36. V. Kroop, Ch. Kammler, and W. Behmenburg, "Polarization Change of Light Scattering Near a $^2P_{3/2} \leftrightarrow {}^2S_{1/2}$ Resonance", Z. Physik A 286, 139 (1978).

37. J. N. Dodd and G. W. Series, "Time-Resolved Fluorescence Spectroscopy", in W. Hanle and H. Kleinpoppen, eds., Progress in Atomic Spectroscopy, Part A, Plenum Press, New York (1978), p. 669.

38. E. B. Alexandrov, "Quantum Beats", in 6th Int. Conf. Atomic Physics, ed. by R. Damburg and O. Kukaine, Plenum Press, New York (1979).

39. A. Denis and J. Desesquelles, "Delayed quantum beats as a method of subnatural-linewidth spectroscopy", Phys. Rev. A, May 1980 (in press).

40. V. P. Chebotayev, "The Method of Separated Fields in Optics", in F. T. Arecchi, R. Bonifacio and M. O. Scully, ed., Coherence in Spectroscopy and Modern Physics, Plenum, New York (1978).

41. J. E. Cahill, "Derivative spectroscopy: understanding its application", American Laboratory, Nov. 1979, p. 79.

42. R. E. Smalley, L. Wharton, and D. H. Levy, "Molecular Optical Spectroscopy with Supersonic Beams and Jets", Acc. Chem. Res. 10, 139 (1977).

43. L. Valyi, Atom and Ion Sources, J. Wiley & Sons, New York (1978).

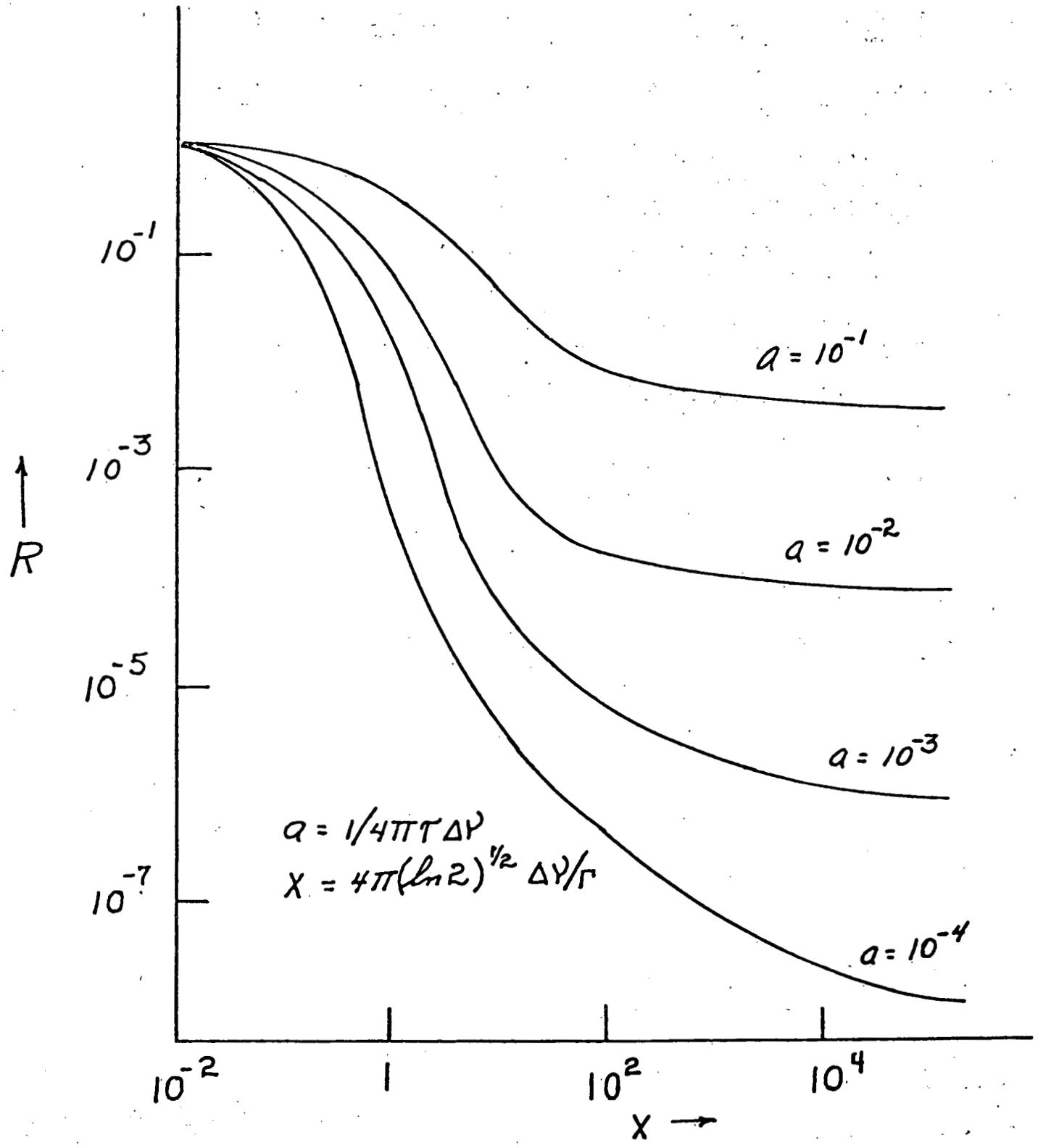


Figure 1. Graph of R vs. x for different values of a.

The Feasibility of Using a Novel Pulsed Neutron Source for in vivo Prompt Gamma Analysis

H. C. BIGGIN and W. D. MORGAN*

Dept. of Applied Physics, Sheffield City Polytechnic, Sheffield S1 1WB, England
*Medical Research Center, Brookhaven National Laboratory, Upton, N.Y.11973,USA

Abstract

This paper outlines the characteristics of a system which incorporates the convenience and availability of isotope neutron sources with the reduction in detection limit achieved by pulsed accelerator beams.

The proposed technique involves the high speed rotation under shielding of one or more ^{252}Cf neutron sources around the circumference of a circle containing an aperture which directs the neutron beam towards the organ of interest. The resulting sequence of collimated neutron pulses are thermalised in the body to induce the emissions of capture gamma rays from a particular element. The emitted radiation is monitored using a detection system which is gated off during the presence of a neutron pulse.

Limitations on neutron pulse length and detector count time require the attainment of a threshold rotational speed which depends on the duty cycle of the system. Analysis of the system characteristics indicates that, in comparison with the corresponding continuous irradiation system, a tenfold reduction in patient dose would result in an increase in detection limit of only 40%.

The stresses produced in the neutron source rotor require currently-available materials with a high strength-to-weight ratio. If safety considerations necessitate working at lower rotational speeds, the detection efficiency per unit dose is reduced due to a proportion of the photons being emitted during the longer neutron pulse, when the detector is gated off. The proportion of lost counts can be calculated for a given neutron pulse length, showing that a tenfold reduction of patient dose is achievable in this more practical situation for a 70% increase in detection limit. Furthermore, by optimising the detector count time to maximise S^2/B, this increase in detection limit is reduced to some 30%, again at the lower dose level.

The system performance depends on precise knowledge of timing relationships between neutron pulse and detector count period. The use of a simple monitor using an inexpensive integrated circuit is described,which makes cycle timing independent of rotor motor stability and precludes the possibility of drift.

* On Leave from Dept. Medical Physics, Singleton Hospital, SWANSEA SA2 8QA Wales

INTRODUCTION

In vivo neutron activation analysis (IVNAA) is an increasingly useful non-invasive technique for measuring partial- or total-body elemental composition.[1] Some elements are determined by off-line counting of induced activities, while others are more amenable to the on-line analysis of prompt neutron capture γ-rays. The latter method has several advantages, and has been successfully applied in the measurement of body nitrogen and organ cadmium.[2]

In essence, the method involves irradiating the body with a beam of fast neutrons which are then slowed down by interactions with body elements (principally hydrogen) to produce a flux of thermal neutrons at depths within the tissues. Since neutron thermalisation occupies a finite time, it is possible to pulse the beam and count capture γ-rays only in the beam off period, thereby reducing the background by avoiding truly prompt events occuring within the beam burst.[3]

Although this pulsed technique has been employed by the Birmingham group using a cyclotron,[4] other workers have developed viable systems based upon the use of constant output isotopic neutron sources such as ^{238}Pu-Be[5-8] and ^{252}Cf.[9] This paper describes a modification to a ^{252}Cf system which combines the convenience and ready availability of an isotope source with the advantages of using a pulsed beam.

The proposal involves the rotation under shielding of one or more neutron sources around the circumference of a circle containing one or more apertures (fig. 1). Such apertures direct the emitted neutrons towards the organ or region of interest. Consequently, a series of neutron pulses are thermalised in the body and prompt capture gamma rays may be observed.

In order to assess the degree of improvement which may be achieved by pulsing it is necessary first to consider what factors determine the detection limit of an element in vivo, and then to evaluate these factors for the proposed system.

FACTORS AFFECTING THE IN VIVO DETECTION LIMIT OF AN ELEMENT

(a) General case:

If the activation of an elemental quantity Q produces S counts in the peak of interest above a background of B, the detection limit is

$$Q_{Lo} = C \frac{\sqrt{B}}{S} Q,$$

where C is a constant related to the degree of statistical confidence required,

In any experimental situation, the values of B and S may be modified for example by changes in detection efficiency and resolution, and by the dose delivered. Let us consider the impact of each of these in turn:

(i) Background modified by a factor R, e.g. change in detector resolution. The new detection limit is

$$Q_L = C \frac{\sqrt{B.R}}{S} .Q = \sqrt{R}.Q_{Lo} \qquad 1$$

(ii) Both signal and background are modified by a factor Δ, e.g. by a change in detection efficiency or in the dose delivered. Now we have

$$Q_L = C \frac{\sqrt{B\Delta}}{S\Delta} .Q = \frac{Q_{Lo}}{\sqrt{\Delta}} \qquad 2$$

Combining equations 1 and 2 we obtain the familiar expression

$$Q_L = \sqrt{\frac{R}{\Delta}} \cdot Q_{Lo} \qquad 3$$

which indicates how the detection limit changes with detector resolution, detector efficiency, and dose delivered (or analysis time).

Finally, in the special case in which S alone is modified by a factor E, i.e. a change in sensitivity without a change in background, then

$$Q_L = C \frac{\sqrt{B}}{SE} \cdot Q = \frac{Q_{Lo}}{E} \qquad 4$$

Therefore, considering all possibilities,

$$Q_L = \frac{1}{E} \cdot \sqrt{\frac{R}{\Delta}} \cdot Q_{Lo} \qquad 5$$

(b) Application to the proposed pulsed system

If the total neutron source strength available for continuous beam operation is divided equally between the n sources (fig. 1) and if the ratio of background with the aperture open and closed is β, then it can be shown that the background modification in the beam off period is

$$R = n/\left[\beta + (n-1)\right] \qquad 6$$

This is a minimum for n = 1, and for a typical system in which $\beta \simeq 5$ we obtain R = 0.2. Using equation 5 it can be seen that if all other parameters remain fixed then the new detection limit $Q_L = 0.45\ Q_{Lo}$.

In practice, the other parameters do not remain fixed: for example, by pulsing the neutron source with a duty cycle $D = \frac{a}{2\pi r}$ (fig. 1), the dose delivered in a fixed time is reduced compared with the continuous beam. Alternatively, the same dose may be given by increasing the analysis time by 1/D. Therefore, in comparing PULSED TO CONTINUOUS irradiation modes,

$\Delta \propto D$ the duty cycle, or dose ratio at a fixed irradiation time and detection efficiency.
$\propto \tau$ the time ratio at fixed dose and detection efficiency.
$\propto \varepsilon$ the detection efficiency ratio at fixed dose and irradiation time.

Hence, $\Delta = D\ \tau\varepsilon$ a cumulative dose/detection efficiency factor.

TIMING RELATIONS IN ROTATING SOURCE MODE

Ideally, we wish to detect all the gamma photons from the induced reaction which are incident on the detector system. Allowing for finite neutron thermalisation in the body, this implies first that there is a maximum neutron pulse length during which no reaction is induced and hence no counts are lost with the detector gated off during this period; and second, that there is a minimum counting period required after each pulse to accumulate all the emitted photons.

With n regularly spaced neutron sources rotating around the circumference of a circle at frequency f and with duty cycle D, the effective period is $\frac{1}{nf}$ and the neutron pulse length is D/f (fig. 1). Clearly, to achieve a

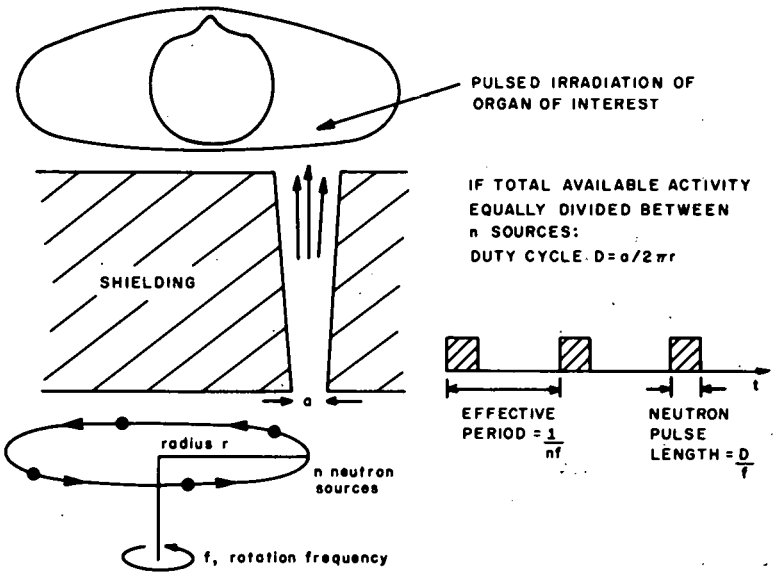
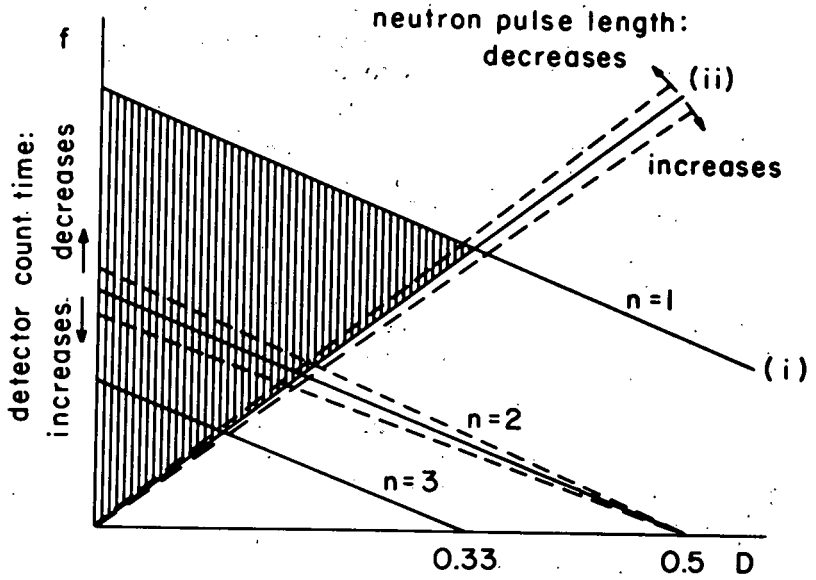


fig. 1: Schematic illustration of the proposed system.

fig. 2

(i)
$$f = \frac{\left(\frac{1}{n} - D\right)}{\text{detector count time}}$$

(ii)
$$f = \frac{D}{\text{neutron pulse length}}$$



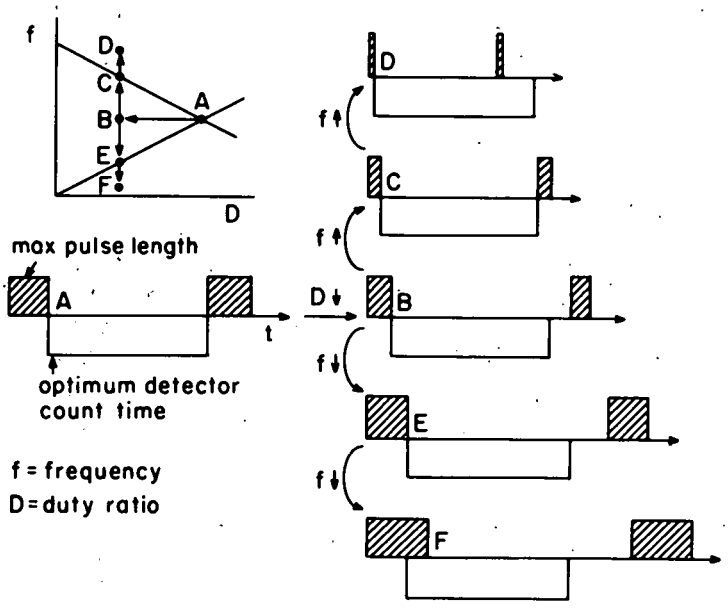


fig. 3: Time relations for different values of D and f.

neutron pulse length less than the maximum allowable,

$$\frac{D}{f} < \text{max. neutron pulse length} \qquad 7$$

The second limitation due to the requirement of a minimum detector count time to enable all counts to be accumulated may be formulated as:

$$\sum_{1\ s} (\text{neutron pulse lengths} + \text{detector count times}) < 1\ s$$

$$\text{or} \quad nf\left(\frac{D}{f} + \text{minimum detector count time}\right) < 1 \qquad 8$$

Combining equations 7 and 8, it can be seen that in order to achieve the desired neutron pulse length and detector count time, the frequency of rotation must satisfy the inequality

$$\frac{D}{\text{maximum neutron pulse length}} < f < \frac{\frac{1}{n} - D}{\text{minimum detector count time}} \qquad 9$$

The allowed frequencies are shown schematically in fig. 2, and the variation with n and D is indicated.

The two timing requirements of equation 9 are satisfied uniquely at point A in fig. 3. A reduction in duty cycle to point B at fixed frequency reduces the pulse length and results in poorer utilisation of irradiation time. An increase in frequency to C then reaches the upper frequency limit to provide the minimum detection period, whereas reduction in frequency to E is the lower frequency limit to maintain a neutron pulse length which will result in no loss of counts. Points D and F are clearly seen to contravene the initial criteria.

Required values of pulse length and count time may be satisfied by a range of D and f. In a solid rotor arm moving round a circle radius r with frequency f the stress produced $\sigma \propto \rho f^2 r^2$ where ρ is the density of the rotor arm. On the lower frequency limit where $f \propto D \propto r^{-1}$, σ is independent of D. However, as can be seen from Fig. 3, the utilisation of time available increases with D. On the other hand, it would be impracticable to reduce D below 0.1 (1/10 continuous dose administered in pulsed mode in a given time) and this is readily achieved with a rotor arm of length $r = 2.4 \times 10^{-2}$m and an aperture 1.5×10^{-2}m in diameter.

[It should be noted here that a reduction in frequency is attainable for given D by introducing a second aperture diametrically opposite the first with the shielding design modified to collimate the neutrons onto the target organ to be irradiated. The original neutron pulse length and detector count time are achieved by halving both the rotational frequency and aperture diameter. Such a modification is equivalent to using two rotating sources but without the associated increase in R. (see equation 6).]

SYSTEM PERFORMANCE IN IDEALISED SITUATION

It is instructive to set up a simplified model initially to calculate the detection limit reductions in pulsed mode. Two assumptions are made as first approximations:

(i) All induced photons may be detected if the neutron pulse length ≤ 25 μs, and the detector count time ≥ 200 μs. The finite neutron thermalisation time and the time dependence of prompt γ-ray emission[3] indicate that such approximations have some validity.

(ii) The neutron pulse is sharp and has a 'square' profile. In practice the profile will resemble a flat-topped normal distribution, the degree of tailing being dependent on the quality of shielding around the aperture.

In this situation with n = 1 and D = 0.1 a rotation frequency of 4 KHz satisfies the restrictions of neutron pulse length and detector count time and the stresses produced in the rotor constructed of high strength-to-weight alloy of Ti or Al will be less than in commercial ultracentrifuge rotors carrying greater mass (mass of Cf source$\sim$4 x 10^{-3}kg).

Table I: COMPARISON OF DETECTION LIMIT QL ATTAINABLE WITH n = 1 AND β = 5 FOR BOTH PULSED AND CONTINUOUS IRRADIATION SYSTEMS

QLo is the detection limit corresponding to a continuous irradiation giving the full dose to the patient and using a standard detector configuration (see equation 5).

	E	R	D	τ	ε	Δ	QL/QLo	COMMENT
PULSED	1	0.2	0.1	1	1	0.1	1.41	1/10 Full Dose
	1	0.2	0.1	10	1	1	0.45	Full Dose
CONTINUOUS	1	2	2	0.1	1	0.1	3.16	1/10 Full Dose
	1	1	1	1	2	2	0.71	Full Dose; 2 x detectors
	1	1	1	1	3	3	0.58	Full Dose; 3 x detectors
	1	1	1	1	4	4	0.50	Full Dose; 4 x detectors
	1	1	1	1	5	5	0.45	Full Dose; 5 x detectors

A comparison of calculated detection limits (Table I) shows that for a given patient irradiation time, the pulsed mode provides a tenfold reduction in patient dose for an increase in detection limit of about 40%. Alternatively, a potential reduction to 45% of the original detection limit could be attained, but this would require a tenfold increase in patient irradiation time. It can be seen that to achieve a detection limit comparable to this latter figure in continuous mode, the efficiency of detection would need to be increased by a factor of five, with the associated expense that this would entail.

REALISTIC SYSTEM PERFORMANCE

A rejection of the simplified assumptions in the ideal system, together with a possible requirement to operate at frequencies below the lower limit necessitates consideration of a situation where the end of the neutron pulse overlaps the onset of photon emission. A varying proportion of available counts are lost due to the detector being gated off during the pulse, as shown in fig. 4, and this results in a reduction in E in equation 5 .

The proportion of lost counts may be calculated by convolution analysis of the thermal neutron response function H(t), essentially the time dependence of prompt γ-ray emission following a 20 μs neutron pulse,[3] with the input neutron pulse length P(t). The time dependence of the induced photon emission is thus obtained:

$$R(t) = \int_0^t P(\tau)\ H\ (t-\tau)\ d\tau$$

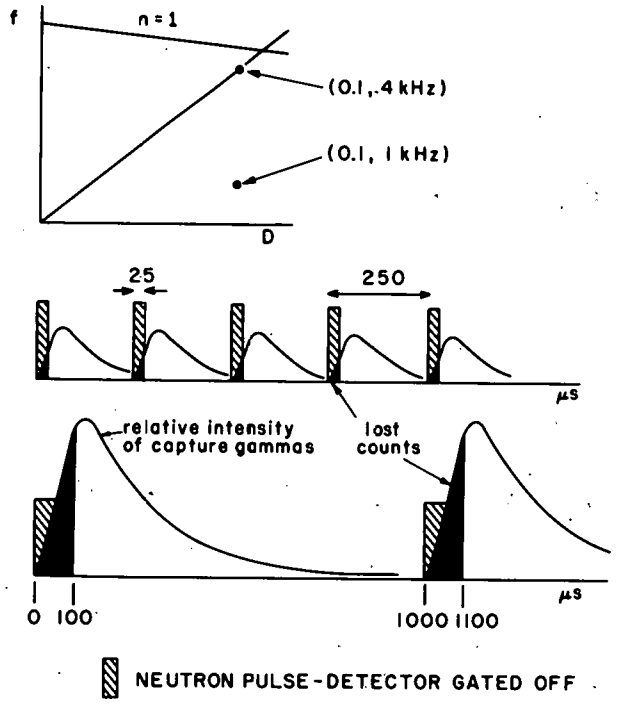


fig. 4: Loss of counts when detector is gated off increases as frequency is reduced (with D kept constant).

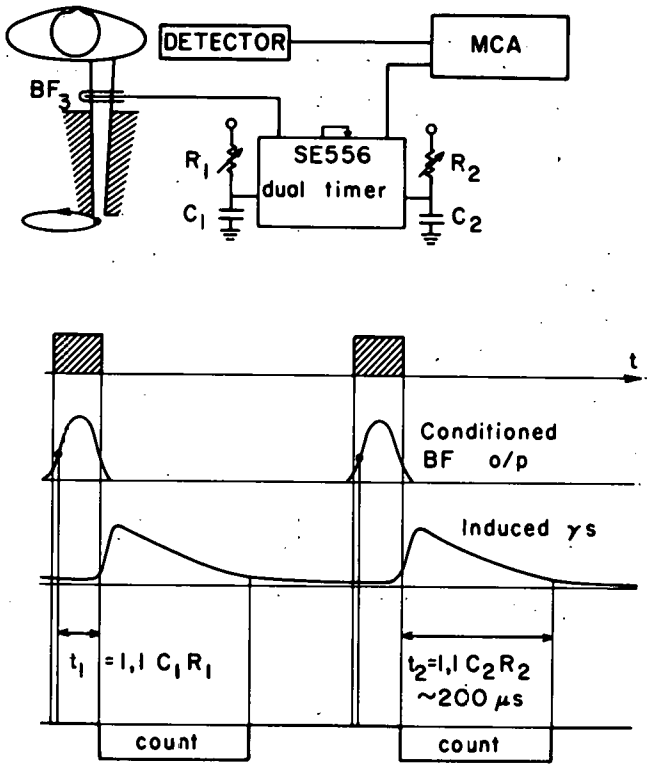


fig. 5: Timing system to gate analyser on and off in synchronism with the neutron pulse.

The analysis shows that the fraction of lost counts increases from 3% for a 20 μs pulse to 40% for a 200 μs pulse. In other words, E decreases from 0.97 to 0.60, with a corresponding increase in detection limit.

Such an increase in detection limit may be partly offset by restricting the detector count time such that S^2/B is maximised. Preliminary results indicate that with f = 1kHz and a neutron pulse length of 100 μs (D = 0.1), 22% of the available counts are lost during the pulse. However, S^2/B is a maximum after a 250 μs count period and during this time 56% of the induced emission may be detected i.e. E = 0.56. Finally, since the detector is gated on for only 250 μs in each 1000 μs, the background is modified by a factor R = 0.2 x 0.25 = 0.05.

Table II: COMPARISON OF DETECTION LIMITS ATTAINABLE IN PULSED AND CONTINUOUS MODES ALLOWING FOR LOSS OF COUNTS DURING FINITE NEUTRON PULSE

	Pulse /μs	f/ kHz	E	R	D	τ	ε	Δ	QL/QLo	COMMENTS
PULSED	100	1.0	0.78	0.2	0.1	1	1	0.1	1.7	1/10 Full Dose; lost counts
	100	1.0	0.78	0.2	0.1	10	1	1	0.57	Full Dose; lost counts
	100	1.0	0.56	0.05	0.1	1	1	0.1	1.27	1/10 Full Dose; S^2/B max.
	60	1.67	0.62	0.05	0.1	10	1	1	0.36	Full Dose; S^2/B max.
	100	1.00	0.56	0.05	0.1	10	1	1	0.39	Full Dose; S^2/B max.
	140	0.71	0.49	0.05	0.1	10	1	1	0.43	Full Dose; S^2/B max.
CONT.			1	1	1	1	5	5	0.45	Full Dose; 5 x detectors
			1	1	1	1	7	7	0.38	Full Dose; 7 x detectors

Table II gives the results of detection limit calculations on this model. It can be seen that for a given patient irradiation time and a neutron pulse of 100 μs(D = 0.1) the pulsed mode yields an increase in detection limit of 70% in comparison to continuous irradiation, for one-tenth of the dose. The alternative of giving the full dose in pulsed mode could lower the limit to 57% of the original.

Also included in the table are calculations based on maximising the S^2/B ratio for a variety of frequencies. The potential benefit of this procedure is apparent in the further reduction in detection limit attainable. The increased detection efficiency required to achieve similar detection limit reductions in continuous mode is again indicated, as in table I.

DETECTOR GATING SYSTEM

The system performance depends on an accurate timing signal to gate the detector off when the neutron beam is present. A simple inexpensive method of maintaining timing relationships at the high frequencies envisaged is shown in fig. 5.

The smoothed output of a BF_3 detector situated in the neutron beam is fed into a SE556 dual timer IC. The BF_3 pulse starts a clock to provide an adjustable time delay $t_1 = 1.1\ C_1R_1$ before initiating the count period at the end of the BF_3 pulse. The count period is similarly adjustable ($t_2 = 1.1\ C_2R_2$) after which the detectors are gated off. Such a system compensates for frequency drift in the drive motor and ensures the integrity of cycle timing.

DISCUSSION

Results in tables I and II are based on a background reduction factor of $\beta = 5$. However, this value was obtained in a static situation with the beam ON and then OFF. In practice, the background immediately after the end of the beam pulse will be greater than this due to thermal neutron capture in hydrogen and other body elements, and therefore β will be correspondingly lower. Nevertheless, the static value of β may be considerably increased by using a greater source-subject distance and by the use of improved shielding materials. In the Brookhaven mobile facility[10] a value of $\beta \simeq 10$ has been measured. It appears, therefore, that the choice of $\beta = 5$ for these calculations is not an unreasonable assumption.

In the only published experimental comparison between pulsed and continuous modes of operation,[11] a reduction in detection limit of about 0.5 was observed by pulsing the cyclotron beam at 6kHz with a duty ratio of $D = 0.1$. This is in very good agreement with the value quoted in Table I, line 2.

At the lower frequencies considered in table II, similar reductions in detection limit are achieved by limiting the count interval appropriate to maximising S^2/B. Although these calculations have assumed a constant background, when in fact a proportion will be varying in the same way as the signal to be measured, nevertheless the tabulated values are a good indication of the degree of improvement likely to be obtained by rotating a single source with a frequency of about 1 kHz.

CONCLUSIONS

This analysis indicates the potential benefits of a rotating source irradiation. Using an optimum frequency of rotation, the detection limit is seen to be approximately halved for the same patient dose as in continuous irradiation mode, or alternatively the detection limit increases by only 40% for one-tenth of this dose (same irradiation time).

Using a lower, more readily-achievable rotation frequency and accepting some loss of signal which occurs during the latter part of the longer neutron pulse and is thus undetected, the detection limit increases by 70% compared with continuous irradiation, again for one-tenth of the patient dose. Further, by reducing the detector count time until S^2/B is maximised, this increase may be reduced to some 30% of that achieved in continuous mode, again at the lower dose level. Thus, the penalty of increase in detection limit is clearly outweighed by the substantial reduction in administered dose, which may well be the overriding concern should sequential studies be envisaged.

The proposed modifications to existing conventional facilities are possible at relatively low cost and could be implemented efficiently by prior testing of subsidiary circuits and components.

ACKNOWLEDGEMENTS

We would like to thank Dr. P. E. Cummins for helpful discussions and comment, and F. C. O'Brien for patience in typing the manuscript.

REFERENCES

1. COHN SH, ELLIS KJ, VARTSKY D, ZANZI I, ALOIA JF, Nuclear Activation Techniques in the Life Sciences; pp 747-761, IAEA-SM-227/63, Vienna (1979).

2. BIGGIN HC, CHEN NS, ETTINGER KV, FREMLIN JH, MORGAN WD, NOWOTNY R, CHAMBERLAIN MJ, Nature New Biol. 236, 187-188 (1972).

3. ETTINGER KV, BIGGIN HC, CHEN NS, CHETTLE DR, FREMLIN JH, HARVEY TC, MORGAN WD, NOWOTNY R, THOMAS BJ, VARTSKY D, Kerntechnik 17, 89-92 (1975).

4. BIGGIN HC, CHEN NS, ETTINGER KV, FREMLIN JH, MORGAN WD, NOWOTNY R, CHAMBERLAIN MJ, in Nuclear Activation Techniques in the Life Sciences; pp 639-649, IAEA-SM-157/15, Vienna (1972).

5. MERNAGH JR, HARRISON JE, McNEILL KG, Phys. Med. Biol., 22, 836 (1977).

6. VARTSKY D, ELLIS KJ, CHEN NS, COHN SH, Phys. Med. Biol., 22, 1085-1096 (1977).

7. VARTSKY D, ELLIS KJ, COHN SH, J. Nucl. Med., 20, 1158-1165 (1979).

8. THOMAS BJ, HARVEY TC, CHETTLE DR, McLELLAN JS, FREMLIN JH, Phys. Med. Biol. 24, 432-437 (1979).

9. EVANS CJ, CUMMINS P, DUTTON J, MORGAN WD, SIVYER A, GHOSE RR, in Nuclear Activation Techniques in the Life Sciences; pp 719-731, IAEA-SM-227/9, Vienna (1979).

10. ELLIS KJ, MORGAN WD, YASUMURA S, VARTSKY D, ZANZI I, COHN SH, p. This Conference (1980).

11. BIGGIN HC, CHEN NS, ETTINGER KV, FREMLIN JH, MORGAN WD, NOWOTNY R, CHAMBERLAIN MJ, HARVEY TC, J. Radioanal. Chem. 19, 207-214 (1974).

NAA as viewed from the Perspective of International Atomic Energy Agency Intercomparison Tests

Rajmund Dybczyński
Laboratory Seibersdorf,
IAEA,
A-1400 Vienna, Austria

ABSTRACT

Results of several IAEA intercomparison runs organized over the last 8 years are analyzed from the point of view of contribution and performance of NAA as compared to other techniques. It is shown that NAA is the method of good accuracy and precision providing on average greater share of results than any other single analytical technique. The prominent position of NAA among other methods used in trace analyses seems to be firmly established and there are no signs that there might be any change of the trend in the nearest future.

INTRODUCTION

The objective comparison of merits and demerits of various analytical techniques used in trace analysis and of their relative significance is extremely difficult due to the complexity of the problem. The problem may be approached in many different ways.

The review of detection limits for instance, provides a valuable insight into the potential possibilities offered by a given method and enables some comparisons between the methods. However, these idealized, calculated values are often difficult not only to attain but even to approximate in the case of real samples.

Practical detection limits may differ by orders of magnitude from idealized values, the gap being dependent both on the method and on the kind of sample.

One can try to compare popularity of various methods by counting the number of publications on a subject, appearing in the literature over a given period of time.

While such numbers undoubtedly reflect the relative research effort in individual areas, it is not certain whether they equally well represent the real contribution of particular methods to trace analysis in every-day applications.

Still too little is known about the accuracy of individual methods partly due to the lack of suitable reference materials for a variety of types of matrices.

On the other hand it is certain that good precision of results demonstrated by a laboratory does not necessarily mean that the results are also accurate (1).

For the majority of radioanalytical chemists it was obvious already long ago that neutron activation analysis (NAA) with its excellent detection limits for most of the elements (2, 3) and rapidly growing literature (4) firmly occupies a prominent place among other methods or inorganic trace analysis.

On the other hand some non-nuclear chemists have not so seldom voiced the opinion that NAA that requires the access to nuclear reactor and quite often also computer data processing of the gamma-ray spectra is a too exotic technique to be really competitive and will constantly lose in value in comparison with other analytical methods. To check whether this opinion might be correct, several IAEA intercomparison runs realized within the past 8 years have been analyzed from the point of view of contribution of NAA as compared with other techniques and the results are reported in this paper.

Contribution of NAA as Compared to Other Methods of Analysis

Some data on contribution and performance of NAA in comparison to other methods of analysis are shown in Tables I and II. As can be inferred from Table I despite the growing competition on the part of other techniques, NAA seems to retain its key role in trace analysis. The number of elements to the determination of which NAA contributed varied from 73 to 100%, depending on the run. The materials analyzed encompassed so diverse matrices as simulated air filters, simulated fresh water samples, geological and environmental samples (soil, lake sediment) and biological materials (fish solubles, milk powder).

NAA contributed on average a greater percentage of the total number of results than any other single analytical method. Depending on the intercomparison, this percentage varied from 21 to 57%, being the lowest for water samples which normally required some preconcentration and/or separation step and could then be conveniently analyzed as solution e.g. by atomic absorption spectrometry (AAS). However, even in this case NAA contributed for some elements (arsenic, barium, selenium and uranium) over 40% of the results and several laboratories were using this technique for the determination of all elements except lead (1). For solid samples in which at least some elements could be determined by purely instrumental NAA the share of NAA results was invariably high (40% - 57 %).

It is worth mentioning that quite often NAA was the only method used by numerous investigators for the determination of a given element. The examples are: Dy, Gd, Ho, Lu, Pr, Sm, Tb, Yb and Hf in soil (5), Eu, Sm, Tb, Yb, Au, Br, Hf and Na in lake sediment (6), and Ag, Au, Cs, Pt, Sb and Sc in milk powder (7). In several cases e.g. when analyzing for: Nd, Sc, Cs, Na, Ta, Th and W in soil, Ce, Dy, La, Lu, Nd, Sc, Cs, Sb, Ta, Th and U in lake sediment and Rb and Se in milk powder, NAA while not being the only method, was still used by the overwhelming majority of laboratories. In general, no such trend as for instance a decrease in the share of NAA results with time could be noted over the past 8 years.

Accuracy and Precision

As can be seen from Table II, the percentage of outlying results by NAA was not excessive and on the average not greater than with the other techniques. In cases when the "true value" was known, i.e. for spiked samples (water and air filters), direct estimation of accuracy was possible. The "true value" considering its own uncertainty was as a rule within the confidence interval (calculated for significance level of $\alpha = 0.05$) of the mean of results obtained by NAA (after rejection of outliers). More detailed analysis of the overall accuracy and precision of individual methods is presented in Table III.

As can also be inferred from Table III, the accuracy of NAA is generally good. With one exception (Zn in water) the percentage deviation of the mean of NAA results from the "true value" was quite small (between 3 and 16%). AAS showed comparable accuracy. Less accurate results were observed with emission spectroscopy (ES), X-ray fluorescence (XRF) and fluorimetry (F).

Overall precision varied quite notably from element to element and from method to method. As a rule the precision was much better for air filters than for water samples, what could be expected as the concentration levels in the latter were two to three orders of magnitude lower. Good overall precision of NAA results was observed when analyzing geochemical materials: Soil-5 and Lake Sediment (cf. Table II). It should be noted that similarly as it was the case with within-laboratory precision, good overall precision by a given method (i.e. low overall relative standard deviation) was not always paralleled by good accuracy and vice versa.

There was generally quite good agreement of results by NAA and AAS. Taking as a provisional criterion for significant difference between the methods that calculated confidence intervals of the means (at a significance level of $\alpha = 0.05$) do not overlap (5) there was only one case where there seemed to exist a systematic difference between the methods. This refers to the determination of manganese in Soil-5 (cf. Table II) where the mean of NAA results was significantly higher than those by AAS and ES, respectively. No explanation for this discrepancy has been found as yet.

General Comments and Conclusions

The results summarized in this paper clearly show that NAA occupies a remarkable place in trace analysis. One could wonder what are the main reasons of this phenomenon.

Obviously in typical multielement analyses such as those listed in Table I, NAA which normally makes possible to determine several elements from one sample was predestinated to be the method of choice for many of those laboratories that had access to nuclear reactor and gamma-spectrometric equipment.

However, there is no doubt that also other merits of NAA must have played a significant role, too.

Favourable detection limits for a great number of elements should be named here first. For traces present in concentration range of parts per billion, NAA is one of very few methods that can still cope with the problem.

On the other hand, traces in the parts per million level can often be determined directly, i.e. omitting any preconcentration or separation steps.

The other remarkable feature of NAA is good accuracy. Because of its nuclear character NAA is relatively free from chemical interferences and virtually free from blank in most instances.

High accuracy of NAA has recently been emphasized by many authors in the context of analysis of biological (2), geological (8, 9), environmental (10) and very pure materials (11). This opinion is confirmed by the present study. It should be added, however, that in inexperienced hands also NAA may yield completely erroneous results as follows from the presence of several outliers in some of the intercomparisons (cf. Table II).

Last but not least, in solid samples quite a number of elements can in many cases be determined non-destructively, among them such elements as Hf, Ta, Th, individual rare earths, Cs and Rb, which usually can be determined only with difficulty by other methods at comparable concentration levels.

Thus the popularity of NAA seems to be well established and justified and one can expect that it will continue to occupy a prominent role among other methods of trace analyses still for many years to come.

One could argue, of course, if the above considerations are not biased because of the fact that IAEA should by definition have closer contacts mostly with organizations dealing with nuclear energy and nuclear methods. The survey of mailing list of our Analytical Quality Control Service (over 1300 addresses) revealed however that only 28.3% of individuals were affiliated with Nuclear or Reactor Institutes, Nuclear Power Plants etc.

The share of addresses from Universities, Technical Universities, Institutes of Academies of Sciences amounted to 23.3%, followed by other Governemental or Industrial Establishements (16.2%), Medical, Biological, Veterinary etc. Institutions (13.1%), Environmental (9.3%), Agriculture, Food,Fisheries etc. (5.1%), and Geological Establishments (4.1%).

Moreover, nuclear centres are normally well equipped with non-nuclear analytical methods, thus having free choice of a technique. Therefore we believe that numbers quoted in this paper fairly adequately reflect contribution of NAA as compared to other methods.

Acknowledgement

The author is indebted to Dr. G.B.Cook for reading the manuscript and making valuable comments.

REFERENCES

1. R. Dybczyński, A. Tugsavul, O. Suschny
Analyst, 103 (1978) 733

2. V.P. Guinn, J. Hoste
Paper IAEA-SM-227/102, International Symposium on Nuclear Activation Techniques in the Life Sciences, Vienna 22 - 26 May, 1978, IAEA, Vienna, 1979.

3. V. Krivan
Angew. Chem. Int. Ed. Engl. 18 (1979) 123.

4. T. Braun, W.S. Lyon, E. Bujdosó
Anal. Chem. 49 (1977) 682 A.

5. R. Dybczyński, A. Tugsavul, O. Suschny
Geostand. Newsl., 3 (1979) 61.

6. R. Dybczyński, O. Suschny
Final Report on the Intercomparison Run SL-1 for the Determination of Trace Elements in a Lake Sediment Sample, IAEA/RL/64, December, 1979.

7. R. Dybczyński, A. Veglia, O. Suschny
(to be published).

8. A.O. Brunfelt, E. Steinnes
Geostand. Newsl. 2 (1978) 3.

9. J.W. Jacobs, R.L. Korotev, D.P. Blanchard, L.A. Haskin
J. Radioanal. Chem., 40 (1977) 93

10. J.M. Ondov, W.H. Zoller, I. Olmez, N.K. Aras, G.E. Gordon, L.A. Rancitelli, K.H. Abel, R.H. Filby, K.R. Shah, R.C. Ragaini
Anal. Chem. 47 (1975) 1102

11. Yu. A. Karpov, I.P. Alimarin
Zh. Anal. Khim., 34 (1979) 1402

Table I

Contribution of NAA as compared to other methods in IAEA intercomparisons.

No.	Intercomparison	Number of elements under investigation	Number of elements determined by NAA	% of results obtained by: *)				
				NAA	AAS	XRF	ES	Other methods
1	Simulated air filters (Air-3) (1972 - 1973)	14	13	53	27	3.8	10	6.2
2	Simulated fresh water (W-3) 1973-1975)	16	15	21.3	53	0.3	7.3	18.1
3	Fish solubles (A-6) (1974 - 1975)	13	12	50	41.8	1.8	0	6.4
4	Simulated fresh water (W-3) (1975 - 1976)	16	15	22.4	50.7	9.9	2.8	14.2
5	Simulated air filters (Air-3) (1975 - 1976)	16	15	45	35	9	9	2
6	Potassium feldspar (F-1) (1976 - 1977)	3	3	46	6	4	6	38
7	Soil (Soil-5) (1976-1978)	60	45	53	19.7	17.1	6.6	3.6
8	Lake sediment (SL-1) (1977 - 1979)	64	52	57	20.1	15.1	3.3	4.5
9	Milk powder (A-11) (1978 - 1980)	40	29	40	38.3	5.7	4	12

*) NAA - neutron activation analysis
AAS - atomic absorption spectrometry
XRF - X-ray fluorescence
ES - emission spectroscopy

Table II

Comparison of the performance of NAA with those by other methods.

No.	Element	Intercomparison	Concen. units	Method	% of outliers by this method	Mean of "accepted"*) results by a given method	Mean of all "accepted"*) results	"True value"
1	Co	Air filter (Air-3)	µg/ filter	NAA	0	4.84± 0.15 (9)	4.65± 0.23 (16)	5.0±0.1
				AAS	0	4.55± 0.57 (5)		
	Co	Water (W-3)	µg/l	NAA	13	13.5 ± 1.1 (7)		
				AAS	0	12.0 ± 1.0 (17)	11.9 ± 0.8 (29)	12.1±0.4
				XRF	0	8.8 ± 2.5 (3)		
	Co	Soil (Soil-5)	µg/g	NAA	4	14.8 ± 0.3 (24)		
				AAS	53	15.4 ± 1.2 (7)	14.8 ± 0.4 (37)	unknown
				ES	25	13.9 ± 2.6 (3)		
	Co	Lake sediment (SL-1)	µg/g	NAA	5	19.0 ± 0.7 (21)		
				AAS	18	22.0 ± 1.6 (9)	19.8 ± 0.7 (35)	unknown
				ES	0	22.3 ± 6.7 (2)		
2	Cr	Air filter (Air-3)	µg/l	NAA	0	2.74± 0.20 (8)		
				AAS	0	1.98± 0.25 (6)	2.35± 0.16 (18)	2.4±0.05
				ES	0	2.61± 0.18 (2)		
	Cr	Water (W-3)	µg/l	NAA	0	11.4 ± 2.3 (7)		
				AAS	0	11.6 ± 1.3 (15)	11.1 ± 1.0 (27)	12.0±0.4
				ES	0	9.5 ± 1.7 (2)		
				XRF	0	6.9 ± 2.2 (2)		
	Cr	Soil (Soil-5)	µg/g	NAA	5	27.6 ± 1.8 (21)		
				AAS	0	26.4 ± 2.5 (15)	28.9 ± 1.4 (44)	unknown
				ES	0	30.3 ± 2.9 (3)		
				XRF	40	41.2 ± 5.1 (3)		
	Cr	Lake sediment (SL-1)	µg/g	NAA	17	111.9 ± 4.5 (15)		
				AAS	15	86.2 ± 8.6 (11)	103.7 ± 4.5 (34)	unknown
				ES	0	114.6 ±19.6 (2)		
				XRF	0	111.1 ±16.7 (4)		

Table II (cont'd)

No.	Element	Intercomparison	Concen. units	Method	% of outliers by this method	Mean of "accepted" results by a given method	Mean of all "accepted" results	"True value"
3	Fe	Air Filter (Air-3)	µg/ filter	NAA	14	205 ± 5 (6)		
				AAS	33	194 ± 5 (6)	200 ± 4 (14)	200 ±4
	Fe	Water (W-3)	µg/l	NAA	40	28.2 ±13.6 (3)		
				AAS	9	37.8 ± 4.1 (20)	33.6 ± 2.7 (25)	32 ±1
				C&S	33	34.0 ± 9.0 (2)		
				XRF	0	29.4 ± 4.9 (2)		
	Fe	Soil (Soil-5)	Wt.%	NAA	4	4.69± 0.07 (22)		
				AAS	55	4.18± 0.18 (19)	4.45± 0.09 (55)	unknown
				XRF	0	4.44± 0.32 (10)		
				VOL	0	4.55± 0.19 (2)		
	Fe	Lake sediment (SL-1)	Wt.%	NAA	10	6.85± 0.11 (19)		
				AAS	23	6.56± 0.15 (10)	6.74± 0.08 (35)	unknown
				XRF	20	6.62± 0.30 (4)		
				VOL	0	6.77± 0.31 (2)		
4	Mn	Air filter (Air-3)	µg/ filter	NAA	0	3.86± 0.17 (9)		
				AAS	0	3.94± 0.29 (8)	4.04± 0.18 (20)	4.0 ±0.1
				ES	0	5.54± 0.09 (2)		
	Mn	Water (W-3)	µg/l	NAA	0	11.2 ± 2.7 (5)		
				AAS	0	11.1 ± 0.5 (11)	10.8 ± 0.6 (30)	12.0 ±0.4
				XRF	0	8.1 ± 1.0 (3)		
	Mn	Soil (Soil-5)	µg/g	NAA	5	935 ±16 (18)		
				AAS	9	807 ±27 (20)	852 ±19 (50)	unknown
				ES	0	740 ±30 (3)		
				XRF	25	888 ±61 (6)		

Table II (cont'd)

No.	Element	Intercomparison	Concen. units	Method	% of outliers by this method	Mean of "accepted" results by a given method *)	Mean of all "accepted" results *)	"True value"
	Mn	Lake sediment (SL-1)	Wt.%	NAA	7	0.337 ± 0.010 (13)	0.346 ± 0.007 (34)	unknown
				AAS	18	0.345 ± 0.010 (14)		
				XRF	17	0.386 ± 0.026 (5)		
5	U	Air filter (Air-3)	µg/ filter	NAA	0	1.13 ± 0.08 (6)	1.22 ± 0.08 (9)	1.03±0.02
				F	0	1.45 ± 0.25 (2)		
	U	Water (W-3)	µg/l	NAA	14	2.7 ± 0.5 (6)	3.5 ± 0.5 (16)	3.2 ±0.1
				F	0	4.1 ± 0.6 (7)		
				XRF	0	1.9 ± 0.01 (2)		
	U	Soil (Soil-5)	µg/g	NAA	0	3.30 ± 0.21 (15)	3.15 ± 0.21 (19)	unknown
				F	0	2.80 ± 1.4 (2)		
				XRF	0	2.38 ± 0.38 (2)		
6	Zn	Air filter (Air-3)	µg/ filter	NAA	0	73.0 ± 3.0 (8)	69.9 ± 1.4 (18)	70.0 ±1.4
				AAS	0	67.8 ± 2.1 (9)		
	Zn	Water (W-3)	µg/l	NAA	17	7.6 ± 2.3 (5)	13.6 ± 1.3 (26)	12.0 ±0.4
				AAS	5	15.2 ± 1.5 (18)		
				XRF	33	11.7 ± 7.3 (2)		
	Zn	Soil (Soil-5)	µg/g	NAA	29	372 ± 5 (10)	368 ± 4 (40)	unknown
				AAS	17	364 ± 6 (19)		
				ES	0	362 ±19 (3)		
				XRF	11	372 ±12 (8)		
	Zn	Lake sediment (SL-1)	µg/g	NAA	40	214 ±11 (6)	223.0 ± 5 (26)	unknown
				AAS	12	226 ± 7 (15)		
				XRF	20	232 ±11 (4)		

*) Results are reported as mean ± standard error, followed by number of "accepted" laboratory means in parentheses.
F - fluorimetry VOL - volumetry. Abbreviations for other methods as in Table I.

Table III

Comparison of accuracy and precision of individual analytical methods for selected elements

No.	Element	Intercomparison	$\frac{100\ (\bar{X}_m - \hat{X})}{\hat{X}}$				$S_{r(m)} = \frac{S_m}{\bar{X}_m}$			
			NAA	AAS	ES	XRF	NAA	AAS	ES	XRF
1	Co	Air filters	-3.2	-9.0	-	-	9.3	27.9	-	-
2	Co	Water	11.6	-0.8	-	-27.3	21.6	34	-	49.2
3	Cr	Air filters	14.2	-17.5	8.8	-	20.8	30.8	9.6	-
4	Cr	Water	-5.0	-3.3	-20.8	-42.5	53.4	43.4	25.3	45.1
5	Fe	Air filters	2.5	-3.0	-	-	6.0	6.3	-	-
6	Fe	Water	-11.9	18.1	6.3	-8.1	83.7	48.4	37.4	23.6
7	Mn	Air filters	-3.5	-1.5	38.5	-	13.2	20.8	2.3	-
8	Mn	Water	-6.7	8.3	-	-32.5	53.9	15.0	-	21.4
9	U	Air filters	9.7	-	[40.8]^F	-	17.7	-	[24.1]^F	-
10	U	Water	-15.6	-	[28.1]^F	-40.6	45.2	-	[38.8]^F	0.7
11	Zn	Air filters	4.3	-3.1	-	-	11.6	9.3	-	-
12	Zn	Water	-36.7	26.7	-	-2.5	67.6	41.8	-	88.0

$\bar{X}_m$ - mean of "accepted" results by a given method

$\hat{X}$ - "true value"

$S_{r(m)}$ - relative standard deviation of results by a given method

F - fluorimetry. Abbreviations for other methods as in Table I.

PIXE analysis of biological and environmental samples using a proton microprobe*

H.R. Wilde, W. Bischof, B. Raith, B. Gonsior

Ruhr-Universität Bochum, D-4630 Bochum, West Germany

1. Abstract

For the investigation of environmental and biological samples a proton microprobe[1] has been built up at the Bochum Dynamitron Tandem Laboratory. By means of PIXE[2] this device is used to measure lateral distributions of a wide range of trace elements in thin samples. Application of this technique to problems in the biological microstructure is of considerable interest, since presence or absence of certain elements at well defined places affects biological properties strongly[3].

2. Experimental

Fig. 1 shows a schematic representation of the microprobe. The diameter of the proton beam coming from the accelerator is reduced to 50 µm by the object diaphragm. A second elliptic diaphragm reduces scattering and defines the divergency of the beam. Then four magnetic quadrupole lenses generate a diminished image of the object diaphragm in the target plane. The x-rays emitted from the irradiated spot of the sample are detected at 90° by a Si(Li)-detector system. The size of the focus strongly depends on the ratio of image to object distance from the lenses according to Liouvilles's theorem. In the lower part of this figure the calcu-

* Supported in part by Bundesminister für Forschung und Technologie, D-5300 Bonn, West Germany

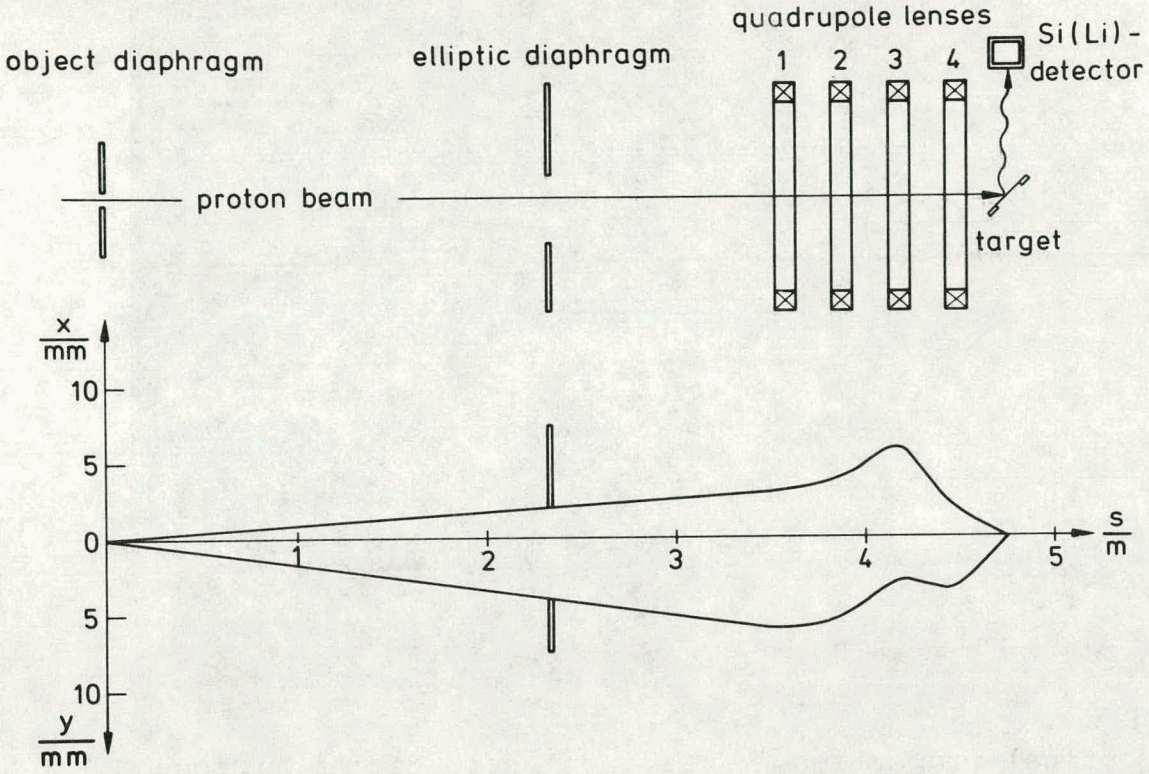


Fig. 1. Schematic representation of the microprobe (upper part) and calculated particle trajectories (lower part).

lated partice trajectories for both x- and y-direction are given. In order to minimize aberrations it is necessary to limit the maximum distance from the axis of the system to the same value in both directions. This is done by an anti-scattering diaphragm between object and image plane. Some results of the beam transport calculations are given in Fig. 2. Based upon the experimental arrangement of the first figure the lower part shows the relation between the four quadrupole currents when the smallest possible focus is generated. The currents of the lenses 2, 3 and 4 are plotted as a function of current 1. In addition the polarity of the lenses is given. The upper part shows the related scale of reduction versus current 1. It is remarkable that there is only one optimum value, i.e. one minimum focus and that it is achieved when the lenses 1 and 2 have the same polarity.

Fig. 3 shows a photo of the microbeam device. On the left hand side of the figure the two quadrupole doubletts are to be seen, which focus the beam into the target chamber in the foreground. This chamber is completely metal sealed and has several ports for detectors and additional equipment. Beneath the scattering chamber

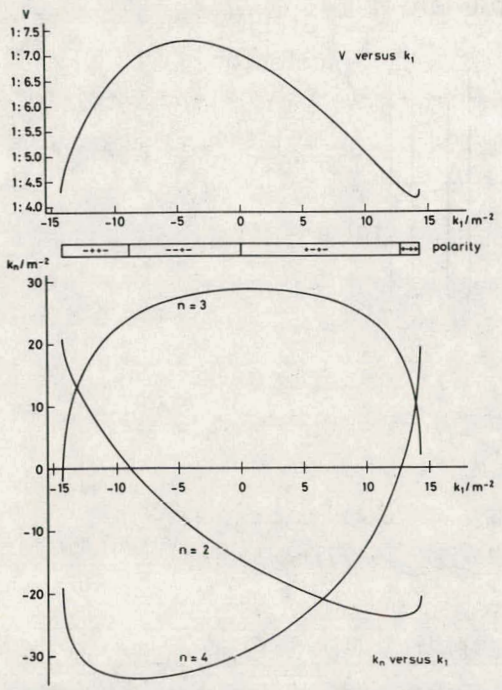


Fig. 2. Ion optical properties of our device. Lower part: the currents of quadrupole lenses 2,3,4 versus current 1. Upper part: scale of reduction versus current 1.

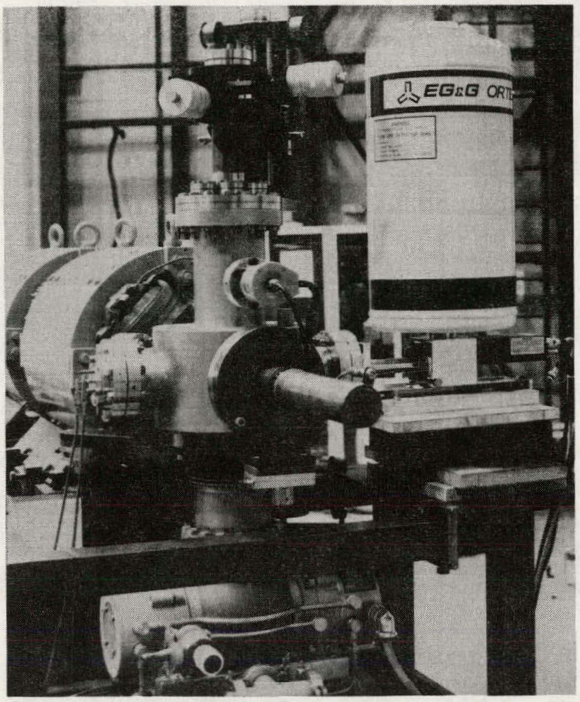


Fig. 3. Photo of the microbeam device. For details see text.

a turbomolecular pump is mounted on a completely separated support to avoid vibration of the sample. On top of the chamber a high precision sample driver is installed. It allows moving of the samples in 3 directions at an accuracy of 1 µm. On the right side the Si(Li)-detector is mounted at 90°, its minimum distance from the irradiated sample is 10 mm. In the 135° port behind the detector the microscope is installed. It is used to determine position and quality of the beam spot. This is done by observing the light output from a thin plastic scintillator foil during fine tuning of the quadrupole currents. Then the beam intensity profile is determined by two crossed tungsten wires, which are moved across the beam. The normalized yield of characteristic x-rays plotted versus the wire position gives the horizontal or the vertical beam profile.

Fig. 4 shows the result of a beam profile measurement. The solid

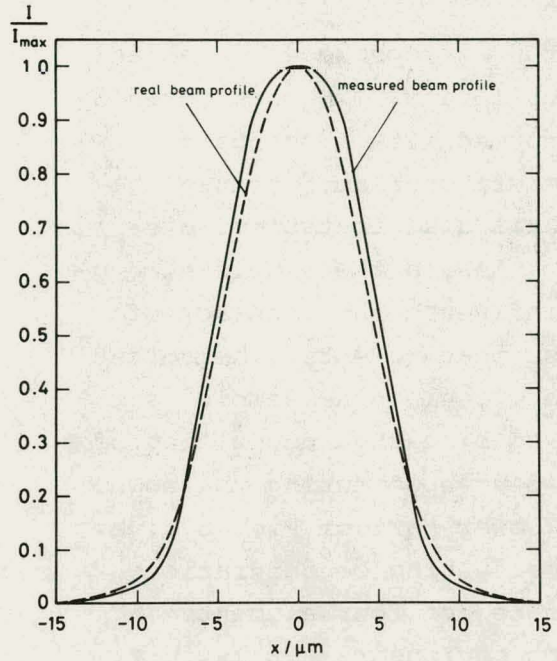


Fig. 4. Measured beam profile (full line) and corrected beam profile.

line gives the normalized x-ray yield from the tungsten wire versus the wire position. This measured beam profile must be corrected, because the beam size and the wire diameter have the same order of magnitude. The broken line gives the corrected beam profile. As a standard beam diameter 10 µm FWHM is achieved regularly within 1 h. 92 % of the beam intensity is concentrated in a beam spot of 20 µm. The beam current normally amounts to <1 nA. A summary of the ion-optical data of our device is given in table 1. To start the measurement the microscope is used to drive the first point of the sample to be analyzed to the position of the beam spot. Then scanning of the sample can be performed in the desired direction.

Table 1

Technical data of the microbeam device

total length	l_o/cm	477	1362
object distance	D_o/cm	351	1236
image distance	D_i/cm	21	21
object diaphragm	d_o/µm	100	57
beam spot size	d_i/µm	16	6.0

3. Measurements

In the field of environmental samples trace element profiles of air samples collected by an impactor have been investigated. The upper part of Fig. 5 shows such an impactor sample after irradiation. The width of the dark line in the middle is about 0.5 mm. It is formed by the air pollutants deposited on a thin nuclepore foil by impact. Investigation of these samples with the

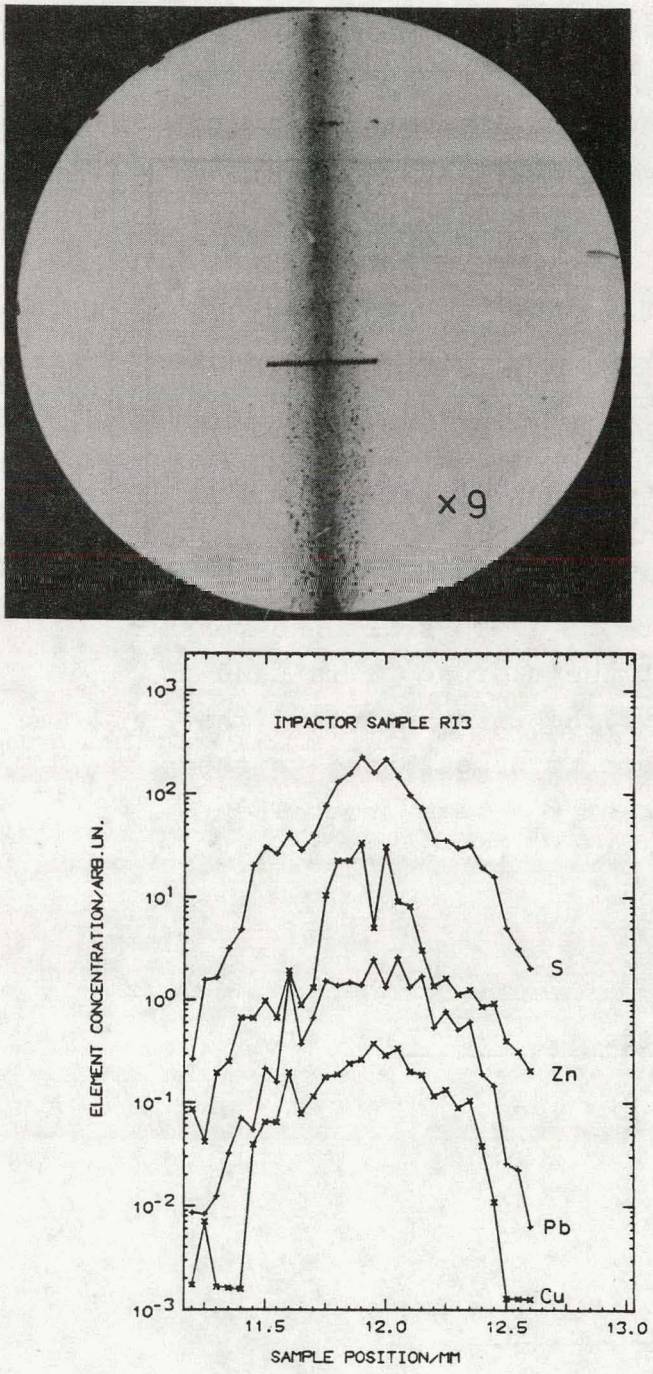


Fig. 5. Upper part: photo of an irradiated impactor sample.
Lower part: concentration profiles of some elements measured by scanning the sample above.

proton microprobe were needed to calibrate PIXE measurements performed with a standard accelerator beam, because the lateral distribution of elements inside the sample strongly influence the accuracy of those measurements. The dotted line crossing the sample is caused by carbon deposition of the beam spot during the scan. The lower part of Fig. 5 gives the resulting concentration profiles of four elements. A first obvious result is that the sample is about two times wider than indicated by the dark line of dust on the foil. Moreover the concentration profiles of different elements have not the same shape, i.e. the relative concentrations are not independent of the sample position. So based upon this result the standard beam measurements mentioned above had to be corrected for this inhomogeneity.

In the field of biological samples measurements of element distributions in thin layers of human skin have been started. The upper part of Fig. 6 shows a 10 µm thick sample of human skin, dyed with an organic agent. It is a depth profile of the skin: on the left the epidermis is to be seen, i.e. the upper layer of the skin, and proceeding to the right the

deeper layers. The total length of the sample is about 1.9 mm. Two questions were of interest in this case: 1. the element concentration in the epidermis, 2. the circular structure in the center of the sample. The two arrows indicate the start and end point of the scan. The result is given in the lower part of Fig. 6. The epidermis is located between 13.3 and 13.6 mm. Whereas iron and clorine concentrations do not vary, the concentrations of sulphur and zinc increase clearly in this range. In the center of the circular structure at position 13.95 mm sulphur increases rapidly, whereas clorine decreases by more than one order of magnitude. This gives rise to the assumption that the circular structure is the root of a hair with the hair in its center.

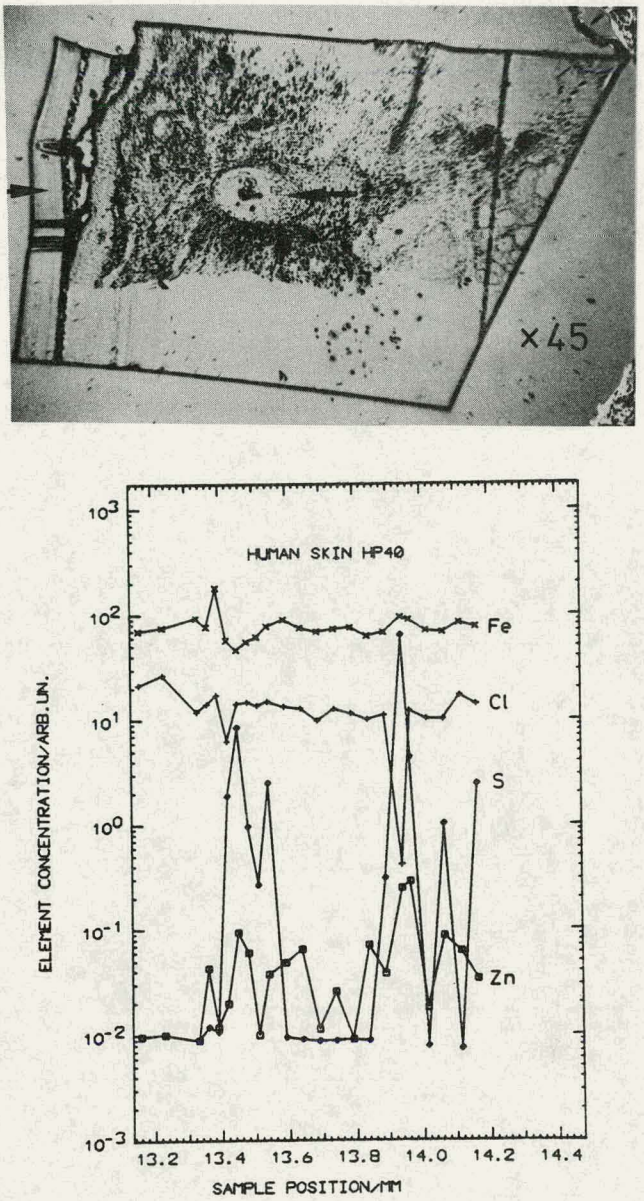


Fig. 6. Upper part: photo of a thin sample of human skin. It has been scanned between the two arrows.
Lower part: Related element concentration profiles.

Concluding one can say that the test measurements done up now have shown that the proton microprobe with its improved technical equipment is a useful tool for the analysis of spatial element distributions. The discussion of the biological aspects of our measurements is still in an early state; but the results will help to learn something about the interdependence between element concentrations at well defined places in an organism and the macroscopic conditions of this organism on the whole.

References

1) Proc. of the III. Int. Conf. on Nucl. Meth. in Environmental and Energy Research, Oct. 1977, Columbia/Mo, p. 99

2) B. Raith, M. Roth, K. Göllner, B. Gonsior, H. Ostermann and C.D. Uhlhorn, Nucl. Instr. and Meth. 142 (1977) 39

3) W. Maenhaut, L. de Reu, H.A. van Rinsvelt, J. Cafmeyer and P. van Espen, Nucl. Instr. and Meth. 168 (1980) 557

ULTRA-SENSITIVE TRACE ELEMENT ANALYSIS OF ENVIRONMENTAL SAMPLES USING ADVANCED TRXRF TECHNIQUES

H. Schwenke, J. Knoth and W. Michaelis

Institut für Physik

GKSS-Forschungszentrum, D-2054 Geesthacht, Germany

Abstract

X-ray fluorescence analysis is a widely adopted technique for measuring elemental concentrations in a variety of sample species. The particular advantages compared to other methods are simplicity in instrumentation, rapidity of measurement and the high degree of automation attainable. In trace element analysis, however, the sensitivity of conventional X-ray fluorescence analysis is often insufficient. The paper describes a new type of energy-dispersive equipment which reveals ultimate performance with respect to detection limits and which thus considerably extends the applicability of XRF analysis.

The essential feature of the system is the utilization of multiple total reflection (TR) of the exciting X-ray beam from polished quartz glass surfaces. Since the refractive index is slightly smaller than 1, total reflection occurs if the radiation strikes the surface at angles of less than 5'. The grazing incident beam from a fine-structure X-ray tube is twice reflected and follows a zigzag path before it is directed to the sample prepared as a thin film on the third quartz glass surface. The direct beam and scattered radiation are eliminated by diaphragms. In this way, a further reduction of the background in the fluorescence spectrum is achieved compared to a previously published version with single reflection of the exciting beam. The performance of the instrument leads to detection limits for aqueous solutions below 10^{-11} g or 0.1 ppb, respectively, for at least 20 elements.

The use of quartz glass blocks as sample supports offers various feasibilities of sample processing on the support itself because of the high chemical and physical resistance of the material. Typical examples are low-temperature ashing of organic matrices in an oxygen plasma chamber and carbamate precipitation of metals onto the quartz surface.

A particular advantage of the spectrometer described is the small amount of sample material needed for the analysis. The method has been successfully applied to the determination of trace elements in a variety of samples relevant to environmental research. Results are presented for air dust collected on polystyrene filters and for filtered stream water. The data obtained are compared with those from other analytical methods.

1. Introduction

X-ray fluorescence analysis is a widely adopted technique for measuring elemental concentrations in a variety of sample species. The particular advantages compared to other methods are simplicity in instrumentation, rapidity of measurement and the high degree of automation attainable. In trace element analysis, however, the sensitivity of conventional X-ray fluorescence analysis is often insufficient. The paper describes a new type of energy-dispersive instrument which reveals ultimate performance with respect to sensitivity and which thus considerably extends the applicability of XRF analysis.

In 1971 Yoneda and Horiuchi [1] for the first time reported on a method to lower the scattered background radiation and thereby to improve the detection limits. They utilized the effect that an X-ray beam which strikes an optical quartz glass flat at a very small angle is totally reflected since the refractive index for X-rays is slightly smaller than 1. Based on this principle, a few years ago a prototype of a total reflection X-ray fluorescence (TRXRF) spectrometer [2] for routine applications was designed and constructed at our laboratory (fig. 1a). The device comprises a variety of essential mechanical improvements compared to earlier experimental arrangements [1, 3]. Detection limits of $50 \cdot 10^{-12}$ or 1 ppb, respectively, have been achieved. A thin sample is prepared on a high-quality quartz glass surface and excited by the radiation of an X-ray tube incident at an angle of a few minutes of arc. The normally occuring coherent and Compton scattered radiation caused by the substratum is nearly completely eliminated, as the exciting radiation virtually does not penetrate into the sample support. The fluorescence radiation, on the other hand, is doubled in intensity because of excitation of the sample by both the incident and the reflected radiation (fig. 1b).

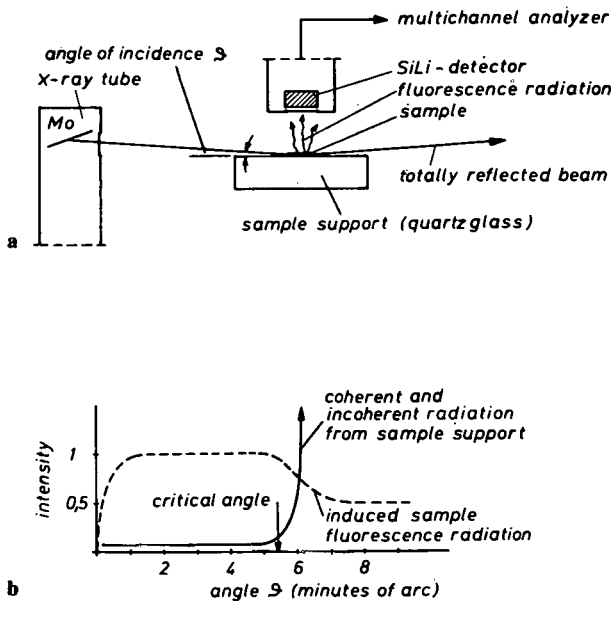


Fig. 1. a Schematic arrangement for X-ray fluorescence analysis with totally reflecting sample support b Angular dependence of scattered and fluorescent radiation.

Since 1977 thousands of multielement analyses of aqueous and organic solutions, dusts, fine powders, emulsions, filters, oils, medical and biological samples have been performed. The instrument has proved to work quite reliably in the daily analytical practice. Even on board ship during a research campaign in the Baltic Sea the device was successfully applied for ultra-trace element analysis of seawater samples. There is no doubt that the method is capable of being also used in mobile environmental monitoring.

2. X-Ray Fluorescence Analysis with Multiple Reflection of the Exciting Beam

Since the construction of the first prototype described above further essential improvements have been achieved with respect to sensitivity, power consumption of the X-ray tube and linear dynamic range by applying multiple reflection of the exciting beam. The specific part of the new version is shown in fig. 2. It consists of a compact and precisely aligned arrangement of three quartz glass mirrors, one of them acting as the sample support. The grazing incident beam from a fine-structure X-ray tube is twice reflected and follows a zigzag path before it is directed to the sample prepared as a thin film on the third quartz glass surface. The mirror system operates as a low-pass filter and cuts off the high-energetic bremsstrahlung of the X-ray tube. The direct beam and scattered radiation are eliminated by diaphragms.

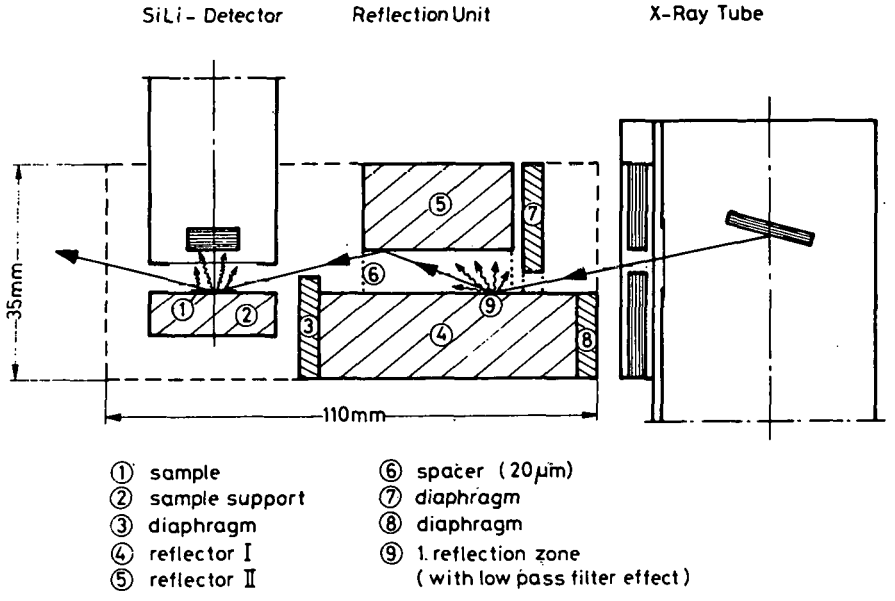


Fig. 2 Schematic view of the multiple reflection X-ray fluorescence spectrometer.

The positions, distances and heights of the reflectors and diaphragms are governed by simple geometric considerations. They are fixed against each other during manufacture by spring load using appropriate spacers between 10 and 50 µm. No subsequent adjustment and periodic recalibrations are needed. The reproducibility of the analytical results with repeated sample preparation was found to be better than 3 %, if an internal standard is used to overcome the residual influence of varying structures of the sample film.

In fig. 3 the detection limits (signal 3 standard deviations above background) are plotted for all elements within the favourable working range of the instrument. The minimum detectable concentrations given are related to a sample volume of 100 µl. The values were obtained with diluted aqueous standard solutions using a molybdenum fine structure tube at 13 mA/60 kV and 1000 sec counting time. For about 20 elements the detection limits are below 10^{-11} g or 0.1 ppb, respectively. The linear dynamic ranges with maximum deviations from linearity of 5 % were determined to about 4 to 5 orders of magnitude.

The multiple reflection spectrometer will be commercially available before long from Rich. Seifert & Co, D-2070 Ahrensburg.

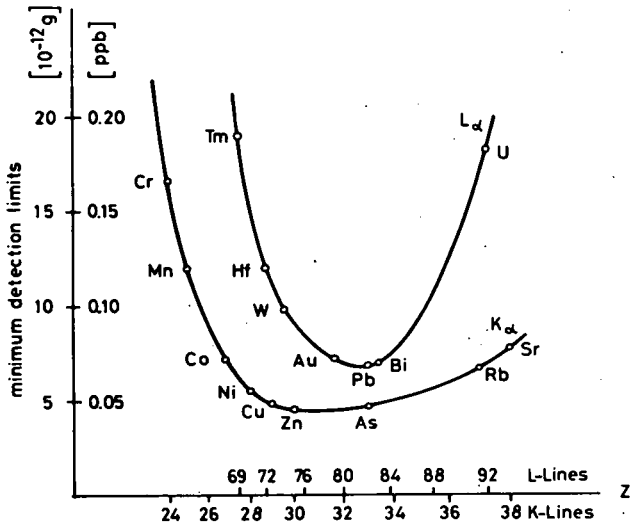


Fig. 3 Minimum detection limits of the TRXRF spectrometer (Mo-tube 13 mA/60 kV ; counting time 1000 s).

3. Applications of the Method

The use of quartz glass blocks as sample supports offers a variety of feasibilities of sample processing on the support itself because of the high chemical and physical resistance of the material. Typical examples are low-temperature ashing of organic matrices in an oxygen plasma chamber and metal chelate precipitation onto the quartz surface.

Low-temperature ashing, for instance, may successfully be applied in multielement analysis of airborne particulate matter [4] collected on polystyrene filters. The results of an interlaboratory test "air dust" are presented in tab. 1. For analysis, from the filters which had been distributed among nine laboratories samples with a diameter of 6 mm were stamped out. These were properly positioned on the quartz glass carriers and soaked with 10 µl of a nickel salt solution as an internal standard. Thus prepared, the quartz supports were put into the asher chamber (model IPC 4000) and exposed to the oxygen plasma for several hours at 20 W. In this way the filter material is oxidized away and the air dust samples are ready for measurement. As can be seen from tab. 1, the analytical results which were achieved in 500 s measuring time agree quite well with the data obtained by neutron activation analysis and with the total interlaboratory mean. Only in the case of bromine which is known to be volatile some losses during sample preparation are observed. This problem may often be overcome by a separate relative measurement of bromine on dust scraped off from the filter using one or several of the absolutely determined dominant elements as a reference. Another promising procedure is wet ashing on the sample support.

A typical X-ray spectrum of air dust is shown in fig. 4. During 1979 600 samples collected in the Greater Hamburg area were analysed in order to study the regional pattern of various elements in air dust. Evaluation of the data is in progress.

Besides rapidity of measurement and associated high sample throughput, a particular advantage of the TRXRF technique is that the small amount of air dust needed for analysis allows short sampling periods. Dust collection for the intercomparison test and the Hamburg environmental programme was essentially deter-

Table 1 Results of an intercomparison test "Air Dust". All values given in $\mu g/cm^2$.

Element	TRXRF (this method)	NAA*)	XRF*) (conventional)	AAS*)	Interlaboratory mean**)
Ti	2.40 ± 0.30	2.02 (1/0)	1.10 (1/1)	-	1.84 ± 0.67 (3)
V	0.77 ± 0.10	0.74 ± 0.10 (3/0)	1.47 ± 0.10 (2/0)	0.50 (1/0)	0.92 ± 0.39 (7)
Cr	0.34 ± 0.07	0.32 ± 0.01 (3/0)	0.40 (1/1)	-	0.34 ± 0.04 (5)
Mn	1.21 ± 0.13	1.59 ± 0.34 (3/0)	1.87 ± 0.94 (2/0)	-	1.62 ± 0.53 (6)
Fe	20.71 ± 2.00	21.69 ± 2.42 (5/0)	19.39 (1/2)	-	21.27 ± 2.17 (7)
Ni	0.375 ± 0.04	0.49 ± 0.15 (3/0)	0.72 ± 0.11 (2/1)	0.615 (1/0)	0.56 ± 0.16 (7)
Cu	0.29 ± 0.04	0.535 (1/0)	0.46 ± 0.20 (2/0)	0.535 (1/0)	0.46 ± 0.10 (5)
Zn	6.04 ± 0.70	6.44 ± 0.37 (3/0)	5.92 ± 0.52 (2/1)	8.65 (1/0)	6.55 ± 1.00 (7)
As	0.35 ± 0.10	0.44 ± 0.02 (3/1)	< 0.3 (-/-)	0.34 (1/0)	0.40 ± 0.05 (5)
Se	0.06 ± 0.02	0.095 ± 0.015 (5/0)	0.19 (1/0)	-	0.10 ± 0.04 (7)
Br	0.53 ± 0.07	0.74 ± 0.12 (3/0)	0.87 ± 0.21 (2/1)	-	0.89 ± 0.34 (6)
Rb	0.125 ± 0.02	0.14 ± 0.03 (3/0)	0.17 (1/0)	-	0.14 ± 0.03 (5)
Sr	0.19 ± 0.02	-	0.23 (1/0)	-	0.21 ± 0.03 (2)
Pb	4.31 ± 0.20	4.72 (1/0)	8.39 ± 2.28 (2/0)	-	6.59 ± 2.26 (4)

*) in parentheses: (number of valid measurements/runaways after Nalimov-test)

**) in parentheses: number of averaged measurements

mined by the requirements of other analytical methods also used. It is expected that TRXRF analysis will yield even better results, if sampling is properly optimized with respect to filter selection and charge.

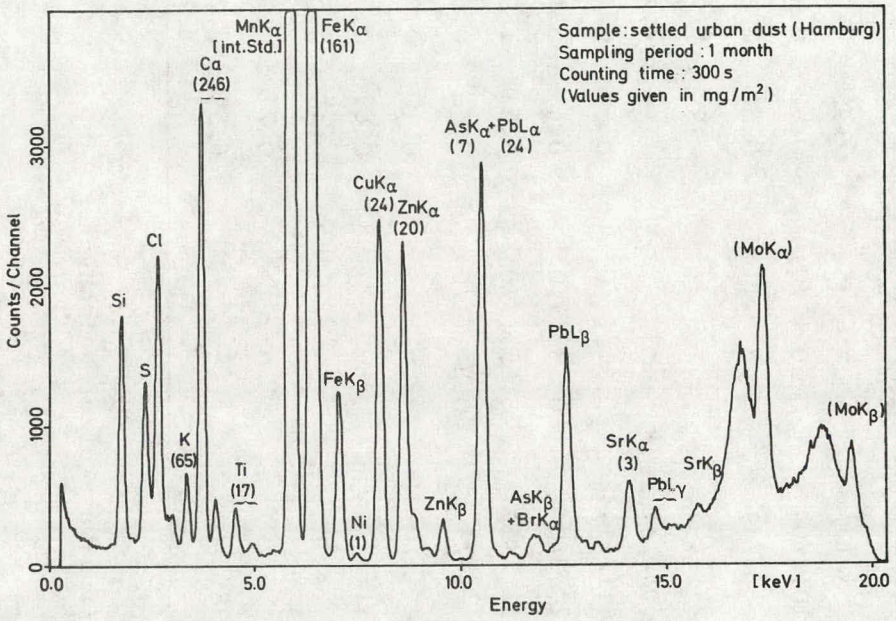


Fig. 4: TRXRF spectrum of urban dust

A second illustration of sample processing on the support is carbamate precipitation onto the siliconized quartz surface with subsequent matrix separation [5]. This method has extensively been used, for instance, for the analysis of filtered water from the German rivers Weser and Elbe. The usual procedure is as follows: An aliquot of 50 ml is spiked with 100 ppb of cobalt or selenium as an internal standard and then adjusted to pH 4 - 5. In order to reduce the influence of blank values the water is condensed by a factor of 5 to 10 using incomplete freeze drying. 50 µl are pipetted onto the quartz support (fig. 5) which was coated before with a silicon solution (Serva,Heidelberg). Into the drop 5 µl of 1 % APDC solution are pipetted. The sample is then allowed to dry. The water-soluble matrix is dissolved by adding 100 µl bi-distilled water to the salt film and is subsequently removed by rinsing with about 3 ml bi-distilled water from a wash bottle. The metal chelates, insoluble in water, remain fixed on the surface of the quartz support and the sample is ready for measurement (fig. 6).

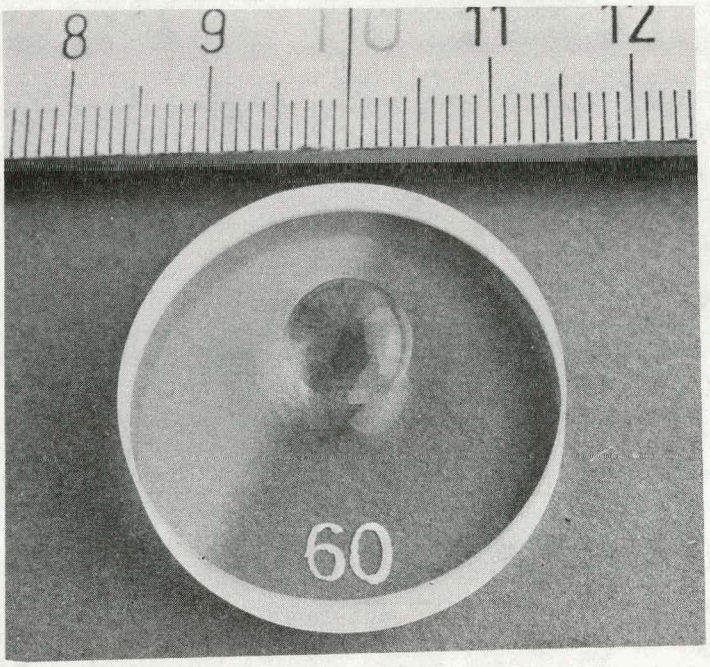


Fig. 5: Photograph of specimen support with 50 µl sample before drying.

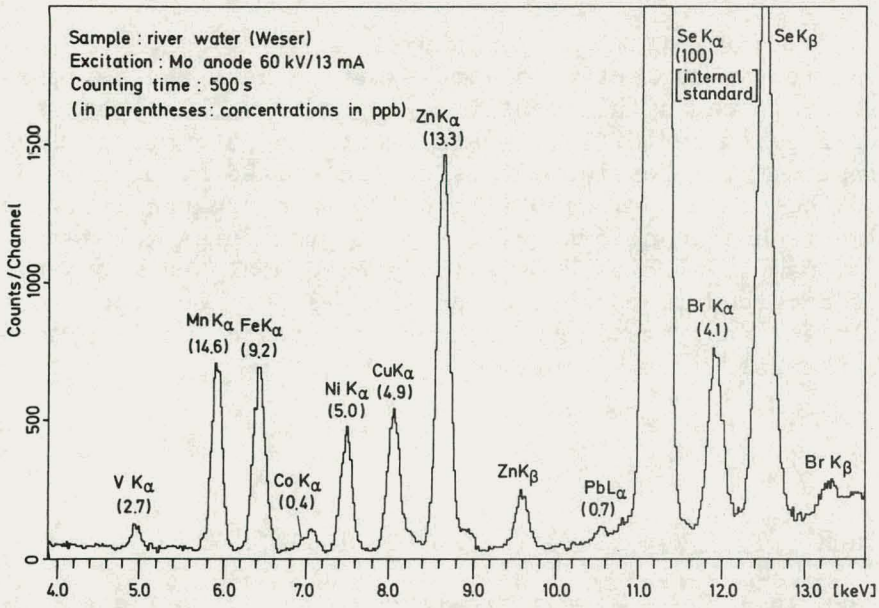


Fig. 6: TRXRF spectrum of filtered river water after matrix removal by the "rinsing method".

Tab. 2 summarizes a few typical results out of a great number of filtered river water analyses. Also, the "rinsing method" described, with the use of a multiple reflection instrument, is compared with a conventional solvent extraction procedure in connection with a single reflection unit. The latter method employs 100 ml samples, APDC as chelating agent, a Chromosorb column and chloroform as the organic phase. The data obtained by the two methods agree very well within experimental errors. This demonstrates that the higher sensitivity of the multiple reflection device may also be utilized to apply rather simple sample preparation procedures instead of more elaborate ones.

Table 2: Analytical results on filtered river water obtained by TRXRF analysis

Element	Metal concentration in µg/l			
	Weser		Elbe	
	A	B	A	B
Fe	7 ± 3	6 ± 2	76 ± 5	73 ± 5
Co	0.3 ± 0.1	0.2 ± 0.1	1.0 ± 0.5	0.7 ± 0.3
Ni	4 ± 1	4 ± 1	11 ± 1	12 ± 1
Cu	4 ± 1	3.5 ± 1	6.5 ± 1	6.8 ± 1
Zn	10 ± 3	14 ± 3	63 ± 5	64 ± 6
Pb	0.3 ± 0.2	0.3 ± 0.2	1.1 ± 0.5	1.1 ± 0.3

A: "rinsing method"; multiple reflection instrument
B: solvent extraction; single reflection instrument.

A detailed comparison of TRXRF techniques, inductively - coupled plasma - excited optical emission spectroscopy and neutron activation analysis in river water monitoring will be published in the near future. Applications of the TRXRF method on human tissue are described elsewhere [6].

4. Conclusions

Using appropriate multiple total reflection of the exciting beam the performance of X-ray fluorescence analysis can significantly be improved with respect to sensitivity without sacrifice in rapidity of measurement and automation. The present status of the instrumental development is characterized by minimum detection limits in aqueous solutions below 10^{-11} g or 0.1 ppb, respectively, for at least 20 elements. The technique allows quite simple procedures for sample preparation. A variety of sample species have already been analysed with great success. Without doubt the method is capable of becoming a powerful tool for ultra-sensitive trace element analyses in environmental research and monitoring as well as in medicine, chemistry and biology.

References

[1] Yoneda, Y., Horiuchi, T.: Rev. Sci. Instr. 42, 1069 (1971)

[2] Knoth, J., Schwenke, H.: Fresenius Z. Anal. Chem. 291, 200 (1978)

[3] Wobrauschek, P., Aiginger, H.: Anal. Chem. 47, 852 (1975)

[4] Freitag, K., Knoth, J., Schwenke, H.: GKSS 79/E/9

[5] Knoth, J., Schwenke, H.: Fresenius Z. Anal. Chem. 294, 273 (1979)

[6] Schwenke, H., Knoth, J.: Proc. 1st Int. Workshop on Trace Element Analytical Chemistry in Medicine and Biology, 26th - 29th April, 1980, Neuherberg, Germany.

MICROAUTORADIOGRAPHY: A USEFUL TECHNIQUE FOR INVESTIGATING RADIONUCLIDE TRANSPORT IN GEOLOGIC MEDIA*

J. L. Thompson, Idaho State University, Pocatello, Idaho 83209
W. R. Daniels, S. Maestas, E. N. Vine, K. Wolfsberg, Los Alamos Scientific Laboratory, Los Alamos, New Mexico 87545

Microautoradiographic techniques have been found to be useful in studies related to the behavior of uranium and transuranics as groundwater solutions in contact with geologic media. Microscopic examination of the alpha particle tracks generated in emulsions by these radionuclides has given insight into the flow patterns of the solutions through rock, allowed the identification of minerals responsible for radionuclide sorption, and identified the tendency of some radioactive species to form aggregates in the aqueous phase. Preparation of the autoradiograms requires only modest amounts of the radionuclide, times of a few days, and relatively simple equipment. Microautoradiography provides information difficult to obtain by other means and is an important supplement to conventional techniques employed to study radionuclide sorption and transport.

*This work was supported by the U. S. Department of Energy

From the very beginning of nuclear science, films and emulsions have been employed to detect and characterize radiation. An extensive review of the applications of emulsions for radiation measurements is contained in a book written by Yogada[5] in 1949. Modern counting equipment has diminished the use of emulsions as detection devices, but they are still used extensively in medical and biological research (and in some other technologies) to determine the location of radionuclides in the materials of interest. In autoradiography, the emulsion is placed in close contact with the substance containing radioactivity and held there until sufficient exposure has occured. On development of the emulsion, the location and relative intensity of the radioactivity is indicated. Individual tracks generated in the emulsion may be viewed with an optical microscope, hence the term "microautoradiography."

We have found a number of ways to apply microautoradiographic techniques to assist in the study of the behavior of certain radionuclides in geologic media, and these methods have been outlined in several reports[1-4]. We have used microautoradiography to study the sorption of U, Np, Pu and Am on a variety of rock types. U and Am have been employed to trace the flow patterns of water through intact and cracked rock cores. Finally, autoradiography has been used to help characterize the state of aggregation of Pu and Am species "dissolved" in groundwater. In all of these studies, the microautoradiographic technique yielded information difficult or impossible to obtain by other experimental methods. Furthermore, the cost of preparing autoradiograms was relatively low, and the time required generally did not exceed a few days.

Polished rock thin sections (about 30 μm thick) were used for the sorption experiments. These were contacted with a solution of the appropriate radionuclide until the sorbed activity was about 10^3 disintegrations min^{-1} cm^{-2}. The contact time ranged from a few hours to a few days. After rinsing off this solution, the thin section was coated with thin layers first of collodion, then of gelatin. Kodak AR.10 strippable emulsion was mounted on the thin section (under darkroom conditions) by the following technique. The strip of emulsion was floated on the surface of a dilute sucrose-KBr solution, and the thin section raised from below, lifting the emulsion onto the thin section surface. The emulsion was dried and stored in a light-tight box for times of several hours to several days, depending on the sorbed activity level. The emulsion was then developed and fixed using standard processes. It remained affixed to the thin section during this treatment. The alpha particle tracks in the developed emulsion generally were viewed at magnification of 100X to 400X using transmitted light, although with particularly dark mineral backgrounds reflected light was sometimes used. Since the emulsion remained in complete registry with the thin section, it was easy to locate the specific minerals on which



Figure 3 (100X) ^{233}U in granite

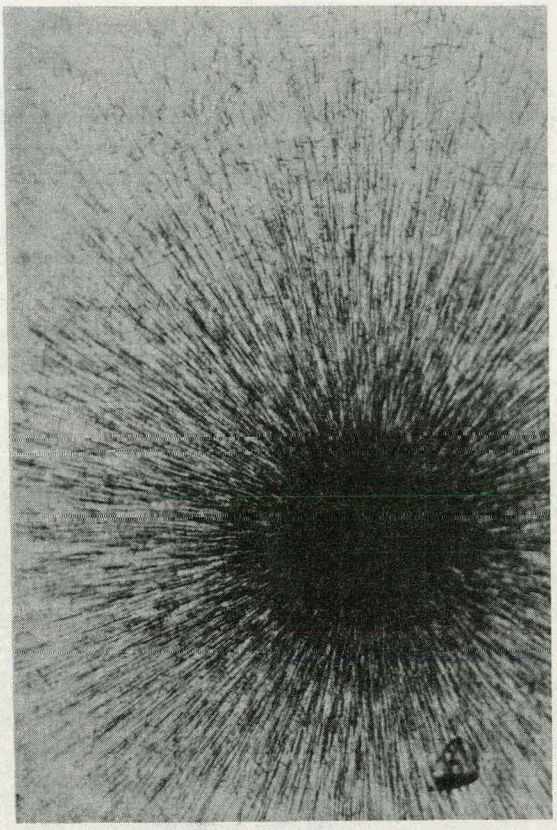


Figure 4 (250X) ^{241}Am on filter

A serious problem encountered by researchers attempting to measure the sorption of transuranic ions on rocks in the pH range of 7-9 units is species characterization. These ions tend to aggregate, forming polymeric groupings which may include thousands of atoms. Filtration is one means of separating these aggregates from the individually dissolved ions. Microautoradiographic examination of the polycarbonate filters (with pore sizes as low as 0.05 μm) which were used proved to be helpful in characterizing the species removed. Aggregates of radionuclides such as ^{239}Pu or ^{241}Am will give rise to "stars" or "giant colloid" patterns on the microautoradiograms. An example of a giant colloid is shown in Figure 4. The filter may be mounted on a glass slide with collodion, and then the emulsion mounted as was done with rock thin sections. Alternatively, the filter may simply be pressed against an emulsion-coated glass slide during the exposure period, then the emulsion developed separately.

In the applications discussed above, the origin of the alpha particle tracks may be accurately located with respect to the material underlying the emulsion. This excellent resolution, plus the qualitative indication of the number of radionuclides located at the origin of the tracks makes this technique extremely useful. The other attractive features include the ease and low

sorption occured, and the track intensity indicated the relative amount of sorption at particular sites. Figure 1 illustrates a situation in which the radionuclide was highly sorbed at several sites. In contrast, Figure 2 shows a fairly uniform distribution of tracks, indicating no strong sorption preference for the minerals present. Since the developed emulsion is transparent,



Figure 1 (400X) ^{233}U on tuff

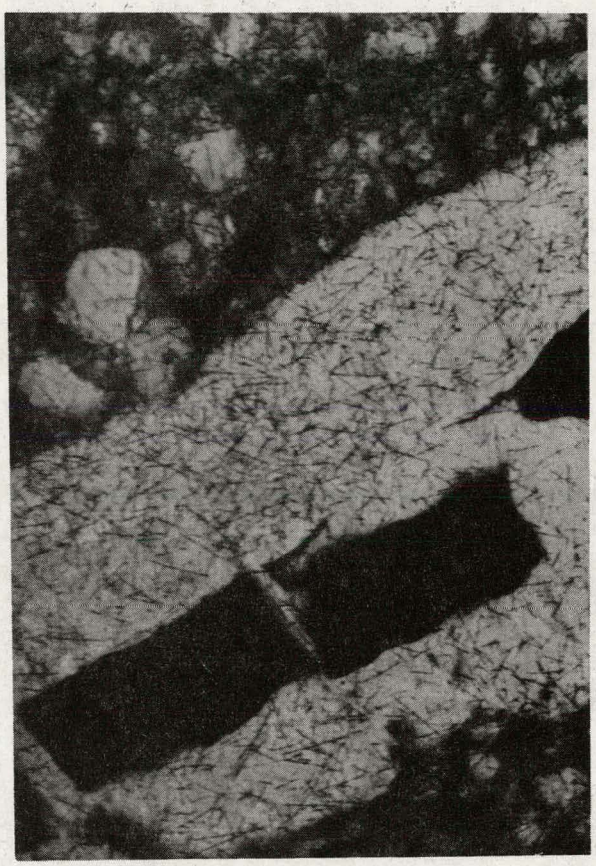


Figure 2 (400X) ^{241}Am on argillite

it does not interfere with the petrographic analysis of the mineral phases present in the thin section. One significant result of these studies is that mineral phases present as minor constituents of the rock often are responsible for the major fraction of the radionuclide sorption which takes place.

Microautoradiography was found to be useful in studying the flow of water through rock cores. In these experiments, groundwater containing ^{233}U or ^{241}Am was forced through the core under controlled conditions, then the core was cut into thin slabs with a rock saw. These slabs were coated with collodion and gelatin, and then coated with either the strippable emulsion mentioned above, or a liquid emulsion. The remainder of the process was the same as that employed with the thin sections. The position and density of the alpha tracks revealed the flow pattern of the solution in the core. Porous rock like tuff showed relatively uniform flow, while in granite cores the flow apparently was confined to tiny crack systems. Figure 3 illustrates this type of flow.

cost with which microautoradiograms may be prepared. We have found microautoradiography to be an important tool for studying radionuclide transport in geologic media.

References:

1. J. L. Thompson and K. Wolfsberg, "Applicability of Microautoradiography to Sorption Studies," Los Alamos Scientific Laboratory report LA-7609-MS (1979).

2. B. R. Erdal (Ed.), "Laboratory Studies of Radionuclide Distribution Between Selected Groundwaters and Geologic Media, Annual Progress Rerport, October 1, 1978 September 30, 1979," Los Alamos Scientific Laboratory report LA-8088-PR (1980).

3. E. N. Vine, R. D. Aguilar, B. P. Bayhurst, W. R. Daniels, S. J. DeVilliers, B. R. Erdal, F. O. Lawrence, S. Maestas, P. Q. Oliver, J. L. Thompson, and K. Wolfsberg, "Sorption-Desorption Studies on Tuff II. A Continuation of Studies with Samples from Jackass Flats, Nevada and Initial Studies with Samples from Yucca Mountain, Nevada," Los Alamos Scientific Laboratory report LA-8110-MS (1980).

4. J. R. Smyth, J. L. Thompson and K. Wolfsberg, "Microautoradiographic Studies of the Sorption of U and Am in Natural Rock Samples," Radioactive Waste Management 1 (in press).

5. H. Yagoda, Radioactive Measurements with Nuclear Emulsions, John Wiley & Sons, Inc., New York, 1949.

INSTRUMENTAL PHOTON ACTIVATION ANALYSIS OF Cd AND Pb IN ZINC ORES, WITH A ROTATING DEVICE FOR INTERMITTENT IRRADIATIONS

by Ch. Berthelot and G. Carraro

Central Bureau for Nuclear Measurements

B-2440 GEEL, BELGIUM

INTRODUCTION

The toxic elements in zinc ores: cadmium and lead, are determined precisely and non-destructively by photon activation using a rotating device for intermittent irradiations of the samples by the same gamma flux. The intact analysis is attractive as difficulties and errors associated with sample dissolution, are eliminated.

The determination of lead by photon activation is more appropriate than by thermal neutron activation, since in the latter case the cross section is extremely low and the ^{209}Pb activation product is a pure β^-emitter.

EXPERIMENTAL

The analyses are performed at the Geel linear accelerator using the bremsstrahlung produced by the impact of an electron beam (45 MeV, 27 μA) on a water-cooled platinum target [1].

Sampling and standard

The zinc ore samples (100 mg), without any pre-treatment, are encapsulated in very pure Al cans (99.999%) of 10 mm $\emptyset_i$. The synthetic standard is prepared by weighing known amounts of metallic oxides in an aluminium can; the standard is mixed and covered by a layer of lithium sulphate, to avoid any loss of the standard during the encapsulation. The composition of the standard is: 79.96 mg ZnO, 9.80 mg Fe_2O_3, 2.20 mg CdO and 8.04 mg PbO. The weights of CdO and PbO are known with a relative accuracy of 0.5%.

Intermittent irradiation arrangement

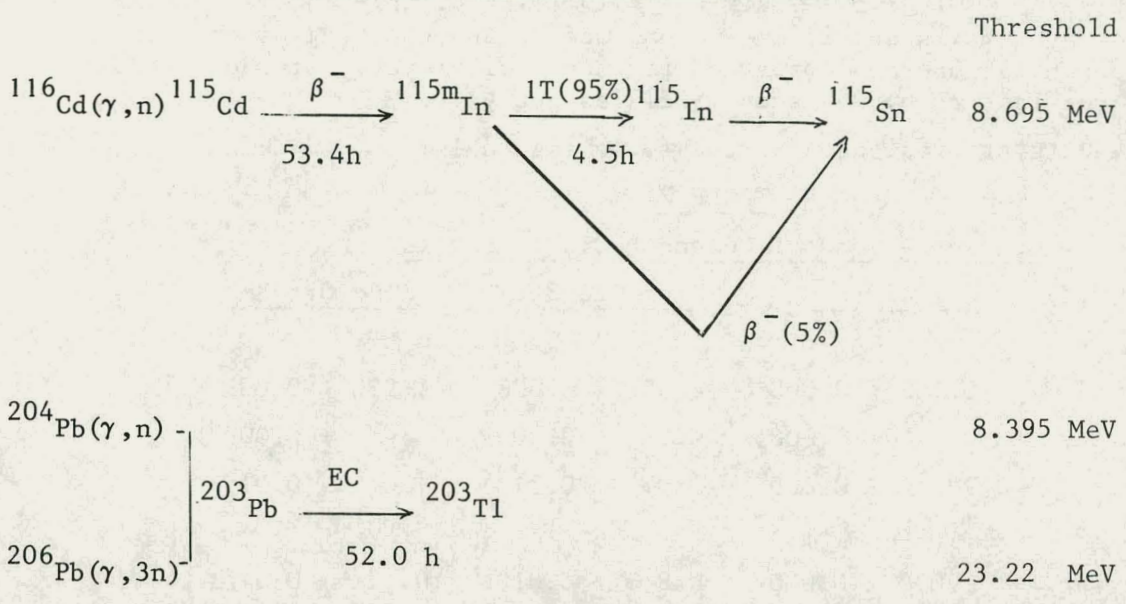
For accurate measurements, the intermittent irradiation arrangement is used instead of the sandwich irradiation arrangement and for that, the axis of the irradiation station is displaced 10 mm from the axis of the electron beam. Using a rotating device (12 rpm) driven by a motor, three zinc ore samples and one standard are placed in a cylindrical Al block at equal distance (10 mm) around the rotation axis and irradiated for a few hours, so that each sample is alternately irradiated by the same gamma flux. In these conditions, the correction for the longitudinal gradient of gamma flux has been calculated to be very small, unlike the sandwich arrangement. The sample holder itself is locked in the head of a cylindrical rabbit (Fig. 1) which is transported by pneumatic transfer from the rotating device to the counting laboratory.

Measurement of activities and counting sequences

Table 1 gives the most interesting photonuclear reactions induced by 45 MeV-bremsstrahlung:

TABLE 1

Photonuclear reactions for Cd and Pb



The induced activities of the radionuclides are measured using a Philips single open-ended coaxial Ge(Li) detector (54.6 cm^3) in conjunction with a Canberra 8180 multichannel analyser (Fig. 2 and 3). A built-in Canberra microprocessor provides the evaluation of the total photopeak area [3] with the associated error. The Cutipie program [4] adapted to the IBM 370 computer, is used for automatic peak searching and for peak fitting.

To avoid having to make corrections for the decay of produced radionuclides whose life times are not accurately known, the standard (R) was counted both before (S^R_1) and after (S^R_2) the zinc sample (S^{Zn}), the time interval between the start of successive counts being equal. The derived rate for the standard during the period when the Zn sample was being counted was then:

$S^R = (S^R_1 \cdot S^R_2)^{1/2}$ and negligible error resulted for the unknown half lives.

An illustration of a sequence of counting is shown in table 2:

TABLE 2

Photopeak areas of Pb and Cd

Gamma-Ray (keV)	Standard t_d = 70.950 h, t_c = 5000 s	Zinc Ore 3 t_d = 72.383 h, t_c = 5000 s	Standard t_d = 73.817 h, t_c = 5000 s
Pb-279.19	968949 ± 1443	1303736 ± 1612	939962 ± 1401
Cd-336.24	278930 ± 984	176578 ± 994	273569 ± 944
Cd-527.76	96545 ± 663	60602 ± 578	93278 ± 603

t_d = time from end of irradiation, t_c = counting time.

RESULTS AND DISCUSSION

The ^{203}Hg - 279.19 keV line from the $^{204}Hg(\gamma,n)^{203}Hg$ ($T_{1/2}$ 46.8 d) reaction can interfere in the determination of lead. However, less than 180 w.ppm of mercury, which can be determined by the reaction $^{198}Hg(\gamma,n)^{197m+197}Hg$, are present in zinc ore 3 and only trace amounts of mercury are

present in the two other zinc ores. In the determination of cadmium with the ^{115m}In-336.24 keV line, the contribution from In and Sn, if present in the samples - ^{115}In(γ,γ')^{115m}In and ^{116}Sn(γ,p)^{115m}In ($T_{1/2}$ 4.5 h)- becomes negligible, when the decay time is sufficiently long before the counting of the samples. The concentrations are corrected for non-stoichiometry of the standard, CdO and PbO by the factors 0.9950 and 0.9921 respectively.

The results are indicated in the following table:

TABLE 3

Concentrations of Cd and Pb in zinc ores

Concentration (w.%)	Zinc Ore 1	Zinc Ore 2	Zinc Ore 3
Cadmium			
conc. ± st. deviat.	0.102 ± 0.008	0.558 ± 0.008	1.222 ± 0.009
weight uncert.	± 0.0005	± 0.003	± 0.006
overall uncert.	± 0.009	± 0.011	± 0.015
Lead			
conc. ± st. deviat.	1.012 ± 0.020	0.805 ± 0.010	10.12 ± 0.015
weight uncert.	± 0.005	± 0.004	± 0.051
overall uncert.	± 0.025	± 0.014	± 0.07

CONCLUSION

The method of intermittent irradiation of the samples and the standard by the same gamma flux, is precise and non-destructive. High concentrations of Cd and Pb in zinc ores are determined with a relative uncertainty of 0.7 - 1.2%. For low concentrations, the relative precision can be improved with a longer time of irradiation.

ACKNOWLEDGEMENT

The authors express their gratitude to Dr. R. Batchelor and Dr.B.Rose for their advice and support to this project and to Dr. H.L. Eschbach for helpful discussions. The samples were prepared by Dr. V. Verdingh, S. Herrmann and H.M. Silvester. The assistance of the Linac machine group is greatly appreciated.

REFERENCES

1. Ch. Berthelot, G. Carraro, V. Verdingh - J. Radioanal. Chem. 50 (1979) 185.
2. C.M. Lederer, V.S. Shirley, eds. - Table of Isotopes, Wiley-Interscience Publ. (1978).
3. P.A. Baedecker - Anal. Chem. 43 (1971) 405.
4. W. Teoh - Nucl. Instr. and Meth. 109 (1973) 509.

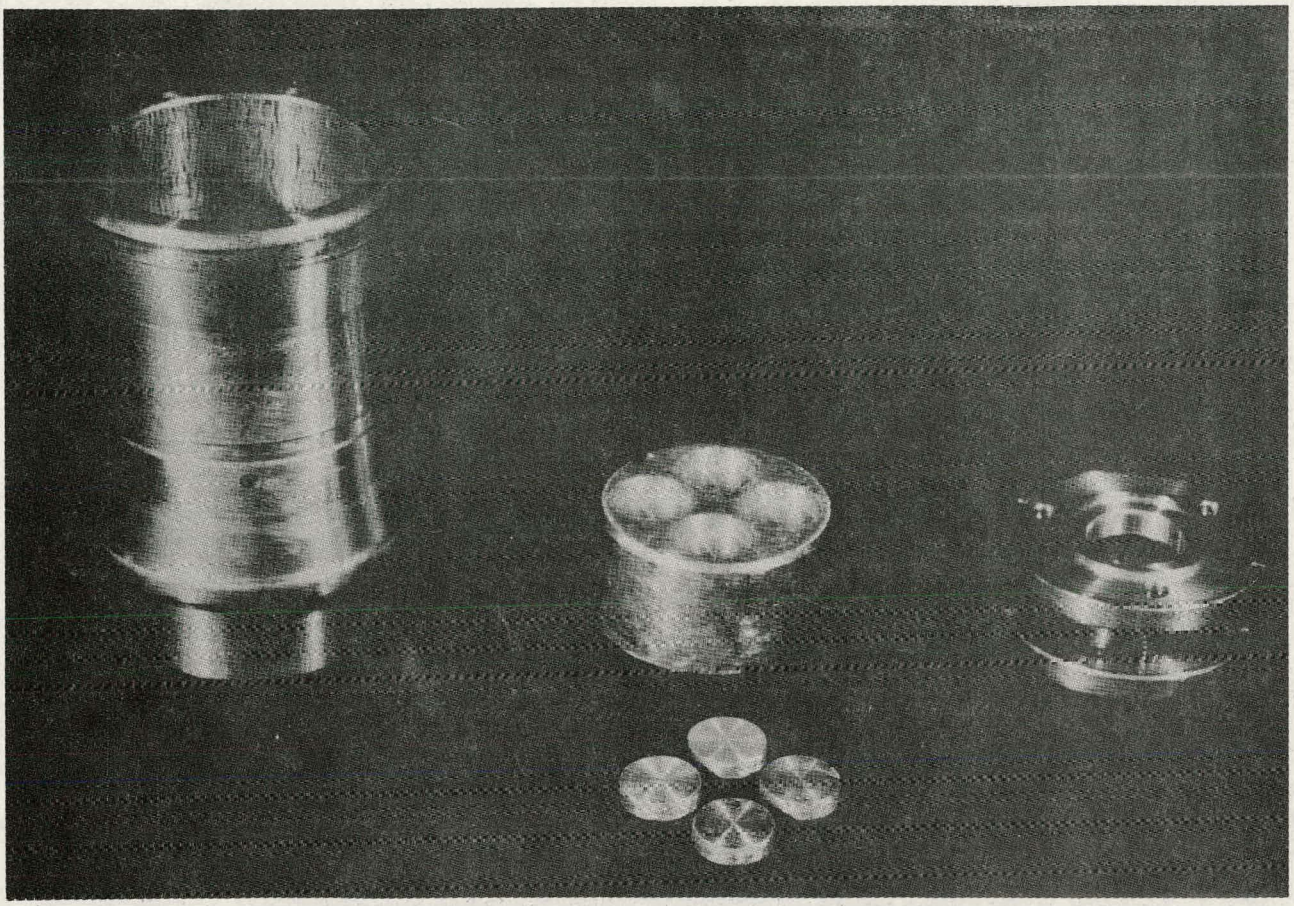
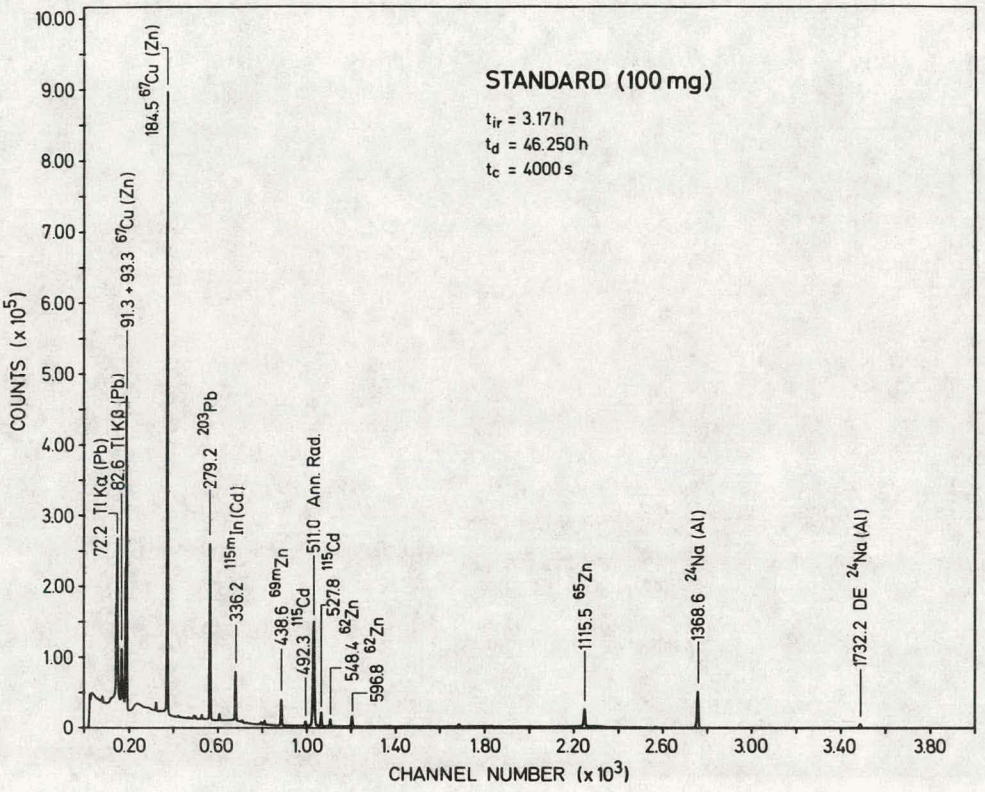


Fig.1 View of different parts of the irradiation container. From left to right: the cylindrical rabbit, the sample holder for intermittent γ-irradiation, and the spring device to lock the sample holder in the rabbit. Below are shown the 4 samples encapsulated in aluminium cans.



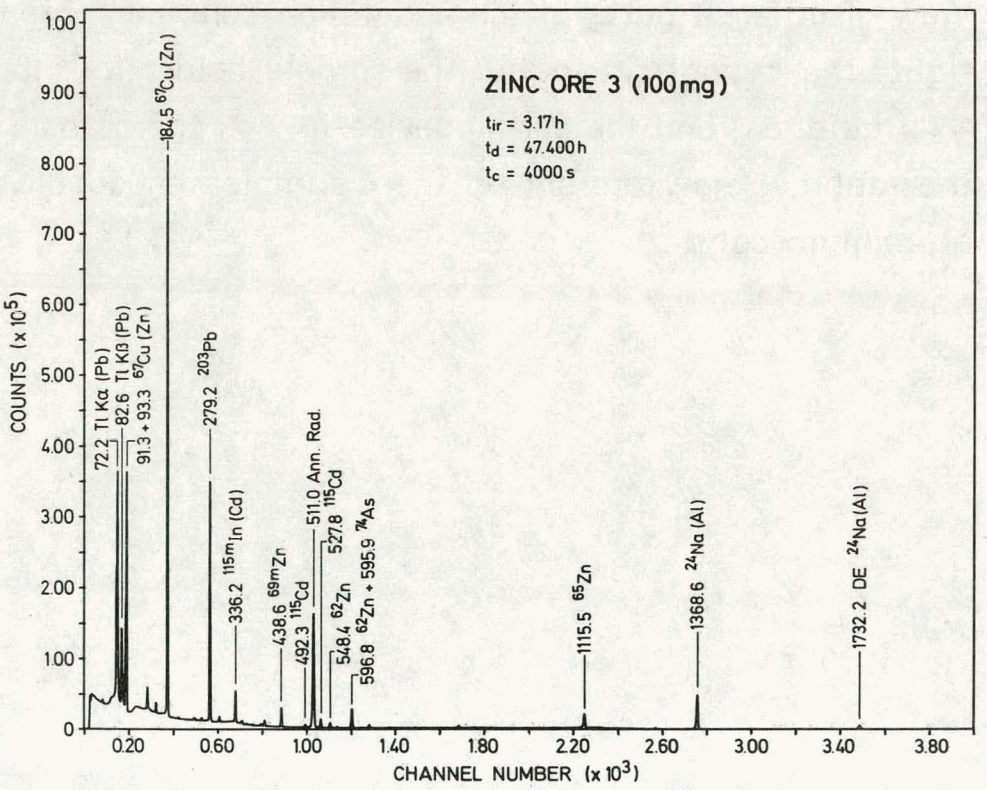
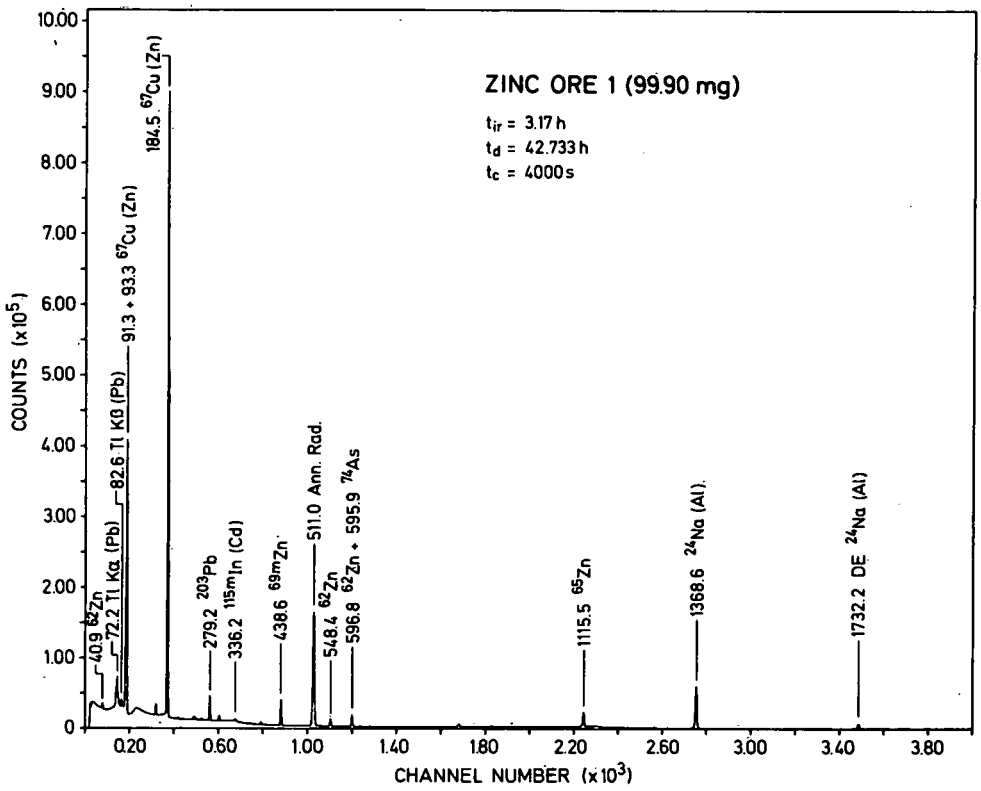


Figure 2 Gamma-ray spectra of standard and zinc ore 3 sample, t_{ir} = irradiation time, t_d = time from end of irradiation, t_c = counting time



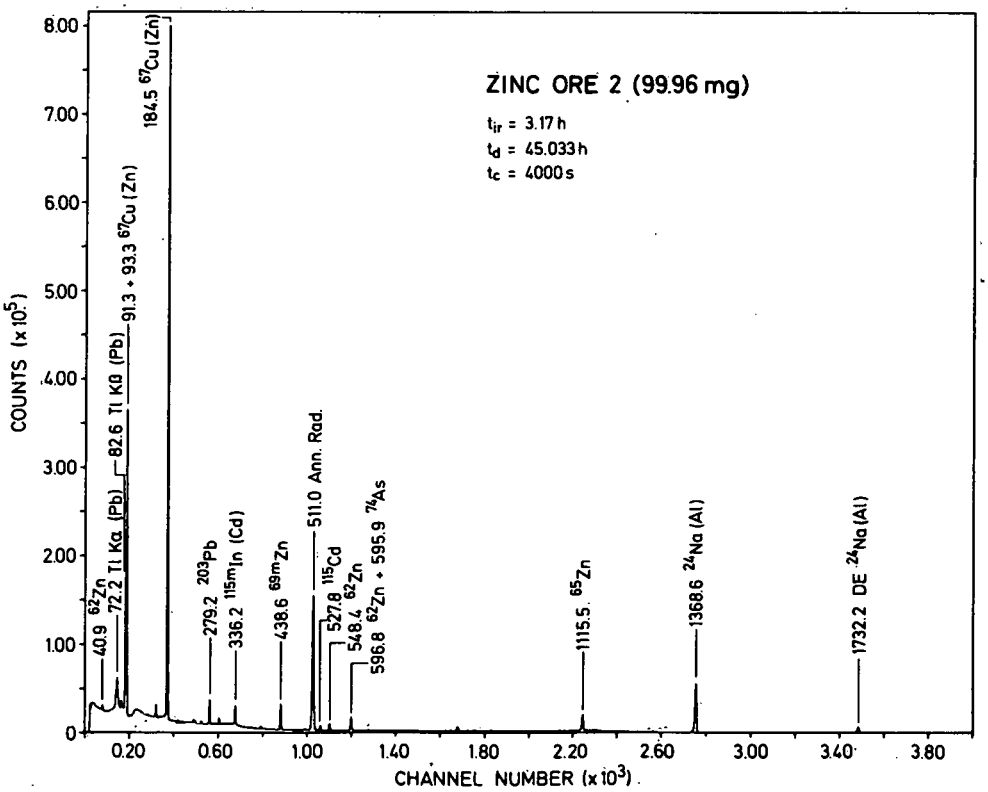


Figure 3 Gamma-ray spectra of zinc ore 1 and 2 samples.

Error-Free Binary Dilution Method for the Preparation of ppb-Level Liquid Standards.

Miguel Wiernik

Institute of Chemistry, State University of Campinas, 13100 Campinas, SP, Brasil

The ways that ppb-level standard solutions are normally prepared and their accompanying dilution errors are studied. A new binary method of dilution that is theoretically error-free is described.

When performing routine activation analysis for trace elements, people normally do not care very much about the accuracy of the standards irradiated together with tne samples because, rather than the exact values, most of the time it is of more interest to know the order of magnitude of the concentration of the element in the sample.

In this kind of routine work, the error normally fluctuates between 3 and 10%. We hope that, in the not too distant future, the quality of the measuring instruments and the stability of the irradiation devices will allow us to easily reach an accuracy of 1% or better at ppb (or ng) levels. Then, we will have to take a serious look at the ways we prepare our standards.

A one ppb standard solution cannot be reasonably prepared directly from the pure element or some simple compound. It will not be very accurate to prepare one liter of solution by weighing one microgram of element, and it will not be very handy to dissolve one milligram of standard in one cubic meter of solvent. So, a mother solution has to be prepared. Let us assume that, using a well calibrated ultramicrobalance, we may weigh 1.000 ± 0.001 mg and dissolve it in a Class A one liter volumetric flask (1000 ± 0.3 ml) producing a one ppm solution (1.10^{-6} ± $1.044\ 10^{-9}$ g/ml) with a probable error of 0.1 %.

This error is very reasonable for any accurate analytical method but, when dilutions are made to reach sub-ppm or ppb levels, customary methods will increase the relative errors of the standard solutions.

In order to calculate the errors produced by each dilution method we must know first which are the probable errors of the Class A volumetric glassware. The values that are relevant to this work are shown in table I.

Table I. Limits of error of Class A volumetric glassware.

Volume	Limit of error	
	Absolute	Relative
ml	ml	%
1	0.006	0.6
5	0.01	0.2
10	0.02	0.2
50	0.05	0.1
100	0.08	0.08
500	0.2	0.04
1000	0.3	0.03

We assume here that these are the maximum errors that glassware may incur in order to be classified as "class A" but that any particular vessel, if well cleaned and properly handled, will always deliver the same volume so long the temperature and, principally, the density and the viscosity of the solutions remain unchanged as is usual with very dilute solutions.

In view of the increasing use of disposable glassware by radiochemists, in order to avoid decontamination processes, we assume that no glassware is recalibrated by the user.

Let us try, now, using the above mentioned mother solution of 1 ppm, to prepare a series of six solutions covering the range: 1 ppm-1 ppb.

The first method to be considered will be the <u>direct</u> one, where the necessary volume of mother solution will be measured with a transfer pipet into a volumetric flask that will be then filled-up with the appropriate solvent. Thus, each dilution will be defined by:

$$C_i = \frac{C_o\ U}{T} \qquad (1)$$

where:

C_i : Concentration of the new solution
C_o : Concentration of the mother solution
U : Used volume of the mother solution
T : Total volume of solution i

and the maximum error of this concentration will be:

$$E_{ci} = C_i \left[\frac{E_{co}^2}{C_o^2} + \frac{E_u^2}{U^2} + \frac{E_t^2}{T^2} \right]^{1/2} \qquad (2)$$

Table II shows the calculations for the above mentioned six dilutions. It may be seen that the maximum practicable dilution is 1/1000 (one ml in one liter) because smaller pipets are not so accurate and larger flasks are not very handy. In this case, the maximum useful dilution increases the original relative error from ~ 0.1 % to 0.61 %.

Table II. Dilutions made by the Direct method.

Number	Mother solution ml (U)	Total volume ml (T)	Concent. g/l	Error Absolute g/l	Error Relative %
0			1.10^{-6}	$1.04\ 10^{-9}$	0.104
1	500 ± 0.2	1000 ± 0.3	5.10^{-7}	$5.79\ 10^{-10}$	0.116
2	100 ± 0.08	1000 ± 0.3	1.10^{-7}	$1.35\ 10^{-10}$	0.135
3	50 ± 0.05	1000 ± 0.3	5.10^{-8}	$7.38\ 10^{-11}$	0.148
4	10 ± 0.02	1000 ± 0.3	1.10^{-8}	$2.28\ 10^{-11}$	0.228
5	5 ± 0.01	1000 ± 0.3	5.10^{-9}	$1.14\ 10^{-11}$	0.228
6	1 ± 0.006	1000 ± 0.3	1.10^{-9}	$6.10\ 10^{-12}$	0.610

In the Chain method, each new solution becomes the "mother" for the next dilution:

$$C_{i+1} = \frac{C_i\ U}{T} \qquad (3)$$

and:

$$E_{c_{i+1}} = C_{i+1} \left[\frac{E_{c_i}^2}{C_i^2} + \frac{E_u^2}{U^2} + \frac{E_t^2}{T^2} \right]^{1/2} \qquad (4)$$

As may be seen from table III, the overall error increases slowly. In addition, this method does not have a practical limit of usefulness as happens with the Direct method. Thus, at first glance it looks as if the Chain method is more accurate, but this is not always the case. As this method does not have volume limitations, it may be easily used to prepare smaller volumes of solutions (10-100 ml); this will save a lot of mother solution and solvent, but the overall errors will increase rapidly.

Both methods imply the use of several pieces of glassware, each one with its own error, but what will happen if, instead of filling up the volumetric flask as we are accustomed to do, we measure the mother solutions and the solvent with the same vessel and mix the measured volumes in a beaker ? If

carefully handled, the same vessel (be it a transfer pipet, volumetric flask, cylinder or even a bucket) will always deliver the same volume if both liquids have the same density and viscosity. Thus, if we mix one volume of the mother solution with exactly the same volume of solvent we will get a new solution whose concentration will be exactly half of that of the previous solution, and its relative error will be the same. In other words; the dilution process will not increase the overall error of the resultant solution relative to that of the mother solution.

Table III. Dilutions made by the Chain method.

Number	Previous solution ml	Total volume ml	Concent. g/l	Error Absolute g/l	Error Relative %
0			1.10^{-6}	$1.04\ 10^{-9}$	0.104
1	500 ± 0.2	1000 ± 0.3	5.10^{-7}	$5.79\ 10^{-10}$	0.116
2	200 ± 0.1	1000 ± 0.3	1.10^{-7}	$1.30\ 10^{-10}$	0.130
3	500 ± 0.2	1000 ± 0.3	5.10^{-8}	$6.95\ 10^{-11}$	0.139
4	200 ± 0.1	1000 ± 0.3	1.10^{-8}	$1.51\ 10^{-11}$	0.151
5	500 ± 0.2	1000 ± 0.3	5.10^{-9}	$7.94\ 10^{-12}$	0.159
6	200 ± 0.1	1000 ± 0.3	1.10^{-9}	$1.69\ 10^{-12}$	0.169

Table IV shows two examples of pure binary dilutions calculated in order to cover the above mentioned range of 1 ppm-1 ppb. It may be seen here that the first example produces some odd concentrations whereas the second example, where the mother solution concentration is a power of 2, produces more handy concentrations.

Table IV. Pure binary dilutions.

Number	Example 1 g/l	Example 2 g/l
0	$1.00000\ 10^{-6}$	$1.024\ 10^{-6}$
1	$5.00000\ 10^{-7}$	$5.120\ 10^{-7}$
2	$2.50000\ 10^{-7}$	$2.560\ 10^{-7}$
3	$1.25000\ 10^{-7}$	$1.280\ 10^{-7}$
4	$6.25000\ 10^{-8}$	$6.400\ 10^{-8}$
5	$3.12500\ 10^{-8}$	$3.200\ 10^{-8}$
6	$1.56250\ 10^{-8}$	$1.600\ 10^{-8}$
7	$7.81250\ 10^{-9}$	$8.000\ 10^{-9}$
8	$3.90625\ 10^{-9}$	$4.000\ 10^{-9}$
9	$1.95312\ 10^{-9}$	$2.000\ 10^{-9}$
10	$9.76562\ 10^{-10}$	$1.000\ 10^{-9}$

Still, both examples need ten dilutions in order to cover the desired concentration range, instead of six as in the two previous methods. However, this problem can be solved if we make a small modification. For instance: if we want to make a dilution 1/5 we may measure and transfer one volume of mother solution and, after carefully cleaning the vessel, do the same four times with the solvent. Table V shows an example of six dilutions covering the range 1 ppm-1 ppb calculated this way. As with the pure binary method, this modification does not increase the relative error of the initial mother solution.

Table V. A modification of the Binary method.

Dilution Number	Previous Concentration units	Solvent units	Total volume units	New Concentration g/l
0				1.10^{-6}
1	1	1	2	5.10^{-7}
2	1	4	5	1.10^{-7}
3	1	1	2	5.10^{-8}
4	1	4	5	1.10^{-8}
5	1	1	2	5.10^{-9}
6	1	4	5	1.10^{-9}

Conclusions

After comparing the advantages and the propagation of errors of several dilution methods, it was shown that the Binary method, pure or modified, does not increase the relative error of the resulting solution above that of the mother solution; in other words; it is an error-free dilution method.

Activation Analysis with Short Lived Nuclides in Environmental Research

F.Grass
Atominstitute, Vienna

With the aid of our fast pneumatic tube system activation analysis with short lived nuclides gives prompt information on certain elements. For this purpose a fast pulse processing system developed in our institute renders it possible to measure radionuclides down to a half life of 20 ms. By means of successive prolonged measurements, the full information of the single irradiation is available. An immediately following longer irradiation with appropriate decay time and successive prolonged measurements delivers activities up to a half life of hours. Cyclic activation with progressive prolonged irradiations and pulse activation may be used to enlarge the sensitivity range.

On-line evaluation enables very rapid analysis. This is demonstrated by examples e.g. activation analysis of lead in an automobile exhaust by the 0.8s Pb-207m, of short lived nuclides in fly ash, in dust samples and in testing filter systems. Boron in fly ash may be determind by the 20ms B-12.

INTRODUCTION

The utilization of short-lived nuclides for AA has many advantages and in my opinion is the only way to make AA attractive for decision-making analysis, as it has the great advantage of producing immediate results. Instead of calling the method AA with short-lived nuclides, one ought to call it short-time activation analysis, because some elements with half-lives of hours may be activated appreciably in many samples, so that their detection is possible even with an activation of a few seconds or by a single reactor pulse.

As short-lived nuclides are utilized and the information density is high, and must be registered within seconds or fractions of seconds, one should use equipment allowing the processing of high count rates.

EXPERIMENTAL TECHNIQUE

The irradiation facility exclusively used in this work was described in (1). It is installed in a beamhole of a TRIGA Mark II reactor and consists of a fast pneumatic tube system which transports samples in 20 ms from the irradiation position (1.3×10^{12}/s and Cd-ratio of 12) to the measuring chamber. In steady state operation, the sample expelled from the irradiation position triggers the measurement of γ-spectra and the multiscaler for Čerenkov counting or γ-decay analysis. In pulse operation, the starting procedure is somewhat different. Expelling the pulse rod starts the multiscaler whereas the measurement of γ-spectra is started as before. It is thus possible to record the whole history of irradiation, flight time and starting of measurement by this procedure.

ELECTRONIC EQUIPMENT

Our team uses a so-called LFC-system developed by Westphal (2 - 7) which allows us to measure γ-spectra up to 500 Kc. This is especially valuable if nuclides with half-lives of less than one second are used for the analysis. In case of lead there is no other choice for instrumental neutron activation analysis.

This system consists of a 70 cc coaxial Ge(Li)-detector, which is DC-coupled to an overload resistant recycling preamplifier. Needle pulses of 200 ns duration produced by a prefilter are used as event detector. Via a delay line and a gated restorer, an integrator produces S-shaped pulses. The pile-up detector opens the ADC-coincidence only for those pulses which are clean of pile-up. The total clean count rate is fed to the Loss Free Counting corrector, and if desired, to a multiscaler to compare the true integral count rate with the converted count rate. In contrast to conventional γ-spectrometers, only clean pulses are converted, but the number of pulses fed into channel i depends on how many pulses have arrived in the time interval from the last conversion. A NOVA 1200 is used as a programmable multichannel analyzer, where 4×1024 channels may be sequentially programmed without any delay or corrected and uncorrected spectra may be registered in 2048 channels each. The repetition rate of the latter mode is at least 11.6 s, determined by the time necessary for data transfer to the PDP-11/34 computer*). The computer is equipped with a 80 K memory and with a Hard Disc and Floppy Discs for programme and data storage. Spectra are evaluated by means of the programme Activa (9), Peak (10), and Alchem (11), whereby different peak detectors are available. Together with a Čerenkov-counter a multiscaler is still a very valuable tool for the decay analysis of lithium and boron.

A test of this LFC-system is shown in Fig.1. In the measurement chamber, a 60 µCi Co-60 source is placed so that it delivers a constant total count rate

*) We are at present constructing a direct memory access system with a transfer time of a fraction of a second (8).

of 50 Kc. A Dy-165m activity produced by a short activation of 100 µg Dy superposes this count rate. Starting with a total count rate of more than 500 Kc, the Dy-165m activity drops to 100 Kc within a few minutes. γ-spectra are taken with a repetition rate if 24 s and the 1173 keV peak is evaluated with fixed peak and background channels. The values of the LFC-corrected peak areas are given in the middle of Fig.1 and the uncorrected ones at the bottom. The LFC-corrected value is constant within the statistical error, which is mainly determined by the number of conversions in the uncorrected spectrum. The mean value is 2.817±.045 Kc. The individual errors are within the dots and amount to 3% at the maximum. This is a very rigorous test for the LFC function up to 500 Kc.

Activation analysis is widely applied in the environmental research field, so that the paper presented is confined to work done at our institute.

Activation analysis is trivial but very valuable in aerosol research, where Dy-165m was used for testing filter systems together with particle size spectrometra. As the results will be published shortly (12), I shall refrain from going into further detail.

Short time activation of dust samples, preferentially with a reactor pulse gives fast information. The radionuclides Na-24m, Cl-38m are measured within 200 ms after the pulse, whereas sequentially prolonged measurements of 6 s allow the evaluation of Sc-46m, In-116m$_1$, Br-79m, Pb-207m, Cl-38m, Cu-66, V-52, F-20, and Al-28, and a further prolonged counting time of 60 s enables the measurement of Mn-56, Cl-38, and Ca-49. As the information about some of the elements is spread over more than one spectrum, it is necessary to calculate the saturation activity of the respective nuclide in the sample and to evaluate the data by a balancing calculation. Figs. 2 - 5 show the spectra after pulse activation of samples from an industrial area in Vienna. The measured elements enable rapid characterization of a certain environmental situation.

Previous work (13) has shown that the molar ratio of halogen and lead in a cold car engine exhaust decreases from 4:1 to 2:1 in the warming up process. A feasibility study was therefore performed testing an engine exhaust by taking samples from different points inside the system. Measuring the ratio of Br, Cl, and Pb should lead to an understanding of the particle fate, as the lead halogen compounds are the most volatile compounds in this system. Somewhat unexpectedly small amounts of In-116m were found, which were deposited inside the system and decreased from the vicinity of the motor to the end of the exhaust.

In Fig.6, γ-spectra samples taken from an exhaust after 60.000 km are shown. It is evident that the halogen-lead ratio has changed appreciably and that no In-116 was found in the last sample. Fig.7 shows the results in µM and their ratios together with a schematic view of the sampling points, which are indicated by dots and the corresponding numbers. Starting at sample 102 in vicinity of the motor, the halogen-lead ratio increases up to a roughly molar ratio of lead:bromine:chlorine indicating PbBrCl, whereas the incoming lead is in large excess. Outside the main stream halogen is relatively enriched, which may be in connection with the coarse structure of the samples, especially in the case of samples 114, 109 and 106 which contain oily constituents. Studies of this type together with a particle size analysis could lead to exhaust constructions where the respirable fraction of lead components could be minimized.

As is the case in many other countries (14 - 17), we have also begun to study the impact by fossil fuel power plants (18). We are interested not only in the ashes, for which there are standard testing procedures, but also in the volatile elements released from exhausts for which there are as yet no standard laboratory procedures. We are using an enlarged water-cooled trap (18 - 20) which should allow us to identify the element and how much of it is volatile and leaves the incinerating chamber, when a given coal sample is heated to the

standard ashing temperature of 760°C . A quartz apparatus (21), Fig. 8, is inserted in a furnace and allows the ashing of coal samples with the off-gases hitting the cold trap in a jet stream. The deposits are scratched (scraped) off the cold trap. Prior to ashing, the surface of the cold trap is covered with carbon black by igniting 0.5ml benzene. The cold trap deposits from ashing Polish soft coal oddly enough contained hardly any Vanadium, but Se, Cl, I, F and Br were found (18).

So a series of experiments are started, incinerating brown coal from an Austrian deposit TRIMMELKAMM, from whose power plant we had already got ash and the fly ash deposit from the electrostatic filter, so that a comparison was possible. In Fig. 9 the deposits of the cold trap using different air flow rates are compared with the deposit on the electrostatic filter. With a change in the flow rate from 1l per min to 14l per min, the selenium deposit remains unchanged, whereas Al, Sc, Hf and V increases with the velocity of the air stream. At high flow rates, the spectra taken from the cold trap and the electrostatic filter are very similar. But in contrast to these, there is a lack of selenium in the fly ash from the power plant. It may therefore be assumed that this element passes the electrostatic filter.

In order to test whether we would determine boron - an element which has only recently come into the focus - we carried out pulse activation on NBS fly ash, two cold trap deposits, and a standard boron sample, and were then able to estimate the boron content by the 20ms B-12 (Fig. 10). This shows that quick results sufficient for many purpose may be gained by means of short activation. If necessary, additional information may then be gained by long-time activation.

I gratefully acknowledge the cooperation of G.P.Westphal, I.Sarac, P.Schindler K.Pongrac, E.Seymann and R.Popp, without whose efforts I could not have presented these results.

LITERATURE

(1) O.BRANDSTÄDTER, F.GIRSIG, F.GRASS and R.KLENK
Nucl. Instr. Methods 104, 45 (1972)

(2) G.P.WESTPHAL, Nucl. Instr. Methods 115, 509 (1974)

(3) G.P.WESTPHAL, ibid. 136, 271 (1976)

(4) G.P.WESTPHAL, ibid. 138, 467 (1976)

(5) G.P.WESTPHAL, ibid. 146, 605 (1977)

(6) G.P.WESTPHAL, 163, 198 (1979)

(7) G.P.WESTPHAL, First International Workshop on Activation Analysis with Short Lived Nuclides, Atominstitut Wien, Feb. 1980, to be published in J. of Radioanalytical Chemistry.

(8) R.POPP and G.P.WESTPHAL, ibid.

(9) I.SARAC, ibid.

(10) K.PONGRAC, Diss. TU Wien 1979

(11) P.SCHINDLER, AIAU 80501, Atominstitut Wien

(12) G.WEBER, see (7)

(13) F.GRASS and G.P.WESTPHAL, Nucl. Instr. Methods 140, (1977), 97

(14) R.DAMS, J.A.ROBBINS, A.RAHN and J.W.WINCHESTER, Anal. Chem. 42, (1970) 861

(15) W.S.LYON, N.E.BOLTON, J.F.EMARY and D.H.KLEIN in J.R.VOGT and W.MEYER (Eds.), Proceedings of Second International Conference on Nuclear Methods in Environmental Research, ANS 1974, p.376

(16) T.V.CRAWFORD and E.L.ALBENESIUS, DP-1455 Savannah River Lab., May 1977

(17) J.M.ONDOY, R.C.RAGAINI and A.N.BIERMANN, in J.R.VOGT (Ed.) Proc. of the Third International Conference Nuclear Methods in Environmental and Energy Research, ANS 1977 p.138

(18) W.GEILMANN, Z. Anal. Chem., 160 (1958), 410

(19) W.GEILMANN and K.NEEB, ibid. 165 (1959), 251

(20) U.PONTA and F.GRASS, unpubl. Results

(21) H.BOCK, I.SARAC and F.GRASS see (7)

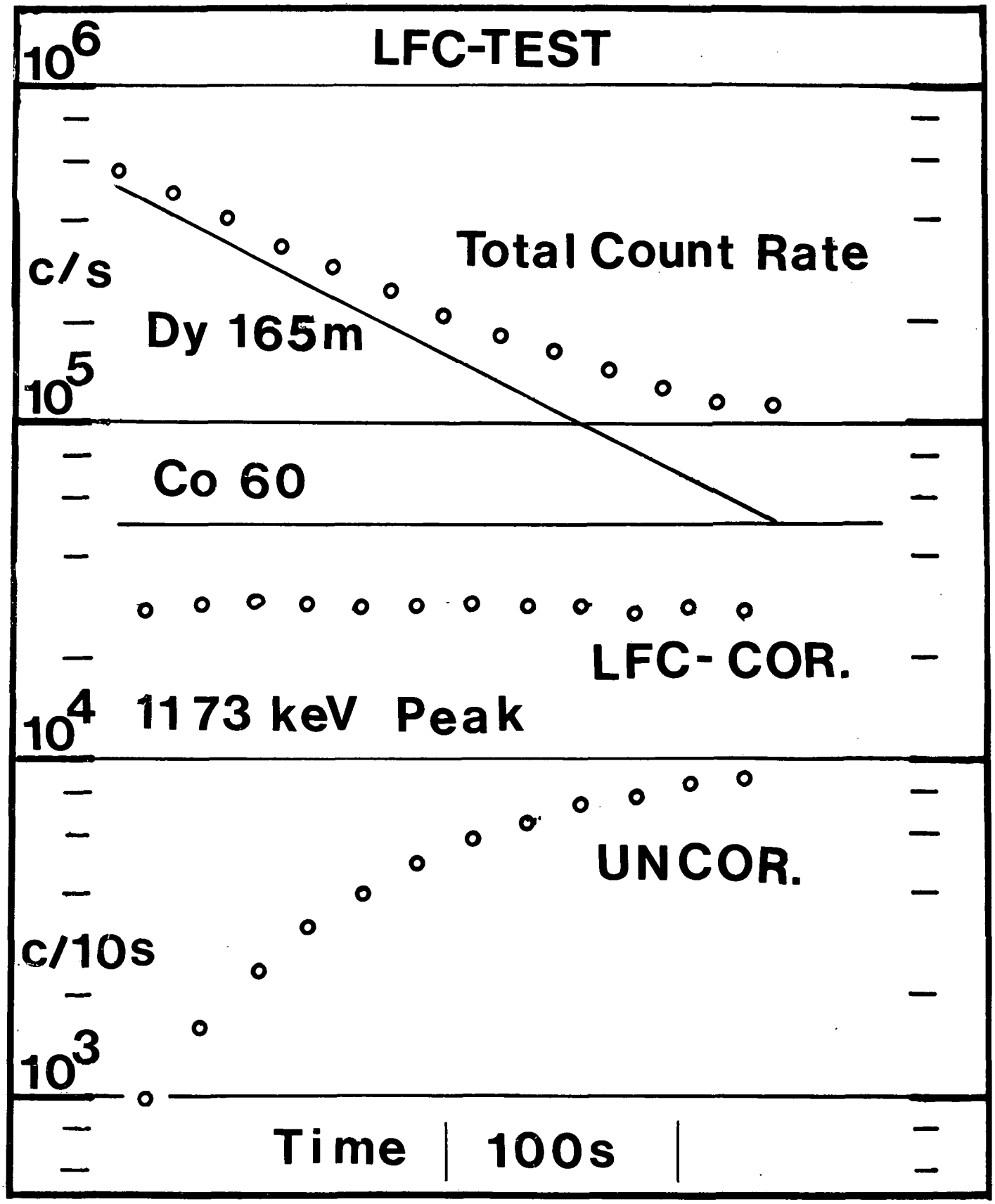


Figure 1. Loss Free Counting-Test
A 60μCi Co-60 source was positioned to give a constant total count-rate of 50 Kc/s which were superposed by a Dy 165m activity. The LFC corrected 1173 keV Co-60 peak which gives a constant mean value of 2.817±0.045 Kc/s whereas the uncorrected value increases from 0.096 to 0.87 Kc/s.

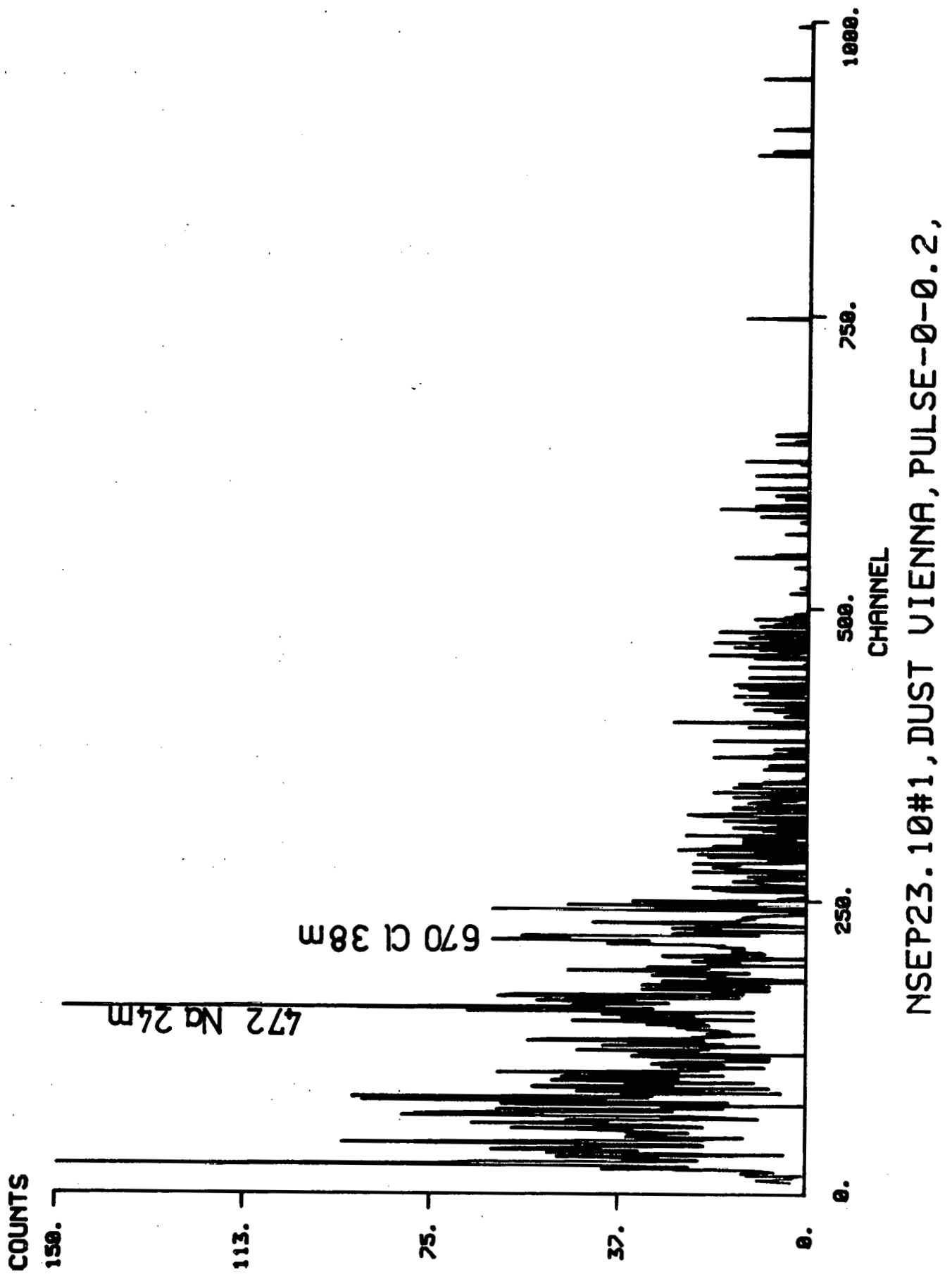


Figure 2. Pulse activation of the dust sample from an industrial area in Vienna collected in a Bergerhoff vessel. Decaytime 0, countingtime 0.3s.

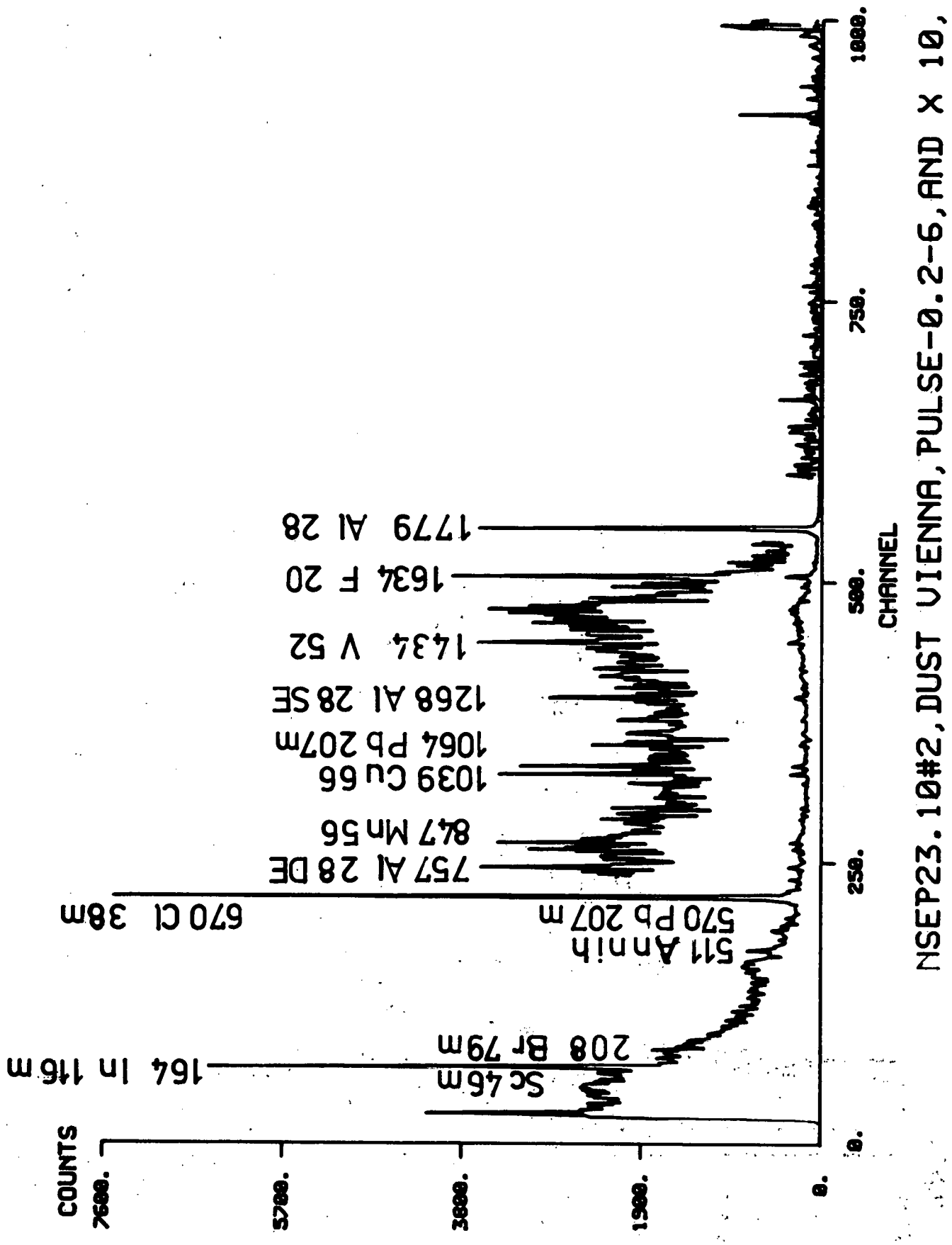


Figure 3. Pulse activation of a dust sample from an industrial area in Vienna collected in a Bergerhoff vessel. Decaytime 0.3s, countingtime 6s.

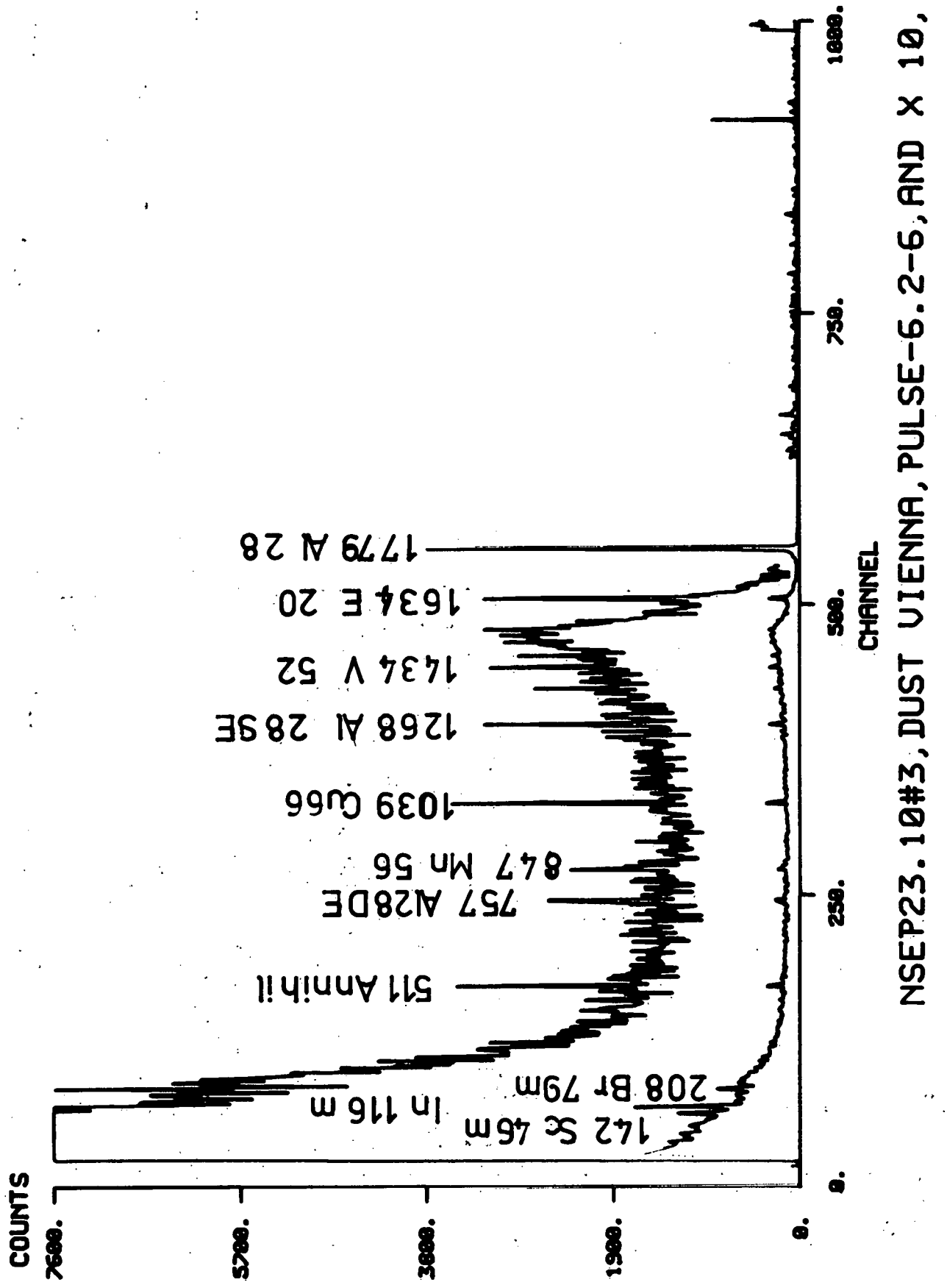


Figure 4. Pulse activation of a dust sample from an industrial area in Vienna collected in a Bergerhoff vessel. Decaytime 6.3s, countingtime 6s.

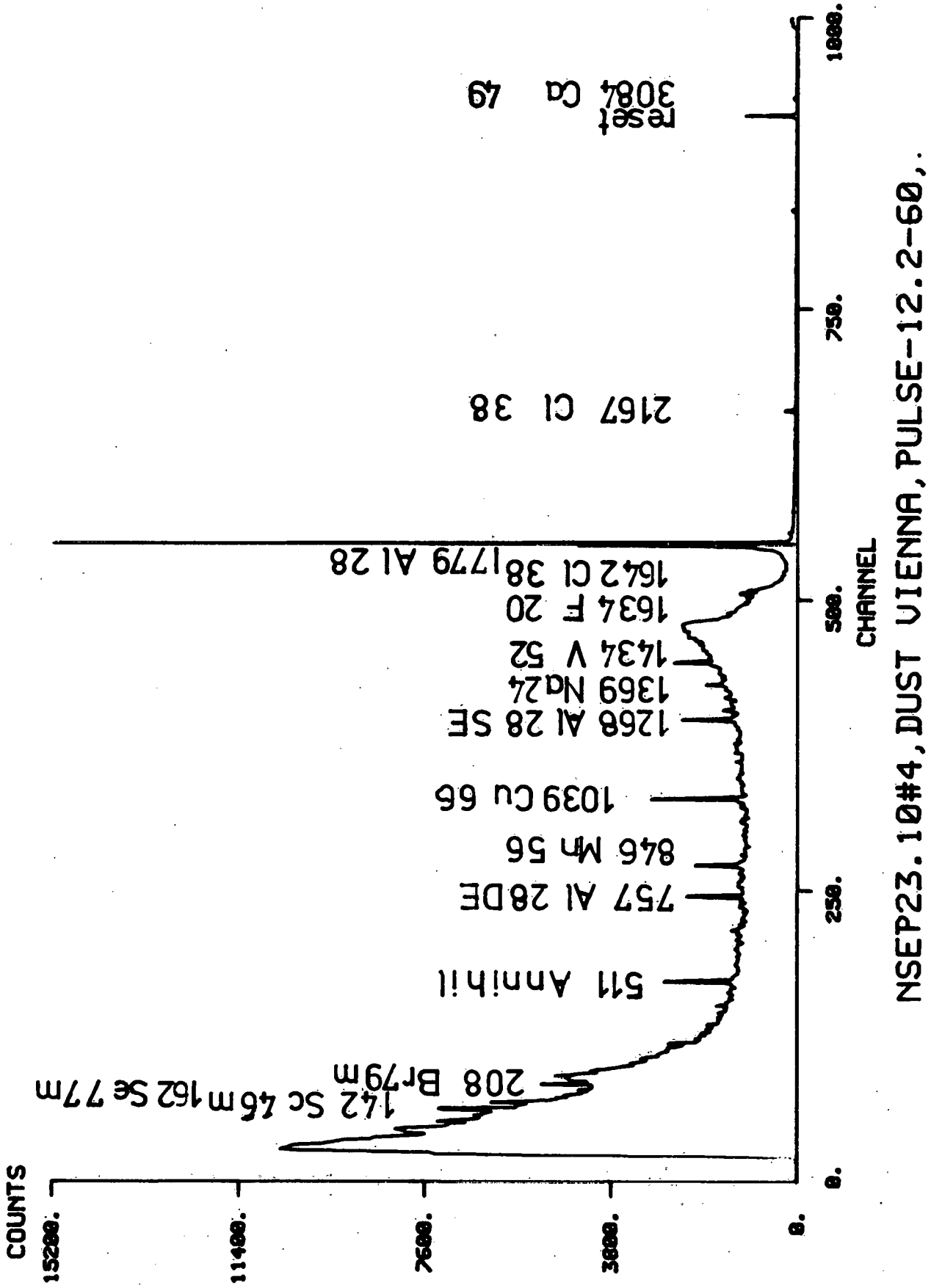


Figure 5. Pulse activation of a dust sample from an industrial area in Vienna collected in a Bergerhoff vessel. Decaytime 12.3s, countingtime 60s.

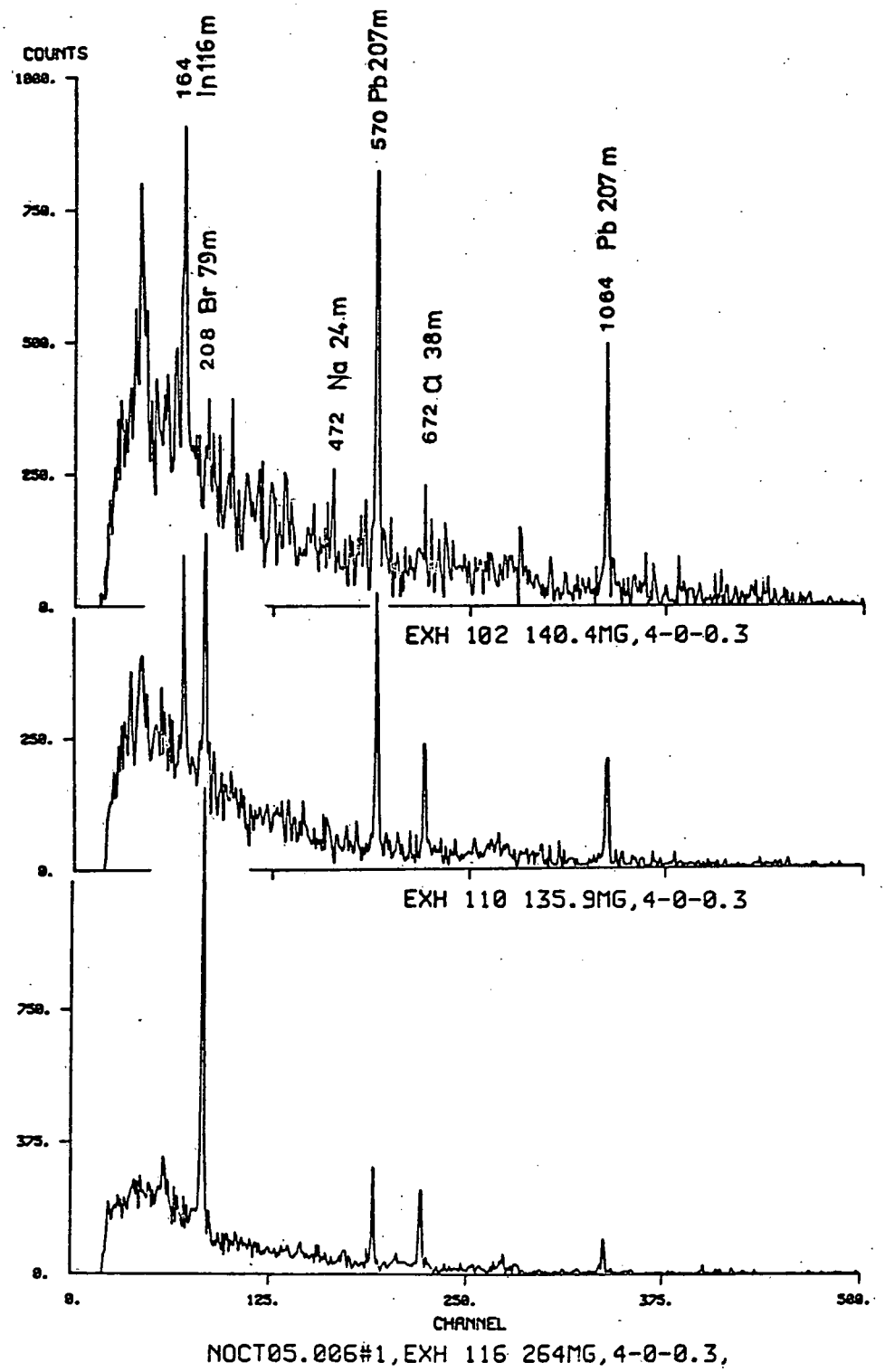


Figure 6. γ-spectra of the deposits of an automobile exhaust. Activation-time 4s, decaytime 0 and countingtime 0.3s. EXH 102 manifold near the motor, upper spectrum. EXH 110 in the muffler middle spectrum. EXH 116 exhaust stack.

SAMPLE	Pb	Br	Cl
102	389±13	5±0.05	27±2
	12	0.15	0.85
103	-	-	-
	-	-	-
104	195±30	6.5±0.05	8.6±1.4
	12.9	0.43	0.57
114	51±11	24±1	25±2
	1	0.5	0.5
112	117±13	17±1	19±2
	3.3	0.47	0.53
109	70±8	24±3	30±3
	1.3	0.44	0.56
105	267±14	40±11	42±2
	3.2	0.49	0.51
110	194±10	36±3	42±6
	2.5	0.46	0.54
106	200±20	70±6	60±5
	1.5	0.54	0.46
115	69±5	44±1.5	38±2
	0.84	0.54	0.46
116	76±4	72±2	59±4
	0.58	0.55	0.45

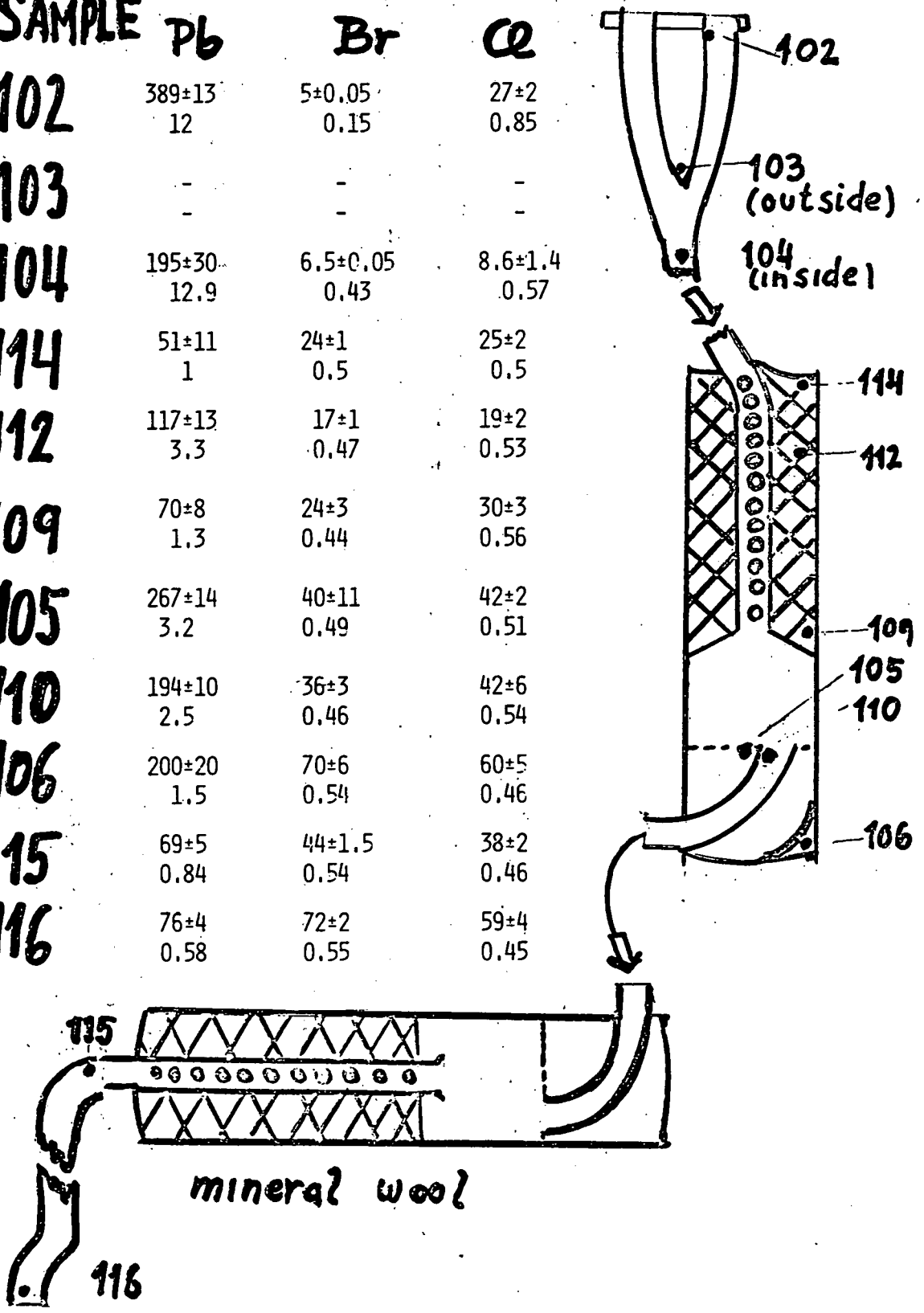


Figure 7. Schematic drawing of an automobile exhaust. Numbers denote sampling point. Values in μM and ratio lead: halogen.

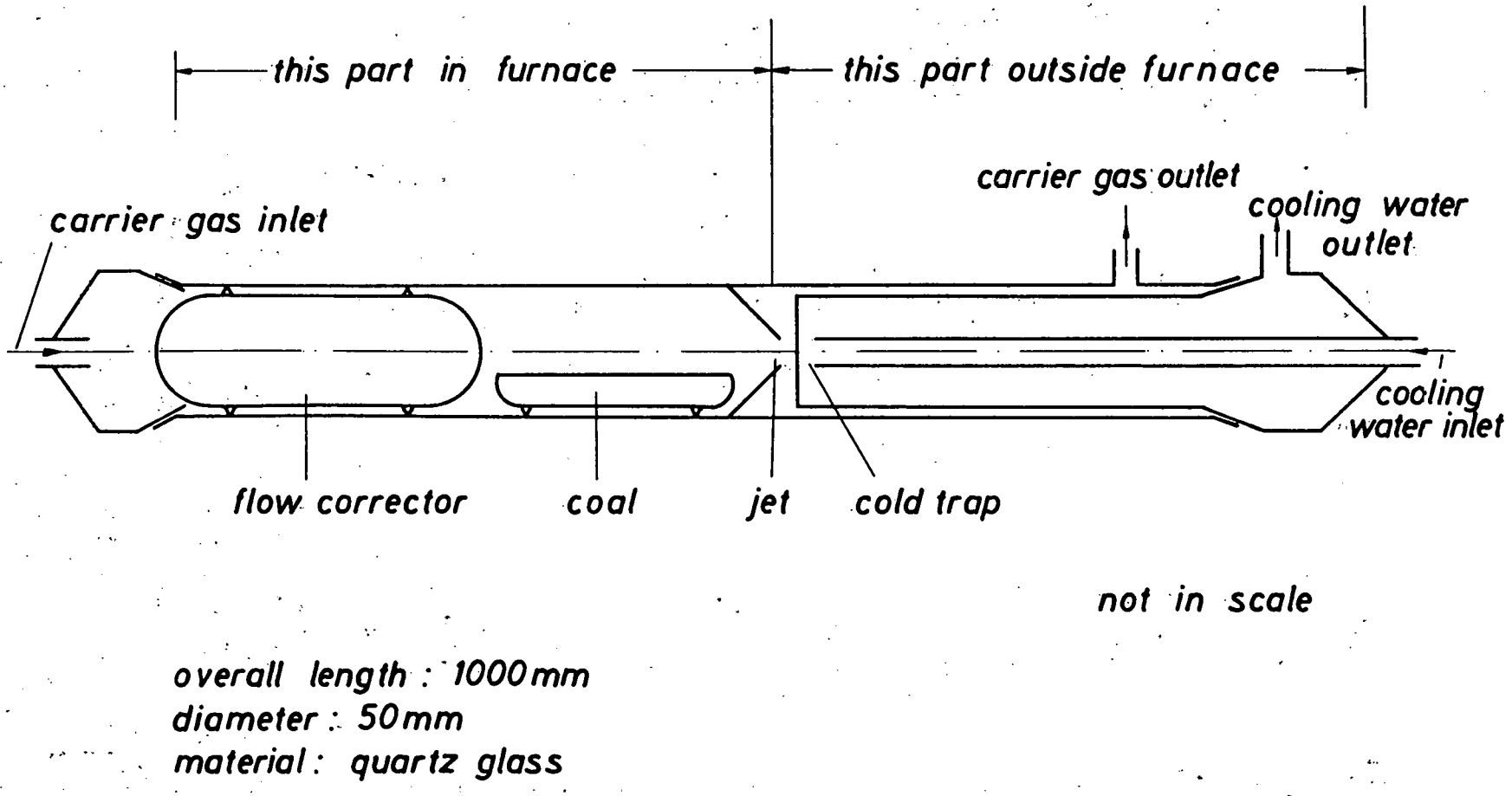


Figure 8. Quartz apparatus for incineration of coal.

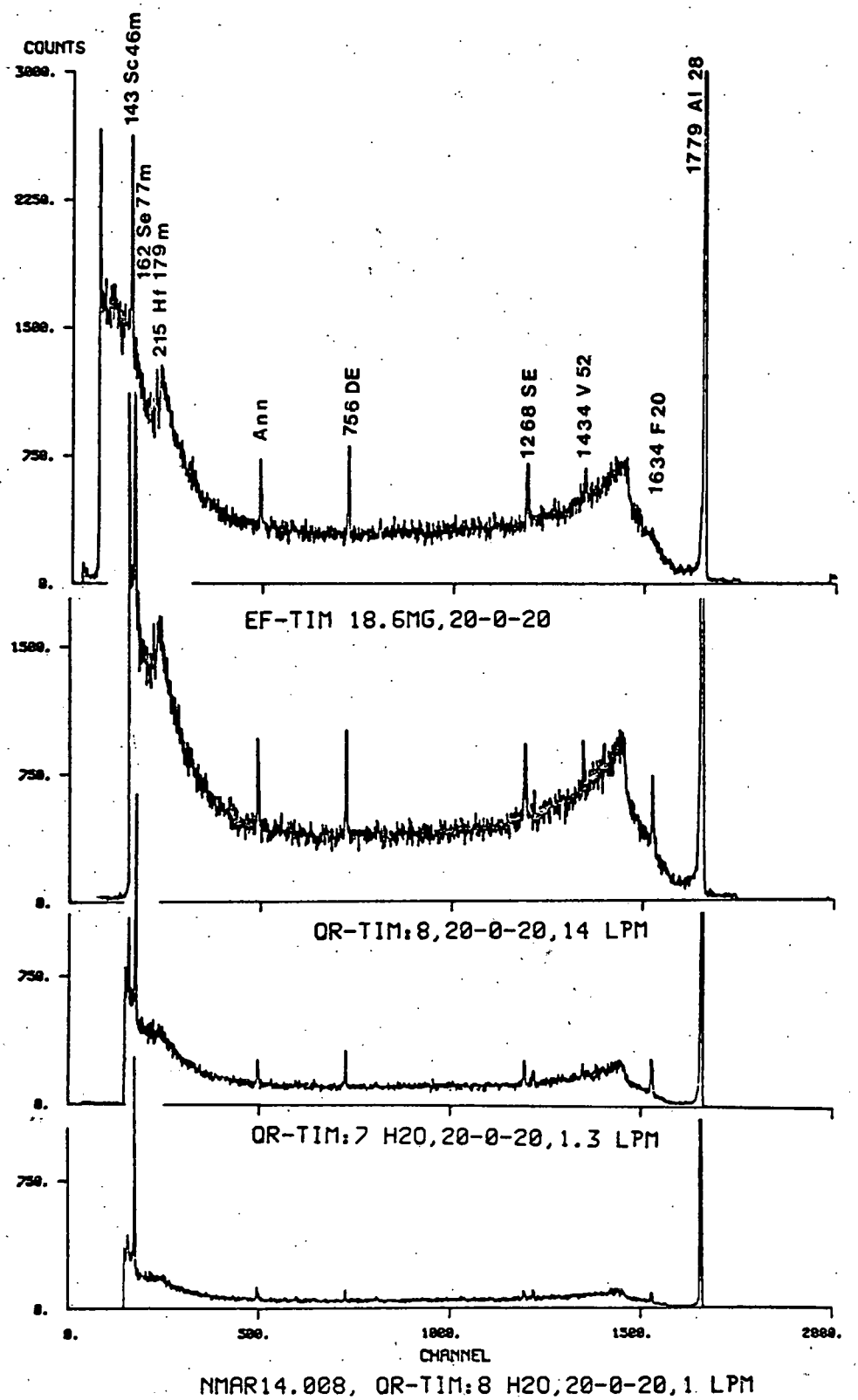


Figure 9. γ-spectra of fly ash from the electrostatic filter of the power plant TRIMMELKAMM and cold trap deposits at different air flow rates 1, 1.3 and 14 Liters per Min. Activationtime 20s, decaytime 0, countingtime 20s.

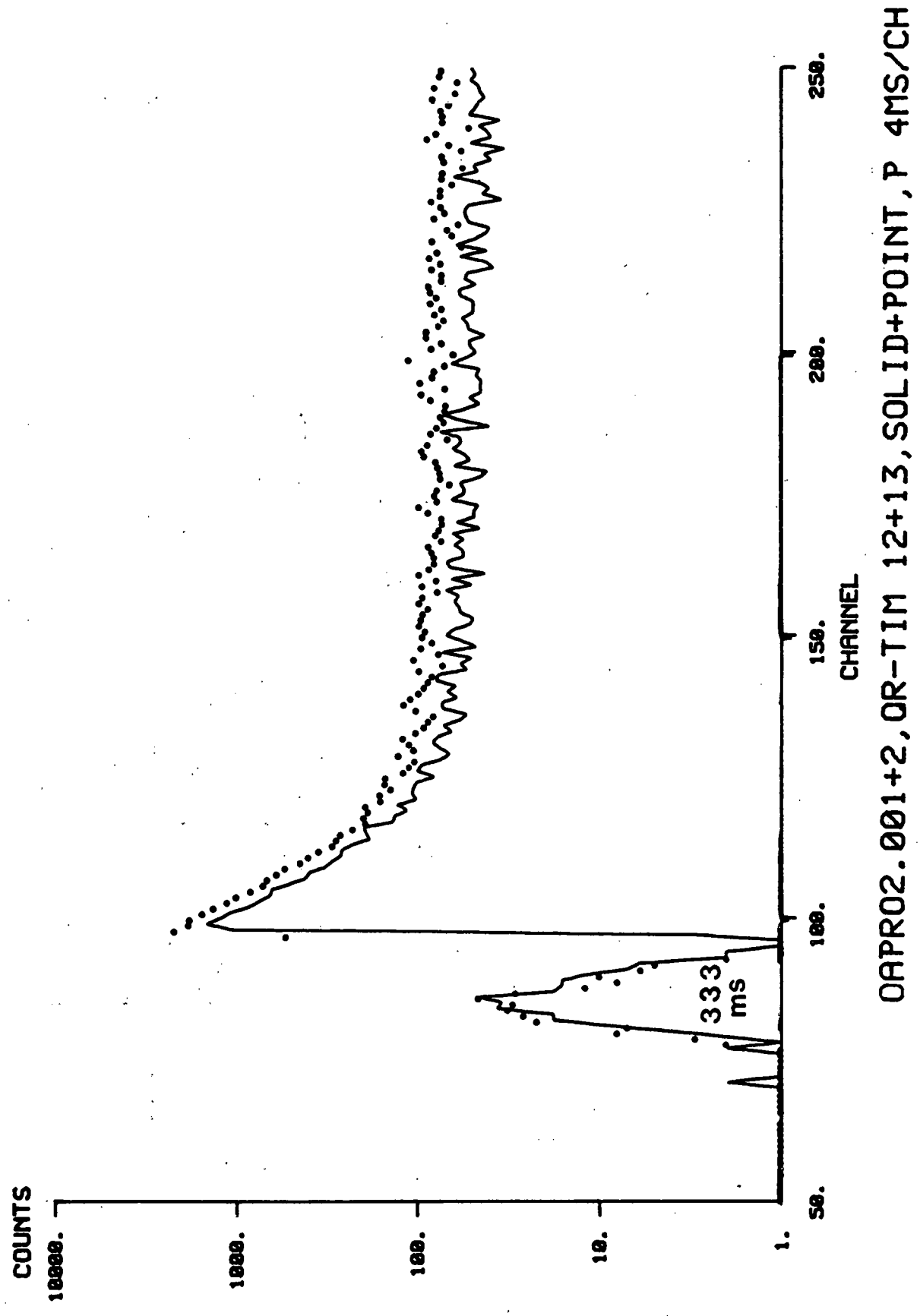


Figure 10a. Pulse activation of NBS-fly ash and a boron standard sample 370 µg measured by Cerencov counting, upper curves.

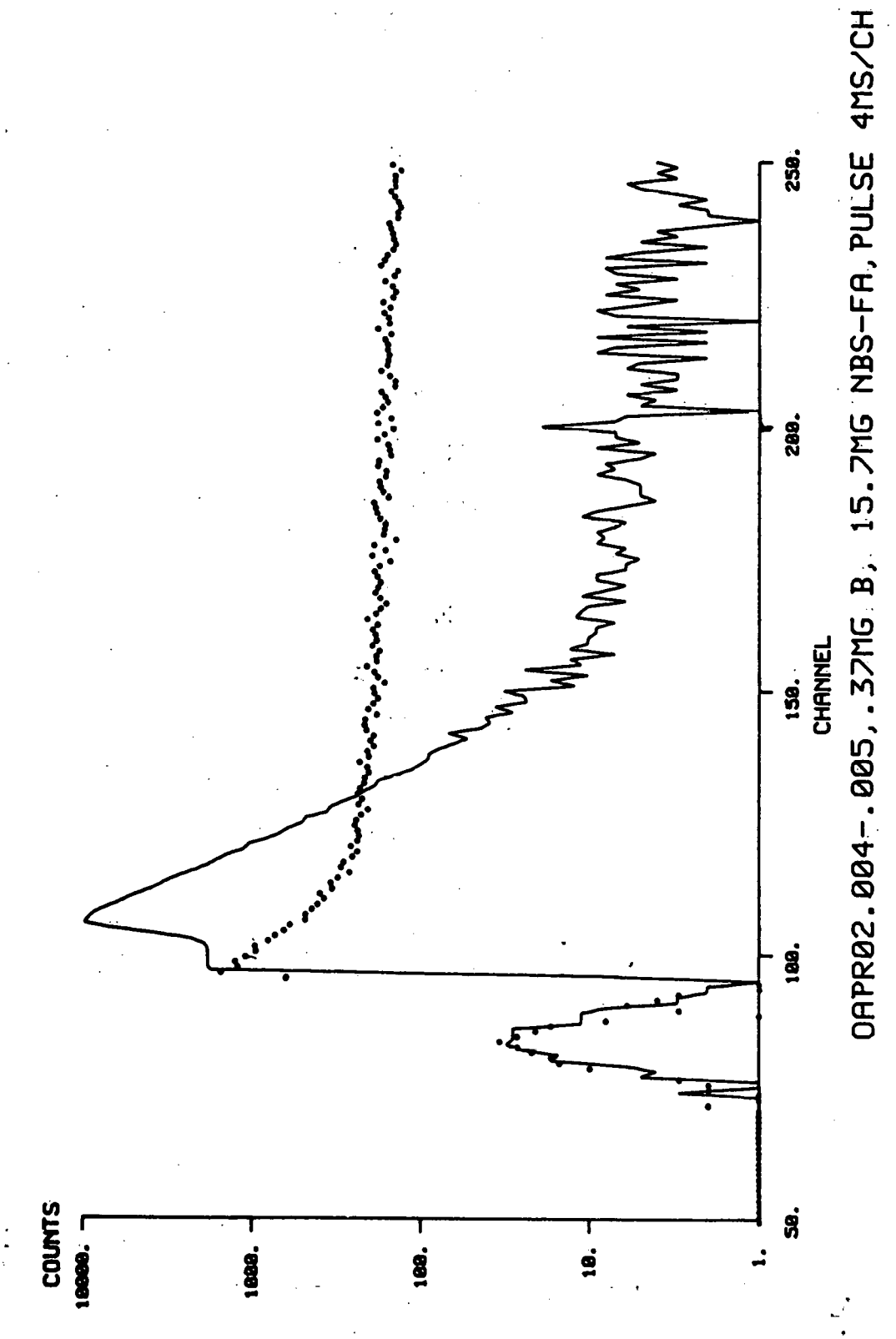


Figure 10b. Cold trap deposits 12 and 13, lower curves. Flow rate of air 6 and 18 Liter per Min. Time seale 4ms/channel.
Multiscaler start coincidently with expelling the pulse rod at channel 0. Reactorpulse ∿ 333 ms later.

NUCLEAR METHODS

IN

BIOLOGY AND MEDICINE

Session Chairmen

W.D. Ehmann

J.M.A. Lenihan

THE CHEMIST IN THE CLINIC

J M A Lenihan

West of Scotland Health Boards
11 West Graham Street
Glasgow G4 9LF
Scotland

ABSTRACT

Nuclear techniques have been useful, psychologically as well as operationally, in studying the impact of the chemical environment, internal and external, on the health of the individual and the community. These studies are characterised by an abundance of answers but not enough meaningful questions. If scientific insight can catch up with technology, important advances can be achieved.

The Chemist in the Clinic

I want to talk this morning about some basic problems in the relationship of the chemical environment - external and internal - to human health. To most people, these problems are of recent origin but, like so many problems in the contemporary world, they have roots that go back far into the past.

It might be thought that, for two centuries or more after the beginning of modern science (in the 17th century) the chemist was not doing very much in the clinic and that, on the contrary, most of the important advances in chemistry as in biology and in physics were being made by medical men. There was however an earlier time when major contributions to medicine - both philosophical and practical - came from chemists. Perhaps it would be more true to say that these advances came from one single chemist - Paracelsus, the greatest of all the alchemists. In the middle ages, the alchemists were apparently obsessed by the making of gold, though this was probably only the bait required to obtain tenure and overhead from their employers in the palaces of Europe. The alchemists were really looking for spiritual purity. The processes of refining and distillation that they developed were the allegories of the spiritual transformation which was to elevate the soul to its eternal life.

Paracelsus had a more practical outlook. The object of alchemy he said is not to make gold but to make drugs for the relief of sickness. Having founded the science of chemotherapy he went on to lay down some important principles. The dose, he said, makes the drug. In other words the administration of medicines should be quantitative rather than qualitative, as it had been until then. The dose must be carefully specified and accurately measured. This was the beginning of measurement in medicine - and indeed the beginning of the scientific approach to chemistry. Paracelsus also insisted on the importance of chemical purity - another concept which, though it seems commonplace to us, marked an important advance in the transformation of chemistry from a craft into a science. After Paracelsus there was, it is true, a rather long interval in which doctors contributed much to chemistry. More recently, chemists have had the chance to start repaying the debt.

In this process nuclear methods of analysis have made a distinctive contribution. Whether these methods can make a large or important contribution to the study and the improvement of human health is not yet clear - but some of the factors which are likely to influence the verdict of history can already be identified.

In the application of any scientific or technical resources to the management of human health we face an immediate difficulty in deciding what we mean by health. The official definition, given by the World Health Organisation is that health is a state of complete physical, mental and social well-being. This is not very useful for it tells us that no one is healthy. We can approach the problem in another way. During the past century advances in hygiene, in living standards and in chemotherapy have made a successful impact on the acute diseases of early and middle life. In the western world, a child born to-day has a much better chance of surviving to middle age than did his ancestors of a hundred years ago. But the expectation of life of a 50 year old person has hardly changed during the past century. So the big problems of medicine are no longer pneumonia, tuberculosis and childhood fevers, but rather the chronic degenerative diseases of middle and later life, including cancer, rheumatic ailments and heart disease. It is in this general area that nuclear methods of analysis and investigation can make a useful contribution.

During the past thirty years the application of nuclear methods in medicine has encouraged the development of many ingenious techniques for the elemental analysis of biological material. These experiments have involved a great variety of activating sources - not always neutrons - and a great variety of procedures for chemical or instrumental separation and assay. A major part of this effort has involved the estimation of various elements in different tissues of the body. One reason for doing this is to establish a range of values which can be used as background in judging the significance of subsequent studies seeking answers to specific questions.

More often the tissue levels of various elements are compared in samples taken from patients and from healthy controls. The purpose of such work, which has been done especially in relation to heart disease and to cancer, is to see whether the concentration of particular elements in particular tissues is different in health and in disease.

Work of this kind is encouraged by the apparent influence of environmental factors and disease. In many parts of the world it is possible to find pairs of neighbouring communities, apparently very similar in genetic, industrial and social background - but with very different experience in the prevalence of heart disease or of cancer. In these situations it is natural to infer that the chemical environment is responsible for the

difference.

Here the search is usually concentrated on the minor elements, including those not yet known to serve any useful purpose in the body. The major chemical elements which are present in virtually every cell and tissue of the body, and a few other elements which, though less abundant, are known to have an essential role, have naturally been rather thoroughly studied. Their concentrations in body tissues are also subject to rather strict physiological control. On the other hand the minor elements, which do not appear to have any particular purpose in the body, occur at widely varying concentrations, influenced mainly by accidents of diet or environment. Sometimes, as in the relation of cadmium to hypertension, the findings appear to be significant. In other enquiries, such as the relationship of minor elements to cancer, the significance of the experimental findings remains elusive.

In all such enquiries, the analytical findings are only the first stage. The essential next step is to find a biochemical process linking the presence or absence of the element concerned with the disease that is being studied. Nuclear methods of analysis are of course not very serviceable in biochemistry, which is largely concerned with organic molecules rather than with inorganic elements. However, the scientific insight of the chemist can still be useful in the later and perhaps decisive stages of the enquiry. In this connection I might mention our current work in Glasgow on mercury hazards in dental practice. This began in the conventional way nearly 20 years ago when we looked at mercury levels in the hair and nails of dentists and dental nurses. There was, not surprisingly, a big difference in mercury levels between dental workers and control subjects.

Subsequent surveys on a larger scale, involving some 1000 dental workers, showed similar results - and led some of our clinical colleagues to wonder whether the psychiatric and neurological illness which they sometimes saw in dentists might be related to exposure to mercury. Two dentists, who were severely ill, were investigated in hospital and the provisional diagnosis of mercury poisoning was soon confirmed. When the patients were treated with penicillamine, a chelating agent, considerable amounts of mercury were mobilised and excreted in the urine. After that, the patients remained in hospital for some time and the daily output of mercury was monitored by activation analysis of beard samples taken with an electric razor. The toxic symptoms - irritability, tiredness and lack of concentration - were relieved while the patients were in hospital but returned shortly after they went back to work.

At this stage it was clear that the brain damage suffered by the dentists could certainly be related to mercury poisoning. We were led to the next stage in the enquiry - that is the finding of a biochemical link - by a report

from a French dentist, Dr Magnaval, who speculated on the possibility that mercury might be methylated in the tissues of the body. This was a novel idea, since the only natural source of methyl mercury known at that time was enzyme action in bacteria in the seabed. Magnaval presented results on four dentists and his findings were not statistically significant. However we were encouraged to pursue the possibility when one of our colleagues, Dr Ian Dale, made an observation which, though obvious in retrospect, had not occurred to us earlier. The symptoms of chronic poisoning by inorganic mercury, as seen in dentists, are very similar to the symptoms of acute poisoning by methyl mercury.

We then decided to measure levels of methyl mercury in the blood of dentists and of control subjects. We spent a year or two in devising a suitable technique, using gas liquid chromatography, for the measurement of methyl mercury in small samples of blood. The results were unambiguous. In dentists' blood, the levels of methyl mercury and total mercury and the ratio of methyl to total mercury were very much higher than in control subjects.

The picture has now become so much clearer than it was 20 years ago when we began these studies. Inorganic mercury circulates in the blood and may be deposited in the kidney or excreted in the urine. The kidney appears to be able to hold quite a lot of mercury before it eventually breaks down, sometimes with fatal results. It seems however that a proportion of the inorganic mercury circulating in the blood is converted to methyl mercury - whether in the gut or in the liver we do not yet know - and can then make its way into cells - particularly in the brain where it survives for a long time.

The signs of chronic mercury poisoning are seldom seen in young dentists; perhaps the brain, like the kidney, can accumulate mercury without any obvious effect until a threshold level at which toxic effects become apparent. These studies are continuing and our clinical colleagues are looking at enzyme systems which suffer a depression of activity in the presence of mercury. We are of course hoping to find the site and the exact mechanism by which inorganic mercury is converted to methyl mercury - but this may take quite a long time.

What we have learned from this work - and indeed from all of our work during the past 25 years on nuclear methods of analysis - is that the chemist must be close to the clinical problem if he is to make an effective contribution. In other words he must take part in formulating the questions, rather than sitting behind a door counting other people's atoms. In this respect, as in other ways, we should be careful not to allow the exuberance of our technology to outweigh the importance of scientific insight. It must of course be acknowledged that the spectacular advances in analytical chemistry during the

past 30 years have had a considerable psychological impetus from activation analysis. It is very seldom that a new technique improves sensitivity by a factor of a thousand or even a million - which was what activation analysis did. The traditional skills of the microanalyst have now been superseded almost entirely by instrumental methods, of which activation analysis was the first. The breakthrough achieved in the 1940s and 1950s had a psychological impact comparable with that of the four-minute mile.

Nuclear methods are important in medicine for another reason. Until the beginning of modern science in the 17th century, medicine was dominated by the teaching of Hippocrates, who insisted that the patient must be viewed as part of his total environment and that disease should be seen as a failure of equilibrium between the patient and his environment. This view was challenged in the 17th century by Descartes, who asserted that man is a machine. During the past century medicine has been essentially Cartesian, based on the proposition that if a patient is ill the correct approach is to find which system or component has gone wrong and then to treat it, remove it or replace it. To-day there is a growing recognition of the importance of environmental practice in medicine. Nuclear methods of analysis can provide a great and lasting service to the community by fulfilling the desire which is so apparent to-day for a bridge between the Hippocratic and the Cartesian approaches to the health of the individual and the community.

Neutron Activation Analysis of Hair from Breast Cancer Patients

Ibrahim Othman and Nicholas M. Spyrou
Medical and Environmental Physics Group, Department of Physics
University of Surrey, Guildford, Surrey, GU2 5XH, U.K.

Abstract

Hair samples from breast cancer patients were collected at the same time as tumour and normal tissues obtained during mastectomy, in order to determine elemental concentrations and investigate whether hair can act as an epidemiological monitor of the disease. Instrumental neutron activation analysis was used and concentrations for Na, Mg, S, Cl, Ca, Mn, Cu, Zn, Br, I, Sb, Ba, Au and Hg in the hair samples measured. No strong correlations were found between the concentrations of Cl, Cu, Zn and Br in hair and those in tumour tissues and in normal tissues. The level of Zn in the patients hair is low and that of Ca very high.

Introduction

About one-fifth of all deaths in the U.K. are caused by cancer. Although the prognoses in some conditions have greatly improved in recent years, there has been little improvemnt for many other cancers, including some of the most common types. In 1977, Sir Richard Doll [1], in a review of environmental hazards with respect to cancer, has said: 'We cannot of course hope to detect hazards efficiently until we know how cancer is produced, so that a policy for detection must include the support of basic biological research'.

The Medical Research Council's Cell Biology and Disorders Board identified in 1978 three subjects to which it wished to give high priority: breast cancer, gastrointestinal cancer and chemotherapy; and a specific priority, repeatedly identified in the past, is the study of the structure and function of the normal human breast, which may yield information relevant to breast cancer, as well as being of more general importance.

Although the vast majority of women do not contract breast cancer, many women (5%) do and the Health Department has mounted a programme of mass breast cancer screening trials in a small number of centres in the U.K. It was through our medical colleagues in the Breast Screening Project in Guildford, one of the centres, that in early 1977 we undertook to study the elemental composition and distribution of normal and abnormal breast tissues, thus contributing to the biomedical research being carried out. Information was required about tissues at the microstructure level and analytical techniques of good sensitivity needed, so that trace quantities can be determined.

In X-ray mammography, the radiographic pattern formed by breast calcifications plays an important rôle in the diagnosis of breast disease. To the eye of the experienced radiologist there is a difference between 'benign' and 'cancer' calcifications, so that when observed together with other positive radiographic signs a true diagnostic rate of $\sim$ 90%, we are told, is achieved. Unfortunately, occult early breast cancer does not manifest positive radiographic signs and the calcifications are often the only clue to disease. The difference then between 'benign' and 'malignant' calcifications is less distinct, so one outcome according to Galkin et al. [2] is that 70% of these patients undergo 'unnecessary' surgery for removal of tissue containing 'benign' calcifications. Price and Gibbs [3], our medical collaborators, suggest that certain types of lesions like in situ intraduct and intralobular carcinomas, when associated with microcalcifications should be regarded as a pre-invasive stage of cancer. The lesions are being discovered with increasing frequency as a result of mammography and as many as 20% of the breast cancers found in screening programmes are at this stage. We therefore have a situation which poses problems of localisation and management for the surgeon and because of the borderline changes between epithelial hyperplasia, in situ carcinoma and invasive carcinoma a difficult responsibility is placed on the pathologist.

In 1978 we reported our preliminary findings [4] that hydroxyapatite crystals formed these calcifications in the analysis of a set of historical samples collected over a number of years at the Regional Hospital, using a transmission and a scanning electron microscope with microprobe facilities. However since these samples were sections prepared originally for histological examination i.e. they were fixed in formaldehyde, dehydrated by methyl alcohol and then embedded in wax we did not attempt to carry out any trace element analysis using neutron activation, since our experience [5] indicated that the value of the concentration of a number of elements would be unreliable due to additions to and losses from the sample having taken place during the dehydration process.

Samples and methods

To study the trace element composition of breast tissues, both cancerous and non-cancerous specimens from the same breast were obtained from patients undergoing mastectomy. In addition we collected for analysis hair samples from these patients in order to investigate whether hair can serve as an epidemiological monitor for the disease by making use of the fact that hair is easy to collect and store and that trace-element constituents in hair are generally more concentrated than in blood or urine, therefore simplifying analytical procedures. The patients undergoing mastectomy were all female aged between 30 and 80 years. The results of instrumental neutron activation analysis (INAA) of normal and cancerous breast tissues have been reported elsewhere [6,7].

Hair samples were clipped with scissors from the left side of the nape about 1 cm from the scalp, for consistency with our established procedures [8] and collected from 28 patients with tumours for activation analysis. A few hairs from the same area were plucked from the root, from some of the patients, and together with a number of strands of cut hair as obtained above, were set aside for electron microprobe analysis.

In preparation for INAA, hair samples were soaked in distilled double deionised water and agitated in an ultrasonic bath for one hour. They were then removed with polyethylene tweezers and placed on filter paper for drying in a laminar flow hood at 25°C for 24 hours. Dry samples were then placed in polyethylene containers ready for irradiation. The following neutron irradiation and gamma-ray counting modes were used at the University of London Reactor Centres facilities:

i) Cyclic activation [9] with 7 cycles of 38s cycling period, giving a total experiment of $\sim$ 266s per sample, for detection of F, Sc, Se, Br, Ag, Ba and Hf using a Ge(Li) detector for counting; in a thermal flux $\sim 2 \times 10^{12} ncm^{-2}s^{-1}$. N.B. A different set of cyclic conditions would be required for the detection of lead via $^{207}Pb^{m}$, when a detection limit of 5 µg/g is achieved.

ii) Short irradiation of duration $\sim$ 20 min, a waiting time of 90s and counting time of $\sim$ 20 min using a Ge(Li) detector for the detection of Na, Mg, Al, S, Cl, Ca, Ti, V, Mu, Cu, Br, Sr, Ba, I and Hg; in a thermal flux $\sim 2 \times 10^{12} ncm^{-2}s^{-1}$.

iii) Long irradiation of duration $\sim$ 30 hrs, a waiting time of 24 hrs and a counting time of 3000s using a Ge(Li) detector for the detection of Na, K, Sc, Co, Fe, Zn, Br, As, Rb, Sb, Ba, La, Hg and Au; in a thermal flux $\sim 1 \times 10^{12} ncm^{-2}s^{-1}$.

The Ge(Li) (Canberra) detector used in photon counting has a resolution of 2.2 keV and an efficiency of6% at 1332 keV; the photon spectra were stored on a LABEN 4k-channel analyser and data stored on magnetic tape for processing using a modified version of SAMPO [10].

Results and Discussion

Table I, gives the concentrations in µg/g of Na, Mg, S, Cl, Ca, Mn, Cu, Zn, Br, I, Sb, Ba, Au and Hg in the hair samples from patients with adenocarcinomas. The range given in the first column, indicates the dispersion in the concentrations determined and in the second column the arithmetic mean and its standard deviation are linked for sample concentrations above the detection limit (typical sample masses were of the order of $\lesssim$ 50 mg). In addition to the arithmetic mean the geometric mean was also calculated, with its standard deviation, shown in the fourth column, as a better representation of the mean

of a skew distribution. The third column listing P, the fraction of samples with elemental concentration above the detection limit is useful in giving the frequency with which an element is detected in the population. Finally in order to include the samples with values below the detection limit, column five presents the median values which take into account all 28 samples of the population.

Frequency histograms were plotted for the elements and those for Mg, S, Ca, Cu, Zn, Br, I, Au and Hg are shown in Fig. 1 (a and b). The frequency histograms for S, Ca, Cu and Zn follow a normal distribution, confirmed by the χ^2-test for best fit with expected frequency. To test for lognormal distributions, cumulative probabilities were plotted on logarithmic probability paper as shown in Fig. 2 for Ca, Cu, Zn, I, Au and Hg. The plots for mercury and gold are straight lines confirming that the distribution of these two elements is of lognormal type, whereas the other elements do not satisfy this condition. To a certain extent these results agree with a suggestion by Liebscher and Smith [11] that essential trace elements follow a normal distribution whereas non-essential trace elements have lognormal ones, although it must be borne in mind that the samples here considered were obtained from cancer patients and the rôle that essential and non-essential trace elements play in the disease is unknown. In the case of mercury and gold this indicates that the rate of accumulation of these elements in the body is not the same as the rate of excretion through hair.

Since we have not yet analysed the hair of a control population, and our experience is limited to the analysis of hair from 'normal' populations selected in Kenya [8,15], students at the University and schoolchildren in the Guildford area, we cannot comment on the levels of elemental concentrations in this sample of breast cancer patients with authority. Nevertheless a few points can be made when the results are compared with other populations: the value of zinc is lower than the reported values for a number of populations [12,13,14] and is about half the amount quoted for the female population in Africa mentioned above. When compared with the latter population, the magnesium concentration is relatively lower and that for manganese is considerably lower although this is generally thought to be consistent with a trend associated with a 'Western' diet in contrast to a manganese rich native one. One can also generally remark that the concentration levels of mercury are relatively low whereas those for sulphur are high but in particular the values of calcium are considerably elevated. The value of copper concentration in patients' hair is similar to the level found in many other communities.

The high excretion rate of calcium is associated with a number of diseases notably those related to bone e.g. osteoporosis and it is of interest to this study since the calcifications in breast tissues were found to be composed of hydroxyapatite crystals.

In an attempt to extract more information about the dependence and interdependence between elements from the results of the analyses of normal and tumour breast tissues and of hair samples from the same person, regression and correlation coefficients were calculated respectively. It was found that there was no correlation between the concentrations of Cl, Cu, Zn and Br in hair with the values of these elements in tumour breast tissue and no correlation was found either with the levels found in normal breast tissue. It must be noted that although calcium was detected in 25 of 28 samples of hair, it was detected in only 4 of the paired breast tissue samples for which hair had been collected. Therefore no statistical information could be extracted.

Conclusion

One of the main problems associated with such a study, where the profound lack of knowledge of structure and function of the normal breast and without which real progress in understanding breast pathology will never be attained, is how to obtain normal tissue. It is easy to obtain hair samples from a control population and compare trace element concentrations found with those in the hair of patients suffering from the disease, however to establish hair as an epidemiological monitor normal breast tissue must also be analysed. Possible future sources of normal tissue may include mammoplasties, coroner's autopsies and thoracoplasties. However in the context of the present investigation, we can conclude that:

i) The level of concentration of a number of elements (Mg, Mn, S and Hg) and in particular that of Zn in the hair of breast cancer patients has exhibited variations when compared with 'normal' levels which may prove to be significant. Ca is in very high concentrations in the hair of the patients suffering from the disease.

ii) No strong correlation was found in the concentration of elements (Cl, Cu, Zn and Br) in tumour and in normal breast tissues with that determined in the hair of the same patient.

iii) The high excretion rate of Ca in the hair of patients who had undergone mastectomy for adenocarcinoma reflected by the concentration of the element, may be a significant indicator to the excretion and formation of calcifications in the breast glands, and should be examined further.

Acknowledgements

We would like to thank our medical colleagues Drs. J.L. Price and N.M. Gibbs and their staff at the Royal Surrey and St. Luke's Hospitals, Guildford, for their interest and advice and for supplying the samples. Our thanks also to Mr. M. Kerridge and his staff, at the University of London Reactor Centre, for use of the irradiation facilities.

Ibrahim Othman is being supported for the session 1979/80 by an MRC contract as post-doctoral fellow.

References

1. Doll, Sir R., Nature 265, (1977) 589.

2. Galkin, B.M., Feig, S.A., Patchefsky, A.S., et al.: A new look at breast cancer calcification, Digest of the Fourth International Conference on Medical Physics, Ottawa, July 1976, Ottawa, Canada. Assoc. Physicists, (1976) 25.3.

3. Price, J.L. and Gibbs, N.M., Clin. Radiol., 29 (1978) 447.

4. Spyrou, N.M., Othman, I., Gibbs, N.M., Price, J.L., Ultrastructure and composition of breast calcification using electron microscopy and microprobe analysis, Euroanalysis III, Dublin (1978).

5. Othman, I., Minski, M.J., Spyrou, N.M., Elemental losses from biological materials using different drying techniques, 5th Symposium on Recent Developments in Activation Analysis, Oxford (1978).

6. Othman, I. and Spyrou, N.M., Composition of breast tissues using neutron activation and electron microscopy, ANS Trans. TANSAO 32 1-832 (1979) 158.

7. Othman, I. and Spyrou, N.M., Elemental Composition of cancerous and non-cancerous breast tissue by instrumental neutron activation analysis (submitted for publication).

8. Spyrou, N.M. and Othman, I., Elemental concentration in the hair of a selected population group from the Machakos District, Kenya, Proceedings 3rd International Symposium on Nuclear Activation Techniques in the Life Sciences, IAEA-SM-227/33 (1978).

9. Spyrou, N.M. and Kerr, S.A., Short-lived isotopes in the analysis of biomedical and environmental samples, J. Radioanal. Chem., 48(1979) 169.

10. Routti, J.T. and Prussin, S.G., Nucl. Inst. and Meth. 72 (1969) 125.

11. Liebscher, K., and Smith, H., Arch. Environ. Health, 17 (1968) 881.

12. Dale, I.M., Lenihan, J.M.A., Smith, H., The environment as reflected in human hair - a comparison, Proceedings 2nd Int. Conf. on Nucl. Meth. in Env. Research, ERDA (1975).

13. Clemente, G.F., Trace element composition of hair in the Italian population, Proceedings IAEA Symposium on Nuclear Techniques in the Life Sciences, SM-227/13 (1978).

14. Imahori et al., A study of trace elements in the hair of some local Japanese population - Part 1, ibid, SM-227/16 (1978).

15. Othman, I., and Spyrou, N.M., Some elements in hair from a population in Kenya, Sci. Tot. Env. (in press).

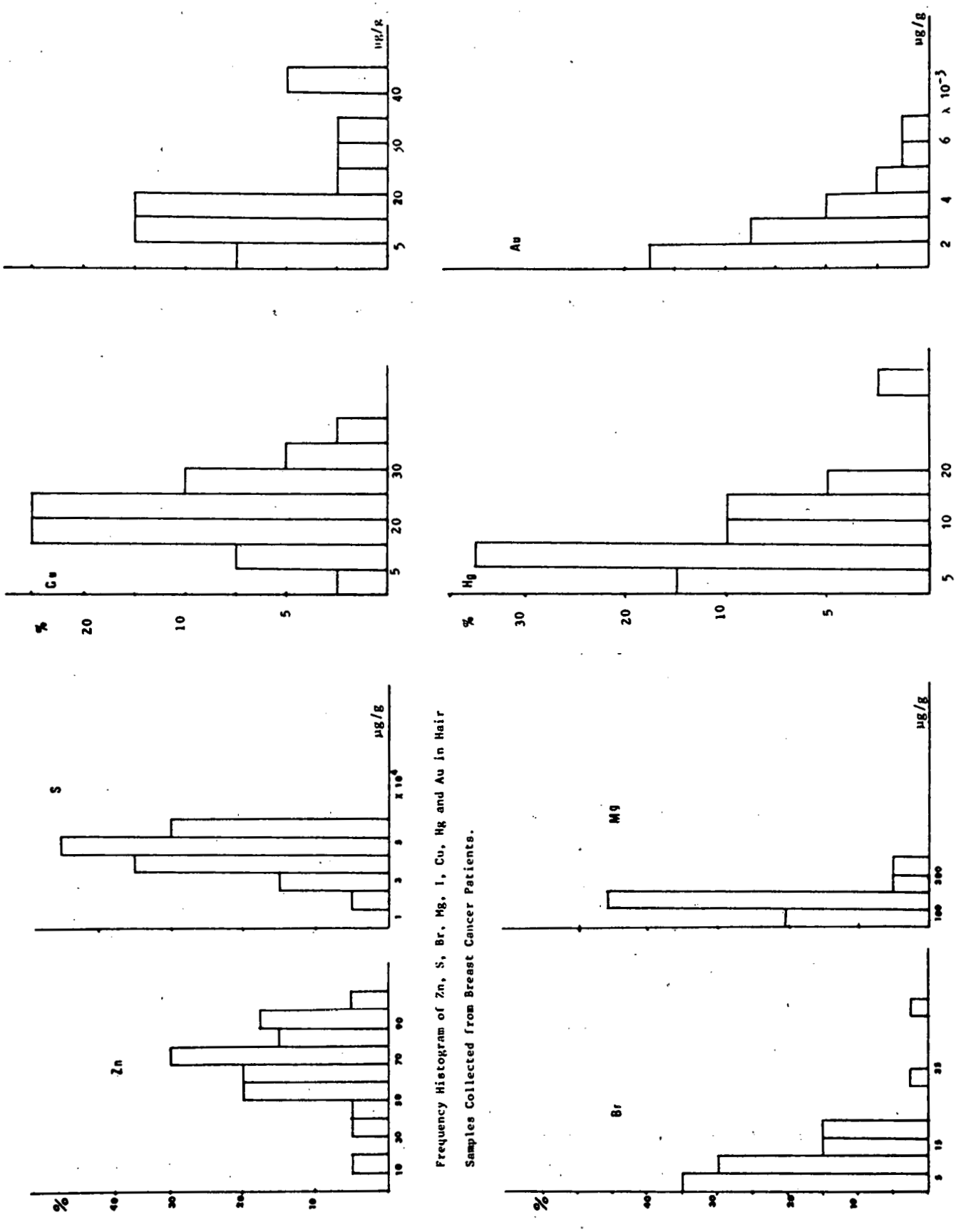


Figure 1 (a and b) Frequency histograms of Zn, S, Br, Mg, I, Cu, Hg and Au in hair samples from breast cancer patients.

Elemental Concentration in μg/g of Hair Samples Collected from Breast Cancer Patients (n = 28)

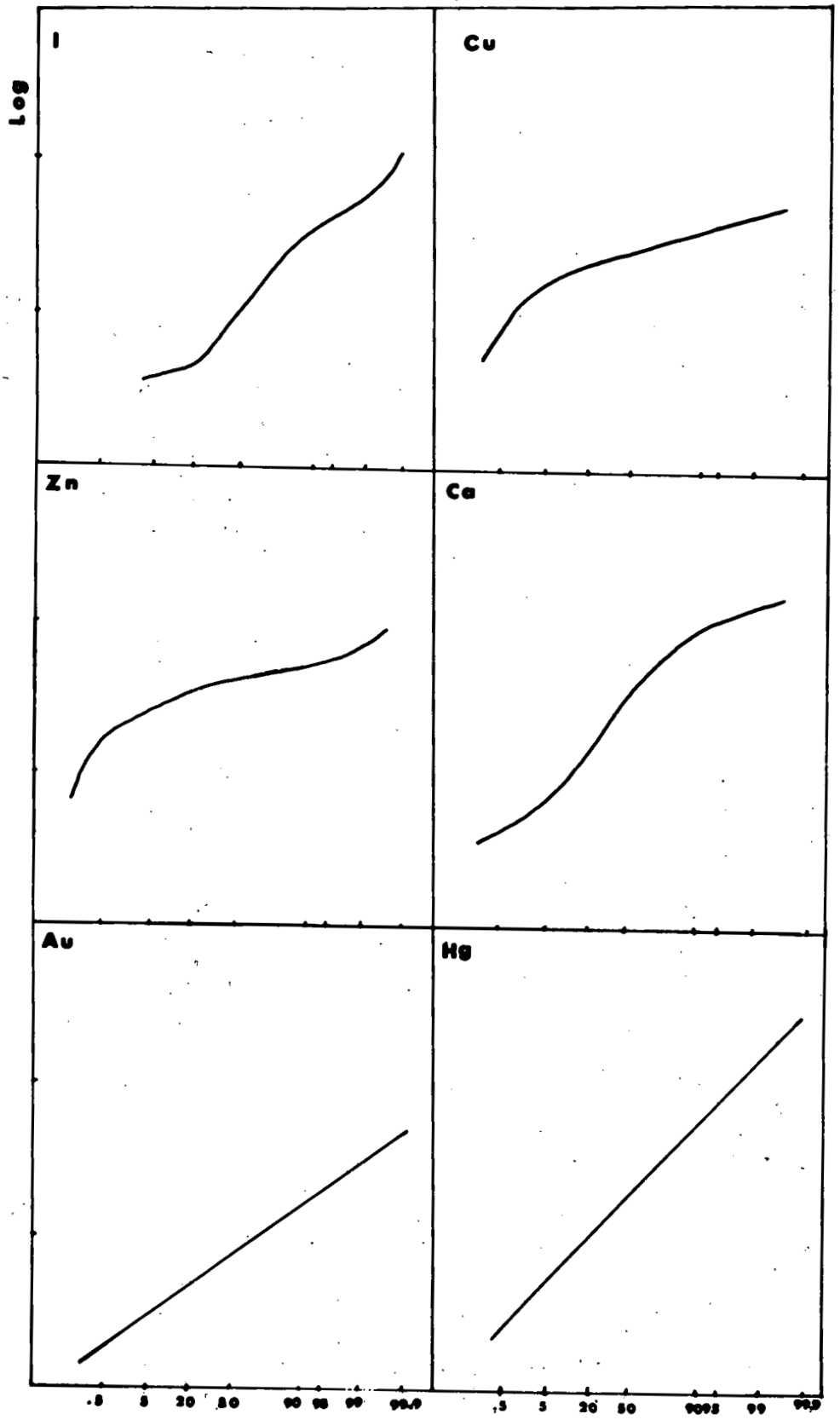
Element	Range	Arithmetic mean ± SD	P	Geometric mean ✕÷ GSD	Median
Na	2-32	*	.48	5.43 ✕÷ 2.5	6.5
Cℓ	90-970	239 ± 23	1.	124 ✕÷ 3.9	154
Mg	63-400	157 ± 107	.59	127 ✕÷ 1.9	150
Mn	.1-1.5	.66 ± .47	.3	.53 ✕÷ 1.9	.46
S	32000-54000	45000 ± 4500	1.	45000 ✕÷ 1.1	45900
Ca	190-10000	4880 ± 1050	.89	1800 ✕÷ 3.1	3944
Cu	9-62	19 ± 11	.93	14.7 ✕÷ 1.8	16
I	.1-6	*	.85	.78 ✕÷ 3.1	.55
Zn	35-100	77 ± 31	1.	70 ✕÷ 1.6	75
Br	.1-60	*	.96	3.9 ✕÷ 5.2	3.6
Sb	.007-.3	*	.29	.106 ✕÷ 8.5	.09
Ba	1.5-40	*	.33	4.6 ✕÷ 2.9	2.9
Au	.006-.08	*	1.	.03 ✕÷ 2.4	.023
Hg	.17-.5	*	.93	.17 ✕÷ 2.3	.16

P is the fraction of samples with concentration above the detection limit set at $\sqrt{B}$

* The arithmetic mean is given only for samples which follow the normal distribution.

Figure 2. The logarithmic concentration versus the cumulative frequency using logarithmic probability peper for I, Cu, Zn, Ca, Au and Hg in hair of breast cancer patients.

TABLE I: The Logarithm of Concentration of I, Cu, Zn, Au, Ca and Hg in Hair Samples Collected from Breast Cancer Patients Plotted Against the Cumulative Frequency Using Logarithmic Probability Papers.



TOXICOKINETIC STUDIES POSSIBLE AFTER ACUTE INHALATION ADMINISTRATION OF COMPOUNDS LABELED WITH SHORT-LIVED ISOTOPES. Ray S. Kutzman*, Geerd-J. Meyer†, and Alfred P. Wolf, Department of Chemistry, Brookhaven National Laboratory, Upton, New York 11973

ABSTRACT

A system has been developed to study the short term pharmacokinetics of inhaled organic pollutants after acute exposure of animals to near carrier free amounts of the radiolabeled compound. The agents tested were labeled with gamma emitting isotopes at very high specific activities. The decay characteristics of these isotopes allows the non-invasive measurement of the amount of radiolabel accumulated by the animal during the exposure period, as well as the amount retained at any time after exposure.

Using a dynamic nose exposure apparatus rats were exposed to selected ^{11}C-labeled compounds to demonstrate the utility of short-lived isotopes as unique new tracers for toxicokinetic studies of environmental agents.

Inhaled ^{11}C-benzaldehyde was rapidly absorbed from the lungs, metabolized, presumably via benzoic acid to hippuric acid, and excreted via the renal system. The removal of benzaldehyde from most tissues was quite rapid and paralleled the removal of radiolabel from the blood.

Inhaled ^{11}C-octanal was also absorbed from the lungs quite rapidly with the greatest concentration of octanal occurring in other tissues at approximately 5 minutes post-exposure. Tissue activities calculated on the basis of administered radiolabel and on the dose retained by the rat until the time of sacrifice indicated a redistribution of the radiolabel as a metabolite of the administered compound. This metabolic fate of inhaled octanal was also reflected in the elimination kinetics of carbon-11 labeled CO_2.

After nose exposure to ^{11}C-acrylic acid 28% of the administered radiolabel was found associated with the exposed animal's nose and bucal cavity. At least part of this material was ingested during the post-exposure period. Experiments were therefore conducted to assess the rate of acrylic acid metabolism when the compound was administered via the pulmonary and gastrointestinal routes to conscious and anaesthetized rats. The physical state of the animal was found to have a greater effect on the expiration of $^{11}CO_2$ from exposed animals than the route by which the agent was administered.

It appears that these techniques may prove very useful for inhalation studies, particularly when substantiating the diposition and metabolic fate of compounds which have only been administered via more convenient, although unrealistic methods, and for assessing the fate of compounds which may present themselves during accidental industrial exposures.

*present address, Medical Department, Brookhaven National Laboratory, Upton, NY
† present address, Institut fur Nuklearmedizin, Medizinische Hochschule, Hannover F. R. Germany

Acute pharmaco- or toxicokinetic studies of inhaled agents have lagged behind similar investigations employing other means of compound administration because of several technical problems. First of all, it is difficult to quantitate the amount of compound actually taken up by an animal during an inhalation exposure. Secondly, it is very difficult to administer sufficient radiolabel during a short exposure period for kinetic studies. It is therefore advantageous to have a system in which the test animal accumulates a high percentage of the available radiolabeled compound without contamination of the animal's fur.

Agents labeled with carbon-11 appeared as likely candidates to aid in overcoming several of these hurdles. This radiotracer holds several significant advantages over traditional carbon-14 and tritium radiolabels. Carbon-11 is a positron emitter, providing body penetrating gamma rays which permit non-invasive monitoring of the administered radiolabel. Also, synthesis of compounds using this cyclotron produced isotope can result in a product that is essentially carrier free (1). These characteristics of carbon-11 labeled compounds were explored in an attempt to develop the necessary techniques for the application of short lived, gamma emitting isotopes as tracers for inhalation experiments. The high specific activity of these compounds provides another advantage, administered quantities of the compound which are so small they are believed to be subphysiological, can be measured. The results obtained in these studies should not then be the consequence of a drug or toxic effect of the agent on the exposed animal.

For administration of radiolabeled agents the apparatus in Figure 1 was developed. The rat to be exposed was lightly anaesthetized (Enflurane) and placed into the glass restrainer. The restrainers were made with the bottle type opening for the nose located above the central axis of the tube. This construction appeared to provide more secure restraint of the rat's head than similar tubes with a central opening. A sliding plunger held the rat forward in the restrainer and a latex mask, with a small hole to permit exposure of the nostrils, was stretched over the animal's nose and held in place with an O-ring. This latex mask provided a seal around the rat's nose and prevented contamination of the animal's fur while holding to a minimum the exposed surface area of the snout. The O-ring which held the mask in place also served as a seal for the glass nose cone which fits over the animal's protruding nose. After the rat was placed into the restrainer and the mask was in place, the assembly was snapped onto the nose cone. A respirator pump provided air at 120 mL/min via the by-pass line while a coiled trap, containing the gas chromatography purified labeled compound, was placed into the delivery line. The rat was then exposed to the radiolabeled compound by redirecting the air flow through the spiral trap in the delivery line. During the exposure period, which was either one or two minutes, depending on the compound being administered, the spiral trap was heated with a hot air gun to aid in the volatilization of test compound. In-line after the nose cone trapping systems were installed to remove any radiolabel from the exhaust line.

Immediately after an exposure period, the restrainer was disconnected and the latex mask and O-ring removed. The glass restrainer containing the rat was then placed into a Capintec ionization chamber to determine the administered dose. After removal of the rat from the restrainer this portion of the exposure apparatus was again inserted into the ionization chamber to check for contamination. Any radioactivity associated with the restrainer would indicate a leak in the nose mask assembly and contamination of the exposed animal's fur.

Because of carbon-11's short half-life, time throughout the experiments was continuously monitored on stopwatches. Time zero for all of the animal studies was assigned to the end of the exposure period. At selected intervals

post-exposure the dose retained by the animal was similarly measured, the rat was killed and the organ distribution of the radiolabel determined. The expired breath of those animals living the longest post-exposure period was monitored for expired $^{11}CO_2$ by placing the rat into a 600 mL chamber (5.5 X 25 cm) immediately after determining the administered dose. Room air was pulled through the animal chamber at one liter per minute. In line between the animal chamber and the vacuum pump were: a two liter NaOH (2N) trap, a CO_2/moisutre trap (barium hydroxide lime), and a flow meter. The sodium hydroxide solution was continuously pumped through a fixed glass coil which was fitted into a Picker sodium iodide well counter. Data accumulation from the Picker counter was in ten second intervals and stored on magnetic tape for later computer analysis.

The compounds selected for study were: benzaldehyde (2), an aromatic aldehyde; octanal, an aliphatic aldehyde; and acrylic acid. The relatively short half-life of carbon-11, 20.4 minutes, necessitates production of the isotope and synthesis of the agent under study for each animal experiment. These individual syntheses resulted in some variation in the chemical yields and specific activities. All of the test compounds (3) were labeled in the carbonyl position and had approximately the following specific activities at the time of animal exposure: benzaldehyde, 7.4 mCi/μm; octanal, 2.7 mCi/μm; and acrylic acid, 5.0 mCi/μm.

Rats exposed to ^{11}C-labeled benzaldehyde for two minutes accumulated an average of 2.5 μg of this aldehyde with the uptake by the animal directly proportional to the amount in the gas chromatograph trap. The inhaled benzaldehyde was rapidly absorbed from the respiratory tissue and at 1.5 minutes post-exposure only 0.8% of the administered radiolabel was resident in the lungs. This aldehyde was quickly distributed to the well profused organs. The peak radioactivity in most of the viscera occurred at 1.5 minutes after exposure. Loss of radiolabel from most tissues was also quite rapid and in most cases paralleled removal of the radiotracer from the blood. The renal system was the obvious route of radiolabel elimination because the kidneys contained 17% of the administered activity at five minutes post-exposure. The excreted labeled compound co-chromatographed with a hippuric acid standard.

When rats were similarly exposed to carbon-11 labeled octanal they took up an average of 17.6 (s.e. $\pm$ 1.7) % of the octanal passing through the nose cone for an average dose of 3.2 μg per animal. For the first several minutes after exposure octanal was rapidly taken up from the lungs. The relative retention (radioactivity per gram of tissue/mean radioactivity per gram of entire animal) of the respiratory tract remained high throughout the post-exposure period.

Gamma emitting radiotracers permit non-invasive measurement of the radioactivity resident in the animal at any time after exposure. Such measurements appeared to be particularly useful when investigating compounds which were rapidly metabolized and eliminated. The information gained from these measurements became evident when the relative distribution and relative retention of tissues were compared (Figure 3). Inhaled octanal was rapidly metabolized, presumably by first being oxidized to the corresponding acid which by β-oxidation was then metabolized to acetyl coenzyme A. Because acetyl CoA is a substrate for a host of metabolic processes, the labeled carbon becomes available for elimination as $^{11}CO_2$ or incorporation into a variety of the biological molecules which may be distributed in a manner very different from the administered octanal. When the radioactivities of the organs were expressed relative to the administered dose, a general clearing was observed. However, when compared to the dose retained at the time of sacrifice the clearing trend became one of relative accumulation after approximately 20 minutes. Presumably this reflected, in part, the redistribution of the radiotracer as catabolic

products of the labeled octanal. The metabolism of octanal was also evidenced by the biphasic nature of $^{11}CO_2$ elimination from the exposed animals (Figure 4). The α phase of $^{11}CO_2$ elimination may reflect the most direct route of octanal to CO_2 while the β phase represents the metabolism of the array of biological compounds synthesized from the ^{11}C-coenzyme A mentioned above.

The mean retained dose of rats killed at 5, 12, 20, and 40 minutes post-exposure are also plotted in Figure 4. These fall very near the plotted $^{11}CO_2$ elimination curve, indicating that the expired breath accounted for essentially all of the radioactivity eliminated by the octanal exposed rats.

Immediately after nose exposure to gaseous ^{11}C-acrylic acid, 28% of the administered radiolabel was associated with the exposed animal's nose and bucal cavity. At 65 minutes after exposure this was reduced to 8% of the administered dose with at least part of the difference having been ingested. To assure total separation of the pulmonary and gastrointestinal routes of exposure, pento-barbital anaesthetized rats were administered ^{11}C-acrylic acid either as a gas via a tracheal cannula, thereby avoiding the bucal cavity, or in an aqueous solution injected directly into the stomach. Conscious rats were nose exposed to acrylic acid for one minute or stomach intubated. The expiration of $^{11}CO_2$ was the only major route of carbon-11 elimination and the rate was more dependent on the physical state of the animal than on the route of acrylic acid administration (Figure 5).

The results reported here indicate that ^{11}C is an excellent tracer for acute inhalation studies. Although the use of short-lived radioisotopes impose certain limitations, these are outweighed by the high specific activity of the synthesized compound and the ability to non-invasively quantitate the amount of radiolabel present in the exposed animal during the course of the experiment. The non-invasive monitoring of radiolabel appears to be particularly useful in studies where the administered compound is rapidly metabolized and eliminated. Extension of these non-invasive techniques to larger animals would allow resolution of the radiolabel in individual organ systems by means of a gamma camera. Such studies would allow continuous dynamic imaging of the radiolabel in the exposed animal. These techniques may also prove to be useful when inhalation studies are used to substantiate the disposition and metabolic fate of compounds which have only been administered via more convenient, although unrealistic methods; and for assessing the fate of compounds which might present themselves during accidental industrial accidents.

References

1. Christman, D. R., Finn, R. D., Karlstrom, K. I., and Wolf, A. P. (1975). Int. J. Appl. Radiat. Isot. 26, 435-442.

2. Kutzman, R. S., Meyer, G.-J., and Wolf, A. P. (1980). Xenobiotica (in press).

3. Tang, D. Y., Lipman, A., Meyer, G.-J., Wan, C.-N., and Wolf, A. P. (1979). J. Label. Cmpds & Radiopharm. 16, 435-440.

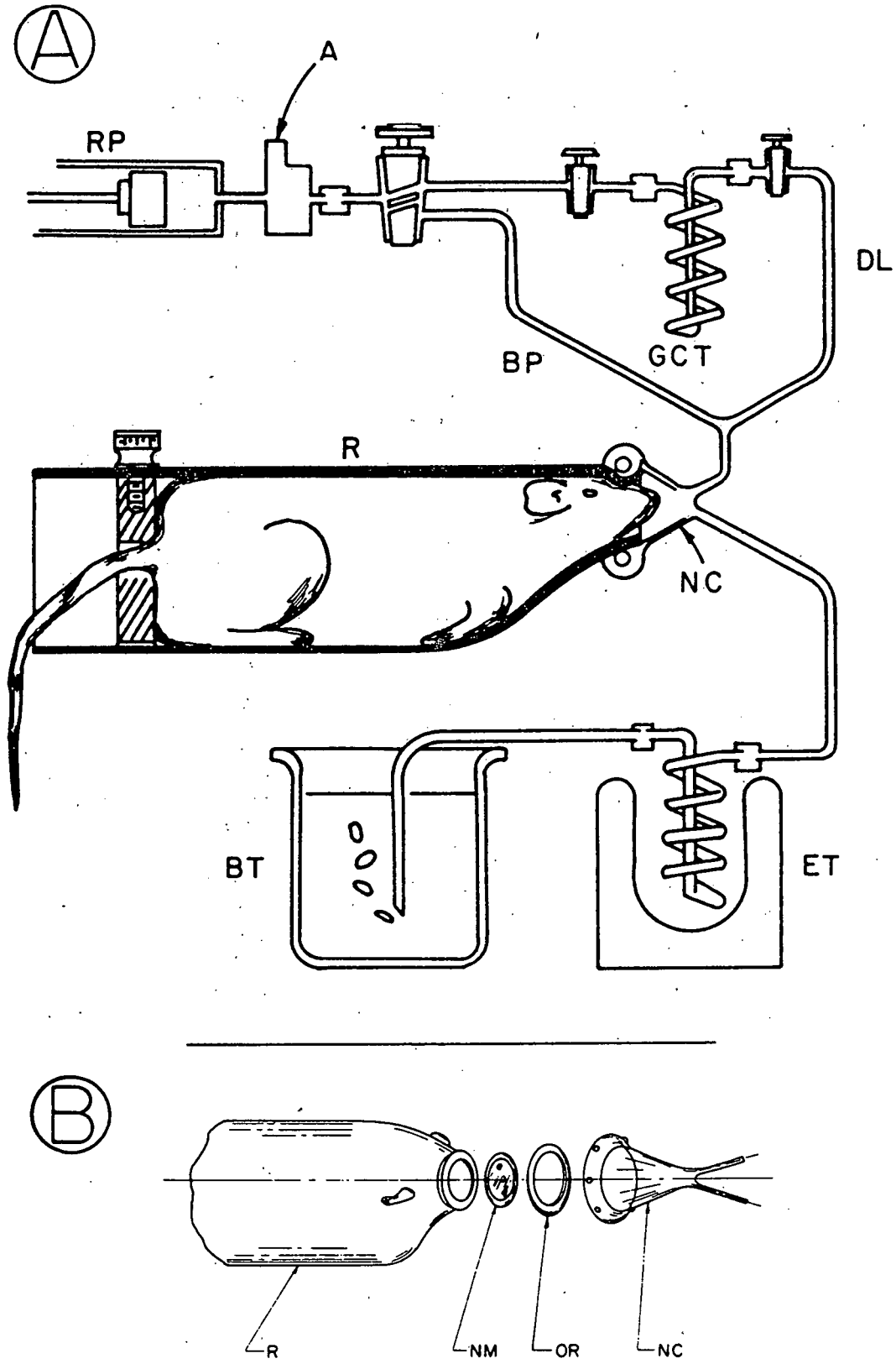


Figure 1. Schematic diagrams of (A) the exposure apparatus used to deliver radiolabeled volatile compounds to rats, and (B) the nose cone assembly of the exposure apparatus. A - air intake; BP - by-pass tubing; BT - bubble trap; DL - delivery line; ET - exhaust trap (cooled with dry ice/acetone); GCT - gas chromatograph trap; NC - nose cone; NM - nose mask, OR O - ring; R - restrainer; RP - respirator pump.

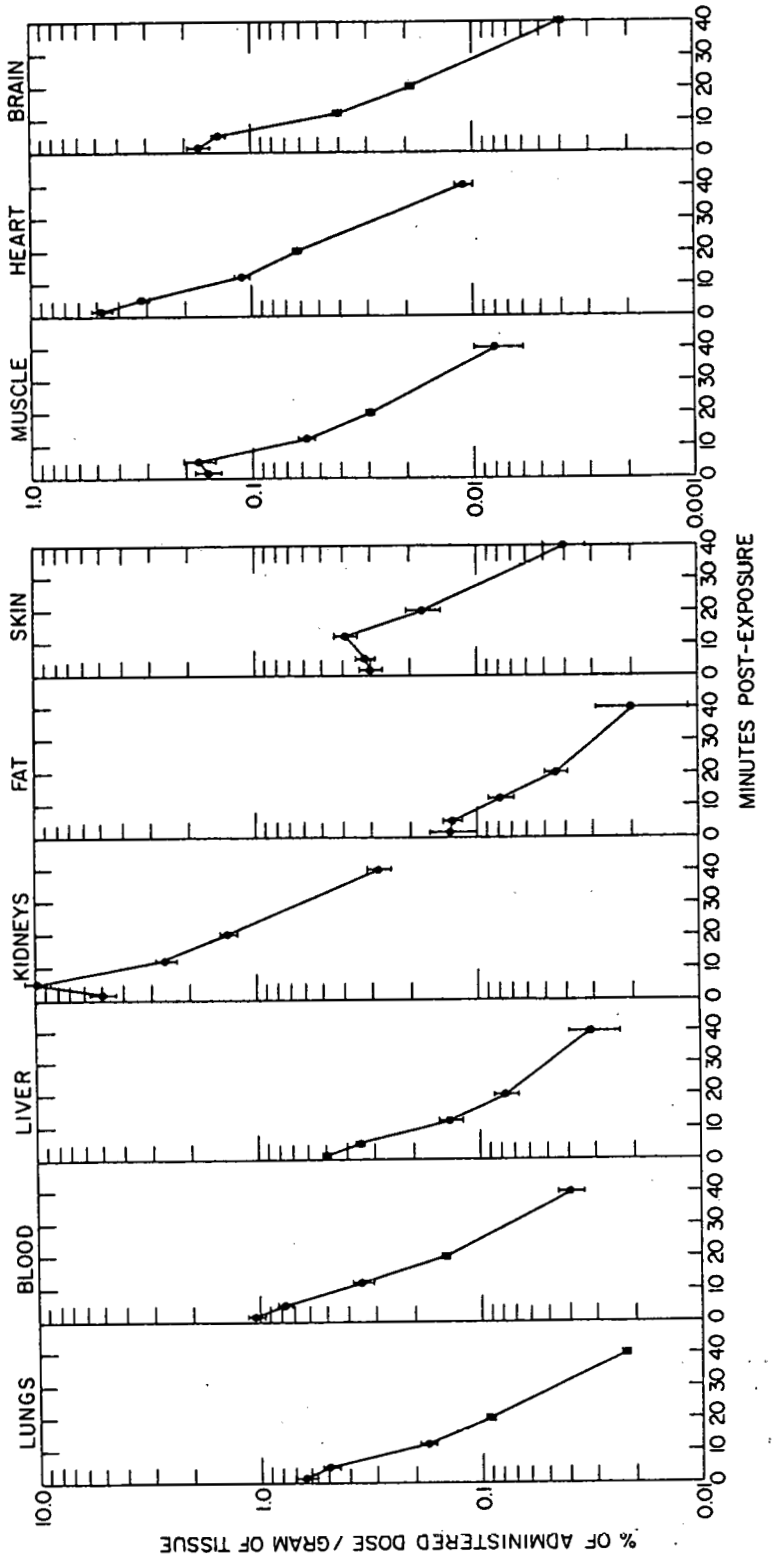


Figure 2. Tissue levels (% of administered dose/gram) of radiolabel at 1.5, 5, 12, 20, and 40 minutes post-exposure to ^{11}C-benzaldehyde. Each point represents the mean ± SE of five rats except the 40 minute skin data where n = 4.

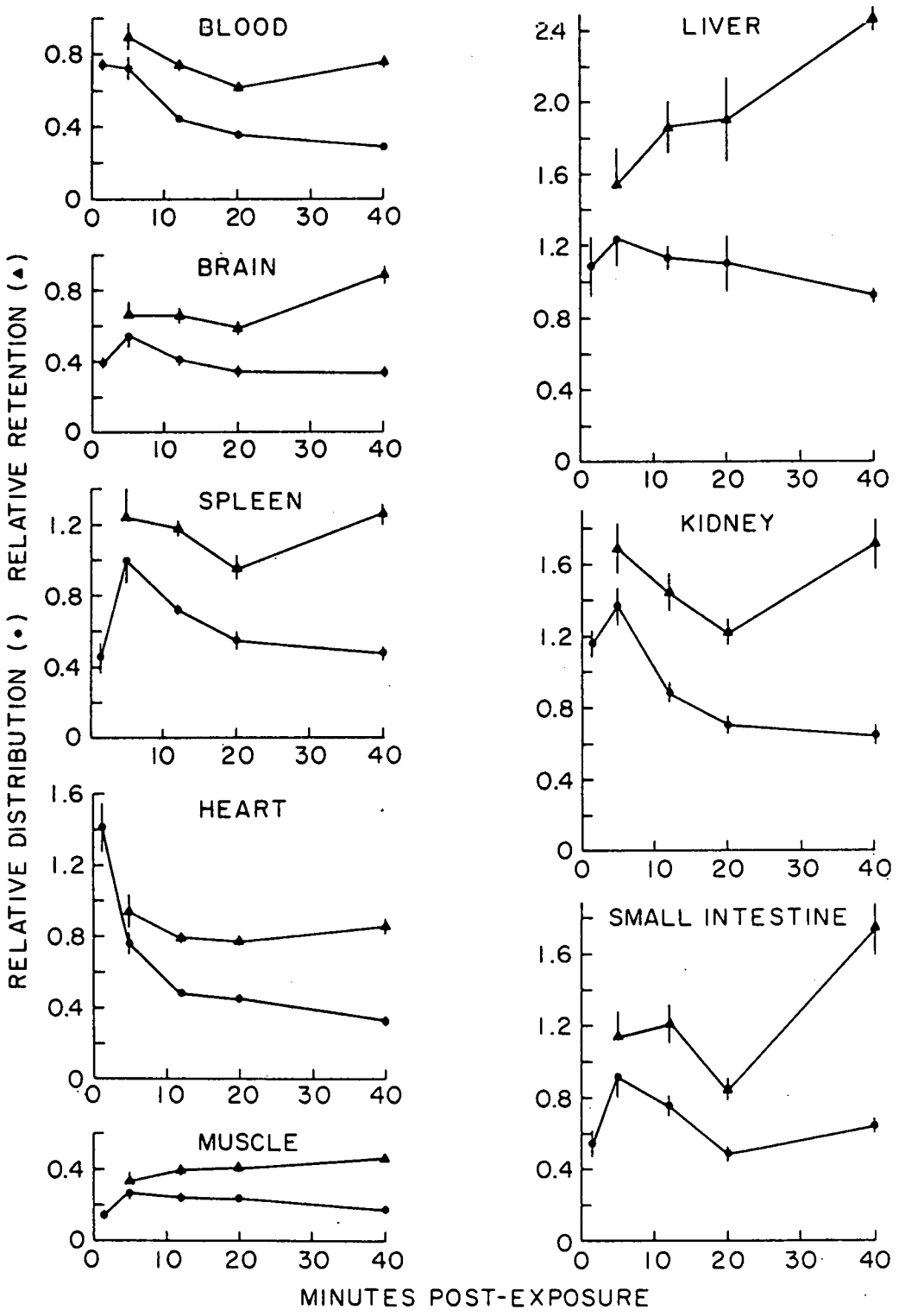


Figure 3. Relative distribution (•) and relative retention (▲) of radiolabel in the tissues of ^{11}C-octanal exposed rats with increasing time post-exposure. Each point represents the mean ± SE of at least five animals.

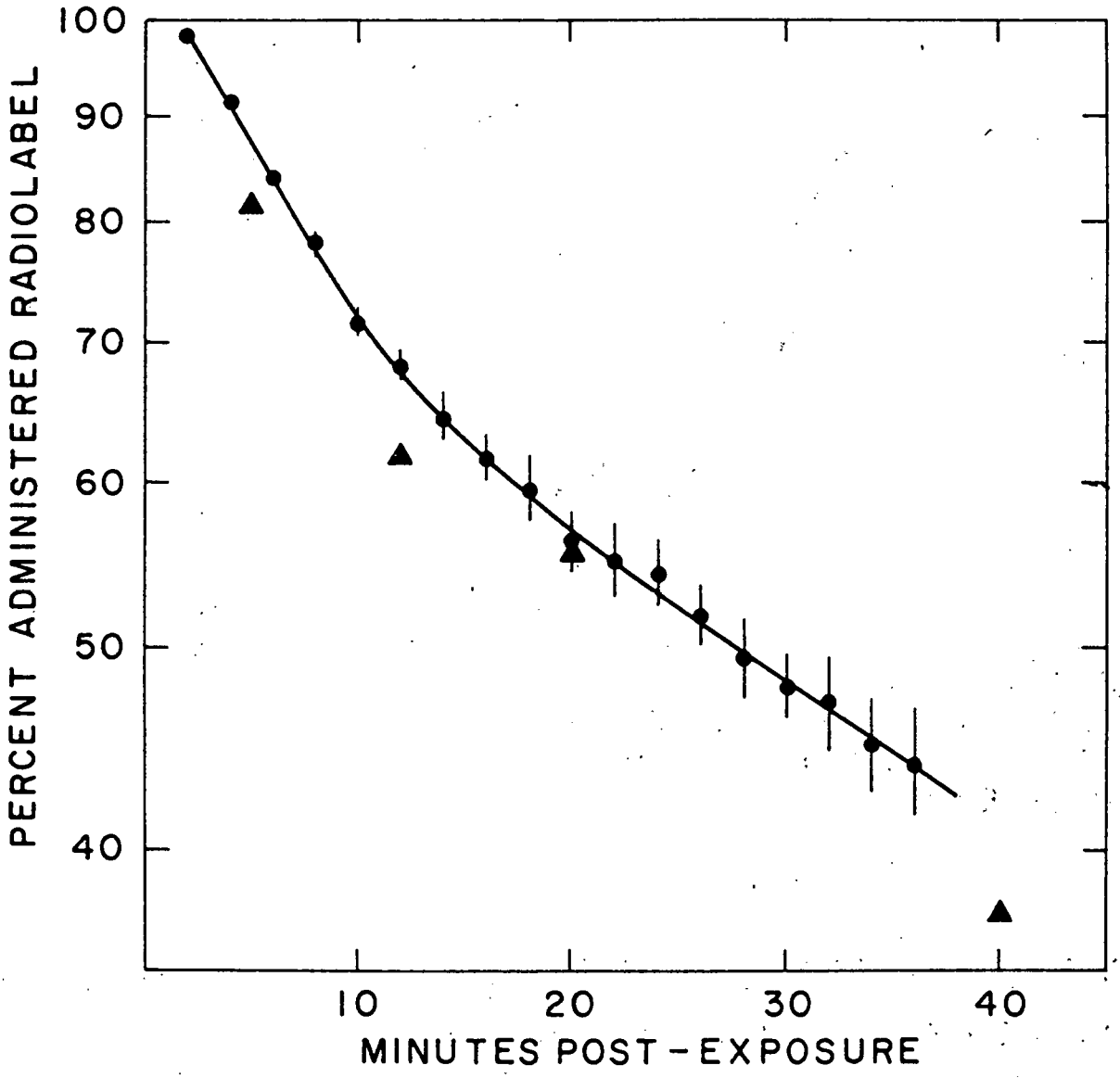


Figure 4. Elimination of radiolabel as $^{11}CO_2$ (•) in the expired breath of ^{11}C-octanal exposed animals (the lines indicate the standard error of five experiments). The mean percent of the administered radiolabel retained by the animals until sacrifice is also plotted (▲).

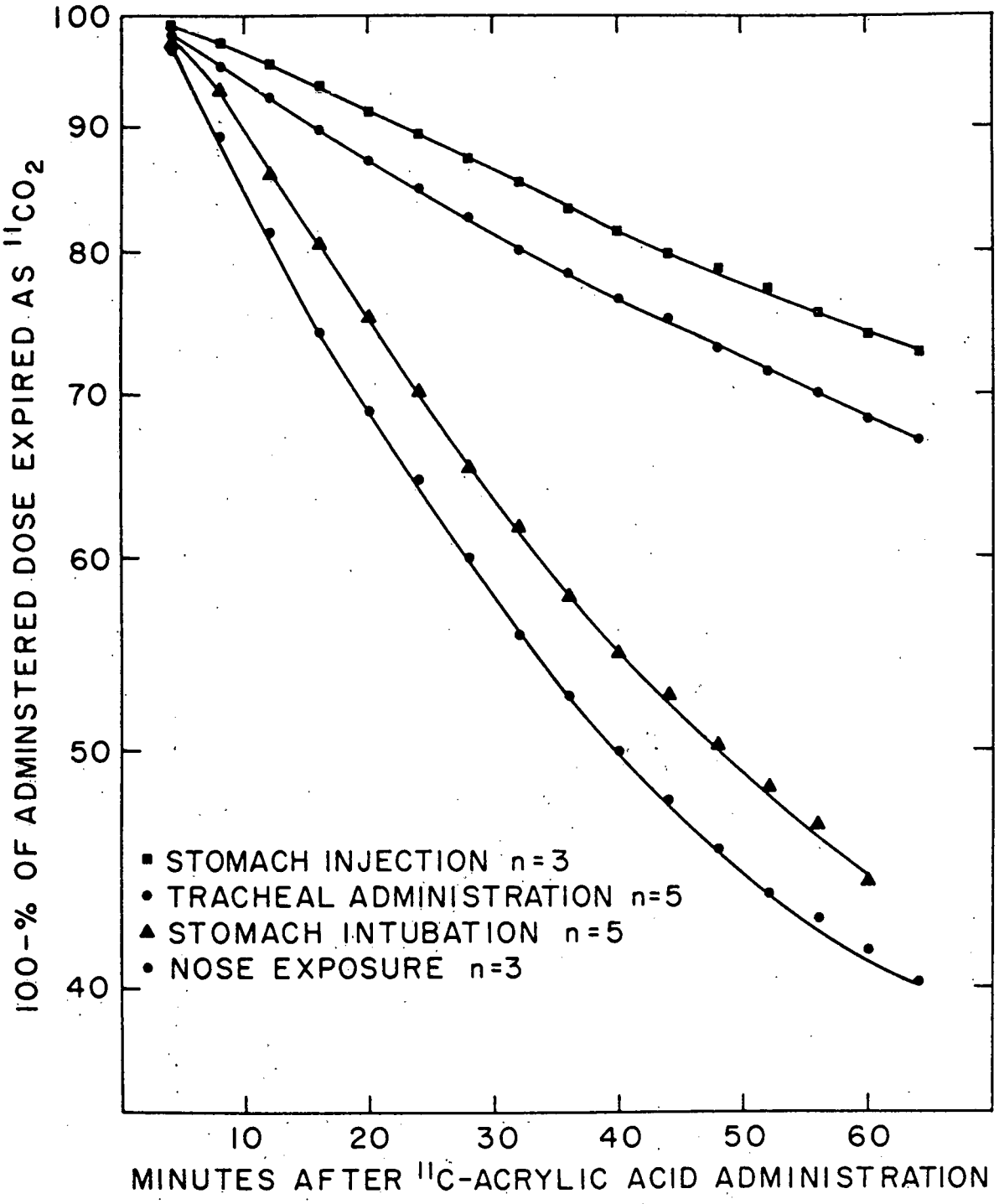


Figure 5. Elimination of radiolabel as $^{11}CO_2$ from rats after administration of ^{11}C-acrylic acid. Animals receiving ^{11}C-acrylic acid by stomach injection and tracheal administration were anaesthetized. Stomach intubated and nose exposed animals were concious.

APPLICATION OF PIXE AND INAA TO BIOLOGICAL MATERIALS : ANALYSIS OF SERUM AND SERUM ALBUMIN

W. Maenhaut[+], L. De Reu and U. Tomza[*]
Instituut voor Nucleaire Wetenschappen, Rijksuniversiteit Gent,
Proeftuinstraat 86, B-9000 Gent, Belgium

and

J. De Roose
Kliniek voor Heelkunde, Rijksuniversiteit Gent (A. Z.),
De Pintelaan 135, B-9000 Gent, Belgium

ABSTRACT

Particle-induced X-ray emission (PIXE) analysis and instrumental neutron activation analysis (INAA) were applied to study the trace element composition of human serum and serum albumin samples. Although most of the elements were present at a concentration level below a few μg/ml, up to 19 elements could be measured in some samples. The precision of the PIXE technique, as determined by analyzing up to 20 targets from one sample, was as low as 3% for those elements where counting statistics were good. A comparison between the PIXE and INAA results showed close agreement, indicating that PIXE can yield data which are accurate to within 10%. In the INAA procedure, the measurement of the elements with short- or medium-long-lived product radionuclides (half-life < 3 d) was seriously hampered by the presence of large ^{38}Cl and ^{24}Na activities. Those elements were normally better determined by PIXE. INAA on the other hand generally proved to be more sensitive than PIXE for the elements which were measured after 3-4 weeks cooling.

+ Research associate of the "Nationaal Fonds voor Wetenschappelijk Onderzoek" (Belgium)

* Permanent address : Institute of Physics, Silezian University, Katowice, Poland

INTRODUCTION

Neutron activation analysis has since long been recognized as a very powerful tool for the determination of trace elements in various samples. When applied to biological materials radiochemical separations are often necessary to obtain maximum sensitivity, but also on a pure instrumental basis (i. e. by INAA) several interesting elements can be measured. In the last five years also particle-induced X-ray emission (PIXE) has found increasing applications in the trace element characterization of biological samples. The major advantages of the PIXE technique are its multi-element capability and its high absolute sensitivity. Even in very small samples ($\sim$ 1 mg) several elements can be determined at the ppm or sub-ppm level.

In this work both INAA and PIXE were applied to study the trace element composition of some human serum and serum albumin samples. The goals of the study were threefold : a) To determine as many trace elements as possible by combining two sensitive analytical techniques ; b) To evaluate the precision and accuracy obtainable with PIXE ; and c) To assess the merits and shortcomings of PIXE and INAA in the analysis of those types of samples.

EXPERIMENTAL

Samples and specimen preparation

The human serum samples were obtained from two patients with haemochromatosis. The medical treatment of these patients includes phlebotomy so that a 400 ml quantity of blood per patient could easily be collected. Procedures described by Versieck et al. [1,2] were followed in taking the blood samples and in separating the serum. The serum was then freeze-dried for 72 h in a Leybold-Heraeus vacuum apparatus. The resulting powder, which represented about 9% by weight of the liquid serum, was homogenized by shaking overnight in a polyethylene container.

Albumin is a protein component of human serum, normally present at a concentration level of about 4 g/100 ml. It plays a role in keeping the blood volume constant and in maintaining the osmotic pressure in the blood vessels. A 20% (w/v) aqueous solution of human albumin is commercially available for the treatment of several diseases. In this work human albumin samples from five different European companies were analyzed. Prior to the analysis similar freeze-drying and homogenization procedures were applied as for the serum samples.

The homogenized freeze-dried material was used as such in the INAA procedure. For the PIXE analysis, however, it was redissolved and doped with silver as an internal standard. The doped liquid was normally obtained by dissolving 0. 1 g of powdered material in 1 ml of an aqueous $AgNO_3$ solution. Aluminized Mylar (thickness 0. 7 mg/cm^2 ; 10 μg Al/cm^2) was used as backing for the PIXE targets. Preliminary experiments with Formvar as a backing film had indicated that charging problems can occasionaly occur, even when the sample thickness does not exceed a few mg/cm^2. By using aluminized Mylar this charging problem was effectively eliminated. The targets were prepared by pipetting 10 μl (or exceptionally 30 μl for some serum targets) of the doped liquid onto an aluminized Mylar backing, which was previously mounted on a polyethylene target frame. The target frames were placed in an evaporation chamber and kept under vacuum for approximately 1 h. Adherence of the dried material was good so that no thin polymer film or glue had to be applied to fix it to the backing.

PIXE analysis

All PIXE analyses were carried out with 2.4 MeV protons. The proton beam was supplied by a compact isochronous cyclotron (CGR-MeV 520), slightly focussed by means of a quadrupole triplet and defined by a tantalum collimator and two carbon collimators. The diameter of the beam at the target was normally 4.5 mm ; only for the targets prepared with 30 µl doped liquid an 8 mm diameter beam was used. The targets were bombarded in vacuo and were therefore placed in a target holder, which made an angle of 67.5° with respect to the beam. Up to ten different targets could be placed in the target holder. After passing through the target the protons were collected in a Faraday cup for beam integration. The X-rays were detected with a 30 mm^2 x 3 mm Kevex Si(Li) detector, which was placed at a backward angle of 135°. The detector was introduced in the irradiation chamber via a side port and vacuum was ensured by means of O-rings around the detector end cap. The solid angle subtended by the detector was 12 msr. The detector's view was restricted to the irradiated target area by means of a cylindrical high-purity aluminum collimator. To cut down the high bremsstrahlung and X-ray intensity in the low-energy region a 660 µm thick Mylar absorber was interposed between target and detector. A Kevex 4525 P amplifier/pulse processor was used in conjunction with the detector. This unit includes a pulse pile-up rejector and live-time correction circuitry to account for the rejected pulses. The energy resolution (FWHM) obtained with the Kevex detector-pulse processor combination was 147 eV at 5.9 keV.

The spectra were accumulated with a Canberra Jupiter system comprising a S-80 multichannel analyzer, a Plessey Micro-1 (PDP-11/03 equivalent) microcomputer and a Plessey dual hard disk unit. Data accumulation was normally done for a preset charge of 40 µC. With a proton current of 50 nA, each analysis took about 15 min. A typical spectrum obtained for a serum target is shown in fig. 1. The PIXE spectra were analyzed for 18 elements (i.e. K, Ca, Ti, V, Cr, Mn, Fe, Ni, Cu, Zn, As, Se, Br, Rb, Sr, Mo, Cd and Pb) by means of an interactive non-linear least-squares fitting program. Details of this program are given elsewhere [3,4]. Fig. 2 shows a fit obtained for a human albumin spectrum.

Two types of standards were used to calibrate the PIXE set-up, i.e. thin mono-element standards obtained from Micromatter Co [5] and multi-element standards prepared in our institute [6]. At the beginning of each PIXE run a few standards were analyzed to check if no drifts or changes in the calibration had occurred. The reproducibility of these checks over several months was of the order of 1-2%.

The biological targets were approximately 4 mg/cm^2 thick and correction for matrix effects was therefore necessary. Two effects were taken into account : X-ray attenuation and proton energy degradation, leading to decreasing cross-sections. The correction factors f_i [7] calculated for the different elements were substantial, between 1.4 and 1.7. However, by using silver as an internal standard only the ratio between the correction factor for the element determined and that for silver (i.e. f_i/f_{Ag}) was needed. That ratio remained for all elements within the range 0.85-1.05.

Instrumental neutron activation analysis

The INAA procedure was similar to that described previously [8]. It involved two separate irradiations and counting of short- and long-lived product radionuclides. A total of 36 elements was looked for. The elements with short-lived products (^{24}Na, ^{27}Mg, ^{28}Al, ^{38}Cl, ^{49}Ca, ^{51}Ti, ^{52}V, ^{56}Mn, ^{66}Cu, ^{87m}Sr,

^{116m}In and ^{128}I) were measured after a 5 min irradiation at a thermal neutron flux of 2.6x10^{12} n.cm^{-2}.s^{-1}. Each sample, consisting of approximately 50 mg of freeze-dried material packed in a polyethylene vial, was irradiated together with a nickel flux monitor, which also served as monitor for the counting position. Sample and flux monitor were counted in identical geometry with a high-resolution Ge(Li) detector. The sample-detector distance was so chosen that the ADC dead-time was less than 20% for both sample and nickel monitor. Live-time correction uncertainties, which could arise from decreasing ADC dead-time during the measurement, were avoided by using a dead-time stabilizer [9, 10]. Errors caused by pulse pile-up losses remain reasonably small as long as the dead-time does not exceed 20%. Multi-element standard pellets were irradiated separately and a similar counting scheme as for the samples was used. The counting geometry for each standard pellet was identical to that of its flux monitor, but not necessarily the same as for the samples. Small differences in the counting position are indeed accounted for by normalizing to the nickel monitor. The standard pellets were prepared by pipetting known amounts from multi-element solutions onto Whatman 41 filter papers, which were dried and pressed into pellets in a die.

The elements with long-lived product radionuclides (^{42}K, ^{46}Sc, ^{51}Cr, ^{59}Fe, ^{60}Co, ^{65}Zn, ^{72}Ga, ^{76}As, ^{75}Se, ^{82}Br, ^{86}Rb, ^{99}Mo, ^{110m}Ag, ^{115}Cd, ^{124}Sb, ^{134}Cs, ^{131}Ba, ^{140}La, ^{141}Ce, ^{153}Sm, ^{152}Eu, ^{177}Lu, ^{187}W and ^{198}Au) were measured after a 32 h irradiation at a flux of 1-2x10^{12}n.cm^{-2}.s^{-1}. Standard pellets and samples were now irradiated together. The sample size was approximately 300 mg of freeze-dried material. NBS bovine liver (SRM-1577) or Bowen's kale powder [11] were also co-irradiated to test the accuracy of the standards and procedures used. Each sample was measured twice, first at 3-5 days and finally at 20-30 days after the irradiation.

All measurements of the short-lived radionuclides were done with a Philips Ge(Li) detector, having a 10.9% detection efficiency and an energy resolution of 2.0 keV at 1332 keV. The same detector and another larger Philips detector (efficiency : 14.2%, resolution 2.1 keV) were used to count the long-lived radionuclides. The Ge(Li) detectors were coupled to Intertechnique Didac 4000-channel analyzers, which were interfaced to a PDP-11/45 computer system. Spectral analysis and calculation of concentrations were done by means of Fortran computer programs [8, 12].

RESULTS AND DISCUSSION

The PIXE and INAA results for the two human serum samples are presented in Table I. All PIXE data in the table were obtained from targets made with 10 µl doped liquid. The uncertainties associated with the data are standard deviations and were calculated from the spread of the individual results for the different targets or subsamples analyzed. For several elements upper limits are reported. These upper limits were obtained according to criteria given by Currie [13, 14]: The net peak area was compared with a critical level L_C = 1.64 x (standard deviation of the net peak area). In case the area was smaller than L_C, the element was considered "not detected" and an upper limit (detection limit) equal to 2 L_C was adopted.

Although we looked for 36 elements in the INAA of the human serum samples, only 9 were actually observed : i.e. Na, Cl, Fe, Co, Zn, Se, Br, Rb and Cs. The analysis by means of short-lived radioactivities was so seriously hampered by the large ^{38}Cl and ^{24}Na activities that no other elements could be measured besides Na and Cl. In the first count after the long irradiation the γ-ray

spectrum was still dominated by the ^{24}Na activity, and to a lesser extent by ^{82}Br, so that only this latter element was measured. The most interesting INAA results were definitely obtained from the count after 3-4 weeks cooling. This last count yielded serum concentration data for Fe, Co, Zn, Se, Rb and Cs, and upper limits down to between ~ 0.1 and ~ 10 ng/ml were obtained for the other elements looked for. The upper limits can certainly be improved by increasing the irradiation time and the neutron flux, but it is very questionable if many more elements will be observed. Versieck et al.[2] irradiated ashed serum samples, corresponding to 100 mg of freeze-dried material, for 12 days at a thermal neutron flux of 10^{14} n. cm^{-2}. s^{-1}, but detected only Ag and Sc in addition to the elements seen in our procedure. For the determination of Cr a distillation procedure was adopted as the 320 keV peak of ^{51}Cr was strongly hindered by the ^{32}P bremsstrahlung, when using a pure instrumental approach.

Of the 18 elements looked for in the PIXE analysis eight (i. e. K, Ca, Fe, Cu, Zn, Se, Br and Rb), including three elements not detected by INAA, could be measured in the serum samples. Most of the elements which were not seen by PIXE were also not seen by INAA, as they had to be measured after the short irradiation or in the first count after the long irradiation. For those elements the PIXE technique yielded detection limits which were up to 400 times lower (i. e. for Sr) than were obtained by INAA. PIXE analysis of serum targets prepared with 30 µl doped liquid (and bombarded for 100 µC) resulted in detection limits which were about 40% lower than those reported in Table I. For the five elements, which were observed by both PIXE and INAA, the sensitivity was clearly superior in the INAA method, with iron being the exception. The PIXE and INAA data for these five elements are in close agreement, indicating that PIXE can yield data which are accurate to within 10%. The reproducibility of the PIXE analysis, as determined by analyzing up to 20 targets from one sample, appears to be very reasonable. Relative standard deviations down to 3% are obtained for those elements where counting statistics are good.

Tables II and III list concentrations measured for three of the five human albumin samples analyzed. Elements, not looked for in the PIXE technique and not observed by INAA in any of the samples, have their upper limits only reported in Table III (i. e. for albumin no. 5). Those elements had very similar upper limits for the other albumin samples. PIXE and INAA combined allowed to measure between 12 and 19 elements in the different samples and both techniques yielded a similar number of trace element concentration data. For albumin no. 2 for example, INAA results for 12 trace elements were obtained in addition to concentration data for Na and Cl, while PIXE analysis yielded data for 11 elements, four of which were not seen by INAA. The precision and accuracy of the albumin PIXE data appear to be as good as those observed for the serum data. The conclusions about the relative sensitivity of PIXE and INAA are also very similar to those drawn from the serum analyses. The elements with atomic number between 18 and 48 have normally lower detection limits in PIXE than in INAA if they have to be measured by means of their short-lived products or in the first count after the long irradiation. However, elements determined in the last count after the long irradiation generally show better sensitivity in INAA than in PIXE. For several elements with $Z > 50$, especially for some rare earth elements, INAA appears to have very low detection limits, but few of those elements are actually observed. From a biological point of view most of the elements with $Z > 50$ are of limited interest, so that PIXE yields practically the same amount of valuable information as INAA. Considering that a PIXE analysis takes about 15 min versus 4 weeks turn-around time for INAA it is clear that PIXE has several advan-

tages over INAA for trace analysis of biological samples, if the elements to be determined are present at levels above 0.1 ppm. For lower levels NAA is definitely superior, but radiochemical separations will be necessary to achieve maximum sensitivity.

ACKNOWLEDGEMENTS

The authors like to thank Prof. Dr. J. Hoste for his interest shown in this work. They are indebted to Dr. J. Versieck from the University Hospital (Gent, Belgium) for providing the serum samples and for stimulating discussions. The technical assistance of J. Cafmeyer, L. Vanballenberghe and G. Lemey is also gratefully acknowledged. This work was supported by the Nationaal Fonds voor Wetenschappelijk Onderzoek and by the Interuniversitair Instituut voor Kernwetenschappen.

REFERENCES

1. J. Versieck, A. Speecke, J. Hoste and F. Barbier, Z. Klin. Chem. Klin. Biochem., 11 (1973) 193
2. J. Versieck, J. Hoste, F. Barbier, H. Steyaert, J. De Rudder and H. Michels, Clin. Chem., 24 (1978) 303
3. P. Van Espen, H. Nullens and W. Maenhaut, in Microbeam Analysis 1979, ed. D. E. Newbury (San Francisco Press, San Francisco, 1979) p. 265
4. P. Van Espen, H. Nullens and F. Adams, Nucl. Instr. and Methods, 142 (1977) 243
5. J. M. Heagney and J. S. Heagney, Nucl. Instr. and Methods, 167 (1979) 137
6. J. Billiet, R. Dams and J. Hoste, X-ray spectrometry, in press
7. W. Maenhaut, L. De Reu, H. A. Van Rinsvelt, J. Cafmeyer and P. Van Espen, Nucl. Instr. and Methods, 168 (1980) 557
8. P. Schutyser, W. Maenhaut and R. Dams, Anal. Chim. Acta, 100 (1978) 75
9. J. Bartosek, G. Windels and J. Hoste, Nucl. Instr. and Methods, 103 (1972) 43
10. J. Bartosek, F. Adams and J. Hoste, Nucl. Instr. and Methods, 103 (1972) 45
11. H. J. M. Bowen, At. Energy Rev., IAEA, Vienna, 13, Nr. 3 (1975) 451
12. J. Op de Beeck and J. De Donder, INWG-CHEM-3 (1977), Internal Report, Institute for Nuclear Sciences, University of Ghent.
13. L. A. Currie, Anal. Chem., 40 (1968) 586
14. L. A. Currie, in X-Ray Fluorescence Analysis of Environmental Samples, ed. T. G. Dzubay (Ann Arbor Science, Ann Arbor, Michigan, 1977), Chapter 25.

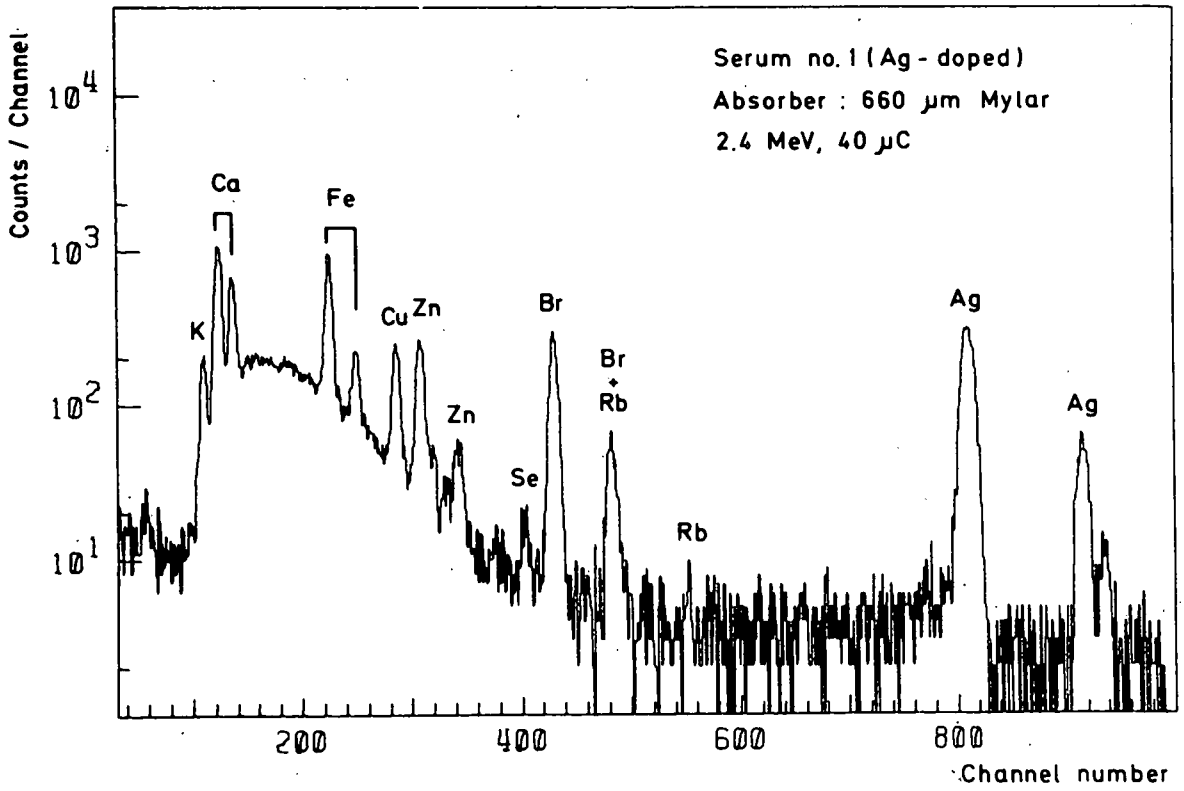


Fig. 1. PIXE spectrum of a human serum target

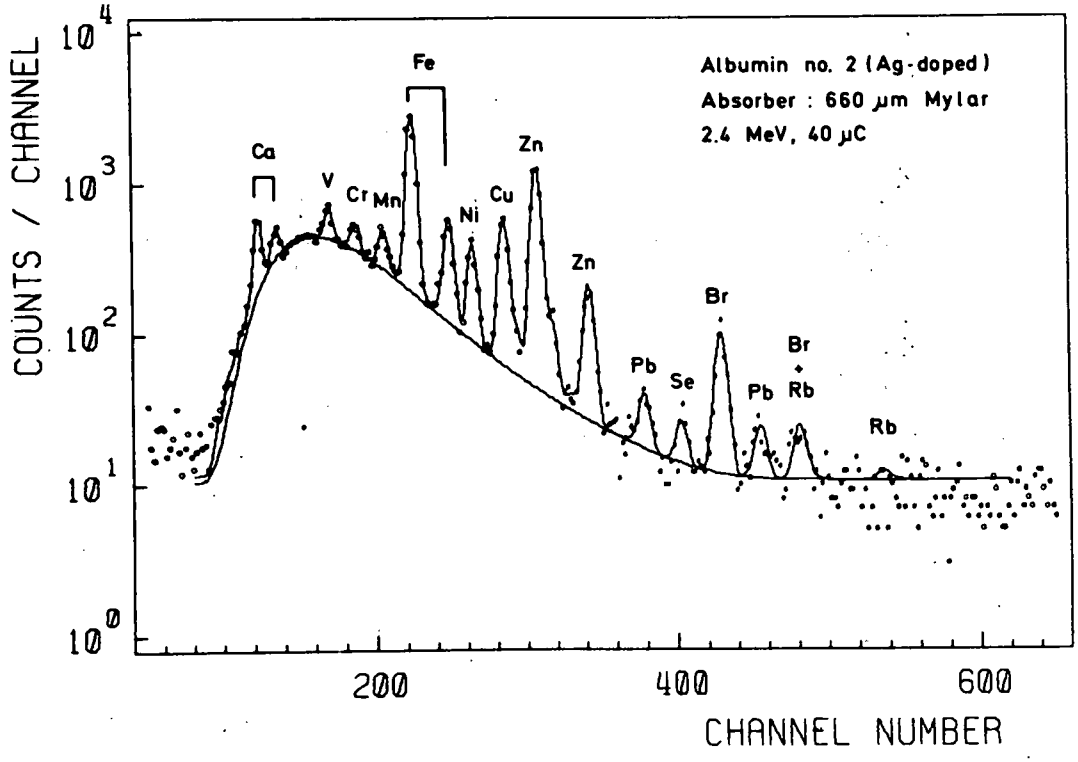


Fig. 2. Fit obtained for a human albumin spectrum. Fitted region : channel 80-620 ; open circles : data points, lower curve : background fit , upper curve : total fit.

TABLE I - Results (in $\mu g.\ ml^{-1}$) for the human serum samples

Element	Patient no. 1		Patient no. 2	
	PIXE (n=14)[a]	INAA (n=3)	PIXE (n=21)	INAA (n=3)
Na		3320±260		3210±270
Mg		<330		<340
Al		<2.9		<2.9
Cl		3490±210		3310±220
K	187±11	<370	170±20	<490
Ca	97±3	<304	92±5	<320
Sc		<0.00005		<0.00004
Ti	<0.4	<29	<0.4	<31
V	<0.22	<0.18	<0.23	<0.18
Cr	<0.15	<0.006	<0.14	<0.007
Mn	<0.09	<1.9	<0.09	<2.2
Fe	2.58±0.07	2.63±0.06	2.20±0.11	2.44±0.07
Co		0.0018±0.0001[b]		0.00231±0.00005[b]
Ni	<0.06		<0.06	
Cu	0.83±0.04	<15	0.84±0.05	<16
Zn	1.10±0.04	0.93±0.02	0.97±0.04	0.83±0.02
Ga		<3.8		<3.6
As	<0.04	<0.2	<0.04	<0.2
Se	0.123±0.020	0.132±0.006	0.088±0.022	0.081±0.002
Br	5.03±0.30	4.57±0.18	3.82±0.22	3.93±0.14
Rb	0.205±0.041	0.176±0.015	0.165±0.051	0.169±0.020
Sr	<0.10	<38	<0.11	<42
Mo	<0.3	<2.2	<0.3	<1.8
Ag		<0.001		<0.001
Cd	<0.8	<3.3	<0.8	<2.9
In		<0.02		<0.02
Sb		<0.0007		<0.0011
I		<1.2		<1.2
Cs		0.0016±0.0005		0.0011±0.0003
Ba		<0.18		<0.19
La		<0.07		<0.07
Ce		<0.006		<0.006
Sm		<0.011		<0.012
Eu		<0.0004		<0.0005
Lu		<0.0002		<0.0002
W		<0.43		<0.44
Au		<0.0001		<0.0001
Pb	<0.14		<0.14	

[a] n indicates the number of targets or samples analyzed

[b] These levels might be artificially elevated as the risk of extraneous Co additions during sample processing is extremely high

TABLE II - Results (in $\mu g.ml^{-1}$) for human albumin samples no. 1 and no. 2

Element	Albumin no. 1		Albumin no. 2	
	PIXE (n=10)	INAA	PIXE (n=7)	INAA
Na		2140±140 (6)[a]		2580±190 (5)
Al		<1.0 (6)		4.77±0.29 (5)
Cl		870±60 (6)		940±60 (5)
K	<36	<630 (2)	<31	<630 (2)
Ca	10.2±0.5	<94 (6)	22.5±1.3	<130 (5)
Sc		0.00092±0.00016 (2)		0.0042±0.0004 (2)
Ti	<0.4	<9 (6)	<0.4	<14 (5)
V	0.42±0.03	0.33±0.03 (6)	1.19±0.05	0.99±0.09 (5)
Cr	0.23±0.03	0.170±0.004(2)	0.35±0.04	0.28±0.02 (2)
Mn	0.19±0.04	<0.6 (6)	0.47±0.04	<0.5 (5)
Fe	2.66±0.16	2.26±0.09 (2)	5.44±0.17	5.2±0.2 (2)
Co		0.0226±0.0011(2)		0.0193±0.0011 (2)
Ni	0.067±0.009		0.68±0.02	
Cu	0.38±0.02	<4.5 (6)	1.48±0.04	<8 (5)
Zn	22.7±0.6	23.4±0.8 (2)	4.14±0.08	4.3±0.3 (2)
As	<0.07	<0.25 (2)	<0.08	<0.27 (2)
Se	0.19±0.04	0.202±0.011 (2)	0.17±0.02	0.178±0.013 (2)
Br	0.24±0.03	0.273±0.043 (2)	1.03±0.05	1.03±0.04 (2)
Rb	<0.16	<0.06 (2)	<0.15	<0.05 (2)
Sr	<0.16	<17 (6)	<0.15	<17 (5)
Mo	<0.4	<1.3 (2)	<0.4	<1.5 (2)
Ag		0.0087±0.0009 (2)		<0.005 (2)
Cd	<1.2	<2.2 (2)	<1.2	<2.5 (2)
Sb		<0.002 (2)		0.019±0.003 (2)
Ba		<0.54 (2)		1.4±0.5 (2)
Au		0.00020±0.00007 (2)		0.00048±0.00006 (2)
Pb	<0.27		0.57±0.04	

[a] Values between parentheses indicate the number of samples analyzed

TABLE III - Results (in $\mu g.\ ml^{-1}$) for human albumin sample no. 5

Element	PIXE (n=8)	INAA
Na		1830±100 (4)
Mg		<130 (4)
Al		34.8±1.4 (4)
Cl		1000±40 (4)
K	<33	<550 (2)
Ca	50.7±2.6	<110 (4)
Sc		<0.0001 (2)
Ti	<0.4	<11 (4)
V	<0.2	<0.06 (4)
Cr	<0.16	0.061±0.006 (2)
Mn	0.59±0.04	<0.8 (4)
Fe	0.52±0.04	<1.0 (2)
Co		0.0141±0.0014 (2)
Ni	0.47±0.04	
Cu	1.48±0.04	<6.3 (4)
Zn	1.03±0.04	0.96±0.02 (2)
Ga		<4 (2)
As	<0.07	<0.2 (2)
Se	0.098±0.022	0.112±0.004 (2)
Br	5.18±0.26	5.65±0.26 (2)
Rb	<0.17	<0.05 (2)
Sr	0.24±0.06	<16 (4)
Mo	<0.4	<1.0 (2)
Ag		<0.005 (2)
Cd	<1.1	<1.8 (2)
In		<0.006 (4)
Sb		<0.001 (2)
I		<0.4 (4)
Cs		<0.001 (2)
Ba		<0.3 (2)
La		<0.07 (2)
Ce		<0.01 (2)
Sm		<0.008 (2)
Eu		<0.001 (2)
Lu		<0.0004 (2)
W		<0.4 (2)
Au		<0.0002 (2)
Pb	<0.3	

IN VIVO MEASUREMENT OF CADMIUM IN AN OCCUPATIONALLY-EXPOSED POPULATION

K. J. Ellis, W. D. Morgan, S. Yasumura*, D. Vartsky, I. Zanzi and S. H. Cohn

Brookhaven National Laboratory, Medical Research Center,
Upton, N.Y. 11973 and *Dept. Physiology,
Downstate Medical Center, Brooklyn, N.Y. 11203

Research supported by DOE Contract No. DE-AC02-76CH00016 and the International Lead Zinc Research Organization

ABSTRACT

Exposure to cadmium is recognized as a potentially serious health problem. A number of clinical abnormalities have been observed in workers occupationally exposed to cadmium. Therefore, it is essential that accurate data on body burdens be available in order to formulate dose-response relationships in man. This report describes the present Brookhaven facility for in vivo measurements of cadmium in man and recent results from a field study to a cadmium production plant.

The cadmium content of the left kidney and concentration in the liver were measured by prompt-gamma neutron activation analysis in 82 occupationally exposed workers and 10 control subjects. Organ content ranged up to 57 mg in the kidney and up to 120 ppm in the liver for the industrial group. By contrast, the values for the control group ranged from 0.4 to 11.8 mg for the kidney and 0.7 to 7.9 ppm for the liver. The geometric means were 3.7 mg for the kidney and 2.7 ppm for the liver in the control group. When the data were analyzed to provide an estimate of the 'critical' concentration for the kidney, a range of 300-400 μg/g for the renal cortex was calculated. These results are compared with the available data in the literature.

INTRODUCTION

The exposure of man to cadmium is recognized as a potentially serious health problem. Both short- and long-term effects of occupational exposure to cadmium have been observed for many years (1-3). Cadmium has been suggested as a possible causitive agent of emphysema, osteomalacia, anaemia, kidney dysfunction and lung carcinoma (1-4). The total accumulation of cadmium in man is dependent on the level of exposure and biological half-life in the body. Once absorbed, the metal is non-uniformly distributed, concentrating primarily in the kidneys and liver. In a normal subject, the kidneys retain the largest absolute amount and also have the highest concentration.

Previously, data on the body burden of cadmium in man has been derived primarily from autopsy studies. The recent development of in vivo measurement techniques (5-8), however, has made it possible to evaluate the status of the active worker. The present report, therefore, describes the continuing improvement of a mobile facility used for the in vivo measurement of kidney and liver cadmium. Preliminary results from a recent field study involving occupationally-exposed workers at a cadmium production plant are also included.

INSTRUMENT AND METHODS

In vivo measurements of small quantities of cadmium in man can be performed by prompt-gamma neutron activation analysis (PGNAA). A detailed discussion of the basic physics of PGNAA can be found in previous publications (5,7). This paper describes modifications and improvements of the original instrument reported at the 1977 Conference (9). These changes include (1) improved shielding, (2) Fe collimator, (3) two 24% Ge(Li) detectors, and (4) reduced organ to detector distance.

A cross-sectional view of the present instrument is shown in Fig. 1. The 78Ci ^{238}PuBe neutron source (2.2×10^8 n/sec) is housed in a 1m x 1m x 0.6m shield constructed mainly of polyethylene bricks doped with Pb and B. An additional 10 cm of Pb covers the shield, except for the area directly below the Ge(Li) detectors which has a 10 cm layer of polyethylene (Pb,B doped) and a 10 cm layer of Bi. No gamma shielding was provided above or to the sides of the detectors which were at the level of the bed. A 1.8 cm thick cap of paraffin (^{6}LiF doped) covered the detectors as an added shield against thermal neutron capture in the detectors.

The collimator opening at the top of the shield was 10 cm x 16 cm and the PuBe source was 59.2 cm below the bed. A 5.1 cm layer of Fe surrounds the source and lines the walls of the collimator. Iron was found to be the best choice of materials for reducing the mean energy of the neutrons by inelastic scattering and therefore increased the probability of capture in the polyethylene shield. The detection system consists of two 24% Ge(Li) detectors positioned approximately 18 cm from the center of the collimator. The signals from the detectors are amplified, passed through an ADC, and stored on magnetic tape for subsequent analysis of the energy region containing the 559keV gamma-ray peak from cadmium.

It is obviously important not only to accurately locate the kidney or liver within the neutron beam (see Fig. 1) but to also have information on its depth within the body. These parameters are vital since the composite sensitivity of the measurement (defined as counts/mg/rem) is dependent on (1) thermal flux distribution within the body, and (2) attenuation of the prompt 559keV gammas.

A series of measurements, therefore, were performed to evaluate the effects of body size on the composite sensitivity of the present instrument.

The calibration curves for different kidney positions are shown in Fig. 2. The posterior depth of the kidney is defined as the z-axis and the lateral depth as the x-axis. As can be seen from Fig. 2, the relative sensitivity for a heavier subject is considerably reduced when compared with a leaner subject. For example, the relative sensitivity at x = 8 cm and z = 6 cm is approximately one-half the value at x = 5 cm and z = 4 cm. These two possibilities are representative of a heavier and average sized subject, respectively. Hence it becomes quite evident that an essential requirement for accurate in vivo measurements of body stores of cadmium is to know the location of the target organ within the body. Therefore, an ultrasonic scan of the lower abdomen is employed to locate the liver and left kidney and to assist in positioning the subject properly in the neutron beam.

The levels of cadmium in the liver are expressed as ppm, as the cross-sectional area of the beam is less than the cross-sectional area of the liver. As the kidney fits within the dimensions of the neutron beam, the total amount of cadmium (in mg) in the kidney is obtained. The dose rate (neutrons and gammas) at the level of the bed is $\sim$0.85 rem/hr (quality factor = 10). The sensitivity of the facility is 444 counts/mg/rem for cadmium in the kidney and 269 counts/mg/rem for cadmium in the liver of an Alderson phantom. For a maximum measurement time of 2000 sec, the dose is $\sim$0.5 rem with a cadmium detection limit (2 SD above background) of 2.2 mg for the kidney and 1.5 μg/g for the liver.

The Alderson phantom was used to determine the interference between the kidneys and liver. The original BNL system was found to have minimum cross-interferences (9). The present facility, however, had cross-interferences between the two organs. The major contributions were: (1) 21% interference from the liver to the left kidney; (2) 9% interference from the right kidney to the left kidney; and (3) 24% interference from both kidneys to the liver. The net counts in each worker's in vivo measurements were adjusted for these contributions. Further investigations have indicated that these cross-interferences were attributable, in part, to the absence of shielding to the sides and above the detectors and to the shorter distance between the organ and detectors.

RESULTS AND DISCUSSION

The first field study involved the in vivo measurement of kidney and liver cadmium in 92 adult males. The industrially exposed group consisted of 82 employees ranging in age from 18 yrs to 85 yrs and work histories from 6 weeks to 45 years. The relationship between kidney cadmium (mg) and liver concentration (ppm) for the industrial workers is shown in Fig. 3. The data points are grouped according to years of employment. The kidney data ranged from 0.9 mg to 57 mg, while liver concentrations ranged from 0.8 ppm to 120 ppm. The seven workers with kidney cadmium levels above 40 mg had been employed at the plant more than 10 years. Forty-two percent (35 workers) had kidney cadmium values greater than 20 mg. No retired workers or active laborer with more than 20 years of employment had a kidney content above 35 mg. The majority of these workers had kidney cadmium values in the 20-30 mg range except for those with liver concentrations above 60 ppm. In general, the kidney content increased with increasing liver concentration until approximately 40 ppm is reached in the liver. As the liver concentration continues to increase further, the kidney cadmium level shows a decrease.

The bi-phasic response between kidney and liver Cd is described by the dashed line in Fig. 3 which is based on a two-component linear model fit to the data. The kidney cadmium value at the 'breakpoint' is 31±9 mg; the associated liver concentration is approximately 35 ppm.

It was difficult to identify an individual worker with any one specific operation at the plant since the limited work force required rotation of the workers among different operations on a routine basis. The total work force, however, was divided into three major categories: laborers (40 active, 21 retired), office workers (8 active, 4 retired), and miscellaneous workers (3 active, 6 retired). The laborers worked in areas of the plant directly involved in the processing of cadmium. The office employees (accountants, clerks, chemist, and management personnel) and miscellaneous workers (machinists, mechanics, security guards, metallurgist) had limited exposures to cadmium. Most of the employees in the miscellaneous group, however, had significant prior work histories as laborers.

The kidney and liver cadmium data had a log-normal distribution, therefore, the mean values were calculated as geometric means and geometric standard deviations. The mean kidney and liver cadmium values by job classification (laborer, office, miscellaneous) and employment status (active vs retired) are given in Fig. 4. The mean kidney cadmium levels for the three occupational groups of active workers were 17.6 mg (laborers), 5.2 mg (office) and 32.4 mg (miscellaneous). The retired workers had mean kidney values of 18.6 mg (laborers), 6.9 mg (office) and 34.4 mg (miscellaneous). The associated liver concentrations were 21.8, 9.3, and 46.5 ppm for the active groups and 38.1, 5.7, and 34.4 ppm for the retired groups, respectively. By contrast, the 10 males in the control group had mean cadmium values of 3.7 mg for the kidney and 2.6 ppm for the liver. These data are in agreement with previous findings for a non-occupationally exposed population (10). In general, there is little difference in the mean kidney and liver cadmium data between the active and retired workers. However, when compared with the control group, the mean kidney and liver values for the office workers were approximately 1.5 to 3 times higher. These differences are even greater for the laborer and miscellaneous categories, ranging from 5 to 9 times higher for the kidney and 8 to 15 times higher for the liver.

The levels of kidney cadmium were also examined in terms of years of employment or retirement (Table I). The average values for laborers with less than 5 yrs employment and for office workers did not differ significantly from the values of the control group. The kidney cadmium value reached a maximum of 30.2 mg in the 5-10 year employment group and remained relatively constant thereafter. Similarly, the mean cadmium level in the liver reached a peak by 10 yrs of industrial exposure, also with insignificant variations thereafter (11).

Further comparisons were based on the kidney cadmium data and urinary levels of β_2-microglobulin. The concentration of β_2-microglobulin (low molecular protein) can be expected to increase in the urine as an early indicator of renal tubular damage. The use of urinary β_2-microglobulin (Uβ-2), therefore, has been proposed as a monitor to assess the renal status of a worker. The relationship between Uβ-2 and kidney cadmium in the present industrial population is shown in Fig. 5. The Uβ-2 data were grouped into three regions: Region I (Uβ-2<400 μg/l), Region II (400 μg/l<Uβ-2<3600 μg/l), and Region III (Uβ-2>3600 μg/l). Uβ-2 values in Region I are within the normal range although kidney cadmium values range up to 57 mg. In Region III, where the Uβ-2 values are significantly elevated above normal (presumably representing an advanced state of proteinuria), the kidney cadium values are generally below 30 mg. Twelve of the workers in Region III also had either elevated serum creatinine or elevated plasma β_2-microglobulin levels (indicates of renal glomerular damage). The 10 workers in Region II can be separated into two groups. The five workers with higher kidney cadmium values had ratios of kidney cadmium to liver concentration similar to the value for workers in Region I. The remaining five workers in Region II had low kidney cadmium values and kidney to liver ratios that would associate them with Region III. Three of these workers also had abnormally high serum creatinine

levels. We propose that the five workers in Region II with the higher kidney cadmium burdens and normal kidney/liver ratios represent an early transitional phase from Region I to Region III before significant cadmium is lost from the kidney. The five workers in Region II with low kidney/liver ratios may represent a prolonged moderate state of proteinuria without excessively elevated Uβ-2 values yet significant lost of cadmium from the kidney. It is important to note, however, that the two subgroups within Region II can be separated solely on the basis of their kidney data and value of the kidney/liver ratio. The five workers in Region II with the higher kidney values have an average kidney content near 32 mg cadmium.

An alternative method of estimating the range of kidney cadmium values associated with normal renal function was based on the kidney data for laborers in only Region I (i.e. normal Uβ-2 levels). The cumulative frequency distribution of kidney cadmium data for the laborers in Region I indicates 38 to 42 mg for the 90th to 95th percentiles. That is, 90 to 95 percent of the workers with normal kidney function (as judged by Uβ-2 levels below 400 μg/l) could be expected to have kidney cadmium burdens below 38 to 42 mg (11). This range, therefore, may be regarded as an upper limit for the critical level in the kidney.

CONCLUSIONS

The accumulation of cadmium in man due to industrial exposures has been determined by an *in vivo* activation technique. These data along with clinical indices of kidney dysfunction have been used to estimate the critical level of cadmium in the kidney. In all cases this critical value would appear to be greater than 30 mg. Although the cadmium content of the whole kidney was measured, the renal cortex concentration was calculated for comparison with data available in the literature (Table II). The WHO Task Group (12) reported a range of 100 to 300 μg/g for the renal cortex, based on autopsy and biopsy data from humans. Nomiyama (13), however, has pointed out that a majority of these subjects had clear evidence of proteinuria and, therefore, presumably had lost significant amounts of cadmium from the kidney. The only other *in vivo* data reported is that of Roels et al (14) where 200-250 μg/g is the estimated range. Our data would indicate 300-400 μg/g for the renal cortex and is in general agreement with the 380-470 μg/g range observed by Nomiyama et al (15).

The importance of an accurate estimate of the critical concentration for the renal cortex is more than an academic issue. For example, the standards for air quality in the work place are calculated on the basis of an allowable body burden. Also, the Swedish Government recently banned cadmium products based, in part, on the WHO recommendation of 200 μg/g as the critical value. The wide range of values presented in Table II would indicate that further studies must be made to evaluate the dose-response relationship in man. These studies should include environmental exposures of the general population and different industrial exposure conditions.

REFERENCES

1. Friberg, L., Piscator, M., Nordberg, G.F., Kjellstrom, T. Cadmium in the environment, 2nd Edition, Cleveland: CRC Press Inc., 1974.

2. Friberg, L. Proc. Int. Cong. Ind. Med. 9, 641, 1948.

3. Kazantzis, G., Flynn, F.I., Spawazi, J.S., Trott, D.G. Q. J. Med. 32, 165, 1963.

4. Criteria (Dose/Effect Relationships) for Cadmium. Comm. of the European Communities, Health and Safety Directorate. New York: Pergamon Press, 1978.

5. McLellan, J.S., Thomas, B.J., Fremlin, J.H., and Harvey, T.C. Phys. Med. Biol. 20, 88, 1975.

6. Evans, C.J., Cummins, P., Dutton, J., Morgan, W.D., Sivyer, A., Ghose, R.R. Nuclear Activation Techniques in the Life Sciences. IAEA, Vienna, 1979, p. 719.

7. Vartsky, D., Ellis, K.J., Chen, N.S., and Cohn, S.H. Phy. Med. Biol. 22, 1085, 1977.

8. Krauel, J.B., Speed, M.A., Thomas, B.W., Baddeley H., and Thomas, B.J. Int. J. Appl. Radiat. Isotopes 31, 101, 1980.

9. Vartsky, D., Ellis, K.J., Chen, N.S., and Cohn, S.H. Third International Conference on Nuclear Methods in Environmental and Energy Research, Columbia, Missouri, 1977, p. 639.

10. Ellis, K.J., Vartsky, D., Zanzi, I., Cohn, S.H., Yasumura, S. Science 205, 323, 1979.

11. Ellis, K.J., Morgan, W.D., Yasumura, S., Zanzi, I., Vartsky, D., and Cohn, S.H. J. Toxicol. Environ. Health (in press).

12. WHO Task Group. Environmental Health Criteria for Cadmium. Geneva: World Health Organization, 1975.

13. Nomiyama, K. J. Toxicol. Environ. Health 3, 607, 1977.

14. Roels, H., Bernard, A., Bucket, J., Goret, A., Lauwerys, R., Chettle, D., Harvey, T., Al Haddad, I. Lancet I, 221, 1979.

15. Nomiyama, K., Nomiyama, H., Nomura, Y., Taguchi, T., Matsui, K., Yotoriyama, M., Akahosi, F., Iwao, S., Koizumi, N., Masaoka, T., Kitamura, S., Tsuchiya, K., Suzuki, T., and Kobayaski, K. Environ. Health Perspect. 28, 223, 1979.

Table I. Relationship of Kidney Cadmium with Occupation and Years of Employment or Retirement.

	Years[a]	No. of Workers (n)	Kidney Cadmium[b] (mg)	p-value, workers vs controls (p)
Controls	-	10	3.7(2.9)	
Active Workers				
Office	1-25[d]	8	5.2(1.5)	n.s.
Laborer	<1	8	5.0(1.7)	n.s.
	1-5	2	16.7(1.1)	n.s.
	5-10	2	30.2(1.2)	<.05[c]
	10-15	9	24.9(1.9)	<.05
	15-20	8	24.5(1.7)	<.05
	>20	11	23.9(1.7)	<.05
Retired Workers				
Office	1-20[d]	4	6.9(1.5)	n.s.
Laborer	<5	12	25.8(1.6)	<.02
	5-10	7	13.7(1.7)	n.s.
	>10	2	10.6(5.2)	n.s.

[a] years of employment or retirement

[b] geometric mean (geom. SD)

[c] t-test, log-normal dist.

[d] All office workers

Table II. Comparison of Different Estimates of Critical Cadmium Concentrations in Kidney Cortex

Range of Critical Concentrations of Cadmium in Kidney Cortex* (µg/g)	References and Methods of Assessment
100-300	WHO Task Group (Autopsies, biopsies; human)
200-250	Roels et al. (In Vivo Activation; human)
380-470	Nomiyama et al. (Autopsies; monkeys)
300-400	PRESENT STUDY (In Vivo Activation; human)

* Assumes kidney weight of 145gm and a cortex cadmium concentration 1.5 times that of the whole kidney.

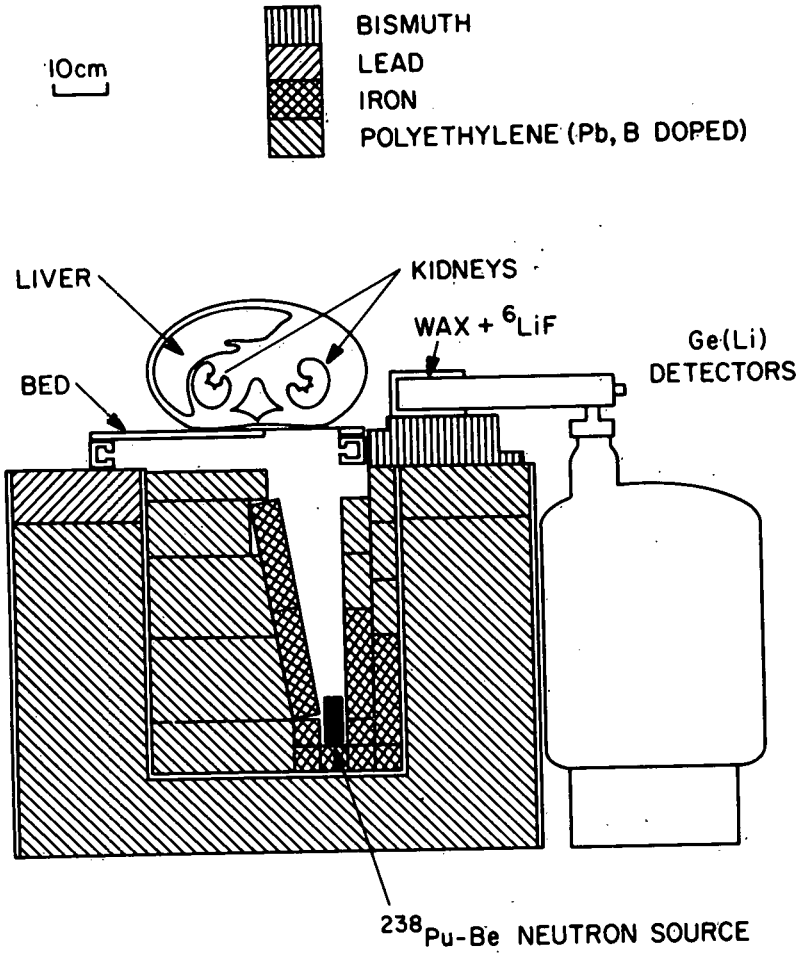


Fig. 1. Cross-Sectional View of In Vivo Measurement Facility.

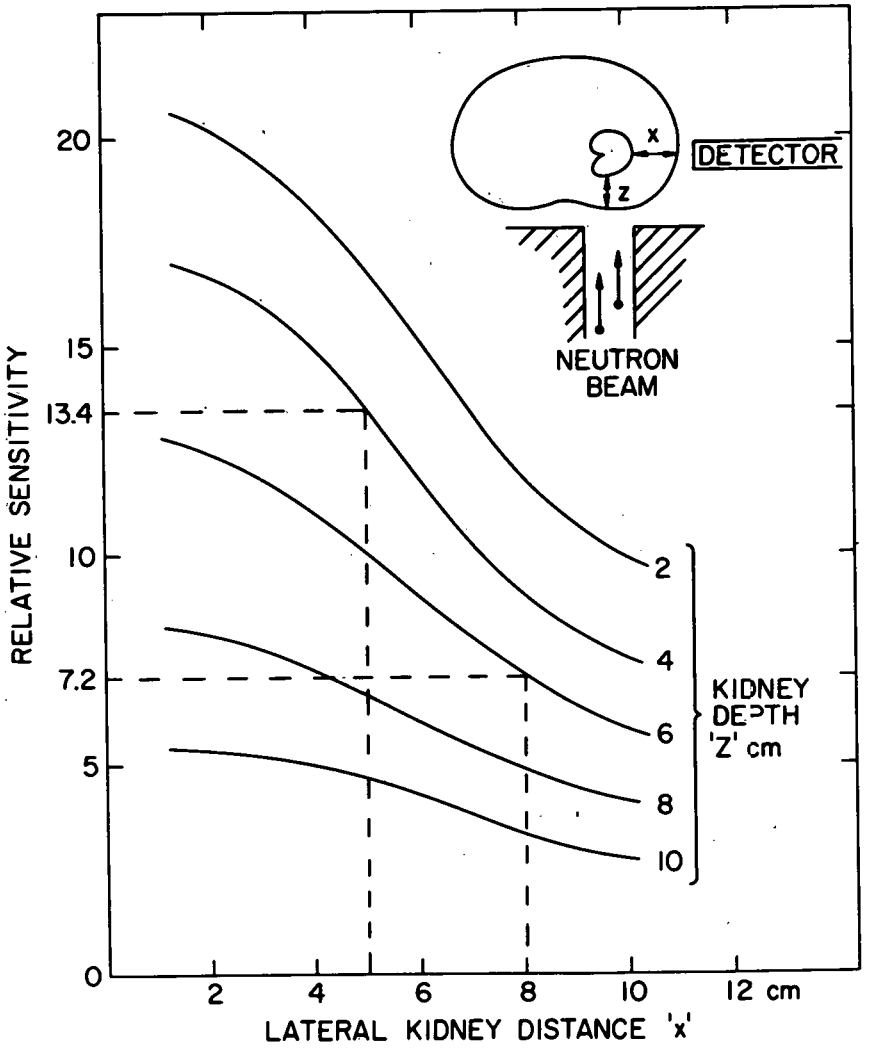


Fig. 2. System sensitivity curves for different kidney positions within the body.

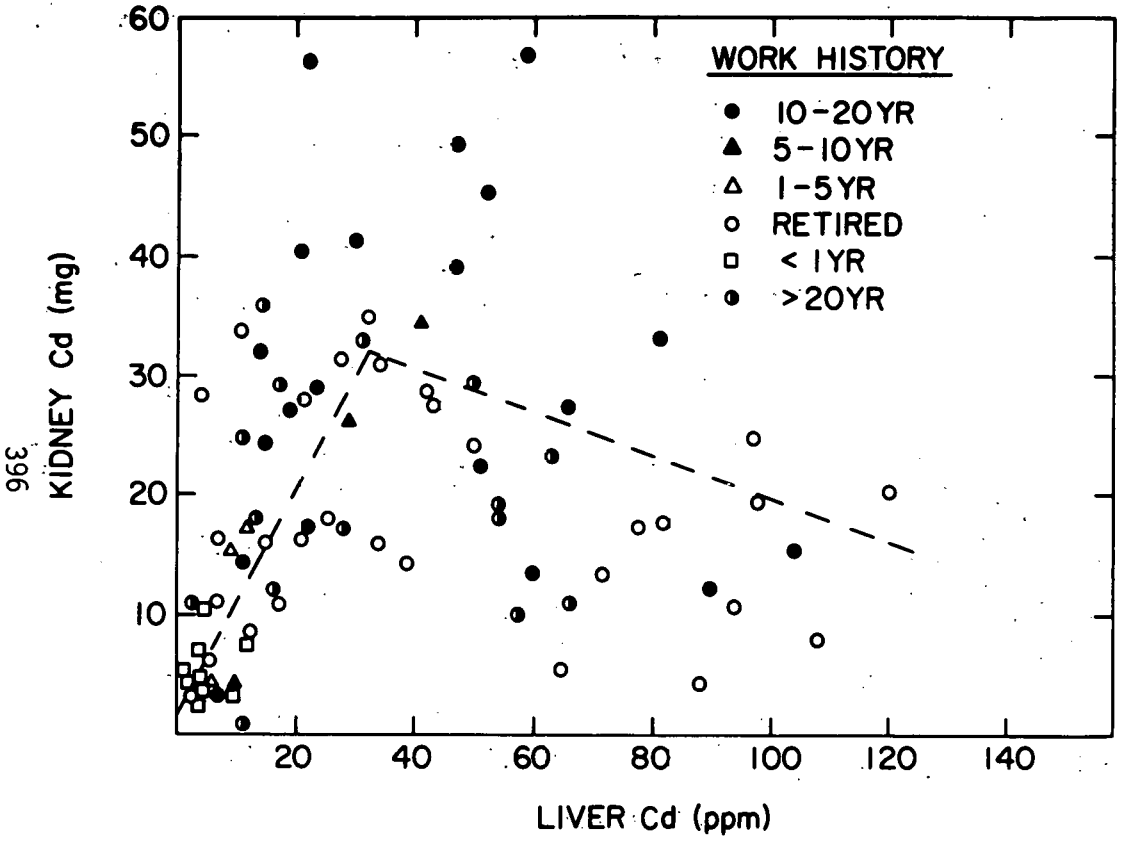


Fig. 3.. Relationship between kidney Cd (mg) and liver Cd (ppm) for industrial workers. The dashed line represents a two-component model fit to the data.

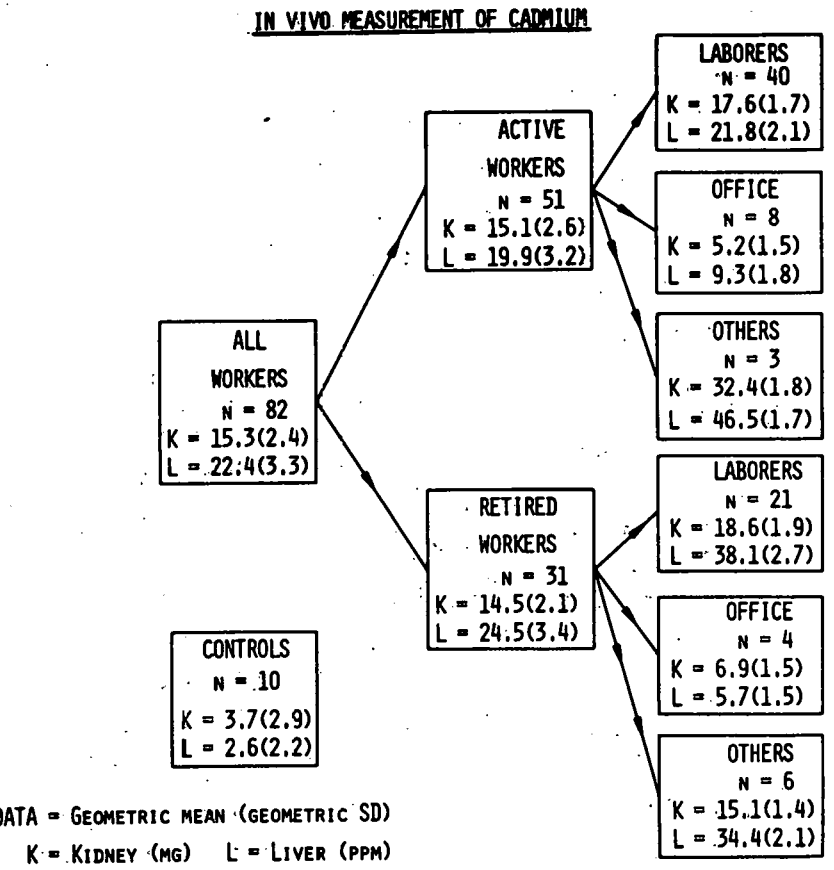


Fig. 4.. Mean kidney and liver cadmium values for different occupational catagories.

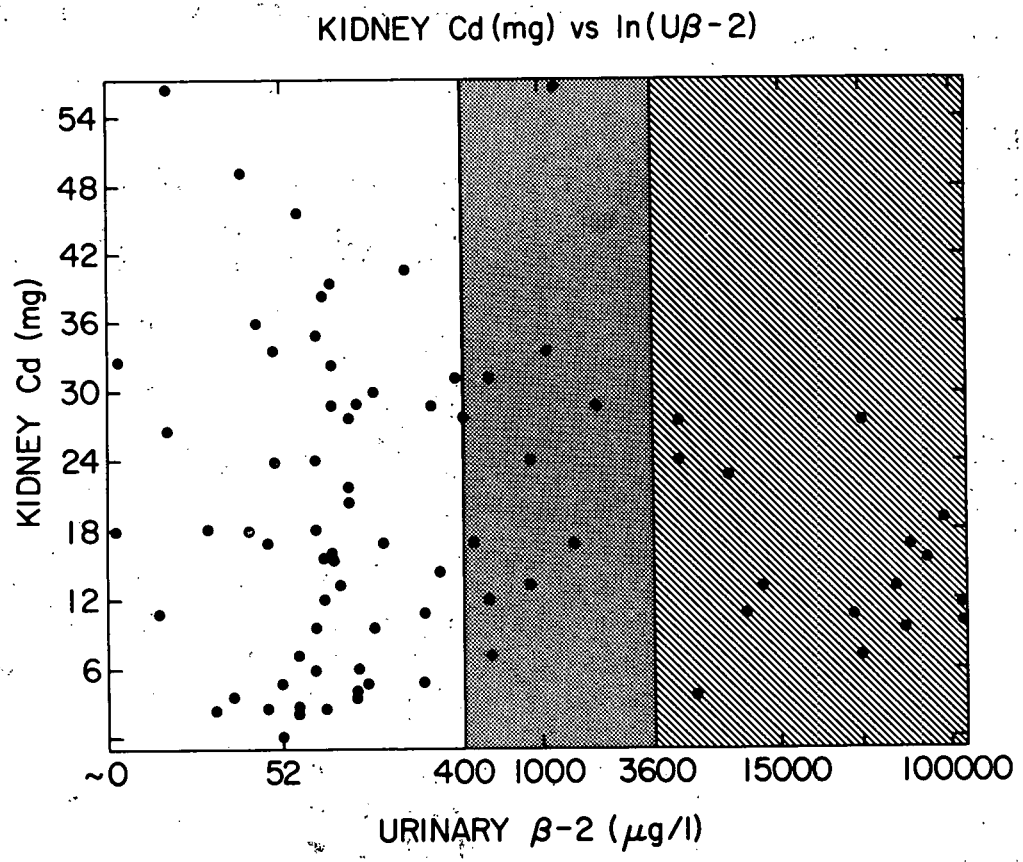


Fig. 5. Relationship between kidney Cd (mg) and urinary β_2-microglobulin (μg/l). The three regions are defined in the text.

A FEASIBILITY STUDY FOR THE IN VIVO MEASUREMENT OF SILICON AND BERYLLIUM BY NUCLEAR TECHNIQUES

K.V.Ettinger,W.D.Morgan,U.Miola,D.Vartsky,K.J.Ellis,L.Wielopolski,S.H.Cohn

Medical Research Center, Brookhaven National Laboratory, Upton, N.Y. 11973,USA

Research carried out under the auspices of the Department of Energy under Contract No. DE-AC02-76CH00016.

Abstract

Silicosis is a chronic fibrosing of the lungs that may develop from exposure to free crystalline silica incurred in a variety of industries including mining, quarrying and stone cutting.

Experiments have been performed to assess the feasibility of measuring silicon *in vivo* by means of the prompt neutron inelastic scattering reaction $^{28}Si(n,n'\gamma)^{28}Si$. The optimum neutron energy in terms of counts per dose delivered to a liquid tissue-equivalent phantom was found to be in the range 5 to 8 MeV.

By pulsing the neutron beam and counting only in the on period it was possible to substantially reduce the background both from thermal neutron interactions in the phantom and also from the fast interfering reaction $^{31}P(n,\alpha)^{28}Si$. In final measurements with a realistic chest phantom no interferences from other prompt inelastic scattering reactions were observed. With one Ge(Li) detector of 19% relative efficiency, a detection limit of 0.6g silicon per rem was obtained. A system comprising six 25% efficient detectors would be capable of measuring normal lung silicon contents of about 0.1g.

Berylliosis, a granulomatous lung disease, has been observed in persons with lung contents ranging from micrograms to tens of milligrams (a "normal" value is 1-2 μg). For gamma photons between 1.665 MeV and 2.225 MeV (the beryllium and deuterium photonuclear thresholds respectively), the production of neutrons is a unique property of beryllium which might be exploited for analysis *in vivo*.

Experiments with a Pb-filtered ^{124}Sb source and an enriched $^{10}BF_3$ counter provided data from which it was projected that a 72-detector array might yield a detection limit of 3.4 mg Be for a lung dose of 2.5 rads. Possible methods for improving this result are discussed.

INTRODUCTION

Silicon, in the form of free crystalline silica, and beryllium, appearing as beryllium oxide dust, are potentially hazardous lung contaminants. Silicosis is a chronic fibrosing of the lungs that may occur from exposure incurred in a variety of industries including mining, quarrying and stone cutting[1]. Berylliosis is a granulomatous disease that may develop after even a very brief exposure to the metal or one of its alloys[2].

The lungs of individuals with silicosis may contain up to 10g of silicon as free silica[1] (compared with a normal level of about 0.1g). With such large amounts of the material, a non-invasive technique for silicon analysis is feasible both for screening exposed workers and also as a research tool for the investigation of the dose-response relationship of the element.

For the analysis of silicon in non-biological samples the fast (n,p) reaction on ^{28}Si to produce ^{28}Al is commonly used. However, in biological specimens, the (n,α) reaction on phosphorus, which also produces ^{28}Al, presents a serious interference to the method. Therefore, for this application it is worthwhile to consider the inelastic neutron scattering reaction ^{28}Si (n,n'γ) ^{28}Si, which has a higher cross-section and is relatively free from phosphorus interference for neutrons in the energy range 2 to 5 MeV. The first excited level of silicon is at an energy of 1778.9 keV, but this level is populated also by the β- decay of ^{28}Al, produced by (n,γ) reaction on ^{27}Al, by (n,α) reaction on ^{31}P, and by (n,p) reaction on ^{28}Si.

The aim of the present investigation is to determine the optimum parameters for maximizing the yield of ^{28}Si (n,n'γ) ^{28}Si *in vivo*, while at the same time minimizing all interferences to this reaction. Finally, the feasibility of performing *in vivo* measurements in human subjects is considered.

The problems associated with *in vivo* measurement of beryllium are more complex than those encountered with silicon, as the quantities are smaller and the response is apparently more variable. Berylliosis has been observed in persons with lung contents ranging from micrograms to tens of milligrams[3]. A normal value is approximately 1-2 μg. There is strong evidence that the human response contains a distinct immunological component and that individual hypersensitivity is an important factor. However, a recent study[4] suggests that a dose-response relationship exists in at least some workers: for these individuals, *in vivo* measurements would be useful.

The only nuclear reaction which might be suitable for the measurement of beryllium is the photonuclear (γ,n) reaction on ^{9}Be, which has a threshold at 1.665 MeV. For photons above this energy level but below 2.225 MeV(the deuterium (γ,n) threshold)the production of neutrons is a unique property of beryllium that might be exploited for analysis *in vivo*.

Since the analysis of silicon and beryllium are dependent upon two quite different nuclear reactions, it is necessary to consider separately the experiments relating to each element. The major effort has been applied to silicon, so this will be considered first.

1. SILICON ANALYSIS

Initial experiments with a 25 μg (5.7×10^7 n/s) ^{252}Cf source in the Brookhaven Mobile Activation Facility[5] confirmed the possibility of utilizing inelastic neutron scattering for the measurement of silicon. Using two 24% Ge(Li) detectors (each of 2.2 keV resolution) and a simple phantom, a detection limit (2 s.d. of the background) of 7.9g silicon was obtained for an administered dose of 1 rem (a quality factor of 10 was assumed).

It was apparent, however, that ^{252}Cf is not an ideal neutron source: a large proportion of the spectrum is of too low an energy to excite the first level of silicon and therefore contributes an unnecessary dose. Similarly, the mean neutron energy of 2.2 MeV is too low to take full advantage of the reaction cross-section.

a) RARAF Experiments

The Radiological Research Accelerator Facility (RARAF) at Brookhaven is based upon a 4 MV Van de Graaff which once served as injector for the Cosmotron. It now operates very reliably in dc mode, to provide beams of monoenergetic neutrons in the range 220 keV to 15 MeV by utilizing a variety of nuclear reactions.

A shield and collimator were assembled at the end of one of the beam lines. The shield consisted of an assembly of paraffin wax, polyethylene bricks and boron-doped polyethylene in a cube of dimension 1 m. The 60 cm long collimator provided an aperture of 0.5 x 5 cm at the target and diverged in the horizontal plane to a size of 10 x 5 cm at the exit. The first 20 cm of the collimator was defined by a 10 cm thickness of iron to reduce the neutron energy by inelastic scattering; and the remaining 40 cm consisted of borated polyethylene.

Total dose measurements at the phantom irradiation position were made with a parallel plate ionization chamber made of Shonka A-150 tissue equivalent (TE) plastic and through which flowed a methane-based TE gas. An identical chamber inserted in the collimator at a distance of 21 cm from the target served as a transmission monitor during the experimental runs. Gamma-ray dosimetry was performed with a compensated Geiger-Muller type dosimeter.

A compilation of the potential interferences which might arise during silicon measurements is shown in table I. The column on the right lists the induced activities including ^{28}Mg ^{28}Al and ^{28}P, which decay via the 1778.9 keV level in ^{28}Si. In the middle column are listed the prompt neutron capture gammas, the majority of which are single or double-escape peaks from full energy lines. Probably the most important column is the one on the left which indicates the most prominent nuclear level transitions that may be induced by neutron inelastic scattering. These include a 1781.3 keV line from ^{70}Ge which is not a significant body element but is present in the detection system. The 1783 and 1783.1 keV lines from ^{110}Cd and ^{48}Ca respectively may be resolvable from ^{28}Si with good resolution detectors. The 1770.2 and 1771.4 keV contributions from ^{207}Pb and ^{56}Fe are also resolvable from ^{28}Si, but the use of these materials for detector shielding is not recommended as their gamma-ray yield is high and hence unnecessarily complicates the accurate determination of low levels of silicon. Consequently, the front face of the neutron shield and collimator was protected by a 2.5 cm thick layer of bismuth. The same material was used to shield the 19% Ge(Li) detector which was situated close to the exit aperture but out of the direct view of the neutron beam.

Experiments were carried out at five neutron energies: nominally 2.15, 3.17, 4.9, 6.8 and 14.8 MeV. Further measurements were made with a 39 Ci $^{238}Pu,Be$ (1.1×10^8 n/s) source placed in the position of the target. This neutron spectrum extends from 0 to 11 MeV, with a mean neutron energy of 4.5 MeV.

For these experiments simple phantoms consisting of polyethylene bottles containing water, waterglass (sodium silicate), sodium phosphate or calcium carbonate were used. At each neutron energy, a water background was obtained, followed by spectra of the silicon, phosphorus and calcium-containing phantoms.

TABLE I

INTERFERENCES TO 1778.9 keV LEVEL IN ^{28}Si

(n,n'γ)		(n,γ)			INDUCED ACTIVITIES	
1770.2	^{207}Pb	1772.7	Al (s)		1771.4	^{56}Co
1771.4	^{56}Fe	1775.2	Zn (s)		1771.8	^{24}Al
1771.8	^{24}Mg	1778.9	Al (F)		1772.0	^{48}K (s)
1772.0	^{48}Ca (s)	1780.2	K (s)		1774.2	^{26}Na
1772.7	^{106}Cd(D)	1781.1	F (F)		1778.0	^{44}K
1774.2	^{26}Mg	1783.1	Mn (s)		1778.9	^{28}Al
1774.6	^{184}W	1783.6	Ca (s)		1778.9	^{28}P
1774.8	^{119}Sn	1783.7	K (D)		1778.9	^{28}Mg
1775.2	^{184}W	1784.4	P (s)		1779.2	^{83}Se (s)
1778.0	^{127}I	1786.9	Na (D)		1783.1	^{48}K
• 1778.0	^{44}Ca					
1778.9	^{28}Si					
1780.0	^{64}Cu					
• 1781.3	^{70}Ge					
1781.7	^{64}Zn (D)					
• 1783.0	^{110}Cd					
• 1783.1	^{48}Ca					
1784.4	^{54}Cr					
1786.1	^{112}Sn (s)					
1786.3	^{110}Cd (D)					
1786.5	^{70}Zn					

(F) = FULL ENERGY PEAK
(S) = SINGLE ESCAPE PEAK
(D) = DOUBLE ESCAPE PEAK

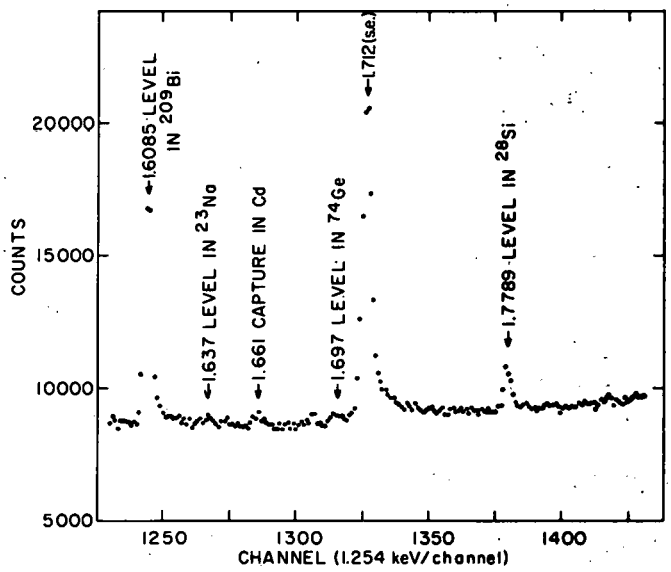


figure 1: Typical spectrum obtained at a neutron energy of 3.17 MeV.

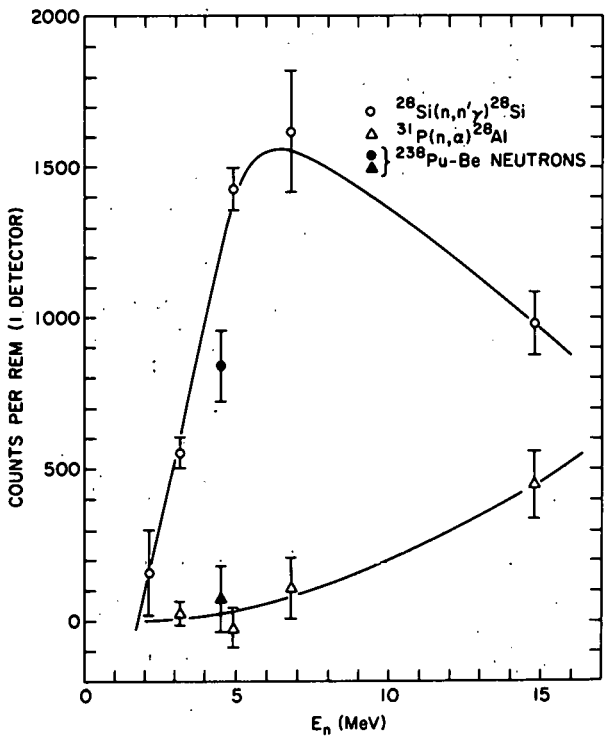


figure 2: Relative yield from hydrogenous phantoms of (n,n') and (n,α) reactions on ^{28}Si and ^{31}P respectively as a function of neutron energy.

Fig. 1 shows a typical spectrum in the region of interest. It was obtained with a waterglass phantom at a neutron energy of 3.17 MeV. The 1778.9 keV peak is prominent, as are the 1712 keV single escape from hydrogen capture at 2223 keV, and the 1608.5 keV level in ^{209}Bi.

A summary of the RARAF experiments is presented in figure 2. The maximum yield (counts/rem) of the $^{28}Si(n,n'\gamma)^{28}Si$ reaction in hydrogenous medium occurs between 5 and 8 MeV, falling thereafter to just under70% of the maximum at the D-T energy. By comparison, the (n,α) reaction on phosphorus rises slowly until about 7 MeV, and reaches a significant level at 14MeV. It is calculated that with the use of two 24% detectors, the 2σ limit of detection at the optimum neutron energy would be 1.2g silicon per rem, a substantial improvement over the initial ^{252}Cf experiment.

b) Tandem Van de Graaff Experiments

Once the optimum neutron energy was determined, any further improvement in detection limit could come only from a reduction in background. It was already known that when a pulse of fast neutrons is directed at tissue or some other hydrogenous material, the maximum flux of thermal neutrons occurs at about 20-30 μs after the beam burst and then gradually diminishes over the next 300 to 500 μs[6]. By pulsing the neutron beam and counting only in the beam off period, one can reduce the background contribution from truly "prompt" events and count only the slow neutron reactions of interest. This technique is the basis for the successful measurement of body nitrogen and cadmium, for example[7].

Conversely, by pulsing the neutron beam and counting only in the beam-on period, one can significantly reduce interferences from slow neutron reactions (predominantly neutron capture in hydrogen) and count only "prompt" neutron inelastic scattering reactions. A further advantage of the pulsed mode of operation is that induced activities are suppressed approximately in the ratio of the pulsing duty cycle. Consequently, the potential interference from ^{28}Al via phosphorus is much reduced, even at 14 MeV neutron energies.

As a result of these considerations, a radio frequency pulser was built for use with the Brookhaven Tandem Van de Graaff accelerator. The shield and collimator was constructed as before. Experiments were carried out with the original phantoms, and also with a more realistic chest phantom. The latter contained a bone-equivalent rib cage, sternum and vertebrae, and two polystyrene lungs each containing 15g silicon. The remaining space was filled with a chemically tissue-equivalent liquid.

Measurements were made with 7 MeV neutrons produced by bombarding a beryllium target with 4 MeV deuterons. The pulsing frequency was 3.7 kHz, with the beam on for 10 μs and off for the following 260 μs. The detection system was gated on for 12 μs after the start of the neutron pulse. While these experiments were restricted by limitations of time and accelerator beam current, the results were, nevertheless, very encouraging. Figure 3 shows a gamma-ray spectrum from the realistic phantom, obtained with only one 19% detector (of diminished resolution) and a total dose of 100 mrem. Only a part of the lung was exposed to the collimated beam, so the effective silicon target was less than 4g.

c) Discussion

From these data, it was concluded that the 2σ detection limit obtained with one 19% detector was 1.9g Si per 100 mrem, or 0.6g Si per rem. With six 25% efficient detectors of typical resolution 3 keV, the detection limit would be improved to 0.15g Si per rem, a value within the normal range of silicon in

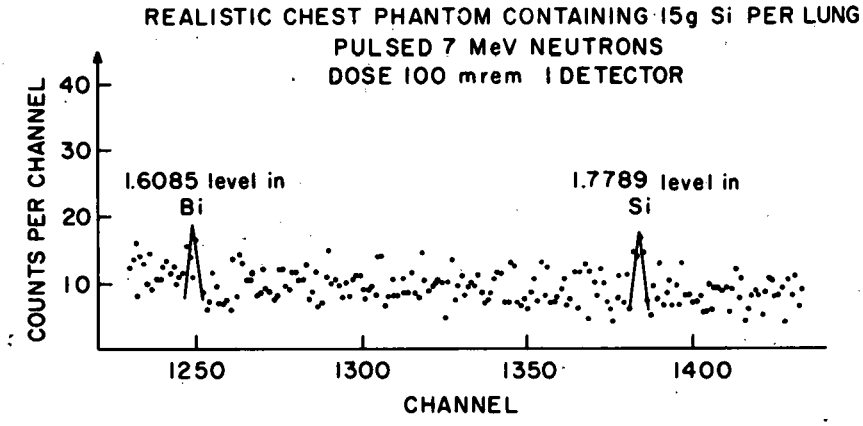


figure 3: Spectrum obtained from realistic chest phantom exposed to a dose of 100 mrem of pulsed 7 MeV neutrons.

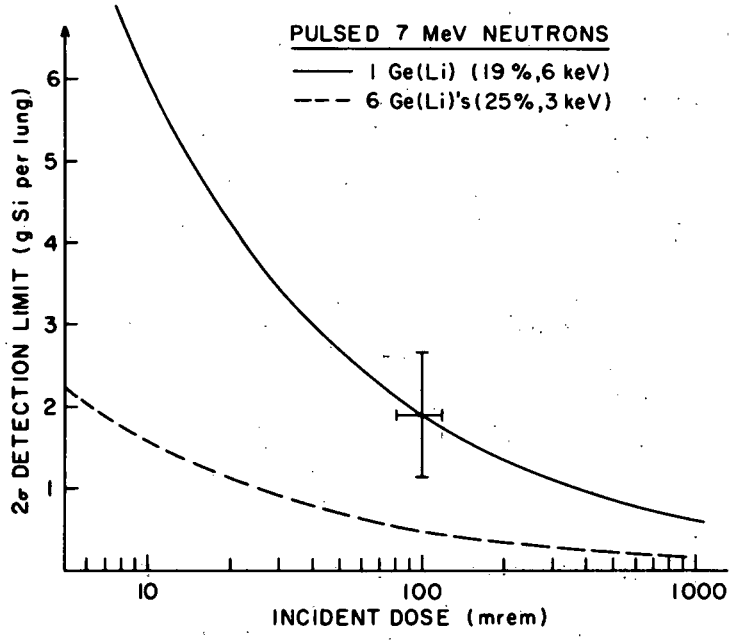


figure 4: Silicon detection limit in vivo as a function of dose and detection efficiency.

the lung. Figure 4 illustrates the variation of the detection limit as a function of dose delivered, as well as the improvement that could be obtained with a more efficient detection system. A 6-detector configuration would provide useful data for doses as low as 40-50 mrem, for screening exposed workers.

Finally, it should be stated that these experiments are of a preliminary nature; further work is needed to optimize the pulsing parameters. Nevertheless, as Figure 3 shows, the first escape peak from hydrogen capture has been greatly reduced, if not removed completely, as the only lines which do appear are the inelastic scattering levels in bismuth and silicon.

2. BERYLLIUM MEASUREMENT

Beryllium is the lightest of all solid and chemically stable substances. Its present industrial uses are numerous, including incorporation in fatigue-resistant alloys, heat-resistant ceramics, electronic and nuclear reactor parts, rocketry and classified weaponry. Although the first report of occupational disease in a beryllium worker appeared in 1933[8], it was not until the early 1940's when light bulb manufacturers began using zinc beryllium silicate as an ingredient of the phosphors in fluorescent tubes, that pulmonary berylliosis was rediscovered and established as an industrial disease.

The diagnosis of berylliosis has posed many problems, particularly as it is difficult to distinguish from other granulomatous disease[2]. The importance of measuring the metal in tissue has been stressed[3], and since measurement is presently dependent upon analysis of biopsy specimens, it is apparent that the development of a non-invasive technique for beryllium would be of considerable value in the diagnosis of beryllium disease.

a) Theoretical Sensitivity

The (γ,n) cross-section for beryllium is shown in Figure 5. It rises to a peak of 1.6 mb ($\pm$15%) at 1.67 MeV photon energy and then falls to a very low value at about 2.0 MeV, before rising again to several maxima of about 5 mb[9,10,11].

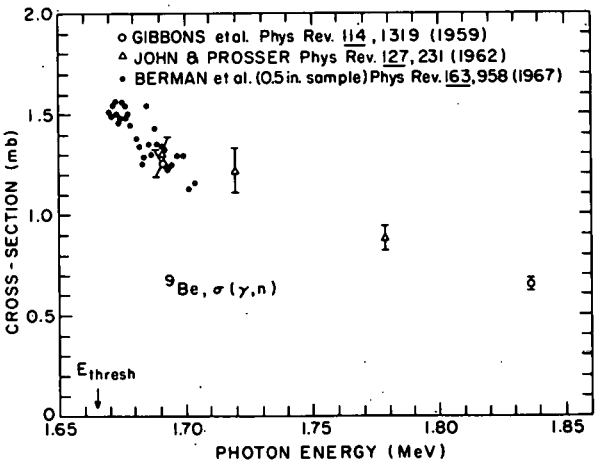


figure 5: The photonuclear cross-section for beryllium-9 near threshold. Data for higher photon energies are given in the references shown.

In order to avoid any possible interference from photoneutron production in deuterium, the ideal photon source should have an energy between 1.665 and 2.225 MeV. Within this range, the beryllium cross-section dictates that a monoenergetic source of 1.67 MeV would be the optimum in terms of photoneutron yield per dose delivered.

It can be calculated that for such an ideal photon source, the neutron yield will be 150 ($\pm$30) neutrons/mgBe/rad.

Therefore, with good n-γ discrimination and a low neutron background it might be possible with a large detection system to measure one milligram for a lung dose of several rads.

b) Photon Sources

In practice it is very difficult to obtain the required monoenergetic photon source. Many isotopes have been considered, but most have been rejected on the grounds of (i) short half-life, (ii) the presence of too many lower energy emissions which contribute to the dose delivered but not to the measurement of Be, and (iii) the presence of significant emissions above the deuterium threshold. Table II lists those isotopes which have been considered in more detail: column 4 lists only those gamma-rays which are above the beryllium threshold. The final column on the right indicates the relative photoneutron yield per unit dose delivered; the factor Avogadro's number divided by the atomic mass of beryllium converts these values to absolute neutron production per gram of beryllium per rad of given dose. The isotopes have been listed according to this figure of merit.

Aluminum-28 approaches the ideal source most closely, but would require the use of a nuclear reactor-based cyclic activation-irradiation system.

Antimony-124 has a more useful half-life, but it also has a significant number of lower energy lines (see table III). However, by filtering the ^{124}Sb spectrum with 4 cm Pb, it is possible to improve the $I\sigma\phi$ value to approximately 1.3, which is more than 60% of the ideal response.

Table III also indicates that the ^{124}Sb spectrum contains nine relatively weak emissions above an energy of 2.225 MeV. The potential interference from these lines due to photoneutron production in deuterium was therefore considered. Assuming a normal chest content of 15 mg deuterium and a lung content of 0.1 mg beryllium, the neutron contribution from deuterium is only 11% of the total (see table IV). Since this level of interference will diminish as the beryllium content is increased, it is not expected to present a serious problem to the measurement of beryllium.

c) Experiments with ^{124}Sb

A simplified diagram of the experimental arrangement is shown in figure 6. A 40 mCi ^{124}Sb source was housed in a cylindrical lead cask of wall thickness 13 cm. The useful beam emerged through a 6.5 cm diameter aperture and was filtered ("hardened") by 4 cm lead before striking the phantom. In cross-section, the chest phantom consisted of a 12 cm thick polystyrene foam lung sandwiched between two 4 cm thick layers of paraffin wax. The beryllium target was a bottle containing 100 g beryllium oxide, equivalent to 36 g beryllium.

Table II: Possible photon sources for beryllium analysis.

Source	Half-Life	Flux Φ (photons/cm^2.rad)	γ-energy (MeV) & intensity (I)		σ (mb)	$I\sigma\Phi$ (x10^{-18})
		(x10^8)				
Ideal		13.3	1.67	(100)	1.6	2.12
^{28}Al	2.24m	13.3	1.78	(100)	0.9	1.2
^{124}Sb	60d	11.3	1.691	(49.1)	1.3	0.74
			2.09	(5.6)	0.3	
^{26}Al	7.5x10^{5}y	8.2	1.809	(100)	0.8	0.62
			2.938	(0.24)	1.2	
^{88}Y	108d	7.8	1.836	(100)	0.7	0.51
^{56}Mn	2.58h	13.3	1.811	(29)	0.8	0.34
			2.11	(15)	0.3	
^{56}Co	77d	6.3	1.76	(15)	1.0	0.19
			2.02	(11)	0.3	
			2.6	(17)	0.5	
			3.26	(13)	0.3	
^{207}Bi	38y	13.9	1.77	(6.8)	0.9	0.09

TABLE III

PRINCIPAL PHOTON ENERGIES FROM

^{124}Sb ($T_{1/2}$ = 60.2 d)

ENERGY (keV)	INTENSITY (%)
602.7	98.3
645.8	7.2
709.3	1.4
713.8	2.4
722.8	11.3
968.3	1.8
1045.2	1.85
1325.5	1.4
1368.2	2.4
1436.7	1.0
1691.0	49.0
2091.0	5.6

PLUS 9 WEAK EMISSIONS ABOVE 2225 keV

TABLE IV

RELATIVE CONTRIBUTIONS OF ^{9}Be AND ^{2}H TO PHOTONEUTRON PRODUCTION USING AN ^{124}Sb SOURCE

	LUNG CONTENT (M)	PHOTON INTENSITY (I)	CROSS-SECTION (σ)	$I\sigma M$
^{9}Be	0.1 mg	60%	1 mb	6.0
^{2}H	15 mg	0.05%	1 mb	0.75

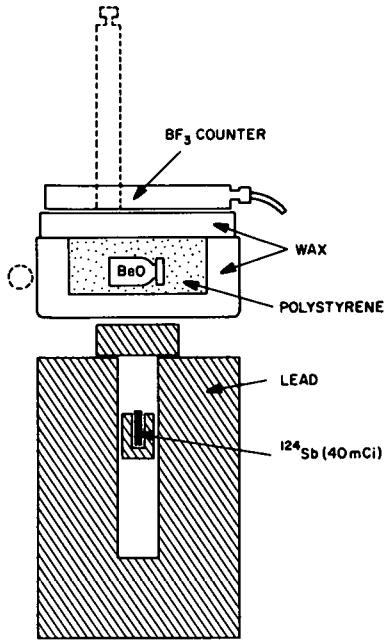


figure 6: Experiment arrangement consisting of ^{124}Sb source, phantom containing beryllium, and $^{10}BF_3$ counter.

The detection system consisted of a 5 cm diameter x 31 cm long counter (model 2033 by LND Inc., Oceanside, N.Y.) filled with 96% - enriched $^{10}BF_3$ to a pressure of 70 cm Hg. Counter efficiency was 49 counts per unit flux. At an operating voltage of 2250 volts the output was fed via an ORTEC 142 pre-amplifier and 572 amplifier to a ND 2400 multichannel analyser. Dosimetry was performed by the use of LiF TLD rods placed in the position of the phantom.

Measurements were made with the counter placed in a variety of positions and orientations around the phantom to determine the optimum geometry. From the results obtained, it was projected that with an array of 72 counters placed perpendicular to the body a yield of 11 counts per milligram of beryllium might be achieved for a lung dose of 5 rads. If this dose was delivered in a period of 10 minutes, the background count-rate (assuming this to be independent of gamma dose-rate) would be approximately 350 counts, and the 2σ detection limit would be 3.4 mg Be.

d) Discussion

The detection limit might be improved by reducing the background and increasing the detection efficiency. For example, the use of a cosmic ray shower detector to disable the counting equipment for about 10 msec on registration of a shower could reduce the cosmic ray neutron component by an order of magnitude. In these experiments the background was found to be largely independent of gamma dose-rate within the range available, namely less than 1 rad/h. However, at the projected dose-rates of 15-30 rads/h, it may be necessary to employ pulse rise time discrimination to reject pile up counts originating from the excitation source.

Since the neutrons emerging from the body have a range of energies from thermal to 24 keV, the use of high pressure $^{10}BF_3$ detectors or ^{3}He proportional counters will improve the detection efficiency of neutrons which are not completely thermalised by about a factor of 2.[12]

An alternative approach is to consider those neutrons which do not emerge from the chest but are captured instead by body hydrogen. By using a pulsed gamma source, which might for example be a filtered bremsstrahlung spectrum

from an electron accelerator, and counting in the beam-off period the neutron-induced (and hence beryllium-produced) capture gamma-rays with a large volume sodium iodide detection system, it may be possible to achieve a slightly better sensitivity of detection than by neutron counting.

3. CONCLUSIONS

These experiments have demonstrated the feasibility of measuring silicon *in vivo* by the method of prompt neutron inelastic scattered gamma ray analysis. A practical system based on the use of 5 to 8 MeV neutrons from a pulsed Van de Graaff accelerator would be capable of detecting normal lung contents of about 0.1 g silicon for a dose of 1 rem. For screening workers suspected of suffering from silicosis, useful data might be obtained for doses of less than 0.1 rem. The technique can be applied with some sacrifice of sensitivity with 14 MeV neutrons from a D-T generator.

The measurement of beryllium *in vivo* is demonstrated by the method of photoneutron detection. The sensitivity of the technique is not as high as one would like, but still it should be possible to detect with a large array of counters 3.4 mg beryllium for a dose of 2.5 rads. With such technical innovations as have been discussed, it may yet be possible to achieve a detection limit of 1 mg beryllium per 2.5 rad dose, but the experimental data so far is unavailable.

Both techniques would be useful in screening exposed workers and as a research tool to evaluate dose-response relationships for these elements.

ACKNOWLEDGEMENTS

We wish to thank the many research groups and individuals who assisted in the setting-up of these experiments. In particular, the help of J. Rothmann, S. Minton, S. Marino, M. Manni, E. N. Carter and F. C. O'Brien is much appreciated.

REFERENCES

1. ZISKIND, M., JONES, R.N., WEILL, H., Am. Rev. Resp. Dis., 113, 643-665 (1976).
2. JONES WILLIAMS, W., J. Soc. Occup. Med., 27, 93-96 (1977).
3. SPRINCE, N.L., KAZEMI, H., HARDY, H.L., Ann. N.Y. Acad. Sci., 278, 654-664 (1976).
4. SPRINCE, N.L., KANAREK, D.J., WEBER, A.L., CHAMBERLAIN, R.I., KAZEMI, H., Am. Rev. Resp. Dis., 119, 237 (1979).
5. ELLIS, K.J., MORGAN, W.D., YASUMURA, S., VARTSKY, D., ZANZI, I., COHN, S.H., These Proceedings, pp. (1980).
6. ETTINGER, K.V., BIGGIN, H.C., CHEN, N.S., CHETTLE, D.R., FREMLIN, J.H., HARVEY, T.C., MORGAN, W.D., NOWOTNY, R., THOMAS, B.J., VARTSKY, D., Kerntecknic, 17, 89-92 (1975).
7. BIGGIN, H.C., CHEN, N.S., ETTINGER, K.V., FREMLIN, J.H., MORGAN, W.D., NOWOTNY, R., CHAMBERLAIN, M.J., Nature New Biology 236, 187-188 (1972).
8. REEVES, A.L., Clin. Toxicol., 10, 37-48 (1977).
9. HUGHES, R.J., SAMBELL, R.H., MUIRHEAD, E.G., SPICER, B.M., Nucl. Phys., A238, 189-198 (1975).
10. BERMAN, B.L., VAN HEMERT, R.L., BOWMAN, C.D., Phys. Rev. 163, 958-963 (1967).
11. JOHN, W., PROSSER, J.M., Phys. Rev., 127, 231-235 (1962).
12. O'DELL, A.A., UCRL-52151 (1976).

EVALUATION OF THE DIAGNOSTIC SENSITIVITY OF SCATTERING MEASUREMENTS OF BONE DENSITY

J.G. Roberts, E. DiTomasso and C.E. Webber

Department of Nuclear Medicine
McMaster University Medical Centre
Hamilton, Ontario, Canada. L8N 3Z5

ABSTRACT

To obtain an indication of the *in vivo* sensitivity of a system for the measurement of os calcis density, we measured the ability of the system to detect the difference in density that exists between groups of subjects of different ages. The detected difference was similar to that observed by other accepted methods for skeletal investigation. Since the Compton scattering technique is the only method available for the non-invasive assessment of weight bearing trabecular bone, their further development and evaluation should be encouraged. A major step in this direction would be an improvement in the availability of high activity sources of ^{153}Gd.

Introduction

The diagnostic sensitivity of tests for the detection of skeletal demineralization depend on many factors. It is often claimed that one of the most important is to make measurements in weight bearing trabecular bone. This claim is based on the fact that the surface area per unit volume of trabecular bone is about five times that of cortical bone (Sissons, Holley and Heighway, 1967). Since bone turnover is a surface related process, the turnover rate of trabecular bone is greater than that of cortical bone (I.C.R.P., 1975) and it is to be expected that a metabolic stress will affect trabecular bone more rapidly. This expectation is supported by the clinical observation that fractures in patients suffering from osteoporosis occur at sites which consist predominantly of trabecular bone. However, it should be noted that the total masses of mineral lost from each type of bone are approximately equal because about 80% of the skeletal mineral is in cortical bone.

This early response of trabecular bone to metabolic stress has prompted a proliferation of Compton scattering methods for the non-invasive measurement of trabecular bone density (Reiss and Steinle, 1973; Clark and Van Dyk, 1973; Garnett, Kennett, Kenyon and Webber, 1973; Piper and Preuss, 1976; Hazan, Leichter, Loewinger, Weinreb and Robin, 1977; Huddleston and Bhaduri, 1979). It has been shown that these systems are accurate and precise when density is measured in inanimate objects. Unfortunately, the sensitivity of density measurements to variations in mineral composition will be compromised by the presence of the non-mineral substances which occupy about 70% of trabecular bone volume. There seems little point in expending further effort on the development of Compton scattering methods until it has been demonstrated that they will be useful clinically. To assess the value of a new diagnostic procedure it is necessary to define its ability to detect, in vivo, a real difference between the mineral composition of bones.

It is well established that throughout adult life there is a net loss of mineral from the skeleton and that the loss is greater in females than in males. This was shown, in vitro, from measurements of density in a number of bones taken from eighty adult skeletons (Trotter, Broman and Peterson, 1960). The studies suggested that the rate of loss of mineral with aging was approximately constant and that it was the same for both trabecular and cortical bone. In vivo surveys of large groups of subjects have shown that the metacarpal cortical width of an 80 year old female is about 70% that of a 40 year old female (Garn, Poznanski and Larson, 1973). The reduction in males was approximately half that observed in females. Similar reductions were detected when the mineral content of cortical bone in the distal radius was measured by photon transmission (Mazess and Cameron, 1973). In vivo measurements of age related loss of mineral from trabecular bone are limited because it has not been possible to examine trabecular bone non-invasively. In a limited study, Meunier and Courpron (1973) showed that in iliac crest biopsies taken from 80 year old females, the mean value of the fractional volume of bone tissue occupied by mineralised matrix was about 66% that of the 40 year old. The corresponding figure for males was 92%. It would seem therefore that a simple preliminary trial of the clinical value of a bone density system would be its ability to detect the differences in density which exist between two populations, the mean ages of which differ by about 40 years.

Materials and Methods

The density of the os calcis was measured in 110 volunteers using the system described by Webber and Kennett (1976). With this system the os calcis is irradiated by a photon beam from a primary source of about 40 GBq ^{153}Sm (103 keV). The fraction of the beam scattered through 90° is measured using a NaI(Tl) detector. Corrections for attenuation are made from measurements of transmission for both the primary source and for a secondary source of about 15 GBq ^{170}Tm (84 keV). For each subject, the density of both os calcii was

measured and the mean value recorded. The long term precision of this system is 1.6% (Adams and Webber, 1978) and the radiation dose per measurement is 1.5 mSv.

The subjects were divided into four groups. Two younger groups acted as controls and consisted of 35 females and 29 males respectively. The means and standard deviations for the ages of each group were 42.0 $\pm$ 3.4 years for the female controls and 42.9 $\pm$ 4.7 years for the male controls. The two older groups consisted of 24 females and 22 males. The corresponding ages were 79.5 $\pm$ 5.6 and 77.1 $\pm$ 6.0 years respectively. All subjects worked either within the Medical Centre or were residents of a local senior citizens home. No subject was suffering from a diagnosed disease or was taking any drug which was known to influence skeletal metabolism. All subjects were ambulatory.

Results

The mean values and standard deviations for os calcis density in the two younger groups were 1.24 $\pm$ 0.04 $g.cm^{-3}$ for females and 1.31 $\pm$ 0.05 $g.cm^{-3}$ for males. The corresponding values for the older groups were 1.12 $\pm$ 0.05 $g.cm^{-3}$ and 1.18 $\pm$ 0.07 $g.cm^{-3}$ respectively. The mean values for all four groups are shown in figure 1. The mean density for each of the older groups was significantly less than that of the younger group ($p < 0.001$).

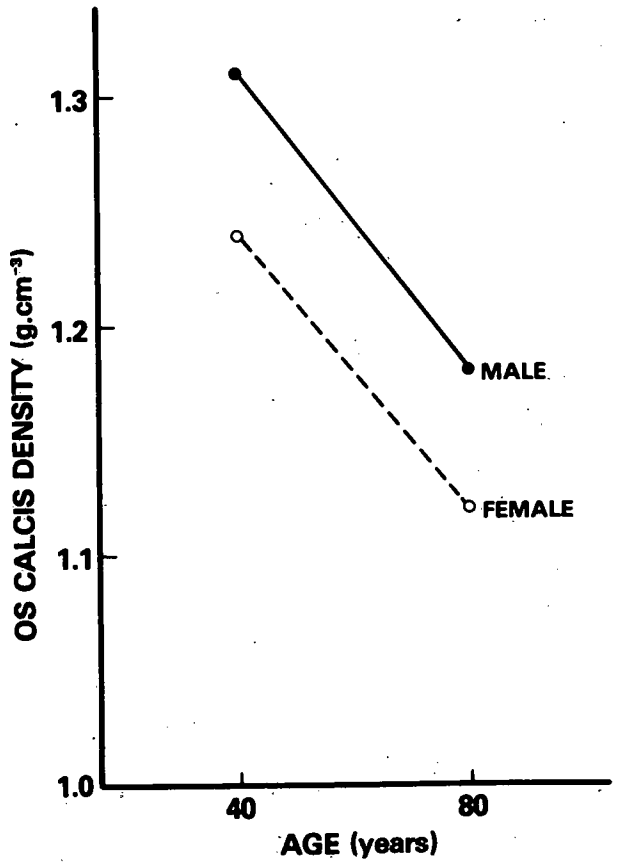


Figure 1 Mean os calcis densities for 40 year old and 80 year old subjects.

The density results are compared in figure 2 with published results from studies using bone biopsies (Meunier and Courpron, 1973), hand radiographs (Garn, Poznanski and Larson, 1973) and measurements of gamma ray transmission (Mazess and Cameron, 1973).

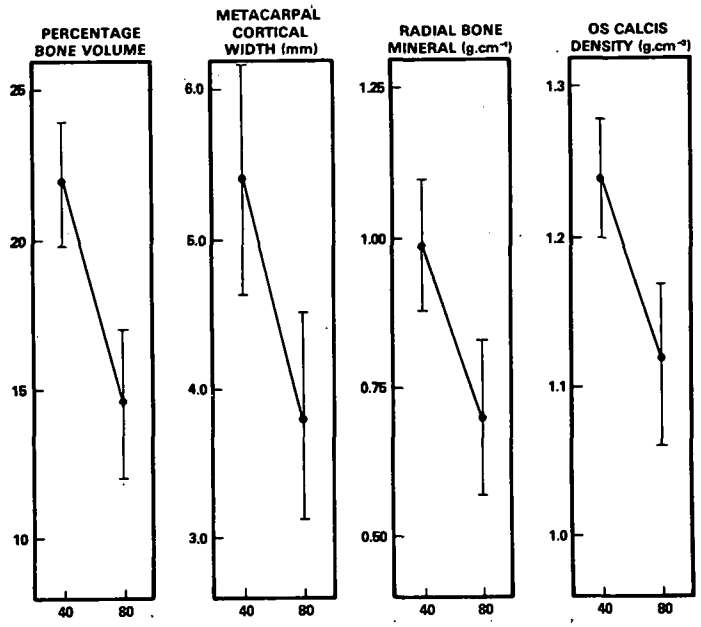


Figure 2 The differences between 40 year old and 80 year old subjects as detected by various techniques for the assessment of bone.

Discussion

The differences in density detected between the 40 and 80 year old subjects were highly significant. It is of interest to note that the differences were similar for each sex whereas the results of other studies have suggested that they are less for males than for females. This may reflect the role of the os calcis in ambulation. While it is not the objective of this work to speculate about the reasons for these differences, the older subjects were probably less active and certainly weighed less. The results do not prove that mineral is lost from bone during life; merely that the os calcis density technique is capable of detecting a real difference that exists between two populations. The difference may be due to many factors and simply reflects the problems associated with all cross sectional surveys (Mainland, 1957; Doyle, 1972).

The comparison with other methods shows that the standard deviations about the mean for both age groups are remarkably similar for all four procedures. Thus it would seem that the loss of sensitivity due to the presence of non-mineral substances within the scattering volume is compensated by the greater sensivity of trabecular bone to a metabolic stress. Of the four, the os calcis density technique is the only method for the non-invasive assessment of weight bearing trabecular bone.

Recently, Elsasser, Hesp, Klenerman, Reeve, Veall and Wootton (1979) used a radioisotope transaxial tomographic technique to distinguish between

changes produced by disease in both the trabecular and cortical bone of the same subject. Their results confirmed that trabecular bone responded to metabolic stress more rapidly than cortical bone. This conclusion is supported, although the evidence is not cited, in recent articles by Mazess (1979a, 1979b). If this is indeed the case and if the os calcis responds to a metabolic stress in the same manner as other trabecular bone, then the scattering technique will be a sensitive diagnostic procedure. Of relevance here are the results of Adams and Webber (1978) who showed that in five of six cadavers the os calcis density was related directly to the density of lumbar vertebrae. However, it should be noted also that the os calcis is not a common site of fracture in patients suffering from osteoporosis.

As an additional test of the diagnostic sensitivity of the density technique we have measured density in a small group of non-ambulatory elderly subjects. The mean age of the 10 female volunteers was 76.6 $\pm$ 6.8 years. The results are shown in figure 3. The mean density of the non-ambulatory

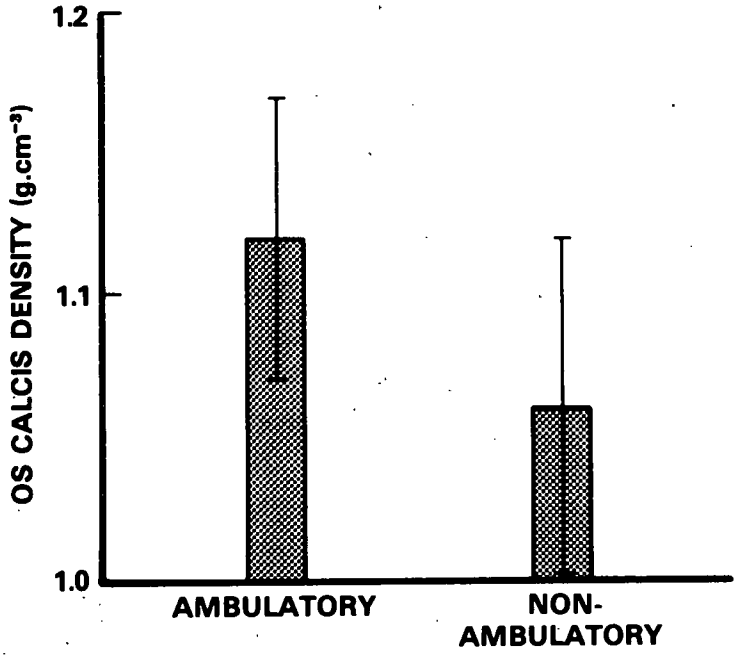


Figure 3 The effect of ambulation on the mean os calcis density of elderly females.

subjects was significantly less than that of the ambulatory elderly females ($p < 0.01$). Since these patients were suffering from a variety of diseases, it cannot be stated that this difference was due solely to the removal from the os calcis of the mechanical stimulus of weight bearing. Nevertheless, these results together with those of the age comparison provide a strong stimulus for the further development and clinical evaluation of gamma ray scattering procedures for the measurement of bone density.

Acknowledgment

We are grateful to the Medical Research Council of Canada for their generous funding of this work.

References

1. Adams, C.H. and Webber, C.E. (1978). Fourth Int. Conf. Bone Measurement, Toronto.
2. Clarke, R.L. and Van Dyk, G. (1973). Phys. Med. Biol., 18, 532.
3. Doyle, F. (1972). Clin. Endocrin. Metab., 1, 143.
4. Elsasser, U., Hesp, R., Klenerman, L., Reeve, J., Veale, N. and Wootton, R. (1979). Clin. Science, 57, 22P.
5. Garn, S.M., Poznanski, A.K. and Larson, K. (1973). Proc. Workshop Bone Morph., Ed. Z.F.G. Jaworski, Ottawa, 367.
6. Garnett, E.S., Kennett, T.J., Kenyon, D.B. and Webber, C.E. (1973). Radiology, 106, 209.
7. Hazan, G., Leichter, I., Loewinger, E., Weinreb, A. and Robin, G.C. (1977). Phys. Med. Biol., 22, 1073.
8. Huddleston, A.L. and Bhaduri, D. (1979). Phys. Med. Biol., 24, 310.
9. I.C.R.P. (1975). International Commission on Radiological Protection, No. 23.
10. Mainland, D. (1957). J. Gerontol., 12, 53.
11. Mazess, R.B. and Cameron, J.R. (1973). Proc. Int. Conf. Bone Min. Measurement, Ed. R.B. Mazess, Chicago, 228.
12. Mazess, R.B. (1979a). Calcif. Tissue Int., 28, 89.
13. Mazess, R.B. (1979b). Osteoporosis II., Ed. U.S. Barzel, Grune and Stratton, N.Y.
14. Meunier, P. and Courpron, P. (1973). Proc. Workshop Bone Morph., Ed. Z.F.G. Jaworski, Ottawa, 100.
15. Piper, D.G. and Preuss, L.E. (1976). Fourth Int. Conf. Med. Physics, Ottawa.
16. Reiss, K.H. and Steinle, B. (1973). Siemens Forsch. U. Entwickl. Ber., 2, 16.
17. Sissons, H.A., Holley, K.J. and Heighway, J. (1967). L'Ostéomalacie. Ed. D.J. Hioco, Masson et Cie, Paris.
18. Trotter, M., Broman, G.E. and Peterson, R.R. (1960). J. Bone Jt. Surg., 42-A, 50.
19. Webber, C.E. and Kennett, T.J. (1976). Phys. Med. Biol., 21, 760.

NUCLEAR MAGNETIC RESONANCE METHOD FOR OBSERVATION OF FERROMAGNETIC PULMONARY CONTAMINANTS

K.V. Ettinger*, D. Vartsky, A. Kronenberg, and S.H. Cohn

Medical Research Center, Brookhaven National Laboratory, Upton, New York 11973 and *Department of Medical Physics, University of Aberdeen, Forester Hill, Aberdeen AB62SD, Scotland

Research supported by DOE Contract No. DE-AC02-76CH00016

ABSTRACT

A method is proposed for measurement of tissue concentration of asbestos and other contaminants containing magnetite. The method uses nuclear magnetic resonance (NMR) of protons as a means of detection of the magnetic particles present in the dust. Results of the study of the effect of concentration of iron particles and particle size on the NMR signal are presented. The NMR signal had linear relationship to the concentration of particles. Experiments with different particle size indicated that the signal was proportional to the mass of particles rather than to their number. Quantitative detection of 7RF02 chrysotile asbestos in gel and in rat lungs was demonstrated.

INTRODUCTION

The carcinogenic potential of asbestos in the environment has become one of the public health concerns of our time. The hazards of asbestos exposure were demonstrated in shipyard workers, miners and mill workers, pipe insulation workers, and automobile brake repairmen (1-4). The presence of asbestos fibers in urban air is now well established (5). There are few data that allow judgement of the relation of the asbestos lung burden to environmental asbestos disease. It is not certain whether the amounts present in lungs as the result of non-occupational exposure are associated with frequent risk. In part, this is a reflection of scarcity of data concerning the asbestos content of lungs in general, including those of asbestos workers. There is a need for quantitative information concerning the asbestos content of the lung in individuals in the general population with relation to age, sex, residence and occupational exposure (5).

Beger (6) estimated from the study of a lung from an asbestos worker that 1cc of lung contained 20 μg of asbestos. Sundius and Bygden (7) analyzed a lung of an asbestos worker and estimated that in both lungs there were about 1.4g of asbestos. Beattie and Knox (8) measured the lung dust in individuals exposed to asbestos and suffering from asbestosis. The concentrations of the dust are shown in Fig. 1a.

Another source of important occupational lung contaminants is welding fumes. Siderosis is the oldest known occupational lung disease among welders. According to chemical lung analyses, iron content is 15-100 times higher in welders than in unexposed subjects (9) (see Fig. 1b).

It is possible by measurement of the amount of the iron oxide, which is present in the asbestos, welding or coal dust, to estimate the amount of the dust in the analyzed lungs. Since one of the oxides, magnetite (Fe_3O_4), has a ferromagnetic behavior it is possible to measure the amount of dust by magnetic measurements. This is the basis of the method used by Cohen, Kalliomaki and Robinson (10,11,12) which consists of magnetizing the magnetic dust by exposing the lungs to a magnetic field and then measuring the remnant magnetic field with a sensitive magnetometer.

In this paper a new way to measure the magnetic contaminants using nuclear magnetic resonance is proposed.

THEORY

The nuclear magnetic resonance of protons has been used extensively as a mean of measurement of the magnitude of magnetic field. Since the proton resonant frequency is directly proportional to the magnetic field in which it is immersed, measurement of the resonance frequency yields immediate information on the field.

Consider now a magnetic particle, introduced into a hydrogenous medium exposed to homogenous magnetic field Ho (Fig. 2). The magnetization alters the field in the vicinity of the particle. The protons in the neighborhood of the particle will experience a modified magnetic field and will therefore resonate at different resonance frequency. The degree of proton frequency change, depends upon the local field and should therefore be a function of such factors as the distance from the particle, particle size and particle magnetic permeability. The net effect is that the frequency of the protons within the particle's volume of influence will be shifted from their normal frequency position causing broadening of the proton resonance peak.

If a magnetic dust is dispersed in a hydrogenous medium, e.g. the lungs or other tissues, the frequency of tissue protons will change for nuclei lying within the field inhomogeneity. The degree of spectrum broadening should reflect the quantity of dust present in the tissue.

MATERIALS AND METHODS

The material used to simulate tissue in which the particles were suspended consisted of gelatine/water solution mixed at 1:10 ratio. The magnetic particles used here were iron particles 1-5μ in size (United Mineral and Chemical Corp.) and 5-10μ in size (Cotronics Corp.). The asbestos was 7RF02 chrysotile obtained from Johns Manville Corp.

For the preparation of the samples, the particles were separated in an ultrasonic bath. The liquid gel was then poured into the beaker which contained the particles, and stirred vigorously for about 15 minutes at room temperature. The gel containing the particles was then transfered to a NMR tube and refrigerated for storage.

In the animal experiment a solution of asbestos was introduced into rat lungs. 0.5cc of saline solution containing 7RF02 asbestos (0.02g asbestos/cc) was instilled intratracheally into two rats. A control animal received 0.5cc saline. The animals were sacrificed immediately and bled through the descending aorta. The trachea was tied below the level of the larynx to prevent expiration of fibers and the lungs and trachea were removed intact. The trachea was separated and the lungs were placed in NMR tubes for examination.

All the spectra were measured using a 60 MHz JEOL NMR spectrometer. The NMR tubes were 5mm thin wall tubes.

RESULTS

1. Effect of Concentration

Fig. 3 shows the effect of spectrum broadening for different concentration of iron particles suspended in gel. At sufficiently high concentrations of magnetic particles (100ppm) the effective width of the proton NMR peak will be so increased as practically to cause the peak to disappear.

A simple way to extract the information from these spectra is to observe the number of protons which did not change their resonance frequency. This will correspond to protons which are outside the regions of influence of the particles. Assuming that in the lung, the number of protons/cc is approximately constant, the fraction of unaffected protons will decrease with increase in the concentration of the magnetic contaminant. This approach eliminates the need for rather complicated calculations of line broadening and makes the analysis simple. The decrease in number of unaffected protons of the gel, as a function of concentration of iron particles is shown in Fig. 4. The figure indicates that this parameter is linearly proportional to the particle concentration.

2. Effect of Particle Size

Calculations of the magnetic field in the vicinity of a spherical particle indicated that the number of protons influenced by the particle should be proportional to the particle mass. This is an important finding since it indicates that if a few particles form a large cluster or condense to form one large particle, the signal should be proportional to the combined

mass of these particles, i.e. it is independent of the spatial density of the particles.

In order to validate these calculations, two groups of iron particles with different diameters, but of the same concentrations were suspended in gel. The particle sizes were 1-5μ and 5-10μ respectively. The plot of the unaffected number of protons versus concentration is shown on Fig. 4 for each group. As can be observed, the plots are identical i.e. for the same mass concentration, the signal has the same value. This indicates that the signal is proportional to the mass of the particles rather than to their number.

3. Asbestos Measurements in Gel

All experiments with asbestos were done using 7RF02 chrysotile asbestos. Chrysotile asbestos may contain 2-5% magnetite particles which adhere tenaciously to the fibers (13). It is therefore suitable for magnetic measurments. In order to check the relationship between concentration of asbestos and NMR signal, different amounts of asbestos was suspended in gel, as explained in Section 2.

Fig. 5 shows the NMR spectra for different concentrations of asbestos in gel. As expected the spectrum gets broader with increased concentration of asbestos. Fig. 6 shows the information extracted from the spectra shown on Fig. 5. One can observe a good linear proportionality between the signal and concentration. A reproducibility study was done by measuring different samples of the same concentrations. The reproducibility results are indicated by the error bars in Fig. 6. Reported asbestos concentration in asbestosis (9) fall in the 200-500 μg/g region which is easily detected by this method.

4. Asbestos Measurements in Animals

A feasibility study of the method was performed using rat lungs. Two rats were contaminated with a large quantity of asbestos as described in section "Materials and Methods". One rat was used as a control. The concentration of asbestos in the lungs of the contaminated rats was about 5000 μg/g. Fig. 7 shows the proton NMR spectrum from the lung of the control animal. It can be observed that the peak is much broader than the peaks obtained from the gel samples. The reason for this intrinsic broadening is most likely due to continuous exchange between bound and unbound water in the tissue. Fig. 8 shows the spectra from contaminated lungs. Since the asbestos concentration is large the peak disappeared completely due to the spectrum broadening.

CONCLUSIONS

The introduction of ferromagnetic particles into a hydrogenous medium causes broadening of the proton NMR spectrum. The degree of broadening can be utilized as a means of quantitative estimation of particle concentration. Experiments with different concentrations of particles indicated linear relationship between the signal and concentration. Investigation of the effect of particle size suggested that the number of protons which are influenced by the particle is proportional to the particle mass. This finding is important since the particles found in the lungs are usually not uniformly distributed, but form clusters of larger concentrations. The study with iron particles indicated that a limit of detection of about 2.5 μg of ferromagnetic material/g is obtainable at present, using this technique.

The feasibility of asbestos measurement was demonstrated for chrysotile, type 7RF02. Since the measurement of asbestos is dependent on the magnetite component, the sensitivity of the method for asbestos is a function of

magnetite percentage. The limit of detection for 7RF02 asbestos in gel was estimated as 50 μg of asbestos/g. Other types of asbestos will be investigated in the near future. A preliminary experiment on rats indicated that the introduction of large quantity of asbestos into the lung produced broadening of the spectrum. However, the measurement of magnetic particles in tissue is complicated by the intrinsic broadening of the line of the tissue protons. It is therefore expected that the limit of detection of asbestos in the lung will be somewhat higher than it was for the gel. A systematic series of experiments using different concentration of particles in animal tissue is planned.

On the basis of these preliminary experiments we conclude that NMR could become a useful technique for direct and rapid estimation of asbestos and other magnetic dust content in biological material. Furthermore, the technique could be applied in-vivo with the use of imaging NMR technique, to provide the content and location of the contaminant in the lung.

ACKNOWLEDGEMENT

We would like to thank Dr. S. Seltzer (Chemistry) for the access to the NMR spectrometer, to Dr. D. Bernstein who helped us with the animal experiment, to Dr. A. Forman for useful discussions, and to Dr. M. LeFevre for the samples of asbestos.

REFERENCES

1. Harries P.G. et al. (1972), Brit. J. Ind. Med. 29, 274.

2. McDonald J.C. et al. (1971), Arch. Environ. Health 22, 677.

3. Selikoff I. J. et al. (1970), In "Proceeding of the International Conference on Pneumoconiosis," 180. Oxford University Press.

4. Hickish E.E. et al. (1970), Ann. Occup. Hyg. 13, 17.

5. Selikoff I.J. et al. (1972), Arch Environ. Health 25, 1.

6. Beger P.J. (1933), Arch. Pathol. Anat. Physiol. 290, 280.

7. Sundius and Bygden (1938), Arch. Gewerbepathol. Gewerbehyg. 8, 26.

8. Beattie J. et al. (1961), "Inhaled Particles and Vapours". C.N. Davies Ed. Pergamon Press, N.Y.

9. Kalliomaki P.L. (1977), MD Thesis, University of Oulu, Finland.

10. Cohen D. (1973) Science, 180, 745.

11. Kalliomaki et al (1976), Scand. J. Work. Environ. Health, 4, 232.

12. Robinson S.E. et al. (1977), The Hahnemann Medical College and Hospital, Philadelphia, Pa., 19102, 103.

13. Badollet M.S. et al. (1961), Canadian Mining and Mettallurgical Bulletin, 54, 547.

14. Nagelschmidt G. (1965), Ann. New York Acad. Sciences, 132, 64.

Fig. 1a

LUNG DUST ANALYSES IN ASBESTOSIS, AFTER BEATTIE AND KNOX (1961)

	Grade of Asbestosis			
	None	Minimal	Moderate	Severe
Number of cases	16	14	8	11
Mineral content mg./gm. dried lung*	4.1	4.3	6.9	5.2
Dust exposure, years	16	18	27	24
Survival, years	3	7	6	10
Dust accumulation, mg./gm. per year exposed	0.27	0.24	0.25	0.21

*Five mg./gm. equals 1 gm. in a pair of lungs of 200 gm. dry weight.

Fig. 1b

WELDING DUST AND ASBESTOS IN LUNGS

GROUP	AMOUNT OF DUST/LUNGS MG	CONC. µG/G	REF.
CHRYSOTILE WORKER (20 Y EXPOSURE)	40	40	BEGER (1933)
AMOSITE (21 Y EXPOSURE)	1400	840	SUNDIUS (1938)
CONTROLS	4 DUST	4	KALLIOMAKI (1978)
STAINLESS STEEL WELDERS	10-600 FUME DUST	10-600	"
FOUNDRY WELDERS	30-600 FUME DUST	30-600	"
CROCIDOLITE ASBESTOS SPRAYERS	10 ASBESTOS	10	"

Fig. 1. Quantity and concentration of asbestos and welding fumes in lungs of occupationally exposed individuals. Concentration calculated assuming 1kg lung weight. Upper table reproduced from Ref. 14.

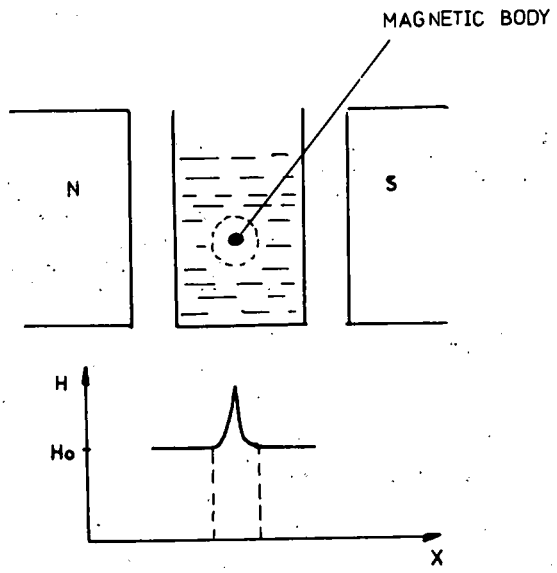


Fig. 2. Schematic representation of a magnetic field in the vicinity of a magnetic particle positioned in an aqueous material and placed in a homogenous magnetic field Ho.

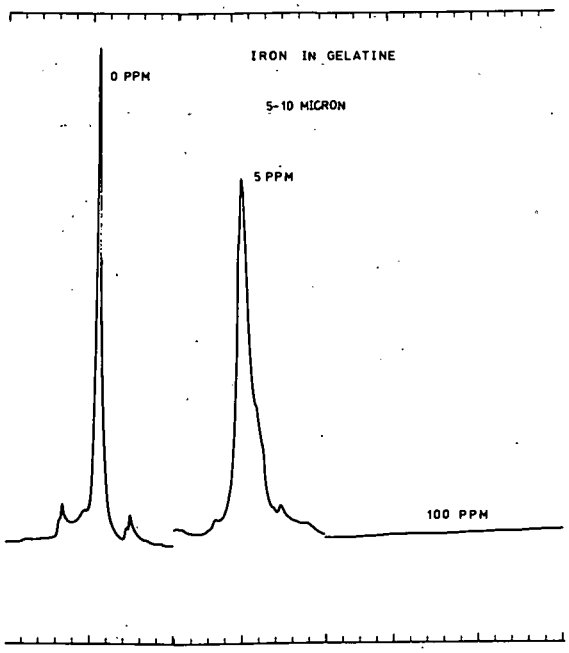


Fig. 3. NMR proton spectra as a function of concentration of iron particles suspended in gel.

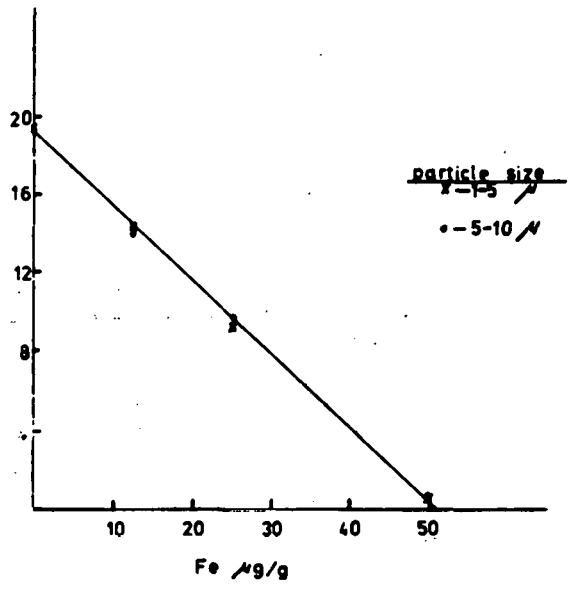


Fig. 4. Number of unaffected protons in gel as a function of iron concentration and particle size.

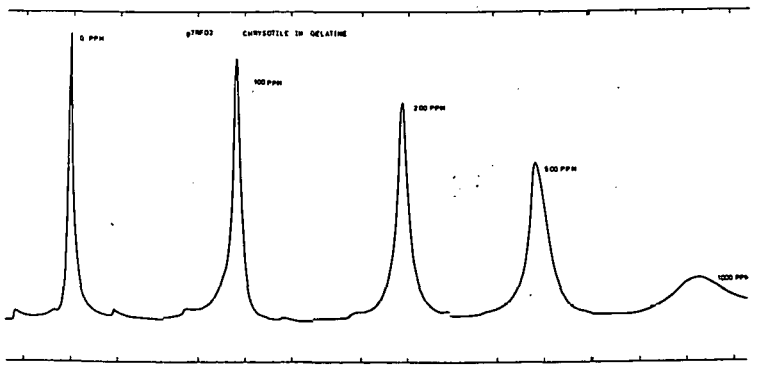


Fig. 5. NMR proton spectra as a function of 7RF02 chrysotile asbestos concentration in gel.

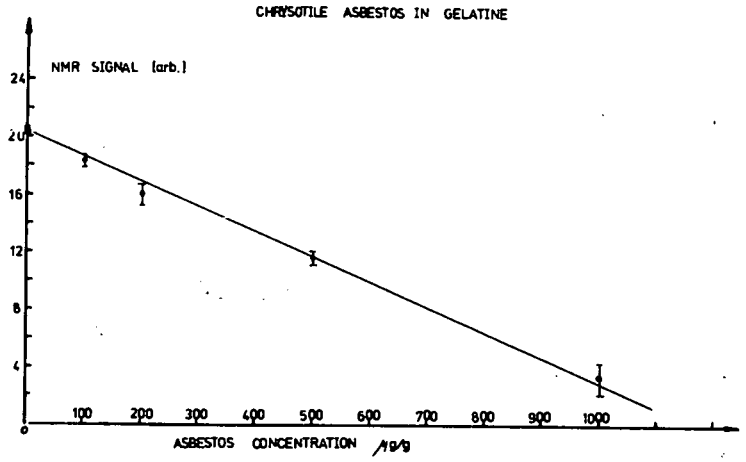


Fig. 6. Number of unaffected protons in gel as a function of asbestos concentration.

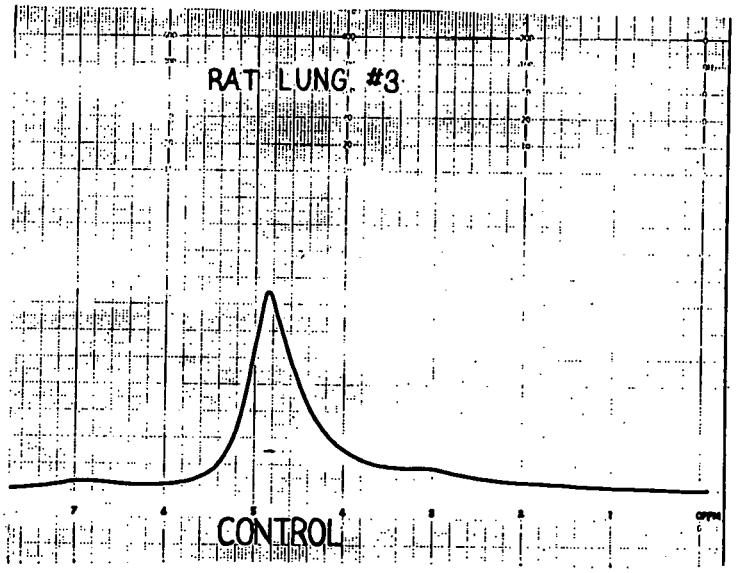


Fig. 7. Proton NMR spectrum of the control rat lung.

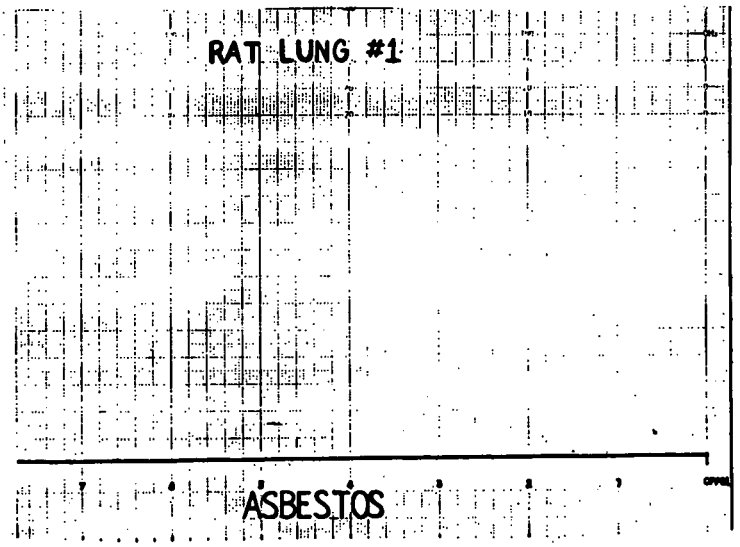


Fig. 8. Proton NMR spectrum of the contaminated rat lung. Concentration 5000 µg asbestos/g.

APPLICATION OF NEUTRON ACTIVATION ANALYSIS IN A REGULATORY AGENCY

William B. Stroube, Jr., and James T. Tanner
U.S. Food and Drug Administration
Washington, D.C. 20204

ABSTRACT

The role of neutron activation analysis in a regulatory agency will be illustrated. Examples of applications to research and short term special problems will be examined.

INTRODUCTION

The Food and Drug Administration maintains an activation analysis unit at the National Bureau of Standards. This group is unique within FDA and as such aids in many analytical problems for both Headquarters and the field laboratories in addition to conducting research. The NAA unit utilizes the 10 MW research reactor at the National Bureau of Standards in Gaithersburg, Maryland for this work. This paper illustrates the variety of projects in which NAA has played an important role.

Multielement Analysis of Animal Waste. For several years sewage sludge has been used as a source of cropland fertilizer. Both sewage sludge and animal waste have recently been used as a source of animal feed. This study involved the determination of twenty-one elements by NAA in animal waste, sewage sludge, and in traditional animal feed. Additional elements were determined by atomic absorption spectroscopy, induction coupled plasma spectroscopy (ICP), and anodic stripping voltammetry. The levels of Al, As, Cd, Co, Cr, Cu, Eu, Fe, Hg, Pb, Sb, Sn, Ti, and Zn were at least a factor of 100 higher in sewage sludge than in feedlot diets. Toxicity could be expected to occur in some animals fed feed with levels of Cd, Cu, Fe, Mn, Pb, Se, and Zn found in the sewage sludge. (1)

Multielement Analysis of Cement Dust. Another multielement project dealing with a cattle feed ingredient involved the analysis of cement kiln dust. Several farmers reported that cattle fed cement kiln dust gained weight at a much faster rate than cattle on normal feeds. These results were verified in a USDA research study. (2) The elements Al, Ca, Cl, Co, Cr, Cs, Cu, Eu, Fe, K, Mg, Mn, Na, Rb, Sb, Sc, Se, and Zn were determined in samples of the dust by NAA. For these elements no toxic levels were found.

Bromine in Beans. An interesting project, although hardly research, involved beans which were being held pending the outcome of analysis, before being released for sale. The beans were suspected of being sprayed with a pesticide containing bromine. Use of this pesticide would prohibit the sale of the beans in this country. Several lots of beans were involved and therefore speedy

analytical results were necessary. The A.O.A.C. procedure for bromine (and the pesticide) was a lengthy time consuming analysis. Samples of each lot of beans were taken, and shipped to Washington for bromine analysis by NAA. The beans with high bromine concentrations were subjected to the lengthier pesticide procedure. These lots were later denied entry into the United States.

Although the determination of bromine is an easy task for NAA, this does illustrate how this technique was used in conjunction with other analytical techniques to "solve" regulatory problems.

Fluorine and Molybdenum in Cattle Feed. Two similar cases involved cattle feed which was contaminated during shipment. In the first case, cattle feed was contaminated with a white crystalline powder. Cattle were dying in the fields and milk production had fallen to one half of its previous level. Chunks of the contaminant were collected along with the feed. Analysis by NAA, ion selective electrode and ICP identified the contaminant as Na_2SiF_6. Later investigation by FDA inspectors revealed that Na_2SiF_6 had been hauled in the boxcar before the feed. The boxcar was apparently not properly cleaned before its use to haul the cattle feed.

A similar case involved the detection of molybdenum in cattle feed. Again it involved the hauling of a contaminant in a boxcar and then hauling a food product in the same car without proper cleaning. In both cases the feed was destroyed after the contaminant was identified.

Chlorine in Rice Oil. Along similar lines, NAA was also used to determine Cl as an indicator of polychlorinated biphenyl (PCB) contamination. About 1000 people in Japan were poisoned as a result of ingestion of rice oil contaminated with PCBs. Values of approximately 1000 ppm for PCBs were obtained by several investigators using gas chromatography. A level of 1050 ppm chlorine was obtained by neutron activation analysis, twice as much as could be accounted for as PCBs. Further investigation by gas chromatography/mass spectrometry identified polychlorinated quaterphenyls to be present. (3) The PCBs were separated by column chromatography and total chlorine by NAA in the fraction was in agreement with the concentration of PCBs.

Survey of GRAS Food Additives. The multielement capability of NAA was used to survey for several elements in samples of "generally recognized as safe" (GRAS) food additives. One result of this NAA work was the identification of high levels of arsenic in one brand of kelp food supplement tablets. The kelp tablets were then removed from the market.

SUMMARY

The use of NAA for many of these projects certainly does not test the limits of the method or even contribute anything new to the analytical methodology; however, without NAA the solution to these problems would have been greatly delayed or may not have been possible. The final conclusion is that NAA has a definite place in a regulatory agency such as the FDA.

REFERENCES

1. S.G. Capar, J.T. Tanner, H.H. Friedman, and K.W. Boyer, "Multielement Analysis of Animal Feed, Animal Wastes, and Sewage Sludge", Environ. Sci. Technol., 12, 785, (1978).

2. T.H. Maugh, "Speaking of Science", Science, 199, 413, (1978).

3. L.R. Kamps, W.J. Trotter, S.J. Young, L.J. Carson, J.A.G. Roach, J.A. Sphon, J.T. Tanner and B. McMahon, "Polychlorinated Quaterphenyls Identified in Rice Oil Associated with Japanese Yusho Poisoning", Bull. Environm. Contam. Toxicol., 20, 589, (1978).

Distribution Pattern of Small and Trace Elements in Human Cancerous Tissues and Normal Human Tissues

M. Terai, M. Yasuda, A. Akabane, M. Matsumoto* and K. Hashimoto*

Department of Chemistry, Faculty of Science, Tokyo Metropolitan University. Fukasawa, Setagaya, Tokyo, Japan 158.

*The Pathological Institute, Juntendo University, School of Medicine. Hongo, Bunkyo, Tokyo, Japan 113.

The concentrations of the seventeen principal elements in six kinds of carcinomatous tissues and their sorrounding non-cancerous tissues have been determined by non-destructive neutron activation analysis. There were difference on the distribution of the Ca, Mg, Fe, Cr, Co and Sc between the cancerous tissues. The consistency of the Ca and Mg in the cancerous tissues were much more than those of sorrounding non-cancerous tissues, in the cases of gastric cancers, cholangiocarcinomas, hepatocellular carcinomas and metastatic carcinoma.

Introduction

Reports of studies on trace constituents in the tissues of organs are increasing. There appears to be a number of trace amounts of elements which play an important role in maintaining the normal physiological status of a living body. On the other hand there are many elements whose physiological effects are not known. The elements termed the essential ones effectively function to maintain the normal processes of the life cycle in an organism, when the amounts of these elements are within the standard levels. However, if the concentrations of these elements are insufficient or excessive, they disturb the metabolic system of the living body(1, 2).

Sometimes the trace elements independently effect physiological functions, but mostly they act mutually. The distribution pattern of the elements was largely similar in every normal tissues analyzed. If the physiological functions in the organism are malfunctioning, the distribution patterns of the elements are rearranged accordingly. In this study, the concentrations of the small and trace elements in human cancer tissues and their surrounding normal tissues, and were examined for a difference in the concentration of the elements between the former and the latter.

Experimental

Samples: The human cancer tissues and their surrounding normal tissues were obtained from 6 autopsy cases examined in the Pathological Institute, Juntendo

University, School of Medicine, Tokyo. The kind of samples were shown in Table 1. The cancer tissue samples were successively taken from the center of cancer to the sorrounding normal tissue at 10 mm intervals. All tissue samples were sliced off and weighed, and dried in the desiccator(P_2O_5) for over 7 days. The dried samples were weighed again and heat-sealed in clean polyethylene bags.

Table 1. The kinds of samples

No. of sample	The kinds of cancer
1- 3, 4- 6	gastric cancer, the stomach
7- 8, 9-14	carcinoma of sigmoid colon, the sigmoid colon
15-17, 17-18	metastatic carcinoma of the liver, the liver
19-20, 20-22	lung cancer, the lung
23-24, 25-27	hepatocellular carcinoma, the liver
28-31, 31-36	cholangiocarcinoma, the liver

Neutron activation and determination and determination of γ-ray: Samples were irradiated in a rotary specimen rack in a TRIGA MARK II reactor(Rikkyo University) with a thermal neutron flux of $5 \times 10^{11} n \cdot cm^{-2} \cdot s^{-1}$. The irradiation period was 3 min for short-lived nuclides, and 24h(intermittent irradiation of 6h a day for 4 days) for long-lived nuclides. Irradiated samples were removed from the polyethylene bag and transferred to new one before measuring the γ-ray spectra. The γ-ray spectra were determined on a Ge(Li) γ-ray detector and 4096 channel pulse height analyzer(Type 8100:Camberra Industies Inc. USA).

Results and Discussion

The concentrations of the small and trace constituents in cancer tissues and their surrounding normal tissues are shown in Table 2(1)-(2). The data was also plotted on the semilogarithmic paper against distance of the cancer tissue from the normal tissue in the axis of abscissa(Fig. 1(1)-(4)). The calculated correlation coefficients are shown in Table 3.

The Characteristics of the Distribution Patterns of the Elements in Human Cancers.

Gastric cancer(No. 1-3, 4-6): Correlation coefficients of the Mg and Ca were significant at the 95% confidence level. These concentrations within cancerous areas(No. 1-3) were higher than the surrounding non-cancerous areas (No. 4-6). The concentrations of Sc, V, Cr, Fe and Co were higher in non-cancerous tissues than cancerous tissues. The concentrations of Na, Mg, Sc, V, Mn, Fe and Co varied in the gastric wall near the gactric cancer. Whereas, those of Cl, Cu, Zn and Se did not vary in any areas of the tissues(Fig. 1(1)-(2)).

Carcinoma of sigmoid colon(No. 7-8, 9-14): The remarkable characteristic on the carcinoma of sigmoid colon was the variance of the Cr concentration. According to the distance from the center of the cancer to the normal tissues, the Cr concentration increases significantly. The Mn concentration is similarly high. Whereas, the Zn and Se concentrations showed the reverse tendency. The Mg V, Mn, Fe, Cu and Br concentrations varied greatly at the boundaries of the cancerous and normal tissues(Fig. 1(1)-(2)).

Metasttic carcinoma of the liver(primary focus is the carcinoma of sigmoid colon)(No. 15-17, 17-18): There were no significant difference of the concentrations of the elements in this cancer and normal tissues. Most of the elemental concentrations varied greatly in any tissues. This might be suggested to be characteristic of a metastatic carcinoma of the liver(Fig. 1(1)-(2)).

Lung cancer(No. 19-20, 20-22): The correlation coefficients of Cu and Fe

concentration decreased according to proximity to the surrounding normal tissue, and were significant at 99% and 95% confidence levels respectively. The Cr concentrations in these tissues were very high compared with those of the 21-30 years old group(3). In the cancerous tissues, the variations of the elemental concentrations were found in most elements except Co and Se. The Mg, Ti, Cr, Mn and Co concentrations fluctuated remarkably at the boundary between the cancer and normal tissues(Fig. 1(3)-(4)).

Hepatocellular carcinoma(No. 23-24, 25-27): Significantly high concentrations of the Mn and Zn have been shown in the carcinomatous tissues. The concentrations of Na, Ca, Cu and Se showed similar tendencies to the Mn and Zn. The concentrations of the Fe, Co and Br varied inversely. The elements Mg, Sc, Ti, Fe, Co, Cu and Br in the tissues of acrcinomas fluctuated widely in concentration(Fig. 1(3)-(4)).

Cholangiocarcinoma(No. 28-31, 31-36): The Na, Cr and Br correlation coefficients were significant at 95% confidence level, and these concentrations decreased with proximity to surrounding normal tissues. The Fe correlation coefficient was also significant at 95% confidence level, and the concentration showed a reverse tendency. The Co, Zn and Se concentrations did not vary in any part of the liver. The Mg, Ti, Mn and Cr concentrations fluctuated widely around the boundary(Fig. 1(3)-(4)).

Conclusion

Na, Mg and Cl which are concerned with the electrolytes in a body fluid, behaved similarly in the cancer and normal tissues. Ca, an another electrolyte, showed similar behaviour to these above mentioned elements in the carcinoma of sigmoid colon and the cholangiocarcinoma. Whereas, Ca showed low concentration in the surrounding normal tissues. The Fe concentration had the tendency of increasing with proximity to the normal tissues, except in the case of the carcinoma of the sigmoid colon. However, the Mn concentration was opposite to that of Fe. The concentration of the Cr was higher in the carcinomatous tissues than their surrounding tissues. The concentrations of the Sc and Co were higher in the cholangiocarcinoma and metastatic carcinoma of the liver than non-cancerous liver tissues.

In the results, the elements such as Na, Mg, Cl and Ca concerning acid-base equilibrium, and Mn and Fe concerning oxidation-reduction equilibrium, have significantly increased or decreased according to the distance from the cancer of carcinomatous tissue to the normal tissues.

Further study on small and trace elements could clarify the role of these elements on the metabolic activity or on the carcinogenecity.

References

(1) Cartwright, G. E.: "Symposium on Copper Metabolism" (W. D. McElroy and B. Glass eds.), p 244, Johns Hopkins Press Baltimore, Maryland, 1950.

(2) Cotzias, G. C.: Physiol. Rev., 38, 503(1958).

(3) Terai, M., Yasuda, M., Matsumoto, M., and Hashimoto, K.: Preprint, 1979 Annual Meeting Radiochemistry, at Osaka Univ., Osaka, Japan(1979).

(4) Terai, M.: Study on Minor Elements in Biological Materials by Neutron Activation Analysis. Dept. Chem., Tokyo Metropolitan University, Tokyo, Japan(1980).

Table 2(1) The concentrations of the small and trace elements in carcinoma of human being

(ppm/dry wt.)

No.	Na	Mg	Cl	Ca	Sc	Ti	V	Cr	Mn	Fe	Co	Cu	Zn	Se	Br
1	440	380	320	2700	0.15	3.0	0.20	3.6	——	9.8	0.20	8.1	77	12	4.2
2	510	260	320	2600	——	0.99	0.23	10	0.13	7.3	0.28	8.0	110	12	6.6
3	470	360	260	2300	0.17	7.3	0.30	6.8	0.32	11	0.28	6.8	78	12	5.4
4	1900	100	340	1400	0.49	11	0.44	18	0.28	20	0.58	5.6	82	11	8.5
5	760	160	490	1800	0.54	2.9	0.79	18	0.18	21	0.54	12	85	18	16
6	390	45	270	1100	0.49	12	0.071	17	0.19	15	0.44	6.9	64	9.6	5.6
7	660	110	650	760	0.21	2.9	0.17	9.3	0.12	20	1.1	9.7	88	13	25
8	750	28	——	780	0.25	7.7	0.22	14	0.097	32	0.67	9.4	84	15	2.8
9	660	210	——	650	0.20	3.1	0.063	7.3	0.030	16	0.69	3.0	63	8.1	20
10	530	250	440	380	0.23	5.4	0.18	19	0.092	20	0.70	2.3	77	13	17
11	590	140	510	520	0.24	7.9	0.13	22	0.12	20	0.70	5.1	77	10	20
12	1500	41	1500	1500	0.16	7.9	0.55	29	0.32	24	0.57	8.3	79	11	——
13	630	93	590	530	0.42	2.6	0.10	55	0.14	13	0.97	14	47	7.4	27
14	1300	190	710	610	0.29	99	0.18	48	0.25	29	1.1	15	54	9.6	32
15	220	55	130	1100	0.27	20	0.90	20	1.8	21	0.70	8.3	74	16	11
16	660	430	610	1200	0.20	4.5	0.24	48	0.051	20	0.61	0.65	75	13	48
17	480	130	590	560	0.21	0.50	0.10	14	0.22	52	0.71	18	120	10	19
18	550	130	630	560	0.26	2.5	0.14	42	0.25	52	0.65	22	80	14	25

1-3:gastric cancer, 4-6:the stomach, 7-8:sigmoid colon cancer, 9-14:the sigmoid colon, 15-17:metastatic carcinoma of the liver, 17-18:the liver.

Table 2(2) (Continued)

No.	Na	Mg	Cl	Ca	Sc	Ti	V	Cr	Mn	Fe	Co	Cu	Zn	Se	Br
19	300	180	230	2000	0.69	17	0.49	49	0.35	65	0.59	12	70	17	14
20	270	390	230	1300	0.71	10	0.68	84	0.11	82	0.90	14	84	14	16
21	430	340	350	1200	1.0	18	0.88	93	0.17	89	1.7	16	90	17	34
22	340	680	280	1300	0.91	26	0.70	79	0.061	92	0.83	19	84	18	311
23	460	75	440	1000	0.12	3.8	0.20	14	0.38	36	0.22	——	90	15	3.0
24	390	55	390	880	0.11	1.4	0.15	15	0.28	34	0.29	180	81	15	6.1
25	450	130	500	780	0.29	3.9	0.21	15	0.24	77	0.63	53	76	14	10
26	400	110	380	780	0.18	6.5	0.24	18	0.23	110	0.44	24	66	13	9.6
27	350	46	360	850	0.089	4.0	0.094	11	0.11	120	0.36	24	69	14	6.0
28	390	27	350	380	0.17	2.6	0.19	27	0.11	18	0.21	5.2	26	6.9	4.5
29	460	79	420	320	0.18	——	9.7	43	0.094	17	0.32	9.0	30	7.2	6.6
30	360	97	350	490	0.21	3.4	0.17	26	0.17	20	0.29	3.3	33	7.3	4.2
31	430	71	390	530	0.13	7.4	0.077	9.5	0.095	33	0.28	8.5	49	14	2.4
32	340	75	350	510	0.19	2.7	0.034	9.4	0.042	40	0.34	14	55	11	2.2
33	280	47	270	340	0.12	2.1	0.036	11	0.029	25	0.21	10	35	6.8	1.5
34	240	27	290	290	——	2.1	0.095	11	0.022	37	0.23	13	45	9.1	1.9
35	140	——	180	180	0.099	2.0	0.10	5.1	0.039	28	0.15	6.8	36	8.7	1.2
36	290	70	350	460	0.19	14	0.22	6.7	0.12	32	0.27	14	52	9.3	2.3

19-20:lung cancer, 20-22:the lung, 23-24:hepatocellular carcinoma, 25-27:the liver,
28-31:cholangio carcinoma, 31-36:the liver

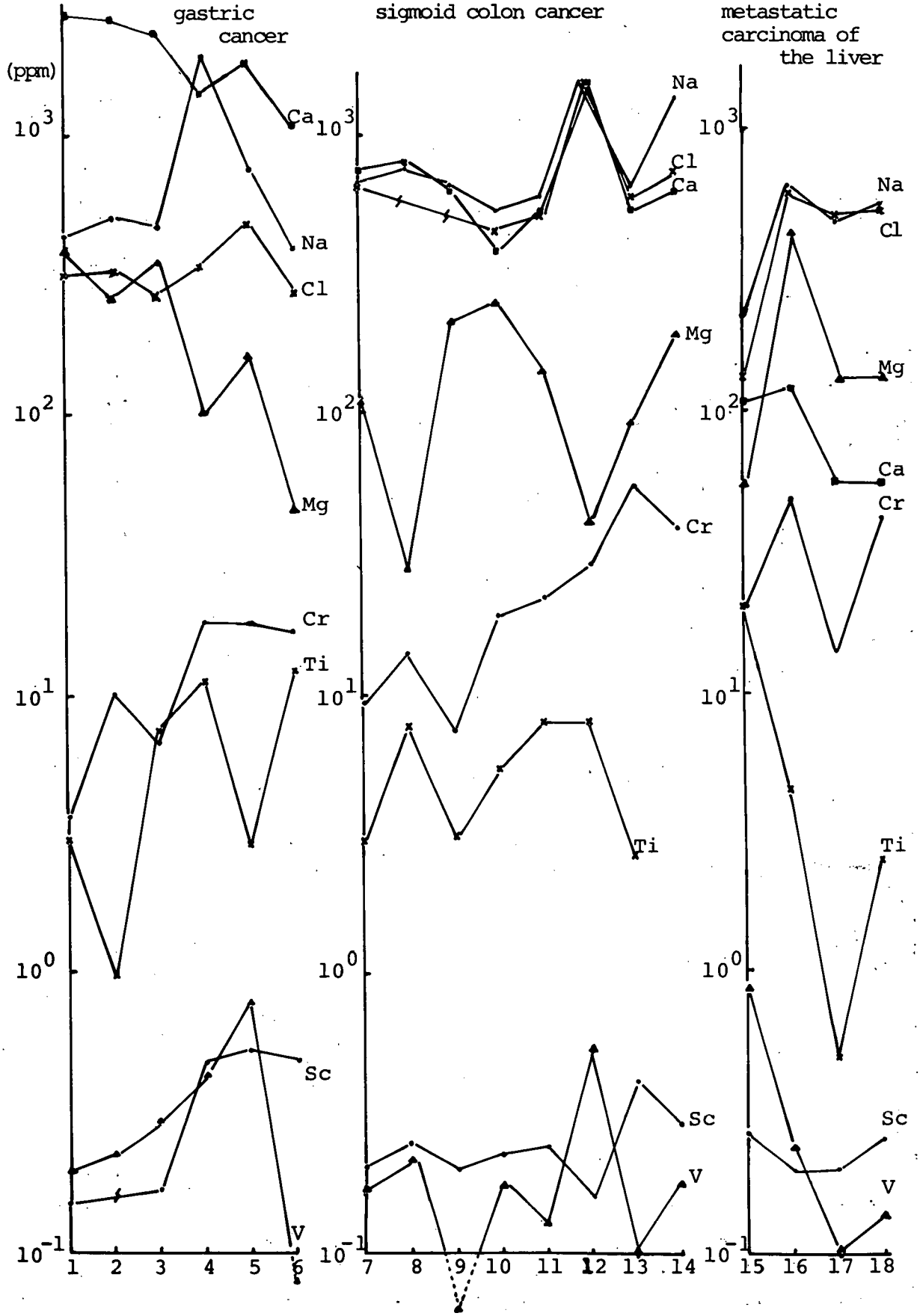


Fig. 1(1). The relationships between the distance from the center of cancer and the concentration of small and trace elements.

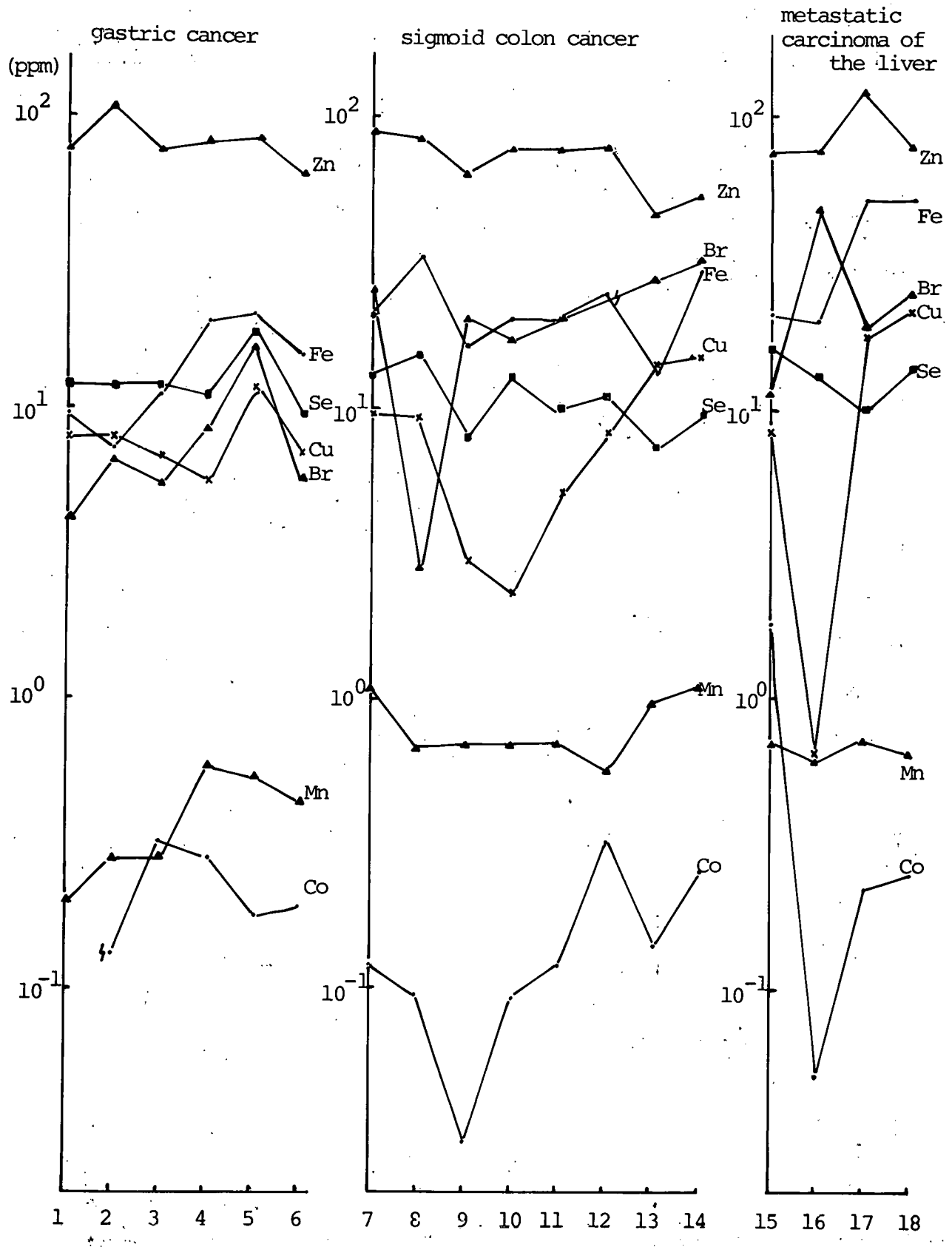


Fig. 1(2). (Continued)

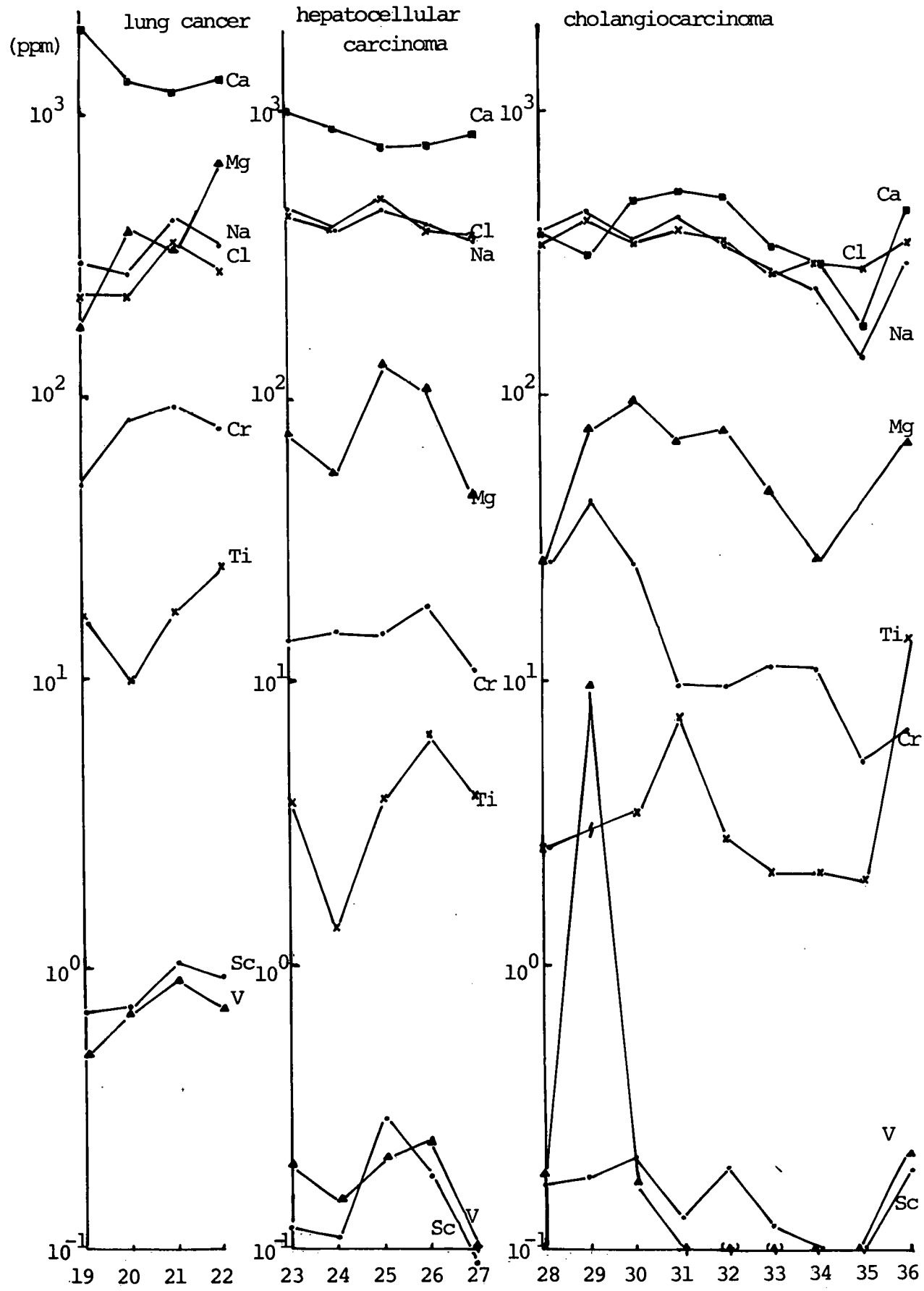


Fig. 1(3). (Continued)

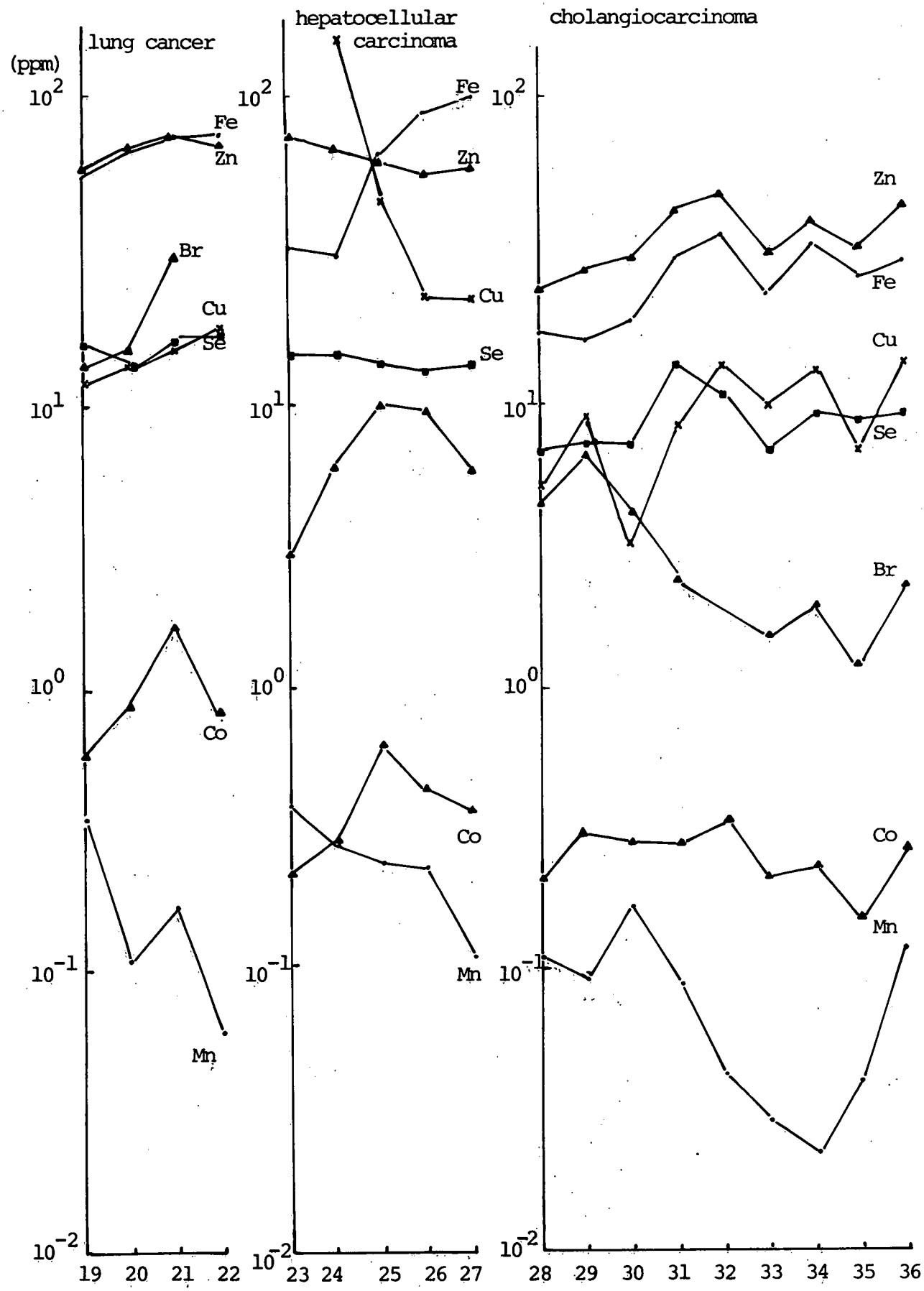


Fig. 1(4). (Continued)

Table 3. Correlation coefficients between the distance from the center of cancer and concentrations of small and trace elements.

Elements	No. 1- 6	No. 7-14	No. 15-18	No. 19-22	No. 23-27	No. 28-36
Na	0.18	0.51	0.57	0.49	-0.73	-0.80**
Mg	-0.87*	0.10	-0.06	0.89	-0.03	-0.06
Cl	0.23	0.22	0.80	0.62	-0.72	-0.65*
K	0.90**	0.37	0.69	———	0.55	0.23
Ca	-0.91**	0.03	-0.86	-0.81	-0.68	-0.12
Sc	0.87*	0.49	-0.03	0.84	0.03	-0.60
Ti	0.64	0.58	-0.82	0.68	0.49	0.20
V	0.25	0.16	-0.83	0.67	-0.32	-0.39
Cr	0.86*	0.90**	0.27	0.67	-0.17	-0.80**
Mn	-0.08	0.64	-0.71	-0.81	-0.96**	-0.05
Fe	0.72	-0.01	0.90*	0.95*	0.96**	0.75*
Co	0.79*	0.03	-0.47	0.42	0.44	-0.29
Cu	0.14	0.49	0.78	0.99**	-0.86*	0.45
Zn	-0.47	-0.74*	0.36	0.74	-0.94**	0.54
Se	0.11	-0.62	-0.36	0.44	-0.73	0.10
Br	0.24	0.31	0.12	0.81	0.50	-0.80**

* : Significant correlation at a 95% confidence level,

** : Significant correlation at a 99% confidence level.

Neutron Activation Analysis Of Copper And Silver In Environmental Samples.

By
Parag K. Shah,
Department of Nuclear Chemistry

and

B.C. Haldar
Environmental Chemistry Laboratory,
The Institute of Science
Bombay-400 032, INDIA

ABSTRACT

A rapid method is described for simultaneous determination of copper and silver in environmental samples by thermal neutron activation analysis involving substoichiometric extraction with HINAP. The time required for radiochemical purification and counting of two samples and one standard does not exceed 2 hours. 1 μg of copper and 0.021 μg of silver could be determined with an accuracy of 11% and 15% respectively.

INTRODUCTION

Heavy metal contamination of the environment has recently been recognized as a serious health hazard problem. Silver has been suspected as a carcinogenic element[1] and excess copper causes Wilson's disease. It is, therefore, necessary to monitor environmental samples for copper and silver so that adequate preventive steps could be taken to protect the human health.

The present paper presents a rapid method for simultaneous determination of copper and silver by neutron activation analysis involving substoichiometric extraction with isonitrosoacetophenone (HINAP). The method has been tested by analyzing oyster homogenate, IRI tobacco, Bowen's Kale and synthetic mixtures and it has been applied to environmental samples.

EXPERIMENTAL

Sampling: Crustaceans and fish (20 animals) were dissected after bringing collection to the laboratory and each of the tissues was lyophilised ground to a fine powder and used for analysis. Animals were separated according to their sex prior to the dissection. Plants were washed with double distilled water, dried at 60°C in an air over, finely powdered, packed in coloured bottles and stored in an air-conditioned room. Sediment and soil were air dried at room temperature before analysis. All analytical data were normalized to the (105°C) dry weight of the sample.

Irradiation: 100-150 mg of the sample and 10 μg of each of copper and silver standards are irradiated for 7-12 days in the CIRUS reactor at BARC, Trombay at a thermal neutron flux of $5\text{-}8\times10^{12}$ n/cm^2/sec.

Procedure: The irradiated sample is dissolved in a mixture of 5 ml of conc. HNO_3 and 1 ml of conc. H_2SO_4 containing 5 mg of each of copper and silver carriers. The solution is evaporated to dryness. The residue is dissolved in dilute HNO_3 and the solution is adjusted to pH 10 with ammonia. Copper is extracted with excess of HINAP in chloroform.

The aqueous phase is brought to pH 1, washed with chloroform, treated with 2 ml of 0.01M EDTA and 3 ml of 0.0093M HINAP in 0.1M NaOH, raised to pH 7.5-8 and equilibrated with 10 ml of O-dichlorobenzene. The organic extract containing silver is scrubbed with water of pH 7.5-8. A 4-ml aliquot of the extract is counted on a gamma-ray spectrometer provided with a well-type 3.8 cm x 3.8 cm NaI (Tl) detector.

Chloroform extract is shaken with 0.5M HNO_3 to re-extract copper into the acid solution. The solution is washed with chloroform, treated with 3 ml of 0.1M NaCN, made to pH 9 and contacted for 2 minutes with substoichiometric amount of HINAP in chloroform. The activity of a suitable aliquot of the organic phase is measured after washing it with water at pH 9.

The standard is treated identically. The amount of the element present in the sample is calculated in the usual way.

RESULTS AND DISCUSSION

The results of decontamination studies with 18 elements in the substoichiometric extraction with HINAP are given in Tables I and II. The decontamination factors for these elements are greater than 10^5.

TABLE - I.
Decontamination Studies In The Substoichiometric Extraction Of Ag(I) With Isonitrosoacetophenone Into O-dichlorobenzene

Decontamination factor greater than.	Element
10^6	Mn(II), Cu(II), Na(I), As(III), Hg(II), W(VI).
10^5	Co(II), Se(IV), Fe(III), Cr(III), Au(III), Sb(III), Cd(II), Zn(II), K(I), Pd(II), Ca(II), Sn(II).

The results of analysis of oyster homogenate, IRI tobacco, Bowen's Kale and synthetic mixtures are given in Table III. The values for copper and silver in these samples are in good agreement with those reported by others.

TABLE - II.
Decontamination Studies In The Substoichiometric Extraction Of Cu(II) With Isonitrosoacetophenone In Chloroform

Decontamination factor greater than.	Element
10^6	Na(I), Ag(I), Fe(III), Se(IV), Co(II).
10^5	Zn(II), Cd(II), Hg(II), Mn(II), Cr(III), Au(III), Sn(II), Sb(III), Ca(II), W(VI), As(III), Pd(II), K(I).

TABLE - III.

Determination Of Copper And Silver By Substoichiometric Neutron Activation Analysis

Sample	Copper (μg/g)		Silver (μg/g)	
	Found*	Reported	Found*	Reported
Oyster homogenate. (MA-M-I)	322 ± 11	285-365[2]	5.6 ± 0.4	5.6-7.0[2]
IRI tobacco	62.9 ± 3.2	70.1 ± 1.6[3] 63.0 ± 1.9[4]	0.22± 0.02	0.17 ± 0.02[5] 0.21 ± 0.03[6]
Bowen's Kale	4.95± 0.20	4.8 ± 0.7[7] Taken	0.032±0.003	0.03[7] Taken
Synthetic mixture	1.00± 0.11	1.00	0.021±0.003	0.020

* Results are reported at 95% confidence limit.

Data for copper and silver in environmental samples are shown in Tables IV and V. The values for copper agree well with those obtained by Ganesan[8] following a different procedure. 1 μg of copper and 0.021 μg of silver could be determined with an accuracy of 11% and 15% respectively. The time required for radiochemical purification and counting of two samples and one standard does not exceed 2 hours. The radiochemical purity of samples was checked by measuring the beta and gamma energies of the separated activity. The half-life of Cu^{64} was also measured.

TABLE - IV.

Simultaneous Determination Of Copper And Silver In Environmental Samples By Neutron Activation Analysis

Sample	Copper (μg/g-dry weight)		Silver (μg/g-dry weight)
	Found*	Reported	Found*
M-m-C	130 ± 4	132	1.03 ± 0.08
G-m-C	324 ± 11	356	1.70 ± 0.08
H-m-C	244 ± 9	225	2.20 ± 0.16
M-f-C	133 ± 4	138	0.64 ± 0.05
G-f-C	568 ± 20	579	1.30 ± 0.09
H-f-C	323 ± 11	342	5.0 ± 0.3
M-Ca	6.0 ± 0.5	5.9	0.48 ± 0.05
G-Ca	40 ± 2	37	1.00 ± 0.06

M-Muscle; G-Gills; H-Hepatopancreas; m-male; f-female; C-Crab; Ca-Catfish.
* Average of 2 results.

TABLE V.
Simultaneous Determination Of Copper And Silver In Environmental Samples By Neutron Activation Analysis

Sample	Copper (μg/g-dry weight) Found*	Reported	Silver (μg/g-dry weight) Found*
Avicennia leaves	44 ± 2	43	0.30 ± 0.02
Avicennia roots.	51 ± 2	53	0.27 ± 0.03
Cynodon grass	51 ± 2	57	0.13 ± 0.01
Sesuvium	17.0± 0.8	18	0.20 ± 0.02
Sediment	25 ± 1	23.6	0.14 ± 0.02
Soil	4.9± 0.3	5.6	0.10 ± 0.01

* Average of 2 results.

REFERENCES

1. T.D. Lucky, B. Venugopal "Metal Toxicity in Mammals", Vol. I, p. 196.
2. R. Fukai, B. Oregioni, D. Vas, Oceanologia Acta, 1, 391 (1978).
3. R.A. Nadkarni, B.C. Haldar, Anal. Chem., 44, 1504 (1972).
4. B.M. Tejam, B.C. Haldar, Radiochem. Radioanal. Letters, 9, 19-26 (1972).
5. B.M. Tejam, B.C. Haldar, Proc. Chem, Symposium, DAE, Dec. 21-23 (1972), Aligarh, p. 55.
6. R.A. Nadkarni, W.D. Ehmann, Radiochem, Radioanal. Letters, 4, 325 (1970).
7. H.J.M. Bowen, "Advances in Activation Analysis", Vol. I, Academic Press, London, 1968.
8. R. Ganesan, Private communication.

We express our sincere thanks to Dr. (Mrs.) Z.R. Turel, K.C. Mahindra Professor of Nuclear Chemistry and Head of the Department of Nuclear Chemistry for her helpful suggestions and interest in the work.

Trace element analysis of human hair by proton induced X-ray excitation PIXE

A.Aframian, H.Shakiba, A.Housseiney
Atomic Energy Organization of Iran, Nuclear Researdh Center
P.O.Box 3327, Tehran, Iran

Abstract

Asimple non-destructive method of trace element analysis has been described based on proton induced X-ray excitation. Preliminary results for fifteen different elements have been presented, with particular reference to Lead as a mostly toxic pollutant. Sub-ppm detection levels have been obtained and possible correlations between the pollution of the biosphere and certain medical ailments considered.

1. Introduction

Pollution of the biosphere with such elements that are found in relatively small concentrations is currently of much significant interest,particularly in relation to the monitoring of toxic or cacinogenic environmental pollutants. Primarily the determinations of initial levels of trace elements in man and the extent of his contamination in areas where certain elements have a natural abundance or there is a preponderance of certain industrial by-products would be expected to show certain anamolies in concentrations. We discuss here an accelerator-based method of trace element analysis using proton induced X-ray excitation, to study the trace element contents as well as the major and minor components ofhuman scalp hair with a view to possible correlation for environmental and medical investigations.

Trace elements may be incorporated into hair from the blood stream as well as through sorption or ion exchange from dust and exhust fumes,sweat etc., as such reflecting both metabolic as well as external contamination processes. Hair generally being an excretory tissue with useful investigative properties, enables the evaluation and the uptake of trace elements from the atmosphere and their storage over relatively long periods of time. Samples can be easily collected, preserved and handeled. It is aimed here to establish overall patterns of elemental contents in scalp hair of normal populations in different geographical (urban and rural) regions in Iran with some emphasis on Lead as a mostly toxic pollutant.

2. Experimental procedure

2.1 Target preparation

Scalp hair samples a few centimeters long were cut with normal medical stainless steel scissors from subjects under study with respect to the regional habitat,age,sex and occupation. Proper care was taken not to use very thick hair while not choosing samples which had been subjected to dyes or various other cosmetics. In particular some samples were taken of professional moulders. Each batch of hair was washed in aceton,water and aceton sequentially with the primary step being from two to three hours and the subsequent steps fifteen minutes each.

Some thirty to forty individual strands cut roughly a centimeter above the distal endwere then strung across a perspex frame which would be left to dry in a dust-

-free atmosphere for up to two hours and then placed directly inside the irradiation chamber,facing a defocussed proton beam of roughly one centimeter in diameter. The proton energy of 2.9 Mev from the 3 MeV Van De Graaff allowed easier identification of the heavier trace elements. Irradiations were made with a 100 nAmp beam intensity for some two to three hours,with the simultaneous recording of the characteristic X-ray spectra using a Si(Li) detector with a resolution of 165 eV at 5.9 KeV. The resulting spectra were then analysed by an on-line PDP-11/05 computer. In some instances longitudinal scans were made to check for uniformity and possible presence of regioal concentrations. Separate irradiations were also carried out for the distal ends (roots) of samples and comparisons made with the spectra of the respective stalks. Reference to the recorded concentration levels of trace elements have been made on a dry weight basis at 12% humidity when samples are assumed to reach equilibrium. However this can vary with respect to the changes in the surrounding humidity.

Due to the inherent porblems in the doping of the hair samples, the relative concentrations of the various constituents quoted have been based on comparison of the respective peak areas of $K_\alpha + K_\beta$ or the $L_\alpha + L_\beta$ of Yttrium nitrate $Y(NO_3)_3.5H_2O$ with those of the trace elements present in each target. The Yttrium being an external standard of a known concentration (e.g. 250 ppm) deposited on a layer of kapton backing . The backing being 7 microns thick. To alleviate the problem a technique is being established with the cooperation of the International Atomic Energy Agency to obtain targets of pulverised hair. Hairs thoroughly washed have been encapsulated in a snap-in type teflon container with a number of teflon balls. Immersion of the container in liquid nitrogen provides freez dried material which can be vibrated(at say 50 rps) at room temperature for some 2-3 minutes. Fine hair powder can be obtained by repeating the above procedure two to three times For greater uniformity a nylon mesh can be used to separate the larger particles for further grinding. This has the added advantage that some 80% of the hair particles are of the order of 50 μm in length ,and roughly equal to the thickness of a normal scalp hair.

3. Analysis of results

3.1 Evaluation of data and normalization

Preliminary observation of the degree of homogeneity

Due to the diverse nature of the sample in terms of a person's metabolic activity,general habitat,dietary, occupation etc., it was expected that there would be a significant measure of inconsistency in terms of the overall levels of major and minor as well as trace elements. The choice of young people (12-35 years) as donors was partly to diminish this inconsistency,since older people would have been exposed to and absorbed larger quantities of artificial material, leading to possible latent or future metabolic disorders. Furthermore hair due to its geometry and variations in thickness (50-100 μm) can not be classified strictly as a thick or a thin target for the purposes of X-ray self-absorption. Additionally its cylindrically formed stalk might have slight variations in density for different subjects,while being partly amorphous. As Such therefore Zinc having been reported[1)] as being constant in both its body weight and relative levels of excretion was selected as a reference material with the other elements reported as relative to zinc.

As a result of the intercomparison of various subjects we can expect to draw a certain conclusion based on preliminary findings regardingthe degree of homogeneietyof the samples examined and the data obtained. Therefore tables (1 and2) indicate relative peak areas with respect to Zinc for a given element.Table (1) being for the Tehran metropolitan area with a population of some five million. Table (2) is representative of a generally urban-come rural agricultural community some 500 miles north of Tehran. Table (3) shows the results specifically for Lead , from two professional moulders with up to 25 years experience. The evident discrepancies for individual subjects and the standard deviations could be associated partly to analytical errors. However to simply reject the outlying data or representation by an overall weighted mean average would not adequately define the true existing fluctuations in elemental concentrations.

3.2 Problem of rejection of outlying results

Results deviating from the population of the other samples met in the intercomprison tests and leading to gross errors are generally due to analytical procedures,instrument calibration,standards used and the calculations employed etc.,and usually vary from element to element. Therefore if reliable values of trace concentrations and their confidence limits are to be arrived at on the basis of intercomparisonsruns an appropriately sensitive method for the detection and rejection of outlying resultsis indispensible. Based on the previous use of this approach for processing of data,in which the "true value" was known the procedure described below seems to assure good selectivity of rejection of outlying results,while not leading to excessive rejections. In table (4) therefor we have compiled the relults for a number of samples analysed, dividing the data into two groups, of high and low mean relative concentrations with respective standard deviations. This then enables the use of even the apparently outlying values without undue interference with the true value. Thus the $\pm 2\sigma$ interval may be taken as an initial estimation of the maximum probable inhomogeneiety. Hence in order to assess with some degree of certainty the true or the relative content of an element, the following criteria had to be fulfilled:

a)-relative uncertainty of the overall mean (at a significance level of $\alpha=0.05$),lower than 20% (trace elements) or 15% (major and minor elements).

b)-relative standard deviation of the overall mean lower than 25% (trace-elements) or 15%(major and minor elements).

c)-where possible,data from at least two different analytical methods could be compared for the calculation of the overall mean.

4. Discussion and conclusion

In this article the results for pulverised hair targets have not beem included. However both the fixed beam analysis and the longitudinal scans showed that amongst all age groups examined (12-40 years) for both male and female, in the metropolitan/urban areas and that for the rural regions the elements sulphur and calcium are the most abundant.There being rather uniform distributions with no regioal concentrations observed for a givenstrand excluding the distal end.

Altogether sixteen elements namely Al,Si,P,S,Cl,Ca,K,Ti,Mn,Fe,Ni,Cu,Sr,Cd and Pb have been investigated.It is observed that elements Ca and S have the highest abundance. Calcium being the major bone substrate is not easily affected by the immediate environment,while superficial deposition of sulphur from the atmosphere can be significant. At the same time the anamolous presence of Sr is probably due to its easily exchangeable nature for calcium. The significant presence of Pb, in the dense traffic area of Tehran along with Cadmium and their near total absence in the rural regions are well demonstrated. The median values for Zinc (165 ± 20 ppm) and Pb (4.3 ± 0.1 ppm) are for average subjects. HOwever that for Pb in professional moulders was found to be of the order of 80 ± 10 ppm, being in reasonable agreement with the results of Stoeppler et al[2]. Similar deposition and/or absorption by ion exchange or various other mechanisms are of course possible perhaps through washing of the hair with cleansing agents, rather than through ingestion of food and/or water, thus adversely affecting natural contents. Similarly the near ansence of Cl and the reduced levels for other elements may point to the presence of a possible distribution or a gradient across the hair diameter. This would then indicate that the core and the cortex have a biased distribution being richer in some and poorer in others and visa-versa. The fact that ionic migration may be forestalled or sharply reduced during or after the cornification process from the distal end upwards lends some weight to such an argument,even though a single hair strand of thickness 70-100 microns can not be regarded as either a thick or a thin target for purposes of self absorption of X-rays.

Table (1). Ratio of the peak areas of various elements respect to Zinc in scalp hair for Tehran metropolitan area

Sample No.	Age	Sex	Al	Si	P	S	Cl	Ca	K	Ti	Mn	Fe	Ni	Cu	Sr	Cd	Pb	comments
1	18	M			1.35	54.5		19.5	1.21	0.07		0.55		3.54				high Cu
2	18	M			1.45	79.42		24.84	1.46	0.16	0.71	0.71		3.36				high Cu
3	15	M			0.9	32.5		35.8	1.35	0.46	0.12	0.35	0.06	0.25	0.06		0.05	
4	40	F			0.25	21.62	12	15.42	12.7		0.1	0.43		0.48		0.11	0.2	
5	12	F		4.7	2.4		29	113	2.54	0.43	0.13	1.35		0.2			0.04	High Ca
6	14	F	0.28		0.53	26.3		45.3	9.8	0.19		0.69	0.07	0.64	0.03	0.13	0.29	
7	35	F				61.4		25.2	2.22			0.44		0.32	0.02			
8	31	F			0.93	23.2		95.34	3.73		0.41			0.24	0.13			High Ca
9	30	F			2.5	77.4		77	1.4		0.13	0.35		0.23	0.04	0.08	0.093	
10	16	M			2.65	70.4		53.93	2.65	0.25	0.06	0.34		0.25		0.02		
11	16	M			3.02	98.1		57.2	1.77	0.11		0.32		1.61	0.06			
12	15	M			0.9	32.5		35.8	1.35	0.46	0.12	0.35	0.06	0.25	0.06		0.05	
weighted mean average concentrations in ppm, (μg/g)																		
					223 ±42	720 ±70		237 ±35	25 ±6	1.2 ±0.1	0.7 ±0.12	2.7 ±0.04	0.41 ±0.07	6.1 ±0.9	0.36 ±0.02	1.1 ±0.1	2.3 ±0.4	
Average high					334 ±61	1452 ±320		386 ±72	73 ±17		2.03 ±0.31	4.5 ±0.74		20.1 ±4.8			3.8 ±0.64	
Average low					93.6 ±15	391 ±65		118 ±21	12.5 ±2.1		0.65 ±0.1	0.35 ±0.3		1 ±0.02	0.28 ±0.03		0.87 ±0.015	

* The elements not quoted are those which have not been detected within a given irradiation time.

Table (2). Ratio of the peak areas of various elements in hair with respect to Zinc for an urban area 500 miles north of Tehran

Sample No.	Age	Sex	Al	Si	P	S	Cl	Ca	K	Ti	Mn	Fe	Ni	Cu	Sr	Cd	Pb	Comments
1	16	F			0.32	11.4		11.26	0.42		0.05	0.09		2.65	0.04			High Cu
2	19	M			0.2	31.6		45.32	2.2		0.14	0.55	0.1	0.21	0.03			
3	16	F			2.8	112.15		96.3	2.3	0.27	0.05	0.66		0.05				
4	17	M			2.3	117.7		103.3	1.74	0.15	0.08	0.27		0.36				
5	17	F			2.71	175		281.1	6.2		1.63	1.08	0.31					High S,Ca,Mn Fe.
6	18	M			1.07	32.3		31.23	0.98			0.55	0.04	0.17	0.04			
7	16	F			1.07	35.4		68.6	1.27		0.51			0.23	0.013			
8	29	F			2.7	67		131.25	3.1		0.24	0.6		0.66	0.08			High Ca,K
9	4	F			0.9	27.04		14.2	1.6			0.31		0.25				
Weighted mean average concentrations in ppm, (μg/g).																		
					230 ±45	1175 ±220		396 ±96	13.6 ±2.8	0.82 ±.06	1.95 ±0.38	2.66 ±.3	0.98 ±.34	4.03 ±.72	0.28 ±.05			
Average high					286 $\pm^{49}$	1752 $\pm^{340}$		618.7 $\pm^{118}$	16.27 ±3.5		1.5 ±.28	3.75 ±.48	1.34 ±.24	2.4 ±.36	0.36 ±.07			
Average low					29.7 ±8.7	408 ±115		107.3 ±22	4.33 ± 1.2		0.4 ±.01	0.87 ±.19	0.26 ±.06	0.78 ±.3	0.15 ±.012			

* The elements not quoted are those that have not been detected within a given irradiation time.

Table (3). Ratios of the peak areas of Lead to Zinc for professional metal moulders

work experience years	Age	Sex	Pb/Zn	concentration ppm
25	49	M	2.45	86± 10
5	25	M	0.82	22± 6

Table (4). Concentrations of a number of major,minor and trace elements in ppm of human scalp hair and corresponding probable inhomogeneiety.

	P	S	Ca	K	Ti	Mn	Fe	Ni	Cu	Sr	Cd	Pb
1)- Location Metropolitan Tehran area	220	854	247	37	1.2	1.13	2.5	0.4	9.07	0.32	1.1	2.3
standard deviation	±98.6	±443	±110	±26	±0.1	±0.64	±1.7	±0.07	±8.07	±0.04	±0.1	±1.2
results laying within 2σ	9/11	11/11	9/11	11/12	7/8	7/8	11/11	3/3	11/12	6/7	5/6	
2)- Rural area ppm	182	1112	374	15	0.82	1.73	2.44	0.86	2.4	0.26		
standard deviation	±110	±550	±210	±1.34	±0.06	±0.23	±1.2	±0.45	±1.33	±0.09		
relultslaying within 2σ	7/9	7/9	8/9	8/9	2/2	6/7	7/8	2/3	6/7	5/5		

It is noteworthy to mention that the existing spread in trace element contents in human hair suggest difficulties in obtaining correlations with medical factors. However the presence of an appreciable discrepancy if any, could indicate a degree of reliability in the hair analysis and would in turn stimulate further analysis of a given subject. In this respect it will be mentioned that correlations between trace element levels and various types of diseases are being intensively studied . The correlations between reduced or enhanced trace element levels and some specific diseases which have been investigated are as follows:

Calcium	bone disease
selenium	cancer
Zinc	skin diseases
"	atherosclerosis
copper	myocardial infarction
"	rheumatoid arthritis
"	wilsons disease
cadmium	hypertension

drug administration and dietary intake will undoubtedly result in an ever changing gradient of trace elements in tissues and blood. However since hair can serve as a suitable register of trace element levels there is room for assumption that it can inthe future be exploited by the medical profession as an indicator of certain human ailments.

References

1)- Cornelis R, J.Radioanal.Chem 15 (1973) 305.

2)- Stoeppler M, paper presented at the IAEA advisory group meeting Vienna January 23-26, 1978.

Acknowledgement

The authors thankfully acknowledge the assistance of the technical staff of the VDG laboratory of the NRC Tehran and to Dr.S.Lodhi, L.Manou and S.Ghahremani for their many helpfull suggestions.

In vivo neutron activation analysis in a study of cadmium and hypertension in South Wales

W.D.MORGAN,[1] P.E.CUMMINS,[2] P.C.ELWOOD,[3] C.J.EVANS,[2] J.DUTTON,[2] A.SIVYER[4]

1 Medical Research Center, Brookhaven National Laboratory, N.Y. 11973 USA
2 Dept. of Physics, University College of Swansea, Swansea SA2 8PP, Wales
3 M.R.C. Epidemiology Unit, 4 Richmond Road, Cardiff CF2 3AS, Wales
4 Dept. of Medical Physics, Singleton Hospital, Swansea SA2 8QA, Wales

Abstract

There is conflicting evidence concerning the influence of cadmium on the incidence of essential hypertension. Some animal experiments have shown that small doses of cadmium can induce hypertension whereas larger doses do not. In humans, post-mortem tissue analyses and blood and urine Cd data also have been contradictory. However, blood and urine are not very good indicators of body burden, and furthermore, the importance in such studies of matching for age and smoking habit has often been overlooked. In this respect, the technique for cadmium measurements *in vivo* by neutron capture prompt gamma analysis has many advantages.

The Swansea instrument contains a 200 μg (4.6×10^8 n/s) ^{252}Cf source, housed in a cylindrical steel vessel 90 cm high and 90 cm in diameter. This vessel is filled with borated paraffin wax except for a vertical collimator system in which the source may be driven to vary the source to subject distance. Various collimators can be inserted into this system to produce different neutron beam profiles, while the beam itself may be switched on or off by means of a rotating mechanical shutter.

Fast neutron irradiation of a subject generates a thermal neutron flux at depths within the body such that capture reactions may occur. These will take place predominantly with hydrogen but also with cadmium and other body elements depending upon their cross-section and tissue abundance. The characteristic 559 keV prompt gamma rays from cadmium are detected using a 21% efficient Ge(Li) detector which is shielded against neutron and gamma radiation emerging both from the source and shield and from the subject. A detection limit (2 s.d. of the background) of 3.2 mg cadmium in the kidney is achieved for an organ dose of 0.3 rem delivered in 33 min.

A study of 30 hypertensive subjects and 30 controls, matched for age, sex and smoking habit, has shown a mean kidney cadmium content of 3.3 ± 2.3 mg in the hypertensives which is not significantly different from the 4.4 ± 2.7 mg in the controls. However, in 13 pairs of non-smokers within the study, the mean value of 2.4 ± 2.5 mg in the hypertensives was significantly ($p<0.05$) lower than the 3.9 ± 1.2 mg observed in the controls. Since the hypertensive patients had been treated for several years this raises the question of whether such therapy has reduced the level of renal cadmium below that which might be found in untreated hypertensives.

Finally, the study confirmed the previously reported association between cigarette smoking and cadmium burden.

INTRODUCTION:

Cadmium has a variety of uses which include electroplating and the manufacture of nickel-cadmium batteries and solar cells. It is not found in the tissues of infants, but accumulates gradually throughout life[1]. This accumulation may be the result of air contamination, of cadmium in the diet, of cigarette smoking, or perhaps, of occupational exposure. Approximately half of the total cadmium absorbed is concentrated in the liver and kidneys where it is bound to a specific protein and excreted only slowly. The toxicity of the metal has been extensively reviewed[2], and although adverse health effects resulting from acute exposures have now been largely eliminated as a result of improved working conditions, concern still exists over the longer term effects on the kidney, in particular, of prolonged exposure either at work or in unusual environmental conditions.

One of the possible harmful effects worthy of further investigation is the influence of cadmium levels in the body on the incidence of essential hypertension, because the evidence to date is conflicting. In experiments with rats, Schroeder[3] showed that small doses of cadmium given orally or by injection produced hypertension, and that removal of some of the cadmium resulted in a return to normal tension. These observations were confirmed by Perry[4], who also discussed possible reasons why other workers were unable to reproduce these findings.

In humans, several investigators[5,6] found higher cadmium levels in patients who had died from hypertensive disease than in non-hypertensive subjects, although the opposite result was reported from a series of biopsy specimens[7]. Other workers[8,9] measured blood levels of Cd, but unfortunately blood and urine analyses are not very accurate indicators of critical organ concentration, and a better method of predicting body burden is required.

It is here that the newer technique of *in vivo* neutron activation analysis is proving to be of value[10]. First described by the Birmingham group who used a cyclotron[11], the method involves irradiating the organ of interest with a collimated neutron beam and counting on-line the prompt 559 keV gamma rays emitted during neutron capture in cadmium. With the realization that adequate neutron fluxes could be provided by isotopic neutron sources, portable instruments have since been developed in at least six laboratories. Most of these systems are based upon the use of ^{238}Pu-Be[12-14], but for reasons which have been previously discussed[15], the Swansea instrument employs a ^{252}Cf source.

DESIGN OF THE SWANSEA INSTRUMENT:

The design features are listed in Table I, and a cross-sectional view of the apparatus is shown in Figure 1.

TABLE I: DESIGN FEATURES OF SWANSEA INSTRUMENT

1. ^{252}Cf neutron source (108 mCi, 4.6×10^8 n.s^{-1})
2. Shutter arrangement
3. Variable source position (compensates partly for ^{252}Cf decay)
4. Interchangeable collimators
5. Right cylindrical shield optimises shield-to-weight ratio
6. Transportability

A 200 μg ^{252}Cf source is mounted in a lead holder on top of a nylon threaded drive mechanism, which permits the source-skin distance to be altered. The shield consists of a cylindrical steel vessel 90 cm high and 90 cm in diameter which contains borated paraffin wax. The vessel was constructed in two halves,

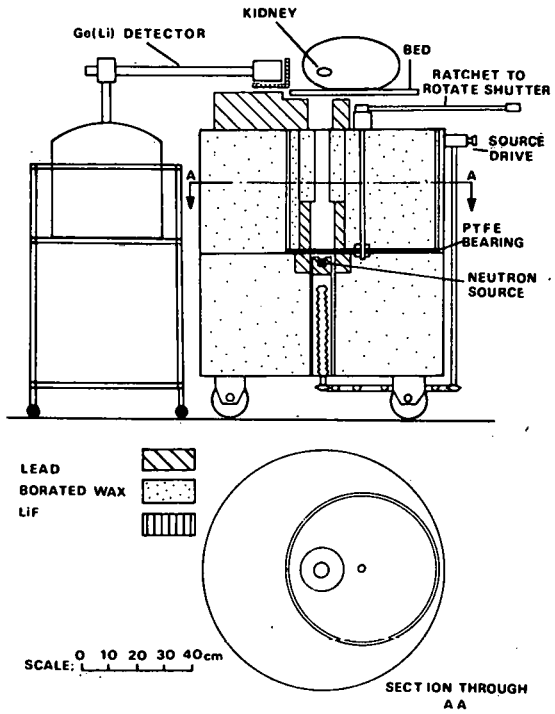


figure 1:

The neutron irradiation facility

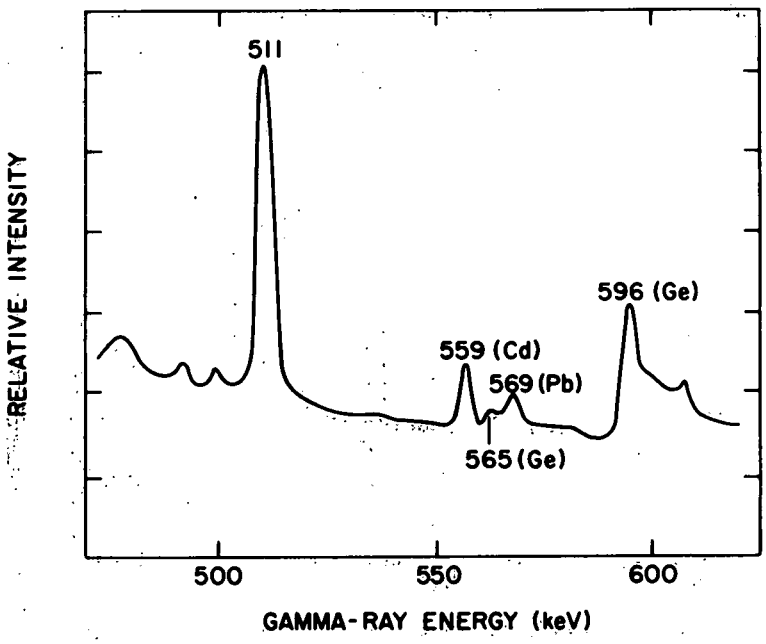


figure 2: A typical Ge(Li) gamma-ray spectrum showing the 559 keV emission from cadmium in the presence of other gamma-rays resulting from neutron interactions with the detector and shielding

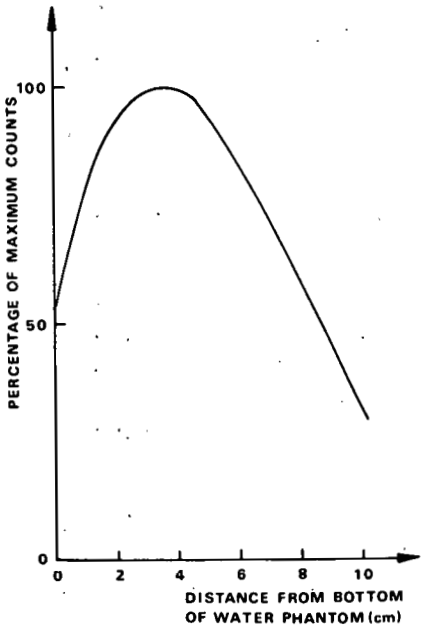


figure 3: Central axis thermal neutron flux distribution from a ^{252}Cf source.

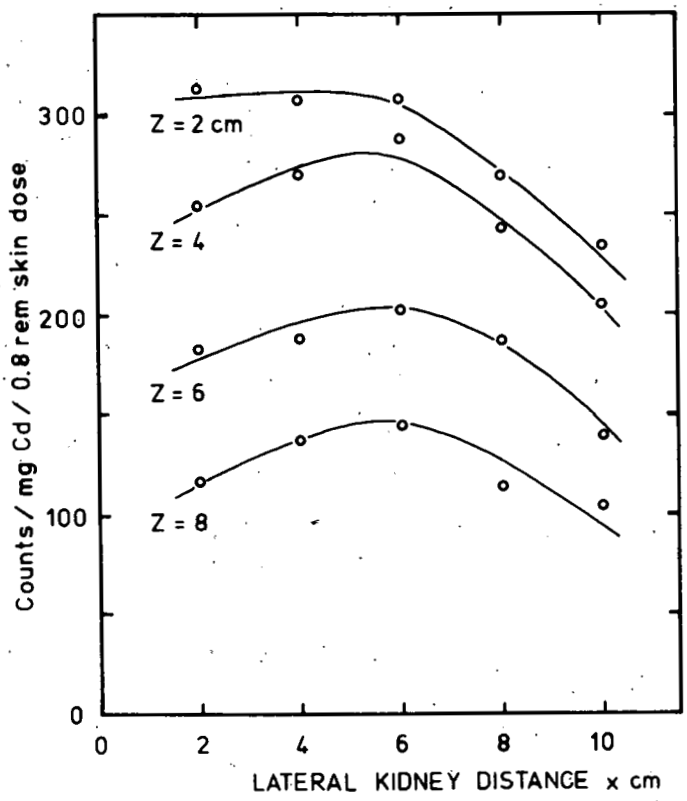


figure 4: Sensitivity of measurement system as a function of posterior kidney depth z and lateral distance x.

the upper half containing a rotatable wax cylinder which enables the neutron beam to be switched on and off. The primary collimator is a 4 mm thick, 15.5 cm diameter steel tube, surrounded along part of its length by a 5 cm thick lead annulus to reduce the gamma emission from the source itself. Secondary collimators may be placed inside this aperture, and in the case of kidney measurements a 6 cm diameter borated wax insert is used.

Particular attention was given to the shielding immediately beneath the detector. Originally, this comprised a layer of lead, but a large proportion of this was replaced by borated wax which further reduced the fast neutron flux reaching the detector. An additional improvement in the gamma shielding was obtained by sandwiching a layer of tungsten between the remaining thickness of lead. This arrangement utilizes the larger inelastic neutron scattering cross-section and better gamma absorption of tungsten compared with lead, but avoids the interference of capture gamma-rays which occur with much higher probability in tungsten.

The detector itself is a coaxial Ge(Li) semiconductor of 21% relative efficiency and 2.6 keV resolution at 1.33 MeV. It is mounted in a vertical dipstick cryostat with a 60 cm long arm to reach across the width of the neutron shield. After preamplification, the signals are fed via a Canberra 2010 amplifier to a Nuclear Data 100 multichannel analyser.

A typical spectrum is shown in Figure 2, which indicates the 511 keV annihilation peak, the 565 and 596 inelastic peaks in germanium and the 569 keV level in $^{207}Pb^{m}$. The cadmium line at 559 keV is resolvable from all interferences.

CALIBRATION MEASUREMENTS:

Fast neutron irradiation of body tissue generates a flux of thermal neutrons at depths within the body as a result of successive neutron collisions with body elements, principally hydrogen. Thermal flux profiles were therefore measured in a water phantom using a 95% ^{6}LiF-ZnS(Ag) scintillator connected to a photomultiplier tube via a perspex light guide. Figure 3 illustrates the variation of these measurements with depth in tissue (or water). It can be seen that for a kidney situated at a depth of more than 4 or 5 cm, it is important to know the exact position of the organ in order to allow for changes in activating flux. Likewise, the lateral position of the kidney is also important since this will determine the attenuation of prompt-gamma rays reaching the detectors. Experiments in which an anthropomorphic kidney phantom was placed at different positions inside a trunk phantom provided the data shown in Figure 4. This indicates the relative sensitivity of the apparatus to kidneys situated at different posterior and lateral depths z and x respectively in the body. The importance of using an ultrasound scanner not only to locate the organ but also to determine the distances z and x is clear from the results.

For typical kidney position, the detection limit of the apparatus is 3.2 mg cadmium in the kidney (2 s.d. of the bkgd) for an organ dose of 300 mrem. This performance may be improved by the use of a better detector(s) (both in terms of efficiency and resolution) and by further attempts to reduce the background, possibly by using lead-and boron-doped polyethylene as a shield, as in the Brookhaven design.

IN-VIVO STUDIES:

The Swansea valley in South Wales has been the subject of an environmental survey of heavy metal contamination[16] - a legacy of the area's importance as a metallurgical centre in the last century - and there is also a higher than average incidence of cardiovascular disease in the region. It seemed appropriate therefore to study the cadmium burdens in the population,

and among hypertensive subjects in particular, to determine whether or not an association exists between cadmium level and high blood pressure.

Sixty patients were selected from two general practices. Thirty of these were long-standing cases of hypertension severe enough to require treatment, and thirty were chosen as controls. The controls, selected at random from an age-sex register, were matched for sex, age and smoking habit. Table II lists the parameters of this study population.

TABLE II PARAMETERS OF STUDY POPULATION

	HYPERTENSIVE SUBJECTS	NORMOTENSIVE CONTROLS
NUMBER	30	30
FEMALE	13	13
MEAN AGE ± S.D.	58.6 ± 9.8 y	58.9 ± 9.7 y
MEAN HEIGHT ± S.D.	166.9 ± 8.1 cm	165.1 ± 8.6 cm
MEAN WEIGHT ± S.D.	75.6 ± 12.7 kg	66.0 ± 14.0 kg
NEVER SMOKED	13	13
PIPE SMOKERS	2	2
SMOKERS & EX-SMOKERS	15	15
CIGARETTE CONSUMPTION IN "PACK-YEARS" ± S.D.	29.1 ± 25.1	33.9 ± 27.0

Each group consisted of 13 non-smokers, 2 pipe-smokers and 15 smokers and ex-smokers. The mean consumption of cigarettes in the last group was approximately 30 pack-years, which is equivalent to smoking 1 pack/day for 30 years or 2 packs/day for 15 years.

Following a full explanation of the nature of the research and the radiation dose involved, each person who agreed to participate was then invited to complete a questionnaire relating to employment history, smoking habits and a broad classification of a normal weekly diet. In this way, it was hoped to identify those persons having an unusual liking for food items such as shellfish and liver and kidney, which contain higher concentrations of cadmium. Blood and urine samples were taken for cadmium estimations by atomic absorption spectroscopy. $Beta_2$-microglobulin, a low molecular weight protein which is indicative of early renal tubular damage was also assayed, although this parameter is more likely to be relevant for studies of occupationally-exposed persons. The left kidney was then located using B-mode ultrasound and finally the *in vivo* measurement was made with the subject lying supine for just over half an hour.

RESULTS:

Table III summarises the values of kidney cadmium which were obtained. Between the two groups as a whole, the controls had more cadmium than the hypertensives, but the difference is not statistically significant. Because of the difficulty of adequately quantifying smoking history, it is instructive to compare the cadmium contents of those persons who were not exposed to this additional source of cadmium. In this group it is seen that the controls do have significantly ($p<0.05$) more cadmium than the hypertensives.

TABLE III

RENAL CADMIUM IN HYPERTENSIVE AND NORMOTENSIVE SUBJECTS

	NO. OF PAIRS	HYPERTENSIVE SUBJECTS	NORMOTENSIVE CONTROLS	CONTROL - PATIENT
ALL PAIRS	30*	3.3 ± 2.3 MG	4.4 ± 2.7 MG	1.1 ± 0.6 N.S.
NEVER SMOKED	13	2.4 ± 2.5 MG	3.9 ± 1.2 MG	1.5 ± 0.7 P<0.05
SMOKERS AND EX-SMOKERS	15	4.0 ± 3.0	4.2 ± 3.1 MG	0.2 ± 0.8 N.S.

* INCLUDES TWO PAIRS OF PIPE SMOKERS

TABLE IV

CORRELATIONS BETWEEN BLOOD, URINE AND KIDNEY CADMIUM

	Cd-U vs Kidney Cd	Cd-B vs Kidney Cd	Cd-U vs Cd-B
Hypertensive subjects	R = -0.16 (N=29)	R = 0.24 (N=28)	R = -0.06 (N=27)
Normotensive controls	R = 0.18 (N=30)	R = 0.27 (N=29)	R = -0.11 (N=29)

IN ALL CASES, P >0.05

TABLE V

BLOOD, URINE AND KIDNEY Cd IN SMOKERS AND NON-SMOKERS

	SMOKERS & EX-SMOKERS	NEVER SMOKED	DIFFERENCE
Cd-B (µg/l)	4.2 ± 1.5 (N=33)	3.0 ± 0.9 (N=24)	1.2 ± 0.3 P <0.001
Cd-U (µg/l)	2.5 ± 1.0 (N=33)	3.3 ± 2.3 (N=26)	-0.8 ± 0.5 N.S.
Kidney Cd (mg)	4.3 ± 3.9 (N=34)	3.3 ± 2.2 (N=26)	1.0 ± 0.8 N.S.

N.S. - P >0.05

Another aspect of the study concerns the possible correlation between blood or urinary concentrations of cadmium, and the body burden. Table IV shows that the correlation coefficients are very small and in no case is the correlation significant at the 5% level of probability.

Table V is a comparison, not between hypertensives and normotensives, but between smokers and non-smokers. Blood cadmium is significantly higher in the smokers, mainly because blood reflects recent, or current exposure to the metal. Similarly, the kidney values are also higher in the smokers but the difference between the two groups is not significant.

However, if the data are plotted in terms of smoking history, (Figure 5) and if the two high cadmium values are excluded on the grounds of probable occupational exposure, and the two extreme values of smoking history as being ex-smokers, then it is possible to obtain a significant correlation between the number of pack-years smoked and the increase in kidney cadmium.

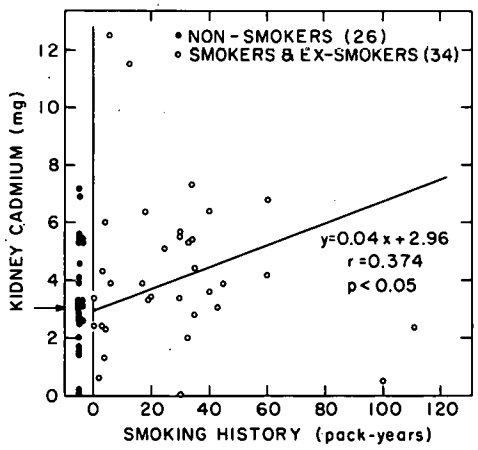


figure 5: Kidney cadmium in relation to smoking history. Four extreme points were excluded from the analysis (see text). Arrow indicates geometric mean (3.0 mg) of cadmium in non-smokers, which coincides with intercept of regression line.

DISCUSSION:

The findings of a higher cadmium content in the normotensives than in the hypertensives is in accord with the *in vitro* measurements of Østergaard who also took care to match for age, sex and smoking habit. However, it should be noted that all of the hypertensive patients were receiving treatment and this might in some way have reduced the amount of cadmium originally deposited in the kidney. For example, Wester[17] reported an increased excretion of cadmium in hypertensives following treatment with chlorthalidone; and McKenzie and Kay[18] observed a greater 24-hour excretion of cadmium in treated hypertensive women compared with a normotensive group.

The present study was not specifically addressed to examining the possibility that raised levels of kidney cadmium might be observed as a result of chronic industrial environmental pollution in the Swansea area. However, it is of interest to report that the mean cadmium levels obtained are comparable with those published by other workers for non-occupationally exposed individuals.[6,7,19] Thus the renal cadmium burdens here reported do not appear to suggest an abnormal environmental exposure to available cadmium.

With regard to cigarette smoking, these results confirm that there is an increase in cadmium body burden in smokers but the increment per pack-year of consumption is less than half of that reported in earlier *in vivo*[19] and *in vitro*[20] studies. However, this is most likely due to the fact that one half of the smokers are in fact ex-smokers who have rejected the habit for periods ranging from a few months to more than ten years. In addition, a further 50% of the group will be hypertensives for whom the question of removal of cadmium by the particular therapeutic regimes has been raised.

CONCLUSIONS:

This *in vivo* study has not demonstrated any increase in kidney cadmium content in hypertensive subjects compared with normotensive controls. On the contrary, the lower values observed in the hypertensive group have raised the question of whether long-term antihypertensive therapy has reduced the quantity of cadmium originally bound in the kidney. Unfortunately, only spot samples of urine were available for cadmium analysis, so it was not possible to state whether the hypertensive group had a higher 24 hour excretion of cadmium than the controls. The possible influence of duration and type of treatment on both kidney and urine measurements is seen as a subject for further investigation.

The lack of correlation between the kidney content and either blood or urine concentrations confirms the unsuitability of either blood or urine sampling to predict the body content of the metal in those subject only to environmental exposure.

The increase in cadmium content of the kidney in smokers is approximately 0.04 mg per pack-year.

In conclusion, the capability of this instrument to detect organ cadmium levels likely to be found in the normal population has been demonstrated. Further studies are planned in areas of higher environmental levels, and a long term follow-up study of occupational exposure is in progress.

ACKNOWLEDGEMENTS:

We are grateful to the two General Practitioners, Dr. D. J. Davies of Gorseinon and Dr. W. O. Williams of Swansea, who kindly provided us with the study population. All the patients and controls, whom we wish to thank for their cooperation, gave their informed consent to the study which was performed in accordance with a protocol approved by the West Glamorgan Ethical Committee and the Neutron Activation Analysis Panel of the Medical Research Council. We are also grateful to Nurse E. Hill who accepted responsibility for all the field work and to Miss H. Cole, Mrs. J. Richter and Mr. J. Dunn for their valuable assistance. We would like to thank Dr. A. C. Ames and Mr. A. Thomas for providing the blood and urine cadmium results, Mrs. J. Davies and Mrs. C. Price for performing the ultrasound scans, and Mrs. F. C. O'Brien for preparing the manuscript.

This investigation was supported in part by the Welsh Scheme for the Development of Health and Social Research, and by the Science Research Council through the award of a CASE Research Studentship for one of us (P.E.C.).

REFERENCES

1. SCHROEDER, H.A., Circulation 35, 570, (1967)
2. FRIBERG, L., in "Cadmium 77" (Ed. Proc. 1st Int. Cadmium Conf., San Francisco, 1977) Metal Bulletin Ltd., London (1978) p. 167
3. SCHROEDER, H.A., VINTON, W.H., Amer. J. Physiol. 202, 595 (1962)
4. PERRY, H.M., ERLANGER, M., PERRY, E.F., Environ. Health Perspect. 28, 251 (1979)
5. NILSSON, R., Aspects of the Toxicity of Cadmium and its Compounds, Ecological Research Committee Bulletin No. 7, Swedish Natural Science Research Council (1970)
6. LENER, J., BIBR, B. Lancet i, 970 (1971)
7. ØSTERGAARD, K., Lancet i, 677 (1977)
8. GLAUSER, S.C., BELLO, C.T., GLAUSER, E.M., Lancet i, 717 (1976)
9. BEEVERS, D.G., CAMPBELL, B.C., GOLDBERG, A., MOORE, M.R., HAWTHORNE, V.M.
10. MORGAN, W.D., Nature 282, 673 (1979) /Lancet ii,1222(1976)
11. BIGGIN, H.C., CHEN, N.S., ETTINGER, K.V., FREMLIN, J.H., MORGAN, W.D., NOWOTNY, R., CHAMBERLAIN, M.J., HARVEY, T.C., J. Radioanal. Chem. 19, 207, (1974)
12. VARTSKY, D., ELLIS, K.J., CHEN, N.S., COHN, S.H., Phys. Med. Biol. 22, 1085 (1977)
13. THOMAS, B.J., HARVEY, T.C., CHETTLE, D.R., MCLELLAN, J.S., FREMLIN, J.H., Phys. Med. Biol., 24, 432 (1979)
14. KRAUEL, J.B., SPEED, M.A., THOMAS, B.W., BADDELEY, H., THOMAS, B.J., Int. J. Applied Radiat. Isotopes 31, 101 (1980)
15. EVANS, C.J., CUMMINS, P., DUTTON, J., MORGAN, W.D., SIVYER, A., GHOSE, R.R., in "Nuclear Activation Techniques in the Life Sciences, 1978," p 719, IAEA, Vienna (1979)
16. GOODMAN, G.T., ROBERTS, T.M., Nature 231, 287 (1971)
17. WESTER, P.O., Acta Med. Scand. 194, 505, (1973)
18. MC KENZIE, J.M., KAY, D.L., N.Z. med. J. 78, 68, (1973)
19. ELLIS, K.J., VARTSKY, D., ZANZI, I., COHN, S.H., YASUMURA, S., Science 205, 323 (1979)
20. LEWIS, G.P., JUSKO, W.J., COUGHLIN, L.L., HARTZ, S., Lancet i, 291, (1972)

INAA Studies of Normal and Diseased Human Brain

W. D. Ehmann, W. R. Markesbery*, M. Alauddin, D. T. Goodin and T.I.M. Hossian

Department of Chemistry
*Department of Neurology and Pathology and Sanders-Brown Research Center on Aging
University of Kentucky
Lexington, Kentucky 40506

Abstract

Several trace elements have been implicated as neurotoxic factors in the human brain disorder known as Alzheimer's disease. In order to study trace element relationships in aging and with this disease, we have developed INAA procedures for the determination of approximately 20 elements in human brain tissue. The analytical approach is based on a series of sequential 14 MeV neutron and reactor thermal neutron irradiations of the same aliquants of freeze-dried brain tissue. The INAA determinations of aluminum at sub-microgram per gram levels posed special problems. Extremely short irradiations were required to minimize interferences from ^{24}Na and ^{38}Cl gamma-ray Compton interactions and high levels of bremsstrahlung radiation from interactions of high energy beta particles produced by the decay of ^{32}P. In addition, the $^{31}P(n,\alpha)^{28}Al$ fast neutron reaction provides a primary interference to the determination of aluminum by the $^{27}Al(n,\gamma)^{28}Al$ thermal neutron reaction. Our approaches to the solution of a number of special analytical problems involved in the application of INAA to brain tissue are presented. Trace element baseline data for neurologically normal individuals have been obtained. Several reports in the literature have contended that exceptionally high values for aluminum abundances in human brain tissues are more common for individuals with Alzheimer's disease and that aluminum may play an etiological role in the disease. The aluminum data we have obtained to date from 136 brain samples derived from 20 control and 11 Alzheimer's patients do not support these contentions. However, a positive correlation of aluminum abundances with age in the control group has been confirmed. Interim data for other trace elements are briefly reviewed.

Introduction

Alzheimer's disease is a term used to describe presenile and senile dementia. These two conditions are now becoming generally regarded as differing only in the age at which they occur. Symptoms are those associated with a progressively deteriorating mental condition. Pathologically, the disease can be identified by atrophy of the cerebral cortex. Histologically, the most common feature is neurofibrillary degeneration (NFD) characterized microscopically by silver positive thickened filaments in neuronal cytoplasm. By electron microscopy the neurofibrillary tangles in Alzheimer's disease are actually shown to be composed of paired helical filaments.[1] Other features of the disease are the presence of senile plaques and granulovacular degeneration. This disease has been implicated as the underlying cause of death for at least 70,000 individuals in the United States each year[2].

It is known that Al metal dust inhalation at high rates can result in brain dysfunction[3]. The first study which claimed to demonstrate a relationship

between Alzheimer's disease and high levels of Al in human brain was that of Crapper et al.[4] They also injected $AlCl_3$ directly into brains of cats and found a significant correlation between brain Al concentrations and poor performance in a one way avoidance response acquisition task.

In 1976 Crapper et al.[5] followed their earlier studies with a much more intensive study which included a control group of seven neurologically normal adults, two children and ten Alzheimer's patients with ages ranging from 50 to 88 years. Six cerebral biopsies were also assayed to determine whether Al accumulation occurs as a terminal event associated with a change in the blood brain barrier. Crapper found Al contents of 1.9 ± 0.7 μg/g dry weight in control brains (208 assays), excluding the olefactory bulb and blood vessel regions. He assumed that the upper limit of normal variation for Al in normal brain would be approximately the control mean plus three standard deviations (4 μg Al/g dry weight). For the Alzheimer's patients, Al concentrations ranged widely from 0.4 to 107.0 μg/g dry weight. The patient with the highest percentage of sampled areas above the 3σ level was found to have the most widespread and highest density of NFD. Overall, for ten Alzheimer's patients, 28% of the assays were above the 3σ level. This suggested to Crapper that Alzheimer's NFD might have an association with elevated brain Al levels.

Niklowitz and Mandybur[6], using dry ashing and atomic absoption spectrophotometry, reported an insignificant difference in Al contents of samples from one Alzheimer's patient and two controls. McDermott et al.[7], also using dry ashing and atomic absorption, analyzed 274 brain samples from ten Alzheimer's patients and nine controls. They concluded that there were no significant differences between control and diseased brains as a whole, or even for those regions high in NFD density. They suggested a positive correlation of brain Al content with age exists, rather than a correlation with dementia. Other less extensive studies of trace element relationships with Alzheimer's disease have lead to suggestions that Mn and Si brain levels may correlate with the disease.[8,9]

In our study we have applied the sensitive multielement technique of instrumental neutron activation analysis (INAA) to determine up to 20 elements in autopsy and biopsy brain tissue samples from approximately 28 adult controls, 4 infant controls and 13 Alzheimer's patients. Sequential 14 MeV neutron, short reactor thermal neutron and long (40 h) reactor thermal neutron irradiations can be performed on the same sample aliquants, avoiding problems of sampling bias. In addition, INAA is much less susceptible than most other analytical techniques to problems associated with reagent and laboratory contamination, an important factor at the extremely low trace element levels in brain tissue.

The elements which may be determined in brain using our 14 MeV and thermal neutron procedures are presented in Fig. 1. Elements in parentheses are seen only rarely, or would require some alteration of the analytical scheme to be determined reliably. At this writing, analytical work has not been completed for all samples and this report will direct its emphasis to a description of the analytical procedures developed and a brief review of the analytical results on elements for which the majority of the analyses have been completed.

Sampling Procedures

Pre-irradiation sample handling procedures are summarized in Fig. 2. The distribution of brain samples by brain region is presented in Table I.

All samples were taken with Suprasil quartz knife, pressed gently between sheets of Whatman 541 hardened, ashless filter paper to remove surface moisture and weighed to determine the fresh, or "wet", weight. Samples for histological studies were simultaneously taken from adjacent areas. For those brain regions

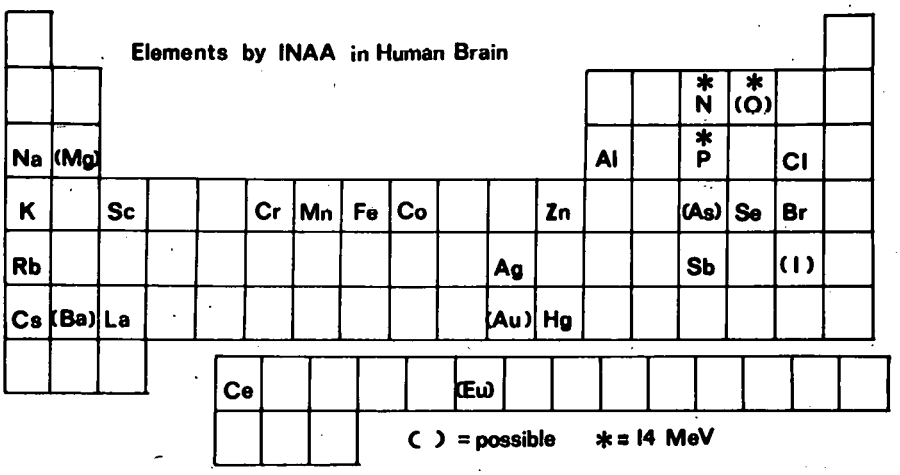
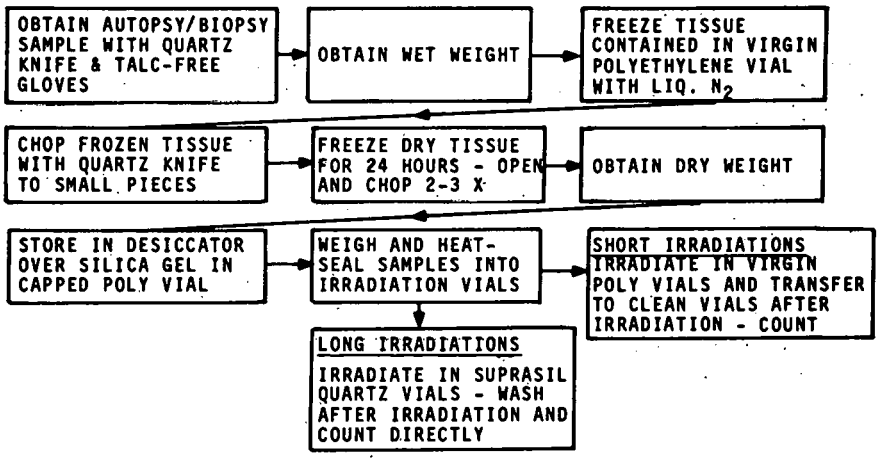


Fig. 1. Elements determined by INAA.



NOTE: SAMPLES ARE HANDLED IN A DUST-FREE ENCLOSURE WHENEVER POSSIBLE.

Fig. 2. Sample handling procedures.

Table I. Distribution of samples by brain region

	Samples	
	Adults	Infants
Anterior frontal lobe	33	3
Middle frontal lobe	42	3
Anterior temporal lobe	28	1
Middle temporal lobe	26	1
Hippocampus	23	0
Amygdala	2	0
Superior parietal lobe	25	2
Posterior occipital lobe	21	2
Caudate	10	1
Thalamus	8	1
Cerebellar vermis	11	0
Cerebellar hemisphere	10	1
Putamen	14	0
Globus pallidus	2	0
Substantia nigra	1	0
Misc. unclassified	2	0
Total samples	258	15
Individual patients (Total sample pool)	44	4

containing both gray and white matter the analytical sample was selected by visual estimate to be a 50 ± 10% mixture. Studies of separated gray and white matter are also planned.

All impliments and containers used in these studies were pre-washed in Ultrex nitric acid (J. T. Baker Chemical Co.), distilled/deionized water and finally in Distilled in Glass methyl alcohol (Burdick and Jackson Laboratories, Inc.). Only quartz or Teflon coated impliments were used to manipulate the samples. Fresh brain samples were placed in zip-lock polyethylene bags and frozen for storage. After freeze-drying, the diced tissues were stored in capped virgin polyethylene scintillation counting vials, which in turn were kept in desiccators over silica gel.

The freeze-drying procedure (LabConCo apparatus) was interrupted several times over the 24 hour drying period to finely dice the brain tissue with a quartz knife. This was found to be necessary, since a semi-impervious surface layer developed on the particles of brain tissue which measureably slowed the rate at which a constant freeze-dried weight could be obtained. Due to the fact that ashing, oven-drying, or freeze-drying procedures can vary considerably among different laboratories, we have chosen to report all of our elemental abundances in terms of fresh, or "wet", weight. Mean freeze-dry (FD) to wet weight ratios obtained for our samples are: adult controls = 0.211, infant controls = 0.159 and Alzheimer's patients = 0.210. Individual FD/WET ratios are calculated for each sample and these values are used to convert our FD abundances to the fresh weight basis.

Irradiation and Counting Procedures

Irradiation times (t_i), delay times (t_d), counting times (t_c), indicator radionuclides, half lives and analytical gamma rays for the elements we have seen commonly in our samples are given in Tables II and III. Most of the irradiations were performed at the University of Missouri Research Reactor

Table II. INAA of brain; Short reactor P-tube irradiations

t_d, t_c	Indicator radionuclide	$t_{1/2}$	Gamma ray, keV
60 s, 120 s	^{28}Al	2.3 m	1779
90 m, 10 m	^{38}Cl	37.2 m	2167
	^{42}K	12.4 h	1525
	^{56}Mn	2.58 h	847
	^{24}Na	15.05 h	1369

50 to 200 mg samples of freeze-dried brain in polyvials irradiated for 5.0 s at a flux density of $\sim 8 \times 10^{13}$ n cm^{-2} s^{-1}.

Facility (MURR) in irradiation positions with a flux density of $\sim 8 \times 10^{13}$ n cm^{-2}s^{-1}. Several early irradiations were conducted at the Georgia Institute of Technology Research Reactor which has a flux density of 8×10^{12} n cm^{-2}s^{-1}.

Determination of Phosphorus

The determination of P is required to correct for the $^{31}P(n,\alpha)^{28}Al$ direct interference reaction when Al is determined by the $^{27}Al(n,\gamma)^{28}Al$ in a reactor facility with a moderately high reactor fast neutron flux. In order to

Table III. INAA of brain; Long reactor irradiations

t_d	Indicator radionuclide	$t_{1/2}$	Gamma ray, keV
1 - 2 d	^{76}As	26 h	559
	^{198}Au	2.7 d	412
	^{82}Br	35 h	776
	^{42}K	12.4 h	1525
14 d	^{86}Rb	18.6 d	1077
30 d	^{110m}Ag	252 d	658
	^{141}Ce	32 d	145
	^{51}Cr	27 d	320
	^{134}Cs	2 y	796
	^{59}Fe	45 d	1099, 1292
	^{203}Hg	47 d	279
	^{124}Sb	60 d	1691
	^{46}Sc	84 d	889
	^{75}Se	120 d	265
60 - 90 d	^{60}Co	5.3 y	1332
	^{65}Zn	244 d	1115

15-20 mg samples of freeze-dried brain in Suprasil quartz vials irradiated for 40 h at a flux density of $\sim 8 \times 10^{13}$ n $cm^{-2}s^{-1}$.

determine Al at the sub-μg/g level in small brain samples, it was necessary to take advantage of the high flux density and ready "rabbit" transfer system accessibility at the University of Missouri Research Reactor. Unfortunately, this facility has an appreciable reactor fast neutron flux which can induce the interference reaction on the high P levels found in brain. Therefore, accurate and precise P determinations are required on the same aliquants that are later used for the Al determinations.

The freeze-dried brain tissues were first packaged in small virgin polyethylene vials which were, in turn, further encapsulated in cleaned new polyethylene "rabbits" for the 14 MeV INAA P determinations. The analytical nuclear reaction used in this study was the $^{31}P(n,\alpha)^{28}Al$ reaction induced by a 4 minute irradiation with 14 MeV neutrons produced by a Kaman A-1250 Cockcroft-Walton neutron generator. A delay time of 15 seconds was used to permit the decay of the majority of the 7.1 second half life ^{16}N, produced by the $^{16}O(n,p)^{16}N$ reaction. A counting time of 4 minutes was used to detect the 1779 keV gamma rays from 2.3 minute half life ^{28}Al. For the majority of the P determinations, a dual 7.6 x 7.6 cm NaI(Tl) scintillation counting system with a uniaxial rotating sample holder was used. This system is illustrated in Fig. 3. A BF_3 proportional neutron counter in a paraffin shield located near the neutron generator was used to monitor the individual neutron doses, so that standard and sample irradiations could be normalized.

Triphenyl phosphate and ammonium phosphate were used as primary standards in the P determinations. NBS SRM 1577, Bovine Liver, served as a secondary comparator standard. The 14 MeV INAA P data were also checked by an alternate technique, derivative thermal neutron activation analysis. Phosphorus was converted to the phosphovanadomolybdate complex and a 1.25 mg ^{252}Cf isotopic neutron source was used for the irradiations to determine V, and by stoichiometry, P[10].

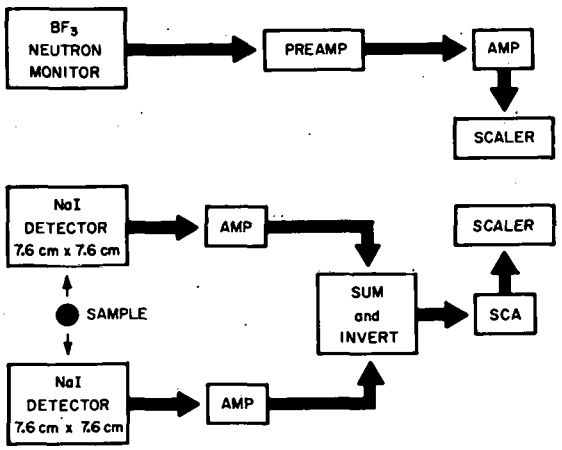


Fig. 3. Counting system for phosphorus determinations.

The derivative NAA technique yielded P data in good agreement with the 14 MeV INAA data on several dozen brain samples and yielded a value of 1.11 ± 0.05% P in replicate analyses of NBS Bovin Liver (NBS uncertified value = 1.1% P). Following the verification of the 14 MeV INAA P technique, the faster INAA procedures have been employed for all recent brain P determination. Nitrogen and oxygen contents of the samples could also be easily determined by 14 MeV INAA, but these determinations have not been included in this study.

The mean P content for the control brain tissues analyzed to date is 0.270 ± 0.042% P (n = 166) and for Alzheimer's patients is 0.281 ± 0.041% P (n = 69), on a fresh weight basis. The error limits quoted are standard deviations for the sample distribution, and do not reflect the errors in the analytical determinations which are estimated to be only of the order of ± 2%, relative. It should also be noted that interferences to the P determinations by the $^{28}Si(n,p)^{28}Al$ nuclear reaction were evaluated and found to be negligible, due to the high P and very low Si contents of brain. This interference can be very serious in geological samples, which are often high in Si.

Determination of Aluminum

The same sample aliquants in which P was determined were used for the determination of Al. The samples were packaged in virgin polyethylene vials and irradiated for 5 seconds in the P-tube facility at MURR. After a one minute delay period during which the freeze-dried tissue was transfered to an unirradiated polyethylene vial, samples and standards were counted for two minutes. The counting system consisted of two 12% efficiency Ge(Li) detectors and amplifiers connected to a multiplexer unit (ORTEC Model 475) that allows two detector systems to operate as a single system with increased counting efficiency.

Pulses from the amplifiers are run through the two separate channels of the multiplexer. Each channel has a gate that must be enabled by a busy signal from the respective amplifier in order for a pulse to be routed to the summed output. The two channel gates have logic circuits that prevent coincident summing of pulse amplitudes. Use of a discriminator before the analyzer ADC restricts the data acquisition to the region of interest around the 1779 keV FEP of ^{28}Al and reduces the analyzer deadtime caused by high levels of ^{24}Na and ^{38}Cl. Two pulsers are operated at different frequencies (60 Hz and 100 Hz) to prevent biased results from rejection of coincidence signals by the multiplexer. A block diagram of the system is given in Fig. 4. A gamma-ray spectrum obtained in the Al analysis of a brain sample is illustrated in Fig. 5.

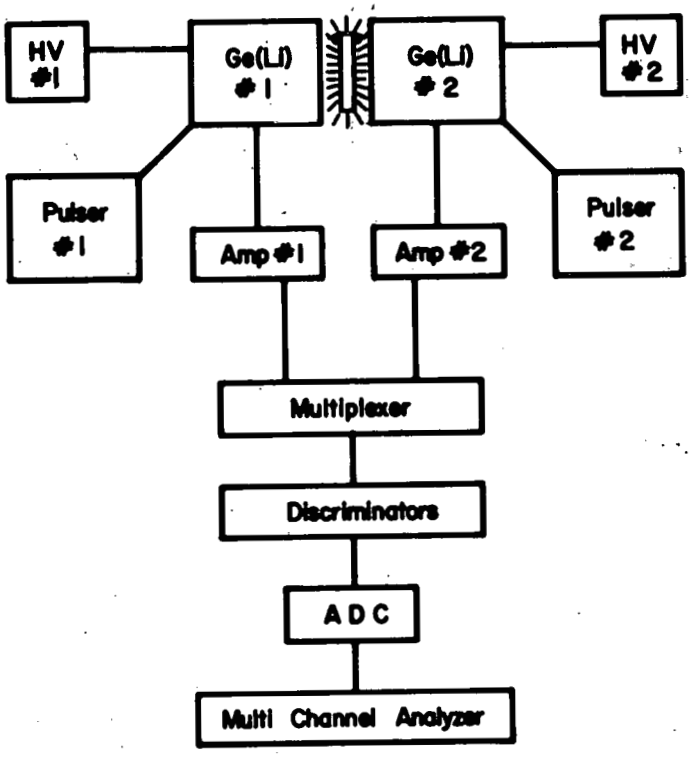


Fig. 4. Two detector multiplexer system for the INAA determination of aluminum in brain tissues.

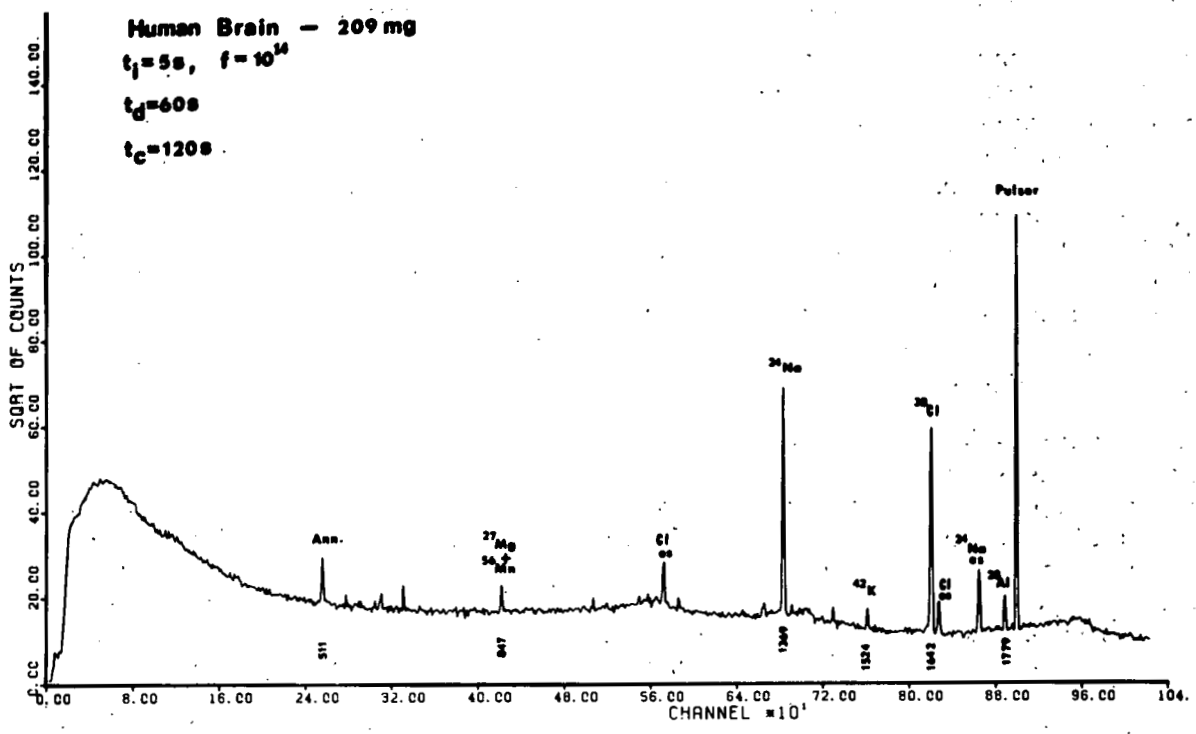


Fig. 5. Gamma-ray spectrum of brain tissue irradiated for 5 s at MURR.

The counting system described above is designed to divide the detector/preamp deadtime between two detectors and permits the placement of the detectors closer to the sample. Compton events generated by the high energy gamma rays emitted by ^{24}Na and ^{38}Cl result in high baseline levels in the region of the ^{28}Al FEP. The relatively short irradiation and counting times were selected to iscriminate against these long lived interferences while the use of the multilexer two detector system and discriminators permitted the sample to be counted in a high counting geometry position without excessive system deadtime. The

pulsers are used to calculate a residual deadtime correction, since the gamma-ray spectra are collected in the clock time mode.

In the early stages of this study the comparator standard used for the determination of Al was aluminum monostearate. This compound is not stoichiometric and was itself standardized against primary standards prepared from high purity aluminum metal. For the majority of the Al analyses, NBS SRM 1570, Spinach Leaves, was used as a primary standard (NBS certified value for Al = 870 ± 50 μg/g). It was experimentally determined that the P and Si contents of this standard contributed a negligible amount (< 1%, relative) to the gross ^{28}Al activity induced under the experimental conditions employed. Samples, primary standards and a variety of secondary standards were irradiated sequentially in the MURR P-tube facility. Primary standards for P were also incorporated into the irradiation sequence (triphenyl phosphate and ammonium phosphate), so that an appropriate correction for the $^{31}P(n,\alpha)^{28}Al$ direct interference reaction could be applied to the brain samples, based on their P content as determined by 14 MeV INAA. Due to the high levels of P in brain, this correction typically accounted for 25 - 30% of the gross ^{28}Al activity observed. Although this correction is large, it should be noted that the P contents of the samples were determined on the same aliquants by the accurate and precise 14 MeV INAA procedure.

The accuracy and precision of our Al determinations for several secondary standards are illustrated in Table IV. At the lower end of the abundance range

Table IV. INAA determinations of Al in secondary standards

Sample	Al content, μg/g This Work	Literature	(Ref.)
NBS SRM 1571 Orchard Leaves	398 ± 24 (n = 18)	410	(11)
Bowen's Kale	48.5 ± 3.4 (n = 9)	38.2	(11)
NBS SRM 1577 Bovine Liver	2.21 ± 0.15 (n = 18)	35.2	(11)
		6	(12)
		1.8	(13)
		2	(14)

NBS SRM 1570, Spinach Leaves, used as a primary standard (Al = 870 ± 50 μg/g, certified).

approaching levels in brain, our value for Al in Bovine Liver is in good agreement with recent literature values obtained by INAA with the use of Cd filters to make the correction for fast neutron reactions[13,14]. Our precision based on analyses of separate aliquants from the same brain region of one individual, is typically ± 5 - 6%, relative. Aluminum contents obtained to date on control group brain samples range from < 0.05 to 3.05 μg/g fresh weight.

Determination of Other Elements

The INAA determination of some 18 additional elements is carried out according to the parameters listed in Tables II and III. For the 40 hour reactor neutron irradiations, splits of the same samples used for the 14 MeV INAA and the reactor P-tube irradiations are encapsulated in Suprasil quartz vials and

irradiated together with NBS standards. NBS certified values in Orchard Leaves and/or Bovine Liver were used in calculating abundances of As, Cr, Fe, Hg, K, Mn, Na, P, Rb, Sb, Se and Zn. NBS non-certified values were used for Br and Cl. Literature values[11] were used for the remaining elements. Gamma-ray spectra of human brain after a 40 h irradiation at MURR and decay periods of 12 and 30 days are shown in Fig. 6 and 7. Zn and Co are ordinarily determined after a 2 to 3 month decay period, to minimize the Sc activity in the region of the Zn FEP. Precision and accuracy are illustrated in Table V by analyses of secondary standard, Bowen's Kale.

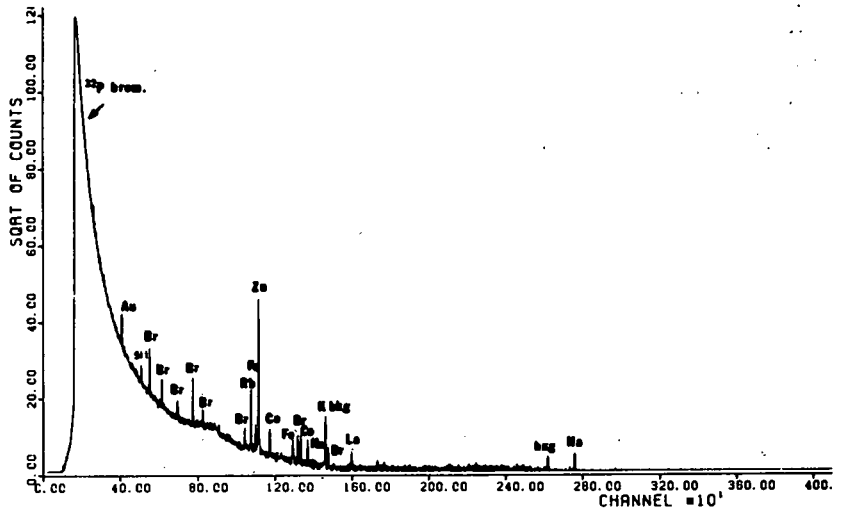


Fig. 6. Human brain tissue irradiated for 40 h at MURR. Decay time = 12 d. Square root of count is plotted.

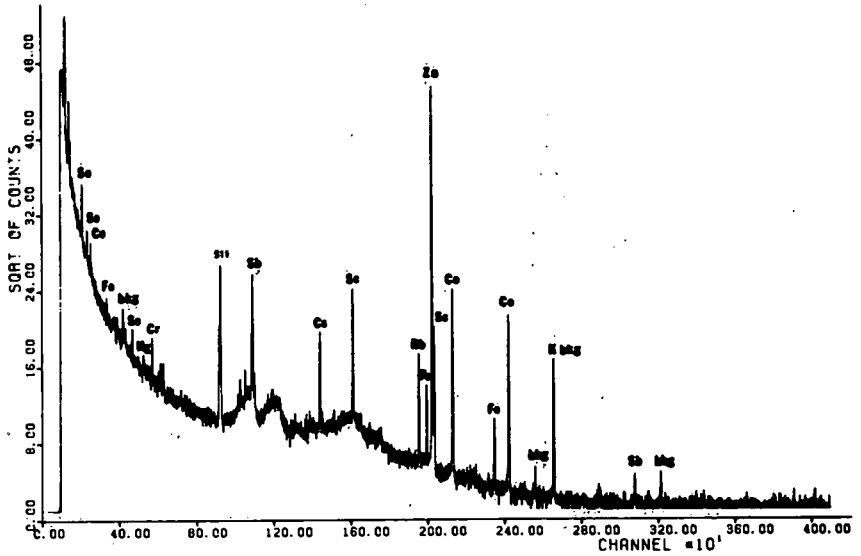


Fig. 7. Human brain tissue irradiated for 40 h at MURR. Decay time = 30 d. Square root of count is plotted.

Table V. INAA determinations in Bowen's Kale

Element,	units	This Work ± σ_m	Analyses	Literature Value
Br	µg/g	26.3 ± 2.0	7	26.1
Cl	%	0.38 ± 0.02	6	0.34
Cs	ng/g	63.9 ± 11.3	3	74.0
Fe	µg/g	108. ± 14.	3	118.
Hg	ng/g	149. ± 10.	4	167.
K	%	2.46 ± 0.07	6	2.46
Mn	µg/g	14.8 ± 0.8	6	14.7
Na	%	0.25 ± 0.01	6	0.25
Rb	µg/g	52.6 ± 3.2	7	52.2
Se	µg/g	0.13 ± 0.02	3	0.12

Several of the analytical gamma rays are subject to spectral interferences which must be corrected for. As an example, the ^{75}Se 279.5 keV gamma ray and the ^{203}Hg 279.2 keV gamma ray are not resolved with our 2.0 keV resolution Ge(Li) detectors. This composite peak is resolved by the peak area ratio method, using the 264.6 keV/279.5 keV gamma-ray ratio for ^{75}Se.

We have found sporadic relatively high levels of Co, Cr, Sb and Sc in blank irradiated (empty) Suprasil quartz vials. Although the mean blank levels are relatively low and blank corrections are made, we plan to transfer samples out of the quartz vials and recount them prior to reporting data on these elements.

Discussion

An abbreviated summary of our determinations of trace elements in human brain is given in Table VI.

Table VI. Abbreviated interim summary of INAA data on trace elements in human brain

Element,	units	Mean Abundances by Sample, Fresh Weight Basis Adult Controls		Alzheimer's		Infants	
Al	µg/g	0.46	(136)	0.40	(66)	0.43	(12)
Ag	ng/g	16.2	(21)	8.4	(28)	2.0	(5)
Br	µg/g	0.71	(78)	1.02	(58)	2.57	(13)
Cl	µg/g	1420.	(170)	1650.	(68)	2540.	(12)
Cs	ng/g	6.7	(46)	5.8	(37)	3.2	(6)
Fe	µg/g	62.5	(66)	75.5	(50)	13.1	(10)
Hg	ng/g	26.6	(18)	112.	(38)	10.7	(8)
K	%	0.257	(173)	0.231	(70)	0.239	(12)
Mn	µg/g	0.265	(160)	0.258	(65)	0.223	(5)
Na	%	0.146	(173)	0.202	(71)	0.247	(12)
P	%	0.270	(166)	0.281	(69)	0.247	(12)
Rb	µg/g	2.02	(96)	1.94	(58)	2.67	(14)
Se	µg/g	0.176	(66)	0.184	(50)	0.149	(10)
Zn	µg/g	13.5	(39)	14.3	(31)	7.4	(5)
FD/WET		0.211		0.210		0.159	
Patients		28		13		4	

Data for the remaining elements and additional samples are still being processed. Therefore, means reported here should be regarded as interim values. A detailed discussion of the data will be published elsewhere, but a brief discussion of the significance of the Al data will be included here.

The Al content of 136 brain samples derived from 20 neurologically normal control individuals is 0.462 ± 0.386 µg/g fresh weight. The error limits are for the sample distribution and are not measures of analytical precision. Al abundances do vary among brain regions, but the means for the memory regions affected by Alzheimer's disease are not significantly different than for the pooled mean for all regions. Calculated on a freeze-dry weight basis this value is 2.2 µg/g dry weight. Crapper, et al.[5] reported a mean value for controls on an oven-dried weight basis of 1.9 µg/g dry weight, in good agreement with our mean.

The Al mean for 66 samples from 11 Alzheimer's patients is 0.403 ± 0.528 µg/g fresh weight. Again, the error limits reflect the dispersion among brain regions, not analytical error. If we apply the statistical approach of Crapper et al.[5], we find that only 2 out of 66 samples exceed 1.62 µg/g fresh weight, which is a limit of 3σ above our mean for the control group. This is only 3% of

the samples, in contrast to the 28% of Alzheimer's samples Crapper et al. reported to exceed their 3σ level. If we use the same 3σ limit used by Crapper et al. (4.0 μg/g dry weight ≈ 0.84 μg/g fresh weight) we still have only 4 of our Alzheimer's samples (6%) above his limit.

When we apply a standard two-tailed analysis of variance test to our data with Al content and Alzheimer's disease as "main effects" and age and sex as "covariates", we obtain an overall "explained" F-statistic of 1.147 with a "significance of F" value of 0.331. Clearly, the null hypothesis is not disproved. However, we do find a relationship of Al content with age in the control group (Pearson correlation coefficient = 0.265, n = 136, P = 0.002). This relationship is illustrated in Table VII. Three premature or newborn infants are included in the 0-19 age group.

Table VII. Variation of Al content with Age - Controls only

Age	Mean Al, μg/g fresh weight By Sample	By Patient	Number of patients
0 - 19	0.291	0.266	3
20 - 39	0.345	0.350	4
40 - 59	0.389	0.404	6
60 - 79	0.458	0.457	6
80 - 99	0.688	0.678	4

Therefore, the Al data we have obtained to date do not support the suggestion of Crapper, et al.[5] that the frequency of high Al contents is greater in Alzheimer's brain tissues. However, our data do support the conclusions of McDermott, et al.[7] that there is a positive correlation of Al content with age in control brains. This correlation could blur conclusions as to possible correlation of Al content with the disease, unless the sample groups were very carefully age matched.

Differences in trace element contents of infant and adult brains, both on a fresh and freeze-dried basis, are noted and these results will be discussed elsewhere.

Acknowledgement - The assistance of Z. Ali-Rumana, G. Richter, D. Johnson and R. Young in early stages of this study is gratefully acknowledged. This work has been supported, in part, by NIH Grant NS14221.

References

1. M. Kidd, Nature 197, 192 (1963).
2. R. Katzman & T. Karasu, Neurological and Sensory Disorder in the Elderly, (ed. W.S. Fields), **Stratton Intercon. Med. Book Corp., New York, 1975.**
3. B. Venugopal & T. Lucky, Metal Toxicity in Mammals, Vol. 2, Plenum Press, N.Y. 1978.
4. D. Crapper, S. Krishnan & A. Dalton, Science 180, 511 (1973).
5. D. Crapper, S. Krishnan & S. Quittkat, Brain 99, 67 (1976).
6. W. Niklowitz & T. Mandybur, J. Neuropath. Exp. Neurol. 34, 445 (1975).
7. J. McDermott, A. Smith, K. Iqbal & H. Wisniewski, The Lancet, **710, Oct. 1, 1977.**
8. R. Banta, D. Clark & W. Markesbery, Neurology 27, 213 (1977).
9. T. Nikaido, J. Austin, L. Trueb & R. Rinehart, Arch. Neurol. 27, 549 (1972).
10. R. Young, Ph.D. Dissertation, University of Kentucky, 1979.
11. R. Nadkarni & G. Morrison, J. Radioanal. Chem. 43, 347 (1978).
12. W. Gooddy, E. Hamilton & T. Williams, Brain 98, 65 (1975).
13. G. Goode, J. Herrington & P. Goddard, Radiochem. Radioanal. Letters 31, 87 (1977).
14. J. Hislop, Private communication quoted in Goode et al. (13).

BIOGEOCHEMICAL PROSPECTING FOR GOLD BY NEUTRON ACTIVATION ANALYSIS

I. M. VALENTE**, M. J. MINSKI**, P. J. PETERSON*

* Department of Botany and Biochemistry,
Westfield College (University of London),
Kidderpore Avenue, London NW3 7ST, U.K.

** University of London Reactor Centre,
Silwood Park, Sunninghill, Ascot,
Berkshire, SL5 7PY, U.K.

ABSTRACT

Shoot material of Chamaespartium tridentatum and Festuca ovina, collected together with soils from a rectangular pattern grid in an area in Spain, was analysed for gold by instrumental neutron activation analysis. Values of gold were found to range from less than 1.0×10^{-3} µg g^{-1} (d.w.) at background sites to 65.4×10^{-3} µg g^{-1} in the leaves of F. ovina in anomalous areas.

The two plants studied were abundant on the site; they exhibited markedly different rooting patterns and they showed a degree of accumulation of gold in proportion to the concentration of the element in the soil. Seasonal variation in the gold concentration was noted.

This work has emphasised the desirability of including plant analytical data in an evaluation of the mineral potential of a given area and should, in the case of gold, place mineral prospecting on an even sounder basis.

INTRODUCTION

Plants can be used as a guide to mineralization either as geobotanical indicators which reveal the nature and properties of the substrate by their presence or absence (1,2,3) or in biogeochemical surveys where plant or humus analysis reveals anomalous metal concentrations in soils or bed rock (4,5,6,7).

The very low gold levels in plants make analysis of plant material difficult and explain why the use of plants as indicators of gold mineralization has not been commonly considered.

Various methods have been reported for the determination of this element in plant material, including fire assay (8), polarography (9), spectroscopy (10) and atomic absorption spectroscopy (11), but they are either time consuming or not sufficiently sensitive and require relatively large samples,

and are therefore not applicable to a large programme of sampling. Minski et al. (12) reported a precise and sensitive method using non-destructive activation analysis for determining gold and arsenic in small samples of dry material. Girling et al. (13,14) using this technique have shown plants to be potential indicators of gold mineralization. The present work describes the results of an orientation survey to assess the potentiality for biogeochemical prospecting for gold in an area of Northern Spain. The approach is based on the analysis of plants providing a mean value for gold concentration within the rooting zone.

Arsenic has long been recognized to be useful in locating gold deposits (15,16). Arsenic plant concentrations were therefore measured simultaneously with gold and the plant arsenic-gold relationship investigated for samples collected. Equivalent soil analysis was carried out to find out the plant to soil content relationship in the area.

Approximately 10-50g of shoot material was collected from up to 10 plants of each species at each sampling site, depending on their frequency, together with approximately 500g of soil from the uppermost horizon (0-10cm). Plant samples were washed and dead material removed prior to oven drying at 60°C (13) for 24 hours.

A homogeneous powder was prepared from the dry shoot material in an electric blender and was stored in plastic vials.

Soil samples were freeze-dried, crushed, sieved and mixed thoroughly before analysis.

In an attempt to find out the distribution of gold as a function of particulate size the soil samples were subsequently sieved through 16, 30, 60, 170 and 350 mesh.

ANALYTICAL PROCEDURES

Duplicate samples of dried homogenised plant material were compressed into pellets (200-300mg) and irradiated in a thermal neutron flux of 1.5×10^{12} n cm^{-2} s^{-1} for 8 hours. A three day decay period followed irradiation in order to obtain optimum resolution of the ^{198}Au peak at 412 keV. Arsenic was determined as ^{76}As at 559 or 656 keV.

Irradiated pellets were transferred to non-irradiated containers before counting to eliminate contamination from ^{198}Au present in the irradiation vials. The γ-emitting nuclides ^{198}Au and ^{76}As were resolved using a Ge(Li) detector linked to a 4000 channel analyzer system. The gold and arsenic concentrations were calculated with reference to National Bureau of Standards Orchard Leaves and chemical standards analysed under identical conditions. The detection limit for plant material under these conditions is 1×10^{-3}μg g^{-1} for Bowen's Kale or samples with high sodium content, but for samples with low sodium e.g. NBS Orchard Leaves it is 1×10^{-4}μg g^{-1}. Soil samples were irradiated under identical conditions but allowed to decay for 4 days. The detection limit is 1.9×10^{-3}μg g^{-1} and the sensitivity of the method for a gold standard is 2.3×10^{-2}ng.

LOCATION AND GEOLOGY OF THE STUDY AREA

The area surveyed is located in the southern part of the Cordilheira Cantrabica Mountains in the Province of Leon (Spain) and lies between 1,375 and 1,425m elevation (Fig.1). The predominant rocks belong to the Cantabric zone

of the Paleozoic Period. The gold vein consisted of a quartz filled tissue averaging 20m in width.

Arsenopyrite and pyrite are associated in the vein and anomalous levels of arsenic and gold have been found in the area.

Both rocks and intrusives are cut by numerous small veins of quartz, some of which show visible gold. The derelict mines of Candin in the area are known to have been exploited by the Romans and some galleries still remain, but mining ceased many years ago.

PLANTS SPECIES AND SAMPLING PROCEDURE

In the area surveyed, the vegetation is principally a heathland community. Two field visits were made to this area. The first sample selection was carried out during the later half of November 1978, while a more detailed study was made late in June, 1979. The sampling procedure involved the collection of a range of plant and soil specimens at intervals on a regular rectangular grid pattern covering the main zone A as shown in Fig(1).

On a first approach shoot material in all the different species available was collected across the transects of the area A at intervals of 10m. The species were common to all transects although some of the species did not occur at all the sampling points. Plants were sampled as far as 110m from the gold vein to provide data on the background values in plants. The eleven plant species collected along the transects are listed in Table I.

RESULTS AND DISCUSSION

From all the species analysed high gold values were reported for Festuca ovina, Halimium alyssoides, Simaethis planifolia and Chamaespartium tridentatum. There seems to be a definite trend to accumulation in all of these plants (Table 1). Two of these plants, the scrub C. tridentatum (leguminosae) and the grass F. ovina (graminae), were chosen for detailed investigation. These were abundant on the site, exhibited markedly different rooting patterns and showed a degree of accumulation of gold in proportion to the element in the soil (Fig. 3). Fig. (2) shows the gold concentration in the C. tridentatum and F. ovina sampled across the quartz vein A. Background values of 1.28×10^{-3} µg g^{-1} and 2.5×10^{-3} µg g^{-1} were determined for C. tridentatum and F. ovina and correspond well with gold concentrations determined by neutron activation analysis in plants from nonauriferous areas: 1.6µg g^{-1} in Orchard Leaves, 2×10^{-3}µg g^{-1} for grass (17) and 2.4×10^{-3}µg g^{-1} for Bowen's Kale standard material (12).

The peak gold concentrations for F. ovina 65.4×10^{-3} µg g^{-1} are the same order of magnitude as peak values reported by Warren and Delavault (19), Cannon et at. (20), Schiller et al. (17) and Girling et al. (14).

The enrichment factors of 10 or 100 (concentration of gold in plants from auriferous areas divided by background sample concentration) quoted from earlier work (14,13,18,19) encompass the range of enrichment in this work. Seasonal variation in the gold concentrations for F. ovina collected in the same transect later in November and early in June was noted. Samples collected in June contained higher concentrations of gold than those collected in November, but background values were similar, confirming that the best time for sampling should be early summer (18).

TABLE I. CONCENTRATION OF AU AND AS IN PLANT SPECIES

Species analyzed	Au ($x10^{-3}$ µg g^{-1}) dry wt.	As (µg g^{-1}) dry wt.
TREE		
Quercus ruber. L.	8.13 (1.31)	0.460 (0.193)
SHRUB		
Vaccinium myrtillus L.	3.55 (1.72)	0.378 (0.255)
Asphodelus albus Miller	10.96 (1.19)	0.679 (0.171)
Halimium alyssoides (Lam.) C. Koch.	23.85 (2.89	0.433 (0.193
Erica australis L.	17.4 (2.30)	0.327 (0.274)
Chamaespartium tridentatum (L.) P. Gibbs	12.17 (1.28)	0.250 (0.152)
HERB		
Digitalis purpurea L.	6.45 (1.30)	1.90 (0.161)
Jasione crispa (Pourr.) Samp.	12.98 (1.19)	0.701 (0.132)
Sedum anglicum Hudson	10.70 (1.18)	0.671 (0.427)
Simaethis planifolia (Vand.) G.G.	14.47 (2.85)	0.704 (0.390)
GRASS		
Festuca ovina L.	65.4 (2.50)	0.352 (0.182)

The background values are between brackets

From our studies it is evident that the analysis of gold in soils is complicated by the erratic occurrence of particulate gold within the material being sampled resulting in large standard deviations. The distribution of gold in sieved fractions of the different sites shows that anomalous concentrations of gold are not necessarily restricted to a single size fraction. However, analysis of a larger number of samples representing each of the mesh sizes may give clearer information on gold distribution and resolve this matter. Fig.(3) represents the average gold values for each site along the first transect on area A. The areas of high gold and arsenic concentrations for F. ovina or any other plant corresponded very well with the high areas shown by soil analysis. Fig. (4) shows concentration contours for the gold content of F. ovina since this is the plant which showed a higher biomagnification.

With the development of a precise and accurate method for the determination of gold in small samples of plant material, the opportunity to undertake biogeochemical surveys is now available. This procedure avoids the problems associated with the sporadic distribution of particulate gold within the soil and the necessity for very large samples required for a geochemical survey.

ACKNOWLEDGEMENT

The authors wish to thank Rio Tinto Finance and Explorations Ltd. for a Research Grant to finance this investigation.

REFERENCES

{1} CANNON, H.L., Science, 132 (1960) 591.

{2} CHIKISHEV, A.G., Plant indicators of soils, rocks and sub-surface waters, N.Y., Consultants Bureau, 209p.

{3} BROOKS, R.R., Geobotany and biogeochemistry in mineral exploration, New York, Harper and Row, 290p.

{4} WARREN, H.V. and DELAVAULT, R.E., Canadian Inst. Mining Metall. Trans. 53 (1950) 236.

{5} MALYUGA, D.P., Biogeochemical methods of prospecting: New York, Consultants Bureau Enterprises, (1964) 205p.

{6} NICOLLS, G.W., PROVAN, D.M.J., COLE, M.M. and TOOMS, J.S., Trans. Inst. Mining. Metall., 74 (1965) 695.

{7} LYON, G.L. and BROOKS, R.R., N.Z. J. Sci., 12 (1969) 200.

{8} WARREN, H.V., DELAVAULT, R.E., Bull. Geol. Soc. Amer. 61 (1950) 123.

{9} CHRISTIAN, G.D., Clin. Chem., 11 (1965) 459.

{10} HERMAN, J., Coll. Czech. Chem. Comm., 6 (1934) 37.

{11} HILDON, M.A., SULLY, G.R., Anal. Chim. Acta., 54 (1971) 245.

{12} MINSKI, M.J., GIRLING, C.A., PETERSON, P.J., Radiochem. Radioanal. Letters 30 (1977) 179.

{13} GIRLING, C.A., PETERSON, P.J., MINSKI, M.J., Sci. Total Environment 10 (1978) 79.

{14}GIRLING, C.A., PETERSON, P.J., WARREN, H.V., Econ. Geology 74 (1979) 902.
{15}CAVENDER, W.S., AIME preprint, 64-2-73, (1964) 16-20.
{16}WARREN, H.V., DELAVAULT, R.E., BARASKO, J., Econ. Geology 59 (1964) 1381.
{17}SCHILLER, P., COOK, G.B., KITZINGER, A., WOLFE, E., Analyst 97 (1972) 601.
{18}SCHILLER, P,, COOK, G.B., KITZINGER, A., WOLFE, E., Radiochem. Radioanal. Letters. 13 (1973) 283.
{19}WARREN, H.V., DELAVAULT, R.E., Geol. Soc. American Bull. 61 (1950) 123.
{20}CANNON, H.L., SHACKLETTE, H.T., BASTRON, H., U.S. Geol. Survey. Bull., (1968) 1278A, 21p.

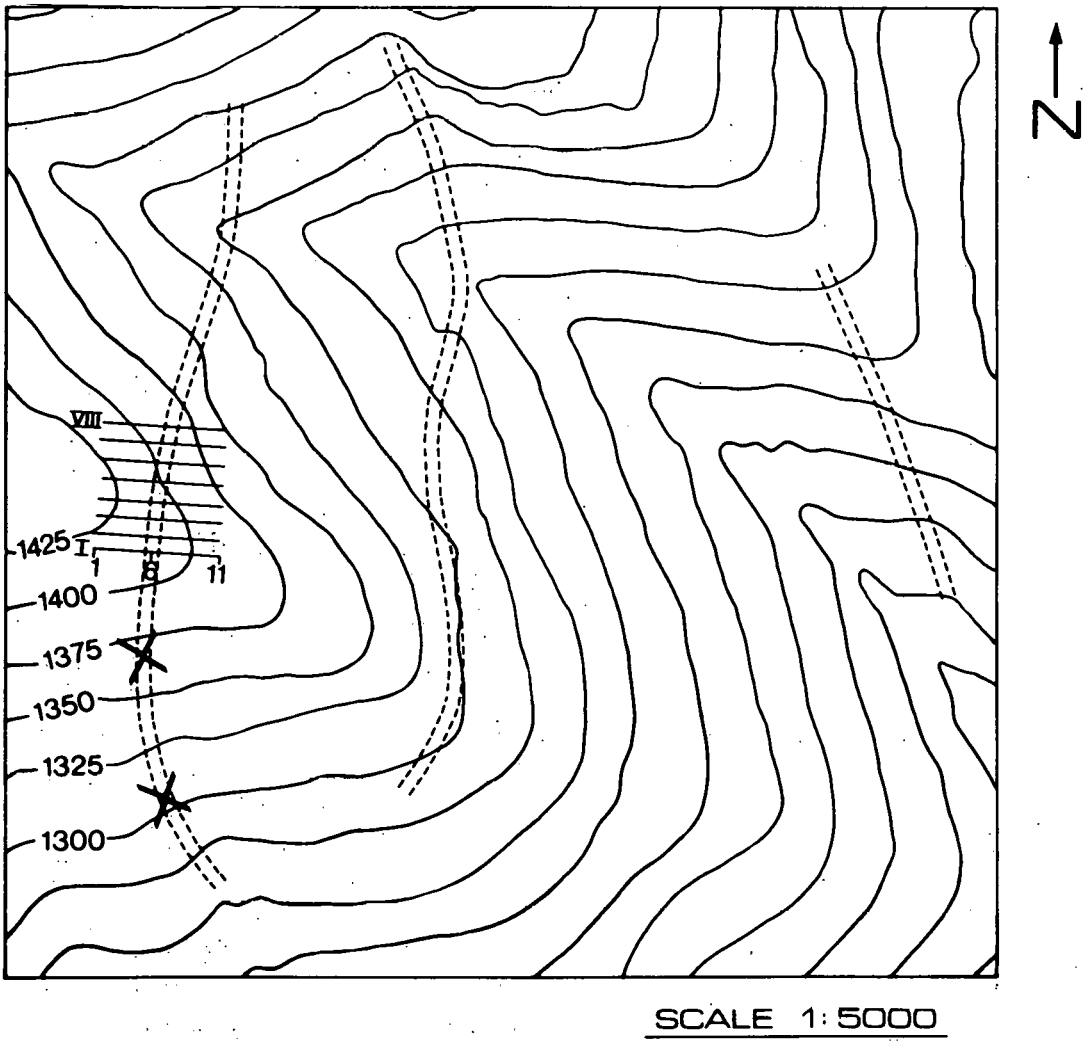


Fig. 1. General view of site location.

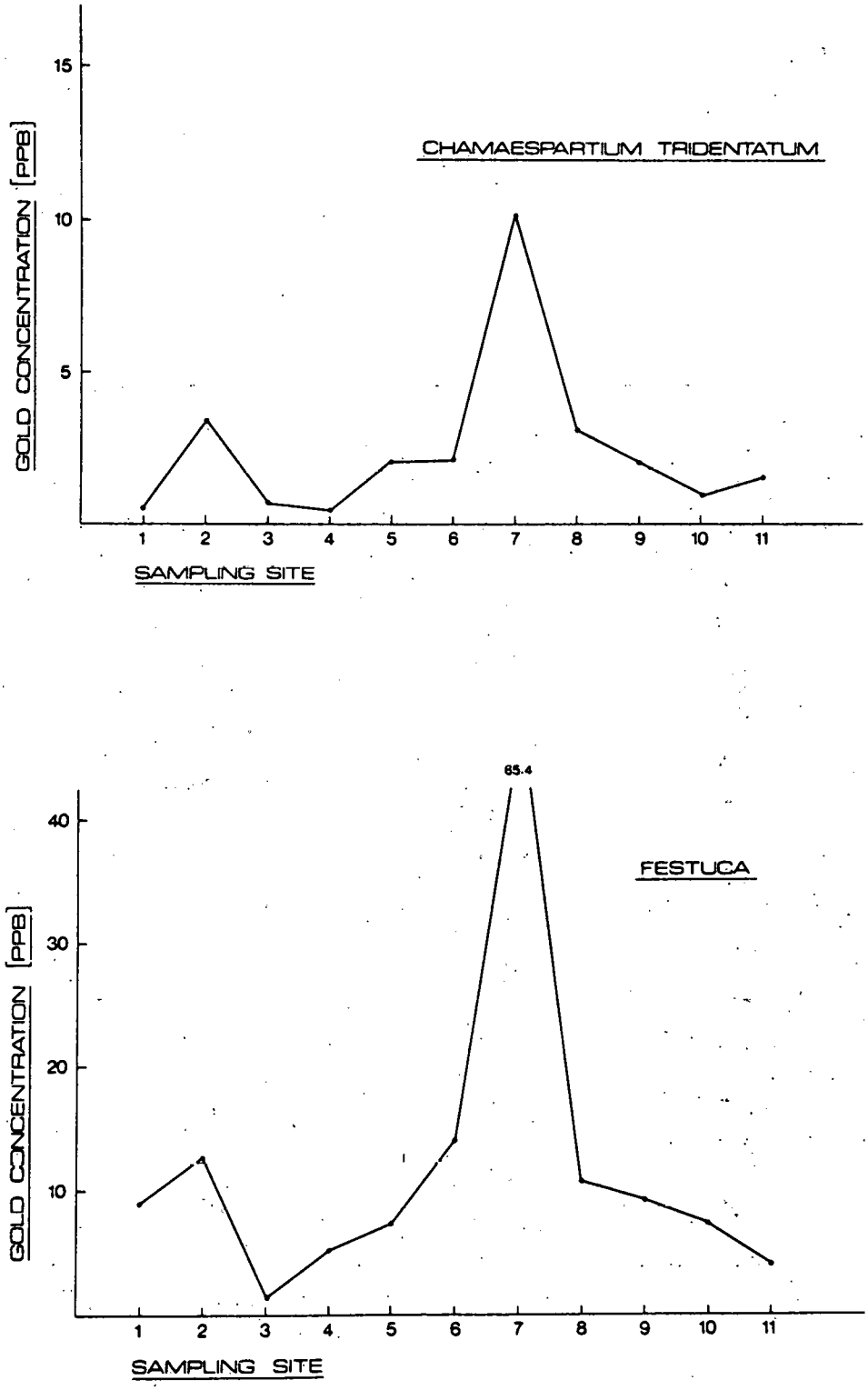


Fig. 2. Gold concentration in the leaves of Festuca ovina and Chamaespartium Tridentatum from transect I. Sampling points are located 10m apart.

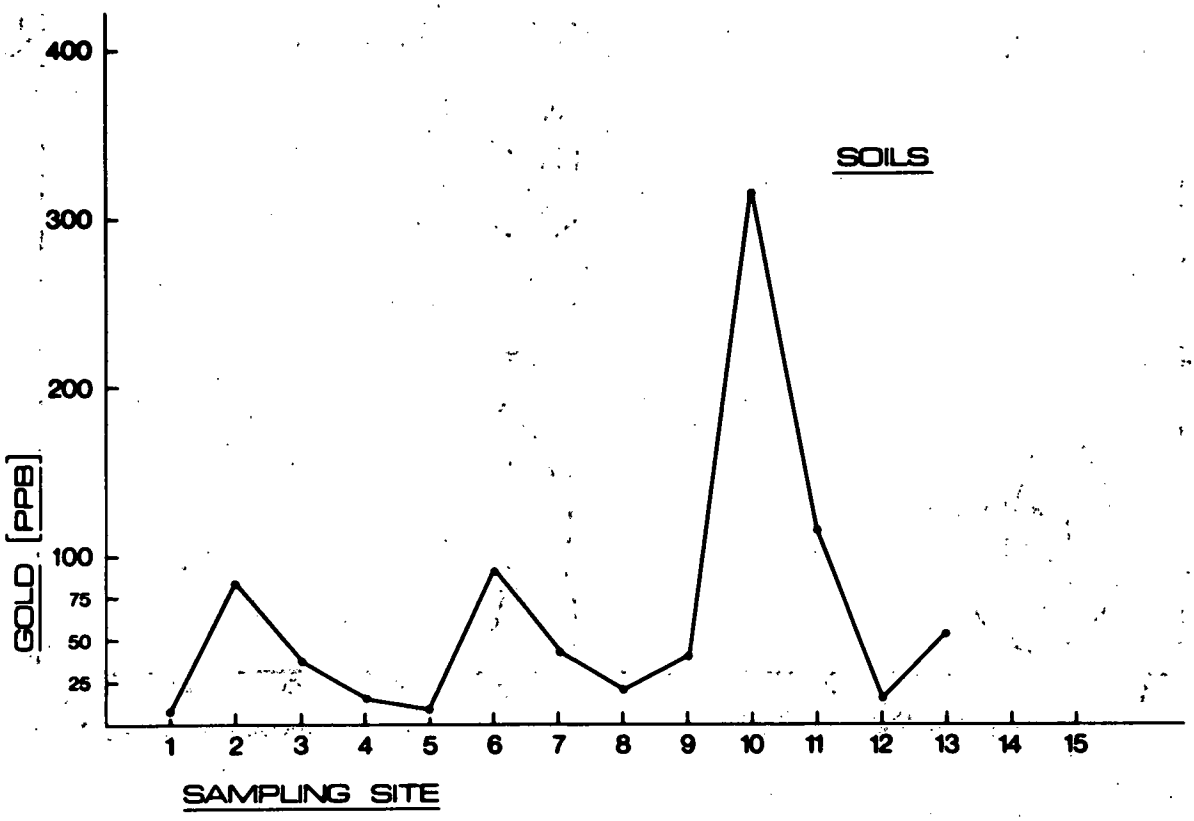


Fig. 3. Gold concentration in soil sample analysed from transect I.

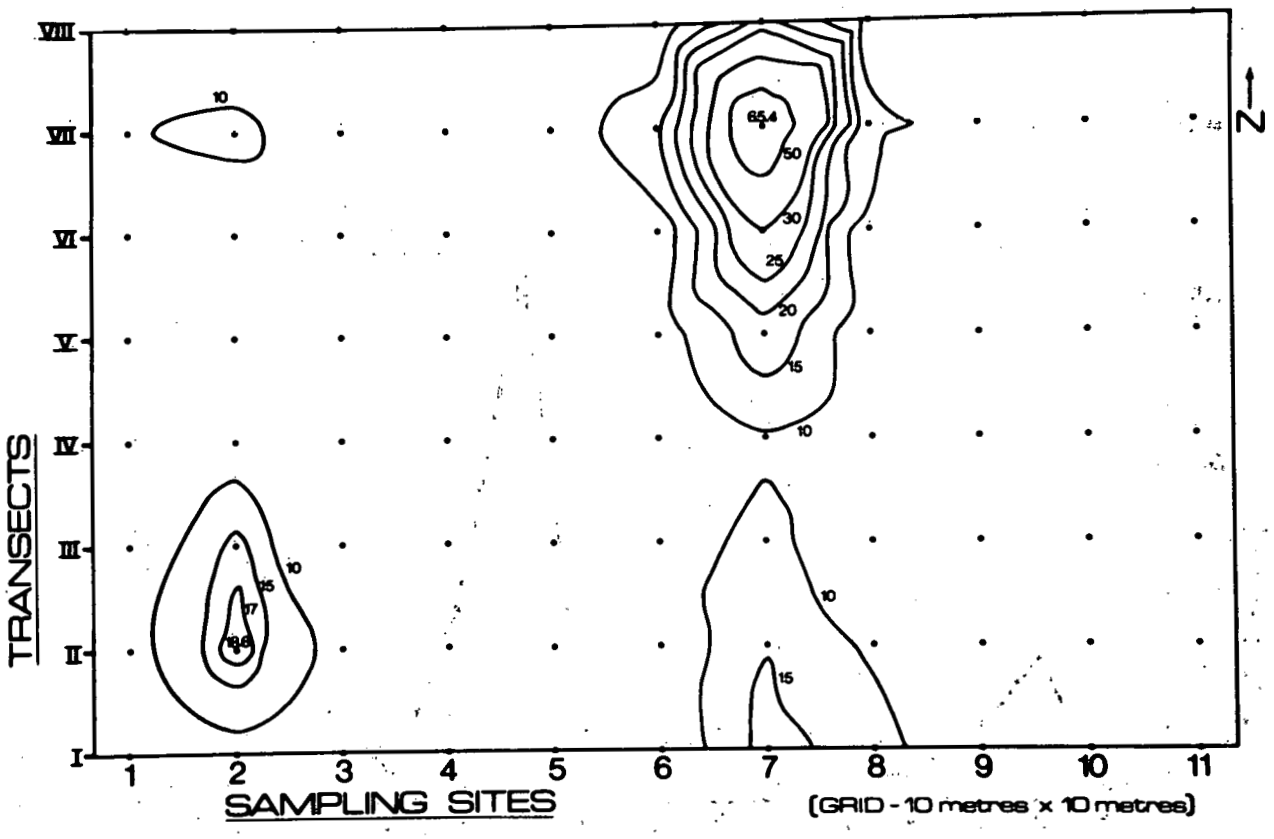


Fig. 4. Gold anomalies indicated by the leaves of F. ovina.

RETENTION OF METABOLIZED TRACE ELEMENTS IN RAT TISSUES: SILVER, CERIUM, CAESIUM, MANGANESE, SCANDIUM AND TIN

G.V.Iyengar, K.Kasperek, L.E.Feinendegen
Nuclear Research Center Juelich GmbH
Institute of Medicine
Post Box 1913, D-517 JUELICH
Federal Republic of Germany

SUMMARY

We investigated the losses of Ag, Ce, Cs, Mn, Sc and Sn during freeze drying and oven drying at 80, 105 and 120 degrees centigrade by incorporating suitable radionuclides into rat tissues. No loss was observed for any of the 6 elements in any of the tissues studied during freeze drying. Whereas, oven drying revealed certain tissue specificity in the retention of these elements and showed the following trend : A significant loss of Sn was observed in muscle even at 80 degrees centigrade and for kidney and liver at 105 degrees centigrade. Also Ce and Mn were lost from heart and muscle at this temperature. Elevating the temperature to 120 degrees centigrade was found to be safe only for Ag and Cs in all the tissues. For the remaining 4 elements the losses seen were about 5 per cent for Ce in brain and heart, for Sc in fur and heart, and for Mn in liver and muscle; up to 10 per cent for Sc in kidney and muscle, and for Sn in blood, fur, heart, liver, ovary and uterus. Losses exceeding 10 per cent were seen for Sn in brain, kidney, lung and muscle.

INTRODUCTION

Very often biological samples need to be dried for trace element analysis. Some of the common procedures employed for this purpose include freeze drying, oven drying and also wet- and dry ashing under various conditions. All these analytical operations are apt to introduce errors. Contamination with and loss of trace elements call for a careful selection of the available procedures. Dehydration and dissolution of the biological samples are chosen according to the nature of the biological sample, major elemental composition of the matrix and various chemical properties. In addition it is also necessary to take into consideration the differences in the behaviour of the trace elements under metabolized conditions. For example, in an earlier communication dealing with Antimony, Cobalt, Iodine, Mercury, Selenium and Zinc, we have shown that there exist tissue specific differences in the retention of these elements, in particular the volatile ones (Iyengar, Kasperek, Feinendegen 1978). In the present investigation similar observations are extended to a further group of elements consisting of Caesium, Cerium, Manganese, Scandium, Silver and Tin.

EXPERIMENTAL

Preparation of the treated water: The radio tracers used were obtained commercially (Amersham Buchler, NEN Chemicals, Germany). The chemical forms of the

Radio-nuclide	Half life	γ-ray energy (keV)	Chemical form	Specific activity	Approximate concentration of the elements in treated water due to the addition of radioactive isotopes
Caesium-134	2.1 y	605	Caesium chloride in water	10 m Ci per mg	100 micro g per litre
Cerium-141	32.5 d	145	Cerium chloride in 0.1 M HCl	2 m Ci per mg	500 micro g per litre
Manganese-54	312 d	835	Managanese chloride in 0.1 M HCl	100 u Ci per ug(carrier-free)	1 micro g per litre
Scandium-46	84.2 d	888 and 1120	As dilute solution in chloride form	3 m Ci per mg	333 micro g per litre
Silver-110m	255 d	658	As solution in nitrate form	3 m Ci per mg	333 micro g per litre
Tin-113	115 d	392 (^{113m}In)	Stannous chloride in 4 M HCl	13.4 m Ci per mg	75 micro g per litre

Table I : Chemicals used for preparing the treated water

elements, their concentration in the treated water, the nuclear data of the radioisotopes chosen and the specific activities are shown in Table I. The labeled water was prepared in one batch by adding required quantities of the radioactive solutions to the drinking water in order to obtain 3 different combinations; 1. Cs, 2. Mn + Sn and 3. Ag + Ce + Sc.

Incorporation of the radionuclides: Three groups of adult wistar rats including both males and females were used. Each group contained 10 animals which were kept in separate cages. Throughout the experimental span of 10 weeks, they were maintained under identical conditions except for the difference in treated water which they drank ad libitum. While group 1 was fed with water containing the radioisotope Caesium-134, 2 and 3 received waters mixed with Manganese-54 + Tin-113, and Silver-110m + Cerium 141, respectively. At the end of the 10th week, the treated waters were replaced with normal water for a period of 3 days. Following this stage blood samples were collected from all the animals by cardiac puncture under ether anesthesia. The animals were then dissected and duplicate sets of samples of brain, faeces, fur, kidney, liver, lung, muscle, ovary, spleen, testis and uterus were collected and prepared for the drying experiments. Blood rich organs were rinsed with water to minimize the detrital blood. Faeces samples were collected directly from the intestine. The specimen denoted as "fur" is actually a piece of outer skin of the rat with a thick bunch of hair. Urine samples were not collected due to technical difficulties.

Drying of the samples and radioactivity measurements: The initial radioactivity of all the samples was measured. The first set of samples was freeze-dried while the second batch was subjected to oven drying at 80 degrees centigrade for 3 days followed by 105 degrees centigrade and 120 degrees centigrade for a day each, respectively. Procedural details concerning various phases of the drying process, equipment used and the radioactivity measurements were essentially same as described elsewhere (Iyengar, Kasperek, Feinendegen 1978). However, one change was introduced in the present experiment by measuring the radioactivity of the samples at the end of each stage of drying instead of counting the samples at the end of each day of drying.

RESULTS AND DISCUSSION

Freeze drying: The results of freeze dried whole blood, brain, faeces, fur, heart, kidney, liver, lung, muscle, ovary, spleen, testis and uterus for the elements Cs, Mn, Sn, Ag, Ce and Sc are shown in Tables II to VII, respectively. As can be seen from these Tables, the recovery values were greater than 98 per cent for all the six elements.

Oven drying: The results for oven dried blood, brain, faeces, fur, heart, kidney, liver, lung, muscle, ovary, spleen, testis and uterus can be seen in Tables II to VII for Cs, Mn, Sn, Ag, Ce and Sc, respectively. A few details concerning the behaviour of individual elements are discussed below.

Caesium: Results obtained for Cs are shown in Table II. As can be seen from the Table, drying up to 105 degrees centigrade poses no danger of losing this element from any of the thirteen samples studied. At 120 degrees centigrade, several tissues showed marginal loss of this element which is reflected by the increased standard deviation in the mean recovery values. However, the losses were not statistically significant.

Manganese: Table III shows the results for this element under different drying conditions. Drying up to 105 degrees centigrade was found to be safe for all the samples with the exception of muscle, which showed a loss of about two per cent, whereas, at 120 degrees centigrade significant loss of Mn was also observed in liver but remained below 5 per cent.

Sample	Fresh	Freeze dried	80°C Day-3	105°C Day-4	120°C Day-5	Number of samples
Blood[a)]	100	98 ± 1.21	99 ± 1.60	98 ± 1.60	97 ± 1.56	6
Brain	100	99 ± 1.22	98 ± 1.65	99 ± 0.56	98 ± 1.00	4
Feces	100	100 ± 0.85	99 ± 1.35	98 ± 1.54	99 ± 1.45	4
Fur[b)]	100	100 ± 1.40	99 ± 1.54	98 ± 1.75	97 ± 1.88	5
Heart	100	98.6± 1.15	98.8 ± 1.60	97 ± 2.00	99 ± 2.11	6
Kidney	100	98 ± 2.24	99 ± 0.66	98 ± 1.05	97 ± 1.44	6
Liver	100	98 ± 1.65	98 ± 1.77	97 ± 2.14	97 ± 2.21	6
Lung	100	99 ± 1.62	97 ± 1.72	98 ± 0.63	98 ± 1.87	6
Muscle	100	100 ± 1.06	100 ± 8.89	99 ± 0.75	99 ± 1.78	6
Ovary	100	98 ± 1.81	98 ± 1.34	98 ± 1.20	99 ± 1.75	4
Spleen	100	99 ± 0.62	98 ± 2.10	98 ± 1.44	97 ± 1.67	4
Testis	100	99 ± 1.11	98 ± 1.84	97 ± 1.26	98 ± 2.48	4
Uterus	100	99 ± 0.50	98 ± 0.84	98 ± 1.62	97 ± 1.55	4

a) Whole blood, b) Skin and Hair together

Table II : Retention of Cs (%) during freeze drying and oven drying

Sample	Fresh	Freeze dried	80°C Day-3	105°C Day-4	120°C Day-5	Number of samples
Blood[a)]	100	100 ± 0.54	100 ± 1.10	99 ± 1.54	98 ± 1.54	6
Brain	100	100 ± 1.00	98 ± 1.71	99 ± 1.22	98 ± 2.44	4
Feces	100	100 ± 1.24	99 ± 2.10	98 ± 2.51	98 ± 1.24	4
Fur[b)]	100	99 ± 1.25	98 ± 1.70	99 ± 0.62	97.5± 1.70	5
Heart	100	99 ± 1.52	99 ± 0.75	98.5± 1.54	98 ± 2.55	5
Kidney	100	99 ± 0.60	98 ± 1.21	98 ± 0.80	97 ± 2.60	6
Liver	100	100 ± 1.20	99 ± 0.70	98 ± 1.22	97.5± 1.52	6
Lung	100	99 ± 1.60	98 ± 1.42	99 ± 0.53	99 ± 1.52	6
Muscle	100	100 ± 0.58	100 ± 1.20	98 ± 0.81	98 ± 1.26	6
Ovary	100	99 ± 1.40	99 ± 1.62	98 ± 0.73	98 ± 1.00	4
Spleen	100	100 ± 0.80	99 ± 0.54	99 ± 1.10	98.5± 1.14	4
Testis	100	98.4± 1.31	98 ± 1.60	98 ± 0.67	97 ± 1.45	4
Uterus	100	99 ± 1.12	98 ± 1.15	98 ± 1.22	97 ± 1.66	4

a) Whole blood, b) Skin and Hair together

Table III : Retention of Mn (%) during freeze drying and oven drying

Sample	Fresh	Freeze dried	80°C Day-3	105°C Day-4	120°C Day-5	Number of samples
Blood[a)]	100	99 ± 1.22	98 ± 1.54	99 ± 2.60	90 ± 3.50	6
Brain	100	98 ± 1.54	99 ± 0.50	97 ± 2.70	86 ± 5.70	4
Feces	100	100 ± 0.50	98 ± 1.80	98 ± 1.30	95 ± 3.00	4
Fur[b)]	100	100 ± 1.15	98 ± 0.85	97 ± 2.64	90 ± 5.32	5
Heart	100	99 ± 2.00	99 ± 1.00	98 ± 1.06	90 ± 3.52	5
Kidney	100	100 ± 1.00	98 ± 1.21	97.4± 1.60	80 ± 6.53	6
Liver	100	100 ± 1.20	99 ± 0.80	96 ± 2.50	90 ± 4.00	6
Lung	100	99 ± 1.56	98 ± 1.25	98 ± 2.55	88 ± 3.75	6
Muscle	100	100 ± 0.82	97 ± 1.85	98 ± 2.54	85 ± 4.70	6
Ovary	100	99 ± 0.55	98 ± 1.47	99 ± 2.20	91 ± 4.20	4
Spleen	100	99 ± 1.20	97 ± 2.14	98 ± 2.53	88 ± 7.20	4
Testis	100	100 ± 0.40	99 ± 1.35	98 ± 2.30	90 ± 6.42	4
Uterus	100	98 ± 1.35	98 ± 0.56	99 ± 1.70	90 ± 2.60	4

a) Whole blood, b) Skin and Hair together

Table IV : Retention of Sn (%) during freeze drying and oven drying

Sample	Fresh	Freeze dried	80°C Day-3	105°C Day-4	120°C Day-5	Number of samples
Blood[a)]	100	98 ± 1.64	99 ± 0.64	98.5± 1.50	97 ± 2.40	6
Brain	100	100 ± 1.22	99 ± 1.42	98 ± 1.84	98 ± 2.21	4
Feces	100	99 ± 0.85	99 ± 0.78	98 ± 0.88	97 ± 2.54	4
Fur[b)]	100	99 ± 1.00	98 ± 1.72	98 ± 0.75	97 ± 1.00	5
Heart	100	99 ± 1.50	99 ± 1.00	98 ± 1.24	97 ± 2.54	5
Kidney	100	98.5± 1.84	99 ± 0.53	99 ± 1.23	96 ± 3.35	6
Liver	100	100 ± 1.10	100 ± 0.46	98 ± 1.40	98 ± 2.16	6
Lung	100	99.2± 2.16	99 ± 1.22	98 ± 1.55	97 ± 2.54	6
Muscle	100	100 ± 0.50	98 ± 0.82	98 ± 1.63	98 ± 1.58	6
Ovary	100	-	-	-	-	-
Spleen	100	99 1.59	98 1.60	99 2.14	97 1.66	4
Testis	100	100 1.34	98 1.85	99 1.34	98 1.27	4
Uterus	100	-	-	-	-	-

a) Whole blood, b) Skin and Hair together

Table V : Retention of Ag (%) during freeze drying and oven drying

Sample	Fresh	Freeze dried	80°C Day-3	105°C Day-4	120°C Day-5	Number of samples
Blood[a)]	100	99 ± 1.00	100 ± 1.32	99 ± 0.64	97.4± 2.15	6
Brain	100	100 ± 0.50	99 ± 1.20	98 ± 1.26	97 ± 1.14	4
Feces	100	100 ± 1.22	100 ± 1.00	100 ± 1.00	98.5± 1.70	4
Fur[b)]	100	99 ± 0.75	100 ± 0.65	98 ± 0.87	97 ± 2.10	5
Heart	100	100 ± 1.00	99 ± 0.56	98.5± 1.2	97 ± 0.60	5
Kidney	100	98 ± 1.50	100 ± 0.85	99 ± 1.35	98 ± 0.80	6
Liver	100	99 ± 0.67	98 ± 1.61	99 ± 1.75	97 ± 1.51	6
Lung	100	99 ± 1.21	98 ± 1.82	99.5± 0.81	98 ± 0.52	6
Muscle	100	98 ± 1.65	99 ± 1.20	98 ± 1.45	98 ± 1.12	6
Ovary	100	-	-	-	-	-
Spleen	100	99 ± 1.31	100 ± 0.61	98.4± 1.21	97 ± 1.80	4
Testis	100	98 ± 1.45	98 ± 1.62	99 ± 0.63	97 ± 1.64	4
Uterus	100	-	-	-	-	-

a) Whole blood, b) Skin and Hair together

Table VI: Retention of Ce (%) during freeze drying and oven drying

Sample	Fresh	Freeze dried	80°C Day-3	105°C Day-4	120°C Day-5	Number of samples
Blood[a)]	100	100 ± 1.15	99 ± 1.21	100 ± 0.50	98 ± 2.60	6
Brain	100	99 ± 0.50	98 ± 1.50	99.5± 1.00	97 ± 1.75	4
Feces	100	100 ± 1.00	99 ± 2.14	98 ± 2.10	98 ± 2.51	4
Fur[b)]	100	100 ± 1.12	99 ± 2.00	99 ± 1.60	96 ± 2.34	5
Heart	100	100 ± 0.50	100 ± 1.00	100 ± 1.10	96 ± 2.61	5
Kidney	100	99 ± 0.80	99 ± 1.85	99 ± 0.81	92 ± 4.50	6
Liver	100	99 ± 1.25	98.5± 1.37	98.5± 1.00	96 ± 3.15	6
Lung	100	98 ± 1.67	99 ± 0.56	98 ± 2.54	96 ± 2.20	6
Muscle	100	99 ± 1.82	100 ± 1.08	99 ± 2.10	93 ± 3.61	6
Ovary	100	-	-	-	-	-
Spleen	100	99 ± 1.45	98 ± 1.74	99 ± 0.80	98 ± 1.60	4
Testis	100	98 ± 1.80	100 ± 1.14	99 ± 1.50	97 ± 1.55	4
Uterus	100	-	-	-	-	-

a) Whole blood, b) Skin and Hair together

Table VII: Retention of Sc (%) during freeze drying and oven drying

Samples	80°C		105°C		120°C		Remarks
	2P<0.02	2P<0.002	2P<0.02	2P<0.002	2P<0.02	2P<0.002	
Blood						Sn^{+}	
Brain					Ce^{o}, Sn^{x}		
Feces							See Table 4
Fur					Sc^{o}, Sn^{+}		
Heart			Ce^{o}		Ce^{o}, Sc^{o}, Sn^{+}		
Kidney			Sn^{o}		Sc^{+}	Sn^{x}	
Liver			Sn^{o}		Mn^{o}	Sn^{+}	
Lung						Sn^{x}	
Muscle	Sn^{o}		Mn^{o}, Sn^{o}		Sc^{+}, Mn^{o}	Sn^{x}	
Ovary						Sn^{+}	
Spleen							See Table 4 and text
Testis							See Table 4 and text
Uterus						Sn^{+}	

^{o} Loss up to 5 per cent
$^{+}$ Loss up to 10 per cent
^{x} Loss up to 15 per cent

Table VIII : Significance Test, Freeze- vs Oven Drying at various temperatures

Tin: The results obtained for Sn are summarized in Table IV. As reflected in the Table, oven drying rat tissues containing metabolized Sn is generally safe for all the samples at 80 degrees centigrade. Although statistically significant losses were seen only for kidney, liver, and muscle at 105 degrees centigrade, it is evident form the increased dispersion tendencies reflected in the mean recovery values (Table IV), that the matrix is no longer stable with respect to tin at this temperature, and is apparently at a critical point that is about to decompose. This is clearly seen with the stepping up of the temperature to 120 degrees centigrade, where all the tissues have lost this element to varying extent. The losses were highly significant in several cases (Table VIII). However, faeces (which is not a tissue) was the only exception that showed a better matrix stability by retaining tin quantitatively.

Silver: Retention of Ag in different samples following drying at different temperatures are presented in Table V. Both 80 and 105 degrees centigrade are very well suited for drying tissues containing metabolized Ag. The tendency seen at 120 degrees centigrade resembles that of Cs at the same temperature with the exception of kidney where some loss was detected (recovery 96 $\pm$ 3.4 %), other samples showed only marginal decline in the recovery values.

Cerium: Table VI shows the retention yields for this element. By and large, drying up to 120 degrees centigrade presented no serious problems for majority of the samples. Although significant losses were recorded for this element in heart and brain at 105 and 120 degrees centigrade, respectively, the losses did not exceed 5 per cent.

Scandium: The results for this element are given in Table VII. Up to 105 degrees centigrade there is no danger of losing this element from any of the thirteen samples. However, drying rat tissues containing metabolized Sc at 120 degrees centigrade was found to be unsuitable for many tissues as illustrated in the Table. While a number of tissues showed tendencies of losing this element, losses observed for fur, heart, kidney and muscle were significant (Table VIII). Only spleen and testis showed better matrix stability at this temperature.

The biological matrix: It has been shown in the earlier communication that most biological matrices decompose above 100 degree centigrade (Iyengar, Kasperek, Feinendegen 1978), and that intrinsically volatile elements such as Hg can be lost very easily. Losses observed for Sn in this experiment confirm this further. Loss of the elements from the decomposed matter varies depending upon the chemical properties of individual elements.

The reader may consult another report for more discussions on the retention of these six elements in different matrices and a comprehensive comparison of the literature data (Iyengar, Kasperek, Feinendegen 1980).

LITERATURE CITED

G.V. Iyengar, K, Kasperek, L.E. Feinendegen
Sci. Total Environ. 10(1978)1

G.V. Iyengar, K. Kasperek, L.E. Feinendegen
Analyst, 1980 (in press)

INFLUENCE OF POST MORTEM CHANGES ON THE ELEMENTAL COMPOSITION OF RAT LIVER STUDIED BY ATOMIC ABSORPTION SPECTROMETRY AND NEUTRON ACTIVATION ANALYSIS

G.V. Iyengar, K. Kasperek[+], L.E. Feinendegen[+]
Department of Radiobiology
The Swedish University of Agricultural Sciences
Box 7031, S-750 07 UPPSALA
Sweden

[+]Nuclear Research Centre Jülich GmbH
Institute of Medicine
Post Box 1913, D-517 JÜLICH
Federal Republic of Germany

SUMMARY

The implication of post mortem changes such as cell swelling, imbibition and autolysis on the elemental composition profiles of body organs has been discussed. Liver has been chosen as an example. Retaining the liver inside the intact body for different periods of time at ambient temperature-induced significant differences in its weight due to post mortem tissue degeneration. Livers from the animals that were frozen at -15°C also showed significant decrease in weight upon thawing on the third day. The effect of these changes on the concentrations of various elements was reflected differently depending upon the association of the elements with extracellular fluids and intracellular components. For example, concentration of K was more affected by the lysis of the cell and sustained losses up to 30 per cent in relation to the control values, while the total content was reduced by more than 40 per cent as a result of both lysis and partial liquefaction. For Na, differences ranging from +10 to -20 per cent in concentrations and +20 to -40 per cent in total content were observed which could be explained by fluid movements in and out of the organ. Among the trace elements, variations observed for Fe ranged from -20 and +40 per cent, while both Cu and Zn were found to fluctuate between -20 and +20 per cent. The loss observed in the total content in liver for the 5 trace elements studied (Cu, Fe, Mn, Rb and Zn) was found to be about 20 to 40 per cent. Rinsing of the liver samples with distilled water depleted the electrolyte concentration up to 30 per cent. Among the trace elements, while Cu, Fe and Zn were relatively unaffected, the losses were up to 20 per cent both for Mn and Rb.

INTRODUCTION

It is well established in the realm of pathology that dead tissues are subject to several post mortem changes. It is also known that such changes are more prevalent at higher temperatures and are best seen in the rapidly metabolizing parenchymal cells of liver, spleen, kidney and heart. These organs whose component cells are severely affected by cell swelling become easily swollen and tend to bulge beneath their capsules. It may be remarked in this

connection that establishment of reliable reference values for elemental concentration in normal human tissues is faced with certain inherent difficulties since only a few samples such as blood, excretory products and occasional biopsy samples are obtainable from living subjects while the remaining ones are sought at autopsy. A recent survey of the literature (Iyengar, Kollmer and Bowen 1978) revealed that elemental concentrations based on autopsy samples generally show great variations in contrast to blood or serum obtained from living subjects (Table I). The elements chosen here are those which do not pose any real analytical difficulties. Regarding the extent of variability illustrated in this Table, such large diviations seen even for the essential bulk elements is rather puzzling since essential elements are generally expected to show narrow limits in their concentration ranges in tissues of similar age, due to physiological control mechanisms. Therefore, the reported discrepancies bring into picture a probable source of error hitherto unidentified by the analytical community. In this connection it should be recognized that autopsy sampling from human cases involves a certain time lapse between death and sample collection due to many reasons and that, immediately after the death of an organism several post mortem changes set in with varying rapidity depending upon such factors as environmental temperature, humidity, body temperature at the time of death, insulating effect provided by the fat layers in the body, time elapsed before the body was put under cooling and the storage time. Of the many changes that occur, cell swelling, tissue dehydration, imbibition, putrefaction and autolysis are of particular significance to the analyst since they influence the "tissue status" as long as the organs remain inside the body. By implication, post mortem changes could have important bearings on the elemental composition profiles of individual organs. Results of an animal model study to assess the impact of such tissue degeneration are presented.

EXPERIMENTAL

Three alternative treatments were chosen: Ambient temperature (25 to 28^{o}C) to follow up tissue autolysis, freezing (-15^{o}C) to inhibit or delay the tissue degeneration and rinsing of the samples with distilled water in order to study the effect of washing. A group of 70 adult, male rats with an average body weight of 160 g (range 155 to 165) was sacrificed by ether anesthesia within a span of one hour. Ten rats were dissected immediately after death and entire livers collected to serve as controls. Care was taken to eliminate blood to the maximum extent by placing the liver sample in a plastic funnel and squeezing it gently with plastic forceps and followed by drainage of blood. Following this, five samples were retained in their original condition while the remaining ones were rinsed once with double distilled water. Wet weights of the unwashed samples were taken. The rest of the 60 rats were divided into two batches of 30 each. While one batch was frozen at -15^{o}C the second one was kept at ambient temperature (25 to 28^{o}C). During the subsequent 3 days ten animals from each batch were dissected to collect the liver samples (Table II). Frozen rats were allowed to thaw before dissection. The samples were oven dried, weighed and prepared for analysis. Elemental concentrations were determined in all the samples. Atomic absorption spectrophotometry was used to determine Ca, Mg, Cu, Fe, Zn, Mn and Rb. K and Na were analysed by atomic emission spectrometry, while Cl was assayed by instrumental neutron activation analysis. NBS bovine liver served as a reference material for checking the analytical steps. The procedural details are described elsewhere (Iyengar 1980a, Iyengar 1980b).

Table I

Variations in the elemental concentrations of normal adult human tissues reported in the literature. Values are expressed in mg per kg fresh tissue and mg per litre fluid (Figures in parentheses represent the ratio maximum/minimum)

Element / Samples	Ca	Cl	Cu	Fe	K	Mg	Na	Zn
Brain[a]	30-130 **(4.3)**	1400-2330[b] **(1.7)**	2-10 **(5)**	30-150 **(5)**	1600-3500 **(2.2)**	130-700 **(5.4)**	1650-1850[b] **(1.1)**	8-33 **(4.1)**
Liver	45-135 **(3)**	840-2000 **(2.4)**	3-22 **(7.3)**	70-390 **(5.6)**	1700-3000 **(1.8)**	170-370 **(2.2)**	560-1750 **(3.1)**	30-120 **(4)**
Muscle	40-150 **(3.8)**	400-1400 **(3.5)**	0.7-4 **(5.7)**	20-50 **(2.5)**	1600-5000 **(3.1)**	170-316 **(1.7)**	400-1800 **(4.5)**	35-70 **(2)**
Blood	57-70 **(1.2)**	2600-3300 **(1.27)**	0.8-1.2 **(1.5)**	350-500 **(1.43)**	1450-2000 **(1.4)**	30-44 **(1.47)**	1700-2050 **(1.2)**	6-9 **(1.5)**
Serum	92-109 **(1.18)**	3300-3800 **(1.15)**	1-1.5 **(1.5)**	0.8-1.5 **(1.87)**	150-180 **(1.2)**	20-24 **(1.2)**	3100-3400 **(1.13)**	0.84-1.5 **(1.79)**

[a] only whole brain considered, [b] limited number of results

Table II

Schematic procedure outlining the sampling schedule

Stage	Day	Tissue Status	Storage Conditions	Number of Animals	Liver	
					Washed	Unwashed
1	0	Fresh	Nil	10	5	5
2	1	Decay-1	25-28°C	10	5	5
			-15°C	10	5	5
3	2	Decay-2	25-28°C	10	5	5
			-15°C	10	5	5
4	3	Decay-3	25-28°C	10	5	5
			-15°C	10	5	5
			Total	70	35	35

RESULTS AND DISCUSSION

Retaining the liver for prolonged periods of time inside the dead body caused fluctuations in its weight (Table III). In rats maintained at ambient temperature, day 1 was characterized by cell swelling and an increase in volume up to 30 per cent with respect to the controls. On day 2, a general shrinkage in the volume ranging from 20 to 50 per cent in relation to control animals was observed. On opening the abdominal cavity a puddle of red tinged plasma released from the circulatory system and blood rich organs (onset of imbibition) was clearly seen. Whereas, on the third day, the tissues appeared pale and supple, and were drenched in the surrounding fluids and degenerated to the extent of partical liquefaction. Among the frozen rats, day 1 animals registered only a slight increase in the weight but the standard deviation of the mean liver weight was higher than that of the controls. This may be partly due to cell swelling since several hours of thawing was necessary before dissection, and partly due to differences in the retention of fluids. Day 2 and Day 3 animals showed a progressive decrease in their liver weights. Livers from these rats appeared black and were surrounded by freely flowing hemolysed blood after thawing.

When the organs from the rats stored at ambient temperature were given a distilled water rinse surface blood was removed efficiently from day 0 and day 1 animals. Whereas, samples from the remaining two days incurred losses of tissue material to varying extent. Frozen livers retained their black colour even after washing.

The overall impact of these changes on the concentration levels and total contents of various elements was reflected differently depending upon the association of the elements with extracellular fluids and intracellular components (Figures 1 to 4).

Rinsing the fresh tissue with distilled water depleted the concentrations of electrolytes up to 30 per cent (Figure 1, A). In unwashed samples stored at ambient temperature, relating the results to dry weight basis led to an initial decline in the concentration level of K during the cell swelling phase while its level remained steady during the remaining two days. With respect to other electrolytes, the concentration levels continued to fluctuate (Figure 1, B). On the other hand, results based on fresh tissue did not yield steady values for K, while the fluctuations seen for Na and Mg were relatively less (Figure 1, C). Concerning Ca, a sharp increase of both concentration and total content up to a factor of 6 in relation to controls was recorded. This is somewhat puzzling since Ca present in blood alone can not account for this entire difference. Since Ca from bone can not be mobilized quickly enough to go into the fluid stream, this implies that the excess Ca came from the decomposing food rests in the GI-Tract by diffusing through the walls of degenerated stomach and intestine. The concentration of Ca in the feed was 1.2 per cent, high by a factor 70 in relation to its level in liver. From practical point of view, the condition leading to the elevated Ca concentrations typically represents one of the several possibilities which may lead to artifacts while dealing with autopsy specimen for elemental analysis. Since in human situations dead bodies obtained from accident cases are usually preferred to acquire samples for establishing normal levels, such influences as observed with Ca can not be ignored.

When the total content in liver is considered, it will be seen that (Figure D) with the exception of the results for fresh tissue (day 0), all other conditions employed in this investigation resulted in lower values for K, and fluctuating values for the remaining ones.

Table III

Changes in liver weight following post mortem tissue degeneration

Sample	wet weight (g)	dry weight (g)	% dry weight (mean)
Control			
Day 0	7.728 ± 0.543	2.056 ± 0.152	27
Surrounding Temperature (25-28°C)			
Day 1	10.282 ± 0.232 ($2p < 0.001$)	2.598 ± 0.140 ($2p < 0.005$)	25
Day 2	5.025 ± 0.277 ($2p < 0.001$)	1.360 < 0.047 ($2p < 0.001$)	27
Day 3	7.242 ± 0.516	1.668 ± 0.124 ($2p < 0.01$)	23
Cold Storage (-15°C)			
Day 1	8.169 ± 0.88	2.216 ± 0.260	27
Day 2	7.790 ± 0.397	2.011 ± 0.111	26
Day 3	6.408 ± 0.332 ($2p < 0.01$)	1.799 ± 0.121 ($2p < 0.05$)	28

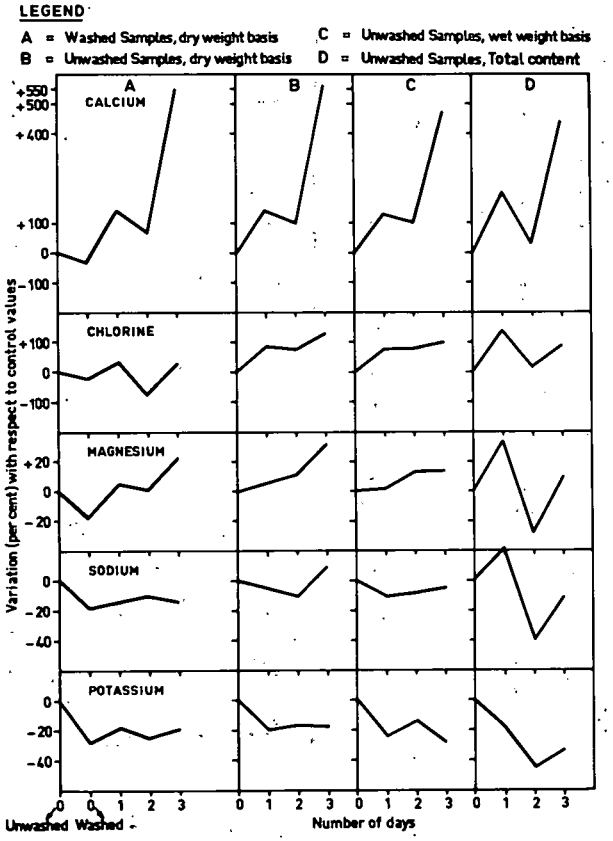


Figure 1. Influence of washing and tissue autolysis on the electrolyte concentration and total content of liver in rats stored at -25 - 28° C.

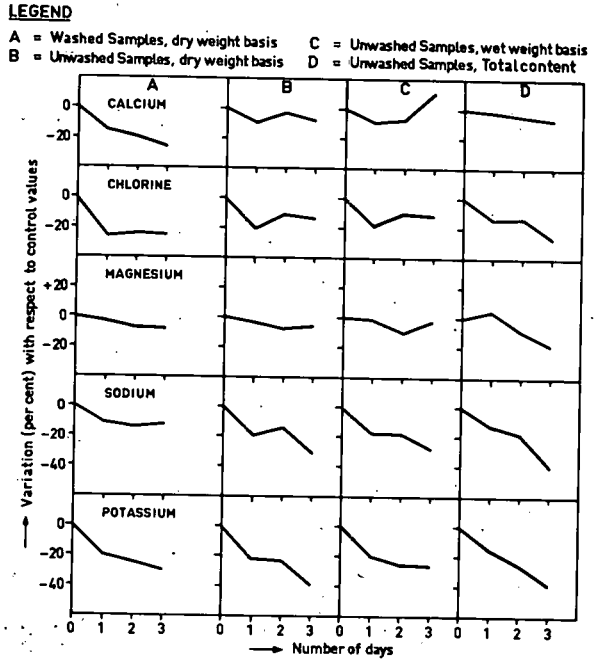


Figure 2. Influence of washing and tissue autolysis on the electrolyte concentration and total content of liver in rats frozen at -15° C.

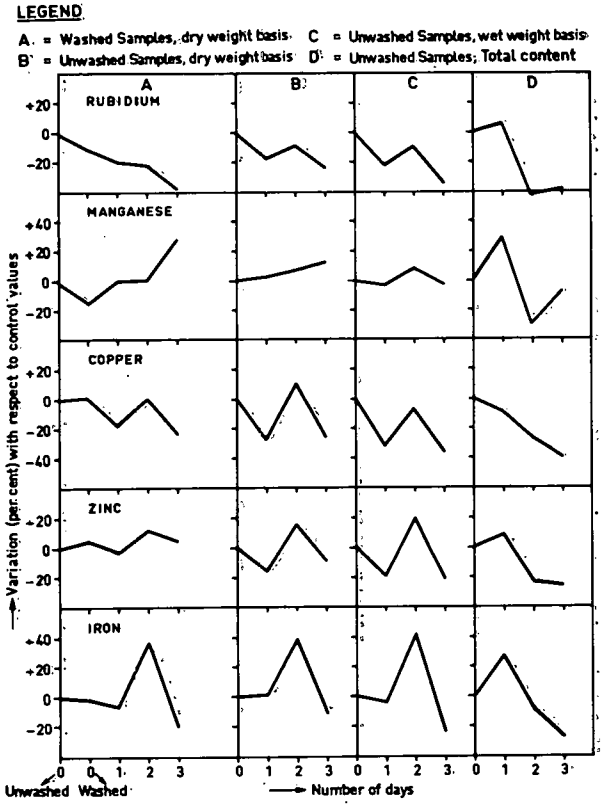


Figure 3. Influence of washing and tissue autolysis on the trace element concentration and total content of liver in rats stored at 25–28°C.

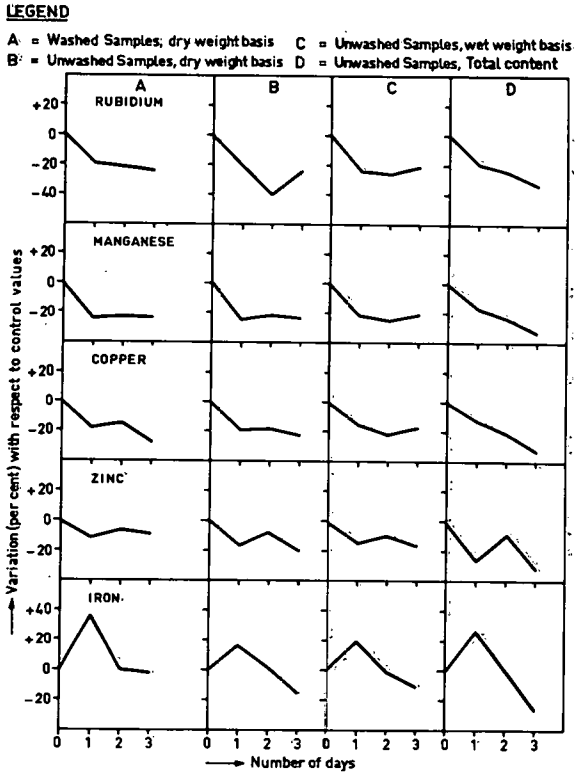


Figure 4. Influence of washing and tissue autolysis on the trace element concentration and total content of liver in rats frozen at –15° C.

In frozen samples, washing effected a general decline of concentrations throughout the entire storage span for all the electrolyte elements (Figure 2). Concentrations based on dry matter in unwashed samples showed lower values for all of them while the loss incurred may extend up to 40 per cent (Figure 2, B). With respect to the findings based on fresh tissues, mainly Na and K showed losses exceeding 20 per cent (Figure 2, C). Regarding the total contents in liver, losses reaching up to 40 per cent were seen for all the electrolytes depending upon the length of storage time (Figure 2, D). It is of interest to note that Ca (Figure 2) is contained within certain limits unlike the previous case (Figure 1).

Trace elements: Rinsing of the fresh liver with distilled water did not affect the concentration levels of Cu, Fe and Zn, while both Rb and Mn showed lower values up to 20 per cent and resembled the electrolytes in this respect (Figure 3, A). In unwashed samples maintained at 25 to 28^{o}C, it is not possible to draw any meaningful conclusion regarding the choice of the basis for expressing results (Figure 3, B and C). Total contents too were subject to serious fluctuations (Figure 3, D). However, with frozen samples, the concentration levels found in washed and unwashed samples were comparable with each other in respect of all the elements (Figure 4). With the exception of Fe around day 1, expressing the results on wet or dry matter basis led to lower values ranging from 15 to 40 per cent (Figure 4, B and C). As for the total content in liver, while Rb, Mn and Cu consistently tended to show losses exceeding 30 per cent, both Fe and Zn were found to be fluctuating and were dependent upon the length of storage time (Figure 4, D). For a comprehensive discussion on the influence of post mortem changes on the elemental composition of autopsy specimens the reader may consult the following reports (Iyengar 1980a, Iyengar 1980b).

CONCLUSIONS

The observations from this study show that there is a need for standardizing sampling time and storage conditions in studies of elemental concentrations after autopsy. It is necessary to avoid excessive time delay between death and sample collection, because even when the body is stored in refrigerator, it only slows down the post mortem events but does not stop them. If these considerations are given due attention in the sampling plans, the true biological variations of the elementary composition of living tissues may be easier to reveal.

LITERATURE CITED

1. G.V.Iyengar, W.E.Kollmer, H.J.M.Bowen. The Elemental Composition of Human Tissues and Body Fluids Verlag Chemie, Weinheim. New York, 1978.

2. G.V.Iyengar. Post mortem changes of the elemental composition of Autopsy Specimens: Variations of K, Na, Mg, Ca, Cl, Fe, Zn, Cu, Mn and Rb in rat liver. Sci.Total Environ., 1980 (in press)

3. G.V.Iyengar. Autopsy Sampling and elemental analysis: Errors arising from post mortem changes. J. Pathology, 1980 (in press).

NUCLEAR METHODS

IN

ENVIRONMENTAL MONITORING

Session Chairman

J.S. Morris

A NEW TECHNIQUE OF RADIATION DOSIMETRY BASED ON LYOLUMINESCENCE

K.V.Ettinger and J.R.Mallard - Department of BioMedical Physics and BioEngineering,University of Aberdeen,Foresterhill,Aberdeen AB9 2ZD,Scotland U.K.

D.Vartsky - Medical Department, Brookhaven National Laboratory,Upton N.Y. USA

Lyoluminescence i.e.emission of light on dissolution by previously irradiated solids has been applied to the needs of radiation dosimetry. The effect can be observed in many categories of organic solids,including carbohydrates,amino acids,proteins and certain polymers. Simple solvents like water can be used for this purpose but higher sensitivity is attained by application of sensitizers e.g.fluorescent dyes or chemiluminescent indicators.

The paper describes the main applications of lyoluminescence dosimetry and gives an outline of the experimental techniques involved in its use.

1. Lyoluminescence is a name given to emission of light when solids,which were previously irradiated,are dissolved in water or other suitable solvent. The action of ionizing radiation on organic solids results in formation of free radicals which may survive for a period of time sufficiently long to be of practical use in radiation dosimetry. After their formation in the bulk of a solid free radicals can disappear only by process of recombination ,which is hindered by the forces binding the solid into a molecular crystal.Even when there is no apparent crystallinity and the solid can be treated as an amorphous one, the radical recombination is a slow process,controlled by diffusion of recombining species. In fact, ionizing radiation usually creates more than one type of radical,but as a consequence of transformations taking place briefly after the irradiation we are left with surviving species of relatively long half-life. E.g. in many saccharides and amino acids the effect of lyoluminescence can be observed after few years since irradiation.In some polymers the decay of radicals is so slow that lyoluminescence may be observable for centuries following the exposure. As expected,the recombination rate of radicals trapped in a solid increases with temperature.

When irradiated solid is dissolved,the radicals are set free to react in solution. The emission of light is a consequence of a considerable amount of energy liberated in free radical reactions. Lyoluminescence dosimetry makes use of this emission of light.The total amount of light produced on dissolution is measured by means of integration of the light reaching suitable detector, usually a sensitive photomultiplier tube. A typical waveform of the light intensity observed when irradiated solid and solvent are brought into contact is shown in Fig.1 .The rise time of the waveform is determined by the response of the recording apparatus and the shape reflects the progressing dissolution of the solid. By analogy with thermoluminescence dosimetry the dissolution waveform is called glowcurve and the solid will be referred as phosphor.

The duration of dissolution depends upon the nature of phosphor-solvent combination and is measured in tens of seconds for saccharides in water.

For some materials e.g.polymers it is necessary to speed up the dissolution by mechanical or ultrasonic stirring.In the latter case it is important to avoid cavitation and sonoluminescence which will interfere with the measurement.

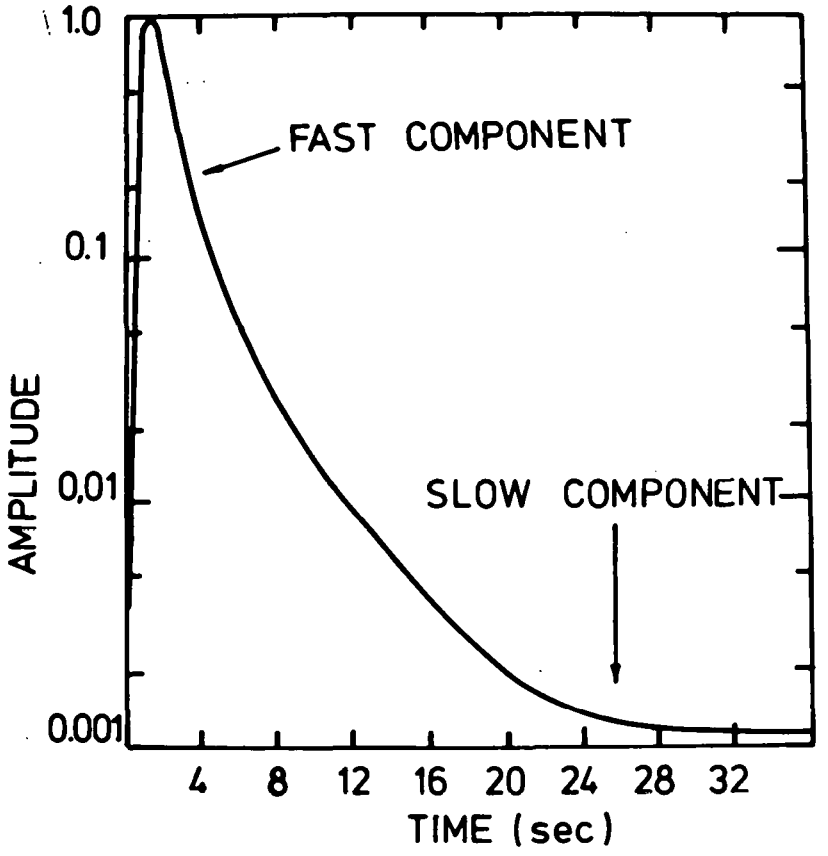


Fig.1 . Glowcurve for mannose dissolved in water. The slow component may have a different chemical origin from the fast one. Only the fast component is integrated for use in dosimetry.

2. Lyoluminescence is a property of a very broad variety of materials. It has been demonstrated in many carbohydrates ,particularly in saccharides and starch,as well as in soluble derivatives of cellulose (ref.1,2). It has been observed in many amino acids (ref.3,4) and in soluble proteins (ref.5).Furthermore,dry preparations of nucleic acids,DNA and RNA, also are lyoluminescent. In fact,quite a number of desiccated organic preparations like powdered foods also exhibits this phenomenon.

Of particular interest for biomedical and environmental applications are phosphors of composition closely related to that of human and animal tissues. The atomic composition of many saccharides e.g.glucose,trehalose,melezitose comes very close to that of soft tissues.As a result,the effective atomic numbers for photoelectric effect and for pair production are fairly close to those of standard muscle.The electron concentration which determines Compton response is also closely coincident. This tissue equivalence holds for all modalities of irradiation e.g.for X- and gamma-rays, for electrons,for heavy charged particles including pi-mesons and, obviously, for neutrons.This equivalence has been verified experimentally (ref.6).Using metalo-organic compounds as phosphors it is possible to broaden the scope of possible responses. E.g.lithium salts of organic acids were used to register thermal neutron beams with much higher sensitivity than for fast neutrons. Similarly,other metalo-organic compounds can be used to obtain response peaking in the photoelectric absorption regions to simulate response of the bone .Starch is a good phosphor for simulating response of plant tissues and finds applications in dosimetry of food processing by radiation.

Radicals trapped within irradiated solids can be detected by electron spin resonance (ESR) and when their concentration is plotted against the imparted dose the resulting curve has a typical shape as shown in Fig.2 .

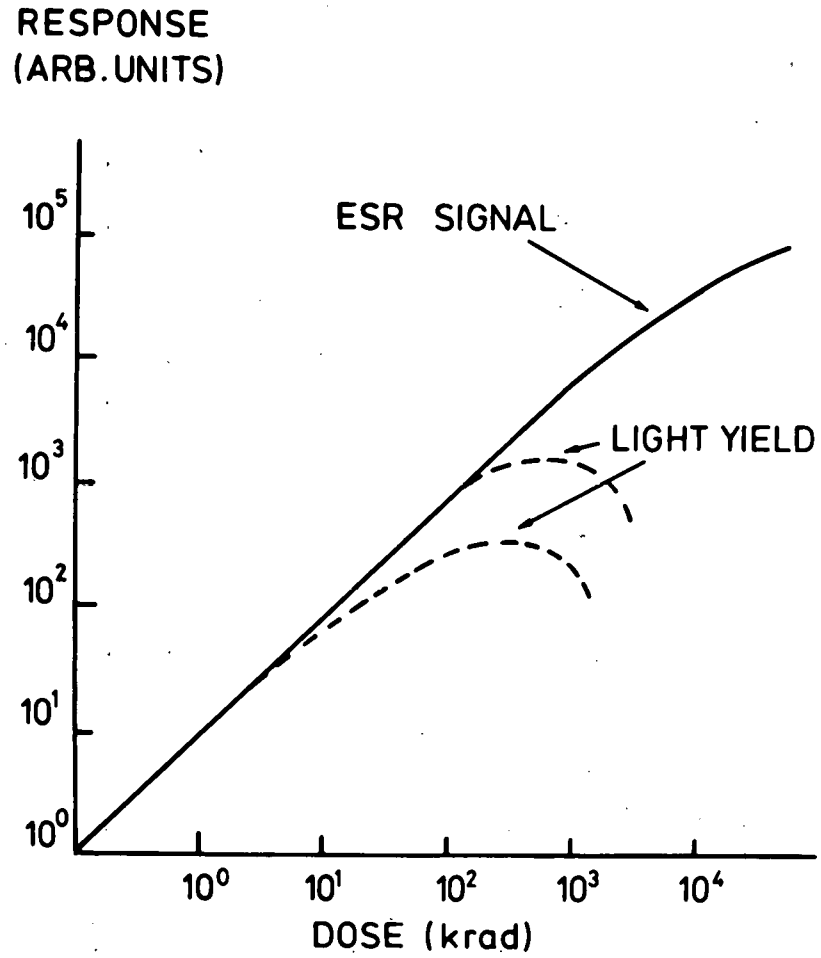


Fig.2. ESR and lyoluminescence signals as function of dose for trehalose dihydrate. Lower broken curve corresponds to water in equilibrium with air; the upper broken curve is for water saturated with O_2. It is evident that the saturation of lyoluminescence is associated with the conditions prevailing during dissolution process. Gamma rays from ^{60}Co were used for irradiation.

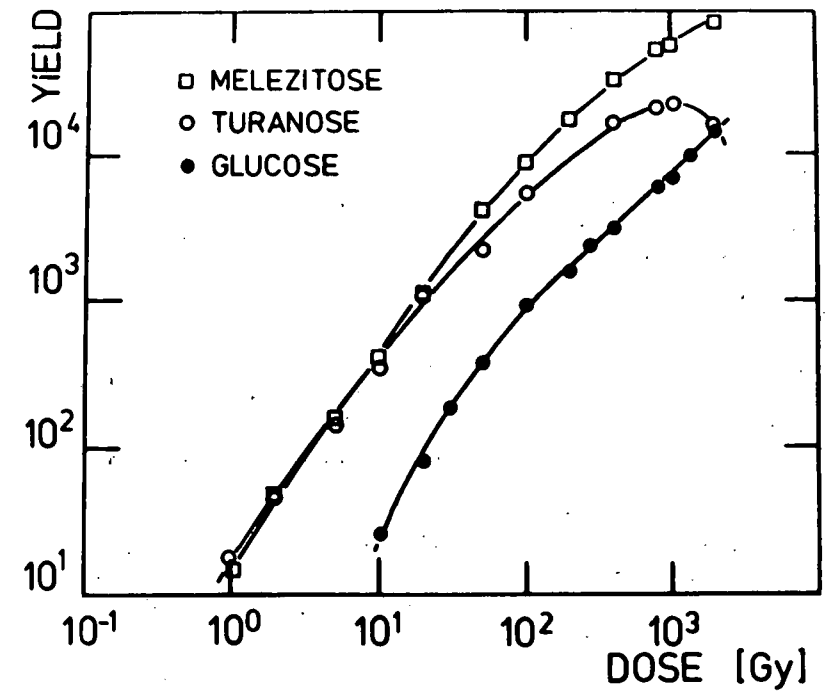
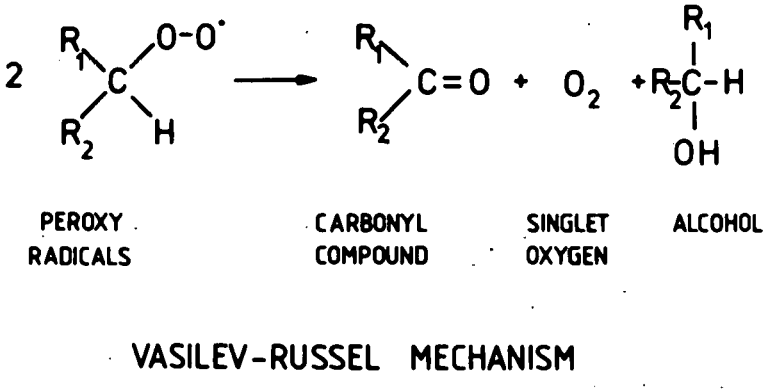


Fig.3. Dose response curves for some saccharides in water. The slope of curves for glucose and melezitose indicates some supra - linearity i.e. response increases faster than the dose. This may be a chemical effect, arising from processes taking place on dissolution.
Response curves were obtained with gamma rays from ^{60}Co.

The upper limit of doses which can be measured with lyoluminescence dosimetry (LLD) is set by the saturation characteristics of the phosphor used.For saccharides this limit is about 600 Gy - 1.5 kGy,soluble starch is suitable up to about 50 kGy and glutamine shows almost linear response up to about 80 kGy. The lower limit of measurable doses depends upon amount of available light reaching photodetector and also on the intensity of spurious luminescence,generated by processes unrelated to the radiation history of the phosphor. This spurious luminescence,called also 'chemical background' depends on the purity of the phosphors,particularly on metallic contaminants as well as on presence of products of autoxidation.Careful preparation of lyoluminescent phosphors enables an experimenter to observe radiation doses well below 0.01 Gy in presence of sensitizers.

3. The chemical mechanism underlying lyoluminescence is not known exactly. Observation of lyoluminescence spectra indicates that emission is concentrated in the region 400 nm - 500 nm in form of a single,broad peak. The most satisfactory explanation is based on the Vasil'ev-Russel scheme,which is known to be responsible for many processes of bioluminescence (ref.7).It is assumed that the radicals originally formed as a consequence of exposure to radiation are oxidised to peroxy radicals (ROO$^{\cdot}$) either in the solid or on dissolution.These peroxy radicals,obviously different for different materials,undergo disproportionation during dissolution. The amount of energy available in this reaction is sufficient to produce singlet oxygen or the carbonyl compound in an excited state,or even both.Light from deexcitation of carbonyl compounds is usually concentrated in the region 400 -520 nm. The transitions of singlet oxygen,observed experimentally,are at 762 and 1269 nm i.e. in the red and infrared parts of the spectrum.



VASILEV-RUSSEL MECHANISM

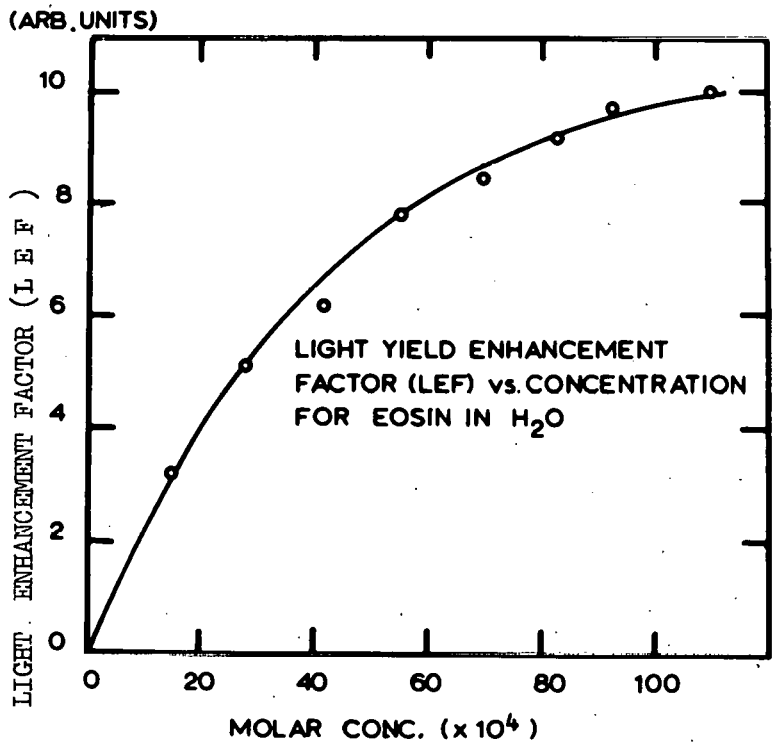


Fig.4. Enhancement of light emission resulting from an addition of a fluorescent dye with high quantum yield.Energy transfer takes place between species produced in excited state in consequence of free radical reactions and dye molecules. Data on which this figure is based were obtained for glucose monohydrate.The read-out system employed EMI photomultiplier type 9635 QA, having an extended bialkali spectral response.

Stauff (ref.8) proposed a hypothetical mechanism of energy pooling of two singlet oxygen molecules, which could produce enough energy to bring the emission to the blue part of the spectrum. The pooling mechanism,even if possible in a liquid medium,cannot nevertheless explain individual differences between lyoluminescence spectra of various phosphors.

4. Enhancement of the amount of light produced during dissolution of LL phosphor results in a simpler reader apparatus and in improved statistical accuracy of results. Various routes leading to the enhancement of emitted light were tried and two most promising methods are : use of fluorescent dyes in solution and use of chemiluminescent indicators. Use of fluorescent dyes results in an enhancement because their quantum fluorescence yield is higher than the original excited species,products of free radical reactions.The light enhancement factor depends upon concentration of the dye and on the spectral characteristics of the photodetector.Enhancements in the range 7 - 90 were obtained with eosin, sodium fluorescein and rhodamine B for glucose monohydrate dissolved in water,alcohols and acetone mixtures. Further details can be found in ref.9 .One should note that energy transfer results in emission spectrum shifted towards longer wavelengths and,correspondingly, the PM tube should have good sensitivity in that region.Photomultiplier type 31034A with a GaAs photosurface (made by RCA) has an extremely useful spectral response,almost flat to 800 nm ,but requires cooling to -30°C for a satisfactory operation.

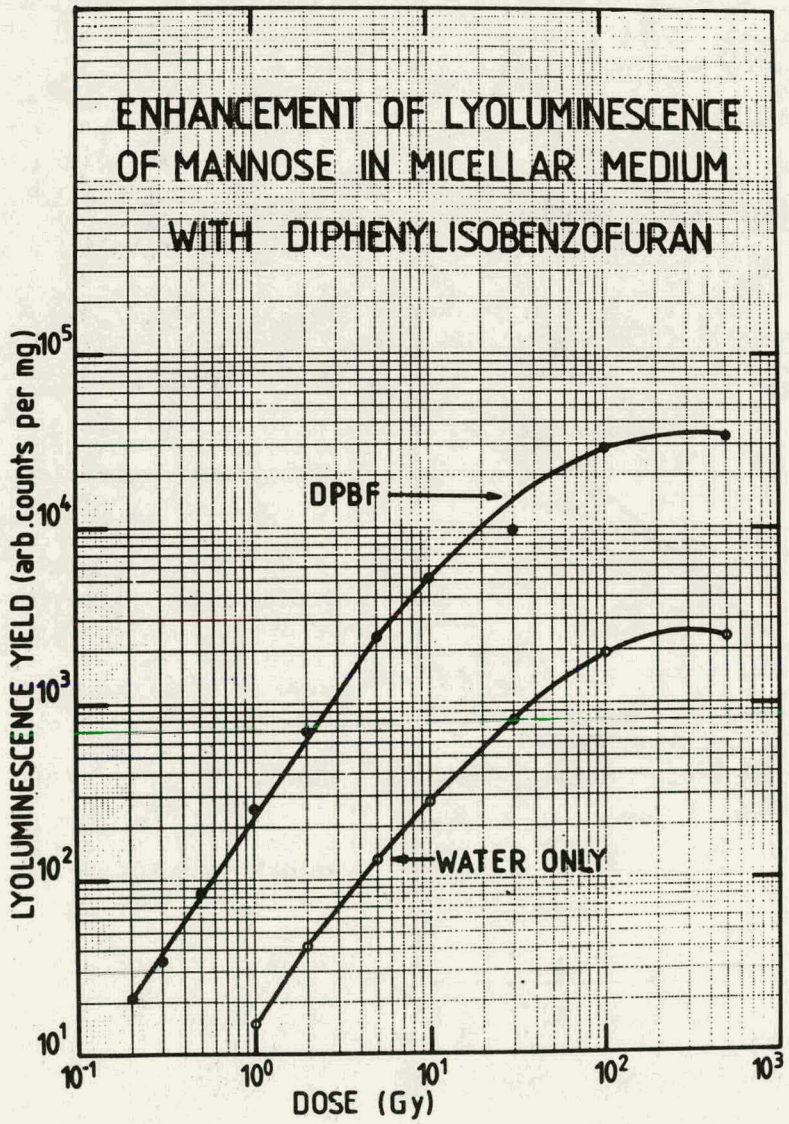


Fig.5. Enhancement of emitted light using 10^{-5}M solution of diphenylisobenzofuran in 10^{-1}M micellar solution of sodium dodecyl sulphate in water. Similar enhancement has been observed for turanose. The light enhancement factor is of an order of 15.Peak of emission spectrum is at 475 nm.

In a recent communication by Laflin and Baugh (ref.10) the use of diphenylisobenzofuran (DPBF) either in aerated aqueous acetone or in an aqueous solution of micelles formed from sodium dodecyl sulphate (SDS) is reported to has significantly enhanced the yield of lyoluminescence of mannose.We have confirmed these results and measured the dose response curves for mannose and turanose in a broad range of doses.(see Fig.5)in DPBF + SDS solution.

The use of luminol (5-amino-2,3-dihydro-1,4-phthalazinedione) to enhance the effect of lyoluminescence has been reported by Atari and Ettinger in the early stage of development of LLD. The mechanism of action of luminol as chemiluminescence indicator has attracted over the last half a century a number of investigators and few explanations were put forward. The light is produced when basic aqueous solutions of luminol are treated with an oxidizing agent. The emission takes place in the blue region of spectrum.The light enhancement factor in solutions of luminol is a function of the concentration,as can be seen from Fig.6. The enhancement of lyoluminescence in solutions of luminol is shared by many compounds, including apparently most of the saccharides and, probably,all water soluble amino acids. Unfortunately for LLD the gain is also a function of pH, temperature of the solution and the oxygen concentration. All these factor must be therefore stabilized in order to attain reproducible results.Furthermore, solutions of luminol exhibit self-glow arising from oxidation of the reagent by oxygen diffusing into solution from the atmosphere. This self-glow is apparently strongly dependent on the presence in solution of very small amounts of foreign ions (e.g.divalent copper) which are known to act as catalysts for the chemiluminescent action of luminol. Lucigenin (N,N-dimethyl-9,9-bi-acridinum nitrate) ,also a chemiluminescence indicator , can be similarly used as an enhancer of lyoluminescence.

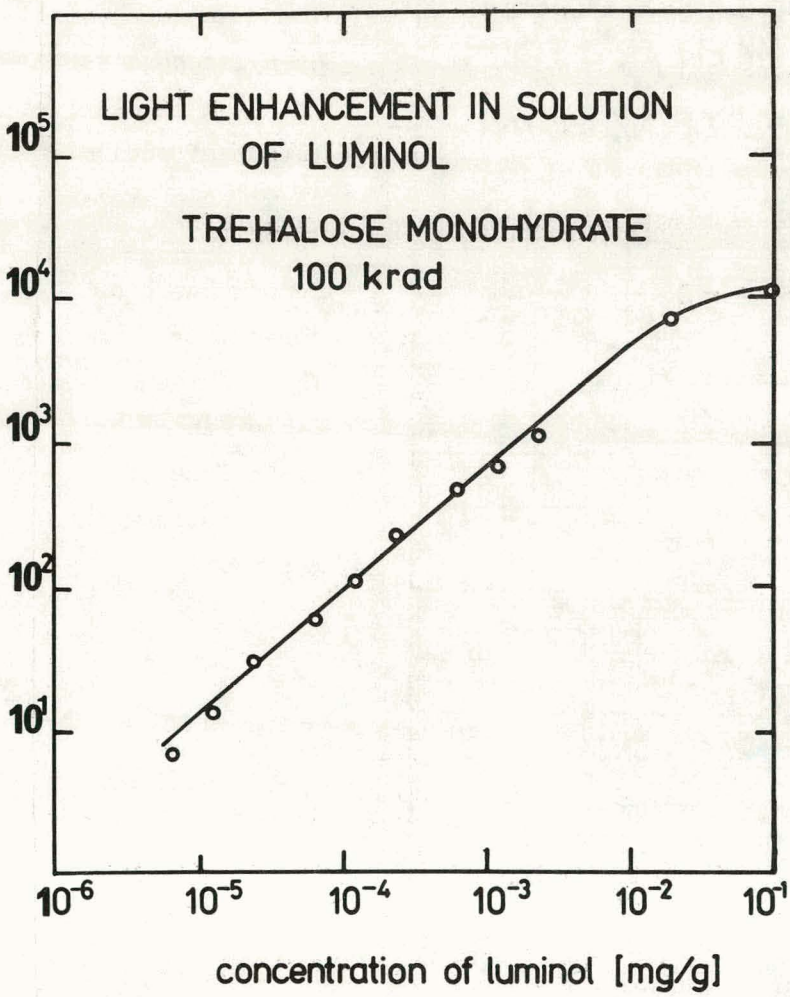


Fig.6. Light enhancement factor as a function of concentration of luminol in water. The figures refer to a freshly prepared solution; it has been observed that luminol solutions change slightly their properties with time.

Instead of dissolving LL phosphor in a solution of sensitizer the sensitizing agent can be incorporated in the phosphor itself. This approach results in less of a self-glow because a very minute amount of sensitizer needs to be involved. Using a process of co-crystallization sensitized phosphors of mannose, glucose and trehalose dihydrate were prepared and their properties investigated. More details can be found in ref.11 . Recently, using very pure materials for synthesis it became possible to measure doses of about 0.005 Gy by this technique. Even higher sensitivities are expected from sensitizers containing rare earth ions and excited in triplet-triplet energy transfers.

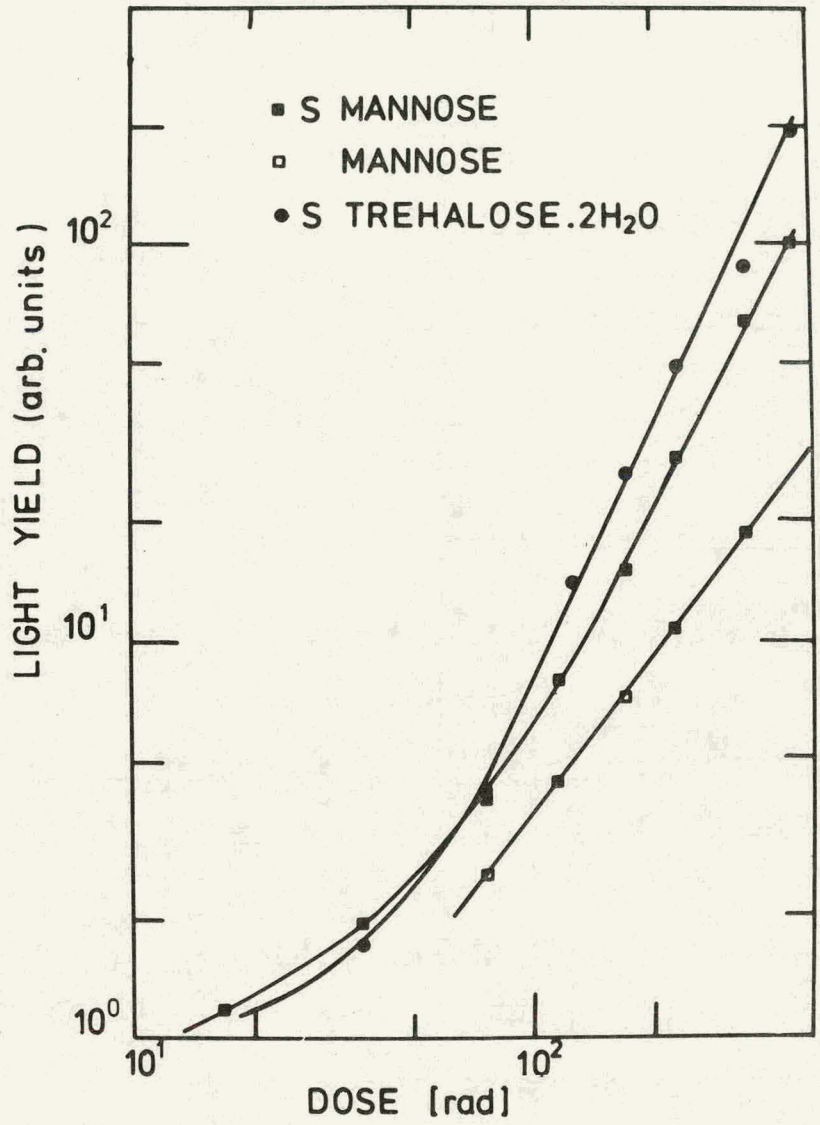


Fig.7. Dose response curves for sensitized mannose and trehalose dihydrate. With sufficiently pure starting materials it is possible to measure smaller radiation doses than shown on the graph.

5. Energy response of LL phosphors depends upon the LET of radiation and for low LET radiations can be calculated from total energy absorption coefficients. The energy response for some saccharides exposed to gamma- and X-rays is shown in Fig.8 .The continuous line is calculated from energy absorption coefficients and each graph is normalized to the calculated value at 1.25 MeV. In addition, energy response of some lyoluminescent phosphors has been measured for 18, 29 and 40 MeV electron beams , for fast and slow neutrons as well as for 10 MeV protons and 30 MeV He-3 ions.(ref.12).

The LET response of some saccharides is shown in Fig.9 ,in which the differences in LET response of various materials have been ignored and an 'average' line drawn through experimental points. The LET response agrees well with the phenomenological theory of R.Katz which predicts such response for single hit detectors.

RELATIVE ENERGY RESPONSE OF SACCHARIDES

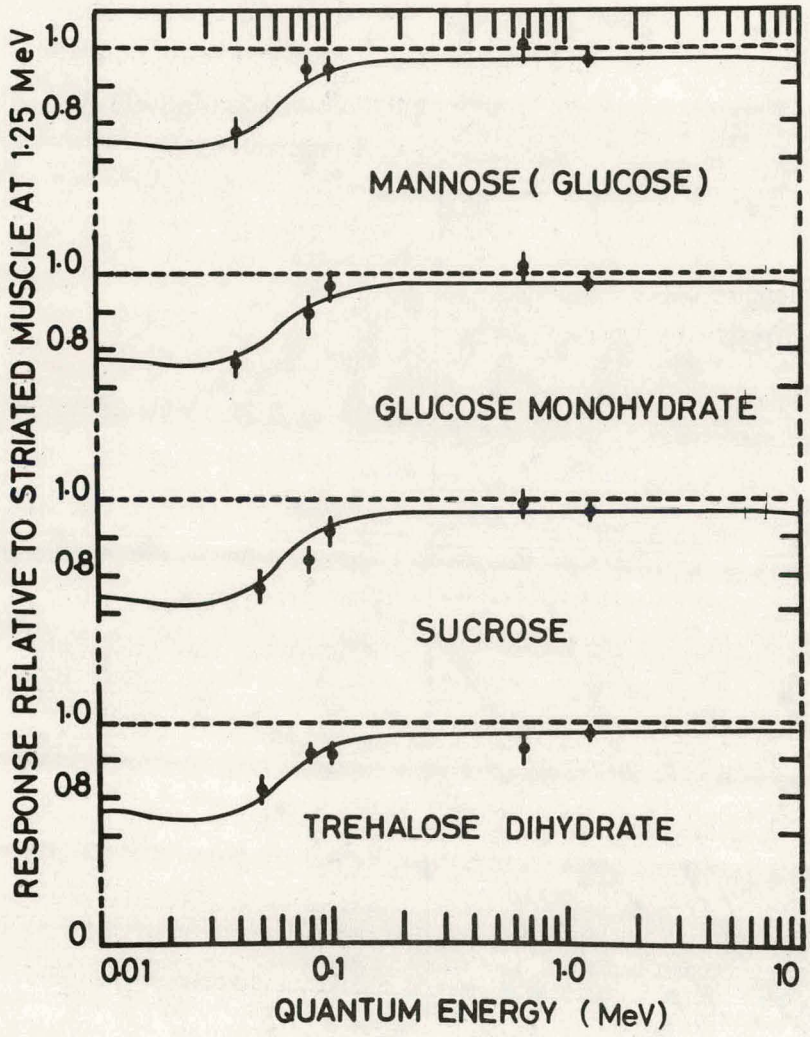


Fig.8.

LL YIELD OF SACCHARIDES AND AMINO ACIDS AS A FUNCTION OF LET

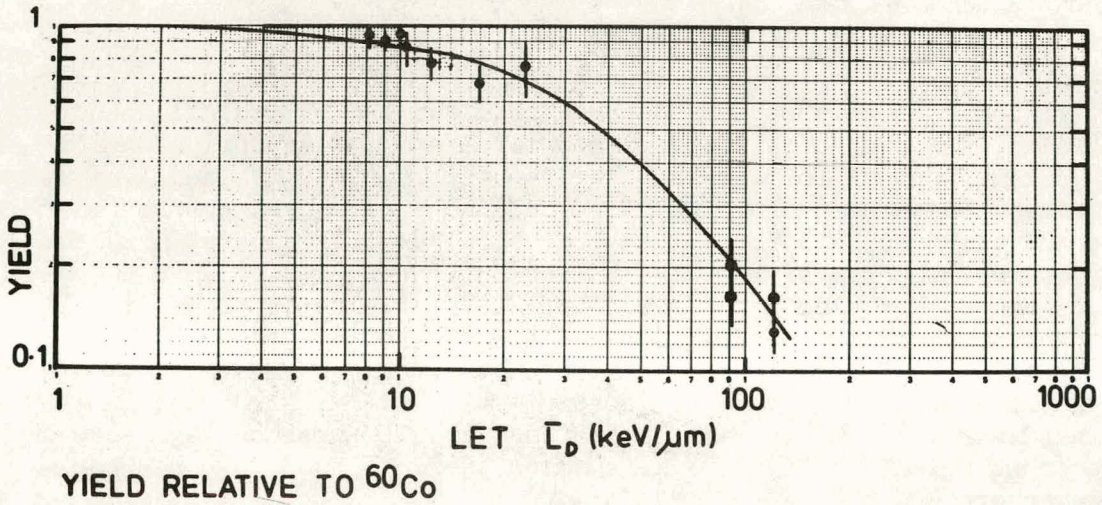


Fig.9.

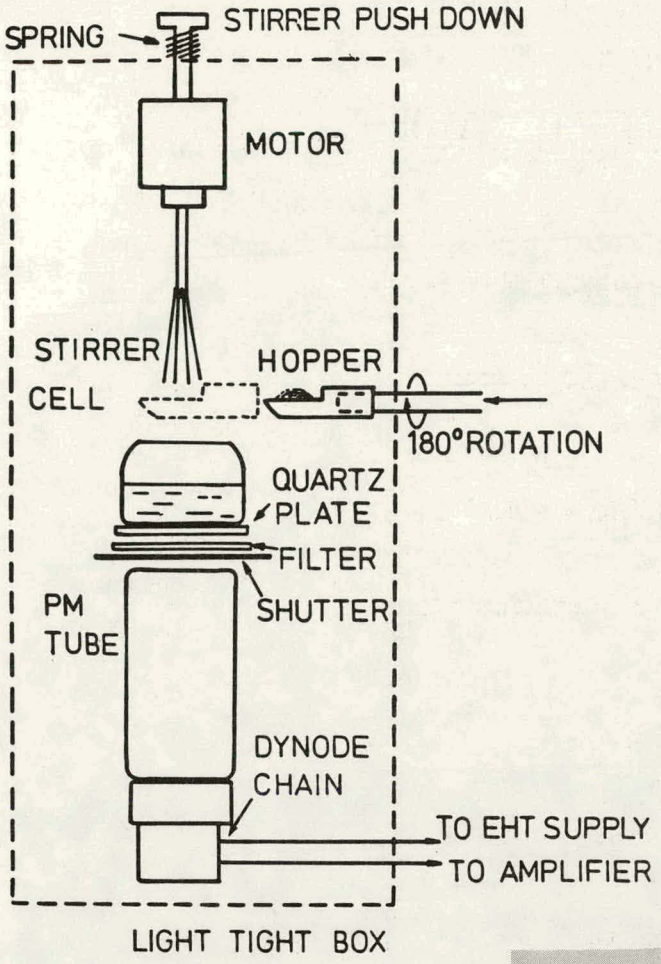


Fig.10. Manually operated LL reader.LL phosphor (10 -40 mg) is placed in a hopper and dropped into the cell.Use of stirrer is optional.Cell contains approx.10 cm^3 of solvent.

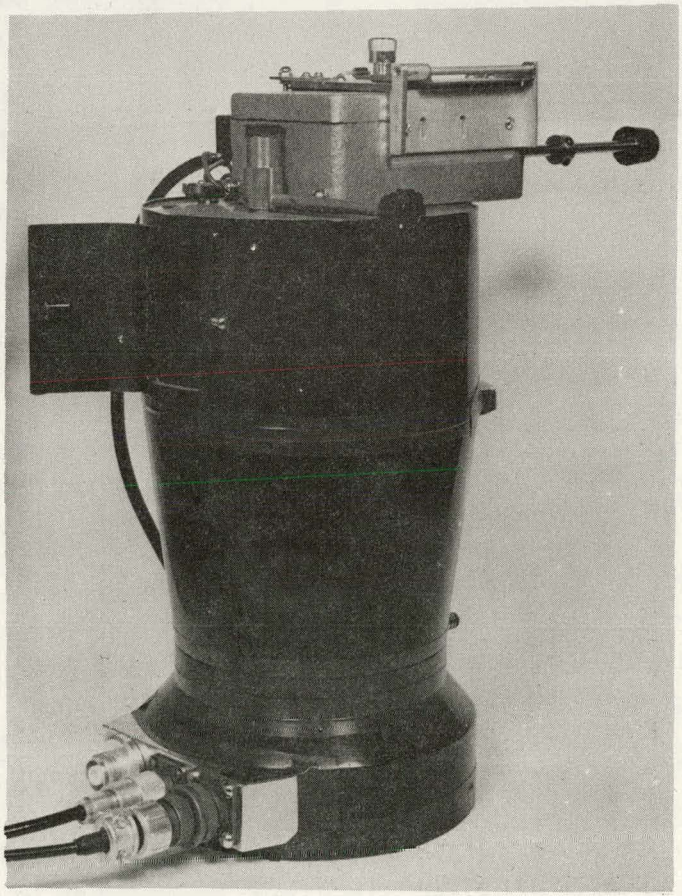


Fig.11. External appearance of manually operated LL reader, which was fabricated from an obsolete liquid scintillation counter.Knob at the right operates the hopper. Knob in the centre rotates the shutter.

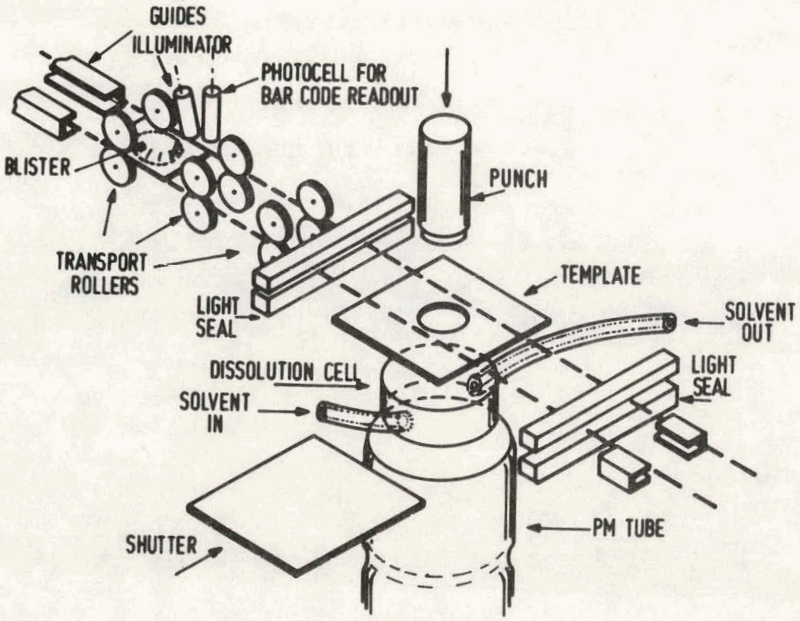


Fig.12. Semiautomatic LL reader for dosimeters encapsulated in blister packs.Blister is punctured by the punch and its content propelled into the dissolution cell. The cell is flushed, cleaned from residuum of the previous run and refilled with solvent by means of a peristaltic pump not shown in the drawing.

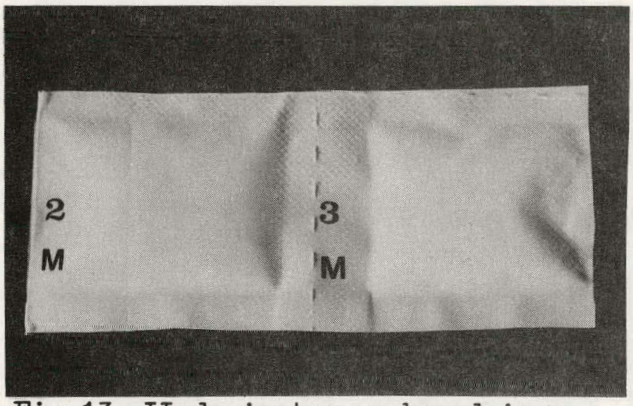


Fig.13. LL dosimeter packaged in a small plastic sachet.It has to be manually opened and its content placed in a hopper of a manually operated LL reader.

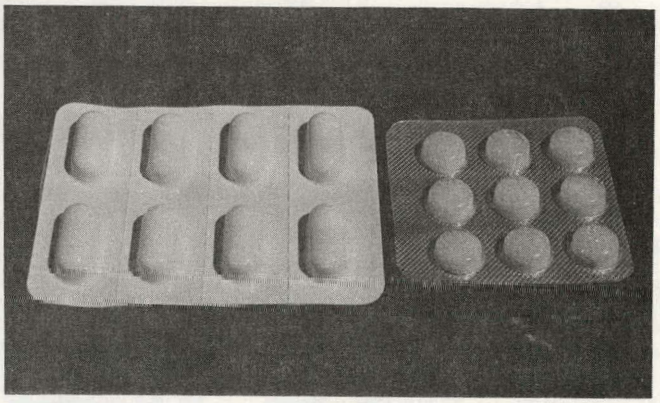
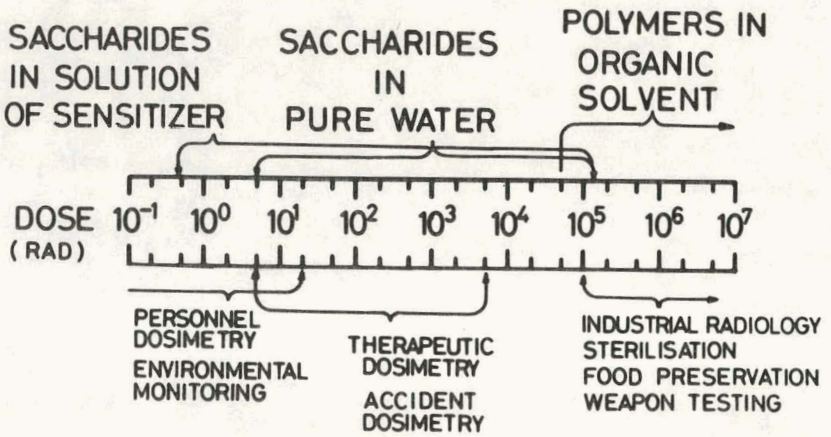


Fig.14. LL dosimeters packaged in plastic blisters of the type used for pharmaceuticals.

Fig.16. Some of the applications of LLD In addition,amino acids can be used for dosimetry in food processing technology.



6. LLD has been successfully tried in a clinical environment as a technique for determination of skin doses at the entry and exit point of a Co-60 therapeutic beam. Delivered doses were in the range of 0.5 to 3.5 Gy. Doses measured by LLD were in a very good agreement with those calculated in the course of treatment planning, usually within 2 - 4%. The standard error of the mean for 3 readouts was about 2 - 3%, which compares very well with TLD.

LLD has been also tried as a technique for measurement of intracavitary doses during radiation therapy. Usual plastic blister packaging was adequate for oral application. A series of small dosimeters placed inside a length of plastic tubing was used for measurements in the lower part of gastro-intestinal tract. In all clinical applications mannose was used as a phosphor.

LLD has been used to determine radiation leakages in accelerator installations as well as leakages through ducts, voids and imperfections in shields of isotopic radiation sources. With glutamine as a phosphor it has been also used for measurements of doses in radiation processing of food. Owing to a very low cost of individual dosimeters it may become a technique of choice for mass irradiation techniques, like food processing or sterilization of sanitary materials and drugs.

Finally, it is worth mention that lyoluminescence of parts of clothing, parts of jewellery and even desiccated tissues (skin flakes, hair) may find application in radiation accident dosimetry.

References:

1. K.V.Ettinger, J.R.Mallard, S.Srirath and A.Takavar. Phys.Med.Biol.22.481.1977

2. K.V.Ettinger, J.R.Mallard, S.Srirath and A.Takavar. "Food Preservation by Irradiation" vol.2 p.345 .IAEA, Vienna 1978.

3. K.V.Ettinger and N.A.Atari .Proc.IV Int.Conf.Luminescence Dosimetry, ed.by T.Niewiadomski p.417. Cracow, 1974

4. D.J.Thwaites, M.Sc.Thesis.University of Aberdeen, 1975 .

5. J.P.Sephton, M.Sc.Thesis ,University of Aberdeen, 1976 .

6. K.V.Ettinger, R.G.Fairchild, C.I.Anunuso, S.Srirath and E.del Vigna Filho, "Lyoluminescent dosimetric materials and their response" Proc.6th.Int.Conf. Solid State Dosimetry, Toulouse 1980. To be publ.in Nucl.Instr.Meth.

7. K.V.Ettinger and G.Buchan "Free Radical Lyoluminescence" in "Radiation Biology and Chemistry" p.127 ed.by H.E.Edwards, S.Navaratnam, B.J.Parsons and G.O.Philips .Elsevier, Amsterdam 1979.

8. J.Stauff Nature 49.58.1966

9. C.I.Anunuso, K.V.Ettinger, A.R.Forrester, C.Hunter, A.Takavar and E.del Vigna , "Enhancement of Lyoluminescence" Report of the Lyoluminescence Laboratory, University of Aberdeen, 1979 .

10. Laflin P. and P.J.Baugh Journ.Chem.Soc.Chem.Comm. 239, 1979

11. A.Burkill M.Sc.Thesis, University of Aberdeen, 1977 .

12. K.V.Ettinger, J.R.Mallard, C.I.Anunuso, E.del Vigna Filho, C.Regan and S.Srirath "Applications of Lyoluminescence" Proc.6th Int.Conf.Solid State Dosimetry, Toulouse 1980. To be publ.in Nucl.Instr.Meth.

Analysis of Fluorine Contamination from Industrial Sources

John M. Skelly, A. Keith Furr, H. Gene Knight, and T. F. Parkinson

Virginia Polytechnic Institute and State University
Blacksburg, VA 24061

Abstract

Foliage samples from corn, pine trees, maple trees and grasses were collected in the vicinity of three industrial plants which process materials containing fluorides. The INAA method was used to measure the fluorine content of the foliage; concentrations ranged as high as 560 ppm (dry weight) in the foliage. Such levels clearly demonstrate that fluorine emissions from industrial plants can cause significant damage to field crops, ornamentals and trees.

Presented at the

Fourth International Conference

on

Nuclear Methods in Environmental and Energy Research

April 14 - 17, 1980

Introduction

Several types of heavy industries, e.g. brick manufacturers and mining operations, process large quantities of fluorine compounds. Some of the fluorine can be discharged as particulate or gaseous emissions. Hydrogen fluoride(HF) is frequently the dominant gaseous species. Field crops and trees in the vicinity of a point source of HF are particularly susceptible to damage. Concentrations as low as 1 part per billion (ppb) can cause perceptible injury to foliage exposed over a 6 week period. While no maximum permissible concentrations have been mandated by the EPA, it has been suggested that feedstuff concentrations should be less than 60 ppm (dry weight) for milk production and less than 100 ppm for beef production. Fluorine analysis of the foliage serves as an "integrating dosimeter" since the elimination of the fluorine from the foliage is very slow. The objective of this work was to use instrumental neutron activation analysis (INAA) to determine fluorine levels in plants growing in the vicinity of three industrial plants that emit fluorine.

Effects of Fluorine on Vegetation

The diagnosis of air pollution injury to vegetation is considered to be difficult even under rather restrictive conditions of point source emissions and symptom expressions in evidence on surrounding plants. Air pollution injury is characterized by foliar symptoms that appear as various forms of chlorosis (yellowing) or some other change in pigmentation, i.e., chronic injury and more severe acute injury as characterized by necrosis of leaf tissues, defoliation and death of entire plants. Many other abiotic and biotic pathogens induce similar symptoms and the separation of each symptom as induced by these incitants must be accounted for in diagnostic procedures (1).

Thus, available methodologies that would assist in separating out the influences of air pollutants amoung other numerous incitants in any particular diagnostic procedure is considered to be of significant value. Tissue analysis for accumulated concentrations of several major phytotoxic air pollutants presents such a group of methodologies (2).

Fluoride, in one or more of its several forms emitted from industrial processes, is one of the most potent phytotoxic air pollutants known. The most severe damage due to fluoride occurs close to its source, often with complete loss of species, larger groups of plants, or even entire plant communities when exposure has occurred continuously at high doses for long periods of time. This pollutant induces local severe problems to vegetation but is of little significance to vegetation growing at distances from point sources.

Most industrial processes that make use of the fluorine-containing minerals of the earth's crust will emit some form of fluoride, especially those utilizing heating, crushing, or treatment with strong acids of such raw material. Minerals containing high fluoride include fluorspars, cryolite, phosphate rock, and silicon tetrafluoride types of sand. The major industrial sources of fluoride in the United States include smelting of ores such as those containing alumina; brick, tile, and glass manufacture; phosphate fertilizer production; and the processes involved in steel manufacture (1, 3).

Of the several forms of fluoride emitted, the gaseous form (hydrogen fluoride) is by far the most phytotoxic. Hydrogen fluoride enters plants via stomata ing normal gas exchange processes of leaf tissues. Fluoride accumulations and translocation to the terminal portions of tissues following various time-concentration exposure have resulted in phytotoxicity and symptom expressions (4).

Fluoride damage is usually very distinctive and since damage is associated with a nearby point source, diagnosis is relatively easy. Chronic symptoms initially appear as yellowing between the veins on hardwoods and as yellowing of needle tips on conifers. Chronic symptoms, however, usually do not remain long and are almost consistently followed by necrosis of tissues. Since fluoride is soluble and therefore easily translocatable, the most severe damage occurs on the leaf margins which become yellow, light brown, darker brown and finally brittle and tattered on broad leaves or reddish brown and brittle in the case of conifers. Some examples of fluorine damage to foliage are shown in figure 1-3. Acute fumigations are followed by dieback and eventual plant death. Particulate fluoride is somewhat phytotoxic when wetted after deposition on a leaf surface. Several specific plants such as black locust (Robinia pseudoacacia L.) or gladiolus (Gladiolus sp.) (6) are sensitive to fluorides and may be planted near a suspected source as part of an analysis system.

Caution must be used in preparing a diagnosis since many other causes of plant stress induce symptoms very much like those of fluoride. Among these are salt damage, drought, winter injury, excessive heat, and several other air pollutants including ozone and chlorine gases. Tissue analysis is also important in the consideration of fluoride content of foliage to be processed into feed for dairy or beef cattle due to the occurrence of the disease termed fluorosis which involves degradation of teeth, muscular tissues, and bone structure (7). Allowable limits of F content in silage for such purposes have been suggested. In addition, the use of tissue analysis as a method to monitor emissions from sources as part of an ambient air quality standard enforcement process has also been suggested (8, 9).

Methodology

Foliage samples from corn, pine trees, maple trees and grasses were collected in the vicinity of three industrial plants: the location of these plants is shown in figure 4. Two of the factories manufacture brick while the other industry is an ore processing facility. Special care was taken in collecting and storing the foliage to minimize contamination.

The INAA method is particularly useful for the determination of fluorine. Because of the short half-life of F-20 (11.41 s.), analytical results can be obtained very quickly. The details of our technique for fluorine analysis are given in reference 10; the data acquisition system is shown in figure 5. Five replicate irradiations were performed on each sample and gamma spectra were recorded over a narrow energy interval to minimize dead time corrections. The gamma spectra were then processed with our VAT-69 software system (11). To calibrate the analytical technique, standards were prepared from teflon. A typical calibration curve is shown in figure 6. From this calibration, the estimated minimum detectable mass of fluorine was 14 μg.

A potentially serious interference with a fluorine determination is the fast neutron activation of sodium: Na-23 (n, α) F-20. In the well-moderated neutron spectrum in our Argonaut reactor, interference from sodium does not constitute a serious problem. To measure the effect of the sodium interference, a solution of $NaHCO_3$ was irradiated and the resulting F-20 was counted. A sensitivity ratio of 263 ± 30: 1 was found for fluorine determined *via* the F-19 thermal neutron activation *vis-a-vis* the equivalent fluorine produced by the fast neutron activation of Na-23. Since we routinely determine the sodium content of the samples, an appropriate correction could be applied if the sodium interference was significant.

Results and Conclusions

The results of our fluorine analysis for sources A, B and C are collected in Tables I, II and III, respectively. From these data it can be seen that fluorine concentrations ranged as high as 560 ppm (dry weight). As expected, fluorine concentrations decreased markedly for samples collected at increasing distances from the pollution source. The normal concentration of fluorine in plants is 5-10 ppm (dry weight).

In conclusion, our measurements demonstrate clearly that certain industrial sources of fluorine can cause significant damage to field crops and trees. The method described is particularly useful for environmental monitoring and source identification of airborne fluorine contamination.

References

1. Skelly, J. M. and S. A. Alexander, Fluoride injury to forest vegetation, Va. Coop. Ext. Serv., VPI&SU, Blacksburg, Va., MRFTD-30, 1977.

2. Jacobson, J. S. and L. H. Weinstein, Sampling and analysis of ambient air, plant, and animal tissues, water, soil and foods, J. Occup. Med. 19: 79-87, 1977.

3. Davis, D. D., Air pollution and plants: Fluorides and evergreens, Coop. Ext. Service., Pa. State Univ., University Park, Pa., 1973.

4. Leone, I. A., E. Brennan, and R. H. Daines, Atmospheric fluoride and its untake and distribution in tomato and corn plants, J. Plant Physiol. 31: 329-333, 1956.

5. McClenahen, J. R. and T. C. Weidensaul, Geographical distribution of fluorides in forage using a bioindicator, J. Env. Qual. 6: 169-173, 1977.

6. Compton, O. C. and L. F. Remmert, Effect of airborne fluoride on injury and fluoride content of gladiolus leaves, Proc. Amer. Soc. Hort. Sci. 75: 663-75, 1960.

7. National Academie of Sciences Committee on Biological Effects of Atmospheric Pollutants: Fluorides, National Acad. Sci., Washington, D.C., 295 p., 1971.

8. Hill, A. C., Air quality standards for fluoride vegetation effects, J. Air Pollution Contr. Assoc. 19: 331-36, 1969.

9. Personal communication

10. Knight, H. G., A. K. Furr and T. F. Parkinson, Determination of fluorine by NAA, Anal. Chem. 49, 11, 1507-10, 1977.

11. Furr, A. K., B. A. Roscoe and T. F. Parkinson, VAT-69, A Software System for Gamma Spectroscopy, Computers in Activation Analysis and Gamma-Ray Spectroscopy, CONF-780421, Dept. of Energy, 352-366, 1979.

Table I

Measured Fluorine Concentration in Foliage Near

Plant A

Plant Species	Estimated Distance (m)	Concentration (PPM, dry weight)
Maple, Red	300	60 ± 10
Maple, Red	310	90 ± 15
Maple, Sugar	400	90 ± 15
Corn	150	560 ± 60
E. White Pine	300	30 ± 10

Table II

Measured Fluorine Concentration in Foliage Near

Plant B

Plant Species	Estimated Distance (m)	Concentration (PPM, dry weight)
E. White Pine	2200	51 ± 10
Pitch Pine	2200	58 ± 12
Maple	2200	92 ± 18
E. White Pine	2200	58 ± 12

Table III

Measured Fluorine Concentration in Foliage Near

Plant C

Plant Species	Estimated Distance (m)	Concentration (PPM, dry weight)
Corn (leaf)	100	360 ± 50
Corn (husk)	100	30 ± 10
Composite Grasses	125	120 ± 15
Composite Grasses	100	400 ± 50
Silage 1	50 - 100	210 ± 25
Silage 2	50 - 100	117 ± 15



Fig. 1. Tissue Damage From Fluorine In Gladiolus

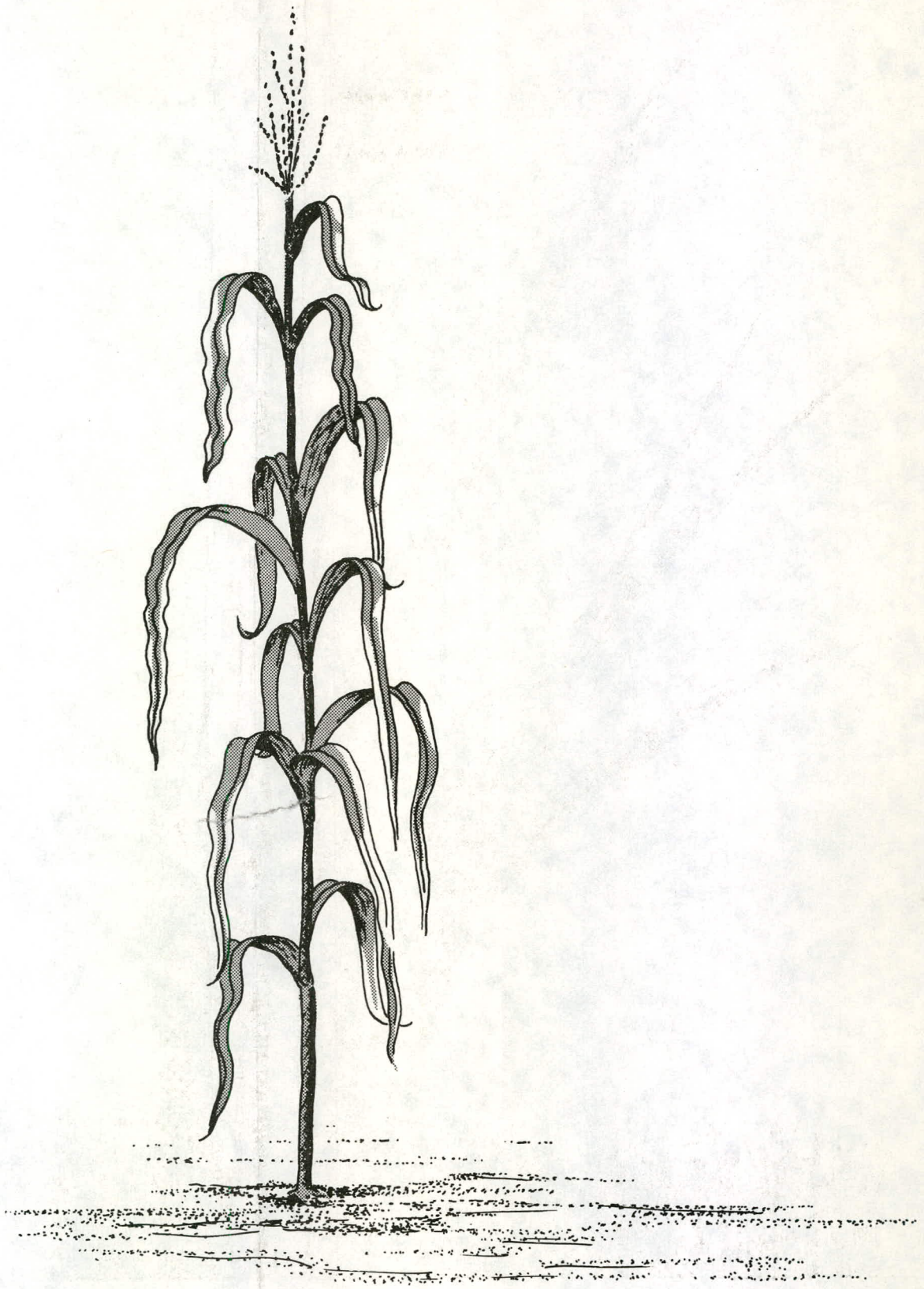


Fig. 2. Tissue Drainage From Fluorine In Corn

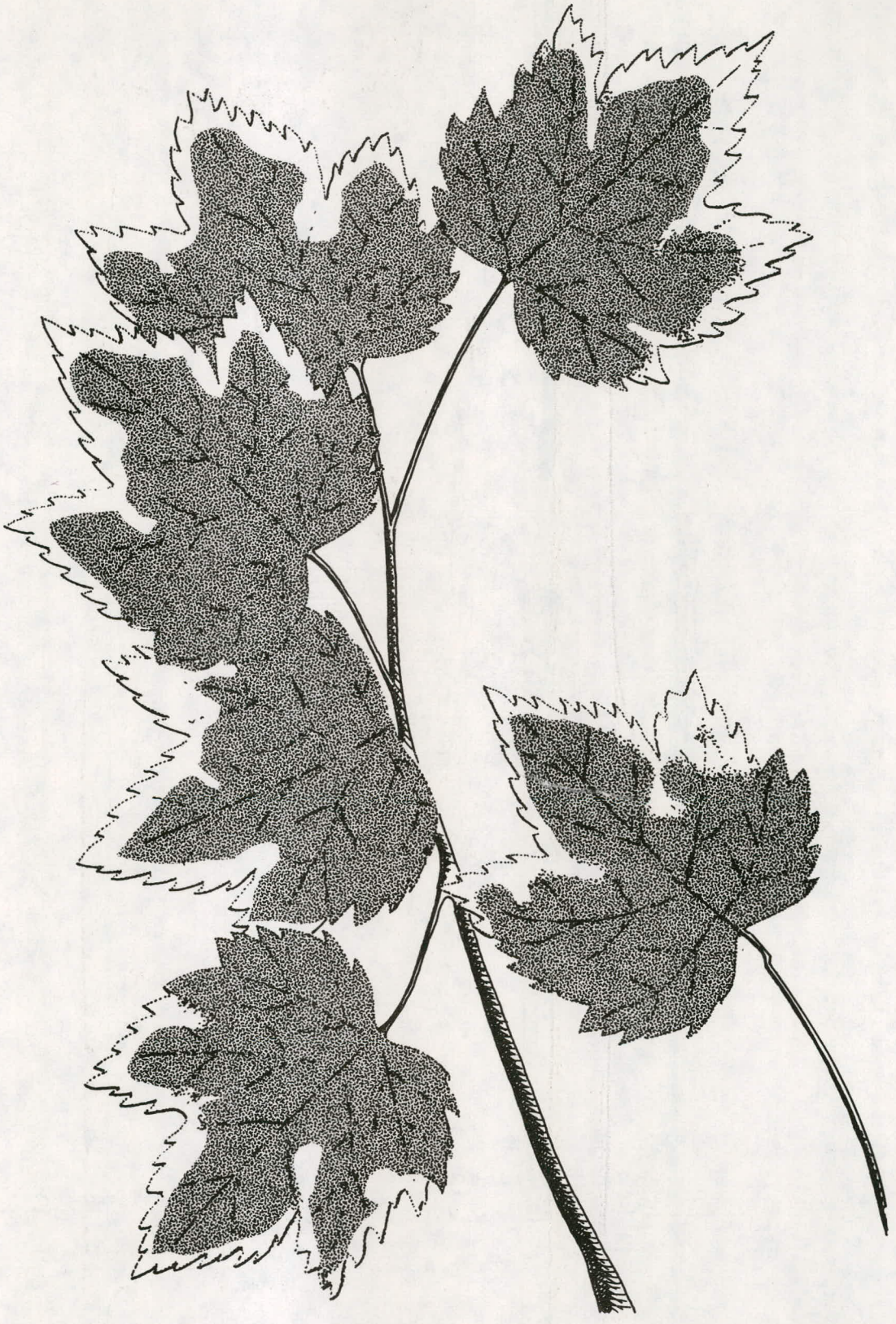


Fig. 3. Tissue Damage From Fluorine In Maple

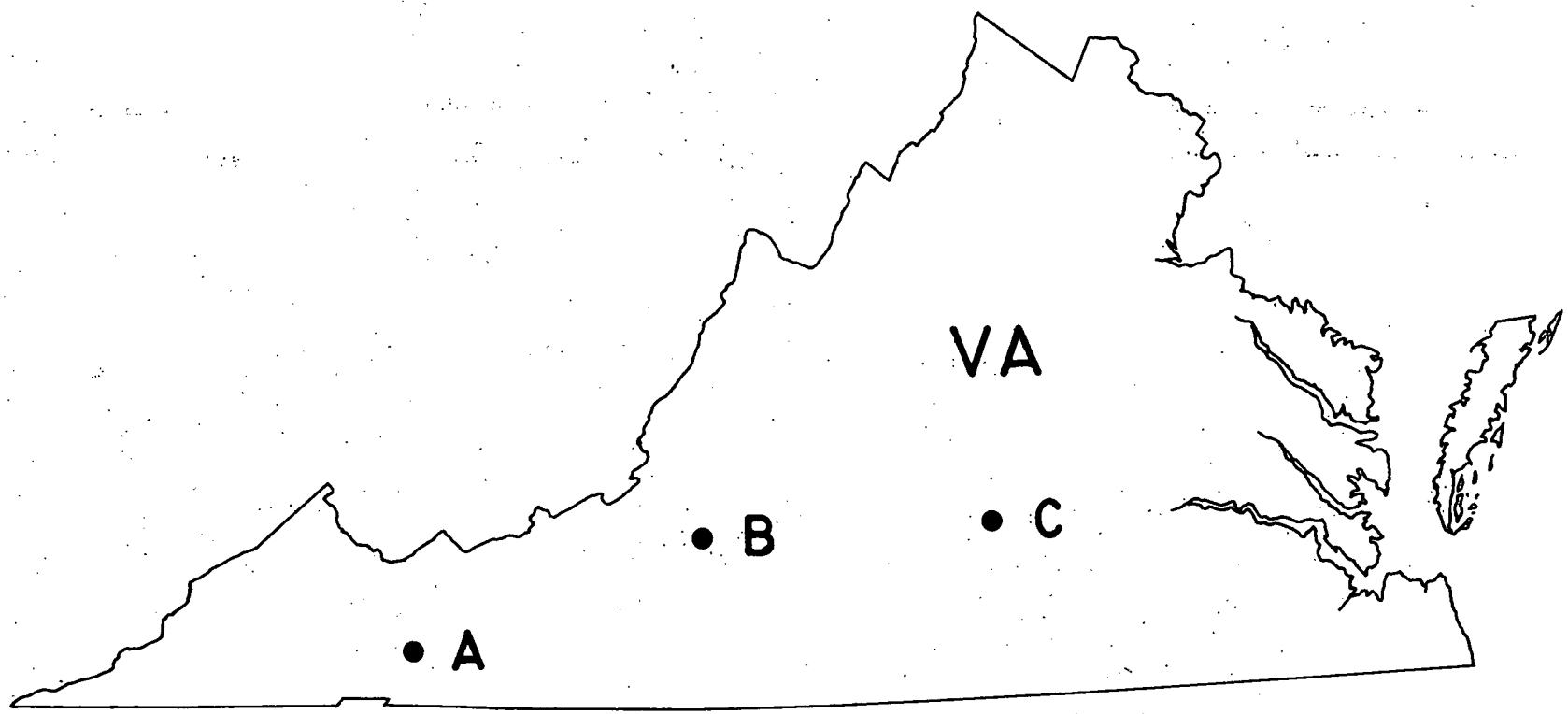


Fig. 4. Locations of Industrial Plants

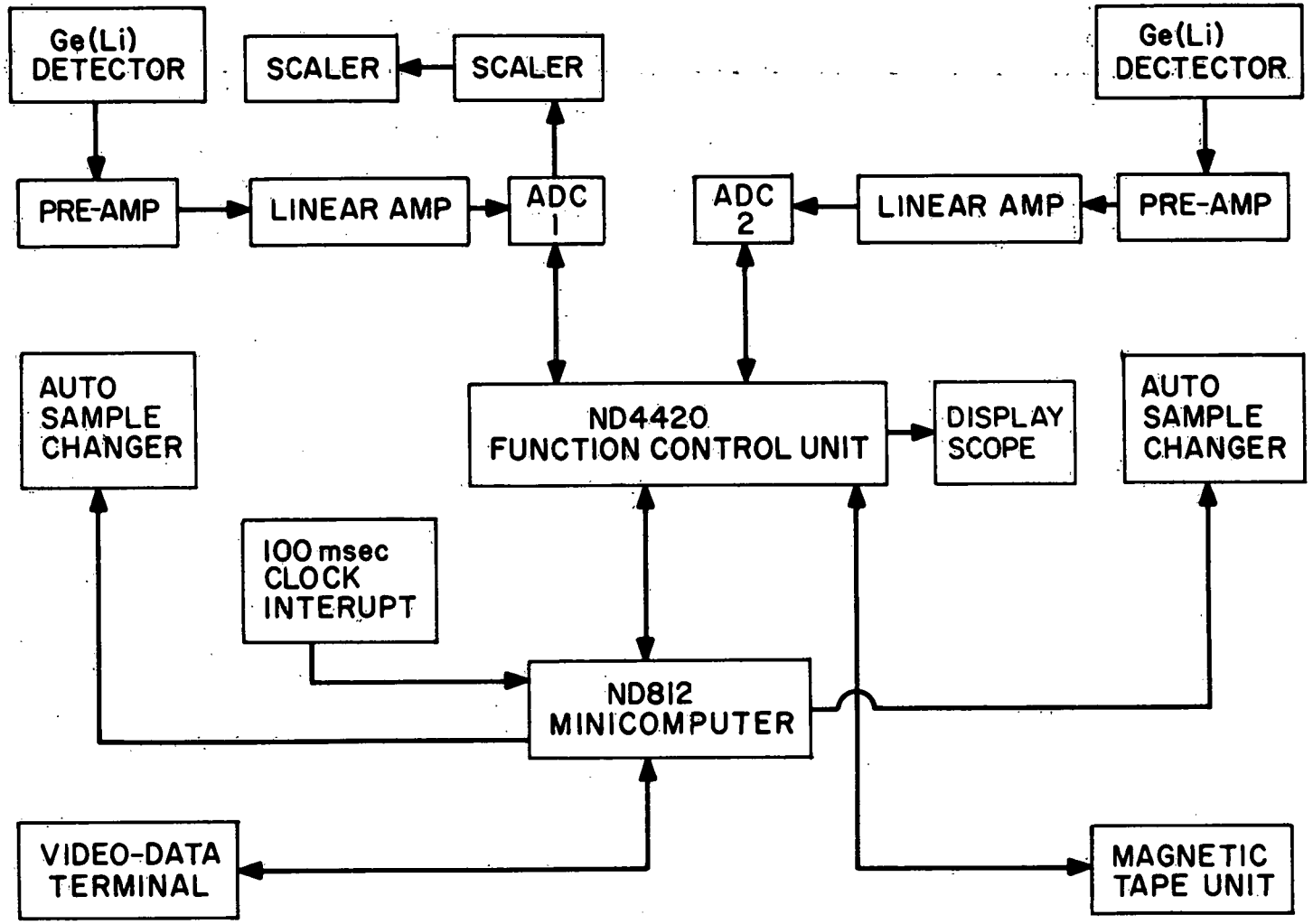


FIGURE 1 : ND4420 COUNTING SYSTEM

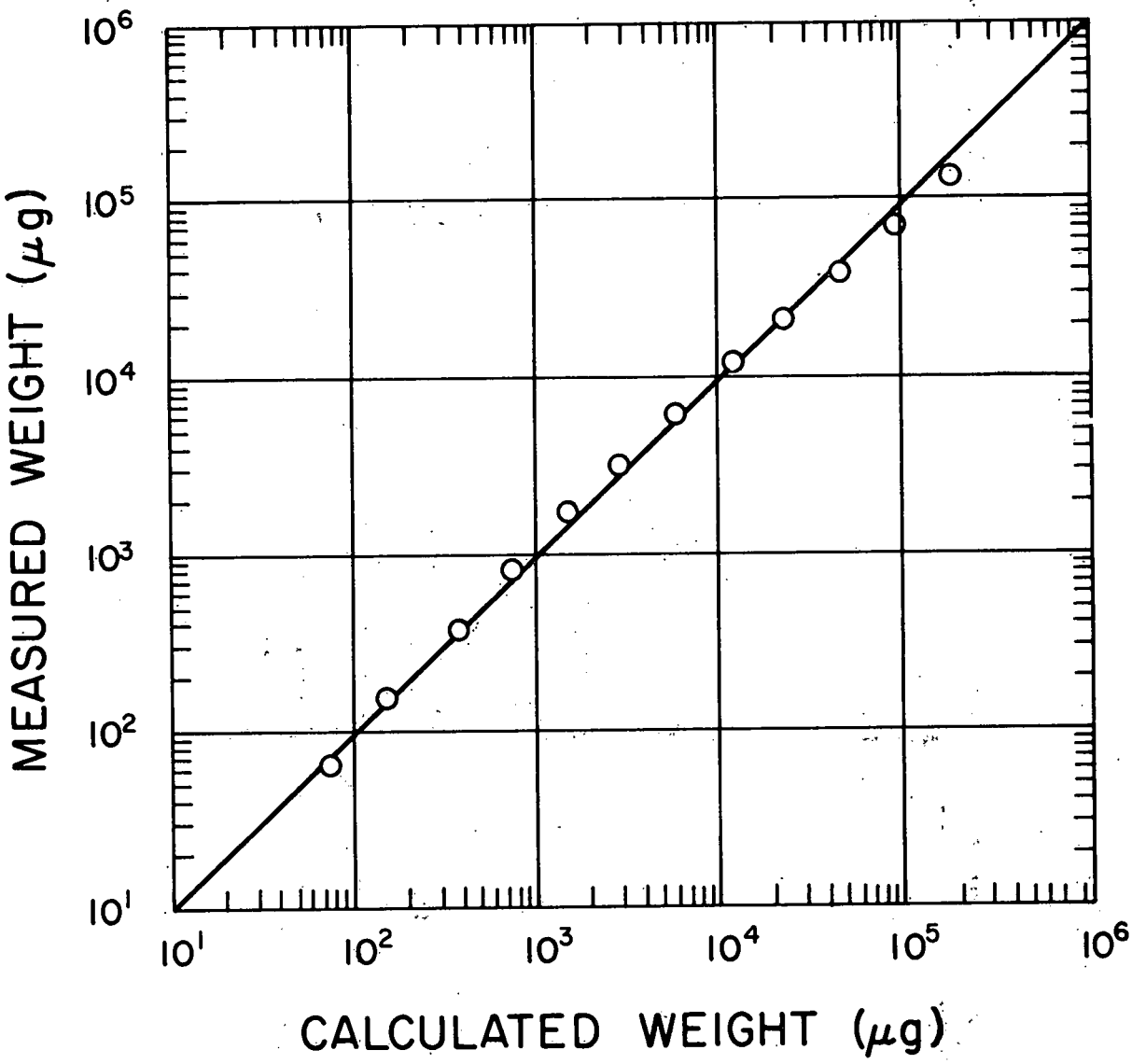


FIGURE 3

COMPARISION OF MEASURED AND CALCULATED WEIGHTS IN C_2F_4

IN SITU DETERMINATION OF TRANSURANIC AND FISSION PRODUCT RADIONUCLIDES*

Michael A. Kay

Rockwell International
Rockwell Hanford Operations
Energy Systems Group
Richland, Washington 99352

ABSTRACT

Waste management requires radionuclide inventory and distribution data as input to the decision-making process for ultimate disposal of the wastes.

If field operations, such as earthmoving, are required, prompt, onsite radioassay capability is necessary to differentiate between contaminated and uncontaminated earth.

To fulfill these requirements, two development vans (Dev Van I and II) have been designed, built, equipped, and field tested on the Hanford Site. Dev Van I is a surface layer radioactivity assay system, and Dev Van II is a borehole, well or drillhole, (a well extends to the groundwater) radioactivity assay system. Both Dev Vans are equipped for solid state X-ray or gamma-ray spectrometry. The Dev Vans will be described and the results of field tests presented. Problems encountered during field testing and the solutions to be implemented will be discussed.

INTRODUCTION

A radiological description of each site being studied is necessary to the waste management decision-making process. This description should include the location, identification, and quantification of any radionuclides present. Carefully selected samples (e.g., from drill hole cores or surface layers) are assayed. The results are combined with other information pertaining to the radiological state of the site, such as hydrology, geology, or radiological history. The product of that process is an estimate of the radionuclide inventory of the site and how it is distributed in three dimensions. The radiological description should relate to current regulations concerning nuclear waste disposal and unrestricted access. Ten nCi/g of transuranic (TRU) elements is the current regulatory limit for TRU waste.[1] Regulatory limits for uncontrolled

---

*Prepared for the United States
Department of Energy (As RHO-SA-156)
Under Contract DE-AC06-77RL01030

release to the environment of other radionuclides are given in ERDA Manual Chapter 0524 Annex A.[2] These limits are our current objectives for the sensitivity of our radionuclide assays.

As part of the Long-Term Transuranic Defense Waste Program, two vehicles have been modified and equipped for in situ radionuclide assay. Development Van I (Dev Van I) is a surface radioactivity analysis system, and Development Van II (Dev Van II) is a borehole radioactivity analysis system.

DEV VAN I

Dev Van I is a mobile data gathering system for surface analysis for X- and γ-ray emitting radionuclides. It has a lithium-drifted silicon [Si(Li)] X-ray spectrometer for surface samples obtained in standard sample containers and a down-looking lithium-drifted germanium [Ge(li)] gamma ray spectrometer for in situ surface assay. Dev Van I contains all equipment necessary to operate these systems in the field and to obtain data on magnetic tape for reduction using the Gamma X-ray Data Reduction (GXDR) System[3] in the laboratory. Limited data reduction is also possible in the field.

The Si(Li) system for plutonium-americium assay handles a standard sample of 65 mℓ of soil in a 64 mm diameter plastic container having a press-fit lid. The minimum determinable amount of plutonium for a 500-second count is 1 nCi/g. (For americium-241, 0.1 nCi/g.)

The Ge(Li) system for fission product assay (represented by cesium-137) is capable of determining a minimum amount of cesium-137 in situ, with a 500-second count, of 1.4×10^{-5} μCi/g (≈0.02 μCi/ℓ).

PLUTONIUM-AMERICIUM ASSAY

The Si(Li) detector is a 200 mm^2 uplooking model with pulsed optical feedback preamplifier. Holding time of the 35 ℓ liquid nitrogen (LN_2) dewar is about five days in the field. Data are collected in a 1024 Channel Pulse Height Analyzer (PHA), and can be printed on a digital recorder, plotted on a X-Y recorder, or stored on cassette magnetic tape.

Since low-energy X- and γ-rays are markedly affected by any matter they must pass through before reaching the detector, definition of a standard sample container is necessary. Because of wide usage on the site, the Olympic Plastics 64-mm diameter, 65-mℓ vial with press-fit lid was chosen. Calibration standards of plutonium of typical Hanford isotopic composition and of National Bureau of Standards (NBS) traceable americium-241 were prepared in clean, sieved Hanford sediments by the Standards Laboratory.

After data acquisition, americium-241 is determined using the 36% abundant 60 KeV γ-ray*, and plutonium is determined using the 17 KeV region X-rays common to plutonium isotopes and americium-241. The contribution of americium-241 to the 17 KeV region is subtracted using the 60 KeV γ-ray peak area and the ratio (17 KeV region area: 60 KeV γ-ray peak area) previously determined from pure NBS traceable americium-241 standards prepared in a Hanford sediment matrix.

---

*All nuclear data are taken from Reference [4].

FISSION PRODUCT ASSAY

A Ge(Li) γ-ray spectrometer with an integral preamplifier is mounted in a down-looking configuration on a supporting tripod. The dewar can go three days between fillings during field work. The detector bias and preamplifier power supplies are battery operated and were constructed on site by the instrument shop. Data are collected in a 4096 Channel PHA. The same options are available for data readout as for the Si(Li) system. Normally, the data are stored on cassette magnetic tape for later reduction by computer.

A barrel calibration standard was prepared for the Ge(Li) detector consisting of homogeneous, spiked Hanford sediment placed in a 30-gallon, bolt-ring, steel drum. The concentrations of radionuclides used in the standard are given in Table 1.

TABLE 1. Ge(Li) Barrel Standard.

Radionuclide	Concentration	
	μCi/g	($\sim\mu$Ci/ℓ)
^{60}Co	5.8×10^{-4}	(0.86)
^{137}Cs	3.5×10^{-4}	(0.51)
^{144}Ce	2.8×10^{-4}	(0.42)
^{152}Eu	1.5×10^{-4}	(0.22)
^{154}Eu	1.1×10^{-4}	(1.60)
^{155}Eu	2.1×10^{-4}	(0.03)

Since the barrel standard weighs about 70 Kg (154 lb.) a smaller set-up source in standard geometry is used for daily instrument checks and discrete sample calibration.

DEV VAN I FIELD TESTS AND RESULTS

Dev Van I was field tested on the Hanford Plateau. During one such test, a series of 500-second counts was made in situ in the area known as Z-19 using the down-looking Ge(Li) detector. Cesium-137 was the only fission product or activation product detected. The mean of all values for cesium-137 was 0.03 μCi/ℓ with a relative standard deviation of ±40%. This large uncertainty occurs because the observed mean of 0.03 μCi/ℓ is just above the determination limit of 0.02 μCi/ℓ.* After the in situ assay was complete, a "cookie-cutter" sampler was used to sample the central 76 mm (3 in.) under the detector to a depth of 25 mm (1 in.) for transuranics. The samples were transferred to standard sample containers. The samples were of extremely low-level so, as an experiment, counting time was extended to 3,000 seconds. These long counts lowered our determination limits to

Pu: 0.3 nCi/g ± 50%

^{241}Am: 0.03 nCi/g ± 25%

No sample exceeded these limits. This was subsequently confirmed by laboratory analysis.

---

*That quantity where the precision of the assay is equal to a specified value, 50% in this case.

Dev Van I has participated in site characterization studies as part of its field testing. Tables 2 and 3 present some typical results encountered during in-field site characterization.

\CLUSIONS AND DISCUSSION

The effectiveness of Dev Van I has been demonstrated. The calibrations of the radiation detectors are traceable through the Analytical Laboratory to primary standards, and so that data taken as part of the field testing of Dev Van I can be included in the site characterization studies. When checked against laboratory analyses of the same sample, TRU assay results are consistent with laboratory results. More direct comparisons are planned to statistically define the relationship between Dev Van I results and laboratory results for TRU assays.

The calibration of the down-looking Ge(Li) detector for in situ measurements is based on a homogeneous matrix. While this is not the case in the field, the relationship between the barrel standard and actual field conditions can be defined. A series of in situ measurements is being made and the location sampled to a 30 cm (one ft) depth with a core sampler. The cores will be divided into segments and each segment analyzed by Dev Van I and the laboratory. Central and peripheral cores will be taken.

The 1 nCi/g sensitivity of the TRU assay is sufficient to meet the regulatory requirement of 10 nCi/g.[1] The sensitivity of the fission product assay is about a factor of 50 above the objectives.[2] In-field radiation detection assay capabilities are being upgraded. Two 34% efficiency, down-looking intrinsic germanium (IG) detectors with ruggedized preamplifiers and mounts are undergoing initial testing and calibration. Two large Si(Li) detectors with ruggedized preamplifiers mounted inside the detector housing have been ordered. Instrument power has already been upgraded by the purchase of an uninterruptable power supply and line conditioner. Data acquisition and reduction capabilities will have to be upgraded to take advantage of the new detectors. The laboratory's GXDR System[3] is currently used for spectra analysis. It is consistent over time, has a history of use on the site, and is well documented. Uncertainty limits are calculated by GXDR based only on counting statistics; many more factors need be considered, such as calibration uncertainties or variations in sample matrix. A conservative estimate is a 50% relative standard deviation for an individual assay with a GXDR calculated uncertainty less than 20%. The milestone for FY 80 is to demonstrate simultaneous in-field data acquisition from at least two detectors using a PHA with two Analog to Digital Converters (ADCs) and interim data storage, such as diskette. Specifications are being written for a high-level microprocesser based PHA system with an FY 81 milestone of in-field data reduction. An outline of the planned capabilities of Dev Van I to be completed by the end of FY 81 follows:

- o Ability to go almost anywhere on the site
- o Simultaneous acquisition of Si(Li) and/or IG spectra
- o Data reduction to a 1 nCi/g sensitivity for TRU radionuclides within 5 minutes after the end of a 10 minute counting period
- o Surface beta assay sensitivity at uncontrolled area limits
- o Environmental Radiation Monitoring at background levels

To allow free access of the Hanford Site, a vehicle with higher clearance, a
ge exhaust system and 4-wheel drive is required.

Dev Van II is a mobile borehole γ-ray spectrometry system designed to gather data on γ-ray emitting fission or activation radionuclides to a depth of 230 m (750 ft). It is a specially designed well-logging truck built by Gearhart-Owen, Inc. (GOI) on a 2 1/2-ton Ford 4-wheel drive chassis. The electrical system operates heating, cooling, fans, and lighting from one generator; and instrumentation from the other. An uninterruptable power supply has been received for installation between the generator and instrumentation to upgrade instrument power. The draw works is a GOI Prospector Hoist Unit operated from a power-take-off unit on the vehicle engine. It is loaded with 230 m (750 ft) of 11 mm (7/16 in.) armored cable with seven single insulated conductors. All hoist controls are on the operator's console. The digital depth monitoring unit was installed by GOI as an integral part of the console.

ELECTRONICS

Dev Van II contains the following rack mounted nuclear instrumentation for γ-ray spectrometry:

- o One powered NIM bin
- o Two live time corrector/pulse pile-up rejectors
- o Two spectroscopy amplifiers
- o One 4096-channel pulse height analyzer
- o One cassette magnet tape unit.

Future 1 shows a block diagram of Dev Van II electronics. The spectroscopy amplifier must be tuned to the output of the preamplifier located in the sonde, and the live time corrector/pulse pile-up rejector (LTC/PPR) then adjusted to give a pulse of optimum shape and timing for analysis by the PHA. The two sondes have greatly different signal characteristics, so one amplifier-LTC/PPR unit was matched to each sonde.

SONDES

The mission of Dev Van II is to position a sonde at a known depth and record the γ-ray spectrum at that depth. Each sonde is a sophisticated intrinsic germanium (IG) γ-ray spectrometer with associated electronic and cryogenic (LN_2) systems. There are two sondes currently used with Dev Van II; they differ in the sensitive volume of the IG detector. Sonde #548 has a coaxial IG detector with a nominal sensitive volume of 100 cm^3; sonde #190 has a planar IG detector with a nominal sensitive volume of 1 cm^3. Both sondes were manufactured by Princeton Gamma-Tech Inc. (PGT) and incorporated PGT detectors and preamplifiers. Each sonde has rechargeable battery operated power and high voltage bias supply units. With the LN_2 cryostat inside the sonde initially full, each sonde will remain operational for about 12 hours. Each sonde is 1.8 m (6 ft) tall by 92 mm (3-5/8 in.) diameter and weighs 27 kg (60 lb) without lead shielding and 73 kg (160 lb) with #1 and #2 lead shields attached. The sondes are water resistant to a depth of 30 m (98 ft) with proper venting of the LN_2 cryostat. All outside surfaces are stainless steel to resist corrosion and contamination. After assembly, lead shields are added, if necessary, the sonde is connected to the cable head, and raised above the well casing. On completion of logging or at the end of the day, the sonde is disconnected from the cable, disassembled, reconnected to the LN_2 feeder, and the electronics - batteries unit is connected to a 110 V 60 Hz power for overnight recharging.

Because radiation levels may vary greatly, even in a signal well, a two-piece lead shield has been constructed for the sondes. It is 38 mm (1-1/2 in.) thick. The shield will reduce the intensity of cesium-137 γ-ray by 1/200; it

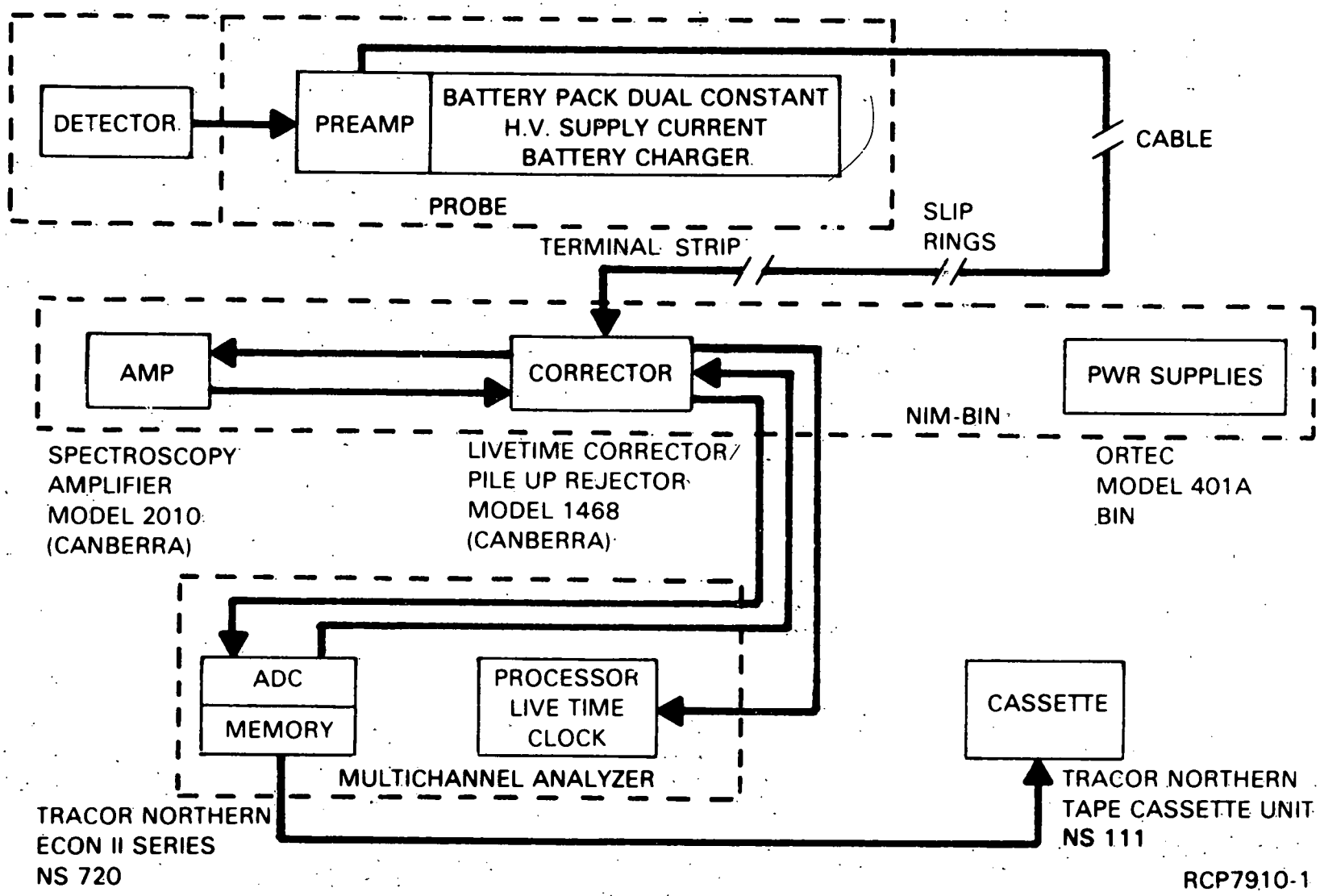


Figure 1. Block Diagram of Dev Van II Electronics

will reduce the intensity of lower energy photons even more. Although very useful, the shields are heavy, about 45 kg (100 lb), and hard to handle. They impose a strain on the draw works brake system, especially with the weight of 50 m (159 ft) of cable added.

Calibration of the sondes is accomplished using a borehole surrounded by a matrix containing a known concentration of radionuclides. Such a facility was constructed. A known amount of liquid from one of the waste tanks was mixed with Hanford backfill sediments and placed in a 1.8 m (6 ft) diameter metal tank having a standard 150 mm (6 in.) well casing welded in the center. A portion of the solution was sent to Pacific Northwest Laboratory (PNL) for detailed radiochemical analysis prior to mixing. The concentrations of radionuclides in the 4-π Fission Product Calibration Facility are given in Table 4.

TABLE 4. 4-π Fission Product Calibration Facility

Radionuclide	Concentration* (μCi/ℓ)
^{106}Ru-^{106}Rh	1.2
^{134}Cs	0.11
^{137}Cs	9.9
^{144}Ce	0.33
^{154}Eu	0.018

*January 1979

The #190 sonde without lead shielding and the #548 sonde with lead shielding can be calibrated directly. The #190 sonde with lead shielding is too insensitive and requires counting longer than the LN_2 will last. The #548 sonde without lead is too sensitive and floods the system at over 10 counts per minute. The #190 with lead and #548 without lead were calibrated by finding suitable places in logged boreholes where calibrated against a directly calibrated sonde could be performed. The calibrations are rechecked routinely for all four configurations, and any necessary updates made in the tables resident in the GXDR system.

The sensitivity of the system depends on the sonde configurations. The minimum determinable amount of several radionuclides has been calculated (Table 5) by the GXDR System for low background conditions. Large amounts of radioactive material will change these limits.

TABLE 5. Dev Van II IG Sondes Sensitivities
(values in μCi/ℓ for a 600 sec count)

Radionuclide	IG#190		IG#548	
	With Lead	Bare	With Lead	Bare
^{60}Co	0.16	0.013	0.0006	0.0002
^{106}Ru-Rh	7.1	0.16	0.072	0.0034
^{137}Cs	0.85	0.018	0.004	0.0002
^{144}Ce	17.0	0.51	0.16	0.079
^{154}Eu	0.46	0.097	0.0013	0.0006

While the sophisticated electronics in Dev Van II have extended the range of radionuclide concentrations that can be assayed, there is still a point at which the pulse pile-up rejector becomes overloaded. For the #190 sonde with lead shields this occurs at a cesium-137 concentration of about 3 millicuries per liter (mCi/ℓ); these levels can only be reported as greater than (>) 3 mCi/ℓ.

DATA REDUCTION AND ANALYSIS

Data from the sondes are processed and stored in 4096 channels in a pulse height analyzer. Since five spectra are normally acquired per hour on logging, computer aided data reduction is necessary. To store data for eventual entry into the laboratory's computer system, cassette magnetic tape is currently used. The operator records the spectrum on tape, enters the position on the tape in the logging record as well as Dev Van II location, well identification, depth, sonde, shielding, date, time, system dead time, and counting period. A log consists of 600-second counts taken every 2 m (or less) over the range of interest.

FIELD TESTS AND RESULTS

Detector sensitivity has been measured to be almost uniform axially for fission products, so all directions are equally represented. Unfortunately, this does not mean the sample is uniform, or that the Dev Van II in situ measurements will agree with laboratory analyses of the core. Both situations have been encountered during field tests. One borehole gave a cesium-137 concentration about 3 mCi/ℓ for two readings 2 m apart. When anomalies were discovered during moisture measurements in the same hole, it was relogged at closer intervals and an exceedingly hot cesium-137 layer (probably a silt lens acting as an ion exchange bed) was found at about the midpoint, reading much greater than 3 mCi/ℓ. That layer was only a few centimeters thick. In situ analyses representing an average over a large sample volume are not expected to agree closely with laboratory analyses of small samples except in the case of uniform distribution of radionuclides. This problem is the subject of a paper on In Situ Sampling.[5] Where comparison has been possible, Dev Van II data are not inconsistent with core sample data. Further comparisons are necessary to explicitly define the relationship. Table 6 presents some data gathered during Dev Van II Field Tests.

TABLE 6. Dev Van II Field Test Well Log
(values in μCi/ℓ)

Depth (m)	^{144}Ce	^{134}Cs	^{137}Cs	^{154}Eu	^{60}Co	Sonde	Time (sec)
8	0.4	0.02	0.01	0.08	0.03	190	600
10	160.0	2.0	3900.0	0.7	0.2	190+Pb	600
12	1.0	0.03	19.0	0.08	0.07	190	3000
14	2.0	0.06	12.0	0.1	0.03	190	600
16	5.0	0.1	38.0	0.2	0.05	190	600
18	1.0	0.03	6.8	0.08	0.03	190	600
20	0.5	0.02	1.2	0.08	0.03	190	600

CONCLUSIONS

Dev Van II has performed satisfactorily during its field tests. The calibration of the sondes can be traced to primary standards, so the data can be used for in situ characterization studies. The total uncertainty of the measurement is great - 50 to 100% - because many variables can affect the assay, such as presence or absence of borehole casing, condition of the borehole casing, existence of voids or vugs behind the casing, and density and moisture content of the matrix. As opportunities arise during drilling operations, Dev Van II logs will be compared with laboratory analyses of core samples to gain further

understanding of the relationship between in situ measurements and laboratory analysis of small samples.

Dev Van II is not a system for continuous logging for total radioactivity. Although sonde #548 without lead shielding is quite sensitive, it still requires 600 seconds to obtain a spectrum at low levels, and it cannot log while the sonde is moving. However, it can identify and assay γ-emitting fission products, something that conventional borehole logging for total radioactivity cannot do. The most efficient use of Dev Van II's sophisticated assay system is in conjunction with conventional γ-scintillation logs. Once areas of radionuclide concentration are found, Dev Van II can be used to log those areas for radionuclide identification and assay. Suspicious areas can be followed over a period of time to establish buildup, decay, or movement of radionuclides. During one day Dev Van II can log about 60 m (197 ft) at 2 m intervals in a single borehole. Fewer measurements can be made if Dev Van II has to reposition for different boreholes.

The electronics of Dev Van II will always require regular attention by instrument maintenance to keep them functioning properly. Operation of Dev Van II currently requires a highly trained, experienced technician.

The #190 and #548 sondes have proved quite serviceable; however, the daily assembly and disassembly are time consuming and inefficient. Two new sondes were ordered, and both returned to their respective manufacturers for modifications to overcome deficiencies discovered during acceptance testing. These sondes are to operate on power supplied from the surface and not require disassembly for LN_2 filling. An LN_2 auto fill system has been ordered, but design difficulties have held up delivery for over a year.

A Canberra Series 80 PHA with data reduction capabilities and a dual floppy diskette system for interim data storage has been acquired and will be used to upgrade Dev Van II's nuclear instrumentation. This will give Dev Van II the capability of in-field radionuclide identification and assay for most situations encountered on the Hanford Site.

The necessity of simplifying the operation of Dev Van II is recognized and action is already underway. A Data Control and Acquisition System (DCAS) has been specified, ordered, and pieces are already arriving. The DCAS will be interfaced to the depth measuring electronics, the PHA, and future instrumentation developed for Dev Van II. While the Dev Van II vehicle is ideally suited for operation on the Hanford Site, two modifications are being made to the mechanical equipment to increase safety and improve operator efficiency. A periscoping boom is being installed to allow easier positioning of the sonde over the well casing, especially where vehicle access is constrained, and to reduce operator wrestling with the 70 kg (154 lb) sondes. At the same time, the hoist's braking capacity is being substantially increased.

The 4-π Fission Product Calibration Facility was not designed to provide a long-lasting standard. The short half lives of ruthenium-106-rhodium-106 and cesium-144 were not taken into consideration years ago when the facility was designed and constructed. The only reliable nuclide left is cesium-137. This provides a standard point for comparison of sondes, but does not allow calibration over the full energy spectrum of fission product radionuclides. The design of a better calibration source for the sondes is a high priority item. This requires careful consideration because it is important to have a solid reference for all field measurements over time.

REFERENCES

1. AEC Manual Chapter 0511, "Radioactive Waste Management," and Appendix 0511,

"Terminology", U.S. Atomic Energy Commission (September 1973).

2. ERDA Manual Chapter 0524, "Standards for Radiation Protection," and Annex A "Concentrations in Air and Water Above Natural Background," U.S. Energy Research and Development Administration (March 30, 1977).

3. Zimmer, W.H., "Gamma, X-Ray Data Reduction System," 1-Gamma, ARH-ST-114-1, Atlantic Richfield Hanford Company, Richland, Washington (December 1974).

4. Lederer, C.M. and V.S. Shirley, Eds., Table of Isotopes, 7th Edition, John Wiley and Sons, Inc., New York (1978).

5. Gilbert, R.O. and M.G. Barnes, "Some Statistical Lessons Learned in Enewetak," TRAN-STAT Number 8, PNL-SA-7655, Pacific Northwest Laboratory, Richland, Washington (April 1979).

EVALUATION OF AIRBORNE RADIOACTIVE IODINE AND NOBLE GAS ENVIRONMENTAL MONITORS USING SHORT-LIVED RESEARCH REACTOR-PRODUCED RADIONUCLIDES

by

W. A. Jester
J. H. Wallace
Nuclear Engineering Department
The Pennsylvania State University

INTRODUCTION

Techniques have been developed in this work to allow for testing of air monitoring systems designed to quantify noble fission gases and airborne iodine and organic iodide under a wide variety of radionuclide concentrations, humidity conditions, and radiation background intensities. These techniques have been successfully employed in the evaluation of a commercial particulate, iodine, and noble gas air monitoring system. The use of research reactor-produced radionuclides having short half-lives facilitates such testing by eliminating waste disposal and system decontamination problems associated with the use of longer-lived fission gases.

DESCRIPTION OF THE SYSTEM BEING EVALUATED

The commercial system being evaluated had the following radiation detection components. The incoming air stream first went through a particulate filter which was monitored by a beta scintillation detector and an alpha solid state detector. The beta detector monitored the gross beta activity deposited on the filter while the alpha monitor provided data on the alpha emitters on the filters resulting from the radon daughters. This data was then used to correct the data from the beta detector for this background component on the particulate filter.

The sampled air then passed through a TEDA-impregnated charcoal cartridge for iodine removal. This cartridge was viewed by a NaI(Tl) detector. The data from this detector was recorded in two regions of the spectrum, namely in a 50 keV window covering the 364 keV peak of iodine-131 and a 50 keV window recording baseline data just above the 364 keV peak. The difference in the counts from these two channels represented the net counts in the iodine peak. The detector contained an ^{241}Am seed and the peak from this radionuclide was used for gain stabilization.

The sampled air then entered a chamber where it was viewed by a beta scintillation detector for the measurement of beta activity of any radioactive noble gases present.

All the detectors were encased in lead shielding to reduce background interference. A GM detector was located external to this shielding as an area

monitor. The data from this detector was also employed to correct the two beta scintillation detectors for gamma background penetrating the shield.

IODINE MONITORING EVALUATION

Iodine-128 point sources were produced by the irradiation of crystals of NH_4I and KI in The Pennsylvania State University's Breazeale Nuclear Reactor. The iodine radioisotope produced in this manner is iodine-128 which has a 25 minute half-life. The two 50 keV windows of the iodine detection system had to be recalibrated to monitor the 441 keV peak of iodine-128 and the baseline data above this peak instead of the 364 keV peak and baseline of iodine-131 for which the system was originally calibrated.

Irradiated iodide salts having a nominal weight of about 10 milligrams were counted as point sources in a Ge(Li) gamma-ray spectroscopy system. This system, being calibrated against IAEA and NBS certified point sources, was able to determine the precise ^{128}I microcuire content of the irradiated samples.

The samples were then transferred to a chemical reaction flask located inside a glove box where the iodine crystals were dissolved and injected into a teflon-lined reaction flask. Inorganic iodine (I_2) or organic iodine (CH_3I) was then generated by the following chemical reactions:

$$2NH_4I + 2KNO_2 + 2H_2SO_4 \rightarrow I_2\uparrow + 2NO + 2H_2O + (NH_4)_2SO_4 + K_2SO_4$$

$$KI + (CH_3)_2SO_4 \rightarrow CH_3I\uparrow + CH_3SO_4K \quad (1)$$

The resulting gas was then mixed into an air stream of known humidity which then flowed into the detector system air inlet.(2) The outlet air from the detector was run through a silver zeolite bed followed by an activated charcoal column to trap any iodine that might break through the charcoal cartridge of the monitor.

Evaluations were made of the iodine detection system resolving time, the iodine loading capacity of the TEDA-impregnated charcoal cartridges, the effects of humidity on the detector efficiency, the distribution of radioactive iodine throughout the system, and its interference on the particulate and noble gas detection systems.

RADIOACTIVE NOBLE GAS MONITOR EVALUATION

A unique approach developed at Penn State is the use of irradiated noble gas clathrates for the calibration of radiation detection equipment.(3) Clathrates are cage-like structures formed from hydroquinone. Each cage can contain a single noble gas atom. Clathrates are stable at room temperature and under the intense irradiation conditions of a nuclear reactor. Thus, single clathrate crystals can be irradiated in a research reactor to produce point radiation series. Argon and krypton clathrates were employed in this project. Argon-41 was produced by the irradiation of the argon clathrates, while krypton-85m was the major radioisotope produced by the irradiation of the krypton clathrates.

Again, the exact microcurie content of each of the irradiated clathrate sources was determined using the calibrated Ge(Li) system.

An irradiated clathrate was placed inside a gas collection bottle which was then placed inside the glove box. The clathrate was then melted by means of a hot air gun. The gas was swept out of the bottle and diluted using a known amount of air of controlled humidity.(2) This air was then allowed to flow through the commercial detector system. The system was then evaluated in

a manner similar to the iodine monitoring system.

HIGH GAMMA BACKGROUND TEST

Tests of the commercial system were also conducted in one of the hot cells located at the Breazeale Nuclear Reactor. These tests involved the positioning of a 100 millicurie cobalt-60 source at various positions around the system. The system's ability to detect and quantify the radioiodine and noble gas under these conditions was determined.

RESULTS

Some of the more significant results from these tests are listed below.

1. Resolving time losses

Using a 0.5 millicurie ^{128}I source inserted into a charcoal cartridge and monitoring its activity as it decayed away, it was found that the resolving time for the instrument was about 140 microseconds for the NaI(Tl) iodine detection system. A typical NaI(Tl) detector would normally have a resolving time of less than one microsecond. Thus, this large resolving time is attributed to the associated electronics used to process and record the pulses. It was found that above a charcoal cartridge loading of about 10 microcuries of iodine-128, a serious error was obtained between the observed iodine recorded by the system and the true iodine content. Considering the system tube non-paralizable, no change in observed iodine activity would occur above a loading of about 100 μCi.

Resolving times for the noble gas and particulate monitors were measured using the split source technique. These two beta scintillation detectors were each found to have resolving times of about 40 microseconds. Again, these values were much higher than should be expected from such detectors.

2. Iodine distribution in the system

Table I gives typical results of one of the tests made to determine iodine distribution in the system. As can be seen, there was a rapid removal of iodine from the reaction flask. No iodine was found to reach the noble gas detectors but a small amount ($\sim$ 0.1%) of the iodine deposited itself on the beta particulate filter. Because of its greater detection efficiency and better counting geometry, this small amount of iodine contributed significantly to the measured particulate activity.

3. Iodine detection efficiency as a function of relative humidity

Table II shows the system calibration as a function of air relative humidity. As can be seen, the detector has a higher efficiency (by about a factor of 2) when the air is dry. In addition, the system has a lower efficiency for methyl iodide than for iodine vapor. The humidity effect can be explained by the loss of absorber sites on the charcoal closest to the detector due to the adsorption of water molecules, thus increasing the average distance between the iodine-128 molecules and the detector. The difference between the detection efficiency of the iodine vapor and the methyl iodide can be attributed to the fact that two different mechanisms are involved in the removal of these two gases by the charcoal.

Table I

^{128}I DISTRIBUTION AS A FUNCTION OF TIME SINCE START OF REACTION*

TIME (MIN)	FLASK (CPMx10^3)	PARTICULATE (CPMx10^{-3})	IODINE (CPMx10^{-3})
0	64.5	0.9	0.02
2	61.6	11.2	0.11
3	54.8	55.2	28.6
4	40.8	111	84.6
5	23.4	150	135
10	1.3	173	197
12	0.05	159	207
16	0.05	156	212
18	0.05	154[1]	211[2]

*Corrected for decay [1]0.1% of ^{128}I [2]99.2% of $^{128}I_2$

4. Iodine breakthrough of charcoal cartridge

An effort was made to determine the amount of iodine that could be loaded onto the charcoal cartridge to cause iodine or methyl iodide breakthrough. Prior to the breakthrough tests, the cartridges were loaded with varying amounts of the gas in question by using nonradioactive iodine salts in the reaction flask. Once the desired loading was achieved, the radioactive iodide salt was introduced into the reaction flask. The silver zeolite bed was monitored at the end of each test for the presence of ^{128}I. In all tests, even with heavily-loaded beds, ^{128}I was detected. This implies that either no breakthrough was taking place or that isotopic exchange was occurring so that when the breakthrough occurred no significant amount of the radioactive gas was reaching the silver zeolite bed.

Table II

IODINE DETECTOR CALIBRATION

FORM	%RH	CALIBRATION (CPM/μG)x10^{-3}
THIS WORK		
$^{128}I_2$	11	8.9
	15	6.1
	15	6.7
	44	5.2
	52	5.0
	54	5.3
	55	4.5
	90	4.4
$CH_3{}^{128}I$	13	5.7
	33	4.4
	81	3.3
	91	3.3
COMPANY DATA		
$^{121}I_2$	?	4.5
	537	

5. Gamma field effects on iodine detectors

Table III shows the effect of the 100 μCi ^{60}Co source on the detection limits of iodine-128. Numbers reported in the gamma channel were obtained with the source located in front of the instrument. The back side of the system was found to be especially poorly shielded, and the count rate in the iodine channel increased by a factor of ten over the values listed if the source was positioned behind the system. The stowed value is that obtained with the source removed from the system and inserted into a lead shielding cask. Thus 0.2 nanocuries represents the limit of detection of this instrument for iodine-128. Using a 95% (2 sigma) confidence level variation in the background.

6. Temperature stability of the iodine monitor

In the past, the authors have experienced difficulties in using ^{241}Am impregnated NaI(Tl) detectors to obtain the required instrument stability in that the apparent calibration energy of the alpha peak would vary with time.[4] With this instrument, no significant peak energy change was observed over an eight-month period during which time the room temperature was kept constant. A test was then conducted by varying ambient temperature. These results are given in Table IV and show a significant peak energy increase by increasing the room temperature to 32°C. The change is large enough to shift the iodine peak out of the 50 keV window.

Table III

GAMMA FIELD EFFECTS ON IODINE DETECTION

SOURCE POSITION (METERS)	GAMMA FIELD (MR/HR)	IODINE CHANNEL ($CPM \times 10^{-3}$)	MINIMUM* DETECTION ($\mu Ci \times 10^{+2}$)
STOWED	0.45	0.017	0.02
3	22	1.89	1.1
2	43	3.40	2.0
1	115	10.4	4.7
0.5	220	20.4	6.5

*Based on 2σ of counts in iodine channel

7. Noble gas monitor calibration

The noble gas detector system provided fewer problems in the various tests than did the iodine monitor. Table V gives the results of the calibration of this system using known amounts of argon-41 and krypton-95m. These results agreed reasonably well with the manufacturer's calibration using xenon-133 and krypton-85.

8. Other comments on system performance

The technical manual was written well enough for the experimenters to operate the instrument without prior instructions on the machine. The mechanical and electrical components of the system held up well during these tests, with the exception of the printer. The printer output consistently differed from keyboard input in the third significant digit, and the printer ink ribbon advance was erratic at times. At the end of a roll of printer paper, the printer continued to operate. In one case, the paper at the end of the roll was taped to the cardboard spindle and thus could not advance beyond that point. The printer continued to operate overnight wearing off a tooth on the platen advance gear.

Table IV

^{241}Am ENERGY TEMPERATURE STABILITY

AMBIENT TEMPERATURE (°C)	APPARENT ^{241}Am ENERGY (MeV)
25	2.38
30	2.69
30.5	2.72
31	2.80*
31	2.74
32	2.80*

*Corresponds to a 63 keV energy shift at the 364.5 keV ^{131}I peak with only a 50 keV window

Table V

NOBLE GAS MONITOR CALIBRATION

	RADIONUCLIDE	CALIBRATION CONSTANT (CPM/$10^{-6}\mu Ci/cc$)
THIS WORK	^{41}Ar	31
	^{85}Kr	26
COMPANY DATA	^{133}Xe	25
	^{85}Kr	52

CONCLUSIONS

The testing procedures described in this paper worked smoothly and could be easily adapted to the testing of other instruments.

The manufacturer of the test instrument was informed of these results and has made a number of system modifications to overcome some of the instrument defficiencies discovered in these tests.

REFERENCES

1. Blatt, A. H., ed. Organic Synthesis, John Wiley & Sons, Inc. New York, 1943.

2. Nelson, Gary O. Controlled Test Atmosphere, Ann Arbor Science Publishers, Ann Arbor, 1971.

3. Stottlemyer, R. R. and W. S. Diethorn. "Preparation of High Capacity Argon Clathrates of Hydroquinone," International Journal of Applied Radiation and Isotopes, vol. 16, pp. 751-752, 1965.

4. Jabs, R. H. and Jester, W. A. "Development of Radioactive Gases," Nuclear Technology, vol. 30, pp. 24-32, July (1976).

AUTORADIOGRAPHIC STUDIES OF ACTINIDE SORPTION IN GROUNDWATER SYSTEMS*

G. D. O'Kelley, G. W. Beall,** and B. Allard†

Oak Ridge National Laboratory
Oak Ridge, Tennessee 37830

ABSTRACT

Autoradiography is a convenient and sensitive technique for the study of spacial distributions of alpha radioactive nuclides on slabs of rock or on other planar surfaces. The autoradiographic "camera" contains an arrangement for placing in firm contact Polaroid sheet film, a plastic scintillator screen, and the radioactive face of the specimen. As an example of the use of the autoradiographic method, a series of sorption experiments were carried out in which synthetic groundwater solutions of americium, neptunium, uranium, and plutonium were contacted with Climax Stock granite under aerated and anoxic conditions at pH 8-9. The sorption observed at specific mineral sites was correlated with data on sorption of these actinides on pure minerals.

INTRODUCTION

The actinide elements are expected to dominate the biological hazards of high-level nuclear wastes at long storage times, from about 300 years after discharge from the reactor up to millions of years. For this reason, the environmental chemistry of actinide elements is a major consideration in the design and safety analysis of geologic repositories for high-level nuclear wastes.

Various concepts of nuclear waste isolation have generated a need for data regarding the sorption behavior of actinides on rocks and minerals. Experiments have most often taken the form of batch equilibration or column measurements on crushed rocks or pure minerals, with the ultimate aim of modeling actinide sorption on whole rocks.

Two objections have been raised to the use of data from batch equilibrations to predict sorption behavior of whole rocks. Some investigators have suggested that studies on pure minerals can not be used for such purposes, because factors such as grain boundary and surface area effects are ignored.

* Research sponsored by the Division of Chemical Sciences, Office of Basic Energy Sciences, U.S. Department of Energy, under contract (W-7405-eng-26) with the Union Carbide Corporation.

**Present address: Radian Corporation, 8500 Shoal Creek Blvd., Austin, TX 78758.

† Present address: Chalmers University of Technology, S-41296 Göteborg, Sweden.

A related objection is that, in the past, many studies on crushed rocks which have attempted to correlate particular sorption mechanisms with the individual minerals contained in them have required rather indirect reasoning, with inconclusive results. These objections prompted the present study, in which an autoradiographic technique was employed to study the sorption of actinide ions on Climax Stock granite in various groundwater systems, from which qualitative comparisons could be made between literature data on pure minerals and the sorption patterns observed. Further details on experimental procedures and results will be found in a forthcoming report (1).

EXPERIMENTAL

All sorption experiments were carried out on the same slab of Climax Stock granite, with dimensions 2.7 x 3.1 x 0.3 cm. Before each experiment, the polished face was cleaned with 6 M HCl, followed by washing with distilled water. Occasionally, an additional step of decontamination was included, using a solution of detergent and EDTA. After final polishing with grade 600 emery paper, the surface was washed again with distilled water, dried with tissue, and mounted in the sorption apparatus. Tests demonstrated that negligible residual radioactive contamination remained on the specimen from one experiment to another.

The aqueous medium used in the sorption experiments was a synthetic groundwater (2) with principal concentrations as listed in Table I. In equilibrium with air, the pH was about 7.8 and was largely determined by the equilibrium between CO_2 and HCO_3^- ion. To conduct experiments under anoxic conditions, N_2

Table I. Composition of Synthetic Groundwater[a] (pH = 7.8)

Species	Concentration (mg/L)	Species	Concentration (mg/L)
HCO_3^-	123	Ca^{2+}	18
SO_4^{2-}	9.6	Mg^{2+}	4.3
Cl^-	70	K^+	3.9
SiO_2 (total)	12	Na^+	65

[a]Reference 2

gas was first bubbled through the solution to remove O_2 and CO_2. In a typical experiment under anoxic conditions, the pH attained a steady value of about 9.3 before the granite specimen was lowered into contact with the solution.

The specimen was immersed in the groundwater solution until the polished face was submerged to a depth of about 2 mm. Contact with the stirred solution was maintained for about 20-21 hours, which yielded K_d values approximately 80% of those obtained in a batch equilibration of five days. Radioactive concentrations, chosen to insure adequate sorption for an autoradiograph, were: ^{233}U, 6×10^{-7} M; ^{237}Np, 4×10^{-5} M; ^{238}Pu, 2×10^{-9} M; and ^{241}Am, 8×10^{-10} M.

Following an experiment, the specimen was washed with distilled water, dried, and installed in the autoradiographic "camera". As sketched in Fig. 1, the camera consisted of a light-tight box with a Polaroid* 4 x 5 film holder,

* Polaroid Corporation, Cambridge, MA 02139.

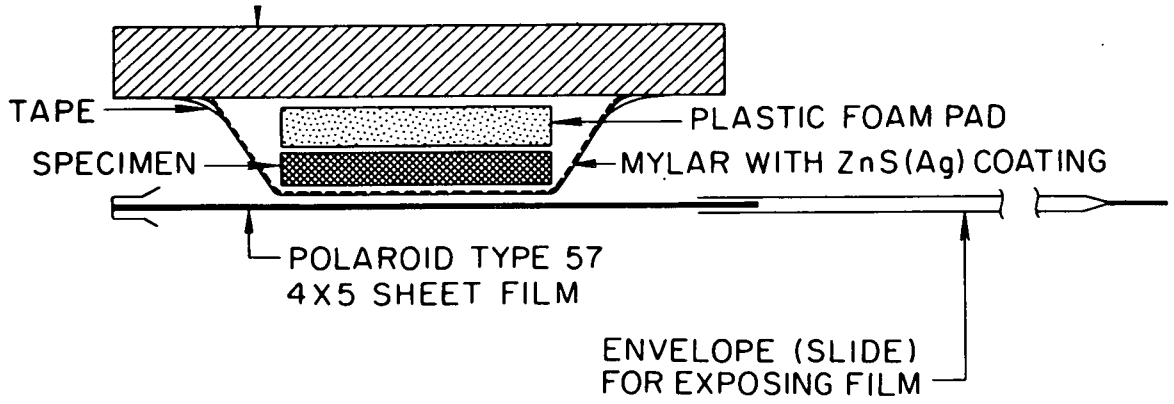


Fig. 1. Simplified diagram of autoradiograph camera, showing essential parts.

a pressure plate on which the specimen was mounted and covered by a scintillator screen, and (not shown) a mechanism for actuating the pressure plate from outside. To load the Polaroid type 57 sheet film, the pressure plate was retracted. When the envelope was pulled back to uncover the film, the pressure plate was then pressed down so the radioactive face of the specimen, the scintillator screen, and the Polaroid film were all in firm contact. Provision was made for constant contact pressure during the exposures.

The high sensitivity of this method for alpha particles arises from the use of the scintillator as a transducer, combined with 3000 ASA panchromatic film. The scintillator sheet** was conventional silver-activated zinc sulfide [ZnS(Ag)] coated on one side of a 0.004-in. (0.1 mm) polyester film, as is used extensively in low-level alpha-particle counting. Several other types of Polaroid film were tried, but type 57 yielded by far the best resolution at the low light levels of these experiments.

The arrangement just described has proved to be very convenient and reproducible. Once the scintillator screen, specimen, and plastic foam pad have been mounted on the pressure plate, any number of autoradiographs can be made without exposing the scintillator to room light. This is an important feature, because after exposure to strong room light about one hour is required for the long-lived phosphorescence in the ZnS(Ag) scintillator to decay to an acceptable level.

RESULTS AND DISCUSSION

As shown in Fig. 2, the Climax Stock granite specimen employed in this study is composed primarily of quartz, feldspar, biotite, and pyrite. In the reflected light optical photograph (Fig. 2a) the white grains are pyrite (FeS_2), the light grey are quartz, the dark grey are feldspars, and the black are biotite. These mineral components are identified in the tracing, Fig. 2b. This particular granite was chosen specifically for its grain size, its reasonably simple, representative mineralogical composition, and its two ferrous minerals. On the basis of mineralogical composition (3) and grain size, this specimen might be more appropriately termed a monzonite. Analytical data also exhibited substantial trace impurities of clay minerals (4) that formed from weathering of the feldspars. These clays appeared to be most abundant along cracks in the granite.

** Available from William B. Johnson & Associates, Inc., Research Park, Montville, NJ 07045.

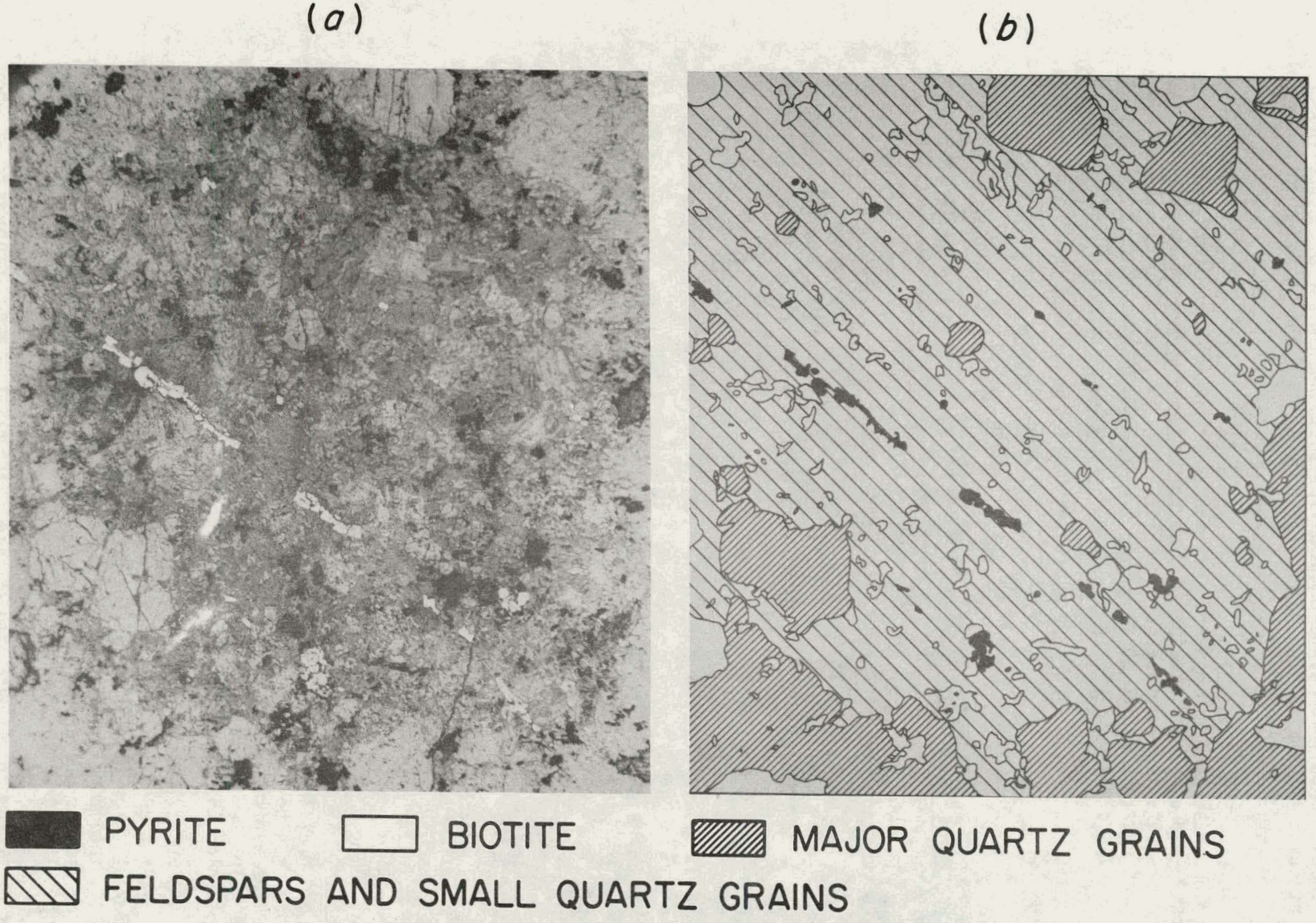


Fig. 2. Mineralogy of the Climax Stock granite specimen. (a) Optical photograph in reflected light; (b) tracing of the photograph coded to identify principal minerals.

The first actinide element chosen for study was americium, since the trivalent state is very stable and a large body of data exists for sorption of americium on pure minerals (2,5).

In Fig. 3 autoradiographs of the specimen are shown after sorption of americium under aerated and anoxic conditions. It appears from these results that slightly reducing conditions (Fig. 3b) do not greatly affect the sorption of americium. A detailed examination shows (cf., Fig. 2) that although there is general sorption over the entire surface, the pyrite and biotite grains sorb most strongly; the feldspars exhibit lower sorption; and finally, quartz shows almost no sorption. This trend for sorption of americium on the whole rock is in excellent qualitative agreement with studies on pure minerals at the same pH and in the same aqueous medium (2).

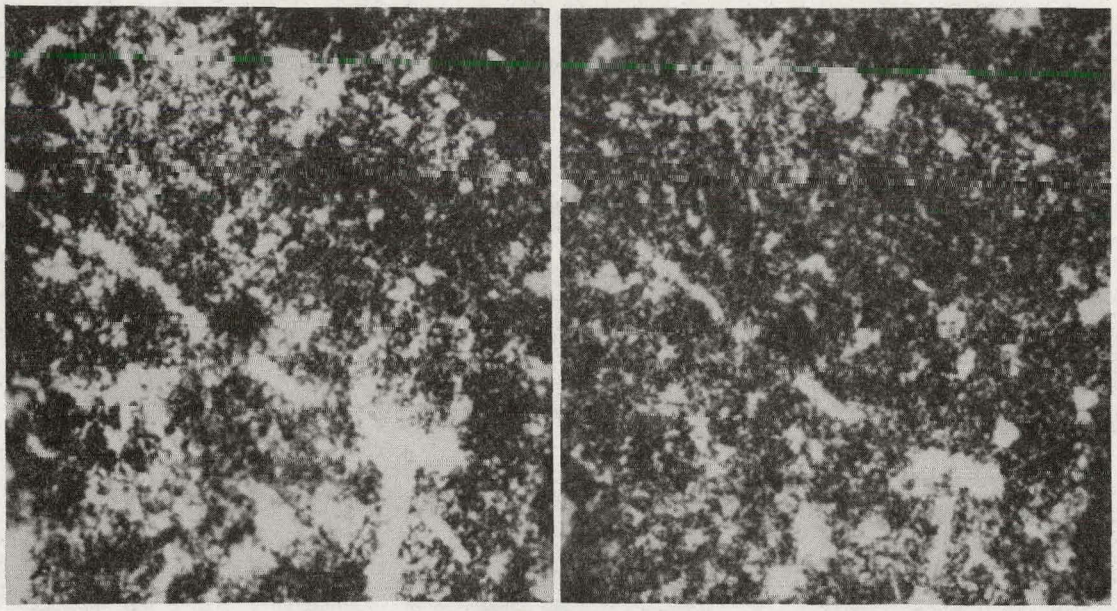


Fig. 3. Autoradiographs after sorption of americium from synthetic groundwater. (a) Aerated solution; (b) solution purged with nitrogen.

No grain boundary effects are evident, but there are obvious features due to cracks. In the optical photo (Fig. 2a) a prominent crack may be seen running from the pyrite grain in the lower right-hand corner of the slab down to the lower edge. The same feature appears in the autoradiographs of Fig. 3, probably due to sorption on the clay minerals present in the crack.

In the solutions employed for these studies, neptunium is expected to be present as the NpO_2^+ ion. Some of the results obtained for sorption of neptunium on Climax Stock granite from aerated and nitrogen-purged solutions are shown in Fig. 4, including a third autoradiograph from an experiment in which the surface of the granite was oxidized with H_2O_2 just prior to exposure to the neptunium solution. The strongly oxidized surface (cf., Fig. 4d) exhibits general sorption over the whole surface that is not specific for any mineral. The sorption of neptunium from an aerated solution (Fig. 4c) shows strong sorption on the Fe(II)-containing minerals pyrite and biotite. Under nearly anoxic conditions (Fig. 4b), even stronger sorption is observed on the pyrite and biotite, and the general

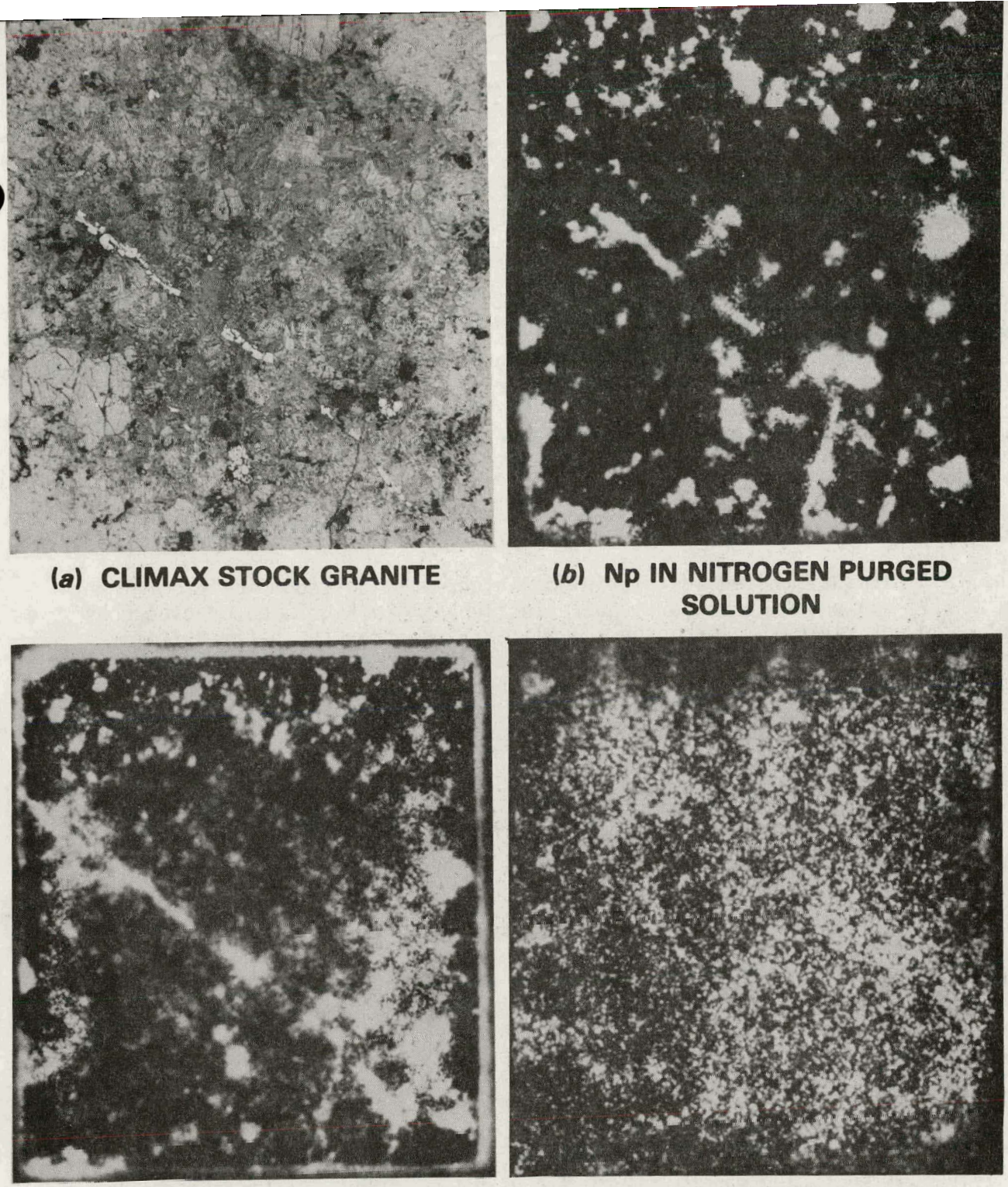


Fig. 4. Sorption of neptunium from synthetic groundwater. (a) Optical photo as in Fig. 2a; (b) autoradiograph after sorption from nitrogen-purged solution; (c) autoradiograph after sorption from aerated solution; (d) autoradiograph after sorption on surface treated with H_2O_2.

background sorption is greatly reduced. These large changes in sorption behavior as the oxidizing or reducing conditions of the solutions change, and the strong correlation of the sorption with the presence of Fe(II)-containing minerals, both

suggest that the mechanism of sorption most likely involves reduction of NpO_2^+ to the much less soluble Np(IV) by the action of Fe(II).

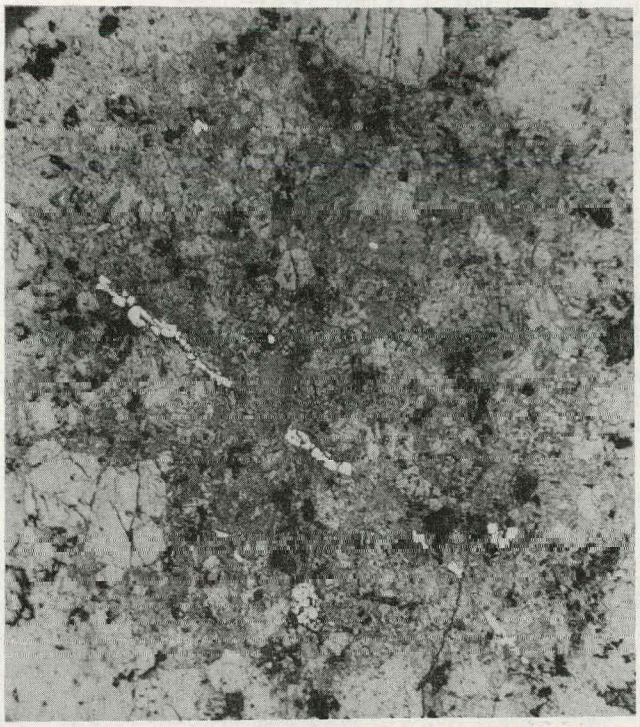
The third element investigated was uranium, expected to exist in solution primarily as the very soluble cation UO_2^{2+}, which generally exhibits low distribution coefficients for most minerals. Analysis of a series of autoradiographs following sorption of uranium on an oxidized granite surface and on an untreated surface from aerated and nitrogen-purged solutions showed that the uranium did not sorb significantly on any of the minerals except biotite. A reduction reaction with Fe(II) was ruled out, because although the Fe(II)-containing mineral biotite sorbed uranium, pyrite did not; moreover, the sorption was not affected by oxidizing or reducing conditions of the solution. The sorption on biotite appears to be related to the layered structure of the mineral and its relatively large cation-exchange capacity. Ion-exchange behavior was supported by an experiment in which uranium was sorbed on the granite from groundwater and an autoradiograph recorded. Then, the groundwater was made 4 M in NaCl and the granite was re-immersed for a time equal to the previous experiment. An autoradiograph taken after this step showed that the uranium had been removed in qualitative agreement with a simple ion-exchange mechanism.

The last element studied was plutonium, which was expected to be predominantly in the (IV) state and, therefore, quite insoluble. In Fig. 5 autoradiographs are presented for plutonium sorbed on the Climax Stock granite specimen from a solution oxidized with O_3, and from aerated and nitrogen-purged solutions. There appears to be little difference in the sorption observed for plutonium under aerated or nitrogen-purged conditions (Fig. 5 c,d). Although some specificity for Fe(II) minerals is observed, the predominant pattern is general sorption across the entire surface. This is consistent with the behavior expected for PuO_2, but implies that some PuO_2^{2+} was also present. Sorption from a solution treated with O_3, in which PuO_2^{2+} should be the dominant species, does exhibit a strong correlation with the Fe(II)-containing minerals, implying a reduction mechanism similar to that seen for NpO_2^+.

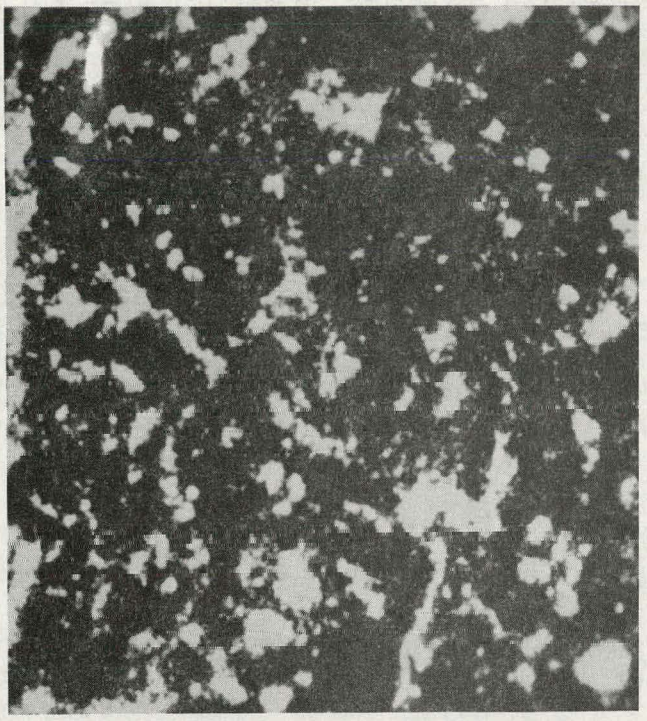
CONCLUSIONS

The results of these sorption experiments demonstrate the importance of the reduction-oxidation potential of the system, Eh, which determines the oxidation state of the ion of interest, and the pH, which determines the degree of hydrolysis. Examination of the trends expected for oxidation states of U, Np, and Pu as functions of reduction-oxidation potential and pH (6) shows that our nitrogen-purged, near-anoxic conditions at pH 8-9 approached the most positive part of the Eh range observed for deep granitic mines (1,7). Our conditions corresponded to potentials in the range of zero to about -0.15 V, while in some deep granitic mines, values of Eh as low as -0.3 to -0.4 V have been reported (7). For such negative values of the potential even UO_2^{2+} is reduced to UO_2, the less mobile form (8).

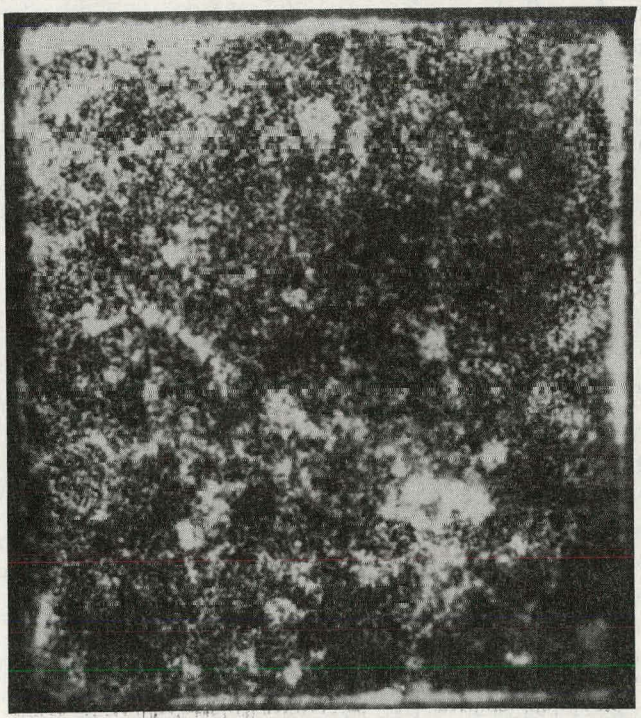
It can be concluded from this work and the earlier work on pure minerals (2) that under aerated conditions, the prevalent oxidation states of the actinides in solution will be Am(III), Pu(IV), U(VI), and Np(V). Under these conditions an appreciable amount of Np(V) appears to be reduced to Np(IV) by Fe(II)-containing minerals. Predominant oxidation states in nitrogen-purged solutions are the same as for the aerated solutions, but the reduction of Np(V) is enhanced. Thus, the autoradiographs obtained with neptunium graphically support the reduction mechanism proposed earlier by Bondietti and Francis (9) for the reduction of neptunium and technetium by Fe(II).



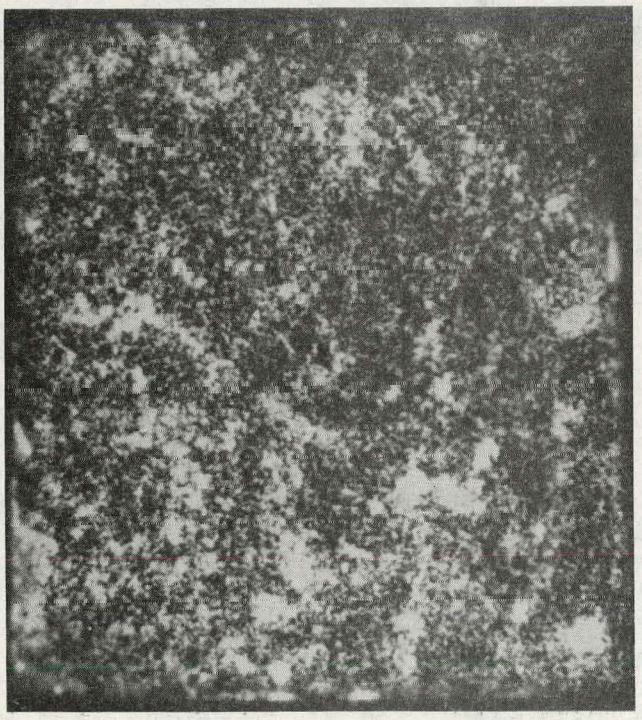
(a) CLIMAX STOCK GRANITE



(b) Pu OXIDIZED WITH O_3



(c) PU IN AERATED SOLUTION



(d) Pu IN NITROGEN PURGED SOLUTION

Fig. 5. Sorption of plutonium from synthetic groundwater. (a) Optical photo of specimen for comparison; (b) autoradiograph of specimen after sorption from a groundwater solution oxidized with O_3; (c) autoradiograph after sorption from an aerated solution; (d) autoradiograph after sorption from a nitrogen-purged solution.

The sorption of americium derived from the autoradiographs also indicates that the sorption data obtained from batch equilibrations of pure minerals can be used to predict sorption on whole rock samples and that grain boundary and surface area effects are not of sufficient importance to alter the sorption markedly.

ACKNOWLEDGEMENTS

The authors wish to express their appreciation to Dr. C. E. Bemis, Jr. for his assistance in the early stages of this work and especially for the design of the autoradiographic camera used. Part of this work was supported (B. Allard) by the Swedish National Council for Radioactive Waste Management and the U. S. Department of Energy, Office of Nuclear Waste Isolation, under contract with Battelle Memorial Institute's Waste Isolation Safety Assessment Program.

REFERENCES

1. G. W. Beall, G. D. O'Kelley, and B. Allard, "An Autoradiographic Study of Actinide Sorption on Climax Stock Granite," Oak Ridge National Laboratory Report ORNL-5617, in press.

2. B. Allard, G. W. Beall, and T. Krajewski, "The Sorption of Actinides in Igneous Rocks," Nuclear Technology, in press, 1980.

3. L. L. Ames, "Controlled Sample Program Publication No. 1. Characterization of Rock Samples," Pacific Northwest Laboratories Report PNL-2797, October, 1978.

4. B. Erdal, Los Alamos Scientific Laboratory, personal communication.

5. J. F. Pelzea, L. L. Ames, R. J. Serne, R. W. Fulton, and C. D. Washburne, Pacific Northwest Laboratories Report PNL-SA-7352, 1979.

6. B. Allard, H. Kipatsi, and J. O. Liljenzin, "Expected Species of Uranium, Neptunium, and Plutonium in Neutral Aqueous Solutions," Journal of Inorganic and Nuclear Chemistry, in press, 1980.

7. B. Allard, J. Rydberg, H. Kipatsi, and B. Torstenfelt, "Disposal of Radioactive Waste in Granitic Bedrock," in S. Fried, ed., Radioactive Waste in Geologic Storage, ACS Symposium Series, American Chemical Society, Washington, D. C., 1979, p. 47.

8. B. Allard, H. Kipatsi, and B. Torstenfelt, "Sorption of Long-Lived Radionuclides in Clay and Rock, Part II," KBS Technical Report 98, Kärnbränslesäkerhet, Stockholm, 1978.

9. E. A. Bondietti and C. W. Francis, Science 203, 1337-1340 (1979).

TRACE ELEMENT ANALYSIS OF WILD RODENT TISSUES USING THE PIXE METHOD

Max W. Hill, Nolan F. Mangelson, John F. Ryder,*
N. Duane Atwood and Benjamin W. Wood

Departments of Botany, Chemistry and Physics and the
Thermochemical Institute Contribution No. 213
Brigham Young University, Provo, Utah 84602 U.S.A.

ABSTRACT

Five species of rodents have been collected in an area near Lake Powell, Utah. Common names of the five species are: Long-tailed Mouse, Small Pocket Mouse, Deer Mouse, Antelope Ground Squirrel and Kangeroo Rat. Liver, lung, kidney and hair tissues from each animal were analyzed for trace element content by proton particle-induced X-ray emission (proton PIXE) analysis. Mean concentrations for the following elements were established for the tissues of each animal type: K, Ca, Ti, Mn, Fe, Ni, Cu, Zn, Se, Br, Rb and Pb.

Analyses of variance were performed on the set of elements common to all tissues. Some significant differences in element concentrations were found between animal species and between tissue types. These differences lead to the following orders based on element concentration: Long-tailed Mouse $\geq$ Antelope Ground Squirrel $\geq$ Kangroo Rat $\geq$ Small Pocket Mouse and liver $\geq$ kidney $\geq$ lung $\geq$ hair.

Linear regression analyses were also performed on mean elemental concentrations in tissues. These analyses lead to several conclusions. First, the pattern of trace element concentrations in each of the four tissues is the same in all five species. Second, the pattern of trace element concentrations is the same in all four tissues of one species with the exception of Ti and Fe in hair. Third, the variation of an element in the hair can not predict the variation of that same element is the other three tissues. Only K, Ca, Ti, Mn, Fe, Cu, and Zn were included in the third study.

INTRODUCTION

While a significant amount of data is available concerning trace element concentrations in tissues of domesticated and laboratory animals very little is known concerning trace element concentrations in the tissues of wild animals. Flynn et al.[1] determined trace element concentrations in the hair of the moose as a function of distance along the hair shaft. Turkstra et al.[2] determined trace elements in the liver of various wild animals indigenous to the African continent. In both of these studies element concentrations were shown to have seasonal changes.

A few studies have been carried out to measure pollutant elements in wild rodents known to be in a contaminated area. Fleming et al.[3] have compared

*esent address: Dow Chemical Co., Midland, MI 48640 U.S.A.

selenium concentrations in the tissues of woodchucks inhabiting fly ash landfills with those in an unpolluted area. Several workers have determined lead and a few other element concentrations in the tissue of small mammals collected from roadside and mining areas.[4-9]

This study concerning the trace element analysis of wild rodents was part of an environmental base-line study conducted in southern Utah near Lake Powell. The specimens were collected northeast of the lake and in the region of sites for the proposed Kaiparowits coal-fired power plant.[10]

EXPERIMENTAL

The rodents for this study were caught in snap traps, classified, and frozen as quickly as possible after collection. They were later thawed out for dissection. Five animal types were collected as are listed in Table I. Four tissues were collected from each animal during dissection: hair, liver, lung, and kidney.

Table I. Rodents collected in this study.[1]

Common name	Species	Notation[2]	No. of sites	No. analyzed
Long-tailed Mouse	Perognathus longimembris	Pl	10	17
Small Pocket Mouse	Perognathus parvus	Pp	2	2
Deer Mouse	Peromyscus maniculatus	Pm	1	1
Antelope Ground Squirrel	Ammospermophilus leucurus	Al	6	8
Kangeroo Rat	Dipodymus ordi	Do	5	5

[1]Rodents were collected in the region west of Lake Powell, Utah between May 3, and August 27, 1973.
[2]Short notation often used when referring to the animal species.

Soft tissues were analysed following a procedure of freeze drying, ashing by excited-oxygen plasma, dissolution in nitric acid and preparing thin samples on Nuclepore filters. The samples were analysed by proton particle-induced X-ray emission (proton PIXE) analysis. Detailed procedures have be reported earlier.[11,12]

A modification of the sample preparation procedure noted above was used for the hair samples. Approximately 100 mg of hair with 50 ml of reagent grade acetone were placed in a clean 250-ml beaker and the beaker was stirred with a magnetic stirrer for fifteen minutes. The hair was then transferred using additional acetone as necessary into an 8-cm Buchner funnel equipped with a filter paper The entire process was repeated a second time. The hair plus 50 ml of distilled-deionized water were then placed in a clean 100-ml beaker with a magnetic stirring bar. After stirring, the hair was again transferred into the funnel. The hair was subsiquently placed in a clean petri dish, dried in an oven at 110°C for two to three hours, cooled to room temperature in a desiccator over calcium sulfate, and then placed into a clean 15-ml polystyrene vial for storage.

For the ashing process approximately 20 mg of the hair were weighed into an aluminum boat and ashed in the excited-oxygen plasma asher. Targets were prepared from the ash as outlined for the other tissues. The target backing material used in the case of the hair was a hydrophilic mylar film[13] rather than a Nuclepore filter. The 6-N nitric acid, used for dissolving the ash, was 4.718×10^{-4} M in Y_2O_3. The Y was used as an internal standard in the anlaysis. The hair preparation methods were developed by Cook[14] and were a modification of the original procedure presented by Allison.[15]

The aluminum boats used in the ashing process were formed on plastic templates using aluminum foil. As many steps as possible were completed in a filtered-air laminar-flow hood to reduce the possiblity of contamination.

PRESENTATION OF DATA

The accuracy of the PIXE analysis system has been previously shown[12] and was further confirmed in this study by preparing samples of National Bureau of Standards (NBS) Standard Reference Material 1577 (bovine liver) which were analyzed simultaneously with the tissue samples. Element concentrations determined in this study agreed well with the NBS certified values.

Mean element concentrations for each of the four tissues types analysed are shown in Table II. The means and standard deviations shown in the table were determined from the mean values of the five animal species collected. All concentrations are in parts per million (ppm) on a dry weight basis. Whenever more than half of the concentrations determined for an element in a tissue were upper limit values the concentration listed in the table is indicated as an upper limit. A complete listing of the mean concentrations for elements detected in each tissue for each individual animal is available.[13]

Figures 1 and 2 are graphical presentations of the trace element data in each of the four tissues. Mean concentrations for each of the five animal species are presented and allow a comparison of the variations and simularities between the species. Figure 3 is a graphical presentation of the mean element concentrations in the four tissues of the Long-tailed Mouse. This figure allows a comparison of element concentrations in the four tissues. The patterns observed are simular to those in the other animal species studied.

Table II. Element concentrations by tissue and averaged over all animal types.

Element	Element concentration (mean ± standard deviation in ppm)[1]			
	Tissue: Hair	Kidney	Liver	Lung
K	<44	11300 ± 2700	10400 ± 2900	10600 ± 2000
Ca	530 ± 220	620 ± 320	820 ± 490	510 ± 110
Ti	8.1 ± 5.2			8.4 ± 8.0
Mn	7.8 ± 3.6	8.0 ± 3.3	10.1 ± 3.2	<2.8
Fe	57 ± 26	480 ± 180	680 ± 300	1050 ± 130
Ni	2.6 ± 1.2	<7.5	<2.8	<1.1
Cu	11.0 ± 4.3	22.4 ± 9.4	19.3 ± 65	11.9 ± 3.0
Zn	170.0 ± 43	98 ± 13	137 ± 37	69 ± 16
Se		<3.9	1.7 ± 0.7	<2.3
Br	<12	6.0 ± 5.1	8.1 ± 5.8	8.8 ± 4.8
Rb	<9	9.6 ± 5.9	7.9 ± 4.2	<6.9
Pb	<16	<12	5.5 ± 4.3	<7.7

[1]The means and standard deviations were determined from the mean values of the five animal species collected and refer to dry tissue weight.

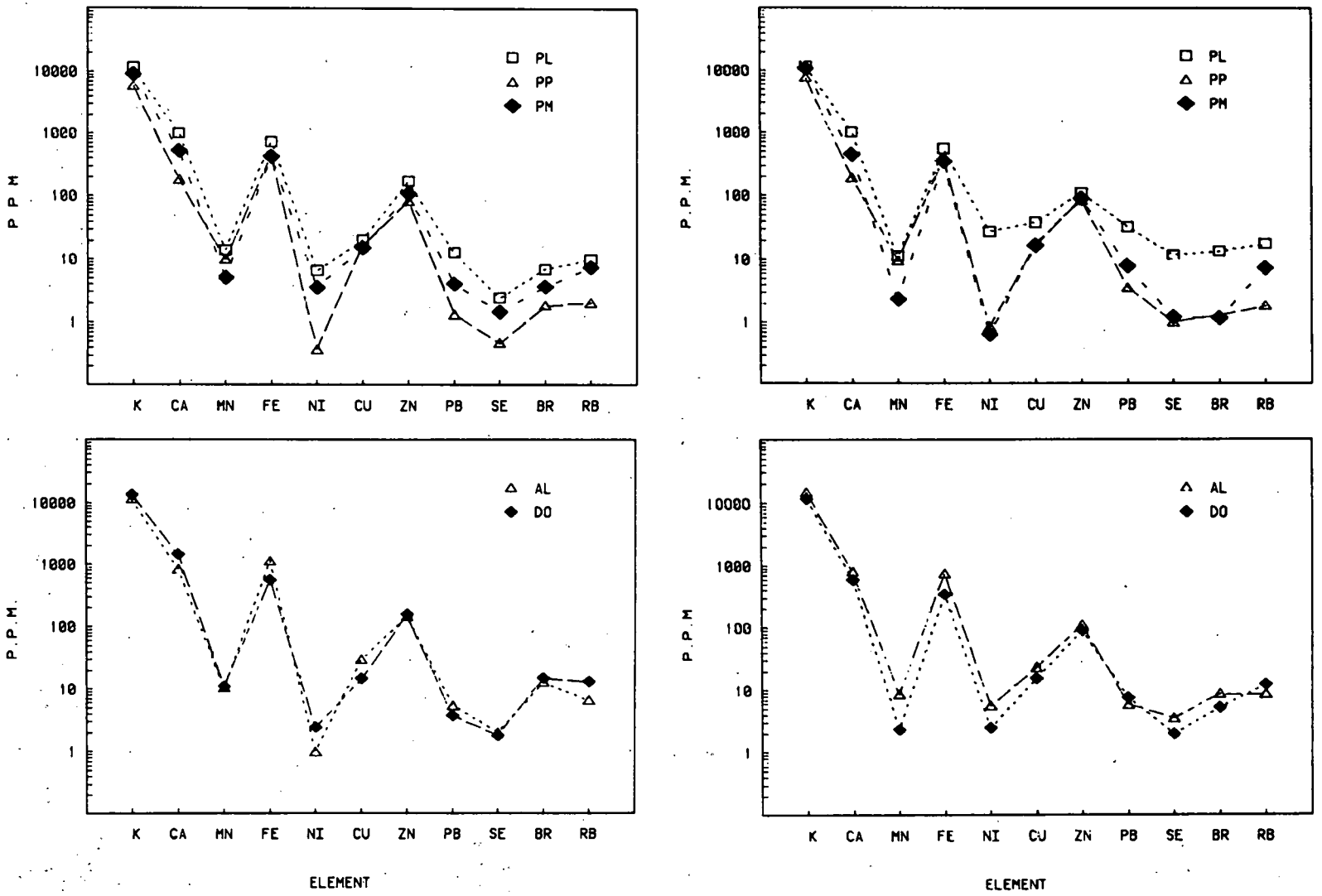


Figure 1. Mean element concentrations in liver (left) and kedney (right). See Table I for an explanation of the symbols representing five rodent species.

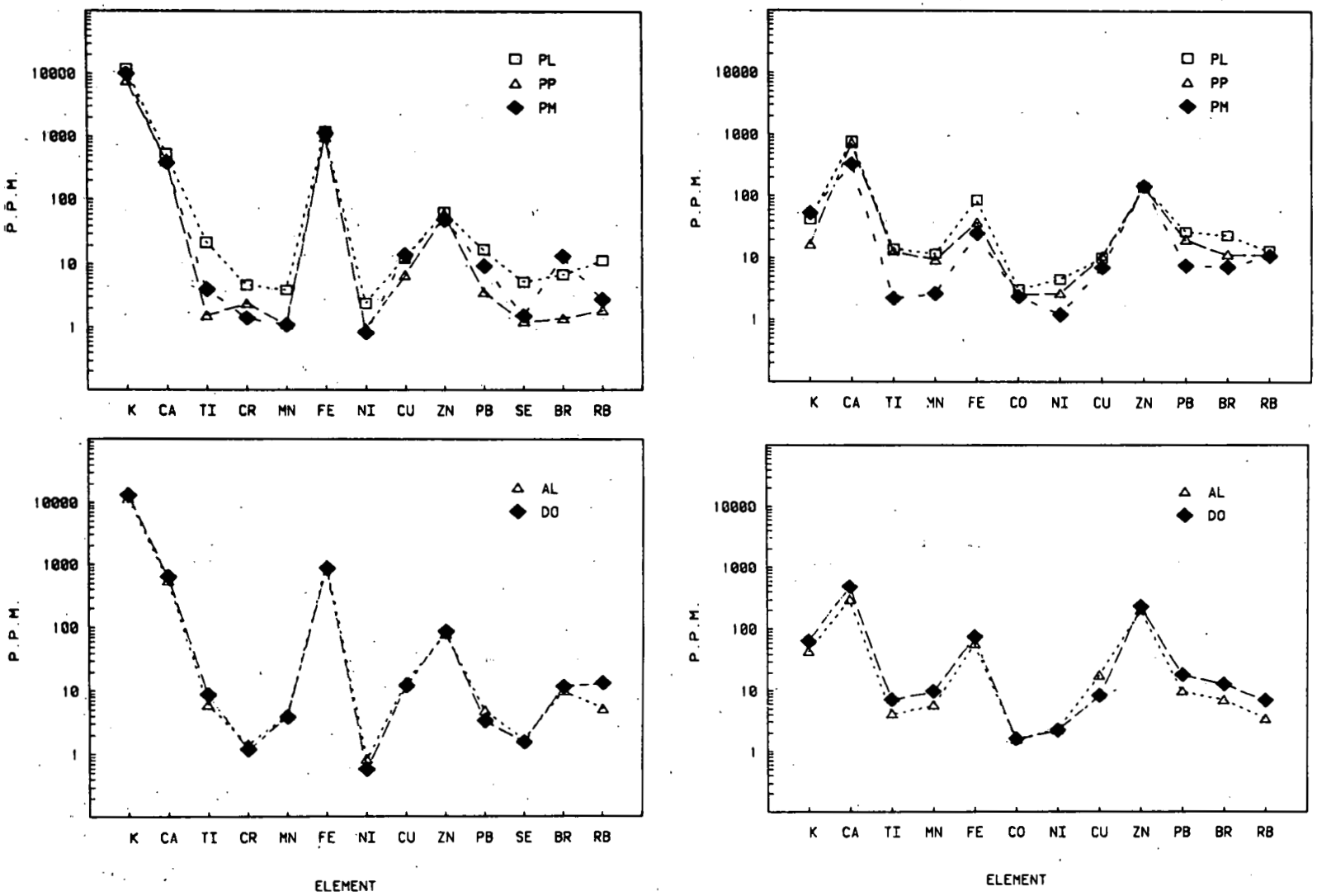


Figure 2. Mean element concentrations in lung (left) and hair (right). See Table I for an explanation of the symbols representing five rodent species.

Highly correlated trace element patterns among the five animal types are evident for all elements detected in each tissue. Further, all elements except K and Fe are seen to correlate well for the four tissues in Figure 3. These correlations are further investigated in the statistical analysis of the data.

DISCUSSION OF RESULTS

Table III lists a comparison of mean elemental concentrations of some elements in the liver, kidney and lung of several laboratory grown rat species and of the Kangaroo Rats captured in the wild. Trace element concentrations for the Kangaroo Rat are in good agreement with concentrations for the other rats in this comparison, however, Ca appears to be considerably higher and Rb seems to be lower.

Table IV is a comparison of mean elemental concentrations between three species of mice from this study and five inbred strains of laboratory mice.[20] The Fe and Zn concentrations appear to be consistant between the two groups when the large standard deviations for the wild species are taken into account. The Rb in the wild mice seems to be low in the comparison which is consistant with the comparison of the rat species.

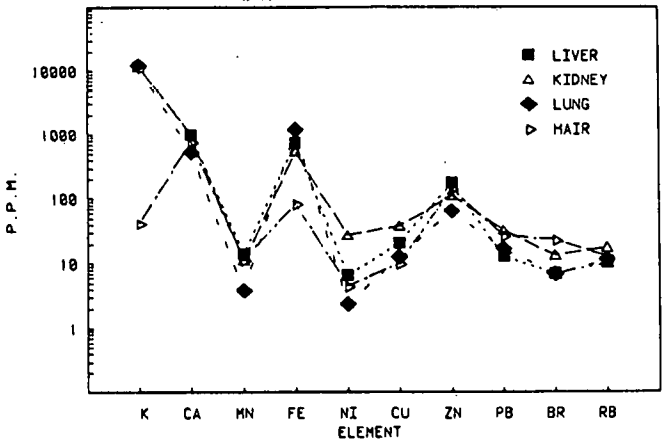


Fig. 3. Mean element concentrations in the tissues of the Long-tailed Mouse (Pl).

Selenium in the liver and lung is about 2 ppm as indicated in Table I. This is higher than the value of 0.4 ppm found for Woodchucks in an unpolluted area and nearly equal that found in the animals captured in fly ash.[3] Lead concentration in the liver was found in this study to be 5.5 ± 4.3 ppm. This agrees well with values of 5 to 8 ppm reported for field mice collected from unpolluted areas.[4]

In order to investigate the correlations observed in Figures 1-3, the elemental concentrations found for the rodents were subjected to an analysis of variance using the computer program, RUMMAGE.[21,22] Only the elements common to all tissues were used in the analyses. These elements were K, Ca, Mn, Fe, Ni, Cu, Zn, Br, Rb and Pb. In addition an analysis was performed on Ti using only data for the lung and hair tissues.

The model for the analysis was

$$Y_{ij} = \mu + T_i + A_j + TA_{ij} + e_{(ij)k}, \qquad (1)$$

where Y_{ij} is the observed elemental concentration in a specific tissue, μ is the mean elemental concentration in all tissues and animals; T_i is the variation of μ to give the mean concentrations in each tissue type; A_j is the variation of μ to give mean concentrations in each animal type; TA_{ij} is the variation of μ to account for interaction between the terms T_i and A_j; and $e_{(ij)k}$ represents the random error due to the individuals in each animal type. Factors T_i and μ were both fixed since the same four tissues were analyzed in each case and the animals were ordered as specific types. The sex and age of the collected animals were not determined and therefore no factors for these variables occur in the statistical model. Also all the animals were collected during the

Table III. Comparison of mean elemental concentrations in tissues of rats.

Tissue	Element	Element concentration (ppm) S.P.F. Male Rats Sherman Strain[1]	White Rat[2]	Sprague-Dawley Rat[3]	Wistar female Rat[4]	Kangeroo Rat[5] (Dipodymus ordi)
Liver	Ca				190 ± 11	1480 ± 476
	Mn	7.50 ± 0.80				10.9 ± 1.6
	Fe	630 ± 100	300	444 ± 54	800 ± 48	557 ± 126
	Cu			11.8 ± 1.2	20.1 ± 1.6	15 ± 3
	Zn	103 ± 10	87.6	109 ± 6	92 ± 3	159 ± 84
	Rb	40.2 ± 3.5			25.1 ± 1.9	13 ± 4
Kidney	Mn	3.10 ± 0.40				8.2 ± 4.0
	Fe	460 ± 100	323	203 ± 14		344 ± 14
	Cu			19.3 ± 0.7		16 ± 3
	Zn	100 ± 8	125	102 ± 4		91 ± 19
	Rb	30.4 ± 3.0				12.4 ± 4.6
Lung	Fe		735	688 ± 70		872 ± 240
	Cu			7.5 ± 0.5		12.1 ± 1.3
	Zn		92	83 ± 4		88 ± 23

[1]Reference 16. [2]Reference 17. [3]Reference 18. [4]Reference 19.

[5]This study; mean ± standard deviation for 5 samples.

summer months so that no seasonal variation in trace element concentrations were determined. The collection of only one or two animals at each sampling site also excluded the determination of any site to site differences in trace element concentrations.

Orthogonal contrasts were established and tested during the execution of the program. Specific contrasts investigated included the following:

1. Trace element concentration differences between animal types: (a) averaged over all tissue types and (b) for each tissue type.

2. Trace element concentration differences between tissue types: (a) averaged over all animal types and (b) for each animal type.

The 95% confidence level ($\alpha = 0.05$) was chosen as the significance level for all tests.

Using the results of the analysis of variance in the study 1. above, that is the trace element differences between animal type, it was found that without exception the animal species could be ordered as follows:

$$Pl \geq Al \geq Do \geq Pp$$

Pm is uncertain for only one speciman was collected.

TABLE IV. Comparison of mean elemental concentrations in tissues of mice.[1,2]

Tissue and Element	Element concentration (ppm) I	II	III	IV	V	Pl	Pp	Pm
Kidney:								
Fe	301±16	214±14	242±30	297±23	261±18	549±163	386±119	352
Zn	75± 6	77± 3	73± 4	68± 4	73± 4	112± 71	84± 17	92.2
Rb	31± 4	33.1±2.4	26±2.8	22.1±2.8	33± 4	17.7±7.2	≤ 1.9	7.3
Liver:								
Fe	468± 63	684± 36	618± 32	1390± 94	382± 41	764±491	460± 57	432
Zn	75± 6	87± 2	107± 4	86± 2	83± 4	179±118	86± 6	113
Rb	40.2± 4	43.5±2.2	33.1± 2	34.3± 2	45.5±2.8	16.2±7.6	≤ 2.0	7.5

[1] I through V represent five inbred strains of laboratory mice: C57L/J(I), BALB/cJ(II), DBA/2J(III), AKR/J(IV) and C57BL/6J(V). Reference 20.

[2] Pl, Pp and Pm represent three species of mice collected in this study. See Table I for animal species and for the number of samples analysed. The mean and standard deviation are given for these three species.

The ">" signs indicate that in some cases element concentrations are significantly different between animal species while in other cases there is significant difference. It is also noted that in general no one element is significantly different in all species. A complete tabulation of the results of these analyses can be obtained.[13]

Using the results of analysis of variance in the study 2. above, that is trace element differences between tissue types, it was found that without exception the tissues could be ordered by element concentration as follows:

$$\text{liver} \geq \text{kidney} \geq \text{lung} \geq \text{hair}$$

except for Ti where

$$\text{lung} = \text{hair} \geq \text{liver} = \text{kidney}$$

The "$\geq$" signs convey the same meaning with respect to tissue type as they did in study 1. above for animal species. A complete tabulation of the results of these analyses can be obtained.[13]

Table V. Correlation coefficients from linear regression analysis of mean elemental concentrations of liver tissues.

Animals tested[1]	Correlation coefficient (r)
Pl vs. Pp	0.998
Pl vs. Pm	0.999
Pl vs. Al	0.999
Pl vs. Do	0.999

[1]See Table I.

Table VI. Correlation coefficients from linear regression analysis of tissues in the Long-tailed Mouse.

Tissue tested	Correlation coefficient (r)
Liver vs. Kidney	1.000
Liver vs. Lung	0.998
Liver vs. Hair	0.999[1]
	0.827[2]
	0.032[3]

[1]Excluding Fe and K concentrations.
[2]Excluding K concentration and including Fe concentration.
[3]Including Fe and K concentrations.

In addition to the analysis of variance just discussed linear regression analyses were used to study several aspects of the trace element data. In one study all element concentrations in the liver of one animal species were compared by linear regression analysis to the concentrations in the liver of each of the other species. The results showed a nearly perfect correlation as indicated in Table V. All other possible correlations between animal species for each of the tissues showed the same high degree of correlation.

In a second linear regression study the correlations evident in the Figure 3 for trace element concentrations in the four tissues of the Long-tailed Mouse (Pl) were examined. The results are shown in Table VI where it can be seen that only K and Fe in the hair fail to show a nearly perfect correlation. It was also deemed desirable to determine if the variation of a trace element in hair could account for the variation of that same trace element in another tissue from the same animal. Therefore, a linear regression analysis, was carried out for each element to compare hair concentrations to that in each of the other tissues. The results of this study show that trace element variation in the hair will not predict the element variation in other tissues for the elements studied in these, apparently normal, animals. Zn variation in the lung shows the most significant correlation but, even here, less than 50% of the Zn variability is predicted by the hair concentration.

ACKNOWLEDGEMENTS

The authors express appreciation to the following for their assistance: G.F. Walters for sample analysis, K.J. Faucette for preparation of hair samples, M.W. Carter, D.O. Richards, A.S. Allen and T.D. Allen for significant direction and help in statistical calculations, Kae Doman for typing the manuscript.

Partial support for the project was provided by Salt River Project, Research Corporation of Arizona Public Service, and Southern California Edison.

REFERENCES

1. A. Flynn, A. W. Franzmann, P. D. Arneson and O. A. Hill, Jr., Determination of past trace element uptake in a wild animal by longitudinal analysis of the hair shaft, Naturwissenschaften, 61, 362, 1974.

2. J. Turkstra, A. M. Harthoorn, P. J. L. Beukes and R. J. N. Brits, The influence of seasonal changes in the concentration of trace elements in liver tissue of various wild animals determined by instrumental neutron activation analysis, J. Radioanal. Chem., 37, 473-481, 1977.

3. W. J. Fleming, W. H. Gutenmann and D. J. Lisk, Selenium in tissues of Woodchucks inhabiting fly ash landfills, Bull. Environ. Contam. Toxicol., 21, 1-3, 1979.

4. R. D. Roberts and M. S. Johnson, Lead contamination of small mammals from abandoned metalliferous mines, Environ. Pollut., 15, 61-69, 1978.

5. D. J. Jefferies and M. C. French, Lead concentrations in small mammals trapped on roadside verges and field sites, Environ. Pollut., 3, 147-156, 1972.

6. G. W. Mierau and B. E. Favara, Lead poisoning in roadside populations of deer mice, Environ. Pollut., 8, 55-64, 1975.

7. H. D. Quarles III, R. B. Hanawalt and W. E. Odum, Lead in small mammals, plants and soil at varying distances from a highway, J. Appl. Ecol., 11, 937-949, 1974.

8. W. R. Welch and D. L. Dick, Lead concentrations in tissues of roadside mice, Environ. Pollut., 8, 15-21, 1975.

9. D. R. Clark, Jr., Lead concentrations: Bats vs. terrestrial small mammals collected near a major highway, Environ. Sci. Tech., 13, 338-341, 1979.

10. N. F. Mangelson, G. M. Allison, D. J. Eatough, M. W. Hill, R. M. Izatt, J. J. Christensen, J. R. Murdock, K. K. Nielson, and S. L. Welsh, Trace element analysis for the environmental baseline studies of the Navajo-Kaiparowits Generating Stations, in: D. D. Hemphill (ed.), Trace Substances in Environmental Health-VII, University of Missouri, Columbia, Missouri, pp. 369-377, 1973.

11. N. F. Mangelson, M. W. Hill, K. K. Nielson and J. F. Ryder, Proton induced X-ray emission analysis of biological samples: some approaches and applications, Nucl. Instr. Meth., 142, 133-142, 1977.

2. N. F. Mangelson, M. W. Hill, K. K. Nielson, D. J. Eatough, J. J. Christensen, R. M. Izatt and D. O. Richards, Proton induced X-ray emission analysis of Pima Indian autopsy tissue, Anal. Chem., 51, 1187-94, 1979.

13. J. F. Ryder, Applications of proton particle-induced X-ray emission analysis to rodent tissue samples and particulate emissions of a copper smelter; development of an automated irradiation chamber. Ph.D. Dissertation, Dept. of Chem., Brigham Young University, Provo, Utah, 1979.

14. W. Cook, Private communication, Brigham Young University, 1978.

15. G. M. Allison, Trace-metal analysis of hair by charged-particle X-ray fluorescence, M.S. Thesis, Dept. of Chem., Brigham Young University, Provo, Utah, 1974.

16. B. Maziére, C. Loc'h, O. Stulzaft, A. Gaudry and D. Comar, Application of neutron activation analysis to the study of the variations of the concentration of trace elements in various organs of rat as a function of age, J. Radioanal. Chem., 37, 617-629, 1977.

17. K. Kostić, R. J. Draśković, M. Ratković, D. Kostić and R. S. Draśković, Determination of some trace elements in different organs of normal rats, J. Radioanal. Chem., 37, 405-413, 1977.

18. M. Chvapil, Y. M. Peng and A. L. Aronson, Effect of zinc on lipid peroxidation and metal content in some tissues of rats, J. Nutr. 104, 434-443, 1974.

19. W. E. Kollmer, P. Schramel and K. Samsahl, Simultaneous determination of nine elements in some tissues of the rat using neutron activation analysis, Phys. Med. Biol., 17, 555-562, 1972.

20. M. P. Siegers, K. Kasperek, H. J. Heiniger and L. E. Feinendegen, Distribution of trace elements in organs of mice of different inbred strains, J. Radioanal. Chem., 37, 421-426, 1977.

21. G. R. Bryce and M. W. Carter, Analysis of variance in unbalanced design--a software package, Comp. stat. 74, in: G. Bruckmann, F. Ferschl, and L. Schmetterer (eds.), Proceedings in Comp. Stat., Vienna, Aust., Physica Verlag, 1974.

22. G. R. Bryce, MAD: analysis of variance program for unbalanced designs, Appl. Stat. (J. Roy. Stat. Soc., Series C), 24, 350-352, 1975.

DETERMINATION OF ^{210}Pb AND ^{210}Po IN THE ENVIRONMENT

W. L. Raines, J. W. Dillard, L. G. Kanipe, B. B. Hobbs

Division of Occupational Health and Safety

Tennessee Valley Authority

ABSTRACT

Measurement of ^{210}Po and ^{210}Pb in environmental samples is a vital part of environmental monitoring programs for regions where uranium is mined or processed. A method for determination of these isotopes in environmental samples is discussed. The key to the procedure is the parent-daughter relationship between ^{210}Pb and ^{210}Po. Lead carrier is added and subsequent formation of several lead compounds is the basis for separation and purification. The ^{210}Po acitivity is determined by alpha spectroscopy after polonium is plated on a nickel disc. The plating technique uses a rotating disc electrode to ensure uniform plates and to reduce plating time substantially. A tracer of ^{208}Po is used to quantitate the plating and alpha counting process. The ^{210}Pb activity is determined from the activity of the daughter ^{210}Po after a 30-day ingrowth period. The measured activity of ^{210}Pb is corrected for the lead chemical yield using a three-point standard addition and anodic stripping voltammetry.

INTRODUCTION

The isotopes ^{210}Po and ^{210}Pb are products of the natural decay series of ^{238}U. These isotopes have become key radionuclides in environmental monitoring programs for regions in which uranium is mined or processed. Before these isotopes could be used in such a program, a suitable chemical procedure had to be developed for their analysis in natural waters, soil, sediment, and vegetation. Several procedures for the analysis of these two radionuclides have been used for a number of years.[1,2] However, these procedures involved complex chemical separations and resulted in lengthy analysis times. In most cases the analysis of ^{210}Po and ^{210}Pb were performed by separate procedures. Often these older procedures were specific for one type of environmental sample. A procedure which could be used to determine the concentrations of both ^{210}Po and ^{210}Pb in all types of environmental samples would reduce overall analysis time and ensure more reproducible results since basically only one procedure is used instead of several. Such a chemical procedure is presented in this paper. This procedure utilizes some of the techniques of older procedures but represents significant improvements in the polonium plating technique and the method of quantitating the lead activity. The procedure also provides a vast reduction in time per analysis and thereby a reduction in cost.

This procedure utilizes the parent-daughter relationship between ^{210}Po and ^{210}Pb. After a few simple separation steps, the activity of the daughter ^{210}Po in the sample is measured. Then, after further separation and purification, the ^{210}Pb concentration is determined from the ingrowth activity of the daughter ^{210}Po.

Separation of ^{210}Po and ^{210}Pb

One liter aliquots of natural water samples are analyzed. No pretreatment is necessary for water samples. Solid samples are dried and ground to a uniform size of ∿65 mesh.

Lead carrier and a ^{208}Po tracer are added to all samples. Solid samples require acid digestion to dissolve the sample. Digestion procedures are given in Table I. The dissolved sample is diluted to 500 ml with deionized water. After these initial steps the procedure is identical for water, soil, sediment or vegetation.

The lead carrier is precipitated as lead sulfate by the addition of 35 ml of sulfuric acid and digested by heating the solution to 70°C. The ^{210}Pb will be precipitated with the stable lead. The ^{210}Po remains in solution. After decanting the supernate, the solution is prepared for plating of the ^{210}Po by adding 1 gm of hydroxylamine hydrochloride and 2 ml of 40-percent citric acid solution. The plating procedure is discussed in detail later in this paper.

The lead sulfate precipitate is dissolved with 20 ml 6N ammonium acetate. The lead is then precipitated as lead carbonate by the addition of 25 ml of 3N sodium carbonate. The lead carbonate must be washed with water to remove any unreacted reagent to ensure that the precipitate will dissolve in the next step. The precipitate is dissolved with 10 ml of 3N nitric acid. The lead is reprecipitated as a carbonate and then dissolved and brought to final volume of about 30 ml with 3N nitric acid. This solution contains the ^{210}Pb and is stored for 30 days to allow ingrowth of ^{210}Po. At the end of ingrowth period, 1 ml of ^{208}Po tracer, 1 gm of hydroxylamine hydrochloride and 2 ml of 40 percent citric acid are added and the ^{210}Po is plated from this solution.

Plating Technique

The ^{210}Po is plated onto a nickel disc by galvanic deposition. A complete discussion of the plating technique has been published in a separate paper.[3] The use of ^{208}Po tracer eliminates the need for exhaustive deposition. Since the electrochemistry of both ^{210}Po and ^{208}Po are identical, proportional quantities of each will be deposited. The only restriction is that enough polonium be deposited to achieve the desired alpha counting statistics. For optimum alpha spectrometry, thin uniform plating of the polonium is extremely desirable. Since peak energy separation between the two isotopes is only 0.19 MeV, thick or nonuniform plates broaden the alpha spectra making it difficult to resolve the two energies and determine the peak areas. Due to its well defined hydrodynamic conditions, the rotating disc electrode used in this procedure is an excellent way of controlling the deposition process to ensure uniformity and predictability of plates.

The nickel electrode discs used in this study are 19.02 mm in diameter and 0.42 mm thick. After descriptive sample information is written on the back side of the electrode, it is sprayed with a light coat of lacquer to ensure permanence of the sample record and to seal the nickel surface. The disc is then pressfit into a Teflon electrode holder. The electrode holder is illustrated in Figure 1. The electrode assembly is attached to a variable speed motor, and the nickel surface of the disc is polished at high rotation speed with 0.1 μm alumina supported on a polishing cloth. After polishing, the disc is cleaned with water and then is primed with 0.5N hydrochloric acid. During the actual deposition, the electrode assembly is rotated at 500 RPM with sufficient immersion into the solution to prevent vortex bubbles from traversing the electrode surface. After plating, the electrode is rinsed in deionized water and is air dried at a fast rotation rate. A hole passing through the entire length of the holder allows for the electrode removal with the use of a ramrod.

Measurement of ^{210}Po by Alpha Spectroscopy

The plated disc is counted by an alpha spectroscopy system consisting of a Princeton Gamma Tech surface barrier detector, coupled by a Nuclear Data 404 preamp and 510 amplifier to a Nuclear Data 2200 multichannel analyzer. A typical alpha spectrum depicting the well-defined peaks of ^{208}Po and ^{210}Po is illustrated in Figure 2. Even with much higher activities of ^{210}Po, there is adequate peak separation from the peak of ^{208}Po to quantitate the activity.

Lead Yield Determination

After ^{210}Po has been plated from the ingrowth solution, the lead chemical yields are determined by anodic stripping voltammetry.[4] The voltammetry system consists of a potentiostatically controlled three-electrode electrochemical cell. The three electrodes are a hanging mercury drop electrode, a

calomel reference electrode, and a platinum counter electrode. The electrochemical cell anodic stripping currents are measured with a Princeton Applied Research model 174 polarographic analyzer.

The final lead solution is transferred to a 50-ml volumetric flask and diluted to volume with deionized water. The supporting electrolyte solution used in this procedure is 10^{-2} M KNO_3. A 50-λ aliquot of the sample is added to the electrochemical cell, and a voltammogram is acquired. Then 50 λ of a standard lead solution is added three times, with a voltammogram obtained after each addition. From these readings a plot of anodic stripping peak current versus standard volume is made. Figure 3 shows a voltammogram and resulting plot for a typical sample. The volume intercept for zero current is determined from the plot, and the lead chemical yield is determined from the equation:

$$\text{Percent yield} = \frac{(\text{volume intercept})\ (\text{standard concentration})\ (100)}{(\text{volume of carrier added})\ (\text{carrier concentration})} \quad (1)$$

Evaluation of the Procedure

The procedure discussed above provides a method of measuring the ^{210}Po and ^{210}Pb concentrations in environmental samples. This method gives good results over a wide range of concentrations. The method can accurately measure levels as low as a few pCi to as high as several hundred pCi. Table II gives a comparison of measured to known concentrations for a group of water samples analyzed by this method.

This method appears superior to procedures used for determination of these isotopes in the past. The sulfate precipitation used in this procedure is simpler and produces better lead yields than the sulfide precipitation used in older procedures. Older plating techniques which used a fixed disc instead of a rotating disc required much longer plating times. In addition, it appears that the plating technique is much more quantitative than older techniques. Tests with known concentrations of ^{210}Po have indicated that this method has a plating efficiency greater than 90 percent.

This procedure is now in routine use for environmental samples analyzed by our laboratory. To date, the data produced by this method have been very satisfactory. Use of this procedure has substantially reduced analysis time and therefore cost.

TABLE I. ACID DIGESTION PROCEDURES

Step Number	Soil and Sediment	Vegetation
1	Weigh 2 gm of sample into a teflon beaker.	Weigh 1 gm of sample into an 800 ml beaker
2	Add 50 ml HNO_3, 3 ml of Pb carrier (50 mg/ml) and 1 ml ^{208}Po tracer.	Add 3 ml of Pb carrier (50 mg/ml) and 1 ml ^{208}Po tracer.
3	Digest the sample until NO_2 is no longer emitted. Continue heating for ∿10 min. Additional HNO_3 should be added to maintain the volume.	Add 10 ml of 4N HNO_3 and 10 ml of HF. Heat to reduce volume to 5 ml. Repeat twice.
4	While sample is warm dilute to 500 ml with deionized water. Filter through Whatman #2 filter into a clean 800 ml beaker. Proceed as directed for a water sample.	Add 10 ml of 4N HNO_3 and heat to reduce volume to 5 ml. Repeat.
5		Proceed as directed in step 4 for soil and sediment samples.

Note: Heat gently and never boil the sample to dryness during digestion. Some forms of ^{210}Po are volatile.

TABLE II. A COMPARISON OF ANALYSIS RESULTS

^{210}Po (pCi/ℓ)		^{210}Pb (pCi/ℓ)	
Found	Added	Found	Added
13.8 ± 1.5	11.3	13.8 ± 1.2	11.3
32.7 ± 3.0	33.7	34.7 ± 2.4	33.7
52.7 ± 4.0	55.7	55.5 ± 3.5	55.7
122.1 ± 8.5	132.0	123.1 ± 7.0	132.0

Values reported as activity found are the average of triplicate analyses.

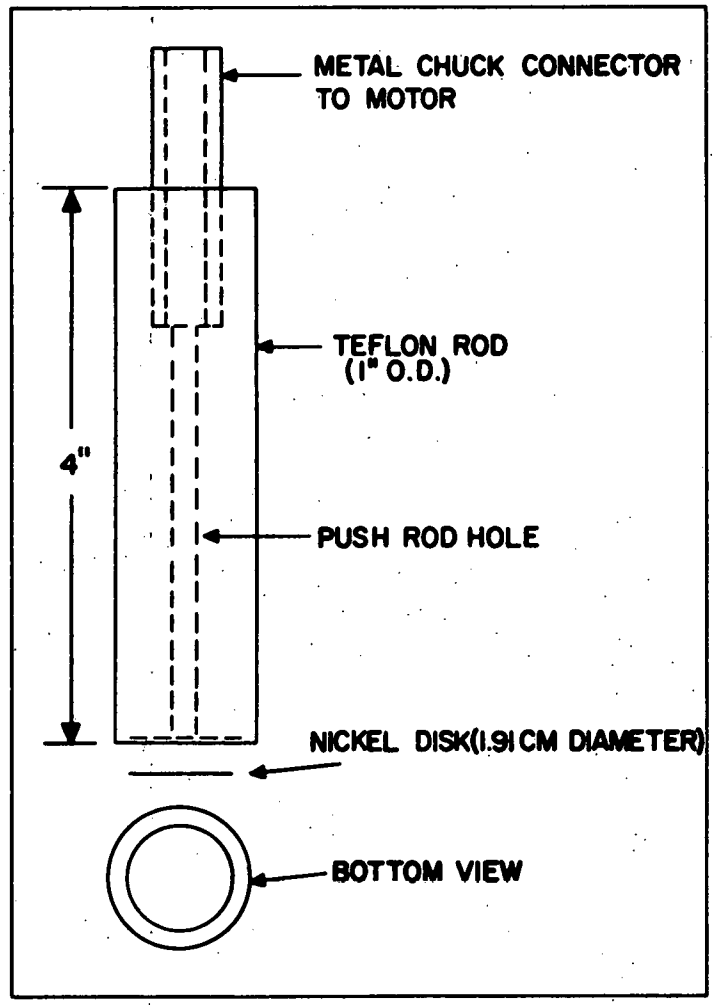


Figure 1. Electrode Holder

Figure 2. Alpha Spectra Generated by Counting a Plated Disc on the Alpha Spectroscopy System

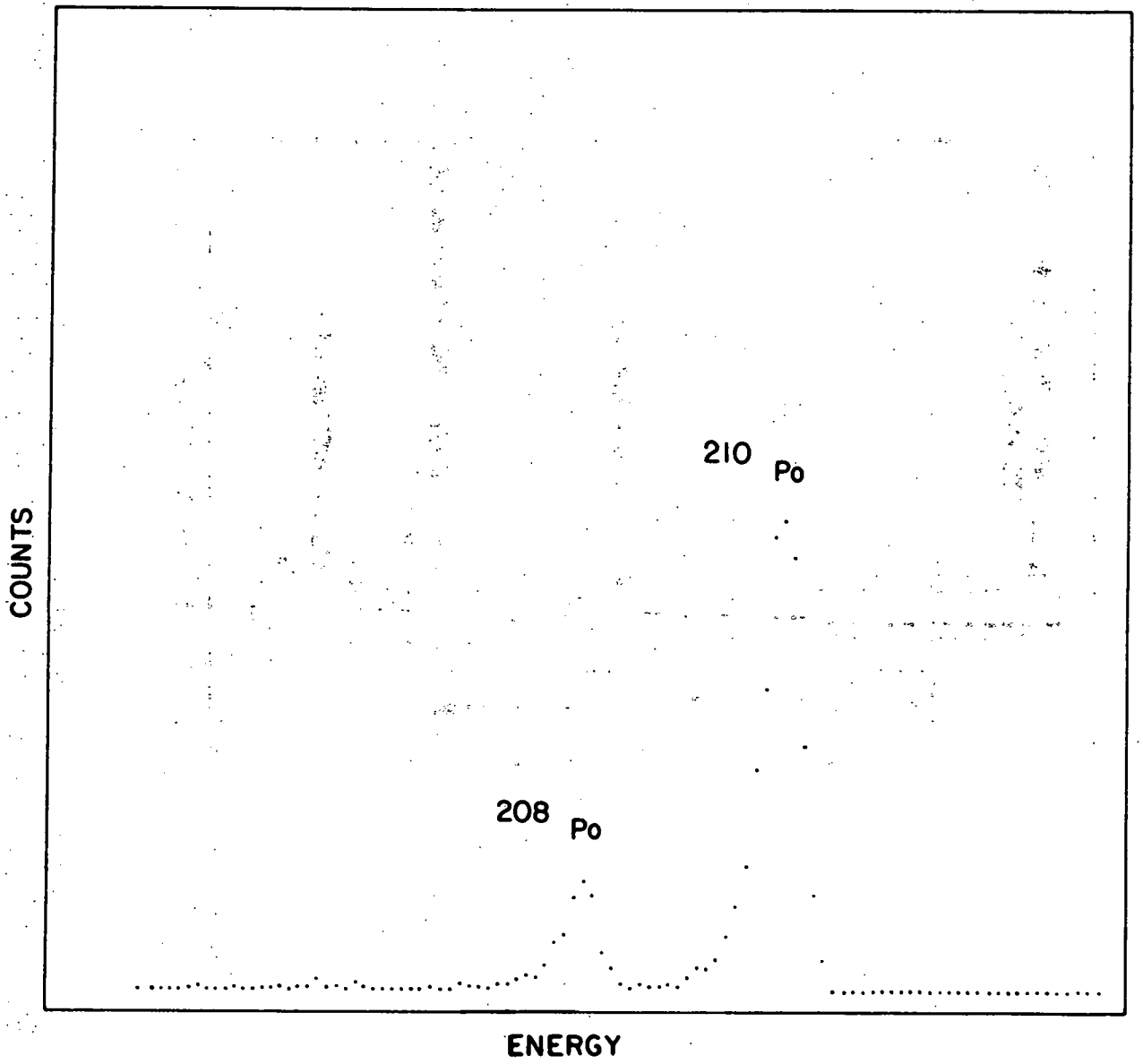
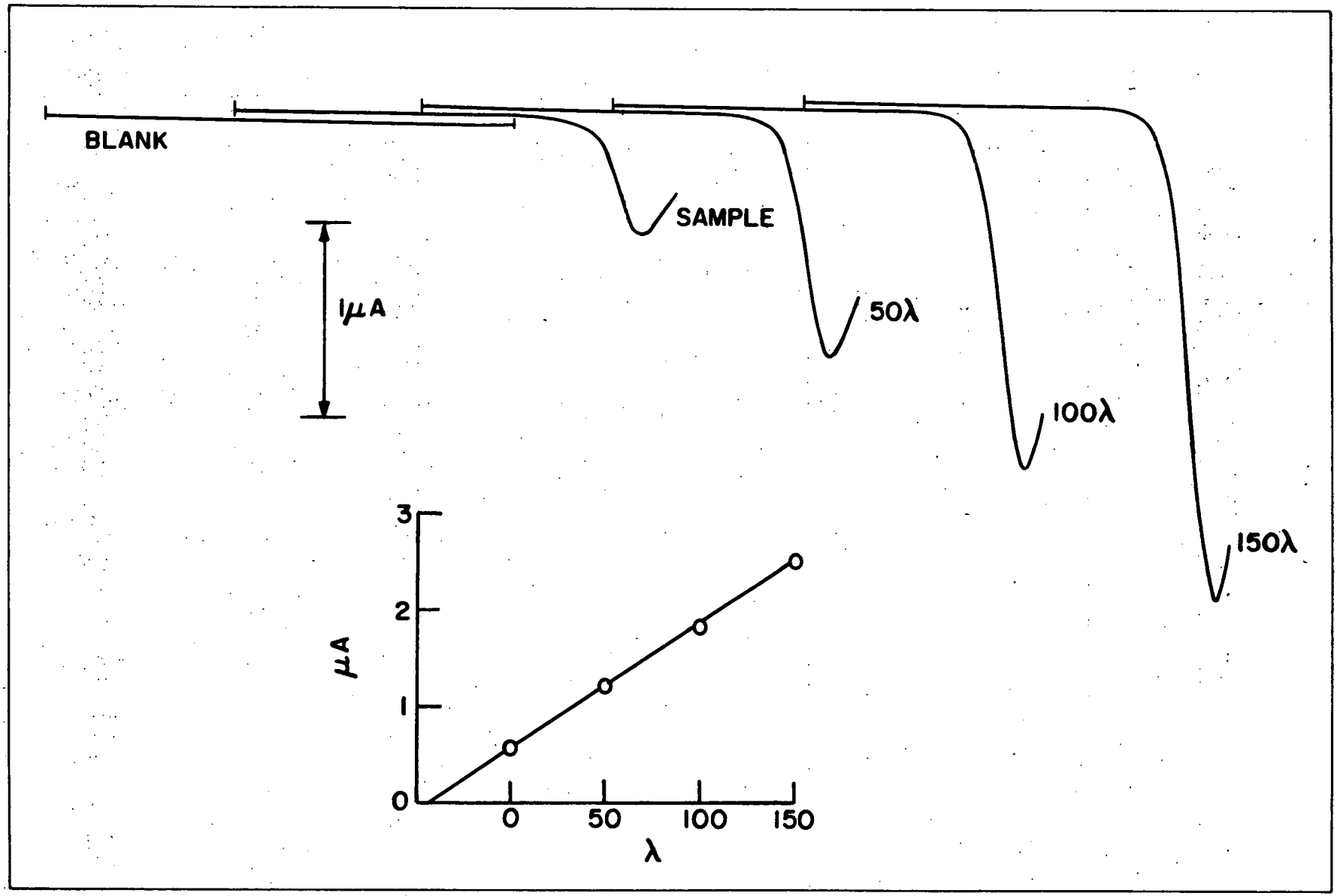


Figure 3. A Voltammogram and Resulting Plot of Anodic Stripping Peak Current vs. Standard Volume for a Typical Sample.



REFERENCES

1. Harley, J. H., ed., HASL-300 Procedures Manual, and Supplements 1-4, Health and Safety Laboratory, U.S. Atomic Energy Commission, New York, 1974.

2. Thatcher, L. L., V. J. Janzer, and K. W. Edwards, Methods for Determination of Radioactive Substances in Water and Fluvial Substances, USGS 024-001-02928-6, 1977.

3. Dillard, J. W., and B. B. Hobbs, Galvanic Deposition of ^{210}Po at a Rotating Nickel Disc Electrode (in press).

4. Copeland, T. R., and R. K. Skogerboe, Anodic Stripping Voltammetry, Anal. Chem. 46 (14), 1257A-1268A, December 1974.

NUCLEAR METHODS
IN
ENERGY RESEARCH

Session Chairman

W.S. Lyon

DEVELOPMENT OF NOVEL RADIOCHROMATOGRAPHIC TECHNIQUES FOR INVESTIGATION OF TRACE ELEMENT BEHAVIOR IN COAL LIQUEFACTION

R. H. Filby, A. K. Das Gupta and D. D. Barbee

Nuclear Radiation Center
Washington State University
Pullman, Washington 99164

ABSTRACT

A Ge(Li) detector and ND 6620 gamma-ray spectrometer system have been coupled to a liquid chromatograph to provide on-line continuous monitoring of radionuclides in the chromatographic effluent. The high resolution of the Ge(Li) detector allows the simultaneous detection and measurement of radionuclides eluting simultaneously from the LC column. The technique has been applied to the separation and determination of ^{65}Ni, ^{60}Co, ^{64}Cu, ^{69m}Zn, and ^{56}Mn by anion exchange on DOWEX 1 in HCl solutions, to the separation of metal chelates on SiO_2, and to the separation of short-lived radionuclides, ^{60m}Co, ^{52}V, ^{27}Mg, and ^{266}Cu on anion exchanger.

INTRODUCTION

For the past five years, this laboratory has conducted a study of the fate of trace elements present in coal in the Solvent Refined Coal (SRC) processes operated on a pilot plant scale by the Pittsburg & Midway Coal Mining Company under contract with the U.S. Department of Energy. The behavior of 34 elements, including the environmentally important elements Hg, Se, As, and Sb, in the SRC I process (solid product) and the SRC II process (liquid products) have been determined by instrumental neutron activation analysis and the results have been reported in the literature (1-5). Recent work (6,7) has shown that the elements Hg, Se, As, Sb, and possibly Co, Ni, Mn and Fe can behave as volatile species in the SRC process and the nature of the volatile species of these elements is not presently known, except for Hg in which there is strong evidence for the presence of Hg^o. In addition, recent work (7) has shown the probable presence of organically combined forms of Ti, V, As, Br, Sb and possibly other elements. Whether these moieties are true organometallic compounds containing C-metal bonds, are chelate type complexes involving O, N, or S functional groups, or are metal salts of organic acids formed in the liquefaction

process is not clear. Table 1 lists potential volatile species of Hg, As, Se, Sb, Fe, Ni, Cr, and Ti and possible organic species of these elements. Considerable research remains to be done to determine the structures and identities of these compounds in liquefaction processes since they have potential environmental importance, play a catalytic role in the process, or may act as catalyst poisons in further treatment of the products (e.g., hydrorefining or hydrodesulfurization).

Table 1: Possible Environmentally Important Forms of Some Trace Elements During Liquefaction

Element	Volatile Species	Organic Species
As	AsH_3, $AsCl_3$, $AsBr_3$ As_2, As_4	$RAsH_2$, RR^1AsH R_3As, $R_4As^+X^-$
Sb	SbH_3, $SbCl_3$, $SbBr_3$	$RSbH_2$, RR^1SbH, R_3Sb
Hg	Hg metal, Hg_s	R_2Hg, RHg^+X^-
Se	H_2Se, Se^o	$R\text{-}Se\text{-}R^1$, $R\text{-}SeO_3H$
Fe	$Fe(CO)_5$, $Fe_2(CO)_9$	$Fe(C_6H_5)_2(CO)_x$, $Fe(C_5H_5)_2$
Ni	$Ni(CO)_4$	Ni-asphaltene bonds
Cr	$Cr(CO)_6$	$Cr(C_6H_6)(CO)_3$, $(C_6H_6)_2Cr$
Ti	$TiCl_4$	$Ti(C_5H_5)_2Cl_2$, $Ti(OC_6H_5)_4$

R and R^1 - aliphatic or aromatic groups

Although some information about organic forms of Ti in SRC I has been obtained from conventional chromatographic separations (e.g., GPC, HPLC) no discrete complexes have been identified. The major problem is that, except for Ti, the concentrations of the individual elements in the SRC products (e.g., solid SRC I, liquid SRC II products) are in the ppb to ppm range which makes the separation, isolation, and identification of individual complexes of elements of interest almost impossible by conventional techniques (e.g., UV spectroscopy). Understanding the chemistry of formation of such metal complexes is also complicated by the lack of knowledge of the actual chemical species of the elements in the original coal. For some minor elements, e.g., Fe, Ti, Ca, Mg, etc., discrete minerals in coals are observed but for most trace elements (e.g., Hg, Se, Sb) discrete minerals may not normally be present and the particular element may exist in several combinations, both organic and inorganic.

In order to study the behavior of trace elements in coal liquefaction a project is underway to study coal liquefaction under controlled laboratory

conditions and to introduce specific compounds or minerals of elements of interest to determine reaction paths and rates. Such compounds or minerals added ll be labelled with a radionuclide of the element obtained either by chemical incorporation or by neutron irradiation. Reaction of the labelled species under controlled hydroliquefaction conditions yields products that may be separated and the reaction products of the labelled elements may be determined uniquely and to a high degree of sensitivity by radiometric determination of the radioactive tag. Since a number of elements (and nuclides) may be involved, high resolution γ-ray spectroscopy with Ge(Li) detectors was the method chosen for radioactivity determination. Both GPC and HPLC have been used for the characterization of metal species in such products for the reasons listed above. A number of element-specific detectors have been developed for GC and HPLC. Such detectors include flame AAS, flameless AAS, electrochemical detectors, and Ar plasma emission spectroscopy. In this paper we report the development of a radioactivity detector for multinuclide determination in GPC or HPLC column effluents.

The technique of radiochromatography is based on the detection of a radiolabelled compound in a mixture separated by conventional chromatographic techniques. Procedures have been reported for radio-GC, radio-TLC, radio-paper chromatography, radio-electrophoresis, and radio-column chromatography (LC, HPLC, GPC, etc.). A recent review has been published by Roberts (8). Most applications have involved compounds labelled with ^{3}H, ^{14}C, ^{32}P or ^{131}I, but several studies involving ion-exchange chromatography have utilized other radionuclides, e.g., rare earth nuclides, transuranium elements. Table 2 lists the major areas of radiochromatography and methods of radioactivity detection. Although most applications to multinuclide (other than ^{3}H, ^{14}C) chromatography have employed collection and analysis of chromatographic fractions, on-line detection systems based on flow-through scintillation detectors (9), GM counters (10) and NaI(Tl) scintillation detectors (11) have been developed. None of the systems reported to date have utilized the extremely high resolution of Ge(Li) spectroscopy for on-line column chromatography. The system reported here was developed for the identification of metal-organic complexes tagged with radionuclides but has also been applied to the anion-exchange separation of Ni, Co, Cu, Zn and Mn and to the rapid separation and measurement of the short-lived radionuclides ^{60m}Co, ^{52}V, ^{27}Mg and ^{66}Cu.

TABLE 2: Types of Radiochromatography

Chromatography Type	Detection Techniques	Applications
Paper (PC)	GM scanner; liquid scintillation; proportional	Mostly to ^{3}H, ^{14}C, or ^{32}P labelled compounds
Thin Layer (TLC)	Autoradiography; liquid scintillation; GM; proportional	Labelled compounds; metabolic studies
Electrophoresis	As for TLC	Labelled compounds ^{3}H, ^{14}C
Gas (GC)	GM; proportional; liquid scintillation; NaI(Tl) on-line measurements	^{14}C and ^{3}H in metabolic pathway studies; pesticides
Column (LC)	Liquid scintillation; NaI(Tl); GM; proportional; on-line measurements possible	Both aqueous and organic phases. Pesticides, drugs, radiopharmaceuticals; ^{3}H, ^{14}C, ^{99m}Tc. Fission products; rare earths; actinides
High Performance (HPLC)	Liquid scintillation - heterogenous and homogeneous; on-line measurement	^{3}H, ^{14}C compounds

EXPERIMENTAL

Radionuclides

Experimental details of the four separation procedures reported here are described elsewhere (12,13,14). In the results reported here, anion exchange on Dowex 1-X8 in aqueous HCl was used for separation of Ni, Cu, Co, Zn, and Mn and for the separation of Mg, V, Cu, and Co. Adsorption chromatography on deactivated SiO_2 was used for the separation of metal acetylacetonates and the separation of Cu chelates in organic solvents. Table 3 lists the separations and pertinent experimental conditions.

All radionuclides were made by irradiation of oxides or carbonates in the WSU TRIGA III type reactor at a neutron flux of 6.0×10^{12} neutrons cm^{-2} sec^{-1} and solutions of species to be separated by anion exchange were prepared in 11 M HCl for Ni^{2+}, Co^{2+}, Cu^{2+}, Mn^{2+}, and Zn^{2+} and in 8M HCl for the separation of Mg^{2+}, VO^{2+}, Cu^{2+} and Co^{2+} after suitable adjustment of valence states. Organic complexes to be separated by SiO_2 adsorption chromatography were prepared as described elsewhere (13).

TABLE 3: Separations Used in Radiochromatographic Experiments

Species Separated*	Substrate	Solvents	Radionuclides Used
$^{2+}$, Co^{2+}, Cu^{2+}, Mn^{2+}, Zn^{2+}	Dowex 1-X8	$HCl-H_2O$	^{65}Ni, ^{60}Co, ^{64}Cu, ^{56}Mn, ^{69m}Zn
Mg^{2+}, VO^{2+}, Cu^{2+}, Co^{2+}	Dowex 1-X8	$HCl-H_2O$	^{27}Mg, ^{52}V, ^{66}Cu, ^{60m}Co
$Cr(acac)_3$, $Co(acac)_3$, $Cu(acac)_2$, $Mn(acac)_3$	SiO_2	Toluene, acac, MeOH, MeCN, Et_3N	^{51}Cr, ^{60}Co, ^{64}Cu, ^{56}Mn
$Cu(acac)_2$, $Cu(DDTC)_2$, $Cu(oxine)_2$	SiO_2	$CHCl_3$, EtOH, MeOH, acac, Et_3N	^{64}Cu

*acac = acetylacetone, $CH_3COCH_2COCH_3$

DDTC = $(C_2H_5)_2NCS_2^-$ Oxine = 8-hydroxyquinoline

Radiochromatography

A schematic diagram of the radiochromatography system is shown in Figure 1. The system consists of a conventional low pressure liquid chromatography unit with solvent reservoirs for gradient elution, column, and a UV monitor set at 254 nm (ISCO Model UA-5). The effluent from the UV monitor then passes to a special flow cell of coiled teflon tubing (0.9 mm id) of 75 µl total volume. This flow cell is mounted on the face of a large volume Ge(Li) detector and designed so that both inlet and outlet tubes are shielded from the detector by Pb shielding. The detector is coupled to an ND 6620 γ-ray spectrometer system as shown in Figure 2.

During the separation of the species of interest, the ND 6620 collected spectral data 0 - 2048 keV in ADC 1 in 30 or 60 sec count intervals (clock time) depending on the flow rate (0.5 - 2.0 ml/min), radionuclide activity, and resolution of the column. After the count period had elapsed the analyzer was switched electronically to ADC 2 and a further count period collected. The contents of ADC 1 memory region were transferred to 9-track IBM compatible tape. The transfer time between ADC 1 and ADC 2 has a maximum value of 100 msec which results in a relative activity loss of <0.33% for a 30 sec count and <0.16% for 60 sec count period. Data collected were stored, analyzed by PKSEARCH (Nuclear [illegible]) and the PKSEARCH data stored. Final data in the form of a chromatogram were obtained by plotting peak areas corresponding to given radionuclides as a

function of time (or volume) after correction for live time and decay or the data were transferred to the WSU Amdahl 470 computer for simulated three-dimensional plots of peak area, peak energy, and time (or volume). A flow diagram of the software is shown in Figure 3.

RESULTS AND DISCUSSION

A chromatogram of the separation of ^{65}Ni, ^{56}Mn, ^{60}Co, ^{64}Cu, and ^{69m}Zn is shown in Figure 4. The chromatogram shows that ^{65}Ni is eluted with 10M HCl, ^{56}Mn and ^{60}Co elute with virtually overlapping peaks with 3.5M HCl, ^{64}Cu elutes with 0.1M HCl and ^{69m}Zn with 3M NH_3. Although the Co and Mn elute together quantitative activities (hence concentrations) were obtained for both radionuclides.

A chromatogram for the separation of short-lived radionuclides is shown in Figure 5. In this it can be seen that ^{27}Mg and ^{52}V elute without absorption (present as cationic specious Mg^{2+} and VO^{2+}) and that ^{60m}Co and ^{66}Cu are well separated.

The application of the technique to the separation of the acetylacetonates of Cr^{3+}, Co^{3+}, Cu^{2+} and Mn^{3+} is shown in Figure 6. Figure 7 shows a similar separation of the Cu^{2+} species $Cu(acac)_2$, $Cu(DDTC)_2$, and $Cu(oxine)_2$. The small peak following the elution of $Cu(DDTC)_2$ is probably due to the formation of a mixed ligand complex.

Efficiency of Detection

Sieswerder, Poppe and Huber (15) have considered flow versus static efficiencies in column radiochromatography using a well-type NaI(Tl) detector. Considering a single radionuclide eluting to give an approximately Gaussian elution curve, the flow efficiency, E_f is given by

$$E_f = \frac{A_t}{A_o}$$

where A_o = Total activity in photons/min of peak of energy E_γ of given nuclide in injected volume

A_t = Integrated area of peak at energy E_γ (in photons/min)

The flow efficiency, E_f, is related to the static efficiency, E_s, by

$$E_s = E_f \frac{F}{V_c}$$

where F = flow rate through the cell (ml/min)

V_c = effective volume of the cell (ml)

and

$$E_s = \frac{E_f}{t_d}$$

where $t_d = \frac{V}{F}$ = mean residence time in the cell.

It can be seen that the flow efficiency is dependent on the flow rate. Calibration curves for the Ge(Li) detector-flow cell system are shown for flow rates 0.67 ml/min and 1.05 ml/min in Figure 8.

Using the calibration data the detection limits for radionuclides separated by anion exchange under the experimental conditions employed are shown in Table 4.

TABLE 4: Detection Limits for Radionuclides Separated by Anion Exchange on Dowex 1-X8

Nuclide	E_γ (keV)	Branching Ratio(B.R)	E_f	Detection Limit(nCi)
^{51}Cr	320	0.098	2.7×10^{-3}	85
^{69m}Zn	439	1.0	2.0×10^{-3}	11
^{64}Cu	511	0.38	1.7 a 10^{-3}	84
^{56}Mn	847	1.0	1.1×10^{-3}	21
^{65}Ni	1115	0.148	0.8×10^{-3}	190
^{60}Co	1173	1.0	0.8×10^{-3}	30

E_f = Flow Efficiency

$$\text{Detection Limit} = \frac{50}{(E_f)\,(B.R)\,(60)(3.7 \times 10)} \text{ nCi}$$

Minimum peak areas detectible = 50 counts/chromatographic peak

REFERENCES CITED

1. R. H. Filby, K. R. Shah, and C. A. Sautter, J. Radioanal. Chem. 37, 693 (1977).

2. R. H. Filby, K. R. Shah, M. L. Hunt, S. R. Khalil, and C. A. Sautter, U.S. Department of Energy Report, FE-496-T-17 (1978).

3. R. H. Filby, S. R. Khalil, and M. L. Hunt, Interim Report on Trace Elements in the SRC Processes, U.S. DOE Report. (In Press.)

4. R. H. Filby and B. S. Carpenter, Trans. Amer. Nucl. Soc. 27, 162 (1977).

5. R. H. Filby and S. R. Khalil, Proc. Symposium on Potential Health and Environmental Effects of Synthetic Fuel Technologies, (ORNL), Gatlinburg, p. 102, U.S. DOE Report CONF-780903 (1979).

6. R. H. Filby, K. R. Shah, F. Yaghmaie, S. R. Khalil, A. K. Das Gupta, C. A. Palmer, C. S. Weiss, M. R. Flatbush, M. L. Hunt, and C. A. Grimm, Determination of the Nature and Amounts of Certain Non-Hydrocarbon Constituents in the Products and By-Products of Prospective Processes for Producing Petroleum Substitutes from Coal and Oil Shale. Final Report to U.S. Env. Prot. Agency. (In Press.)

7. R. H. Filby, unpublished data.

8. T. R. Roberts, "Radiochromatography," J. Chromatography Library Volume 14 Elsevier (1978).

9. L. Schutte and E. B. Koenders, J. Chromatography 76, 13 (1973).

10. M. C. Corfield, S. Dilworth, J. C. Fletcher, and R. Gibson, Int. J. Appl. Radiat. Isotop. 5 , 42 (1959).

11. W. Weinlander and G. Hohlein, Kerntechnik 10, 563 (1968).

12. A. K. Das Gupta, Ph.D. Thesis, Department of Chemistry, Washington State University (1980).

13. A. K. Das Gupta, R. H. Filby, and D. B. Barbee, Anal. Chem. (in preparation).

14. A. K. Das Gupta, D. B. Barbee, and R. H. Filby, J. Radioanal. Chem. (in preparation).

15. G. B. Sieswerda, H. Poppe, and J. F. K. Huber, Anal. Chim. Acta 78, 343 (1975).

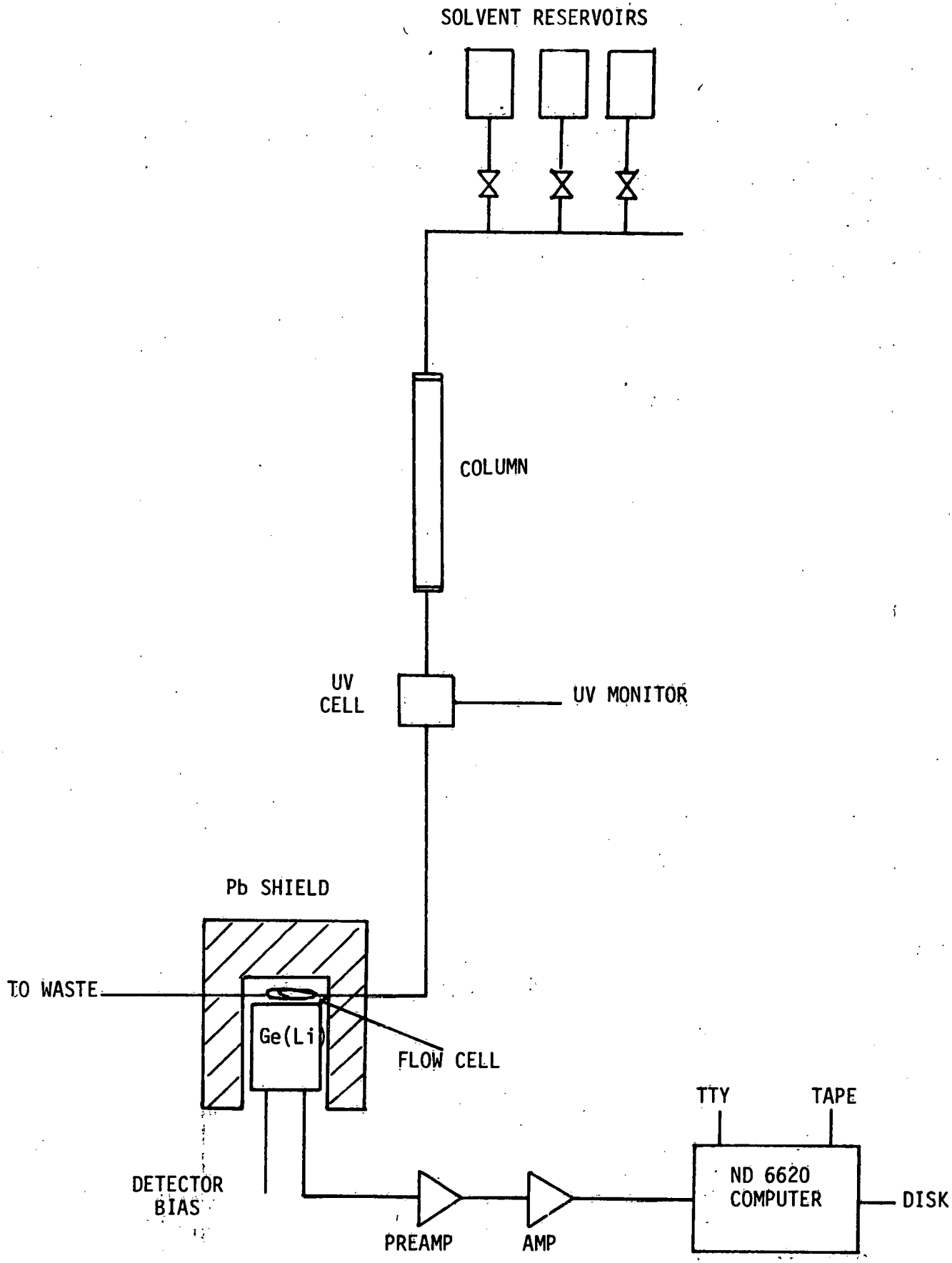


Figure 1: Schematic Diagram of ND6620-Based Radiochromatography System.

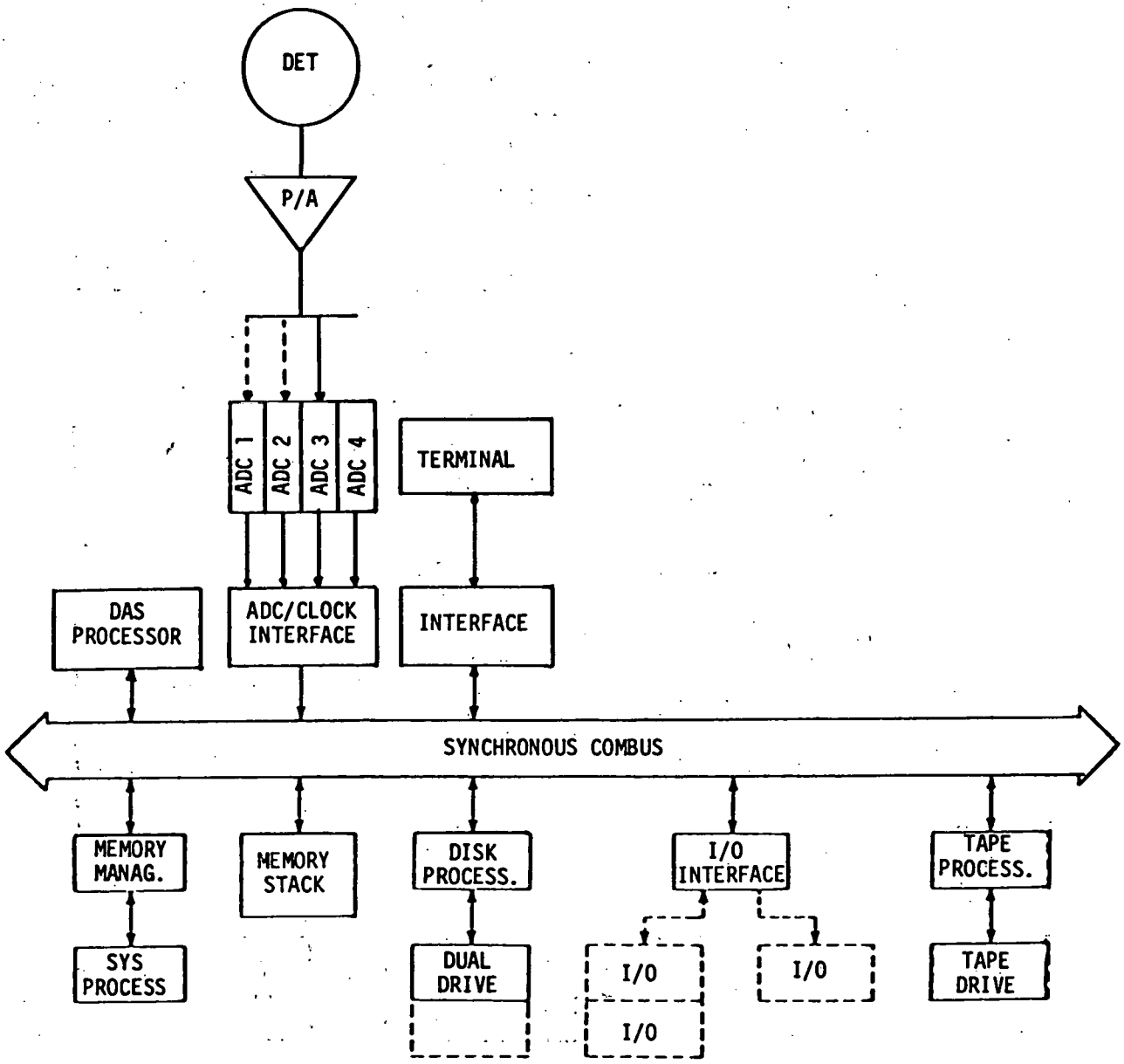


Figure 2: Schematic Diagram of the ND6620 Gamma-Ray Spectometer

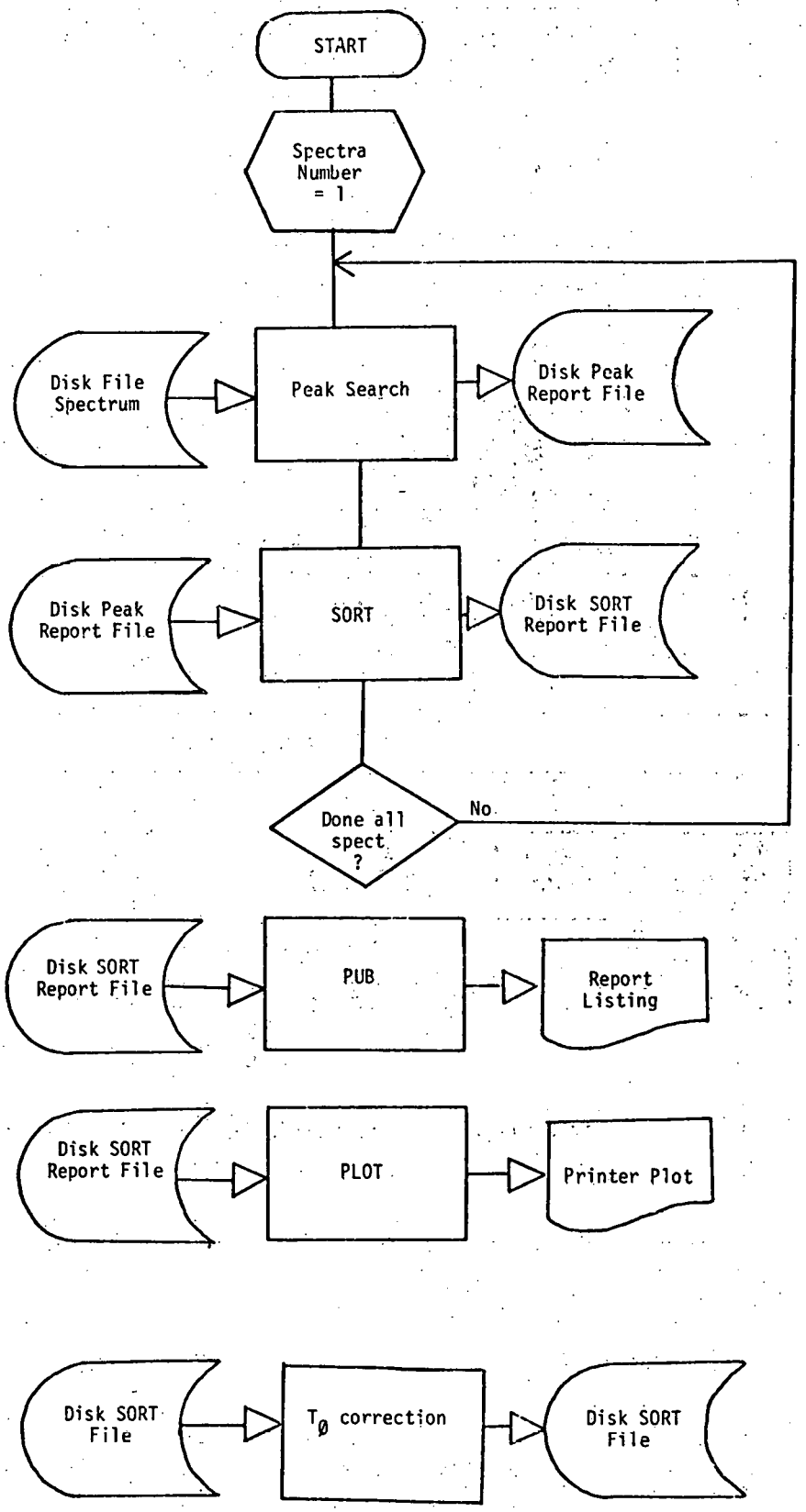


Figure 3: Flow Diagram of ND6620 Software Used in Radiochramatography

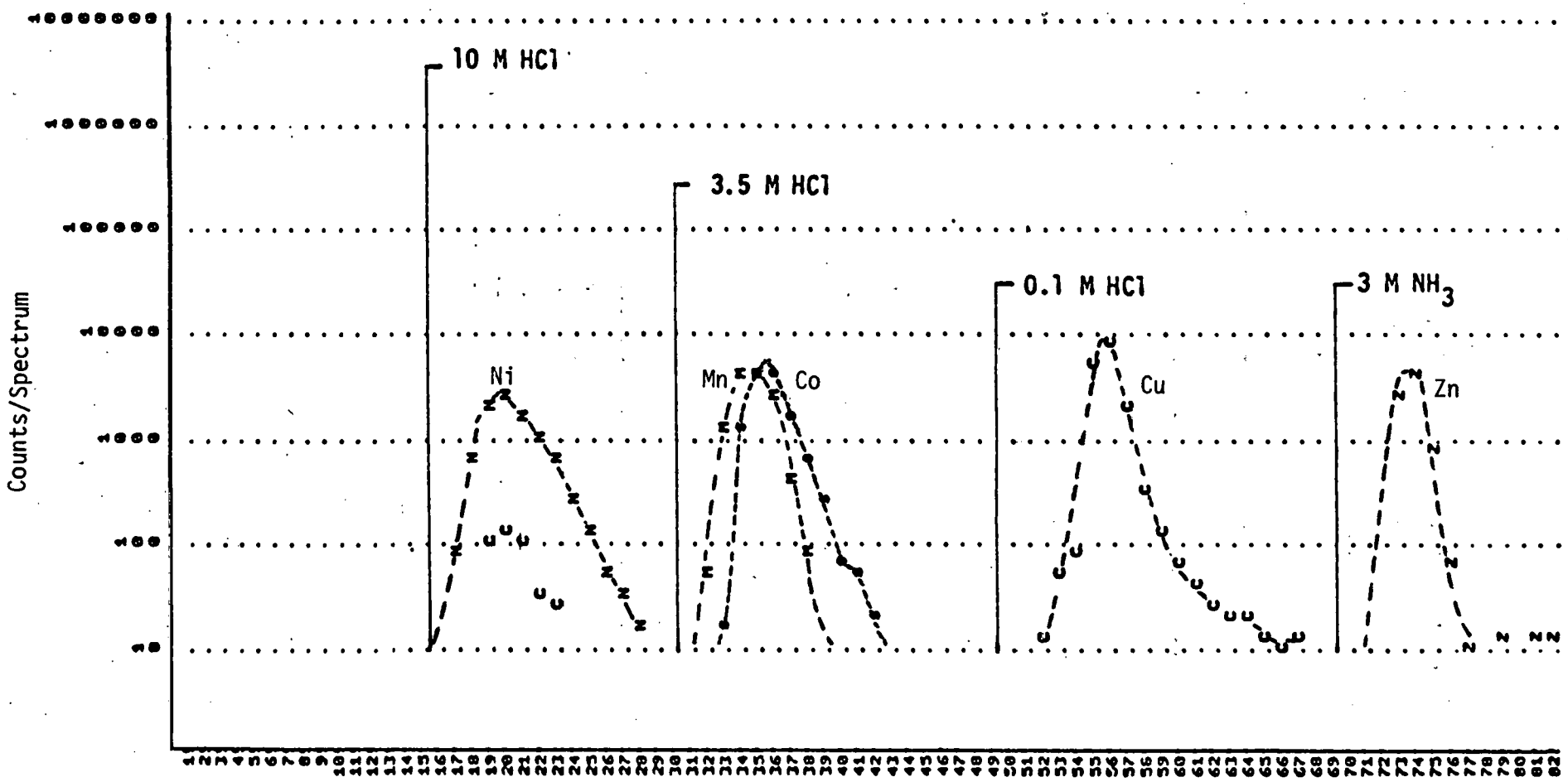


Figure 4: Elution Chromatogram for Ni, Mn, Co, Cu and Zn on Dowex-1 in HCl-H_2O

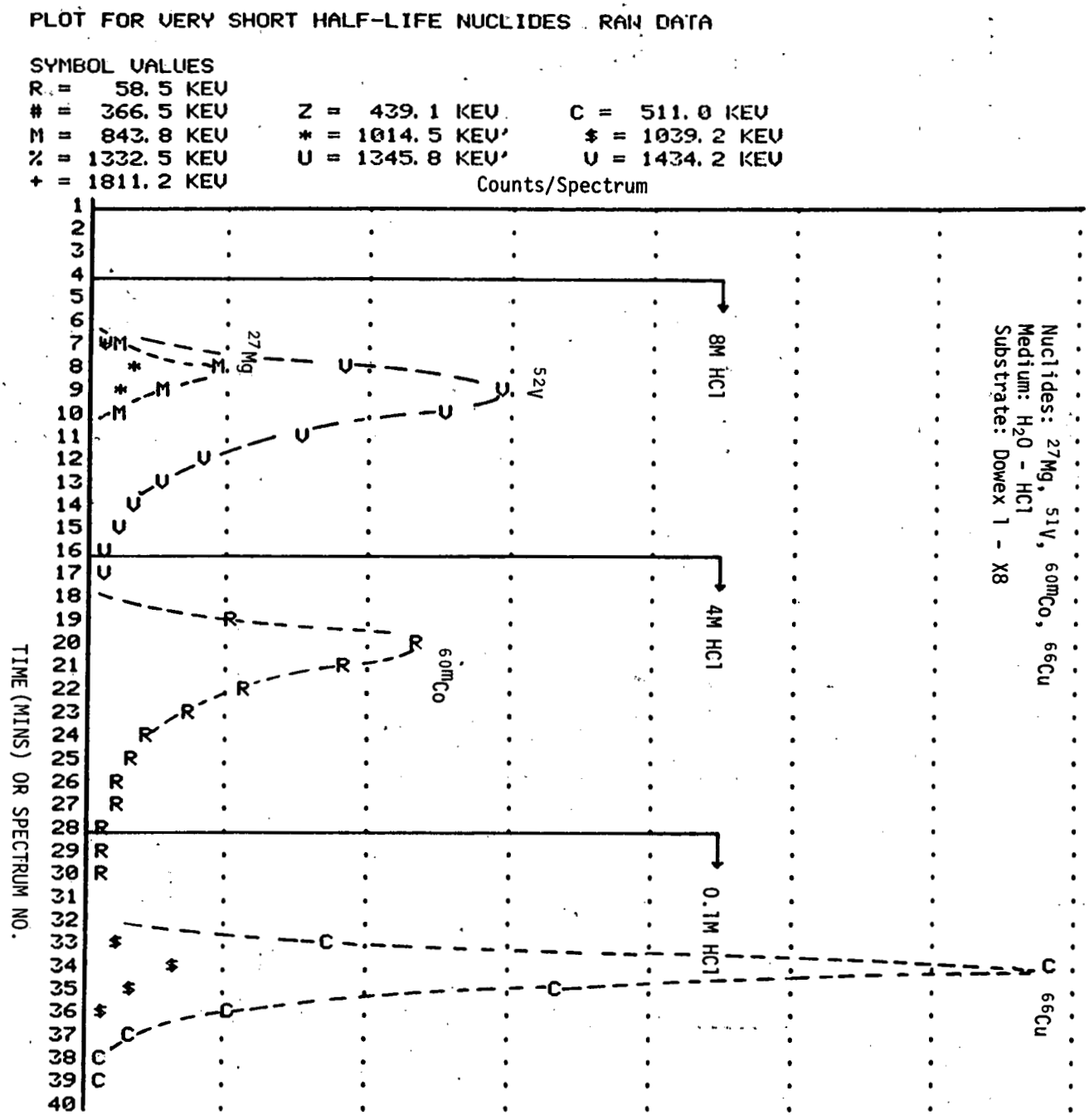


Figure 5: Elution Chromatogram of V, Mg, Co, and Cu on Dowex-1 in HCl-H_2O

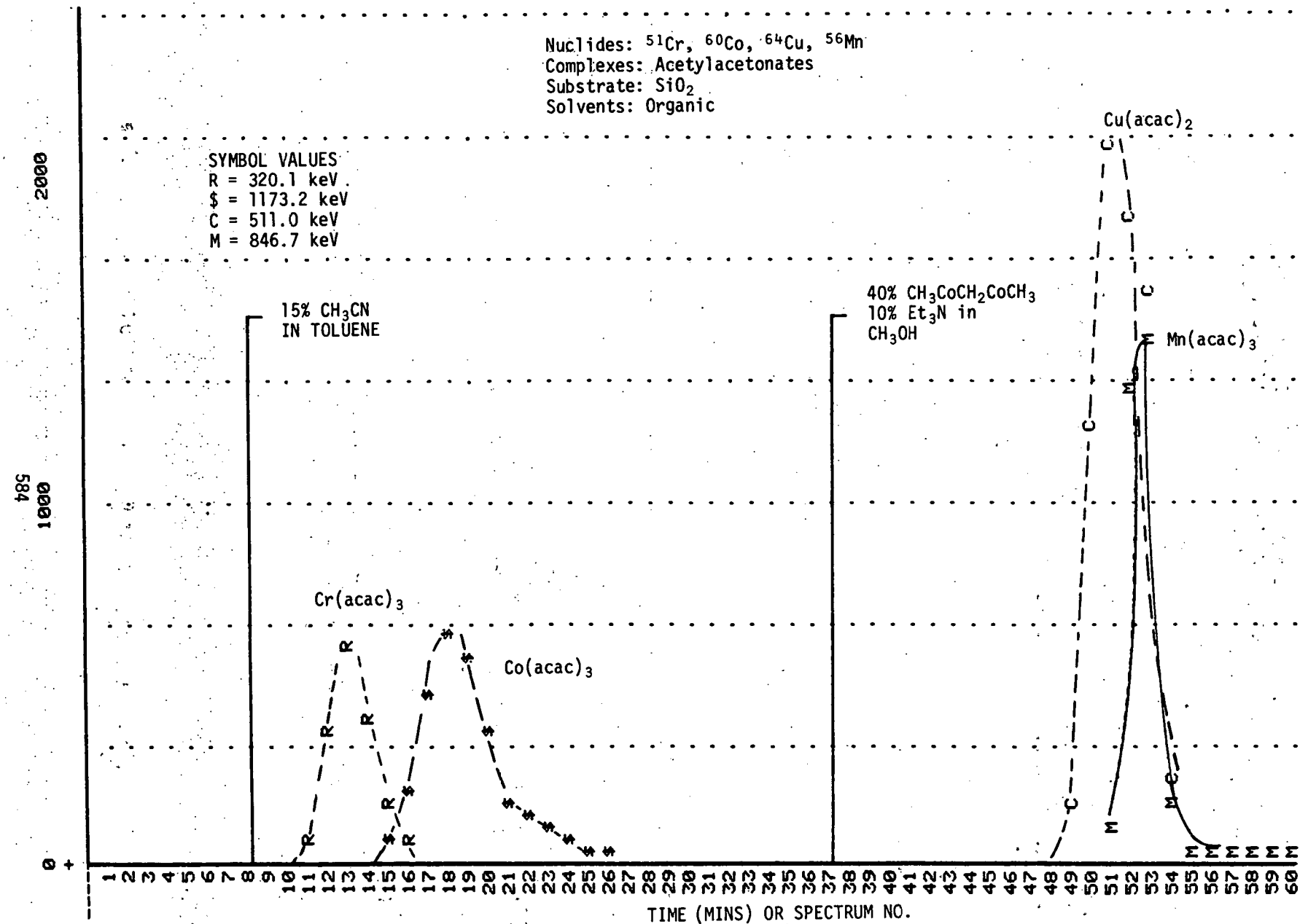


Figure 6: Elution Chromatogram of Acetylacetonates of Cu, Cr, Co, and Mn and SiO_2

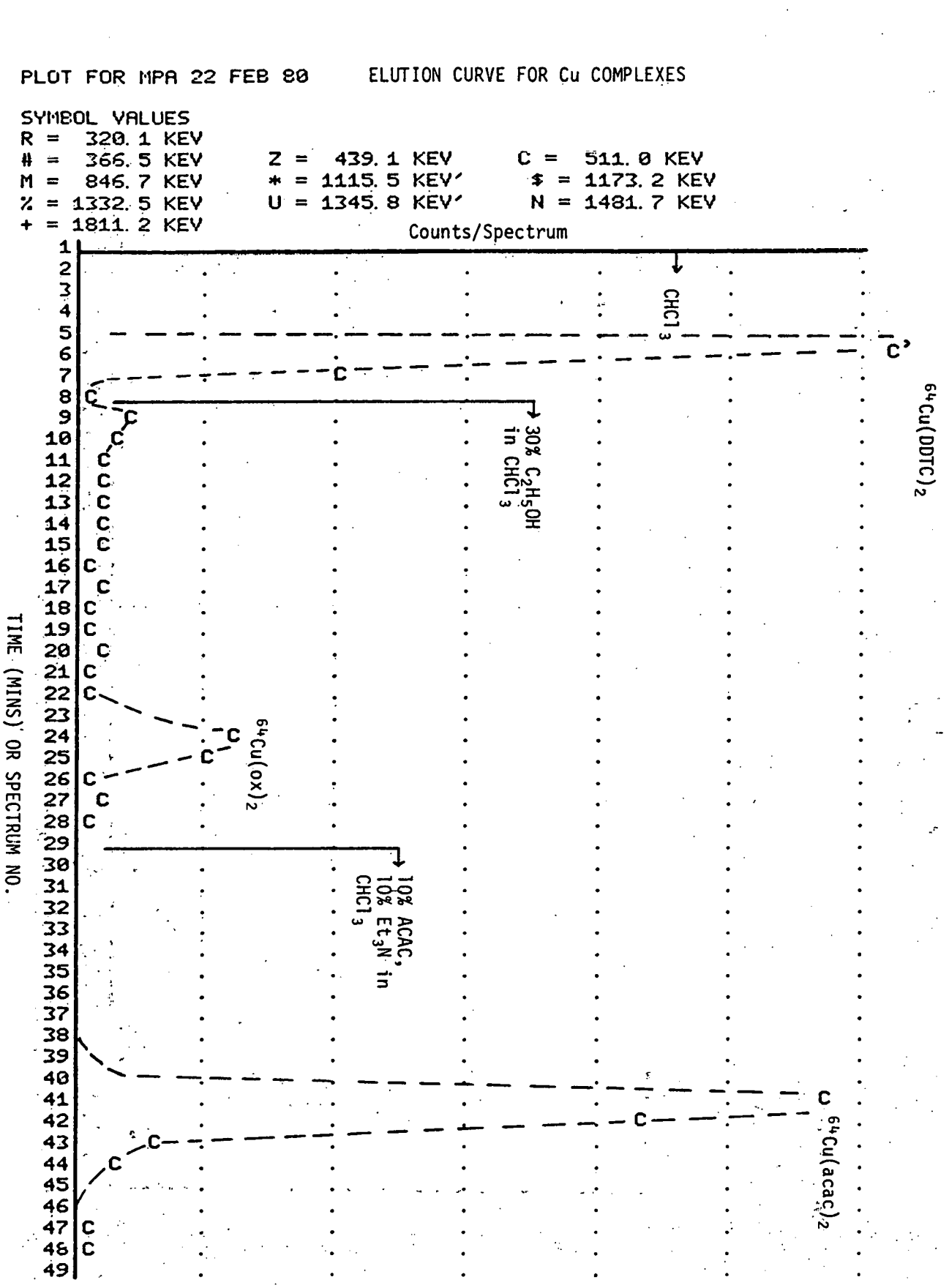


Figure 7: Elution Chromatogram of $Cu(acac)_2$, $Cu(DDTC)_2$ and $Cu(oxine)_2$ Compexes on SiO_2

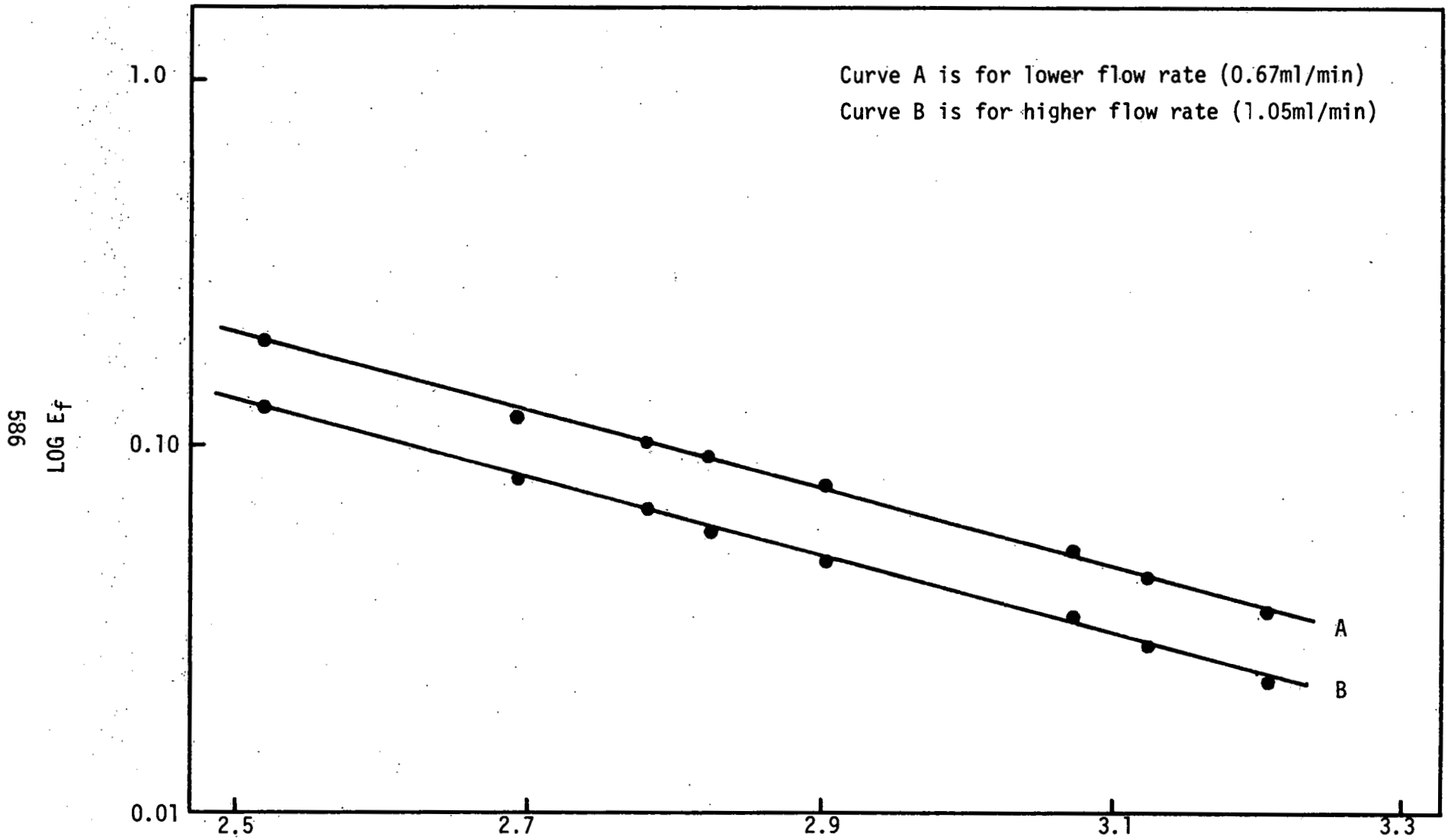


Figure 8: Calibration Curve for Ge(Li) Detector at Two Flow Rates

NUCLEAR METHODS IN COAL RESEARCH

W. S. Lyon
Analytical Chemistry Division
Oak Ridge National Laboratory*
Oak Ridge, TN 37830

ABSTRACT

Nuclear methods, particularly neutron activation analysis (NAA) provide useful information about elemental constituents in coal and fly ash, but often other techniques are required to supplement NAA data. Spark source mass spectrometry and atomic absorption have been studied as methods for determination of certain elements in coal that are not easily measured by NAA. In work concerned with the chemical speciation of elements in fly ash, a number of analytical techniques have been used; these include NAA, chemical etching and separation, optical and electron microscopy and x-ray diffraction.

INTRODUCTION

Coal is to become increasingly important in energy production in this country. Nuclear methods of analysis are making significant contributions to our understanding of coal composition, coal combustion, and the structure and composition of fly ash. Neutron activation analysis (NAA) is the most useful and universally applied nuclear analytical technique, but the complex chemical problems associated with coal utilization are not going to be solved by application of NAA or any other single technique. Rather, instead, the analytical chemist must be knowledgeable in many aspects of his discipline and should be able to choose from a battery of methods those that can best help solve his problem.

This paper presents examples of two such multi-disciplinary approaches: (1) comparison of several analytical methods for trace elements in coal difficult to determine by NAA and (2) use of old fashioned wet chemistry, optical and scanning microscopy, and chemical inference for the elucidation of the chemical speciation of elements in fly ash.

STATISTICAL STUDY OF METHODS FOR SOME DIFFICULT ELEMENTS

In the course of a 15-month study of trace elements in coal from three different steam plants (1), we decided to make some comparisons between several analytical techniques that might be used for elements not easily determined by NAA.

*Research sponsored by the Office of Energy Research, U. S. Department of Energy under contract W-7405-eng-26 with the Union Carbide Corporation.

Isotope dilution spark source mass spectrometry (IDSSMS) was compared with instrumental neutron activation analysis (INAA) for determination of Ba, Cr, Sr, and As. For IDSSMS a known weight of a mixture of stable isotopes to be used as tracers was added to a sample of ground coal. The stable isotopes plus sample were homogenized and then fired in the RF arc of the spark source mass spectrometer. The intensities of the lines of the isotopes present were measured, and the concentrations of these elements in the coal were obtained by comparing the intensities of the lines from the known added enriched stable isotopes to those of lines from the sought elements. An underlying assumption in this method is that sample and spike both volatilize in an identical manner.

Mercury was determined by flameless atomic absorption (AA). Arsenic was determined by an arc emission, atomic absorption method described in (3).

In a second series of special comparisons, AA was compared with IDSSMS for determining Zn, Cu and Pb. These data were not combined with the other since the comparisons were not run over the full 15 months.

Table I summarizes the results of a statistical comparison of the values obtained on coal samples by these methods. As can be seen from the significance probabilities, the agreement between INAA and IDSSMS is

TABLE I
Comparison of INAA with IDSSMS for Determination of Ba, Cr, and Sr, and with He Arc Emission for Determination of As

Procedure	N	$\bar{\chi}$ μg/g	σ	χ_{min} μg/g	χ_{max} μg/g	t	Significance Probabilities*
				Ba			
INAA	42	155.6	42.3	94	232	3.19	0.01
IDSSMS	42	132.3	46.0	40	220		
				Cr			
INAA	45	29.54	6.6	21	59	2.61	0.011
IDSSMS	45	24.91	10.6	7	48		
				Sr			
INAA	43	115.7	31.7	46	185	0.097	0.923
IDSSMS	45	114.9	37.6	44	230		
				As			
INAA	31	29.66	11.8	12.4	58	5.61	0.001
He Arc	31	36.24	13.3	16.2	65		

*Probability that the t value is due to chance alone. Values $\leq .01$ are taken as indicating a significant difference in the calculated means of the analytical results for a given element.

marginal for Ba and Cr but excellent for Sr. Barium is determined by activation through measurement of the 166 keV gamma-ray of 86-minute ^{139}Ba after a 20-minute decay. The Compton background is large due to the presence of other short-lived activities, and this could be a cause for error in the INAA method. Chromium is determined by measuring the 320 keV gamma-ray from 27.8 day ^{51}Cr after a long decay. No obvious explanation can be found for why this INAA value should be high. A possible cause for low values in IDSSMS is failure to volatilize spike and sample element at the same rate. Both the IDSSMS and INAA laboratories run the NBS coal standard (SRM #1632) and agreement between the laboratories for both Ba and Cr is usually within a few percent.

The INAA values for arsenic are all consistently lower than the He arc values, and although we have no explanation for this, we believe the AA values to be more reliable.

Table II gives results obtained on a 6-month trial comparison of AA versus IDSSMS for three elements. The purpose of this test was to see if AA could be used to reduce some of the sample load on the mass spectrometer. Here the significance probabilities show that the methods do give comparable results. Thus, it appears that the simpler and less expensive AA technique can replace IDSSMS for determinations of Cu, Zn, and Pb.

TABLE II
Comparison of AA and IDSSMS for Determination of Cu, Zn, and Pb in Coal

Procedure	N	$\bar{\chi}$ μg/g	σ	χ_{min} μg/g	χ_{max} μg/g	t	Significance Probabilities*
				Cu			
AA	23	21.77	1.73	17.3	25.0	1.18	0.25
IDSSMS	23	20.2	6.03	12	42		
				Zn			
AA	23	24.90	7.87	14.2	40	0.34	0.74
IDSSMS	23	24.09	8.46	10	40		
				Pb			
AA	23	13.22	4.67	8.2	30	1.33	0.19
IDSSMS	23	11.43	4.44	5.0	21		

*(See Table IV for explanation)

RESEARCH METHODS FOR STUDY OF THE CHEMICAL SPECIATION OF FLY ASH

At the Third International Conference on Nuclear Methods in Environmental and Energy Research (1977), this author stated, "Of these (problems) probably the most urgent, difficult and important is the development of speciation techniques". Since that time very little information has appeared on chemical speciation of trace elements in fly ash. In our group at ORNL Lester Hulett and co-workers have taken an indirect

approach to this problem. There is no "magic spectroscopy" with which one can unambiguously detect elements such as Cr, Ni, As, Pb, at the 100 ppm level and directly determine their chemical state. Therefore, Hulett used classical methods of chemical inference, taking the solids apart by physical (size fractionation and magnetic separation) and chemical (HF etching) methods. NAA was the primary tool then used to analyze these fractions. It is our thesis, based on chemical inference, that chemical species of trace elements in fly ash are largely determined by the matrix in which the elements are dissolved.

Fly ash from four TVA power plants was studied in these experiments, complete details of which are given in reference 4. These four plants used different firing conditions and different coals but results from all four were essentially the same. Ash was separated according to size and magnetic character. Most of the work reported here was done on four nonmagnetic 100-200 μm fractions and their 100-200 μm magnetic counterparts. One sample of nonmagnetic ash size <37 μm was also studied, and results agreed qualitatively with those obtained on the larger size samples. We, therefore, think our conclusions are applicable to all sizes of particles.

Seen before etching under the optical microscope the particles were qualitatively the same for all four ashes. We categorized them into four types:

1. Spheres and spherical shards--some were transparent and translucent, some were white-opaque, having solid cores, some were of the hollow cenosphere types.

2. White opaque oblong shapes--these had the general appearance of miniature pebbles.

3. Nonfused quartz sand particles--these particles had sharp edges and fracture surfaces. X-ray diffraction confirmed that they were quartz.

4. Carbon-cinder particles--these are very high in carbon and sulfur. Type-4 particles constitute a rather large weight percentage of the 100-200 μm size fraction for all four ashes.

The effect of etching was also qualitatively the same for the four different specimens studied. Concentrated HF consumed almost all the mineral components, leaving only the type-4 particles. In this manner we accounted for the carbonaceous material, so we could estimate the total aluminosilicate content of the four specimens.

Particles were etched with a 1% HF solution for 16-20 hours. The material removed by the etch is believed to be primarily glass; the noncarbonaceous residue is mostly crystalline mullite. Type-3 and 4 particles were relatively unaffected by the 1% HF etch. A large number of the type-1 and type-2 particles retained their overall shapes through the etching process, even though large percentages of their masses had been removed. We isolated collections of type-1 and type-2 particles for x-ray diffraction and scanning electron microscopy energy dispersive x-ray fluorescence (SEM-EDX) analysis. For all four ashes we found that the etched type-1 and type-2 particles produced very strong diffraction patterns corresponding to mullite. Some patterns also had weaker lines corresponding to quartz. The SEM-EDX spectra showed, for all four ashes, that the Si:Al ratio was reduced to a value corresponding to

mullite compositions. It is also significant that the hardness of the etched type-1 and type-2 particles was much less than for the unetched. The etched particles were easily crushed; the glass phase which cemented the mullite crystals together and gave the particles their strength was removed by the etching. Most of the nonetched particles resisted crushing. It is beyond the scope of this paper to discuss the morphology of these particles, but it is interesting to see the changes wrought in one of them by etching. Figure 1 shows an etched type-1 particle that contains a clustering of mullite crystals having the needle-form habit (acicular form). Etching has changed the Al:Si ratio in this particle from about 1:2 to 3:1, which is the ratio in mullite.

Glass and crystal phases of the nonmagnetic matrices were isolated from each other for separate elemental analyses. The dilute HF etching procedure was used for dissolving the glass phases, leaving mullite-quartz and C residues. The mullite quartz phases were then removed from the C with 48% HF. Aliquots of these extracts were evaporated to dryness in specially designed capsules and submitted for NAA. Portions of the remaining solutions were analyzed by atomic absorption. Element distributions between glass and mullite-quartz phases for Bull Run fly ash are listed in columns 1-2 of Table III. Weighted averages of columns 1-2 are entered in column 3, labeled "Mass Balance." These were calculated by multiplying the concentrations in columns 1 and 2 by the respective weight fractions of glass and mullite-quartz and summing. The mass balance data of column 3 of Table III can be compared with the total analysis data of columns 4 and 5. The data of column 4, labeled "Total Aluminosilicate" were obtained by extracting samples with 48% HF, in which all mineral matter was dissolved, leaving C behind. The concentrations of column 5 were measured by activation analysis only of combined aluminosilicate plus C.

Table III shows that the mullite-quartz phase is relatively pure and free of most of the trace elements. All of the alkali and rare earth elements are clearly more concentrated in the glass phases. All of the alkaline earth elements are also more concentrated in the glass phases with the exception of Mg. We think the Mg concentrations for the crystalline phases are too high. They do not agree with analyses of individual crystallites by SEM-EDX, in which no Mg was found. This discrepancy was probably caused by the extraction of Mg from C during the 48% HF dissolution of the quartz-mullite phase. We, therefore, make the generalization that the mullite-quartz phase is free of all +1 and +2 valent elements. This means that the majority of trace elements in the aluminosilicate matrix of fly ash are concentrated in the glass phases.

There are certain trace elements having +3 and +4 valences that are notable for their high concentrations in the mullite-quartz phases: Ti, V, Cr, Fe, Ga, and Zr. Vanadium is about equally distributed in the glass and crystalline phases while Cr and Ga are predominantly contained in the crystalline. All of these elements have ionic radii small enough to allow isomorphic substitution in the mullite lattice. Therefore we have the following inference about the chemical species of certain of the trace elements:

TABLE III

BULL RUN FLY ASH: ELEMENT DISTRIBUTIONS IN ALUMINOSILICATE PHASES
CONCENTRATIONS IN μg/g

	Glass Phase	Mullite-Quartz	Mass Balance	Total Alumina-silicate	Alumino-Silicate Plus carbon
Al	86262	203532	135513	143356	150700
Fe	19582	3358	12849	12644	13100
Si*	343000	287000	------	------	------
Na	1711	256	1107	1004	1000
K	25057	5274	16847	16333	17100
Rb	532	12	316	62	93
Cs	0	0	0.3	3	8
Mg	10418	15498	12526	12689	13900
Ca	------	0	------	-----	1800
Sr	798	174	539	889	180
Ba	319	69	215	163	365
Sc	31	7	21	20	18
Ti	10874	4626	8281	8378	8480
V	176	127	155	166	171
Cr*	169	311	227	255	225
Mn	87	9	55	56	53
Co	25	2	16	16	14
Ni*	174	78	134	172	------
Cu*	144	17	91	144	------
Zn*	209	17	129	155	------
Ga	0	12	8	0	7
As	42	2	26	25	24
Se	54	7	35	26	3
Mo	0	3	1	0	20
Cd*	0.32	0.27	0.3	0.5	------
Hf	6	3	5	4	6
Ta	3	1	2	2	2
W	4	1	3	3	4
Hg	8	1	5	3	0
Pb*	35	2	21	12	------
La	61	0	36	18	82
Ce	119	6	72	18	135
Eu	2	0	1	0	3
Tb	5	0	3	0	2
Dy	10	0	6	0	9
Yb	4	0	2	0.4	0
Th	5	0	3	2	21
U	13	1	8	4	9

*Asterisk indicates that atomic absorption spectroscopy was used. All others were determined by neutron activation spectroscopy. Silicon concentration calculated by difference.

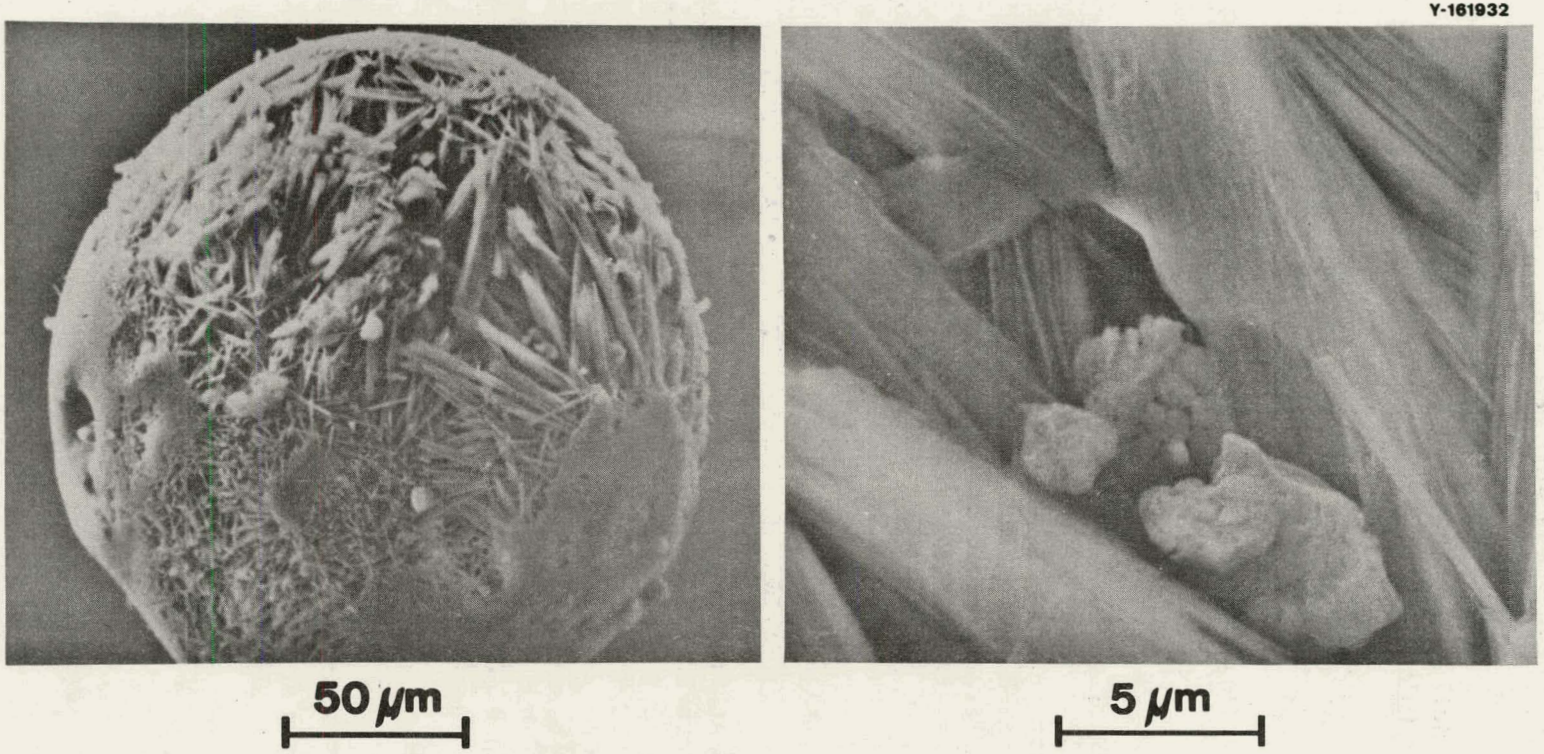


FIGURE 1: **FLY ASH PARTICLE, GLASS PHASES REMOVED, ACICULAR (NEEDLE) MULLITE SKELETON**

Trace elements contained in the mullite matrix of fly ash are in the form of isomorphic substitutions:

$$3(Al_{2-x}O_3).2(Si_{1-y}O_2).M_x^{+3}.M_y^{+4}$$

$$M^{+3} = V, Cr, Fe, Ga$$

$$M^{+4} = Ti, Zr,$$

There are no quantitative data on Zr because they were not credible. We did, however, examine the mullite-quartz phase qualitatively by x-ray fluorescence and found large concentrations of Zr. We have not been able to completely physically isolate the magnetic component of fly ash. The magnetic portions consisted of "strongly magnetic" and "weakly magnetic" fractions. We have been able to isolate the nonmagnetic matrix from the magnetic, but not vice versa. It appears, however, that the nonmagnetic and strongly magnetic fractions are appreciably different in kind with respect to trace element distributions. The first two columns of Table IV compare distributions of elements for the aluminosilicate matrix to magnetic matrix for Bull Run. The first-row transition elements tend to be more concentrated in the strongly magnetic fractions. This suggests that the chemical species of some of the trace elements may be as substitutions in spinels. There is, however, an appreciable concentration of alkali, alkaline earth, and rare earth elements in the magnetic material that is unexplainable, except to presume that they are dissolved in aluminosilicate material that is sintered to or occluded in the magnetic phase.

An attempt was made to isolate the magnetic phases by dissolving them in 12 *M* HCl over a steam bath for a period of about three weeks, but the magnetic material was only partially dissolved. Aliquots of the 12 *M* HCl solutions were evaporated in specially constructed capsules and analyzed by neutron activation analysis. Remaining portions of the liquid extract were analyzed by atomic absorption spectroscopy. Results are listed in column 3 of Table IV. The differences between the magnetic and aluminosilicate phases are now much more apparent. The most significant features of the magnetic phases are as follows:

1. Al and Fe were extracted in about the same mole ratios.

2. All alkaline earth elements are absent in the extracted magnetic phase. Presumably the Na, K, and Cs that were extracted were in the form of carbonates or other soluble surface species.

3. Except for Ce and La, all of the rare earth elements are absent from the magnetic phase.

4. The first-row transition elements V, Cr, Mn, Co, Ni, Cu, and Zn are concentrated in the magnetic phase by factors as high as 10-50.

Concentrations listed in the third columns of Table IV were calculated by assuming stoichiometric equivalents of O for Al and Fe. The results of this work indicate that the magnetic component of fly ash is not magnetite, Fe_3O_4, as is commonly reported, but an aluminum-substituted ferrite. Further work is needed to support this interpretation. Presently our evidence is as follows: Al was extracted in high concentrations, along with Fe, for all four specimens. One might argue that Al was

TABLE IV

BULL RUN FLY ASH: COMPARISON OF ELEMENT DISTRIBUTIONS IN ALUMINOSILICATE AND MAGNETIC PHASES
CONCENTRATIONS IN μg/g

	Total Alumino-silicate	Magnetic Physically extracted	Magnetic (HCl extract)
Al	143356	76300	86641
Fe	12644	385000	605344
Na	1044	501	2078
K	16333	8200	3587
Rb	62	180	229
Cs	3	3	0
Mg	12689	8500	0
Ca	1800	1700	0
Sr	889	150	0
Ba	163	208	0
Sc	20	17	15
Ti	8378	3480	0
V	166	165	150
Cr*	255	273	1374
Mn*	56	501	1038
Co	16	172	251
Ni*	172	----	2270
Cu*	144	----	496
Zn*	155	----	382
Ga	0	15	0
As	25	50	0
Se	26	28	38
Mo	0	79	0
Cd*	0.5	----	1.2
In	0	0.2	0
Sb	0	4	0
Hf	4	3	0
Ta	2	1	0
W	3	4	0
Hg	3	0	0
Pb*	12	----	5.1
La	18	37	14
Ce	18	66	141
Eu	0	1	1
Tb	0	1	0
Dy	0	5	0
Yb	0.4	0	0
Th	2	11	5
U	4	7	4

*Asterisk indicates atomic absorption analysis

extracted as Al_2O_3, but x-ray diffraction studies of the unextracted material showed no peaks corresponding to Al_2O_3. The diffraction peaks that were found indicated a compound with spinel structure, but the lattice parameter was significantly smaller than that of Fe_3O_4. Assuming that all of the HCl-extracted Al and Fe were associated with each other as ferrite materials, we calculate compositions varying from $Fe_{1.68}Al_{1.22}O_4$ to $Fe_{2.27}Al_{0.73}O_4$. We could not find lattice constants for ferrites having Al concentrations this high, but we did find a constant (5) for the compound $Fe_{2.78}Al_{0.22}O_4$. Mossbauer spectra (6) of some of these magnetic fractions were taken. They were considerably different from that of pure magnetite. It is well known that magnetitite and ferrites can accept the transition metal ions V, Cr, Mn, Co, Ni, Cu, and Zn as isomorphic substitutions of the type:

$$Fe_{3-x}M_xO_4.$$

Possibly this accounts for their chemical states and is an explanation of why they are so heavily concentrated in the magnetic phase.

CONCLUSION

We have used NAA in conjunction with other analytical techniques to study trace elements in coal and fly ash. IDSSMS and AA were shown to give satisfactory results for elements not easily determined by NAA. Etching studies of fly ash support our thesis that chemical species of trace elements are defined to a large extent by the matrix in which they are dissolved.

ACKNOWLEDGEMENTS

Many people have aided in the accumulation and interpretation of these data; it is impossible to name them all. Special thanks, however, go to Lester Hulett, Juel Emery, Joel Carter, and Marion Ferguson, of the Analytical Chemistry Division.

REFERENCES

1. W. S. Lyon, et al, *Nuclear Activation Techniques in the Life Sciences*, 1978, IAEA, Vienna (1979).

2. W. S. Lyon, *Trace Element Measurements at the Coal Fired Steam Plant*, CRC Press, Cleveland, 23 (1977).

3. C. Feldman, *Anal. Chem.* 49, 825 (1977).

4. L. D. Hulett, A. J. Weinberger, N. M. Ferguson, K. J. Northcutt, W. S. Lyon, "Chemical Speciation of Fly Ash Part I: Characterization of Solids", EPRI Report R. P. 1061, EPRI, Palo Alto, Calif. (1979).

5. R. F. Pearson, *J. Phys. Radium*, 20, 409 (1959).

6. L. D. Hulett, J. F. Emery, J. M. Dale, A. J. Weinberger, H. W. Dunn, C. Feldman, E. Ricci, J. O. Thomson, "Proceedings: Advances in Particle Sampling and Measurement", EPA-600/7-79-065, p. 355, February 1979.

INSTRUMENTAL PROMPT GAMMA ACTIVATION ANALYSIS OF ENERGY-RELATED SAMPLES AND STANDARDS*

D. L. Anderson, M. P. Failey, G. E. Gordon and W. H. Zoller
Department of Chemistry
University of Maryland
College Park, Maryland 20742

ABSTRACT

Instrumental thermal neutron prompt-gamma activation analysis (PGAA) is a powerful method for multi-elemental characterization of fuels and related materials. Samples of several types of fuels were irradiated and counted at the University of Maryland's PGAA facility at the National Bureau of Standards (NBS) reactor. The beam extraction system consists of a lower beam thimble and shutter apparatus extending from atop the reactor to a location in the D_2O moderator next to the core. An upper beam tube provides neutron shielding and a location for sample placement. Sample sizes ranged from 0.1 to 2.5 g, and irradiation times were typically 4 to 20 hours, with a thermal [Cd(Au) ratio = 55] beam flux of 2 x 10^8 n/cm^2-sec. The detection system consisted of a Ge(Li) of 24% relative efficiency surrounded by a large, split-annulus NaI detector, permitting the simultaneous accumulation of singles, Compton-suppressed, and pair spectra from 0.05 to 11 MeV. Coals, fuel oils, fly ashes and several other energy-related sample types may be analyzed for some or all of the following elements: H, B, C, N, Na, Mg, Al, Si, S, Cl, K, Ca, Ti, V, Mn, Fe, Cd, Nd, Sm and Gd. Thus, the PGAA technique can readily provide information on the environmentally important elements N and S, as well as other elements that are measures of the ash, moisture and heat content. Also, in the case of coal, the method can be used to determine concentrations of the trace elements B, Nd, Sm and Gd. These measurements are all non-destructive and many of them can be done in real time on fossil-fuel streams in plants.

---

*Work was in part supported by the U. S. Department of Energy under Contract No. DE-AS05-76ERO-5173-M0003.

INTRODUCTION

The use of neutron-capture prompt γ-ray activation analysis (PGAA) for determining elemental concentrations in coal has been demonstrated in several recent studies (1-5). Gladney, Jurney and Curtis at Los Alamos have obtained measurements of the elements B and Cd (1), S (2), and N, H, and C (3) in coal samples irradiated in a reactor thermal column (high neutron flux) by observing prompt γ rays with a Ge(Li) detector located outside of the shielding. Fay et al. (4) at Ames Laboratory used a low flux (ϕ_{th} = 6 x 10^5n/cm^2-sec) beam and NaI detectors to obtain prompt γ-ray spectra from coal samples weighing about 200 g. In a recent paper, the University of Maryland-

National Bureau of Standards group (5) demonstrated the multielement capabilities of PGAA in coal samples. Pouraghabagher and Profio (6,7) measured sulfur in bulk quantities of fuel oil using a ^{252}Cf source and NaI(Tl) detector. An excellent summary by E. S. Gladney (8) should be consulted for a comprehensive list of references on PGAA in fuels analysis.

The present study shows results of the analyses of National Bureau of Standards Standard Reference Material (SRM) coals and #6 fuel oil, as well as several other types of samples. The work was done at the University of Maryland neutron beam facility at the National Bureau of Standards Reactor in Gaithersburg, Maryland.

EXPERIMENTAL SETUP

Samples are irradiated in a vertical neutron beam with a thermal neutron flux of 2 x 10^8 n/cm^2-sec and a Cd(Au) ratio of 55/1. The detection system consists of a large volume Ge(Li) detector (24% efficient relative to 7.6 cm x 7.6 cm NaI at 1.33 MeV) surrounded by a 30- x 38-cm split-annulus NaI(Tl) crystal which can be used for Compton suppression and pair spectrometry. The anti-Compton and pair modes were not employed for the analyses presented here, so the results give an indication of what can be attained in a simple external beam-Ge(Li) set-up.

Massive neutron and γ-ray shielding was employed in the upper beam tube and around the detectors. More detailed descriptions of the set-up are given in references 5, 9 and 12. Data were accumulated and analyzed on Tennecomp TP-5000 analyzer which is built around a PDP 11/34 minicomputer. Two spectra were taken for each sample, one over 8192 channels covering the energy range 0.05-4 MeV, and one over 4096 channels covering the range of 3.5 to 11.0 MeV. The number of γ rays used for analysis varied with the element and with the irradiation length, but a general listing of those used has been previously given (5).

SAMPLES

The SRM coal samples and one oil shale sample were formed into pellets weighing 0.8 to 2.0 g and sealed between layers of 0.0025-cm Teflon film. The fly ash samples were loose powders packaged in Teflon film. The remaining coal sample and all of the oil samples were placed in 2/5-dram snap-top polyethylene vials ("polyvials") and were all of about 1 g in mass. All samples were held in place in the sample holder by thin nylon fish line. Targets were centered by the use of template external to the sample position.

STANDARDS

The standards varied in mass and form depending on the neutron cross section and convenient matrices (see Ref. 5). All were irradiated packaged in Teflon film, but several standards were also run in polyvials. It appears that the considerable amount of hydrogen in the walls of the polyvial causes some distortion of the thermal neutron spectrum, probably by preferential removal of very low energy neutrons (~0.01 eV). Most elements, which have flat excitation functions in the thermal region from 0.01 to 0.03 eV are unaffected, but elements with rising cross sections at low energy are not activated as strongly inside of the polyvial. In particular, the count rates observed from the S and Ti standards are depressed by about 5 and 12%, respectively, relative to the bare standards, whereas those of Al and other elements are depressed by less than 2%.

RESULTS

Results of the study are presentcd in Tables I to IV. Table I indicates that PGAA is very effective for the analysis of up to 17 elements in the NBS SRM coals. The coal sample obtained from a local power plant was subjected to a much shorter irradiation, but could still be readily analyzed for B, Na, Al, S, Cl, K, Ti, Fe, Sm and Gd. Results for hydrogen are not indicated only because of the very high polyvial blanks. (The containment volumes of the polyvials are well within the central, uniform portion of the neutron beam, but the solid end sections are not.)

Table II groups the SRM fly ash results with those for oil shale samples obtained from C. Wilkerson (11), as both have roughly "crustal" compositions. Again, the agreement with other measurements is very good. The hydrogen value reported for the oil shale was obtained from a single irradiation, that of the pellet in Teflon film. All other shale results are averages of two 2.5-hr irradiations (one as pellet in Teflon film and one as a powdered sample in a polyvial). Again, there is good agreement between the values obtained here with certified and other values for up to 17 elements.

Sulfur and V measurements produced excellent results for SRM 1634 (#6 fuel oil). Table III also shows the analyses of single samples of high- and low-sulfur fuel oil obtained from a local power company. Sulfur and V were measured in a relatively short (1-1.2 hr) count of high sulfur fuel, but V was not observable in a long count (18 hrs) of the low sulfur variety. Table IV indicates the results of the analysis for B, N and S in two shale oils, one type obtained from the processing of above ground shale deposits, the other from in situ deposits. The results for each are averages of two 18-hr irradiations of approximately 1.1-g oil samples in 2/5-dram polyvials. The comparative results listed under "other" in this table and in Table III (for oil shale) are the mean values of preliminary results from several laboratories (11). The shale oil and shale samples were obtained from Dr. C. L. Wilkerson, Battelle Northwest Laboratories.

DISCUSSION

The PGAA technique is an effective way to determine concentrations of many important elements in fuel-related materials. Sulfur can be readily measured at concentrations normally found in coal, coal fly ash, oil shale, shale oil and fuel oils. Hydrogen is an important indication for hydrocarbons in oil shale, and this method provides for the determination of this element at low levels (down to ~30 ppm in most geologic materials). For coal and crustal-type materials, PGAA is an excellent non-destructive major element analytical technique for H, C, N, Na, Mg, Al, Si, S, K, Ca, Ti, Mn and Fe. The measurement of these elements provides important practical information about the quality of coal. Nitrogen and sulfur are important because of their relationships to the release of NO and SO_2 during combustion. Several elements, e.g., Al, Si, Ti, can be related to the total ash content. As noted by Sowerby and Watt (this Conference), the heat content of most coals is proportional to the carbon content. If a proportionality between H and C content of the carbonaceous portion of the coal has been established, hydrogen in excess of the amount predicted from the carbon will be an approximate measure of the moisture content. The PGAA method is also useful for measuring the trace elements B, Cd, Sm and Gd in these sample types. The technique is also capable of measuring S and V in fuel oil and B, S, and N in shale oils.

REFERENCES

1. E. S. Gladney, E. T. Jurney and D. B. Curtis, Anal. Chem. 48, 2139 (1976).

2. E. T. Jurney, D. B. Curtis and E. S. Gladney, Anal. Chem. 49, 1741 (1977).

3. E. S. Gladney, D. B. Curtis and E. T. Jurney, Anal. Chim Acta 110, 339 (1979).

4. D. A. Fay, A. Pazirandeh, R. G. Strauss, M. A. Wechter and A. F. Voigt, J. Radioanal. Chem. 43, 263 (1978).

5. M. P. Failey, D. L. Anderson, W. H. Zoller and G. E. Gordon, Anal. Chem. 51, 2209 (1979).

6. A. R. Pouraghabagher, M.S. Thesis, University of California, Santa Barbara, 1973.

7. A. R. Pouraghabagher and A. E. Profio, Anal. Chem. 46 1223 (1974).

8. E. S. Gladney, Los Alamos Scientific Laboratory Report, LA-3028-MS, Sept. 1979.

9. D. L. Anderson, M. P. Failey, W. B. Walters and W. H. Zoller, Nucl. Inst. Meth. (in preparation) (1980).

10. M. S. Germani, I. Gokmen, A. C. Sigleo, G. S. Kowalczyk, I. Olmez, A. Small, D. L. Anderson, M. P. Failey, M. C. Gulovali, C. E. Choquette, E. A. Lepel, G. E. Gordon and W. H. Zoller, Anal. Chem. 52 , 240 (1980).

11. C. L. Wilkerson, Battelle Northwest Laboratories, private communication (1980).

12. G. E. Gordon, D. L. Anderson, M. P. Failey, W. H. Zoller, W. B. Walters and R. M. Lindstrom, in Proc. of the Third Int. Conf. on Nuclear Methods in Environmental and Energy Research, J. R. Vogt, ed. (University of Missouri, Columbia, MO, 1978), TID Document CONF 771071, pp. 83-89.

Table I. Concentrations of Elements in Coals as Determined by PGAA

Element	SRM 1632		SRM 1632a		SRM 1635[a]		Chalk Point Power Plant Coal
	PGAA[a]	Other[b]	PGAA[a]	Other[c]	PGAA[a]	Other[c]	PGAA[d]
H (%)	4.02±0.05	4.3	3.7±0.1	-	3.96±0.03	-	-
B (μg/g)	42.1±0.7	47.0	53±2	-	105±3	-	10.7±0.5
C (%)	70±5	73	71±4	-	59±3	-	-
N (%)	1.3±0.2	1.2	1.27±0.08	-	1.0±0.1	-	-
Na (%)	-	0.041	-	0.085	0.270±0.005	0.244	0.15±0.05
Al (%)	1.68±0.04	1.85, 1.74	3.01±0.13	3.07, 2.91	0.34±0.04	0.32, 0.30	1.6±0.3
Si (%)	2.95±0.06	3.2, 3.92	5.8±0.1	-	0.52±0.02	0.56	-
S (%)	1.29±0.03	1.32	1.59±0.02	1.64, 1.8	0.32±0.01	0.33	2.41±0.03
Cl (μg/g)	895±15	890	784±17	780	26±2	26	740±30
K (%)	0.275±0.010	0.28	0.42±0.02	0.42	0.0097±0.0006	0.0117	0.21±0.03
Ca (%)	0.33±0.05	0.35	0.24±0.02	0.24	0.54±0.02	0.55	-
Ti (μg/g)	890±35	800, 890	1550±40	1750, 1620	190±20	200, 205	880±30
Mn (μg/g)	43.5±2.4	40±3	29±5	28±2	24±7	21.4±1.5	-
Fe (%)	0.84±0.02	0.87±0.03	1.11±0.06	1.11±0.02	0.22±0.01	0.239±0.005	1.75±0.19
Cd (μg/g)	0.18±0.02	0.19±0.03	0.21±0.03	0.17±0.02	-	0.03±0.01	-
Nd (μg/g)	11.3±2.0	8.7	11.8±0.4	-	-	-	-
Sm (μg/g)	1.53±0.02	1.7	2.10±0.07	-	0.25±0.01	-	2.1±0.2
Gd (μg/g)	2.20±0.08	-	3.00±0.05	-	0.35±0.02	-	2.8±0.4

[a]Five or more determinations per value, counting times 16-20 hours.
[b]Underlined values from NBS Certificate of Analysis (Information values are those given with no errors.) Other values from various studies (see Ref. 5).
[c]NBS values as in footnote b. Other values from Ref. 10.
[d]One sample, 2.75-hr count.

Table II. Concentrations of Elements in NBS Fly Ashes (SRM 1633 and SRM 1663a) and in Oil Shale

Element	SRM 1633		SRM 1633a		Oil Shale	
	PGAA[a]	Other[b]	PGAA[a]	NBS[b]	PGAA[c]	Other[d]
H (%)	-	-	-	-	1.7±0.1	1.50±0.03
B (μg/g)	433±4	434, 493	39.2±0.7	-	76±2	94±2
Na (%)	0.30±0.02	0.32, 0.28	0.21±0.06	0.17±0.01	1.69±0.09	1.71±0.03
Mg (%)	1.5±0.2	1.8, 1.78	-	0.455±0.010	3.62±0.05	3.5±0.1
Al (%)	12.6±0.2	12.7, 12.3	14.0±0.2	14	4.0±0.1	3.8±0.1
Si (%)	21.8±0.3	21, 17	22.2±0.4	22.8±0.8	15.9±1.2	14.2±0.9
S (%)	0.39±0.04	0.44	0.27±0.02	-	0.66±0.06	0.65±0.05
K (%)	1.76±0.05	1.72, 1.61	1.97±0.04	1.88±0.06	1.59±0.06	1.66±0.07
Ca (%)	4.75±0.08	4.7, 4.69	1.29±0.11	1.11±0.01	9.8±0.2	10.1±0.7
Ti (%)	0.72±0.02	0.74, 0.70	0.84±0.01	0.8	0.155±0.010	0.18±0.02
V (μg/g)	190±50	214±8	360±40	300	-	84±14
Mn (μg/g)	480±25	493±7	190±15	190	-	313±7
Fe (%)	6.1±0.1	6.2, 6.7	9.7±0.2	9.40±0.10	1.97±0.09	2.03±0.05
Cd (μg/g)	1.50±0.07	1.45±0.06	1.07±0.05	1.0±0.15	0.7±0.3	0.63±0.02
Nd (μg/g)	62.1±2.4	58, 81	65.6±5.4	-	-	19±2
Sm (μg/g)	12.1±0.4	12.4	16.0±0.2	-	2.8±0.2	3.08±0.07
Gd (μg/g)	17.5±0.3	-	23.5±0.3	-	3.1±0.2	-

[a]Five irradiations of approximately 18 hours each.
[b]Underlined values from NBS Certificate of Analysis (Information values are given without errors indicated.) Other values are from various studies (see Ref. 5 for details).
[c]Two irradiations of 2.5 hours each.
[d]C. L. Wilkerson, Battelle Northwest, private communicaton, 1980.

Table III. Concentrations of Sulfur and Vanadium in #6 Fuel Oils

Element	SRM 1634		High Sulfur		Low Sulfur	
	PGAA[a]	NBS[b]	PGAA[c]	Other[d]	PGAA[e]	Other[d]
S (%)	2.21±0.07	2.14±0.02	2.24±0.11	2.3	0.67±0.10	0.5
V (μg/g)	309±11	320±15	420±170	-	-	-

[a]Three irradiations of approximately 18 hours each.
[b]Certified values.
[c]One 1-1/2 hour irradiation.
[d]S values supplied by Potomac Electric Power Company.
[e]One 18-hour irradiation.

Table IV. Concentrations of Boron, Nitrogen and Sulfur in Shale Oils

Element	Above Ground Shale Oil		In situ Shale Oil	
	PGAA[a]	Other[b]	PGAA[a]	Other[b]
B (μg/g)	1.0±0.2	-	0.5±0.2	-
N (%)	1.33±0.05	-	0.83±0.02	-
S (%)	0.81±0.02	0.82	0.71±0.05	0.72

[a]Two irradiations of 18 hours each.
[b]C. L. Wilkerson, Battelle Northwest, private communication, 1980.

Assessments of Accuracy and Precision of Multi-Element Determinations in Whole Coal by Non-destructive Neutron Activation Analysis

George E. Miller, Don R. Burtner, and Paul A. Jerabek
Department of Chemistry
University of California, Irvine
Irvine, California 92717

Abstract

Factors affecting the accuracy and precision of element determinations of samples of coal using instrumental neutron activation analysis are examined in some detail. In the case of nitrogen determination using 14-MeV neutrons, it is concluded that several "correction" factors for interference reactions must be determined fairly precisely in order that the analytical technique can be applied routinely to samples of widely varying composition.

Methods for analysis of coals are receiving considerable attention in relation to the current drive to develop methods and techniques for conversion of coals to other fuels. In spite of the fact that methods for determination of the major, minor, and trace elements in geological matrices are well developed, there appear to be unique problems in designing fast, reliable methods for the widely varying coal matrix. Neutron activation methods using thermal neutrons have been in use for some time, particularly because of the high sensitivity for important trace elements (see, for example, Ref. 1). Recently more attention has been given to the possibility of determining both trace, minor, and major elements using entirely activation methods.[2] In addition, the determinations of the very important oxygen and nitrogen contents using fast (14 MeV) neutron activation have been rather extensively explored.[3,4]

Some of the requirements for analysis of coal are that the methods have a high productivity. This is necessary because to a first approximation, no two samples of coal are alike! It thus becomes imperative that the minimum amount of effort is required for an individual sample, with the maximum possible data yield. In order that the data be useful, however, they must be reliable, and to accomplish this, considerable effort is needed to evaluate the parameters influencing the accuracy and precision. It appears to us (and others) that the neutron activation methods are capable of filling much of this requirement. We have begun to re-examine, as far as the capability of our laboratory facilities will permit, the determinations of elements in coal matrices setting boundary conditions that "reasonable" data for modest sized samples should be obtained with the minimum number of sample handling steps, and that both accuracy and precision should be fully assessed for a uniform set of analytical procedures that can, hopefully, be used for the whole spectrum of "coal" materials.

In this work, we have found that it is necessary to re-investigate some of the more obvious problems that have arisen in previous determinations of certain elements. We have established a uniform sample size (about 1.6 grams), with a single packaging step as our initial working parameter.

Table I illustrates the different factors that influence accuracy and precision, and others have discussed these extensively, particularly as related to "fast" neutron utilization.[5] It is clear that most of the precision requirements are related to instrumentation provisions, once we restrict considerations to reproducibility of measurement of one specific sample. Problems of coal sample preparation are not trivial, especially as related to standardization of moisture content[6], but they are not the main emphasis here.

Table I

Factors Affecting Activation Analysis Determinations

Precision - Single Sample
Sample/standard Irradiation Geometry
Flux Variation
Sample/standard Counting Geometry
Timing Reproducibility
Counting Statistics

Accuracy
Primary Interferences
Secondary Interferences (γ rays)
Background Interferences
Flux Depletion and Self-absorption
Standard Preparation

To minimize many of these factors, our 14 MeV neutron activation system utilizes a dual sample, dual axis rotating irradiator, dual NaI detectors, and a multiplexed multichannel analyzer. An electronic timer/programmer controls the sequencing. When needed, flux monitoring is possible using a separate transfer port or a BF_3 neutron counter. The equipment utilized for thermal neutron activation is[3] familiar to most. Because of concerns regarding homogeneity of the large samples used, we have experimented with a sample spinner during gamma-ray assay with the Ge-Li detector, but find no significant improvement in precision. In any event, since the thermal neutron data are intended at this stage to provide only information for establishment of corrections for interferences in the determinations using 14 MeV neutrons, high precision is not always needed.

The remainder of this article concerns the application of instrumental 14 MeV neutron activation analysis to coals.

In the determination of oxygen in coal and other matrices via the $^{16}O(n,p)^{16}N$ reaction, interferences are practically nonexistent. The determination is essentially "perfect" as activation analysis methods go and accuracy and precision within the limits of counting statistics have been attained in our laboratory and by other groups. With our dual simultaneous comparator system, agreement to 0.2% relative is frequently achieved, for determinations requiring only a few minutes.

For all other elements, longer irradiations and more complex counting sequences are required and the interferences found vary from mild to severe. It may be feasible, however, to obtain quantitative information on nitrogen, silicon, iron and magnesium in coal samples following a five minute irradiation in our system.

Determination of nitrogen has recently been examined for a number of matrices[4,7], utilizing the $^{14}N(n,2n)^{13}N$ reaction and determining the ^{13}N activity by counting the 511 keV annihilation radiation produced from the positrons emitted in its decay. Other groups have chosen to do this by coincidence counting methods to lower the backgrounds observed. We have elected to employ straightforward gamma-ray spectrometry in order that simultaneous information can be accumulated for other elements.

The major potential interferences in the use of this reaction are summarized in Table II. Groups have differed in their approach to correction for these effects. Our earlier attempts[8] involved preparation of special "blanks" for comparison, in an attempt to simulate the specimen under examination, but without the nitrogen content. Standards were prepared from piperine (72% C; 6.7% H; 16.8% O; 9% N), roughly comparable in C, H, and O content to many coals. Measurements corrected in this manner were in satisfactory agreement with results from Kjeldahl nitrogen determinations provided that the ash (inorganic) component of the sample was limited. The corrections were inadequate when a wide variation in inorganics or oxygen content was encountered because of the magnitude of the interference contribution in this case.

Table III illustrates the nature of the problem involved in applying these determinations routinely to coal samples from varied origins. Methods need to be devised to ensure adequate corrections for interferences over a very wide range of sample compositions. It should be emphasized, too, that all correction factors applied must be determined for each facility and for any variation in sample irradiation geometry or beam energy since the relative cross sections for neutron reactions at around 14 MeV can vary rapidly with neutron energy. The latter varies not only with accelerator voltage, but also as a function of angle from sample to target.

Table II

Possible Interferences in Nitrogen Determination by the $^{14}N(n,2n)^{13}N$ Reaction

Reaction	Target Abundance	Cross Section mb	Product Half-Life min	Interference
$^{14}N(n,2n)^{13}N$	99.63	5.7	9.96	β^+ (511 kev)
$^{16}O(p,\alpha)^{13}N$	99.76	?	9.96	β^+
$^{13}C(p,n)^{13}N$	1.11	?	9.96	β^+
$^{12}C(p,\gamma)^{13}N$	98.89	?	9.96	β^+
$^{39}K(n,2n)^{38}K$	93.09	4	7.71	β^+, p-p'n*
$^{31}P(n,2n)^{30}P$	100	11	2.50	β^+
$^{63}Cu(n,2n)^{62}Cu$	69.10	550	9.76	β^+
$^{79}Br(n,2n)^{78}Br$	50.52	1141	6.46	β^+
$^{28}Si(n,p)^{28}Al$	92.27	235	2.31	p-p'n
$^{27}Al(n,p)^{27}Mg$	100	80	9.50	p-p'n
$^{30}Si(n,\alpha)^{27}Mg$	3.12	46	9.50	p-p'n
$^{56}Fe(n,p)^{56}Mn$	91.68	103	154.6	p-p'n
$^{54}Fe(n,2n)^{53}Fe$	5.84	15	8.50	β^+

* Pair production in sample, detector, or shielding by high energy gamma-ray.

Table III

Variation of Selected Elements in Coal

114 Illinois Basin Coals†

Element	Mean Concentration	Max Conc / Min Conc
	%	
Al	1.2	7
Mg	0.05	17
Si	2.4	8
K	0.17	14
Fe	2.0	9
Br	13 (ppm)	87
C	70	1.3
H	5	1.4
N	1.3	1.9
O	8.2	3.3

† Gluskoter, H. J., Ruch, R. R., Miller, W. G., Cahill, R. A., Dreher, G. B., Kuhn, J. K. Illinois State Geological Survey Circular, 1977, 489.

The relative magnitudes of the more significant correction parameters are shown in Table IV. These data are for a 5 minute irradiation, 11 minute delay, and 10 minute count sequence.

Table IV

Element	C	O	H	S	Si	N	Al	Fe	K	P
%, composition	67	15	5	2.7	2.7	1.3	1.1	1.7	0.2	< 0.1
mg in sample	1443			43.2	43.2	20.8	17.6	27.2	3.2	< 1.6
"counts" *	1440+			0	0	4740	0	170	117	< 30

* In the nitrogen "peak" (511 KeV)

\+ Determined for a 1443 mg sample of benzoic acid (C:69%, O:26%, H:5%).

The largest correction to be applied is that generated from the C, H, and O content. This arises (see Table II) from proton reactions, the protons being predominantly "knocked-on" by fast neutron collisions. This complex phenomenon has been the subject of several investigations and has recently been reviewed.[9] The conclusions of the earlier investigations were that the effect of the $^{16}O(p,\alpha)^{13}N$ reaction for samples containing oxygen were about an order of magnitude larger than the contribution from ^{13}C reactions leading to ^{13}N and that an apparently linear relation was observed for the ^{13}N yield as a function of the product of the hydrogen and oxygen concentrations in the sample.

To simplify the problem of this "blank correction", most published work on nitrogen determination has employed a single subtraction of the ^{13}N obtained from a sample containing roughly similar C, H, O concentrations. We ourselves have used benzoic acid data for this purpose. We have re-examined this problem in an effort to ascertain how precisely this correction can be estimated over a wide range of organic sample compositions.

Two series of mixtures of pure organic compounds were prepared (Table V), such that a constant hydrogen content was maintained in one, and a constant oxygen content in the other. The compounds used were recrystallized and very thoroughly mixed before use.

Table V

	%C	%O	%H
1. "Constant H"			
3 : 4 dimethoxybenzoic acid $C_9H_{10}O$	59.34	35.13	5.53
Benzophenone, $C_{13}H_{10}O$	85.69	8.78	5.53
2. "Constant O"			
1 : 4 Naphthoquinone, $C_{10}H_6O_2$	75.94	20.23	3.82
1 : 4 Diethoxybenzene, $C_{10}H_{14}O_2$	72.26	19.25	8.49

Samples of the mixtures were analyzed for "apparent" nitrogen content, relative to piperine and other nitrogen standards. For the series of "constant oxygen content" samples, results were constant within experimental uncertainty. The data for the other series is shown in Figure 1, and shows a clear non-linearity at lower oxygen concentrations. Further work is needed to establish whether there are other subtle effects that might need to be applied to coal, such as differences between oxygen in a mineral phase vs. that in the organic phase of coal.

Coal samples can be analyzed for both silicon and iron at the same time. In the former case, the interferences to the $^{28}Si(n,p)^{28}Al$ given by the $^{27}Al(n,\gamma)^{28}Al$ and the $^{31}P(n,\alpha)^{28}Al$ reaction appear to be 1% or less for typical coals. For the iron determination, utilizing the $^{56}Fe(n,p)^{56}Mn$ reaction, the $^{27}Al(n,p)^{27}Mg$ reaction, yielding gamma radiation at a very similar energy (847 vs. 840 KeV) generates about three times the total counts in a typical sequence, swamping the iron activity. Alterations in the counting cycle or accurate determination, via thermal neutron activation, of the aluminum content of the sample will be needed so that this procedure could be utilized for routine iron determination in coal.

References

1. J. N. Weaver, "Neutron Activation Analysis of Trace Elements in Coal, Fly Ash and Fuel Oils", Chapter 12 in Analytical Methods for Coal and Coal Products, Volume 1, C. Karr, ed., Academic Press, New York, 1978.

2. M. S. Germani, Inci Gokmen, A. C. Sigleo, G. S. Kowalczk, Ilhan Olwez, A. M. Small, D. L. Anderson, M. P. Failey, M. C. Golovali, C. E. Choquette, E. A. Lepel, G. E. Gordon, and W. H. Zoller, Anal. Chem., 52, 240 (1980).

3. A. Volborth, G. E. Miller, C. K. Garner, and P. A. Jerabek, "Material Balance in Coal. 2: Oxygen Determination and Stoichiometry of 33 Coals", Fuel, 57, 49 (1978).

4. C. E. Hamrin, A. H. Johannes, W. D. James, G. H. Sun, and W. D. Ehman, "Determination of Oxygen and Nitrogen in Coal by Instrumental Activation Analysis", Fuel, 58, 48 (1979).

5. S. S. Nargolwalla and E. P. Przybylowicz, "Activation Analysis with Neutron Generators", Wiley Interscience, New York, 1973.

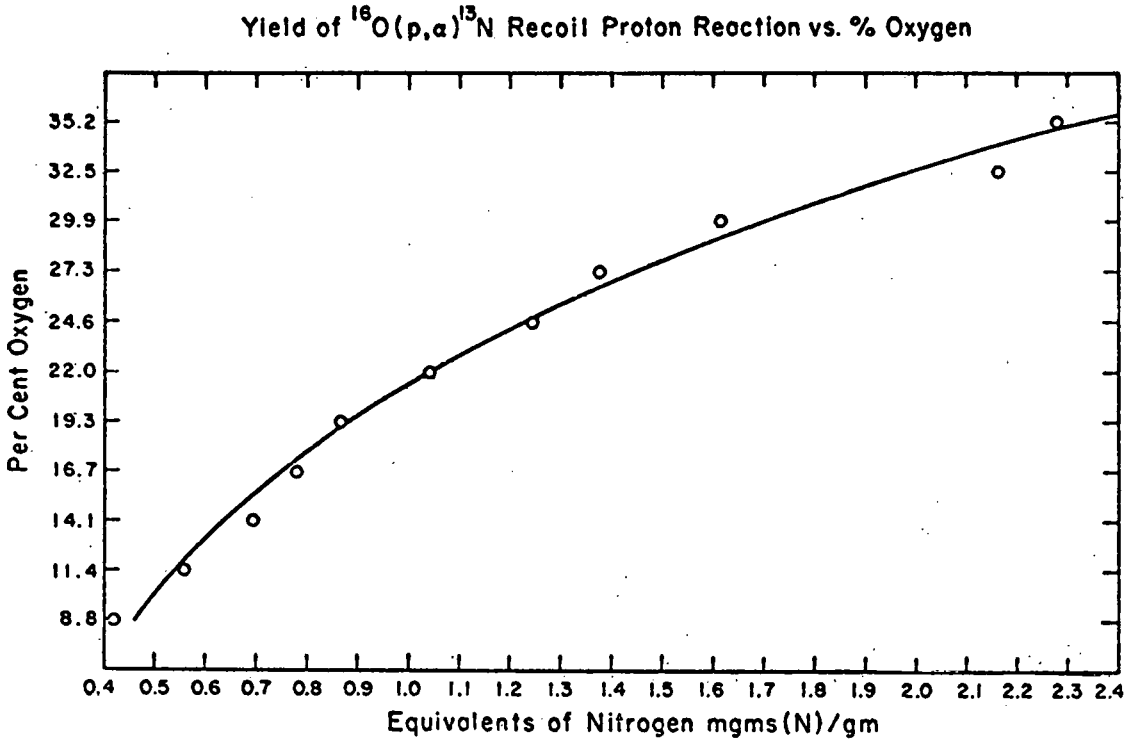
6. G. E. Miller and A. Volborth, "Use of 14 MeV Generator in Analysis of Coal and Coal Derivatives", Proceedings of 4th Conf. Appl. Small Accelerators, Denton, Texas, 1976, 288-292.

7. L. S. Chuang, D. A. Miller, W. P. Lay, and W. Y. Chiu, "The 14 MeV Neutron Activation Analysis of Chinese Foodstuffs for Protein Content", J. Radioanalytical Chemistry, 38, 279 (1977).

8. R. R. Ruch, G. E. Miller, and A. Volborth,"Nitrogen Determination in Coal and Related Products", in preparation.

9. C. M. Buczko and M. Varadi, "Role of Secondary Nuclear Reactions in the Determination of Nitrogen", Radiochem. Radioanal. Letters, 30, 319 (1977).

Figure 1


Yield of $^{16}O(p,\alpha)^{13}N$ Recoil Proton Reaction vs. % Oxygen
Per Cent Oxygen
35.2
32.5
29.9
27.3
24.6
22.0
19.3
16.7
14.1
11.4
8.8
0.4 0.5 0.6 0.7 0.8 0.9 1.0 1.1 1.2 1.3 1.4 1.5 1.6 1.7 1.8 1.9 2.0 2.1 2.2 2.3 2.4
Equivolents of Nitrogen mgms(N)/gm

A STUDY OF COAL OXIDATION BY CHARGED PARTICLE ACTIVATION ANALYSIS

David J. Schlyer and Alfred P. Wolf
Chemistry Department
Brookhaven National Laboratory
Upton, New York 11973

It has been possible, using the technique of changed particle activation analysis, to follow the time course of the oxidation of coal exposed to air. The kinetics have been studied and seem to be consistent with a rapid initial uptake of oxygen containing molecules followed by slow diffusion into the surface of the coal particles. In this latter regard a study has been undertaken to study the depth profile of the oxygen into the coal particle surface. The depth of penetration of the activating particle is determined by the incident energy and therefore, by comparison to the appropriate standards, the depth profile may be determined either by varying the incident energy or by varying the particle size. Both approaches have been used and give consistent results. The depth to which a significant amount of oxygen penetrates varies from about 3 μm for very high rank coals to about 20 μm for low rank coals. This diffusion depth seems to be related to the porosity of the coals. A model for the low temperature air oxidation of coal has been developed to explain the results from the above mentioned experiments.

INTRODUCTION

The interaction between coal and air has been the focal point of a great deal of study over the past fifty years. This interaction is of importance since air exposure can cause significant alteration of the processing characteristics of the coal. This is especially true of low rank coals.

Both the primary interaction of air with coal and how this interaction affects the characteristics of the coal have been addressed by previous studies.[1] The kinetics of adsorption have been measured on both coal[2] and brown coal chars.[3] Adsorption isotherms have been determined for oxygen and water on coal either calorimetrically[4] or gravimetrically.[5] The desorption under reduced pressure has also been studied.[6] It has been noted that coal particles develop a discoloration near the surface.[7] This "oxidation rim" is directly related to the behavior of the coal.

The purpose of this study is to determine the characteristics of this oxidation process in more detail. The parameters to be determined are 1) the kinetics of the adsorption of oxygen-containing species, 2) what the elemental composition of the oxide layer is and how deeply it extends into the surface, and 3) the number of reactive sites on the surface. In order to accomplish this task the technique of charged particle activation analysis (CPAA) has been employed. Extensive use of this technique in a variety of experiments gives a relatively clear description of the coal oxidation process.



EXPERIMENTAL

The technique of Charged Particle Activation Analysis has been described previously.[8] In the study of the kinetics of the coal oxidation a slight modification of the procedure was used. The coal was ground to an average particle size of 45 micron (325 mesh) in a Spex mixer utilizing a steel ball and container under an inert (He or Ar) atmosphere. The distribution of particle sizes was such that about 80% of the particles were between 38 and 60 microns in diameter as determined by sieving the crushed coal in a separate experiment. The samples were dried at 100°C under vacuum for 18 hours to remove moisture. The samples were then exposed to air in a controlled humidity room (relative hymidity 45%, temperature 20°C) for a given period of time and either sealed directly into 1 mil aluminum packets or were returned to the vacuum oven, dried and then sealed into the packets. These packets, along with a set of standards, were then irradiated with a 10 MeV He-3 beam for 300 seconds at a beam current of 0.3 microamperes. The samples were placed in a Searle model 1185 automatic gamma counter where each sample was counted every 20 minutes for 5 hours. A paper tape of these data was analyzed with a PDP-11/34 minicomputer to determine the oxygen to carbon ratio for each coal sample.

To determine the equilibrium oxygen depth profile at room temperature, the coal samples were ground as in the kinetic study. The particles were then sorted according to particle size using standard sieves (35 to 400 mesh). After sieving, the samples were exposed to air in the controlled temperature and humidity room for 60 days. The samples were stirred from time to time to ensure even exposure of the coal. These samples and a set of standards were then sealed into the aluminum packets and irradiated. By determining the oxygen to carbon ratio as a function of particle size, it is possible to determine the equilibrium oxygen depth profile. In order to carry out this determination, it is necessary to know the variation in the cross-section ratio for the production of F-18 compared to that for C-11 as a function of depth of penetration into the particle (i.e., as the He-3 energy decreased). The cross-section ratio was determined by constructing "sandwiches" of a film of Mylar, a film of polyethylene and another film of Mylar. The Mylar films represented the oxide layer and the polyethylene film represented the coal. These "sandwiches" were irradiated and counted in the same manner as the coal samples.

A series of control experiments were done to ensure that the variation in the oxygen to carbon ratio with particle size was not an artifact of the system. Each type of coal used in these experiments was ground under an argon atmosphere, placed in a dry box and sieved. The samples were then sealed into the irradiation packets in the dry box so that they were never exposed to air after crushing. The samples were then irradiated and counted as in the previous experiments. In two of the three coals analyzed, the O/C was constant for all sizes of coal particles. In one case (NDL) there was a small variation of approximately 5% for which a correction was made in analyzing the results.

Coal samples have also been oxidized using a fluidized bed while varying both the temperature and the composition of the gas mixture. The coal was Belle Ayr coal which was about 70% carbon by weight (low rank). These experiments were carried out at Gulf Research in Pittsburgh and the samples were then sent to Brookhaven for analysis. In only two cases was an attempt made to determine the depth profile of these samples.

In addition to varying particle size to determine the depth profile it is also possible to determine this profile by varying the incident energy of the particle as long as there is a standard irradiated at the same energy. Results from these experiments were consistant with those obtained by varying the particle size of the coal. The scatter in the data was significantly greater however and therefore the results reported in this paper are exclusively those obtained by varying the particle size of the coal.

A third set of experiments were performed using molecules labelled with O-15 to determine the nature of the interaction between small amounts of oxygen and the coal. Gas chromatography columns were prepared from three ranks of coal. These coals were North Dakota Lignite, New Mexico Sub-bituminous and Pennsylvania Anthracite. The columns were stainless steel tubes ¼ inch in diameter and 1 foot long with coal particles in the column of 100 to 200 mesh. These columns were placed in the oven of a radio-gas chromatograph. The detectors for this gas chromatograph included a thermal conductivity detector followed by a flow proportional counter. A flow of helium was started and the column was allowed to equilibrate at 40°C for about 20 minutes. Molecular nitrogen containing a small amount of molecular oxygen labelled with oxygen-15 was then injected onto the column. The column was maintained at 40°C for 2 minutes to allow the injected gas to pass through the column and the oxygen to become adsorbed. The temperature of the column was then gradually raised to 250°C and both the mass and activity trace recorded. The experiment was then repeated with molecular oxygen from the air added to the gas sample. Thus limits could be placed on the number of active sites for oxygen adsorption on the coal surface.

The oxygen-15 used in these experiments was prepared from the $^{15}N(p,n)^{15}O$ nuclear reaction using N_2 as a target gas. The samples contained less than a few parts per million of molecular oxygen.

RESULTS

Kinetic Experiments. The curves derived from the kinetic experiments are shown in Figure 1. The three coal types all follow the same general behavior, a rapid uptake of oxygen followed by a more gradual uptake which continues for a considerable amount of time in the case of the low rank coal. The lower curve in each case is the uptake of oxygen after the sample had been placed in the vacuum oven at 65°C for 3 hours and then irradiated. In all cases this uptake is slower and in the case of Anthracite the oxygen to carbon ratio remains nearly constant after about 15 minutes. In the case of Lignite, the irreversible uptake (after heat and pumping) appears to increase for a long period of time. This may be due to the chemical oxidation of the coal itself.

High temperature oxidation. The results from the coal samples oxidized at higher temperatures are given in Table 1. The numbers in this table with the greatest uncertainty associated with them are those for the weight percent moisture. The determinations were made at the end of the experiment at Gulf and there is some evidence to indicate that the values were slightly different after shipment. The samples with very little moisture increased in moisture content while those with a great deal of moisture seem to have decreased in percent moisture. The oxygen to carbon ratio data suggest that two processes are occurring as temperature is increased. The first is a drying of the coal particle as water is desorbed from the interior of the coal particle (reducing the oxygen to carbon radio). The second is a chemical oxidation penetrating into the coal particle (increasing the oxygen to carbon ratio).

Oxygen Depth Profile. In order to analyze the results from the oxygen depth profile measurements in a quantitative manner, a model of the coal particle must be assumed. In the analysis of these data, a simple model was found to replicate the experimental results reasonably well. It has been assumed the coal particle is a sphere which has a diameter $2r_p$ and an oxide layer on the exterior of the particle which has a thickness r_o. The volume of the oxide layer compared to the volume of the total particle can then be compared to the experimental oxygen to carbon ratio to determine the approximate thickness of the outer layer. This model and the resulting curves are depicted in Figure 2. The variation in the oxygen to carbon ratio within this oxidized layer will effect the numerical value of the oxygen to carbon ratio, but the depth of the layer is determined from the shape of the curve and is relatively insensitive to variations in the oxygen content as long as the particle diameters sampled are greater than the oxide layer depth. The experimental results from the New Mexico Sub-bituminous are given in Figure 3 along with the model curves. The model curves have been corrected for the measured cross-section ratio as a function of depth of penetration. The best fit to the measured data is for an oxide layer of approximately 7 microns. In the case of the North Dakota Lignite the layer depth is about 10 microns and for Pennsylvania Anthracite the depth is 4 microns.

Oxygen-15 adsorption. When a few milliliters of oxygen labelled with a trace of O-15 were injected onto the Pennsylvania Anthracite, all of the activity initially taken up was desorbed during the heating cycle. When trace quantities (10^8 molecules) of labelled O_2 and CO_2 in a few milliliters of N_2 were injected onto the North Dakota Lignite, all of the activity was retained on the coal even at 250°C. When a few milliliters of O_2 gas was added to this mixture, the O_2 activity was not retained but the CO_2 activity was retained. When carrier CO_2 was added, essentially all of the activity was removed from the column (i.e., the coal) during the heating cycle. These results suggest that CO_2 is more strongly adsorbed that O_2.

DISCUSSION

The data from these studies using radiochemical techniques are in essential agreement with the previous work done on the low temperature air oxidation of coal. The kinetics of oxygen adsorption follow Elovich kinetics, i.e. a rapid uptake followed by a more gradual uptake.[9] It has also been found that oxygen can chemically react with low rank coals[10,11] as is suggested by the CPAA kinetic results and the retention of oxygen-15 labelled oxygen in the North Dakota Lignite. The fact that a few sites in the coal are very reactive is also consistent with the observation that the apparent activation energy for oxidation is very low.[12] Recent modelling studies [13,14] have demonstrated the equivalence of Elovich kinetics with diffusion and adsorption in microporous solids. These studies tend to support solid state diffusion and the fairly low activation energies associated with this process, as the rate limiting step in coal oxidation by air.

The data collected seem to be most consistent with the following mechanism for the oxidation of coal by air. Oxygen is adsorbed weakly onto the surface of the coal. This adsorbed oxygen can then migrate across the surface of the coal to a reactive site at which point it becomes chemically bound to the surface. As the surface becomes saturated with oxygen, this oxygen will diffuse through pores and react with active sites within the coal particle. This constitutes the second, slower part of the adsorption process. At equilibrium (in the low temperature case) a layer of definite depth is formed which resists any further oxidation from the exterior of the particle. The exact distribution of oxygen within this layer cannot be determined at the present time since to do so would require separating extremely fine coal particles which are

impossible to sort using sieves. The most likely candidate for this distribution would be an expotential decrease in the oxygen to carbon ratio going into the particle since this distribution is representative of a chemical potential barrier to further oxidation within the particle. As the temperature is raised the diffusion can occur to greater depths. At higher temperatures (150°C) there is no observable oxygen gradient left. The oxygen has become evenly distributed throughout the coal particle.

REFERENCES

1. See for example Dryden, I. G. C. in Chemistry of Coal Utilization, Supplementary Volume (Ed. H. H. Lowry), Wiley, New York, 1963, Ch. 6, p. 272.
2. T. Wood, J. Appl. Chem. 8 (1958) 565.
3. D. J. Allardice, Carbon 4 (1966) 255.
4. K. K. Bhattacharyya, FUEL 51 (1972) 214.
5. D. J. Allardice and D. G. Evans, FUEL 50 (1971) 201,236.
6. O. D. Mahajan and P. L. Walker, Jr., FUEL 50 (1971) 308.
7. P. Dugan and V. J. Moran, FUEL 49 (1970) 415.
8. D. J. Schlyer, T. J. Ruth, and A. P. Wolf, FUEL 58 (1979) 208.
9. J. O. Newman et al., Nature 213(1967) 280.
10. B. S. Ignosiak et al., FUEL 51 (1972) 280.
11. P. D. Swann and D. G. Evans, FUEL 58 (1979) 276.
12. I. G. C. Dryden in Chemistry of Coal Utilization, Supplementary Volume (Ed. H. H. Lowry), Wiley, New York, 1963, Ch. 6, p. 277.
13. J. A. Harris and D. G. Evans, FUEL 54 (1975) 276.
14. K. A. Debelak, private communication.

ACKNOWLEDGMENT

The authors wish to express appreciation to the Electric Power Research Institute and Gulf Research and Development for their cooperation in providing coal samples. This research carried out at Brookhaven National Laboratory under contract with the U. S. Department of Energy and supported by its Office of Basic Energy Sciences.

FIGURE LEGENDS

Figure 1. Plot of oxygen adsorption versus time for three ranks of coal. Circles represent total oxygen adsorption. Triangles represent the oxygen adsorbed on coal after heating under vacuum for 3 hours at 65°C.

Figure 2. Plot of volume of oxide layer versus particle diameter in model used to analyze oxide layer depth. The diameter of the coal particle is $2r_p$ and the oxide layer depth is r_o. The family of curves represent various oxide layer depths.

Figure 3. Plot of experimental oxygen to carbon ratio versus particle diameter for the New Mexico Sub-bituminous. The model curves, corrected for the nuclear cross-section ratio, are plotted for comparison.

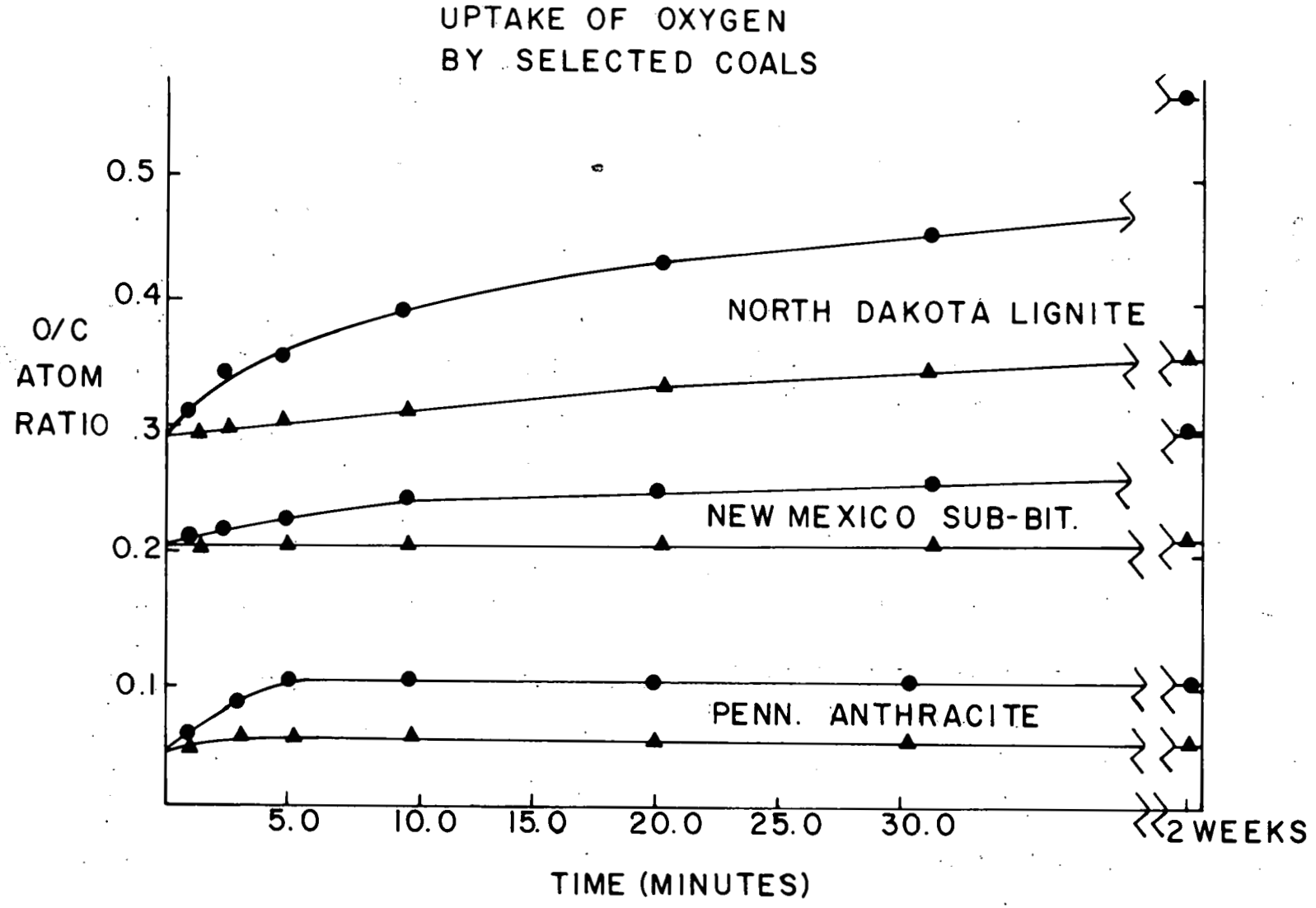

UPTAKE OF OXYGEN
BY SELECTED COALS
O/C
ATOM
RATIO
0.5
0.4
.3
0.2
0.1
NORTH DAKOTA LIGNITE
NEW MEXICO SUB-BIT.
PENN. ANTHRACITE
5.0
10.0
15.0
20.0
25.0
30.0
2 WEEKS
TIME (MINUTES)

Figure 1:

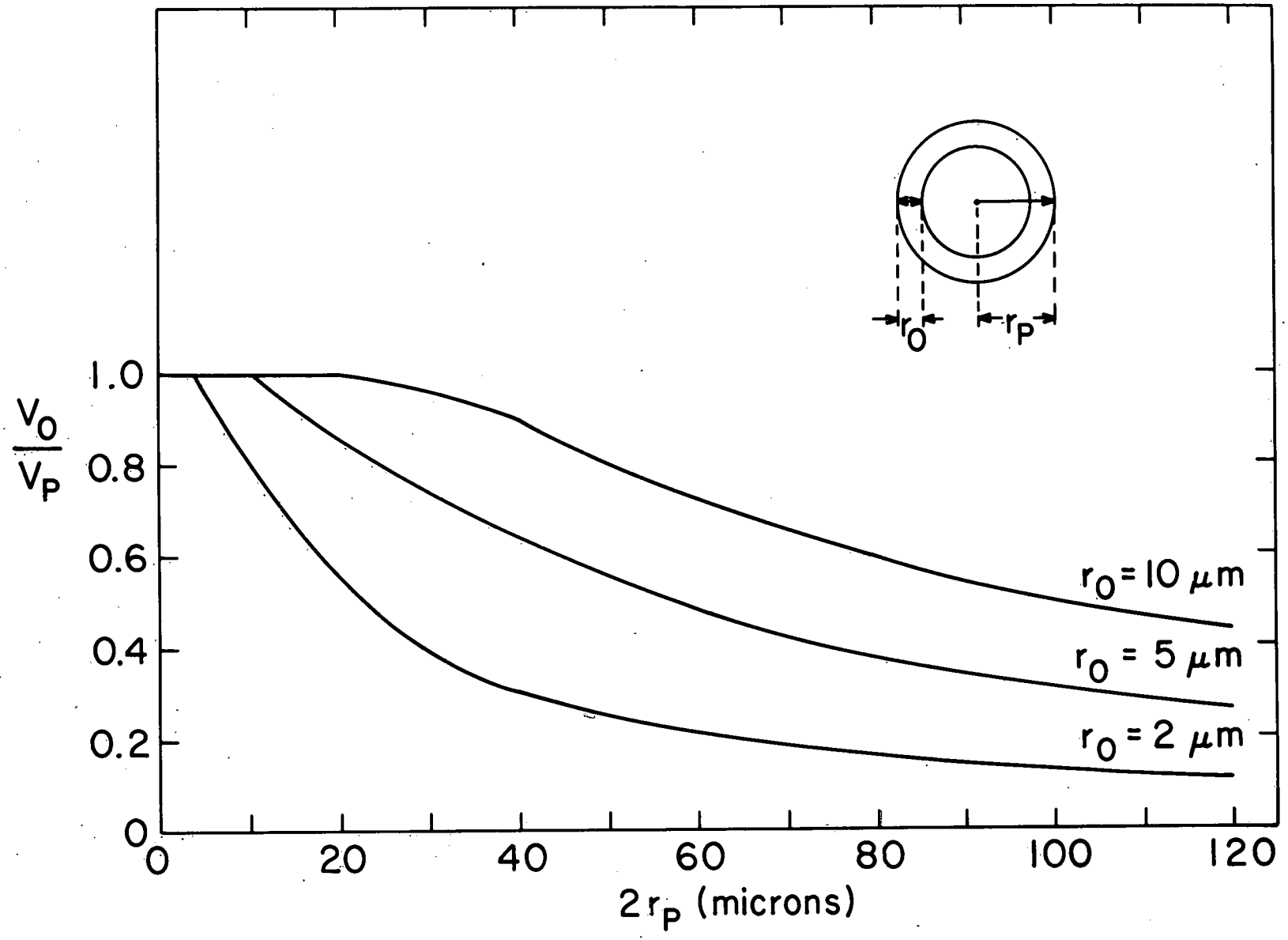

r_0
r_P
$\frac{V_0}{V_P}$
1.0
0.8
0.6
0.4
0.2
0
0
20
40
60
80
100
120
$2r_P$ (microns)
$r_0 = 10\ \mu m$
$r_0 = 5\ \mu m$
$r_0 = 2\ \mu m$

Figure 2

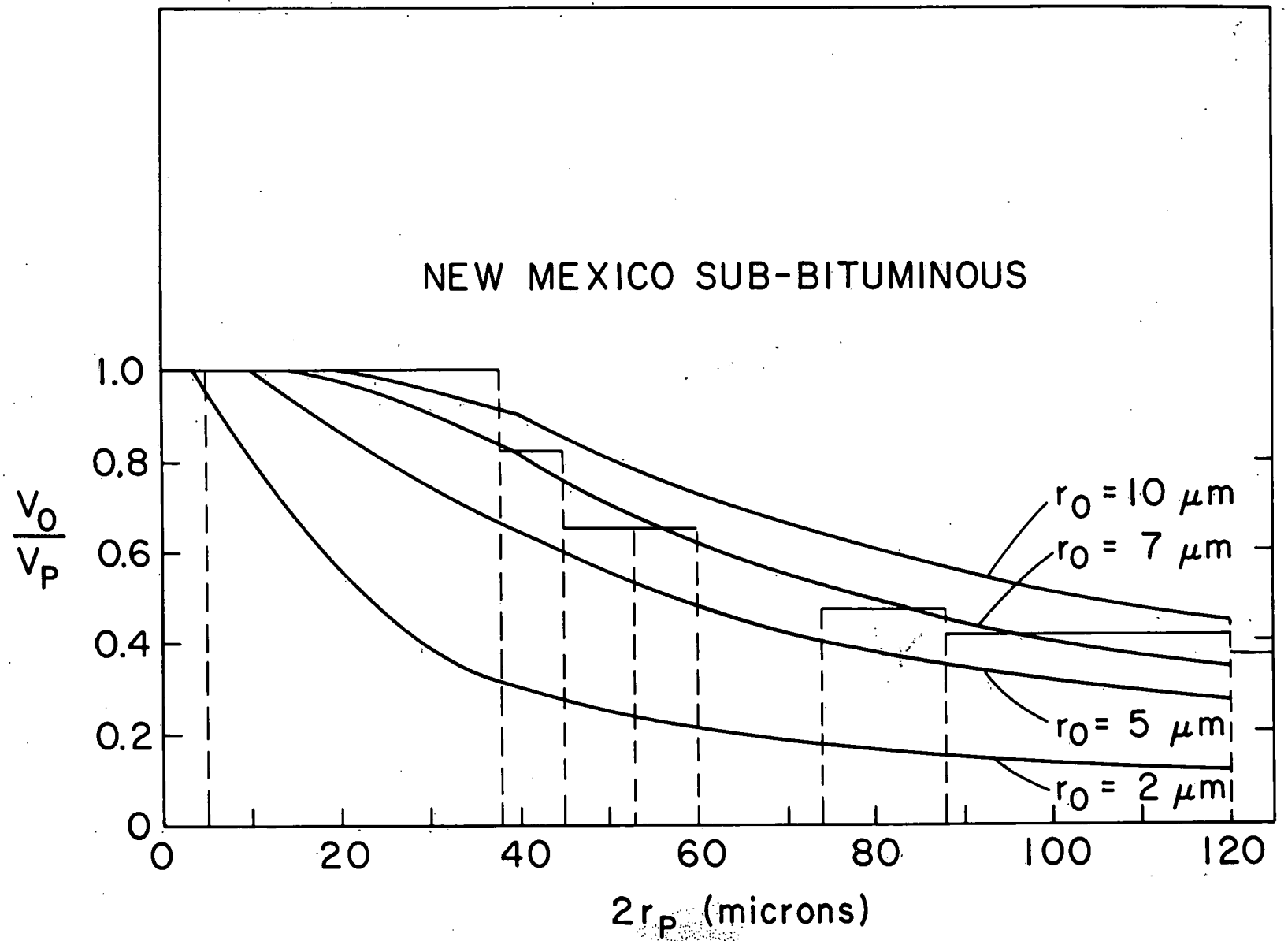

NEW MEXICO SUB-BITUMINOUS
1.0
0.8
0.6
0.4
0.2
0
$\frac{V_O}{V_P}$
0
20
40
60
80
100
120
$2r_P$ (microns)
r_O = 10 μm
r_O = 7 μm
r_O = 5 μm
r_O = 2 μm

Figure 3

Table 1. EP Series Coal Samples

Sample	Mesh	Temp °C	Gas	Time	Moisture (wt %)	Atomic O/C	Corr O/C
A2	84+	none	---	----	27.5	0.799	0.616
B2	84+	vac. oven	---	----	0.0	0.268	0.268
EP-85	84+	50	Air	10	24.0	0.627	0.467
EP-126	84+	100	N_2	60	0.3	0.272	0.270
EP-42	84+	125	MG*	15	12.7	0.378	0.293
EP-48	84+	125	MG*	60	0.5	0.315	0.312
EP-54	84+	150	Air	60	0.6	0.334	0.330
EP-68	140 x 230	50	MG*	30	12.0	0.413	0.333
EP-67(D2)	140 x 230	50	MG*	120	3.0	0.314	0.294
EP-80(J2)	140 x 230	50	Air	30	10.5	0.400	0.330
EP-60	140 x 230	100	N_2	30	0.6	0.328	0.324
EP-65(P2)	140 x 230	100	MG*	30	1.2	0.272	0.264
EP-64	140 x 230	100	MG*	60	----	0.304	0.304
EP-66(Q2)	140 x 230	100	MG*	120	1.2	0.312	0.304
EP-92(R2)	140 x 230	100	Air	5	5.3	0.275	0.240
EP-127	84 x 230	100	Air	5	5.4	0.311	0.275
EP-77	140 x 230	125	N_2	60	0.1	0.330	0.329
EP-71(V2)	140 x 230	150	Air	15	0.2	0.272	0.271
EP-73(X2)	140 x 230	150	Air	120	0.0	0.296	0.296
EP-25(Z2)	140 x 230	200	Air	30	1.4	0.319	0.310

*MG is a mixture of 10% O_2 and 90% N_2.

CLASSIFICATION OF COAL BY TRACE ANALYSIS USING INAA-CLUSTERANALYSIS AND LEACHING OF PRECIPITATOR ASH

H.A. van der Sloot
Netherlands Energy Research Foundation
Petten, The Netherlands

Abstract

In The Netherlands the coal used for energy production is imported from many different countries. This implies a great variability of the (trace) element levels in the ash produced which in turn has implications for disposal and the preferred application in industry (e.g. road filling, brick-and concrete production). To get hold of this variability in precipitator ashes obtained from coals of different origin a classification of coal was performed with clusteranalysis using the elemental composition (CLUSTAN-1C package).
In addition to the measurement of elemental concentrations in coal and ash, leaching experiments were performed with precipitator ash. Elements which are leached appreciably are the halogens, SO_4^{2-}, Mo, W, Cd and Hg. Arsenic and selenium are hardly leached from the alkaline ash studied.

Introduction

At present approximately five percent of the Dutch energy demand is supplied by coal combustion. It is expected that the contribution of coal combustion to the total energy demand in the year 2000 may rise to about 20%. As the Dutch coal reserves can not be exploited economically by the present techniques, coal used for energy production has to be imported from many different countries. This poses serious restrictions to the boiler type used in coal-fired power plants and implies rather great variability in the resulting (precipitator) ash with respect to the major- and minor element composition.
This forms a limitation to the application of these (precipitator) ashes in industry (e.g. brick and concrete production).
In a small, densily populated country with a high ground water level as the Netherlands application of a significant part of the ash produced is a mere necessity. Although knowledge on the impact of ponded precipitator ash on the quality of ground- and surface water is still incomplete, critical factors seem to be SO_4^{2-}, Mo, W, Sb and possibly some other anionic species.
The impact of coal-derived ashes on ground- and surface water is the subject of a project started in 1979 at the Netherlands Energy Research Foundation. It includes the following items:

- The developement of analytical procedures for the accurate measurement of (trace) elements in coal, precipitator ash, bottom ash, fly ash, flue gas and effluents.
- the classification of coals of different origin
- the relation between ash composition (bottom, precipitator and fly ash), coal composition and firing conditions and the mass-balance.
- the leaching characteristics of typical ash samples under natural conditions
- the interaction of ash leachate with bottom sediments (not yet started)

Parts of this project are discussed below.

Analysis

The developement of accurate methods for the analysis of major- and trace constituents in representative samples of coal, bottom ash, precipitator ash, fly ash, flue gas and effluents is a first requirement. Neutron activation analysis employing thermal, epithermal- and fast neutrons covers a great deal of the required analysis [1,2,3]. After a simple preconcentration effluent samples can also be analysed properly [4,5]. The earth alkali elements Ca, Mg and heavy metals Pb, Cu, Cd and Zn are best analysed by atomic absorption, while ion-chromatography is suitable for anions like SO_4^{2-}, NO_3^-, F^-, Cl^- and Br^-. In figure 1 the flow diagram of present capabilities is shown. A considerably overlap of element analysis is maintained for comparison of data obtained with totally different techniques. A high quality (accuracy and precision) is further maintained by analysing home standards and whenever available reference samples or standard reference samples together with actual samples. As far as coal and ash analysis is concerned the Standard Reference Materials of the National Bureau of Standards are best qualified. In Table I

our results for Subbituminous coal 1635, Bituminous coal 1632 A and Coal Fly ash 1633 A are compared with the NBS certified and proposed values. The agreement is generally good.

ıssification

After analysing some 140 coal samples by instrumental neutron activation analysis data were obtained for 20-30 delements. Since a data matrix of this size can only be handled with sophisticated computerprograms, the clustering package CLUSTAN-IC (D. Wishart, Computer Centre, University College London) has been applied to classify the samples (cases).

The program used for calculation of the element concentrations produces punched cards with sample codes and element concentrations in fixed format. These cards have been used as input to CLUSTAN. Elements showing large analytical errors or elements detected occasionally were eliminated. Ultimately seventeen elements were used in the classification. To avoid bias towards variables with large variances the data have to be standardised prior to hierarchic fusion. Starting with n clusters (here n = 134), each containing a single case, the method completes (n-1) fusion steps in which the two clusters which are most "similar" are combined.

Several methods using either similarity or dissimalarity type correlations were tried. In the optimization the best results were obtained with procedure Centroid using product-moment correlations. A random start, as suggested by Everitt [6], to test the stability of the clusters obtained, proved to have no influence on the number of clusters, the clustersize or composition. The omission of a few variables or part of the samples neither. This may indicate that stable clusters have been obtained.

Starting with a classification into 30 clusters obtained with procedure Centroid procedure Relocate was activated, in which each sample is considered in turn by iterative relocation and its similarities with all 30 clusters are computed. Whenever its simularity with the parent cluster is smaller than with one of the other clusters the sample is moved to the other cluster and centroids are recomputed. Scanning down to 11 clusters showed a considerable relocation of samples at a classification in 18 clusters. In table II the number of relocations after succesive iterations is given for each number of clusters between 30 and 11.

Table II. Results of procedure RELOCATE

Number of clusters	Relocations at iteration 1	2	3	4	Number of clusters	Relocation at iteration 1	2	3	4
30	0				20	1			
29	0				19	0			
28	4	2			18	8	19	8	1
27	1	1			17	0			
26	1				16	1			
25	1				15	5	2		
24	0				14	0			
23	1				13	0			
22	1	2	1		12	0			
21	2				11	1			

Ri; introducing replicate analyses of one and the same sample (AUS1-4, ZA1-4) is possible to give an estimate of insignificant differences caused by the analytical error resulting from the analytical method used to obtain the data (Dotted line in figure 2). For the 134 coal samples this reduces the maximum number of clusters from 134 to about 66. Going from 1 to 134 clusters a

relative sharp increase in the number of clusters is noted at similarity measure +0.5, which corresponds to some 20 clusters.

In figure 2 the classification obtained with Centroid sorting is shown. The identification of samples is as follows:

Aus	= Australian	Duits	German
Can	= Canadian	Ruhr	German
Eng	= English	Aken	German
ZA	= South-African	Pool	= Polish
Rus	= Russian	Chin	= Chinese
Amer	= American	India	= Indian
Tjech	= Czech	Ned	= Dutch

It should be stated that the coal samples used in the classification were obtained through power plants purchasing at the international market. Unfortunately the precise origin of the samples is often unknown. Using the American classification system most of these coals fall in the rank low- and medium volatile bituminous. In the classification shown here two distinct groups are identified within the samples from South-Africa. Obviously, there are at least two distinct coal basins. Although the number of samples used in the classification should be larger, the identification of coal samples by their trace element content is working satisfactory. Since the trace element composition of precipitator ash obtained by burning one type of coal in a powder-coal fired boiler is remarkably constant, it seems possible to estimate the effect of firing certain types of coals on ash composition in advance. A further extention would be to relate ash leachability characteristics to coal composition and boiler-type.

Leaching

In general results obtained from leaching experiments are difficult to compare, because widely different conditions are used to measure leachability. Variables are the weight ratio of ash to "water", the choice of the leach solution, the experimental set-up: column- or batch-wise leaching [7,8,9,10,11].

We have tried to compare the results of a relatively time-consuming column-experiment with data obtained from rapid shaking experiments using mildly neutron activated ash. In both experiments the same ash was used, collected from the electrostatic precipitatorsof a powder coal-fired power plant burning a (2:1:1) mixture of German, Polish and South-African coals at the time. Due to the relatively high Ca-content the ash is strongly alkaline, thus imposing a pH of 12 upon any natural leaching solution (e.g. rainwater, surface water, groundwater). Therefore all experiments were carried out with demineralized water.

- In the shaking experiments portions of 10 g ash were irradiated during 10 hours at a thermal neutron flux of 10^{11} n.cm^{-2}s^{-1}. The irradiated ash samples were transferred to 250 ml centrifuge bottles and to each sample 100 ml of demineralized water was added. At subsequent time intervals a bottle was taken from the shaking machine centrifuged and supernatant withdrawn. The solution was filtered through a 0.45 µm membrane filter and split in two fractions. One fraction of 5 ml was measured directly and the other fraction (70-80 ml) was used for preconcentration of trace elements of interest on active carbon or by coprecipitation with $Fe(OH)_3$. In this way interfering ^{24}Na, ^{82}Br and ^{42}K-activities were eliminated [12]. In figure 3 the leaching characteristics of Br, Mo, W, Na, Cr en K are given showing that equilibrium is obtained after a contact-time of $\sim$ 24 hours. The percentage leached is expressed as the fraction of the total amount of the element present in the ash. In figure 4 the leaching characteristics of As, Se and Sb are given. These three elements are showing a markedly different behaviour. After an initial release of these elements from the ash resorption occurs after a longer contact-time between ash and solution. Tracer experiments with "cold" ash using ^{75}Se, ^{74}As and ^{125}Sb tracers showed a rapid decrease of the soluble fraction of the added tracer. The curves for antimony are identical in both leaching and tracer experiment.

- In the column experiments approximately 16.5 kg of precipitator ash was transferred dry to a column of 300 mm diameter and 150 mm height. To avoid clogging and inclusion of airbubbles up-flow was applied. At the very slow flow-rate of 1 l demineralized water a day this column was leached. The effluents collected were analyzed by atomic absorption, ion-chromatography and neutron activation analysis, both instrumental and after preconcentration of trace elements by adsorption to active carbon or coprecopitation with iron hydroxide. The results obtained are given in figures 5 to 8 showing the leaching characteristics of Ca, K, Na, SO_4^{2-}, Cl, W, F, Fe, Cu, Pb, Ni, Te, Zn, Se, As, Mo, Cr^{3+}, V, Hg, Cr^{6+}, Al, Sb and La. Here the actual concentrations measured in the effluents are given. In table III a summary of both experiments in terms of percentage leachable relative to the total concentration in the ash is given. For comparison the total concentration in the ash is included.
The agreement between the batch- and column experiments is generally good. The proces of resorption of arsenic, selenium and antimony in the batch tests is confirmed in the column experiments by the extremely low leaching percentages. The extremely low leaching of arsenic is in contradiction with some published data stating that at high pH arsenic is released to a considerable extent [7]. Our data agree with those of Dreesen [10]. In the long run other processes tend to release antimony again. The elements leached most are the halogens, Mo, W, Cd and Hg. From the shape of the leaching curves shown in figures 5 to 8 it may be concluded that SO_4^{2-}, F, Pb, Ni, Te, Se, As, Mo, Cr and to a lesser extent Ca, V and Hg are concentrated on the surface of the precipitator ash particles. This seems to be related to the volatility of the elements during the coal-burning proces. The less volatile components form the matrix of the ash particles which are covered by a condensate of volatile components in the cooler parts of the boiler installation.
The elements Fe, Cu and Zn show a more or less constant leaching, whereas Na, K, Cl and Br (not shown) are removed immediately, which is in agreement with the speed in which equilibrium is attained in the batch experiments. Tungsten, Al, Sb and La leachability is initially low but shows a sharp increase after about one bed volume, then reaching a more or less constant level. This type of behavior might be related to solubility limitations. At present a similar study is undertaken with an acidic ash.

References

1. C. Block and D. Dams, Anal. Chim. Acta, 68 (1973) 11.
2. E. Steines and J.J. Rowe, Anal. Chim. Acta, 87 (1976) 451.
3. W.S. Lyon, Trace element measurements at the coal-fired steam plant, CRC-Press (1977).
4. H.A. van der Sloot, ECN-1, Petten (1976).
5. G.D. Wals, et al., to be published in J. Radioanal. Chem.
6. B. Everitt, Cluster analysis, H.E.B., London (1977).
7. T.L. Theis and J.L. Wirth, Environ. Sci. Technol., 11 (1977) 1096.
8. W.D. James, M. Janghorbani and T. Baxter, Anal. Chem. 49 (1977) 1944.
9. E.A. Crecelius, Marine Chem., 8 (1980) 245.
10. D.R. Dreesen, et al, Environ. Sci. Technol., 11 (1977) 1017.
11. Radian Corporation, PB-252 090 (1975).
12. H.A. van der Sloot, et al., Anal. Chem., 52 (1980) 112.

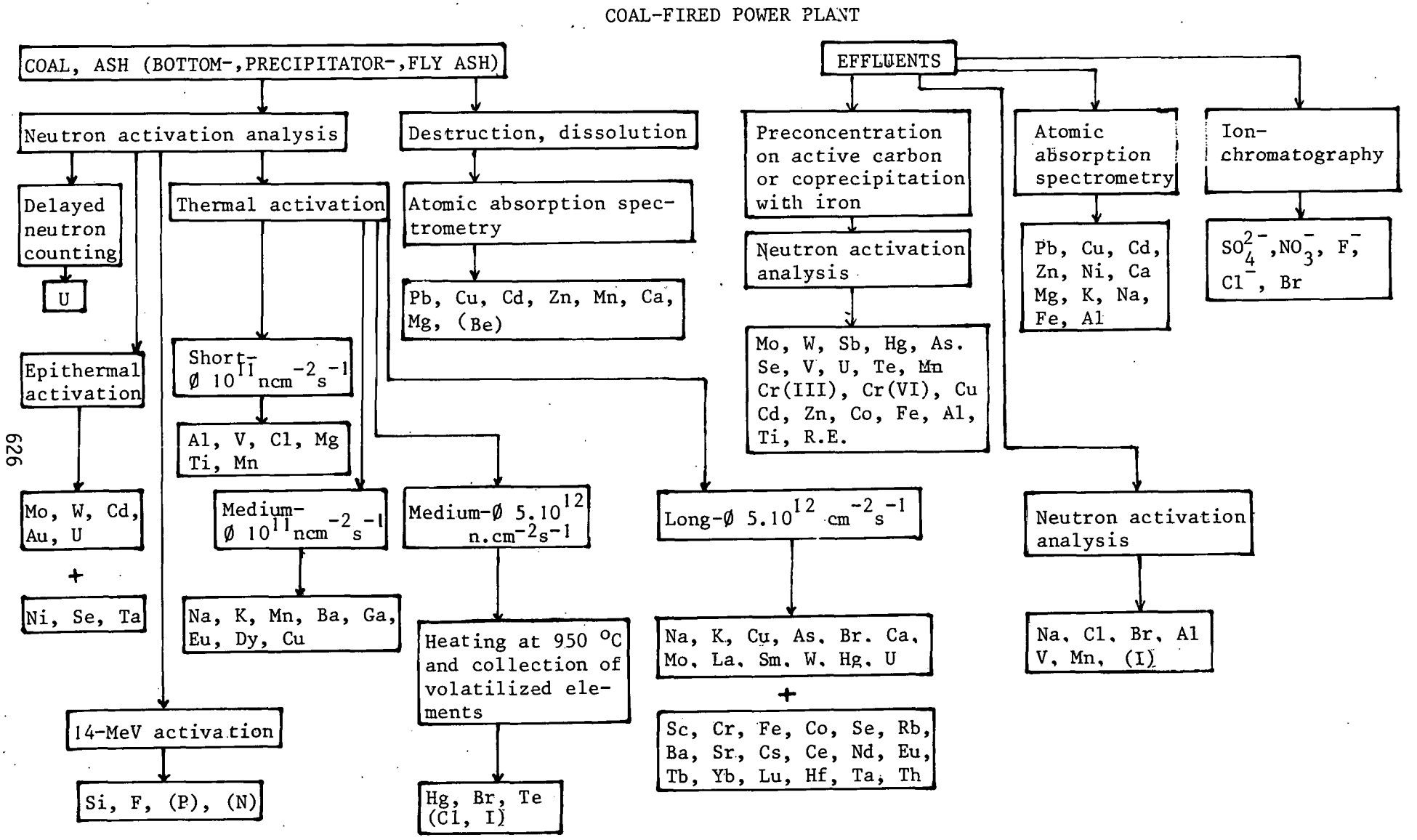


Fig. 1. Flowsheet of analytical procedures

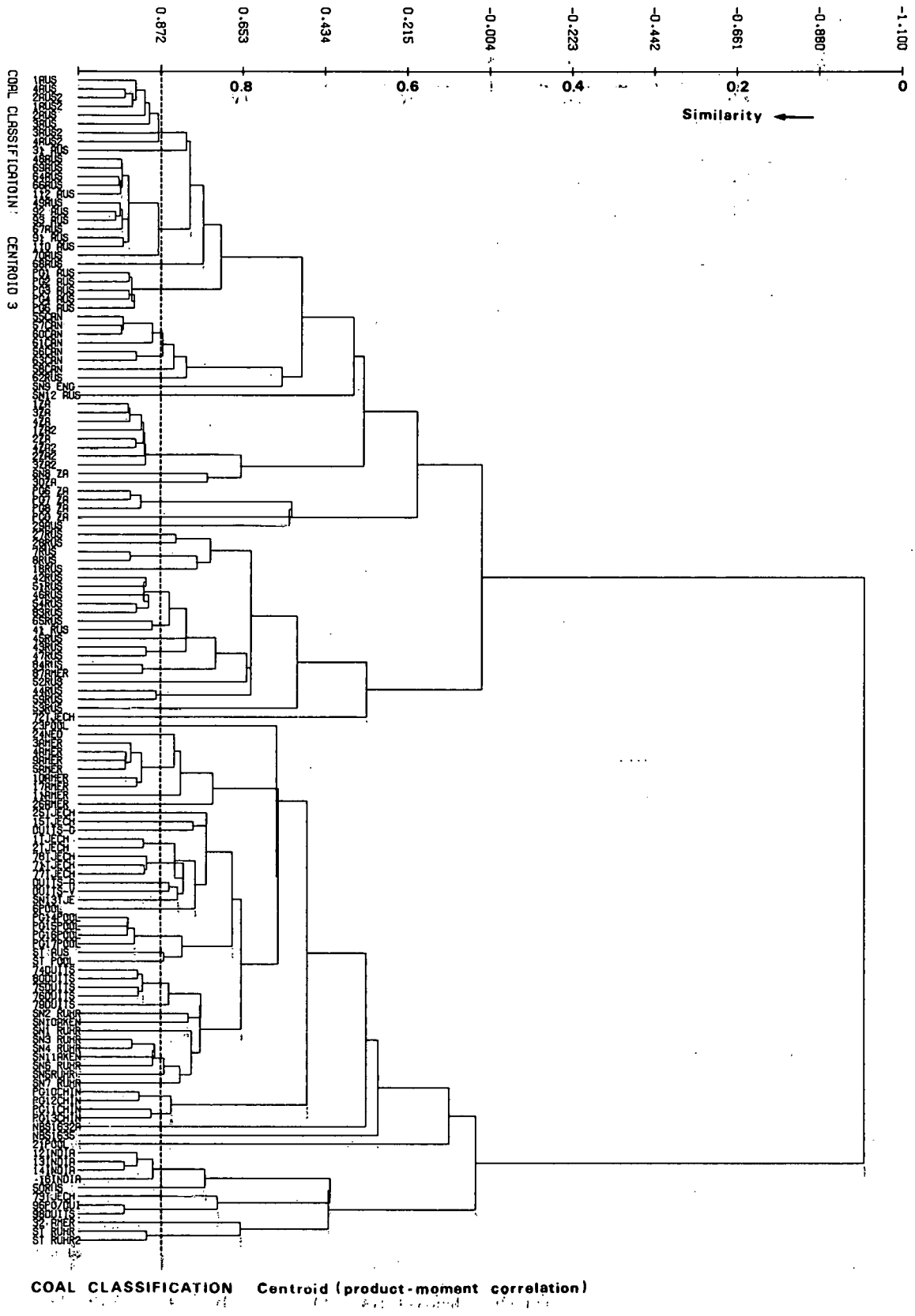
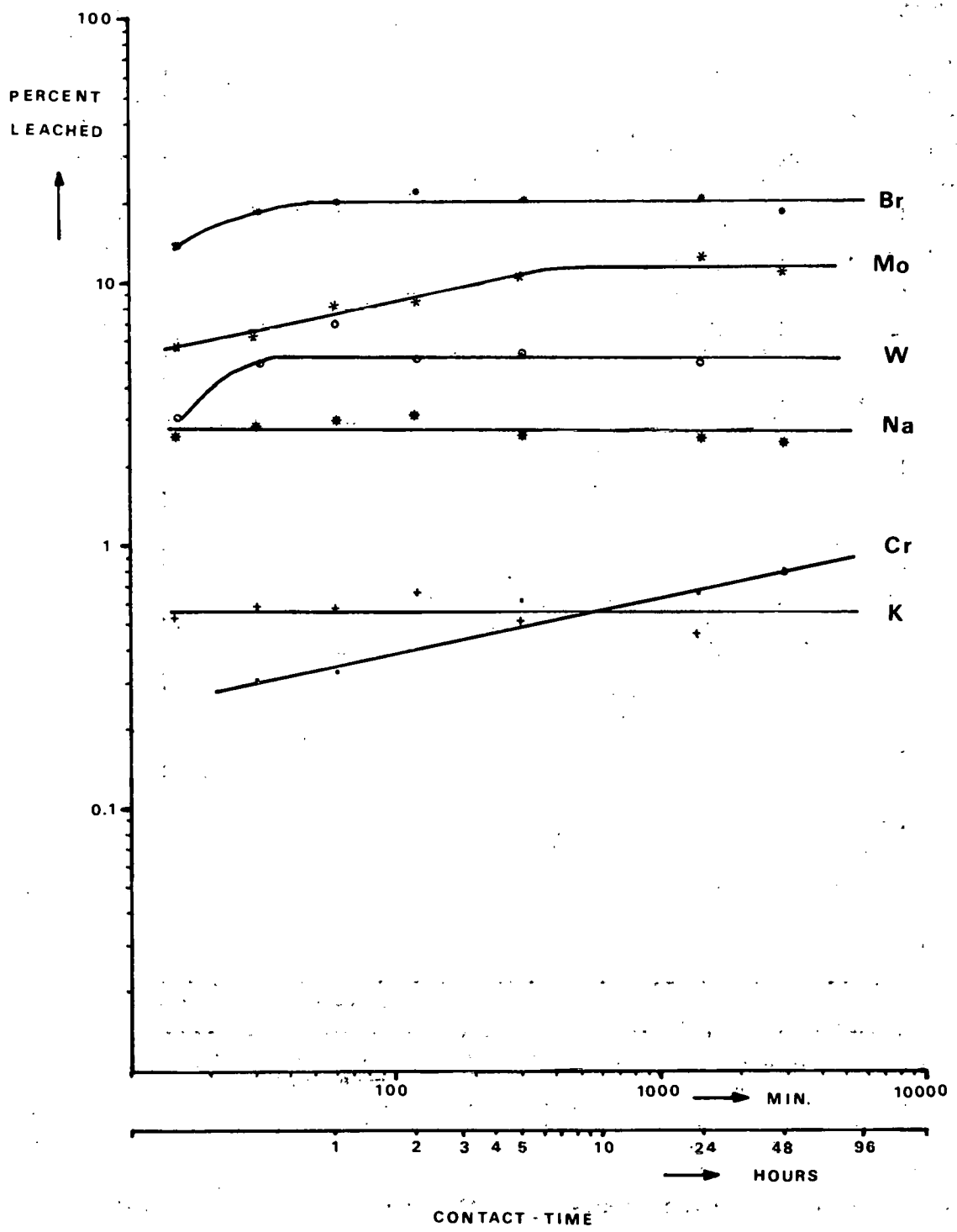
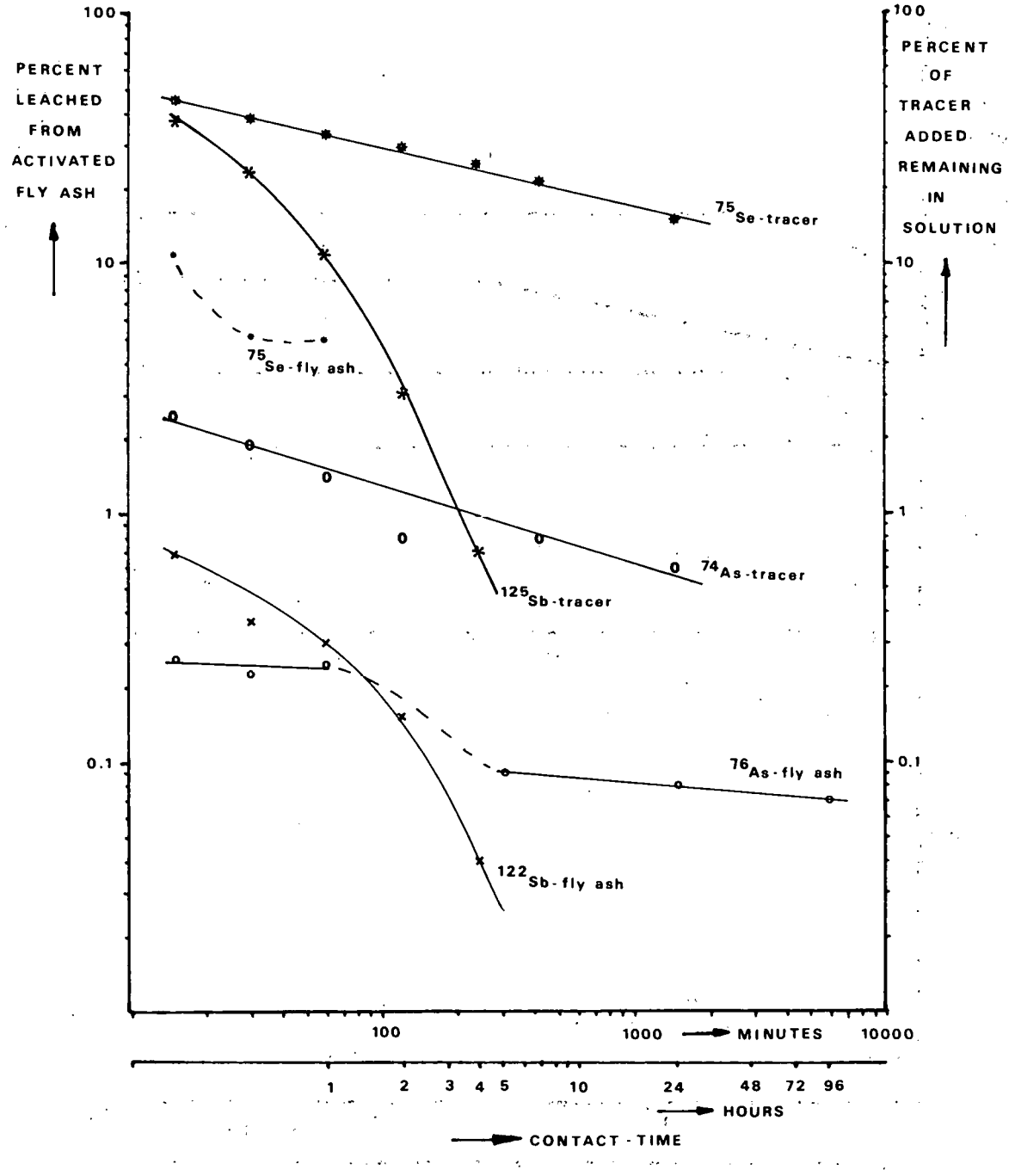

0.872
0.653
0.434
0.215
-0.004
-0.223
-0.442
-0.661
-0.880
-1.100
0.8
0.6
0.4
0.2
0
Similarity
COAL CLASSIFICATION: CENTROID 3
COAL CLASSIFICATION Centroid (product-moment correlation)

Fig. 2



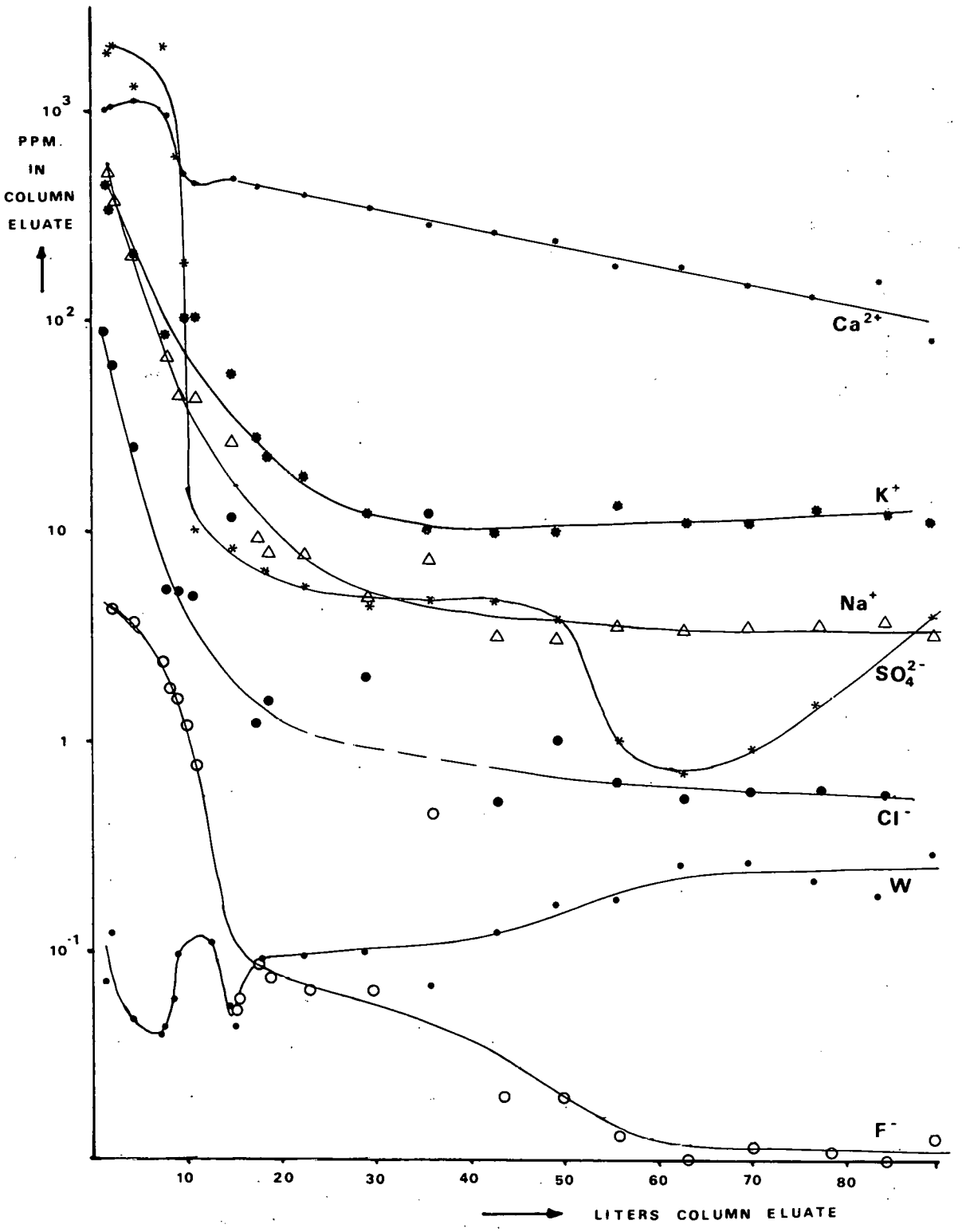
Leaching of fly ash in 1:10 ratio with demineralized water.

Fig. 3



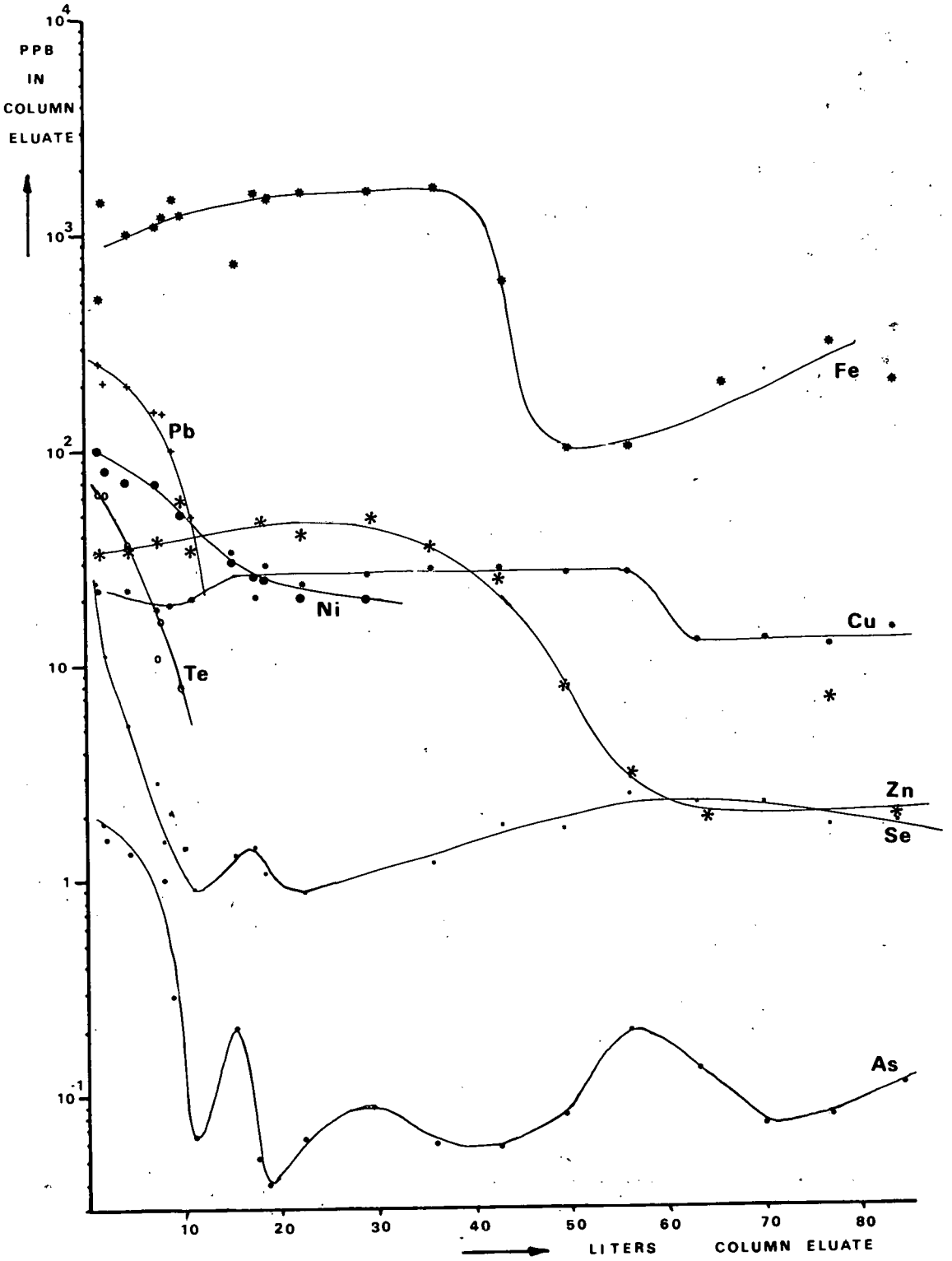
Leaching and tracerexperiments with fly ash in a 1:10 ratio with demineralized water

Fig. 4



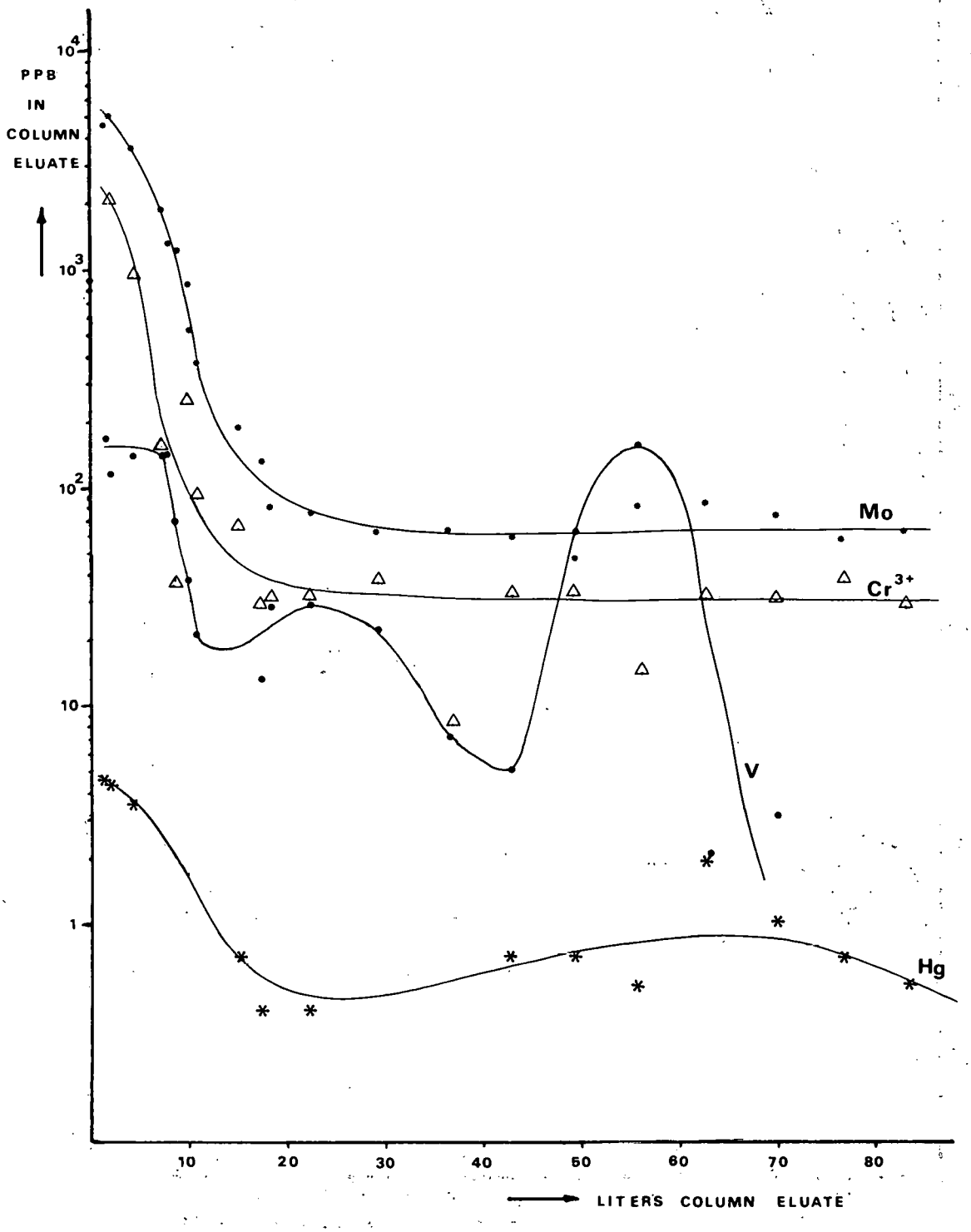
Leaching of a 16-kg fly ash column at 1 liter per day.

Fig. 5



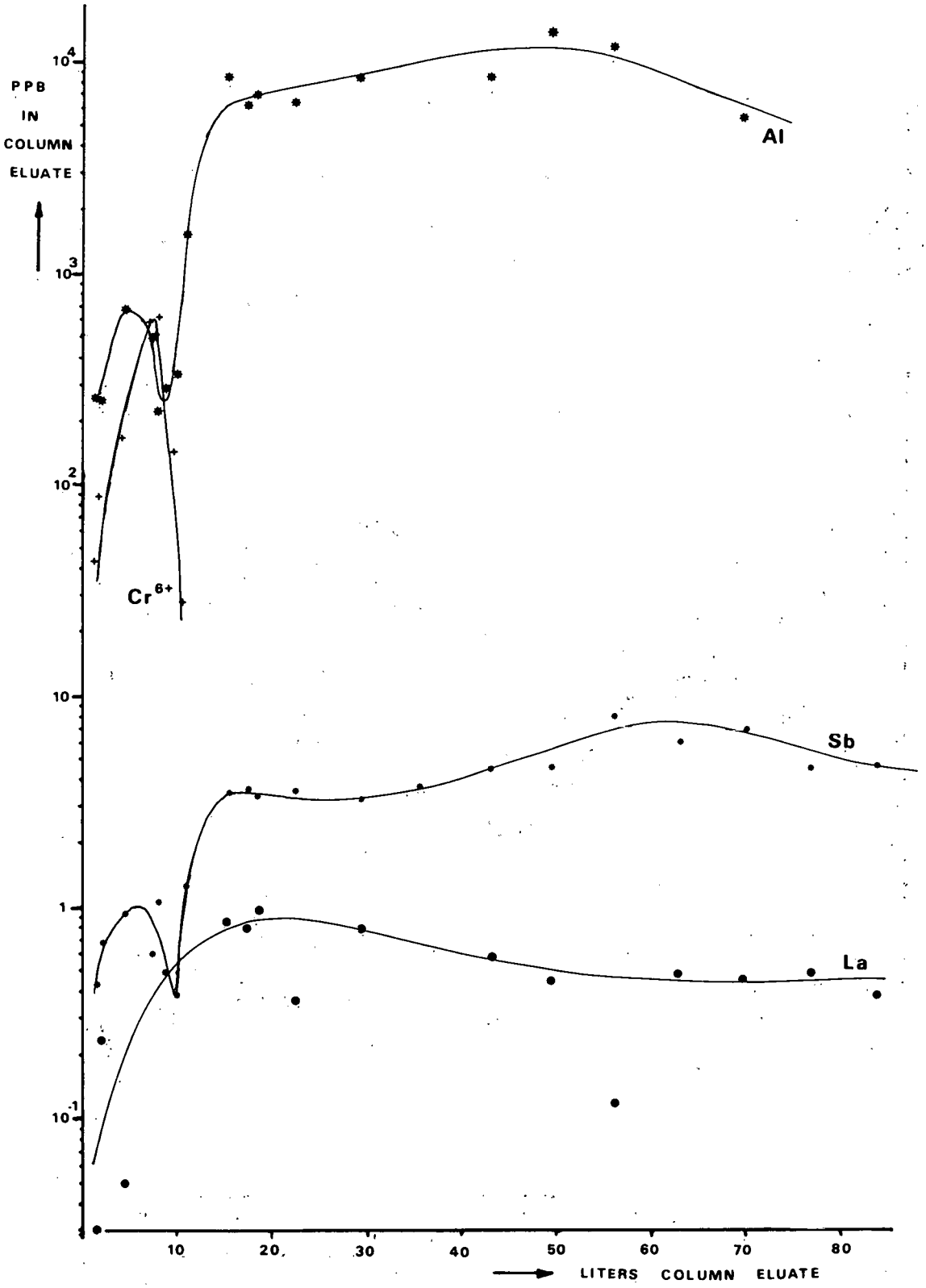
Leaching of a 16-kg fly ash column at 1 liter per day.

Fig. 6



Leaching of a 16-kg fly ash column at 1 liter per day.

Fig. 7



Leaching of a 16-kg fly ash column at 1 liter per day.

Fig. 8

Table I. Analytical data on NBS Standard Reference materials

	NBS 1632 A Bituminous coal		NBS 1635 Subbituminous coal		NBS 1633 A Coal Fly ash	
Element	ECN	Certified	ECN	Certified	ECN	Certified
Na(%)	0.0905±0.0015	0.085±0.0045	0.2180±0.001	0.2440±0.02	0.167±0.002	0.17±0.01
K (%)	0.44±0.01	0.42±0.02	-	-	1.73±0.05	1.88±0.06
Fe(%)	1.14±0.02	1.11±0.02	0.20±0.01	0.24±0.005	9.40±0.05	9.4±0.1
Si(%)						22.8±0.8
As	10.6±0.2	9.3±1.0	0.73	0.42±0.15	141±1	145±15
Ba	150±40		80±10		1350±200	(1500)
Br	43±0.5		0.81±0.10		2.0±0.1	
					3.6 (chem)	
Ce	34±1	(30)	3.4±0.2	(3.6)	190±1	(180)
Co	6.07±0.03	(6.8)	0.58±0.03	(0.65)	42.6±0.5	(46)
Cs	2.2±0.1	(2.4)	-	-	9.7±0.3	(11)
Cr	34±1	34.4±1.5	3.1±0.05	2.5±0.3	188±5	196±6
Eu	0.50±0.02	(0.54)	0.044±0.003	(0.064)	3.6±0.1	(4)
Hf	1.37±0.04	(1.6)	0.27±0.07	(0.29)	6.6±0.2	(7.6)
Hg	-	0.13±0.03	-	-	0.14 (chem)	0.16±0.01
La	13.5±0.2		1.54±0.04		72±0.5	
Lu	0.18±0.01		0.023		1.20±0.02	
Mo	-		-		46	(29)
Ni	-		-		130±20	127±4
Nd	13	12±3	-	1.4	95±10	
Rb	25±1	31	-	-	127±5	131±2
Sb	0.72±0.05	(0.58)	0.15	(0.14)	7.1±0.1	(7)
Sc	6.05±0.02	(6.3)	0.50±0.02	(0.63)	36.6±0.1	(40)
Se	3.8	2.6±0.7	0.9	0.9±0.03	10.5±1.0	10.3±0.6
Sm	2.80±0.05	2.1	0.27	0.25	16.7±0.2	
Sr	-		150±50		1000±200	830±30
Ta	0.33		-		1.7±0.1	
Tb	0.35±0.07		-		2.6±0.1	
Th	4.6±0.1	4.5±0.1	0.41±0.05	0.62±0.04	26±1	24.7±0.3
Tm	-		-		3.7	
U	-	1.28±0.02	-	0.24±0.02	8.1±0.3	10.2±0.1
W	0.94±0.02	-	0.19	-	5.4±0.8	
Yb	1.24±0.10		0.15		7.45±0.05	
Zn	25	28±2	-	4.7±0.5	260±50	220±10

Tabel III

Leaching experiments with fly-ash (column-batch)

Element	Percent Leachable				
	Column (16.5 kg percolation at 1 l demineralized water per day)		Batch (10 g in 100 ml demineralized water)		Total concentration in fly ash
	After 10 l	After 90 l	after 15 min	after 2 days	
Na	2.2	2.6	2.6	2.6	0.52%
K	0.5	0,8	0.53	0.50	2.2%
Ca	0.018	0.053	-	-	3.6%
Fe	0.001	0.005	-	<0.07	6.23%
Mg	0.0031	0.0060	-	-	2.03%
Br	33	41	20	28	6ppm
Cu	0.009	0.072	-	<0.1	210ppm
Cd	0.61	0.72	-	-	2.5ppm
Co	0.0016	0.005	-	-	55ppm
Mn	0.00003	0.0007	-	-	1045ppm
Zn	0.000006	0.00003	-	<0.2	430ppm
Ni	0.012	0.018	-	-	120ppm
Pb	0.049	0.068	-	-	205ppm
As	0.0025	0.0045	0.27	0.07	26ppm
Se	0.0007	0.002	12	<1	6.2ppm
Sb	0.003	0.2	0.7	0.02	14.4ppm
Mo	6.7	8.1	5.6	11	25ppm
W	0.07	1.4	3	5	6.7ppm
Cr(III)	0.26	0.4	0.2	0.8	} 162ppm
Cr(VI)	0.14	0.15			
Au	0.013	0.07	-	-	~0.3ppm
La	0.0003	0.0005	-	-	65ppm
Hg	0.18	0.73	-	-	0.6ppm
pH	12.5	12.4	12.5	12.5	

Studies of Oxygen and Nitrogen in Coal Conversion Liquids by 14 MeV INAA

Samir R. Khalil, David W. Koppenaal* and William D. Ehmann

*Institute of Mining and Minerals Research and
Department of Chemistry, University of Kentucky,
Lexington, KY 40506

Abstract

Fast neutron activation analysis has been used for the direct determination of oxygen and nitrogen in coal conversion liquids. The technique is based on the $^{16}O(n,p)^{16}N$ and $^{14}N(n,2n)^{13}N$ reactions induced by 14 MeV neutrons produced by a Cockcroft-Walton neutron generator. Multiscaler counting of the 6.13 and 7.12 MeV ^{16}N photopeaks is used for the oxygen analyses. The detection system consists of two 7.6 x 7.6 cm NaI(Tl) scintillation detectors, mounted at 180° and connected to a summing amplifier. The samples are rotated uniaxially in both the irradiation and counting positions. Multiscaler coincidence counting of 0.511 MeV annhilation photons from the positron decay of ^{13}N is used for the nitrogen analyses. Oxygen and nitrogen contents in coals and coal conversion liquids are highly variable. Differences in gamma-ray self-absorption of the low average atomic number organic matrix in coal liquids and the higher average atomic number USGS BCR-1 and NBS $K_2Cr_2O_7$ oxygen standards normally used for oxygen determinations in geochemical matrices have been observed. Therefore, two separate sets of organic liquids were selected and evaluated for use as oxygen or nitrogen standards in the analyses of coal-derived liquids. Dilutions with n-hexane, or mixtures of two compounds from the selected liquid standard sets make it possible, if desired, to "fine tune" oxygen and nitrogen levels in the standards to values corresponding to those anticipated in the coal conversion liquids being studied. The standard liquids are selected using criteria of high boiling point, high purity, consistent stoichiometry, a non-hygroscopic nature, and simple CHO or CHN elemental composition. Possible interferences from recoil proton reactions on carbon and oxygen are considered for the nitrogen determinations. Excellent agreement between the 14 MeV INAA experimental data and calculated stoichiometric values has been demonstrated for organic liquids over a wide range of oxygen and nitrogen contents. Variations in oxygen and nitrogen contents at intermediate stages of coal conversion processes are being studied.

Introduction

The precise and accurate determination of oxygen and nitrogen in coals and coal conversion liquids is of considerable current interest. Organic oxygen containing sites in coal are suggested to be active sites in the conversion processes and low oxygen contents of the conversion liquids are used as gauges of the efficiencies of the conversion processes. The presence of nitrogen in fuels presents numerous technological and environmental problems. The environmental ramifications of utilizing high nitrogen fuels include the release of NO_x compounds to the atmosphere[1]. These NO_x pollutants may then contribute to the formation of acid rain. Various other nitrogen gases, such as molecular nitrogen, ammonia, and hydrogen cyanide are released under reducing conditions

of coal gasification and liquefaction processes[2].

Oxygen has traditionally been determined by performing analyses for C, N, H and S in a dried coal sample, correcting for ash content and assuming the mass difference to be the organically bound oxygen content of the coal[3]. Direct determinations of total oxygen in different matrices have recently been achieved using the instrumental 14 MeV neutron activation analysis (INAA) technique[4-8]. USGS Standard Rock BCR-1 and NBS Standard Reference Material 136b, $K_2Cr_2O_7$, were commonly used oxygen standards for oxygen determinations in small solid samples.

Nitrogen is ordinarily determined by the time-consuming Kjeldahl method which requires sample dissolution. The 14 MeV INAA technique has been used in the determination of nitrogen in a variety of matrices[9-11]. Several different comparator standards have been used to calculate the nitrogen contents in various matrices[11]. N-1-naphthylacetamide (7.56% N) was used as a primary comparator in coal nitrogen determinations[4] because it has a bulk elemental composition very similar to bituminous coals.

Several problems exist in the use of solid standards for the determination of oxygen and nitrogen in coal conversion liquids by the 14 MeV INAA technique. These include the geometry and density differences between the liquid samples and the solid standards which have been previously used. In order to obtain comparable detector responses for samples and standards while retaining uniform irradiation and counting geometries, liquid standards of widely varying oxygen or nitrogen content are desired. The average atomic numbers and densities of the liquid standards chosen should be close to those for typical coal conversion liquids in order to minimize both neutron and gamma-ray self-absorption effects when large samples are used to achieve greater sensitivity.

In the present study, two sets of selected organic liquids have been evaluated for use as oxygen and nitrogen standards in the analysis of coal conversion liquids. These liquids have been used as both primary and reference standards to demonstrate the precision of oxygen and nitrogen determinations in a number of coal conversion liquids and fuel and shale oils. The accuracy and precision of the technique have been further confirmed by replicate analyses of NBS Standard Reference Materials and USGS standard rocks using NBS $K_2Cr_2O_7$ as primary standard for oxygen and N-1-napthylacetamide for nitrogen.

Experimental

Oxygen contents were determined in this study by an instrumental 14 MeV neutron activation technique similar to that described by Morgan and Ehmann[12]. The technique is based on the $^{16}O(n,p)^{16}N$ reaction induced by the exposure of the sample to the 14 MeV neutrons produced by a Cockcroft-Walton neutron generator, which is coupled to an automatic sample transfer and counting system[4,8]. A 10.2 cm x 10.2 cm NaI(Tl) well-type scintillation detector was originally used[4,6,7] to measure the radioactivity of the 7.35 s half life ^{16}N product which emits highly energetic γ-rays of 6.13 and 7.12 MeV. With the large coal liquid samples required to be used for increased analytical sensitivity, a portion of the sample extended outside of the most efficient region of the well-type detector. Therefore, to improve the counting efficiency, a new counting system consisting of two solid 7.6 cm x 7.6 cm NaI(Tl) detectors mounted at 180° with respect to a uniaxially spinning sample holder is employed. Each detector is connected through a linear amplifier to a sum/invert amplifier. The output is fed to a single channel analyzer which is gated to the energy region between 5 and 8.0 MeV. Neutron flux density is monitored every 0.8 seconds with a BF_3 neutron proportional counter for flux variation correction. Both the output of BF_3 counter and the single channel analyzer are gated to a ND 2200 multichannel analyzer operating in the multiscaler mode. The recorded time spectrum

from the analyzer is computer processed to yield the oxygen data.[12] **Exclusive of the time required to package the samples in the polyethylene "rabbits", it is possible to analyze up to 200 samples in one working day.**

Nitrogen contents are determined by a 14 MeV INAA technique similar to that described by James et al[4]. The technique is based on the ^{14}N (n,2n) ^{13}N nuclear reaction induced by exposing the sample to the 14 MeV neutrons. The ^{13}N product decays via positron emission with a 9.96 m half life, and the nitrogen content is determined by coincidence of counting the 0.511 MeV annihilation photons using the two solid 7.5 cm x 7.6 cm NaI(Tl) detectors. Each detector is connected through a linear amplifier to a single channel analyzer. These two analyzers are each gated on the 0.511 MeV radiation triggering a fast coincidence unit, and the output of this unit is fed to a scaler. To discriminate against the potential interference from the annihilation radiation of ^{30}P produced by ^{31}P (n,2n) ^{30}P reaction, a 12.5 m delay time was selected before counting for 20 m. Other significant potential interferences due to proton recoil reactions, $^{12}C(p,\gamma)^{13}N$, $^{13}N(p,n)^{13}N$ and $^{16}O(p,\alpha)^{13}N$ were evaluated experimentally by using appropriate standards.

All samples are packed in previously cleaned 2-dram virgin polyethylene vials under an inert atmosphere of helium. If only oxygen determinations are required, samples may be packaged under a nitrogen atmosphere.

For use as standards in the determination of oxygen and nitrogen contents in coal conversion liquids, two separate sets of organic liquids were selected by using criteria of high boiling point, well-defined stoichiometry, high purity, non-hydroscopic nature[13] and simple C-H-O or C-H-N elemental composition. These standards are listed in Tables I and II, along with their

Table I

Selected standards for INAA oxygen determinations in coal conversion liquids

Samples	Formula	% Oxygen by stoichiometry
Methyl alcohol	CH_3OH	49.49
1,2,5-Trihydroxyhexane	$HOCH_2CH(OH)(CH_2)_4OH$	35.77
1,5-Pentanediol	$HO(CH_2)_5OH$	31.30
2-(2-n-Butoxyethoxy) ethanol	$CH_3(CH_2)_3OCH_2CH_2OCH_2CH_2OH$	29.59
2-Propanol	C_3H_7OH	26.68
1-Butanol	$CH_3CH_2CH_2CH_2OH$	21.62
2-Propanol and 1-Octanol mixture (1:1)	--	19.87
4-Methyl-2-pentanol	$(CH_3)_2CHCH_2CH(OH)CH_3$	16.39
1-Octanol	$CH_3(CH_2)_7OH$	13.05
Benzyl ether	$(C_6H_5CH_2)_2O$	8.88
Benzyl ether and n-hexane mixture (2:5)	--	3.55

Table II

Selected standards for INAA nitrogen determinations in coal conversion liquids

Samples	Formula	% Nitrogen by stoichiometry
Dimethylcyanamide	$(CH_3)_2$ NCN	39.96
1,2-propanediamine 97%	$CH_3CH(NH_2)CH_2NH_2$	36.66
Dimethylcyanamide and aniline mixture (3:2)	--	29.98
Dimethylcyanamide and quinoline mixture (2:3)	--	22.23
Pyridine 99%	C_5H_5N	17.53
Aniline 99.9%	$C_6H_5NH_2$	15.02
N-heptylamine 99%	$CH_3(CH_2)_6NH_2$	12.04
Di-n-butylamine 99%	$NH[(CH_2)_3CH_3]_2$	10.81
Quinoline 96%	C_9H_7N	10.41
Di-n-octylamine 97%	$NH[(CH_2)_7CH_3]_2$	5.63
Quinoline and n-hexane mixture (2:9)	--	1.89

molecular formulae and stoichiometric O or N contents. Mixtures of standards, or dilutions with n-hexane were used to fill gaps or to extend the range to lower levels.

Results and Discussion

Oxygen Determinations

The oxygen content of each selected organic compound or mixture was first determined with using NBS Standard Reference Material $K_2Cr_2O_7$ and USGS Standard rock BCR-1 as comparator standards. These standards are normally used in the analyses of silicate rocks. As expected, the plot of experimental oxygen values versus stoichiometric oxygen contents indicated that a strictly linear relationship existed, but the least squares fitted line did not pass through the origin. This deviation was interpreted to be due to the irradiation and counting geometry factors and also neutron and gamma-ray self-absorption differences between the organic liquids and solid standards related to varying matrix densities and compositions. A single geometry/self-absorption correction factor was calculated and was applied to all the experimental data. Excellent agreement between the final experimental values and calculated stoichiometric oxygen contents was obtained. The least squares fitted line, corrected to pass through the origin, yielded a correlation coefficient of 0.9995 for ten different compounds or mixtures covering a range of 3.55 to 49.94% in oxygen content. Compared to the single 10.2 cm x 10.2 cm well-type NaI(Tl) detector system which had been used in our previous work[4,6,8], the new paired detector system resulted in a 1.31 ± 0.05 times improvement in the analytical sensitivity.

The precision and accuracy of our technique for the determination of oxygen in several pure organic liquid samples are shown in Table III. For ten replicate analyses, standard deviations of the mean of ± 0.3 to 1.1% relative, were observed. Variations of the INAA experimental means from the stoichiometric oxygen contents were in the range of ± 0.2 to 2.3%, relative.

Table III

Precision and accuracy of INAA oxygen determinations on organic liquids

Determination No.	Experimental % oxygen 2-(2-n-Butoxyethoxy) ethanol	1-Butanol	1-Octanol	Benzyl ether and n-hexane (2:5)
1	29.53	21.96	12.60	3.63
2	30.14	22.33	13.07	3.57
3	29.53	22.38	13.39	3.51
4	30.00	21.89	13.17	3.51
5	29.73	21.13	12.81	3.62
6	29.60	21.19	12.85	3.84
7	29.92	22.21	12.96	3.82
8	29.19	21.35	13.62	3.56
9	29.45	21.56	12.71	3.48
10	29.53	22.04	13.64	3.52
mean	29.66	21.80	13.08	3.61
std. dev. of mean	±0.09	±0.15	±0.12	±0.04
% oxygen by stiochiometry	29.59	21.62	13.05	3.55

*Benzyl ether and 1,5-pentanediol were used as standards.

The method has recently been applied to typical coal conversion liquids and other conversion by-products. The means of five replicate determinations on several coal conversion products are given in Table IV. The data exhibit a precision of better than ± 1.54%, relative, over a range of oxygen contents from 3.88% to 28.89% and ∿ 3%, relative, for H-coal process sample with lower O contents.

Nitrogen Determinations

For each pure compound or mixture selected, the nitrogen contents were first determined by using N-1-naphthylacetamide as a primary standard and NBS SRM 912 urea and 148 nicotinic acid as secondary reference standards. Important interferences are due to "Knock-on reactions" where the incident 14 MeV neutrons undergo collisions with protons in the polyethylene vials and in the sample itself and generate a flux of high energy protons. These protons may generate the desired indicator radionuclide, ^{13}N, by nuclear reactions on carbon and oxygen. Corrections have been made for these interferences by irradiating and counting pure hydrocarbons (n-hexane and naphthalene), quartz and deionized water samples under the nitrogen determination conditions. The correction factors would be expected to be dependent on the specific packaging and irradiation configurations used and should be determined independently for each system. The experimentally determined factors in our system are 1.48×10^{-4} "apparent gN"/gC for carbon and 1.30×10^{-3} "apparent gN"/gO for oxygen.

Table IV

Representative data for oxygen in coal liquids and by-products

Sample description	Experimental oxygen, % ± σ_m^*
Gross liquid product[a]	12.94 ± 0.16
Centrifuged liquid product[a]	5.08 ± 0.07
Centrifuge residue[a]	14.13 ± 0.07
Coal liquid product[b]	5.16 ± 0.03
Filtered liquid product[b]	3.88 ± 0.03
Liquid filtrate[b]	28.89 ± 0.39
Atmospheric still overheads[c]	1.42 ± 0.04
Atmospheric still bottoms[c]	1.70 ± 0.04
Vacuum still overheads[c]	1.50 ± 0.04
Vacuum still bottoms[c]	9.48 ± 0.13

*standard deviation of the mean for five replicate determination

(a) Samples obtained from Pittsburgh Energy Technology Center 400 lb/day fixed-bed liquefaction unit.

(b) Sample obtained from Solvent Refined Coal Pilot Plant, Wilsonville, Alabama.

(c) Samples obtained from H-Coal process development unit, Hydrocarbon Research, Inc., Trenton, NJ.

After the blank and recoil proton interference corrections have made, the nitrogen contents of the organic liquids were calculated by using the N-1-naphthylacetamide standards. As in the case of oxygen, the systematic deviation in the plot of these experimental values versus stoichiometric nitrogen contents of the selected liquids was observed. A single geometry/self-absorption correction factor was computed and applied to the raw data to allow the experimental regression line to pass through the origin. Excellent agreement between the final corrected experimental values and the known stoichiometric nitrogen contents was obtained. A correlation coefficient of 0.9999 was calculated for eleven different compounds or mixtures, covering a range of nitrogen contents from 1.89 to 39.96%.

The accuracy and precision of the technique was tested by analyses of a set of nitrogen in residual fuel oil standards prepared by the Japan Petroleum Institute and several pure organic compounds and mixtures as illustrated in Table V. Except for the lowest nitrogen content oil sample, S-250, the precision for four replicate determinations are in the range of ± 4.5 to 5.2%, relative, over the range of 0.111 to 1.86% nitrogen. For the higher nitrogen content (14.86 to 26.74% N) compounds, the relative error is even smaller. The variation of the experimental means from the stoichiometric nitrogen values for the organic compounds is less then ± 1.64%, relative, and from the certified values in the residual fuel oils did not exceed ± 7.8%, relative, for samples above 0.1% N. For samples below 0.1% N, larger detectors and/or larger sample sizes would be required to obtain better statistics. The method has also been applied to four typical coal conversion liquids, shale oil and a petroleum

residuum. These replicate determinations are presented in Table VI. The precision varied in the range of ± 1.14 to 3.67%, relative, for the liquid samples while it is ± 5.69%, relative, for the residuum.

Table V

Precision and accuracy of INAA nitrogen determinations using a liquid standard*

Determination No.	S-250[1]	S-251[1]	S-252[1]	Aniline	1,2-Propane-diamine	Quinoline and n-hexane (2:9)
1	0.0440	0.126	0.325	14.45	37.01	1.73
2	0.0174	0.108	0.260	15.05	36.60	2.01
3	0.0234	0.101	0.269	15.01	36.25	2.00
4	0.0433	0.111	0.291	14.92	37.09	1.68
5	0.0690	-	-	-	-	-
6	0.0350	-	-	-	-	-
Mean ± σ_m	0.039 ±0.007	0.111 ±0.005	0.286 ±0.015	14.86 ±0.14	36.74 ±0.19	1.86 ±0.09
Certified, or stoichiometric value	0.052	0.103	0.303	15.02	36.66	1.89

*Standard used is dimethylcyanamide, 39.96% N.

[1]Japan Petroleum Institute, standard samples, Lot No. 75N9502, 75N1002 and 75N3002, respectively.

Summary

We have shown that 14 MeV INAA, using **organic liquids as standards**[15,16], can yield precise and accurate data for oxygen and nitrogen contents of coal conversion liquids and related by-products over a wide analytical response range. Sensitivities can be further improved over those presently obtained by use of larger sample sizes and larger volume NaI(Tl) scintillation detectors with anticoincidence background reduction circuitry and adequate shielding.

For laboratories with access to a 14 MeV neutron generator, this technique can be a time-efficient and inexpensive method for routine oxygen and nitrogen analyses in coal and coal conversion products. For laboratories without a generator facility, external analyses by 14 MeV INAA can be used to monitor internal analyses done by more traditional techniques.

Table VI

Nitrogen determinations in liquid fossil fuels and conversion products*

Run #	ASOH[1]	ASB[1]	VSOH[1]	VSB[1]	Shale oil[2]	Petroleum Residuum[3]
1	0.693	0.601	0.881	2.48	1.79	0.202
2	0.703	0.625	0.851	2.26	2.04	0.177
3	0.717	0.693	0.922	2.15	2.05	0.210
4	0.681	0.655	0.860	2.13	1.93	0.248
5	-	0.556	-	-	-	0.218
Mean	0.699	0.626	0.879	2.26	2.00	0.211
$\pm \sigma_m$	±0.008	±0.023	±0.016	±0.08	±0.03	±0.012

*Dimethylcyanamide (39.96% N) used as standard

[1]Coal liquefaction products obtained from Hydrocarbon Research Institute H-Coal[R] Process Development Unit. ASOH = atomspheric still overhead; ASB = atmospheric still bottom; VSOH = vacuum still overhead; VSB = vacuum still bottom.

[2]Sample obtained from Lawrence Livermore Laboratory Retort.

[3]Nitrogen as determined by Kjeldahl procedure[14] is 0.195 wt. %.

REFERENCES

1. D.H. FINE, S.M. SLATER, A.F. SAROFIM, G.C. WILLIAMS, Fuel, 53 (1974) 120.
2. A.V. SLACK, Sulfur Dioxide Removal from Waste Gases, Pollution Central Review, 1971.
3. ASTM Method D3176-74, Annual Book of ASTM Standard, Part 26, American Society for Testing Materials, 1978.
4. W.D. JAMES, W.D. EHMANN, C.E. HAMRIN, L.L. CHYI, J. Radioanal. Chem., 32 (1976) 195.
5. C. BLOCK, R. DAMS, J. Anal. Chim. Acta, 71 (1974) 53.
6. C.E. HAMRIN, A.H. JOHANNES, W.D. JAMES, G.H. SUN, W.D. EHMANN, Fuel, 58 (1979) 48.
7. W.D. JAMES, W.D. EHMANN, G.H. SUN, C.E. HAMRIN, Proc. 4th Conference of Scientific and Industrial Applications of Small Accelerators, Inst. for Electrical and Electronic Engineers, Inc., 1976, p. 281.
8. W.D. EHMANN, Proc. 3rd Int. Conf. on Nuclear Methods in Environmental and Energy Research, Columbia, MO (Oct. 1977) ERDA CONF-771072, 1978, p. 284.
9. H. SEVINLI, H. OZYOL, E. BARUTCUGIL, S. DINGER, Turk A.E.C., Tech. J., 1 (1974) 15.
10. C.L. SYA, M.S. Thesis, University of Kentucky, 1973.
11. D.M. BIBBY, H.M. CHAMPION, Radiochem. Radioanal. Letters, 18 (1974) 177.
12. J.W. MORGAN, W.D. EHMANN, Anal. Chim. Acta, 49 (1970) 287.
13. ALDRICH Catalog/Handbook of Organic and Biochemicals, 1978.
14. H.V. DRUSHEL, Exxon Research and Development Laboratories. Baton Rouge, Louisiana, private communication (1980).
15. S.R. KHALIL, D.W. KOPPENAAL, W.D. EHMANN, J. Radioanal. Chem., In press, 1980.
16. W.D. EHMANN, S.R. KHALIL, D.W. KOPPENAAL, To be published.

FOURTH INTERNATIONAL CONFERENCE ON NUCLEAR METHODS IN ENVIRONMENTAL AND ENERGY RESEARCH

NUCLEAR TECHNIQUES FOR THE ON-LINE BULK ANALYSIS OF COAL

B.D. Sowerby and J.S. Watt

Research Establishment, Australian Atomic Energy Commission,
Private Mail Bag, Sutherland, New South Wales, 2232, Australia.

ABSTRACT

Several research projects are being undertaken at the Australian Atomic Energy Commission (AAEC) on the development of neutron, γ-ray and X-ray techniques for bulk coal analysis. Two projects described in the present paper are the development of neutron techniques for the determination of carbon and specific energy, and the development of X-ray techniques for the determination of ash.

Recent research has led to the development of a method for simultaneously determining the specific energy, ash and moisture contents of coal. This method is based on the measurement of neutron inelastic scatter γ-rays from carbon and neutron capture γ-rays from hydrogen combined with a separate 'matched' measurement of γ-ray scattering. Laboratory tests on ~ 50 kg coal samples containing > 70% wt % C have shown that the method can be used to determine the carbon, specific energy, hydrogen and ash contents of coal to within relative errors of 0.5, 0.8, 1.4 and 6.4% respectively. Promising applications include the on-line determination of the specific energy of coal being fed to power stations and the determination of carbon in coal slurries. Laboratory measurements show that the method can be used to determine the carbon content to better than 1.5% relative in both these applications.

Current research on X-ray techniques is aimed at use of high energy X-rays to average ash content determination over large volumes of coal. Experiments being undertaken use ^{241}Am (60 keV), ^{153}Gd (~ 100 keV), and ^{133}Ba (mainly 356 keV) with backscatter, scatter-transmission and collimated beam transmission geometries viewing 100 kg samples of coal. The effective depth of coal seen by the backscatter assembly has been matched for the three energies by use of collimation which also has the advantage of increasing the effective depth seen for ^{241}Am by a factor of three compared with an uncollimated assembly. Preliminary data processing of results shows that ash content is most accurately determined using ^{153}Gd in the backscatter assembly by taking the ratio of intensities of backscattered X-rays in a high and a low energy channel. Root mean square errors obtained for suites of coal a) 5-18 wt % ash and 6-12.6 wt % iron in the ash, b) 5-26.5 wt % ash and 3-19 wt % iron and c) 10-31 wt % ash and 0.6-4.5 wt % iron were respectively 0.80, 2.14 and 1.1 wt % ash.

1. INTRODUCTION

There are large potential savings from the use of on-line analysis techniques in the coal industry, particularly in the control of coal washeries and in the more efficient operation of coal-fired power stations. Three important parameters for which on-line analysis is required are specific energy, ash and moisture. Ash is the oxidised incombustible residue from the combustion of coal and corresponds closely to the mineral matter content. Radioisotope X-ray techniques have been developed for the analysis of the ash content of coal [1 - 6]. They are based on the difference in absorption of X-rays in the coal matter and the higher atomic number constituents of the mineral matter. Neutron techniques can be used to measure the concentration of some specific elements such as C and H in the coal. The measurement of specific energy, ash and moisture then depends on the correlation of the particular parameter with the measured elemental composition.

Two of the research projects being undertaken at the AAEC Research Establishment on the development of neutron and X-ray techniques for bulk coal analysis [6, 7] are described in the present paper. The aim of these projects is to carry out research, development and field testing of radioisotope techniques of analysis which have potential applications in Australian industry. Once commercial design can be undertaken, the AAEC usually licences an outside organisation to manufacture and market the analysis system, thus ensuring that equipment becomes available to the mineral industry. Two projects which have, in the past, been successfully carried through to a stage of commercial development are radioisotope on-stream analysis of mineral slurries using X-ray techniques [8] and bulk analysis of copper and nickel ores using γ-ray resonance scattering [9].

2. NEUTRON TECHNIQUES OF COAL ANALYSIS

2.1 Determination of Carbon and Hydrogen

The specific energy, ash and moisture contents of bulk coal samples can be determined simultaneously by a method based on the accurate measurement of carbon and hydrogen contents. The method for carbon and specific energy depends on a combination of a measurement of 4.43 MeV ^{12}C γ-rays from neutron inelastic scattering with a separate ^{60}Co γ-ray scattering measurement. The response of the neutron and γ-ray gauges was 'matched' to measure over essentially the same sample volume by using a relatively large source-to-sample separation for the γ-ray gauge. The γ-ray scattering measurement corrects the neutron gauge for variables such as sample bulk density, bulk density gradients and sample thickness. By matching the response of the two gauges, an accuracy can be obtained that is higher than has been previously reported for bulk coal samples. Ash and moisture are determined by combining the above measurements with a simultaneous measurement of hydrogen content using 2.22 MeV H neutron capture γ-rays.

The method has been tested by laboratory measurements on many $\sim$50 kg coal samples from coalfields in southern New South Wales, Australia using the gauges shown in Figure I. The count rates measured on the neutron gauge are summarised in column A of Table I.

Root mean square deviations between chemical laboratory and nuclear gauge assays are summarised in Table II. These results show that the method can be used to determine the carbon and specific energy contents of coal to within about 1.4% relative for a wide range of coal compositions and to within about 0.8% relative for coals with a carbon content in excess of 70 wt %.

Moisture can be determined to within about 0.2 wt % provided that the carbon/hydrogen ratio in the coal matter remains constant.

2.2 Application to the Analysis of Power Station Feed

2.2.1 Background

One promising application of the above method is the on-line determination of the specific energy of coal being fed to coal-fired power stations. Measurement of specific energy to within ± 1% relative is required within a few minutes of the coal being fed to the boilers. The advantages seen for this application include improved and safer boiler control and possibly reduced NO_x emissions.

At power stations operated by the Electricity Commission of New South Wales, coal is fed from bunkers through vertical stainless steel chutes to gravimetric feeders. Coal from the gravimetric feeders passes to grinding mills from which it is blown into the boilers. Residence time in the grinding mills is about 2 minutes. There are 6 to 8 gravimetric feeders and mills for each boiler and typically 4 boilers to a power station.

The most favourable measuring point appears to be at the stainless steel chutes. These chutes typically have an internal diameter of 610 mm, a wall thickness of 9.5 mm and an unobstructed length of approximately 2.5 m. The chutes are full of coal having a maximum particle size of about 20 mm. It is highly undesirable to place windows in the chutes or to obstruct the coal flow.

Determination of the specific energy to within about 1% relative requires either measurement of the carbon content to 1% relative, as described in Section 2.1, or measurement of both the ash and moisture to within about 0.7 wt %. However, the accurate analysis of ash by high energy X-ray techniques is not feasible through 9.5 mm thick steel walls.

2.2.2 Experimental Details

The neutron and γ-ray gauges used in the present experiments are shown in Figures 2(a) and 2(b). The measured depth penetration for these gauges is shown in Figure 3 together with a depth penetration for the neutron gauge with a reduced source-to-sample separation (i.e. reduced d_1). A gauge with small d_1 has the advantage of greater depth penetration but the disadvantage of poorer matching with the γ-ray gauge.

The count rates measured in the geometry shown in Figure 2(a) are summarised in column B of Table I. The ratio of 4.43 MeV photopeak count rate to background under the photopeak is about 15% lower than was obtained in Figure 1(a), primarily because of the larger sample and the thick-walled steel sample container.

Calculations show that if the measured count rates are increased by a factor of about 4 (using a larger detector and/or source), the carbon content of the coal can be determined to within 1.2% relative with a 3 minute counting time. The method is being tested in the laboratory using 24 bulk samples ($\sim$ 200 L each) from a New South Wales power station.

2.3 Application to the Analysis of Coal Slurries

2.3.1 Background

A new method for the pipeline transportation and beneficiation of coking

coal is being developed [10, 11]. Previous technology associated with long distance slurry transportation of coals for power generation could not be used for Australian coking coals owing to the product not meeting specifications for existing operations. The main problems with this technology are the small particle size and the coating of coal particles by fine clays. These problems have been overcome by an agglomeration technique in which oil or an oil/water emulsion is added to the slurry before sending it through the pipeline. For control of this system, oil needs to be added in proportion to the amount of coal matter.

The analytical problem is, therefore, to determine the coal matter or carbon content in a slurry containing about 50 wt % solids (range 20 - 70%) before the addition of oil. The maximum particle size is about 3 mm and oil will be added to about 10% by weight of the dry coal. An accuracy of determination of about 1 wt % C is required.

2.3.2 Experimental Details

The application of neutron inelastic scatter and capture techniques to the determination of carbon in slurries has been examined in the laboratory. Slurries were prepared with solid weight fractions from 10 to 50% using bulk coal samples of fine particle size (> 90% minus 2 mm). The slurries were measured in drums of diameter 380 mm and height 580 mm. A high speed stirrer (2800 rev/min) of diameter 48 mm was used in conjunction with a deflection baffle to achieve uniform mixing. However, uniform mixing could not be achieved using this assembly on slurries with solid weight fractions in excess of about 55%.

Measurements were made on 13 slurry samples from 3 solid coal samples and on water in geometries similar to those shown in Figure 1. Counting times under neutron irradiation were either 10 or 20 minutes per sample. The net γ-ray count rates from a typical slurry sample are summarised in column C of Table I. Thermal neutron flux was also measured with a ^{3}He detector located near the slurry sample.

The results of the measurements of the 4.43 MeV count rate for the slurry samples are plotted in Figure 4. The results of single parameter linear regression fits to the data are summarised in Table III. Multiple parameter regression fitting with either the γ-ray backscatter count rate or the ^{3}He count rate did not significantly improve the r.m.s. deviations shown in Table III. A regression fit between calculated slurry bulk density and γ-ray backscatter intensity showed an r.m.s. deviation of 0.012 g cm^{-3}.

As shown in Table III, the measured 2.22 MeV count rate can be used to determine the carbon and hydrogen contents of coal slurries to within 0.28 and 0.035 wt %, respectively, which are equivalent to relative errors of 1.1% and 0.40%. However, the error in determining carbon using the measured 4.43 MeV count rates is 1.22 wt % C. This increased error is due mainly to mixing problems as sedimentation occurred near the lower edge of the slurry container. The 2.22 MeV thermal neutron capture γ-rays originated deeper in the sample than the 4.43 MeV γ-rays and were therefore less sensitive to this deposition. The above errors should be further reduced by improving the slurry mixing by means of a large diamter, slower speed stirrer.

The preliminary results indicate that it is technically feasible to determine the carbon content of coal slurries accurately using neutron inelastic scatter and capture techniques.

Increased count rates and more uniform mixing should enable the carbon content to be determined to within 1% relative with analysis times of less than 2 minutes.

3. X- AND γ-RAY TECHNIQUES TO DETERMINE ASH

3.1 Potential Applications

The development of techniques for the on-line determination of ash content of coal should lead to large financial savings in the coal industry. Their use could improve the efficiency of:

(a) coal washeries both in the gravity separation process for the coarse coal fraction and in the flotation process for the fine fraction,

(b) blending of different coal streams to give a constant ash content in the product stream,

(c) power stations, and

(d) coal mining, especially by providing a rapid warning of mining inadvertently off the coal seam.

Continuous on-line determination of ash content to 0.5 - 1.0 wt % (r.m.s.) is highly desirable in all of these applications.

3.2 Radioisotope X-Ray Techniques

The techniques for determining the ash content of coal involve measuring the intensity of X-rays or low energy γ-rays transmitted through, or backscattered by the coal, and often but not always a high energy γ-ray measurement which determines bulk density. The absorption of X-rays per unit weight of coal can be used to determine ash content because the effective atomic member (Z) of ash constituents ($Z \sim 11$-12) is considerably higher than that of the coal matter ($Z \sim 6$), and X-ray absorption is Z dependent. A single determination of X-ray absorption per unit weight of coal has been reported to determine ash content accurately in Germany [1], Japan [2] and the USSR [3].

The above techniques are not accurate if the iron content of the coal varies considerably. Iron interferes because, per unit weight, it absorbs several times as much as the principal ash constituents silica and alumina. Workers in the United Kingdom [4,5] have overcome this problem by compensating the intensity of backscattered X-rays by a simultaneous measurement of the intensity of iron K X-rays. However, iron K X-rays are absorbed in about one millimetre of coal, and hence the overall system for sampling the coal process line, crushing and sample presentation is complex and expensive.

The AAEC is developing a different approach to alleviate the problem of iron and other interfering elements [6]. This technique depends on measuring the relative absorption per unit weight of coal at two different X-ray energies. For example, if two radioisotopes emitting X-rays of different energies are used, separate measurements of intensities of part or all of the detected energy spectra can be combined to give ash content. Alternatively, if one X-ray source only is used, measurements of intensity can be made in two or more energy regions of the same spectrum of detected X-rays. These are combined to give ash content. Whichever alternative is used, a third measurement using high energy γ-rays is often required to compensate for changes in bulk density of the coal.

The technique based on two radioisotope X-ray sources has been shown to determine ash content to 0.6 - 1 wt % r.m.s. if the X-ray energies are $\lesssim$ 35 keV [6]. The use of higher energy X-rays is desirable because of their increased penetration. Ash determination would then be averaged over larger volumes of coal and the effect of variations of particle size of coal is made less. However, it has been shown [6] that ash content could not be determined accurately using narrow beams of high energy X-rays unless the iron varied over a relatively small range of concentration. We have, however, calculated that it may be possible to use high X-ray energies in broad beam geometries and determine ash accurately, even though the iron concentration varies considerably. The reason for the use of broad beam geometries is to reduce the effect of Compton scatter relative to photoelectric absorption.

3.3 Ash Determination Using High Energy X-rays

3.3.1 Introduction

The general approach to the choice of X-ray energies and the design of experimental equipment is summarised as follows:

(a) Coal samples have density gradients and localised variations due to particle size and packing. Hence, to determine ash representatively, analysis should be averaged over large volumes of coal. This is accomplished using high energy X-rays ($\sim$60 keV from ^{241}Am and $\sim$100 keV from ^{153}Gd) and by scanning along and around the coal sample.

(b) To minimise the handling of large volumes of coal, many measurements are made on the same sample of packed coal. For each of the geometries being considered for on-line analysis (Figure 5), nine separate measurements of intensity were made on each sample with the radioisotopes ^{241}Am, ^{153}Gd and ^{133}Ba placed sequentially in positions shown in Figure 5.

(c) Since measurements of intensity for the three radioisotopes used in the same geometry are to be combined to determine ash content, the effective volume of coal 'seen' should be approximately the same for each measurement This would minimise errors in ash determination arising from density gradients and localised variations of bulk density of the coal. This was easily achieved for the two transmission geometries. However, the geometry of source, shield and detector of the backscatter assembly had to be carefully designed as discussed in the next action.

3.3.2 Matching of effective volumes seen by the backscatter assembly

The effective volumes of coal seen have been closely matched for the three radioisotopes. This has been achieved by using some collimation by placing shields near the source and the detector. The effect of this collimation has been to increase the depth (and hence volume) of coal seen by a factor of about three over uncollimated backscatter measurement for ^{241}Am X-rays, and, to a lesser extent, for ^{153}Gd X-rays.

In Figure 6, the normalised count rates for various depths of coal and water are plotted. It can be seen that the sensitive depth of coal effectively overlaps for the three radioisotopes.

3.3.3 Experimental

Measurements of intensity of γ- and X-rays have been made with the back-scatter, scatter -transmission and collimated beam geometries shown schematic-

in Figure 5. Sodium iodide crystals of diameter 50 mm and height 50 mm were used in each scintillation detector. Details of radioisotope sources are as follows:

Source	Activity (mCi)	Filter over source (S) or detector (D)	X- or γ-ray energy (keV)
^{241}Am	300	-	59.5
^{153}Gd	12	0.3 mm tin (S)	97,103
^{133}Ba	7	1.3 mm Cd (D)	356 (mainly)

Each source was mounted on a steel cylinder which could be put in and taken out of the measurement positions shown in Figure 5. Count rate reproducibility on replacement was better than 0.1%. Only one source was used at a time. Backscattered and collimated beam measurements were made simultaneously, but scatter-transmission measurements were done separately.

Coal was contained in a 100 L polythene container of internal diameter, height and wall thickness respectively 350, 1030 and 7 mm. The container was rotated about its axis continuously, and the source-detector systems were scanned vertically, parallel to the container-axis, for a distance of 630 mm. This ensured that intensity measurements were averaged over much of the coal.

Coal samples were obtained from Utah Development Company's Blackwater mine in Queensland's Bowen Basin and from twelve mines on the South Coast of New South Wales, which supply coking coal to Australian Iron and Steel Pty. Ltd. at Port Kembla.

3.3.4 Results and discussion

Some analyses for coal samples used in experiments, and errors in ash for X-ray techniques, are summarised in Table 1V. The Blackwater samples are given in two groups, those with less than 18 wt % ash and all samples. The first group has a moderate range of iron concentrations in the ash (6-11 wt %), and the second has a very wide range of 3-19 wt % iron. Comparison of errors in ash determination for the two groups shows the effect of variations of iron concentration on accuracy of ash determination.

Calculations and experimental results for collimated transmission beams (Table 1V) show relatively large errors except for the Blackwater group of samples with $\leq$ 18 wt % ash. The calculations have been based on tabulated mass absorption coefficients and chemical assays of each coal sample for C, H, Al, Si, Fe, water and ash. It has been assumed that Al, Si and Fe are present as Al_2O_3, SiO_2 and Fe_2O_3 respectively. These compounds make up about 85 wt % of the ash. Much of the error in ash determination using collimated beams is often due to the relatively high absorption of X-rays by iron. This can be checked by using an additional term '$a_3 . C_{Fe}$' to the calculated collimated beam equation (Table 1V) where C_{Fe} is the iron concentration in the coal. The resulting calculated errors in ash determination are 0.23, 0.32 and 0.51 wt % respectively for $\leq$ 18 wt % ash and all Blackwater samples, and South Coast samples. However, these errors underestimate the real errors in ash (assuming iron content is known) because of the effect of uncertainties due to the unaccounted-for elements making up the remaining 15 wt % ash. Addition of the iron concentration term to the experimental results for collimated beam decreased the error in ash by only a small amount.

The best results have been obtained with backscattered X-rays from ^{153}Gd, comparing count rates in the two energy regions shown in Figure 7. The r.m.s. errors in ash determination of 0.80 wt % ash for Blackwater samples of less than 18 wt % ash, and 1.1 wt % ash for the New South Wales South Coast samples, are probably acceptable for some applications of on-line analysis of coal streams. However, the error for all the Blackwater samples would not be acceptable.

The results in Table 1V are preliminary because data processing of most of the spectra taken with backscatter and scatter-transmission geometries has not yet been undertaken. The long-term program will include measurements on many more samples, and full details of the present and further experiments will be published at a later date.

ACKNOWLEDGEMENTS

Section 2 of this paper describes work being undertaken by B.D. Sowerby, G. Gray, W.K. Ellis and N. Ngo, and Section 3 by J.S. Watt, V.L. Gravitis, R.A. Fookes, C. Campbell and E. Steffner, all of the AAEC. The authors wish to thank Australian Iron and Steel Pty. Ltd., N.S.W., and Utah Development Co., Queensland for supplying the samples of coal used in the experiments.

REFERENCES

[1] TROST,A., Radioisotope Instruments in Industry and Geophysics (Proc. Symp. Warsaw, 1965) 1, IAEA, Vienna (1966) 435.

[2] KATO, M., Proc. 2nd Symp. on Low Energy X- and Gamma Sources and Applications, Austin, Texas, March 1967, ORNL-11C-10, 2 (1967) 723.

[3] VASILEV,A.G. et al, Koks i Khimiya 5 (1974) 52.

[4] BOYCE,I.S., CLAYTON,C.G., PAGE,D., Nuclear Techniques and Mineral Resources 1977, IAEA, Vienna (1977) 135-165.

[5] CAMMACK,P., BALINT,A., AIME Annual Meeting, Las Vegas, Nevada (1976) Preprint No. 76-F-24.

[6] FOOKES,R.A., GRAVITIS,V.L., WATT,J.S., Nuclear Techniques and Mineral Resources 1977, IAEA, Vienna (1977) 167-182.

[7] SOWERBY,B.D., Nuclear Instrum. Methods 160 (1979) 173.

[8] WATT, J.S., Nuclear Techniques and Mineral Resources 1977, IAEA, Vienna (1977) 569.

[9] SOWERBY, B.D., ELLIS, W.K., GREENWOOD-SMITH, R., Nuclear Techniques and Mineral Resources, IAEA, Vienna, (1977) 499.

[10] RIGBY, G.R., CALLCOTT, T.G., B.H.P. (Broken Hill Proprietary Company Limited) Technical Bulletin 21 (1977) 2.

[11] RIGBY, G.R., CALLCOTT, T.G., Paper E5, Fifth Internat. Conference on Hydraulic Transport of Solids in Pipes, Hanover, 8-11 May, 1978.

TABLE I

Count rates measured in three applications of neutron techniques to the determination of carbon and hydrogen in bulk coal samples.

Column Identification	A	B	C
Sample	Crushed coal	Crushed coal	Coal slurry
Sample size (approx.)	50 kg	150 kg	50 L
Geometry	Figure 1 (a)	Figure 2 (a)	Similar Figure 1(a)
Neutron source strength (4 Π) (neutrons/s)	2×10^7	7.7×10^6	7.7×10^6
Carbon content (wt.%)	69	78	30
Net count rates (counts/s)			
4.43 MeV γ-ray	830	194	105
2.22 MeV γ-ray	920	358	534
Total count rate (counts/s)	72,000	25,000	5,800

TABLE II

Summary of results of 85 measurements of 23 coal samples from various mines in southern N.S.W., Australia. Experimental assays for carbon and specific energy were obtained by a combination of the intensities of 4.43 MeV γ-rays and γ-ray backscatter. Experimental assays for hydrogen, moisture and ash were obtained by a combination of the intensities of 2.22 MeV and 4.43 MeV γ-rays and γ-ray backscatter.

	r.m.s. deviations between chemical laboratory and experimental assays *	
	For all 23 samples	For samples with carbon content > 70 wt.%.
Carbon	0.92	0.38
Specific energy	0.44	0.26
Hydrogen	0.071	0.058
Moisture	0.85	0.19 **
Ash	1.42	0.81

* Assays quoted as wt.% on an "as received" basis (a.r.) except for specific energy which is quoted in MJ/kg (a.r).

** Measurements on a single coal sample with added moisture up to 23.4 wt.%.

TABLE III

Root mean square deviations in carbon and hydrogen obtained by single parameter linear regression between chemical assays and measured count rates of 4.43 and 2.22 MeV γ-rays for coal slurries of solid weight fraction 20 to 50%.

	Using only the 4.43 MeV count rate	Using only the 2.22 MeV count rate
Carbon	1.22 wt.% C	0.28 wt. % C
Hydrogen	-	0.035 wt. % H

TABLE Iv

ROOT MEAN SQUARE ERRORS IN ASH DETERMINATION USING RADIOISOTOPE X-RAY TECHNIQUES

Origin of Sample	Blackwater, Queensland		South Coast, NSW
Number of samples	13	24	15
Ash content (wt %)			
Range	5-18	5-26.5	10-31
Mean	11.1	16.4	17.9
r.m.s.	4.1	6.9	6.5
Iron (wt % in ash)			
Range	6-12.6	3-19	0.6-4.5
Mean	9.1	9.0	2.4
r.m.s.	2.1	3.6	1.0
r.m.s. error (wt % ash) in ash determination by radioisotope X-ray techniques			
a) Collimated beam			
Calculated: $C_{ash} = a_1 + a_2 \mu_{Am}/\mu_{Ba}$	1.15	4.36	2.2
Experiment (I_{Am}, I_{Ba})*	0.95	2.22	1.93
b) Backscatter			
Integral counts using I_{Am} and I_{Ba}*	1.69	2.39	1.85
^{153}Gd: $C_{ash} = a_1 + a_2(I_{HE}+a_3)/(I_{LE}+a_4)$	0.80	2.14	1.10

* $C_{ash} = a_1 + a_2 \log I_{Am} + a_3 \log I_{Ba}$

where C_{ash} is wt % ash in coal, I is intensity, where subscripts Am, Ba, HE and LE refer to Am, Ba, and high and low energy channels respectively for ^{153}Gd (see Figure 7), μ_{Am} and μ_{Ba} are mass absorption coefficients in the coal for 60 and 356 keV γ-rays respectively, calculated from tables for μ and know elemental abundances in the coal, and subscripted values of 'a' are constants obtained from least squares methods to minimise errors in ash.

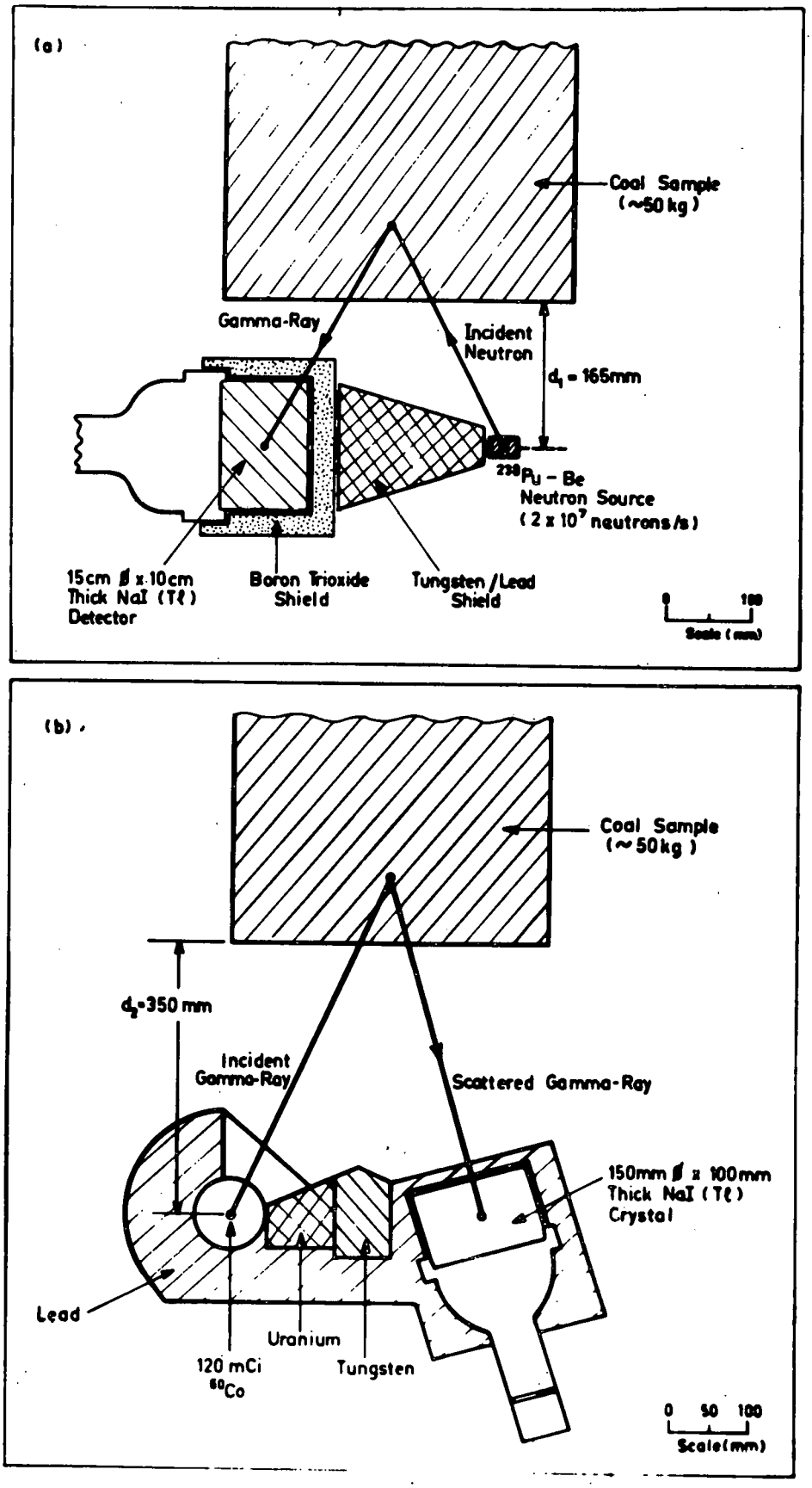


Figure 1: Cross-sectional views of (a) the neutron gauge and (b) the γ-ray gauge used for the analysis of bulk coal samples (1).

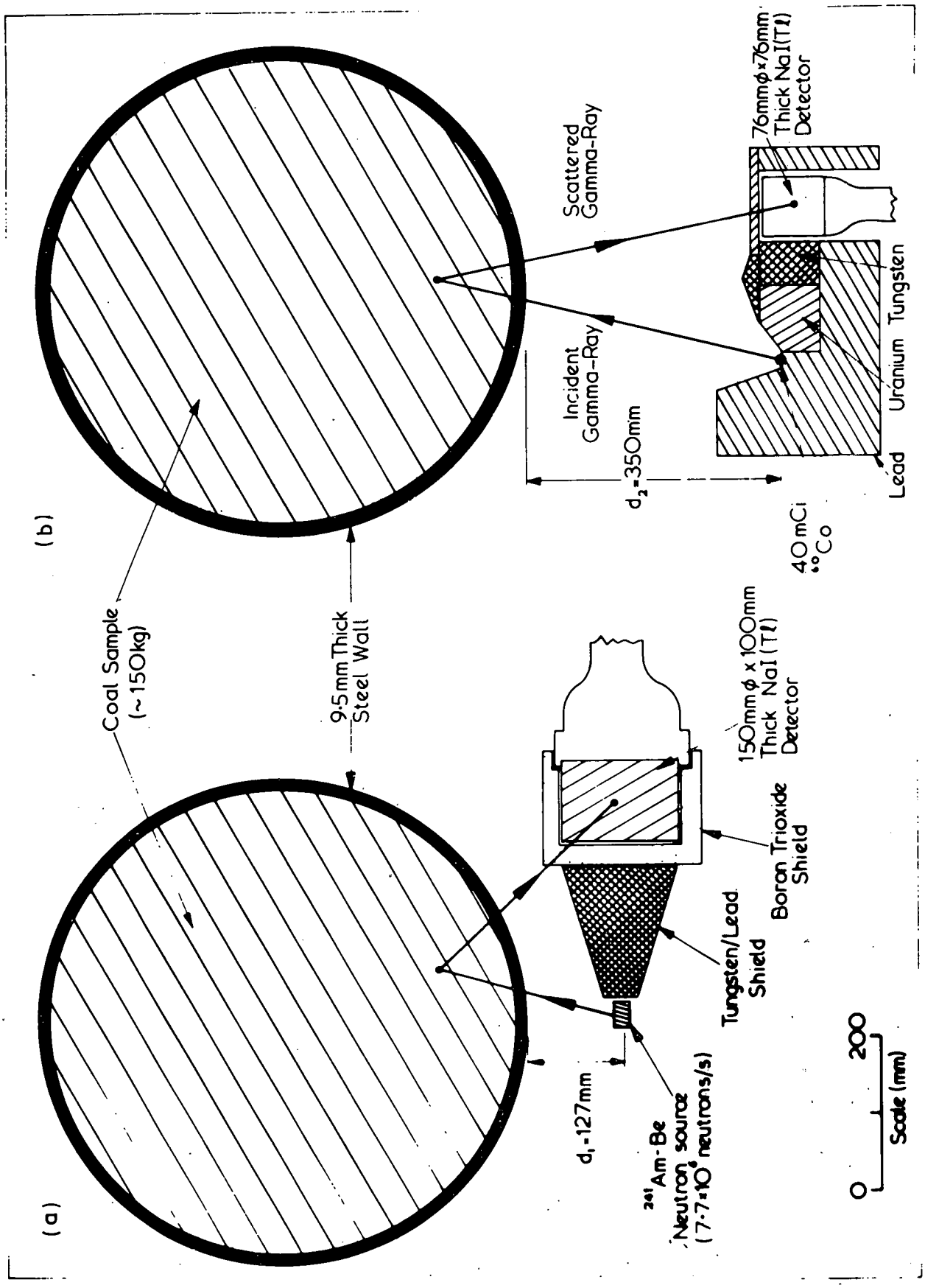


Figure 2: Cross sectional views of (a) the neutron gauge and (b) the γ-ray gauge used for laboratory experiments on the application of neutron techniques to the on-line analysis of power station feed.

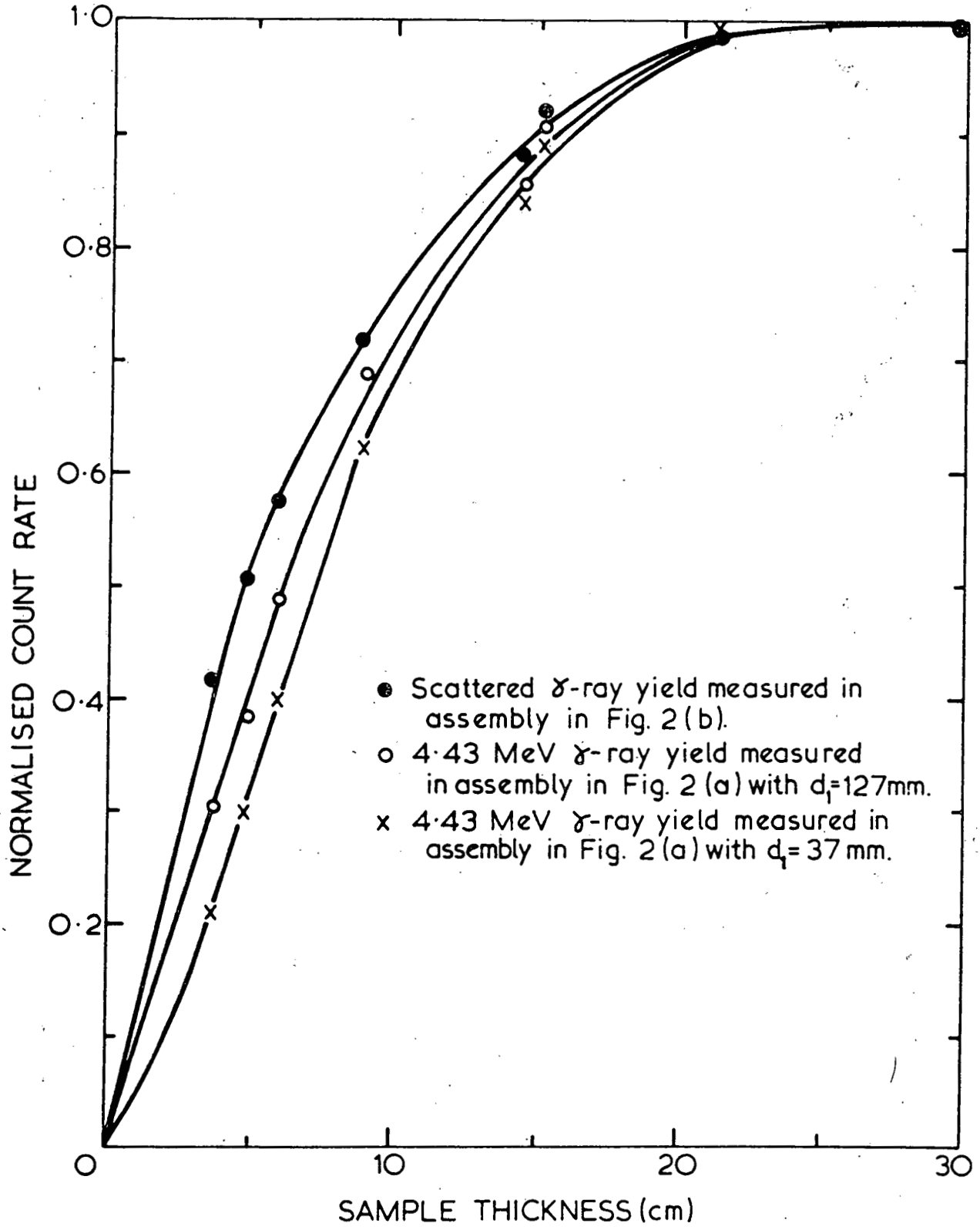


Figure 3: Experimental count rates measured as a function of sample thickness for a coal sample in a half drum in the assemblies shown in Figures 2(a) and 2(b).

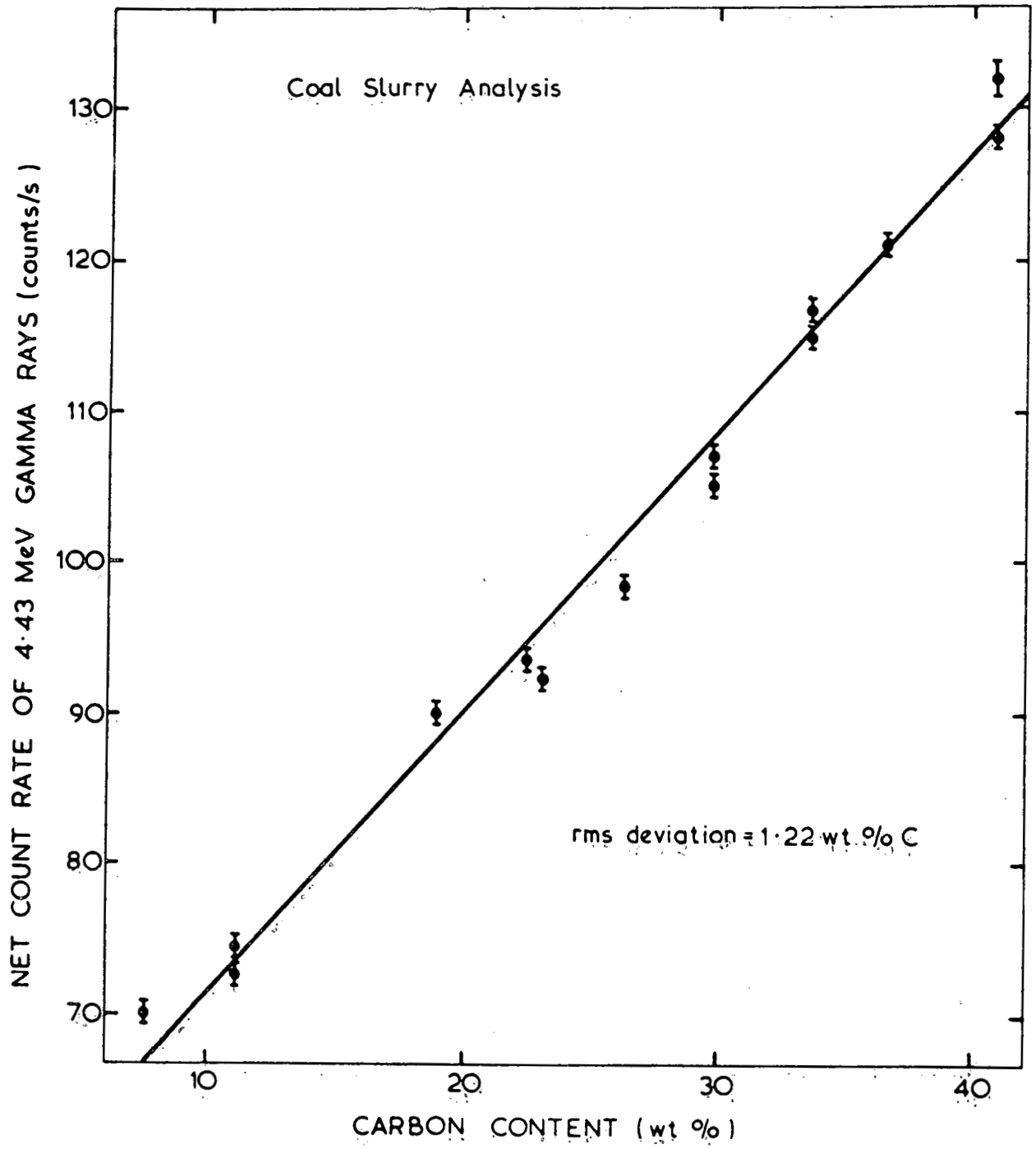


Figure 4: Measured net photopeak count rate of 4.43 MeV γ-rays versus chemical assays of carbon in coal slurries.

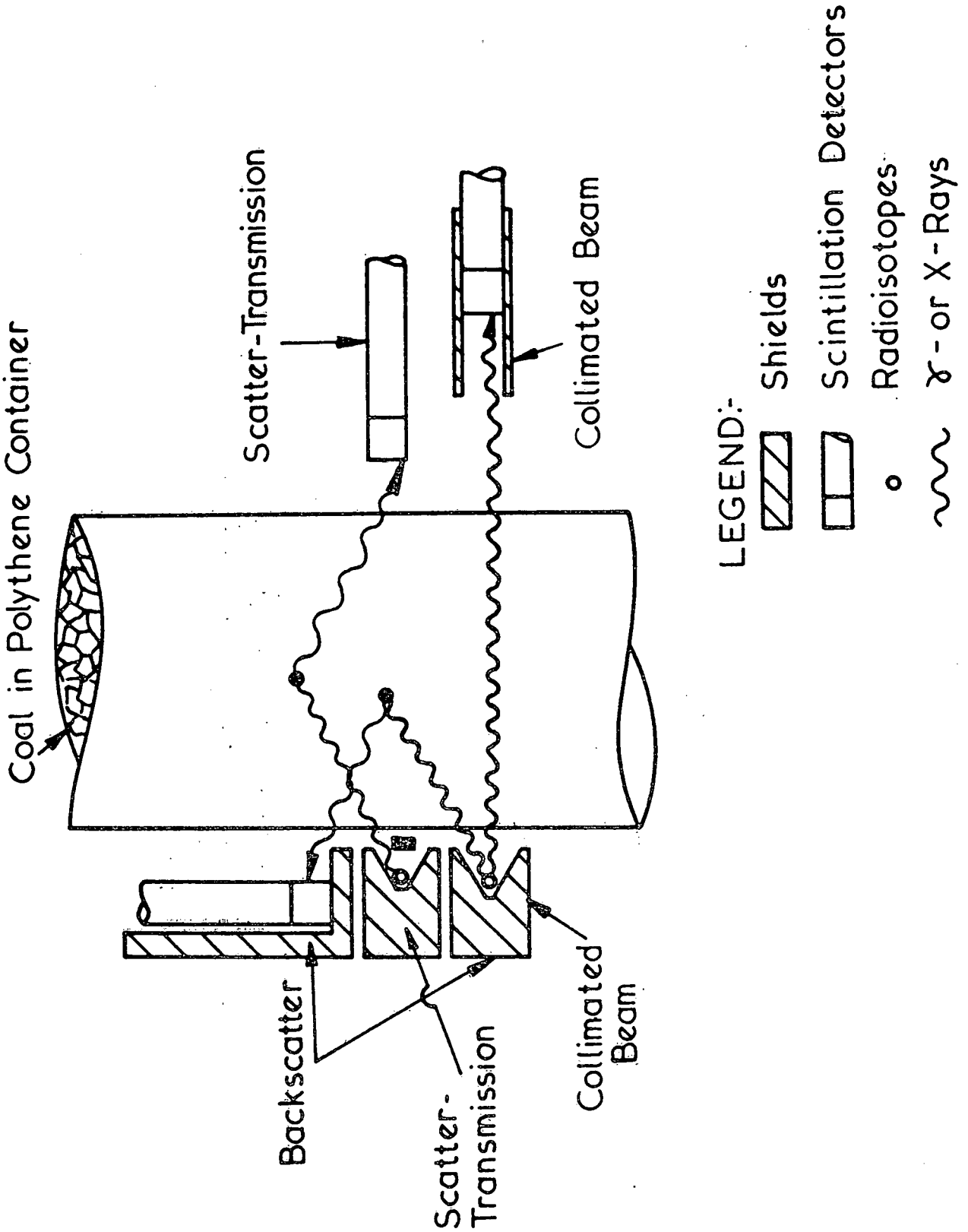


Figure 5: Schematic diagram of X-ray backscatter, scatter-transmission and collimated beam transmission assemblies as mounted about the container of coal used in experiments to determine ash content of coal.

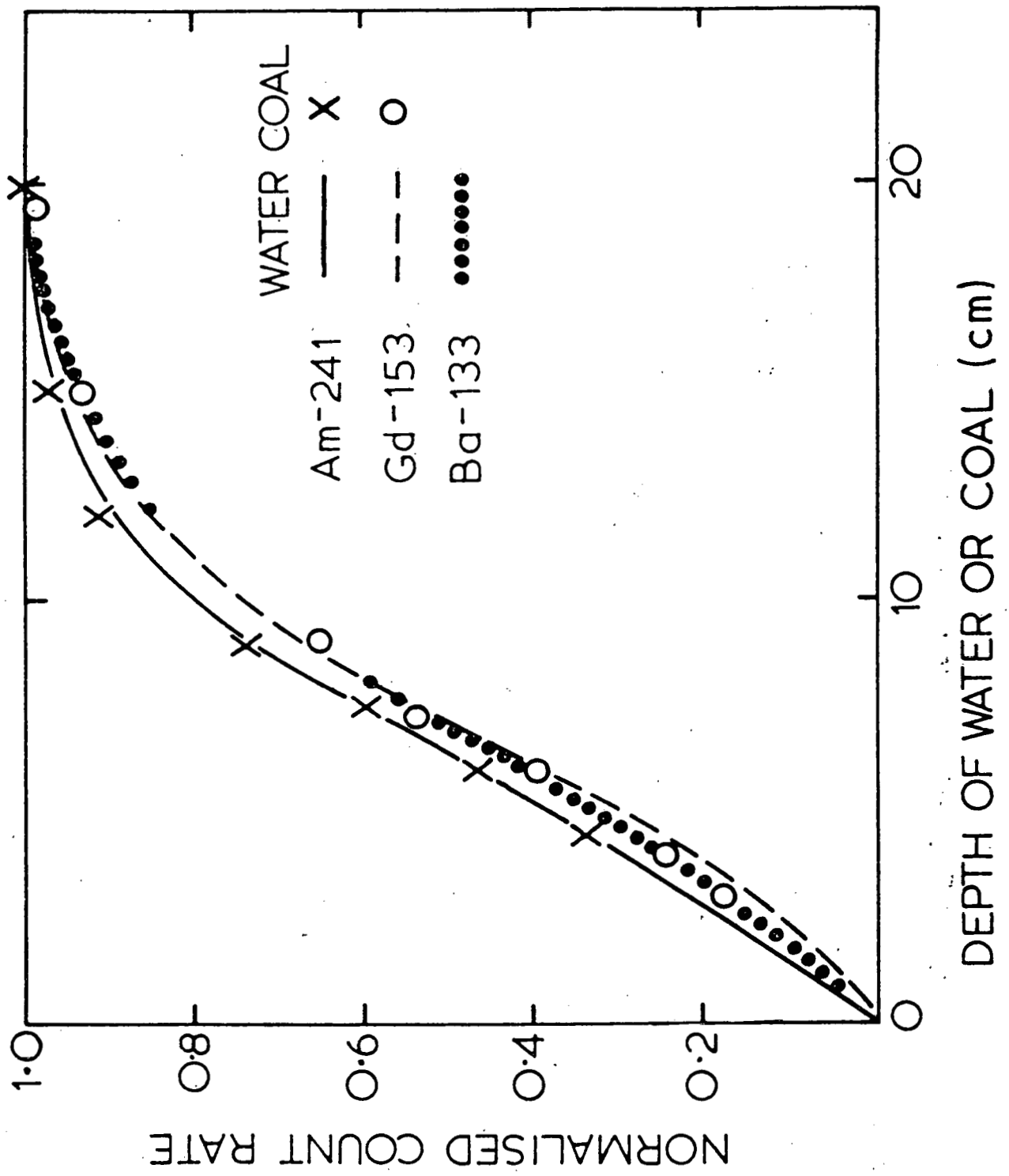


Figure 6: Experimental count rates measured as a function of sample thickness for water and for a coal sample 10 wt % ash) using a X-ray backscatter assembly.

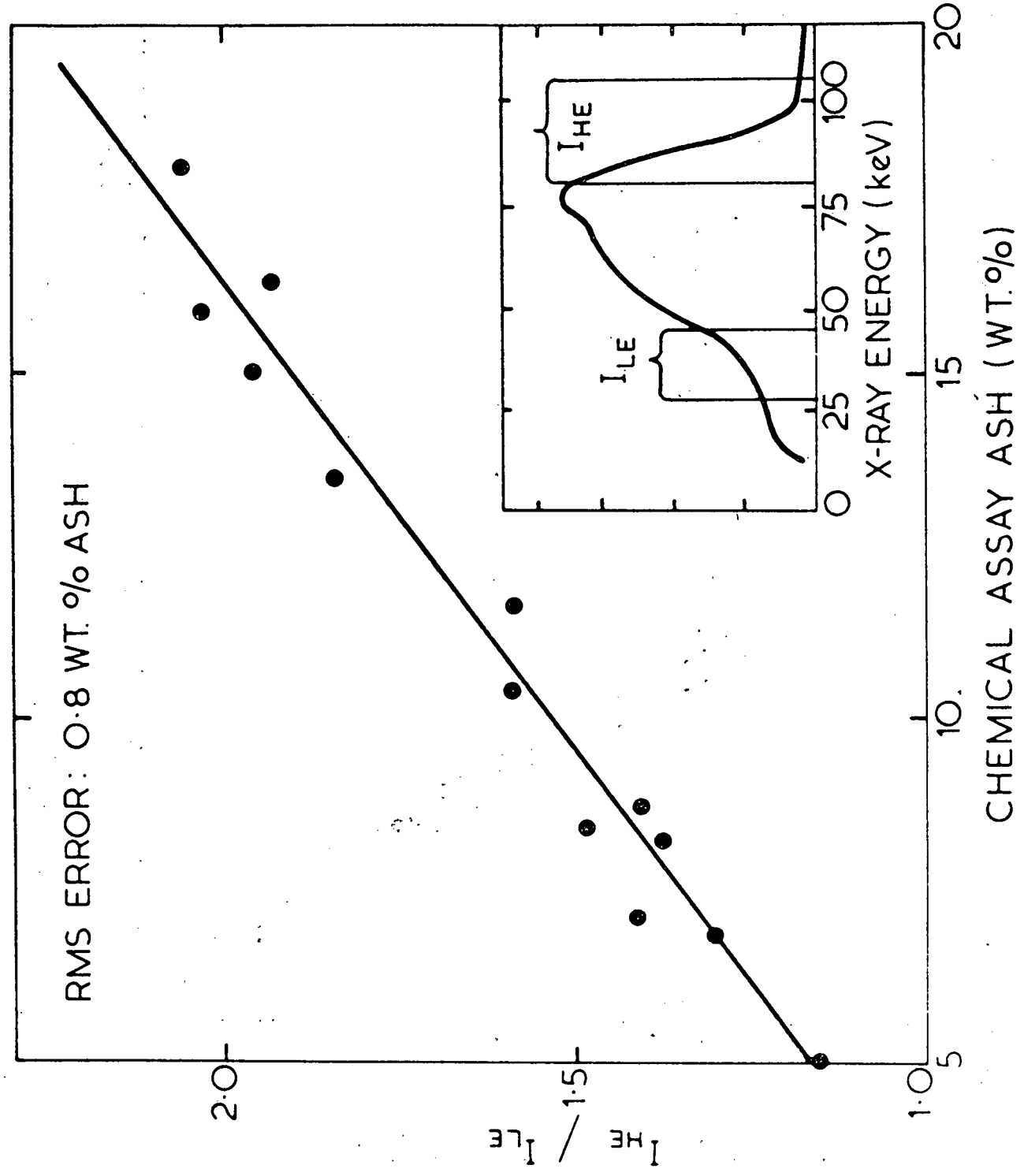


Figure 7: Comparison of chemical assay for ash in coal and the ratio of intensities of two energy regions in the spectrum (see inset) of backscattered X-rays from ^{153}Gd for Blackwater samples of < 18 wt % ash.

Radiochemical-NAA Studies of Biological Samples in Connection with Marine Production of Petroleum

by

Keith de Lancey and Vincent P. Guinn
Department of Chemistry
University of California
Irvine, California 92717

Abstract

A previous NAA radiochemical-separation procedure for Ba-139 has been modified to also recover Sr-87m quantitatively (precipitated together as the sulfates), and, via extraction with a chloroform solution of $Bi(DDC)_3$, to recover Cu and Hg. After removal of Na-24 from the aqueous phase with HAP, other activities, such as Zn-69m, can be measured in it.

Several years ago, with the support of the Bureau of Land Management (BLM) of the U.S. Department of the Interior, a project was begun to measure, among other things, levels of various elements prior to proposed offshore drilling for oil along the Southern California coast. The primary project objective was to obtain a reference baseline against which future comparisons could be made to assess potential changes in the marine ecosystem.

During the course of normal offshore drilling operations, quite a few elements (including Ba, Cd, Cr, Cu, Pb, Fe, Zn, Al, Ti, As, Mn, V, and Ni) are likely to be injected into the marine environment. Two of these, Ba and V, were the only ones chosen by BLM in the early phases of the project to be determined by neutron activation analysis (NAA). It has been previously reported[1] that an NAA post-irradiation separation procedure for Ba-139 in biological materials had been developed and tested in this study. The purpose of the current work was to ascertain whether the Ba procedure could be carried a few steps farther with a minimum amount of effort to determine additional elements of interest.

For a typical analysis, approximately 100 mg of biological material is used. This is the maximum amount of organic material allowable in the 25 ml Parr teflon-lined acid digestion bomb used for wet-ashing the samples. All irradiations were done in the rotary specimen rack of the U.C. Irvine TRIGA Mark I nuclear reactor, where the thermal-neutron flux is 1.0×10^{12} n cm^{-2} s^{-1}. After irradiation and digestion, non-radioactive carriers are added to the sample solution and the well known method of $BaSO_4$ precipitation is employed, as described previously.

Strontium Determination

In the Ba separation procedure, it is clear that $SrSO_4$ precipitates along with the $BaSO_4$. However, if the determination of Sr is of interest, a few basic questions need to be answered:

(1) Is the simultaneous precipitation of $SrSO_4$ quantitative?

(2) Can accurate, reproducible values for Sr concentrations be obtained?

(3) Will the present Ba determination procedure provide good values for Sr also, or will modifications be necessary?

In search of answers to these questions, radiotracer experiments were performed to measure Sr recovery. The results of these ex-

periments (shown in Table I) indicated that in order to obtain the desired results for Sr, it is necessary to adjust the pH of the sample solution up into the range of 4-6 pH units. A series of analyses of reference materials showed that the simultaneous determination of Ba and Sr seems quite capable of yielding accurate results, and that those for Sr can be obtained with little additional work. The results of these analyses for Sr are presented in Tables II and III.

Determination of Additional Elements

During the radiochemical procedure for the determination of Ba and Sr, the sulfates are precipitated and a filtrate is collected. At this point, attention was directed toward the possibility of analyzing this filtrate for additional elements, and of developing a routine procedure for such an analysis. Typically, biological material irradiated in a flux of thermal neutrons will show Na-24, Cl-38, K-42, Mn-56, Br-80, and Br-82 as the principal induced (n,γ) product activities. These elements can be determined quite easily, instrumentally, in most biological samples. However, in the majority of cases these activities are unwanted interferences, due to their much larger specific activities compared to the elements of interest. Three of these interferences, Cl-38 ($t_{1/2}$ = 37.3 m), Mn-56 ($t_{1/2}$ = 2.58 h), and Br-80 ($t_{1/2}$ = 17.6 m) have relatively short half lives, and hence can be simply allowed to decay out, leaving, however, substantial levels of Na-24 ($t_{1/2}$ = 15.0 h), K-42 ($t_{1/2}$ = 12.4 h), and Br-82 ($t_{1/2}$ = 35.3 h) from which most elements of interest must be separated.

Bi(DDC)$_3$ Extraction. After precipitating $BaSO_4/SrSO_4$ with dilute H_2SO_4, the pH of the filtrate is readjusted into the range of 3-5 pH units. This solution is then extracted with shaking in a separatory funnel for 10 minutes with 35 ml of 3.2 M Bi(DDC)$_3$ in $CHCl_3$ (DDC = diethyldithiocarbamate anion).[2] The organic phase is then washed with H_2O to remove suspended impurities and this wash is added to the original aqueous phase. Copper and, to a certain extent, mercury DDC complexes are now present in the organic phase, which is counted for 30 minutes on a 90 cm^3 Ge(Li) detector. This extraction is very selective, and allows one to use the very sensitive 511 keV γ-ray peak for the determination of Cu.

Bromine Separation. After the copper and mercury activities are separated from the sample solution, objectionable quantities of Br-82 and Na-24 activities remain. In order to remove Br-82, an oxidation-extraction scheme is carried out. This procedure is outlined below:

(1) Bromide carrier is added in the form of NH_4Br.

(2) Permanganate is added as an oxidizing agent in the form of $KMnO_4$.

(3) The solution is heated gently, and concentrated HCl is added dropwise until the solution turns clear.

(4) Three equivolume extractions with CCl_4 are performed.

It is important to be aware of the possibility that some elements of interest may be removed along with the bromine. In particular, one must be concerned about the group As, Se, and Sb, each of which has a tendency to form bromides (e.g. $SeBr_4$) that might be somewhat soluble in the CCl_4 layer. To test this possibility, experiments were performed in which solutions containing As, Se, and Sb tracers were processed through the oxidation-extraction scheme and the aqueous and organic phases counted. In the cases of all three elements, the amount of activity present in the organic phase was less than 3%.

Sodium Removal. In order to remove the large interference due to Na-24 activity from the sample, the well known Girardi method of passing the sample solution (12 M in HCl) through a column of Hydrated Antimony Pentoxide (HAP) was employed.[3] The sample solution is collected with the elements of interest intact, while sodium is quantitatively retained on the column.

Results

As a means of testing these methods, analyses of two biological reference materials, NBS Bovine Liver and NBS Orchard Leaves, were performed, and the results are presented in Table IV. For each analysis, approximately 0.1 g of material is irradiated in a flux of 1.0×10^{12} n cm^{-2} s^{-1} for one hour, then wet-ashed immediately after irradiation. After dissolution of the sample, 5.00 mg each of Ba, Sr, Cu, Hg, and Zn carriers are added and the radiochemical separations described above are begun. The $BaSO_4/SrSO_4$ precipitate and the DDC complexes in $CHCl_3$ are counted as soon as possible, while the filtrate (minus Na-24 and Br-82) can be count-

ed at various decay times, depending upon the elements of interest. One or more solution standards are activated, processed, and counted in an identical manner. Samples and standards are counted as solutions in 125 ml erlenmyer flasks.

References

1. V.P. Guinn, E.R. Christensen, K. de Lancey, W.W. Wadman III, J.H. Reed, N. Hansen, A. Abu Samra, and V.J. Orphan, Third Intl. Conf. on Nuclear Methods in Envir. and Energy Research, University of Missouri, 1977, 303.

2. S. Bajo and A. Wyttenbach, Anal. Chem., 48 (1976) 902.

3. F. Girardi and E. Sabbioni, J. Radioanal. Chem., 1 (1968) 169.

TABLE I

Sr Recovery Experiment

	% Sr-87m in Filtrate	% Sr-87m Ppt'd as $SrSO_4$
Trial #	%	%
1	3.0	97.0
2	3.0	97.0
3	3.1	96.9
4	3.4	96.6

TABLE II

Sr in Bowen's Kale

Experimentally Determined Concentration		Best Value from H.J.M. Bowen
Original $BaSO_4$ procedure:	58.0 ± 4.4 ppm*	
Modified $BaSO_4$ procedure (with pH adjustment):	87.8 ± 6.5 ppm$^{\Delta}$	96.5 ± 26.5 ppm

*1 sample wet-ashed, 3 aliquots analyzed, 90% C.L.

$^{\Delta}$2 samples wet-ashed, 6 aliquots analyzed, 90% C.L.

TABLE III

Bovine Liver Spiking Experiment*

Experimentally Determined Sr Concentration (ppm)	Amount of Sr Spike Added (ppm)
0.25 ± 0.46**	(No Spike)
55.1 ± 11.1	60.2 ± 3.0**
47.4 ± 1.3	51.6 ± 2.6
100. ± 13.5	117 ± 6.0

*Bovine Liver is a Standard Reference Material which contains a negligible amount of Sr.

**All the ± values represent a 90% C.L., based upon 3 measurements in each case.

TABLE IV

Reference Material	This Study (ppm)*		NBS Certified Values (ppm)	
	Cu	Zn	Cu	Zn
Bovine Liver	205 ± 1	144 ± 32	193 ± 5	130 ± 6
Orchard Leaves	10.7 ± 0.1	36 ± 13	12 ± 2	25 ± 3

*Dry-weight basis; error shown is one standard deviation.

SUBSTOICHIOMETRIC ISOTOPE DILUTION ANALYSIS OF TIN IN COAL FLY ASH

Nobuo Suzuki and Hisanori Imura

Department of Chemistry, Faculty of Science,
Tohoku University, Sendai 980, Japan

ABSTRACT

An accurate and precise analytical method for traces of tin by substoichiometric isotope dilution has been investigated. The present method consists of the extraction of tin(IV) as iodide into benzene, the complex formation of tin(IV) with the substoichiometric amount of salicylideneamino-2-thiophenol in the benzene phase. The reproducibility of the substoichiometric separation is satisfactorily good, and the determination of tin in microgram order can be expected. The high selectivity of this method has been ascertained by adding 17 foreign metals and 11 radioactive tracers to the tin(IV) solution. The present method has been applied to the determination of tin in environmental materials, NBS Coal Fly Ash (SRM 1633) and fly ash from coal-fired power plant in Japan.

INTRODUCTION

Recent works on the substoichiometry in this laboratory has been concerned with an extensive application to many elements and with a development of selective substoichiometry. As(III), Sb(III) and methylmercury have been determined selectively with high accuracy [1-3], and the substoichiometric isotope dilution analysis has been applied for the determination of Ca and Fe in biological materials [4], and U in phosphate rock [5].

Tin occurs extensively but irregularly in nature in traces. Recently, it has been reported that tin may be one of the essential elements for higher animals[6]. We are interested in behaviour of this element in biosphere together with problems of environmental pollution. The need for a reliable analytical method has long been apparent. In an interlaboratory comparison for trace analyses of environmental samples such as coal, fly ash, gasoline, and residual fuel oil, the reported values of tin which was determined by spark source mass spectrometry, optical emission spectrometry, and instrumental neutron activation analysis have varied by more than one order of magnitude in these samples. Hence, the necessity for more thorough investigation on analytical methods of tin has been pointed out[7].

It is the purpose of this paper to develope a substoichiometric isotope dilution analysis for traces of tin. This analytical method has great advantages as follows[8,9]; (1) the quantitative separation and recovery of an element in question from the matrix are not required, (2) the element in question can be determined by measuring only the radioactivity of the substoichiometric extract without any standard references or calibration curves, (3) by comparison with general instrumental methods, consequently, the more accurate and the precise determination of the element can be expected. The main sources of errors appeared in this method are considered to be the statistical errors in counting the radioactivity, which can be reduced to less than a few tenth percentage as the relative standard deviation (RSD), e.g., the RSD calculated for 100,000 counts is only 0.3%.

In the present paper, the substoichiometric isotope dilution analysis of trace tin with salicylideneamino-2-thiophenol (SATP), has been investigated. It has been reported that the appreciable reaction of tin(IV) with SATP in an aqueous solution does not proceed untill the mole ratio of SATP to tin(IV) attains to at least 10-fold[10]. This suggests the quantitative reaction of tin(IV) with SATP in the aqueous solution under substoichiometric conditions would not be expected. Accordingly, the complex formation of tin with a substoichiometric amount of SATP in a nonaqueous medium has been studied. It is well known that the extraction of tin(IV) from iodide solutions is highly selective[11,12], and this extraction system has been adopted as the procedure of the transfer of tin(IV) into a nonaqueous medium. The overall process of substoichiometric separation of tin(IV) can be summarized as three steps, viz., the iodide extraction of tin(IV) into benzene, the substoichiometric complexation with SATP in the benzene phase, and the back-extraction of an excess of tin(IV) from the tin(IV)-SATP chelate in the organic phase. The substoichiometric isotope dilution analysis using the present procedure has been applied to the determination of tin in environmental samples, the National Bureau of Standards (NBS) coal fly ash (SRM 1633) and the coal fly ash obtained from a coal-fired electric power plant in Japan.

EXPERIMENTAL

Reagents and Apparatus

Potassium hydrogen sulphate used as a flux and hydrofluoric acid were of a ultra high purity (Suprapur, E. Merck). Sulphuric acid was of a ultra high purity (Wako Pure Chemical Ltd.). A series of buffer solutions used for phase washing consisted of 0.1 M HCl - 0.1 M sodium acetate at the pH region below 4 and of 0.1 M acetic acid - 0.1 M sodium acetate - 0.1 M sodium hydroxide at the pH region between 4 and 8.

A standard tin(IV) solution was prepared by dissolving its high purity metal (99.999%) in concentrated H_2SO_4 on a hot plate, being adjusted to the 6 M H_2SO_4 solution. The concentration of tin(IV) was 4.109×10^{-2} M (4877 μg/ml).

A radioisotope, ^{113}Sn was obtained from the New England Nuclear (USA), being appropriately diluted with 2.5 M H_2SO_4. Its specific activity was enough high as 19 Ci/g Sn.

Radioactive tin(IV) spike solutions were prepared by adding a few drops of the ^{113}Sn(IV) solution to the standard tin(IV)

solution and by diluting with 2.5 M H_2SO_4 to a volume. The resulting solutions were allowed to stand for over a day in a series of fundamental investigations. The concentration of the radio-tin(IV) stock solutions used were 4.1×10^{-3}, 4.1×10^{-4}, and 4.1×10^{-5} M, and the specific activity of those solutions, above ca. 0.5 μCi/ml. In practical application, a 1.027×10^{-5} M (1.219 μg/ml) radio-tin(IV) spike solution was prepared and immediately added to a sample solution containing unknown amounts of tin(IV). The isotopic equilibrium was achieved perfectly by heating at about 90 °C over night.

Radioactive tracers of ^{54}Mn, ^{57}Co, ^{57}Ni, ^{67}Cu, ^{74}As, $^{120,122}Sb$, and ^{203}Pb used in experiments for the interference were prepared by photon irradiation with maximam bremsstrahlung energy of 30 and 60 MeV using the Tohoku University electron linear accelerator. Other tracers, ^{51}Cr, ^{59}Fe, and ^{65}Zn were purchased from the New England Nuclear (USA).

SATP was obtained from the Dojin Chemical Laboratory, its purity (better than 98%) was checked by elemental analysis of C, H, N, and S. The 10^{-5} - 10^{-3} M SATP solution was prepared by dissolving it in absolute ethanol (99.5%) containing 1% ascorbic acid as a stabilizer in a blown volumetric flask. A 10% pyridine-ethanol solution was prepared by diluting with absolute ethanol. Benzene was purified by usual method.

The γ-activity of $^{113}Sn(^{113m}In)$ was measured with a 50 x 50 mm NaI(Tl) well-type scintillation detector connected to a single-channel analyser (Nippon Atomic Industry Group Ltd.)

Preparation of Sample Solution

A coal fly ash sample was dried in a desiccator over P_2O_5 untill a constant weight was obtained. In a platinum crucible, the weighed sample (about 1 g) was taken, and 1-2 ml of water, 0.05 ml of H_2SO_4, and 4 ml of HF were added. The contents were heated on a hot plate (adjusted to about 80 °C) for 1-2 h. After 0.5 ml of HF was added, the resulting solution was evaporated to dryness untill the H_2SO_4 fume was evolved. Three to four g of $KHSO_4$ was added in the platinum crucible, and the contents were gradually heated with care. After the contents thoroughly fused, further the heating (at ca. 400-600 °C) was continued for 15 to 30 min. After cooling, the fused mass resulted was placed in a conical flask together with a 5-ml portion of the radioactive tin(IV) spike solution (6.097 μg of tin) and about 40 ml of 3.5 M H_2SO_4. The resulting solution was heated at 90-95 °C for 8-11 h to achieve completely the isotopic equilibrium between radioactive tin(IV) and non-active. Into a 100-ml separatory funnel, about 50 ml of the resulting sample solution was transfered together with 6 ml of 5 M NaI and 20 ml of benzene, and then the contents were shaken for 1-2 min. Tin(IV) extracted into the organic phase was back-extracted with 10 ml of 2.5 M H_2SO_4.

Substoichiometric Separation of Tin(IV)

In a 50-ml centrifuge tube with a ground-glass stopper, 10 ml of the sample solution prepared above (or 10 ml of the radioactive tin(IV) spike solution), 8 ml of 5 M $NaClO_4$, and 13 ml of benzene were placed. Immediately after 2 ml of 5 M NaI was added, the contents were vigorously shaken for 30 sec. After centrifugation, a 5-ml portion of the benzene phase containing tin(IV) iodide was pipetted into a 30-ml centrifuge tube with a ground-glass stopper. The substoichiometric amount of SATP in ethanol (1 ml of 2.5×10^{-5} M

SATP-ethanol in practical application) for the amount of tin(IV) carrier in the organic phase, and 0.1 ml of 10% pyridine-ethanol were added in this order. The contents were moderately mixed for each addition, and then allowed to stand for 10 to 30 min. They were vigorously shaken with 5 ml of a buffer solution of pH 3.8-4.0 containing 2.5×10^{-5} M tartrate for 1 h. After centrifugation, a 3-ml portion of the organic phase was pipetted into a glass test-tube with a fitted cap and allowed to stand for 18 h in order to achieve the radioactive equilibrium for $^{113}Sn(T_1=115d)$-$^{113}In(T_1=1.66\ h)$. The γ-activity was measured by using a scintillation counter set. The pH value of the aqueous phase was checked before and after shaking.

RESULTS AND DISCUSSION

Iodide Extraction of Tin(IV)

We have examined the iodide extraction of tin(IV) to transfer it from a sample solution acidified with sulphuric acid to an organic medium, and this must be effective in separating tin from some interfering elements and in accelerating substoichiometric complexation with SATP in the nonaqueous solvent medium. The results are shown in Fig. 1 together with the extraction conditions. It was ascertained that the distribution ratio of tin(IV) did not depend on its concentration from 10^{-6} to 10^{-3} M. In higher acidic solutions, larger amounts of iodine produced by air-oxidation was extractable into benzene, hence the extraction of tin(IV) was carried out from H_2SO_4 solutions in the concentration as low as possible. As previously reported in the $HClO_4$-NaI-benzene system [11], an addition of $NaClO_4$ significantly enhanced the extraction of tin(IV) into benzene; it makes possible the extraction in lower acidity of the aqueous phase. As shown in Fig. 1, the distribution ratio of tin(IV) increases by two orders of magnitude in the presence of 2.0 M $NaClO_4$. In the presence of about 0.1 M HCl, on the contrary, it decreases by an order of magnitude due to the formation of relatively stable chloro complexes in the aqueous phase, so that the use of HCl in the dissolution of samples must be avoided.

Tin(IV) extracted as iodide into benzene can be readily back-extracted with aqueous solutions of various pH values. This washing procedure can be applied to remove an excess of tin(IV) from the SATP chelate in the recommended procedure.

Formation of Tin(IV)-SATP Chelate in Nonaqueous Medium under Substoichiometric Conditions

In iodide extraction system iodine produced might interfere the quantitative reaction with a substoichiometric amount of SATP with tin(IV) in the organic medium. Practically, however, the stock solution of SATP was prepared with addition of ascorbic acid as a stabilizer for SATP, and this ascorbic acid served also as a reducing agent for I_2 extracted in the organic phase. The results showed that I_2 may be readily reduced with ascorbic acid added with SATP as the ethanol solution, and no influence on the complex formation of tin(IV) with a substoichiometric amount of SATP was observed below 3 M H_2SO_4.

Inasmuch as a constant amount of tin(IV) must be isolated as the SATP chelate, the washing for removing of extra tin(IV) iodide from the organic phase but for remaining of the SATP chelate in

the organic phase has been investigated. In this phase washing the following phenomena were observed, that is the tin(IV)-SATP complex in the organic phase transfer into the aqueous phase by short time shaking for a few sec, and at that time the aqueous phase turned slightly yellow colour, then the radioactivity of ^{113}Sn in the organic phase increased with shaking and soon attained to a constant value. These observations may be explained on the assumption that the 1:1 complex of tin(IV)-SATP is formed instantaneously in the nonaqueous medium under substoichiometric conditions, and then the phase washing with an appropriate pH buffer causes the rearrangement to 1:2 complex of tin(IV)-SATP which is finally re-extracted into the organic phase. An extraction behaviour of tin(IV) with SATP was thoroughly investigated[13].

The influence of pH on the substoichiometric extraction with 2.0×10^{-4} M SATP is clearly seen in Fig. 2. By reaction with a constant but substoichiometric amount of SATP a fixed amount of tin(IV) must remain in the organic phase. The constant radioactivity is observed at pH 2.5-5.3, with the relative standard deviation (RSD) of the activity as amall as 0.38%. This plateau pH region, as expected, broadens with the increase in the shaking time. The similar results were obtained in the substoichiometric system with different concentration of SATP, e.g., with 2.0×10^{-5} M SATP a plateau region appeared at pH 2.5-4.5 by shaking for 1.5 h. When the pH values are adjusted below 2 with 0.1 M HCl, as shown in Fig. 2, an extra tin(IV) remains in the organic phase, while with 0.05 M H_2SO_4, such an abnormality is not observed. This may be attributed to the formation of a mixed ligand complex of Sn(IV)-Cl^--SATP. Such a mixed complex was ascertained in the extraction of tin(IV) with 8-hydroxyquinoline(oxine) or N-benzoyl-N-phenylhydroxylamine(BPHA), being $SnCl_2(oxine)_2$[14] or $SnCl_2(BPHA)_2$[15].

Reproducibility of the Substoichiometric Separation

A substoichiometric separation of tin(IV) by a combination of the iodide extraction and the complexation with a substoichiometric amount of SATP in the nonaqueous medium was applied to a series of solutions containing different amounts of tin(IV) labelled with ^{113}Sn. As shown in Fig. 3, the radioactivity of the organic phase increases with the increase in the amounts of labelled tin(IV) untill the equivalent point corresponding to the ratio of tin(IV) to SATP of 1:2. Beyond this point, that is, under the substoichiometric conditions, a constant amount of tin(IV) remains in the organic phase, and the reproducibility is very satisfactory. The precision obtained for the substoichiometric separation under various conditions is summarized in Table 1. The precision of the radioactivity measurement, which practically governs that of the substoichiometric determination, is sufficiently high. From the table, it is also expected that the present method can be applied to the determination of tin in microgram order.

Effect of Diverse Metal Ions

The effect of other metal ions on the substoichiometric separation of tin(IV) was investigated by adding each non-active ion in 10- to 400-fold amounts for tin(IV) to 10 ml of the aqueous solution containing 49 μg of tin(IV). The radioactivity of ^{113}Sn obtained in the presence of the interfering ion was compared with that obtained in the absence of the interfering ion. The results showed many elements other than Fe(III), Cu(II), and V(V) do not interfere the substoichiometric isolation of tin(IV). An interference of Fe(III) can be prevented by reducing to Fe(II) with

ascorbic acid prior to the iodide extraction. Generally the interference can be avoided by separating tin(IV) from I_2, for example by repeat extraction, that is, tin(IV) extracted as iodide is back-extracted with 2-3 M H_2SO_4, and extracted again into benzene as iodide, and followed by substoichiometric chelate formation with SATP. In this procedure no interference is observed. To be sure of the selectivity of the overall extraction procedure the degree of decontamination from foreign metal ions labelled with appropriate radioactive isotope was examined. As shown in Table 2, foreign metals other than As(III) and Sb(III) are thoroughly separated from tin(IV) in the iodide extraction, and then contamination of As(III) and Sb(III) is almost eliminated by the substoichiometric separation with SATP. Practically, inasmuch as the iodide extraction is repeated twice as described above, it is stated that the present procedure has higher selectivity for the determination of tin(IV).

Determination of Tin(IV) in a Synthetic Mixture

The accuracy and the precision of the substoichiometric isotope dilution analysis for tin(IV) proposed here can be evaluated by determining tin in a synthetic mixture containing a known amount of tin and large amounts of other metals. The results are summarized in Table 3. The reproducibility of the substoichiometric isolation of tin(IV) is seen in fourth and fifth column in this table, being enough high as 0.25 and 0.32% respectively. The errors in the determination of tin by the isotope dilution principle are influenced also by the isotopic dilution ratio of the amount of tin in the sample to that of labelled tin spiked, the RSD obtained in the present experiments, 0.63% is very satisfactory. The mean value, 16.16 $\pm$ 0.10 μg is very consistent with the amount added, 16.25 μg within the deviation of 0.56%. The present method is highly accurate and precise, and can be applied to practical samples.

Determination of Tin in Coal Fly Ash

The coal fly ash samples were obtained from the NBS and a coal-fired electric power generation plant in Japan. The latter was the finest part (ca. 80% of it passed through a 300-mesh screen) of the fly ash treated stepwise with electrostatic precipitators. Table 4 shows the analytical result of the domestic sample together with the analytical conditions. The overall deviation of the determined value are as little as 1.8%, consequently, the present procedures including the decomposition of the sample, the isotopic dilution, and the substoichiometric separation, are considered to be adequate for the determination of tin in fly ash. The blank analysis was carried out over all the procedures, thereby, it was ascertained that the blank contamination of tin from reagents and glass ware etc. was negligible as less than 0.01 μg.

The results for the NBS SRM 1633 coal fly ash are summarized in Table 5. The reproducibility of the substoichiometric separation from each sample solution (see in fourth column of this table) is very satisfactory; the mean values of the RSD is 0.76%. Nevertheless, the precision for the overall mean value of tin is 10.0% and does not seem to be very good. Recalling the high precision of the independent experiment, the scatter of the analytical values among individual samples may be responsible for relatively large errors of the overall mean value. Recently, it has been pointed out that the concentration of elements in coal fly ash is varied remarkably with the particle size[16]. The scatter found for the NBS fly ash may be ascribable to the sampling statistical

or the inhomogeneity of the sample rather than the randam errors in the present analytical method.

CONCLUSIONS

The substoichiometric isotope dilution analysis for tin proposed here has enough high accuracy and precision. This may be appreciated by the characteristic of the present method: The element can be determined by measuring only the radioactivity separated substoichiometrically without any calibration curves, and the quantitative recovery of the element in question is not required. It is stated that the present method is reliable analytical one of tin down to μg/g range not only in the routine works but in the reference work to assess the results given by other methods.

REFERENCES

1. Y. Kanda and N. Suzuki, Radiochem. Radioanal. Lett., 1979, 39, 221.
2. Y. Kanda and N. Suzuki, ibid., 1979, 37, 183.
3. Y. Kanda and N. Suzuki, Anal. Chem., to be published.
4. N. Suzuki, S. Nakamura and H. Imura, J. Radioanal. Chem., in press (1980).
5. N. Suzuki, H. Imura and K. Yoshida, Presented at the 17th Annual Meeting on Radioisotopes in the Physical Science and Industry, 1980, Tokyo, Japan.
6. K. Schwarz, D.B. Milne and E. Vinyard, Biochem. Biophys. Res. Comn., 1970, 40, 22.
7. D.J. Von Lehmden, R.H. Jungers and R.E. Lee, Jr., Anal. Chem., 1974, 46, 239.
8. J. Ruzicka and J. Stary, Substoichiometry in Radiochemical Analysis, Pergamon, Oxford, 1968, p. 43.
9. K. Kudo and N. Suzuki, J. Radioanal. Chem., 1975, 26, 327.
10. G.R.E.C. Gregory and P.G. Jeffery, Analyst, 1967, 92, 293.
11. D.D. Gilbert and E.B. Sandell, Microchem. J., 1960, 4, 491.
12. A.R. Byrne and D. Gorenc, Anal. Chim. Acta, 1972, 59, 81.
13. H. Imura and N. Suzuki, Anal. Chim. Acta, in press.
14. A.R. Eberle and M.W. Lerner, Anal. Chem., 1962, 34, 627.
15. M. Koeva, Anal. Chim. Acta, 1979, 104, 161.
16. J.A. Campbell, J.C. Laul, K.K. Nielson and R.D. Smith, Anal. Chem., 1978, 50, 1032.

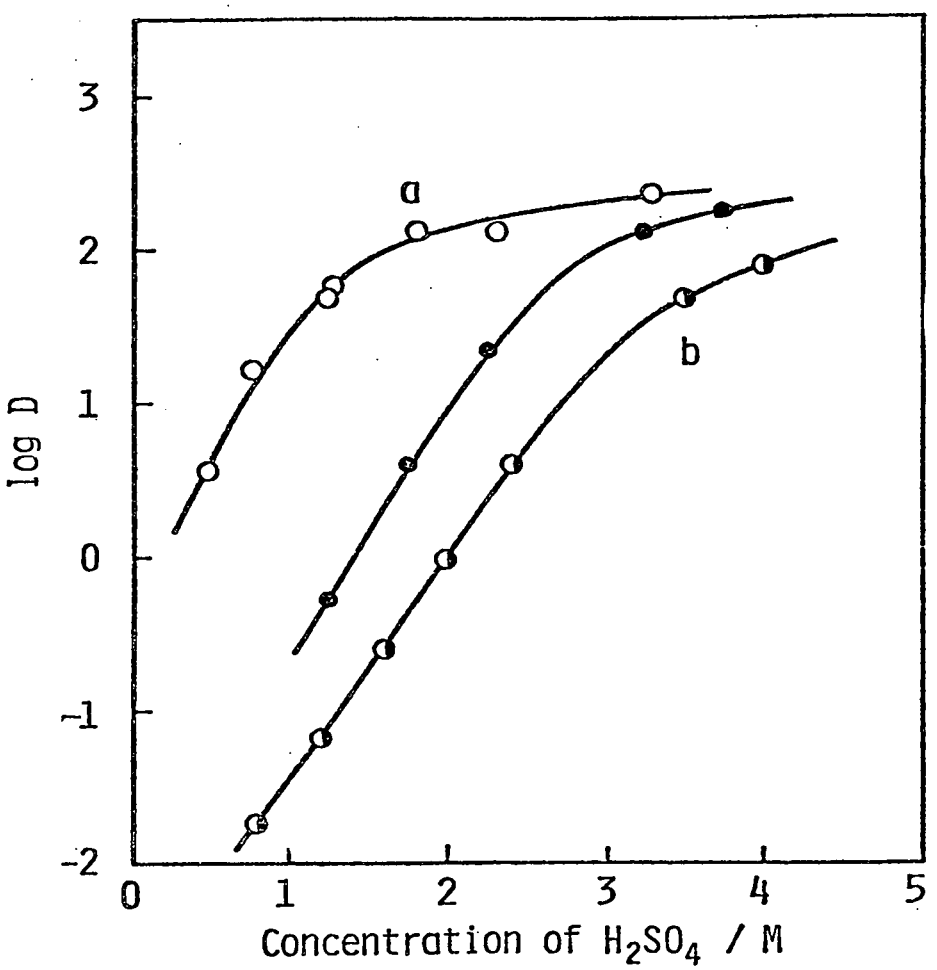
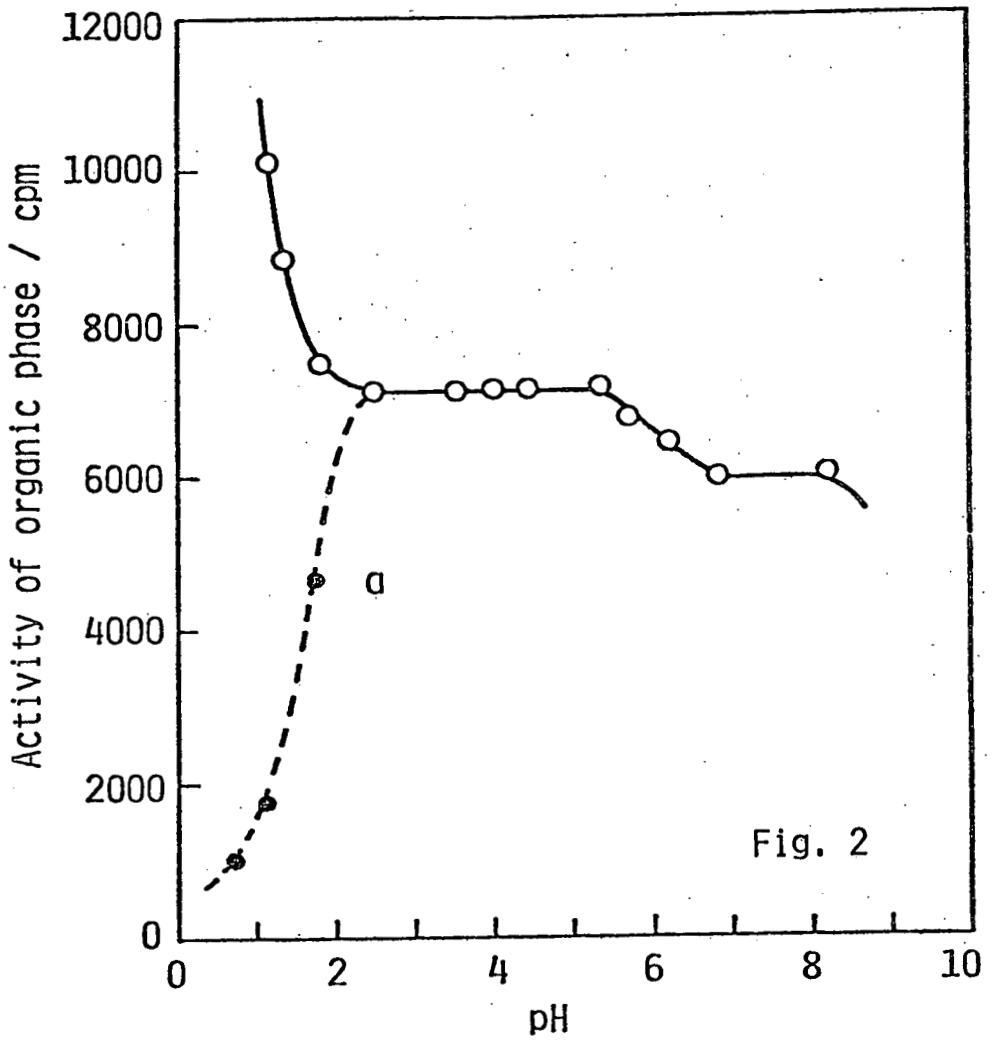
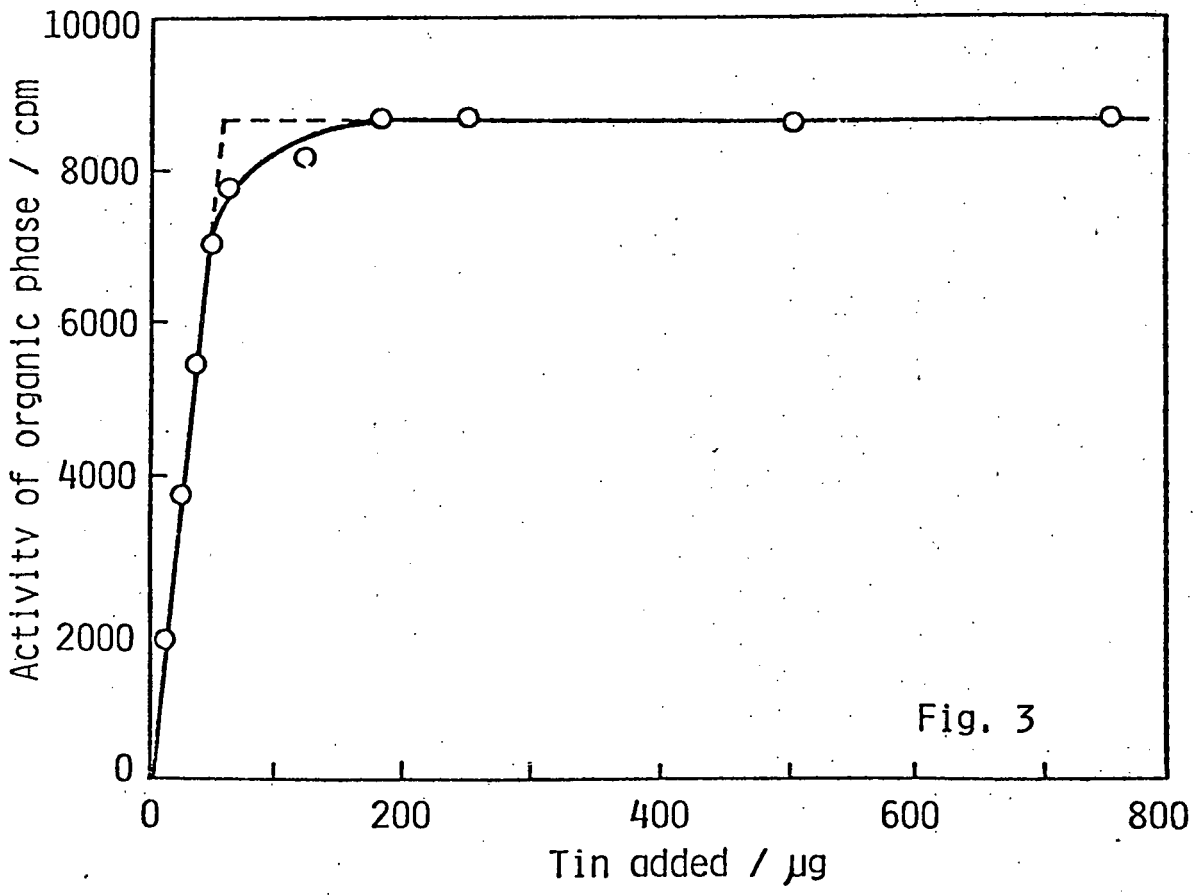


Fig. 1

Extraction of tin(IV) from H_2SO_4 solutions containing 0.5 M NaI to benzene. $[Sn(IV)] = 10^{-5}$M, shaking time = 1-2 min.
(a) Extraction in the presence of 2.0 m $NaClO_4$.
(b) Extraction in the presence of 0.1 M HCl.



Dependence of the substoichiometric separation of Sn(IV)-SATP complex on the pH value.
Conditions; [Sn(IV)] = 4.1 x 10^{-4}M, [SATP] = 2.0 x 10^{-4}M,
[Tart] = 1.0 x 10^{-3}M, shaking time = 1 h.
(a) The pH values are adjusted with 0.05 M H_2SO_4 without chloride.



Reproducibility of the substoichiometric separation of tin(IV) with SATP after the iodide extraction.
Conditions; [SATP] = 2.0×10^{-4}M. [Tart] = 1.0×10^{-3}M, pH = 3.6-3.9, shaking time = 2 h.

Table 1. Reproducibility of the substoichiometric separation under various conditions

2.0×10^{-4} M SATP*		2.0×10^{-5} M SATP†		2.0×10^{-6} M SATP§	
Tin taken µg/5 ml	Activity of organic phase cpm	Tin taken µg/5 ml	Activity of organic phase cpm	Tin taken µg/5 ml	Activity of organic phase cpm
1219	7174	121.9	9202	12.19	10865
731.6	7181	73.16	9226	7.32	10682
487.7	7143	48.77	9167	4.88	11184
365.8	7153	36.58	9083	3.66	11489
304.8	7085	30.48	9141	3.05	11082
243.9	7096	24.39	9199	2.44	11255
243.9	7074	18.29	9224	1.22	11218
182.9	7048	12.19	9190		
mean $\pm$ σ = 7115 $\pm$ 46 cpm		mean $\pm$ σ = 9179 $\pm$ 48 cpm		mean $\pm$ σ = 11111 $\pm$ 266 cpm	
%RSD = 0.64		%RSD = 0.52		%RSD = 2.39	

Experimental conditions;

* [Tart] = 10^{-3} M, pH = 3.9, shaking time = 1 h.

† [Tart] = 10^{-4} M, pH = 3.9, shaking time = 1 h.

§ [Tart] = 10^{-5} M, pH = 3.9, shaking time = 1.5 h.

Table 2. Selectivity of the substoichiometric separation of tin(IV) with SATP after the iodide extraction

Radioactive tracer added cpm		Carrier added mg	Activity of iodide extract cpm	Activity of substoichiometric extract cpm	Decontamination factor*
^{51}Cr,	439,813	5.2	0	0	$> 10^6$
^{54}Mn,	418,827	5.5	0	0	$> 10^6$
^{59}Fe	458,005	5.6	7	7	7×10^4
^{57}Co,	942,706	5.9	0	1	$> 10^6$
^{57}Ni-^{57}Co,	1,636,008	1.4	2	1	$> 10^6$
^{67}Cu,	2,263,951	6.4	4	1	$> 10^6$
^{65}Zn,	480,246	6.5	0	1	$> 10^6$
^{74}As,	94,172	0.7	4295	30	3×10^3
$^{129,122}Sb$,	1,935,160	0.9	78953	68	3×10^4
^{203}Pb,	909,408	1.7	30	0	$> 10^6$

Experimental conditions; tin taken = 49 µg/10 ml of aqueous phase, [SATP] = 2.0×10^{-5} M [Tart] = 10^{-4} M, pH = 3.9, shaking time = 1 h.

* Decontamination factor = (Activity taken)/(Activity of substoichiometric extract).

Table 3. Determination of tin in a synthetic mixture by the substoichiometric isotope dilution analysis with SATP

Tin taken μg	Other metals present mg		Active tin spiked μg (M_s)	Activity from spike soln. cpm (A_s)	Activity from test sample cpm (A_x)	Tin found μg (M_x) *
16.25	Al (III), 1.3	Co (II), 2.9	16.25	21298	10726	16.11
	V (V), 2.5	Ni (II), 2.9		21374	10707	16.17
	Cr (III), 2.6	Cu (II), 3.2		21402	10663	16.30
	Mn (II), 2.8	Zn (II), 3.3			10741	16.06
	Fe (III), 2.8					

Mean value ± σ = 16.16 ± 0.10 μg. %RSD = 0.63. Deviation from tin taken = -0.56%.

Table 4. Determination of tin in a domestic coal fly ash by the substoichiometric isotope dilution analysis with SATP

Sample weight g	Amounts of $KHSO_4$ g	Active tin spiked μg	Activity from spike soln. cpm	Activity from test sample cpm	Tin found μg	Concentration μg/g
1.0228*	4.0	6.097	12434	7223	4.40	4.30
1.0399†	3.5	6.097	32973	19090	4.43	4.27
1.0500†	3.0	6.097	32973	18719	4.64	4.42

Mean value ± standard deviation = 4.33 ± 0.08 μg/g. %RSD = 1.8.

* The isotopic equilibrium was achieved by heating for 8 h. † for 11 h.

Table 5. Determination of tin in the NBS coal fly ash (SRM 1633) by the substoichiometric dilution analysis with SATP

Sample weight g	Active tin spiked µg	Activity from spike soln. cpm	Activity from test sample cpm	Tin found µg	Concentration µg/g
0.9931*	6.097	25358	12263	6.51	6.56
			12183	6.59	6.64
1.0445*	6.097	25358	13286	5.54	5.30
			13575	5.29	5.07
0.9882*	6.097	12237	6439	5.49	5.56
			6522	5.34	5.41
0.9314*	6.097	8706	4536	5.61	6.02
1.0689†	6.097	12434	6540	5.50	5.14
			6490	5.58	5.22
0.9488†	6.097	12434	6346	5.85	6.17
			6378	5.79	6.10

overall mean value ± standard deviation = 5.74 ± 0.57 µg/g. %RSD = 10.0.

* Fusion with 3.5 g flux. † Fusion with 4.0 g flux.

VARIATION OF MINOR AND TRACE ELEMENTS IN COALS FROM KNOWN GEOLOGIC SETTINGS

BAILEY, A., Department of Geology, Marshall University Huntington, WV, 25701, USA and JONES, J., Phoenix Memorial Laboratory, University of Michigan, Ann Arbor, MI, 48109, USA.

ABSTRACT

To determine chemical differences between coals formed in different environments, samples of West Virginia Pocahontas No. 3 and Pocahontas No. 2 coals were analyzed for a wide range of elements using neutron activation, x-ray and atomic absorption analysis. The samples consisted of the <1.55 specific gravity fraction of core taken from an area where the geologic environments have been determined as part of a recent doctoral dissertation. Specifically, rocks associated with the coals show that the Pocahontas No. 2 in this area was formed in a swamp that developed on a uniform platform open to marine influences, while the Pocahontas No. 3 was influenced by a river system and protected from marine influences by barrier bars that developed between the sea and the platform.

Results from this study indicate that the Pocahontas No. 3 has higher concentrations of Al, Si, Sc, Ti, La, Ce, Eu, Yb, Hf, Th, and U in this area, while the No. 2 has higher concentrations of pyritic sulfur, Fe, Co, Zn, and As. The enrichment of the eleven elements in the No. 3 appears to be due to higher concentrations of some of these elements in fresh water (in clastic and/or dissolved form) being added to the No. 3 swamp, while enrichment of the five elements in the No. 2 is probably due to the formation of sulfides in the more brackish environment. Some of these chemical differences also appear between suites of coals from similar pairs of environments collected in other areas, indicating some generality for the relationships.

In addition to these distinctions between the seams, values for the concentrations in the Pocahontas No. 2 have narrow distributions, while values for many elements in the No. 3 have wider distributions and increase toward the northeast, toward a major wedge of clastic material within the No. 3. If the clastic material represents a splay deposit (wedge of clastic material deposited from water flowing through a break in the natural levee system of the main river) then the trends may be related to increased supplies of these elements from water flowing through the break in the levee system.

These relationships between the chemistry of the coal and its environment of formation may be used in developing predictive models for mine planning, chemical surveys, and reserve estimation. Examples of possible application include prediction of partings and design of sampling plans.

INTRODUCTION

A great deal of work has been devoted to the determination of trace and minor constituents in coals. These constituents may be incorporated into the coal by a number of processes (Zubovic, 1966). Many of these processes are related to geologic conditions around the coal-forming swamp. Where this is the case, there should be relationships between the inorganic chemistry of the coals and their paleoenvironments, as indicated by associated rocks. A major objective of the present research is to examine relationships between the inorganic chemistry of coal and its paleoenvironments, as inferred from associated rocks. Such information is needed for a basic understanding of the geochemistry of coals and may be used in constructing predictive models of use during the development of coal resources.

In order to examine relationships between the chemistry of coals and their paleoenvironments, coals from known paleoenvironments are needed. The present work is based on two coal seams in southern West Virginia that have been studied as part of a recent doctoral dissertation (Baganz, 1979). These two coal seams are the Pocahontas No. 3 and the Pocahontas No. 2. At present, the data consist of analyses of drill core samples taken from an area of about seven by eight kilometers. Relative locations are shown in Figure 1.

Extensive core and mine data allowed Baganz to construct the following series of events for the formation of the Pocahontas No. 2 and the Pocahontas No. 3 in the study area:

1) Formation of a stable sandstone platform in a shallow sea.
2) Formation of an accumulation of organic material that later formed the Pocahontas No. 2.
3) Inundation of the area with clastic material and possible marine incursion.
4) Formation of an accumulation of organic material that later formed the Pocahontas No. 3. This swamp was cut by river systems.
5) Inundation of the area with clastic material and for mation of barrier bars which isolated the swamp from the sea to some extent.

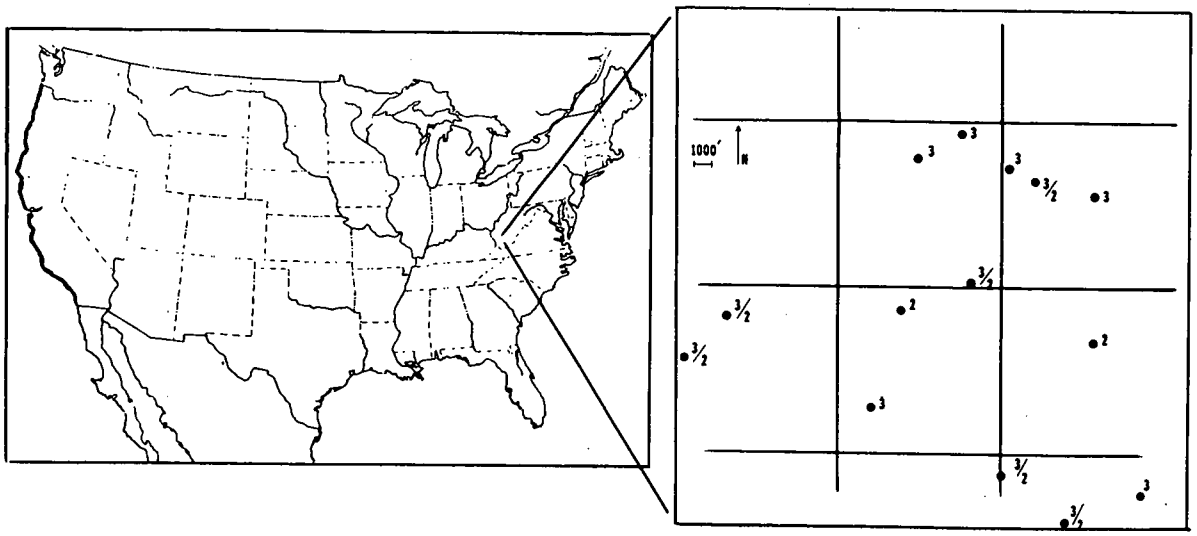


Figure 1. Relative locations of samples used in this study. Number indicates seam sampled at that location.

From this data the two seams have different environments of formation. The Pocahontas No. 2 swamp, which formed on the open platform, was subject to marine influences. The Pocahontas No. 3 was influenced by river systems and formation of a barrier bar system blocked off later marine incursions. The fluvial influence can be seen in the northeastern part of the study area. Here the No. 3 contains a major wedge of clastic material (see Figure 2). This may represent a crevasse splay deposit, formed when the river system broke through the natural levee system and spilled out into the swamp, carrying material in the form of clastic particles and in solution out into the deposit of organic debris.

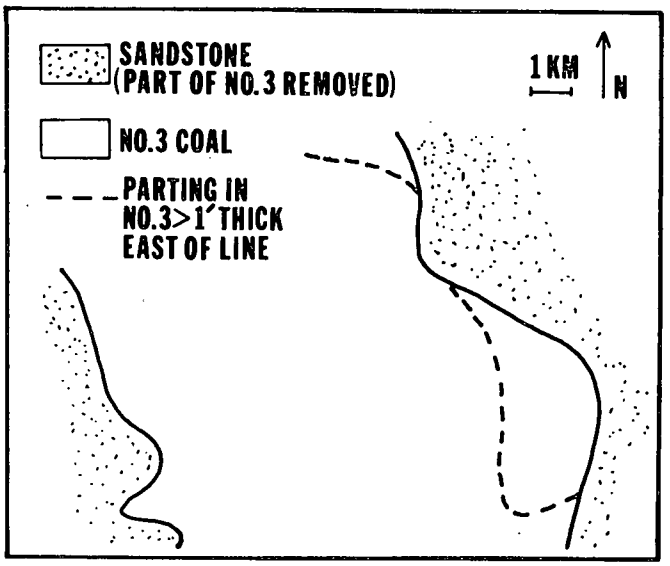


Figure 2. Parting in No. 3 coal (After Baganz, 1979).

METHODS

At present, 12 core samples of No. 3 and 8 core samples of No. 2 have been analyzed for a variety of constituents. These samples, consisting of the <1.55 specific gravity portion, have been analyzed using three techniques: atomic absorption spectroscopy (AAS), x-ray fluoresence (XRF), and neutron activation analysis (NAA). Cu, Zn, Ca, Mg, Ni, Cr and Mn were determined using AAS and Si, Al, K, Ti and Fe by XRF. Ce, Se, Hf, Tb, Sc, Co, Eu, Sb, Sm, Lu, U, Th, Ba, Nd, As, Br, Na, La, V and Cl were determined by NAA. Several other elements were sought but were present in concentrations too low to be determined by these methods. These include Ag, Au and Cs. In addition to the above thirty-two elements, pyritic sulfur (PyS) was determined using a leaching technique and 500° ash by combustion in a muffle furnace. The analytical procedures are summarized in the flow chart shown in Figure 3.

In order to verify the results of the analytical methods used in this study, a sample analyzed by the USGS was also analyzed using techniques used in the present study. Results obtained in this study and those obtained by the USGS are given in Table I.

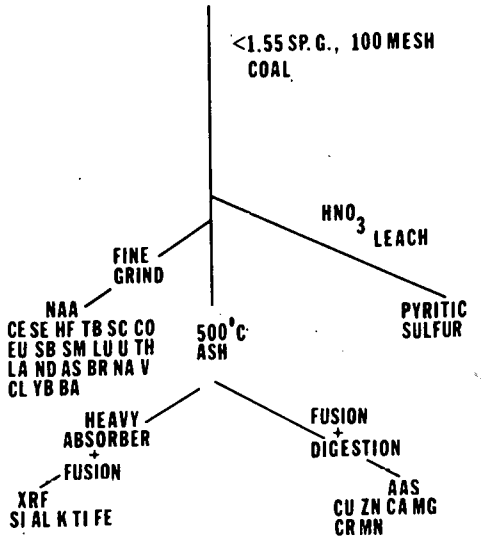


Figure 3. Flow chart showing procedures used in the study.

Table I. Comparison of results obtained in this study with those obtained by the USGS for a sample of Herrin (No. 6) Coal.

	NA μG/G	MG %	AL	SI	CL	K	CA	SC μG/G	CR
THIS STUDY	679	0.064	1.2	2.9	—	0.2	0.51	3.0	14
USGS	—	—	1.2	2.9	0.016	0.2	0.50	2.4	13.8

	MN	FE %	CO μG/G	CU	ZN	LA	CE	ND	SM
THIS STUDY	24	1.83	4.7	2	30	5	10	23	1.0
USGS	36	1.80	3.9	8.7 (6.4)	33.8	5	9	30	0.8

	EU	TB	YB	LU	HF	AS	SE	BR
THIS STUDY	0.24	0.24	0.6	0.09	0.6	1.4	1.9	1.43
USGS	0.18	0.15	0.6	0.10	0.4	1.5	1.9	2.15

	SB	BA	TH	U	TI %
THIS STUDY	0.1	84	2.5	0.83	0.065
USGS	0.2	47	2.7	0.85	0.066

RESULTS

Results consist of whole-coal concentrations for 33 constituents in the two seams. As a first step in processing the data, means and standard errors were calculated for the two seams. Using this data, t-statistics were calculated for the differences between the means for the two seams. The means for the thirty-three elements for the two seams are given in Table II. Those elements that display a statistical difference at the 5% level are starred.

Table II. Means for the whole-coal concentrations of the thirty-three elements determined in the Pocahontas No. 3 and No. 2 Coals. Those elements displaying statistically valid differences at the 5% level are starred.

	NA μG/G	MG%	*AL	*SI	*PYS	CL	K	CA	*SC μG/G
NO.3	465	0.024	1.1	1.5	0.18	0.109	0.06	0.05	3.9
NO.2	253	0.016	0.80	1.1	0.55	0.079	0.05	0.06	3.0

	*TI%	V μG/G	CR	MN	*FE%	*CO μG/G	CU	*ZN	*LA
NO.3	0.07	64	26	3	0.24	6.1	33	8	14
NO.2	0.04	28	12	4	0.80	8.5	31	17	8

	*CE	ND	*SM	*EU	TB	*YB	LU	*HF	*AS
NO.3	30	13	2.7	0.68	0.63	1.07	0.18	0.71	15
NO.2	18	11	2.0	0.49	0.51	0.95	0.20	0.46	27

	SE	BR	SB	BA	*TH	*U
NO.3	3.6	51.4	1.8	54	3.8	2.07
NO.2	3.5	52.4	1.9	50	2.1	1.18

From Table II, it can be seen that the No. 3 is higher in Al, Si, Sc, Ti, La, Ce, Sm, Eu, Yb, Hf, Th and U. These will be referred to as Group A elements. The No. 2 is higher in PyS, Fe, Co, Zn and As. These will be referred to as Group B elements. In addition, the dispersion among the individual value was found to be greater in the No. 3 than the No. 2. If the geographic distributions of Group A elements in the No. 3 are examined (Figure 4) it can be seen that all except Ti, Yb and Hf are higher in the northeast portion of the study area.

CONCLUSIONS AND DISCUSSION

From the above data the marine-influenced No. 2 is higher in PyS, Fe, Co, Zn and As and the fluvial-influenced No. 3 is higher in Al, Si, Sc, Ti, La, Ce, Sm, Eu, Yb, Hf, Th and U. In the No. 3, most of the Group A elements are higher in the northeast samples and lower in the southwest samples. These features can be explained in terms of several possible modes of incorporation. Definite statements about the mode of incorporation are difficult to make without mineralogical studies such as those by Gluskoter (1967), Ward (1978) and Finkelman and Stanton (1978). However, these probably include addition to the coal-forming swamp as clastic material, addition as dissolved material

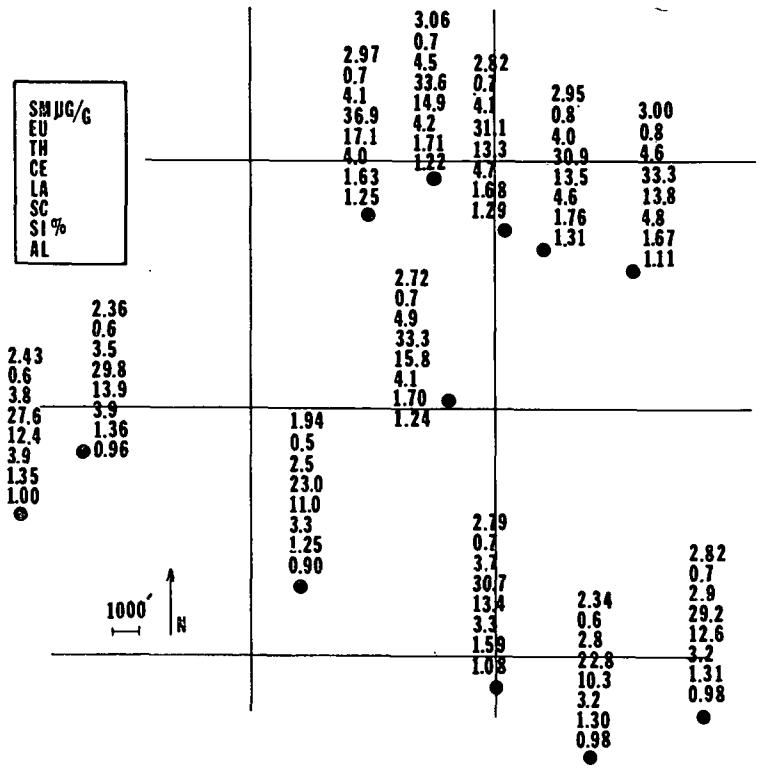


Figure 4. Concentrations of some Group A elements in the No. 3 Coal

followed by precipitation, and addition in solution followed by precipitation aided by micro-organisms. In particular, Group A elements were probably introduced into the coal-forming swamp as clastic particles carried by the river system and/or as dissolved materials whose concentrations would be higher in freshwater. This may have been followed by direct precipitation under new chemical conditions or utilization by plants, followed by release from the organic debris and precipitation. Regardless of the exact mechanism, concentrations of these elements would be higher in the No. 3 because of the greater fluvial influence. Within the No. 3, Group A elements are generally higher in the northeast because, as stated previously, the presence of the crevasse splay deposit in the northeast indicates addition of material to the No. 3 swamp from this direction.

Fe and PyS in Group B elements are higher in the No. 2 Coal because more marine conditions in the No. 2 coal-forming swamp favored microbial activity that was involved in the precipitation of iron disulfides. Arsenic is sometimes associated with pyrite (Minkin, et al.; 1979) and might be higher in the No. 2 because of this association. Zn and Co incorporation may also be due to sulfide precipitation, promoted by higher pH's and

microbial activity, but less is known about this.

In general, many of these differences are also displayed by another group of samples from marine-influenced and fluvial paleoenvironments. In particular, Al, Si, Ti, La, Ce, Yb and Hf were found to be higher in fluvial Kittanning Coals from the Appalachian Basin, while marine-influenced coals were found to be higher in Fe, PyS and Zn. Necessary data for examination of Sc, Co, As, Th and U were not available. Sm, Eu and Yb did not give statistically valid differences in the Kittanning study. However, differences between sample and coal types may explain these different results.

These relationships between the coal chemistry and paleoenvironments, as indicated by associated rocks, suggest possible applications. Among these are use of chemical features as an aid in determining the paleogeographic position of a suite of coals. This, in turn, may be used as an aid in mine development. Further application includes anticipation of chemical features from the paleogeographic setting for the coal. Finally, such information contributes to the basic understanding of geochemical processes associated with coal.

REFERENCES CITED

BAGANZ, B., 1979, Paleoenvironmental model for the Pocahontas No. 1, No. 2 and No. 3 Coal Seams, Southern West Virginia: Ph.D. Thesis, University of South Carolina.

FINKELMAN, R.B. AND R.W. STANTON, 1978, Identification and significance of accessory minerals from a bituminous coal: Fuel, vol. 57, p. 763-768.

GLUSKOTER, H.J., 1967, Clay minerals in Illinois coals: J. Sediment. Petrol., vol. 37, p. 205-214.

MINKIN, J.A., FINKELMAN, R.B., THOMPSON, C.L., CECIL, C., STANTON, R.W., AND CHAO, E., 1979, Arsenic-bearing pyrite in Upper Freeport Coal, Indian County, Pennsylvania: Abs. of papers Ninth International Congress of Carboniferous Stratigraphy and Geology, p. 140.

WARD, C.R., 1978, Mineral matter in Australian bituminous coals: Proceedings Australasian Institute of Mining and Metallurgy, No. 267, p. 7-25.

ZUBOVIC, P., 1966, Physiochemical properties of certain minor elements as controlling factors in their distribution in coal: In Coal Science. Advances in Chemistry Series 55, Chapt. 13.

DETERMINATION OF MINERAL MATTER IN COAL BY TARGET TRANSFORMATION FACTOR ANALYSIS

Bradley A. Roscoe and Philip K. Hopke
Institute for Environmental Studies and
Nuclear Engineering Program
University of Illinois
Urbana, Illinois 61801

ABSTRACT

There is an increasing need to determine the nature of mineral matter in coal. The mineral matter is composed of all inclusions in the coal whether or not they are distinct from the coal. The need for this information is based on the increased use of coal and the problems associated with its use such as boiler tube fouling, air pollution, and coal liquifaction. By utilizing target transformation factor analysis, it is possible to identify the number of mineral phases that may be present in the coal as well as the composition of these mineral phases including major, minor, and trace elements. It is thus possible to determine the mineral phases and reconstruct the minerology of the coal sampled such that general characteristics of the mineral phases can be determined. From this information, insight into the formation of the coal can be obtained and better methods of utilizing the coal can be devised.

INTRODUCTION

With the increased utilization of coal for power production, more emphasis has been placed on the problems associated with coal. Problems such as boiler tube fouling, air pollution, and acid rain are all linked to the mineral matter inclusions in the coal. By learning more about the mineral phases that are present, insight can be gained in how to best approach the solutions to these problems.

Factor analysis is a statistical technique that can be utilized to produce additional information about the mineral matter inclusions in coal. This technique is used to determine the minimum number of variables needed to reproduce the various characteristics of a large set of data. It has been used in the areas of psychological and sociological research (4), mass spectroscopy (7), chemistry (2), and environmental analysis (5).

TARGET TRANSFORMATION FACTOR ANALYSIS

To perform a factor analysis, a set of n coal samples for which the concentration of m elements are known is required. The data set must include at least as many samples as there are representative factors in the data. The more redundant data that is available, the better the factor analysis will be, assuming that the data is reliable.

The approach of the analysis is based on a justifiable assumption that a coal sample is a mixture of materials from a number of independent sources that have relatively constant compositions. Thus, the amount of any given element present in a sample can be expressed as the sum of contributions from each of these sources. For example, the total mass of silicon present in a sample of coal is the sum of the mass of silicon in each independent source present in that sample. Mathematically, the total mass of silicon, M(Si), may be represented as

$$M(Si) = M_1(Si) + M_2(Si) + \ldots + M_k(Si) \quad (1)$$

where $M_k(Si)$ is the mass of silicon present contributed by the k^{th} source. Since each source contributes a total mass of material, F_k, of which only a fraction is silicon, $M_k(Si)$ can be represented by

$$M_k(Si) = a_k(Si)\ F_k \quad (2)$$

where $a_k(Si)$ is the concentration of silicon in the k^{th} source material.

Expanding equation 2 to encompass multiple samples with a number of elements present yields

$$x_{ij} = a_{i1}f_{1j} + a_{i2}f_{2j} + \ldots + a_{ip}f_{pj} \quad (3)$$

where x_{ij} is the concentration of the i^{th} element in the j^{th} sample and p is the number of factors. Each data point, x_{ij}, is represented as the product of a_{ik} and f_{kj}, where a_{ik} is the concentration of the i^{th} element in the k^{th} factor while f_{kj} is the amount of source k in sample j. In matrix notation, equation 3 may be written as

$$X = AF \quad (4)$$

where A is a m × p matrix containing the concentration profiles for each of the p sources and F is a p × n matrix containing the amount that each source contributes to each sample.

The goals of factor analysis are threefold: 1) to determine p, the number of factors needed to correctly reproduce the data, 2) to determine A, the elemental source profiles of the factors that reproduce the data, and 3) to determine F, the contribution of each source to each sample. A detailed description of factor analysis may be found in Hopke, Lamb, and Natusch (5),

Alpert and Hopke (1), and Malinowski (6).

DATA

Coal data reported by the Illinois State Geological Survey in their Circular 499 was utilized for this study (3). Circular 499 reports data for 60 elements on 172 separate coal samples from the major coal producing states with the majority of the data being from the Illinois area. For this study, Herrin (No. 6) coal was selected from this data file since there was an abundance of data on the coal from this seam. Since several specific elements had missing values for a large fraction of the samples, these elements were deleted from the analysis. Some samples that were missing many elements were also deleted. Zinc and oxygen were deleted since their uncertainties were very high. Data for carbon was also deleted since it was found to confuse the analysis. Sulfur values in the data are divided into 3 groups: pyritic sulfur, sulfate sulfur, and organic sulfur. Thus, the data analyzed consisted of 40 samples and 31 observations per sample.

PROCEDURE AND RESULTS

The first step of factor analysis is to determine the number of independent factors required to reproduce the data. Since this step can be difficult, several tests were used to ascertain the number of factors required. The tests used include the eigenvalue, chi-square, and exner function tests whose descriptions can be found in the literature (1,5). As can be seen in Table I, there is a large decrease in the magnitude of the eigenvalues after 6 factors. In addition, a large decrease in the chi-square and exner tests was observed at 6 factors. Thus the analysis was approached on the basis of 6 factors being required to reproduce the data.

As has been described in other reports (1,5), the analysis does not directly provide factors that can be associated with physically real mineral phases. In order to determine the mineral phases present and their compositions, a target transformation rotation (1,5,6) was employed. In this procedure, suggested composition vectors are tested by rotating a factor axis toward the test vector by the method of least-squares. By this process, elemental profiles representing specific mineral phases can be found that are good representations of the factors in the system. Thus, suspected sources may be either kept or eliminated from further consideration. The sources tested included minerals that are normally found in coal including galina, pyrite, calcite, iron sulfate, siderite, barite, sphalerite, quartz, gypsum, and various clays. In addition, each element was tested to see if it was present as a unique source. The sources that were found to fit the data were

refined such that they fit the data better by replacing the original test vector value with the predictions obtained from the rotated factor. In this manner, the distributions of the minor and trace elements become evident in the source profiles. The concentrations found by the target transformation may not be the absolute concentration of the elements in the mineral phases. For this reason, scaling factors were calculated using a multiple regression analysis to ensure that all the mineral matter is taken into account (5).

Utilizing target transformation, six sources were found that fit together to reproduce the data: organic fraction, organic sulfur, alumino-silicate, calcite, pyrite and miscellaneous iron. The refined and scaled source profiles are given in Table II. From these vectors and the original data, the mass contribution of each source to each sample can be calculated as shown in Table III. Table IV summarizes the total calculated mass after scaling of each sample and the error associated with it. The source contributions to the average sample may be seen in figure 1.

The organic fraction source obtained by TTFA is indicative of bituminous coal. Bituminous coal has an average composition of 84.2% carbon, 8.7% oxygen, 5.6% hydrogen, and 1.5% nitrogen which is consistant with the results obtained by the factor analysis even though data for carbon and oxygen were omitted from the analysis. Because of the large variance in the organic sulfur values, organic sulfur was treated as a unique factor, even though it is in the organic fraction.

Circular 499 reports organic affinity of certain elements as determined by washability tests. According to the results of these tests, beryllium and antimony have a high organic affinity and manganese, arsenic, molybdenum, and iron have high inorganic affinity. The factor analysis reproduces these results for the elements of high inorganic affinity. However, the factor analysis did not reproduce the organic affinity of beryllium and antimony. Antimony was divided among the inorganic sources and was not found in the organic fraction. Beryllium, while having higher concentrations in the inorganic sources, had its largest mass contribution from the organic fraction due to the large relative abundance of the organic fraction in the sample.

The sources attributable to the inorganic fraction, alumino-silicate, calcite, pyrite, and miscellaneous iron, gave reasonable results. As shown in Table II, the sum of the concentrations for a single source is less than 100%. A large portion of the undetermined fraction of each source can be attributed to oxygen present as oxides. Since the inorganic sources are deposited in a carbon matrix, it is assumed that the rest of the undetermined fraction of each source is carbon. This is justified in that during the formation of coal, the nucleation and growth of the inorganic minerals would entrap other minerals in their crystal structure. During crystalization of a mineral phase, certain

elements may be either enriched or depleted in a localized area depending on the solubility of the matter present. For this reason, it is not surprising that the factor analysis produced varying concentrations of aluminum and silicon in the sources other than the alumino-silicate. This is evident by the silicon to aluminum ratios in the inorganic factors: 1.0 for calcite, 3.3 for alumino-silicate, and 6.2 for pyrite.

A major point of interest is how the minor and trace elements are distributed in the different mineral phases. Several of the metals were only contributed from the inorganic sources. These elements include titanium, vanadium, magnesium, chromium, molybdenum, lead, arsenic, selenium, and antimony. On the other hand, phosphorus was only contributed by the organic fraction. Chlorine was contributed primarily by the organic fraction but had a minor contribution from the miscellaneous iron source, probably in the form of an iron chloride ($FeCl_2$ or $FeCl_3$). Most of the arsenic present was contributed by the pyrite and miscellaneous iron sources implying some relationship between iron and arsenic. It is evident from the results that each source has its own distinct source profile of minor and trace elements.

CONCLUSIONS

This study has shown that factor analysis may be a useful approach to the determination of mineral matter in coal. The results produced in this study show that the total mass of a source can be accounted for, even with 80% of the sample mass not included in the raw data. The ability of factor analysis to resolve mineral source contributions of a whole coal sample is an encouraging accomplishment in factor analysis. The benefits of TTFA are enhanced by its ability to resolve minor and trace elements without previous knowledge of their distribution.

REFERENCES

1. Alpert, D.J., and Hopke, P.K., "A Quantitative Determination of Sources in Boston Urban Aerosol", Atmospheric Environment, (in press).

2. Duewer, D.L., and Kowalski, B.R., Anal. Chem., 48, 2002-2010, 1976.

3. Gluskoter, H.J., Ruch, R.R., Miller, W.G., Cahill, R.A., Dreher, G.B., and Kuhn, J.K., Trace Elements in Coal: Occurance and Distribution, Illinois State Geological Survey, no. 499, 1977.

4. Harman, H.H., Modern Factor Analysis, University of Chicago Press, Chicago, 1976.

5. Hopke, P.K., Lamb, R.E., and Natusch, D.F.S., Environmental Science and Technology, 1977.

6. Malinowski, E.R., and McCue, M., Analytical Chemistry, 49, 284-287, 1977.

7. Rozett, R.W., and Petersen, E.M., American Laboratory, 107-116, February 1977.

TABLE I
Reproduction Summary

Factors	Eigenvalue	Chi-square	Exner	% Error
1	38.540	1.460	.213	71.0
2	.730	.730	.151	63.2
3	.258	.472	.121	59.7
4	.156	.316	.099	61.9
5	.137	.179	.075	60.8
6	.113	.066	.045	51.6
7	.029	.037	.034	49.5
8	.020	.017	.023	44.9
9	.011	.006	.014	40.0
10	.005	.001	.006	31.4

TABLE II
Refined Source Profiles
(percent)

Element	Organic Fraction	Alumino-silicate	Calcite	Organic Sulfur	Misc. Iron	Pyrite
Aluminum	.633	6.65	6.48	0.	0.	1.17
Bromine	.00181	0.	.00749	0.	.00127	0.
Calcium	0.	0.	53.5	0.	0.	0.
Chlorine	.218	0.	0.	0.	.51	0.
Iron	0.	0.	0.	0.	18.4	23.1
Phosphorus	.00583	0.	0.	0.	0.	0.
Potassium	.123	.758	0.	0.	.192	.265
Silicon	0.	21.9	6.48	0.	2.67	7.31
Titanium	0.	.429	.293	0.	.190	.2201
Vanadium	0.	.0226	.0265	0.	.00543	.0102
Magnesium	0.	.346	.125	0.	.0947	.209
Manganese	0.	.0324	.243	0.	.0255	.0378
Sodium	.0636	.255	0.	0.	.392	0.
Copper	.00102	.00244	.00558	0.	.00412	.00226
Cobalt	.00077	0.	.00366	0.	.00207	0.
Nickel	.00098	.0133	.0168	0.	.00213	0.
Beryllium	.00017	0.	.00127	0.	.00093	.00026
Chromium	0.	.0121	0.	0.	.00876	.00342
Molybdenum	0.	.00152	.00271	0.	0.	.00664
Lead	0.	0.	.0355	0.	.0405	.0220
Arsenic	0.	.00080	.00350	0.	.0131	.00563
Gallium	.00026	.00012	.00091	0.	.00113	.00030
Mercury	.00002	0.	.00017	0.	.00005	.00008
Selenium	0.	.00174	.00093	0.	0.	.00045
Fluorine	.00119	.0446	0.	0.	0.	.0146
Antimony	0.	0.	.00327	0.	.00178	.00055
Hydrogen	6.20	0.	0.	0.	0.	0.
Nitrogen	1.61	0.	0.	0.	0.	0.
Organic S	0.	0.	0.	95.8	0.	0.
Pyritic S	0.	0.	0.	0.	0.	25.8
Sulfate S	0.	0.	0.	0.	4.39	0.
Total	8.9	30.5	67.3	95.8	26.9	58.2

TABLE III
Average Elemental Concentrations
(ppm)

Element	Organic Fraction	Alumino-Silicate	Calcite	Organic Sulfur	Misc. Iron	Pyrite	Average Predicted	Average Observed	Average % Error
Aluminum	4990.	6180.	924.	0.	0.	757.	12900.	13200.	7.
Bromine	14.3	0.	1.07	0.	0.21	0.	15.5	15.0	64.
Calcium	0.	0.	7630.	0.	0.	0.	7630.	7630.	5.
Chlorine	1720.	0.	0.	0.	83.1	0.	1800.	1710.	315.
Iron	0.	0.	0.	0.	2990.	15200.	18200.	18100.	1.
Phosphorus	46.0	0.	0.	0.	0.	0.	46.0	45.8	169.
Potassium	969.	704.	0.	0.	31.2	174.	1980.	1690.	16.
Silicon	0.	20310.	924.	0.	435.	4790.	26500.	26300.	1.
Titanium	0.	399.	41.8	0.	30.9	144.	616.	680.	17.
Vanadium	0.	21.0	3.78	0.	0.89	5.71	32.4	32.4	24.
Magnesium	0.	321.	17.8	0.	15.4	137.	491.	500.	21.
Manganese	0.	30.1	34.7	0.	4.16	24.7	93.6	52.0	139.
Sodium	502.	237.	0.	0.	63.8	0.	802.	662.	130.
Copper	8.01	2.27	0.80	0.	0.57	1.48	13.2	13.0	24.
Cobalt	6.03	0.	0.52	0.	0.34	0.	6.89	5.60	54.
Nickel	7.72	12.4	2.39	0.	0.35	0.	22.8	22.0	35.
Beryllium	1.31	0.	0.13	0.	0.15	0.17	1.81	1.49	56.
Chromium	0.	11.2	0.	0.	1.43	2.24	14.9	19.5	51.
Molybdenum	0.	1.41	0.39	0.	0.	4.35	6.15	8.96	95.
Lead	0.	0.	5.07	0.	6.61	14.5	26.1	25.1	243.
Arsenic	0.	0.74	0.50	0.	2.15	3.69	7.08	6.08	142.
Gallium	2.04	0.12	0.13	0.	0.18	0.20	2.67	3.11	25.
Mercury	0.13	0.	0.02	0.	0.01	0.05	0.21	0.17	66.
Selenium	0.	1.62	0.13	0.	0.	0.29	2.04	2.15	33.
Fluorine	9.34	41.4	0.	0.	0.	9.56	60.3	63.	22.
Antimony	0.	0.	0.47	0.	0.29	0.36	1.12	0.95	184.
Hydrogen	48900.	0.	0.	0.	0.	0.	48900.	48800.	1.
Nitrogen	12700.	0.	0.	0.	0.	0.	12700.	13000.	14.
Organic S	0.	0.	0.	16300.	0.	0.	16300.	16300.	3.
Pyritic S	0.	0.	0.	0.	0.	16900.	16900.	16900.	2.
Sulfate S	0.	0.	0.	0.	714.	0.	715.	871.	248.
								Average:	71.

TABLE IV
Error in Predicted Sample Mass

Sample	Masses Act.	Masses Pred.	% Error	Sample	Masses Act.	Masses Pred.	% Error
Coal-12831	100.0	100.3	.3	Coal-15717	100.0	99.5	-.5
Coal-12942	100.0	103.8	3.8	Coal-15791	100.0	100.7	.7
Coal-13324	100.0	95.9	-4.1	Coal-15868	100.0	94.9	-5.1
Coal-13433	100.0	96.1	-3.9	Coal-15872	100.0	97.1	-2.9
Coal-13464	100.0	98.2	-1.8	Coal-15999	100.0	95.7	-4.3
Coal-13895	100.0	101.0	1.0	Coal-16030	100.0	98.5	-1.5
Coal-13975	100.0	103.6	3.6	Coal-16139	100.0	96.0	-4.0
Coal-14574	100.0	106.0	6.0	Coal-16265	100.0	100.3	.3
Coal-14613	100.0	104.8	4.8	Coal-16317	100.0	94.7	-5.3
Coal-14630	100.0	94.6	-5.4	Coal-16501	100.0	105.0	5.0
Coal-14684	100.0	101.0	1.0	Coal-16543	100.0	102.7	2.7
Coal-14721	100.0	92.3	-7.7	Coal-16741	100.0	98.3	-1.7
Coal-14970	100.0	94.1	-5.9	Coal-16993	100.0	95.9	-4.1
Coal-14982	100.0	99.7	-.3	Coal-17016	100.0	100.7	.7
Coal-15038	100.0	100.1	.1	Coal-17279	100.0	107.4	7.4
Coal-15117	100.0	99.7	-.3	Coal-18044	100.0	103.9	3.9
Coal-15231	100.0	103.5	3.5	Coal-18320	100.0	106.5	6.5
Coal-15432	100.0	97.7	-2.4	Coal-18368	100.0	96.3	-3.7
Coal-15436	100.0	101.5	1.5	Coal-18493	100.0	99.0	-1.1
Coal-15456	100.0	97.1	-2.9	Coal-18560	100.0	93.7	-6.3

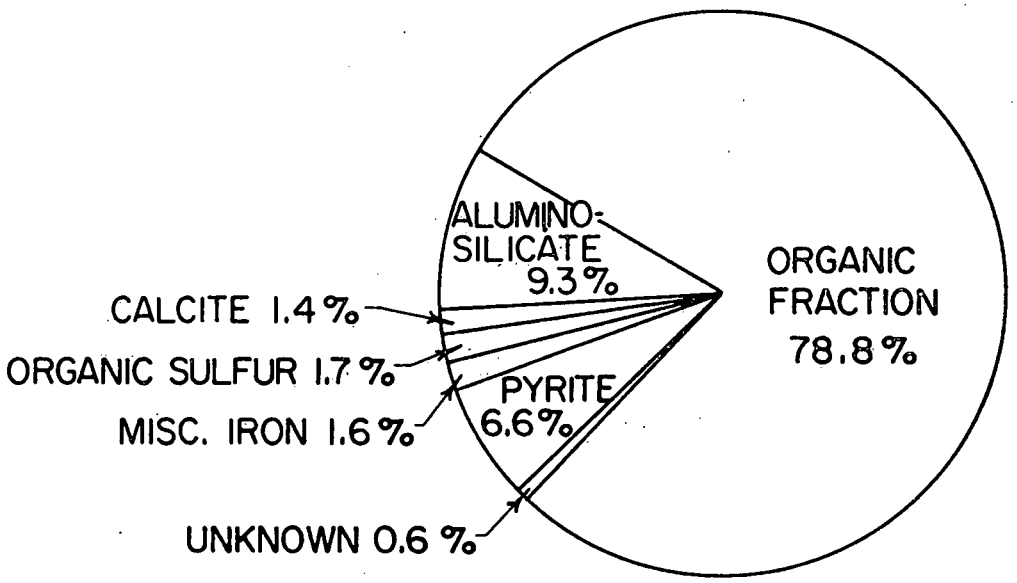


Figure 1: Source contribution to the average Herrin #6 coal sample.

TABLE I
Reproduction Summary

Factors	Eigenvalue	Chi-square	Exner	% Error
1	38.540	1.460	.213	71.0
2	.730	.730	.151	63.2
3	.258	.472	.121	59.7
4	.156	.316	.099	61.9
5	.137	.179	.075	60.8
6	.113	.066	.045	51.6
7	.029	.037	.034	49.5
8	.020	.017	.023	44.9
9	.011	.006	.014	40.0
10	.005	.001	.006	31.4

TABLE II
Refined Source Profiles
(percent)

Element	Organic Fraction	Alumino-silicate	Calcite	Organic Sulfur	Misc. Iron	Pyrite
Aluminum	.633	6.65	6.48	0.	0.	1.17
Bromine	.00181	0.	.00749	0.	.00127	0.
Calcium	0.	0.	53.5	0.	0.	0.
Chlorine	.218	0.	0.	0.	.51	0.
Iron	0.	0.	0.	0.	18.4	23.1
Phosphorus	.00583	0.	0.	0.	0.	0.
Potassium	.123	.758	0.	0.	.192	.265
Silicon	0.	21.9	6.48	0.	2.67	7.31
Titanium	0.	.429	.293	0.	.190	.2201
Vanadium	0.	.0226	.0265	0.	.00543	.0102
Magnesium	0.	.346	.125	0.	.0947	.209
Manganese	0.	.0324	.243	0.	.0255	.0378
Sodium	.0636	.255	0.	0.	.392	0.
Copper	.00102	.00244	.00558	0.	.00412	.00226
Cobalt	.00077	0.	.00366	0.	.00207	0.
Nickel	.00098	.0133	.0168	0.	.00213	0.
Beryllium	.00017	0.	.00127	0.	.00093	.00026
Chromium	0.	.0121	0.	0.	.00876	.00342
Molybdenum	0.	.00152	.00271	0.	0.	.00664
Lead	0.	0.	.0355	0.	.0405	.0220
Arsenic	0.	.00080	.00350	0.	.0131	.00563
Gallium	.00026	.00012	.00091	0.	.00113	.00030
Mercury	.00002	0.	.00017	0.	.00005	.00008
Selenium	0.	.00174	.00093	0.	0.	.00045
Fluorine	.00119	.0446	0.	0.	0.	.0146
Antimony	0.	0.	.00327	0.	.00178	.00055
Hydrogen	6.20	0.	0.	0.	0.	0.
Nitrogen	1.61	0.	0.	0.	0.	0.
Organic S	0.	0.	0.	95.8	0.	0.
Pyritic S	0.	0.	0.	0.	0.	25.8
Sulfate S	0.	0.	0.	0.	4.39	0.
Total	8.9	30.5	67.3	95.8	26.9	58.2

TABLE III
Average Elemental Concentrations
(ppm)

Element	Organic Fraction	Alumino-Silicate	Calcite	Organic Sulfur	Misc. Iron	Pyrite	Average Predicted	Average Observed	Average % Error
Aluminum	4990.	6180.	924.	0.	0.	767.	12900.	13200.	7.
Bromine	14.3	0.	1.07	0.	0.21	0.	15.5	15.0	64.
Calcium	0.	0.	7630.	0.	0.	0.	7630.	7630.	5.
Chlorine	1720.	0.	0.	0.	83.1	0.	1800.	1710.	315.
Iron	0.	0.	0.	0.	2990.	15200.	18200.	18100.	1.
Phosphorus	46.0	0.	0.	0.	0.	0.	46.0	45.8	169.
Potassium	969.	704.	0.	0.	31.2	174.	1880.	1690.	16.
Silicon	0.	20310.	924.	0.	435.	4790.	26500.	26300.	1.
Titanium	0.	399.	41.8	0.	30.9	144.	616.	680.	17.
Vanadium	0.	21.0	3.78	0.	0.89	6.71	32.4	32.4	24.
Magnesium	0.	321.	17.8	0.	15.4	137.	491.	500.	21.
Manganese	0.	30.1	34.7	0.	4.16	24.7	93.6	52.0	139.
Sodium	502.	237.	0.	0.	63.8	0.	802.	662.	130.
Copper	8.01	2.27	0.80	0.	0.67	1.48	13.2	13.0	24.
Cobalt	6.03	0.	0.52	0.	0.34	0.	6.89	6.60	54.
Nickel	7.72	12.4	2.39	0.	0.35	0.	22.8	22.0	35.
Beryllium	1.31	0.	0.18	0.	0.15	0.17	1.81	1.49	56.
Chromium	0.	11.2	0.	0.	1.43	2.24	14.9	19.5	51.
Molybdenum	0.	1.41	0.39	0.	0.	4.35	6.15	8.96	95.
Lead	0.	0.	5.07	0.	6.61	14.5	26.1	25.1	243.
Arsenic	0.	0.74	0.50	0.	2.15	3.69	7.08	6.08	142.
Gallium	2.04	0.12	0.13	0.	0.18	0.20	2.67	3.11	25.
Mercury	0.13	0.	0.02	0.	0.01	0.05	0.21	0.17	66.
Selenium	0.	1.62	0.13	0.	0.	0.29	2.04	2.15	33.
Fluorine	9.34	41.4	0.	0.	0.	9.56	60.3	63.	22.
Antimony	0.	0.	0.47	0.	0.29	0.36	1.12	0.95	184.
Hydrogen	48900.	0.	0.	0.	0.	0.	48900.	48800.	1.
Nitrogen	12700.	0.	0.	0.	0.	0.	12700.	13000.	14.
Organic S	0.	0.	0.	16300.	0.	0.	16300.	16300.	3.
Pyritic s	0.	0.	0.	0.	0.	16900.	16900.	16900.	2.
Sulfate S	0.	0.	0.	0.	714.	0.	715.	871.	248.
								Average:	71.

TABLE IV
Error in Predicted Sample Mass

Sample	Masses Act.	Masses Pred.	% Error	Sample	Masses Act.	Masses Pred.	% Error
Coal-12831	100.0	100.3	.3	Coal-15717	100.0	99.5	-.5
Coal-12942	100.0	103.8	3.8	Coal-15791	100.0	100.7	.7
Coal-13324	100.0	95.9	-4.1	Coal-15868	100.0	94.9	-5.1
Coal-13433	100.0	96.1	-3.9	Coal-15872	100.0	97.1	-2.9
Coal-13464	100.0	98.2	-1.8	Coal-15999	100.0	95.7	-4.3
Coal-13895	100.0	101.0	1.0	Coal-16030	100.0	98.5	-1.5
Coal-13975	100.0	103.6	3.6	Coal-16139	100.0	96.0	-4.0
Coal-14574	100.0	106.0	6.0	Coal-16265	100.0	100.3	.3
Coal-14613	100.0	104.8	4.8	Coal-16317	100.0	94.7	-5.3
Coal-14630	100.0	94.6	-5.4	Coal-16501	100.0	105.0	5.0
Coal-14684	100.0	101.0	1.0	Coal-16543	100.0	102.7	2.7
Coal-14721	100.0	92.3	-7.7	Coal-16741	100.0	98.3	-1.7
Coal-14970	100.0	94.1	-5.9	Coal-16993	100.0	95.9	-4.1
Coal-14982	100.0	99.7	-.3	Coal-17016	100.0	100.7	.7
Coal-15038	100.0	100.1	.1	Coal-17279	100.0	107.4	7.4
Coal-15117	100.0	99.7	-.3	Coal-18044	100.0	103.9	3.9
Coal-15231	100.0	103.5	3.5	Coal-18320	100.0	106.5	6.5
Coal-15432	100.0	97.7	-2.4	Coal-18368	100.0	96.3	-3.7
Coal-15436	100.0	101.5	1.5	Coal-18493	100.0	99.0	-1.1
Coal-15456	100.0	97.1	-2.9	Coal-18560	100.0	93.7	-6.3

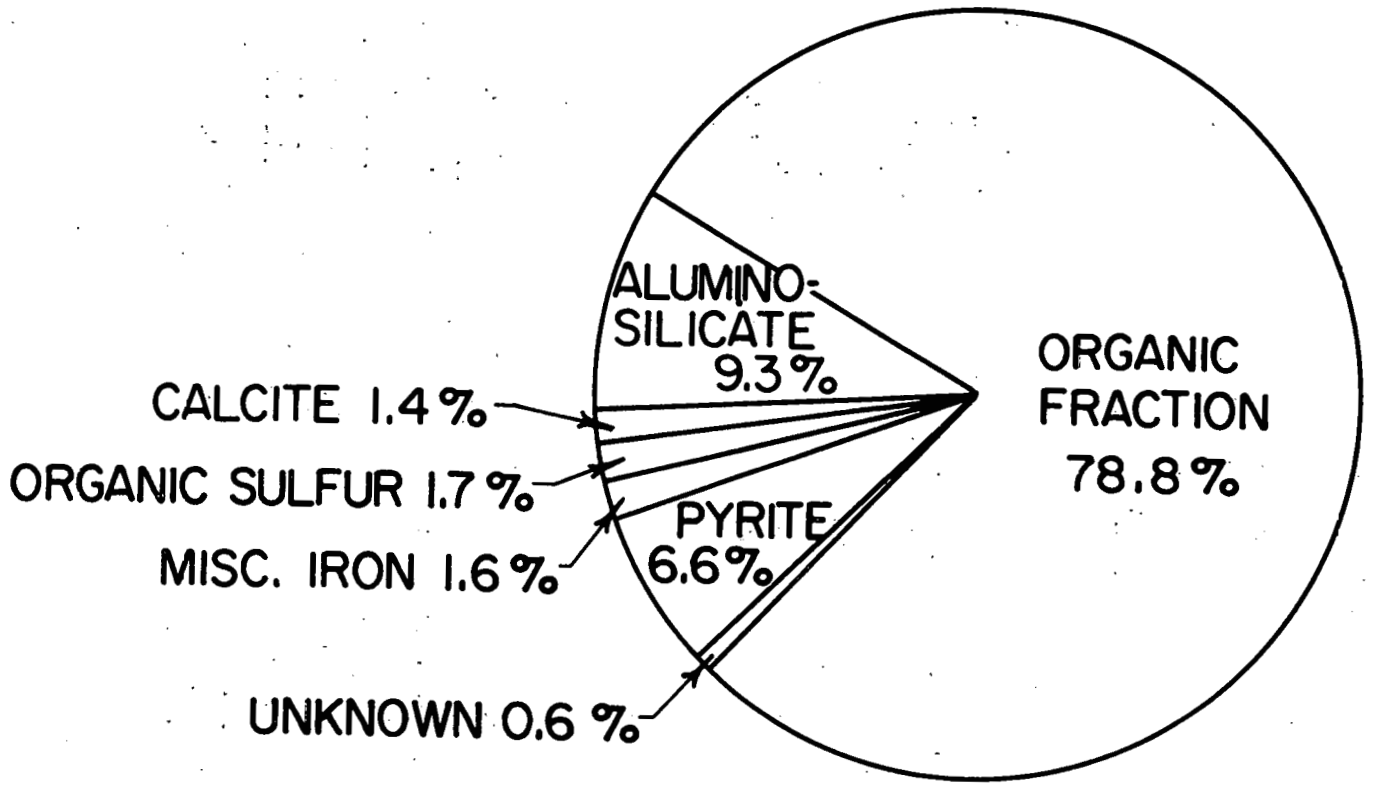


Figure 1: Source contribution to the average Herrin #6 coal sample.

ON-LINE MONITORING OF PLUTONIUM IN MIXED URANIUM-PLUTONIUM SOLUTIONS

K. J. Hofstetter, T. V. Rebagay, and G. A. Huff*

Allied-General Nuclear Services
Post Office Box 847
Barnwell, South Carolina 29812

ABSTRACT

The measurement of the total and isotopic plutonium concentrations in mixed uranium-plutonium solutions blended with highly radioactive fission product nuclides and other radionuclides (e.g., Cs-137 and Co-60) has been investigated at the Barnwell Nuclear Fuel Plant (BNFP). An on-line total and isotopic plutonium monitoring system is being tested for its ability to assay the plutonium abundances in solutions as might be found in the process streams of a light water reactor (LWR) spent fuel processing plant. The monitoring system is fully automated and designed to be maintained remotely. It is capable of near real-time inventory of plutonium in process streams and provides the basis for on-line computerized accounting of special nuclear materials.

INTRODUCTION

Recent concerns over the proliferation of nuclear weapons have stimulated interest in the identification of fuel recycling technologies that offer less proliferation risk than the traditional (conventional) Purex process in which plutonium is separated from uranium and decontaminated from fission products. The coprocessing of plutonium with uranium has been suggested as an alternative. (1, 2, 3) This option is considered to have the advantages of permitting both fuel recycling capabilities and proliferation resistance. A technically feasible coprocessing flowsheet has been proposed which could accomplish these objectives. (4) The incorporation of highly radioactive, gamma-emitting radionuclides into the fuel through incomplete removal of the fission products during reprocessing or by adding spikes to the fuel during fabrication has been suggested as an additional deterrent.

Design concepts (5) for proliferation-resistant fuel alternatives have been developed based on the Barnwell Nuclear Fuel Plant (BNFP) model which was designed for reprocessing light water reactor (LWR) spent fuel using Purex processing technology. Diversion resistance of special

---

*Work supported by the United States Department of Energy, Fuel Cycle Projects Office under Contract No. DE-AC09-78ET-35900.

nuclear materials (uranium and plutonium) can be enhanced by producing a mixed-nitrate coprocessed product that is highly radioactive due to the retention of some fission products. In addition, the coprocessing flowsheet has alternatives for high- and low-fission product decontamination of the mixed nitrates. The low-fission product decontamination alternative is envisioned to increase diversion resistance of the fuel cycle.

This study is focused on the nondestructive assay of plutonium in solutions that might be found in a reprocessing plant using a coprocessing flowsheet. Verification and quantification of plutonium are essential to protect against covert substitution and operating errors as well as for inventory and process control. The nondestructive assay of plutonium is vital to the implementation of a dynamic materials control system, frequently being the only available means for timely measurement of in-process plutonium. Toward this end, an on-line total and isotopic plutonium concentration monitor has been developed and tested for its performance at the BNFP. The on-line monitoring system, which has been previously evaluated in the BNFP laboratory, used highly purified plutonium nitrate solutions of varying concentrations and its performance as a potential safeguard monitoring device has been considered excellent. (6) The present work now addresses the response and operational characteristics of this system to mixed uranium-plutonium solutions in highly radioactive environments. This study may provide a basis for upgrading and improvement of the monitor to accurately measure plutonium in the presence of high radiation fields caused by the incorporation of fission products. The quantitative extent of the effects of this highly radioactive environment on the sensitivity and accuracy of the monitoring system is assessed.

EXPERIMENTAL

The on-line total and isotopic plutonium concentration monitoring system used in this study has been described in detail elsewhere. (7) This system is capable of near real-time inventory of plutonium and could provide the basis for on-line computerized accounting of the plutonium in the process streams of a light water reactor spent fuel reprocessing plant. (8) Briefly, the system includes a high-resolution lithium-drifted germanium detector, a multichannel pulse-height analyzer, a dedicated minicomputer, and the sample cell assembly. The cell is equipped with a 0.02-inch brass absorber to reduce the background contribution of low-energy gamma and X-rays (E <60 keV) and a built-in Cd-109 source for an overall check of the system performance and stability and for energy calibration. The system is fully automated and designed to be maintained remotely.

The feed and product solutions were formulated based on the composition of LWR spent fuel. (9, 10, 11) Natural and enriched uranium (3.5% U-235) were utilized for the uranium component of the blends while plutonium of typical LWR grade isotopic composition was used. The uranium/plutonium ratio (based on elemental content) was varied from 99/1 for feed compositions to 75/25 for product solutions. Control solutions consisting of highly purified uranium nitrate and plutonium nitrate were also prepared for comparison.

Different levels of fission products and spikes were mixed with the simulated uranium/plutonium coprocessing solutions consistent with the levels suggested for enhanced proliferation resistance without affecting

the characteristics of the blends when refabricated as nuclear fuel. The fission products studied were Ru-106/Rh-106, Ce-144/Pr-144, Zr-95/Nb-95, and Ru-103 while the spikes were Co-60 and Cs-137. While Cs-137 is invariably present as a fission product, it is also considered a spike in this study due to its long half-life and availability when compared to the other shorter lived fission products. Table 1 shows the compositions of the blends studied.

Sampling was done by drawing the test solutions into the counting cell of the monitoring system. Since the system was designed for remote control and operation, the radiological safety of the analyst in making the plutonium determinations is assured. Two 1-hour countings of each sample were made and the resulting plutonium values were averaged.

The total and isotopic compositions of plutonium in the different blends were determined by measuring the absolute intensities of the gamma rays characteristics of the Pu-238, Pu-239, and Pu-241 by direct gamma-ray spectroscopy and computer analysis of the spectral data. (12) Plutonium gamma rays in the energy range of 120 to 250 keV were analyzed (129.3 keV peak for Pu-239, 152.7 keV peak for Pu-238, and 148.6 keV peak for Pu-241; the 208.0 keV peak due to U-237 daughter of Pu-241 was also analyzed in the case of "aged" plutonium) while the 185.6 keV gamma line due to U-235 was used for the detection of uranium. To determine the extent of spectral interference of fission products and spikes on the determination of plutonium, the control solutions were analyzed under parallel conditions as the test solutions. Figures 1 through 3 show some representative gamma-ray spectra of the test solutions and control solutions obtained in the energy region of interest.

RESULTS AND DISCUSSION

Coprocessing is technically feasible for any mixture of uranium and plutonium and plays an important role in the development of a proliferation-resistant fuel cycle. The laboratory protocol in this investigation was designed to demonstrate the sensitivity and accuracy of the on-line isotopic concentration monitoring system in measuring plutonium in the presence of high quantities of fission products and other strong gamma-ray emitters. The results of the laboratory experiments were then evaluated to determine its utility as a safeguards and accountability device for a reprocessing plant with a coprocessing flowsheet.

A summary of the data for the response of the monitor to plutonium is presented in Table 2. Included in the table are the plutonium concentrations measured by isotope dilution mass spectrometry and controlled potential coulometry. Two different isotopic batches were studied. The gamma-ray spectra of the test solutions and the control solutions consisting of LWR-grade, highly purified plutonium nitrate and/or uranium nitrate are depicted in Figures 1 through 3.

As can be seen in Figure 1b, the control solution containing plutonium nitrate only (2.08 grams plutonium/liter) has a barely discernible photopeak at 152.7 keV indicating that, at this plutonium concentration, the calculated Pu-238 value would be suspect. It can be concluded that the abundance of Pu-238 in the plutonium nitrate used to formulate the simulated product stream is extremely low. All the other photopeaks (129 keV, 149.6 keV, and 208 keV gamma lines) are well-defined and

sufficiently delineated from the background radiation. Similarly, the 185.6 keV gamma line due to U-235 does not have sufficient intensity (Figure 1) for the quantitative assay of uranium although the uranium nitrate used had been enriched with U-235 (3.5% enrichment). The uranium concentration is in the range calculated for complete fuel dissolution. (11) It is interesting to note that the background radiation of the uranium isotopes appears to have no effect on the general shape of the plutonium spectra at the energy region of interest (120 to 250 keV).

The question posed by denaturing plutonium with fission products or other strong gamma-emitting radionuclides is whether these denaturants improve or hinder the accuracy of the nondestructive assay measurement. Thus, our analyses of the various coprocessing solutions denatured by blending with these selected denaturants are focused on the reliability and accuracy of the monitoring system to measure plutonium only. The extent of spectral interference or enhancement, if any, was evaluated for each denaturant to resolve the problem.

All the fission products (Ru-106/Rh-106, Ru-103, Ce-144/Pr-144, and Zr-95/Nb-95) employed as denaturants appear in every step of the nuclear fuel cycle. Each fission product was of known activity and concentration.* Aliquot portions of these radionuclides were measured quantitatively such that their concentrations lie in the range from 0.1 to 5.0 Ci per gram of fissile material required for proliferation deterrence. (13) The use of nominal amounts of ruthenium and cobalt as denaturants is not expected to adversely affect fuel performance. (14) Ruthenium-106 and Ce-144 are not present in sufficient quantities in spent nuclear fuels to produce the maximum radiation dose rate level required for proliferation deterrence, but they have shown very little effect on the refabrication of the coprocessed solution and its fuel properties. They also exhibit amenability to reprocessing. (13) Although Zr-95/Nb-95 and Ru-103 are not recommended as denaturants due to their short half-lives, they were included to determine if they may cause difficulty in the nondestructive assay of plutonium if present in coprocessing solutions.

In spite of the undesirability of Cs-137 as a spike due to its low retention (low boiling point) during fuel refabrication and corrosive effects, it was also considered because it is invariably present in partially separated uranium-plutonium mixtures. (10) Cobalt-60, a strong gamma-emitter, has been recommended as a suitable denaturant to reduce proliferation risk. Fission products have limited usefulness as denaturants but Ce-144 and Ru-106 together with Co-60 could provide semilethal dose rates for limited diversion. The effect of adding Np-237 to the coprocessing solution was also evaluated for its use as a heat spike in another proposed alternative fuel cycle. (15)

The analytical evalutions of the sensitivity of the detection system to plutonium isotopes in the presence of the selected fission products and/or denaturants are listed in Table 2 and the gamma-ray spectra corresponding to representative cases of the various blends are shown in Figures 1 through 3. All the spectral analyses of Pu-238, Pu-239, and

*Radiochemical Center, Amersham, England.

Pu-241 were conducted in the intermediate energy region (120 to 250 keV) of the plutonium gamma-ray spectra. No similar analysis was done in the higher energy regions for it has been reported that strong gamma-ray emitters used as denaturants could effectively mask the higher energy gamma lines of plutonium (13) rendering the calculated plutonium values meaningless. Further, an earlier investigation, (16) which dealt with the feasibility of determining the isotopic composition of plutonium by gamma-ray spectrometry, revealed that the plutonium photopeaks most seriously affected are those in the 600 to 800 keV region where the intense gamma-rays of Cs-137 and Zr-95 are very close to the Pu-239 photopeaks.

The levels of the background radiations of the test solutions on which the plutonium photopeaks are superimposed are slightly increased, but the general shape of the observed spectra resembles the control spectra (spectra of the solution containing plutonium nitrate only) suggesting that the fission products (except Ce-144) and/or denaturants have no gamma lines or Compton edges (distribution) in the region of analysis. The peak/background ratios differed slightly from the control ratio, but the discrepancies may be attributed in part to counting errors. That the increase in the background radiation did not diminish the sensitivity of the monitor could be deduced from the test peak area/control peak area ratios. The slight enhancements (approximately 10%) of these ratios may be due to other experimental errors in addition to the counting errors. Consequently, no significant loss of accuracy or precision in the plutonium measurements is expected. This is borne by the good agreement of the values obtained by the monitor with those gathered by the chemical methods.

Although it was reported (16) that the 133-keV line of Ce-144 may cause serious interference if present in any quantity, our results indicated that the amount of Ce-144 added to the coprocessing solutions (which is substantial) did not cause any interference in the analysis of the nearby plutonium photopeaks (129.3-keV line of Pu-239 and 148.6-keV line of Pu-241). The closest plutonium photopeak, the 129.3-keV Pu-239 photopeak, is clearly distinct and well separated from the 133-keV Ce-144 photopeak. The integrated absolute intensity of this line was not very different from the absolute intensity of the 129-keV line of the plutonium control solution.

As mentioned earlier, the 152.7-keV photopeak of Pu-238 does not possess sufficient intensity for accurate evaluation in the case of the simulated product solution of the coprocessing technology. However, this photopeak can be resolved without difficulty in the simulated feed solutions (>1.5% plutonium). Hence, the Pu-238 contents of the feed solutions are given.

The investigation showed that at the levels of fission products and/or denaturants added to the uranium-plutonium coprocessing feed and product solutions, no spectral interference could be detected from these proliferation deterrents in the nondestructive direct gamma-ray spectroscopy of plutonium. It clearly demonstrated the usefulness of the on-line isotopic concentration monitor to assay accurately small quantities of plutonium even in highly radioactive environments. This valuation of the system's performance may help in design concepts aimed t determining the detection pattern in plutonium-bearing streams of a reprocessing plant with a coprocessing flowsheet.

REFERENCES

1. Hammelman, J. E., and Nguyen, T. D., "Technical Feasibility Studies of Partial Plutonium-Uranium Separation in Nuclear Fuel Reprocessing," SAI-78-730-WA (1978).

2. Till, C. E., and Chang, Y. I., "Survey of Alternative Fuel Cycle Options Without Plutonium Separations," Trans. America Nuclear Society, 27, 428 (1977).

3. Pobereskin, M.; Kok, K.; and Madia, W. J., "Coprocessing to Ameliorate the Proliferation and Waste Management Problems," Trans. America Nuclear Society, 27, 428 (1977).

4. Hammelman, J. E.; Nguyen, T. D.; and Mostillar, R. D., "Coprocessing: Technical Feasibility and Radioactivity Impacts of Partial Plutonium-Uranium Separation," Trans. American Nuclear Society, 30, 303 (1978).

5. Hall, J. C., "Studies and Research Concerning BNFP: Engineering Evaluations of Alternative for Processing Uranium-Based Fuels," AGNS-35900-4.1-25 (1979).

6. Hofstetter, K. J.; Huff, G. A.; Gunnink, R.; Evans, J. E.; and Prindle, A. L., "On-Line Measurement of Total and Isotopic Plutonium Concentrations by Gamma-Ray Spectrometry," Analytical Chemistry in Nuclear Fuel Reprocessing, W. S. Lyon (ed.), Science Press, Princeton, 1978, pp 266-274.

7. Gunnink, R.; Prindle, A. L.; Niday, J. B.; Van Lehn, A. L.; and O-Brien, D. W., Operations Manual for the TASTEX Gamma Spectrometer System, Tokai Advanced Safeguards Technology Exercise, Lawrence Livermore Lab, M-106 (ISPO-67), March 13, 1979.

8. Hofstetter, K. J.; Rebagay, T. V.; and Huff, G. A., "Studies and Research Concerning BNFP: Plutonium Measurement Systems Using the On-Line Isotopic Concentration Monitor," Allied-General Nuclear Services, AGNS-35900-2.4-58 (1979).

9. Pobereskin, M.; O'Hara, F. A.; Madia, W. J.; Zeilenback, W. J.; and Yates, K. R., "Evaluation of Coprocessing as an Alternative Fuel Cycle," American Nuclear Society Education Division, American Nuclear Society Annual Meeting, San Diego, California, June 21, 1978, p 10.

10. Denatured Plutonium: A Study of Deterrent Action, Electric Power Research Institute, EPRI 310, Final Report, July 1975.

11. Alternate Fuel Cycle Technologies, Composite Quarterly Report, April-June 1977, Savannah River Lab, DPST-AFCT-77-2-2.

12. Gunnink, R., and Evans, J. E., "In-Line Measurement of Total and Isotopic Plutonium Concentrations by Gamma-Ray Spectrometry," Lawrence Livermore Laboratory, UCRL-52220 (1977).

13. Weinstock, E. V., "The Spiking of Special Nuclear Materials as a Safeguards Measure," Brookhaven National Lab, September 19, 1975.

14. Selle, J. E.; Angelini, P.; Rainey, R. H.; Federer, J. I.; and Olsen, A. R., "Practical Considerations of Nuclear Fuel Spiking for Proliferation Deterrence," ORNL/TM-6483, October 1978.

15. Waltz, W. R., and Godfrey, W. L., "Fuel Cycle Utilizing Pu-238 as a Heat Spike," Allied-General Nuclear Services, AGNS-35900-3.1-5 (1979).

16. Banham, M. F., "The Determination of the Isotopic Composition of Plutonium by Gamma-Ray Spectrometry," United Kingdom Atomic Energy Authority, AERE-R-8737, June 1977.

TABLE 1

COMPOSITIONS OF FEED AND PRODUCT SOLUTIONS
IN URANIUM-PLUTONIUM COPROCESSING OF LWR FUEL

Materials	Feed		Product	
	A	B	A	B
Pu (g/L)	4.4	2.08	50.0	1.04
U (g/L)	393.3	192.0	139.3	64.0
Np (g/L)	0.54	0.54	0.18	0.18
Cs-137 (mCi/L)	0.829	0.37	0.64	0.64
Co-60 (mCi/L)	0.176	0.146	0.878	0.878
Ru-106/Rh-106 (mCi/L)	3.53	0.88	0.011	0.011
Ce-144/Pr-144 (mCi/L)	4.03	1.08	2.93	2.93
HNO_3, M	3	3	0.3	0.3
Uranium/Plutonium,* Approximate	99:1	99:1	75:25	98:2

*Based on total metal content.

TABLE 2

PLUTONIUM ABUNDANCES IN
URANIUM-PLUTONIUM COPROCESSING SOLUTIONS

Sample	Total Plutonium, g/l		
	Method of Analysis		
	This Work	Mass Spectrometry	Dilution**
1. Product Control (aged)	0.99	1.401	1.50
2. Product Solution + Ru-106	0.94	0.951	0.87
3. Product Solution + Co-60	1.10	0.982	0.87
4. Product Solution + Np-237	0.90	1.157	1.02
5. Product Solution + Ce-144	1.06	1.132	1.02
6. Product Solution + Cs-137	1.00	0.971	0.87
7. Composite (aged)	1.21	1.959	1.67
8. Product Solution	0.93	1.145	1.04
9. Product Solution + Ce-144	1.04	1.089	0.93
10. Product Control + Ce-144	1.14	1.178	0.98
11. Feed Solution + Ce-144	1.27	2.787	3.00
12. Feed Solution + Ru-106	1.20	1.990	1.73
13. Feed Solution (aged)*	--	4.191	4.41
14. Feed Solution (aged)*	--	3.940	4.28
15. Feed Solution + Ce-144	1.08	1.596	1.58
16. Feed Control + Ce-144	1.09	1.286	1.73

*Solutions used for calibration.

**Stock solutions analyzed by controlled potential coulometry.

TABLE 3

THE EFFECTS OF DENATURIZATION ON THE RESPONSE OF THE ON-LINE MONITORING SYSTEM TO PLUTONIUM

	Plutonium Photopeaks Analyzer*							
	Pu-239 (129 keV)		Pu-238 (152 keV)		Pu-241 (148 keV)		Pu-241-U-237 (208 keV)	
Solutions	S/B	S/C	S/B	S/C	S/B	S/C	S/B	S/C
	Feed Solution (2.08 g/L Pu)							
Feed Only	3.56		2.06		3.80		16.26	
Feed + Np-237	2.88	1.08	1.37	0.81	3.38	1.18	14.0	1.01
Feed + Co-60	2.18	1.11	1.28	1.08	2.94	1.05	12.2	0.94
Feed + Co-137	2.48	0.99	1.54	0.87	3.99	0.98	17.9	1.07
Feed + Ru-106	2.76	1.08	1.62	0.87	4.47	0.98	15.4	1.03
Feed + Ce-144	2.85	1.11	1.64	1.08	4.63	0.92	17.3	0.97
Composite	2.13	0.96	1.30	1.08	4.22	1.11	16.5	1.04
	Product Solution (1.04 g/L Pu)							
Product Only	2.95		1.42		3.59		16.9	
Product + Np-237	2.83	1.05	1.78	1.44	2.90	1.02	14.4	1.04
Product + Co-60	2.66	1.07	1.59	1.00	3.35	1.00	13.8	1.11
Product + Cs-137	2.10	1.04	1.40	0.57	2.25	1.00	4.05	0.98
Product + Ru-106	2.68	1.04	1.38	0.30	3.43	1.00	15.4	1.06
Product + Ce-144	2.09	1.02	1.49	0.98	2.72	1.13	8.36	1.06
Composite	2.14	1.14	1.18	1.17	3.25	1.23	14.3	1.24

*S/B represents the ratio of the sample peak counts to the background counts, and S/C is the ratio of the integrated area of the sample photopeak to the integrated area of the control.

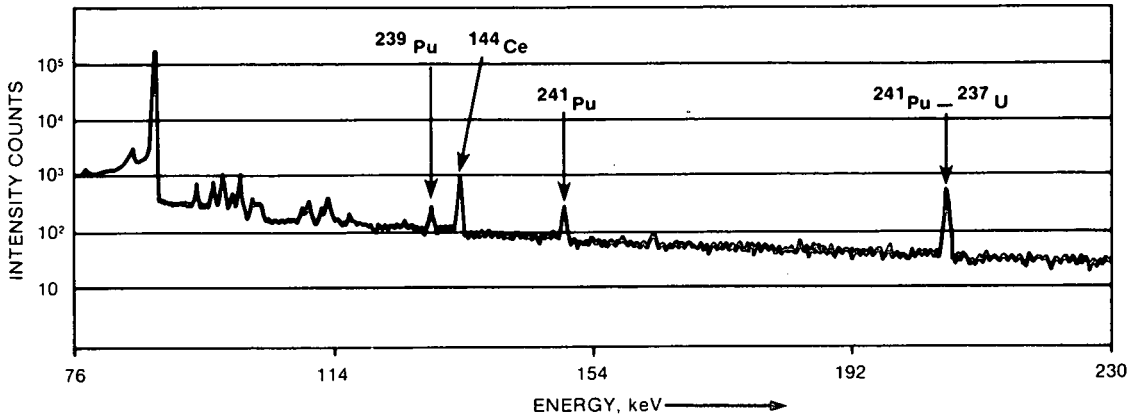


Figure 1A
Feed Solution

Solution Composition: Freshly Separated Pu, enriched natural uranium, Np-237, Cs-137, Ru-103, Ru-106/Rh-106, Ce-144/Pr-144, Co-60, and Zr-95/Nb-95 in 3M HNO_3

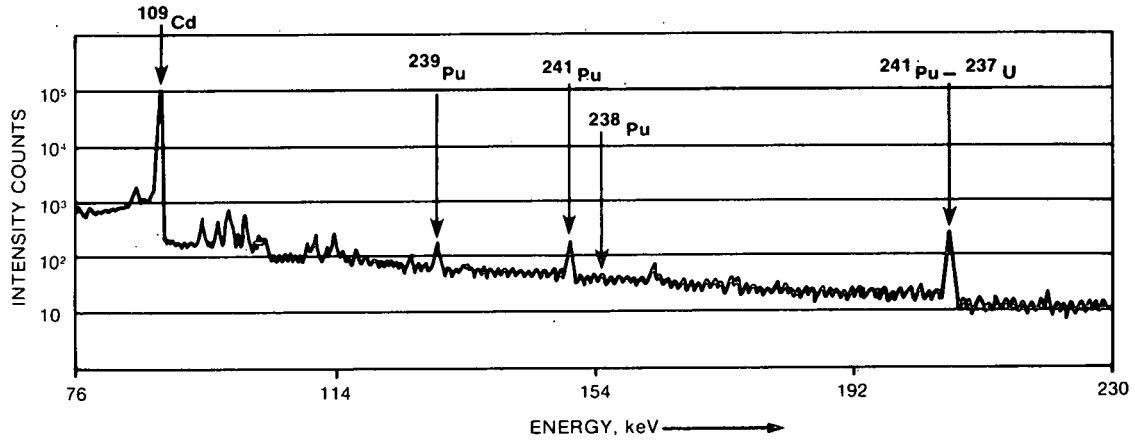


Figure 1B
Feed Control Solution

Solution Composition: Freshly Separated Pu (2.08 g/L) in 3M HNO_3

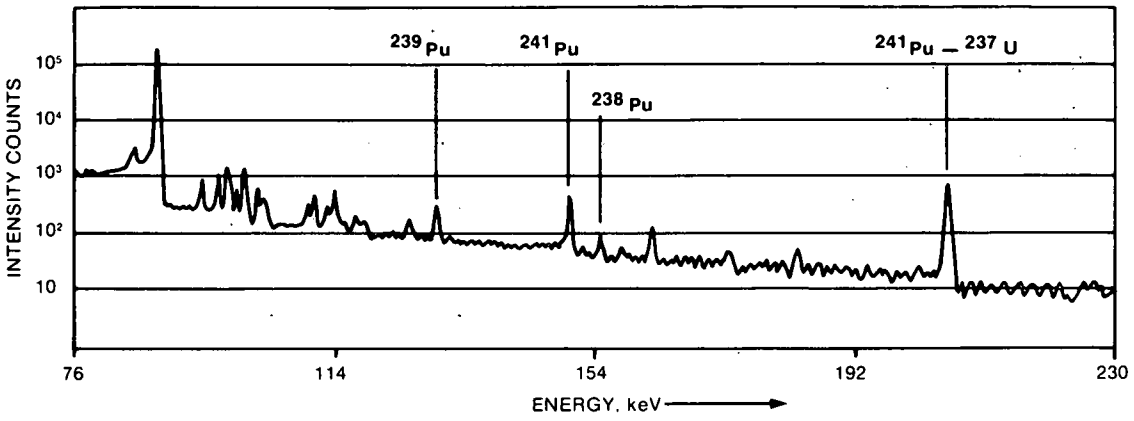


Figure 2A
Plutonium Control Solution (1% Pu, No U)

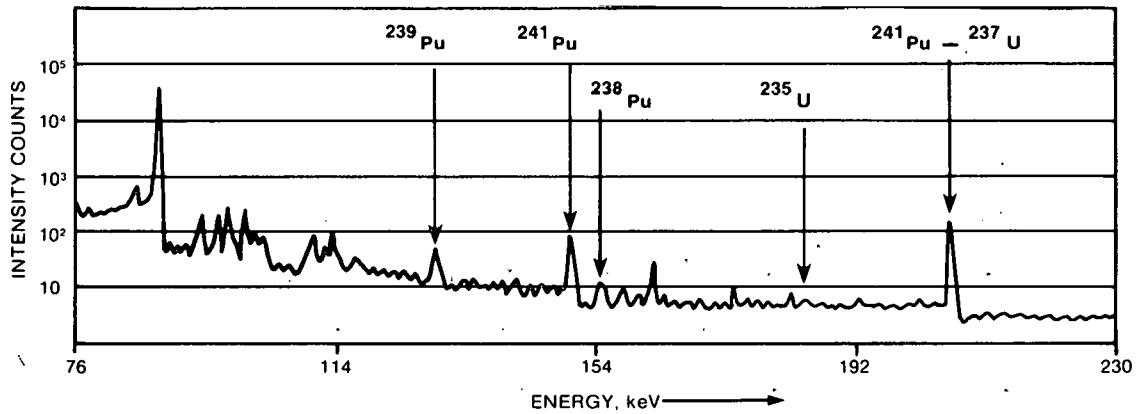


Figure 2B
Uranium (99%) - Plutonium (1%) Solution

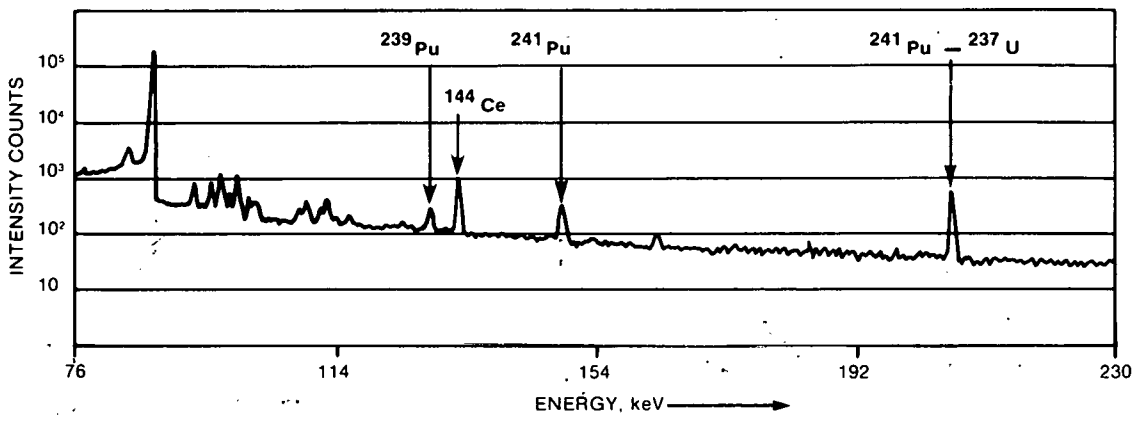


Figure 2C
Feed Solution

Solution Composition: "Aged" Pu (3.0 g/L), natural U, Np-237, Co-60, Cs-137, Ce-144/Pr-144, Ru-103, Ru-106/Rh-106, Zr-95/Nb-95

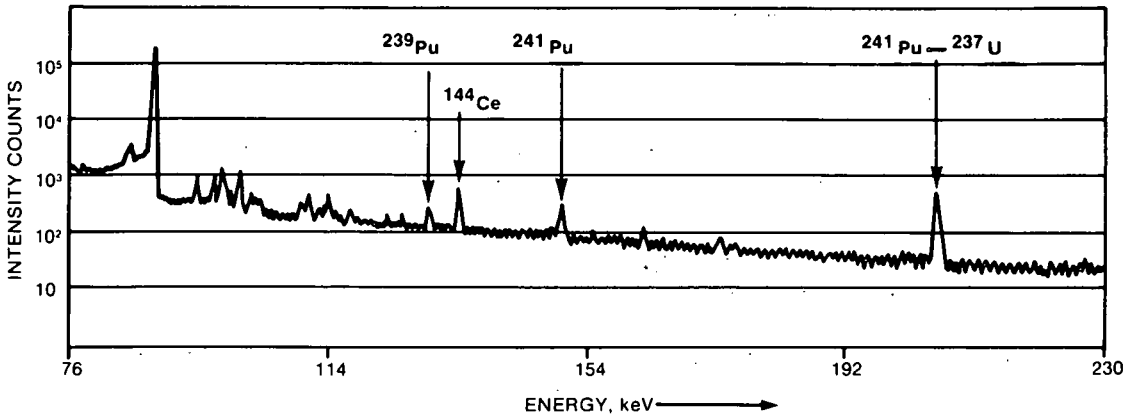


Figure 3A
Control Solution with Denaturants

Solution Composition: Pu (1.0 g/L), Np-237, Co-60, Cs-137, Ru-103, Ru-106/Rh-106, Zr-95/Nb-95, in 3M HNO_3 - no uranium added.

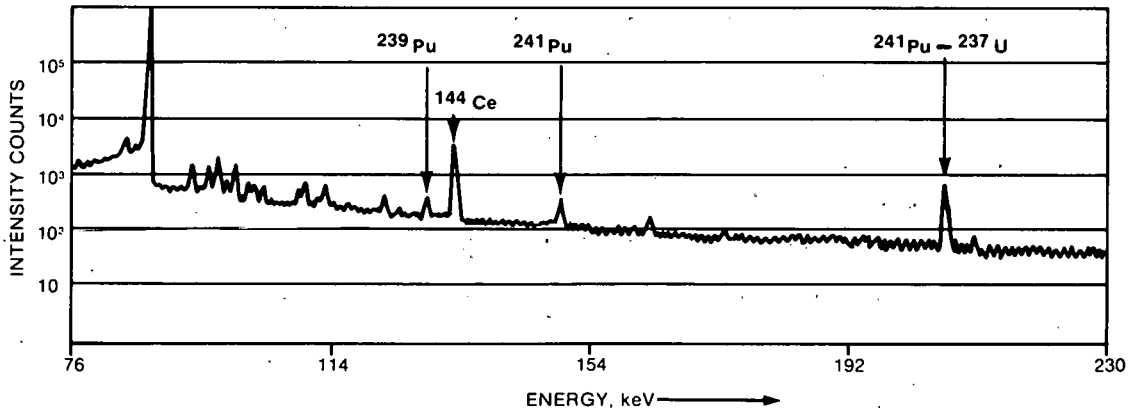


Figure 3B
Product Solution

Solution Composition: Pu (1.0 g/L), U(64 g/L), Np-237, Co-60, Cs-137, Ru-103, Ru-106/Rh-106, Zr-95/Nb-95, in 3M HNO_3

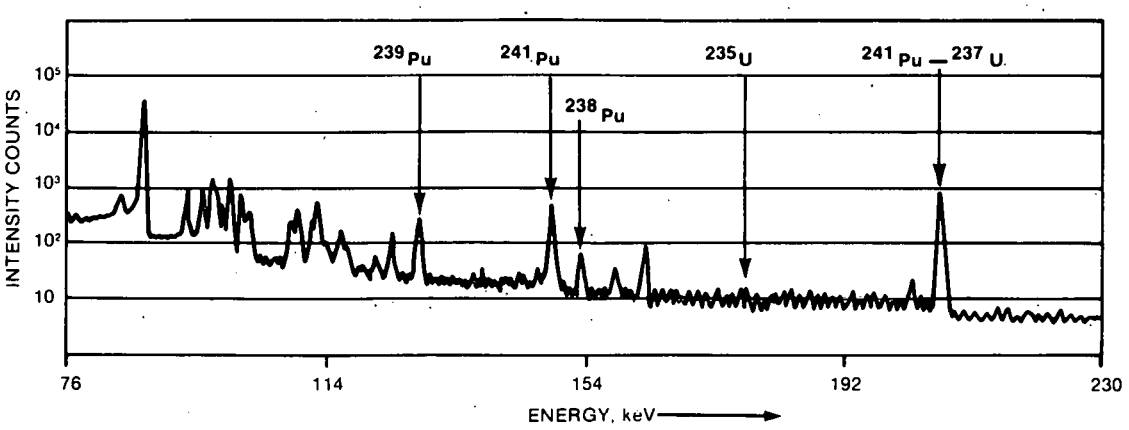


Figure 3C
Product Solution: Uranium (75%) - Plutonium (25%)

NUCLEAR METHODS

IN

TRACER STUDIES

Session Chairman

W.D. James

PLUTONIUM AS A TRACER FOR STUDIES OF SETTLING PROCESSES IN A SLOW BODY OF RUNNING WATER

M. Pimpl, H. Schüttelkopf

Kernforschungszentrum Karlsruhe
Hauptabteilung Sicherheit / Radioökologie

Summary

The mechanism of plutonium settling in a slow body of running water was investigated by the example of plutonium activity released from the Karlsruhe Nuclear Research Center into the Altrhein, an old branch of the river Rhine. It was found that the plutonium distribution in the sediments depends on the distance of the location under consideration from the point of discharge and the sediment density which, in turn, is influenced by the width of the Altrhein and hence by the flow velocity. In the topmost sediment layers over the first 3.5 km an isotope ratio Pu-238/P-239+240 of 0.64 was found, in the bottom layers a ratio of 0.36. It is supposed that the contamination of the bottom layers is caused by sinking in of the oldest plutonium contamination in a highly liquid sediment, whilst the topmost layer is characterized by the plutonium emission of the recent years. The plutonium concentration is equally distributed over the depth. Shortly after the point of discharge water and filterable suspended matter show an increased plutonium contamination although the plutonium content quickly decreases with increasing distance from the point of discharge and reaches the reference value already after 3.5 km, this value being determined in samples from the same water upstream of the point of discharge. The total amount of plutonium deposited in the main canal was estimated from the sediment contaminations and the amounts of sediment. In the sediments located below the water surface 94% of the plutonium, which have been released from the Nuclear Research Center into the Altrhein, was found again. This means that the majority of plutonium emitted together with the liquid effluents is still present in the Altrhein. This proves that resuspension in plutonium transport in the Altrhein plays but a minor role.

The discharge of industrial waste waters into brooks and rivers over extended periods automatically leads to a pollution of these waters. This might cause a disturbance of the ecological equilibrium due to the enrichment of heavy metals in the sediments. The settling processes, which, depending on waterspecific parameters, give rise to this enrichment, have been investigated insufficiently ly, so that at present model concepts of a general validity, which would allow to take preventive measures, are not available. The experimental in situ

investigation of sedimentation processes with the aim of preparing such models is very expensive and often impossible because a suitable tracer is not available. We profited from the situation that, since startup of the Karlsruhe Reprocessing Plant, low amounts of radionuclides have been discharged with the liquid effluents into a river system in order to study the settling processes as a function of the waterspecific parameters such as width, distance from the point of discharge, flow velocity, etc. Plutonium was considered as the best suitable tracer and was therefore used for this investigation.

The annual rates of plutonium emission with the clarified and purified waste waters from the Nuclear Research Center and the Karlsruhe Reprocessing Plant have been recorded since 1973 within the frame of emission monitoring (Table 1). The waste waters are discharged into the Altrhein, a branch of the Rhine before it has been corrected, which, due to its low flow velocity, is a suitable main canal and they reach the Rhine after some 23 km. On this way the greater part of the solid particles suspended in the liquid effluents gets settled. This applies also to the fractions with the lower grain sizes. Plutonium, which is present in the neutral aqueous solution as a nearly insoluble plutonium (IV) hydroxide, is settled together with these suspended materials. If the plutonium concentration in water and in the suspended materials as well as the distribution in the sediments are determined and this values are related to the waterspecific parameters, the time- and location- dependent settling behavior of plutoniun can be estimated in a manor, which is representative of the water insoluble heavy metals.

Table 1: Pu-238 and Pu-239+240 releases with the liquid effluents from the Karlsruhe Nuclear Research Center

Year	Release of Plutonium (mCi/a)		Isotope ratio
	Pu-238	Pu-239+240	Pu-238/Pu-239+240
1973*	0.37	1.09	0.34
1974	0.14	0.28	0.50
1975	0.13	0.21	0.59
1976	0.49	0.37	1.32
1977	0.16	0.21	0.79
1078	0.07	0.07	1.07
1979**	0.07	0.08	0.80
Total	1.43	2.31	Mean: 0.62

* July to December 1973; ** January to June 1979

In two preliminary experiments longitudinal profiles were recorded of the sediment contamination appearing in the middle of the river. It was found that in the range of the first 3.5 km after discharge the highest plutonium contamination occurred, 250 fCi/g of dry material at the maximum. Subsequently, this part of the main canal was subjected to a more detailed investigation. At 23 sampling positions alongside the Altrhein downstream of the point of discharge, three to nine individual samples were taken from the topmost sediment layer on profiles transverse to the flow direction. In addition to the width of the Altrhein at the individual locations the following characteristics were determined at each point of sampling: water depth, flow velocity, thickness of sediment layer and density of the sediments. At one sampling location three depth profiles were taken down to 70 cm depth, at another 14 locations, 24 sediment samples in total from the bottom sediment layer.

Sampling of water and suspended materials took place from May to December 1979 using automated instruments. A pump, driven by a dry battery, aspirated regularly a defined amount of water through a hose from the middle of the Altrhein about 30 cm below the water surface. It was passed through a filter where the suspended materials were collected and then caught in a supply vessel. The instrument had been so adjusted that 50 l water were collected per month by each automated instrument. Downstream of the point of discharge a total of 6 automated instruments were installed on the river bank at 20 m, 600 m, 2.0 km, 3.5 km, 5.5 km and 13.0 km distance. An additional automated instrument was installed to collect reference samples 500 m upstream of the point of discharge.

The sediment and suspended material samples were dried at 110°C and then ashed at 600°C after addition of nitric acid. The water samples were reduced to about 200 ml in an evaporator. The whole sampling material was used for analysis in case of water and suspended material samples, whilst 100 g of ash were used in case of the sediment samples. After addition of Pu-236 as the internal standard for evaluation of the yield the samples were boiled with 8 M nitric acid. The plutonium dissolved in this way was then separated from the other substances in three steps - extraction with TOPO, co-precipitation with LaF_3, anionic exchange - subsequently purified and then electroplated from hydrochloric oxalate solution and measured by alpha spectrometry. With a measuring time of 1000 minutes a detection limit of 0.2 fCi plutonium/l was reached for water and suspended material samples, for sediments 0.1 fCi plutonium/g of ash.

The results of the preliminary experiments are represented in Fig. 1. It is clearly apparent that the maximum plutonium contamination in the sediments is attained over the first 3.5 km of the Altrhein. The average contamination

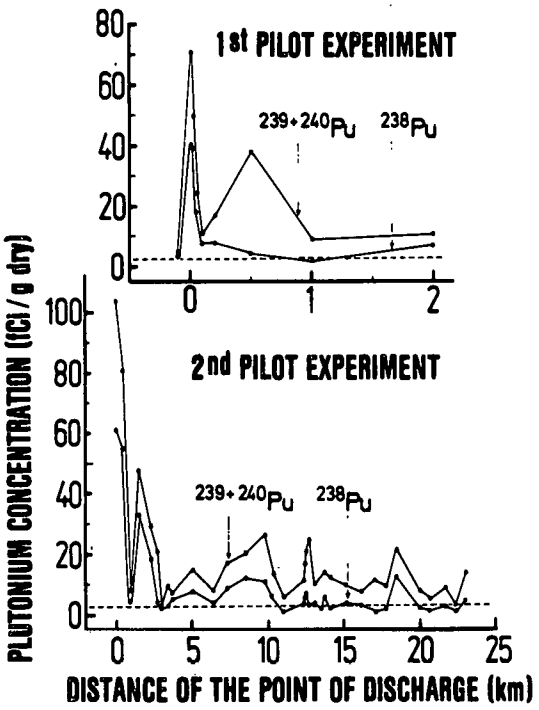


Fig. 1: Pu-238 and Pu-239 + 240 concentrations of the sediments of the Altrhein river. Samples were collected in June 1977 and November 1978 (---Fallout-level)

decreases subsequently also it remains well above the fallout background, until the main canal discharges into the Rhine river. The considerable depths in the concentration profile were identified as constrictions of the Altrhein and junctions of tributaries. The mean isotope ratio Pu-238/Pu-239+240 of 0.62 in the liquid effluents of the Nuclear Research Center is found again in the topmost sediment layer over the first 3.5 km. It is strongly reduced over the next 10 km, although it remains clearly above the fallout value of 0.025.

The distribution of plutonium in the topmost sediment layer over the first 3.5 km of the Altrhein appears from Fig. 2.

The longitudinal profile, i.e., the plutonium distribution in the sediments of the river with increasing distance from the point of discharge is very highly influenced by four constrictions in the course of the river. In this way, four successive settling basins are formed, in which plutonium settles as a function of the respective flow velocity. At points characterized by a high flow velocity, i.e., the constrictions in the course of the river, always low plutonium depositions are measured whilst at the wide points, where the flow velocity is low, maxima of the plutonium concentration always occured (Fig. 3). However, since the flow velocity and the sediment density are proportional to each other (Fig.4), inversely proportional relation exists between the density of the sediment and

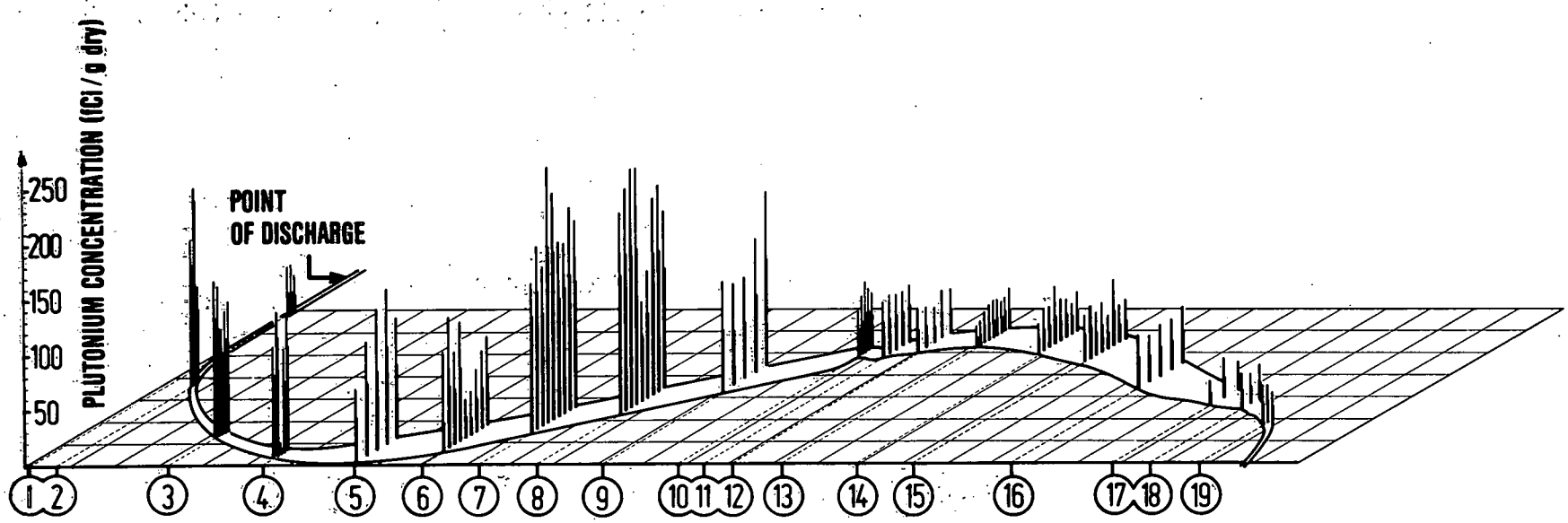


Fig. 2: Pu-238 and Pu-239 + 240 concentrations of samples of the surface layer of the sediments in the Altrhein river near Linkenheim in relationship to the sampling positions (═══ Pu-239 + 240, ——— Pu-238)

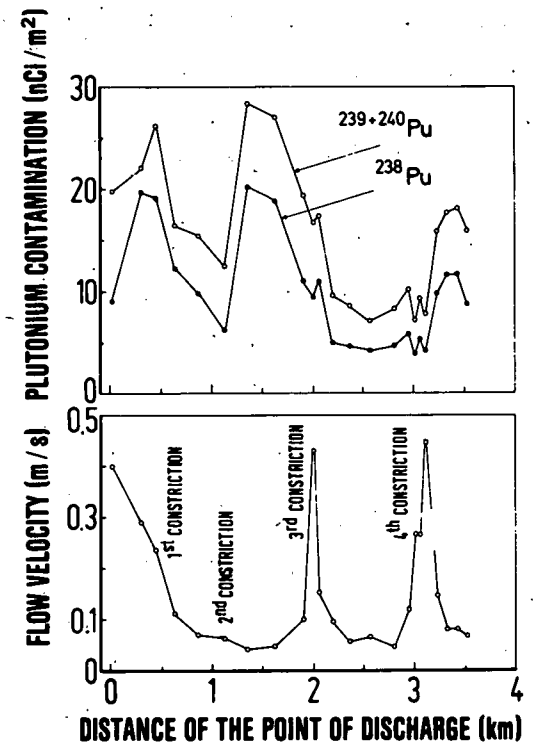


Fig. 3 : Correlation between the plutonium deposition in the Altrhein river near Linkenheim and the flow velocity

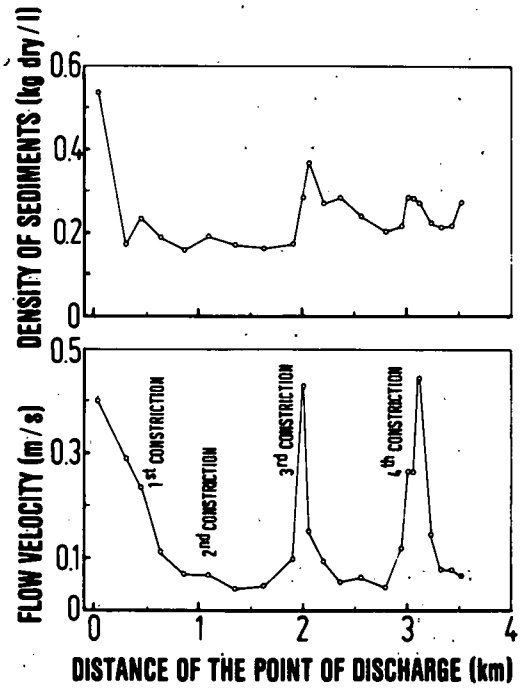


Fig. 4 : Correlation between the density of sediments and the flow velocity in the Altrhein river near Linkenheim

the plutonium contamination. At locations with a low flow velocity the stay time of the suspended materials over a given settling space is so long that even finely grained suspended materials may settle. These finer suspended materials which result in a lower density of a sediment must be preferred carriers of plutonium. Therefore at the points of low flow velocity and hence little density of the sediments, high plutonium deposition take place.

It is comprehensible from these considerations that the contamination of the sediment in a longitudinal profile does not decrease steadily with the distance from the point of discharge, but that minima of plutonium contamination must occur at the constrictions and maxima at the broadest locations of the individual settling basins.

The plutonium contamination in the transverse profiles, i.e., the profiles normal to the flow direction, was equally distributed, in case the course of the river was in the middle of the river bed. In a long drawn left turn, where the course of the water is at the outmost radius of the river bed, contamination maxima were measured at the border of the river course. Also in this case a relationsship can be observed between the density of the sludge and the plutonium contamination.

At the point in the river course where the maximum plutonium contamination was found - at location 8 - depth profiles were recorded in the middle and at both river banks (Fig. 5). It was found that the plutonium contamination reaches down to the bottom layer of the sediments lying at 70 cm depth. The isotope ratio Pu-238/Pu-239+240 in the topmost sediment layer takes a value of 0.64 and thus corresponds to the average isotope ratio in the liquid effluents of the Nuclear Research Center, but it decreases with increasing sediment depth and in the bottom sediment layer it reaches the value of 0.36, i.e., almost the value found in the liquid effluents in 1973 (see Table 1). The analysis of another 24 samples, taken from the bottom sediment layer, confirmed the presence of plutonium in the bottom sediment layer along the whole Altrhein.

Also in case of the depth profiles a dependence was found of the plutonium contamination on the sediment density. Conversion of the plutonium concentrations into the pCi/l sediment value, which is independent of the density, allows to demonstrate that the concentration of the total plutonium present is equally distributed over the depth of the sediments. Since it is improbably that the whole sediment layer of 70 cm has been deposited during the last eight years, the plutonium can not be deposited there by jointly settling with the suspended materials. It must rather be assumed that at the date of startup of the Karls-

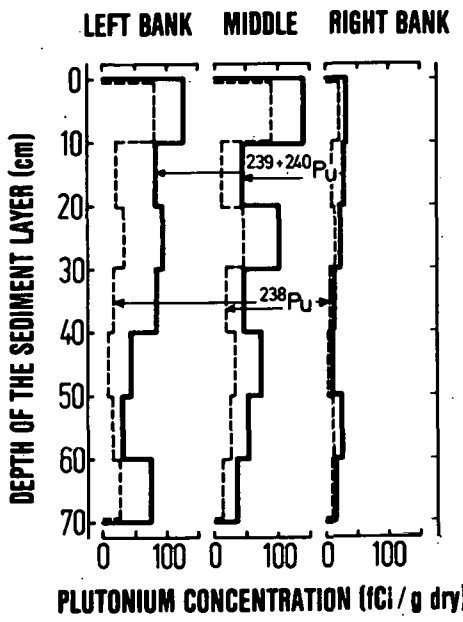


Fig. 5 : Pu-238 and Pu-239 + 240 concentrations of the sediments of sampling position 8 as a function of the depth of the sediment layer

ruhe Reprocessing Plant the Altrhein and its sediments had been in equilibrium. This implies that the sediments filled up all cavities and that only the topmost sediment layer was subject to changes by deposition and resuspension. The plutonium particles settled then on this topmost layer. Although they had been slightly whirled up by resuspension and carried on, the majority sank slowly into the relatively highly liquid sludge. Therefore, the contamination of the bottom sediment layers is due to the sinking of the oldest plutonium contamination whilst the topmost layer is rather characterized by the plutonium releases over the recent years.

The water samples collected in the Altrhein from May to December 1979 contained 1 to 6 fCi Pu-238/l and 1 to 7 fCi Pu-239+240/l immediately downstream of the point of discharge. Alongside the Altrhein the plutonium concentration in water decreases and after 3.5 km the maximum values of 1.4 fCi Pu-238/l and 1.6 fCi Pu-239+240/l are the same values as measured at the reference location upstream of the point of discharge. These measured values take the same order of magnitude as the soluble plutonium amount which can be estimated from the solubility product for plutonium hydroxide (pk = 44). For neutral, aqueous solutions the values 1.5 fCi Pu-239/l and 5.5 fCi Pu-240/l are obtained.

The content of suspended materials in water at the same sampling locations is subject to great monthly variations. However, a systematic course, which can be

found for the samples taken during the same month, is repeated. The maximum content of filterable suspended materials - up to 24 times of the reference measurement - was obtained always immediately downstream of the point of discharge. With increasing distance from the point of discharge the content of suspended materials decreased and after 3.5 km it reached the value of the reference sample. The plutonium contamination of the suspended materials showed the same location and time dependent behavior. After passage through the Altrhein near Linkenheim, the plutonium concentration in the suspended materials filtered from a water sample remains relatively constant and is approximately twice as high as in the filtered water.

To obtain a statement as to the percentage of plutonium transport caused by resuspension, it is necessary to estimate the fraction of the total discharged plutonium which has remained in the Altrhein. If resuspension were of high significance, only a little fraction of the total plutonium activity released should be found in the Altrhein. To calculate the activity deposited in the sediments of the Altrhein the plutonium concentration (fCi/g of dry material) measured at the different sampling locations were multiplied by the respective density (kg of dry material/l of sediment). These values (pCi/l of sediment) were multiplied by the depth of the sediments and the average was taken of the transverse profiles. The mean plutonium activities so found per unit area were averaged with the values obtained in a similar way at the neighbouring locations and subsequently multiplied by the area of the watercovered Altrhein. The multiplication yields the minimum of plutonium deposit in the Altrhein (Table 2). Comparison of these values with the total plutonium emission with the liquid effluents (see Table 1) gives a minimum deposition of 94%.

Table 2: Estimation of the total quantity of plutonium deposited in the main canal

Range of the main canal (km)	Quantity of plutonium in the main canal			
	mCi		% of the emitted Pu	
	Pu-238	Pu-239+240	Pu-238	Pu-239+240
-0.5 to 0	0.04	0.08	3	3
0 to 3.5	0.98	1.52	69	66
3.5 to 23	0.30	0.60	21	26
Total	1.32	2.20	93	95

Since the total river bed is completely filled with water only during the high water period, e.g. four weeks per year at the maximum, and the water level in the Altrhein is relatively constant otherwise, the amount of plutonium actually deposited in the Altrhein should be slightly more than 94% of the total amount discharged.

This estimate shows that the plutonium emitted with the liquid effluents is practically completely deposited in the sediments of the Altrhein. This means, however, that the resuspension plays but a minor role in plutonium transport. This is also evident from the fact that the suspended materials carried in the flowing water after 3.5 km shows only very low plutonium contaminations.

The studies will be continued with the aim of obtaining a mathematical model for plutonium deposition in a flowing water, which will be representative of other heavy metals.

Finally it should be mentioned that also the emission of plutonium with the liquid effluents has caused a clearly detectable contamination of the Altrhein, its size is insignificant, if one consideres that the mean plutonium activity is well below 1% of the natural alpha activity found in the local soil and sediment samples.

APPROACH TO CADMIUM SPECIATION IN NATURAL WATERS USING ^{109}Cd AS RADIOTRACER

L. Maggi*, V. Caramella-Crespi°, N. Genova°, S. Meloni°

* Laboratorio di Radiochimica - Istituto di Chimica Generale e Inorganica - Università di Pavia - 27100 Pavia (Italy)

° Centro di Radiochimica e Analisi per Attivazione del Consiglio Nazionale delle Ricerche - Istituto di Chimica Generale e Inorganica - Università di Pavia - 27100 Pavia (Italy)

ABSTRACT

The present study was undertaken to evaluate to which extent cadmium present in natural waters is associated to organic matter and/or to large inorganic molecules and suspended particulate, whose size is below 0.45 μm. Cadmium behaviour was investigated by adding to the original waters carrier-free ^{109}Cd as a tracer. A simpler approach to the identification and, possibly, characterization of organic and large inorganic species of cadmium was established by fractionating inorganic and organic matter in natural waters (Po and Lambro rivers in Northern Italy) with the ultrafiltration technique.

Cadmium content and distribution were correlated to organic carbon content, inorganic and organic phosphorus content and to soluble silica concentration. A preliminary evaluation of the strength of ligands in the water fractions was obtained by batch and column experiments with Chelex resins. Results, behaviours and trends are reported and discussed.

INTRODUCTION

Recently a great effort has been devoted in environmental research programs to investigations of the different chemical forms of elements in natural waters (1-5). Cadmium is known to be a highly hazardous pollutant and its interaction and toxicity in the environment are strictly related to its chemical species (6-7). It is possible by calculation to work out a list of inorganic species in natural waters knowing pH, total cadmium and Cd^{++} concentration and the content of some relevant anions such as HCO_3^-, CO_3^{--} and Cl^-(16-17). On the other hand information on organic forms of Cd or, at least, on the amount of Cd linked to them, is quite poor. In addition the concentration of cadmium in unpolluted surface waters is very low, in the range 1-10 µg/l, (8) and this rises detection and contamination problems.

The present study was undertaken to evaluate to which extent cadmium present in natural waters is associated to organic matter and/or to large inorganic molecules and suspended particulate, whose size is below 0.45 µm.

In this work cadmium behaviour was investigated by adding to the original waters carrier free ^{109}Cd as a tracer. A simpler approach to the identification and, possibly, characterization of organic and large inorganic species of Cadmium was established by fractionating inorganic and organic matter in natural waters with the ultrafiltration technique (9).

EXPERIMENTAL

Materials and methods

REAGENTS - All chemicals used were certified ACS reagent grade. A ^{109}Cd carrier-free solution was obtained commercially (Radiochemical Centre-Amersham U.K.), with specific activity >50 µ Ci/µg Cd.

All the containers used throughout this work were manufactured with Nalgène (linear polyethylene) (10). Before their use, they were soaked in 1 M HNO_3 for 24 h, then filled with double distilled-deionized water and left four days.

Chelex-100 resins (sodium form , 50-100 mesh) were obtained commercially (Bio.Rad.Laboratories). Before their use they were suspended in double distilled deionized water.

NATURAL WATERS - Surface fresh waters were collected from the Po river (the major Italian river flowing in the North, East-bound, through an industrial and

agricoltural area) and from the Lambro river, which is a left side tributary of the Po river and flows Southward and collects large amounts of industrial and municipal liquid wastes.

Usually 5 liters samples were collected and pH, alkalinity and hardness quickly measured. The water samples were then filtered through a 0.45 μm pore size membrane filter and the filtrate stored at 4°C for further investigations.

APPARATUS - A Millipore 90 mm High-Flux cell Ultrafiltration system was employed using membranes with a nominal molecular weight limit of 1000 (PSAC), 10000 (PTGG), 100,000 (PTHK) and 1,000,000 (PSVP).

Radioactivity measurements were carried out by gamma-ray spectrometry using a well-type NaI(Tl) detector and a multichannel pulse height analyzer. The 22 Kev Ag X-ray emitted in the decay of ^{109}Cd was measured.

Total cadmium determination was carried out by atomic absorption spectrometry equipped with a carbon rod atomizer. Total organic carbon (TOC) determinations were made with a gas chromatographic apparatus, measuring the carbon dioxide released after oxidation with potassium persulfate and phosphoric acid (11).

Absorbance spectra for nitrogen, phosphorus, ionic and non-ionic detergents and silica determination were performed with a UV-Visible spectrophotometer. Complexation capacity with respect to copper was carried out by potentiometric measurements using a copper ion-selective electrode.

Preliminary experiments with ^{109}Cd

Preliminary experiments were carried out to test the possibility of using ^{109}Cd as radio-tracer in the study of cadmium distribution in the different fractions from the ultrafiltration step.

Aliquots of a carrier-free ^{109}Cd standard solution were added to water samples collected from the Lambro river, which contained cadmium levels easily detectable by AAS, after filtration through 0.45 μm pore size membrane filters.

The traced solutions were left to sit at 4°C, periodically submitted to ultrafiltration and ^{109}Cd activity measured in each fraction. The cadmium distribution thus obtained was compared with the one obtained by AAS on samples of the same river water which had been processed as above described but for the ^{109}Cd addition. Results show that the two distributions are in an acceptable agreement within the experimental errors, after equilibration times of 25 days, as it is

reported in Table 1.

Table 1.: Cadmium distribution after 25 days equilibration time, as determined by radioactivity measurements and by AAS

Fraction (M W u)	Cadmium distribution %	
	radioactivity measurements	A.A.S.
$>10^6$	9.9	5.1
10^5-10^6	2.9	<0.1
10^4-10^5	5.2	6.5
10^3-10^4	11.6	13.0
$<10^3$	70.4	75.3

Ultrafiltration

The fractionation of river water samples coming from 0.45 µm filtrations was carried out by the ultrafiltration technique. This method separates, by the use of membrane filters of known pore size, the solutes according to their sizes which are related to their molecular weights. Five fractions were collected: 1--containing solutes whose molecular weights are greater than 10^6; 2-containing solutes with molecular weights in the range 10^5-10^6; 3-containing solutes with molecular weights in the range 10^4-10^5; 4-containing solutes with molecular weights in the range 10^3-10^4; 5-contaizing solutes whose molecular weights are lower than 10^3.

A check of the reliability of the ultrafiltration method was carried out by submitting to ultrafiltration a solution of a protein BSA (Bovine Serum Albumine) of known molecular weight (67000). As expected 95% and more of the protein was found in the fraction containing solutes with molecular weights in the range 10^4-10^5.

Investigations on Po and Lambro rivers water samples

The determination of some quality parameters in water samples from Po and Lambro rivers was carried out in order to define the type of water under study. These parameters were: inorganic and organic phosphorus, ionic and non ionic deter

gents, soluble silica, inorganic and organic nitrogen, complexation capacity with respect to copper, TOC and, of course, cadmium content. They were determined according to methods reported in the literature (12-15). The measurement of the parameters was repeated on the last fraction from ultrafiltration.

Known amounts of the high specific activity carrier free ^{109}Cd solution were added to water samples; as ^{109}Cd was added as a HCl solution, it was necessary to add proper aliquots of NaOH solution to bring back pH to the original value of the river water. The traced solutions were left to reach equilibrium for at least 25 days.

After the equilibration time expired the traced water samples were submitted to ultrafiltration at room temperature. Fractions from ultrafiltration and membrane filters were submitted to radioactivity measurements to evaluate cadmium distribution.

Not traced river water subsamples were ultrafiltrated as well and in each fraction the previous parameters determined.

It is likely that cadmium in the different fractions, expecially in those containing solutes with molecular weights greater than 10^3, is present as a complex species, either adsorbed on large colloidal molecules or complexed by inorganic and organic ligands. In order to establish a relative strength of these complex species, the ^{109}Cd traced fractions from ultrafiltration were equilibrated with Chelex-100 resins by column and batch experiments, and results compared with the behaviour, under the same working conditions, of cadmium complexes of known stability such as those with cysteine and EDTA. The complexes were prepared using ^{109}Cd tracer (Cd^{++} 1×10^{-5} M, cysteine 4×10^{-4} M and EDTA 2×10^{-4} M in a buffered medium) and waiting the proper time to reach equilibrium.

The column experiments were run with polyethylene columns (I.D. 0.5 cm, height 7 cm) at a flow rate of 1.5 cm^3/min.

RESULTS

The selected parameters measured in water samples from Po and Lambro rivers after filtration at 0.45 μm and after the last step in the ultrafiltration are shown in Table 2.

Tables 3 and 4 give the percent distribution of cadmium in the different fractions of ultrafiltered water samples from Po and Lambro rivers respectively, as

obtained by radioactivity measurement. The table also reports the percent distribution of some selected parameters, which were measured in order to verify a possible correlation with cadmium distribution.

The Chelex-100 resins equilibration experiments carried out with Cd-EDTA and Cd-cysteine solutions have shown that cadmium uptake with EDTA is quite limited 3-4% and no difference occurs between column and batch experiments, and that cadmium uptake with cysteine is about 77% in column experiments and about 94% in batch experiments.

The results of chelex-100 equilibration experiments carried out with the ultrafiltration fractions of the water samples from Po and Lambro rivers are reported in Table 5.

DISCUSSION

A criticism free procedure to afford distribution and speciation studies of trace elements in complex systems such as natural waters is not yet available. The problem must be faced with a trial-and-error procedure introducing alterations, as little as possible, of natural equilibria.

The approach to speciation studies is better achieved if an experimental procedure is worked out, capable to divide the initial sample in simpler subsamples without drastically changing the natural equilibria among the different components of the system. The ultrafiltration technique yields different fractions of the initial sample each containing mainly solutes having molecular weights above a given limit and its operational conditions assure that natural equilibria, as those depending from major components as HCO_3^-, CO_3^{--} Cl^- etc, remain almost unaltered. The combined use of radiotracers and ultrafiltration provides a better operational answer to difficulties encountered in speciation studies. When using radiotracers two basic considerations must be pointed out: 1- the added radiotracer must be in a carrier-free form and have an high specific activity, thus adding only neglectable amounts of element and meeting the sensitivity requirements after the ultrafiltration fractionation; 2- the time necessary to reach equilibrium with natural trace elements has to be investigated and, possibly, controlled in the course of experiments.

These requirements were fulfilled in the present work by using a high specific activity carrier-free ^{109}Cd solution and evaluating the time of the reached

equilibration between the added tracer and the natural cadmium when cadmium distribution in the ultrafiltration fractions of a not traced water sample, evaluated by AAS, showed the same trend as the one determined by radioactivity measurement. The similarity in the distribution trend was obtained after 25 days of equilibration time as shown in Table 1 and confirmed later when investigations on the Lambro river water samples were carried out. The choice of 25 days time period for equilibration was based on the fact that after that time about 90% of added cadmium radiotracer behaves as natural cadmium, as shown by the last three fractions in Table 1. Differences, about 10%, refer to the first two fractions, expecially the first one. It has been observed that the ^{109}Cd radiotracer content in the first fraction ($>10^6$ M W u) is initially high and decreases with time and it may be worthwhile to investigate the ^{109}Cd sorption and desorption from large molecules as those retained in the first ultrafiltration step. The use of traced samples has moreover allowed to point out that not neglectable amounts of cadmium (3-5%) are strongly adsorbed on the filters and thus subtracted to the next fractions. Corrections were thereafter applied in the evaluation of cadmium distribution.

Cadmium level and the selected parameters of the original Po and Lambro river waters samples are shown in Table 2. The choice of these parameters was based on the assumption that large amounts of cadmium in the river waters are associated to organic matter and in order to select some parameters to which correlate cadmium distribution after ultrafiltration.

Most of the parameters have a greater value for the Lambro river, thus confirming that this river is highly polluted, due to large urban and industrial discharges. It was suprising that TOC had a higher value in the Po river, possibly due to the fact that in the Lambro river a great amount of organic pollutants may be found in particulate form not passing through the 0.45 μm filters.

Column 3 and 5 of Table 2 report also the same parameters measured in the solution after the last ultrafiltration step (solutes having M W less than 10^3). The values, in this case, are usually lower than in the initial water samples. In two cases, referred to Lambro river (complexation capacity and anionic deterents), it is possible to observe a drastic decrease in the measured values, indicating the presence in that river of organic species having large dimensions.

The cadmium distribution among the different fractions of the ultrafiltration

is quite similar in the water samples of the two investigated rivers. About 87% is found in the last two fractions which contain solutes with molecular weights in the range 10^3-10^4 and lower than 10^3 respectively. A minor difference between the rivers may be observed about the cadmium level in the 4-th fraction. The remaining 13% of cadmium is homogeneously distributed among the other three fractions, with a higher cadmium level in the first fraction, the one with solutes having molecular weights higher than 10^6.

The distribution indicates that the great majority of cadmium is not associated to very large molecules or adsorbed on large colloidal solutes, whereas it is likely that cadmium be present, inorganically or organically bound to small molecules, or as the free ion, Cd^{2+}. A theoretical evaluation of the probable inorganic species of cadmium in the pH and hardness conditions of the Lambro river points out that the major forms are $CdCO_3$, Cd^{2+}, $CdHCO_3$. All these species would therefore concentrate in the last ultrafiltration fraction. On the other hand the data concerning the other parameters reported in Tables 3 and 4, show that there is a direct correlation between cadmium distribution and the distribution of the values of those parameters that may be considered indicators of the occurrence of organic matter (TOC, organic phosphorus, organic nitrogen). Accordingly one might foresee that a great part of cadmium be linked to organic matter. An independent and reliable determination of the free-ion Cd^{2+}, is expected to be quite indicative of the relative abundances of inorganic and organic species of cadmium.

The experiments carried out with the Chelex-100 resins (Table 5) show that in the last four fractions of the ultrafiltration cadmium complex species are in most cases strongly adsorbed, this pointing out that these complex species are weaker than the Cd-Chelex complex. In the fraction which contains solutes with molecular weights greater than 10^6, cadmium uptake shows a difference between the Po and Lambro rivers. In the water sample from the Po river cadmium uptake is quite limited, about 20%, showing that most of the complex cadmium species are stronger than the Cd-Chelex complex. Cadmium uptake from Lambro river water samples is about 75%, a value quite similar to the one that can be obtained by adsorption of the Cd-cysteine complex. Adsorption of the Cd-EDTA complex yields a cadmium uptake of about 4%.

The fact that in the above mentioned fraction cadmium uptake is lower than

100% may be accounted for the presence of very large molecules having strong absorption or complexing capacities with respect to cadmium, and for the occurrence of particulate inorganic forms of cadmium.

ACKNOWLEDGMENT

The authors wish to thank Dr. M.T. Ganzerli Valentini for performing complexation capacity measurement and Dr. M. Di Casa for A.A.S. measurement.

REFERENCES

1. Batley, G.E. and Florence, T.M. - Mar. Chem. 4, 347-63 (1976).

2. Benes, P. and Steines E. - Water Res. 9, 741-9 (1975).

3. Figura, P. and Mc Duffle, B. - Anal. Chem. 51, 120-125 (1979).

4. Hart, B.T. and Davies, S.H.R. - Aust. J. Mar. Freshwater Res. 28, 105-112 (1977).

5. Bowen, H.J.M., Page, E., Valente, I. and Wade R.J. - J. Rad. Chem. 48, 9-16 (1979).

6. Cearley, J.F., Coleman, R.L. - Bull. Environ. Contam. Toxicol. 11, 146-151 (1974).

7. Ball, I.R. - Water Res. 1, 805-806 (1967).

8. Calamari, D., Marchetti, R. - Nuovi Annali d'Igiene e Microbiologia, vol. XXVIII, n° 6, 425-436 (1977).

9. Smith, R.G. Jr. - Anal. Chem. 48, 74-76 (1976).

10. Subramanian, K.S., Chakrabarti, C.L., Sueiras, J.E. and Maines, I.S. - Anal. Chem. 50, 444-448 (1978).

11. Peterson, G.N. and Montgomery, J.R. - Anal. Chim. Acta 113, 395-397 (1980).

12. Weatherburn, M.W. - Anal. Chem. 39, 971-974 (1967).

13. Florence, F. and Miener, D.F. - Analyst, 104, 378-381 (1979).

14. Pantani, F., Raconelli, E., Legittimo, P. - Inquinamento 14, 13-20 (1972).

15. Campbell, P.G.C., Bisson, M., Gagné, R. and Tessier, A. - Anal. Chem. 49, 2358-2363 (1977).

16. Baudoin, M.F. and Scoppa, P. - Publ. no. 901 of the Biology Directorate of the European Communities Commission (1973).

17. Zirino, A. and Yamamoto, S. - Limnol. Oceanogr. 17, 661-671 (1972).

Table 2.: Selected parameters of Po and Lambro rivers water samples

Parameters \ Samples	Po river a)		Lambro river b)	
	after filtration at 0.45 μm	After filtration at 10^3 M W u.	After filtration at 0.45 μm	After filtration at 10^3 M W u.
Cadmium (μg l^{-1})	1.5	0.9	2.4	1.6
Complexation capacity (μg Cu l^{-1})	16.9	12.3	566	21
Total organic carbon (TOC) (mg l^{-1})	3.6	2.7	1.2	0.8
Organic phosphorus (mg l^{-1})	0.02	0.02	0.57	0.19
Inorganic phosphorus (mg l^{-1})	0.22	0.06	1.65	0.64
Organic nitrogen (mg l^{-1})	-	-	1.24	1.08
Inorganic nitrogen (mg l^{-1})	0.37	0.32	4.53	3.95
Soluble silica (mg l^{-1})	3.6	3.5	-	-
Non ionic detergents (μg BRIJ l^{-1}) c)	70	70	245	130
Anionic detergents (μg ABS l^{-1}) d)	18	11	130	23

a) pH = 7.15 Hardness = 167 (mg $CaCO_3$ l^{-1}) Alkalinity = 144 (mg $CaCO_3$ l^{-1})

b) pH = 8.12 Hardness = 253 (mg $CaCO_3$ l^{-1}) Alkalinity = 188 (mg $CaCO_3$ l^{-1})

c) BRIJ - 35 $\left[CH_3-O-(C_2H_4O)_{12}-C_{12}H_{25}\right]$ M W = 728

d) ABS [sodiumalkylarylsulphonate] average E W = 348

Table 3.: Po river: percent distribution of cadmium and other selected parameters in the fractions from ultrafiltration

Fraction (M W u)	Cadmium		Total organic carbon	Phosphorus		Complexation capacity
	solution	filter		organic	inorganic	
$> 10^6$	3.5	1.4	2.0	0.7	1.6	< 0.1
10^5-10^6	1.7	0.3	0.4	0.8	1.8	< 0.1
10^4-10^5	2.4	0.3	0.5	0.9	2.0	12.4
10^3-10^4	18.1	3.1	21.7	1.2	44.2	14.8
$< 10^3$	69.2	-	75.4	11.7	35.4	72.8

Table 4.: Lambro river: percent distribution of cadmium and other selected parameters in the fractions from ultrafiltration

Fraction (M W u)	Cadmium		Total organic carbon	Phosphorus		Organic nitrogen
	solution	filter		organic	inorganic	
$> 10^6$	4.1	0.8	7.8	5.6	4.5	< 0.1
10^5-10^6	2.0	0.7	1.8	0.6	1.4	< 0.1
10^4-10^5	2.0	0.6	1.6	< 0.1	3.8	< 0.1
10^3-10^4	8.4	1.1	25.3	12.7	23.7	6.4
$< 10^3$	80.3	-	63.5	10.9	36.8	93.6

Table 5.: Percent cadmium uptake by chelex-100 resins in the different fractions of the ultrafiltration of Po and Lambro rivers water samples.

Fraction	Po river		Lambro river	
(M W u)	column	batch	column	batch
$> 10^6$	23	19	76	72
10^6-10^5	100	100	52	100
10^5-10^4	100	100	100	100
10^4-10^3	100	100	77	100
$< 10^3$	100	100	100	100

SOIL HOMOGENEITY EVALUATION BY RADIONUCLIDE TRACER BREAKTHROUGH CURVE INTERPRETATION

by

J. S. Brenizer, Jr.
A. R. Jarrett
W. A. Jester

INTRODUCTION

Increasing concern about the environmental impact of hazardous waste disposal has made site evaluation and site selection difficult and expensive. Pollutants, assumed to be absorbed by the soil immediately surrounding the burial trench, have been detected far from sites. Discrepancies between predicted migration distances based on indirect methods such as laboratory and computer modeling and and those observed at the field site are often significant.

The homogeneity of subsurface media, often assumed in laboratory and modeling studies, is seldom found in the field. The use of tracers to determine the flow characteristics of a potential disposal site involves time and expense, but offers a direct evaluation of solute transport and eliminates the assumptions inherent in indirect methods.

Current modeling of solute transport in nonhomogeneous porous media is limited by the quantification of input parameters. Several general models, such as those developed by Duguid and Reeves (1976) and Segol (1976), can predict solute transport in saturated-unsaturated media from low-level disposal sites if the hydraulic characteristics and chemical reactions expected in each unique water-solute-media system can be defined.

The objective of this research was to develop a method of evaluating potential shallow-land burial waste disposal sites by interpreting tracer breakthrough curve structure with respect to the hydrologic properties of the media at the potential disposal site. This methodology will be helpful in evaluating the potential performance of many types of shallow-land waste burial sites such as low-level radioactive waste disposal, surface disposal of flyash, chemical waste disposal, waste sedimentation ponds, and sanitary landfills.

BACKGROUND

The evaluation of contaminant movement through soil, rock or other porous media requires an understanding of both water and solute transport phenomenon. Solute transport in a hydrogeologic system is controlled by (1) advection or convection of the moving groundwater, (2) hydrodynamic dispersion, and (3) chemical reactions between the solute, groundwater, and porous media, (Papadopulous and Winograd, 1974).

Fracture Effects on Advection

Advective transport rates, predicted from homogeneous media parameters, are often several orders of magnitude slower than observed in media containing perturbations. Actual leachate travel times from the disposal site to monitoring points are much shorter than predicted when based on homogeneous analysis using an

average hydraulic conductivity or effective permeability, or the continuous approach. This method gives good results if perturbations react hydraulically as granular media, (Freeze and Cherry, 1979). Similarly, media containing small sand lenses are easily modeled using the continuous approach. If, however, the fractured density is small, or large sand lenses are present, the continuous approach will not predict the earliest arrival of the leachate from the disposal site.

Nonhomogeneities oriented in a particular direction will cause the media to be anisotropic. This may cause leachate to be directed away from the monitoring wells.

While it is obvious that accurate modeling of regional water movement is required to predict the advective transport of leachate, definition of and mathematical modeling of nonhomogeneous systems is difficult. Even where models are designed to handle nonhomogeneities, input parameters, such as hydraulic conductivity for the fractures, may not be definable.

Fracture Effects on Hydrodynamic Dispersion

Evaluation of the biological and environmental hazards of solute migration requires an estimate of dilution which occurs as the solute moves from the disposal site to the point of interest. Nonhomogeneities, such as factures with rapid hydraulic conductivities, have different dispersion properties than the surrounding homogeneous media. When contaminates are transported through large fractures, the amount of dispersion is reduced. However, Levy (1972) reports that where flow is principally through very small fractures, the velocity varience will be greater and hence, more dispersion will occur.

Fracture Effects on Solute Reactions

Another important factor in determining the value of a potential waste disposal site is the amount of contaminant adsorption which will occur as the leachate migrates through the media. Solute adsorption slows the migration rate and thus increases the time required for contamination to reach critical locations. The correct estimation of radionuclide migration rates is critical when predicting the occurrence of radioactive decay before contaminants reach site boundaries, ground water aquifers, or other points of interest.

The presence of nonhomogeneities in the porous media has two important effects on the adsorption of the migrating solute. First, the exposed surface of the nonhomogeneity will probably be smaller than that of the surrounding media making available less total surface area per unit volume of soil for adsorptive processes. Secondly, the velocity of contaminant migration may be too rapid to permit equilibrium to occur.

BREAKTHROUGH CURVE INTERPRETATION

Tracers have been utilized for many years to study ground water flow. One tool used for the analysis of tracer arrival is the breakthrough curve. The breakthrough curve is the graphical relationship between the relative concentration of the tracer and the elapsed time since introduction.

The most direct method of obtaining ground water velocity in a field study is to introduce a non-reactive tracer at one point in the flow field and monitor its arrival at other points in the flow. By correcting for dispersion, the velocity of the water can be computed from the travel time and the distance of travel. Many tracers have been employed for this purpose including salts, radioisotopes such as hydrogen-3, iodine-131, cobalt-60, and bromine-82, and fluorescent dyes. Numerous examples of this direct method of subsurface water velocity determination can be found in the literature.

The advantage of using tracers in nonhomogeneous media is that non-reactive tracers are transported with the water along the most rapid path of ground water movement. If injection and monitoring wells are correctly placed, the tracers will indicate the existence of a direct link of one point in the media with

another via a 'short circuit'. Therefore, where detailed knowledge of potential contaminant migration is required, the use of tracers is a viable technique for potential site evaluation.

Correlation of tracer breakthrough curve structure and the media's hydraulic properties is difficult in field studies. The advective, dispersive, and chemical properties of the media-solute system will influence the shape and relative concentration of the breakthrough curve. Haaser, et al. (1978) presents a discussion on breakthrough curve analysis and the affects of various hydrogeologic properties and processes on breakthrough curve structure.

Hackenberry, et al. (1971) used an iodine tracer to investigate the ground water velocity and the dispersion coefficient in a Nevada field study. The tracer was introduced as a potassium iodide pulse source and the arrival time of the maximum peak concentration was used to calculate flow velocities. The breakthrough curves were single peaked, although some curves did show different recession rates after the peak. While the flow velocities and flow patterns were calculated, no estimate of the dispersion coefficients was possible.

Thus, tracer breakthrough curves have been successfully used to determine ground water velocities, flow patterns, and the media's effective porosity. However, only a few attempts have been made to interpret breakthrough curves structure and shape to determine other hydrologic properties of a solute-media system. These attempts have had only limited success in field studies.

The tracer used in this study was chosen to be adaptable to both laboratory and future field studies. The bromide ion best meets these requirements, as radioactive bromine-82 for the laboratory study and as activatable bromine for the field work. Bromine can be introduced in large concentrations in the field without violating pollution regulations. Laboratory and field studies by Jester and Uhler (1974), Schmotzer (1970), and Osmin (1977) indicate that the bromine ion moves faithfully with ground water and the bromide ion concentration in a water sample can be determined using neutron activation. Details of the neutron activation analysis procedure are presented by Osmin (1977) and Haaser, et al. (1978).

THEORETICAL CONSIDERATIONS

Before an experimental set-up was developed to generate breakthrough curves, two problems required consideration. First, the water flow net inside the experimental column was not defined. Consequently, the experimental results were not easily interpreted. Secondly, each run required a minimum of ten days for decay of the tracer, with more time required to modify the column. To aid in the analysis of the experimental results and to optimize the experimental time available, a computer model of the experimental system was developed.

Two requirements were placed on the model, namely, it should be relatively simple, and yet have the capability of handling the initial field study. Models of the general type were reviewed, but most were too complex and required large core storage and long computer run times. A simple finite element model, developed by Pall, et al. (1978), could easily handle water infiltration in one dimension. It had been extended to two dimensions and benchmarked to experimental data presented in the literature, (Pall, et al. 1979a and 1979b). The model was developed in Cartesian coordinates for unsaturated water flow but cylindrical coordinates and the capability to handle saturated-unsaturated solute flow were needed to model the experimental set-up. Thus, it was necessary to modify and extend the Pall method to a three-dimensional cylindrical coordinate, saturated-unsaturated solute flow model.

The first objective of the model was to determine the water velocity spatial distribution for steady state flow. The Darcy equation can be written in one direction as

$$v = \frac{\Delta Q}{\Delta t} = -K\,(\Psi_m)\,A\,\frac{\Delta \Psi_t}{\Delta L} \qquad (1)$$

where

v = Darcy velocity, cm/sec
ΔQ = volume flow rate, cm^3/sec
t = time, sec
$K(\Psi_m)$ = hydraulic conductivity, a function of matric potential, cm/sec
A = area perpendicular to flow, cm^2
Ψ_t = total potential, cm
L = distance of flow, cm

Assuming the total potential is the sum of the matric potential, Ψ_m, and the gravitational potential, Ψ_g, the volume flow rate between two elements in the horizontal direction can be written as

$$\frac{\Delta Q}{\Delta t} = -K(\Psi_m)A \frac{(\Psi m_2 - \Psi m_1)}{L_2 - L_1} \tag{2}$$

In the vertical direction, the volume flow rate between two elements is

$$\frac{\Delta Q}{\Delta t} = -K(\Psi_m) A \frac{(\Psi m_2 + \Psi g_2 - \Psi m_1 - \Psi g_1)}{L_2 - L_1} \tag{3}$$

If Darcy's law is assumed to be valid, using equation (2) and (3) and a material balance, the water flow can easily be determined by explicit calculation if

$$\frac{K(\Psi_m)}{C(\theta)} \frac{\Delta t}{\Delta L^2} \leq 0.5$$

where

$$C(\theta) = \frac{\partial \theta}{\partial \Psi_m}$$

is evaluated at saturated conditions.

The experimental system to be modeled was a cylindrical soil column. The column can be divided in the vertical direction, z, into equal elements of length, Δz. These are numbered consecutively beginning at z = 1 at the top of the column. The horizontal direction is divided into segments of equal angular width in the ϕ direction but with varying radial width in the r direction. A sample element is illustrated in Figure 1. Thus, while each element is identical in dimension in the ϕ and z directions, the element width can vary in the r direction. An element is located by the ϕ, r, and z numbers. The horizontal segments are numbered consecutively in the counter-clockwise direction from the interior of the column to the outer boundary. The amount of core storage is reduced by identifying an element by a segment number in the horizontal plane in the computer program.

The flow into and out of any element can be calculated using equations (2) and (3). For example, the flow of element ϕ to element $\phi + 1$ in the ϕ direction would be

$$\Delta Q_{\phi \text{ to } \phi+1} = \frac{-K(\bar{\Psi}_m)(R\phi+1 - R\phi)\ \Delta z\ (\Psi_{m\phi+1} - \Psi_{m\phi})\Delta t}{((R_{\phi+1}+R_\phi)/2)\phi'} \tag{4}$$

where

$\bar{\Psi}_m$ = weighed average matric potential of the two elements, cm
$R_{\phi+1}$ = outer radius of element i and element i+1, cm
$R\phi$ = inner radius of element i and element i+1, cm
Δz = thickness of the element. cm

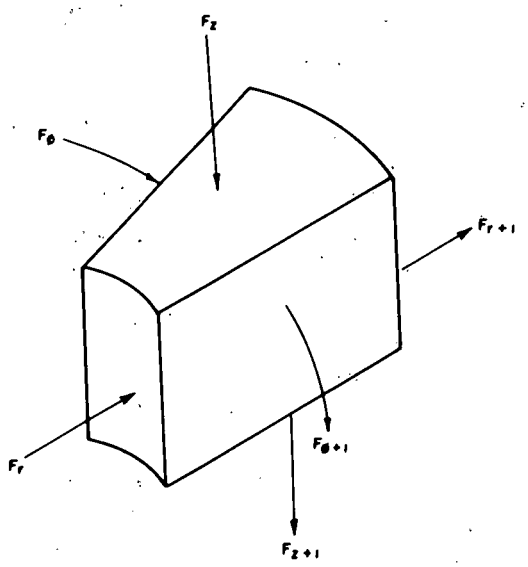


Figure 1. Three-dimensional view of an element with solute flow in the ϕ, r, and z directions.

$\Psi_{m\phi}$ = matric potential of element i, cm
$\Psi_{m\phi+1}$ = matric potential of element i + 1, cm
ϕ' = angular width of the elements, rad
Δt = time step, sec

For vertical flow from element z to element z + 1 the equation would be written as

$$\Delta Q_{z \text{ to } z+1} = \frac{-K(\bar{\Psi}_m)V_z(\Psi_{z+1} - \Psi_z)\,\Delta t}{(\Delta z)^2} \qquad (5)$$

where

V_z = volume of element, cm^3
Ψ_z = total potential of element, cm
Ψ_{z+1} = total potential of element, cm

Similar equations can be written for flow to or from each element in the radial direction as $\Delta Q_{r \text{ to } r+1}$.

The net flow for a given element can be expressed as

$$\text{Net flow} = \Delta Q_{\phi+1} - \Delta Q_\phi + \Delta Q_{r+1} - \Delta Q_r + Q_{z+1} - \Delta Q_z \pm IC \qquad (6)$$

where

$\Delta Q_{\phi+1}$ = volume of flow out of the element in the counter-clockwise ϕ direction
ΔQ_ϕ = volume of flow into the element in the counter-clockwise ϕ direction
ΔQ_{r+1} = volume of flow out of the element in the outward radial direction
ΔQ_r = volume of flow into the element in the outward radial direction
ΔQ_{z+1} = volume of flow out of the element in the downward vertical direction
ΔQ_z = volume of flow into the element in the downward vertical direction
IC = boundary conditions of flow into or out of the element

The change of storage in the element is

$$\text{change in storage} = V(\phi,r,z)\quad \Delta\theta(\phi,r,z) \qquad (7)$$

where

$V(\phi,r,z)$ = element volume, cm^3

$\Delta\theta(\phi,r,z)$ = change in moisture content of element

Employing the conservation of mass principle, the net flow must equal the change in storage. Thus the change in moisture content can be calculated from

$$\Delta\theta(\phi,r,z) = \frac{\Delta Q_{\phi+1} - \Delta Q_{\phi} + \Delta Q_{r+1} - \Delta Q_{r} + \Delta Q_{z+1} - \Delta Q_{z} \pm IC}{V(\phi,r,z)} \quad (8)$$

The moisture content of the element for the next time step can be determined from

$$\theta(\phi,r,z,t) = \theta(\phi,r,z,t-1) + \Delta\theta(\phi,r,z) \quad (9)$$

The moisture content of the element at time t-1 is obtained from the moisture characteristic curve (θ vs Ψ_m) which relates the moisture content and the matric potential in the media. After calculating the moisture content of the element for the next time step, t, the matric potential for the element at time is calculated, again using the media's characteristic curve.

This process is repeated for all the elements in the model. When the calculation of the matric potentials for the next time step are completed, the time is incremented and the process repeated. This cycle continues until an equilibrium is established, i.e. a steady-state flow condition exists in the model. Once the matric potentials of each element are determined for equilibrium flow, the Darcy velocity, moisture content, and average linear velocity of flow are known.

Solute Flow

Solute flow through the column can be calculated if the solute is assumed to be non-reactive. An explicit method similar to that used for the water flow calculation can be developed. A three-dimensional view of an element is shown in Figure 1. The mass of solute per unit time per unit cross-sectional area entering the element is

$$F_{\phi}A_{\phi} + F_{r}A_{r} + F_{z}A_{z}$$

where

A_i = cross-sectional area perpendicular to solute flow in the i direction

The solute flow out of the element would be

$$F_{\phi+1}\,A_{\phi+1} + F_{r+1}\,A_{r+1} + F_{z+1}\,A_{z+1}$$

The matric and gravitational potentials at equilibrium flow are first calculated using the water flow model described above. Initially all dispersion was assumed to be due to longitudinal dispersion. It was further assumed that the longitudinal dispersion is independent of direction and moisture content. However, the value for the dispersion coefficient may vary between different elements. The net solute flow per unit cross-sectional area per unit time is

$$F_{total} = \left\{ \left[v(\phi+1,r,z)C(\phi+1,r,z) - D_{ave}\theta_{ave} \frac{C(\phi+1,r,z) - C(\phi,r,z)}{\phi'(R_{inner}+R_{outer})/2} \right] - \left[v(\phi,r,z)C(\phi,r,z) - D_{ave}\theta_{ave} \frac{C(\phi,r,z) - C(\phi-1,r,z)}{\phi'(R_{inner}+R_{outer})/2} \right] \right\} (R_{outer}-R_{inner})\Delta z$$

$$+\left\{\left[v(\phi,r+1,z)C(\phi,r+1,z)-D_{ave}\theta_{ave}\frac{C(\phi,r+1,z)-C(\phi,r,z)}{(R_{outer+1}-R_{inner})/2}\right]\phi' R_{outer}\Delta z\right.$$

$$\left.-\left[v(\phi,r,z)C(\phi,r,z)-D_{ave}\theta_{ave}\frac{C(\phi,r,z)-C(\phi,r-1,z)}{(R_{outer}-R_{inner-1})/2}\right]\phi' R_{inner}\Delta z\right\}$$

$$+\left\{\left[v(\phi,r,z+1)C(\phi,r,z+1)-D_{ave}\theta_{ave}\frac{C(\phi,r,z+1)-C(\phi,r,z)}{\Delta z}\right]\right.$$

$$\left.-\left[v(\phi,r,z-1)C(\phi,r,z-1)-D_{ave}\theta_{ave}\frac{C(\phi,r,z)-C(\phi,r,z-1)}{\Delta z}\right]\right\}\frac{V(\phi,r,z)}{\Delta z}\pm F_{IC}$$

where

F_{total} = total solute flow per unit time per area, gm/cm^2-sec
$v(\phi,r,z)$ = velocity in the element, cm/sec
$C(\phi,r,z)$ = concentration of the element, gm/cm^3
D_{ave} = average dispersion coefficient of the two elements where flow is occurring, cm^2/sec
θ_{ave} = average moisture content of the elements where flow is occurring
R_{inner} = inner radius of the element, cm
R_{outer} = outer radius of the element, cm
ϕ' = angular width of the element, rad
Δz = vertical depth increment, cm
F_{IC} = flow of solute into the element by initial or boundary conditions
$V(\phi,r,z)$ = volume of the element, cm^3

Flow in a clockwise, radially outward, or vertically downward direction is considered to be out of the element. The change in solute concentration in the element (ϕ,r,z) can be written as

$$\Delta C(\phi,r,z) = \frac{F_{total}\ \Delta t}{V(\phi,r,z)\ \theta(\phi,r,z)}$$

where

$\Delta C(\phi,r,z)$ = change in solute concentration

The solute concentration for the next time step is equal to the concentration for the current time step plus the change in concentration, or

$$C(\phi,r,z,t) = C(\phi,r,z,t-1) + \Delta C(\phi,r,z)$$

This calculation is repeated for all elements at each time increment, giving the solute concentration as a function of space and time.

After the model has been debugged and tested, improvements will be made in the calculation of the average metric potential and average dispersion coefficient. The model will permit calculation of solute breakthrough curves for many different nonhomogeneous column packings. The model will be benchmarked with the breakthrough curves obtained from the experimental system.

APPARATUS AND PROCEDURE

An experimental soil system was developed to generate structured breakthrough curves caused by various media nonhomogeneities. The experimental setup is shown in Figure 2. The soil column was constructed by welding a steel plate on the bottom of a piece of 0.91-m diameter corrugated steel pipe 1.52 m in length. Holes, 0.64 cm in diameter, were drilled on 30° centers around the bottom of the column. A water reservoir was formed by setting the column in a 30.5-cm deep pan 122 cm in diameter. A Tygon tube was placed vertically along

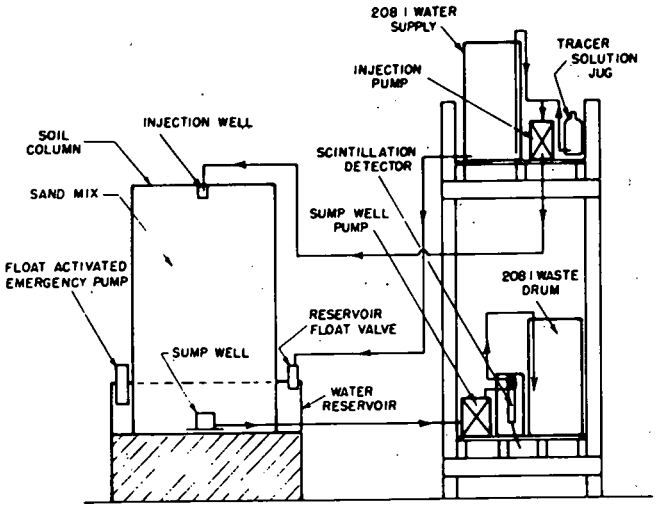


Figure 2. Experimental set-up of soil column system.

the column and enters the column at the bottom to indicate the elevation of the saturated zone. After attaching a sump well (7.6 cm in diameter x 10.2 cm high) to the inside center of the bottom, mortar sand was packed in the column to a bulk density of 1.73 gm/cm^3. The sand was chosen for its availability and rapid hydraulic conductivity which decreases in the amount of time required for each experimental run.

An 10.7-cm long by 2.54-cm diameter injection well was inserted flush with the soil surface. A finger pump maintains a 100 ml/min flow of tap water from a 208-L water supply. A pulse tracer injection can be bled into the suction side of the water supply line without disrupting the water flow. Water from the 208-L supply is fed through a float valve to the reservoir at the bottom of the column to maintain a constant water level in the reservoir.

A second pump draws water from the sump well at the column bottom, past a scintillation detector into a second storage drum. The counts over each 60-sec interval are stored in a 8100 channel Tracor Northern Multichannel Scaler permitting continuous monitoring of the tracer activity during a 64-hour run. At the conclusion of the run, data can be displayed graphically on a CRT, printed on paper or punched on paper tape for subsequent computer analysis.

Initially, the 0.64-cm holes around the bottom of the column were plugged to eliminate flow from the reservoir into the bottom of the column. The value of the 208-L supply was closed, and thus, the reservoir remained dry. The only input into the column was the injection well. The sand was initially homogeneous; no layering or other nonhomogeneities were intentionally introduced into the column. Local tap water was introduced into the injection well until the water level at the bottom of the column reached a depth of 30 cm when the sump well pump was turned on at approximately the same flow rate as the injection well pump. The column was maintained in this condition over a period of 12 to 24 hours.

When the column had reached flow equilibrium, tap water tagged with radioactive bromine-82 tracer (half-life of 35.4 hours) was introduced into the shallow injection well. Thus there was infiltration of the tagged water into the top of the column at the injection well and a drawdown of the water table in the lower section of the column. After the tracer spike had been introduced, injection of non-tagged tap water into the injection well continued. This drives the system and maintains an established flow pattern. The outflow from the sump well was ıtinuously monitored for the activity of the bromine-82 tracer.

EXPERIMENTAL RESULTS

The breakthrough curve obtained from the homogeneous sand column is shown in Figure 3. The single peak implies no layering or channeling was introduced into the column during packing. The rapid rise in activity and subsequent fall off is similar to breakthrough curves obtained in smaller laboratory test columns using mortar sand. The width of the peak implies that the tracer remained essentially as a slug, undergoing only a small amount of dispersion.

After the initial homogeneous column run, a nonhomogeneity consisting of a closed cylinder 7.6 cm in diameter and 63.5 cm in length, made from aluminum screen and covered with cheese cloth inserted vertically 13 cm directly below the injection well. The resulting breakthrough curve is shown in Figure 4. The peak indicated that solute flow was not affected by the cylinder. Water flow probably did not enter the cylinder because the surrounding sand was not saturated. The curve is almost identical in shape to the curve obtained from the homogeneous column, Figure 3.

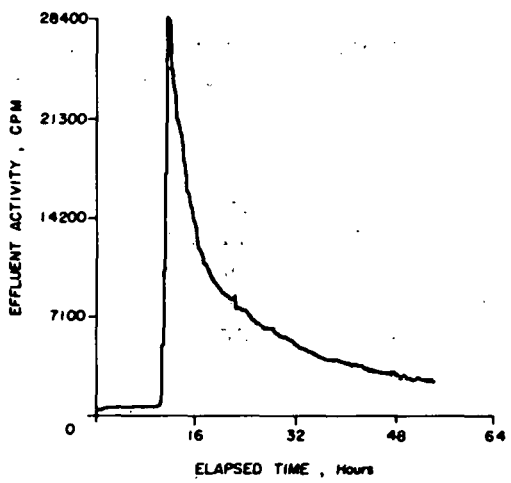


Figure 3. Breakthrough curve obtained with homogeneous packing of sand column.

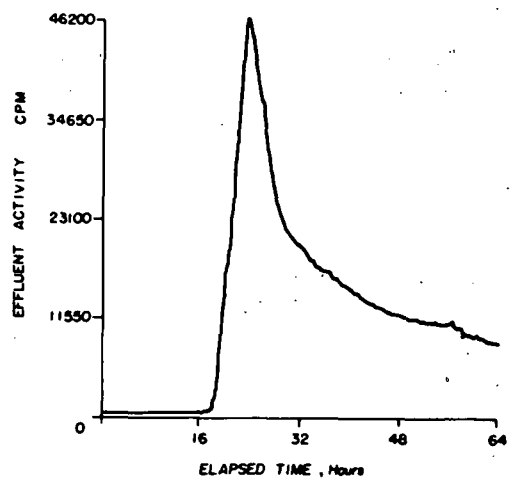


Figure 4. Breakthrough curve obtained with cylindrical nonhomogeneity introduced 12.7 cm below injection well in sand column.

To force the water flow through both the cylinder and the homogeneous sand, a perched water table was created above the cylinder by the addition of a circular plastic sheet 30.5 cm in diameter with a 5 cm hole and was placed directly on top of the cylindrical nonhomogeneity in a concave shape. The perched water table drained directly into the cylinder which created a shorter path to the sump well, while some of the water flowed through the homogeneous sand (a longer path). This resulted in a multi-peaked breakthrough curve shown in Figure 5.

SUMMARY

Recent field studies indicate tracer breakthrough curves exhibit structures which may be caused by nonhomogeneities present in the porous media. This structure should provide a direct method of determining some of the geohydrologic

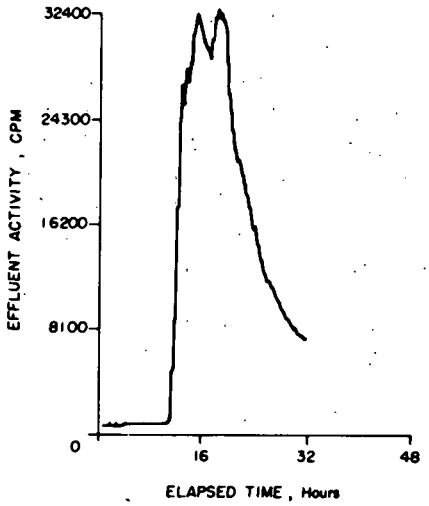


Figure 5. Breakthrough curve obtained with perching layer and cylindrical nonhomogeneity introduced 12.7 cm below injection well in sand column.

properties of a potential disposal site. An experimental system has been constructed which simulates the hydraulic conditions which could exist at a disposal site. A mathematical model of the experimental soil column has also been developed to aid in analysis of curves obtained in the experimental study and to generate additional breakthrough curves. A nonhomogeneity was introduced in the column. The structure of the resulting breakthrough curve indicated multi-peaking.

REFERENCES

Duguid, J. and Reeves, M. "Material Transport Through Porous Media: A Finite Element Galerkin Model." ORNL-4928, Oak Ridge National Laboratory, Oak Ridge, Tennessee, 1976.

Freeze, R. A. and Cherry, J. A. Groundwater. Englewood Cliffs: Prentice Hall, 1979.

Haaser, F. G.; Jester, W. A.; Heald, W. R.; Rogowski, A. S.; and Pionke, H. B. "Use of Neutron Activatable Tracers for Simulating Water and Chemical Flow Through Porous Media." The Pa. State Univ. Institute for Research on Land and Water Resources, 1978.

Hackenberry, P. S.; Nork, W. E.; and Essington, E. H. "Determination of a Coefficient of Dispersion Under Field Conditions Interim Report." NVO-1229-178, Teledyne Isotopes Nevada Operations, Las Vegas, Nevada, October 1971.

Jester, W. A. and Uhler, K. A. "Identification and Evaluation of Water Tracers Amenable to Post-Sampling Neutron Activation Analysis." Research Public. No. 85, The Pa. State Univ. Institute for Research on Land and Water Resources, 1974.

Levy, H. B. "On Evaluating the Hazards of Groundwater Contamination by Radioactivity from an Underground Nuclear Explosion." UCRL-51278, Lawrence Livermore Laboratory, Livermore, California, 1972.

Osmin, W. L. "Groundwater Tracing with Post-Sampling Activation Analysis Using Bromide and Iodide Ions Injected Simultaneously into a Shallow-Well System." M.S. Thesis, The Pa. State Univ., University Park, Pennsylvania, 1977.

Pall, R; Jarrett, A. R.; and Morrow, C. T. "A Simple Finite Element Method of Infiltration." Paper presented at the Summer 1978 American Society of Agricultural Engineers Meeting, Utah State University, Logan, Utah, June 1978.

Pall, R.; Jarrett, A. R.; and Morrow, C. T. "Explicit Numerical Method of Infiltration for Layered Soils." Paper presented at the Summer 1978 American Society of Agricultural Engineers and Canadian Society of Agricultural Engineers Meeting, University of Manitoba, Winnipeg, Canada, June 1979.

Pall, R.; Jarrett, A. R.; and Morrow, C. T. "Two-Dimensional Infiltration by an Explicit Method." Paper presented at the Winter 1979 American Society of Agricultural Engineers Meeting, New Orleans, Lousiana, December 1979.

Papadopulous, S. S. and Winograd, I. J. "Storage of Low-Level Radioactive Wastes in the Ground: Hydrogeologic and Hydrochemical Factors." EPA-520/3-74-009, 1974.

Schmotzer, J. K. "Ground Water Tracing with Post Sampling Activation Analysis." M.S. Thesis, The Pa. State Univ., University Park, Pennsylvania, 1970.

Segol, G. "A Three-Dimensional Galerkin Finite Element Model for the Analysis of Contaminant Transport in Variably Saturated Porous Media. User's Guide." PG-291 326, Waterloo University, Toronto, Canada, June 1976.

New Developments in the Use of Stable Activable Tracers in Environmental Science*

W. Loveland, K. Keasler, L. Ghannam and A. Borovik
Dept. of Chemistry, Oregon State University
Corvallis, OR 97331

ABSTRACT

Recent developments in the use of stable activable tracers(SATs) in environmental science are reported. (A stable activable tracer is a stable material injected into a system under study and whose concentration is measured by post-sampling activation analysis.)The activable nuclear parts of the tracers studied have been rare earth nuclides with short-lived activation products or Cu. To trace the fate of fluid-bound pollutants(and/or water masses) in marine waters, we have used anionic DTPA complexes of the rare earths. These tracers were shown to be stable (80-90% nondissociated) in extensive laboratory tests involving solutions of the tracer in estuarine water including large amounts of marine sediments. Results of a field study in which the flushing time and other hydrological characteristics of an estuarine marina were measured by simultaneously using a fluorescent dye and a SAT are presented. To trace the path of potentially toxic organic molecules, three stable activable tracers, dysprosium(III)-trisacetylacetonate ($Dy(acac)_3 \cdot 3H_2O$), dysprosium(III)-trisdibenzoylmethane($Dy(dbm)_3 \cdot H_2O$) and copper oxinate $Cu(C_9H_6ON)_2$ were synthesized. Their octanol/water partition coefficients and their solubility in water were measured and used to correlate the tracer species and its biological activity with that of known toxic materials. In a project to demonstrate the simple use of SATs to trace the origin of common insecticides and herbicides, seven common insecticides and herbicides were marked with anionic rare earth DTPA complexes and shown to be detectable at dilutions of 1 part in 10^{12}. Two arsenical herbicides were chosen for further study and the tracer/herbicide ratio was shown to remain constant in samples of herbicide material collected on plant surfaces and runoff waters in the environment for long periods.

I. Introduction

A survey of the history of environmental science will show that tracers are important tools for the environmental scientist. They have been used in efforts to measure flow rates and dispersion coefficients, to follow the movement of materials through the atmosphere, hydrosphere, and biosphere and to characterize pollutant sources. Three principal types of tracer have been used in environmental science; (a) chemical tracers, such as NaCl, $KHSO_4$, K_2CO_3,etc. (b) radioactive tracers, such as ^{3}H, ^{32}P, ^{82}Br,etc. and (c) fluorescent dyes, such as fluorescein, Rhodamine B, Rhodamine WT, etc. Use of each of these tracer types has been beset by certain problems. The chemical tracers are difficult to detect except in the highest concentrations whereupon their use leads to a modification of the system under study. The uncontrolled use in the environment of the radiotracers poses real or imagined safety problems (with their associated delays) and in the case of short-lived radionuclides, the duration of the experiment is limited by the tracer half-life. The use of fluorescent dyes may lead to aesthetically objectionable modifications of water or air color("the red-tide syndrome"), and significant alterations

of the tracer concentrations by photochemical decay. In general, the dyes are inapplicable in highly colored media.

To overcome many of these problems and to open new possibilities of tracer use for the environmental scientist, there has been renewed interest in developing stable activable tracer technologies that will be attractive alternatives to conventional tracers.

A stable activable tracer (SAT) is a stable material that is injected into a system under study and whose concentration in the system is measured by post-sampling activation analysis. One may inquire as to the advantages of such "artificial" tracers as compared to the "naturally occurring" trace elements in various systems that act as "natural" tracers. The artificial tracer has the advantages of having a controlled emission rate (either pulse or continuous injection) and control of the amount injected, both of which are valuable in model verification studies. Artificial tracers can be injected in amounts sufficient to insure easy detection in the system under study and lend themselves better to simultaneous tracing of several similar pollutant sources.

What advantages do stable activable tracers possess in general or when compared, in specific situations to fluorescent dyes, radiotracers or conventional chemical tracers? The advantages are: (1) The tracers are non-toxic[1,2,3] at concentrations encountered in environmental studies. (2) The detection sensitivity of these tracers is very good. For example, for Dy, one can readily detect amounts of 10^{-12} g. This allows pollutant tracing over very long distances. Stable activable tracers can be chosen such that their naturally occurring concentrations are very small. (3) The tracers can be bound as EDTA or DTPA complexes and thus not suffer any adsorption by sediments,etc. (4) The detection of these tracers is not affected by the presence of water color or the occurrence of photochemical or radioactive decay of the tracer. (5) According to our estimates[4], the rare earth stable activable tracers are cost competitive with the use of radiotracers and fluorescent dyes. (6) Effluents from specific pollutant sources can be marked with a given "fingerprint" (fixed ratio of tracer elements) and the effluent from several sources traced simultaneously. By the careful selection of the elements and their ratio used in any one "fingerprint", results can be obtained that can be analyzed in one day or less in the laboratory. This avoids the traditional problem of activation analysis-based methods, i.e., one of long analysis times.

Because of these advantages, stable activable tracers have been used widely in the environmental sciences in recent years. They have been used to track the movements of pollutants in river systems,[5] to monitor ground water flow[6], to measure the movement of oily waste[7], to measure dispersion of materials in the atmosphere[8,9], to study precipitation scavenging[10], and in a wide variety of industrial applications.[11] In all these applications, the SAT was used to mimic the physical behavior of materials in the environment (aerosols,rainwater, etc.)wherein the segments of the environment being measured were easily ameniable to activation analysis.

In this paper, we report the application of stable activable tracers in three new applications; (a) the tracing of fluid bound pollutants in marine waters (b) the tracing of environmentally significant organic molecules (c) the simple tracing of herbicides. In all of these applications, we emphasize the central issues in the use of SATs, i.e., the verification of tracer stability and its conservative nature and the determination of the chemical and physical properties of the tracer to verify its expected environmental behavior. In addition, we report the extension of SAT usage to media not readily ameniable to activation analysis and report the use of SATs to mimic the chemical and biological behavior of materials in the environment.

II. Tracing of Fluid-Bound Pollutants in Marine Waters

Following the pioneering work of Channell and Kruger[12] and extending our own work in fresh water systems[4], we undertook to develop appropriate

SATs for tracing fluid bound pollutants in marine waters. Based upon the previous work[4], we chose anionic DTPA complexes of the rare earths as the SATs for fluid bound pollutants.

To collect the tracer from seawater it was coprecipitated with the mixed hydroxides and carbonates of Mg and Ca. This was accomplished by adding NaOH to seawater. We found that 99% of the tracer is collected when the pH of the solution is raised to 13 or greater. However, in river water or less saline estuarine water, there is not enough material present to co-precipitate the tracer successfully (collection efficiency at pH 13 is only 39%). This difficulty was overcome by adding a different poorly activable rare earth carrier (Pr) to the solution for these cases. Following activation, it was necessary to chemically separate the coprecipitated rare earths from any residual contamination. To test the stability of these tracers in the marine environment, CeDTPA complexes were added to Yaquina Bay,Oregon estuarine water in a series of laboratory experiments. The solutions contained 4.8ug of Ce, 15g of dry Yaquina Bay sediment and 100ml of estuarine water. The solutions were agitated at a constant temperature of 10°C for periods up to 22 days. Samples were withdrawn from the solutions each day and their Ce content measured. Control experiments were performed under similar conditions using uncomplexed Ce. The results (see Figure 1) show that the CeDTPA complex remains 80-90% nondissociated and soluble in Yaquina Bay water containing sediments with the amount of uncomplexed tracer in solution dropping to 7% of its original value within 2 days.

To test the performance of these tracers in the field, a study was made of the hydraulic characteristics (and related water quality) of a small boat marina located in a marine estuary, Yaquina Bay, Oregon. Yaquina Bay is located at Newport, Oregon; the boat basin is located on the south side of the entrance channel to the Yaquina estuary, as shown in Figure 2. The tidal prism of the estuary inland from the marina is 10^9 ft^3.(Ref. 13) The entrance to the marina is directly off the main channel, so that the entire tidal prism flows by and has a strong influence on the hydraulic parameters in the basin. To study the flushing characteristics of this basin, a known conservative tracer, Rhodamine B, and a stable activable tracer, Dy(DTPA) were injected into the marina and the flushing of these tracers was followed for several tidal cycles.

If C_0=initial spatial average tracer concentration and C_i the average tracer concentration after i tidal cycles, we define the fraction exchanged per cycle,E, as

$$E = 1 - (C_i/C_0)^{1/i}$$

Isolines of equal exchange coefficient for this marina are shown in Figure 3. In general, the flushing of the marina seems adequate. The changes in C_i/C_0 as a function of time tend to agree with a simple box model of the estuary. While further field studies of this tracer are planned, we feel that the potential usefulness of the tracer has been established.

III. Tracing Environmentally Significant Organic Molecules

The current emphasis on the environmental impact of agricultural and industrial organic chemicals has resulted in a need to assess their physical and chemical behavior in the environment. Often, the need for such an assessment may pose problems because of the extreme toxicity of the chemical in question, a fact which hampers widespread field experiments with these chemicals. We report the use and testing of stable activable tracers which are not toxic at the concentrations used in field experiments, to mimic the physical and chemical behavior of toxic, biologically significant molecules in the environment.

In choosing the tracer species, we have relied on the fact that the n-octanol/water partition coefficients and solubility in water of substances

have proven useful[14-17] as a means to predict soil adsorption, biological uptake, lipophilic storage and biomagnification of a wide variety of chemicals including aliphatic and aromatic hydrocarbons, aromatic acids, organochlorine and organophosphate pesticides. Thus, our general plan is to obtain or synthesize metal chelates whose central metal atom is easily detectable using neutron activation analysis and to compare the n-octanol/water partition coefficient and solubility in water for these species with known values of these quantities for environmentally significant organic molecules.

Three such stable activable tracers, dysprosium (III)-trisacetylacetonate ($Dy(acac)_3 \cdot 3H_2O$), dysprosium(III) trisdibenzoylmethane ($Dy(dbm)_3 \cdot H_2O$) and copper oxinate $Cu(C_9H_6ON)_2$ have been prepared[18-21] and their n-octanol/water partition coefficients and their solubility in water have been measured.

The results of this measurement for the copper oxinate and $Dy(dbm)_3 \cdot H_2O$ tracers are shown in Table I along with known values[15] of these quantities for environmentally significant organic molecules. Upon examination of the data in Table I, one can see that the solubility of copper oxinate in water is similar to the organophosphorus insectides Methyl Pirimiphos and Phosalone. The value of its n-octanol/water partition coefficient, P, is depressed relative to the known systematics of these values[15]. However, recent semiempirical considerations[22] have indicated that this depression in the value of log P is to be expected due to the presence of the metal atom in the complex compared to the pure organic compounds. Since biological uptake, lipophilic storage, etc., are most closely related to solubility[15], we believe that copper oxinate should behave like Methyl Pirimiphos in the environment. Reasoning in a similar manner for the organodysprosium compounds would suggest their analogs to be lower chlorinated pesticides.

In order to test this equivalence and the overall conservative properties of the tracer, certain laboratory tests have been made to study the behavior of these tracers in the marine environment. Using copper oxinate as a model tracer, the stability of the tracer in seawater was measured by mixing known concentrations (ppm) of the tracer material in contact with seawater for period of up to seven days, withdrawing samples periodically and measuring tracer loss or decomposition as a function of time. The separation of the tracer metal chelate from seawater was done using a solvent extraction involving n-octanol. (only the chelated tracer (and not the Cu ions) are soluble in n-octanol). This separation also eliminates Na and Cl from the tracer sample, a fact which aids in the activation analysis of the tracer. The tracer abundances were measured by instrumental neutron activation analysis involving coincidence counting of the annihiliation radiation from the decay of 12.8 hour ^{64}Cu. The concentration of tracer remaining in solution after seven days was 90% of the initial tracer concentration.

The adsorption properties of the copper oxinate tracer in sediments were also measured, in particular, the relative adsorption of the tracer into the wnterstitial water and solid matrix.

Bioaccumulation of the tracer and its toxic organic analog, Methyl Pirimiphos, was tested using oysters as a model system. (The copper is not toxic to oysters in its chelated form.) Oysters are being exposed to a range of copper oxinate concentrations (ppb-ppm) over a period of 1-7 days. After sacrificing the oysters, the Cu concentrations in the gills and digestive system are measured. Preliminary results support the Methyl Pirimiphos-copper oxinate equivalence.

IV. Quick and Dirty Herbicide Tracing

In addition to the orderly development described in Section III of tracers for environmentally significant organic molecules, the current controversies concerning the dispersal of herbicides used in forestry have demanded the immediate implementation of tracer techniques to be used in connection with herbicide dispersal. This development caused us to develop a "quick and dirty" tracer technology to meet this demand. The success of our effort has certain consequences concerning strategies for monitoring herbicide dispersal and

Table I

n-Octanol/Water Partition Coefficient(P) and Solubility(S) of Organic Molecules

Compound	log S (S(umole/l))	log P
Benzene	4.02	2.13
Toluene	3.71	2.69
Fluorobenzene	4.21	2.27
Chlorobenzene	3.60	2.84
Bromobenzene	3.45	2.99
Iodobenzene	3.22	3.25
p-Dichlorobenzene	2.73	3.38
Naphthalene	2.36	3.37
Diphenylether	2.05	4.20
Chloroform	5.20	1.97
Carbon Tetrachloride	4.72	2.64
2,4,5,2',5' PCB	-1.51	6.11
2,4,5,2',4',5' PCB	-2.59	6.72
4,4' PCB	-0.56	5.58
Malathion	2.64	2.89
Fenitrothion	1.92	3.38
Dicapthon	1.22	3.58
Parathion	1.85	3.81
Dichlorofenthion	-0.11	5.14
Methyl Parathion	5.42	2.04
Pentachlorophenol	5.42	5.01
Copper Oxinate	1.03	2.70
$Dy(dbm)_3 \cdot H_2O$	0.60	1.59
Methyl Pirimiphos	1.05	4.25
Phosalone	0.95	4.30

establishing legal responsibility for its consequences.

The activable tracer used to monitor herbicide dispersal was Dy(DTPA). In an initial test, seven common herbicides and insecticides were purchased, prepared in their recommended concentrations and spiked with 150 ug/l tracer. The products involved were: (a)a 20.2% solution of monosodium acid methane-arsonate (b) sodium cacodylate(1.98%) ,(c) amitrole(21.1%),(d) prometone(3.3%), (e) 2,4,-D(6.3%) (f)carbaryl(23.4%),(g) malathion(50.0%),(h)diazinon(12.5%). Instrumental neutron activation analysis of the samples revealed the tracer to be easily detected in the concentrations given above. Two arsenic-based herbicides ((a) and (b)) were chosen for further study and spiked with 150ng/l Dy(DTPA). Plots of grass of area 300 ft^2 were treated withthe spiked herbicide in a manner recommended by the manufacturer and grass clippings collected over a one week period. Analysis of the clippings revealed the As/Dy ratio in the clippings remained constant over this period of time, indicating that the tracer and herbicide were behaving similarly. In a second experiment, runoff water from the sprayed grass was collected for over week and analyzed. Once again we found the As/Dy ratio to be constant in the runoff water, with the absolute values indicating 3% removal of the herbicide/tracer by rainwater.

While it is quite true that to trace the movement of the herbicides studied in this work in the environment, one need only measure the As content of the various samples, the results do have potential usefulness in monitoring herbicide dispersal. Quite frequently, the problem is not to establish whether herbicides are present, but to establish who was responsible for the presence of the herbicide. Thus, drawing on this work and previous work involving multiple source tracing in fresh water[4], one should be able to simply mark a given application of herbicide with a unique "fingerprint" of rare earth DTPA tracers (spiking at the levels used herein and with concentrations of the elements in the "fingerprint" differing by a factor of 3).

V. Summary

We have described three applications of stable activable tracers in environmental science and technology. Each example was intended to illustrate a separate aspect of tracer use. The tracing in marine waters shows the details of how such tracers might be employed in a difficult medium, seawater. The tracing of organic molecules is intended to show how tracers can be created to mimic not only the physical behavior of a material in the environment, but also its chemical and biological behavior. Finally, the examples of herbicide tracing are discussed to indicate how quick and dirty application of current technology can lead to the solution of otherwise intractable problems of a controversial legal nature.

References

*This work was supported by the U.S. Department of the Interior through the Water Resources Research Institute at Oregon State University and the OSU Sea Grant College Program of NOAA under Grant No. 04-8-M01-144.

1. T.J. Haley, J. Pharmaceutical Sciences,54,683 (1965)
2. G.C. Kyker,E.A. Cress, A.M.A. Arch. Industr. Health, 16, 475 (1957)
3. J.G. Graca, F.C. Davison,J.B. Feavel, Arch. Environ. Health, 5,437 (1962)
4. S.W.K. Chick and W. Loveland, Nuclear Methods in Environmental and Energy Research, J.R. Vogt,Ed. (CONF-771072) p.233
5. See W. Loveland, Hydrospheric Trace Elements and their Application in Tracing Water Pollutants, Oregon State University Water Resources Research Institute Report WRRI-59 (July,1978) and references cited therein.
6. H. Behrens, H. Moser, and E. Wildner, J. Radioanal. Chem. 38, 491,(1977)
7. D.L. McCown, Water Research, 13, 1065 (1979)
8. H. Nakasa and H. Ohno,in Radioisotope Tracers in Industry and Geophysics (IAEA,Vienna,1967) p.239
9. Y.S.Shum, W. Loveland and E.W. Hewson, J.Air Pollut.Control Assoc.25,1123

10. A.N. Dingle, D.F. Gatz, and J.W. Winchester, J.Appl. Meteor.,8,236(1969)
11. A. Van Dalen and J. Wijkstra, J. Radioanal. Chem. 38,223(1977)
12. J.K. Channell and P. Kruger, Modern Trends in Activation Analysis, NBS, Washington,D.C., 1968
13. C.R. Goodwin, E.W. Emmett, and B. Glenne, Bulletin No. 45, Engineering Experiment Station, Oregon State University, Corvallis,OR, May,1970
14. R.N. Dexter and S.P. Parton, Marine Chemistry, 6,41 (1978)
15. C.T. Chiou, V.H. Freed, D.W. Schemedding, and R.L. Kohnert, Env. Sci. Tech.,11,475 (1977)
16. C. Hansch, Acc. Chem. Res., 2,232 (1969)
17. C. Hansch and T. Fujita, J- Am. Chem. Soc.,86,1616(1964)
18. J.G. Stities, C.N. McCarthy, and L.L. Quill,J. Am. Chem. Soc.,70,3142(1948)
19. G.W. Pope, J.F. Steinbeck, and W.F. Wagner, J. Inorg. Nucl. Chem.,20, 304(1961)
20. R.G. Charles and A. Perrotto, J. Inorg. Nucl. Chem.,26,373(1964)
21. R.E.Whan, and G.E. Crosby, J. Mol. Spectroscopy, 8,315,(1962)
22. C.T. Chiou (private communication)
23. E.P. Richey and N.K.Skjelbreia, Technical Report No. 56, Dept. of Civil Engineering, University of Washington, Seattle, WA, January , 1978.

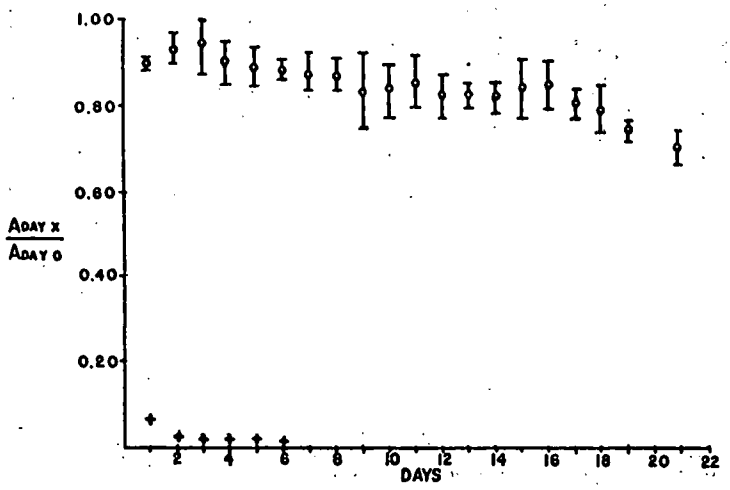


Figure 1. The fraction of the SAT remaining in solution after contact with sediments in estuarine waters. + Ce, o CeDTPA

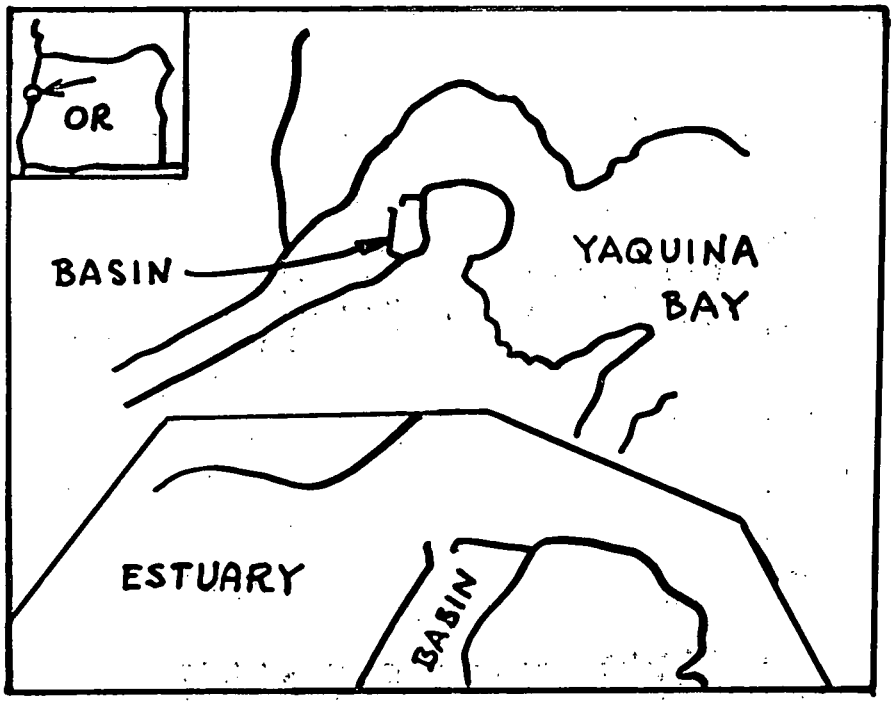


Figure 2. Map showing the location of the Yaquina Bay, Oregon small boat basin studied in this work.

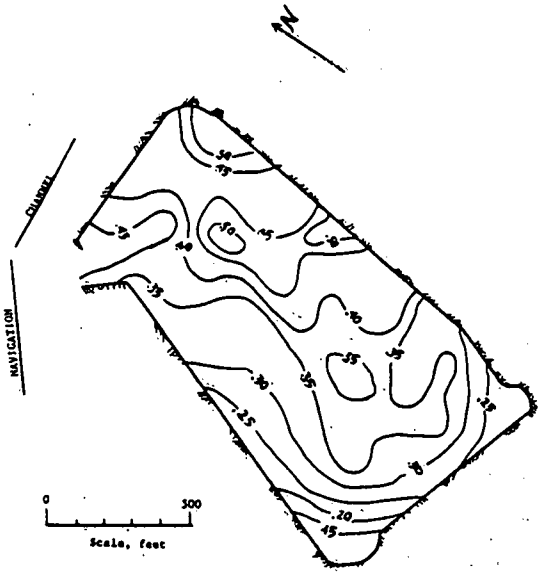


Figure 3. A contour plot of exchange coefficient isolines (6' range) in the Yaquina small boat basin.

Fourth International Conference

on

NUCLEAR METHODS IN ENVIRONMENTAL AND ENERGY RESEARCH

April 14-17, 1980
Columbia, Missouri

LIST OF PARTICIPANTS

AHMAD, AZIDDIN
University of London
Reactor Centre
Silwood Park
Sunninghill, ASCOT SL5 7PY
England

ALGER, DON
Research Reactor
University of Missouri
Columbia, Mo. 65211

ALPERT, DAN J.
214 Nel
University of Illinois
Urbana, IL 61801

ANDERSON, DAVID L.
University of Maryland
Chemistry Department
College Park, MD 20742

ANDERSON, HAROLD
Dept. of Natural Sciences
Stephens College
Columbia, MO 65205

ARAS, XAMIK K.
Dept. of Chemistry
University of Maryland
College Park, MD 20742

AFRAMIN, A.
Atomic Energy Organization
of Iran
Nuclear Research Centre
P.O. Box 3327
Tehran, Iran

BAEDECKER, PHILLIP A.
U.S. Department of Interior
Geological Survey
Mail Stop 924
Reston, VA 22092

BAHRUDIN, Y.B.
PUSPATI, Ministry of Science
Technology & the Environment
No. 4, JALAN 1/3K
Bandar Baru Bangi
Bangi, Selangor,
Malaysia

BAILEY, ALAN
Geology Department
Marshall University
Huntington, W. VA 25701

BAXTER, TERRY
Research Reactor
University of Missouri
Columbia, MO 65211

BEALL, G.W.
Oak Ridge National Laboratory
P.O. Box X
Oak Ridge, TN 37830

BERTHELOT, CHARLES A.
B-2440 Geel
Central Bureau for Nuclear Measurement
Belgium

BIGGIN, H.C.
Sheffield City Polytechnic
Pond St. Sheffield
U.K.

BLOTCKY, ALAN J.
V.A. Medical Center
Medical Research
4101 Woolworth Ave.
Omaha, Neb. 68105

BOULDIN, DENNIS
IBM Corporation
Dept. 326, Bldg. 970
Essex Jct., VT 05452

BRUGGER, ROBERT
Research Reactor
University of Missouri
Columbia, MO 65211

BRUNK, ROBERT
Nuclear Data Inc.
Golf and Meacham Rd.
Schaumburg, IL 60196

CAHILL, RICHARD A.
Ill. State Geological Survey
322 Nat. Research Bldg.
Urbana, IL 61801

CARNI, JAMES
Research Reactor
University of Missouri
Columbia, MO 65211

CAWLEY, CHARLES N.
205 MVR
Cornell University
Ithaca, N.Y. 14850

CEKORICH, A.
NDH Industries
Monrovia, CA 91016

CHATT, A.
Dalhousie University
Trace Analysis Research Center
Chemistry Department
Halifax, N.S.
B34 4J1
Canada

CHICK, STEPHEN W.D.
Kansas Dept. of Health &
Environment
7740 Frobes Bldg.
Topeka, KS 66620

CHRISTENSEN, ERIK R.
University of Wisconsin
Dept. of Civil Engineering
5430 W. Radcliffe Dr.
Milwaukee, WI 53223

COLLINS, THOMAS
University Hall
University of Missouri
Columbia, MO 65211

CROWSON, SANDRA
Willoughby Creek #10
3133 S.E. Indian St.
Sutart, Fla. 33494

de BRUIN, M.
Interuniversity Reactor Institute
Mekelweg 15
Delft
The Netherlands

de LANCEY, KEITH
University of California-
Irvine
Chemistry Department
30801 S. Coast Highway #556
Laguna Beach, CA 92651

DEICH, HERBERT
NDH Industries
426 Duarte Rd.
Monrovia, CA 91016

DYBCZNSKI, RAJMUND
IAEA
Vienna International Center
Karntner Ring 11,
P.O. Box 590
Uno City, Vienna, Austria

EDEN, YEHUDA
University of California-
Irvine
127 Pergola
Irvine, CA 92715

EHMANN, WILLIAM D.
Department of Chemistry
University of Kentucky
Lexington, Kentucky 40506

ELLIS, KATHERINE
Bedford Instit. of Ocean.
Dartmouth, Nova Scotia
Canada

EMERY, JUEL F.
Oak Ridge National Lab.
Oak Ridge, TN 37830

EMMONS, ARDATH
Nuclear Engineering
University of Missouri
Columbia, MO 65211

ERNST, PETER
McMaster University
Hamilton, Ontario
Canada L85 4K1

ETTINGER, K.V.
Dept. of BioMedical Physics
University of Aberdeen,
Foresterhill, Berdeen
AB9 2ZD, Scotland
U.K.

FANGER, HANS-ULRICH
Jahnstr 8, D-2057 Reinbek,
F.R. Germany

FENZL, FRIEDRICH
DWK
Buntewegz D-300
Hanover, West Germany

FILBY, ROYSTON
Nuclear Radiation Center
Washington State University
Pullman, WA 99163

FROST, JOYCE K.
320 Natural Resources Bldg.
Illinois Geological Survey
Urbana, IL 61801

GLASCOCK, MICHAEL
Research Reactor
University of Missouri
Columbia, MO 65211

GOEDERS, MINA NASSIRI
5615 Verano Place
Irvine, CA 92715

GORDON, BARRY M.
Brookhaven National Laboratory
Upton, N.Y. 11973

GORDON, GLEN E.
Department of Chemistry
University of Maryland
College Park, MD 20742

GRAHAM, CHRISTOPHER
Research Reactor
University of Missouri
Columbia, MO 65211

GRASS, FRIEDRICH
A-1020 Schuttelstr
115 Vienna, Austria

GREV, DENNIS M.
Columbia College
Columbia, MO 65216

GRIFFIN, LEONARD H.
Shell Development Co.
P.O. Box 1380
Houston, TX 77001

GUINN, VINCENT P.
Department of Chemisty
University of California-
Irvine
Irvine, CA 92717

HASSAN, AZZAHARI
Washington University
4001 Gravois
St. Louis, MO 63130

HENKELMANN, RICHARD
Technische Universitat Munchen
Institut Fur Radiochemie
D 8046 Garching
West Germany

HOFSTETTER, K.J.
Allied General Nuclear Services
P.O. Box 847
Barnell, S.C. 29812

HOPKE, PHILIP
University of Illinois
Environmental Research Lab.
100 W. Western Ave.
Urbana, IL 61801

HOSSAIN, TIM
University of Kentucky
Chemistry Department
Lexington, Kentucky 40506

HUFF, G.G.
Allied General Nuclear Services
P.O. Box 847
Barnwell, S.C. 29812

HUSAIN, JAVED
Physics Department
University of Missouri-Rolla
Rolla, MO 65401

INOUYE, T.
Toshiba R & D Center
Komukai Tashiba-Cho
Saiwai-KU
Kawasaki 210
Japan

IYENGAR, G. VENKATESH
Institute of medicine
Kerivforschungs anlage
D-517
Julich, F.R. Germany

JAMES, WILLIAM D.
Trace Analysis Center
Texas A&M University
College Station, TX 77840

JERVIS, R.E.
University of Toronto
Dept. of Chem. Engineering
Toronto MSS1A4, Canada

JESTER, WILLIAM A.
Breazeal Nuclear Reactor
Pennsylvania State University
University Park, PA 16802

JOSNI, S.R.
National Water Research Instit.
P.O. Box 5050
Burlington, Ontario L7R 4A6,
Canada

KAY, M.A.
Dept. of Chemistry
Reed College
Portland, OR 97202

KELLY, KERRY
Dow Chemical
1602 Bldg.
Midland, MI 48640

KHAJEH-NASSIRI MINA
Department of Chemistry
University of California
Irvine, CA 92717

KHALIL, SAMIR R.
University of Kentucky
Department of Chemistry
Lexington, Kentucky 40506

KNIGHT, H. GENE
NAA Lab. VPI & SU
Blacksburg, VA 24061

KOROTEV, RANDY
Washington University
St. Louis, MO 63130

KORTHOVEN, P.J.M.
Interuniversity Reactor Institute
Mekelwag 15
Delft
The Netherlands

KOSZYKOWSKI, REBECCA
P.O. Box 5507 L-453
Lawrence Livermore Lab.
Livermore, CA 94550

KRSTOFF, LJERKA
Metro Sanitary Dist. of Greater
Chicago
5915 W. Pershing Rd.
Cicero, IL 60650

KUTZMAN, RAYMOND
Brookhaven National Lab.
Medical Department-490
Upton, N.Y. 11973

KUYENDALL, W.E.
Texas A&M University
College Station, TX 77843

LARSEN, INGVAR LAUREN
P.O. Box X
Oak Ridge National Lab.
Oak Ridge, TN 37830

LENIHAN, J.M.A.
West of Scotland Health Boards
Dept. of Clincial Physics
11 W. Graham St.
Glasgow G4 9LA
Scotland

LEPEL, ELWOOD
Physical Sciences Department
P.O. Box 999
Battelle N.W.
Richland, WA 99352

LESLIE, JEANNE C.
University of California-
Irvine
Chemistry Department
Irvine, CA 92717

LINDSTROM, RICHARD
National Bureau of Standards
Analytical Chemistry Division
Reactor Building
Washington, D.C. 20234

LINDSTROM, DAVID J.
Washington University
Dept. of Earth & Planetary Sc.
St. Louis, MO 63130

LOVELAND, WALTER
Oregon State University
Radiation Center
Covallis, OR 97331

LURIE, NORMAN
7650 Convoy Ct.
IRT Corporation
San Diego, CA 92111

LYON, WILLIAM S.
Analytical Chem. Div.
Oak Ridge National Lab.
P.O. Box X
Oak Ridge, TN 37830

MAC MAHON, D.
Silwood Park
Sunninghill
Ascot Berkshire
SL5 7PY, England

MAENHAUT, WILLY
Instituut Nucleaire Wetenschappen
Proeftuinstraat 86
B-9000 Gent, Belgium

MANGELSON, NOLAN F.
Bringham Young University
Provo, Utah 84602

MARSHALL, J.H.
MDH Industries
Monrovia, CA 91016

MAY, MELANIE
Oak Ridge National Lab.
P.O. Box X
Oak Ridge, TN 37830

McKOWN, DAVID M.
U.S. Geological Survey
Denver Federal Center
Denver, CO 80225

McFARLAND, ROBERT H.
University of Missouri-Rolla
309 Christy Dr.
Rolla, MO 65401

McDANIEL, DARREL
Nuclear Data, Inc.
Golf & Meacham Rds.
Schaumburg, IL 60196

MELONI, SANDRO
Laboratorio de Radiochimica
Instituto di Chimica Generale
Universita di Pavia
27100 Pavia
Italy

MEYER, WALTER
Nuclear Engineering
University of Missouri
Columbia, MO 65211

MEYERS, THOMAS
Nuclear Data, Inc.
Golf & Meacham Rds.
Schaumburg, IL 60196

MICHAELIS, WALFRIED
GKSS Research Center
D-2105 Seevetal 2
Elbring
F.R. Germany

MILLER, GEORGE
Department of Chemistry
University of California
Irvine, CA 92717

MORGAN, GARY
Nuclear Data, Inc.
Golf & Meacham Rds.
Schaumburg, IL 60196

MORGAN, W.D.
Brookhaven National Lab.
Medical Research Center
Upton, N.Y. 11973

MORRIS, J. STEVEN
Research Reactor
University of Missouri
Columbia, MO 65211

NAEUMANN, ROGER
Dept. of Chemistry
University of California-
Irvine
Irvine, CA 92717

NAKAZAWA, LEIKO
4921 Verano Place
Irvine, CA 92715

O'CONNOR, JOHN T.
University of Missouri
Dept. of Civil Engineering
Columbia, MO 65211

PASCHOA, ANSELMO S.
PUC/RJ - Rio De Janeiro
C.P. 38071 - Depto De. Fisica
Rio De Janeiro, R.J.
Brazil 22453

PECEQUILO, BRIGITTE R.S.
Instituto de Pesquisas Energeticas e
Nucleares COURP/AFN
Cx. Postal 11049 - Pinheiros
01000 Sao Paulo, Brazil

PERSSON, GUNNAR
SSI, Natl. Instit. of Rad.
Protection
BOX 60204
S-104 01 Stockholm
Sweden

PHILLIPS, GARY
U.S. Naval Research Lab
Code 6603M
Washington, D.C. 20375

PIMPL, MAX
Kernforschungszentrum
Karlsruhe
Abt. Sicherheit/Radiogekolgie
Box 3640
D-7500 Karlsruhe
West Germany

RAINES, WILLIAM L.
Tennessee Valley Authority
R.O.B.
Muscle Shoals, AL 35660

REINGROVER, SCOTT W.
University of Maryland
Chemistry Department
College Park, MD 20742

RIGOT, WARD
University of Michigan
3104 Phoenix Memorial Lab.
Ann Arbor, MI 48109

RIGGS, CHARLES
Rockwell International
Rocky Flats Plant
P.O. Box 464
Golden, CO 80401

ROSCOE, BRADLEY A.
University of Illinois
110 E. Michigan Ave.
Urbana, IL 61801

SALGETTI, FAUSTO
CISE
P.O. Box 3986
20100 Milano
Italy

SCHLEGEL, STEVE
Research Reactor
University of Missouri
Columbia, MO 65211

SCHLYER, DAVID
Bldg. 555A
Brookhaven National Laboratory
Upton, N.Y. 11973

SCHMITT, BERNHARD F.
Bundesanstalt fur Materialpruefung
Unter den Eichen 87
D 1000 Berlin 45
F.R. Germany

SCHNEIDER, ERIC
General Motors Research Lab
Warren, MI 48090

SCHNIER, CHRISTIAN
GKSS Forschungszentrum
Reaktor Str. 4
D2054 Geesthact
West Germany

SHAH, P.K.
15E, Jaybharat Society
111 RD Road, Khar
Bombay--400052
India

SINGH, JAG J.
NASA
Mail Stop-235
Langley Research Center
Hampton, VT 23665

SIVYER, A.
Dept. of Medical Physics
Singleton Hospital
Swansea SA2 8OA
Wales, U.K.

SOWERBY, B.D.
Australian Atomic Energy Comm.
Research Estab.
Private Mail Bag
Sutherland, N.S.W. 2232
Australia

SPATE, VICKIE
Research Reactor
University of Missouri
Columbia, MO 65211

SPYROU, NICHOLAS M.
Medical & Environmental Physics
Group
Department of Physics, University
of Surrey
Guildford, Surrey
England GU25XH

STEINNES, EILIV
University of Trondheim
7055 Dragvoll
Norway

STOKELY, JAMES R.
Oak Ridge National Lab.
P.O. Box X
Oak Ridge, TN 37830

STRAUSS, MICHAEL G.
Argonne National Lab.
9700 S. Cass Ave. Bldg. 818
Argonne, IL 60439

STROUBE, WILLIAM B.
Food & Drug Admin.
200 "C" St., S.W.
Washington, D.C. 20204

SUZUKI, NOBUO
Tohoku University
Dept. of Chemistry
Faculty of Science
Sendai 980, Japan

TAKEDA, YASUSHI F.
Tohoku University
Aramaki-aza-Aoba
Sendai, Japan

TERAI, MINORU
Tokyo Metro. University
2-1-1 Fukazawa, Setagaya, Tokyp
Japan 158

THOMPSON, JOSEPH L.
Los Alamos Scientific Lab.
1642 Monte Vista Dr.
Pocatello, ID 83201

TROUTNER, DAVID
Department of Chemistry
University of Missouri
Columbia, MO 65211

TUREL, MRS. Z.R.
Institute of Science
15 Madame, Cama Rd.
Bombay, India

VALENTE, I.
University of London
Westfield College
Kidelspire Ave.
London, England

VAN DE STEEG, G.E.
Kerr-McGee Corp.
P.O. Box 25861
Oklahoma City, OK 73120

VARTSKY, DAVID
Brookhaven National Lab.
Medical Research Center
Upton, N.Y. 11973

VAN DER SLOOT, HANS A.
Energy Research Foundation Netherlands
P.O. Box 1
The Netherlands

VOGT, CORA
Environmental Trace Substances
University of Missouri
Columbia, MO 65211

VOGT, JAMES R.
Research Reactor
University of Missouri
Columbia, MO 65211

VOKERT, WYNN A.
University of Missouri
Dept. of Radiology
Columbia, MO 65211

WALFRIED, MICHAELIS
GKSS Research Center
D-2054 Geethacht, Germany

WEATHERS, GENE
Francis Howe H.S.
Weldon Springs, MO 64870

WEBBER, C.E.
McMaster University
Hamilton, Ontario,
Canada

WIERNIK, MIGUEL
Universidade Estadual de
Campinas
Institute of Chemistry
13100 Campinas - S.P.
Brazil

WILDE, HANS RUDOLF
Ruhr Universitaet
D-463 Bochum
West Germany

WILLIAMS, ROBERT E.
University of Illinois
3956 E. Ave. #5
Livermore, CA 94550

ZOLLER, WILLIAM H.
University of Maryland
Chemistry Department
College Park, MD 20742

☆U.S. GOVERNMENT PRINTING OFFICE: 1981-740-145/2134